Química de moléculas orgánicas en regiones de formación de estrellas masivas

Centro de Astrobiología. INTA-CSIC
Departamento de Astrofísica Molecular. ICMM

Departamento de Física Teórica
Facultad de Ciencias
Universidad Autónoma de Madrid

Memoria para acceder al grado de Doctor realizada por:

Alicia López Jiménez

Directores:

Prof. José Cernicharo Quintanilla

Departamento de Astrofísica Molecular. ICMM

Dra. Belén Tercero Martínez

Cuerpo de Astrónomos del Estado

Tutora: **Patricia Sánchez-Blázquez**
Departamento de Física Teórica. UAM

Junio 2017

Índice de Materias

Abstract **1**

1 Prólogo y Objetivo de la investigación **4**
1.1 Introducción . . . 5
1.2 Objetivos de la investigación . . . 8

2 Región de formación de estrellas: Nube de Orión **10**
2.1 Contexto: Nube de Orión-KL . . . 11
2.1.1 Componentes de la nebulosa de Orión-KL . . . 12
2.2 Formación de estrellas masivas . . . 19
2.2.1 Formación estelar . . . 19
2.2.2 Formación de estrellas OB . . . 21
2.3 Región de formación de estrellas y Química Interestelar . . . 22
2.3.1 Formación estelar y su efecto en la química . . . 22

3 Moléculas orgánicas complejas interestelares **24**
3.1 Moléculas orgánicas complejas interestelares . . . 26
3.1.1 Temperatura de las regiones del ISM y las transiciones observadas . . . 27
Condiciones físicas del ISM . . . 29
3.1.2 Parámetros físico-químicos . . . 30
3.2 Espectroscopía de moléculas . . . 35
3.2.1 Moléculas interestelares trompo-asimétricas . . . 36
3.3 Observación de las COMs en el ISM . . . 37
Moléculas prebióticas . . . 38
Moléculas en núcleos fríos y envolturas circumestelares de estrellas evolucionadas 39
Moléculas complejas en PDRs . . . 39
Moléculas en nubes difusas . . . 40
Moléculas en outflows . . . 40
Moléculas complejas extragalácticas . . . 40
Moléculas a alto redshift . . . 40
3.4 Reacciones moleculares: Química interestelar . . . 40
Reacciones interestelares dominantes en el ISM . . . 43
3.4.1 Algunos precursores para la formación de las moléculas interestelares . . . 43
Papel del H_2 . . . 43
Papel de H_3^+ . . . 43
Papel del CH_3OH . . . 44
3.4.2 Reacciones térmicas y no-térmicas . . . 44
3.4.3 Velocidad de la reacción . . . 45
3.5 Formación de las COMs en los *hot cores* . . . 45
3.5.1 Modelos de química . . . 46
3.6 Polvo interestelar y química . . . 47
3.6.1 Escala de tiempo de colisión de las moléculas con los granos de polvo . . . 47
3.6.2 Composición química de los granos de polvo . . . 47
PAHs: diminutos granos de polvo carbonáceos . . . 48

3.6.3 Manto de hielo de los granos de polvo . . . 48

4 Metodología: Radioastronomía y Laboratorio **50**
Observaciones . . . 51
Análisis . . . 52
4.1 Interacción entre materia y radiación . . . 52
4.1.1 Mecanismos de población de niveles energéticos . . . 53
4.1.2 Aproximaciones . . . 57
4.2 Radioastronomía . . . 58
4.2.1 La atmósfera terrestre . . . 58
4.2.2 Radiotelescopios . . . 59
4.2.3 Reducción de las observaciones: el problema de la banda imagen . . . 62
4.3 Técnicas de análisis específicas . . . 63
4.3.1 Diagramas de población o rotación . . . 63
4.3.2 Modelización con MADEX . . . 65
4.4 Metodología: Análisis de Laboratorio . . . 66
4.4.1 Espectroscopía rotacional en el laboratorio . . . 66
4.4.2 Espectroscopía (sub)milimétrica (QUIFIMA-UVA) . . . 66
4.4.3 Procedimiento: predicción de frecuencias de las líneas rotacionales . . . 68

5 Trabajos publicados **69**
5.1 Caracterización en el laboratorio y detección astrofísica de estados vibracionalmente excitados de cianuro de etilo . . . 69
5.2 Caracterización en el laboratorio y detección astrofísica de estados vibracionalmente excitados de cianuro de vinilo en Orión-KL . . . 84
5.3 Descubrimiento de acetato de metilo y de *gauche* formiato de etilo en Orión . . . 125
5.4 Buscando *trans* etil metil éter en Orión-KL . . . 132
5.5 Isómeros de C_2H_4O en Orión-KL: Formiato de metilo, Ácido acético y Glicolaldehído. Una visión de conjunto de ALMA y de IRAM 30 m . . . 141
5.6 Resultados globales . . . 172
5.6.1 Identificación de líneas . . . 172
5.6.2 Sumario de los resultados . . . 173
5.6.3 Moléculas prebióticas . . . 181
5.6.4 Trabajos publicados . . . 182

6 Conclusiones y Perspectivas **183**
6.1 Conclusión de los resultados . . . 183
6.2 Conclusiones globales de la tesis . . . 183
6.3 Perspectivas futuras . . . 184

Material Adicional **185**

A *Daly et al. 2013, ApJ, 768, 81* **186**

B *López et al. 2014, A&A, 572, A44* **272**

C *Tercero et al. 2013, ApJ, 770, L13* **386**

D *Tercero et al. 2015, A&A, 582, L1* **408**

E *Lopez et al. 2017, en preparación* 445

Bibliografía 482

Abstract

Resumen de los resultados de la tesis

La espectroscopía de las moléculas orgánicas, consideradas complejas desde un punto de vista interestelar cuando tienen más de 6 átomos, es la herramienta principal utilizada en este trabajo, tanto en el ámbito de laboratorio (en algunos casos con el laboratorio de espectroscopía molecular QUIFIMA-UVA), como en l observacional (con datos del telescopio de antena única de 30 m de IRAM, y en algunos casos, con los del interferómetro ALMA). La radioastronomía, necesita información de los laboratorios de espectroscopía molecular, para la caracterización e identificación de moléculas abundantes en las nubes moleculares del medio interestelar, en el caso concreto de este trabajo, la nube molecular asociada con Orión-KL. La temperatura de esta región de formación de estrellas masivas hace que se exciten los estados vibracionales más bajos de muchas de estas moléculas. Por lo tanto, además de isotopólogos, contamos con la detección de algunos de sus modos vibracionales. Esto ha sido posible gracias a las medidas en el dominio de las ondas milimétricas y submilimétricas realizadas durante mi estancia en el laboratorio de espectroscopía del Profesor José Luis Alonso de la Universidad de Valladolid. A partir de la información obtenida en el laboratorio, podemos afrontar el estudio de los estados vibracionalmente excitados que contribuyen con una gran cantidad de líneas rotacionales a nuestro espectro interestelar. Para ello, nos basamos en un grupo de familias de moléculas que contienen nitrógeno (CH_3CH_2CN y CH_2CHCN) y otras que contienen oxígeno (CH_3OCOH e isómeros; CH_3OCOCH_3 y CH_3CH_2OCOH; $CH_3CH_2OCH_3$; $CH_3CH_2OCH_3$), con el fin de estimar las condiciones físico-químicas de la nebulosa de Orión-KL.

En los casos en los que se dispone de datos de ALMA, se pueden establecer sub-componentes de la nube con una alta resolución espacial. Esto nos ofrece una valiosa información acerca de posibles mecanismos de formación/destrucción de moléculas interestelares, y nos define los parámetros físicos de cada sub-región de la nube, para modelizar las líneas de las moléculas detectadas con el radiotelescopio de 30 m de IRAM. El análisis astrofísico combinado con el análisis de laboratorio, ha permitido la detección interestelar de nuevos estados excitados por primera vez en Orión-KL: CH_2CHCN v_{11}=2,3; CH_3CH_2CN v_{12}=1 y v_{20}=1; CH_3COOH, CH_2OHCHO; trans-CH_3CH_2OCOH; y por primera vez en el espacio: CH_2CHCN (v_{10}=1)⇔(v_{11}=1,v_{15}=1); CH_3COOH v_t=1,2; CH_3OCOCH_3; *gauche*-CH_3CH_2OCOH; *trans*-$CH_3CH_2OCH_3$. Con todas las moléculas observadas y analizadas en esta tesis, aportamos un total de más de 9 600 características espectrales, contribuyendo a reducir el número de líneas sin identificar en el espectro de Orión-KL de manera muy significativa, y a inferir posibles rutas químicas para la formación de dichas moléculas. Este trabajo, ha permitido caracterizar el espectro de este prototipo de *hot core*, y tendrá una alta relevancia en la detección e identificación de líneas moleculares con ALMA en otras regiones de formación de estrellas masivas.

Para el diagnóstico de la región de Orión-KL, es necesario obtener información acerca de la estructura y dinámica de la fuente, utilizar toda la información relevante obtenida en trabajos previos por otros autores, y emplear códigos de transferencia de radiación adecuados, para determinar las condiciones fisico-químicas de la nube. Para ello, utilizaremos varias herramientas para interpretar la emisión observada en términos de propiedades físicas (códigos LVG, diagramas rotacionales; *ver* Cap. 2), así como la modelización de los procesos químicos responsables de la formación de las moléculas (*ver* Cap. 3). Asímismo, en este manuscrito abordamos la metodología tanto experimental (laboratorio) como

observacional (radioastronomía), y el procedimiento de análisis astrofísico para moléculas orgánicas complejas con un espectro denso y poblado de líneas rotacionales que emergen de la nube y alcanzan nuestros radiotelescopios (*ver* Cap. 4). La nube molecular seleccionada, Orión-KL, es una región de formación de estrellas masivas cercana y referente para el tipo de moléculas tratadas en esta tesis. Finalmente, los artículos incluidos en este trabajo organizados por grupos de familias de moléculas conteniendo nitrógeno y oxígeno, componen la estructura principal de esta tesis con la finalidad de aportar un paso más en el conocimiento de las regiones de formación estelar masiva, y por ende, de la complejidad química en este tipo de regiones y, con ello, en el medio interestelar (*ver* Cap. 5).

Abstract of results of the dissertation

The spectroscopy of organic molecules, which from an interstellar point of view are considered to be complex when they have more than six atoms, is the main tool used for this work, both in the area of the laboratory (sometimes with the QUIFIMA-UVA molecular spectroscopy laboratory) and in the field of astronomical observations (with data from the single-dish 30 m telescope of IRAM and in some cases, those of high-spatial resolution of the ALMA interferometer). Radioastronomy needs information from the laboratory for the spectral characterization and identification of abundant molecules in the Orion-KL molecular cloud. The temperature of this high-mass star forming region causes many of the low-lying vibrational states of these molecules to be excited so that, in addition to lines from rare isotopologues, we have to identify lines arising from vibrationally excitd states, thanks to the availability of laboratory measurements in the millimeter and submillimeter domains. Thus, we tackle the study of vibrationally excited states that contribute with a significant number of rotational lines to th observed spectra of Orion-KL. We have selected a family of nitrogen-bearing molecules (CH_3CH_2CN y CH_2CHCN) and oxygen-bearing molecules (CH_3OCOH and their isomers; CH_3OCOCH_3 y CH_3CH_2OCOH; $CH_3CH_2OCH_3$; $CH_3CH_2OCH_3$), in order to estimate the physico-chemical conditions of Orion-KL nebula.

In those cases in which ALMA data are available, it is possible to set out the cloud sub-components with high spatial resolution, which provides a very valuable information about possible formation/destruction mechanisms of interstellar molecules and allow us to constrain the physical parameters of each sub-region by modeling the lines detected with the IRAM 30 m radio-telescope. Astrophysical analysis combined with laboratory analysis has allowed the interstellar detection of new vibrationally excited states for the first time in Orion-KL: CH_2CHCN v_{11}=2,3; CH_3CH_2CN v_{12}=1 y v_{20}=1; CH_3COOH, CH_2OHCHO; trans-CH_3CH_2OCOH; and for the first time in space: CH_2CHCN (v_{10}=1)⇔(v_{11}=1,v_{15}=1); CH_3COOH v_t=1,2; CH_3OCOCH_3; gauche-CH_3CH_2OCOH; trans-$CH_3CH_2OCH_3$−tentative detection. With all the molecules of this dissertation, we provide a total of more than 9 600 spectral features contributing to significantly reduce the number of unidentified lines in the Orion-KL spectra and infer possible chemical routes to their interstellar formation. This work has permitted to characterize the spectrum of this prototypical hot core and will be of great importance to detect and identify molecular lines using ALMA in other high-mass star forming regions.

For the diagnosis of the Orion-KL region it is necessary to have information about its structure and dynamics, and to rely on the previous work performed by other authors. The tools that we have used to determine the physico-chemical conditions of the cloud, are described in Chap. 2 and the analysis of the molecules responsible for such emission in Chap. 3. Likewise, in this manuscript we have adopted both experimental (laboratory) and observational (radio astronomy) methodologies, and have carried out an analysis of the spectrum of Orion-KL, which is densely populated by rotational lines of complex organic molecules (see Chap. 4). Orion-KL is the closest high-mass star forming region and

a benchmark for the chemical study of the molecules treated on this thesis. Finally, the scientific papers in this work, organized by group of families of molecules containing nitrogen and oxygen, make up the main structure of this dissertation with the aim of contributing to the knowledge of the regions of massive star formation, and therefore of the chemical complexity in this type of regions and, therefore, in the interstellar medium(see Chap. 5).

Capítulo 1

Prólogo y Objetivo de la investigación

Las moléculas interestelares abundan en todos los entornos. Especialmente en aquellos, asociados a las regiones de formación estelar, es decir, las nubes moleculares; lugares donde se concentra la mayor parte del gas molecular. En la emisión de sus líneas rotacionales, y en algún caso en vibracionales (H_2), radica su importante labor como refrigerantes de las nubes, influyendo en los procesos de formación estelar. Buscarlas en los entornos donde nacen las estrellas, es una oportunidad para investigar la complejidad química que se desarrolla en el medio interestelar, definiendo una disciplina científica que engloba esencialmente a la química y a la astrofísica, es decir, la Astroquímica o Astrofísica Molecular. Y como si de una técnica fotográfica se tratase, la radioastronomía es capaz de captar ese crisol de moléculas que se forman durante periodos de tiempo enormes, comparados con aquellos asociados a la química en la Tierra, y nos proporcionan la información esencial sobre su composición, estructura, así como de los procesos físicos y químicos que están aconteciendo en un momento determinado. Para caracterizar nuestra fuente objeto de estudio, debemos afrontar el desafío de comprender la evolución química del medio interestelar, desde las nubes difusas a las nubes densas. Los estudios acerca del medio interestelar, al fin y al cabo, pueden desembocar en el estudio de otros sistemas planetarios, lo cual puede permitirnos obtener información sobre la formación de nuestro Sistema Solar y nuestro planeta, así como el rol que jugó la atmósfera primitiva de la Tierra, heredera en parte de la composición del disco protosolar, en la evolución química de nuestro planeta, hasta alcanzar el mayor grado de complejidad mostrado por cualquier sistema: la vida.

El experimento de Miller y Urey (Miller 1953; Miller and Urey 1959) considera la sopa química compuesta por H_2, H_2O, CH_4 y NH_3, como moléculas precursoras implicadas en la química prebiótica, bajo las condiciones de la atmósfera primitiva de la Tierra, como los aminoácidos, o los azúcares como la glucosa. Estos mismos ingredientes de la sopa química son constituyentes básicos de los hielos interestelares que inundan las regiones del medio interestelar. Es natural pensar que es posible que existan determinadas condiciones físicas y químicas interestelares, que lleven a sintetizar algunas de las moléculas prebióticas en el espacio.

El medio interestelar está en continuo reciclaje. Así, cada vez que muere una estrella, su material químico se dispersa por el entorno inmediato, impulsado por los fenómenos físicos asociados a la fase de gigante roja, de estrellas de masa inferior a 8 masas solares, o a los procesos altamente energéticos asociados a las supernovas en la estrellas masivas. Aunque aparentemente la muerte de un estrella solo deja un remanente que contribuye a las fases difusas del medio interestelar, el colapso de éstas, millones de años después, será el preámbulo de una fase densa, donde tendrán lugar las próximas generaciones de estrellas. El hecho de que la nueva generación se trate de estrellas masivas o poco masivas, y de que puedan o no tener planetas a su alrededor, dependerá de diversos factores críticos que conciernen a las condiciones iniciales de la nube molecular y su evolución durante millones de años.

Son muchos los estudios de la nebulosa de Orión-KL, un cercano lugar (418 pc ó unos 1300 a.l.) dominado por estrellas masivas[1] que perturban el medio circundante, ocasionando una gran variedad de procesos físico-químicos que permiten la formación de moléculas complejas. La región de Orión-KL

[1]Nos referimos a estrellas de más de 8 masas solares y de tipo espectral OB

muestra en el espectro milimétrico y submilimétrico una gran cantidad de líneas espectrales de especies abundantes como el dimetil éter, el formiato de metilo, el cianuro de etilo, el ácido acético, entre otras. Estas moléculas actúan como testigos de la región, y su estudio nos revela conocimientos cada vez más precisos de la estructura y condiciones fisicas y químicas del medio.

En primera instancia, podríamos pensar que la nebulosa de Orión-KL es la protagonista de nuestro trabajo por sus propiedades, pero se puede esperar que otras nubes moleculares con la misma tasa de formación estelar y similares condiciones físicas, tengan la misma firma espectral que Orión-KL. La importancia del estudio de esta nebulosa, radica principalmente en su cercanía a nosotros y en que puede ser considerada como un prototipo de zona de formación de estrellas masivas. De hecho, es necesario destacar que todas las regiones de formación de estrellas masivas, incluidas las de masa más baja como los *hot corinos*, poseen un espectro milimétrico y submilimétrico bastante similar al de Orión.

Para saber qué molécula aparece en la nebulosa de Orión-KL, debemos desarrollar un trabajo conjunto entre la astrofísica, la espectroscopía de laboratorio, la química y la física. El trabajo de laboratorio y el análisis astrofísico, se aúnan para descodificar la información de las moléculas que encontramos en el medio interestelar.

El título de esta tesis podría haber sido ”Moléculas orgánicas, el lenguaje de las nubes interestelares”. Es por ello, por lo que en este trabajo, vamos a interpretar lo que nos dicen las moléculas, para indagar en qué tipo de entorno estamos y qué tipo de química se está desarrollando en este laboratorio interestelar, que posteriormente podría llegar a formar futuros sistemas planetarios.

El papel del polvo interestelar es el de arbitrar muchos fenómenos astrofísicos que ocurre en todo el medio interestelar. Su presencia es tan esencial, que sin él las estrellas no se formarían, y como consecuencia las moléculas, y por tanto, nosotros no existiríamos. Si no fuese por este crucial ingrediente, las estrellas serían tan masivas como en los inicios de nuestro universo, y su duración sería tan fugaz, que si se pudiesen formar planetas, la vida en estos si es que la hubiese, sería efímera. Es por ello, que el polvo interestelar como catalizador de moléculas merece una especial atención.

Las observaciones radioastronómicas, nos muestran cómo las moléculas se detectan en casi todas las direcciones donde apuntemos nuestros radiotelescopios y exista un poco de gas interestelar. De hecho, la astroquímica nos invita a descubrir un mundo molecular, revelándonos el verdadero significado de la evolución química del Universo.

El contenido de esta tesis sirve de guía del trabajo desarrollado en los artículos publicados, en los cuales se detalla el procedimiento de análisis para la detección de diversas moléculas con O y N en Orión-KL. Para ello, la síntesis de esta tesis conforma los siguientes capítulos de *Región de formación de estrellas: Nube de Orión*, *Moléculas Orgánicas Complejas Interestelares*, *Metodología: Radioastronomía y Laboratorio*, *Trabajos publicados*, y *Conclusiones y Perspectivas*.

1.1 Introducción

Para empezar, deberíamos indagar acerca de la importancia que tienen las moléculas en el medio interestelar. Si echamos una ojeada a los tipos de nubes interestelares que se conocen, vemos que se tiene que dar una serie de condiciones críticas para que sean ”simples” nubes, que aún no muestran

actividad de formación de estrellas, o bien el lugar idóneo donde la evolución dinámica de la nube ha permitido la aparición de condensaciones pre-estelares o incluso de estrellas. Los granos de polvo actúan de catalizadores de reacciones dando lugar a refrigerantes importantes, como el CO y el H_2O. Pero el papel más relevante desde el punto de vista químico, es la formación del hidrógeno molecular en la superficie de dichos granos. Obviamente, el resto de las moléculas que se forman sobre el polvo y se desorben a la fase gas, a pesar de encontrarse en menor abundancia, también enfrían la nube a través de la emisión de sus líneas rotacionales, lo cual compensa el calentamiento producido por los rayos cósmicos, el colapso gravitatorio y la radiación UV procedente de fuentes externas y de las propias estrellas recién formadas, cuando estas consigan limpiar su entorno de gas y polvo.

Antes de hablar de moléculas orgánicas complejas como las que trataremos en esta tesis, vamos a remontarnos al origen de los elementos en la historia del Universo. Pero para ello, deberíamos recordar algo esencial acerca de la composición fundamental de las moléculas orgánicas, y es que son entidades o compuestos químicos constituidos por carbono (C) e hidrógeno (H), aunque además pueden tener oxígeno (O), nitrógeno (N) y otros elementos como azufre (S), fósforo (P), silicio (Si) y en algunos casos metales como Al, K, Na y Mg, en su composición. De todos estos elementos, H, O, C y N resultan ser los más abundantes en el Universo, y lo más interesante es que, además, son los cimientos que dan estructura a las moléculas prebióticas (aquellas relacionadas con el origen de la vida).

Observar la tasa de la formación estelar (SFRate, "Star Formation Rate") desde las épocas más tempranas del Universo, es crucial para comprender la formación y evolución de galaxias. La evolución de la SFRate a través del tiempo, nos induce a conocer su historia, la información cronológica de lo que aconteció en el Universo, pudiendo acceder a la evolución química en la que ha estado implicada la historia de la formación estelar. La creciente disponibilidad de datos observacionales de galaxias a redshifts (z) cada vez más altos, nos permite el estudio de la historia de la formación estelar a escala cósmica, pudiendo acercarnos a la época de la Reionización, donde comenzó a encenderse la primera población de estrellas masivas ($7 \leq z \leq 30$). Con el tiempo, el medio interestelar se ha ido reciclando y enriqueciéndose de elementos químicos, formados en el corazón de las estrellas a través de las reacciones de nucleosíntesis, que pasarán a formar parte de una gran cantidad de especies moleculares que pueblan todas las nubes moleculares densas.

A pesar de que los procesos químicos encontrados en los entornos estelares poco masivos y en los masivos es similar[2], la importancia del estudio de las estrellas masivas radica en la temperatura a la que someten al gas de su entorno inmediato, calentándolo a temperaturas de hasta unos 300 K, lo que favorece la evaporación de los mantos de hielo de los granos de polvo, activando algunas reacciones que proceden lentamente a baja temperatura, y desencadenando una química compleja que produce una gran cantidad de moléculas poliatómicas, contribuyendo a la densidad espectral hasta el punto que se puede alcanzar el límite de confusión y dificultar el proceso de identificación de las moléculas. Las especies moleculares existentes es posible detectarlas en fase gas a través de su espectro rotacional, en el dominio de las ondas de radio (microondas/(sub)milimétricas e IR-lejano) mediante sus líneas de emisión. Esta química compleja se asocia a la fase denominada "*Hot Core*" (núcleo caliente), y su estudio es el objetivo principal de esta tesis doctoral.

[2]Las condiciones iniciales para la obtención de las moléculas orgánicas complejas en *hot core* y *hot corinos*, pueden no ser similares a causa de la diferente deuteración de las especies moleculares en las primeras etapas y la envoltura externa implicada, con lo que la química que encontrásemos en ambas regiones podría variar en algunas especies, aunque los procesos físicos sean prácticamente los mismos.

Orión-KL (*Kleinmann Low*, Kleinmann and Low 1967) en la nube molecular OMC-1, localizada en la Nebulosa de Orión, es la región de formación de estrellas masivas más próxima a nuestro Sistema Solar. La química encontrada en esta nube es muy rica en moléculas complejas, fruto de la evaporación de los mantos de los granos de polvo en las zonas más calientes de la región; también en esta nube se encuentran distintas componentes del gas debidas a la interacción de los violentos procesos de formación de las estrellas masivas con su entorno (ver, por ejemplo, Genzel and Stutzki 1989; Zapata et al. 2011). El espectro de esta región en el dominio de las ondas milimétricas, se caracteriza por una gran densidad de líneas en emisión de moléculas complejas, como el formiato de metilo (CH_3OCOH), cianuro de etilo (CH_3CH_2CN), dimetil éter (CH_3OCH_3), cianuro de vinilo (CH_2CHCN) y un largo etcétera.

La diferenciación química dentro de la región de Orión-KL, como cualquier otro *"hot core"*, depende de su historia previa, es decir, de la etapa *fría* que ocurrió antes del colapso de la nube. Dicha etapa, representa las condiciones fisico-químicas iniciales, pertenecientes al proceso de formación de estrellas en esta región. Dado que no todo el gas de la nube es utilizado en la formación de estrellas, dichas condiciones iniciales se aplican a todas las componentes del gas en la región. Algunas de estas componentes, aún siguen mostrando prácticamente las mismas abundancias moleculares y los mismos parámetros físicos que al principio de la evolución de la nube molecular (el *extended ridge*). Otras sin embargo, muestran una alteración extraordinaria de las condiciones fisico-químicas, y corresponden a regiones sometidas a choques y/o iluminadas por las estrellas recién formadas.

Los niveles de vibración de las moléculas complejas más abundantes en la nebulosa de Orión, como CH_3OCOH, CH_3CH_2CN, CH_2CHCN, tienen energías relativamente bajas y son poblados bajo las condiciones físicas de la región de Orión-KL (Demyk et al. 2008; Daly et al. 2013; López et al. 2014). Sin embargo, la falta de estudios espectroscópicos sobre todos estos estados, hace imposible la detección de las líneas moleculares provenientes de estas especies, con lo que el número de líneas sin identificar en las observaciones de los espectros milimétricos y sub-milimétricos de las nubes moleculares es muy abundante, impidiendo un completo análisis de estas regiones. En la actualidad, la colaboración entre los laboratorios de espectroscopía molecular y los astrofísicos moleculares está cambiando esta situación, y es en esta dirección en la que se ha basado el trabajo que conforma una buena parte de esta tesis doctoral.

El barrido espectral de Orión-KL se tomó con el radiotelescopio de 30 m de IRAM, apuntando hacia la fuente infrarroja IRc2 en las ventanas espectrales de 3, 2 y 1.3 mm (Tercero et al. 2010). El análisis de más de 15 000 líneas espectrales detectadas en este barrido, requiere de una colaboración estrecha entre astrofísicos, espectroscopistas, físicos teóricos y químicos. Dada la multitud de líneas, el análisis fue focalizado en dos direcciones: por un lado dividiendo el análisis en distintas familias de moléculas y, por otro, detectando nuevas especies gracias a las frecuencias proporcionadas a través de los laboratorios. De esta manera, es posible profundizar en la información de las condiciones físicas y químicas de la región.

Además, disponemos de datos de alta resolución espacial, obtenidos con el interferómetro ALMA (*Atacama Large Millimeter/Submillimeter Array*) de Chile, procedentes de 16 de las antenas de 12 m operando en el rango de frecuencias de la banda 6 (213.715−246.627 GHz). En esta nueva era de la radioastronomía que estamos viviendo con la puesta en marcha del interferómetro ALMA, es esencial la estrecha colaboración entre diversas áreas del conocimiento, que confluyen en la Astrofísica molecular o Astroquímica, para una adecuada interpretación de estas nuevas observaciones.

Las primeras moléculas en el espacio, detectadas en la década de los años 30 del siglo pasado, fueron los radicales CH y CN, y el ión CH^+, y su detección se obtuvo mediante espectroscopía óptica. Hubo que esperar hasta el año 1963, para que se detectase la primera molécula en la región de las ondas de radio, el radical OH. A partir de ese momento, el observatorio de Kitt Peak (radiotelescopio de 11 m, Arizona, USA) impulsó la era de la radioastronomía con el descubrimiento de un número considerable de moléculas interestelares a bajas frecuencias. A partir de 1984, los telescopios americanos cedieron protagonismo al radiotelescopio de 30 m de IRAM (Granada, España), instrumento creado para la observación en la región milimétrica y submilimétrica del espectro. De manera paralela, la caracterización de los espectros moleculares en el laboratorio, ha sido fundamental para poder asegurar cualquier detección molecular en el espacio. Es interesante destacar, que el estudio de laboratorio del primer espectro microondas, se llevó a cabo con la molécula de NH_3 en 1934. Sin embargo, la sinergia entre la observación radioastronómica y la experimentación de laboratorio, con la finalidad de detectar nuevas especies moleculares en los entornos astrofísicos, comenzó varias décadas después, cuando se detectaron las primeras moléculas en el dominio de las ondas de radio.

Hasta la fecha (junio 2017), se han detectado cerca de 200 moléculas en el medio interestelar y en las envolturas circumestelares. El monóxido de carbono (CO), es la segunda molécula interestelar más abundante después del hidrógeno molecular (H_2), y ambas, junto con los granos de polvo, tienen especial relevancia en la síntesis de las moléculas orgánicas más complejas, detectadas en una gran diversidad de nubes moleculares.

Debido a la importancia del polvo en la formación de las especies moleculares, es necesario dedicar un apartado a la composición de los mantos de los hielos de los granos de polvo, puesto que de ellos depende que las reacciones químicas se desarrollen en una dirección u otra, ofreciendo una diferenciación química de los diferentes grupos funcionales.

En esta tesis, un estudio conjunto de las moléculas nitrogenadas y oxigenadas, nos permite determinar la abundancia molecular en las componentes que constituyen nuestra nebulosa de una manera precisa, puesto que se trata de moléculas abundantes y, por tanto, fieles testigos de las condiciones físicas y químicas de nuestra nube molecular. Los mapas de emisión para las diferentes moléculas, revelan su distribución espacial, lo cual nos aporta una valiosa información sobre los procesos de formación de cada especie. Para completar esa información, debemos incluir en nuestro estudio las moléculas precursoras, a partir de las cuales se originan las moléculas de nuestro trabajo, como pueden ser metanol, acetona, formaldehído, etc.

La naturaleza de *hot core*, hace que la *"alta"* temperatura favorezca unas nuevas condiciones, para la producción de las moléculas más complejas que se han encontrado en el medio interestelar. Sin embargo, no hemos detectado todavía el aminoácido más simple (glicina), lo cual podría tener su explicación, en que la presencia de los ingredientes precursores de este tipo de moléculas prebióticas, necesitan mucho más tiempo para llegar a formarse.

1.2 Objetivos de la investigación

La importancia de la presente investigación, radica en los resultados obtenidos a través de la combinación de los datos de laboratorio, con aquellos procedentes de la observación radioastronómica.

El estudio de las moléculas de interés astrofísico en el ámbito de la experimentación de laboratorio, acompañada con cálculos teóricos, es un complemento necesario para la detección de especies moleculares en el medio interestelar, y para la interpretación de las observaciones. Las regiones de formación de estrellas masivas, presentan una gran densidad de líneas en sus espectros debido a complejidad de la química que allí tiene lugar, y a las altas abundancias relativas al hidrogeno molecular de dichas especies moleculares. Estudiar las propiedades físicas y químicas de dicha región a través de la emisión espectroscópica de las moléculas más abundantes, nos ofrece una visión de la evolución de este tipo de regiones, así como de su importancia en la generación de una química prebiótica.

El objetivo de esta investigación, es obtener las condiciones físicas y químicas de la nebulosa de Orión-KL, además de la caracterización de nuevas especies en el laboratorio, con el fin de reducir el número de líneas sin identificar en los espectros observados y facilitar así la caracterización físico-química de la región bajo estudio. Para ello, hemos llevado a cabo un estudio espectroscópico de las transiciones rotacionales de las moléculas que emiten en Orión-KL, identificando también líneas de nuevas especies, gracias al trabajo conjunto de las medidas de laboratorio (cálculos mecano-cuánticos, medidas experimentales en el rango mm/submm) y el análisis de las observaciones. En definitiva, las observaciones que se van a analizar en este trabajo, van a proporcionar estimaciones de la temperatura, densidad volúminica, abundancias moleculares, cinemática y dinámica de las zonas de Orion-KL sometidas a la interacción con las estrellas masivas. Las condiciones de temperatura y densidad obtenidas, nos permite inferir la evolución y estructura de la fuente, trazar las rutas químicas de formación de las especies moleculares encontradas, y determinar el contenido molecular de estos objetos.

Las medidas de laboratorio permiten obtener las constantes espectroscópicas (constantes rotacionales efectivas, constantes de distorsión centrífuga y demás términos de corrección del hamiltoniano) de las moléculas orgánicas en su estado fundamental y sus estados excitados vibracionalmente, y así poder determinar las frecuencias de las transiciones, que nos van a permitir detectar y analizar esas especies en nuestro espectro de la nebulosa de Orión-KL.

Las moléculas objeto de estudio son CH_3OCOH, CH_3CH_2CN, CH_2CHCN, CH_3COOH, y CH_3OCOCH_3. Los isómeros de la molécula de formiato de metilo (CH_3OCOH), ácido acético (CH_3COOH) y glicolaldehído (CH_2OHCHO), incluyendo sus estados torsionales, nos dan una visión acerca de la importancia de la isomerización en el medio interestelar, para deducir rutas de formación molecular. Además, hemos observado y estudiado el acetato de metilo (CH_3OCOCH_3) y su isómero, gauche-formiato de etilo (g-CH_3CH_2OCOH), así como una molécula de 12 átomos detectada en nuestra fuente, el etil metil éter ($CH_3CH_2OCH_3$).

Capítulo 2

Región de formación de estrellas: Nube de Orión

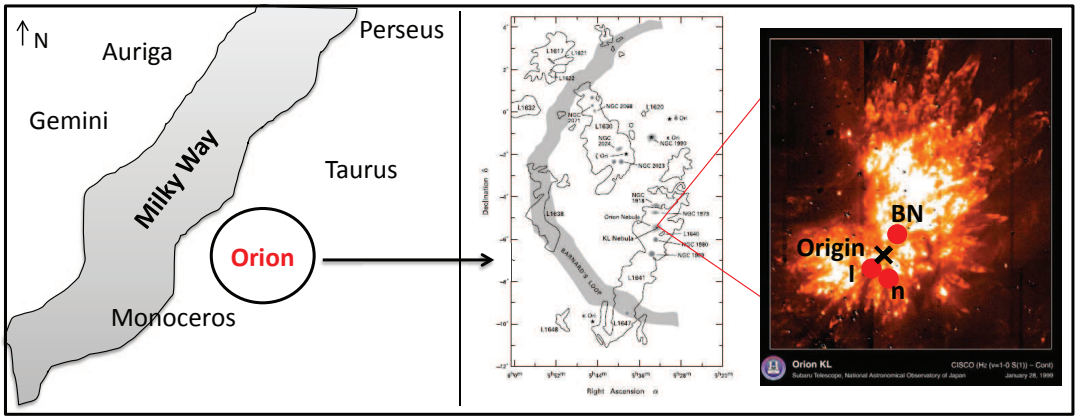

Figura 2.1: Contexto de la nebulosa de Orión-KL. *Fuente: Basado en Bally et al. 2015 y en el libro de Stahler and Palla 2004. Imagen de Orión-KL: CISCO, Telescopio de 8.3m-Subaru, NAOJ*

Durante la evolución estelar, el ISM sufre importantes modificaciones, a causa de las grandes cantidades de masa y energía eyectados al inicio y final de los ciclos vitales de las estrellas, fundamentalmente mediante sus vientos estelares y eyecciones masivas de materia, producidos por eventos sumamente energéticos como explosiones de supernova.

La nebulosa de Orión, es una nube molecular gigante con regiones de formación estelar masiva, en las que los objetos estelares jóvenes inmersos en la nube (YSOs, por sus siglas en inglés *Young Stellar Objects*), calientan, ionizan e interacionan con el medio interestelar, caracterizando diferentes fases de las nubes en base a sus propiedades de densidad, temperatura y composición química. En estas regiones, hay cúmulos densos, filamentos, cirros, nubes difusas, traslúcidas, densas y oscuras, proplidos (discos protoplanetarios o planetarios sometidos a un campo UV intenso).

Esta región, es de gran interés por su cercanía (414±6 pc, Menten et al. 2007, Kim et al. 2008), y en ella se produce la interacción de las estrellas masivas recién formadas con la materia interestelar de la nube parental, dando lugar a la Nebulosa de Kleimann-Low, situada en la Nube molecular de Orión-1 (OMC-1), que a su vez está inmersa dentro de la gran nube molecular de Orión-A (Genzel and Stutzki 1989). La interacción de dichas estrellas con el medio circundante, da lugar a una gran complejidad química, producto de una serie de rutas químicas de formación/destrucción, tanto en fase gas como sobre los mantos de hielo de los granos de polvo.

El estudio de las condiciones físicas y químicas de la Nebulosa de Orión-KL, puede trazarse por medio de la emisión de las moléculas presentes, especialmente a través de las más abundantes. Por ejemplo, la anchura de nuestras líneas espectrales, pueden ser consecuencia de la energía cinética transferida por la turbulencia generada por los ”outflows” de las estellas masivas recién formadas y

todavía embebidas en la nube (*ver por ej.* Beichman et al. 1986, Myers et al. 1988), y posiblemente por la turbulencia aportada por los campos magnéticos y gravitatorios (*ver por ej.* Li et al. 2014). Las estrellas masivas que han conseguido limpiar su entorno de gas y polvo, son estrellas de tipo espectral OB, tienen unas $\approx 10^5$ luminosidades solares, y una edad de unos cuantos millones años (Lada and Kylafis 2012a).

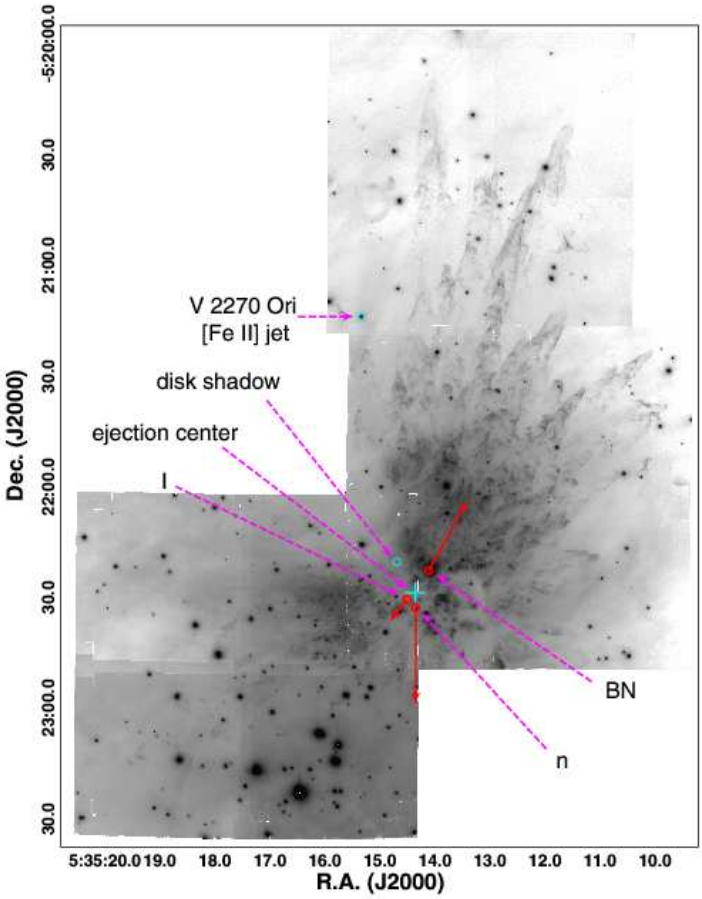

FIGURA 2.2: IMAGEN DEL *outflow* DE OMC-1 EN H_2 CON LOS MOVIMIENTOS PROPIOS (VECTORES ROJOS, GÓMEZ ET AL. 2008) DEL OBJETO BN Y LAS FUENTES DE RADIO I Y *n*. LA CRUZ MUESTRA EL CENTRO DE EJECCIÓN DEL GAS DETERMINADO POR LOS MOVIMIENTOS PROPIOS DE DICHAS FUENTES. (*Fuente: Bally et al. 2015*)

2.1 Contexto: Nube de Orión-KL

La diferenciación química de las distintas componentes cinemáticas que constituyen la nube de Orión-KL, es una clara evidencia de las diferentes condiciones iniciales de formación estelar. Debido al rango de temperaturas de las componentes de la nube, además de las especies debidas a una química en fase gas; en la que incluso se obtienen moléculas producto de eficientes procesos endotérmicos con barreras de activación, o tiene lugar la destrucción de otras originadas en las etapas previas, también existe una química en superficie sobre los granos, que contribuye significativamente al aumento de la abundancia de las moléculas orgánicas en fase gas.

Franco et al. (1988) propusieron un modelo para la formación del complejo de Orión-Monoceros, a partir de una colisión de nubes a gran velocidad hace unos $6{\times}10^7$ años desde el hemisferio sudeste de la Galaxia hacia el disco Galáctico, en la que las fuerzas de marea provocaron la fragmentación de la nube en el complejo de Orión y en el de Monoceros (fig. 2.3 arriba). El complejo molecular de Orión consta de nubes difusas, oscuras, densas, núcleos pre-estelares, regiones HII, PDRs, etc. El complejo molecular sur se corresponde con la nube de Orión A (Kutner et al. 1977), y está centrado de manera aproximada en la nebulosa de Orión (NGC1976). La nube molecular gigante de Orión (*ver* Fig. 2.3 abajo) está asociada a una gran cantidad de material molecular, que nos ofrece información acerca de la distribución del gas en la nube, así como de su evolución en el tiempo y su cinemática. La nube molecular de Orión 1 (OMC-1) es el cúmulo molecular o núcleo denso predominante de la región de Orión A, en el que se están ocurriendo fenómenos de formación estelar, y contiene estrellas embebidas que emiten en el dominio de las ondas de radio y/o IR, las cuales pueden estar produciendo la expansión de la región HII (M42, Orión A)[1], que rodea a las estrellas OB del Trapecio y comprime la nube de OMC-1 (Genzel and Stutzki 1989).

El núcleo denso OMC-1 en el que se encuentra la nebulosa de Kleimann-Low o nebulosa de Orión-KL (Kleimann & Low 1967), es el contexto principal de esta tesis, cuyo principal mecanismo de calentamiento es radiativo (Goldsmith et al. 1983). La nebulosa IR de Kleimann-Low está caracterizada por una serie de fuentes de emisión en radio e IR embebidas, y son responsables del fenómeno energético que domina la región (Genzel and Stutzki 1989). Entre ellas, destacan la fuente de radio I y las fuentes de infrarrojo IRc2, n y BN (Becklin and Neugebauer 1967, Menten and Reid 1995, Zapata et al. 2011). IRc2 es la fuente predominante de la región (Wynn-Williams et al. 1984). En esta fuente, los objetos compactos que emiten en el IR y el radio, aportan una luminosidad total de unas $\approx 10^5\, L_\odot$. IRc2 es la fuente seleccionada para el barrido espectral realizado con el radiotelescopio de 30-m de IRAM, objeto de este trabajo. La figura 2.4 muestra un mapa de emisión del continuo de Orión-KL en la ventana milimétrica de 1.3 mm (Wu et al. 2014).

Por el momento, no hay un consenso acerca de si el calentamiento del *Hot Core* de Orión-KL es interno, ocasionado por estrellas embebidas, o por otras fuentes extensas (Genzel and Stutzki 1989, Blake et al. 1996, Kaufman et al. 1998, De Vicente et al. 2002, Zapata et al. 2011, Bally et al. 2015). Como se ha mencionado anteriormente, el calentamiento del *Hot Core* de Orión-KL parece no estar producido por la presencia de una proto-estrella, sino más bien por el impacto de material a gran velocidad hace unos 500 años, en el que el gas acelerado a alta velocidad (un fenómeno trazado especialemente por líneas de CO) desencadenó el calentamiento de la nube y, en consecuencia, el *Hot Core* de Orión-KL (Zapata et al. 2011, Bally et al. 2017).

2.1.1 Componentes de la nebulosa de Orión-KL

Entre las condensaciones densas y calientes de Orión-KL (Tabla 5.1, *basado en* Blake et al. 1987), nos encontramos el *plateau*, el *extended ridge* o nube ambiente, el *compact ridge*, y el *hot core*. El *hot core* se caracteriza por la elevada temperatura, a consecuencia de la actividad de la formación estelar, y el *plateau*, por la presencia de *outflows* en la región. La componente asociada al *extended ridge* presenta una menor temperatura cinética. Por otro lado, en el *compact ridge* también se observan regiones de gas caliente de temperaturas un poco menores que las de las componentes de *hot core*, pero

[1]El complejo de Orión está constituido por diversos objetos, entre los cuales nos encontramos con la Gran Nebulosa de Orión (M42) y la nebulosa Cabeza de Caballo.

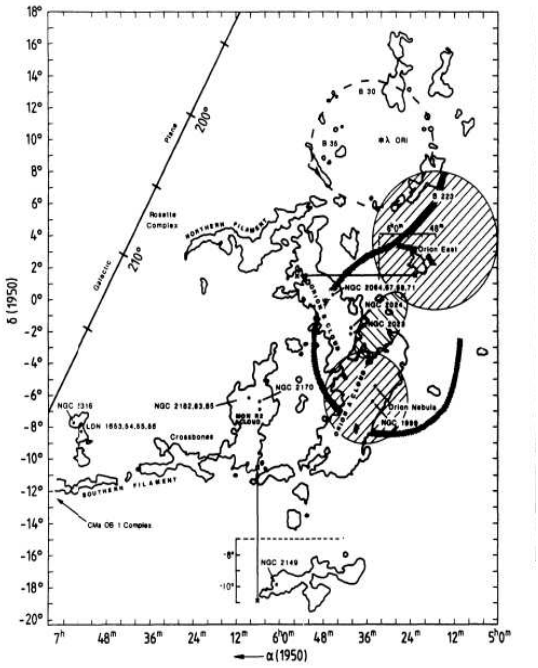

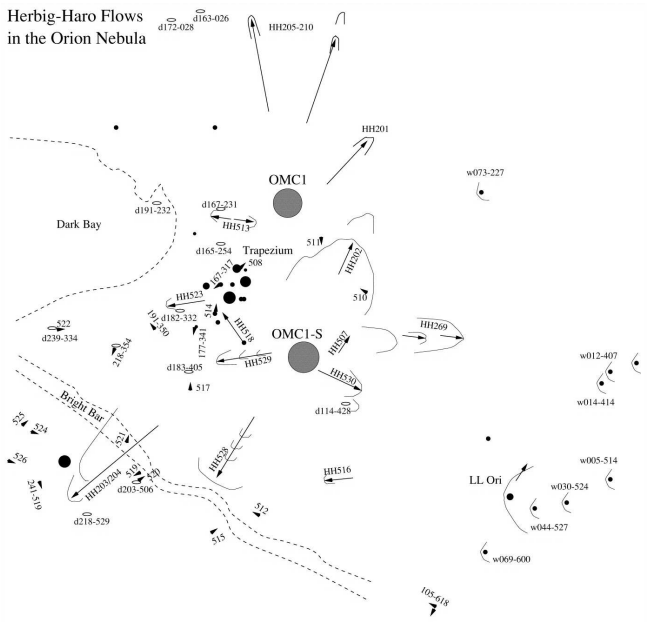

FIGURA 2.3: *Arriba*: FIGURA QUE MUESTRA LA DISTRIBUCIÓN ESPACIAL DE LA NUBE DE ORIÓN, EN LA QUE SE APRECIAN NUBES Y ZONAS DE FORMACIÓN ESTELAR A GRAN ESCALA, EN LOS COMPLEJOS MOLECULARES DE ORIÓN Y MONOCEROS (*Genzel and Stutzki 1989*). *Abajo*: ILUSTRACIÓN DEL ENTORNO DE LA NEBULOSA DE ORIÓN (NEBULOSA DE *M*42), EN LA QUE LOS FLUJOS (U *outflows*) DE LOS OBJETOS HERBIG-HARO SE REPRESENTAN COMO VECTORES "HH(SEGUIDO DE UNA NUMERACIÓN)" Y LOS GLÓBULOS DE BOK COMO CÍRCULOS SÓLIDOS. SE PUEDEN OBSERVAR LAS ESTRELLAS DEL TRAPECIO, ASÍ COMO LA FUENTE OMC-1 AL NORESTE, EN CUYA POSICIÓN COINCIDE LA NEBULOSA DE ORIÓN-KL. *Fuente: Bally et al. 2000*

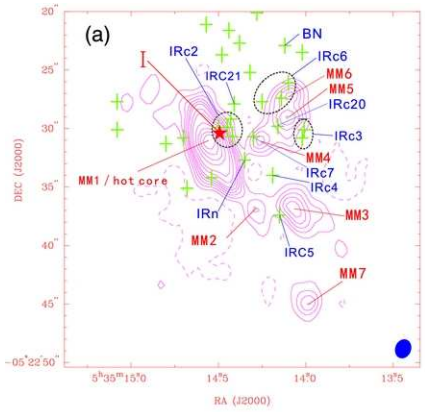

FIGURA 2.4: MAPA DE EMISIÓN DEL CONTINUO DE LA NEBULOSA DE ORIÓN-KL EN LA VENTANA MILIMÉTRICA DE 1.3 MM (*Wu et al. 2014*). LOS NIVELES DE CONTORNO VARÍAN ENTRE -0.05 Y 1.3 JY·BEAM^{-1}, LA NOTACIÓN MM1-7 SE CORRESPONDE CON NÚCLEOS DE EMISIÓN DEL POLVO Y LAS CRUCES VERDES REPRESENTAN LAS FUENTES DE IR CERCANO.

con una química diferente.

TABLA 2.1: COMPONENTES CLÁSICAS DE LA NUBE DE ORIÓN-KL.

COMPONENTE	n (cm^{-3})	T_{rot} (K)	d_{fuente} (")	v_{LSR} (kms^{-1})	Δv (kms^{-1})	Origen (emisión)
plateau	$\geq 10^6$	95-150	≤20"	7-8	≥20-25	*outflows*−choques−regiones
extended ridge	$\approx 10^5$	55-60	extensa	9	4	*outflows*−choques−regiones
compact ridge	$\geq 10^6$	80-140	≤30"	7-8	3-5	nube ambiente−*outflows*
hot core	$\geq 10^7$	150-300	≤10"	3-5	5-10	formación estelar activa

Nota. Esta tabla muestra las diferentes componentes de la nube, las cuales representan las condiciones típicas o clásicas de la nebulosa de Orión-KL (*basado en* Blake et al. 1987).

A continuación se describen las propiedades físicas más importantes[2] que caracterizan cada región clásica de la nube de Orión-KL. Para más detalle de las componentes de la nube de Orión, remitimos a Blake et al. 1987 y a la Tesis doctoral de B. Tercero ().

• *Plateau*:

La emisión de la componente del *plateau* es producida por moléculas simples como CO, CS, SiO, SO, SO_2, OCS, H_2S, HDO, H_2CO, HCN, HC_3N (Blake et al. 1987). La emisión molecular de esta región está caracterizada por unas anchuras de línea de 30 a 100 km s^{-1}; a causa de la alta velocidad del *outfllow*. A partir de estudios interferométricos se pudo inferir un tamaño de la fuente de unos 20". La densidad de H_2 en este objeto se estimó a partir de la observación de transiciones de moléculas de fuerte momento dipolar, como SO_2. La temperatura cinética del gas, 100 K y la densidad de columna, $\leq 10^{23}$ cm^{-2}, se determinaron a partir de los diagramas de rotación de SO_2 y otras especies, aunque hay una gran variación de temperaturas y de densidades de columna en función de la posición en el *outflow* (Plambeck et al. 1982, Blake et al. 1987). Las moléculas que se destruyen fácilmente en los choques, como el formaldehído, están confinados en condensaciones densas y de pequeño tamaño embebidas en el

[2]Tomadas de Blake et al. 1987 y de la Tesis doctoral de B. Tercero ()

outflow, mientras que las moléculas menos frágiles, como el óxido de azufre, suelen trazar una delgada envoltura de material de baja velocidad en los límites de la cavidad, donde el *outflow* está decelerado debido a la interacción con la densa nube molecular. El material de alta velocidad se expande más fuertemente a lo largo de los gradientes de densidad más rápidos dentro de la cavidad (Blake et al. 1987). La anchura de las líneas Δv en esta componente de ≈1' de diámetro (centrado en la nebulosa de Orión-KL), está entre los ≈30-100 km^{-1}, (Tercero). Zuckerman and Palmer 1975 sugirieron que la emisión procedía de una región cercana a la nebulosa de Orión-KL y al objeto BN. Posteriormente Zuckerman et al. y Kwan and Scoville la observaron en la transición J=1 → 0 del CO en 1976. Sin embargo, la interpretación de ambos autores acerca del motivo de la anchura anormal de las líneas fue diferente, para los primeros la emisión parecía surgir de un objeto jóven que aún no ha entrado en la secuencia principal y para los segundos como si esa emisión surgiese de la expansión de la envoltura debida a un posible evento explosivo. El material del *outflow* a baja velocidad ($\Delta v \approx 35\,km^{-1}$) puede ser trazado con transiciones rotacionales de moléculas como SiO, HCN, SO_2 y SO, y máseres de H_2O de baja velocidad (producidos en la interfase y debido a las ondas de choque), de SiO y de OH, y se extiende del NE al SO prácticamente a lo largo de la componente de *extended ridge* (para más detalle sobre el origen de los *outflows* de Orión-KL remitimos a Beuther and Nissen 2008). Genzel and Downes (1983) sugieren un flujo simétricamente esférico en base a los picos de emisión de los máseres de SiO y H_2O, localizados en los lados anterior y posterior de la envoltura en expansión. Es probable que el gas se encuentre en forma de condensaciones, debido a que las intensas líneas de emisión de las transiciones observadas requerirían densidades elevadas para su excitación (Stutzki et al. 1988). La fuente I es la precursora del flujo de baja velocidad (Beuther and Nissen 2008; Plambeck et al. 2009), y se refleja en el cambio del centroide de velocidad desde 5 kms^{-1} (emisión de los máseres de SiO y H_2O de baja velocidad localizados a ≤1" de la fuente I y la emisión térmica de SiO) a 9 kms^{-1} (emisión de los máseres de OH y H_2O localizados a 5" de la fuente I). En esta última región nos encontramos una abundancia mayor de moléculas sulfuradas, como SO y SO_2. Las temperaturas rotacionales, radios y densidades de esta región de *plateau* se situan entre 60-250 K, 10-30" y ≥10^6-10^7 cm^{-3}, respectivamente (Tercero).

El material del *outflow* a alta velocidad ($\Delta v \leq 250\,kms^{-1}$) se extiende del NO al SE, perpendicular al *outflow* de baja velocidad, tal y como se observa con el máser de SiO, teniendo el pico de emisión cercano a la fuente IRc2 (Wright and Plambeck 1983). Hay muchos autores que han trazado esta componente a través de las transiciones de CO (*ver por ej.* Kwan and Scoville 1976; Kuiper et al. 1981; Zapata et al. 2011; Marcelino et al. 2011), con el centroide de la emisión al norte de IRc2. Erickson et al. (1982) la describió como una componente con estructura marginalmente bipolar. La fuente submilimétrica SMA situada entre los objetos I y n, es considerada la precursora de esta componente de flujo de alta velocidad, en base a las observaciones combinadas con el interferómetro SMA (*SubMillimeter Array*)[3] y el radiotelescopio de 30 m de IRAM de la transición J=2→1 de $C^{18}O$ (Beuther and Nissen 2008). Aunque, observaciones realizadas por otros autores con CARMA (*Combined Array for Research in Millimeter-wave Astronomy*)[4] consideraron este *outflow* de alta velocidad como una parte de aquel de baja velocidad (Plambeck et al. 2009). No obstante, Zapata et al. 2009, partiendo de observaciones de H_2 y CO con el SMA, concluyeron que el *outflow* de alta velocidad procedía del evento explosivo anteriormente mecionado (*ver* Fig. 2.2).

Muchas de las líneas de algunas de nuestras moléculas orgánicas se excitan en las condiciones de la

[3]Es un interferometro constituido por 8 antenas de 6 metros situadas en la cima del Maunakea en Hawaii que operan en la región de de frecuencias entre 180−418 GHz.

[4]Era un interferómetro que comprendía 23 antenas de 3.5, 6.1 y 10.4 m que operó hasta abril de 2015, fundamentalmente en las ventanas milimétricas de 1 y 3 mm, a una altura media de unos 2200 m.

componente del *plateau*.

• *extended ridge*:

También denominada nube ambiente, es la componente que describe la emisión extensa de las nubes menos activas en formación estelar cercanas a Orión-KL, y está caracterizada por tener una velocidad v_{LSR} de unos 9 kms^{-1} y anchos de línea pequeños, $\Delta v \approx$3-4 kms^{-1}, encontrándose en el centro de la nube OMC-1 (Blake et al. 1987). Esta componente se caracteriza por la emisión de moléculas simples como CO, CN, CS, SO, C_2H, C_3H2_2, HCO^+, HCS^+, HNC, HCN, HC_3N y con la molécula orgánica compleja trompo-simétrica de CH_3CCH (Blake et al. 1987). A partir de la observación de las transiciones rotacionales de estas especies, se pudo obtener un tamaño para esta componente de unos 8'. La temperatura cinética está entre los 50-60 K, sin embargo, los estudios previos de diferentes autores (Johansson et al. 1984; Blake et al. 1987) indican que las temperaturas de excitación para las moléculas de HCO^+ y HCN (que poseen momentos dipolares altos) están subtermalizadas (15-20 K). Partiendo de una cantidad significativa de líneas rotacionales de varias especies, se determinan densidades críticas de $\approx 10^5$ cm^{-3} (Blake et al. 1987). La emisión se extiende espacialmente de norte a sur en la nube de Orión-KL, con velocidades radiales que rondan los 8 kms^{-1} en el *SO* y los 10 km^{-1} en el *NE*. Hasegawa et al. (1984) propusieron que esa diferencia de velocidades, a pequeña escala, era consecuencia de la rotación diferencial y colapso de un disco molecular, basándose en observaciones de CS. Del mismo modo, Vogel et al. (1985) apuntaron hacia la misma hipótesis a partir de observaciones interferométricas de la molécula de HCN. Diversos autores (Ho and Barrett 1978; Bastien et al. 1981; Padman et al. 1985; Womack et al. 1993) interpretaron el gradiente de velocidad del *extended ridge*, que parecía diverger por ambos lados en las proximidades de la fuente IRc2, como resultado de la colisión de dos nubes moleculares. Una conclusión que se afianzó a patir de observaciones de NH_3, H_2CO, CS y NNH^+ (Ho and Barrett 1978; Bastien et al. 1981; Padman et al. 1985; Womack et al. 1993, respectivamente).

Las líneas de algunas de nuestras moléculas orgánicas también se detectan en esta zona. Esta componente está caracterizada por una química en fase gas basada en reacciones ión-molécula (Herbst and Klemperer 1973), en la que abundan las moléculas ricas en carbono (CS, CN, CCH), mientras que las ricas en oxígeno muestran una abundancia menor (Harwit 1982).

La densidad de columna de H_2 para el *extended ridge* se estima en $\approx 10^{22}$ cm^{-2} (Tercero et al. 2010).

• *compact ridge*:

Es una fuente compacta, en la que abundan las moléculas que contienen oxígeno, tanto simples como complejas, tales como HDO, OCS, H_2CO, H_2CCO, HCOOH, CH_3OH, CH_3OCOH, CH_3OCH_3 (Blake et al. 1987). Los diagramas rotacionales de algunas de estas moléculas ricas en oxígeno, incluyendo también la molécula de H_2CS, proporcionan una temperatura rotacional entre los 90-140 K. La molécula de CH_3OH presenta una gran cantidad de líneas, cuyos niveles superiores de energía cubren un amplio rango. A partir de la obsevación de esta molécula, Blake et al. 1987 pudieron determinar una gran variación de la anchura de las líneas y de la temperatura cinética del gas a lo largo del compact ridge. Así, las de baja energía se caracterizan por un $\Delta v \approx$3.3 kms^{-1} y una T_{rot} entre 120-140 K, mientras que las de energías más altas (incluyendo el v_t=1) tienen valores de $\Delta v \approx$6.5-9.5 kms^{-1} y una $T_{rot}>$200 K. Las tasas de emisión espontánea de las líneas de sus estados torsionalmente excitados, requieren de unas densidades de hidrógeno $\geq 10^7$ cm^{-3} para que se pueblen los niveles superiores por colisiones (aunque también podría ser radiativamente). Las condiciones físicas del *compact ridge*, se determinan a partir

de la observación de las transiciones de moléculas con un largo rango de momentos dipolares y de energías de los niveles superiores. Además de CH_3OH, la molécula de cianuro de metilo, CH_3CN, ha sido utilizada para estas determinaciones (Bell et al. 2014). Esta fuente parece mostrar propiedades físicas (gradiente de temperatura, velocidad radial, distribución espacial) y químicas entre las de nube ambiente, o *extended ridge*, y aquellas del *plateau*, en el cual el *outflow* de la fuente IRc2 interacciona con la componente de la nube a 8 Kms^{-1} comprimiéndola, calentándola y modificando su composición química (Johansson et al. 1984; Irvine and Hjalmarson 1984; Bell et al. 2014). De esta manera, el *compact ridge* podría considerarse como una componente del *extended ridge* que ha sido sometida a choques y otros procesos energéticos; es decir, como una componente compacta del *extended ridge*. Esta fuente puede considerarse una componente compacta del *extended ridge*. El tamaño de esta componente es <40" y se sitúa a unos 20" al *S* de BN. Favre et al. (2011) muestran mapas de intensidad integrada para la molécula de CH_3OCOH obtenidos con el interferómetro de Plateau Bure[5], a partir de la suma de varias transiciones a ≈223 GHz en el rango de velocidades de 5 a 12 kms^{-1}. En dichos mapas, la componente de *compact ridge* se sitúa al *SO* de la estructura en forma de *V*. Estos autores sugieren que el flujo UV/IR procedente de la fuente I, produce un calentamiento de los granos de polvo y la evaporación de sus mantos de hielo de CH_3OH, H_2CO, H_2O, CO, NH_3, etc. Una vez estas moléculas se encuentran en la fase gaseosa, se pueden formar otras especies como CH_3OCOH (la cual también ha podido ser formada en los granos de polvo).

Las líneas tienen una anchura también muy pequeña, rondando los 3-5 kms^{-1}, cuyos picos de emisión caen entorno a los 7-8 kms^{-1}. La densidad de columna de H_2 para el *compact ridge* se estima en $\approx 10^{22}$ cm^{-2} (Tercero et al. 2010).

- *hot core*:

Se trata de una región caliente, densa y compacta del material inmediatamente adyacente (2" al *S*) a la fuente IRc2 (*ver* por ejemplo, la fig. 2.4). Los valores de v_{LSR} y Δv no están tan definidos como lo pueden estar en las componentes del *ridge*, pero suelen situarse entorno a los 4-6 kms^{-1} y 10-15 kms^{-1}, respectivamente. En esta componente abundan las moléculas complejas que contienen nitrógeno como CH_3CN, CH_3CH_2CN y CH_2CHCN, y además se puede trazar con moléculas simples como CO, HDO, H_2CO, HNCO (Blake et al. 1987). En el rango milimétrico, submilimétrico e IR-lejano, esta componente se caracteriza por transiciones que tienen una profundidad óptica elevada. Por su proximidad a la fuente IRc2, hay un amplio rango de temperaturas. Desde temperaturas cinéticas del orden de >300 K que excitan niveles de alta energía cerca de la fuente (prácticamente centrados en ella), como ocurre con moléculas como CH_3CN y HC_3N, hasta temperaturas cinéticas del orden de los 100-200 K trazadas a partir de transiciones de J más bajas de CH_3CH_2CN y CH_2CHCN. El tamaño de la fuente con alta temperatura cinética es de 3-5", mientras que la de baja temperatura cinética es de unos 10". La temperatura del polvo en esta región ronda los 150 K. En los mapas de Favre et al. (2011) que mencionamos antes, la componente del *hot core* se encuentra en el este de la estructura en forma de *V*. Se estima una densidad de columna de H_2 de $\approx 10^{24}$ cm^{-2} (Blake et al. 1987), que corresponde a unas densidades altas de H_2 (10^7-10^8 cm^{-3}). A partir de las observaciones de NH_3 con el VLA[6] (Genzel et al. 1982; Pauls et al. 1983; Hermsen et al. 1988), se dedujo la estructura física de esta región como un conjunto de condensaciones de ≤1" no asociadas con los picos de emisión IR.

[5]Es otro observatorio de IRAM, que consiste en un interferómetro compuesto por 6 antenas de 15m que operan en las ventanas milimétricas de 3,2,1.2 y 0.8 mm y se sitúa a 2550 m en el Plateau de Bure en los Alpes franceses.

[6]Es un interferómetro compuesto por 27 antenas de 25m distribuidas en una configuración en forma de Y que opera en la región de 1.2-96 GHz, situado en las llanuras de San Agustín, Nuevo Méjico

La fase gas es rica en especies hidrogenadas, consecuencia de la evaporación de los mantos de hielo de los granos de polvo (Sweitzer 1978; Tielens and Hollenbach 1985; Blake et al. 1987; Walmsley et al. 1987; Brown et al. 1988). Es interesante destacar, que para varias moléculas la relación de abundancias relativas de D/H es ≈2 órdenes de magnitud mayores que aquella del medio interestelar (*ver por ej.*, Plambeck and Wright 1987; Walmsley et al. 1987). Una alta abundancia de especies deuteradas, puede indicar que ha ocurrido fragmentación química[7] en la nube fría (como *por ej.* la deuteración del formaldehído y del metanol, Ceccarelli et al. 2001). Algunas moléculas que contienen deuterio se pueden formar mediante reacciones en fase gas (*por ej.* Rodgers and Millar 1996), o tras la evaporación de moléculas formadas en la superficie de los granos de polvo durante la etapa de gas frío en el entorno de las nubes calientes (*por ej.* van der Tak et al. 2002). Sin embargo, a excepción del metanol, se conoce poco acerca de la deuteración de moléculas orgánicas complejas en el medio interestelar, especialmente en regiones de formación de estrellas masivas (Gerin et al. 1992, Daly et al. 2013, Neill et al. 2013, Esplugues et al. 2013, Coudert et al. 2013, López et al. 2014, Belloche et al. 2016). Diversos autores (Walmsley et al. 1987, Brown et al. 1988 y Plambeck and Wright 1987) proponen que el *hot core* ha sido calentado recientemente ($\leq 10^4$ yr) de manera que aún refleja la composición inicial de los granos de polvo.

Diversos autores han especulado sobre la naturaleza de *hot core* de Orión-KL. Se ha propuesto que el *hot core* está siendo calentado por un flujo explosivo asociado con la desintegración dinámica de un sistema estelar masivo, que resultó en tres objetos que se alejan unos de otros *BN*, *n* e *I* (*ver Fig.2.2* que muestra la emisión en el IR cercano obtenida recientemente por Bally et al. 2015; *ver* también Bally et al. 2017); estas fuentes emiten en radio continuo y formaron un grupo estelar en el pasado, hace ≈500 años (Zapata et al. 2011). Detrás de la región HII (0.1 pc) producida por el flujo UV de las estrellas OB del Trapecio, está la región de Orion-KL que contiene un clúster de fuentes IR de $\approx 10^5$ luminosidades solares cerca del centro del núcleo más denso de la nube molecular (Lada and Kylafis 2012b; Genzel and Stutzki 1989). Genzel and Stutzki (1989) sugieren que la fuente IRc2 está entre las fuentes con mayor tempertura de los granos de polvo.

Zapata et al. (2011) interpretan esta componente como producto del choque del gas acelerado por una explosión hace ≈500 años (en el seno de varios objetos estelares en formación) contra una región densa del *extended ridge*, calentándolo y favoreciendo la formación del *hot core*. Aunque comparte similitudes con las condiciones físicas de la componente del *compact ridge*, experimenta una química diferente, probablemente por las distintas condiciones iniciales de los granos de polvo.

La caracterización de las componentes clásicas o típicas de la región de Orión-KL, son el resultado del análisis de los perfiles de las líneas de emisión molecular de la nebulosa (ver Tabla 5.1, Blake et al. 1987). Con el tiempo y la mejora de las resoluciones espectrales y espaciales, se ha encontrado que las componentes de la nube de Orión-KL se subdividen en subcomponentes adicionales.

[7] *ver* Sec. 3.1.2

2.2 Formación de estrellas masivas

2.2.1 Formación estelar

Es importante destacar, que la mayor parte de la formación estelar en la Vía Láctea tiene lugar en las nubes moleculares gigantes (GMCs *Giant Molecular Clouds*, $\geq 10^5$-$10^6 M_\odot$, $\approx 10^7$ años, >150 pc)[8] (Blitz 1993, Blitz and Williams 1999). En estas GMCs albergan regiones de formación de estrellas masivas, y en ellas nos encontramos una gran variedad de condiciones físicas y químicas (nubes difusas, oscuras, densas, núcleos pre-estelares, regiones HII, PDRs, etc). La fig. 2.6 es una representación de las diferentes fases del medio interestelar y la química que nos encontramos asociada (basada en Kwok 2007).

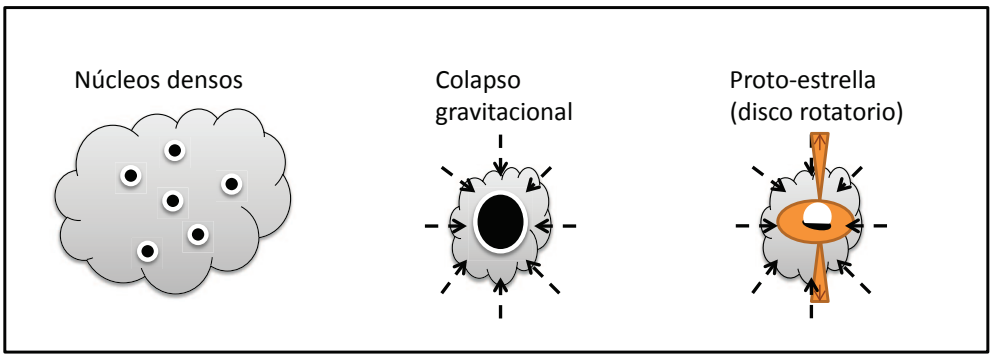

FIGURA 2.5: ESQUEMA GENERAL PARA EL PROCESO DE FORMACIÓN DE ESTRELLAS A PARTIR DE NÚCLEOS DE CONDENSACIÓN DENTRO DE LA NUBE (DE IZQUIERDA A DERECHA). LAS PROTO-ESTRELLAS TARDAN EN FORMARSE ALREDEDOR DE LOS 10^6 AÑOS. LAS NUBES MOLECULARES DONDE SE FORMAN LAS ESTRELLAS SE DISIPAN EN TORNO A LOS 10^7 AÑOS.

El mecanismo básico de formación estelar (*ver por ej.* Shu et al. 1987) parte del movimiento sistemático de ”parcelas” de gas en la nube, considerando a este como un fluido, ya que las distancias en las que se producen esos movimientos sistemáticos son significativamente mayores que el recorrido libre medio de las partículas. Esto confiere al gas propiedades de fluido, es decir, que puede ser caracterizado con unas variables macroscópicas como densidad (ρ), velocidad (v), temperatura (T) y presión (P). Estos parámetros se pueden determinar a partir de observaciones moleculares. De este modo, el movimiento del gas en la nube se puede modelizar a partir de las leyes de conservación del momento (con la ecuación de movimiento), de la energía (con la aproximación adiabática) y de la masa (con la ecuación de continuidad).

Dentro de una nube molecular gigante, puede haber zonas de elevada densidad o núcleos que no pueden soportar su propia gravedad, con lo que la nube comienza a contraerse aumentando la velocidad angular y fragmentándose en partes (lo que dará lugar a la escisión de los núcleos en cúmulos que precederán al comienzo de la formación estelar), para terminar colapsando y generando proto-estrellas. Este proceso se conoce como inestabilidad gravitacional (*ver por ej.* Jeans 1902, Bonnor 1956). El teorema de Virial relaciona la energía cinética y potencial involucradas en tal fenómeno, proporcionando

[8] Estos valores típicos de GMCs pueden variar teniendo en cuenta la no uniformidad de las propiedades del gas interestelar en diferentes posiciones de la galaxia. Así, por ejemplo, cerca del radio central de Nuestra galaxia la presión del gas es unos 3 órdenes de magnitud mayor que en la vecindad local.

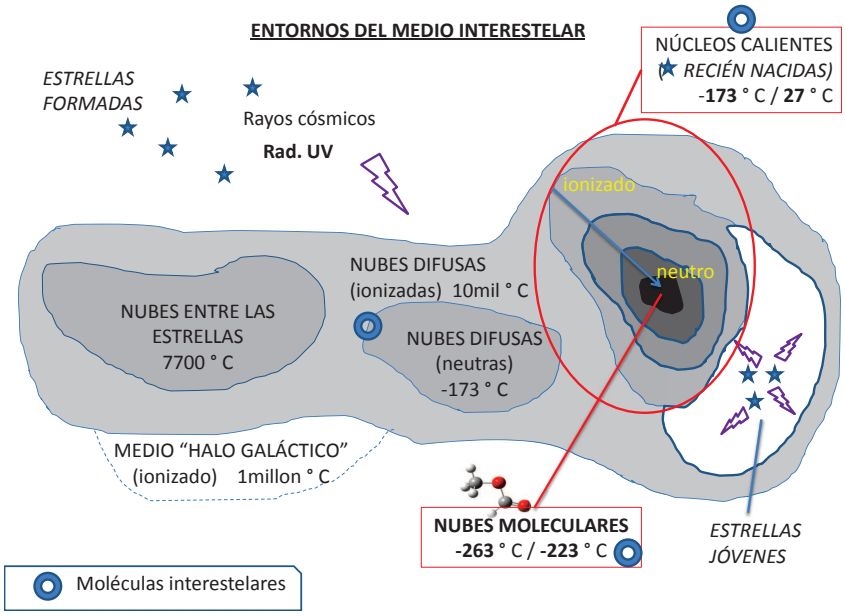

FIGURA 2.6: ESTA FIGURA MUESTRA LOS ENTORNOS O FASES DEL MEDIO INTERESTELAR Y SU IMPLICACIÓN EN LA QUÍMICA. LA NEBULOSA DE ORIÓN-KL SE SITÚA DETRÁS DE LA REGIÓN HII, Y CONTIENE EL NÚCLEO MÁS DENSO EN LA NUBE Y UN CLÚSTER DE ESTRELLAS INFRARROJAS MUY LUMINOSAS, DE LAS CUALES IRC2 ES LA FUENTE DOMINANTE. LOS *donuts* REPRESENTAN LAS MOLÉCULAS INTERESTELARES Y EN LA FIGURA APARECEN LOS LUGARES EN LOS QUE SE DETECTAN. *Fuente: basado en Kwok 2007*

la masa de Jeans (M_J)[9], la cual ofrece una idea de la masa crítica de gas que se necesita para que ocurra el colapso gravitacional.

La función inicial de masas (IMF, *Initial Mass Function* por sus siglas en inglés, *ver por ej.* Miller and Scalo 1979, Figer 2005) permite establecer la distribución inicial de masas para una población de estrellas que comienzan a tener reacciones nucleares de fusión de hidrógeno, es decir, que entran en la secuencia principal. La distribución de masas en una nube molecular, puede expresarse mediante una ley de potencias[10] (Kroupa 2001).

También hay que tener en consideración, que la turbulencia y los campos magnéticos tienen un papel esencial en el mecanismo de formación estelar (Larson 1981, Ostriker 1997, Pudritz et al. 2014, Mac Low and Klessen 2004, Ballesteros-Paredes et al. 2007, Cortes et al. 2016). El colapso gravitacional de la nube molecular puede estar asociado a procesos de fragmentación de la nube, dando lugar a la formación de estrellas de forma aislada o en grupos. Los mecanismos básicos que implican la fragmentación de la nube (*ver por ej.* Klessen and Burkert 1999, Inutsuka 2012), se basan principalmente en el efecto de la gravedad y en la turbulencia, la cual hace que las masas o "parcelas" de gas colisionen y compriman el gas, volviéndose opacas y pasando de ser isotermas a adiabáticas, para generar núcleos proto-estelares en la nube.

[9] M_J ($M_\odot$)=C$\frac{P^{3/2}}{G^{3/2}\rho^2}$=C$(\frac{kT_k}{\mu G})^{3/2}\frac{1}{\rho^{1/2}}$, donde la C depende del exponente adiabático y la μ es el peso molecular del gas. Si la M_{nube}>M_J entonces la nube terminará colapsando gravitacionalmente puesto que la presión del gas no es suficientemente elevada como para contrarrestar el efecto de la gravedad. Así, cuanto mayor sea la densidad inicial a elevada temperatura, menor será la M_J, y por tanto, mayor probabilidad de formación de estrellas masivas.

[10] $dN/dlnM \propto M^{-\alpha}$, donde α depende del entorno astrofísico por la composición del medio.

En el proceso de formación de las proto-estrellas (*ver por ej.* Shu et al. 1987), el gas en caída libre libera energía cinética y como consecuencia aumenta la presión y la temperatura centrales, convirtiéndose en fuentes que emiten en la región IR del espectro. Generalmente se forma un disco en rotación alrededor de cada objeto central. Estos discos pueden evolucionar dando lugar a sistemas planetarios. Los procesos que conducen a la acreción de suficiente material a través del colapso gravitatorio, generan flujos bipolares que emergen del núcleo proto-estelar. De este modo, las estrellas quedan embebidas en la nube parental y calientan el entorno inmediato, como por ejemplo, las estrellas del Trapecio de la nebulosa de Orión.

Los campos magnéticos, actúan como fuentes de presión sobre el gas de la nube provocando la contracción de la misma o actuando de freno, aunque para ello se requiere que haya gas ionizado (*ver por ej.* Pudritz 2002, Inutsuka 2012). El teorema de Virial incluye esta influencia por medio de la energía magnética, la cual marcará el modo en que se fragmenta la nube en función de la relación entre la energía gravitatoria y cinética (*ver por ej.* Shu et al. 1987). De este modo, se establece una masa crítica (M_{cr})[11] que depende directamente de la intensidad del campo magnético (B) e inversamente de la densidad del gas de la nube (ρ).

2.2.2 Formación de estrellas OB

Las estrellas OB son estrellas masivas, que tienden a formarse en clústers (*ver por ej.* Pudritz 2002), con una vida media relativamente corta (en comparación con las estrellas menos masivas del clúster), cuyo color espectral varía entre el azul (O) y el blanco-azulado (B), y son excelentes indicadores de formación estelar reciente. El complejo que constituye la asociación de estrellas OB, está asociado a nubes moleculares gigantes, en las que ocurren procesos de formación tanto de estrellas de baja y alta masa. Las estrellas de tipo espectral OB asociadas a la región de Orión-KL, tienen luminosidades de $\approx 10^5\, L_\odot$, masas de $\geq 10\, M_\odot$ y edades de unos $\approx 10^6$ años. La asociación OB de esta región consta de 56 estrellas de tipo espectral de O6 a B2 (Blaauw 1964). La presencia de estrellas de diferentes edades en el complejo, se atribuye a la formación de dichas estrellas en etapas progresivas desencadenadas quizá por fenómenos de explosión de supernovas en el pasado, resultado como consecuencia de la fragmentación de la nube molecular parental (Blaauw 1964). Las estrellas masivas suelen estar caracterizadas por una región de ionización HII (o esfera de Strömgren), a causa de la intensa radiación UV en el entorno de la nube molecular, en la que la nebulosa de Orión-KL es una de las remanentes de la asociación de estrellas OB objeto de esta tesis.

Las estrellas OB asociadas a la nube de Orión-KL se encuentran en el centro del clúster del Trapecio. Aunque aún queda mucho para comprender sobre la formación de estrellas masivas, Bally and Zinnecker (2005) respaldan un mecanismo de formación mediante acreción a partir de un disco circumestelar. La región HII asociada a la región de Orión se encuentra en una fase poco evolucionada. Esto indica que los objetos estelares asociados a Orión-KL, como es la fuente I, se encuentran en una etapa temprana de proto-estrella masiva asociada a un disco de acreción (Reid et al. 2007; Testi et al. 2010; Plambeck et al. 2013).

Genzel and Stutzki (1989) son los autores de referencia para la anatomía de la región de Orión-KL. Numerosos estudios relacionados con esta nebulosa, han llevado a analizar el posible origen y evolución de este objeto (como por ejemplo, Johansson et al. 1984; Sutton et al. 1985; Blake et al.

[11] $M_{cr}\ (M_\odot) = \frac{5^{3/2}}{48\pi^2}\frac{B^3}{G^{3/2}\rho^2}$ (*Referencia*: Mac Low and Klessen 2004)

1987; Turner 1989, Tercero et al. 2010, 2011; Comito et al. 2005). La distribución espacial del gas molecular en la región de Orión-KL se ha obtenido a partir de diferentes trazadores moleculares que emiten principalmente en la región de las ondas mm/sub-mm del espectro (como por ejemplo, Blake et al. 1986; Favre et al. 2011; Brouillet et al. 2013; Tercero et al. 2015).

La vida de una estrella no está marcada únicamente por las condiciones en las que nace, sino por su interacción continua con el entorno. Por ese motivo, la tendencia a encontrarnos estrellas masivas formando parte de clústers, hace que su historia sea diferente a la de las estrellas de baja masa. La observación de discos y *outflows*, una forma evidente de liberación de exceso de momento angular, en estrellas masivas ha inducido al estudio de sus mecanismos de formación mediante teorías de acreción −acreción del núcleo y acreción competitiva, *ver por ej.* Tan et al. 2014− las cuales se basan en un aumento del campo gravitatorio ($GM_{\odot}/R^2$) que supere la elevada presión de radiación (κ L/($4\pi R^2$c), donde κ es la opacidad del gas). La tendencia de las estrellas masivas a formarse en grupos, puede estar también originada en colisiones entre nubes y fusiones de estrellas (Bonnell et al. 1998).

Con el tiempo, las estrellas que en un principio se han formado en clusters o en grupos terminan dispersándose al cabo de los pocos millones de años. Sin embargo, y debido a que el tiempo de vida de las estrellas masivas es corto (*ver por ej.* Lada 1991), estas estrellas suelen encontrarse casi siempre en asociaciones (*ver* por ej. Blaauw 1964, 1991 (Orión)). En los diagramas de color-magnitud, este tipo de estrellas en clusters suelen tomarse de referencia para medir distancias[12].

Las condiciones físicas del disco circumestelar que rodea a una estrella masiva (*ver* por ej. Hirota et al. 2014) se espera que sean diferentes a las de las estrellas poco masivas, especialmente en la temperatura alcanzada en el disco, un factor clave a tener en cuenta a la hora de analizar la posible formación de planetas en base a la temperatura que son capaces de soportar los granos de polvo, material esencial para la formación de planetas rocosos.

2.3 Región de formación de estrellas y Química Interestelar

La diferenciación química de la nube de Orión-KL, marca las diferentes condiciones físicas y químicas que tuvieron lugar en el proceso de formación estelar, y que han conducido a una química definida en distintas subcomponentes de la nebulosa. Por lo tanto, es necesario abordar los mecanismos físicos de formación estelar desde los primeros estadios hasta que llegan a una etapa en la que las jóvenes estrellas han interaccionado con su entorno, modificando las condiciones químicas y formando especies moleculares cada vez más complejas.

2.3.1 Formación estelar y su efecto en la química

Las nubes difusas y las regiones de fotodisociación (PDRs) están iluminadas por el intenso campo UV de las estrellas jóvenes próximas a ellas, por lo que la química que presentan será muy diferente (*ver* Cap. 3.3) de que aquella que tiene lugar en las regiones más internas y densas de las nubes asociadas a núcleos de condensación molecular. En estos núcleos densos y protegidos de la radiación UV,

[12] El módulo de la distancia considera que los objetos que constituyen el clúster están a la misma distancia debido a que en general los clústers están muy lejos de nuestro sistema de referencia, $m-M=A+5log(d/10)$ (donde m es la magnitud aparente y M la magnitud absoluta, medidas a la distancia estándar de 10 pc; A es la extinción interestelar; d es la distancia.

los rayos cósmicos juegan un papel esencial a la hora de establecer los ingredientes que desencadenan reacciones interestelares más complejas, como es la formación de H_3^+ a partir de H_2 y H_2^+, este último producido por la colisión de H_2 con un rayo cósmico. En las nubes difusas, la química que se desarrolla se encuentra en un estado cuasi-estable, debido a que las escalas de tiempo para los procesos de las recciones químicas que tienen lugar son más rápidos que el resto de cambios dinámicos que puede haber en la nube, como por ejemplo el colapso y la congelación (*freeze out*) de las especies sobre los granos de polvo (Fraser et al. 2002). Sin embargo, la mayor densidad que caracteriza a las regiones con núcleos densos dentro de nubes moleculares, implica que los procesos químicos y los cambios dinámicos ocurran a una escala de tiempo comparable, impidiendo que no se establezca un estado cuasi-estable durante la evolución de tales nubes (Fraser et al. 2002).

La química de los *hot cores*, así como la de los *hot corinos*, regiones donde se están experimentando las fases iniciales de colapso para la formación de estrellas, conlleva una serie de etapas que conducen a la formación de moléculas interestelares complejas, y se basan esencialmente en una química de superficie y en una síntesis de moléculas en fase gas, ambas interrelacionadas con una etapa de desorción de las moléculas de los hielos a la fase gas (Herbst 2005, 2006). En los artículos presentados en esta tesis, podemos ver la estructura física de Orión-KL vista en diferentes transiciones rotacionales de diversas moléculas, presentada en forma de mapas de intensidad integrada de la emisión de líneas moleculares. Anteriormente, hemos visto como la figura 2.4 muestra un mapa de emisión del continuo de Orión-KL.

En la figura 2.6 podemos observar los entornos o fases del medio interestelar y su implicación en la química interestelar.

Capítulo 3

Moléculas orgánicas complejas interestelares

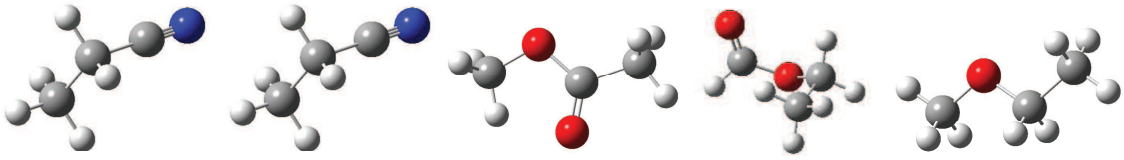

(a) EtCN (b) VyCN (c) cis-AcMe (d) g-EtF (e) t-EME

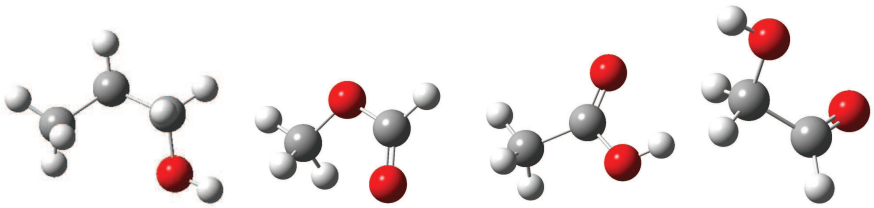

(f) gt-n-PropOH (g) cis-MF (h) trans-AA (i) cis-GLY

FIGURA 3.1: MOLÉCULAS ORGÁNICAS COMPLEJAS (COMS) INTERESTELARES QUE ABARCAN ESTA TESIS. *EtCN: Cianuro de Etilo; VyCN: Cianuro de Vinilo; cis-AcMe: cis-Acetato de Metilo; g-EtF: gauche-Formiato de Etilo; t-EME: trans-Etil Metil Éter; gt-n-PropOH: gauche-trans-n-Propanol; cis-MF: cis-Formiato de Metilo; trans-AA: trans-Ácido acético; cis-GLY: cis-Glycolaldehído*

Las reacciones químicas implicadas en la producción de moléculas en el medio interestelar, están regídas por procesos físicos bajo condiciones de baja presión, temperatura y densidad, en un entorno altamente hostil. El medio interestelar no es un lugar tranquilo, los violentos procesos asociados con las últimas etapas de la vida de las estrellas (eyección de materia en los procesos de pérdida de masa de las gigantes rojas, la explosión de supernovas, los vientos de las estrellas masivas, etc.), marcan las condiciones de temperatura y densidad en el gas interestelar, pudiendo hacer que el gas alcance velocidades de cientos de kilómetros por segundo en las zonas asociadas a choques, mientras que en las zonas densas alrededor de las proto-estrellas, estas velocidades se reducen a unos cuantos kilómetros por segundo (Williams and Herbst 2002).

Para estudiar esa química compleja y poder estimar las condiciones físicas y químicas de esos objetos, se deben utilizar las regiones del espectro donde emiten las moléculas: el dominio de las ondas milimétricas, submilimétricas, microondas e infrarrojo lejano. La mayor parte de las nubes interestelares, están muy protegidas de la radiación UV de las estrellas por los granos de polvo que absorben dicha radiación. La Figura 3.2 muestra una de dichas nubes, el glóbulo de Bok B68. En esta nube se puede percibir el enrojecimiento de las estrellas conforme penetramos en la misma, hasta que estas desaparecen

completamente debido a la enorme absorción A_v, a unos segundos de distancia del borde de *B68* (Fig. 3.2)[1].

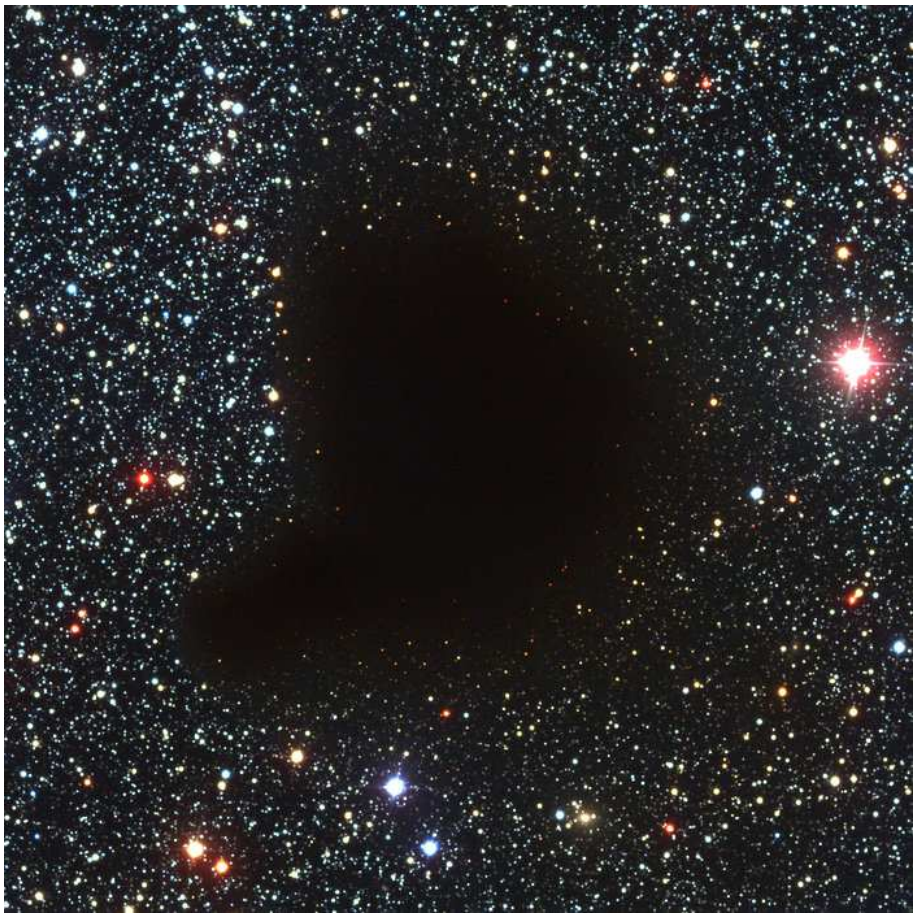

FIGURA 3.2: BARNARD 68 (B68 O LDN 57) ES UN GLÓBULO DE BOK, DE UNOS 7 MESES LUZ DE DIÁMETRO (≈0.2 PC), QUE SE ENCUENTRA A UNA DISTANCIA DE UNOS 500 AÑOS LUZ HACIA LA CONSTELACIÓN DE OFIUCO, Y REPRESENTA EL EJEMPLO MÁS CARACTERÍSTICO DE NUBE MOLECULAR O NEBULOSA OSCURA. CONSIDERADO ANTAÑO COMO UN "AGUJERO EN EL CIELO", ESTAS NUBES MOLECULARES SON UNO DE LOS OBJETOS MÁS FRÍOS DEL UNIVERSO (RONDANDO LOS 10 K), Y ES EL LUGAR DONDE NACEN LAS ESTRELLAS. ESTA NUBE PARECE ESTAR EN SU ETAPA MÁS TEMPRANA DE COLAPSO. LA IMÁGEN (N ARRIBA, E A LA IZQUIERDA) ES UNA COMPOSICIÓN EN COLOR CON UNA EXPOSICIÓN EN TRES COLORES (B, V, I–*blue, green-yellow, near-infrared*, RESPECTIVAMENTE) OBTENIDA CON EL ESPECTRÓGRAFO FORS1 DEL TELESCOPIO *Antu* DEL *Very Large Telescope* (VLT) EN 1999. *Fuente:* https://www.eso.org/public/spain/images/eso9924a/

La gran complejidad molecular observada en el medio interestelar, particularmente en los *hot cores* (condensaciones moleculares asociadas a estrellas masivas) y *hot corinos* (los análogos asociados a estrellas poco masivas), ha impulsado en los ultimos 40 años, una intensa búsqueda de nuevas especies moleculares, para comprender el grado de complejidad química y los procesos que dan lugar a la formación de moléculas en entornos tan rarificados. En la base de datos del *"The Cologne Database for Molecular Spectroscopy"* podemos encontrar una lista de moléculas detectadas en el medio interestelar y circumestelar, así como en objetos extragalácticos, ordenados según el número de átomos de las moléculas.

[1]Condiciones físicas de *B68*: Temperatura cinética (basada en observaciones de transiciones de inversión de NH_3)=10 K (Hotzel et al. 2002, Bergin et al. 2006); Densidad (central)=10^6 cm^{-3} (Bergin et al. 2006).

Las bajas temperaturas y densidades que nos encontramos en las nubes interestelares en comparación con las condiciones terrestres, se compensan por el largo tiempo de vida de las nubes moleculares que, protegidas por los granos de polvo, permiten que tenga lugar la formación de moléculas complejas. En las nubes moleculares oscuras y frías, las temperaturas rondan los 10-20 K y los procesos moleculares no ocurren en equilibrio termodinámico. De manera que, se requiere un aporte de energía externo suplido por los rayos cósmicos, que ionizan la materia interestelar, desencadenando una química ión-neutro que da lugar a un gran número de moléculas complejas.

A pesar de que las transiciones moleculares emiten en la región visible/UV (transiciones electrónicas), infrarroja (transiciones vibracionales) y de radio (transiciones rotacionales), para estudiar los fenómenos astrofísicos que están aconteciendo en las regiones de formación estelar, debemos recurrir al diagnóstico de las líneas en la región milimétrica/submilimétrica del espectro. En esta región, las nubes interestelares son transparentes y permiten analizar las diferentes zonas de emisión de la nube. La emisión de energía de las moléculas a través de sus transiciones moleculares, hace que se les considere importantes refrigerantes de la nube interestelar, lo cual puede ayudar al colapso de la nube (Fraser et al. 2002).

3.1 Moléculas orgánicas complejas interestelares

Gracias a las extensas escalas de tiempo de vida de las nubes moleculares, y a pesar de las condiciones físicas extremas, se puede esperar que determinadas reacciones químicas suficientemente rápidas, permitan la formación de moléculas complejas. En las constantes de equilibrio que caracterizan las reacciones químicas, influyen las variables termodinámicas; tales como la energía libre de Gibbs, la entalpía y la entropía. Dichas constantes, son significativas en entornos de densidades y temperaturas elevadas; características de atmósferas de estrellas, objetos subestelares y planetas gigantes gaseosos (Agúndez 2009). Sin embargo, evaluar el estado de equilibrio químico de las moléculas en las nubes moleculares resulta complicado. La variación de la abundancia de las especies moleculares con el tiempo, es la variable que nos permite determinar la viabilidad de una reacción química. Para evaluar el equilibrio cinético de las reacciones interestelares en las nubes moleculares[2], debemos utilizar las velociades de reacción[3], las cuales dependen de la temperatura y de la energía de activación del sistema.

Dependiendo del número de átomos que poseen las moléculas, se las considera simples, cuando tienen menos de 6 átomos, o complejas, en el caso contrario (Herbst and Van Dishoeck 2009).

La formación del H_2 se produce por procesos de catálisis en la superficie en los granos de polvo, ya que esta molécula es la más abundante y de ella depende la formación del resto de moléculas interestelares. Sin embargo, el desencadenante de la complejidad química en el medio interestelar es el ión H_3^+ (Geballe and Oka 1996), producto de la ionización del H_2 por los rayos cósmicos que penetran

[2]reacciones ión-molécula, neutro-neutro, asociación radiativa, recombinación disociativa, fotodisociación y fotoionización, reacciones a tres cuerpos, disociación colisional, recombinación radiativa, recombinación de asociación radiativa, intercambio neutro, reacciones en superficie (catálisis heterogénea, adsorción, desorción térmica, impacto por radiación UV/ión/electrón), reacciones de insercción de carbono, reacciones de agregación de granos de polvo y moléculas grandes, escisión de los granos de polvo, etc.

[3]asociadas a temperaturas cinéticas a causa de colisiones moleculares elásticas, las cuales se caracterizan por establecer una distribución de velocidades maxwelliana

en las densas nubes de gas y polvo.

Cuanto más grandes son las moléculas, mayor complejidad espectral poseen. Las funciones de partición rotacionales que las caracterizan, cuando adquieren valores grandes, conllevan a una disminución en la población de los niveles rotacionales individuales, incluso a las bajas temperaturas de los núcleos fríos (Smith 2011). Thaddeus (2006) especuló la posibilidad de la existencia de un límite para la observación de moléculas interestelares grandes mediante espectroscopía milimétrica, debido a la complejidad espectral que las caracteriza.

La primera vez que se aplicaron las técnicas de espectroscopía microondas con el fin de observar moléculas poliatómicas, fue con la emisión de la molécula de NH_3 hacia el centro galáctico (Cheung et al. 1968). Desde entonces, el interés por conocer la naturaleza molecular del medio interestelar, no ha hecho nada más que aumentar. La primera molécula orgánica poliatómica que se observó en el medio interestelar, fue el formaldehído (H_2CO), haciendo uso del radiotelescopio de 140 pies (≈43 m) de diámetro de Green Bank de la NRAO en el año 1969 (Snyder et al. 1969), al mismo tiempo que el vapor de agua H_2O (Cheung et al.). La ubicuidad de esta molécula en numerosas fuentes astrofísicas, indujo a considerar que los procesos de evolución química eran mucho más complejos de lo que se pensaba en aquel momento.

Los grupos funcionales detectados en el medio interestelar son extremadamente variados. La fig. 3.3 muestra los grupos funcionales detectados en Orión-KL: éteres (CH_3OCH_3, $CH_3OCH_2CH_3$), ésteres (CH_3OCOH, CH_3OCOCH_3, CH_3CH_2OCOH), alcoholes (CH_3OH, CH_3CH_2OH, $OHCH_2CH_2OH$), aldehídos (H_2CO, CH_3CHO, CH_2OHCHO), cetonas (CH_3COCH_3), ácidos carboxílicos (HCOOH, CH_3COOH), cetenas (H_2CCO), óxidos cíclicos (c-CH_2OCH_2), aminas (CH_3NH_2), amidas (NH_2CHO), cianuros (CH_3CN, CH_3CH_2CN, CH_2CHCN, $(CH_3)_2CHCN$), isocianuros (CH_3NC, CH_3CH_2NC, CH_2CHNC, HCCNC), isocianatos (CH_3NCO), cianopoliinos (HC_nN, n=3,5), mercaptanos (CH_3SH). Debemos tener en cuenta, que también hay que incluir en esta lista los isotopólogos y estados vibracionalmente excitados de la mayoría de estas moléculas. Como el eje central de esta tesis se enfoca en las moléculas de cierta complejidad química, en la figura se han omitido las moléculas de naturaleza más simple como H_2O, H_2, CO, CO_2, SO, SO_2, NH_3, HCO^+, HCN, CN, SiO, SiS, HCS^+, OCS, H_2CS, CH_3O, CO^+, NS, SH_2, CCS, CCH, HNCO.

Seguramente aún haya muchas moléculas interestelares que no han sido detectadas todavía, bien porque tengan un momento dipolar eléctrico pequeño o nulo, en el caso de especies con el centro de carga coincidente con el centro de la distribución de cargas, una abundancia pequeña, o incluso porque su identificación requiera un arduo trabajo de laboratorio, que facilite su asignación espectroscópica fiable. Además, para poder tener una base de datos de reacciones completa, habría que considerar a las moléculas que reaccionan muy rápidamente con otras especies, y cuya abundancia instantánea es baja, pero juegan un papel importante en la evolución química del gas.

3.1.1 Temperatura de las regiones del ISM y las transiciones observadas

Mientras que la mayoría de las moléculas se detectan a través de su espectro de emisión en la región milimétrica/sub-milimétrica (mm/sub-mm), los granos de polvo se detectan en la región Infraroja (IR) del espectro electromagnético (granos calientes) o submilimétrica (granos fríos). Los granos emiten como un cuerpo gris, donde el coeficiente de absorción y emisión está determinado

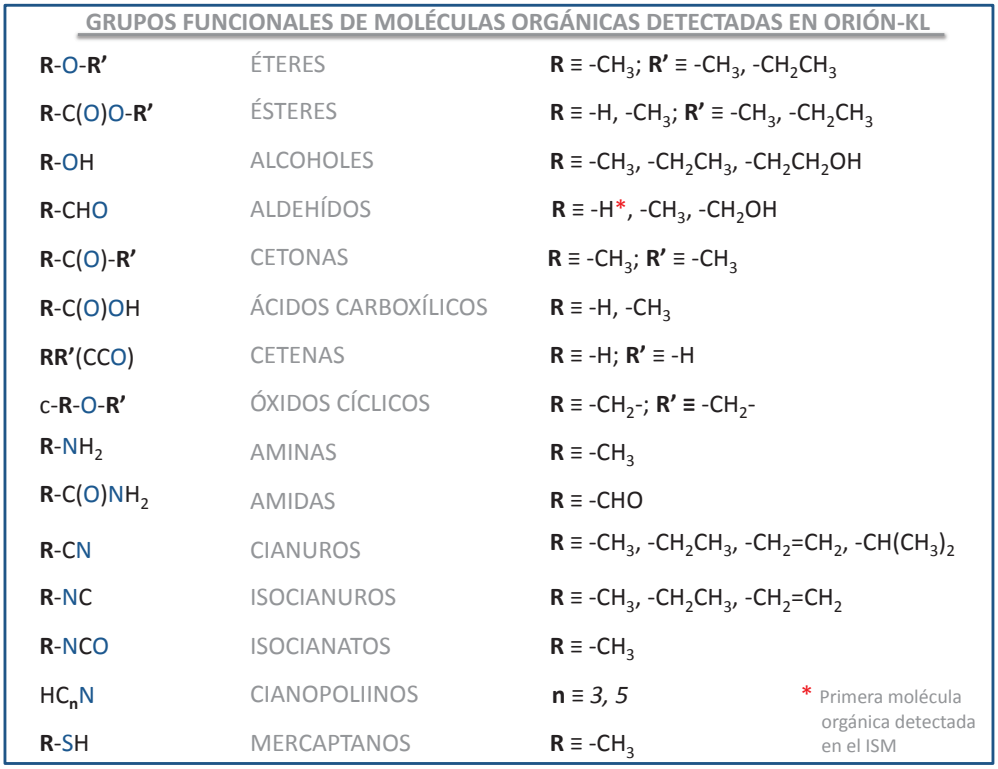

FIGURA 3.3: LAS MOLÉCULAS ORGÁNICAS OBSERVADAS EN LA NUBE DE ORIÓN-KL MUESTRA LA DIVERSIDAD DE GRUPOS FUNCIONALES QUE SON POSIBLES DETECTAR EN EL ISM. LAS MOLÉCULAS NITROGENADAS Y AQUELLAS QUE CONTIENEN OXÍGENO MARCAN UNA DIFERENCIACIÓN QUÍMICA EVIDENTE ENTRE LAS DIFERENTES COMPONENTES DE LA NUBE PREDOMINANTEMENTE EN EL ENTORNO DEL *hot core* Y DEL *compact ridge*. EN ESTA FIGURA APARECEN LAS MOLÉCULAS ORGÁNICAS DE CIERTA COMPLEJIDAD QUÍMICA Y OMITIMOS AQUELLAS DE NATURALEZA MÁS SIMPLE COMO EL CO, NH_3, HCN, OCS, ETC.

por las propiedades eléctricas de su superficie. Por otro lado, si quisieramos obtener información acerca de los estados electrónicos de las moléculas en el medio interestelar, tendríamos que recurrir a observaciones en el dominio de las ondas ultravioleta (UV). Pero el principal problema de ese estudio sería el ”oscurecimiento” por el polvo interestelar, que impediría ver lo que hay detrás de la región que quisieramos observar. Estas técnicas se han utilizado en las nubes difusas (van Dishoeck 1998, Yamamoto 2017).

La aproximación de Born-Oppenheimer separa los movimientos rotacionales, vibracionales y electrónicos de las moléculas. De esta manera, se puede resolver la ecuación de Schrödinger para cada uno de esos movimientos separadamente, facilitando el cálculo del operador Hamiltoniano. Para cada nivel electrónico, hay que tener en cuenta toda la estructura vibracional y rotacional. Las transiciones electrónicas, vibracionales y/o rotacionales, respectivamente, que ocurren entre los diferentes niveles energéticos vendrán determinadas por la energía interna disponible en la molécula. En una transición electrónica, los electrones cambian de orbital molecular. Las energías asociadas son generalmente de varios eV. En una transición vibracional, los núcleos cambian de frecuencia de vibración entre ellos. Las frecuencias fundamentales de vibración oscilan entre los más de 4 000 cm^{-1} del hidrógeno molecular a unas decenas de cm^{-1} para la torsión de algunas moléculas con grupos CH_3. Finalmente, el cambio de velocidad de rotación de la molécula corresponde a energías de unos Kelvin a centenas de Kelvin, dependiendo de los números cuánticos involucrados en la transición.

Las transiciones rotacionales poseen los coeficientes de Einstein de emisión espontánea más bajos, y los niveles rotacionales involucrados tienen energías muy bajas. Esto implica que se puedan poblar bajo condiciones de temperatura mucho más bajas, típicas del medio interestelar, concretamente entre los pocos y los cientos de grados Kelvins. Además, como el espaciado entre los niveles de energía rotacionales guardan relación con los momentos de inercia principales de la molécula (I_i, i=a,b,c), la predicción de las frecuencias de las transiciones rotacionales se realiza a través de sus constantes rotacionales (A,B,C), y constantes de distorsión centrífuga.

Condiciones físicas del ISM

Las nubes interestelares se caracterizan por desidades desde los $10 \geq n_H \geq 10^6$ cm^{-3}, y temperaturas cinéticas de $10 \leq T_k \leq 300$ K. Aproximadamente, la mitad de la materia interestelar (constituida por un 99% gas interestelar y el resto polvo interestelar) se encuentra en las densas nubes moleculares (Gargaud 2011).

Condiciones típicas de las nubes interestelares

Nubes difusas ($T_k \approx 100$ K, $A_v \approx$ 1-3 mag, $n_H \approx 10^2$ cm^{-3}, *Composición*: HI (H atómico), *Química interestelar*: moléculas simples −diatómicas,...−)

Nubes traslúcidas ($50 < T_k < 100$ K, $A_v \approx$ 2-5 mag, $n_H \approx 10^2$-10^3 cm^{-3}, *Composición*: interfase HI/H_2, *Química interestelar*: Química de nubes difusas/moleculares)

Nubes oscuras ($T_k \approx$ 10-20 K, $A_v \approx$ 1-5 mag, $n_H \approx 10^4$-10^5 cm^{-3}, *Composición*: H_2, *Química interestelar*: moléculas simples y complejas, así como cianopoliinos e hidrocarburos de naturaleza no terrestre)

Glóbulos de bok ($T_k \approx 10$ K, $A_v \approx 10$ mag, $n_H \approx 10^4$ cm^{-3}, *Composición*: H_2, *Química interestelar*: moléculas simples y complejas)

Nubes densas ($T_k \approx$ 10-50 K, $A_v \approx$ 5-10 mag, $n_H \approx 10^3$-10^6 cm^{-3}, *Composición*: H_2, *Química interestelar*: moléculas simples y complejas)

Núcleos calientes ($T_k \approx$ 100-300 K, $A_v \approx 10^2$-10^3 mag, $n_H > 10^6$ cm^{-3}, *Composición*: H_2, *Química interestelar*: química compleja ”COMs”)

Las temperaturas que hacen falta para que se exciten las transiciones de una molécula y las podamos observar en una región u otra del espectro electromagnético, dependerán de las tasas de colisión con H_2 y He, las cuales dependen de la temperatura. Todas las moléculas pueden ser excitadas rotacional, vibracional o electrónicamente. La energía rotacional E_{rot}, vibracional E_{vib} y electrónica E_{elec}, contribuyen a la energía total del sistema, junto con la energía traslacional (E_{tras})[4]. A continuación,

[4]La energía traslacional aporta un valor constante a la energía total del sistema, de ahí que las frecuencias de la transición puedan estimarse como $E_{TOT} = h\nu = \Delta E_{rot} + \Delta E_{vib} + \Delta E_{elec}$

detallamos las características principales de las diferentes transiciones moleculares, así como el motivo por el cual se observan unas transiciones y no otras en el medio interestelar.

• **Transiciones rotacionales** (MW, milimétrico/sub-milimétrico, IR-lejano): están implicadas en los movimientos de rotación respecto a los ejes principales de las moléculas. Las transiciones rotacionales tienen coeficientes de Einstein pequeños, entre 10^{-8} a 10^{-3} s^{-1}, por lo que una vez excitada la molécula a un nivel determinado permanece un tiempo considerable en él. Esto implica que se puedan poblar o excitar los niveles rotacionales con facilidad en el medio interestelar, alcanzando incluso la termalización para densidades moderadas de H_2, como es el caso de todas las moléculas con bajo momento dipolar (por ejemplo CO). El espaciado entre los niveles rotacionales (ΔE=ΔE_{rot}) es pequeño (unos pocos meV), y las energías de los niveles rotacionales se encuentran en el orden de los 1-10^2 K ($\approx 10^{-3}$ eV, ≈1-100 cm^{-1}, ≈30-3000 GHz), es decir, dentro de los valores de la temperatura cinética de las nubes oscuras, densas y condensaciones moleculares asociadas a formación estelar. Las transiciones rotacionales más bajas o más altas trazarán el gas más frío o más caliente, respectivamente. El nivel rotacional máximo que puede ser poblado, J_{max}, dentro de un mismo nivel vibracional, vendrá caracterizado por las constantes rotacionales y las energías de las transiciones implicadas.

• **Transiciones vibracionales** (IR): están implicadas en los movimientos de vibración y los ángulos entre los átomos de las moléculas. El espaciado entre los niveles vibracionales (ΔE=ΔE_{rot}+ΔE_{vib}) es mayor que los rotacionales, y sus energías se encuentran entre 100 y 5000 K (≈1-5×10^{-1} eV, ≈100-4000 cm^{-1},≈3000-120000 GHz), típico de condensaciones moleculares calientes (>10^2 K) y de las regiones más próximas al entorno que circunda las estrellas recién formadas. Los coeficientes de Einstein de las transiciones vibracionales, oscilan entre un fracción de segundo y varios segundos, dependiendo de la derivada del momento dipolar con respecto a las direcciones y ángulos asociados a la vibración.

• **Transiciones electrónicas** (IR-cercano, UV, vis): están implicados en los cambios en la configuración electrónica de las moléculas y, como consecuencia, de la fortaleza de los enlaces covalentes o iónicos. El espaciado entre los niveles electrónicos (ΔE=ΔE_{rot}+ΔE_{vib}+ΔE_{elec}) es mucho mayor, y sus energías son >10^4 K (≈5-10 eV, ≈10^4 cm^{-1}, ≈3×10^5 GHz), típico de gas coronal, plasma, explosiones de supernovas, y atmósferas estelares en general. Los niveles electrónicos no están poblados bajo las condiciones interestelares.

3.1.2 Parámetros físico-químicos

La **densidad de columna** (N), es la densidad de moléculas por cada unidad de superficie (en cm^2) contenida en una columna de longitud equivalente a la distancia entre la fuente y el observador. Es el parámetro libre estimado en la modelización astrofísica, y se mide en unidades de cm^{-2}. Es una medida del número de átomos o moléculas a lo largo de la línea de visión (ec. 3.1-3.6, Gordy and Cook 1984, Mangum and Shirley 2015). Dependiendo de diversos factores observacionales como el diámetro del telescopio (d_{telesc}), la velocidad observada de las líneas respecto al sistema local de reposo (v_{LSR}) y la anchura a media altura de las líneas gaussianas (v_{FWHM}, por las siglas en inglés "Full Width at Half Maximum"), así como la temperatura de las diferentes componentes de la nube, la densidad de columna

dependerá de cada molécula considerada, y tendrá que ser determinada a partir de la observación de una gran número de transiciones moleculares que permitan trazar las diferentes condiciones físicas de la nube (temperatura, densidad de H_2 y abundancia de las moléculas).

Densidad de columna (n=átomo o molécula en el nivel superior n; tot=población total):

$$N_n = \int_0^s n_n ds \tag{3.1}$$

$$\tau_\nu = \int_0^s \alpha_\nu ds = \int_0^s k_\nu \rho ds \tag{3.2}$$

$$k_\nu \rho = \frac{h\nu}{4\pi}(n_m B_{mn} - n_n B_{nm})\phi_\nu = \frac{c^2}{8\pi\nu^2}\frac{g_n}{g_m} n_m A_{nm}(1 - \frac{g_m n_n}{g_n n_m})\phi_\nu \tag{3.3}$$

$$\frac{n_n}{n_m} = \frac{g_n}{g_m} e^{-h\nu/kT} \tag{3.4}$$

$$\frac{\mathbf{N_{tot}}}{N_n} = \frac{Q_{rot}}{g_n} e^{E_n/kT} \tag{3.5}$$

$$\Rightarrow \mathbf{N_{tot}} = \frac{3h}{8\pi^3 \mid \mu_{mn} \mid^2} \frac{Q_{rot}}{g_n} e^{E_n/kT}(e^{h\nu/kT} - 1)^{-1} \int_0^s \tau_\nu dv \tag{3.6}$$

$$donde\ \tfrac{dv}{\nu} = \tfrac{dv}{c}$$

La **abundancia relativa** (X=N_a/N_b), es la densidad de columna de una molécula referida a la densidad de columna de otra especie que se toma como referencia. Este parámetro, resulta muy útil para hacer comparaciones entre la emisión de moléculas orgánicas complejas (COMs) provenientes de diferentes fuentes, o incluso para comparar COMs en diferentes posiciones dentro de la misma nube. El metanol (CH_3OH), como indican Herbst and Van Dishoeck (2009), se utiliza como molécula de referencia para las COMs, ya que es abundante en las nubes moleculares. Del mismo modo, nuestra molécula de referencia para estimar abundancias relativas de todas las moléculas en las nubes moleculares, es el H_2.

La **fraccionación química** es un proceso por el cual, las reacciones químicas producen razones o relaciones de abundancias entre los isotopólogos diferente de las relaciones de abundancia elementales actuales (Herbst and Van Dishoeck 2009). Los isotopólogos interestelares se usan para determinar relaciones de abundancia elementales, como por ejemplo D/H y $^{13}C/^{12}C$. Las abundancias de los isótopos de los átomos, es un parámetro es muy importante para estudiar la evolución química galáctica, ya que varía con la distancia al centro galáctico.

Cuando la mayor parte de las líneas de la molécula que se busca están recubiertas o solapadas con líneas de otras especies, no es posible confirmar su presencia, y en ese caso, solo se puede obtener un **límite superior** a su abundancia (o a su densidad de columna). Lo mismo ocurre cuando suficientes líneas están libres de recubrimientos, pero no se detectan. En el primer caso, el límite superior se establece por el valor del límite de confusión espectral, y en el segundo, por la sensibilidad de las

observaciones. En la mayor parte de las observaciones de este trabajo, el límite de confusión espectral está 4-5 veces por encima de la sensibilidad de las observaciones. Eso quiere decir, que por mucho que se integre a las frecuencias de búsqueda de la especie molecular en cuestión, nunca podremos mejorar la determinación de su abundancia. La **detección tentativa** de una especie molecular, se puede aportar en el caso de tener un número significativo de líneas detectadas.

Desde el punto de vista de la transferencia radiativa, se hará hincapié en qué tipo de información nos ofrecen las líneas moleculares. La intensidad de las líneas espectrales se ve afectada por las condiciones del medio interestelar, especialmente en cuanto a su **opacidad** (τ). Las líneas ópticamente transparentes (τ<1), hacen que la radiación que nos llega de la molécula nos permita obtener información de manera directa acerca de su densidad de columna y temperatura de excitación. Hablamos de líneas ópticamente opacas (τ>1), cuando la radiación que nos llega de la molécula no es representativa de la densidad de columna total ni de la temperatura de excitación. Un análisis de los isótopos de las moléculas que estamos estudiando (isotopómeros e isotopólogos) −como en el artículo del CH_2CHCN de esta tesis− nos puede ayudar a conocer la opacidad de nuestras líneas, para así proceder a la corrección necesaria para la obtención de las abundancias.

La **Temperatura vibracional** (T_{vib}) nos indica como están poblados los niveles vibracionales de la molécula. La densidad de columna de la molécula, tanto en su estado fundamental como excitado, definen su temperatura vibracional a través de la ecuación de Boltzman (T_{vib}=-[E_{v_x}/ln($Q_v N_{v_x}/N_{TOT}$)], x=nivel vibracional, $N_{TOT}=Q_v \cdot N_{g.s.}$). Los niveles vibracionales se pueblan por colisiones con otras moléculas, o bien mediante la radiación IR aportada por los granos de polvo interestelares.

Los **mecanismos de población** de los niveles de energía (*ver* Sec. 4.1.1) estados asociados a los diferentes fenómenos de interacción de la radiación con la materia, es decir, de la radiación electromagnética y de su interacción colisional con átomos y moléculas. Considerando estados estacionarios, tanto vibracionales, como rotacionales y electrónicos, pueden tener lugar tres procesos de absorción/emisión de la radiación entre dos estados (m y n) separados una cierta energía ΔE (con E_m<E_n), con los que establecemos las tasas de variación de la población (dN_n/dt): absorción inducida, emisión espontánea, y emisión inducida o estimulada. En ocasiones, hay que considerar la emisión de los átomos como el carbono y el oxígeno atómico, que poseen líneas de estructura fina en el dominio sub-milimétrico e IR-lejano. Asimismo, la interacción colisional con H_2, He, y con electrones, puede modificar la población de los niveles de energía, y estos efectos deben incorporarse las ecuaciones de equilibrio estadístico local (dN_n/dt=0). El mecanismo de población de los niveles energéticos de las moléculas, permite definir dos temperaturas de excitación, una rotacional y otra vibracional, que caracterizarán cómo estan poblados los niveles rotacionales dentro de cada nivel vibracional. Si ambas temperaturas coinciden, posiblemente la población de los niveles de la molécula en cuestión estén regidos por colisiones con otras moléculas del gas. Sin embargo, si la temperatura vibracional supera a la cinética, es posible que el bombeo de radiación IR (*"IR-pumping"*), por parte del polvo interestelar, sea el mecanismo dominante que puebla los niveles vibracionales.

Para que haya una termalización de las líneas de la molécula, todas las temperaturas de excitación tienen que ser las mismas, es decir, la temperatura rotacional (T_{rot}) de las líneas debe ser igual a la temperatura cinética (T_k). Y es, de este modo, como se comportarían las líneas bajo condiciones de equilibrio termodinámico local (ETL o LTE, *"Local Thermodynamic Equilibrium"* por sus siglas en inglés).

Otro parámetro que define las propiedades de las moléculas en cuanto a la contribución de la población de los diferentes estados de la molécula, es la **función de partición**, $Q(T)$ o $f(T)$. La función de partición engloba el peso estadístico, la energía del estado (vibracional, rotacional, o electrónico) de la molécula y la temperatura de rotación y vibración de la misma. Dependiendo del nivel electrónico, vibracional o rotacional del que queremos obtener la contribución de la población en el nivel considerado, nos referimos a la función de partición electrónica, vibracional o rotacional, respectivamente.

A continuación, se muestran las ecuaciones necesarias para llevar a cabo el cálculo de las funciones de partición vibracional (ec. 3.10) y rotacional (ecs. 3.11 y 3.12) en el marco de nuestro contexto (nube de Orión-KL asociada a la región de formación estelar masiva). En la nube de Orión-KL, la población de moléculas excitadas en los estados electrónicos no se contempla, debido a que, a pesar de que la temperatura cinética del gas en Orión puede alcanzar los 300 K, los niveles de energía electrónicos se encuentran a varios eV (varias decenas de miles de grados).

La función de partición total (ec. 3.9) describe la distribución de la energía interna de la molécula entre los diferentes estados electrónicos, vibracionales y rotacionales, cuyas energías correspondientes están separadas (E_{elec}>E_{vib}>E_{rot}), de ahí que se pueda considerar como el producto de las funciones de partición electrónica, vibracional y rotacional, evaluándo dichas funciones por separado.

Un parámetro importante que va a caracterizar el valor de los coeficientes de Einstein para cada transición molecular, es la fuerza de línea[5], $S_{nm}{\cdot}\mu^2_{nm}$, que es el valor medio del operador momento dipolar entre el estado inicial y final de la transición bajo estudio. Las fuerzas de línea se calculan a partir de las funciones de onda de los niveles de energía, y se obtienen a partir del Hamiltoniano que caracteriza los niveles de energía de cada molécula.

. . . . . .

Forma de la función de partición Q_{tot} (ecuación de Boltzmann):

$$N_{tot} = \frac{N_{g.s.}}{g_{g.s.}} \sum_{i=0}^{\infty} g_x \exp\left(-\frac{E_x}{kT}\right) = \frac{N_{g.s.}}{g_{g.s.}} Q_{tot} \tag{3.7}$$

$$N_i = \frac{N_{tot}}{Q_{tot}} g_i \exp\left(-\frac{E_i}{kT}\right) \tag{3.8}$$

x=estado molecular excitado (electrónico, vibracional o rotacional)

$N_{g.s.}$*=densidad de columna en el estado fundamental*

$g_{g.s.}$*=grado de degeneración del estado fundamental*

Función de partición total:

$$Q_{tot} = f_{tot} = Q_{elec} \cdot Q_{vib} \cdot Q_{rot} \rightarrow Q_{tot} = Q_{vib} \cdot Q_{rot} \tag{3.9}$$

$$\textit{donde,} \quad Q_{elec} = f_{elec} \rightarrow 1 \quad y \quad 1 < Q_{vib} < 100$$

[5]Es la fuerza del oscilador a partir de la cual se establecen los coeficientes de einstein asociados a las transiciones radiativas, y es una medida de la intensidad de la transición de frecuencia ν, desde el nivel superior n al nivel inferior m. Este parámetro es la sección eficaz de absorción a lo largo de la línea de visión.

Función de partición vibracional (donde el 1=ZPE):

$$Q_{vib} = f_{vib} = (1 - e^{E_{v_1}/kT})^{-d_1} \cdot (1 - e^{E_{v_2}/kT})^{-d_2} \cdot (1 - e^{E_{v_3}/kT})^{-d_3} \cdots \tag{3.10}$$

d_x=*grado de degenerción del modo vibracional x (bending, stretching,...)*

E_{v_x}=*energía del nivel excitado vibracionalmente* (v_x=1,2,...)

Aproximaciones para la función de partición rotacional:

$$\textit{Rotores trompo-asimétricos,} \quad Q_{rot} = f_{rot} = [\frac{\pi(kT)^3}{h^3ABC}]^{1/2} \tag{3.11}$$

$$\textit{Con un rotor interno,} \quad Q_{rot} = f_{rot} = Q_{rot}(A) + Q_{rot}(E) = 2[\frac{\pi(kT)^3}{h^3ABC}]^{1/2} \tag{3.12}$$

Fuerza de línea ($S_{nm} \cdot \mu_{nm}^2$)[6]:

$$S_{nm} \cdot \mu_{nm}^2 = \frac{8\pi^3 \nu_{nm} \mid \mu_{nm} \mid^2 g_m}{3hcQ_{tot}} (e^{-E_m/kT} - e^{-E_n/kT}) \tag{3.13}$$

Los **modos de vibración** de las moléculas influyen en los ángulos y longitudes de enlace entre los átomos que la constituyen, y en los espectros se refleja el comportamiento de esas modificaciones, de manera que cada modo normal de vibración aparece a una frecuencia determinada. De la caracterización de los modos vibracionales, se encarga la espectroscopía Raman e IR, sin embargo, para la detección de las transiciones rotacionales dentro de cada uno de esos modos vibracionales en el espectro interestelar, se recurre a la espectroscopía microondas/(sub)milimétrica.

Considerando una molécula constituida por N átomos, las coordenadas de los átomos−x, y, z−describen la modificaciones en los desplazamientos, de ahí que haya "3N" grados de libertad, de los cuales 3 movimientos son traslacionales y, en el caso de las moléculas lineales, 2 son los movimientos internos rotacionales de los ángulos, o, para el caso de las moléculas no-lineales, 3 son los movimientos internos rotacionales de los ángulos correspondientes con la orientación de la molécula en función de sus ejes. De este modo, si la molécula es lineal tiene 3N-5 modos normales de vibración, mientras que si es no-lineal tiene 3N-6 modos normales de vibración. Estos modos actúan como osciladores normales e independientes que pueden estar excitados individualmente o colectivamente, produciendo un espectro infrarrojo notable rico. Las temperaturas necesarias para excitar por colisiones esos modos, están generalmente por encima de los 200 K. Los modos de las moléculas diatómicas están entre 300 (las más pesadas con enlaces iónicos) y 6000 K (para las más ligeras con enlaces covalentes).

Hay que tener en cuenta la estructura de la molécula para evaluar los modos de vibración capaces de excitarse, y determinar si son o no activos (a causa del cambio del momento dipolar). Los modos de vibración pueden ser de tensión o estiramiento (*stretching*), y de flexión (*bending*), y pueden ser desplazamientos vibracionales de los enlaces de manera simétrica o antisimétrica. Las moléculas de los artículos presentados en esta tesis pertenecen al grupo puntual de simetría C_s, cuyos elementos de simetría son la operación identidad (E) y la operación reflexión en un plano especular horizontal (σ_h), y las especies de simetría son A' (simétrica) y A" (antisimétrica) con respecto al plano de simetría de la

[6] *Referencia*: Waters 1976 (*ver* Verdes et al. 2005 y Mangum and Shirley 2015 para más detalles).

molécula, tal que cada modo normal de vibración se corresponde con una especie de simetría A' o A", de frecuencia característica en función de los desplazamientos de los átomos que componen la molécula (C-C, C=C, C≡N, CCN, CCO, C-N, C-O, C=O, C-H, ...).

3.2 Espectroscopía de moléculas

Para abordar este apartado, la bibliografía esencial tomada como referencia fue la siguiente: Gordy and Cook 1984, Hollas 2004, y Atkins and De Paula 2008.

La condición principal para poder observar las transiciones de las moléculas en el dominio de las ondas de radio, es que la molécula tenga un momento dipolar permanente no nulo. Por otra parte, si nos referimos al tipo de espectroscopía de mayor trascendencia por su relación con el campo de la radioastronomía, la "espectroscopía rotacional pura" cuyas transiciones rotacionales se hallan dentro del mismo nivel vibracional ($\Delta v=0$), estamos dejando a un lado tanto la espectrocopía vibracional (es decir, las transiciones entre niveles rotacionales de diferentes niveles vibracionales, con los que se obtienen espectros IR y/o Raman), como la espectroscopía electrónica (es decir, aquella en la que las transiciones rotacionales y vibracionales ocurren entre diferentes estados electrónicos, con los que se obtienen espectros UV e IR). Las transiciones entre los niveles rotacionales tienen lugar con el cambio de unidad del momento angular de rotación J, es decir entre J consecutivos ($\Delta J=\pm 1$, donde +1:rama *R*; -1:rama *P*), aunque también existen en algunos casos transiciones con $\Delta J=0$ (rama *Q*), y si además la molécula está en un campo magnético, el efecto Zeeman influye en el desdoblamiento de los momentos magnéticos de cada nivel de rotación, para los cuales las reglas de selección son $\Delta M_J=0, \pm 1$.

La distorsión centrífuga produce, debido a la fuerza centrífuga generada por la rotación de la molécula, una modificación de la posición promedio de los núcleos atómicos. Además, influye en la frecuencia a la que se observan las transiciones rotacionales de las moléculas en el espectro. Este fenómeno se incluye en los Hamiltonianos moleculares a través de las constantes de distorsión centrífuga, añadiendo complejidad al cálculo del operador Hamiltoniano de la molécula.

La resolución del operador Hamiltoniano efectivo se utiliza principalmente para obtener las frecuencias de las líneas y sus intensidades, y así llevar a cabo la caracterización de la molécula para su identificación espectral en el medio interestelar. El operador Hamiltoniano efectivo[7], se trata de una expansión de términos dependiente de los momentos angulares de la molécula, y está asociado a las constantes espectroscópicas. El Hamiltoniano permite obtener las energías y autovalores para determinar las frecuencias de las transiciones, así como la intensidad a la que aparecen. Las constantes espectroscópicas, además, permiten predecir las frecuencias de líneas (no medidas en el laboratorio). No obstante, la incertidumbre en las frecuencias predichas de líneas con números cuánticos rotacionales más elevados que las de las líneas medidas en el laboratorio, puede llegar a ser muy grande, principalmente por el limitado número de constantes de distorsión que pueden determinarse cuando las medidas de laboratorio no son completas.

Cuanto más grandes son las moléculas, más denso es su espectro, debido a que sus momentos de inercia son mayores y, por ende, las constantes rotacionales que las describen son más pequeñas. Además, las moléculas que poseen rotación interna o torsión debido a la presencia en su estructura de

[7] *Ver* Gordy and Cook 1984 para expresiones detalladas.

grupos torsionales, como el grupo metilo (-CH_3), contribuyen a un aumento en la densidad de líneas espectrales, ya que los movimientos de torsión y de rotación interaccionan. Además, pueden tener varios mínimos de energía potencial asociados a la existencia de diferentes confórmeros de la molécula (trans, gauche, ...). Un ejemplo de ello, es una de las moléculas de la presente tesis, formiato de metilo (CH_3OCOH). Otra de las moléculas también estudiadas en este trabajo, el cianuro de etilo, CH_3CH_2CN tiene tal cantidad de líneas, que representan un bosque densamente poblado en nuestro espectro de la nebulosa de Orión-KL, lo cual dificulta la identificación espectral, por solapamientos con otras especies moleculares, de nuevas moléculas de gran interés astrofísico. Los estados excitados vibracionalmente, así como los isotopólogos, de especies moleculares que presentan alguna de estas características, forman también parte de esa contribución al denso bosque de líneas. Ese ”bosque” genera un espectro de confusión, en el que muchas transiciones de las moléculas identificadas y aquellas que quedan por identificar se entremezclan. Además, al límite de confusión espectral se añaden las especies moleculares que están presentes al nivel de la señal-ruido del espectro (es decir, una desviación estándar de unos 3σ que varía en función de la ventana milimétrica que estemos considerando y el tiempo de observación dedicado a cada ventana del espectro).

3.2.1 Moléculas interestelares trompo-asimétricas

Inspeccionar las pautas que se repiten a lo largo del espectro rotacional de la molécula, es crucial para la asignación fiable de las transiciones rotacionales y, por ende, de sus frecuencias, con el fin de obtener unas constantes rotacionales o espectroscópicas que describan de manera adecuada la estructura geométrica de la molécula, y con ello los niveles rotacionales.

Las constantes rotacionales (A, B, C) describen la estructura geométrica de todas las moléculas, y son inversamente proporcionales a los momentos de inercia que se proyectan sobre los tres ejes principales (I_a, I_b, I_c)[8], en orden decreciente del valor del momento de inercia asociado a cada eje principal. De este modo, la magnitud de las constantes rotacionales es: $A>B>C$.

Existen diferentes estructuras geométricas de las moléculas poliatómicas, las cuales se clasifican según su simetría: rotores lineales, rotores esféricos, rotores simétricos y asimétricos. La mayoría de las moléculas son rotores asimétricos ($A\neq B\neq C$). A partir del parámetro de asimetría (denominado parámetro de Ray k, Ray 1932) se pueden definir un tipo de rotores próximos al límite de simetría *prolate* (k cerca de -1, pues $A>B\approx C$), y con ello nos referimos a *near-prolate asymmetric tops*[9]. Dicho valor del parámetro k es dependiente de los valores de las constantes rotacionales (A,B,C). La notación de King-Hainer-Cross permite caracterizar las transiciones en base a tres números cuánticos ($J_{K_{-1},K_{+1}}$, donde K_{-1}: $k\rightarrow$-1; K_{+1}: $k\rightarrow$+1). Los números cuánticos rotacionales de J son momentos angulares totales de la molécula, y las K son pseudonúmeros cuánticos que se corresponden con la proyección de J sobre los ejes de simetría para los casos límite de rotores simétricos *prolate* y *oblate* (Gordy and Cook 1984).

Las moléculas de esta tesis, presentan una estructura correspondiente a la del rotor trompo-asimétrico con $k\approx$-1 (CH_3CH_2CN, CH_2CHCN, CH_3OCOH, CH_3COOH, CH_2OHCHO, CH_3CH_2OCOH,

[8] Los movimientos de vibración de las moléculas hace que los momentos de inercia dependan de los estados vibracionales, ya que los cambios en los ángulos y distancias de enlace son diferentes para cada modo normal de vibración.

[9] El otro tipo de rotores posee una geometría próxima al límite de simetría *oblate* y se define como *near-oblate asymmetric tops* (k cerca de +1, pues $A<B\approx C$), pero es menos frecuente.

CH_3OCOCH_3, $CH_3CH_2OCH_3$). En el caso de las moléculas trompo-asimétricas, el cálculo de los niveles de energía rotacionales y, por ende, de los Hamiltonianos efectivos, es considerablemente más intrincado que para el caso de las moléculas trompo-simétricas (donde los niveles que se corresponden con las $k\approx$-1 y $k\approx$+1 están degenerados, de ahí su notación J_K), especialmente para niveles rotacionales cada vez más altos. Para niveles rotacionales bajos, las ecuaciones que describen los niveles de energía y las frecuencias de las transiciones, son expresiones analíticas a partir de las constantes de rotación y de distorsión.

El orden de las transiciones rotacionales, respecto a los números cuánticos rotacionales (J) de las moléculas, varía dependiendo de las reglas de selección correspondientes a la geometría de la molécula, pues difiere según la disposición de los momentos dipolares (μ_a,μ_b,μ_c). Así, en el caso de las moléculas trompo-asimétricas, las transiciones rotacionales las caracterizamos como de tipo *a*, *b* y *c*, las cuales a su vez pueden pertenecer a varios tipos de ramas en función de las reglas de selección para los números cuánticos rotacionales J, es decir la rama P (ΔJ=-1), la rama Q (ΔJ=0) y la rama R (ΔJ=+1). Dependiendo del tipo de molécula, las transiciones de tipo a, b ó c de la rama P, Q o R serán unas más intensas que otras, dependiendo de la fuerza de la línea S_{nm} (o más bien $S_{nm}\cdot\mu_{nm}^2$) y del momento dipolar involucrado en la transición. Así, por ejemplo, en el caso de una de las moléculas de esta tesis, cianuro de etilo (CH_3CH_2CN), las transiciones tipo ${}^aR$ dependen más de las constantes *B* y *C*, mientras que las transiciones de tipo ${}^bQ$ dependen más de la constante rotacional *A*. Este comportamiento es válido para todas las moléculas trompo-asimétricas, y se ha de tener en cuenta para realizar las medidas correspondientes en el laboratorio. En esas medidas de laboratorio, se han de interpretar los espectros rotacionales buscando patrones entre las distintos tipos de transiciones rotacionales, con el fin de establecer una pauta y poder caracterizar los niveles de energía de la molécula.

En las moléculas trompo-asimétricas, las distorsiones centrífugas de las transiciones rotacionales hace que no se siga un patrón constante en el espectro, las correcciones a tal efecto dependen fuertemente de *J*, K_- y K_+. Además de los efectos ocasionados por la distorsión centrífuga, puede haber efectos causados por la resonancia de Fermi y acoplamientos de Coriolis (Kisiel et al. 2012).

Las reglas de selección para la espectroscopía rotacional de las moléculas trompo-asimétricas, son: ΔJ=0,±1 (cada J tiene (2*J* + 1) subniveles rotacionales discretos); $\mu_i\neq0$ (*i*=*a*,*b*,*c*); transiciones tipo-a: ΔK_{-1}=**0**,±2 y ΔK_{+1}=±**1**,±3; transiciones tipo-b: $\Delta K_{-1}=\Delta K_{+1}$=±**1**,±3; transiciones tipo-c: ΔK_{-1}=±**1**,±3 y ΔK_{+1}=**0**,±2. Estos valores de las variaciones en los pseudonúmeros cuánticos Δ*K*, se refieren a las transiciones permitidas (más intensas en negrita) para una componente del momento dipolar determinado, *a*, *b* ó *c*. Así, para las moléculas trompo-asimétricas cercanas al límite *prolate*, las transiciones más significativas son las que ocurren cuando ΔK_{-1}=0,±1.

3.3 Observación de las COMs en el ISM

Aunque muchas moléculas detectadas en el espacio no son corrientes en la Tierra (radicales carbonados por ejemplo), la mayor parte de ellas son bien conocidas en los laboratorios terrestres. El monóxido de carbono (CO), moléculas como el etanol (CH_3CH_2OH), el cianuro de hidrógeno (HCN), o el cinuro de etilo (CH_3CH_2CN) son abundantes en el espacio y se encuentran con gran facilidad en la Tierra. Sin embargo, los procesos químicos que dan lugar a esas especies moleculares en el espacio y en nuestro planeta son muy diferentes.

Desde 1937 hasta ahora (junio 2017), se han detectado cerca de 200 moléculas en el medio interestelar y circumestelar (de las cuales unas 5 son tentativas), y 60 moléculas en objetos extragalácticos (incluyendo una tentativa). Alrededor de 1/3 de las moléculas detectadas en el ISM son moléculas complejas, refiriéndonos a aquellas ≥6 átomos. De todas las moléculas detectadas en el ISM, unas 50 han sido detectadas en nuestra fuente de Orión-KL, a los que hay que añadir los isotopólogos y estados vibracionales, y todas son bien conocidas en diferentes procesos químicos en la Tierra.

Las moléculas orgánicas complejas se han detectado en el medio interestelar, tanto en *hot cores* como en *hot corinos*. Ambos tipos de condensaciones (*hot cores* y *hot corinos*) tienen una composición de COMs similar. Pero las diferentes escalas de tiempo y gradientes de temperatura que les definen, hacen que el estudio de la composición química específica de las COMs y sus abundancias, se puedan utilizar para distinguir entre ciertos aspectos de la formación estelar de baja y alta masa.

Las regiones de formación estelar masiva, SgrB2 y Orión-KL se consideran las fuentes de referencia para el estudio de las COMs. Sin embargo, la distancia a ambas es extraordinariamente diferente, lo que hace que la cercanía (a unos 414 pc ó 1300 a.l.) de la nebulosa de Orión-KL a nuestro Sistema Solar, sea considerada la fuente prototipo capaz de proporcionar medidas más precisas en relación a la resolución espacial que se obtiene con los radiotelescopios. Por otro lado, son muchos los objetos de similar naturaleza (*hot cores*) que muestran una gran variedad de COMs, como W3(H2O) (≈2000 pc), W3 IRS5 (<3000 pc), NGC 7538 (<3000 pc), NGC 6334 (≈1300 pc), G301.12-0.20 (≈4400 pc), G31.41+0.31 (≈7900 pc), IRAS18089-1732 (≈3600 pc), entre otros. En objetos de baja masa (*hot corinos*), cabe destacar la proto-estrella tipo-solar IRAS16293-2422 (≈120 pc), NGC1333-IRAS4A (≈220 pc), entre otras fuentes.

La nube de SgrB2, es la región de formación estelar más masiva de la Galaxia (a unos 8000 pc de nuestro Sistema Solar o 27000 a.l.), y en ella se ha encontrado la primera molécula orgánica ramificada, cianuro de isopropilo $(CH_3)_2CHCN$, un importante *building block* para los aminoácidos (Belloche et al. 2014). Por el momento, la molécula orgánica más compleja detectada en el espacio (concretamente en SgrB2) es el cianuro de n-propilo (n-$CH_3CH_2CH_2CN$). La molécula de etil metil éter ($CH_3CH_2OCH_3$), ha sido recientemente detectada en el espacio (concretamente en Orion-KL, Tercero et al. 2015).

Moléculas prebióticas

Son aquellas moléculas relacionadas con una Química Prebiótica o con el origen de la vida (*building blocks*), puesto que pueden ser consideradas los escalones intermedios con probabilidad de conducir a moléculas como el ADN, los aminoácidos o los azúcares. Las primeras que se detectaron fueron hacia el centro galáctico, SgrB2(N): glicolaldehído CH_2OHCHO (Hollis 2000), etilenglicol $OHCH_2CH_2OH$ (Hollis et al. 2002), cianuro de vinilo CH_2CHCN (Gardner and Winnewisser 1975), acetamida CH_3CONH_2 (Hollis et al. 2006), aminoacetonitrilo NH_2CH_2CN (Belloche et al. 2008), cianuro de isopropilo $(CH_3)_2CHCN$ (Belloche et al. 2014). De todas estas moléculas, la del cianuro de isopropilo es la única molécula orgánica ramificada, cuya detección despierta posibles indicios acerca de la presencia de aminoácidos en el ISM (H_2N-CHR-COOH), a causa de la naturaleza ramificada de la cadena lateral R (radical isopropil, $(CH_3)_2CH-$).

En discos protoplanetarios se habían detectado moléculas simples, pero el interferómetro ALMA es capaz de acceder a la tenue radiación que nos llega de las líneas espectrales de moléculas orgánicas más complejas. De hecho, la abundancia de moléculas como CH_3CN, HC_3N y HCN, detectadas en el disco protoplanetario de la estrella MWC 480 (de unas dos veces la masa solar, en la región de formación estelar de Tauro a unos 455 a.l.), revelan una alta tasa de eficiencia en la formación de COMs en discos protoplanetarios alrededor de estrellas jóvenes en escalas de tiempo cortas, lo cual permite que puedan sobrevivir en cometas u otros cuerpos helados del sistema protoplanetario (Öberg et al. 2015). Walsh et al. (2014) llevaron a cabo una modelización que incluía una red química análoga a la de los *hot cores* (en cuanto a reacciones en superficie sobre los granos de polvo, en fase gas e interacciones entre los granos de polvo), y concluyeron que las COMs (como CH_3CHO, CH_3CH_2OH, CH_3OCH_3, CH_3COCH_3, CH_3COOH, etc) son eficientemente formadas sobre los mantos de los granos de polvo, bajo las condiciones fisico-químicas del plano medio del disco protoplanetario mediante reacciones de superficie, y después son liberadas a la fase gas mediante procesos de desorción no-térmicos (fotodesorción y/o rayos cósmicos).

Moléculas en núcleos fríos y envolturas circumestelares de estrellas evolucionadas

En estos entornos predominan moléculas de naturaleza exótica: aquellas que no encontramos de manera estable en la Tierra, como radicales (*ver* por ej. Cernicharo et al. 2004). Las cadenas carbonadas cianopoliinos (HC_nN, n=3-5,7,9) y los carbinos poliinos (C_nH, n=2-6,8) se detectan en entornos fríos y en las envolturas circumestelares de estrellas evolucionadas. TMC-1 (*Taurus Molecular Cloud*, Ohishi and Kaifu 1998, Smith et al. 2004) es una nube oscura fría ($\approx$10 K) donde se han observado este tipo de moléculas de estructura insaturada, así como en la envoltura circumestelar de la estrella evolucionada AGB rica en carbono IRC+10216 (Kawaguchi et al. 1995). Aunque no abundan, también se encuentran especies moleculares saturadas (Remijan et al. 2005), como el metanol o el acetaldehído.

El cianopoliino más largo detectado en el espacio es el $HC_{11}N$ (Bell et al. 1997). Además los aniones de cadena carbonada (C_nH^-), como aquellos con n=4 (Cernicharo et al. 2007), 6 (McCarthy et al. 2006), 8 (Brünken et al. 2007), se han detectado en este tipo de regiones. Los entornos de TMC-1 y las capas más externas de IRC+10216, parecen tener un inventario molecular similar (Olofsson 2005), así como el de la nebulosa protoplanetaria CRL 618 (Pardo et al. 2007).

Moléculas complejas en PDRs

Las regiones de fotodisociación (PDRs, *Photodissociation Regions or Photon-Dominated Regions* por sus siglas en inglés) son el único entorno del ISM de gas molecular denso, donde la robusta molécula de CO es fotodisociada. En estas regiones, se da uno de los procesos de calentamiento más relevante del medio interestelar, el calentamiento fotoeléctrico. Las PDRs son la interfase entre las regiones frías y neutras, y las expuestas directamente a la radiación UV, en las que se desarrolla una fotoquímica capaz de destruir una buena parte de las moléculas, pero también de formar otras especies complejas (Cernicharo et al. 2004). Esta química se basa en moléculas fotodisociadas (potenciales de ionización< 13.6 eV) en escalas de tiempo tan rápidas (<1 yr) que incluso pueden llegar a ser calentadas a temperaturas cercanas a los 10^3 K, de modo que, además de los vibracionales, se pueden excitar los niveles electrónicos, dando lugar a reacciones endotérmicas con relativa facilidad. En general, las moléculas simples e iones característicos de las PDRs, son CO^+, HCO^+, CH^+, C_3H^+, HCN^+, H_2CO^+, CS^+, HCN, CS, HCO, etc, aunque también existen moléculas COMs como CH_3CN. En la PDR de la

cabeza de caballo en Orión las temperaturas son bastante bajas (20-30 K), lo cual implica una química basada en reacciones de desorción no térmicas. Aunque hay moléculas orgánicas tan complejas como en los *hot cores* o *hot corinos*, se han detectado COMS en esta fuente tales como HCOOH, CH_2CO, CH_3CHO y CH_3CCH (Guzmán et al. 2014, Cuadrado 2017 in prep.).

Moléculas en nubes difusas

Este tipo de nubes están expuestas a radiación UV estelar, pero en el interior de las mismas el gas está algo más protegido del campo de radiación, permitiendo la presencia de moléculas simples como H_2, CO, OH, CN, CH^+, entre otras.

Moléculas en outflows

Los *outflows* son los flujos de gas procedentes de estrellas en formación, albergan una química de alta temperatura producida por los choques entre el *outflow* y el gas ambiente (*shocked gas* en inglés). CH_3OH, en las cercanías de YSOs de baja masa, es una molécula que posee una abundancia mayor que en los núcleos fríos (Bachiller et al. 1995, Jørgensen et al. 2004).

También se han encontrado las moléculas complejas de CH_3OCOH y CH_3CH_2OH hacia la posición del pico B1, en el lóbulo del *outflow* protoestelar L1157 con una abundancia, relativa a CH_3OH, comparable a aquella encontrada en hot cores y en nubes del centro galáctico (Arce et al. 2008).

Moléculas complejas extragalácticas

Aproximádamente, son 60 las moléculas detectadas hasta la fecha en fuentes extragalácticas. Las moléculas más complejas encontradas en galaxias externas, hasta el momento, están constituidas por 7 átomos: metil acetileno CH_3CCH (Mauersberger et al. 1991), y metilamina CH_3NH_2 y formaldehído CH_3CHO (Müller et al. 2011).

Moléculas a alto redshift

Hace unos 20 años, la tecnología permitía acceder al conocimiento del espacio a unos 6×10^9 yr después del Big-Bang, lo que equivale a un redshift $z\approx1$. Sin embargo, actualmente somo capaces de explorar el Universo alcanzando un redshift $z>7$, es decir, cerca de unos 800×10^6 yr después del Big-Bang. Aunque, la galaxia más lejana detectada hasta el momento, EGS8p7, se acerca a unos 700×10^6 yr después del Big-Bang ($z\approx8.68$, *Ly*α). Los datos proporcionados por radiotelescopios de alta sensibilidad, como ALMA, podrán llevarnos a trazar el gas molecular de galaxias cada vez más lejanas.

3.4 Reacciones moleculares: Química interestelar

En el Capítulo 5, podemos ver los casos particulares de las reacciones químicas con las moléculas interestelares observadas en este trabajo. La detección de nuevas especies en el medio interestelar nos aporta información acerca de los posibles mecanismos de formación/destrucción de

FIGURA 3.4: SISTEMAS PLANETARIOS EN FORMACIÓN EN LA NEBULOSA DE ORIÓN *(Fuente: http://apod.nasa.gov/)*. MUCHOS DE LOS DISCOS PROTO-PLANETARIOS EN FORMACIÓN POSIBLEMENTE EVOLUCIONARÁN HASTA LLEGAR A FORMAR PLANETAS.

moléculas, con el fin de completar la intrincada red de rutas químicas interestelares. Además, los mapas de emisión de las líneas rotacionales de las moléculas de la región astrofísica, nos ayudará a deducir los reactantes más probables implicados en la obtención de las especies moleculares presentes en el medio interestelar.

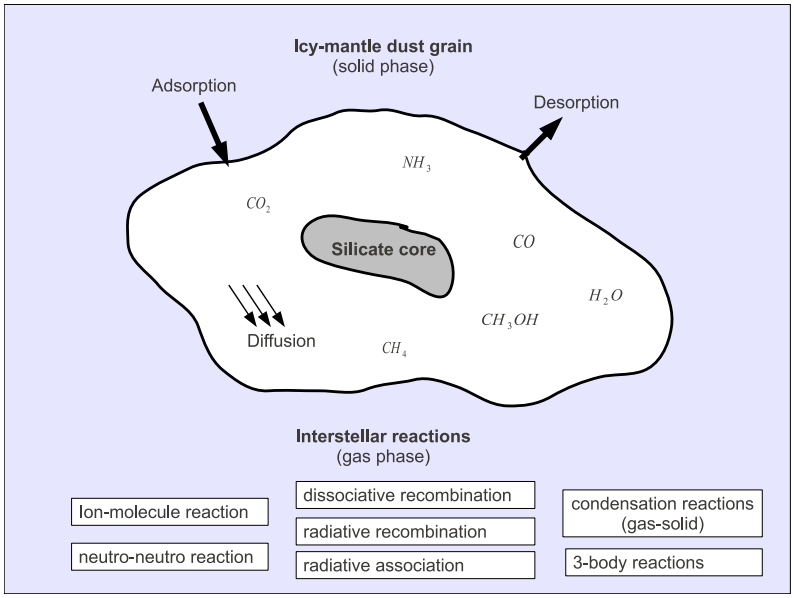

FIGURA 3.5: MECANISMOS DE REACCIÓN PRINCIPALES EN ASTROQUÍMICA (*Ehrenfreund et al. 2005; Fraser et al. 2002*).

Las condiciones de baja presión, temperatura y densidad se corresponden con una química fría en la que las reacciones tienen lugar gracias a las extensas escalas de tiempo de vida de las nubes ($\approx 10^7$ años). Dependiendo del entorno en el que nos encontremos, dominarán unas reacciones u otras. La principales reacciones que se producen en las nubes moleculares son reacciones de recombinación, de

fotodisociación, reacción neutro-neutro, reacción ión-molécula, ionización por rayos cósmicos, etc (*ver* Fig. 3.5). La comprensión de las reacciones que ocurren en el medio interestelar, nos aporta una valiosa información acerca del tipo de química que está aconteciendo en cada entorno astrofísico (regiones de formación estelar, envolturas circumestelares, atmósferas planetarias,...).

Hay que destacar el importante papel que tiene el polvo interestelar, ya que proteje al gas de la radiación UV y actúa de catalizador, permitiendo una mayor complejidad en los procesos químicos y la formación de COMs (*ver* fig. 3.5).

A continuación, se describen brevemente las reacciones significativas en el marco de nuestra fuente de *hot core*, tomando como guía Duley and Williams 1984.

En las colisiones **ión(A^+)-molécula(BC) (o ión-neutro)**, el campo eléctrico del ión induce un dipolo eléctrico en la molécula produciéndose una fuerza de atracción entre ambos, cuyo potencial de interacción depende de la polarizabilidad de la molécula (α), la cual depende linealmente del momento dipolar inducido. Estas reacciones pueden ser de transferencia de protón, abstracción, insercción y condensación de hidrógeno, de transferencia de carga (como por ejemplo $CO^+ + CH_4 \rightarrow CO + CH_4{}^+$).

$$A^+ + BC \rightarrow AB^+ + C$$

En las colisiones **neutro(A)-neutro(BC)**, ambas partículas se inducen mutuamente un dipolo eléctrico al interaccionar, produciéndose una fuerza de atracción (mediante fuerzas de van der Waals) entre ambas y cuyo potencial de interacción depende de la polarizabilidad de ambas especies implicadas. La mayor parte de las reacciones neutro-neutro dependen de la temperatura, ya que suelen poseer energías de activación.

$$A + BC \rightarrow AB + C$$

Hay procesos químicos en los que las partículas implicadas (A y B) interaccionan, y se genera un estado excitado intermedio (AB*) que puede decaer radiativamente a la especie AB (las reacciones a 3 cuerpos que podrían estabilizar a la especie AB* no son eficaces en las condiciones de densidad del medio interestelar). A este proceso se llama **asociación radiativa**.

$$A + B \rightarrow AB^* \rightarrow AB + h\nu \qquad \text{(r. asociación radiativa)}$$

En el medio interestelar es muy probable tener especies cargadas positivamente (AB^+ o ABC^+) que terminan interaccionando con un electrón, en lo que se conoce como **recombinación radiativa**; o bien, rompiendo enlaces y obteniendo especies más simples, es decir, mediante **recombinación disociativa**. Ambos procesos son dependientes de las condiciones de temperatura del entorno.

$$AB^+ + e^- \rightarrow AB + h\nu \qquad \text{(r. recombinación radiativa)}$$

$$ABC^+ + e^- \rightarrow A + BC \qquad \text{(r. recombinación disociativa)}$$

Reacciones interestelares dominantes en el ISM

En química de superficie dominan tres tipos de mecanismos: Langmuir-Hinshelwood (o de difusión), Eley-Rideal, y el *hot atom* o átomo caliente (Herbst and Van Dishoeck 2009). El primero de ellos, es el más ampliamente estudiado e incluido en los modelos de astroquímica (Kolasinski 2012). En el mecanismo de Langmuir-Hinshelwood, la difusión ocurre por efecto túnel o salto térmico sobre la barrera de energía potencial entre centros o lugares de unión/enlace por parte de átomos y radicales, que al caer en el mismo mínimo, reaccionan liberando el exceso de energía. En el mecanismo de Eley-Rideal, las especies de la fase gas se adsorben sobre un átomo o radical de la superficie del polvo y reacciona con él. Y en el mecanismo de átomo caliente (una variante del mecanismo de Eley-Rideal), las especies de la fase gas se adsorben sobre la superficie del polvo y se mueven antes de que se haya termalizado para colisionar con el átomo o el radical que encuentren (Herbst 2002; Herbst and Van Dishoeck 2009).

Los fenómenos de fisisorción y quimisorción que ocurren sobre la superficie de los granos de polvo, dependen de su composición y su temperatura, para contribuir a la formación de los mantos de hielo sobre sus superficies. La fisisorción sobre la superficie de los granos de polvo ocurre mediante las fuerzas de van der Waals. La quimisorción ocurre a través de enlaces químicos.

Para determinar las reacciones dominantes en fase gas, vamos a explicar la formación de las COMs en nuestro contexto, los *hot cores* (*ver* Sec. 3.5).

3.4.1 Algunos precursores para la formación de las moléculas interestelares

Papel del H_2

Toda la química que tiene lugar en el medio interestelar, además de los granos de polvo, actuando como catalizadores y protectores esenciales, depende de la presencia del hidrógeno molecular (H_2). La molécula más abundante del Universo, el hidrógeno molecular (H_2), antes de encontrarse en la fase gase, es eficientemente formada sobre la superficie de los granos de polvo.

Respecto a la detección de la molécula de H_2, debido a que no posee momento dipolar permanente (μ=0), carece de transiciones dipolares eléctricas. Esta especie tan dominante en el medio interestelar puede ser detectada mediante sus transiciones cuadrupolares eléctricas, así como mediante su espectro de rotación-vibración (Herbst 2001). Por este motivo, la distribución del gas en la Galaxia se traza mediante el segundo gas más abundante en el medio interestelar, el monóxido de carbono (CO).

Papel de H_3^+

El catión trihidrógeno o hidrógeno molecular protonado (H_3^+) sería la segunda molécula más abundante del ISM, sin embargo su presencia es efímera debido a que reacciona inmediatamente con átomos de O y C, actuando, de ese modo como iniciador de las reacciones ión-molécula en las nubes moleculares. Una vez que se forma el H_2^+ por efecto de los rayos cósmicos, rápidamente se forma el H_3^+, resultado de la interacción del H_2^+ con H_2; H_3^+ puede reaccionar con otras especies diferentes a las moléculas de H_2, principalmente mediante reacciones ión-neutro para dar lugar a especies protonadas (Herbst 2001).

Papel del CH_3OH

La acreción del CO (formado en la fase gas) sobre los granos de polvo puede llevar a cabo una secuencia de reacciones, pasando por la producción de formaldehído (H_2CO), que conducen a CH_3OH tras su hidrogenación, una molécula compleja que favorece la formación de moléculas aún más complejas, como el dimetil éter (CH_3OCH_3) y el formiato de metilo (CH_3OCOH) (*ver por ej.* Garrod and Herbst 2006). Sin embargo, la química previa a la formación de la molécula de CH_3OH marcará la síntesis de un tipo de moléculas u otras bajo las condiciones físicas de las diferentes componentes de la nube, un fenómeno que influirá en la diferenciación química observada en nuestra fuente de Orión-KL. De este modo, el *hot core*, caracterizado por moléculas esencialmente nitrogenadas, y el *compact ridge*, dominado por especies que contienen oxígeno, reflejan esa diferenciación. Es posible que la mayor temperatura del gas y del polvo (superficie de los granos) para el caso del *hot core*, implique que las especies se enlazan débilmente a los granos de polvo, con lo que no permanecen el tiempo suficiente para reaccionar (Caselli et al. 1993). La menor temperatura para el caso del *compact ridge*, hace que se obtengan especies más pesadas que permanecen sobre los granos de polvo y reaccionan con otras especies (Caselli et al. 1993).

3.4.2 Reacciones térmicas y no-térmicas

Los CRs se asocian principalmente a explosiones de supernovas, y son una fuente de ionización principal en las nubes moleculares.

La fracción de ionización controla la química de las nubes moleculares y el acoplamiento del gas con el campo magnético, por lo que los CRs contribuyen a la dinámica del ISM favoreciendo la evolución del gas molecular. Además, los CRs representan una importante fuente de calor para las nubes moleculares, debido a que la energía de los electrones primarios y secundarios producidos por el proceso de ionización, se convierte en gran parte en calor por colisiones inelásticas con los átomos y las moléculas del ISM. Los CRs no sólo ionizan el gas de las nubes (átomos y moléculas), sino que también rompen enlaces químicos. La ionización por parte de los CRs, hace que el gas de las nubes moleculares se caliente como consecuencia de la transferencia de energía a los electrones eyectados. Además, unido a que los fotones secundarios (γ-R, electrón-positrón, neutrinos) producidos por los CRs conllevan a la fotoionización e ionización del gas, hace que se se mantenga una tasa de ionización considerable (Viti et al. 2013).

La tasa de ionización inducida por rayos cósmicos, es del orden de los $\approx 10^{-16}$–10^{-17} s^{-1} (Padovani et al. 2009). Las pruebas directas de las tasas de ionización en nubes densas, son las moléculas de HCO^+ y $H_3{}^+$. La fracción de ionización es un parámetro fundamental a la hora de distinguir los diferentes regímenes que ocurren en el medio interestelar.

La importancia de la presencia de los CRs resulta evidente, especialmente si nos centramos en las reacciones ión-molécula desencadenadas por moléculas simples como $H_2{}^+$ o $H_3{}^+$, las cuales son las responsables de la síntesis de moléculas más complejas en el ISM.

3.4.3 Velocidad de la reacción

La mayoría de las reacciones (tanto reversibles con unidireccionales) están regidas por las tasas de los coeficientes de la reacción, o también llamada constante de velocidad (k) según la Ley de Arrhenius, k=$A(T)$ $exp(-E_a/k_BT)$ (donde k está en unidades de $cm^3 \cdot s^{-1}$, $A(T)$ es el factor pre-exponencial o de frecuencia de colisiones de los reactivos, que es dependiente de la temperatura; E_a es la energía de activación en $J \cdot molecula^{-1}$; k_B es la constante de Boltzman en JK^{-1}). En las nubes densas con unas temperaturas de unos 10 K, las reacciones con E_a (o barrera de activación) no ocurren de manera eficiente.

La mayoría de las reacciones exotérmicas ión-molécula no tienen barrera de activación, suelen regirse por la ecuación de Langevin, $k_{ion-molecule} = 2\pi e(\alpha/\mu)^{1/2}$ (donde e, carga electrónica; α, polarizabilidad; μ, masa reducida de los reactivos), cuyo valor es mayor cuando la molécula es de naturaleza polar. Los intervalos de tiempo entre las colisiones de moléculas en el ISM suelen ser grandes, pero aún así dichas colisiones generan una química interestelar. Los rangos de valores típicos de k en función de la región del ISM −especialmente en nubes oscuras y regiones de formación estelar− adquiere los siguientes valores (Caselli 2005):

k (ión-molécula): 10^{-9} cm^3 s^{-1}
k (neutro-neutro): 10^{-12}-10^{-10} cm^3 s^{-1}
k (recombinación disociativa): 10^{-6} cm^3 s^{-1}
k (asociación radiativa): 10^{-16}-10^{-9} cm^3 s^{-1}
k (fotodisociación): 10^{-9} cm^3 s^{-1}
k (transferencia de carga): 10^{-9} cm^3 s^{-1}

Las reacciones ión-molécula son considerablemente más eficientes produciendo moléculas en el ISM que las reacciones neutro-neutro.

3.5 Formación de las COMs en los *hot cores*

Los escenarios propuestos para la formación de COMs en los *hot cores*, presentan etapas previas de formación de los núcleos pre-estelares fríos (≈10 K), en los que los átomos y las moléculas formadas en fase gas, condensan sobre la superficie de los granos de polvo para producir especies moleculares más complejas mediante hidrogenación (Bacmann and Faure 2014).

Es de esperar que las COMs no se formen en las fases previas de la formación de los *hot cores*, es decir, en el caso de los núcleos pre-estelares, puesto que las condiciones de temperatura son muy bajas, ≈10 K (Bacmann and Faure 2014), a excepción del metanol, CH_3OH (Friberg et al. 1988; Tafalla et al. 2006). Sin embargo, la presencia de moléculas orgánicas con oxígeno, tales como CH_3CHO, CH_3OCH_3, CH_3OCOH, en fríos núcleos pre-estelares dominadas por bajas energías térmicas, indican que este tipo de moléculas de naturaleza terrestre no son únicas de los *hot cores* o *hot corinos* (Cernicharo et al. 2012; Bacmann et al. 2012).

A raíz de encontrar COMs en nubes frías, se ha desarrollado el estudio de nuevas rutas químicas para los mecanismos de formación de moléculas en fase gas (Vasyunin and Herbst 2013). Estos últimos autores, proponen un escenario en el que moléculas precursoras como metanol (CH_3OH), radical metoxi (CH_3O) y formaldehído (H_2CO), se desorben de los mantos de hielo de modo no-térmico mediante *desorcion reactiva*, un proceso en el que parte de la energía exotérmica procedente de las reacciones químicas sobre la superficie de los granos, se utiliza como energía cinética para la ruptura del enlace entre el producto y el hielo. Posteriormente, se desencadenarán las reacciones en fase gas para obtener las COMs.

Una vez se ha formado la proto-estrella, la evaporación de los mantos de hielo desarrolla una química rica y compleja en fase gas (química de *hot core*/*hot corino*), íntimamente relacionada con los procesos de la química de superficie de los granos de polvo en la etapa precedente.

La diferencia entre los objetos estelares jóvenes de baja masa y aquellos masivos, radica en que estos últimos cubren una mayor fracción de la envoltura a una temperatura más alta, y además los núcleos pueden estar siendo calentados por estrellas jóvenes cercanas (van Dishoeck and Blake 1998). El proceso de desorción o evaporación de los mantos de hielo alrededor de las proto-estrellas, ocurre de manera más eficiente para las especies volátiles que han constituido la capa de hielo sobre los granos de polvo (CO, O_2, N_2, CO_2), formadas a mayores densidades, que la capa de hielo constituida por especies polares (H_2O, CH_4, NH_3), las cuales fueron antes condensadas sobre los hielos (van Dishoeck and Blake 1998). Desde las observaciones en el IR de Willner et al. (1982), la composición de los mantos de hielo en las envolturas de los YSOs masivos ha sido estudiada con más detalle que para aquellos de baja masa, dada la dificultad de encontrar fuentes infrarrojas brillantes en este caso.

3.5.1 Modelos de química

UMIST *Database for Astrochemistry* (UDfA 2012) es una base de datos consistente en modelos de química, asociados a una base de datos de reacciones químicas. UDfA contiene un conjunto de 6173 reacciones en fase gas, que involucra 467 especies. Además, incluye 1171 reacciones que implican aniones y todas las tasas de los fotones (”*photorates*”) actualizadas y revisadas. Todas las tasas de fotodisociación de las reacciones, se han actualizado en esta base de datos. También considera las tasas de los coeficientes de reacciones deuteradas específicos de cada estado de espín del H_2, reacciones de intercambio de deuterio y una lista de energías de enlace de superficie para muchas especies neutras. Las tasas de los coeficientes de la reacción comprenden un amplio rango de temperaturas: $\leq$10 K (núcleos preestelares), $\approx 10^2$ K (núcleos moleculares calientes), $\approx 10^3$ K (gas post-choque).

Debido a que existe mucha incertidumbre asociada a la química de superficie relacionada con los granos de polvo, la base de datos UDfA sólo considera reacciones en fase gas. Los datos y códigos asociados a este entramado de reacciones se puede encontrar en `http://www.udfa.net`. La modelización química se aplica a una nube oscura y a la envoltura rica en carbono de una estrella AGB, sin embargo, se puede usar en un amplio rango de entornos astrofísicos. Así, los núcleos moleculares calientes se pueden modelizar incluyendo química de superficie sobre los granos de polvo. Es interesante destacar que los primeros modelos de química para los hot cores fueron desarrollados por Brown et al. en 1988. La versión más actualizada para la base de datos que incluye las propiedades cinéticas para la red de reacciones entre especies de interés en astroquímica, *KInetic Database for Astrochemistry* se

encuentra en la web: *http://kida.obs.u-bordeaux1.fr/* (KIDA, Wakelam et al. 2015).

3.6 Polvo interestelar y química

El polvo interestelar en las fases finales de las estrellas, conformándose en base a los elementos pesados que se generan en las recciones nucleares estelares (Mg, Fe, C, Si,...). El polvo interestelar puede proceder del material eyectado de estrellas de la rama asintótica de las gigantes, bien aquellas ricas en carbono o bien en oxígeno, de modo que la composición de los granos de polvo varía en función de la naturaleza de la estrella (*ver por ej.* Gail and Sedlmayr 1986, 1987; Mathis 1990; Sedlmayr 1994). La masa de nuestra Galaxia se constituye en un 20-30% de gas y polvo interestelar. Este último, se corresponde con una fracción muy pequeña, pues apenas constituye el 1% de la materia interestelar, pero resulta en un elemento esencial para la química interestelar y la formación de estrellas y planetas (*ver por ej.* Charnley et al. 1992; Ehrenfreund and Charnley 2000).

Los granos de polvo contribuyen en gran medida a la refrigeración de la nube, incluso antes de que esta llegue a ser densa. De hecho, es el principal sistema refrigerante (*ver por ej.* Bodenheimer 2011).

3.6.1 Escala de tiempo de colisión de las moléculas con los granos de polvo

Dentro de las nubes, el tiempo de colisión de las moléculas con los granos de polvo es del orden de los 10^5 años (en densidades típicas de n_H=10^4 cm^{-3} (Schutte et al. 1996, Schutte and Greenberg 1991). Para $T_{granos}\approx$10 K, las moléculas y átomos más pesados que He se pegarán (”*stick*”) a los granos de polvo con una eficiencia de cerca del 100%. De este modo, el polvo tiene una mezcla de especies que van formando su manto de hielo (Schutte et al. 1996).

3.6.2 Composición química de los granos de polvo

La espectroscopía en el rango de longitudes de onda del IR, revela la composición química de los granos de polvo basándonos en las transiciones vibracionales de las moléculas presentes en los granos de polvo (núcleo + manto de hielo). Dichos modos vibracionales aparecen en absorción en el caso de las nubes moleculares. Los mantos de hielo de los granos de polvo envuelven, núcleos de silicatos o materiales carbonáceos en función de su procedencia.

El tiempo que tarda el ISM en destruir los granos de polvo es relativamente corto, por lo que la población de granos de estructura amorfa es significativamente mayor que aquellos de estructura cristalina, los cuales requieren de temperaturas elevadas. Los granos de polvo que proceden de estrellas ricas en oxígeno suelen tener una naturaleza silicatada con materiales como las olivinas[10]. Estos cristales diminutos, además de encontrarse en el polvo cometario y en estrellas evolucionadas (gigantes rojas y nebulosas planetarias), se han observado en discos proto-planetarios, concretamente en la envoltura de un sistema estelar jóven constituido por un objeto a medio camino entre enana marrón y planeta gigante en la constelación de Camaleón (HD 100546, Acke and van den Ancker 2006) (*ver* por ejemplo Huss

[10]La estequiometría de la olivina es $(Mg,Fe)_2SiO_4$, cuya composición está basada en los minerales fosferita (Mg_2SiO_4) y fayalita (Fe_2SiO_4)

et al. 2001; Bouwman et al. 2003).

Los materiales carbonáceos, procedentes de estrellas ricas en carbono, pueden presentarse en forma de Hidrocarburos Policíclicos Aromáticos, carbonos amorfos hidrogenados, hidrocarburos alifáticos, o incluso en su forma cristalina como diamantes o grafitos.

PAHs: diminutos granos de polvo carbonáceos

Los Hidrocarburos Policíclicos Aromáticos (PAHs, "*Policiclic Aromatic Hydrocarbons*" por sus siglas en inglés) son considerados otro tipo de granos de polvo (carbonáceos) aunque de menor tamaño. Los PAHs son moléculas constituidas por anillos aromáticos (benceno, como unidad básica) y tienen bandas de emisión en 3.3, 6.2, 7.7, 8.6 μm (Gillett et al. 1973; Russell et al. 1977). De hecho, la banda 7.7 μm es un trazador de SFR's ("Star Forming Regions"). Su espectro, en función de la fase del ISM en la que se encuentra (fría, caliente, templada,...), abarca el dominio de las ondas IR y mm. Dicho espectro permite obtener principalmente abundancias y carga eléctrica de los PAHs en el ISM (Guessoum et al. 2010).

Estos compuestos se suelen encontrar asociados a las interfases entre un medio difuso y un medio denso (pues son generados en regiones de fotodisociación), en las nebulosas planetarias (PNs), en Regiones HII y en AGNs. Se observan los modos vibracionales que son debidos a la presencia de uniones C-C y C-H.

3.6.3 Manto de hielo de los granos de polvo

Los mantos de hielo de los granos de polvo se corresponden con la envoltura que se desarrolla alrededor de ellos, y representa la interfase transitoria entre la fase sólida y la fase gas. Su presencia se confirma por las características espectrales de absorción procedentes de las nubes densas del ISM, debidas principalmente a hielos de H_2O, CO, CO_2 y CH_3OH (Herbst 2001).

Gibb et al. 2004 mostraron la composición química de los mantos de hielos de los granos de polvo (que básicamente contienen H_2O, CO, CO_2, CH_3OH, y CH_4) perteneciente a diversas fuentes (objetos jóvenes de alta y baja masa en nubes oscuras y difusas) con el espectrómetro del telescopio ISO (*Infrared Space Observatory* por sus siglas en inglés), en la que se han identificado, entre otras, moléculas de OCS, H_2CO, and HCOOH. La evolución química de los mantos de hielo, así como la temperaura de los granos y el campo de radiación en la nube molecular, determinarán la composición y estructura de los hielos (Watanabe et al. 2007). La acreción de moléculas en fase gas sobre la superficie de los granos de polvo, así como procesos fotoquímicos in-situ, también contribuyen a definir la composición de los granos (Allamandola et al. 1999). Los mantos de hielo estarán constituidos esencialmente por moléculas simples, sin embargo, la irradiación y los procesos térmicos a los que puedan estar sometidos, inducirán a la producción de moléculas más complejas (Allamandola et al. 1999).

La dependencia de la composición química de los mantos de hielo con el entorno astrofísico, se hace evidente en las diferentes características espectrales que se muestran en el UV con la banda ancha de absorción a 217.5 nm, debida a los granos de polvo carbonáceos en las nubes difusas, y en el IR con las bandas de absorción/emisión de los silicatos a 10 y 20 μm típicas de regiones calientes. Estas bandas

aparecen en absorción en regiones frías (Herbst 2001). Los hielos polares, dominados por hielos de H_2O, se evaporan generalmente alrededor de los 90 K bajo las condiciones del entorno y pueden sobrevivir en regiones calientes cerca de la estrella (Ehrenfreund and Charnley 2000; Tielens and Whittet 1997).

Capítulo 4

Metodología: Radioastronomía y Laboratorio

A comienzos del siglo XX, la radioastronomía dio sus primeros pasos con la búsqueda de interferencias en las radiotransmisiones transatlánticas por parte del físico e ingeniero estadounidense Karl Guthe Jansky (nombre que recibe la unidad de intensidad de la radiación en su honor, Jy), pues descubrió señales procedentes del centro de nuestra Galaxia. Posteriormente, el ingeniero Grote Reber continuó con el trabajo de Jansky observando el espacio con un radiotelescopio casero de 9 m de diámetro y, más tarde, Martin Ryle desarrolló la técnica de síntesis de apertura que permite llevar a cabo observaciones interferométricas, con muy alta resolución angular.

Es necesario remarcar que la **radioastronomía** es una herramienta fundamental, no sólo para el estudio de las moléculas interestelares, sino para la investigación de las galaxias más lejenas del universo conocido, la materia oscura, la radiación de fondo cósmico, así como para todos los demás objetos astronómicos, como por ejemplo los planetas del Sistema Solar. Además, las moléculas interestelares no nos informan únicamente de las condiciones fisico-químicas del gas, sino también de la radiación de fondo, la radiación infrarroja ambiente o el campo UV galáctico (Cernicharo et al. 1999). En la investigación de las moléculas interestelares, la radioastronomía se vale de las líneas espectrales de moléculas en fase gas procedentes de la región astrofísica de interés, las cuales experimentan procesos de relajación o excitación desde distintos niveles de energía.

En este capítulo, se presentan los métodos y técnicas utilizadas para el análisis y producción de los resultados presentados en esta tesis. En líneas generales, podemos resumir el procedimiento de obtención de resultados según las siguientes etapas:

- Observación de la fuente astrofísica de interés.
- Reducción de los datos observacionales.
- Análisis y modelización astrofísica.
- Trabajo de laboratorio.

Los artículos presentados en esta tesis se basan, principalmente, en análisis de los datos obtenidos del barrido espectral de Orión-IRc2 (en el complejo Orión-KL) con el radiotelescopio de IRAM-30 m (Tercero et al. 2010; Tercero). En este barrido espectral se han detectado alrededor de 16 000 características espectrales correspondientes a unas 40 moléculas y a más de 200 especies diferentes (teniendo en cuenta distintos isotopólogos y estados vibracionalmemte excitados). Sin embargo, durante las primeras fases del análisis de este barrido espectral, muchas de las líneas detectadas (alrededor de 8 000) no pudieron identificarse con ninguna especie conocida, principalmente porque las frecuencias a las que aparecen las transiciones de un gran número de isotopólogos y estado excitados de especies abundantes en nuestra fuente eran desconocidas. Esta incertidumbre en la asignación de un número tan elevado de líneas, suponía una fuerte limitación para poder llevar a cabo un análisis profundo del objeto de estudio. Por este motivo, se inició una estrecha colaboración con expertos en el ámbito de la espectroscopía molecular, con el fin de poder identificar estas líneas. Cerca de 2 000 líneas fueron

identificadas gracias a estas colaboraciones (*ver* Tercero) en las que se estudió en el laboratorio los isotopólogos principales de formiato de metilo (CH_3OCOH) y de cianuro de etilo (CH_3CH_2CN). Este trabajo supuso la primera detección en el espacio de 9 especies diferentes y, gracias a ello, se logró un análisis más profundo de la región Orión-KL. Por otro lado, dado el gran número de características espectrales presentes en el estudio, se procedió al análisis en base a distintas familias moleculares. Los primeros trabajos fueron dedicados a las moléculas que presentaban el grupo −CS (Tercero et al. 2010) y las que contenían Si (Tercero et al. 2011).

En esta tesis y puesto que todavía existían gran cantidad de líneas sin identificar y de especies moleculares sin analizar, se ha tratado de dar continuidad a este trabajo. Por un lado, se ha continuado trabajando con los laboratorios de espectroscopía molecular para lograr identificar nuevas especies y, por otro, se han realizado análisis físico-químicos de la fuente con diferentes familias de moléculas.

Observaciones

Las **ventanas atmosféricas** en las cuales hemos observado la nube de Orión-KL abarcan las longitudes de onda de 3 mm a 0.9 mm, aproximadamente desde los 80 GHz hasta los 307 GHz de frecuencia, en el dominio de las ondas milimétricas y sub-milimétricas.

A continuación, vamos a describir los datos de los que disponemos, procedentes de los radiotelescopios involucrados en este trabajo:

Los **datos observacionales** se obtuvieron con el radiotelescopio de 30 m de IRAM (Granada, España), apuntando hacia la fuente Orión-IRc2 (α_{2000}=$5^h35^m14.5^s$, δ_{2000}=-5°22′30”) y usando cuatro receptores superheterodinos con mezclador SIS (Superconductor-Aislante-Superconductor) operando a 3 mm (80-115 GHz), 2 mm (130-180 GHz) y 1.3 mm (197-280 GHz). La resolución espectral es de 1-1.25 MHz. Asimismo, disponemos de otro set de datos obtenidos posteriormente con el mismo telescopio pero ampliando los rangos de frecuencias con uso del receptor EMIR (*Eight MIxer Receiver*): 80.7-116, 122.7-161.2, 199.7-306.7 GHz, con una resolución espectral de 0.2 MHz.

IRAM-30 m, es un radiotelescopio de antena única, con una superficie de alta precisión localizado a 2850 m de altura en Sierra Nevada, en la provincia de Granada, España.

Los cartografiados de emisión molecular nos permiten caracterizar espacialmente la emisión molecular de un objeto. En el caso de un único apuntado, solo tenemos información promediada sobre el haz principal del telescopio (eqivalente a 1 píxel). En un mapa *on-the-fly* (OTF) se realiza un barrido espacial con múltiples apuntados, para registrar la emisión en distintas direcciones a lo largo del objeto que estamos estudiando.

Además, en este trabajo también se han analizado datos de Orión-KL con una alta resolución espacial (2”) obtenidos con el interferómetro ALMA (*Atacama Large Millimeter/Sub-millimeter Array*) en el desierto de Atacama en Chile, con 16 de las antenas de 12m operando en el rango de frecuencias de la Banda 6 (entre 213.715 y 246.627 GHz). La resolución espectral obtenida es de 0.488 MHz.

ALMA, es un interferómetro que puede revolucionar el campo de la detección de moléculas orgánicas complejas en regiones de formación estelar, al superar los límites de detección de los teslescopios

actuales. Está situado en el desierto de Atacama en Chile, un lugar muy seco donde se reduce significativamente el efecto del vapor de agua atmosférico, y a unos 5000 m de altura, para atenuar el efecto que tiene el oxígeno atmosférico en las señales espectrales. En esta tesis, los datos de los que disponemos se corresponden principalmente con los datos del ALMA *Science Verification (SV)* en la ventana atmosférica de 1 mm. La combinación de estos datos con aquellos procedentes del radiotelescopio de 30 m de IRAM resulta esencial para un análisis completo de los datos, debido a que los mapas de emisión que se obtienen con datos de ALMA SV revelan las componentes de la nube de Orión-KL con una elevada resolución espacial.

Análisis

El **análisis y la reducción** de los datos, es posible gracias al uso del paquete de software GILDAS[1]. Para el estudio de las transiciones rotacionales de las moléculas que emiten en la región de Orión-KL y obtener las condiciones físicas y químicas que definen la misma, llevamos a cabo una modelización físico-química, haciendo uso de un código de excitación y transporte de radiación, MADEX, desarrollado por J. Cernicharo (Cernicharo 2012). Todo esto, acompañado del uso de catálogos espectrales moleculares para identificar las líneas moleculares y determinar los posibles solapamientos con otras especies que emiten en frecuencias similares.

El trabajo desarrollado en el **laboratorio**, es crucial para la detección e identificación de especies moleculares en el espacio. Por ello, para algunas de las moléculas de la tesis, se investigó en el Laboratorio de espectroscopía milimétrica de la Universidad de Valladolid, el cual desarrolla sus investigaciones a través del análisis de los datos obtenidos con distintos instrumentos, entre los que se encuentra un espectrómetro que opera en la región microondas/(sub)milimétrica.

De todas las moléculas que comprende esta tesis, CH_3CH_2CN y CH_2CHCN son las que han sido estudiadas en el laboratorio de Valladolid para proceder a la detección interestelar de los estados vibracionales de más baja energía de las mismas. Dicho trabajo de laboratorio, tuvo lugar entre los meses de noviembre de 2011 a febrero de 2012.

4.1 Interacción entre materia y radiación

Los átomos y las moléculas son sistemas cuánticos, que interaccionan con los fotones de la radiación electromagnética, absorbiendo cuantos de energía ($E=h\nu$)[2]. Dicha energía, es equivalente a la diferencia entre los dos estados o niveles energéticos ($\Delta E=E_m-E_n$) por los que pasa el sistema al cambiar de estado energético, excitándose a un nivel superior o desexcitándose y relajándose a un estado inferior, emitiendo un fotón. Las líneas espectrales, consecuencia de las transiciones que resultan de la absorción o emisión de la radiación, aparecen en posiciones del espectro correspondientes a las frecuencias características de cada transición.

Las condiciones del medio interestelar, influyen en la intensidad que recibimos de las líneas moleculares en nuestro espectro. La **profundidad óptica** del medio mide la capacidad del gas del medio

[1] https://www.iram.fr/IRAMFR/GILDAS/

[2] La energía de las ondas electromagnéticas se propaga a la velocidad de la luz, y viene determinada por la relación $E = h\nu = hc/\lambda$.

interestelar, para bloquear la luz en la nube en base al recorrido libre medio, que pueden tener los fotones de la luz que recibimos en su interacción con las partículas del gas.

El medio es ópticamente transparente (τ<1), si la emisión molecular que nos llega de la nube sufre pocas interacciones con otras partículas. En estos casos, podemos calcular la densidad de columna de la especie detectada, así como la temperatura a la que se excitan sus líneas. Si el medio es ópticamente opaco (τ>1), las interacciones entre la radiación emitida con las demás partículas del medio, son importantes (habrá habido muchos procesos de absorción y dispersión) y dará lugar a unas líneas saturadas, con lo que perdemos información respecto a la abundancia de la especie emisora.

Las especies muy abundantes en la región, suelen presentar líneas ópticamente opacas. Es por ello, que el cálculo de las abundancias de estas moléculas, se hará a través de los isotopólogos menos abundantes. Éstos, no se ven afectados generalmente por problemas de opacidad, y mediante ellos se pueden estimar las abundancias del isotopólogo principal a través de las razones isotópicas.

En nuestro trabajo hemos utilizado MADEX, un código de transporte de radiación desarrollado por J. Cernicharo (2012), para caracterizar y modelizar la región estudiada. MADEX permite realizar una modelización, para la obtención de las condiciones físicas y químicas de la nube, simulando los espectros observados. Este código de transporte radiativo opera en aproximación LTE o LVG, cuando la molécula cuenta con coeficientes colisionales.

4.1.1 Mecanismos de población de niveles energéticos

El análisis de las líneas de emisión moleculares observadas, nos aporta información acerca de los mecanismos por los que se pueblan los niveles de energía de las moléculas. Así, en las regiones donde se forman las estrellas, las moléculas interestelares pueden excitarse de diversas formas: por el calentamiento del gas y el polvo presentes en la nube a causa de la radiación de una estrella que se está formando, debido a las ondas de choque procedentes del flujo de material de una protoestrella, por la radiación emitida por el polvo interestelar al interaccionar con la radiación de las estrellas, o incluso por la radiación de fondo de microondas (CMB, $T_{background}\approx$2.7 K). Las moléculas del gas no sólo son excitadas en procesos radiativos, sino también colisionales. Por ejemplo, el medio denso propio de la región de formación estelar estudiada, presenta condiciones favorables para que las colisiones entre moléculas (principalmente con la molécula más abundante, H_2) dominen los mecanismos de excitación.

Para estimar las propiedades físicas de la nube, recurrimos a las aproximaciones de equilibrio termodinámico local LTE, o LVG (*Large Velocity Gradient*, en el que los fotones en una zona no interaccionen con el resto de la nube). Estas dos hipótesis permiten resolver las ecuaciones de transporte radiativo y de equilibrio estadístico de manera simultánea.

La figura 4.1, ilustra los procesos de excitación/desexcitación moleculares, que dan lugar a las transiciones colisionales y radiativas en el marco de la interacción de la radiación con la materia. A continuación, se muestran las ecuaciones de equilibrio estadístico (ecs. 4.1−4.3), la forma de las transiciones radiativas (ecs. 4.4−4.9) y colisionales (ecs. 4.10−4.12) en el equilibrio, así como ambas contribuciones radiativas y colisionales (ecs. 4.13−4.14), y por último, las ecuaciones de transporte radiativo principales (ecs. 4.15−4.23) esenciales para llevar a cabo un análisis de poblaciones de niveles energéticos.

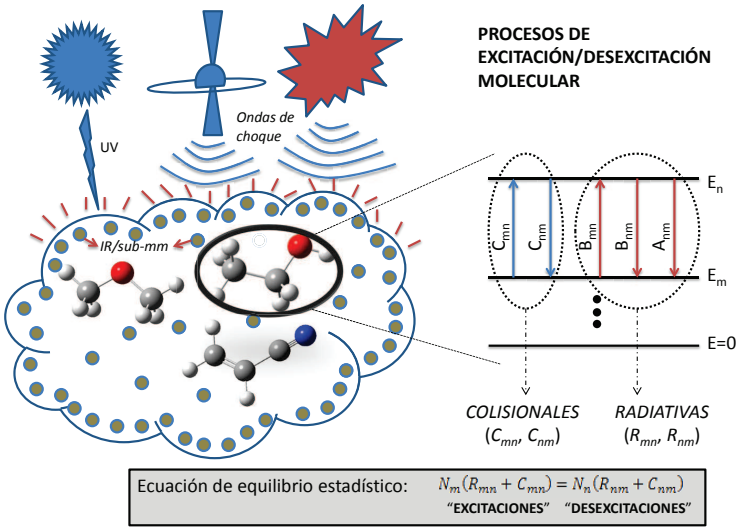

FIGURA 4.1: LOS DIFERENTES MECANISMOS DE EXCITACIÓN Y DESEXCITACIÓN DE LOS NIVELES ENERGÉTICOS DE LAS MOLÉCULAS EN LA NUBE. EN LA ECUACIÓN DE EQUILIBRIO ESTADÍSTICO SE CONSIDERA TANTO LAS TRANSCIONES COLISIONALES COMO LAS TRANSICIONES RADIATIVAS.

► Transiciones radiativas en el equilibrio:

Las ecuaciones básicas de equilibrio estadístico, describen el balance entre los procesos que pueblan y despueblan los niveles de energía de un sistema, permitiendo determinar las poblaciones del estado n (superior), N_n, y m (inferior), N_m. Así, refiriéndonos a la parte radiativa, las expresiones son las siguientes:

(*I*) Absorción inducida: $\frac{dN_n}{dt}=N_m B_{mn}\rho(\nu)$ (ec. 4.1)

(*II*) Emisión inducida o estimulada: $\frac{dN_n}{dt}=-N_n B_{nm}\rho(\nu)$ (ec. 4.2)

(*III*) Emisión espontánea: $\frac{dN_n}{dt}=-N_n A_{nm}$ (ec. 4.3)

Según una de las expresiones de *Milne-Einstein* los coeficientes de emisión/absorción inducida se relacionan tal que $g_n B_{nm}=g_m B_{mn}$.

$$N_m B_{mn}\rho(\nu)-N_n B_{nm}\rho(\nu)=(N_m-N_n)B_{nm}\rho(\nu) \qquad \text{(ec. 4.4)}^{3}$$

Los tres procesos (ecs. 4.1–4.3) ocurren a la vez, cuando las poblaciones de niveles han alcanzado sus valores de equilibrio, con lo que las tasas o velocidades de emisión y absorción de la radiación se igulan ($\frac{dN_n}{dt}=0$):

[3] Al contrario que ocurre con la emisión espontánea, la emisión estimulada o inducida es coherente (o está en fase) con la radiación incidente, con lo que contribuye al cómputo de la radiación absorbida neta, haciendo que $B_{nm}\approx B_{mn}$.

$$\frac{dN_n}{dt}=(N_m-N_n)B_{mn}\rho(\nu)-N_nA_{nm}=0 \qquad \text{(ec. 4.5)}$$

Población de niveles (ley de distribución de Boltzmann):

$$\frac{N_n}{N_m}=\frac{g_n}{g_m}e^{-\frac{\Delta E}{kT}} \qquad \text{(ec. 4.6)}$$

Densidad de radiación espectral (o de energía):

$$\rho(\nu)=\frac{8\pi h\nu^3}{c^3}\frac{1}{e^{h\nu/kT}-1} \qquad \text{(ec. 4.7)}$$

Relaciones de *Milne-Einstein*:

$$A_{nm}=\frac{8\pi h\nu^3}{c^3}B_{nm} \qquad g_nB_{nm}=g_mB_{mn} \qquad \text{(ec. 4.8)}$$

$$B_{nm}=\frac{1}{(6\varepsilon_o\hbar^2)}\cdot|\mu_{nm}|^2 \qquad A_{nm}=\frac{(16\pi^2\nu^3/c^3)}{(6\varepsilon_o\hbar)}\cdot|\mu_{nm}|^2 \qquad \text{(ec. 4.9)}$$

donde $|\mu_{nm}|^2$ es la probabilidad de transición radiativa.

► Transiciones colisionales en el equilibrio:

De igual modo, en equilibrio, los dos procesos (ecs. 4.1−4.3) ocurren a la vez, con lo que las tasas o velocidades de emisión y absorción se igulan ($\frac{dN_n}{dt}=0$):

$$\frac{dN_n}{dt}=(N_m-N_n)NC_{nm}-N_nA_{nm}=0 \qquad \text{(ec. 4.10)}$$

N=densidad de partículas colisionantes

Excitación/Desexcitación colisionales:

$$N_mC_{mn}=N_nC_{nm} \qquad \text{(ec. 4.11)}$$

Población de niveles (ley de distribución de Boltzmann):

$$\frac{C_{nm}}{C_{mn}}=\frac{g_m}{g_n}e^{-\frac{\Delta E_{mn}}{kT}} \qquad \text{(ec. 4.12)}$$

► Transiciones radiativas y colisionales-Ecuaciones de equilibrio estadístico (estado estacionario):

$$\frac{dN_n}{dt}=-N_n\sum_{m\neq n}[R_{nm}+C_{nm}]+\sum_{m\neq n}(N_m[R_{mn}+C_{mn}])=0 \qquad \text{(ec. 4.13)}$$

Donde las probabilidades de transición de desexcitación/excitación radiativas y colisionales son R_{nm} o R_{mn} y C_{nm} o C_{mn}, respectivamente.

$$R_{nm}=A_{nm}+B_{nm}\rho_\nu \qquad R_{mn}=B_{mn}\rho_\nu \qquad \text{(ec. 4.14)}$$

El valor umbral de la densidad, en la cual las transiciones colisionales son igual de importantes que las radiativas ($C_{nm}\approx R_{nm}$), proporciona la densidad crítica. Este valor nos indica el mecanismo dominante,

por el que se pueblan los niveles energéticos en una determinada región.

► Ecuaciones de transporte radiativo:

La intensidad de la radiación I_ν (o intensidad específica) describe el campo de radiación electromagnética como la energía dE de un intervalo de frecuencia $d\nu$ que se transporta dentro de un ángulo sólido[4] $d\Omega$ a través de un área $d\sigma$ en un tiempo dt a lo largo de la línea de visión s, tal que $I_\nu = dE/dtd\sigma cos\theta d\Omega d\nu$. De modo que, $I_\nu cos\theta d\Omega$ se corresponde con el flujo de la radiación $\frac{dI_\nu}{ds}$. La I_ν promediada o integrada sobre todas las direcciones a través del angulo sólido es la intensidad media J_ν. La densidad de energía ρ_ν tiene la misma forma que la intensidad media, sólo que es la intensidad de radiación propagada a la velocidad de la luz, es decir I_ν/c, con lo que $\rho_\nu = \frac{4\pi}{c} J_\nu$.

Intensidad media de la transición $m \leftarrow n$ (J_{nm}):

$$J_{nm} = \frac{1}{4\pi} \int d\Omega \int I_{nm} \phi_{nm}(\nu) d\nu \qquad \text{(ec. 4.15)}$$

El parámetro ϕ_{nm} es el perfil de la línea espectral, da cuenta de la probabilidad de absorción en torno a la frecuencia central de la línea ν_0.

La ecuación de transporte (ec. 4.16) evalúa el cambio de la intensidad al atravesar un medio a lo largo de la línea de visión, y se escribe en función de un término de atenuación (α_ν) y otro de incremento de la intensidad (j_ν). El flujo de radiación a través de la materia (ec. 4.16), tras integrar, da como solución la ec. 4.17 (4.1.1):

$$\frac{dI_\nu}{ds} = \frac{dI_\nu^{abs} - dI_\nu^{emit}}{ds} = -\alpha_\nu I_\nu + j_\nu \qquad \text{(ec. 4.16)}$$

$$I_\nu(\tau_\nu) = I_\nu(0) e^{-\tau_\nu} + S_\nu(1 - e^{-\tau_\nu}) \qquad \text{(ec. 4.17)}$$

Según la ley de Kirchoff en el equilibrio termodinámico las absorciones se igualan a las emisiones, por lo que la ecuación de transferencia se anula ($dI_\nu/ds = 0$) y, además, $I_\nu = B_\nu$, de modo que, $j_\nu/\alpha_\nu = B_\nu$. En LTE, la función fuente será igual a la función de Planck del cuerpo negro $B_\nu = S_\nu$. Esta función fuente S_ν se define como:

$$S_\nu = \int_{4\pi} I_\nu \cos\theta d\Omega = \frac{j_\nu}{\alpha_\nu} = \frac{\epsilon \cdot \rho}{k_\nu \cdot \rho} \qquad \text{(ec. 4.18)}$$

j_ν=coeficiente de emisión ; ϵ=emisividad

k_ν=coeficiente másico de absorción

$$j_\nu = \frac{dI_\nu^{emit}}{ds} = \frac{h\nu}{4\pi}(N_n A_{nm})\phi_\nu \qquad \text{(ec. 4.19)}$$

$$\alpha_\nu = k_\nu \rho_\nu = -\frac{1}{I_\nu}\frac{dI_\nu^{abs}}{ds} = \frac{h\nu}{4\pi}(N_m B_{mn} - N_n B_{nm})\phi_\nu \qquad \text{(ec. 4.20)}$$

[4] $d\Omega = d\sigma/r^2$, σ es el área proyectada del cono geométrico que contiene la energía que recibe el receptor o que se emite desde la fuente, y r la distancia entre la fuente y el receptor. La intensidad específica recibida es igual a la intensidad emitida, lo que hace que esta magnitud sea independiente de la distancia que separa la fuente del receptor r. Así, el ángulo sólido para toda la esfera es $\Omega = 4\pi r^2/r^2 = 4\pi$.

La profundidad óptica u opacidad depende del coeficiente de absorción a lo largo de la línea de visión s, por lo que es proporcional a la densidad de columna del medio ($\int \rho ds = \int n_i ds = N_i$), e influye en la atenuación e incremento de la intensidad de las líneas moleculares:

$$\text{Opacidad: } \tau_\nu = \int_0^s \alpha_\nu ds \text{ ; } \alpha_\nu = \text{coeficiente de absorción} = k_\nu \rho \qquad \text{(ec. 4.21)}$$

$$dI_\nu^{abs} = -\alpha_\nu I_\nu ds = -k_\nu \rho I_\nu ds \qquad \text{(ec. 4.22)}$$

$$\alpha_\nu = 1/l_\nu \text{ ; } l_\nu = \text{recorrido libre medio de los fotones} \qquad \text{(ec. 4.23)}$$

4.1.2 Aproximaciones

En condiciones de LTE, las poblaciones siguen una distribución de Maxwell-Boltzmann ($N_n/N_m \approx exp(-\Delta E/kT)$, población de niveles donde $T = T_{kinetic} = T_{excit}$). La temperatura de excitación del gas bajo LTE, equivale a la temperatura cinética o rotacional, dado que las transiciones se termalizan a la temperatura cinética del gas.

Asumiendo la aproximación de Rayleigh-Jeans ($\lambda >> hc/kT$ o $h\nu << kT$), la función de Planck del cuerpo negro queda de la forma $B_\lambda \approx 2ckT/\lambda^4$ o $B_\nu \approx 2\nu^2 kT/c^2$.

A continuación se muestran las ecuaciones principales para el balance de energía y poblaciónes en LTE (ecs. 4.24–4.26).

► Ecuaciones de equilibrio termodinámico local (LTE):

(*I*) Población de cada nivel de energía (Ecuación de Boltzmann):

$$N_{upp} = \frac{N}{Q_{rot}} g_u e^{-E_{upp}/kT} \qquad \text{(ec. 4.24)}$$

(*III*) Ecuación de Maxwell (distribución de velocidades):

$$f(v) = \left(\frac{m}{2\pi kT}\right)^{3/2} e^{(-mv^2/2kT)} \qquad \text{(ec. 4.25)}$$

(*IV*) Densidad crítica[5]:

$$N_{cr} = \frac{A_{nm}}{\gamma_{mn}} \text{ , "competición procesos radiativos/colisionales"} \qquad \text{(ec. 4.26)}$$

Si $N_i > N_{cr}$: población de niveles termalizado ($T_{exc} = T_k$)

Si $N_i < N_{cr}$: población de niveles subtermalizado ($T_{exc} < T_k$)

Para un medio isotermo, en condiciones de LTE, la solución para la ecuación de transporte en la aproximación de Rayleigh-Jeans es la siguiente: $T_B(\tau_\nu) = T_B(0)e^{-\tau_\nu} + T(1 - e^{-\tau_\nu})$ (*ver por ej.* Lequeux 2005). De modo que, para un medio ópticamente transparente ($\tau_\nu << 1$), en LTE y con emisión del

[5] Transición sin excitación radiativa: $N_i N_x \gamma_{mn} = N_n N_x \gamma_{mn} + N_n A_{nm}$; donde x=partícula o molécula con la que colisiona, e i=nuestra molécula.

continuo ($T_B(0)$) débil la ecuación de transporte se puede aproximar a: $T_B(\tau_\nu)=T\ \tau_\nu$.

Debido a que la opacidad del medio τ_ν está directamete relacionada con la densidad de columna N, la T_B (o bien T_A o T_{MB}) sería proporcional a la N.

En la aproximación de LVG, la región se considera homogénea, isoterma y con un gran campo de velocidades que permite desacoplar radiativamente las distintas regiones de la nube. En la aproximación LVG, también denominado método de Sobolev (Sobolev 1960), se establece un gradiente de velocidades desacoplando radiativamente regiones físicamente próximas, a causa del desplazamiento en frecuencia de la línea por efecto Doppler (dν/ν=dv/c). Esta aproximación se utiliza para estimar las condiciones físicas del gas bajo un estado de excitación de "no-LTE", en el que la población de los niveles energéticos está determinada por diferentes temperaturas de excitación y en el que la población de niveles no está termalizada. En este caso, la función fuente (S_λ) ya no es equivalente a la función de Planck de la radiación del cuerpo negro (B_λ).

4.2 Radioastronomía

4.2.1 La atmósfera terrestre

La **transmisión de la radiación electromagnética** que procede del espacio en los rangos de frecuencia o ventanas atmosféricas de nuestro estudio, depende principalmente de diversos factores como el perfil de temperatura y presión con la altura, la cantidad de vapor de agua en la atmósfera y el de otras especies minoritarias como O_3, SO_2, CO, etc. Las observaciones radioastronómicas pueden realizarse desde tierra, gracias a la transparencia de la atmósfera en la región del espectro en el que ocurren la mayor parte de las transiciones rotacionales de las moléculas que detectamos en el espacio. Sin embargo, para especies ligeras cuyas transiciones ocurren en el dominio del infrarrojo lejano, o cerca de las frecuencias de las transiciones de H_2O, nuestra atmósfera es ópticamente opaca. La Fig. 4.2 muestra la opacidad de la atmósfera a lo largo del espectro electromagnético.

Las **moléculas atmosféricas** relevantes que absorben y emiten en el espectro milimétrico y submilimétrico son principalmente: O_2, H_2O, O_3 (Pardo 1996, Cernicharo 1985, Pardo et al. 2001). El vapor de agua contenido en las nubes dispersa y absorbe la radiación, por lo que resulta importante situar radiotelescopios en lugares con condiciones atmosféricas locales estables, con baja cantidad total de agua precipitable y gran altitud.

El código para el modelo de transmisión atmosférica en el rango microondas ATM (*Atmospheric Transmission Model*, *ver* Cernicharo 1985; tesis de Cernicharo 1988; Pardo 1996; Pardo et al. 2001) modeliza el espectro de la atmósfera terrestre para simular la transferencia radiativa en este rango de frecuencias. Este código es válido para frecuencias entre 0 y 2 THz (Pardo et al. 2001) proporcionando el espectro atmosférico en condiciones de cielo despejado para la radioastronomía y otras aplicaciones científicas, y con el que se calibra la escala de intensidad de las observaciones. Por ejemplo el código de ATM, permite simular el modelo de transmisión atmosférica para el telescopio de 30 m de IRAM, en las cuatro bandas de frecuencias de operación, para unas condiciones climáticas con una cantidad de vapor de agua precipitable determinada.

La masa de aire que atraviesa la radiación influye en la opacidad o profundidad óptica (τ, ec. **??** y **??**)

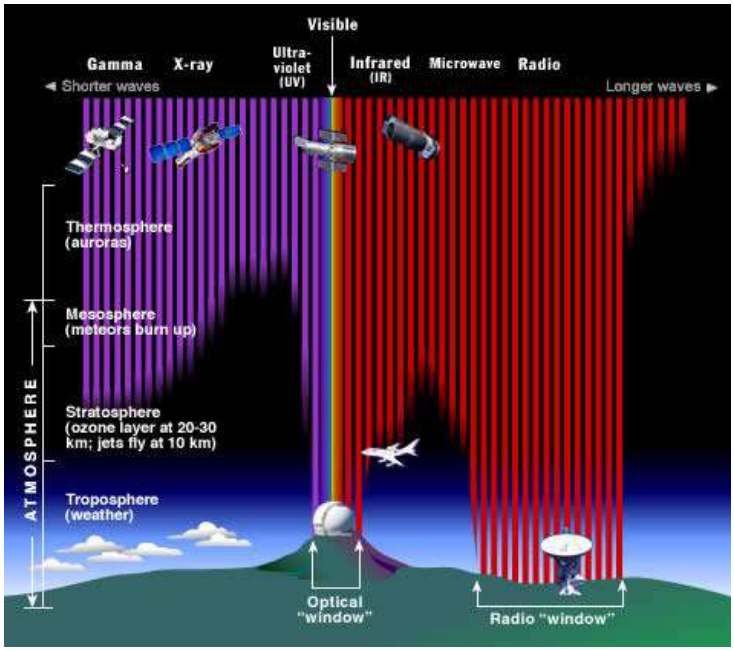

FIGURA 4.2: REPRESENTACIÓN DE LA TRANSMITANCIA/ABSORBANCIA DE LA RADIACIÓN ELECTROMAGNÉTICA A TRAVÉS DE LA ATMÓSFERA TERRESTRE Y LA INSTRUMENTACIÓN UTILIZADA PARA RECURRIR A LA REGIÓN DEL ESPECTRO DE INTERÉS. *Fuente: STScI/JHU/NASA* https://imagine.gsfc.nasa.gov/

a lo largo de la línea de visión (s) −desde el extremo de la atmósfera (s=0) hasta la antena (s=s_0)−, la cual depende de las condiciones de temperatura (T) y presión (P) atmosféricas, así como de la densidad del gas (ρ), haciendo que la intensidad de la radiación recibida se vea modificada.

Las observaciones radioastronómicas, proporcionan la intensidad de la radiación en términos de T_A^*, es decir, de la temperatura de antena corregida de los efectos de la atmósfera. Dichos efectos, se estiman a partir de las variables locales de temperatura, presión y cantidad de vapor de agua y del código ATM.

4.2.2 Radiotelescopios

El principio de funcionamiento de un radiotelescopio (basado en el telescopio de 30 m de IRAM) se basa en la detección y recepción de las ondas de radio, de manera que las señales que proceden de la fuente astrofísica sobre la que se realiza el apuntado, son captadas por la antena primaria (que es el reflector principal), que a su vez las redirige a un espejo secundario (subreflector), el cual focaliza las señales a los receptores situados dentro de la antena. Para que las señales puedan ser amplificadas, los receptores las convierten en señales de frecuencias más bajas, para lo que se combinan con una señal producida por un oscilador local, a una frecuencia similar a la señal original. A la salida del mezclador, se obtiene una señal a la frecuencia intermedia del sistema y con una intensidad proporcional a la señal incidente (ν_{IF}, *Intermediate Frequency*), es decir, la diferencia entre las dos frecuencias entrantes (la del cielo y la inyectada por el oscilador local, $|\nu_{sky}-\nu_{LO}|=\nu_{IF}$), de modo que se obtiene una frecuencia suficientemente baja como para ser amplificada convenientemente por amplificadores de muy bajo ruido y alta ganancia.

El receptor que se usa actualmente en el radiotelescopio de IRAM 30 m es EMIR (*Eight MIxer Receiver*), cuyos mezcladores son de doble banda-lateral (o *sideband*), 2SB, que ofrecen 8 GHz de ancho

de banda lateral por cada SB (*Lower Side-Band* o LSB, y otro *Upper Side-Band* o USB) y polarización (horizontal H y vertical V). Cada ancho banda de 8 GHz se divide en dos sub-bandas de 4 GHz cada una, Inner Lower/Upper SB y Outer Lower/Upper SB, y teniendo en cuenta las dos polarizaciones H y V quedan ocho sub-bandas que pueden ser transportadas a los espectrómetros cubriendo un total de 32 GHz de ancho de banda instantánea (es decir 16 GHz de ancho de banda por cada polarización). EMIR opera en cuatro bandas (o cuatro ventanas atmosféricas) correspondientes a, aproximadamente, E090 (3 mm), E150 (2 mm), E230 (1.3 mm), E330 (0.9 mm). Cada una proporciona dos canales de polarización lineal sintonizados a la misma frecuencia. Los espectrómetros utilizados en nuestro caso, son los *Fast Fourier Transform Spectrometers* con 200 KHz de resolución espectral. Las observaciones en la banda E330, sólo pueden reallizarse bajo condiciones climáticas muy buenas debido a la alta absorción de la atmósfera terrestre a dichas frecuencias. Es necesario remarcar que, la escala de intensidad de las observaciones se calibran usando el modelo de transmisión atmosférica citado anteriormente (ATM, *ver* Cernicharo 1985; Cernicharo 1988; Pardo 1996; Pardo et al. 2001).

A continuación, vamos a describir brevemente las propiedades fundamentales de los radiotelescopios (*ver* 4.3), basándonos en Wilson et al. 2009, Baars 2007, Kwok 2007 y Kraus 1988.

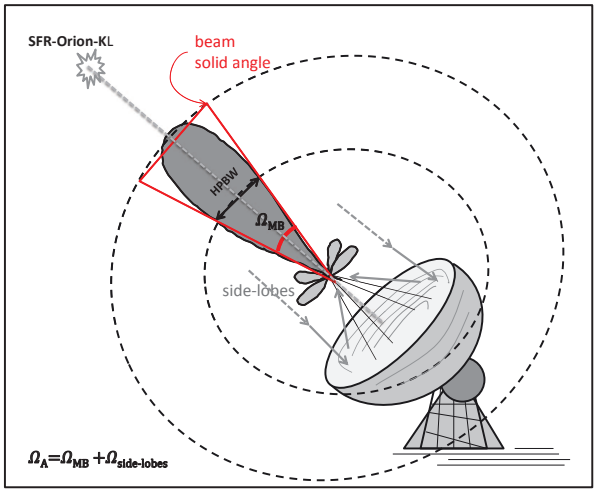

FIGURA 4.3: VISUALIZACIÓN DE ALGUNOS PARÁMETROS DE LA ANTENA.

• **Diagrama de radiación**: el diagrama de radiación o patrón de energía de una antena ($P(\theta,\phi)$) representa la cantidad de energía transmitida o recibida por ángulo sólido en la dirección (θ,ϕ), donde θ es la coordenada en latitud y ϕ en longitud. El diagrama se representa en términos del patrón de energía normalizado (con respecto a su valor máximo), tal que $P_n(\theta,\phi)=P(\theta,\phi)/P_{max}$. El patrón de energía de una antena tiene la forma de un patrón de Airy, que consiste en un área central brillante que se corresponde con el haz principal del patrón de difracción (que constituye ≈84% de la energía difractada procedente de la fuente, Goldberg and Mc Culloch 1968), rodeado por anillos oscuros y brillantes o lóbulos laterales del patrón de difracción.

En el patrón de radiación de la antena o diagrama de radiación para radiotelescopios de antena única, aparece un lóbulo principal muy destacado, que es donde recae la mayor parte de la intensidad de la radiación, y otros secundarios o laterales (*side-lobes*). En el caso de los interferómetros, poseen un diagrama de radiación que es el producto de la interferencia entre las ondas que conforman los diagramas de las antenas individuales, con una separación entre ellos que depende de la distancia

espacial (la distancia entre las antenas o línea-base). Es decir, en lugar de lóbulo principal y secundarios se habla de "franjas" (*ver* Fig. 4.4). Las posiciones de los mínimos de un patrón de difracción se sitúan en los valores $\theta \propto \lambda/D$, que se corresponden con el límite de difracción (θ, o tamaño del haz) y establecen la resolución espacial del instrumento. Cuanto mayor es el diámetro D del telescopio, mayor energía se colecta, mejor es la resolución espacial del telescopio, y mayor es la capacidad para resolver detalles pequeños. Algo que se consigue de forma muy eficaz, con la disposición interferométrica de radiotelescopios individuales, que simulan el tamaño de un radiotelescopio equivalente a la distancia entre los radiotelescopios individuales implicados, como el interferómetro ALMA.

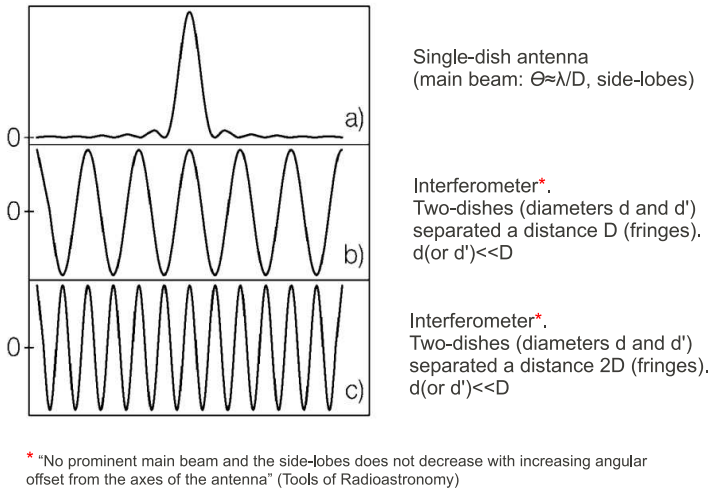

FIGURA 4.4: ESTA FIGURA MUESTRA EL PATRÓN O DIAGRAMA DE RADIACIÓN PARA DIFERENTES CONFIGURACIONES DE ANTENA– ANTENA ÚNICA (A) E INTERFERÓMETRO (B,C). *Fuente: Tools of Radioastronomy, Wilson et al. 2009*

• **Anchura del haz a media potencia**: La mayor fracción de la energía colectada por la antena recae en el lóbulo central. Este lóbulo principal se define por la anchura del haz a media potencia *HPBW* (*Halph-Power Beam Width*), es decir, el ángulo del haz pincipal donde el patrón de la radiación disminuye a la mitad del valor máximo (nivel de $-3dB$)[6], siendo $HPBW \propto \lambda/D$). Para el telescopio de 30 m de IRAM, $HPBW(") = 2460/\nu(GHz)$ (*fuente*: http://www.iram.es/IRAMES/mainWiki/Iram30mEfficiencies), con lo que el tamaño del haz principal varía entre 31"(80 GHz) y 8"(307 GHz).

• **Ángulo sólido del haz principal y de antena**: El ángulo sólido del haz principal (Ω_{MB}, ec. 4.27) es aquel que se obtiene intengrando el diagrama de radiación para todo el haz principal (o lóbulo principal). El ángulo sólido de la antena (Ω_A) comprende tanto el ángulo sólido del haz principal, como el de los lobulos secundarios, correspondiéndose con aquel ángulo integrado para toda la esfera (ec. 4.28).

$$\Omega_{MB} = \int\int_{main-lobe} P_n(\theta,\phi) sen\theta d\theta d\phi = \int\int_{main-lobe} P_n(\theta,\phi) d\Omega \tag{4.27}$$

$$\Omega_A = \int_0^{2\pi}\int_0^{\pi} P_n(\theta,\phi) sen\theta d\theta d\phi = \int_0^{2\pi}\int_0^{\pi} P_n(\theta,\phi) d\Omega \tag{4.28}$$

[6]El nivel del decibelio consiste en la relación logarítmica $dB = 10 log_{10} P_n(\theta,\phi)$ (Kraus 1988)

• **Eficiencia del haz pincipal**: La eficiencia del haz principal (η_{MB}) relaciona el ángulo sólido del haz principal y el de la antena, tal que η_{MB}=Ω_{MB}/Ω_A, indicando la fracción de energía concentrada en el haz principal. La calidad de una antena se mide básicamente por la capacidad que tiene de colectar la mayor parte de la energía en el haz principal.

• **Área efectiva**: El área o apertura efectiva (A_e) de la antena es la fracción entre la cantidad de potencia radiada por la antena (P_e) y la densidad de energía que intercepta la antena $|< S >|$. Este parámetro define la sensibilidad de la antena, y se relaciona con la directividad o ganancia del telescopio a través de D=$4\pi\ A_e/\lambda^2$=$4\pi/\Omega_A$. La eficiencia de la apertura (η_A) indica la relación entre el área efectiva y al área geométrica de la antena.

• **Temperatura de antena**: La intensidad de las líneas espectrales se miden en unidades de temperatura. Para definir la temperatura de antena (T_A), partimos del concepto de cuerpo negro y de la temperatura de brillo (T_b=$[c^2/(2\nu^2 k)]B_\nu$), que es la temperatura que tendría un cuerpo que emite a la misma intensidad y frecuencia que la fuente, I_ν=$B_\nu(T_b)$. Es importante destacar que T_b no es la temperatura física de la fuente. La T_A (ec. 4.29) será la convolución de la temperatura de brillo de la fuente con el diagrama del haz del telescopio.

$$T_A = \frac{\int_0^{2\pi}\int_0^{\pi} T_b(\theta,\phi)P_n(\theta,\phi)sen\theta d\theta d\phi}{\int_0^{2\pi}\int_0^{\pi} P_n(\theta,\phi)sen\theta d\theta d\phi} = \frac{1}{\Omega_A}\int_0^{2\pi}\int_0^{\pi} T_b(\theta,\phi)P_n(\theta,\phi)d\Omega \qquad (4.29)$$

Al tener en cuenta los efectos de transmisión de la atmósfera en dirección a la fuente (mediante $e^{-\tau_{atm}}$), la expresión de la temperatura de antena queda corregida como: T_A=$T_{MB}\eta_{MB}e^{-\tau_{atm}}$, donde η_{MB} es la eficiencia del haz principal (Lequeux 2005). La temperatura de brillo se puede igualar a la del haz principal en el caso de que la fuente observada cubra exactamente la dimensión del haz principal.

4.2.3 Reducción de las observaciones: el problema de la banda imagen

Un descripción completa de la estrategia de reducción de los datos obtenidos en el barrido espectral de Orión-KL se puede encontrar en Tercero et al. (2010) y Tercero ().

En este apartado, y relacionado con la recepción de la señal en radioastronomía, nos centraremos en el problema de la banda imagen.

Para una frecuencia del oscilador local dada (ν_{LO}), el mezclador (un dispositivo no lineal) amplificará dos bandas de frecuencia diferente para una frecuencia del oscilador local dada. Estas dos bandas corresponden a la banda ”señal” y a la banda ”imagen”, y son aquellas separadas de ν_{LO} por un valor $\pm\nu_{IF}$, siendo ν_{IF} la frecuencia intermedia. La banda de frecuencias de la banda imagen se corresponde con la frecuencia de la señal ν_s incrementada un valor igual al doble de la frecuencia intermedia, es decir, ν_{imagen}=ν_s+$2\nu_{IF}$.

En el radiotelescopio de IRAM 30 m los receptores atenúan la señal de la banda imagen de manera eficaz, sin embargo, debido a que Orión-KL es una de las fuentes más brillantes en el milimétrico, líneas intensas en la banda imagen aparecen en la banda señal con una intensidad significativa. Por ejemplo, aquellas líneas pertenecientes a moléculas abundantes como CO, SO y SO_2.

Con el fin de detectar y eliminar estas características espectrales procedentes de la banda imagen, se realizan dos observaciones donde se sintonizan frecuencias ligeramente diferentes en el oscilador local, en nuestro caso correspondiente a una diferencia de 50 MHz respecto a la frecuencia central previa. La Fig. 4.5 muestra un ejemplo de líneas procedentes de la banda "imagen"; serán aquellas que aparecen desplazadas 100 MHz al superponer ambos espectros. Para obtener el espectro reducido final, se anulan los canales en los que aparecen las líneas de la banda imagen en ambos espectros (desplazado y sin desplazar 50 MHz), y a continuación se suman los espectros.

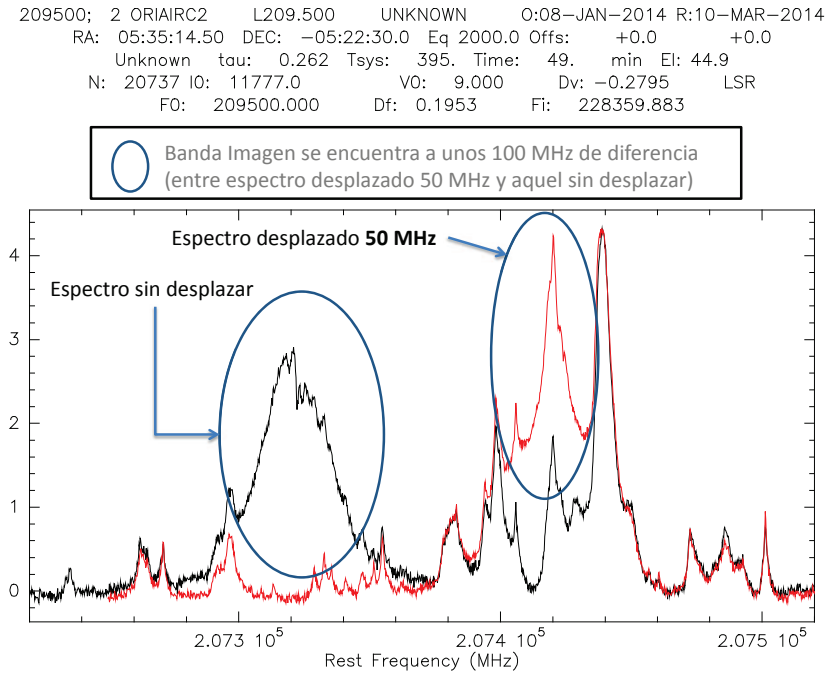

FIGURA 4.5: EJEMPLO DE LA BANDA IMAGEN TRAS SUPERPONER LOS ESPECTROS DE EMISIÓN OBTENIDOS MEDIANTE EL MÉTODO DE OBSERVACIÓN *wobbler switching*. LA LÍNEA NEGRA SE CORRESPONDE CON EL ESPECTRO SIN DESPLAZAR Y LA ROJA CON EL ESPECTRO DESPLAZADO 50 MHZ RESPECTO A LA FRECUENCIA CENTRAL. LA BANDA IMAGEN APARECE A 100 MHZ DE DIFERENCIA ENTRE AMBOS ESPECTROS (NEGRO−207320 MHZ Y ROJO−207420 MHZ). EL ESPECTRO RESULTANTE SE OBTIENE DESPUÉS DE ELIMINAR LAS LÍNEAS DE LA BANDA IMAGEN DE LOS ESPECTROS DESPLAZADO Y SIN DESPLAZAR, Y A CONTINUACIÓN, SUMAR DICHOS ESPECTROS.

4.3 Técnicas de análisis específicas

4.3.1 Diagramas de población o rotación

Los **Diagramas de Rotación (D.R.)** o también denominados diagramas de población, son representaciones gráficas de la población de niveles de las moléculas en función de su energía ($ln(N_u/g_u)$ vs. E_{upp}/k). En condiciones de LTE, como hemos visto, la población de niveles sigue una distribución de Boltzmann y los niveles están termalizados, por lo que la temperatura de excitación que se obtendría a partir de la pendiente es equivalente a la T_k. Este método se usa en primera aproximación para obtener la densidad de columna (N) y la temperatura (T_{rot}). Estos diagramas se construyen utilizando líneas no solapadas con otras moléculas o, al menos, lo más aisladas posibles.

Los diagramas de rotación se pueden hacer para cada componente que vemos en los perfiles de las líneas espectrales, ofreciéndonos información acerca de las propiedades físicas de la región. En la siguiente lista de ecuaciones (ecs. 4.30−4.39), se relacionan los parámetros observacionales y teóricos que se necesitan para la construcción gráfica de los diagramas rotacionales (*ver* Tabla 4.3.1). Se obtendrá T_{rot} a partir de la pendiente, y la densidad de columna del gas (N) a partir del eje de ordenadas ($\ln(N_u/g_u)$ (cm^{-2}), donde $N_u/g_u=[(8\pi k\nu^2 W_{obs})/(hc^3 A_{ul} g_u b \eta_{MB})]$). En el caso de transiciones ópticamente transparentes, la densidad de columna es directamente proporcional a la temperatura de antena (T_A) o del haz principal (T_{MB}).

► Diagrama de rotación-población $\ln(N_u/g_u)$ (cm^{-2}) vs. (E_{upp}/k (K)):

$$\ln\left(\frac{N_u}{g_u}\right)=\ln\left[\frac{8\pi k\nu^2 \mathbf{W}}{hc^3 A_{ul} g_u}\right]=\ln\left[\frac{3kW}{8\pi^3 \nu \mu^2 S_{ul} g_i g_k}\right]=\ln\left(\frac{N}{Q_{rot}}\right)-E_{upp}/kT= \quad \text{(ec. 4.30)}$$

$$=\ln\left(\frac{\mathbf{N_{(W_{obs})}}}{Q_{rot}}\right)-E_{upp}/kT\mathbf{+ln(b\cdot\eta_{MB})} \quad \text{(ec. 4.31)}[7]$$

$$=\ln\left[\frac{8\pi k\nu^2 \mathbf{W_{obs}}}{hc^3 A_{ul} g_u}\left(\frac{1}{\mathbf{b}}\right)\left(\frac{1}{\eta_{\mathbf{MB}}}\right)\right]=\ln\left(\frac{\mathbf{N}}{Q_{rot}}\right)-E_{upp}/kT \quad \text{(ec. 4.32)}$$

$$\ln(\mathbf{N_{(W_{obs})}})=\ln(N)-\ln(b\cdot\eta_{MB}) \quad \text{(ec. 4.33)}$$

• Factor de dilución del telescopio para haz y fuentes gaussianas:

$$b=\frac{\theta_{sou}^2}{\theta_{sou}^2+\theta_{beam}^2} \; ; \; \theta_{beam}=HPBW \quad \text{(ec. 4.34)}$$

• Temperatura de antena corregida de la dilución (K):

$$T_A^{obs}=T_A^{sou}\left(\frac{\theta_{sou}^2}{\theta_{sou}^2+\theta_{beam}^2}\right)=T_A^{sou}\cdot b \quad \text{(ec. 4.35)}$$

• Temperatura del haz principal (K): $T_{MB}=T_A\left(\frac{1}{\eta_{MB}}\right)$; $T_{MB}^{obs}=T_{MB}^{sou}\cdot b$ (ec. 4.36)

• Factor de eficiencia del telescopio: $\eta_{MB}=\frac{B_{eff}}{F_{eff}}$ (ec. 4.37)

Tabla para obtener los factores de eficiencia:

http://www.iram.es/IRAMES/mainWiki/Iram30mEfficiencies

• Área integrada de la línea ($K\cdot cm\cdot s^{-1}$):

$$W(\text{en } T_{MB})=\int T_{MB}^{sou} dv=\int T_{MB}^{obs} dv\cdot\left(\frac{1}{b}\right)=\int T_{MB}^{obs} dv\left(\frac{\theta_{sou}^2+\theta_{beam}^2}{\theta_{sou}^2}\right)=W^{obs}\cdot\left(\frac{1}{b}\right) \quad \text{(ec. 4.38)}$$

$$W(\text{en } T_A)=\int T_{MB}^{sou} dv=\int T_A^{sou} dv\cdot\left(\frac{1}{\eta_{MB}}\right)=\int T_A^{obs} dv\cdot\left(\frac{1}{b}\right)\left(\frac{1}{\eta_{MB}}\right)=W^{obs}\cdot\left(\frac{1}{b}\right)\left(\frac{1}{\eta_{MB}}\right) \quad \text{(ec. 4.39)}$$

[7] Se introduce el factor de dilución (b) a causa de que la fuente observada tiene un tamaño menor que el diámetro del haz principal del radiotelescopio.

► Parámetros espectroscópicos y observacionales necesarios para el D.R.:

▷ Parámetros teóricos: Subestado de simetría (A, E, AA, EE,..), transición (J,K_a,K_b,K_c,v,...), frecuencia ν(MHz), fuerza de línea S_{ul}, $S_{ul}\mu_i^2$ (i=a,b,c), energía del nivel superior $\mathbf{E_{upp}}$(K), coeficiente de einstein $A_{ul}(s^{-1})$, peso estadístico g_u.

▷ Parámetros observacionales: diámetro de la fuente d_{sou}("), área integrada de la línea $W(\mathrm{K\cdot cm\cdot s^{-1}})=\int T_{MB}dv$

▷ Resultados (D.R.): $\mathbf{T_{rot}(K)}$, $\mathbf{N(cm^{-2})}$.

4.3.2 Modelización con MADEX

En el procedimiento para el análisis astrofísico, a la hora de realizar la modelización usando códigos de transporte de radiación, lo primero que debemos considerar es la **espectroscopía de la molécula**. En MADEX (Cernicharo 2012) se han introducido estos datos para más de 1 200 familias de moléculas (incluyendo las variantes isotopólogas y los estados vibracionales son más de 5 800 especies). Con ello, para todo ese número de especies, disponemos en un mismo código de la información acerca de las constantes de rotación, las frecuencias de las transiciones, las energías de las transiciones, las fuerzas de línea y, en algunos casos, los coeficientes de colisión de la molécula (sin este dato, el cálculo del transporte radiativo sólo puede evaluarse en aproximación LTE).

El código MADEX está desarrollado, de manera que, introduciendo las condiciones físicas del medio y las características del telescopio, obtenemos el espectro de la molécula que elijamos bajo esas condiciones: el código calcula las temperaturas de excitación, las profundidades ópticas y la intensidad de la línea. MADEX es el código que hace de nexo entre los parámetros teóricos de laboratorio y aquellos observacionales o astrofísicos, permitiendo desarrollar modelos físico-químicos de nuestro objeto de estudio de nuestro mediante el ajuste del espectro sintético generado a la observación. Además, podemos sumar la contribución de todas las componentes físicas de la nube a la intensidad de una línea (algo muy útil en el caso de Orión-KL).

Para poder obtener los resultados de las densidades de columna promediados sobre el tamaño de la fuente, fijamos el diámetro de la misma con un modelo que supone una estructura de capas esféricas. Otro parámetro que fijaremos es el diámetro del telescopio; con ambos parámetros, el código calcula la dilución.

De este modo, teniendo en cuenta las características de la molécula y los parámentros que hemos fijado para las condiciones físicas de las componentes de Orión-KL, podemos reproducir los espectros observados variando únicamente la columna de densidad y la temperatura. Este proceso también tendrá un carácter iterativo, y tanto los parámetros físicos (como la temperatura o la densidad del medio) como los observacionales (velocidades radiales y anchuras de las líneas) podrán irse refinando en sucesivos ajustes.

4.4 Metodología: Análisis de Laboratorio

4.4.1 Espectroscopía rotacional en el laboratorio

Identificar especies moleculares en el medio interestelar haciendo uso de radiotelescopios, requiere conocer las frecuencias de sus transiciones rotacionales que se pueden asignar gracias al trabajo de laboratorio. El procedimiento de laboratorio para la caracterización de moléculas con interés astrofísico, consiste en un laborioso trabajo experimental que incluye cálculos mecano-cuańticos y la evaluación de las condiciones óptimas que garanticen la obtención de un espectro teórico fiable. Muchas de las líneas no identificadas en el espectro de nuestra fuente astrofísica, se corresponden con estados excitados vibracionalmente e isotopólogos de moléculas que son abundantes en el ISM, de las cuales no se conocía de manera precisa su espectroscopía. Esto nos llevó a estudiar en el laboratorio los estados excitados de CH_3CH_2CN y CH_2CHCN.

La estructura de las moléculas determina su espectroscopía, que dependerá de parámetros estructurales como los ángulos de enlace y las distancias internucleares entre los átomos que constituyen la molécula. Esto afecta a los momentos de inercia y a los momentos dipolares eléctricos de la misma.

4.4.2 Espectroscopía (sub)milimétrica (QUIFIMA-UVA)

En el laboratorio, podemos caracterizar el espectro rotacional (en nuestro caso) de un gas mediante el uso de espectroscopía microondas/milimétrica/submilimétrica, a partir de una muestra (una vez sometida a condiciones de P y T óptimas en un sistema de refrigeración y vacío) en una celda de absorción de un espectrómetro microondas (Fig. 4.6*a*). El espectrómetro se basa en una fuente de radiación monocromática coherente que atraviesa una celda de absorción (de 2 m de longitud), de modo que un detector situado a la salida de la misma mide el nivel de potencia de la radiación, la cual es amplificada y enviada a un detector síncrono para obtener el espectro en función de la frecuencia de barrido. La fuente de radiación microondas se trata de un oscilador de onda regresiva (BWO, *Backward-Wave Oscilator*[8]) o bien un oscilador de tecnología Agilent. La fuente de radiación se sincroniza con respecto a un oscilador de referencia o sintetizador mediante un lazo de fase. Esta técnica puede hacer uso de tres opciones de modulación de la señal en el rango de 8 a 100 GHz: la modulación por efecto Stark, la modulación por frecuencia, y la modulación por doble resonancia. Los rangos de frecuencia medidos dependen del detector a la salida de la celda.

A través de esta técnica, se calculan las constantes rotacionales, que se utilizan para predecir las frecuencias de las líneas pertenecientes a diferentes estados de energía. Además para ampliar el rango de frecuencias del espectrómetro, se recurre a una fuente de modulación de ondas milimétricas (MMW, Fig. 4.6*b*) que opera con una configuración de haz doble o sencillo entre 50 y 1080 GHz (QUIFIMA-UVA). Para este sistema la fuente de radiación es un generador de señal modulada por frecuencia. El procedimiento general para detectar estados excitados vibracionalmente, consiste en barrer el espectro en el rango en el que está el estado fundamental. Posteriormente seleccionamos un rango de frecuencias

[8]Son osciladores de onda regresiva y actúan de fuentes de radiación microondas al producirse la interacción de un haz electrónico (electrones acelerados que emiten radiación termoiónica) y una estructura helicoidal que provoca una modulación de velocidad en el haz, de manera que agrupa los electrones en intervalos regulares de una determinada longitud de onda, para que se muevan hacia el colector. Los campos eléctricos que se generan aparecen fuera de la hélice y el potencial de aceleración de los mismos hace que se produzca una onda de retroceso en la hélice, generando así una señal microondas/(sub)milimétrica a una frecuencia de oscilación bloqueada a un armónico concreto.

para buscar un estado excitado. Esta búsqueda se realiza en función de las predicciones iniciales de las constantes rotacionales y se van mejorando con nuevas asignaciones.

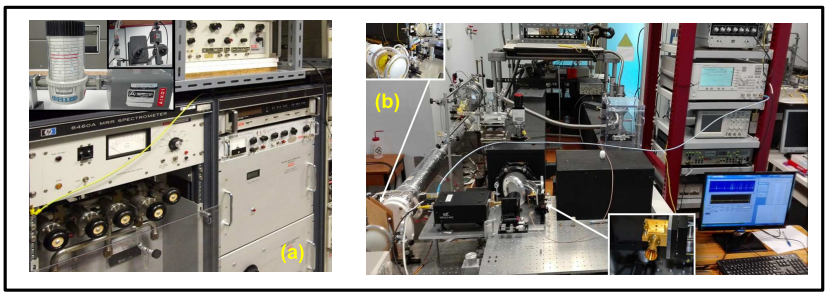

FIGURA 4.6: ESPECTRÓMETROS UTILIZADOS PARA EL ESTUDIO DE MOLÉCULAS EN EL ISM: (*a*) ESPECTRÓMETRO DE MICROONDAS (MODULACIÓN STARK), Y (*b*) DE ONDAS MILIMÉTRICAS Y SUBMILIMÉTRICAS (FUENTE DE MODULACIÓN).

Vamos a mostrar las características principales de las tres opciones de modulación de la señal, que tienen como objetivo principal convertir la señal a la salida del detector en voltaje de salida.

Por un lado, la modulación por efecto Stark o **modulación Stark** se basa en la perturbación de niveles por efecto Stark mediante la aplicación de un voltaje determinado (debido a la aplicación de un campo eléctrico entre el séptum metálico −debajo del centro de la celda− y las paredes de la celda de absorción), suministrando un campo de onda cuadrada en la celda de absorción. Esta modulación no es válida para pequeñas diferencias de energía entre transiciones, y por tanto es adecuado para medir transiciones con números cuánticos rotacionales de J pequeños.

Otro tipo de modulación, es la **modulación por frecuencia**, una técnica a la cual se recurre para realizar medidas de números cuánticos rotacionales de J grandes, es decir para frecuencias elevadas, de modo que, acoplado a un sistema de modulación microondas o milimétrica, se sitúan unos preamplificadores unidos a la modulación de frecuencias.

Y la otra técnica de modulación, es la **modulación por doble resonancia**. El fundamento de la doble resonancia es sustraer la señal de las transiciones $K-$dobletes que nos interesan del resto de señales, para lo cual suministramos una radio-frecuencia en señales de onda cuadrada, modulando señales ON/OFF de 33.333 KHz. Consta de un generador de radio-frecuencias acoplado a una celda de Stark, y consiste en el bombeo de niveles o transiciones degeneradas por modulación de radio-frecuencia de resonancia. Esta técnica se utiliza en el caso de espectros complejos de rotación o bien con gran cantidad de líneas, y es válida para pequeñas diferencias de energía entre las transiciones. La radio-frecuencia utilizada para modular las transiciones del estado fundamental sirve también para modular los estados excitados vibracionales, puesto que la separación energética de niveles permanece prácticamente inalterada. Una alternativa en el caso de los $K-$dobletes en la que los niveles de rotación se sitúan como los niveles de la frecuencia adjunta, es utilizar una radiofrecuencia o frecuencia modulada en AM (amplitud modulada), de manera que module únicamente dicha transición en el espectro de rotación.

El osciloscopio nos ayuda a optimizar la línea haciendo uso de un generador de onda cuadrada. En

el caso de un generador de onda cuadrada externo (Stark externo) se modifica el voltaje para buscar el máximo de intensidad de la línea. Normalmente se suele coger una línea intensa y conocida, como la frecuencia de un estado fundamental, y se optimiza. Aunque también podría hacerse con la transición de un estado excitado, que acabasemos de detectar, y optimizar al máximo sus condiciones.

Respecto a la introducción de la muestra en el sistema, es necesario que permanezca en fase gas en el sistema para llevar a cabo experimentos de absorción. Para ello, inicialmente la muestra en estado líquido es sometida a una serie de ciclos de presión (con llave de vacío) y temperatura (con N_2 líquido) óptimas que permiten tener la muestra lo más pura posible. Asímismo, las ventanas para transmitir la radiación en la región microondas o milimétrica deben ser de mica y situarse en cualquiera de los extremos de la celda de absorción.

4.4.3 Procedimiento: predicción de frecuencias de las líneas rotacionales

Los cálculos ab-initio resuelven el hamiltoniano efectivo por medio de métodos computacionales, tras aplicar una serie de aproximaciones que simplifican su expresión.

La predicción de las frecuencias de las transiciones rotacionales durante el trabajo de asignación e identificación de las líneas espectrales de las moléculas, incluyendo la asignación de los modos vibracionales, es en definitiva un proceso iterativo partiendo de los cálculos mecano-cuánticos para mejorar el hamiltoniano efectivo que describe a la molécula, al ir introduciendo transiciones rotacionales significativas (en cuanto a sus números cuánticos) y constantes de distorsión centrífuga, e incluso correcciones séxticas y ócticas, en el ajuste de las líneas de laboratorio (SPFIT/SPCAT). Un procedimiento que, como ya se ha indicado, al completarse con el análisis astrofísico, puede ayudar a confirmar la asignación de ciertas líneas espectrales de una molécula y sus estados vibracionales e isotopólogos.

Capítulo 5

Trabajos publicados

En este capítulo mostraré los trabajos publicados en los que he participado a lo largo de mi periodo de estudiante de doctorado. La tesis se presenta en formato publicaciones, pues pensamos que estos artículos son la mejor prueba del trabajo realizado. Las explicaciones más rigurosas de la investigación que hemos llevado a cabo están contenidas en estos trabajos y es allí donde se encuentra la magnitud de todo el trabajo realizado. Sin embargo, al comienzo de cada artículo incluiremos una breve introducción al mismo, donde resaltaremos las aportaciones más destacadas del trabajo que se presenta. Tras la presentación de todas las publicaciones, se llevará a cabo una breve discusión de los resultados y las conclusiones más importantes de estos trabajos.

5.1 Caracterización en el laboratorio y detección astrofísica de estados vibracionalmente excitados de cianuro de etilo

El artículo veremos a continuación fue publicado en la revista *The Astrophysical Journal* en el año 2013. Como ya hemos indicado en la introducción, uno de los principales objetivos del análisis del barrido espectral sobre Orión-KL de Tercero et al. (2010), era la identificación de multitud de características espectrales detectadas, que no correspondían con ninguna especie cuya espectroscopía fuera conocida. En los artículo de Demyk et al. (2007) y Margulès et al. (2009) se detectaron en Orión-KL y por primera vez en el espacio las especies correspondientes a los isotopólogos ^{13}C y ^{15}N de CH_3CH_2CN (cianuro de etilo) por medio de más de 800 líneas previamente no identificadas en el barrido espectral. Con ello quedó demostrado que los isotopólogos y estado excitados de baja energía de especies abundantes en la región, contribuirían con un gran número de características espectrales en los barridos espectrales de este tipo de regiones.

En este punto, el siguiente paso consistía en la caracterización de los estados vibracionalmente excitados de CH_3CH_2CN en el laboratorio. Como también hemos apuntado previamente, las condiciones físicas de las regiones de formación de estrellas masivas, son favorables para que se produzca la población de niveles excitados. El estado v_{13}/v_{21} cuya energía se encuentra a 315.4 K sobre el estado fundamental, ya había sido detectado en Sgr B2 (región de formación de estrellas masivas en el centro de la galaxia) por Mehringer et al. (2004). En el presente artículo se caracterizaron los niveles $v_{20} = 1$ y $v_{12} = 1$ que se encuentran a una energía de 531.2 y 763.4 K respecto al estado fundamental, respectivamente. Para desarrollar este trabajo, realicé una estancia de tres meses en el Laboratorio de Espectroscopía Molecular de la Universidad de Valladolid.

Tras el trabajo de laboratorio y una vez obtenido el espectro rotacional de CH_3CH_2CN $v_{20} = 1$ y $v_{12} = 1$, detectamos por primera vez en el espacio y en el barrido espectral de Orión-KL estas especies. Este resultado supuso, por un lado, una contribución muy importante para el análisis de fuentes similares en el medio interestelar, ya que contribuimos a mitigar el número de líneas sin identificar en los espectros obtenidos. Esto es particularmente relevante para las observaciones de alta sensibilidad, como las que se pueden llevar a cabo con el interferómetro ALMA. Por otro lado, mediante la detección de una gran cantidad de isotopólogos y estados vibracionalmente excitados de una molécula, se puede llevar a cabo un

estudio riguroso sobre las condiciones físicas de la fuente. Esto es lo que hicimos en la segunda parte del artículo, mediante la construcción de diagramas rotacionales y de la modelización del espectro observado usando MADEX. Con ello fuimos capaces de derivar tanto temperaturas rotacionales y abundancias, como abundancias isotópicas o temperaturas vibracionales. Todo ello nos proporciona una visión más profunda de la región de estudio.

A continuación mostramos este artículo. En él se puede encontrar la descripción detallada del trabajo realizado. En el Apéndice A se muestran las tablas que forman parte del contenido *online* del artículo y que se pueden encontrar en la base de datos CDS (centro de datos astronómicos de Estrasburgo)[1].

[1] http://vizier.cfa.harvard.edu/viz-bin/VizieR?-source=J/ApJ/768/81

The Astrophysical Journal, 768:81 (13pp), 2013 May 1 doi:10.1088/0004-637X/768/1/81

LABORATORY CHARACTERIZATION AND ASTROPHYSICAL DETECTION OF VIBRATIONALLY EXCITED STATES OF ETHYL CYANIDE

A. M. Daly[1], C. Bermúdez[1], A. López[2], B. Tercero[2], J. C. Pearson[3], N. Marcelino[4], J. L. Alonso[1], and J. Cernicharo[2]
[1] Grupo de Espectroscopia Molecular (GEM), Edificio Quifima, Área de Química-Física, Laboratorios de Espectroscopia y Bioespectroscopia, Unidad Asociada del CSIC, Universidad de Valladolid, E-47005 Valladolid, Spain; adammichael.daly@uva.es, cbermu@qf.uva.es, jlalonso@qf.uva.es
[2] Department of Astrophysics, CAB, INTA-CSIC, Crta Torrejón, E-28850 Torrejón de Ardoz, Madrid, Spain; lopezja@cab.inta-csic.es, terceromb@cab.inta-csic.es, jcernicharo@cab.inta-csic.es
[3] Jet Propulsion Laboratory, California Institute of Technology, 4800 Oak Grove Dr., Padadena, CA 91109, USA; John.C.Pearson@jpl.nasa.gov
[4] National Radio Astronomy Observatory, 520 Edgemont Road, Charlottesville, VA 22903, USA; nmarceli@nrao.edu
Received 2012 October 10; accepted 2013 February 11; published 2013 April 17

ABSTRACT

Ethyl cyanide, CH_3CH_2CN, is an important interstellar molecule with a very dense rotational–vibrational spectrum. On the basis of new laboratory data in the range of 17–605 GHz and ab initio calculations, two new vibrational states, ν_{12} and ν_{20}, have been detected in molecular clouds of Orion. Laboratory data consist of Stark spectroscopy (17–110 GHz) and frequency-modulated spectrometers (GEM laboratory in Valladolid: 17–170, 270–360 GHz; Toyama: 26–200 GHz; Emory: 200–240 GHz; Ohio State: 258–368 GHz; and JPL: 270–318, 395–605 GHz). More than 700 distinct lines of each species were measured in J up to 71 and in K_a up to 25. The states were fitted with Watson's S-reduction Hamiltonian. The two new states have been identified in the interstellar medium toward the Orion Nebula (Orion KL). The ground state, the isotopologues of CH_3CH_2CN, and the vibrationally excited states have been fitted to obtain column densities and to derive vibrational temperatures. All together, ethyl cyanide is responsible for more than 2000 lines in the observed frequency range of 80–280 GHz.

Key words: ISM: abundances – ISM: individual objects (Orion KL) – ISM: molecules – line: identification – surveys

Online-only material: color figures, machine-readable tables

1. INTRODUCTION

Ethyl cyanide, CH_3CH_2CN, was first identified by Johnson et al. (1977) in the Orion Nebula and has subsequently been identified in several other high-mass star-forming regions (Miao & Snyder 1997; Cazaux et al. 2003). The isotopologues ^{13}C and ^{15}N in their ground state have been detected in Orion (Demyk et al. 2007; Margulès et al. 2009) using the line survey between 80 and 280 GHz carried out with the 30 m radio telescope of the Institute de Radio Astronomie Millétrique (IRAM; Tercero et al. 2010, 2011, 2012). The density of lines in this source, as observed with the 30 m telescope, makes this frequency survey a line confusion-limited one, despite very short integration times, and produces a forest of lines arising from isotopologues and vibrationally excited states of abundant species such as ethyl cyanide, methyl formate (Carvajal et al. 2009; Margulès et al. 2010; Kobayashi et al. 2007; Demyk et al. 2008; Tercero et al. 2012), methanol, SiS, SiO, OCS, CS, HCO^+, etc. (see, e.g., Tercero et al. 2010, 2011). If all the weak lines produced by these species are not identified and assigned, the quest for chemical complexity stops for line intensities larger than 1 K in sources such as Orion, and the detection of new molecular species becomes a very hard task. In Orion, Tercero and collaborators used values for the intensity of lines that are above the confusion limit of 0.03, 0.05, and 0.1 K (in antenna temperature) at 3, 2, and 1.3 mm wavelengths, respectively; values that are reached in a few minutes of observing time. The number of features in the line survey above these limits exceeds 15,000, and after assignment of the obvious features to the most abundant species (45 molecules), 4000 lines remain to be identified.

The detection of the isotopic species of ethyl cyanide (Demyk et al. 2007; Margulès et al. 2009) and the very intense spectrum measured of the parent species suggests that highly excited vibrational states of ethyl cyanide could be present in this source. This has been the case for objects with similar physical conditions such as Sgr B2, where Mehringer et al. (2004) have reported the detection of the in-plane bending vibration, $\nu_{13} = 1$, and the $\nu_{21} = 1$ torsional state toward Sgr B2(N-LMH). The increase in sensitivity of instruments such as ALMA and the opening of new spectral windows from space observatories (*Herschel*) will rely on the assignment of the low-lying vibrational states of abundant molecules to penetrate the line forest they produce. Without this spectral information, the full power of line surveys will be strongly limited and the data produced by new instruments will not be fully exploited. High-resolution spectroscopic work has been done for the ground state isotopologues of abundant species, but reliable rotational constants for a large number of low energy vibrational modes of polyatomic molecules, such as ethyl cyanide, have yet to be published. While the emission from isotopologues will depend on the isotopic abundances (e.g., $\simeq$40–50 for $^{12}C/^{13}C$), the emission from low energy vibrationally excited states will depend on the vibrational temperature. In hot cores with $T_K \simeq 200$ K, the levels around 150–200 cm^{-1} above the ground state will have line intensities 1/3–1/5 of those of the ground state. A systematic study of the effect of temperature on the spectrums from 210 to 270 GHz and 570 to 645 GHz of this molecule has been performed by Fortman et al. (2010a, 2010b), who measured 9962 strong lines of ethyl cyanide in the range of 575–645 GHz and 3000 strong lines from 210 to 260 GHz in the laboratory. Not all of these states could be assigned to known vibrational states of ethyl cyanide, highlighting the importance of systematic studies that can identify vibrational states.

The ground state rotational a-type and b-type transitions of the parent ethyl cyanide have been assigned up to $J = 120$, with measurements in the laboratory reaching 1.6 THz

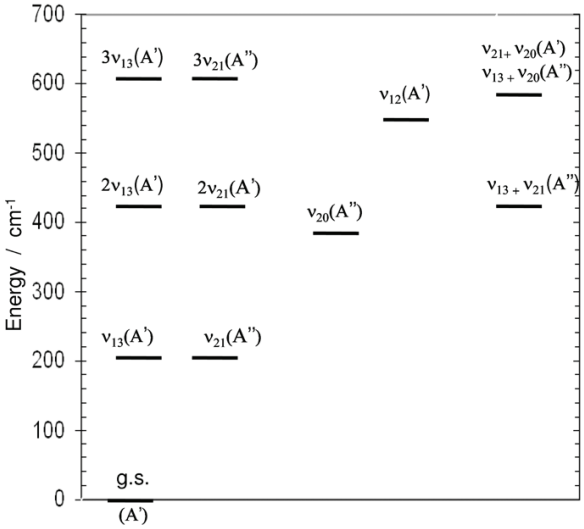

Figure 1. Vibrational states of ethyl cyanide below 700 cm^{-1}, excluding states made by difference.

(Pearson et al. 1994; Brauer et al. 2009). The dipole moments have been measured recently by Krasnicki & Kisiel (2011). Early observations of microwave transitions from excited vibrational states were assigned by Duncan & Janz (1955) and the gas-phase structure supporting the C_s symmetry was reported by Lerner & Dailey (1957). These states were identified by Laurie (1959) to arise from the two lowest energy states, the torsion (ν_{13} at 206 cm^{-1}) and in-plane bend (ν_{21} at 212 cm^{-1}) states, and were assigned to the A′ and A″, respectively, in Heise et al. (1981). The states below 700 cm^{-1} are shown in Figure 1 with their respective symmetries. The two overtone and combination bends also contribute to further complicating the spectrum. The first relatively unperturbed state was assigned and studied for the first time by Fukuyama et al. (1999); this was ν_{20} at 373 cm^{-1}. This study included the ground, ν_{13}, ν_{21}, and ν_{20} in a four-state fit, and μ_a and μ_b transitions were assigned up to $J = 16$ and $K_a = 4$. As part of our investigation of unassigned states of ethyl cyanide in the interstellar medium, we have continued the assignment of this state to obtain accurate spectroscopic constants for positive identification. The state ν_{12} at 534 cm^{-1} lies well above the three states of $2\nu_{13}$, $2\nu_{21}$, and $\nu_{13} + \nu_{21}$ at 410 cm^{-1} and just below the states at 570 cm^{-1} : $\nu_{13} + \nu_{20}$ and $\nu_{21} + \nu_{20}$ (see Figure 1). To disentangle these states, low frequency measurements using the Stark modulation spectrometer in Valladolid were performed. This technique is ideally suited for the identification of vibrational states due to the high sensitivity and distinct shape of the Stark pattern for each transition type. The vibrational satellite pattern around the ground state transition was modeled using ab initio calculations to help identify new states assigned in the Stark spectra. Fits of a previously unassigned state, ν_{12}, and additional measurements of ν_{20} up to 360 GHz have provided accurate rotational and distortion constants that have greatly aided the identification of two new states in the clouds of Orion. Subsequently, we combined data from the published studies of Toyoma (26–200 GHz; Fukuyama et al. 1999), OSU (210–270 GHz; Fortman et al. 2010a), and JPL (440–530 GHz; Pearson et al. 1994; Brauer et al. 2009) and previously unpublished measurements at OSU (258–368 GHz), Emory (200–240), and JPL (270–318, 395–605 GHz) to create a fit that includes transitions up to $J = 71$ and $K_a = 25$.

The new assignments of ν_{20} and ν_{12} were used successfully to identify both states for the first time in Orion using the data provided by the IRAM telescope. We have included data from this study, previously published data of the coupled state of ν_{21} and ν_{13}, and isotopic data in the ground vibrational state to present an analysis of the relative densities of vibrationally excited states to isotopologues in the ground vibrational state. We provide a wide analysis of the molecule and column densities have been calculated for all species detected from ethyl cyanide in a consistent way.

2. EXPERIMENTAL

Ethyl cyanide was purchased from Sigma Aldrich and was used without further purification. The sample was placed into a glass cell and degassed using the common freeze-pump-thaw method to remove air from the sample. Sample pressure was maintained between 2–3 $\times$ 10^{-2} mbar or about 20 mTorr. Experiments were performed first in the frequency range of 26–40 GHz using a newly configured computer-controlled Stark-modulated spectrometer whose principle components have been described in Lessari et al. (1991) and extended to 50–110 GHz by incorporation of multipliers and detectors from Virginia Diodes, Inc., which will be described in detail in a later publication. For most measurements, an accuracy of 50 kHz for peak frequencies is given, as unresolved ^{14}N-nuclear quadrupole splitting is present in our measurements. Voltages ranging from 100 to 700 V were used to sufficiently separate the modulated signals to obtain reliable determination of the center frequency. Scans were performed in both directions and the sum of both scans was used for frequency determination.

The experiments performed in Valladolid with frequency modulation (FM) from 110 to 170 GHz and 240 to 360 GHz were carried out in a static free space glass cell with Teflon windows fitted with ports to evacuate and maintain pressures of 20 mTorr with a 2 m length and 12 cm diameter (Alonso et al. 1993). Active multipliers and detectors from Virginia Diodes were used to obtain 240–360 GHz using FM modulation, and those detected at 2*f* will be described in detail soon. Software written in LabVIEW was used to control the synthesizer (13–20 GHz) and record the signal capable of scanning 30 GHz in 10 hr in 1 GHz sections with a step size of 50 kHz. Scans were performed in both directions, and the average of both directions was used for frequency measurements with an accuracy of 50 kHz. The spectra were imported into AABS (Kisiel et al. 2005), and frequencies were determined using a fit from a Gaussian line shape.

Additional measurements covering 270–318 GHz and 395–605 GHz were performed at the Jet Propulsion Laboratory (JPL) using the spectrometer described in Drouin et al. (2005) and Pearson et al. (2011) and at the Ohio State University with the FASSST spectrometer covering 268–368 GHz (Petkie et al. 1997). Some additional spectra covering 200–240 GHz were collected at Emory University and (the study peak list of Fukuyama et al. 1996) covering 26–200 GHz was utilized. Lines measured at JPL and Emory were peak picked and are assumed to be accurate to 50 kHz, with strong isolated lines being significantly more accurate. The spectrum in the JPL measurements above 270 GHz is line confused, assuring that lines are almost never isolated. The FASSST lines were collected with an early version of the system and are only accurate to 200 kHz. Agreement between common measurements suggests that the asserted accuracies are, on average, reasonable.

Table 1
Scaled Values of ab initio Predictions for the Ground State and the Vibrational States ν_{20} and ν_{12}

	G.S.	ν_{20}	ν_{12}
ΔE (cm^{-1})	0	369	530
A (MHz)	27663.7	28374.9	27423.1
B (MHz)	4714.2	4716.6	4708.3
C (MHz)	4225.1	4240.8	4229.0

Note. Method MP2/6−311++G(d,p).

3. ASSIGNMENT OF THE EXCITED STATES

3.1. Identification of ν_{12}

Ethyl cyanide, $\mu_a = 3.816(3)$ D and $\mu_b = 1.235(1)$ D (Krasnicki & Kisiel 2011), has a strong a-type spectra and is dominated by strong a-type R-branch transitions in the region below 700 GHz. For this reason, long scans with the Stark spectrometer experiments were performed at room temperature at pressures of 20 mTorr concentrated on the $K_a = 1$ transitions of $J = 2$–8. As expected, several signals with the same Stark shape as the ground state transition were observed. Using the Fukuyama data, transitions assigned to ν_{13}, ν_{21}, and ν_{20} were readily identified. Unknown signals were recorded and preliminary fits were made. To help understand which vibrational states may be present, optimization and frequency calculations were performed with MP2/6−311++G** in the Gaussian09 (Frisch et al. 2009) suite using an anharmonic potential. This calculation will give the first-order correction to the ground state rotational constants and can be used to simulate the data with columns, $\alpha_i^A \alpha_i^B \alpha_i^C$. Vibrationally averaged rotational constants are given as the sum, $A_e - \sum_{i=0}^{n} (\alpha_i^A)(v+1/2)$. Since the ground state rotational constants are well known, the difference between the predicted and calculated rotational constants can be added to each state to effectively shift all the states equally. This is summarized in Table 1 for the states $\nu_{20} = 1$ and $\nu_{12} = 1$.

An example spectrum is shown in Figure 2 with the simulated spectrum produced from ab initio calculations using MP2/6−311++G** (Frisch et al. 2009) for the 7_{17}–6_{16}. The intensities of the lines were estimated using the vibrational partition function and are scaled by the ground state to 1.

A comparison of the ab initio predicted values shows both excellent predictions for the assigned ν_{20} and ν_{13} states in the frequency up to $J = 8$, and a poor prediction of the placement of the ν_{21} state. The poor prediction for the ν_{21} state is due to a $\Delta K = 2$ resonance with $\nu_{13} = 1$, which the ab initio calculation does not take into account. Also, it is clear from the spectra that there are no equally spaced progressions for any of the assigned states. The rotational transitions from the three states assigned by Fukuyama et al. (1999) are consistently higher in frequency than the ground state as measured up to $J = 8$. A transition consistently lower in frequency was observed. A fit was made of A, B, C as adjustable parameters with the distortion constants fixed to the ground state values given in Brauer et al. (2009) using SPFIT (Pickett 1991). The rotational constants obtained were consistent with the predicted values of ν_{12}. At a given transition, the ν_{12} CCC bending state lies at lower frequency than the ground state and all the other known low-lying vibrational states. Additionally, it exhibits no measurable torsional splittings in any of the transitions observed. As a result, the transitions are all single lines, giving them comparable intensity to torsionally split transitions lying 200 cm^{-1} lower in energy. The a-type R-branch is well separated from the ground state, which makes the assignments relatively straightforward.

Table 2
Summary of s-representation

	Experimental	
	ν_{12}	ν_{20}
A (MHz)	28081.9841(95)	27445.4006(86)
B (MHz)	4707.35767(23)	4715.64665(32)
C (MHz)	4228.63011(19)	4240.78292(31)
$D_J \times 10^3$ (kHz)	2.980519(84)	3.01522(19)
D_{JK} (kHz)	−48.3584(50)	−46.5397(26)
D_K (kHz)	582.3(15)	518.14(94)
d_1 (kHz)	−0.680293(43)	−0.68374(11)
d_2 (kHz)	−0.033681(40)	−0.027800(27)
H_J (kHz)	0.009274(13)	0.009299(59)
H_{KJ} (Hz)	−0.956(27)	−1.330(11)
H_{JK} (Hz)	...	−0.1430(30)
H_K (Hz)	−976. (23)	−296.(26)
h_1 (Hz)	0.0037837(71)	0.003950(40)
h_2 (Hz)	0.0003052(68)	...
h_3 (Hz)	0.0000431(38)	...
L_J (mHz)	...	−0.0000456(61)
L_{JJK} (mHz)	−0.00781(15)	...
L_{JK} (mHz)	−2.1412(39)	...
L_K (mHz)	8232. (71)	...
l_1 (mHz)	...	−0.0000276(44)
l_2 (mHz)	...	0.0000538(10)
l_3 (mHz)	...	0.00001561 (63)
P_{JK} (μHz)	0.0562 (14)	...
σ_{fit} (MHz)	0.087	0.095
σ_{rms} (MHz)	1.60	1.65
$N_{total}/N_{excluded}$	1109/128	971/180

Note. Lines excluded based on a measured frequency greater than five times the assigned uncertainty.

We were able to include lines from ν_{20} in the Stark spectrum after re-fitting the Fukuyama et al. (1999) data with several blended lines removed. This state was included in a global fit in that study, but the reference uses a structural model that does not allow for easy calculation of unmeasured transitions. Transitions of a-type R-branch and b-type Q-branch were measured for both states in the region of 17–110 GHz using Stark spectrometer data and 110–170 GHz using FM modulation. Predictions were made for the region of 240–360 GHz and a record of this range was made. These data were fit with the Watson S-reduction (Watson 1977) using SPFIT, with 265 transitions eventually included in the fit using the combined Stark and FM modulation data up to 360 GHz.

3.2. Assignment of ν_{12} and ν_{20} to 605 GHz

We have compiled the data from several sources in the literature of OSU (Fortman et al. 2010b) combined with Fukuyama et al. (1996), Pearson et al. (1994), and Brauer et al. (2009), which allowed us to extend the fit to JPL 605 GHz including transitions up to $J = 71$, $K_a = 25$ using the S-reduction. Both reductions were shown to give similar results in the study of the ground state.

These assignments were fit using the Hamiltonian in the S-reduction, including the octic (P^8) and a single decic term, P_{JK}, which are centrifugal constants for a semi-rigid molecule, and are given in Table 2. Tables of all the assigned transitions are given in the online journal for both states (tables sorted

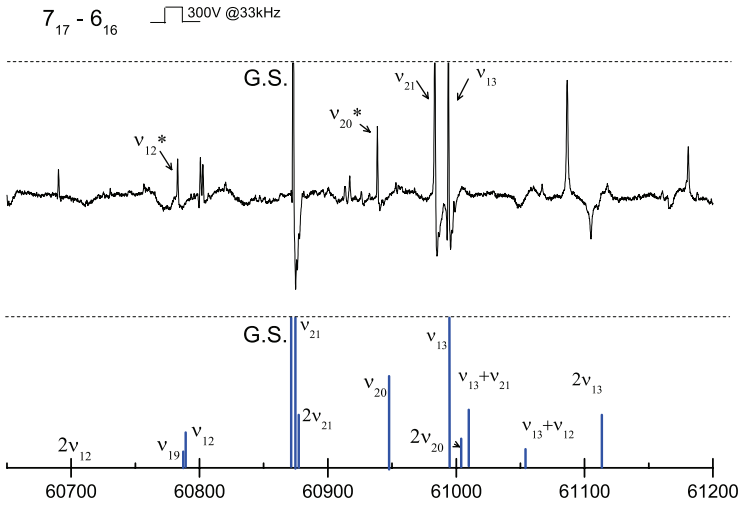

Figure 2. Plot of the 7_{17}–6_{16} scan using the Stark spectrometer and ab initio simulation of the data, above and below, respectively. Rotational constants used to predict the transitions are shifted by the ground state difference between prediction and experimental. Intensities are estimated using the vibrational partition function and have been scaled to the ground state. The graph is expanded to show the excited states.

(A color version of this figure is available in the online journal.)

by frequency and quantum number for ν_{20} and ν_{12} given in Tables 4–7). Excluding internal rotation and other types of coupling, are given as

$$\begin{aligned} H = {} & A J_a^2 + B J_b^2 + C J_c^2 - D_J J^4 - D_{JK} J^2 J_c^2 \\ & - D_K J_c^4 + d_1 J^2 (J_+^2 + J_-^2) + d_2 (J_+^4 - J_-^4) \\ & + H_J J^6 + H_{JK} J^4 J_c^2 + H_{KJ} J^2 J_c^4 + H_K J_c^6 \\ & + h_1 J^4 (J_+^2 + J_-^2) + h_2 J^2 (J_+^4 - J_-^4) + h_3 (J_+^6 - J_-^6) \\ & + L_J J^8 + L_{JJK} J^6 J_c^2 + L_{JK} J^4 J_c^4 + L_{KKJ} J^2 J_c^6 \\ & + L_K J^8 + l_1 J^6 (J_+^2 + J_-^2) + l_2 J^4 (J_+^4 - J_-^4) \\ & + l_3 J^2 (J_+^6 - J_-^6) + l_4 (J_+^8 - J_-^8) + P_{JK} J^6 J_c^4. \end{aligned}$$

In the ν_{20} and ν_{12} states, there are several K_a states that were found to be perturbed and have significant deviation from the fit or are split due to internal rotation. Lines were not included in the fit if the difference between predicted and assigned was found to be more than five times the assigned uncertainty. Torsional splittings were observed in all ν_{20} b-type transitions reported by Fukuyama et al. (1999), and they are observed in a-type transitions with $K_a = 2$, $K_a = 3$, and $K_a = 12$–14. Significant deviations for small ranges of J are observed for ν_{20} in $K_a =$ 4,6,7,11,12,14,15,16 and for the states $K_a = 12,13$ in ν_{12}. The torsional effects observed in ν_{20} are an order of magnitude larger than those observed in the ground state. It is known that the couplings between ν_{20} and $2\nu_{21}$ and ν_{20} and $2\nu_{13}$ are weak. However, it is possible that there is a much stronger interaction with the same symmetry combination band $\nu_{21} + \nu_{13}$ that leads to the deviations in the K_a states. If the interaction originates from a quanta in the torsional state, the splitting, which has been ignored in this study, might be inverted relative to the normal ground state. The spectrum of ν_{20} and ν_{12} up to 605 GHz has been fit to be independent of any coupling from another torsion state ($2\nu_{21}$ 412 cm^{-1}, $2\nu_{13}$ 414 cm^{-1} and $\nu_{13} + \nu_{21}$ 419 cm^{-1}, and ν_{20}+ ν_{13} 570 cm^{-1} and ν_{20}+ ν_{21} 574 cm^{-1}, respectively). The lowest three states are most likely coupled with ν_{20} and the upper two are suspected to be coupled with ν_{12}. Future studies with clear assignments of $2\nu_{21}$, $2\nu_{13}$, and $\nu_{13} + \nu_{21}$ may reveal the extent of coupling for the excited vibrational state of ν_{20}. A similar exercise would be required for $\nu_{20} + \nu_{13}$ and $\nu_{20} + \nu_{21}$ to determine the extent of interactions with ν_{12}, but for the purposes of astronomical assignments of the a-type spectrum to 300 GHz, these difficult steps can be neglected—though at higher frequencies than reported here ν_{12} clearly becomes perturbed.

There are several important points in utilizing the present analysis for astronomical searches. First, we have neglected the torsional splittings of the b-type transitions in the ν_{20} state. The b-type transitions in the ν_{20} state are all split by a few MHz, and the constants will give what we believe is the A-state line. Confirming that it is in fact the A-line will require understanding the origin of the torsional splittings, which is beyond the scope of the present effort. Second, interactions with higher states were neglected and very few b-type transitions changing K were included. As such, the H_K and L_K constants are not going to accurately predict the higher K b-type transitions. It is known that assignment of the high frequency b-type R-branch spectrum based on the present work is impossible. Finally, the spectrum becomes progressively more perturbed with increasing J, with the interactions spreading rapidly to lower K values. However, the majority of a-type R branches are predicted sufficiently well for astronomical assignments.

4. CH_3CH_2CN IN ORION KL

4.1. Observations and Overall Results of the Line Survey

Astronomical observations were carried out with the IRAM 30 m telescope from 2004 September to 2007 January in four different sessions, pointing toward the IRc2 source at $\alpha_{2000.0} = 5^h35^m14^s.5$, $\delta_{2000.0} = -5°22'30''.0$ (J2000.0). Four SiS receivers were operating simultaneously at 3, 2, and 1.3 mm. Image side band rejections and system temperatures were in the ranges of 13–27 dB and 100–800 K, respectively, for all the frequency range covered. The calibration of the intensity scale was performed using two absorbers at different temperatures and

Table 3
Physical-chemical Conditions of Orion-KL from CH_3CH_2CN

	Hot Core 1	Hot Core 2	Hot Core 3
d_{sou} ($''$)	4	10	25
Offset ($''$)	5	5	5
v_{exp} (km s^{-1})	5	13	22
v_{LSR} (km s^{-1})	5	3	3
T_{ETL} (K)	275	110	65
$N(CH_3CH_2CN)$ (cm^{-2})	$(3.0 \pm 0.9) \times 10^{16}$	$(8 \pm 2) \times 10^{15}$	$(3.0 \pm 0.9) \times 10^{15}$
$N(CH_3CH_2CN\ v_{13} = 1/v_{21} = 1)$ (cm^{-2})	$(4 \pm 1) \times 10^{15}$	$(1.1 \pm 0.3) \times 10^{15}$	$(4 \pm 1) \times 10^{14}$
$N(CH_3CH_2CN\ v_{20})$ (cm^{-2})	$(1.7 \pm 0.5) \times 10^{15}$	$(4 \pm 1) \times 10^{14}$	$(1.7 \pm 0.5) \times 10^{14}$
$N(CH_3CH_2CN\ v_{12})$ (cm^{-2})	$(6 \pm 3) \times 10^{14}$	$(1.6 \pm 0.5) \times 10^{14}$	$(6 \pm 3) \times 10^{13}$
$N(^{13}CH_3CH_2CN)$ (cm^{-2})	$(7 \pm 2) \times 10^{14}$	$(1.9 \pm 0.6) \times 10^{14}$	$(7 \pm 2) \times 10^{13}$
$N(CH_3^{13}CH_2CN)$ (cm^{-2})	$(7 \pm 2) \times 10^{14}$	$(1.9 \pm 0.6) \times 10^{14}$	$(7 \pm 2) \times 10^{13}$
$N(CH_3CH_2^{13}CN)$ (cm^{-2})	$(7 \pm 2) \times 10^{14}$	$(1.9 \pm 0.6) \times 10^{14}$	$(7 \pm 2) \times 10^{13}$
$N(CH_3CH_2C^{15}N)$ (cm^{-2})	$(2 \pm 1) \times 10^{14}$	$(5 \pm 3) \times 10^{13}$	$(1.7 \pm 0.8) \times 10^{13}$
$N(A\text{-}CH_2DCH_2CN)$ (cm^{-2})	$\leqslant 6 \times 10^{14}$	$\leqslant 2 \times 10^{14}$	$\leqslant 6 \times 10^{13}$
$N(S\text{-}CH_2DCH_2CN)$ (cm^{-2})	$\leqslant 7 \times 10^{14}$	$\leqslant 1 \times 10^{14}$	$\leqslant 6 \times 10^{13}$
$N(CH_3CHDCN)$ (cm^{-2})	$\leqslant 6 \times 10^{14}$	$\leqslant 2 \times 10^{14}$	$\leqslant 6 \times 10^{13}$

Note. Physical-chemical conditions of Orion-KL from the analysis of ethyl cyanide emission lines in the range of 80–280 GHz.

the atmospheric transmission model (Cernicharo 1985; Pardo et al. 2001b). Observations were made in the balanced wobbler-switching mode, with a wobbling frequency of 0.5 Hz and a beam throw in the azimuth of $\pm 240''$. Quasars 0420−014 and 0528+134 were used to check pointing and focus. All spectra have 1 or 1.25 MHz of spectral resolution. As backends, two filter banks with 512 × 1 MHz channels and a correlator providing two 512 MHz bandwidths and 1.25 MHz resolution were used.

For further description of the observations and data reduction see Tercero et al. (2010).

Within the frequency domains 80–115.5, 130–178, and 196–281 GHz (168 GHz bandwidth covered), more than 15,000 spectral features have been detected. We found a total of 45 molecules, including 191 different isotopologues and vibrationally excited states. To date, more than 4000 spectral features are still unidentified (Tercero et al. 2010, 2011).

In the analysis of the emission lines of this line survey by Gaussian fits, we mainly found, in agreement with previous works, four different components characterized by different physical and chemical conditions (see Blake et al. 1987, 1996; Tercero et al. 2010, 2011, and references therein): (1) the *extended ridge* or ambient cloud ($T_k \simeq 60$ K, $n(H_2) \simeq 10^5$ cm^{-3}) at $v_{LSR} \simeq 9$ km s^{-1} and $\Delta v \simeq 4$ km s^{-1} traced by emission of simple molecules such us CO, CS, NS, or CCH; (2) the *compact ridge* ($v_{LSR} \simeq 8$ km s^{-1}, $\Delta v \simeq 3$ km s^{-1}, $T_k \simeq 110$ K, $n(H_2) \simeq 10^6$ cm^{-3}), a compact region rich in oxygen bearing and complex molecules such as $HCOOCH_3$, CH_3OH, and CH_3OCH_3 that was identified for the first time by Johansson et al. (1984); (3) the *plateau*, a mixture of outflows, shocks, and interactions with the ambient cloud ($v_{LSR} \simeq$ 6–10 km s^{-1}, $\Delta v \gtrsim 25$ km s^{-1}, $T_k \simeq$ 150 K, $n(H_2) \simeq 10^6$ cm^{-3}). This component is traced by molecules produced in shock chemistry (SO, SO_2, or SiO); and (4) a *hot core* component ($v_{LSR} \simeq 5$ km s^{-1}, $\Delta v \sim 10$ km s^{-1}, $T_k \simeq 225$ K, $n(H_2) \simeq 5 \times 10^7$ cm^{-3}) characterized by a N-rich chemistry. Molecules such as ethyl cyanide come mainly from this component.

4.1.1. 2D Survey Observations

In addition to the single pixel line survey of Orion KL, we also performed a 2D line survey between 210 and 275 GHz in 2008 and 2010. The maps covered an area of 140 × 140 arcsec^2 with a sampling of 4 arcsec. The observations were performed using the On-The-Fly mapping mode with reference position 10 arcmin west of Orion KL. This 2D line survey has been used to select different transitions of CH_3CH_2CN and to study the spatial extent of its emission. The EMIR single pixel heterodyne receivers were used for all observations except for the 220 GHz frequency setting, for which the HERA receiver array was used. The WILMA backend spectrometer was used for all observations, with a total bandwidth of 4 GHz and a spectral resolution of 2 MHz, corresponding to velocity resolutions of 5.4–2.5 km s^{-1} at 110 and 239 GHz, respectively. The telescope pointing was checked every 2 hr and found to have errors of typically less than 3 arcsec. The data were processed using the IRAM GILDAS software package.[5] Data reduction consisted of removing bad pixels, checking for image sideband contamination and emission from the reference position, and fitting and removing first-order baselines.

4.2. Detection of Excited Vibrational States and Isotopologues

4.2.1. Detection

The new laboratory and theoretical work presented above allows us to detect two new species (v_{20} and v_{12} vibrationally excited states of ethyl cyanide) in our line survey and for the first time in space. In the following sections, we will focus on the analysis of the detected spectral features from all species of ethyl cyanide (ground state, isotopologues, and vibrationally excited states). This analysis follows the proceedings of our previous works (Tercero et al. 2010, 2011, 2012; Demyk et al. 2007; Margulès et al. 2009, 2010; Carvajal et al. 2009; Motiyenko et al. 2012).

Ethyl cyanide (CH_3CH_2CN) shows emission from a large number of lines in this frequency band. Line detections in our survey include the ground vibrational state of five isotopologues (CH_3CH_2CN, $^{13}CH_3CH_2CN$, $CH_3^{13}CH_2CN$, $CH_3CH_2^{13}CN$, $CH_3CH_2C^{15}N$; Demyk et al. 2007; Margulès et al. 2009), plus four vibrationally excited states of the main isotopologue ($v_{13} = 1/v_{21} = 1$; v_{12}: torsion in the plane; and v_{20}:

[5] http://www.iram.fr/IRAMFR/GILDAS

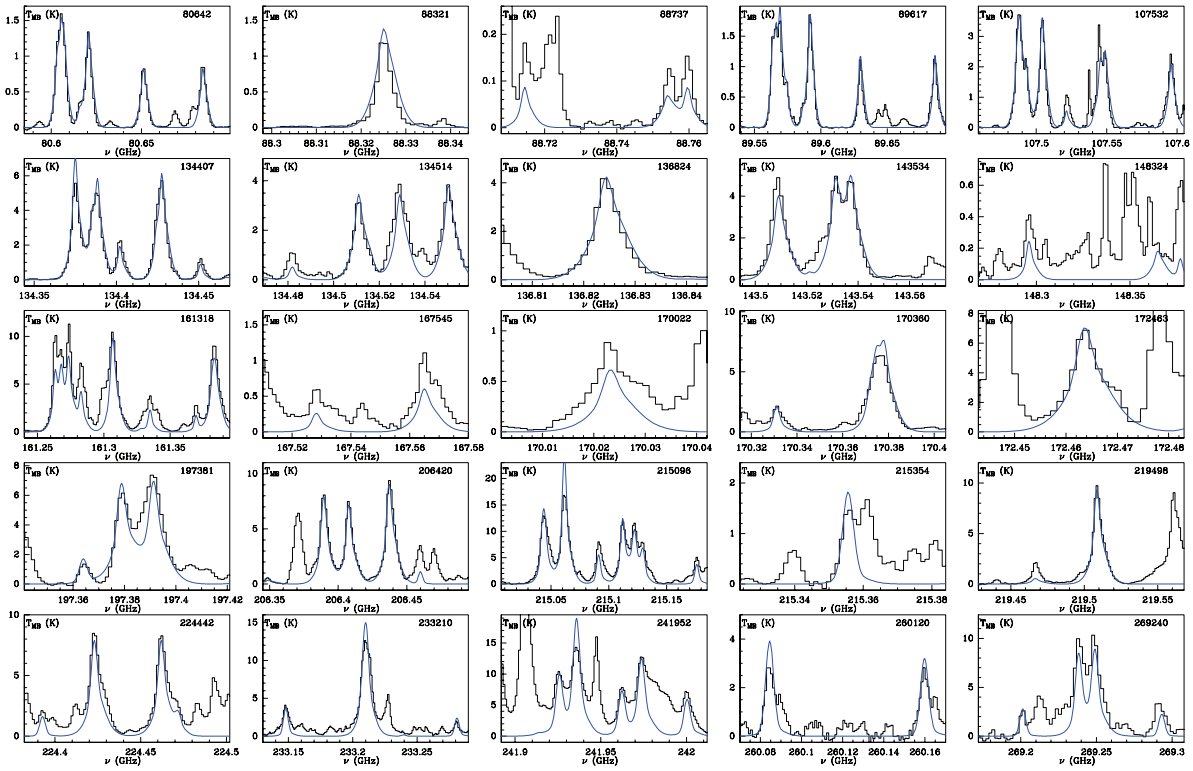

Figure 3. Observed lines from Orion KL (histogram spectra) and the model (thin curves) of ethyl cyanide in the ground state.
(A color version of this figure is available in the online journal.)

torsion out of the plane). The last two were detected here for the first time in space. Only a tentative detection is presented for the deuterated species, A/S-CH_2DCH_2CN and CH_3CHDCN (Margulès et al. 2009), because of the weakness of the features and/or their overlap with other spectral lines.

Isotopologue species have been characterized in Demyk et al. (2007) and Margulès et al. (2009). Here, we present observed line parameters and intensities, as well as the predicted frequencies, for all lines that are not strongly blended with other species from the vibrationally excited states (Tables 8–10 in the online version). In this paper, we provide a wide analysis of the molecule, and the column densities have been calculated in a consistent way for all species detected from ethyl cyanide.

The rotational constants were implemented in the MADEX code (Cernicharo 2012), which was used to calculate the emerging spectrum from the four cloud components. Table 10 gives the line intensity derived from the model predictions. In Tables 8–10, the observed brightness temperature has been obtained from the peak emission channel in the spectra. For that, the observed main beam temperature of weak blended lines is affected by the emission of the molecules that overlap in the same feature and this value, in those cases, has to be considered an upper limit. Hence, we have not showed highly blended lines in those tables. Nevertheless, the predicted intensities agree with the observations of the detected lines (see below, Figure 4).

For strong non-blended lines, we also provide the parameters of the lines derived by fitting Gaussian profiles with CLASS software.[6] We note that the line parameters for these stronger lines match those of the hot core component. For the two new detected vibrationally excited states, ν_{20} and ν_{12}, we assigned 66 and 56 unblended lines, respectively.

Figures 3 and 4 show selected detected lines of ethyl cyanide in the ground state and in the three detected vibrational states, respectively, together with our best-fit-model line profiles.

Figure 4 shows many detected lines of CH_3CH_2CN ν_{20} and ν_{12} without blending with other species. The good fit between model and observations appears to be the first detection in space of both ethyl cyanide vibrationally excited states.

5. ASTRONOMICAL MODELING OF CH_3CH_2CN IN ORION KL

5.1. CH_3CH_2CN Maps

From the 2D survey data of Orion KL, maps of the integrated intensity of four ground state transitions of CH_3CH_2CN at different velocity ranges are shown in Figure 5 (line 1 to 4: $30_{2,28}-29_{2,27}$, $31_{2,30}-30_{2,29}$, $32_{0,32}-31_{0,31}$, and $32_{1,32}-31_{0,31}$, respectively). The velocity structure of the CH_3CH_2CN emission shows the contribution from two cloud components: a compact component at the position of the hot core and a more extended component. Note that there is not a spatial displacement of the emission peak with velocity. Particularly interesting is the spatial distribution of the red and blue wings at the largest

[6] http://www.iram.fr/IRAMFR/GILDAS

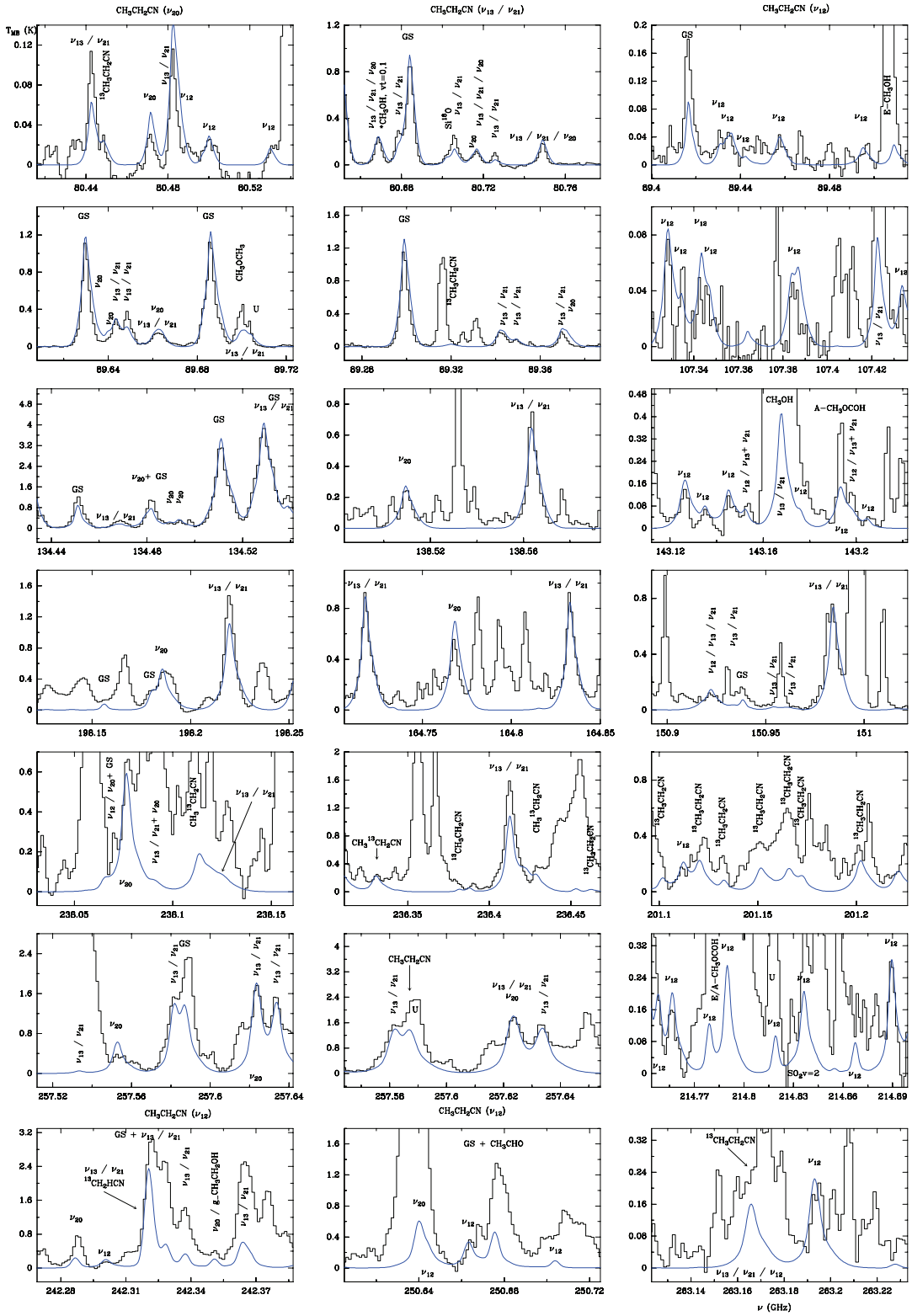

Figure 4. Observed lines from Orion KL (histogram spectra) and the model (thin curves) of vibrationally excited ethyl cyanide. (A color version of this figure is available in the online journal.)

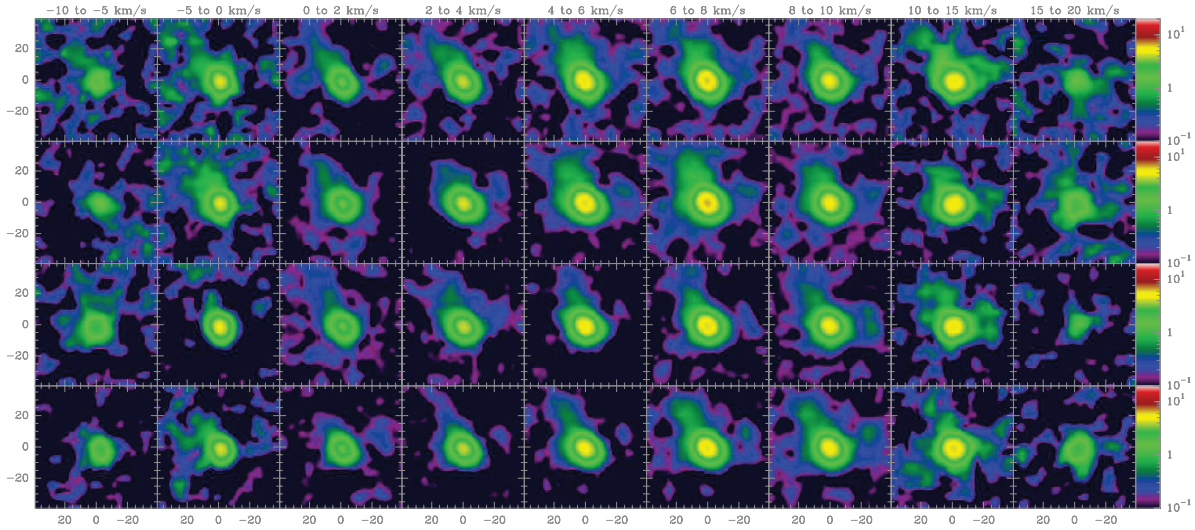

Figure 5. Integrated intensity of four transitions of ethyl cyanide (line 1 to 4: $30_{2,28}-29_{2,27}$, $31_{2,30}-30_{2,29}$, $32_{0,32}-31_{0,31}$, and $32_{1,32}-31_{0,31}$, respectively) at different velocity ranges (indicated in the top of each column). For each box, axes are in units of arcseconds ($\Delta\alpha$, $\Delta\delta$). Color logarithm scale is the integrated intensity ($\int T_A^* dv$) in units of K km s^{-1}.

(A color version of this figure is available in the online journal.)

velocities where we note the contribution of the plateau centering at the hot core position. The extended component appears at the northeast, at velocities from −5 to 15 km s^{-1}, following the delineation of the extended ridge (see, e.g., Wright et al. 1996). The observed structure in all transitions is in agreement with previous maps made with interferometric arrays by Wright et al. (1996) and Blake et al. (1996) in the 3 and 1.3 mm domains, respectively.

5.2. The Model

Radial velocities and line widths of the ethyl cyanide lines present in this line survey, together with the velocity maps shown above, suggest that the emission of these species comes mainly from the hot core. In addition, modeling the emission from the ^{13}C and ^{15}N isotopologues of ethyl cyanide (Demyk et al. 2007; Margulès et al. 2009), we found that the sum of two components, the hot core component and the plateau, is sufficient to reproduce all line intensities and profiles reasonably well.

For all detected ethyl cyanide species, column densities were calculated using an excitation and radiative transfer code developed by J. Cernicharo (Cernicharo 2012).

Owing to the lack of collisional rates for ethyl cyanide, we used LTE approximation. Nevertheless, as most of the emission comes from the hot core (a component with high density and temperature, see Section 4.1), the LTE approximation must work reasonably well. We assumed uniform physical conditions for the kinetic temperature, density, radial velocity, and line width (Table 3). These values are derived from the data analysis: the large number of transitions in a wide range of frequency allows us both to constrain these physical values by means of Gaussian fits and to attempt to simulate the line profiles with an LTE code. In addition, we performed a rotational diagram (Goldsmith & Langer 1999) of CH_3CH_2CN in its ground state (Figure 6), including 127 lines (transitions) free of blending with energies of the upper level from 23.5 to 449.2 K for two different Gaussian components of the emission lines. To quantify the beam telescope dilution, we considered a source diameter of 5″ and 10″ for the emitting region responsible for the narrow and broad profiles of the emission lines, respectively.

We have introduced a stratification of the hot core component to fit all the lines arising from ethyl cyanide species with the same physical source model (following the $T_{\rm rot}$ results of the rotational diagram). We considered three layers with different temperatures. Sizes and offsets from the pointing position (IRc2) of each component are taken into account in our model (maps of ethyl cyanide obtained with the 2D survey of Orion, N. Marcelino et al., in preparation, allow us to provide these parameters), and beam dilution is corrected for each line depending on their frequency. We did not observe any contributions from the error beam as most of cloud components are compact and lie inside the telescope beam. This setup gives the column density as the only free parameter. Sources of uncertainty are described in Tercero et al. (2010).

5.3. CH_3CH_2CN Column Densities

Column density results are shown in Table 3. Owing to the low intensity of the lines belonging to deuterated ethyl cyanide, implying larger overlap problems, we can only obtain upper limits for their column density. We estimate the uncertainty to be about 30% for the results of CH_3CH_2CN, CH_3CH_2CN $\nu_{13} = 1/\nu_{21} = 1$, CH_3CH_2CN ν_{20}, and the ^{13}C isotopologues, whereas for CH_3CH_2CN ν_{12} and $CH_3CH_2C^{15}N$ we estimate the uncertainty to be 50% (due to the weakness of the observed lines for these species).

Figures 3 and 4 and Table 10 (in the online journal) show the comparisons between model and observations. Observed line intensities from all lines free of blending agree with the model predictions. For weaker observed lines, the lack of a good agreement is caused by overlap with other species.

Differences between column densities obtained with the rotational diagram and those derived from the model are mostly due to the source diameter considered in each component. We consider that this model fits these results better when taking into account all data introduced in it (rotational diagram results,

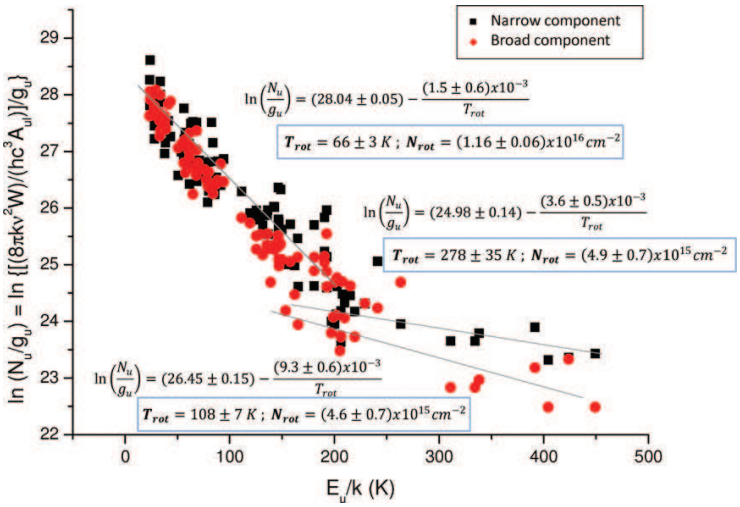

Figure 6. Rotational diagram of CH_3CH_2CN in its ground state.
(A color version of this figure is available in the online journal.)

Table 4
Measured Transitions of ν_{20} of Ethyl Cyanide Sorted by Frequency

J'	K'_a	K'_c	J''	K''_a	K''_c	ν_{obs}[a] (Hz)	ν_{obs}-ν_{cal}[b] (Hz)	Given Error[c] (Hz)	Flag[d]	Blended?[e]	Weighted Average Peak (Hz)
3	0	3	2	0	2	26839.519	−0.007	0.05			
3	1	2	2	1	1	27576.759	−0.067	0.05			
6	1	5	6	0	6	28352.470	−0.161	0.05			
7	1	6	7	0	7	30319.440	−0.087	0.05			
8	1	7	8	0	8	32665.470	−0.076	0.05			
6	0	6	5	1	5	33867.010	0.272	0.05	*		
4	1	4	3	1	3	34861.170	−0.083	0.05			
9	1	8	9	0	9	35422.430	0.011	0.05			
4	0	4	3	0	3	35751.461	0.021	0.05			
4	2	3	3	2	2	35820.625	−0.089	0.05			

Notes.
[a] Observed Frequency.
[b] Difference between observed and calculated frequencies.
[c] Error in ν.
[d] Non-fitted lines.
[e] Blended lines.

(This table is available in its entirety in a machine-readable form in the online journal. A portion is shown here for guidance regarding its form and content.)

diameters of the components following the 2D survey of Orion, velocity components from Gaussian fits, etc.).

We obtained a total column density of ethyl cyanide in the ground state of 4.1×10^{16} cm^{-2}. This result coincides with previous calculations: the source-averaged (hot core) CH_3CH_2CN column density was obtained by Comito et al. (2005) and Schilke et al. (2001) in their Orion surveys at high frequency (795–903 GHz and 607–725 GHz, respectively). However, Sutton et al. (1995) obtained a corrected-source-averaged column density of 2.4×10^{15} and 4.0×10^{15} for the hot core and compact ridge, respectively. In our line survey, we do not distinguish the spectral characteristic of the compact ridge in the ethyl cyanide lines.

For CH_3CH_2CN $\nu_{13} = 1/\nu_{21} = 1$, the derived column density (the same for each state) is one order of magnitude less than the derived column density of ethyl cyanide in the ground state. We obtained a total column density of $\simeq 2 \times 10^{15}$ and $\simeq 8 \times 10^{14}$ cm^{-2} for the ν_{20} and ν_{12} states, respectively.

5.4. Isotopic Abundances

From the derived column densities quoted above, we can now estimate the isotopic abundance ratios.

$^{12}C/^{13}C$. We obtained the same column density ratio for each ^{13}C isotopologue and cloud component: $\simeq 42 \pm 13$. Hence, no isotopic fractionation is found for these isotopologues of ethyl cyanide.

We obtain a factor of two lower than the solar isotopic abundance ($^{12}C/^{13}C = 90$; Anders & Grevesse 1989). This ratio is understood to be a direct measurement of the primary to secondary nuclear processing in stars (see Martín et al. 2010, and references therein) and is considered a sensitive indicator of the degree of galactic chemical evolution. Solar isotope value reflects conditions in the interstellar medium at an earlier epoch (Savage et al. 2002; Wyckoff et al. 2000).

In agreement with our study, Tercero et al. (2010) found an average value of $^{12}C/^{13}C = 45 \pm 20$. This result indicates a

Table 5
Measured Transitions of v_{20} of Ethyl Cyanide[a]

J'	K'_a	K'_c	J''	K''_a	K''_c	ν_{obs}[b] (Hz)	ν_{obs}-ν_{cal}[c] (Hz)	Given Error[d] (Hz)	Flag[e]	Blended?[f]	Weighted Average Peak (Hz)
3	0	3	2	0	2	26839.519	−0.007	0.05			
4	0	4	3	0	3	35751.461	0.021	0.05			
5	0	5	4	0	4	44633.991	0.016	0.05			
6	0	6	5	0	5	53480.380	0.012	0.05			
7	0	7	6	0	6	62284.613	0.013	0.05			
8	0	8	7	0	7	71041.824	−0.011	0.05			
9	0	9	8	0	8	79748.976	0.065	0.05			
10	0	10	9	0	9	88404.817	0.023	0.05			
11	0	11	10	0	10	97010.865	0.007	0.05			
12	0	12	11	0	11	105570.915	0.039	0.05			

Notes.
[a] Lines sorted by type of transition: type of branch: R and Q; dipole moment: μ_a and μ_b; quantum number K_a; quantum number J.
[b] Observed Frequency.
[c] Difference between observed and calculated frequencies.
[d] Error in ν.
[e] Non-fitted lines.
[f] Blended lines.

(This table is available in its entirety in a machine-readable form in the online journal. A portion is shown here for guidance regarding its form and content.)

Table 6
Measured Transitions of v_{12} of Ethyl Cyanide Sorted by Frequency

J'	K'_a	K'_c	J''	K''_a	K''_c	ν_{obs}[a] (Hz)	ν_{obs}-ν_{cal}[b] (Hz)	Given Error[c] (Hz)	Flag[d]	Blended?[e]	Weighted Average Peak (Hz)
2	1	2	1	1	1	17393.370	0.002	0.05			
2	0	2	1	0	1	17864.600	−0.002	0.05			
2	1	1	1	1	0	18350.740	−0.039	0.05			
3	1	3	2	1	2	26085.360	−0.038	0.05			
4	1	3	4	0	4	26097.404	−0.031	0.05			
5	1	4	5	0	5	27406.956	0.125	0.05			
3	1	2	2	1	1	27521.430	0.065	0.05			
6	1	5	6	0	6	29035.680	0.085	0.05			
7	1	6	7	0	7	31012.870	0.027	0.05			
6	0	6	5	1	5	33131.490	−0.042	0.05			

Notes.
[a] Observed Frequency.
[b] Difference between observed and calculated frequencies.
[c] Error in ν.
[d] Non-fitted lines.
[e] Blended lines.

(This table is available in its entirety in a machine-readable form in the online journal. A portion is shown here for guidance regarding its form and content.)

low opacity in the CH_3CH_2CN lines. Previous studies found a similar $^{12}C/^{13}C$ ratio in Orion (Johansson et al. 1984; Blake et al. 1987; Savage et al. 2002; Persson et al. 2007).

$^{14}N/^{15}N$. Our values of this ratio are very similar in all components. The $^{14}N/^{15}N$ average abundance ratio of our study is found to be 148 ± 74. In agreement with previous authors (Blake et al. 1987; Margulès et al. 2009) and within the observational errors, ^{15}N abundance obtained in this work appears to be similar to its terrestrial value ($^{14}N/^{15}N \simeq 274$; Anders & Grevesse 1989). Adande & Ziurys (2012) found that the $^{14}N/^{15}N$ ratio exhibits a distinct positive gradient with increasing distance from the Galactic center (toward 11 molecular clouds). This gradient is consistent with predictions of Galactic chemical evolution models in which ^{15}N has a secondary origin in novae.

D/H. We found a column density ratio for all deuterated species of 0.020 ± 0.010 in all considered components. In close agreement with our values, Tercero et al. (2010) found an $N(HDCS)/N(H_2CS)$ column density ratio of 0.05 ± 0.02 for the hot core component. Depending on the considered molecule and component, we found different values from the work of other authors: using $N(HDO)/N(H_2O)$, Pardo et al. (2001a) found an abundance ratio in the range 0.004–0.01 in the plateau component, and Persson et al. (2007) derived 0.005, 0.001, and 0.03 for the large velocity plateau, the hot core, and the compact ridge, respectively. Schilke et al. (1992) derived the DCN/HCN column density ratio in the hot core region, obtaining 0.001. A recent study of time dependence D/H fractionation from prestellar to protostellar cores (Aikawa et al. 2012) found that, even in warm regions, neutral species with high D/H ratios

Table 7
Measured Transitions of ν_{12} of Ethyl Cyanide[a]

J'	K_a'	K_c'	J''	K_a''	K_c''	ν_{obs}[b] (Hz)	ν_{obs}-ν_{cal}[c] (Hz)	Given Error[d] (Hz)	Flag[e]	Blended?[f]	Weighted Average Peak (Hz)
2	0	2	1	0	1	17864.600	−0.002	0.05			
4	0	4	3	0	3	35670.530	0.008	0.05			
5	0	5	4	0	4	44533.415	−0.032	0.05			
6	0	6	5	0	5	53360.500	−0.108	0.05			
7	0	7	6	0	6	62145.961	−0.045	0.05			
8	0	8	7	0	7	70884.747	−0.022	0.05			
9	0	9	8	0	8	79573.643	0.009	0.05			
10	0	10	9	0	9	88211.405	0.014	0.05			
11	0	11	10	0	10	96799.224	0.052	0.05			
12	0	12	11	0	11	105340.472	−0.003	0.05			

Notes.
[a] Lines sorted by type of transition: type of branch: R and Q; dipole moment: μ_a and μ_b; quantum number K_a; quantum number J.
[b] Observed Frequency.
[c] Difference between observed and calculated frequencies.
[d] Error in ν.
[e] Non-fitted lines.
[f] Blended lines.

(This table is available in its entirety in a machine-readable form in the online journal. A portion is shown here for guidance regarding its form and content.)

Table 8
Detected Lines of CH_3CH_2CN $\nu_{13} = 1/\nu_{21} = 1$

Transition[a] $J_{K_a,K_c,\nu} - J'_{K'_a,K'_c,\nu'}$	Predicted Frequency (MHz)	S_{ij}	E_u[b] (K)	ν_{LSR}[b,c] (km s^{-1})	$\delta\nu^2$ (km s^{-1})	T_{MB}[(2)] (K)	Area[b] (km s^{-1})
$9_{1,9,1}$–$8_{1,8,1}$	80481.139	15.20	330.5	4.3[(1)]		0.13	
$9_{2,8,0}$–$8_{2,7,0}$	80481.228*	15.20	330.5	4.6[(1)]		0.13	
				4.4 ± 0.5	10.6 ± 1.5	0.12	1.4 ± 0.2
$9_{2,8,1}$–$8_{2,7,1}$	80481.228*	15.20	330.5	0.7[(1,3)]		0.09	
$9_{3,7,0}$–$8_{3,6,0}$	80590.893	14.10	325.7	6.6[(1,3)]		0.09	
$9_{3,7,1}$–$8_{3,6,1}$	80592.859*	14.10	325.7	6.0[(1,4)]		0.13	
$9_{3,6,0}$–$8_{3,5,0}$	80715.621	14.10	325.6	6.6[(1,4)]		0.13	
$9_{4,6,0}$–$8_{4,5,0}$	80715.791*	14.10	325.6	4.0[(1,4)]		0.22	
$9_{4,5,2}$–$8_{4,4,2}$	80747.552	12.60	333.0	4.8[(1,4)]		0.22	
$9_{4,6,1}$–$8_{4,5,1}$	80747.778*	12.40	333.0	5.4[(1,4)]		0.22	

Notes.
[a] The line transition in the format $J_{K_a,K_c,\nu} - J_{K'_a,K'_c,\nu'}$. The ν quantum number defines A and E states: $\nu = 0$ is A for the bend and $\nu = 3$ is A for the torsion; $\nu = 1$ and 2 are E for the bend and $\nu = 4$ and 5 are E for the torsion.
[b] The observed parameters are shown when the line is not blended with other molecule and no uncertainty is provided. Calculated parameters have uncertainties and mean the line can not be fitted like a Gaussian or there is some contribution from other molecule. (Narrow component (N), Wide component(W).)
[c] (1) peak line observed velocity. (2) peak line intensity. (3) blended with U-line. (4) blended with CH_3CH_2CN $\nu_{20} = 1$. (5) blended with $(CH_3)_2CO$. (6) blended with $HC^{13}CCN$. (7) blended with $HC^{13}CCN$ $\nu_7 = 1$. (8) blended with E-CH_3OD. (9) blended with $Si^{18}O$. (10) blended with E-$HCOOCH_3$. (11) blended with t-CH_3CH_2OH. (12) blended with $^{33}SO_2$. (13) blended with CH_3CHO $\nu_t = 2$. (14) blended with $SO^{18}O$. (15) blended with SO_2 $\nu_2 = 1$. (16) blended with HCOOH. (17) blended with $CH_3CH_2C^{15}N$. (18) blended with CH_2CHCN $\nu_{11} = 1$. (19) blended with CH_2CHCN $\nu_{15} = 1$. (20) blended with $^{34}SO_2$. (21) blended with HCCCN. (22) influence of CH_3CH_2CN $\nu_{12} = 1$. (23) blended with CH_3CH_2CN. (24) blended with A-$HCOOCH_3$. (25) blended with CH_3OH, $\nu_t = 0, 1$. (26) blended with g-CH_3CH_2OH. (27) blended with $^{13}CH_3OH$ $\nu_t = 0, 1$. (28) blended with $CH_2{}^{13}CHCN$. (29) blended with CH_3OCH_3. (30) blended with $SO^{17}O$. (31) blended with A-$HCOO^{13}CH_3$. (32) blended with E-$HCOO^{13}CH_3$.

(This table is available in its entirety in a machine-readable form in the online journal. A portion is shown here for guidance regarding its form and content.)

reflect the D/H ratio of those species that were injected from dust mantles (where icy material is highly deuterated by surface reactions with D atoms) to the hot gaseous medium. This is in agreement with other studies of hot core deuterium chemistry (Rodgers & Millar 1996). On the other hand, various complex organics (such us methyl formate) are formed via both gas-phase and grain surface reactions. Their high deuteration is mainly due to their formation from molecules with high deuteration (Aikawa et al. 2012). For ethyl cyanide, as a complex organic molecule, the process of deuteration most likely is the later case.

5.5. Vibrational Temperatures

We can estimate vibrational temperatures from

$$\frac{\exp\left(-\frac{E_{\nu_x}}{T_{\rm vib}}\right)}{f_\nu} = \frac{N(CH_3CH_2CN\ \nu_x)}{N(CH_3CH_2CN)}, \quad (1)$$

where E_{ν_x} is the energy of the vibrational state (315.4, 531.2, and 763.4 K for ν_{21}, ν_{20}, and ν_{12}, respectively), $T_{\rm vib}$ is the vibrational temperature, f_ν is the vibrational partition function,

Table 9
Detected Lines of CH_3CH_2CN ν_{20}

Transition[a] $J_{K_a,K_c} - J'_{K'_a,K'_c}$	Predicted Frequency (MHz)	S_{ij}	E_u[b] (K)	v_{LSR}[b,c] (km s^{-1})	δv^2 (km s^{-1})	T_{MB}[(2)] (K)	T_{MB}[(2)b] (K)
$9_{2,8}$–$8_{2,7}$	80470.356	8.55	567.6	4.7[(1)]		0.03	
				5.8 ± 0.7	11.3 ± 1.5	0.03	0.40 ± 0.05
$9_{6,4}$–$8_{6,3}$	80470.356	8.55	567.6	2.0[(1,3)]		0.25	
$9_{6,3}$–$8_{6,2}$	80665.506	5.00	602.9	2.0[(1,3)]		0.25	
$9_{5,5}$–$8_{5,4}$	80665.506*	5.00	602.9	7.6[(1,3)]		0.25	
$9_{5,4}$–$8_{5,3}$	80668.091*	6.22	590.8	7.6[(1,3)]		0.25	
$9_{7,3}$–$8_{7,2}$	80668.091*	6.22	590.8	5.7[(1,3)]		0.25	
$9_{7,2}$–$8_{7,1}$	80669.367*	3.56	617.2	5.7[(1,3)]		0.25	
$9_{2,7}$–$8_{2,6}$	80669.367*	3.56	617.2	6.1[(1,4)]		0.07	
$9_{1,8}$–$8_{1,7}$	81319.905	8.55	567.7	6.1[(1)]		0.05	

Notes.
[a] The line transition in the format $J_{K_a,K_c} - J_{K'_a,K'_c}$.
[b] The observed parameters are shown when the line is not blended with other molecule and no uncertainty is provided. Calculated parameters have uncertainties and mean the line can not be fitted like a Gaussian or there is some contribution from other molecule. (Narrow component (N), Wide component (W).)
[c] (1) peak line observed velocity. (2) peak line intensity. (3) blended with CH_3OH $\nu_t = 0, 1$. (4) blended with $H_2C^{17}O$. (5) blended with U-line. (6) blended with ^{18}OCS. (7) blended with E-$HCOOCH_3$. (8) blended with CH_3CH_2CN ν_{13}/ν_{21}. (9) blended with A-$H^{13}COOCH_3$. (10) blended with E-$H^{13}COOCH_3$. (11) blended with $HCC^{13}CN$ $\nu_7 = 1$. (12) blended with SHD. (13) blended with $CH_3CH_2{}^{13}CN$. (14) influence of CH_3CH_2CN $\nu_{12} = 1$. (15) blended with A-$HCOOCH_3$. (16) blended with CH_3OCH_3. (17) blended with $(CH_3)_2CO$. (18) blended with CH_3CHDCN. (19) blended with $HCOO^{13}CH_3$. (20) blended with $^{33}SO_2$. (21) blended with $HC^{13}CCN$ $\nu_6 = 1$. (22) blended with CH_3-$^{13}CH_2CN$. (23) blended with $H^{15}NCO$.

(This table is available in its entirety in a machine-readable form in the online journal. A portion is shown here for guidance regarding its form and content.)

Table 10
Detected Lines of CH_3CH_2CN ν_{12}

Transition[a] J_{K_a,K_c}–$J'_{K'_a,K'_c}$	Predicted Frequency (MHz)	S_{ij}	E_u (K)	Observed Frequency[b] (MHz)	v_{LSR}[(1)] (km s^{-1})	Observed T_{MB} (K)	Model T_{MB} (K)
$9_{2,8}$–$8_{2,7}$	80288.056	8.55	799.3	80290.1	1.5	0.01	0.02
$9_{8,1}$–$8_{8,0}$	80495.806	1.89	867.3	80496.5	6.4	0.02	0.01
$9_{8,2}$–$8_{8,1}$	80495.806*	1.89	867.3	80496.5	6.4	0.02	0.01
$9_{4,6}$–$8_{4,5}$	80498.676	7.22	813.0	80499.8	4.8	0.02	0.02
$9_{4,5}$–$8_{4,4}$	80499.106*	7.22	813.0	80499.8	6.4	0.02	0.02
$9_{3,7}$–$8_{3,6}$	80528.735	8.00	805.0	80530.5	2.4	0.02	0.02
$9_{3,6}$–$8_{3,5}$	80560.434	8.00	805.0	80562.0	3.2	0.02	0.02
$9_{2,7}$–$8_{2,6}$	81129.013	8.55	799.5	81130.5	3.5	0.03	0.02
$10_{1,10}$–$9_{1,9}$	86693.722	9.90	799.6	86694.4[(2)]	6.8	0.05	0.02
$10_{0,10}$–$9_{0,9}$	88211.372	9.98	799.0	88212.5	5.1	0.01	0.03

Notes.
[a] The line transition in the format $J_{K_a,K_c} - J_{K'_a,K'_c}$.
[b] (1) peak line observed velocity. (2) blended with U-line. (3) blended with ^{33}SO. (4) blended with A-$HCOOCH_3$. (5) blended with c-C_2H_4O. (6) blended with CH_2CHCN $\nu_{11} = 2$. (7) blended with CH_3CH_2CN ν_{13}/ν_{21}. (8) blended with NH_2D. (9) blended with H_2CCO. (10) blended with CH_3-$^{13}CH_2CN$. (11) blended with SO_2 $\nu_2 = 1$. (12) blended with E-$HCOOCH_3$. (13) blended with $^{13}CH_3CH_2CN$.

(This table is available in its entirety in a machine-readable form in the online journal. A portion is shown here for guidance regarding its form and content.)

$N(CH_3CH_2CN\ \nu_x)$ is the column density of the vibrational state, and $N(CH_3CH_2CN)$ is the total column density of ethyl cyanide. Taking into account that $N(CH_3CH_2CN) = N(\text{ground}) \times f_v$, we only need the energy of each vibrational state and the calculated column densities to derive the vibrational temperatures.

We obtained the same T_{vib} in all cloud components for each vibrationally excited level, being $\simeq 160 \pm 50$ K, $\simeq 185 \pm 55$ K, and $\simeq 195 \pm 95$ K, for ν_{13}/ν_{21}, ν_{20}, and ν_{12}, respectively.

The values for ethyl cyanide $\nu_{13} = 1/\nu_{21} = 1$, ν_{20}, and ν_{12} in all components are similar to the averaged kinetic temperature we adopted in this model ($\simeq 150$ K). We assumed that both gases (ground state and vibrationally excited) are spatially coincident, so the calculated vibrational temperatures have to be considered as lower limits.

We note that the obtained T_{vib} for all levels is larger than the T_{rot} in the coldest component, pointing to an inner and hotter emitting region (shown in our model) for vibrationally excited ethyl cyanide. Comparing both temperatures is not an easy task, as temperature and density gradients in the region are required for the vibrational excitation. Collisional rates are necessary to ascertain whether either molecular collisions or IR dust photons dominate the vibrational excitation of ethyl cyanide.

6. CONCLUSION

Very sensitive low frequency Stark modulation experiments have been used to conclusively identify the excited vibrational state ν_{12} of ethyl cyanide. On the basis of fits made from

this work and the previously assigned ν_{20}, reliable rotational and distortion constants were obtained by measurements up to 605 GHz for both states.

The line survey of Orion KL with the IRAM 30 m telescope permitted the assignment of 66 and 56 free of blending spectral features that correspond to the first detection of the ethyl cyanide ν_{20} and ν_{12} species, respectively. The new detection of vibrationally excited ethyl cyanide, together with that of the three ^{13}C and the ^{15}N isotopologues and the tentative detection of deuterated ethyl cyanide (Demyk et al. 2007; Margulès et al. 2009) contributes more than 1000 lines in the 80–280 GHz domain covered by the Orion line survey of Tercero et al. (2010).

The present work clearly shows that the spectroscopic catalogs for heavy species could include the predicted spectra for all their vibrationally excited states with energies below three to four times the kinetic temperature of the gas. For vibrationally excited states with energies similar to the kinetic temperature of the gas, the intensities of their rotational lines will be much larger than those of the isotopologues of the ground state. For example, in Orion $^{12}C/^{13}C \simeq 50$, a vibrational level with $E_{vib} = T_K$ will have a population $\simeq 1/3$ of the ground state. The analysis of the spectral complexity of hot sources such as Orion requires a detailed laboratory study of the vibrational levels below 800 cm^{-1} of the most abundant species (CH_3CN, CH_2CHCN, CH_3CH_2CN, CH_3OH, CH_3OCOH, CH_3OCH_3, HCOOH, HNCO, and so on). Without this information, the analysis of future data coming from more sensitive instruments such as ALMA will be extremely limited.

A.L., J.C., and B.T. thank Spanish MICINN for support under grants AYA2006-14786 and AYA2009-07304. C.B., A.M.D., and J.L.A. thank the Spanish MICINN for the FPI grant (BES-2011-047695) associated with the CTQ2010-19008 project. The Spanish authors also thank the CONSOLIDER program "ASTROMOL" CSD2009-00038 for support. A portion of this work was performed at the Jet Propulsion Laboratory, California Institute of Technology, under contract with NASA. J.C.P. thanks the NASA Astrophysics Research and Analysis program for support.

REFERENCES

Adande, G. R., & Ziurys, L. M. 2012, ApJ, 744, 194
Aikawa, Y., Wakelam, V., Hersant, F., Garrod, R. T., & Herbst, E. 2012, ApJ, 760, 40
Alonso, J. L., Lessari, A. G., Leal, L. A., & López, J. C. 1993, JMoSp, 162, 4
Anders, E., & Grevesse, N. 1989, GeCoA, 53, 197
Blake, G. A., Mundy, L. G., Carlstrom, J. E., et al. 1996, ApJL, 472, L49
Blake, G. A., Sutton, E. C., Masson, C. R., & Philips, T. H. 1987, ApJ, 315, 621
Brauer, C. S., Pearson, J. C., Drouin, B. J., & Yu, S. S. 2009, ApJS, 184, 133
Carvajal, M., Margulès, L., Tercero, B., et al. 2009, A&A, 500, 1109
Cazaux, S., Tielens, A., Ceccarelli, C., et al. 2003, ApJL, 593, L51
Cernicharo, J. 1985, Internal IRAM Report (Granada: IRAM)
Cernicharo, J. 2012, in ECLA-2011: Proc. European Conf. on Laboratory Astrophysics, ed. C. Stehlé, C. Joblin, & L. d'Hendecourt (European Astronomical Society Publications Ser., Vol. 58; Cambridge: Cambridge Univ. Press), 251
Comito, C., Schilke, P., Philips, T. G., et al. 2005, ApJS, 165, 127
Demyk, K., Mäder, H., Tercero, B., et al. 2007, A&A, 466, 255
Demyk, K., Wlodarczak, G., & Carvajal, M. 2008, A&A, 489, 589
Drouin, B. J., Maiwald, F. W., & Pearson, J. C. 2005, RScI, 76, 093133
Duncan, N. E., & Janz, G. J. 1955, JChPh, 23, 434
Fortman, S. M., Medvedev, I. R., Neese, C. F., & De Lucia, F. C. 2010a, ApJ, 714, 476
Fortman, S. M., Medvedev, I. R., Neese, C. F., & De Lucia, F. C. 2010b, ApJ, 725, 1682
Frisch, M. J., Trucks, G. W., Schlegel, H. B., et al. 2009, Gaussian 09, Revision A.02 (Wallingford, CT: Gaussian, Inc.)
Fukuyama, Y., Odashima, H., Takagi, K., & Tsunekawa, S. 1996, ApJS, 104, 329
Fukuyama, Y., Omori, K., Odashima, H., Takagi, K., & Tsunekawa, S. 1999, JMoSp, 193, 72
Goldsmith, P. F., & Langer, W. D. 1999, ApJ, 517, 209
Heise, H. M., Winther, F., & Lutz, H. 1981, JMoSp, 90, 573
Johansson, L. E. B., Andersson, C., Elldér, J., et al. 1984, A&A, 130, 227
Johnson, D. R., Lovas, F. J., Gottlieb, C. A., et al. 1977, ApJ, 218, 370
Kisiel, Z., Pszczolkowski, L., Medvedev, I. R., et al. 2005, JMoSp, 233, 231
Kobayashi, K., Ogata, K., Tsunekawa, S., & Takano, S. 2007, A&A, 657, L17
Krasnicki, A., & Kisiel, Z. 2011, JMoSp, 270, 83
Laurie, V. W. 1959, JChPh, 31, 1500
Lerner, R. G., & Dailey, B. P. 1957, JChPh, 26, 678
Lessari, A. G., Charro, M. E., Villamañán, R. M., et al. 1991, JMoSp, 149, 317
Margulès, L., Huet, T. R., Demaison, J., et al. 2010, ApJ, 714, 1120
Margulès, L., Motiyenko, R., Demyk, K., et al. 2009, A&A, 493, 565
Martín, S., Aladro, R., Martín-Pintado, J., & Mauersberger, R. 2010, A&A, 522, 62
Mehringer, D. M., Pearson, J. C., Keene, J., & Phillips, T. G. 2004, ApJ, 608, 306
Miao, Y. T., & Snyder, L. E. 1997, ApJL, 480, L67
Motiyenko, R., Tercero, B., Cernicharo, J., & Margulès, L. 2012, A&A, 548, 71
Pardo, J. R., Cernicharo, J., Herpin, F., et al. 2001a, ApJ, 562, 799
Pardo, J. R., Cernicharo, J., & Serabyn, E. 2001b, ITAP, 49, 12
Pearson, J. C., Drouin, B. J., Maestrini, A., et al. 2011, RScI, 82, 093105
Pearson, J. C., Sastry, K., Herbst, E., & Delucia, F. C. 1994, ApJS, 93, 589
Persson, C. M., Olofsson, A. O. H., Koning, N., et al. 2007, A&A, 476, 807
Petkie, D. T., Goyette, T. M., Bettens, R. P. A., et al. 1997, RScI, 68, 1675
Pickett, H. M. 1991, JMoSp, 148, 371
Rodgers, S. D., & Millar, T. J. 1996, MNRAS, 280, 1046
Savage, C., Apponi, A. J., Ziurys, L. M., & Wyckoff, S. 2002, ApJ, 578, 211
Schilke, P., Benford, C. J., Hunter, T. R., Lis, D. C., & Philips, T. G. 2001, ApJS, 132, 281
Schilke, P., Walmsley, C. M., Pineau Des Forets, G., et al. 1992, A&A, 256, 595
Sutton, E. C., Peng, R., Danchi, W. C., et al. 1995, ApJS, 97, 455
Tercero, B., Cernicharo, J., Pardo, J. R., & Goicoechea, J. R. 2010, A&A, 517, 96
Tercero, B., Margulès, L., Carvajal, M., et al. 2012, A&A, 538, 119
Tercero, B., Vincent, L., Cernicharo, J., Viti, S., & Marcelino, N. 2011, A&A, 528, 26
Watson, J. K. G. 1977, in Vibrational Spectra and Structure, Vol. 6, ed. J. Durig (Amsterdam: Elsevier), 1
Wright, M. C. H., Plambeck, R. L., & Wilner, D. J. 1996, ApJ, 469, 216
Wyckoff, S., Kleine, M., Peterson, B. A., Wehinger, P. A., & Ziurys, L. M. 2000, ApJ, 535, 991

5.2 Caracterización en el laboratorio y detección astrofísica de estados vibracionalmente excitados de cianuro de vinilo en Orión-KL

Este artículo fue publicado en 2014 en la revista *Astronomy and Astrophysics*. Este trabajo sigue la misma línea de estudio del que hemos presentado anteriormente. En este caso, nos centramos en los estados excitados de baja energía del cianuro de vinilo (CH_2CHCN). El cianuro de vinilo es una molécula muy abundante en nuestra fuente. La emisión de esta especie parece estar relacionada con aquella de CH_3CH_2CN y otros cianuros. En el espectro de Orión-KL se encuentran velocidades radiales y anchuras de línea similares para todas estas especies. Por este motivo, en esta publicación, además de realizar un trabajo análogo al llevado a cabo para CH_3CH_2CN, decidimos hacer un estudio donde se abarcara el análisis de todos los cianuros e isocianuros en la fuente de estudio. De esta manera podríamos caracterizar la emisión de toda una familia de especies moleculares.

El estudio de laboratorio se centró en caracterizar por primera vez 9 estados vibracionales del cianuro de vinilo por encima del nivel $v_{11} = 2$. Este trabajo se llevó a cabo en parelelo al trabajo de laboratorio realizado para el CH_3CH_2CN, durante mi estancia en el Laboratorio de Espectroscopía Molecular de la Universidad de Valladolid. La posterior identificación de estados excitados de hasta una energía cercana a 1000 K en los datos del barrido espectral de Orión-KL con el telescopio de IRAM de 30 m, prueba, una vez más, la importancia de realizar la caracterización de los espectros rotacionales de estas especies. He de insistir en que estos datos de laboratorio se incorporan a los catálogos disponibles para toda la comunidad científica. Con ello hemos contribuido de manera muy significativa a la interpretación de los espectros que se obtienen en observaciones realizadas con instrumentos de última generación, como las que se realizan con ALMA.

Además de resaltar los logros que conseguimos con el trabajo en el laboratorio, quiero señalar que nuestro principal objetivo en todos estas publicaciones es la caracterización físico-química de Orión-KL. En este artículo, una vez identificadas todas las especies de CH_2CHCN que presentan emisión en el barrido de Orión-KL, se llevó a cabo un detallado análisis físico de la región. Hay que señalar que, a pesar de basarnos en datos de antena única, somos capaces de constreñir de manera muy precisa la determinación de distintas componentes de emisión, abundancias y temperaturas. Esto es debido a varios factores: en primer lugar, el amplio rango de frecuencias observado permite el estudio de diferentes regímenes de emisión (por ejemplo, los datos a 3 mm trazan mejor la emisión de las regiones más templadas mientras que a 1 mm las regiones más calientes dominan la emisión); en segundo lugar, nuestros modelos de la fuente son autoconsistentes, en el sentido de que se analiza de manera simultánea la emisión observada tanto del isotopólogo principal como de los isotopólogos menos abundantes y de los estados vibracionalmente excitados. En la segunda parte de este artículo podemos encontrar los resultados obtenidos para el análisis de la emisión global de CH_2CHCN.

Como ya hemos apuntado, en este trabajo también se realizó un estudio comparativo de la emisión de las moléculas que contienen el grupo −CN en la región. Uno de las cuestiones principales que surgen al estudiar estas especies en el medio interestelar es la de si la emisión de sus isómeros (especies con el grupo −NC) puede ser correlacionada. Con ello, se pueden obtener posibles rutas químicas de isomerización en el medio. En este trabajo analizamos la emisión de los isómeros de todas las especies detectadas en Orión-KL que contienen −CN. Con este trabajo, se pudo llevar a cabo un amplia discusión sobre la emisión de los cianuros y los isocianuros en Orión-KL.

Finalmente, gracias a la colaboración en el artículo de Hannah Calcutt y Serena Viti, se modelizaron químicamente las abundancias de estas especies. Para ello se hizo uso del código UCL-CHEM que opera en dos fases: una fase donde se simula la gase gaseosa en condiciones de colapso gravitacional y una segunda donde el núcleo colapsado se calienta y se produce la evaporación de los mantos de los granos de polvo. Con estos modelos se visualiza la evolución de las abundancias moleculares en función del tiempo cuando se introducen una serie de parámetros como, por ejemplo, la masa de la estrella en formación o las abundancias atómicas iniciales.

En las siguientes páginas mostramos el artículo que aquí hemos presentado. Siguiendo con la estructura de esta tesis, en él se puede encontrar la descripción detallada de los estudios realizados. En el Apéndice B se muestran las tablas que forman parte del contenido *online* del artículo y que se pueden encontrar en la base de datos CDS[2].

[2] http://vizier.cfa.harvard.edu/viz-bin/VizieR?-source=J/A+A/572/A44

A&A 572, A44 (2014)
DOI: 10.1051/0004-6361/201423622

Astronomy & Astrophysics

Laboratory characterization and astrophysical detection of vibrationally excited states of vinyl cyanide in Orion-KL⋆,⋆⋆

A. López[1], B. Tercero[1], Z. Kisiel[2], A. M. Daly[3,4], C. Bermúdez[4], H. Calcutt[5], N. Marcelino[6], S. Viti[5], B. J. Drouin[3], I. R. Medvedev[7], C. F. Neese[8], L. Pszczółkowski[2], J. L. Alonso[4], and J. Cernicharo[1]

[1] Centro de Astrobiología (CSIC-INTA), Departamento de Astrofísica Molecular, Ctra. de Ajalvir Km 4, 28850 Torrejón de Ardoz, Madrid, Spain
e-mail: lopezja@cab.inta-csic.es
[2] Institute of Physics, Polish Academy of Sciences, Al. Lotników 32/46, 02-668 Warszawa, Poland
[3] Jet Propulsion Laboratory, California Institute of Technology, 4800 Oak Grove Dr., Pasadena, CA 91109, USA
[4] Grupo de Espectroscopia Molecular (GEM), Unidad Asociada CSIC, Edificio Quifima, Laboratorios de Espectroscopia y Bioespectroscopia, Parque Cientfico UVa, Universidad de Valladolid, 47011, Valladolid, Spain
[5] Department of Physics and Astronomy, University College London, Gower Street, London WC1E 6B, UK
[6] NRAO, 520 Edgemont Road, Charlottesville, VA 22902, USA
[7] Wright State University, 3640 Colonel Glenn Hwy, Dayton, OH 45435, USA
[8] Ohio State University, 191 W. Wooddruff Ave., Columbus, OH 43210, USA

Received 11 February 2014 / Accepted 12 July 2014

ABSTRACT

Context. We perform a laboratory characterization in the 18–1893 GHz range and astronomical detection between 80–280 GHz in Orion-KL with IRAM-30 m of CH_2CHCN (vinyl cyanide) in its ground and vibrationally excited states.
Aims. Our aim is to improve the understanding of rotational spectra of vibrationally excited vinyl cyanide with new laboratory data and analysis. The laboratory results allow searching for these excited state transitions in the Orion-KL line survey. Furthermore, rotational lines of CH_2CHCN contribute to the understanding of the physical and chemical properties of the cloud.
Methods. Laboratory measurements of CH_2CHCN made on several different frequency-modulated spectrometers were combined into a single broadband 50–1900 GHz spectrum and its assignment was confirmed by Stark modulation spectra recorded in the 18–40 GHz region and by ab-initio anharmonic force field calculations. For analyzing the emission lines of vinyl cyanide detected in Orion-KL we used the excitation and radiative transfer code (MADEX) at LTE conditions.
Results. Detailed characterization of laboratory spectra of CH_2CHCN in nine different excited vibrational states: $v_{11} = 1$, $v_{15} = 1$, $v_{11} = 2$, $v_{10} = 1 \Leftrightarrow (v_{11} = 1, v_{15} = 1)$, $v_{11} = 3/v_{15} = 2/v_{14} = 1$, $(v_{11} = 1, v_{10} = 1) \Leftrightarrow (v_{11} = 2, v_{15} = 1)$, $v_9 = 1$, $(v_{11} = 1, v_{15} = 2) \Leftrightarrow (v_{10} = 1, v_{15} = 1) \Leftrightarrow (v_{11} = 1, v_{14} = 1)$, and $v_{11} = 4$ are determined, as well as the detection of transitions in the $v_{11} = 2$ and $v_{11} = 3$ states for the first time in Orion-KL and of those in the $v_{10} = 1 \Leftrightarrow (v_{11} = 1, v_{15} = 1)$ dyad of states for the first time in space. The rotational transitions of the ground state of this molecule emerge from four cloud components of hot core nature, which trace the physical and chemical conditions of high mass star forming regions in the Orion-KL Nebula. The lowest energy vibrationally excited states of vinyl cyanide, such as $v_{11} = 1$ (at 328.5 K), $v_{15} = 1$ (at 478.6 K), $v_{11} = 2$ (at 657.8 K), the $v_{10} = 1 \Leftrightarrow (v_{11} = 1, v_{15} = 1)$ dyad (at 806.4/809.9 K), and $v_{11} = 3$ (at 987.9 K), are populated under warm and dense conditions, so they probe the hottest parts of the Orion-KL source. The vibrational temperatures derived for the $v_{11} = 1$, $v_{11} = 2$, and $v_{15} = 1$ states are 252 ± 76 K, 242 ± 121 K, and 227 ± 68 K, respectively; all of them are close to the mean kinetic temperature of the hot core component (210 K). The total column density of CH_2CHCN in the ground state is $(3.0 \pm 0.9) \times 10^{15}$ cm^{-2}. We report the detection of methyl isocyanide (CH_3NC) for the first time in Orion-KL and a tentative detection of vinyl isocyanide (CH_2CHNC). We also give column density ratios between the cyanide and isocyanide isomers, obtaining a $N(CH_3NC)/N(CH_3CN)$ ratio of 0.002.
Conclusions. Laboratory characterization of many previously unassigned vibrationally excited states of vinyl cyanide ranging from microwave to THz frequencies allowed us to detect these molecular species in Orion-KL. Column density, rotational and vibrational temperatures for CH_2CHCN in their ground and excited states, and the isotopologues have been constrained by means of a sample of more than 1000 lines in this survey.

Key words. ISM: abundances – ISM: molecules – stars: formation – line: identification – methods: laboratory: molecular – radio lines: ISM

⋆ The full Tables A.6–A.14 are only available at the CDS via anonymous ftp to cdsarc.u-strasbg.fr (130.79.128.5) or via http://cdsarc.u-strasbg.fr/viz-bin/qcat?J/A+A/572/A44

⋆⋆ This work was based on observations carried out with the IRAM-30 m telescope. IRAM is supported by INSU/CNRS (France), MPG (Germany), and IGN (Spain).

A&A 572, A44 (2014)

1. Introduction

The rotational spectrum of vinyl cyanide (CH_2CHCN) was first studied in 1954 by Wilcox and collaborators and then later by Costain & Stoicheff (1959), who also investigated the singly-substituted ^{13}C species, as well as the ^{15}N, and the CH_2CDCN species. This molecule was detected for the first time in the interstellar medium (ISM) in 1973 toward the Sagittarius B2 (Sgr B2) molecular cloud (Gardner & Winnewisser 1975). Since then, CH_2CHCN has been detected toward different sources, such as Orion (Schilke et al. 1997), the dark cloud TMC-1 (Matthews & Sears 1983), the circumstellar envelope of the late-type star IRC+10216 (Agúndez et al. 2008), and the Titan atmosphere (Capone et al. 1981). CH_2CHCN is one of the molecules, whose high abundance and significant dipole moment allow radioastronomical detection even of its rare isotopologue species. Thus, vinyl cyanide makes an important contribution to the millimeter and submillimeter spectral emissions covered by high sensitivity facilities, such as ALMA and the *Herschel* Space Telescope. However, there has not yet been a comprehensive study of its low-lying vibrational excited states.

Vinyl cyanide is a planar molecule (six internuclear distances and five independent bond angles) and is a slightly asymmetric prolate rotor with two non-zero electric dipole moment components, which lead to a rich rotational spectrum. The first detailed discussion of the vinyl cyanide microwave spectrum was in 1973 by Gerry & Winnewisser. Subsequent studies of the rotational spectrum of vinyl cyanide resulted in the determination of its electrical dipole moment components by Stolze & Sutter (1985); these values were later improved by Krasnicki & Kisiel (2011) who reported the values $\mu_a = 3.821(3)$ D, $\mu_b = 0.687(8)$ D, and $\mu_{TOT} = 3.882(3)$ D. Additional studies upgraded the molecular structure as Demaison et al. (1994), Colmont et al. (1997), and Krasnicki et al. (2011) successively derived more refined structural parameters from the rotational constants. The ^{14}N nuclear quadrupole hyperfine structure has been studied by Colmont et al. (1997), Stolze & Sutter (1985), and Baskakov et al. (1996).

Kisiel et al. (2009a) updated the rotational constants by simultaneously fitting the rotational lines of CH_2CHCN in its ground and lowest excited state $v_{11} = 1$. They fit the ground states of the ^{13}C and the ^{15}N isotopologues. More detailed analysis of the isotopologue spectra was later reported by Krasnicki et al. (2011). The ground state rotational *a*-type and *b*-type transitions of the parent vinyl cyanide have been assigned up to $J = 129$ with measurements in the laboratory reaching 1.67 THz (Kisiel et al. 2009a). They showed the influence of temperature on the partition function and consequently on the spectrum of vinyl cyanide. Figure 1 of Kisiel et al. (2009a) identifies this effect and the dominance of the millimeter and submillimeter region by the ^aR-type transitions. However, the *b*-type *R*-branch rotational transitions are one order of magnitude more intense than those of *a*-type due to smaller values of the rotational quantum numbers *J* at high frequencies (THz region).

The rotational transitions of CH_2CHCN in several of the lowest vibrational excited states, $v_{11} = 1,2,3$ and $v_{15} = 1$, were assigned by Cazzoli & Kisiel (1988), and the measurements were extended by Demaison et al. (1994) ($v_{11} = 1$ and the ground state). The data for $v_{11} = 3$ was more limited by hindering the determination of all sextic or even quartic constants. Recently, the analysis of broadband rotational spectra of vinyl cyanide revealed that there are perturbations between all pairs of adjacent vibrational states extending upwards from the ground state (g.s.), see Fig. 2 of Kisiel et al. (2009a). Kisiel et al. (2012) covered a broader frequency region (90–1900 GHz) identifying and

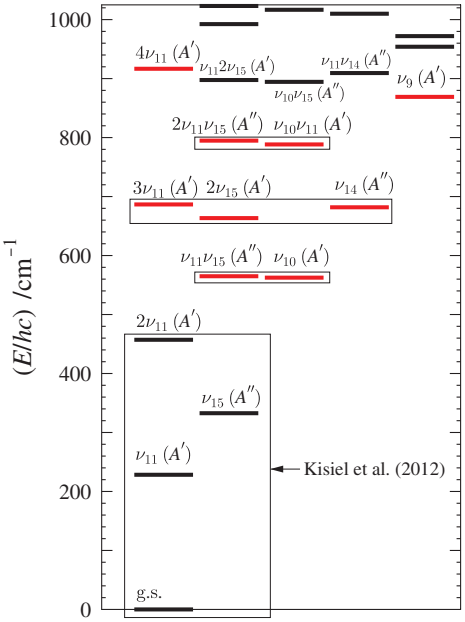

Fig. 1. All vibrational levels of vinyl cyanide up to 1000 cm^{-1}. The levels in red are those for which rotational transitions have been analyzed in this work. The boxes identify sets of levels treated by means of coupled fits accounting for interstate perturbations.

fitting the perturbations in frequencies of rotational transitions due to *a*-, *b*- or *c*-axis Coriolis-type or Fermi type interactions between the four lowest states of vinyl cyanide (g.s., $v_{11} = 1$, $v_{15} = 1$, and $v_{11} = 2$). The need for perturbation treatment of the $v_{10}/v_{11}v_{15}$ dyad at about 560 cm^{-1} and the $3v_{11}/2v_{15}/v_{14}$ triad of states at about 680 cm^{-1} was also identified, and initial results for the dyad were reported in Kisiel et al. (2011). Thus a meticulous analysis aiming toward an eventual global fit of transitions in all states of vinyl cyanide is necessary. The low resolution, gas-phase infrared spectrum of vinyl cyanide and its vibrational normal modes were studied by Halverson et al. (1948) and by Khlifi et al. (1999). Partial rotational resolution of the vibration-rotation spectrum of the two lowest wavenumber modes was also reported in the far-infrared study by Cole & Green (1973).

The first detection in the ISM of vinyl cyanide was in 1973 by means of the 2_{11}–2_{12} line in emission in Sgr B2 and was confirmed in 1975 by Gardner & Winnewisser (1975), suggesting the presence of the simplest olefin in the ISM, CH_2=CH_2 (ethylene) based on the evidence of the reactive vinyl radical. Betz (1981) observed the non-polar organic molecule CH_2=CH_2 toward the red giant C-rich star IRC+10216, for the first time; specifically, this is the v_7 band in the rotation-vibration spectral region (28 THz). Owing to the symmetry of ethylene the dipole rotational transitions are forbidden, and Occhiogroso et al. (2013) estimated a column density of 1.26×10^{14} cm^{-2} in standard hot cores for this molecule based on the abundance of its derivative molecule, hydrocarbon methylacetylene (CH_3CCH).

The dense and hot molecular clouds, such as Orion and Sgr B2, give rise to emission lines of vibrationally excited states of vinyl cyanide. Rotational transitions in the two lowest frequency modes v_{11} and v_{15} were detected in Orion by Schilke et al. (1997) (as tentative detection of three and two lines,

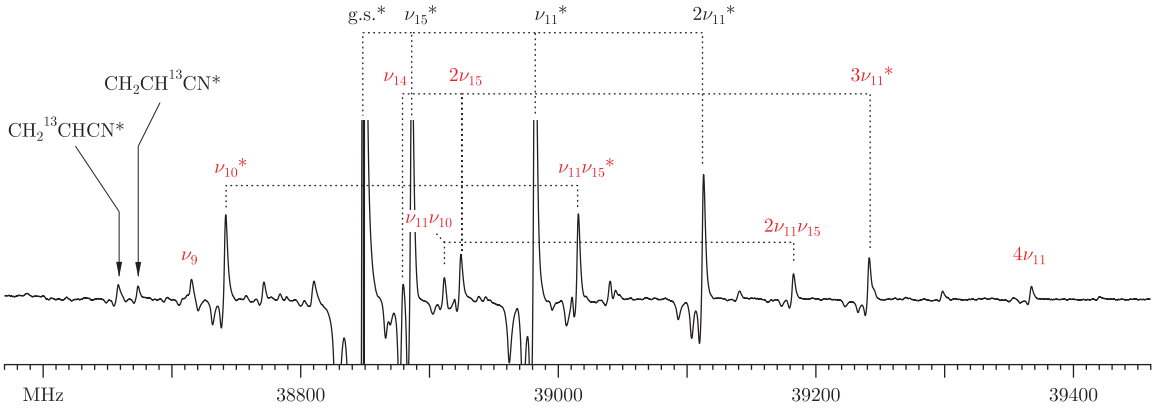

Fig. 2. Room-temperature laboratory spectrum of vinyl cyanide in the region of the $4_{13}-3_{12}$ rotational transition recorded with a Stark modulation spectrometer. All marked lines are for the $4_{13}-3_{12}$ transition in a given vibrational or isotopic species and display a characteristic pattern of negative lobes due to the non-zero field cycle of Stark modulation. Dotted lines connect vibrational states analyzed as perturbing polyads, red denotes vibrational states analyzed in the present work, and asterisks identify states detected presently in Orion-KL. It can be seen that laboratory analysis is now available for excited vibrational state transitions that are comparable in room-temperature intensity to those for ^{13}C isotopologues in terrestrial natural abundance.

respectively) and in Sgr B2 by Nummelin & Bergman (1999) (64 and 45 identified lines, respectively). The latter authors also made the tentative detection transitions in the $2v_{11}$ mode (five lines). Recently, Belloche et al. (2013) detected six vibrational states in a line survey of Sgr B2(N) (v_{11} = 1, 2, 3,v_{15} = 1, 2, v_{11} = v_{15} = 1) among which they detected the higher-lying vibrational states for the first time in space.

On the other hand, the ground states of rare isotopologues have been well characterized in the laboratory (Colmont et al. 1997; Müller et al. 2008; Kisiel et al. 2009a; Krasnicki et al. 2011). All monosubstituted species containing ^{13}C, ^{15}N, and D, and those of all ^{13}C-monosubstituted species of H_2C=CDCN of both cis- and trans- conformers of HDC=CHCN, HDC=CDCN, and D_2C=CDCN have been characterized. The double ^{13}C and $^{13}C^{15}N$ species have also been assigned by Krasnicki et al. (2011). The detection of ^{13}C species of vinyl cyanide in the ISM was carried out toward Sgr B2 by Müller et al. (2008) with 26 detected features.

The millimeter line survey of Orion-KL carried out with the IRAM-30 m telescope by Tercero and collaborators (Tercero et al. 2010, 2011; Tercero 2012) presented 8000 unidentified lines initially. Many of these features (near 4000) have been subsequently identified as lines arising from isotopologues, and vibrationally excited states of abundant species, such as ethyl cyanide and methyl formate, thanks to a close collaboration with different spectroscopic laboratories (Demyk et al. 2007; Margulès et al. 2009; Carvajal et al. 2009; Margulès et al. 2010; Tercero et al. 2012; Motiyenko et al. 2007; Daly et al. 2013; Coudert et al. 2013; Haykal et al. 2014). In this work, we followed the procedure of our previous papers, searching for all isotopologues and vibrationally excited states of vinyl cyanide in this line survey. These identifications are essential to probe new molecular species which reduce the number of U-lines and help to reduce the line confusion in the spectra. At this point we were ready to begin the search for new molecular species in this cloud by providing clues to the formation of complex organic molecules on the grain surfaces and/or in the gas phase (see the discovery of methyl acetate and *gauche* ethyl formate in Tercero et al. 2013, the detection of the ammonium ion in Cernicharo et al. 2013, and the first detection of ethyl mercaptan in Kolesniková et al. 2014).

We report extensive characterization of 9 different excited vibrational states of vinyl cyanide (see Fig. 1) positioned in energy immediately above v_{11} = 2, which, up to this point, has been the highest vibrational state subjected to a detailed study (Kisiel et al. 2012). The assignment is confirmed by using the Stark modulation spectrometer of the spectroscopic laboratory (GEM) of the University of Valladolid and ab initio calculations. The new laboratory assignments of v_{11} = 2, v_{11} = 3, and v_{10} = 1 ⇔ (v_{11} = 1,v_{15} = 1) vibrational modes of vinyl cyanide were used successfully to identify these three states in Orion-KL; the latter for the first time in the ISM. We also detected the v_{11} = 1 and v_{15} = 1 excited states in Orion-KL, as well as the ground state, and the ^{13}C isotopologues (see Sect. 4.2.1).

Because isomerism is a key issue for a more accurate understanding of the formation of interstellar molecules, we report observations of some related isocyanide isomers. Bolton et al. (1970) carried out the first laboratory study of the pure rotation (10–40 GHz) spectrum of vinyl isocyanide and also studied its 200–4400 cm^{-1} vibrational spectrum. Laboratory measurements were subsequently extended up to 175 GHz by Yamada & Winnewisser (1975) and the hyperfine structure of cm-wave lines was measured by Bestmann & Dreizler (1982). In Sect. 4.5, we searched for all isocyanides corresponding to the detected cyanides in Orion-KL: methyl cyanide (Bell et al. 2014), ethyl cyanide (Daly et al. 2013), cyanoacetylene (Esplugues et al. 2013b), cyanamide, and vinyl cyanide. In this study, we have tentatively detected vinyl isocyanide (CH_2CHNC) in Orion-KL (see Sect. 4.5). In addition, we observed methyl isocyanide (CH_3NC) for the first time in Orion-KL, which was observed firstly by Cernicharo et al. (1988) in the Sgr B2(OH) source, and we provide a tentative detection of ethyl isocyanide and isomers HCCNC and HNCCC of isocyanoacetylene. After the detection of cyanamide (NH_2CN) by Turner et al. (1975) in Sgr B2, we report the tentative detection of this molecule in Orion, as well as a tentative detection for isocyanamide.

Finally, we discuss and summarize all results in Sects. 5 and 6.

A&A 572, A44 (2014)

Table 1. Spectroscopic data sets for excited vibrational states of CH_2CHCN acquired in this work.

Excited state	E_{vib}[a] (cm^{-1})	ΔE[b] (cm^{-1})	N_{fitted}[c]	$N_{unfitted}$[d]	σ_{fit}[e] (MHz)	σ_{rms}[f]	J range	K_a range	Frequency range[g] (GHz)
v_{10}	560.5	0	2135[h]	55	0.324	1.446	2–99	0–22	37.0–1893.4
$v_{11}v_{15}$	562.9	2.391494(5)	1837[h]	136	0.382	1.872	3–100	0–20	39.0–1783.5
$2v_{15}$	663.5	0	1329[i]	52	0.265	1.980	1–70	0–17	18.6–1191.3
v_{14}	681.8	18.31812(2)	1287[i]	53	0.228	1.467	5–70	0–18	58.3–1891.1
$3v_{11}$	686.6	23.16415(3)	1250[i]	81	0.309	2.329	2–69	0–17	28.0–1196.5
$v_{10}v_{11}$	787.5	0	842[j]	3	0.137	1.289	3–68	0–12	37.1–639.3
$2v_{11}v_{15}$	793.9	6.44502(3)	860[j]	7	0.164	1.551	3–69	0–12	37.3–640.0
v_9	869.0		373	7	0.167	1.665	1–63	0–7	18.5–570.3
$4v_{11}$	916.7		225	17	0.250	2.496	3–43	0–5	37.4–410.9

Notes. [(a)] Estimated vibrational energy (see text in Sect. 3.2). [(b)] Energy difference relative to the lowest level in the relevant polyad obtained from the perturbation analysis. [(c)] The number of distinct frequency fitted lines. [(d)] The number of confidently assigned lines rejected from the fit at the 10σ cutoff criterion. [(e)] Deviation of fit for the vibrational subset. [(f)] Unitless deviation of fit for the vibrational subset. [(g)] Frequency coverage of transitions in the data set. [(h,i,j)] Transitions fitted jointly in a single fit accounting for interstate perturbations.

2. Experimental

The present spectroscopic analysis is based largely on the broadband rotational spectrum of vinyl cyanide compiled from segments recorded in several different laboratories. That spectrum provided a total of 1170 GHz of coverage and its makeup was detailed in Table 1 of Kisiel et al. (2012). In the present work, the previous spectrum has been complemented by two additional segments: 50–90 GHz and 140–170 GHz recorded at GEM by using cascaded multiplication of microwave synthesizer output. The addition of these segments provides practically uninterrupted laboratory coverage of the room-temperature rotational spectrum of vinyl cyanide over the 50–640 GHz region, which is key to the analysis of vibrational state transitions.

Another laboratory technique brought in by GEM is Stark spectroscopy at cm-wave frequencies. The Stark-modulation technique has the useful property of preferentially recording a given low-J rotational transition by a suitable choice of the modulation voltage. This is particularly the case for the lowest-J, $K_a = 1$ transitions. Due to asymmetry splitting, these transitions are significantly shifted in frequency relative to other transitions for the same J value. An example spectrum of this type is shown in Fig. 2 where all, but some of the weakest lines, correspond to the $4_{13}-3_{12}$ transition in either a vibrational state of the parent vinyl cyanide or the ground state of an isotopic species. Such spectra are particularly useful for an initial assignment since vibrationally induced frequency differences from the ground state are near additive. Relative intensities of transitions also give an immediate measure of relative population of assigned vibrational states and isotopic species.

The analysis of the spectra was carried out with the AABS graphical package for Assignment and Analysis of Broadband Spectra (Kisiel et al. 2005, 2012), which is freely available on the PROSPE database (Kisiel, 2001)[1]. The AABS package was complemented by the SPFIT/SPCAT program package (Pickett 1991)[2] used for setting up the Hamiltonian, fitting, and prediction.

Supporting ab initio calculations were carried out with GAUSSIAN 09[3] and CFOUR[4] packages. The key parameters for vibrational assignment are vibrational changes in rotational constants, which require relatively lengthy anharmonic force field calculations. Two strategies were used for this purpose: a relatively long basis set combined with a basic electron correlation correction (MP2/6-311++G(d,p)) and a more thorough correlation correction with a relatively simple basis set (CCSD(T)/6-31G(d,p)). The final results minimally favored the second approach but, in practice, both were found to be equally suitable.

3. Laboratory spectroscopy

3.1. Analysis of the excited vibrational states

An overview of the results of the spectroscopic analysis is provided in Table 1 and the determined spectroscopic constants necessary for generating linelists are given in Tables 2 and A.1–A.4.

The initial assignment was based on a combination of several techniques: (1) inspection of Stark spectra such as that in Fig. 2; (2) the use of the concept of harmonic behavior of rotational constant changes on vibrational excitation (linear additivity of changes); and (3) ab initio calculations of vibration-rotation constants. The final assignment of vibrational states is confirmed by the comparison of values of experimental vibration-rotation changes in rotational constants relative to the ground state with computed ab initio values, as listed in Table A.5.

Preliminary studies revealed a multitude of perturbations in rotational frequencies that necessitate the use of fits that account for interactions between vibrational states. The grouping of energy levels visible in Fig. 1 suggests that it was possible to break the treatment down into three isolated polyads above the last state studied in detail, namely $2v_{11}$. The symmetry classification of vibrational states (A' and A'', C_s point group) is marked in

[1] http://info.ifpan.edu.pl/~kisiel/prospe.htm
[2] http://spec.jpl.nasa.gov

[3] Frisch, M. J.; Trucks, G. W.; Schlegel, et al., Gaussian 09, Revision B.01; Gaussian: Wallingford, CT, 2010.
[4] Stanton, J. F., Gauss, J.; Harding, M. E. et al., CFOUR, a quantum chemical quantum package with integrated packages MOLECULE (Almlof, J.; Taylor, P. R.) and ECP routines (Mitin, A. V.; van Wüllen, C.), http://www.cfour.de

Table 2. Spectroscopic constants in the diagonal blocks of the Hamiltonian for the $v_{10} \Leftrightarrow v_{11}v_{15}$ and the $v_{11}v_{10} \Leftrightarrow 2v_{11}v_{15}$ dyads of vibrational states in vinyl cyanide compared with those for the ground state.

	Ground state	v_{10}	$v_{11}v_{15}$	$v_{11}v_{10}$	$2v_{11}v_{15}$
A/MHz	49850.69655(43)[a]	49550.03(63)	49890.72(61)	48861.72(62)	49124.87(56)
B/MHz	4971.212565(37)	4965.6692(98)	4992.6723(70)	4984.979(32)	5011.494(25)
C/MHz	4513.828516(39)	4509.6228(13)	4531.6029(13)	4517.9357(31)	4540.0924(32)
Δ_J/kHz	2.244058(13)	2.20646(19)	2.26839(18)	2.24034(23)	2.28278(27)
Δ_{JK}/kHz	−85.6209(35)	−89.854(83)	−80.615(83)	−88.79(17)	−63.97(17)
Δ_K/kHz	2715.4213(94)	2591.5(31)	2522.4(31)	2225.(16)	1842.(15)
δ_J/kHz	0.4566499(32)	0.44642(11)	0.465487(70)	0.46094(18)	0.47422(18)
δ_K/kHz	24.4935(22)	22.099(24)	25.225(14)	25.212(82)	24.683(96)
Φ_J/Hz	0.0064338(17)	0.006345(26)	0.006244(26)	0.006038(38)	0.005952(39)
Φ_{JK}/Hz	−0.00425(40)	0.0541(96)	0.0324(86)	−0.126(17)	−0.244(23)
Φ_{KJ}/Hz	−7.7804(39)	−5.74(11)	−5.18(11)	0.59(23)	1.52(22)
Φ_K/Hz	384.762(63)	399.73(71)	−86.8(11)	428.(396)	−1858.(389)
ϕ_J/Hz	0.00236953(79)	0.002405(22)	0.0021005(36)	0.002185(23)	0.002136(22)
ϕ_{JK}/Hz	0.14283(40)	0.1151(27)	0.1698(18)	0.145(13)	0.135(14)
ϕ_K/Hz	37.011(58)	51.4(12)	38.0(11)	17.1(27)	−5.6(38)
L_J/mHz	−0.000026315(71)	−0.0000263(15)	−0.0000202(14)	[0.]	[0.]
L_{JJK}/mHz	−0.001077(29)	−0.01178(86)	−0.00659(91)	[0.]	[0.]
L_{JK}/mHz	0.4279(30)	−0.0703(85)	[0.]	[0.]	[0.]
L_{KKJ}/mHz	0.012(12)	4.00(18)	−9.63(17)	[0.]	[0.]
L_K/mHz	−61.41(17)	−55.6(29)	462.9(45)	[0.]	[0.]
l_J/mHz	−0.000011602(36)	−0.0000165(13)	[0.]	[0.]	[0.]
l_{JK}/mHz	−0.000956(20)	[0.]	[0.]	[0.]	[0.]
l_{KJ}/mHz	−0.1436(46)	−1.79(11)	−0.86(12)	[0.]	[0.]
l_K/mHz	8.91(18)	[0.]	9.21(43)	[0..]	[0.]
P_{KJ}/mHz	−0.0000156(31)	−0.000147(14)	[0.]	[0.]	[0.]
P_{KKJ}/mHz	−0.0001977(57)	[0.]	[0.]	[0.]	[0.]
P_K/mHz	0.00867(15)	0.0286(23)	−0.3457(49)	[0.]	[0.]
ΔE^b/MHz		0.0	71695.20(16)	0.0	193216.69(90)
ΔE/cm^{-1}		0.0	2.391494(5)	0.0	6.44502(3)
$N^c_{\rm lines}$	4490,0	2135,55	1837,136	842,3	860,7
$\sigma^d_{\rm fit}$/MHz	0.144	0.324[e]	0.382[e]	0.137[f]	0.164[f]
$\sigma^d_{\rm rms}$	0.713	1.446	1.872	1.289	1.551

Notes. [(a)] Round parentheses enclose standard errors in units of the last quoted digit of the value of the constant; square parentheses enclose assumed values. [(b)] The fitted vibrational energy difference relative to the lowest vibrational state in the respective dyad. [(c)] The number of distinct frequency fitted lines and the number of lines rejected at the 10σ fitting criterion of the SPFIT program. [(d)] Deviations of fit for the different vibrational subsets. [(e)] The coupled fit for the $v_{10} \Leftrightarrow v_{11}v_{15}$ dyad encompasses 3978 lines, at an overall $\sigma_{\rm fit}$ of 0.352 MHz and requires also the use of constants reported in Table A.2. [(f)] The coupled fit for the $v_{11}v_{10} \Leftrightarrow 2v_{11}v_{15}$ dyad encompasses 1702 lines, at an overall $\sigma_{\rm fit}$ of 0.151 MHz and requires also the use of constants reported in Table A.2.

Fig. 1 and states of different symmetry need to be connected by a- and b-type Coriolis interactions, while states of the same symmetry are coupled via c-type Coriolis and Fermi interactions. The Hamiltonian and the techniques of analysis used to deal with this type of problem have been described in detail in Kisiel et al. (2009a, 2012). This type of analysis is far from trivial, but its eventual success for the polyads near 560, 680, and 790 cm^{-1} is confirmed in Table 1 by the magnitudes of the deviations of fit in relation to the numbers of fitted lines and their broad frequency coverage. In the most extensive of the present analyses, for the $v_{10} = 1 \Leftrightarrow (v_{11} = 1, v_{15} = 1)$ dyad, the fit encompasses almost 4000 lines in addition to ^aR-type transitions that include ^bQ- and ^bR-types. We use the 10σ cutoff criterion of SPFIT to prevent lines perturbed by factors outside the model from unduly affecting the fit, and a moderate number of such lines (191) are rejected for this dyad. These are confidently assigned lines, generally in high-J tails of some transition sequences for higher values of K_a, but their incompatibility suggests that there is hope for a final global fit with coupling between the polyads. At the present stage, the success of the perturbation fits is further reflected by additive vibrational changes in values of quartic centrifugal distortion constants and by the relative changes in perturbation constants between the two dyads listed in Table A.2, which are similar to those found for the well studied case of $ClONO_2$ (Kisiel et al. 2009b).

Unlike the situation in the ground state of vinyl cyanide (Kisiel et al. 2009a), the perturbations visible in the presently studied polyads are not a spectroscopic curiosity but affect the strongest, low-K_a, ^aR-type transitions. Such transitions occur in the mm- and submm-wave regions which are normally the choice for astrophysical studies. This effect is illustrated by the scaled plots in Fig. 3, which would have the form of near horizontal, very smoothly changing lines in the absence of perturbations. Perturbations lead to the marked spike shaped features in

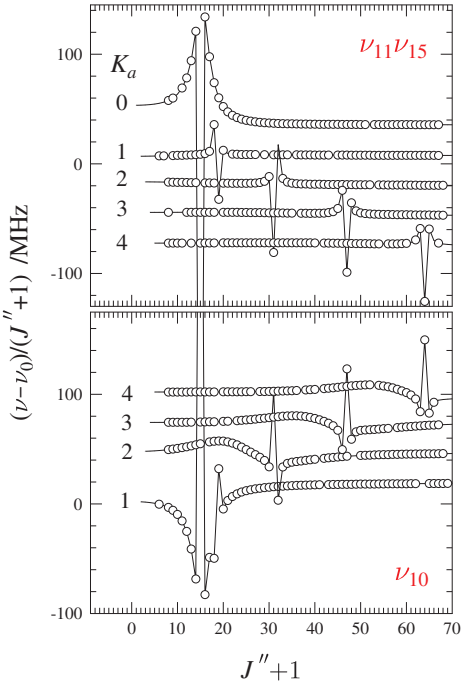

Fig. 3. Effect of vibration-rotation perturbations on frequencies of the strongest rotational transitions in the $v_{10} \Leftrightarrow v_{11}v_{15}$ dyad of vibrational states. The plotted quantities are scaled frequency differences relative to the same transitions in the ground state. Continuous lines are predictions from the final fit; circles mark assigned lines and traces in each panel have added vertical shifts to improve clarity.

these plots. Since evaluation of the Hamiltonian is made in separate blocks for each value of J, the perturbations affecting the two coupling states should have a mirror image form, as seen in Fig. 3. The scaled nature of these plots hides the reason that perturbations to the frequencies of many lines are considerable. For example, the peak of the rightmost spike in Fig. 3 corresponds to a perturbation shift of close to 50 × 64 MHz, namely 3.2 GHz. The frequencies of ^aR-transitions corresponding to the maximum perturbation peaks visible in Fig. 3 are 154.1, 183.4, 301.4, 456.5, and 620.8 GHz for v_{10}, and 131.9, 174.9, 290.3, 443.3, 604.9 GHz for $v_{11}v_{15}$. A significant number of transitions around such peaks are also clearly perturbed. The perturbations are not limited to frequency but also extend to intensities, which are often significantly decreased for pure rotation transitions near the perturbation maxima. The considerable energy level mixing in these cases leads instead to the appearance of transitions between the perturbing vibrational states. These transitions could only be predicted accurately in the final stages of the perturbation analysis but were easily found in the compiled broadband laboratory spectrum and are explicitly identified in the data files. Fortunately, the line lists generated from perturbation fits with the use of the SPCAT program reflect both frequency and intensity perturbations. Accounting for such effects at laboratory experimental accuracy is therefore the key to successful astrophysical studies.

Above the $v_{10}v_{11} \Leftrightarrow 2v_{11}v_{15}$ dyad, the density of vibrational states rapidly increases. The complexity of a thorough analysis appears to be too forbidding at this stage, but it is possible to check how successfully some of these states can be encompassed by single state, effective fits. The v_9 vibrational state seems to be the most isolated, and its analysis could be taken up to $K_a = 7$ and transition frequencies of 570 GHz. In contrast, the easy to locate $4v_{11}$ state exhibited very incomplete sequences of transitions even at low values of K_a, so that its analysis could only be taken up to $K_a = 5$. The very fragmentary nature of line sequences for this state illustrates the limitations of single state approaches, but it nevertheless provides a useful starting point for any future work. The complete results of fit and the primary data files for the SPFIT program for all coupled and single-state effective fits are available online[5], while the predicted linelists will be incorporated in the JPL database.

3.2. Vibrational energies

In Table 1 we report a consistent set of vibrational energies for the studied excited states of vinyl cyanide, which are evaluated by taking advantage of results from the various perturbation analyses. The values for $3v_{11}$ and $4v_{11}$ are from v_{11} and the anharmonicity coefficient $x_{11,11}$ from Kisiel et al. (2012). The value for $v_{11}v_{15}$ comes from v_{11} and v_{15} augmented by $x_{11,15}$, which is calculated at the CCSD(T)/cc-PVDZ level that was benchmarked in Kisiel et al. (2012) as the optimum level for evaluating this type of constant for vinyl cyanide. The remaining vibrational energies in the lower dyad, and the triad are evaluated using the precise ΔE values from the perturbation analyses. Finally, $v_{10}v_{11}$ comes from v_{10} and v_{11} augmented by ab initio $x_{10,11}$. A double check of this procedure is provided by an alternative evaluation for $2v_{15}$ based on ab initio $x_{15,15}$, which gives a result within 0.5 cm^{-1} of the more reliable tabulated value. Only the vibrational energy for v_9 comes from the low resolution gas phase infrared spectrum (Halverson et al. 1948).

4. Astronomical detection of vinyl cyanide species

Thanks to these new laboratory data, we identified and detected the $v_{10} = 1 \Leftrightarrow (v_{11} = 1, v_{15} = 1)$ vibrational modes of CH_2CHCN for the first time in space. A consistent analysis of all detected species of vinyl cyanide have been made to outline the knowledge of our astrophysical environment. We also report the detection of methyl isocyanide for the first time in Orion KL and a tentative detection of vinyl isocyanide and calculate abundance ratios between the cyanide species and their corresponding isocyanide isomers.

4.1. Observations and overall results

4.1.1. 1D Orion-KL line survey

The line survey was performed over three millimeter windows (3, 2, and 1.3 mm) with the IRAM-30 m telescope (Granada, Spain). The observations were carried out between September 2004 and January 2007 pointing toward the IRc2 source at $\alpha_{2000.0} = 5^h35^m14.5^s$ and $\delta_{2000.0} = -5°22'30.0''$. All the observations were performed using the wobbler switching mode with a beam throw in azimuth of ±120″. System temperatures were in the range of 100–800 K from the lowest to the highest frequencies. The intensity scale was calibrated using the atmospheric transmission model (ATM, Cernicharo 1985; Pardo et al. 2001a). Focus and pointing were checked every 1–2 h. Backends provided a spectrum of 1–1.25 MHz of spectral resolution. All

[5] http://info.ifpan.edu.pl/~kisiel/data.htm

spectra were single-side band reduced. For further information about observations and data reduction, see Tercero et al. (2010)[6].

All figures are shown in main beam temperature (T_{MB}) that is related to the antenna temperature (T_A^*) by the equation: $T_{MB} = T_A^*/\eta_{MB}$, where η_{MB} is the main beam efficiency which depends on the frequency.

According to previous works, we characterize at least four different cloud components overlapping in the beam in the analysis of low angular resolution line surveys of Orion-KL (see, e.g., Blake et al. 1987, 1996; Tercero et al. 2010, 2011): (i) a narrow (∼4 km s^{-1} line-width) component at $v_{LSR} \simeq 9$ km s^{-1} delineating a north-to-south *extended ridge* or ambient cloud or an extended region with $T_k \simeq 60$ K, $n(H_2) \simeq 10^5$ cm^{-3}; (ii) a compact ($d_{sou} \simeq 15''$) and quiescent region, or the *compact ridge*, ($v_{LSR} \simeq 7$–8 km s^{-1}, $\Delta v \simeq 3$ km s^{-1}, $T_k \simeq 150$ K, $n(H_2) \simeq 10^6$ cm^{-3}); (iii) the *plateau*, or a mixture of outflows, shocks, and interactions with the ambient cloud ($v_{LSR} \simeq 6$–10 km s^{-1}, $\Delta v \gtrsim 25$ km s^{-1}, $T_k \simeq 150$ K, $n(H_2) \simeq 10^6$ cm^{-3}, and $d_{sou} \simeq 30''$); (iv) a *hot core* component ($v_{LSR} \simeq 5$ km s^{-1}, $\Delta v \simeq 5$–15 km s^{-1}, $T_k \simeq 250$ K, $n(H_2) \simeq 5 \times 10^7$ cm^{-3}, and $d_{sou} \simeq 10''$). Nevertheless, we found a more complex structure of that cloud (density and temperature gradients of these components and spectral features at a v_{LSR} of 15.5 and 21.5 km s^{-1} related with the outflows) in our analysis of different families of molecules (see, e.g., Tercero et al. 2011; Daly et al. 2013; Esplugues et al. 2013a).

4.1.2. 2D survey observations

We also carried out a two-dimensional line survey with the same telescope in the ranges 85–95.3, 105–117.4, and 200.4–298 GHz (N. Marcelino et al. priv. comm.) during 2008 and 2010. This 2D survey consists of maps of 140 × 140 arcsec^2 area with a sampling of 4 arcsec using a On-The-Fly mapping mode with a reference position 10 arcmin west of Orion-KL. The EMIR heterodyne receivers were used for all the observations except for 220 GHz frequency setting, for which the HERA receiver array was used. As backend, we used the WILMA backend spectrometer for all spectra (bandwidth of 4 GHz and 2 MHz of spectral resolution) and the FFTS (Fast Fourier Transform Spectrometer, 200 kHz of spectral resolution) for frequencies between 245–259, 264.4–278.6, and 289–298 GHz. Pointing and focus were checked every 2 h giving errors less than 3 arcsec. The data were reduced using the GILDAS package[7] by removing bad pixels, checking for image sideband contamination and emission from the reference position, and fitting and removing first order baselines. Six transitions of CH_2CHCN have been selected to study the spatial extent of their emission with this 2D line survey.

4.2. Results

4.2.1. Detection of CH_2CHCN: its vibrationally excited states and its isotopologues in Orion-KL

Vinyl cyanide shows emission from a large number of rotational lines through the frequency band 80–280 GHz. The dense and hot conditions of Orion-KL populate the low-lying energy excited states. Here, we present the first interstellar detection of the $v_{10} = 1 \Leftrightarrow (v_{11} = 1, v_{15} = 1)$ vibrational excited state.

Figures 4–8 and A.1 show selected detected lines of the g.s. of vinyl cyanide and five vibrationally excited states of the main isotopologue CH_2CHCN: in plane C-C≡N bending mode ($v_{11} = 1$, 228.1 cm^{-1} or 328.5 K), out of plane C-C≡N bending mode ($v_{15} = 1$, 332.7 cm^{-1} or 478.6 K), in plane C-C≡N bending mode ($v_{11} = 2$, 457.2 cm^{-1} or 657.8 K), in a combination state ($v_{10} = 1 \Leftrightarrow (v_{11} = 1, v_{15} = 1)$, 560.5/562.9 cm^{-1} or 806.4/809.9 K), and in plane C-C≡N bending mode ($v_{11} = 3$, 686.6 cm^{-1} or 987.9 K). The latter is in the detection limit, so we do not address the perturbations of this vibrational mode.

In addition, we detected the following isotopologues of vinyl cyanide in its ground state: $^{13}CH_2CHCN$, $CH_2{}^{13}CHCN$, and $CH_2CH^{13}CN$ (see Fig. 9). For $CH_2CHC^{15}N$ and the deuterated species of vinyl cyanide, DCHCHCN, HCDCHCN, and CH_2CDCN (see Fig. A.2), we only provided a tentative detection in Orion-KL because of the small number of lines with an uncertainty in frequency less than 2 MHz (up to $K_a = 7, 5, 15$ for DCHCHCN, HCDCHCN, and CH_2CDCN, respectively), the weakness of the features, and/or their overlap with other molecular species.

Tables A.6–A.13 show observed and laboratory line parameters for the ground state, the vibrationally excited states, and the ^{13}C-vinyl cyanide isotopologues. Spectroscopic constants were derived from a fit with the MADEX code (Cernicharo 2012) to the lines reported by Kisiel et al. (2009a, 2012), Cazzoli & Kisiel (1988), and Colmont et al. (1997). For the $v_{10} = 1 \Leftrightarrow (v_{11} = 1, v_{15} = 1)$ state, spectroscopic constants are those derived in this work; dipole moments were from Krasnicki & Kisiel (2011). All these parameters have been implemented in MADEX to obtain the predicted frequencies and the spectroscopic line parameters. We have displayed rotational lines that are not strongly overlapped with lines from other species. Observational parameters have been derived by Gaussian fits (using the GILDAS software) to the observed line profiles that are not blended with other features. For moderately blended and weak lines, we show observed radial velocities and intensities given directly from the peak channel of the line in the spectra, so contribution from other species or errors in baselines could appear for these values. Therefore, the main beam temperature for the weaker lines ($T_{MB} < 0.1$ K) must be considered as an upper limit.

From the derived Gaussian fits, we observe that vinyl cyanide lines reflect the spectral line parameters corresponding to hot core/plateau components (v_{LSR} between 2–3 km s^{-1} for the component of 20 km s^{-1} of line width, and 5–6 km s^{-1} for the component of 6 km s^{-1} of line width). As shown by Daly et al. (2013) there is a broad component associated to the hot core that limits the accuracy of the derived velocities for the hot core and this broad component. Our velocity components for CH_2CHCN agree with those of CH_3CH_2CN obtained by Daly et al. (2013). Besides, for the vibrationally excited states, we found contribution of a narrow component with a v_{LSR} of 3–6 km s^{-1} and a line width of ≃7 km s^{-1}.

We rely on catalogs[8] to identify possible contributions from other species overlapping the detected lines (Tercero 2012), but it should be necessary to perform radiative transfer modeling with all the known molecules in order to precisely assess how much the contamination from other species influences the vinyl cyanide lines.

[6] The data of the IRAM-30 m line survey of Orion-KL are available is ASCII format on request to B. Tercero and J. Cernicharo and will be available on the IRAM web page.

[7] http://www.iram.fr/IRAMFR/GILDAS

[8] Cernicharo private catalogs, CDMS (Müller et al. 2001, 2005), and JPL (Pickett et al. 1998).

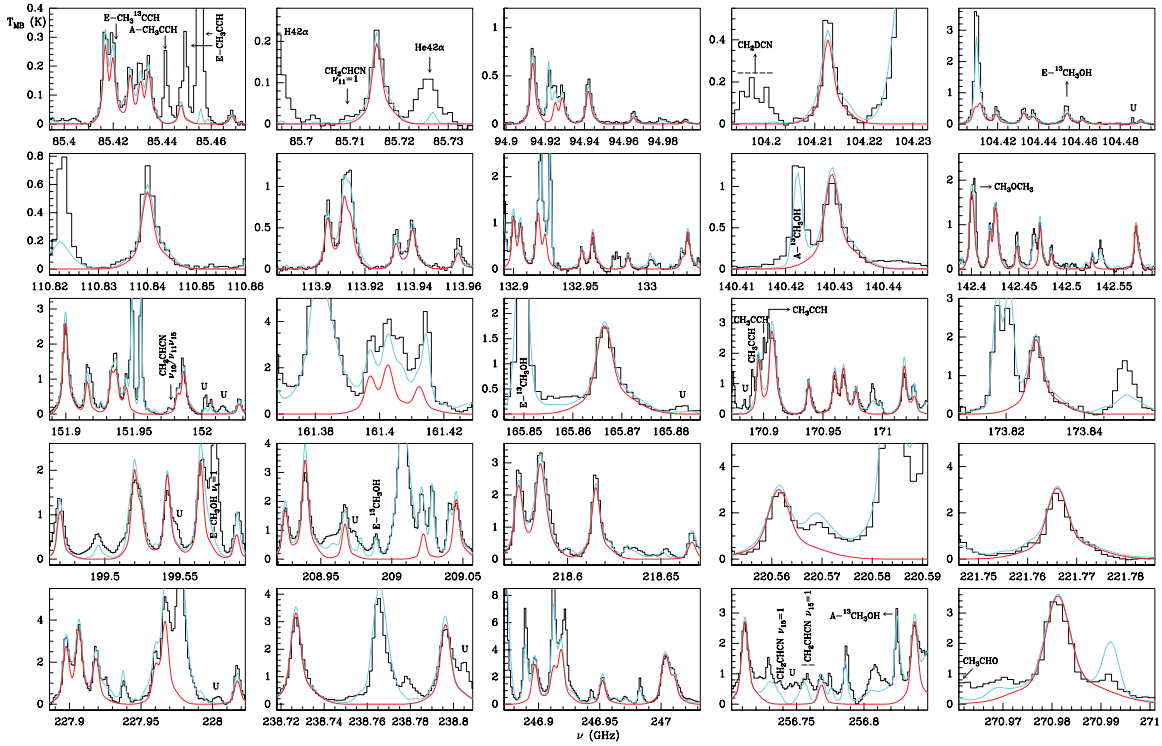

Fig. 4. Observed lines from Orion-KL (histogram spectra) and model (thin red curves) of vinyl cyanide in the ground state. The cyan line corresponds to the model of the molecules we have already studied in this survey (see text Sect. 4.4.2), including the CH_2CHCN species. A v_{LSR} of 5 km s^{-1} is assumed.

Table 3. Number of identified lines of CH_2CHCN species.

Species	Detectable	Unblended	Partially blended	Totally blended
CH_2CHCN g. s. (a-type)	350	204 (59%)	85 (24%)	61 (17%)
CH_2CHCN $v_{11}=1$	307	111 (36%)	75 (25%)	121 (39%)
CH_2CHCN $v_{11}=2$	253	59 (23%)	35 (14%)	159 (63%)
CH_2CHCN $v_{11}=3$	245	30 (12%)	33 (14%)	182 (74%)
CH_2CHCN $v_{15}=1$	287	68 (24%)	62 (22%)	157 (55%)
CH_2CHCN $v_{10}=1 \Leftrightarrow (v_{11}=1, v_{15}=1)$	474	65 (14%)	64 (14%)	345 (73%)
(^{13}C)-CH_2CHCN	348	102 (29%)	115 (33%)	131 (38%)

Table 3 shows the number of lines of vinyl cyanide identified in this work. Our identifications are based on a whole inspection of the data and the modeled synthetic spectrum of the molecule we are studying (where we obtain the total number of detectable lines) and all species already identified in our previous papers. We consider blended lines when these are close enough to other stronger features. Unblended features are those, which present the expected radial velocity (matching our model with the peak channel of the line) (see, e.g., lines at 115.00 and 174.36 GHz in Fig. 5 or the line at 247.55 GHz in Fig. 8), and there are not another species at the same observed frequency (±3 MHz) with significant intensity. Partially blended lines are those which present either a mismatch in the peak channel of the line or significant contribution from another species at the peak channel of the feature (see, e.g., the line at 108.16 GHz in Fig. 8). Generally, these lines also present a mismatch in intensity; see, e.g., line at 152.0 GHz in Fig. 6. If we do not found the line for the unblended frequencies we are looking for, then we do not claim detection, so we do not accept missing lines in the detected species. For species with quite strong lines (g.s., $v_{11}=1$, and $v_{15}=1$), most of the totally and partially blended lines are weaker due to the high energy of their transitions (see Tables A.6, A.8, and A.11). We observed a total number of ≃640 unblended lines of vinyl cyanide species. Considering also the moderately blended lines, this number rises to ≃1100. We detected lines of vinyl cyanide in the g.s. with a maximum upper level energy value of about 1400–1450 K by corresponding to a $J_{max}=30$ and a $(K_a)_{max}=24$. For the vibrational states we observed transitions with maximum quantum rotational numbers of $(K_a)_{max}=20,15,17,16,15$ from the lowest energy vibrational

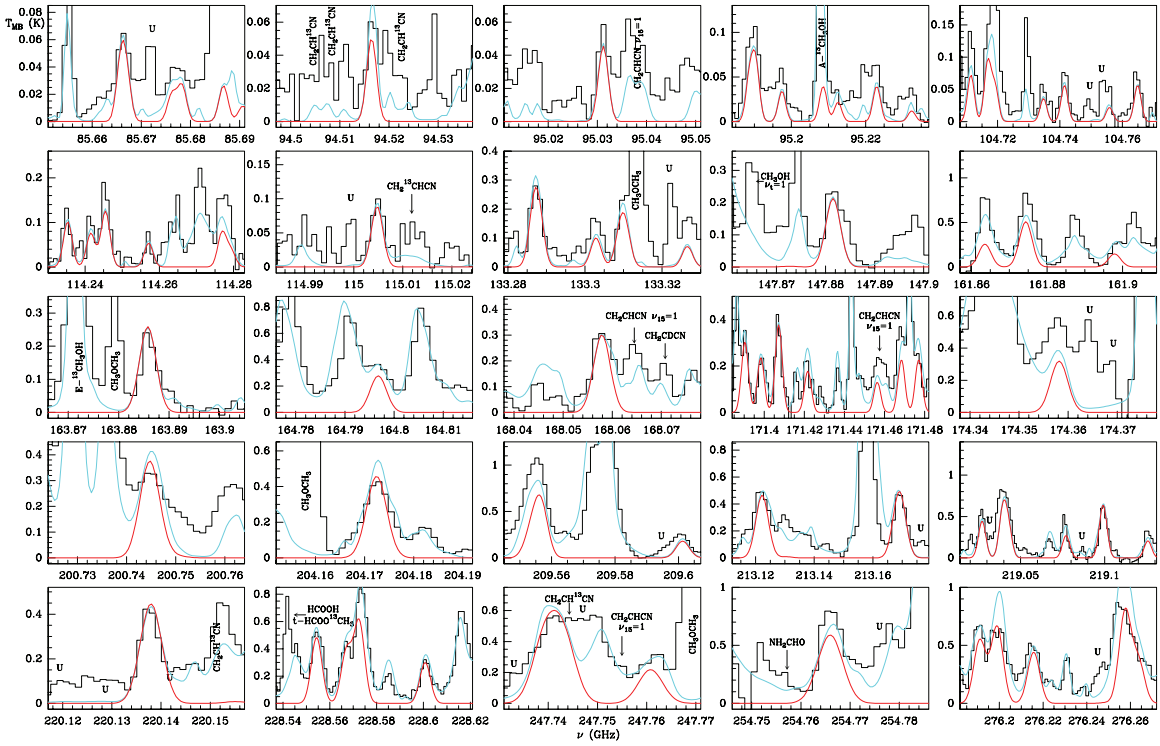

Fig. 5. Observed lines from Orion-KL (histogram spectra) and model (thin red curves) of CH_2CHCN of v_{11} = 1. The cyan line corresponds to the model of the molecules we have already studied in this survey (see text Sect. 4.4.2), including the CH_2CHCN species. A v_{LSR} of 5 km s^{-1} is assumed.

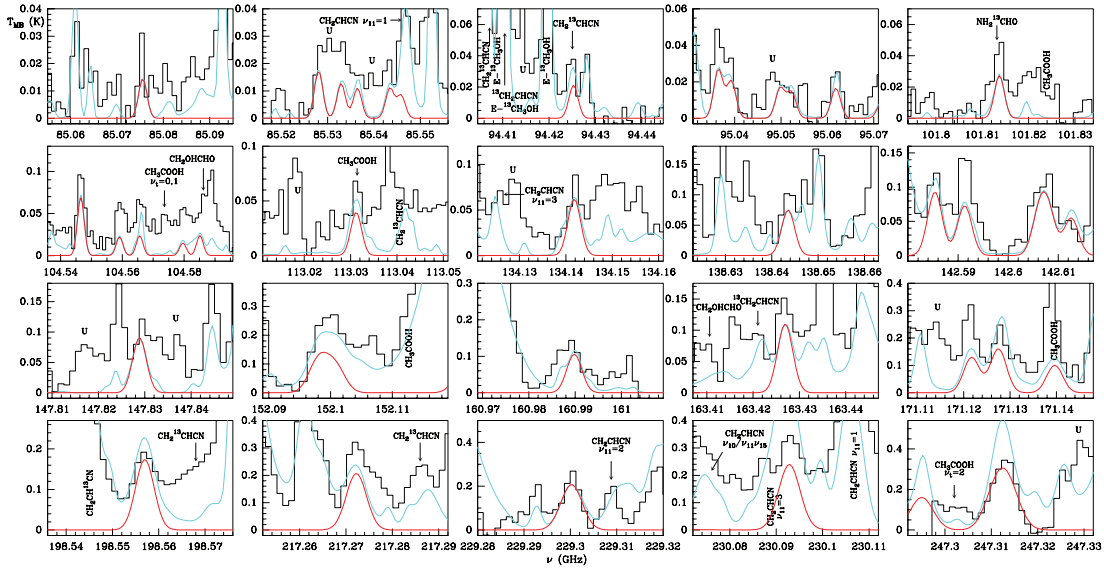

Fig. 6. Observed lines from Orion-KL (histogram spectra) and model (thin red curves) for the v_{15} = 1 vibrational state of CH_2CHCN. The cyan line corresponds to the model of the molecules we have already studied in this survey (see text Sect. 4.4.2), including the CH_2CHCN species. A v_{LSR} of 5 km s^{-1} is assumed.

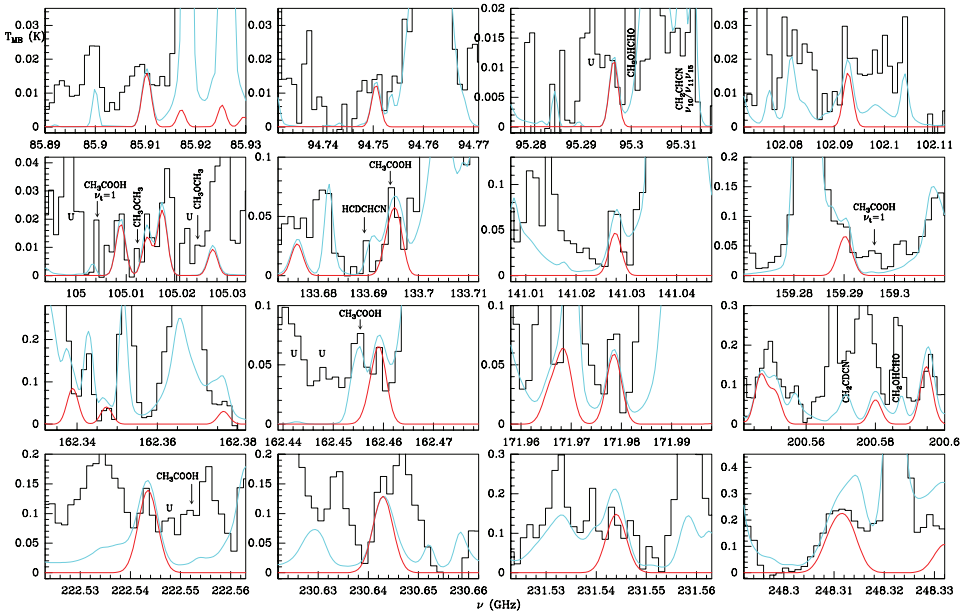

Fig. 7. Observed lines from Orion-KL (histogram spectra) and model (thin red curves) for the $v_{11} = 2$ vibrational state of CH_2CHCN. The cyan line corresponds to the model of the molecules we have already studied in this survey (see text Sect. 4.4.2), including the CH_2CHCN species. A v_{LSR} of 5 km s^{-1} is assumed.

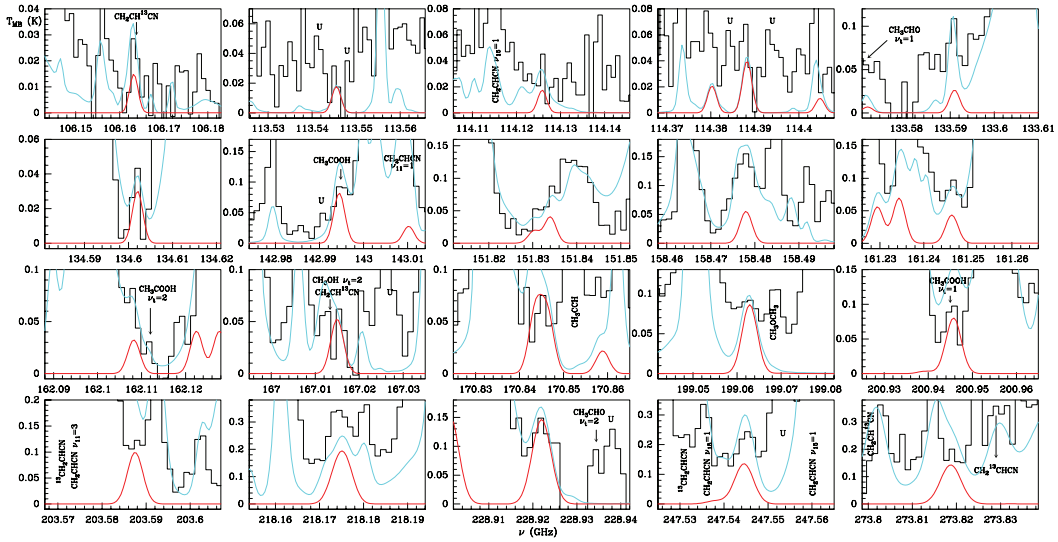

Fig. 8. Observed lines from Orion-KL (histogram spectra) and model (thin red curves) for combined vibrationally excited states of CH_2CHCN in the $v_{10} = 1 \Leftrightarrow (v_{11} = 1, v_{15} = 1)$ dyad. The cyan line corresponds to the model of the molecules we have already studied in this survey (see text Sect. 4.4.2), including the CH_2CHCN species. A v_{LSR} of 5 km s^{-1} is assumed.

state to the highest (i.e., from $v_{11} = 1$ to $v_{11} = 3$) and the same $J_{max} = 30$ value up to the maximum E_{upp} between 1300–1690 K.

4.2.2. CH_2CHCN maps

Figure 10 shows maps of the integrated emission of six transitions in the g.s. of CH_2CHCN at different velocity ranges. From line 1 to 6: $12_{1,12}$–$11_{1,11}$ (110 839.98 MHz, E_{upp} = 36.8 K), $24_{0,24}$–$23_{0,23}$ (221 766.03 MHz, E_{upp} = 134.5 K), $24_{2,23}$–$23_{2,22}$ (226 256.88 MHz, E_{upp} = 144.8 K), $26_{1,26}$–$25_{1,25}$ (238 726.81 MHz, E_{upp} = 157.4 K), $26_{2,25}$–$25_{2,24}$ (244 857.47 MHz, E_{upp} = 167.9 K), and $24_{10,15}$–$23_{10,14}$ and $24_{10,14}$–$23_{10,13}$ (228 017.34 MHz, E_{upp} = 352.0 K). These maps reveal the emission from two cloud components: a component

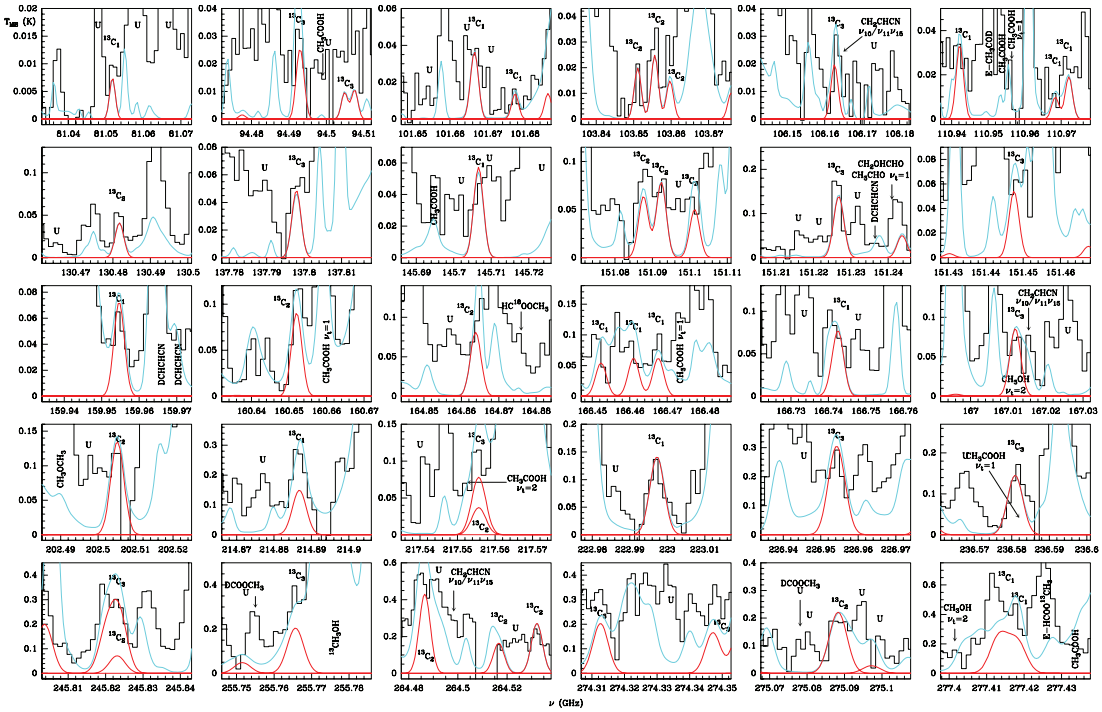

Fig. 9. Observed lines from Orion-KL (histogram spectra) and model (thin red curves) of ^{13}C isotopes for CH_2CHCN in the ground state. The subindex in $^{13}C_i$ (i = 1, 2, 3) corresponds to the position of the isotope in the molecule ($^{i_1}CH_2^{i_2}CH^{i_3}CN$). The cyan line corresponds to the model of the molecules we have already studied in this survey (see text Sect. 4.4.2), including the CH_2CHCN species. A v_{LSR} of 5 km s^{-1} is assumed.

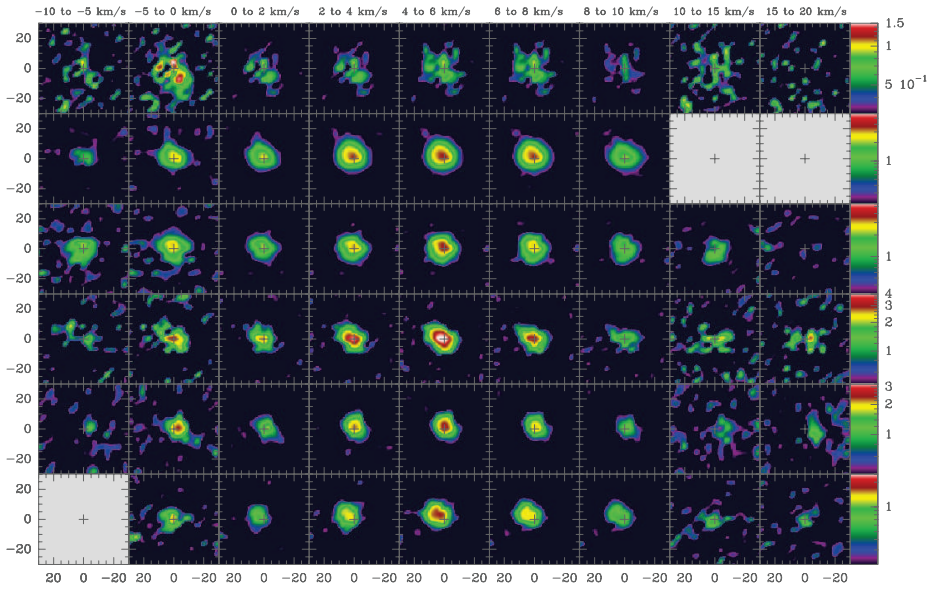

Fig. 10. Integrated intensity maps for 6 ground state transitions of vinyl cyanide. From line 1 (*top row*) to 6 (*bottom row*): $12_{1,12}$–$11_{1,11}$ (110 839.98 MHz, 36.8 K), $24_{0,24}$–$23_{0,23}$ (221 766.03 MHz, 134.5 K), $24_{2,23}$–$23_{2,22}$ (226 256.88 MHz, 144.8 K), $26_{1,26}$–$25_{1,25}$ (238 726.808 MHz, 157.4 K), $26_{2,25}$–$25_{2,24}$ (244 857.47 MHz, 167.9 K), and $24_{10,15}$–$23_{10,14}$ and $24_{10,14}$–$23_{10,13}$ (228017.34 MHz, 352.0 K) at different velocity ranges (indicated in the top of each column). Three boxes have been blanked because the emission at these velocities was blended with that from other well known species. For each box axis are in units of arcseconds ($\Delta\alpha$, $\Delta\delta$). Color logarithm scale is the integrated intensity ($\int T_A^* \mathrm{d}v$) in units of K km s^{-1}.

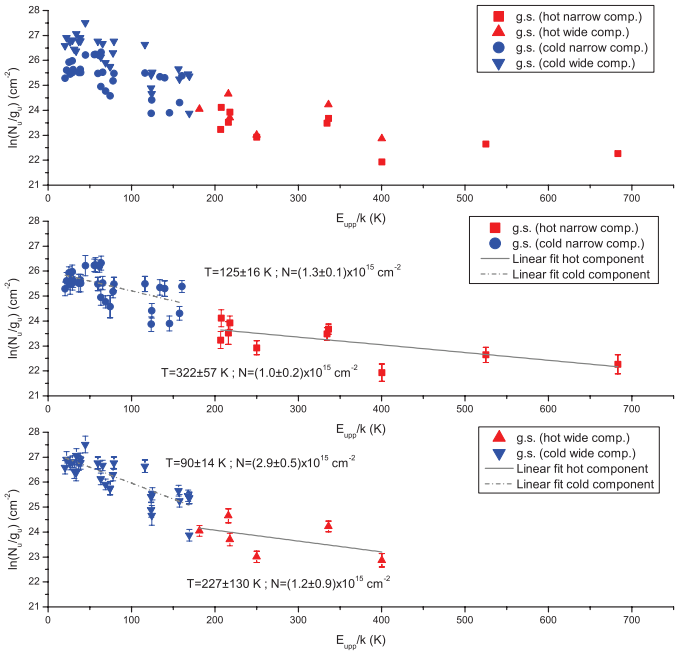

Fig. 11. Rotational diagram of CH_2CHCN in its ground state. The *upper panel* displays the two components derived from the line profiles. The *middle panel* shows two linear fits to the narrow component points; these linear regressions yield temperatures and column densities of $T_{\rm rot} = 125 \pm 16$ K and $N = (1.3 \pm 0.1) \times 10^{15}$ cm^{-2} ($Q_{\rm rot} = 7.06 \times 10^3$), and $T_{\rm rot} = 322 \pm 57$ K and $N = (1.0 \pm 0.2) \times 10^{15}$ cm^{-2} ($Q_{\rm rot} = 2.92 \times 10^4$). Likewise, the *bottom panel* shows another two linear fits to the points corresponding to the wide component. The results of these fits are rotational temperatures of $T_{\rm rot} = 90 \pm 14$ K and $T_{\rm rot} = 227 \pm 130$ K, and column densities of $(2.9 \pm 0.5) \times 10^{15}$ cm^{-2} ($Q_{\rm rot} = 4.31 \times 10^3$) and $(1.2 \pm 0.9) \times 10^{15}$ cm^{-2} ($Q_{\rm rot} = 1.73 \times 10^4$), respectively.

at the position of the hot core at velocities from 2 to 8 km s^{-1} and a component with a slight displacement of the intensity peak at the extreme velocities. The intensity peak of the central velocities coincides with that of the -CN bearing molecules found by Guélin et al. 2008 (maps of one transition of ethyl and vinyl cyanide) and Daly et al. (2013) (maps of four transitions of ethyl cyanide). We note a more compact structure in the maps of the transitions at 352.0 K. Our maps do not show a more extended component found in the ethyl cyanide maps by Daly et al. (2013). We have obtained an angular source size between 7″–10″ (in agreement with the hot core diameter provided by different authors; see, e.g., Crockett et al. 2014; Neil et al. 2013; Beuther & Nissen 2008) for central and extreme velocities by assuming emission within the half flux level and corrected for the size of the telescope beam at the observed frequency. These integrated intensity maps allow us to provide the offset position with respect to IRc2 and the source diameter parameters needed for modeling the vinyl cyanide species (see Sect. 4.4.1).

4.3. Rotational diagrams of CH_2CHCN (g.s., $v_{11} = 1$, 2, and $v_{15} = 1$)

To obtain an estimate of the rotational temperature ($T_{\rm rot}$) for different velocity components, we made rotational diagrams, which related the molecular parameters with the observational ones (Eq. (1); see e.g., Goldsmith & Langer 1999) for CH_2CHCN in its ground state (Fig. 11) and for the lowest vibrationally excited states $v_{11} = 1$, 2, and $v_{15} = 1$ (Fig. 12). Assumptions, such as LTE approximation and optically thin lines (see Sect. 4.4.4), are required in this analysis. We have taken the effect of dilution of the telescope into account, which was corrected by calculation of the beam dilution factor (Demyk et al. 2008, Eq. (2)):

$$\ln\left(\frac{N_{\rm u}}{g_{\rm u}}\right) = \ln\left(\frac{8\pi k\nu^2 W_{\rm obs}}{hc^3 A_{\rm ul} g_{\rm u}}\right) = \ln\left(\frac{N}{Q_{\rm rot}}\right) - \frac{E_{\rm upp}}{kT_{\rm rot}} + \ln b, \quad (1)$$

$$b = \frac{\Omega_{\rm S}}{\Omega_{\rm A}} = \frac{\theta_{\rm S}^2}{\theta_{\rm S}^2 + \theta_{\rm B}^2}, \quad (2)$$

where $N_{\rm u}$ is the column density of the considered vinyl cyanide species in the upper state (cm^{-2}), $g_{\rm u}$ is the statistical weight in the upper level, $W_{\rm obs}$ (K cm s^{-1}) is the integrated line intensity ($W_{\rm obs} = \int T_{\rm MB_{obs}}(v)dv$), $A_{\rm ul}$ is the Einstein A-coefficient for spontaneous emission, N (cm^{-2}) is the total column density of the considered vinyl cyanide species, $Q_{\rm rot}$ is the rotational partition function, which depends on the rotational temperature derived from the diagrams, $E_{\rm upp}$ (K) is the upper level energy, and $T_{\rm rot}$ (K) is the rotational temperature. In Eq. (2), b is the beam dilution factor, $\Omega_{\rm S}$ and $\Omega_{\rm A}$ are the solid angle subtended by the source and under the main beam of the telescope, respectively, and $\theta_{\rm S}$ and $\theta_{\rm B}$ are the angular diameter of the source and the beam of the telescope, respectively. We note that the factor b increases the fraction N_u/g_u in Eq. (1) and yields a higher column density than if it were not considered.

For the g.s., we used 117 transitions free of blending with upper level energies from 20.4 to 683.1 K with two different velocity components: one with $v_{\rm LSR} = 4$–6 km s^{-1} and $\Delta v = 4$–7 km s^{-1} and the second one with $v_{\rm LSR} = 2$–4 km s^{-1} and

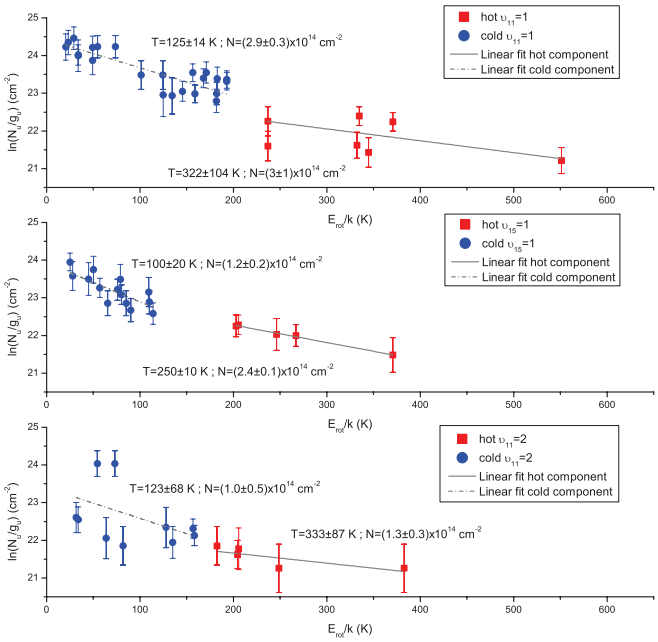

Fig. 12. Rotational diagrams for the vibrationally excited states of vinyl cyanide $v_{11} = 1$, $v_{15} = 1$, and $v_{11} = 2$ as a function of rotational energy (upper level energy corrected from the vibrational energy of each state), which sorted by increasing vibrational energy *from top to bottom*.

Δv = 14–20 km s^{-1}. For the vibrationally excited states, we considered 43 (40–550 K), 24 (30–380 K), and 33 (25–370 K) transitions with line profiles that can be fitted to a single velocity component ($v_{\rm LSR}$ = 4–6 km s^{-1} and Δv = 5–7 km s^{-1}) for v_{11} = 1, 2, and v_{15} = 1, respectively.

The scatter in the rotational diagrams of CH_2CHCN g.s. is mainly due to the uncertainty of fitting two Gaussian profiles to the lines with the CLASS software. Rotational diagrams of the vibrationally excited states (v_{11} = 1 and v_{15} = 1) are less scattered because there is only one fitted Gaussian to the line profile. For the rotational diagram of the v_{11} = 2 state, the scatter is mostly due to the weakness of the observed lines for this species. We have done an effort to perform the diagrams with unblended lines; however, some degree of uncertainty could come from non-obvious blends. The individual errors of the data points are those derived by error propagation in the calculated uncertainty of $\ln(N_{\rm u}/g_{\rm u})$, taking only the uncertainty of the integrated intensity of each line (W) provided by CLASS and an error of 20% for the source diameter into account. The uncertainty of the final values of $T_{\rm rot}$ and N has been calculated with the statistical errors given by the linear least squares fit for the slope and the intercept.

We assumed the same source diameter of 10″ for the emitting region of the two components for the g.s. and the single component of the vibrationally excited states. In Fig. 11, the upper panel shows points in the diagram related with the wide and narrow components for the CH_2CHCN g.s. We observed two tendencies in the position of the data points up to/starting from an upper state energy of ≃200 K. From the narrow component, we derived two different rotational temperatures and column densities, $T_{\rm rot} = 125 \pm 16$ K and $N = (1.3 \pm 0.1) \times 10^{15}$ cm^{-2}, and $T_{\rm rot} = 322 \pm 57$ K and $N = (1.0 \pm 0.2) \times 10^{15}$ cm^{-2}. Likewise, from the wide component, we have determined cold and hot temperatures of about $T_{\rm rot} = 90 \pm 14$ K and $T_{\rm rot} = 227 \pm 130$ K, and column densities of $N = (2.9 \pm 0.5) \times 10^{15}$ cm^{-2} and $N = (1.2 \pm 0.9) \times 10^{15}$ cm^{-2}, respectively.

To quantify the uncertainty derived from the assumed source size, we also have performed the rotational diagram of CH_2CHCN g.s. by adopting a source diameter of both 5″ and 15″. The main effect of changing the source size on the rotational diagram is a change in the slope and in the scatter. Table 4 shows the derived values of N and $T_{\rm rot}$ by assuming different source sizes. Therefore, as expected, derived rotational temperatures depend clearly on the assumed size with a tendency to increase $T_{\rm rot}$ when increasing the source diameter. The effect on the column density is less significant also due to the correction on the partition function introduced by the change in the rotational temperatures; in general, these values increased or decreased when we decreased or increased the source size, respectively (see Table 4).

In Fig. 12, the panels display the rotational diagrams of the three vinyl cyanide excited states v_{11} = 1, v_{15} = 1, and v_{11} = 2, which are sorted by the vibrational energy from top to bottom. In the x-axis we show the rotational energy which has been corrected from the vibrational energy to estimate the appropriate column density. We also observed the same tendency of the data points quoted above. The rotational temperature and the column density conditions for the v_{11} = 1 were $T_{\rm rot} = 125 \pm 14$ K and $(2.9 \pm 0.3) \times 10^{14}$ cm^{-2}, and $T_{\rm rot} = 322 \pm 104$ K and $N = (3 \pm 1) \times 10^{14}$ cm^{-2}. For the v_{15} = 1 state we determine $T_{\rm rot} = 100 \pm 20$ K and $N = (1.2 \pm 0.2) \times 10^{14}$ cm^{-2}, and $T_{\rm rot} = 250 \pm 10$ K and $N = (2.4 \pm 0.1) \times 10^{14}$ cm^{-2}. For the v_{11} = 2 state we find that $T_{\rm rot} = 123 \pm 68$ K and $N = (1.0 \pm 0.5) \times 10^{14}$ cm^{-2}, and $T_{\rm rot} = 333 \pm 87$ K and $N = (1.3 \pm 0.3) \times 10^{14}$ cm^{-2}. Owing to the weakness of the emission lines of the v_{11} = 3 and v_{10} = 1 ⇔ (v_{11} = 1,v_{15} = 1) vibrational modes, we have not performed rotational diagrams for these species.

Table 4. N and T_{rot} from rotational diagrams of CH_2CHCN g.s. which assumes different source sizes.

	Hot narrow comp. v_{LSR} = 4–6 km s^{-1}	*Cold narrow comp.* Δv = 4–7 km s^{-1}	*Hot wide comp.* v_{LSR} = 2–4 km s^{-1}	*Cold wide comp.* Δv = 14–20 km s^{-1}
d_{sou} = 5″	$N = (2.3 \pm 0.7) \times 10^{15}$ cm^{-2} $T_{rot} = (334 \pm 89)$ K	$N = (3.8 \pm 0.8) \times 10^{15}$ cm^{-2} $T_{rot} = (100 \pm 20)$ K	$N = (1.1 \pm 0.9) \times 10^{15}$ cm^{-2} $T_{rot} = (210 \pm 132)$ K	$N = (4.8 \pm 0.5) \times 10^{15}$ cm^{-2} $T_{rot} = (71 \pm 5)$ K
d_{sou} = 10″	$N = (1.0 \pm 0.2) \times 10^{15}$ cm^{-2} $T_{rot} = (322 \pm 57)$ K	$N = (1.3 \pm 0.1) \times 10^{15}$ cm^{-2} $T_{rot} = (125 \pm 16)$ K	$N = (1.2 \pm 0.9) \times 10^{15}$ cm^{-2} $T_{rot} = (227 \pm 130)$ K	$N = (2.9 \pm 0.5) \times 10^{15}$ cm^{-2} $T_{rot} = (90 \pm 14)$ K
d_{sou} = 15″	$N = (6.9 \pm 1.9) \times 10^{14}$ cm^{-2} $T_{rot} = (326 \pm 85)$ K	$N = (1.0 \pm 0.2) \times 10^{15}$ cm^{-2} $T_{rot} = (166 \pm 55)$ K	$N = (9 \pm 6) \times 10^{14}$ cm^{-2} $T_{rot} = (250 \pm 125)$ K	$N = (1.0 \pm 0.1) \times 10^{15}$ cm^{-2} $T_{rot} = (100 \pm 10)$ K

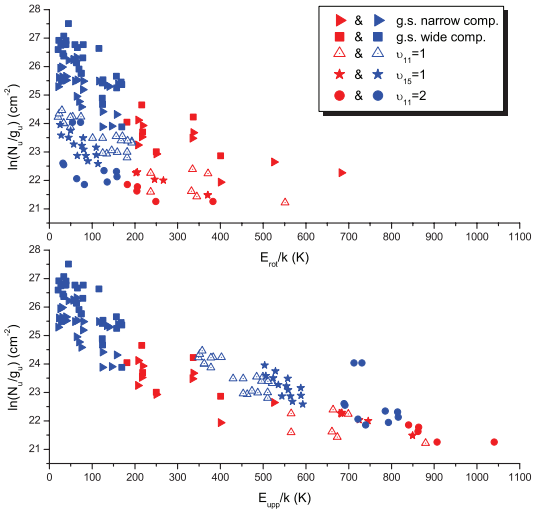

Fig. 13. Rotational diagram of CH_2CHCN in its ground and excited states as shown as a function of rotational energy corrected from the vibrational energy in the *upper panel*, while the *bottom panel* displays the ground state followed by CH_2CHCN $v_{11} = 1$, $v_{15} = 1$, and $v_{11} = 2$ excited states as a function of the upper level energy.

Figure 13 displays the combined rotational diagram for the ground state of CH_2CHCN and $v_{11} = 1$, $v_{15} = 1$, and $v_{11} = 2$ excited states. The upper panel is referred to the rotational level energies of the vinyl cyanide states, whereas the bottom panel shows the positions of the different rotational diagrams in the upper level energies when taking the vibrational energy for the excited states into account.

Owing to the large range of energies and the amount of transitions in these rotational diagrams we consider the obtained results (T_{rot}) as a starting point in our models (see Sect. 4.4.1).

4.4. Astronomical modeling of CH_2CHCN in Orion-KL

4.4.1. Analysis: the Model

From the observational line parameters derived in Sect. 4.2.1 (radial velocities and line widths), the displayed maps, and the rotational diagram results (two components, cold and hot, for each derived Gaussian fit to the line profiles), we consider that the emission of CH_2CHCN species comes mainly from the four regions shown in Table 5, which are related with the hot core (those with Δv = 6–7 km s^{-1}) and plateau/hot core (those with Δv = 20 km s^{-1}) components. Daly et al. (2013) found that three components related with the hot core were enough to properly fit their ethyl cyanide lines. The named "Hot Core 1" and "Hot Core 3" in Daly et al. (2013) are similar to our "Hot narrow comp." and "Cold wide comp." of Table 5, respectively. Interferometric maps performed by Guélin et al. (2008) of ethyl and vinyl cyanide and those of Widicus Weaver & Friedel (2012) of CH_3CH_2CN (the latter authors affirm that in their observations CH_3CH_2CN, CH_2CHCN, and CH_3CN are cospatial) show that the emission from these species comes from different cores at the position of the hot core and IRc7. The radial velocities found in the line profiles of vinyl cyanide (between 3–5 km s^{-1}) in this work with the cited interferometric maps could indicate that the four components of Table 5 are dominated by the emission of the hot core. For the vibrationally excited states and for the isotopologues, we found that two components (both narrow components) are sufficient to reproduce the line profiles (see Table 5). We note that we need a higher value in the line width for $v_{11} = 1$ and $v_{15} = 1$. This difference is probably due to a small contribution of the wide component in these lines.

Spectroscopic (Sect. 2) and observational parameters, such as radial velocity (v_{LSR}), line width (Δv), temperature from rotational diagrams (T_{rot}), source diameter (d_{sou}) and offsets from the maps, were introduced in an excitation and radiative transfer code (MADEX) in order to obtain the synthetic spectrum. We have considered the telescope dilution and the position of the components with respect to the pointing position (IRc2). The LTE conditions have been assumed by owing to the lack of collisional rates for vinyl cyanide, which prevents a more detailed analysis of the emission of this molecule. Nevertheless, we expect a good approximation to the physical and chemical conditions due to the hot and dense nature of the considered components. Rotational temperatures (which coincide with the excited and kinetic temperatures in LTE conditions) have been slightly adapted from those of the rotational diagrams to obtain the best fit to the line profiles. These models allow us to obtain column density results for each species and components independently. The sources of uncertainty that were described in Tercero et al. (2010) have been considered. For the CH_2CHCN g.s., $v_{11} = 1$, and $v_{15} = 1$ states we have adopted an uncertainty of 30%, while we have adopted a 50% uncertainty for the ^{13}C isotopologues and the $v_{11} = 2$, $v_{11} = 3$, and $v_{10} = 1 \Leftrightarrow (v_{11} = 1, v_{15} = 1)$ states. Due to the weakness and/or high overlap with other molecular species, we only provided upper limits to the column densities of monodeuterated vinyl cyanide and the ^{15}N isotopologue.

4.4.2. Column densities

The column densities that best reproduce the observations are shown in Table 5 and used for the model in Figs. 4–9 and A.2. Although the differences between the intensity of the model and that of the observations are mostly caused by blending with other molecular species, isolated vinyl cyanide lines confirm a good

Table 5. Physico-chemical conditions of Orion-KL from ground and excited states of CH_2CHCN.

	Hot narrow comp.	*Cold narrow comp.*	*Hot wide comp.*	*Cold wide comp.*
d_{sou} (")	5	10	5	10
offset (")	2	2	0	0
Δv_{FWHM} (km s^{-1})	6(7*)	6(7*)	20	20
v_{LSR} (km s^{-1})	5	5	3	3
T_{rot} (K)	*320*	*100*	*200*	*90*
$N_{CH_2CHCN(g.s.)}$ (cm^{-2})	$(3.0 \pm 0.9) \times 10^{15}$	$(1.0 \pm 0.3) \times 10^{15}$	$(9 \pm 3) \times 10^{14}$	$(1.3 \pm 0.4) \times 10^{15}$
$N_{CH_2CHCN(v_{11}=1)}$(cm^{-2})	$(9 \pm 3) \times 10^{14}$	$(2.5 \pm 0.8) \times 10^{14}$	...	...
$N_{CH_2CHCN(v_{11}=2)}$(cm^{-2})	$(2 \pm 1) \times 10^{14}$	$(5 \pm 2) \times 10^{13}$	...	...
$N_{CH_2CHCN(v_{11}=3)}$(cm^{-2})	$\leq(2 \pm 1) \times 10^{14}$	$\leq(5 \pm 2) \times 10^{13}$	...	...
$N_{CH_2CHCN(v_{15}=1)}$(cm^{-2})	$(4 \pm 1) \times 10^{14}$	$(1.0 \pm 0.3) \times 10^{14}$	...	...
$N_{CH_2CHCN(v_{10}=1 \Leftrightarrow (v_{11}=1, v_{15}=1))}$(cm^{-2})	$(4 \pm 2) \times 10^{14}$	$(8 \pm 4) \times 10^{13}$	...	...
$N_{^{13}CH_2CHCN}$(cm^{-2})	$(4 \pm 2) \times 10^{14}$	$(5 \pm 2) \times 10^{13}$	...	...
$N_{CH_2^{13}CHCN}$(cm^{-2})	$(4 \pm 2) \times 10^{14}$	$(5 \pm 2) \times 10^{13}$	...	...
$N_{CH_2CH^{13}CN}$(cm^{-2})	$(4 \pm 2) \times 10^{14}$	$(5 \pm 2) \times 10^{13}$	...	...
$N_{CH_2CHC^{15}N}$(cm^{-2})	$\leq(1.0 \pm 0.5) \times 10^{14}$	$\leq(2 \pm 1) \times 10^{13}$	...	...
$N_{HCDCHCN}$(cm^{-2})	$\leq(4 \pm 2) \times 10^{14}$	$\leq(4 \pm 2) \times 10^{13}$	...	...
$N_{DCHCHCN}$(cm^{-2})	$\leq(4 \pm 2) \times 10^{14}$	$\leq(4 \pm 2) \times 10^{13}$	...	...
N_{CH_2CDCN}(cm^{-2})	$\leq(3 \pm 1) \times 10^{14}$	$\leq(3 \pm 1) \times 10^{13}$	...	...

Notes. Physico-chemical conditions of Orion-KL from vinyl cyanide (see text 4.4.1). * 7 km s^{-1} is only considered for $v_{11} = 1$ and $v_{15} = 1$ states.

agreement between model and observations. We found small differences between the column density values from the model and those from the rotational diagram, likely because of the source diameters that are considered in the determination of the beam dilution for the two components.

In Figs. 4–9, 15, 16, and A.1–A.5, a model with species all already studied that have been in this survey is included (cyan line). The considered molecules and published works containing the detailed analysis for each species are as follows: OCS, CS, H_2CS, HCS^+, CCS, CCCS species in Tercero et al. (2010); SiO and SiS species in Tercero et al. (2011); SO and SO_2 species in Esplugues et al. (2013a); HC_3N and HC_5N species in Esplugues et al. (2013b); CH_3CN in Bell et al. (2014); CH_3COOCH_3 and t/g-CH_3CH_2OCOH in Tercero et al. (2013); CH_3CH_2SH, CH_3SH, CH_3OH, CH_3CH_2OH in Kolesniková et al. (2014); ^{13}C-CH_3CH_2CN in Demyk et al. (2007); $CH_3CH_2{}^{15}N$, CH_3CHDCN, and CH_2DCH_2CN in Margulès et al. (2009); CH_3CH_2CN species in Daly et al. (2013); ^{13}C-$HCOOCH_3$ in Carvajal et al. (2009); $DCOOCH_3$ and $HCOOCH_3$ in Margulès et al. (2010); ^{18}O-$HCOOCH_3$ in Tercero et al. (2012); $HCOOCH_2D$ in Coudert et al. (2013); ^{13}C-$HCOOCH_3$ $\nu_t = 1$, and $HCOOCH_3$ $\nu_t = 1$ in Haykal et al. (2014); NH_2CHO $\nu_{12} = 1$ and NH_2CHO in Motiyenko et al. (2007); CH_2CHCN species in this work; $HCOOCH_3$ $\nu_t = 2$ and CH_3COOH from López et al. (in prep.).

We obtained a total column density of vinyl cyanide in the ground state of $(6 \pm 2) \times 10^{15}$ cm^{-2}. This value is a factor 7 higher than the value in the Orion-KL hot core of Schilke et al. (1997), who detected the vinyl cyanide g.s. in the frequency range from 325 to 360 GHz with a column density (averaged over a beam of 10″–12″) of 8.2×10^{14} cm^{-2} and a T_{rot} of 96 K. The difference between both results is mostly due to our more detailed model of vinyl cyanide which includes four components, two of them with a source size of 5″ (half than the beam size in Schilke et al. 1997). Sutton et al. (1995) also derived a column density of 1×10^{15} cm^{-2} (beam size of 13.7″) toward the hot core position. These authors found vinyl cyanide emission toward the compact ridge position but at typical hot core velocities. Previous authors derived beam averaged column densities between 4×10^{13} and 2×10^{14} cm^{-2} (Johansson et al. 1984; Blake et al. 1987; Turner 1991; Ziurys & McGonagle 1993).

The column density of CH_2CHCN $v_{11} = 1$, $(1.0 \pm 0.3) \times 10^{15}$ cm^{-2} is four times smaller than that derived for the ground state in the same components. Moreover, we derived a column density of $(3 \pm 2) \times 10^{14}$, $\leq(3 \pm 2) \times 10^{14}$, $(5 \pm 2) \times 10^{14}$, and $(5 \pm 2) \times 10^{14}$ cm^{-2} for the $v_{11} = 2$, $v_{11} = 3$, $v_{15} = 1$, and $v_{10} = 1 \Leftrightarrow (v_{11} = 1, v_{15} = 1)$ states, respectively. Schilke et al. (1997) did not give column density results for the tentative detection of $v_{11} = 1$ and $v_{15} = 1$ bending modes. We also obtained a column density of $(4 \pm 2) \times 10^{14}$ cm^{-2} for each ^{13}C-isotopologue of vinyl cyanide.

4.4.3. Isotopic abundances

It is now possible to estimate the isotopic abundance ratio of the main isotopologue (^{12}C, ^{14}N, ^{1}H) with respect to ^{13}C, ^{15}N, and D isotopologues from the obtained column densities shown in Table 5. For estimating these ratios, we assume the same partition function for both the main and the rare isotopologues.

^{12}C/^{13}C: the column density ratio between the normal species and each ^{13}C isotopologue in Orion-KL, when the associated uncertainties are considered, vary between 4–20 for the hot narrow component and between 10–43 for the cold narrow component. The solar isotopic abundance (^{12}C/^{13}C = 90, Anders & Grevesse 1989) corresponds roughly to a factor 2–22 higher than the value obtained in Orion. The ^{12}C/^{13}C ratio indicates the degree of galactic chemical evolution, so the solar system value could point out earlier epoch conditions of this region (Wyckoff et al. 2000; Savage et al. 2002). The following previous estimates of the ^{12}C/^{13}C ratio in Orion-KL from observations of different molecules have been reported: 43±7 from CN (Savage et al. 2002), 30–40 from HCN, HNC, OCS, H_2CO, CH_3OH (Blake et al. 1987), 57 ± 14 from CH_3OH (Persson et al. 2007), 35 from methyl formate (Carvajal et al. 2009, Haykal et al. 2014), 45 ± 20 from CS-bearing molecules (Tercero et al. 2010), 73 ± 22 from ethyl cyanide (Daly et al. 2013), and ≃3–17 from cyanoacetylene in the hot core (Esplugues et al. 2013b). Considering the weakness of the ^{13}C lines, the derived ratios are compatible

A&A 572, A44 (2014)

Table 6. Line opacities.

			Hot narrow comp.	Cold narrow comp.	Hot wide comp.	Cold wide comp.
			d_{sou} = 10″	d_{sou} = 15″	d_{sou} = 10″	d_{sou} = 15″
Transition	Freq. (MHz)	E_{upp} (K)	$N = 1.6 \times 10^{15}$ cm^{-2}	$N = 3.6 \times 10^{14}$ cm^{-2}	$N = 8.2 \times 10^{13}$ cm^{-2}	$N = 9.2 \times 10^{14}$ cm^{-2}
$11_{0,11}$–$10_{0,10}$	103 575.4	29.9	$\tau = 2.76 \times 10^{-3}$	$\tau = 8.99 \times 10^{-3}$	$\tau = 1.22 \times 10^{-4}$	$\tau = 8.70 \times 10^{-3}$
$14_{3,11}$–$13_{3,10}$	133 030.7	67.3	$\tau = 3.83 \times 10^{-3}$	$\tau = 9.72 \times 10^{-3}$	$\tau = 1.58 \times 10^{-4}$	$\tau = 9.03 \times 10^{-3}$
$18_{0,18}$–$17_{0,17}$	167 728.4	77.1	$\tau = 6.33 \times 10^{-3}$	$\tau = 1.51 \times 10^{-2}$	$\tau = 2.57 \times 10^{-4}$	$\tau = 1.39 \times 10^{-2}$
$23_{0,23}$–$22_{0,22}$	212 788.7	123.8	$\tau = 8.89 \times 10^{-3}$	$\tau = 1.55 \times 10^{-2}$	$\tau = 3.31 \times 10^{-4}$	$\tau = 1.35 \times 10^{-2}$
$25_{4,21}$–$24_{4,20}$	237 712.0	182.8	$\tau = 8.78 \times 10^{-3}$	$\tau = 1.02 \times 10^{-2}$	$\tau = 2.93 \times 10^{-4}$	$\tau = 8.39 \times 10^{-3}$
$28_{0,28}$–$27_{0,27}$	257 646.2	181.4	$\tau = 1.10 \times 10^{-2}$	$\tau = 1.30 \times 10^{-2}$	$\tau = 3.68 \times 10^{-4}$	$\tau = 1.07 \times 10^{-2}$
$30_{0,30}$–$29_{0,29}$	275 588.1	207.4	$\tau = 1.25 \times 10^{-2}$	$\tau = 1.15 \times 10^{-2}$	$\tau = 3.71 \times 10^{-4}$	$\tau = 9.20 \times 10^{-3}$
			d_{sou} = 5″	d_{sou} = 10″	d_{sou} = 5″	d_{sou} = 10″
Transition	Freq. (MHz)	E_{upp} (K)	$N = 3.0 \times 10^{15}$ cm^{-2}	$N = 1.0 \times 10^{15}$ cm^{-2}	$N = 9.0 \times 10^{14}$ cm^{-2}	$N = 1.3 \times 10^{15}$ cm^{-2}
$11_{0,11}$–$10_{0,10}$	103 575.4	29.9	$\tau = 5.07 \times 10^{-3}$	$\tau = 2.50 \times 10^{-2}$	$\tau = 1.37 \times 10^{-3}$	$\tau = 1.23 \times 10^{-2}$
$14_{3,11}$–$13_{3,10}$	133 030.7	67.3	$\tau = 7.06 \times 10^{-3}$	$\tau = 2.70 \times 10^{-2}$	$\tau = 1.78 \times 10^{-3}$	$\tau = 1.28 \times 10^{-2}$
$18_{0,18}$–$17_{0,17}$	167 728.4	77.1	$\tau = 1.16 \times 10^{-2}$	$\tau = 4.19 \times 10^{-2}$	$\tau = 2.89 \times 10^{-3}$	$\tau = 1.96 \times 10^{-2}$
$23_{0,23}$–$22_{0,22}$	212 788.7	123.8	$\tau = 1.64 \times 10^{-2}$	$\tau = 4.30 \times 10^{-2}$	$\tau = 3.72 \times 10^{-3}$	$\tau = 1.91 \times 10^{-2}$
$25_{4,21}$–$24_{4,20}$	237 712.0	182.8	$\tau = 1.62 \times 10^{-2}$	$\tau = 2.84 \times 10^{-2}$	$\tau = 3.30 \times 10^{-3}$	$\tau = 1.19 \times 10^{-2}$
$28_{0,28}$–$27_{0,27}$	257 646.2	181.4	$\tau = 2.02 \times 10^{-2}$	$\tau = 3.61 \times 10^{-2}$	$\tau = 4.14 \times 10^{-3}$	$\tau = 1.51 \times 10^{-2}$
$30_{0,30}$–$29_{0,29}$	275 588.1	207.4	$\tau = 2.14 \times 10^{-2}$	$\tau = 3.20 \times 10^{-2}$	$\tau = 4.18 \times 10^{-3}$	$\tau = 1.30 \times 10^{-2}$
			d_{sou} = 2″	d_{sou} = 5″	d_{sou} = 2″	d_{sou} = 5″
Transition	Freq. (MHz)	E_{upp} (K)	$N = 8.0 \times 10^{15}$ cm^{-2}	$N = 4.8 \times 10^{15}$ cm^{-2}	$N = 2.5 \times 10^{14}$ cm^{-2}	$N = 4.4 \times 10^{15}$ cm^{-2}
$11_{0,11}$–$10_{0,10}$	103 575.4	29.9	$\tau = 1.35 \times 10^{-2}$	$\tau = 1.20 \times 10^{-1}$	$\tau = 3.80 \times 10^{-4}$	$\tau = 4.16 \times 10^{-2}$
$14_{3,11}$–$13_{3,10}$	133 030.7	67.3	$\tau = 1.88 \times 10^{-2}$	$\tau = 1.30 \times 10^{-1}$	$\tau = 4.94 \times 10^{-4}$	$\tau = 4.32 \times 10^{-2}$
$18_{0,18}$–$17_{0,17}$	167 728.4	77.1	$\tau = 3.11 \times 10^{-2}$	$\tau = 2.01 \times 10^{-1}$	$\tau = 8.02 \times 10^{-4}$	$\tau = 6.64 \times 10^{-2}$
$23_{0,23}$–$22_{0,22}$	212 788.7	123.8	$\tau = 4.36 \times 10^{-2}$	$\tau = 2.06 \times 10^{-1}$	$\tau = 1.03 \times 10^{-3}$	$\tau = 6.48 \times 10^{-2}$
$25_{4,21}$–$24_{4,20}$	237 712.0	182.8	$\tau = 4.31 \times 10^{-2}$	$\tau = 1.37 \times 10^{-1}$	$\tau = 9.16 \times 10^{-4}$	$\tau = 4.01 \times 10^{-2}$
$28_{0,28}$–$27_{0,27}$	257 646.2	181.4	$\tau = 5.39 \times 10^{-2}$	$\tau = 1.73 \times 10^{-1}$	$\tau = 1.15 \times 10^{-3}$	$\tau = 5.10 \times 10^{-2}$
$30_{0,30}$–$29_{0,29}$	275 588.1	207.4	$\tau = 5.71 \times 10^{-2}$	$\tau = 1.54 \times 10^{-1}$	$\tau = 1.16 \times 10^{-3}$	$\tau = 4.40 \times 10^{-2}$

Notes. Opacities for some lines of CH_2CHCN g.s. at different frequencies that consider different source diameters and column densities (see text, Sect. 4.4.4).

with a $^{12}C/^{13}C$ ratio between 30–45, which are found by other authors. Nevertheless, our results point out a possible chemical fractionation enhancement of the ^{13}C isotopologues of vinyl cyanide. The intensity ratios derived in Sect. 4.4.4 also indicate this possibility. This ratio might be underestimated if the lines from the g.s. were optically thick. However, our model for the assumed sizes of the source yields values of τ (optical depth) that are much lower than unity (see Sect. 4.4.4). In Sgr B2(N), Müller et al. (2008) derived from their observations of CH_2CHCN a $^{12}C/^{13}C$ ratio of 21 ± 6.

$^{14}N/^{15}N$: we obtained an average lower limit value for $N(CH_2CHC^{14}N)/N(CH_2CHC^{15}N)$ of ≥33 for the two involved components. In Daly et al. (2013) (see Appendix B), we provided a $^{14}N/^{15}N$ ratio of 256 ± 128 by means of ethyl cyanide, which agree with the terrestrial value (Anders & Grevesse 1989) and with the value obtained by Adande & Ziurys (2012) in the local interstellar medium. The latter authors performed an evaluation of the $^{14}N/^{15}N$ ratio across the Galaxy (toward 11 molecular clouds) through CN and HNC. They concluded that this ratio exhibits a positive gradient with increasing distance from the Galactic center (which agree with chemical evolution models where ^{15}N has a secondary origin in novae).

D/H: for a tentative detection of mono-deuterated forms of vinyl cyanide we derived a lower limit D/H ratio of ≤0.12 (for HCDCHCN and DCHCHCN) and ≤0.09 (for CH_2CDCN) for the hot narrow component, whereas we obtain ≤0.04 (for HCDCHCN and DCHCHCN) and ≤0.03 (for CH_2CDCN) for the cold component. Studies of the chemistry of deuterated species in hot cores carried out by Rodgers & Millar (1996) conclude that the column density ratio D-H remains practically unaltered during a large period of time when D and H-bearing molecules are released to the gas phase from the ice mantles of dust grains. These authors indicate that the observations of deuterated molecules give insight into the processes occurring on the grain mantles by inferring the fractionation of their parent molecules. Furthermore, the fractionation also helps us to trace the physical and chemical conditions of the region (Roueff et al. 2005). Values of this ratio were given by Marguléès et al. (2010) from observations of deuterated methyl formate at obtained $N(DCOOH_3/HCOOCH_3)$ = 0.04 for the hot core; Tercero et al. (2010) estimated an abundance ratio of $N(HDCS)/N(H_2CS)$ being 0.05 ± 0.02, which is also for the hot core component. Neil et al. (2013) provided a $N(HDCO)/N(H_2CO)$ ratio in the hot core of ≤0.005. Pardo et al. (2001b) derived a value between 0.004–0.01 in the plateau by means of $N(HDO)/N(H_2O)$. Persson et al. (2007) also for $N(HDO)/N(H_2O)$ derived 0.005, 0.001, and 0.03 for the large velocity plateau, the hot core, and the compact ridge, respectively, and Schilke et al. (1992) provided the DCN/HCN column density ratio of 0.001 for the hot core region.

4.4.4. Line opacity

The MADEX code gives us the line opacity for each transition for the physical components assumed in Table 5. Table 6 shows the opacities for the four cloud components shown in Table 5, which are obtained by varying the source diameter

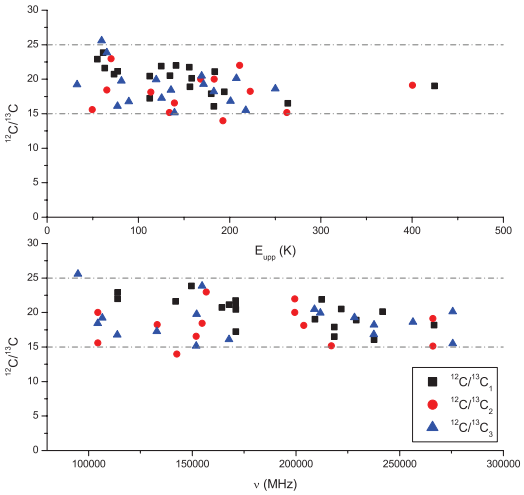

Fig. 14. $^{12}C/^{13}C$ ratios of the observed line intensities for a given transition as a function of the upper level energy (*top panel*) and the frequency (*bottom panel*).

and the column density (the last in order to obtain a good fit between the synthetic spectra and the observations). When we decreased the source diameter, we have to increase the column densities to properly fit the observations and, therefore, the opacities of the lines increment. The extreme case, where the hot and cold cloud components have diameters of 2″ and 5″, respectively, allow us to obtain the maximum total opacity of ≃0.26 (sum of the opacity of all cloud components) for the $30_{0,30}$–$29_{0,29}$ transition at 275 588 MHz. This value corresponds with a maximum correction of about 3–5% for our column density results. Column densities have to rise a factor 4 to obtain a total opacity of ≃0.95, which implies a large mismatch (a factor ≃3–4 in the line intensity) between model and observations.

Figure 14 shows the $^{12}C/^{13}C$ ratios of the observed line intensities for a given transition against its upper level energy and its frequency. As for the rotational diagrams, unblended lines have been used for deriving these ratios. We observe that most of these ratios are between 15 and 25, and we do not observe a clear decline of this ratio with either the increasing of upper state energy or the increasing of the frequency. In case of optically thick lines, we should expect these large opacities for lines at the end of the 1.3 mm window (240–280 GHz) where the upper state energies are above 150 K even for transitions of K_a = 0,1. Figure 14 suggests that the CH_2CHCN g.s. lines have $\tau < 1$. Nevertheless, if the bulk of the emission comes from a very small region (<1″), opacities will be larger than 1.

From Fig. 14 we can estimate the average intensity ratios for each ^{13}C isotopologue being 20 ± 6, 18 ± 5, and 19 ± 6 for $^{12}C/^{13}C_1$, $^{12}C/^{13}C_2$, and $^{12}C/^{13}C_3$, respectively. These results with the $^{12}C/^{13}C$ column density ratio derived in Sect. 4.4.3 suggests possible chemical fractionation enhancement of the ^{13}C isotopologues of vinyl cyanide.

4.4.5. Vibrational temperatures

We can estimate the vibrational temperature between the different vibrational modes of the vinyl cyanide according to

$$\frac{N(CH_2CHCN\ v_x)}{N(CH_2CHCN)} = \frac{\exp\left(-\frac{E_{vx}}{T_{vib}}\right)}{f_v}, \quad (3)$$

where v_x identifies the vibrational mode, E_{v_x} is the energy of the corresponding vibrational state (328.5, 478.6, 657.8, 806.4/809.9, and 987.9 K for v_{11} = 1, v_{15} = 1, v_{11} = 2, v_{10} = 1 ⇔ (v_{11} = 1,v_{15} = 1), and v_{11} = 3, respectively), T_{vib} is the vibrational temperature, f_v is the vibrational partition function, $N(CH_2CHCN\ v_x)$ is the column density of the vibrational state, and $N(CH_2CHCN)$ is the total column density of vinyl cyanide. Considering the relation $N(CH_2CHCN) = N_{g.s.} \times f_v$ and assuming the same partition function for these species in the ground and in the vibrationally excited states, we only need the energy of each vibrational state and the calculated column density to derive the vibrational temperatures. The vibrational temperature (T_{vib}) is given as a lower limit, since the vibrationally excited gas emitting region may not coincide with that of the ground state.

From the column density results, the T_{vib} in the hot narrow component for each vibrationally excited level were ≃268 ± 80 K, ≃246±74 K, ≃265±132 K, ≃402±201 K, and ≃385±192 K for v_{11} = 1, v_{15} = 1, v_{11} = 2, v_{10} = 1 ⇔ (v_{11} = 1,v_{15} = 1), and v_{11} = 3, respectively. In the same way, the T_{vib} in the cold narrow component for each vibrationally excited level were ≃237±71 K, ≃208 ± 62 K, ≃220 ± 110 K, ≃324 ± 162 K, and ≃330 ± 165 K for v_{11} = 1, v_{15} = 1, v_{11} = 2, v_{10} = 1 ⇔ (v_{11} = 1,v_{15} = 1), and v_{11} = 3, respectively. The average vibrational temperature for v_{11} = 1, 2, and v_{15} = 1 from both narrow components was 252 ± 76 K, 242 ± 121 K, and 227 ± 68 K, respectively. In the case of v_{10} = 1 ⇔ (v_{11} = 1,v_{15} = 1) and v_{11} = 3, the derived T_{vib} is larger than the T_{rot} in the hot narrow component (320 K), which could suggest an inner and hotter region for the emission of these vibrationally excited states of vinyl cyanide. Moreover, a tendency to increase the vibrational temperature with the vibrational energy of the considered state is observed. Vibrational transitions imply ro-vibrational states that may be excited by dust IR photons or collisions with the most abundant molecules in the cloud. Nevertheless, collisional rates are needed to evaluate the excitation mechanisms. The observed differences between T_{rot} and T_{vib} indicate either a far-IR pumping of the highly excited vibrational levels or the presence of a strong temperature gradient toward the inner regions. Some internal heating might be reflected in temperature and density gradients due to processes such as, for example, star formation.

4.5. Detection of isocyanide species

We searched for the isocyanide counterparts of vinyl, ethyl, and methyl cyanide, cyanoacetylene, and cyanamide in our line survey. In this section, we report the first detection toward Orion-KL of methyl isocyanide, and a tentative detection of vinyl isocyanide. The first to sixth columns of Table 7 show the cyanide and isocyanide molecules studied in Orion-KL, their column density values in the components where we assumed emission from the isocyanides, the column density ratio between the cyanide and its isocyanide counterpart, the same ratio obtained by previous authors in Sgr B2 and TMC-1 sources, and the difference of the bond energies between the -CN and -NC isomers.

Vinyl isocyanide (CH_2CHNC) is an isomer of the unsaturated hydrocarbon vinyl cyanide. The structure differences between the vinyl cyanide and isocyanide are due to the CNC and CCN linear bonds and their energies, where CCN displays shorter bond distances. The bonding energy difference between vinyl cyanide and isocyanide is 8658 cm^{-1} (24.8 kcal mol^{-1}) (Remijan et al. 2005) with the cyanide isomer being more stable than the isocyanide. We have tentatively detected vinyl isocyanide in our line survey (Fig. 15) with 28 unblended

A&A 572, A44 (2014)

Table 7. Column densities of the isocyanide species and N(-CN)/N(-NC) ratios.

Molecule	N_{TOTAL} (cm^{-2})	[N(-NC)/N(-CN)]			Isomerization energy
		Orion-KL	Sgr B2	TMC-1	(cm^{-1})
CH_2CHCN	$(4 \pm 1) \times 10^{15}$				
CH_2CHNC	$\leq(4 \pm 2) \times 10^{14}$	$\leq(1.0 \pm 0.5) \times 10^{-1}$	5×10^{-3} [a]		8658 [a]
CH_3CN	$(3.2 \pm 0.9) \times 10^{16}$				
CH_3NC	$(6.0 \pm 3.0) \times 10^{13}$	$(2 \pm 1) \times 10^{-3}$	2×10^{-2} [a] $(3–5) \times 10^{-2}$ [b]	$\geq 9 \times 10^{-2}$ [c]	9486 [a]
CH_3CH_2CN	$(7 \pm 2) \times 10^{16}$				
CH_3CH_2NC	$\leq(2.0 \pm 0.6) \times 10^{14}$	$\leq(3 \pm 2) \times 10^{-3}$	$\leq 3 \times 10^{-1}$ [a]		8697 [a]
HCCCN	$(4 \pm 1) \times 10^{15}$				
HCCNC	$\leq(3 \pm 1) \times 10^{13}$	$\leq(8 \pm 4) \times 10^{-3}$		$(2–5) \times 10^{-2}$ [d] 8×10^{-3} [e]	6614 [d]
HNCCC	$\leq(3 \pm 1) \times 10^{13}$	$\leq(8 \pm 4) \times 10^{-3}$		$(2–6) \times 10^{-3}$ [f] 1×10^{-3} [e]	17 745 [d]
NH_2CN	$\leq(3 \pm 1) \times 10^{13}$				
NH_2NC	$\leq(5 \pm 2) \times 10^{13}$	...	...	...	18 537 [g]

Notes. Derived column densities for the cyanide and isocyanide species (Col. 2). Columns 3–5 show the ratio between the cyanide and its isocyanide isomer in this work and that derived from other authors in Sgr B2 and TMC-1. Column 6 gives the energy difference for the isomerization between the isocyanide species and its corresponding cyanide.

References. [a] Remijan et al. (2005). [b] Cernicharo et al. (1988) . [c] Irvine & Schloerb (1984). [d] Kawaguchi et al. (1992a). [e] Ohishi & Kaifu (1998) . [f] Kawaguchi et al. (1992b). [g] Turner et al. (1975).

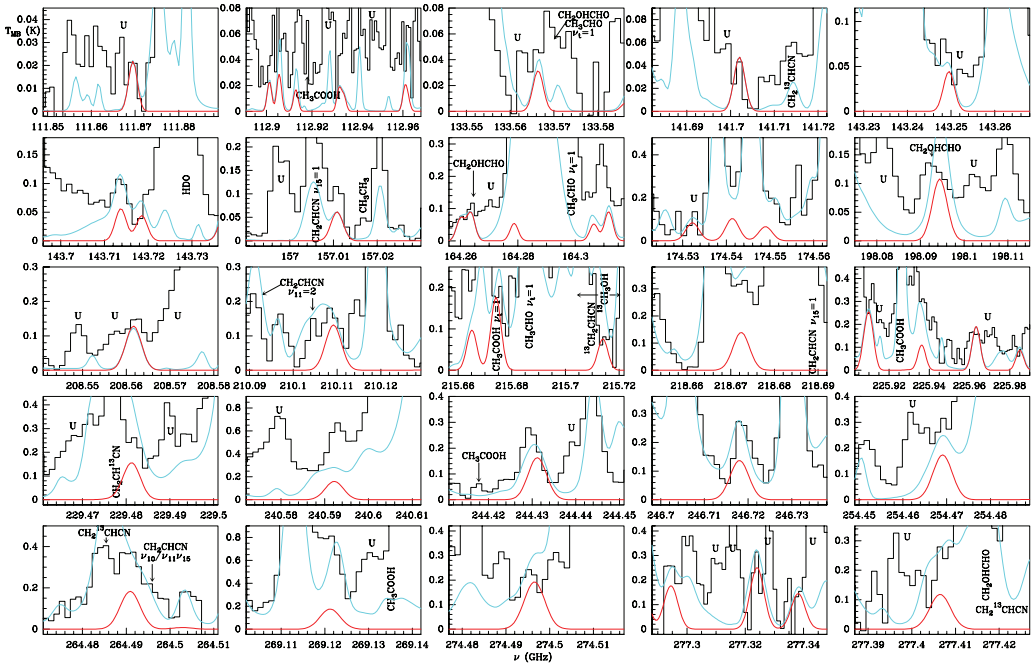

Fig. 15. Observed lines from Orion-KL (histogram spectra) and model (thin red curves) of vinyl isocyanide in its ground state. The cyan line corresponds to the model of the molecules we have already studied in this survey (see text Sect. 4.4.2) including the CH_2CHCN species. We consider the detection as tentative. A v_{LSR} of 5 km s^{-1} is assumed.

lines and 26 partially blended lines from a total of 96 detectable lines. This detection is just above the confusion limit. In Table A.14 we show spectroscopic and observational parameters of detected lines of vinyl isocyanide. Rotational constants were derived fitting all experimental data from Bolton et al. (1970), Yamada & Winnewisser (1975), and Bestmann & Dreizler (1982); the dipole moments were from Bolton et al. (1970). For modeling this molecule, we assume the same physical conditions as those found for the vinyl cyanide species (where we consider both narrow components). We derived a column density of $\leq(3 \pm 2) \times 10^{14}$ cm^{-2} (hot narrow component) and $\leq(5 \pm 3) \times 10^{13}$ cm^{-2} (cold narrow component). We estimate a $N(CH_2CHNC)/N(CH_2CHCN)$ ratio of $\leq 0.10 \pm 0.05$, while Remijan et al. (2005) derived a ratio of about $\leq$0.005 toward Sgr B2 with an upper limit for the vinyl isocyanide column density of $\leq 1.1 \times 10^{13}$ cm^{-2}.

Methyl cyanide (CH_3CN) is a symmetric rotor molecule whose internal rotor leads to two components of symmetry A

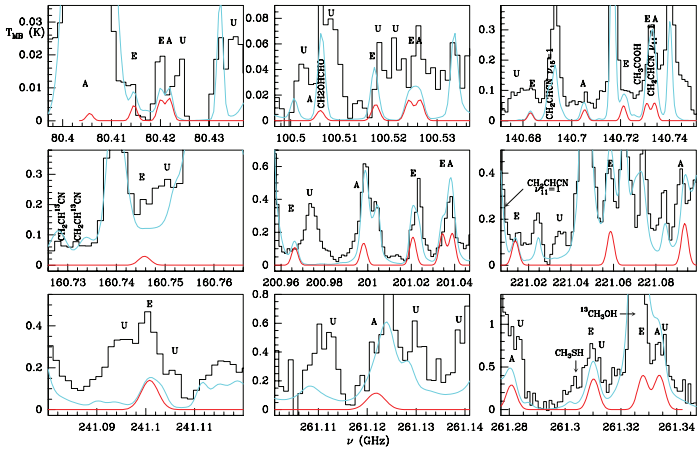

Fig. 16. Observed lines from Orion-KL (histogram spectra) and model (thin red curves) of methyl isocyanide in its ground state. The cyan line corresponds to the model of the molecules we have already studied in this survey (see text Sect. 4.4.2) including the CH_2CHCN species. A v_{LSR} of 5 km s^{-1} is assumed.

and E. The column densities of the ground state obtained for both A and E sub-states using an LVG model were derived by Bell et al. (2014) in Orion-KL. They separately fitted different series of K-ladders transitions (J = 6–5, J = 12–11, J = 13–12, J = 14–13). We averaged the model results for these four series at the IRc2 position deriving a column density of 3.1×10^{16} cm^{-2} and a kinetic temperature of ≃265 K. The CH_3CN molecule has a metastable isomer named methyl isocyanide (CH_3NC) that has been found in dense interstellar clouds (Sgr B2) by Cernicharo et al. (1988) and Remijan et al. (2005). The bonding energy difference between methyl cyanide and isocyanide is 9486 cm^{-1} (27.1 kcal mol^{-1}) (Remijan et al. 2005). We observed methyl isocyanide in Orion-KL for the first time (Fig. 16). For modeling the weak lines of methyl isocyanide we assume a hot core component (T = 265 K, d_{sou} = 10″, offset = 3″, v_{LSR} = 5 km s^{-1}, Δv = 5 km s^{-1}) that is consistent with those derived by Bell et al. (2014). Rotational constants were derived from a fit to the data reported by Bauer & Bogey (1970), Pracna et al. (2011). The constants H_J, L_J, and L_{JKKK} have been fixed to the values derived by Pracna et al. (2011). The constants A and D_K were from Pliva et al. (1995). Dipole moment was that of Gripp et al. (2000). We derived a column density of (3.0 ± 0.9) × 10^{13} cm^{-2} for each A and E symmetry substates. We determined a $N(CH_3NC)/N(CH_3CN)$ ratio of 0.002 which is a factor 15–25 lower than the value obtained by Cernicharo et al. (1988) toward Sgr B2. DeFrees et al. (1985) by means of chemical models predicted this ratio in dark clouds in the range of 0.1–0.4.

Ethyl cyanide (CH_3CH_2CN) is a heavy asymmetric rotor with a rich spectrum. In our previous paper (Daly et al. 2013), three cloud components were modeled in LTE conditions to determine the column density[9] of this molecule. We obtained a total column density of (7 ± 2) × 10^{16} cm^{-2} for this species.

The bonding energy difference between ethyl cyanide and isocyanide is 8697 cm^{-1} (24.9 kcal mol^{-1}) (Remijan et al. 2005). The spectroscopic parameters used for ethyl isocyanide (CH_3CH_2NC) were obtained from recent measurements in Lille up to 1 THz by Margulès et al. (in prep.). For CH_3CH_2NC we provide an upper limit to its column density of (2 ± 1) × 10^{14} cm^{-2}. Then, we derived a $N(CH_3CH_2NC)/N(CH_3CH_2CN)$ ratio of 0.003. This value is 100 times lower than the upper limit value obtained by Remijan et al. (2005) toward Sgr B2 of ≤0.3.

We observe that the upper limit for the CH_2CHNC column density is 5 times higher than the value of methyl isocyanide and holds a similar order of magnitude relationship with the upper limit column density of the tentatively detected ethyl isocyanide.

Cyanoacetylene (HCCCN) is a linear molecule with a simple spectrum. Its lines emerge from diverse parts of the cloud (Esplugues et al. 2013b), although mainly from the hot core. The model of the HCCCN lines was set up using LVG conditions. The authors determined a total column density of (3.5 ± 0.8) × 10^{15} cm^{-2}.

Isocyanoacetylene (HCCNC) is a stable isomer of cyanoacetylene and has an energy barrier of 6614 cm^{-1} (18.9 kcal mol^{-1}). Owing to high overlap problems in our data, we only found one line of HCCNC free of blending at 99 354.2 MHz. To obtain an upper limit for its column density we assumed the same physical components as those of Esplugues et al. (2013b). Spectroscopic parameters were derived by fitting the lines reported by Guarnieri et al. (1992); the dipole moment was taken from Gripp et al. (2000). We obtained an upper limit to the HCCNC column density of ≤(3 ± 1) × 10^{13} cm^{-2}. We estimated an upper limit for the $N(HCCNC)/N(HCCCN)$ ratio of ≤0.008. The molecule HCCNC was observed for the first time toward TMC-1 (three rotational lines in the frequency range 40–90 GHz) by Kawaguchi et al. (1992a). They obtained a $N(HCCNC)/N(HCCCN)$ ratio in the range 0.02–0.05 in that dark cloud, which is around 2–6 times higher than our upper limit. Ohishi & Kaifu (1998) provided an upper limit value of ≤0.001 also in TMC-1. This molecule has also been detected in the envelope of the carbon star IRC+10216 by Gensheimer (1997).

The other carbene-type isomer of HCCCN is 3-imino-1, 2-propadienylidene (HNCCC) that was predicted to have a relative energy of about 17744.6 cm^{-1} with respect to HCCCN (Kawaguchi et al. 1992b). We provided a tentative detection of this isomer in our survey (Fig. A.3). Its column density,

[9] We found a typographical error that is twice the difference in the column density of the hot core component 1 for the ground and excited states in our previous paper (Daly et al. 2013) hence the isotopic abundance has to be modified. We have attached the tables of column densities and that of isotopic abundance for CH_3CH_2CN in Appendix B.

$(3 \pm 1) \times 10^{13}$ cm^{-2}, has been obtained by assuming the same cloud components as those of Esplugues et al. (2013b). Spectroscopic parameters were derived from a fit to lines reported by Kawaguchi et al. (1992b) and Hirahara et al. (1993), and three lines observed in IRC+10216 with an accuracy of 0.3 MHz. The dipole moment was determined from Botschwina et al. (1992). We derived a N(HNCCC)/N(HCCCN) upper limit ratio of 0.008. Kawaguchi et al. (1992a) obtained a N(HNCCC)/N(HCCCN) ratio in the range 0.002–0.006 in TMC-1.

After the detection of cyanamide (NH_2CN) by Turner et al. (1975), Cummins et al. (1986), and Belloche et al. (2013) in Sgr B2, we report a tentative detection of cyanamide (NH_2CN) in Orion-KL (see Fig. A.4). Frequencies, energies, and line intensities for O^+-NH_2CN and O^--NH_2CN were those published in the JPL catalog (based on the works of Read et al. 1986 and Birk 1988). We estimated a column density $\leq(3 \pm 1) \times 10^{13}$ cm^{-2} (O^++O^-) by assuming that its lines are coming only from one component (hot core) at 200 K (v_{LSR} = 5 km s^{-1}, Δv = 5 km s^{-1}, d_{sou} = 10″, offset = 2″). NH_2CN has an isomer differing only in the CN group, so that, the isomerization energy between the cyanamide and isocyanamide (NH_2NC) is 18 537 cm^{-1} (Vincent & Dykstra 1980). In this work, we also provided only an upper limit column density of isocyanamide (O^++O^-) being $\leq(5 \pm 1) \times 10^{13}$ cm^{-2}. Spectroscopic parameters were derived fitting the rotational lines reported by Schäfer et al. (1981). the dipole moment was determined by Ichikawa et al. (1982) from ab-initio calculations.

In Table 7, we give values of interconversion energies between cyanide and isocyanide molecules. These interconversion barriers are high, and under astronomical environments, such as the hot cores, it is unlikely that the isocyanide isomers are produced by rearrangement of the corresponding cyanide species. Remijan et al. (2005), proposed that non-thermal processes (such as shocks or enhanced UV flux in the surrounding medium) may be the primary route to the formation of interstellar isocyanides by the conversion of the cyanide to its isocyanide counterpart. Nevertheless, other formation routes have to be explored to explain their presence in environments dominated by thermal processes. Dissociative recombination reactions on the gas phase probably lead to the formation of the cyanide or isocyanide molecules. Depending on the structure of the protonated hydrocarbon and the branching ratios of the dissociative recombination pathway, the molecule $H_2C_3N^+$ might produce cyanoacetylene and isocyanoacetylene, and similarly, the molecule $C_2H_4N^+$ could yield methyl cyanide and methyl isocyanide (Green & Herbst 1979). DeFrees et al. (1985) found that the calculated ratio of the formation of the protonated precursor ions (CH_3CNH^+ and CH_3NCH^+) agrees with the detection of CH_3NC in dark clouds (Irvine & Schloerb 1984). In the same way, the recombination reaction of the molecule $C_2H_6N^+$ could give ethyl isocyanide (Bouchoux et al. 1992). Once the isocyanides are formed, they remain as metastable species due to the high barrier quoted above supporting the possible existence of isolated isocyanides (Vincent & Dykstra 1980). On the other hand, a recent experimental study of the interaction of the diatomic radical CN and the π-system C_2H_4 confirms that the possible pathway to CH_2CHNC becomes negligible even at temperatures as high as 1500 K (Balucani et al. 2000; Leonori et al. 2012). Since the cyanide molecules are strongly related to the dust chemistry (Blake et al. 1987; Charnley et al. 1992; Caselli et al. 1993; Rodgers & Charnley 2001; Garrod et al. 2008; Belloche et al. 2013), we also can infer a probable origin for the isocyanides from reactions on grain mantles.

5. Discussion

5.1. Abundances and column density ratios between the cyanide species

Table 8 shows the ground state abundances in the hot core (or hot core + plateau) component of the studied species in this work and the column density ratios between vinyl cyanide and other cyanide molecules. Results provided by different authors in Orion-KL, the well-studied star forming region Sgr B2, the star forming complex G34.3+0.2 (hot core), and the dark molecular cloud TMC-1 are also given in this table.

For Orion-KL, our study covers a wide frequency range allowing detailed modeling of the molecular emission. Moreover, the molecular abundances obtained from other authors, which are shown in Table 8, are often obtained with different telescopes and different assumptions on the size and physical conditions of Orion-KL. For this reason, these abundances are given in Table 8 for comparison purposes, but we focus on the results obtained in this work that have been derived from a common set of assumptions, sizes, and physical conditions for Orion-KL.

To estimate molecular abundances for the cyanide and isocyanide species, we assume that the column density of H_2 (N_{H_2}) is 4.2×10^{23} cm^{-2} for the hot core, 2.1×10^{23} cm^{-2} for the plateau, and 7.5×10^{22} cm^{-2} for the compact ridge and for the extended ridge, as derived by Tercero et al. (2010).

The total abundance for the CH_2CHCN ground state, as derived from all the components (hot core + mix hot core-plateau) (see Table 5), was $X(N_{CH_2CHCN}/N_{H_2}) = (2.0 \pm 0.6) \times 10^{-8}$. By means of the derived vibrational temperatures, we can estimate the vibrational partition function that follows the Eq. (4) for a Boltzmann distribution in both narrow components (1.7 and 1.5 for hot and cold narrow components, respectively) and correct the ground state column density to the total one (see Sect. 4.4.5). Considering these results for the vibrational partition function, we obtained $X_{CH_2CHCN} \simeq (3.1 \pm 0.9) \times 10^{-8}$.

$$f_v = 1 + \sum_{x=1}^{n} d_x \exp\left(-\frac{E_{vx}}{T_{vib}}\right), \quad (4)$$

where d_x is the degeneracy of the vibrational mode x and the low T_{vib} leads to $f_v \simeq 1$.

Assuming the column density values of CH_3CN of Bell et al. (2014), the abundance for CH_3CN ground state in the hot core component was $\simeq(1.0 \pm 0.3) \times 10^{-7}$. To estimate the correction of the column density of CH_3CN from excited vibrational states, we have derived the column density of this molecule in its $v_8 = 1$ lower energy state (525.2 K) and found a $N(CH_3CN, v_8 = 1) \simeq 1.4 \times 10^{15}$ cm^{-2} and $T_{vib} \simeq 159$ K (considering only the hot core and plateau components). Hence, the vibrational partition function is ~1.04 and $X_{Total} \simeq X_{ground}$ for methyl cyanide.

For ethyl cyanide we use the column density results of Daly et al. (2013) (see Appendix B). We determine the $X(N_{CH_3CH_2CN}/N_{H_2})$ ratio being $(1.8 \pm 0.5) \times 10^{-7}$ for the ground state. Assuming the vibrational temperatures obtained in Daly et al. (2013) $\simeq$160 ± 50 K, $\simeq$185 ± 55 K, and $\simeq$195 ± 95 K for v_{13}/v_{21} (E_u = 306.3/315.4 K), v_{20} (E_u = 531.2 K), and v_{12} (E_u = 763.4 K), respectively, the estimated vibrational partition function is 1.4, so we derived an abundance ratio $X \simeq (2.5 \pm 0.8) \times 10^{-7}$ for ethyl cyanide.

Esplugues et al. (2013b) derived an abundance of 7.3×10^{-9} for HC_3N (hot core + plateau) in the ground state.

Assuming a mean vibrational temperature of 360 K in the hot core that is calculated by these authors, the vibrational partition function from v_5 (E_u = 954.48), v_6 (E_u = 718.13), v_7 = 1

Table 8. Column density ratios and molecular abundances.

Molecule	Orion-KL		Sgr B2		G34.3+0.2		TMC-1	
	X	R	X	R	X	R	X	R
CH_2CHCN	$(2.0 \pm 0.6) \times 10^{-8\,\dagger}$ $1.5 \times 10^{-9\,a}$ $1.8 \times 10^{-9\,b}$	...	$6.2 \times 10^{-8\,j}$ $6.0 \times 10^{-8\,k}$	...	$3.0 \times 10^{-10\,n}$	...	$1.0 \times 10^{-9\,p}$	...
CH_3CN	$(1.0 \pm 0.3) \times 10^{-7\,\dagger\,d}$ $4.0 \times 10^{-9\,a}$ $7.8 \times 10^{-9\,b}$ $5.1 \times 10^{-9\,c}$	$0.20^{\dagger\,d}$ 0.39^{a} 0.23^{b} 1.7^{e} $0.18–1.8^{f}$ 0.48^{g}	$3.0 \times 10^{-8\,k}$	0.40^{e} 2.0^{k} 3.4^{l} 0.40^{m} 0.37^{o}	...	...	$7.5 \times 10^{-10\,p}$	1.3^{p}
CH_3CH_2CN	$(1.8 \pm 0.5) \times 10^{-7\,\dagger\,h}$ $3.0 \times 10^{-9\,a}$ $9.8 \times 10^{-9\,b}$	$0.11^{\dagger\,h}$ 0.50^{a} 0.18^{b} 0.15^{e} 0.14^{f} 0.06^{g}	$6.0 \times 10^{-10\,k*}$	0.72^{e} 11^{l} 0.67^{m} 1.7^{n} 0.40^{o}	$1.0 \times 10^{-8\,n}$	0.20^{n}	...	$>2.00^{q}$
HCCCN	$(7 \pm 2) \times 10^{-9\,\dagger\,i}$ $1.8 \times 10^{-9\,a}$ $1.6 \times 10^{-9\,b}$ $1.8 \times 10^{-9\,c}$	$2.9^{\dagger\,i}$ 0.86^{a} 1.1^{b} 2.11^{e} $0.6\text{-}1.5^{f}$ 0.16^{g}	$5.0 \times 10^{-9\,k}$	0.13^{e} 12^{k} 61^{o}	...	...	$7.5 \times 10^{-8\,p}$	0.01^{p}
NH_2CN	$\leq(7 \pm 2) \times 10^{-11\,\dagger}$	$\geq 286^{\dagger}$ 30^{e}	$9.0 \times 10^{-11\,k*}$	1.4^{e} 14^{o}	...	...	...	...

Notes. Abundances (X) and column density ratios between vinyl cyanide and some studied cyanides (R) in Orion-KL and other sources. [(†)] Values from this work. [(a)] Sutton et al. (1995), hot core, telescope beam ~13.7″. [(b)] Blake et al. (1987), hot core, telescope beam ~30″. [(c)] Persson et al. (2007), hot core, source size 10″. [(d)] Bell et al. (2014), hot core (different components between 5–10″) + plateau (10″). [(e)] Turner (1991). [(f)] Johansson et al. (1984). [(g)] Schilke et al. (1997). [(h)] Daly et al. (2013), hot core (4–10″) and mix hot core-plateau (25″). [(i)] Esplugues et al. (2013b) hot core (7–10″) and plateau (20″). [(j)] Müller et al. (2008). [(k)] Nummelin et al. (2000) small source-size averaged. [(k*)] Nummelin et al. (2000) beam averaged. [(l)] Remijan et al. (2005). [(m)] Belloche et al. (2009). [(n)] Mehringer & Snyder (1996). [(o)] Belloche et al. (2013). [(p)] Ohishi & Kaifu (1998). [(q)] Minh & Irvine (1991).

(E_u = 320.45), and v_7 = 2 (E_u = 642.67) is ~2.6 for the hot core components. Applying this correction in the hot core, we obtained a total abundance of $X_{HC_3N} \simeq 1.3 \times 10^{-8}$ (hot core + plateau).

For NH_2CN, we determine a molecular abundance $X(N_{NH_2CN}/N_{H_2})$ of $\leq(7 \pm 2) \times 10^{-11}$.

The column density ratio between the unsaturated hydrocarbon CH_2CHCN and other -CN bearing molecules, such as CH_3CH_2CN, CH_3CN, HC_3N, and NH_2CN, $N(CH_2CHCN)/N$(X-CN), could be used to track a possible different evolutionary state described by different chemical models and to provide inputs for the chemical modeling of the cloud.

We obtain an abundance ratio $N(CH_2CHCN)/N$(X-CN)<1 for the saturated cyanide molecules (CH_3CH_2CN and CH_3CN); these ratios related with methyl and ethyl cyanide obtained by different authors are lower (in general) in Orion-KL than in the galactic center (Sgr B2). We also note that the relative abundance of CH_3CH_2CN with respect to vinyl cyanide in Orion is twice as much as in the hot core G34.3+0.2. In contrast, in the dark cloud TMC-1 vinyl cyanide is more abundant than the saturated -CN hydrocarbons.

The relative abundance between CH_2CHCN and HC_3N follows an opposite tendency than that of methyl and ethyl cyanide: HC_3N is less abundant than CH_2CHCN in Orion-KL and Sgr B2, whereas HC_3N is at least two orders of magnitude more abundant than CH_2CHCN in TMC-1. Nevertheless, we want to remark that we only address the hot core (or hot core + plateau) abundances in our work in Table 8. For vinyl and ethyl cyanide and cyanamide, these abundances correspond with the total abundance in the ground state in Orion-KL. However, cyanoacetylene appears in all the Orion-KL components, so its total abundance is higher than that of vinyl cyanide when we consider the whole Orion-KL region covered by our observations.

Finally, we find an lower limit of 286 for $X(CH_2CHCN)/X(NH_2CN)$.

The formation routes of the cyanide molecules in several environments have been extensively discussed by different authors. As ethyl cyanide was mainly detected in hot core regions (Johansson et al. 1984; Sutton et al. 1985; Blake et al. 1987), the grain surface production (by hydrogenation of HC_3N) seemed to be the main formation mechanisms for this molecule (Blake et al. 1987; Charnley et al. 1992; Caselli et al. 1993). On the other hand, vinyl cyanide has been detected in the dark could TMC-1 (Matthews & Sears 1983) and in hot cores (where appeared correlated with ethyl cyanide emission), indicating that gas phase production was also important for forming these species. Chemical models of Charnley et al. (1992) and

A&A 572, A44 (2014)

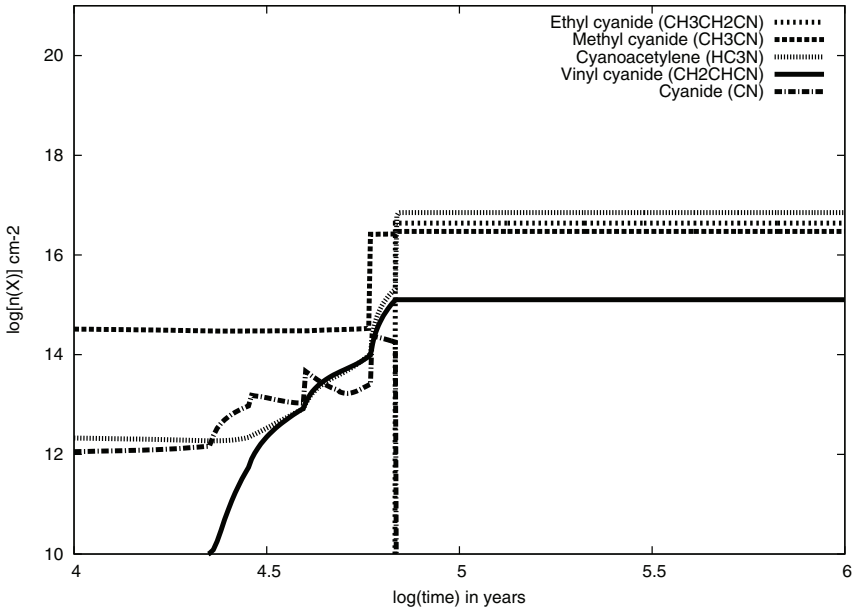

Fig. 17. Time evolution of the column densities of CH_2CHCN, CH_3CN, CH_3CH_2CN, HC_3N, and CN for a hot core chemical model.

Caselli et al. (1993) in hot cores predicted that CH_2CHCN forms in gas phase reactions involving CH_3CH_2CN. Caselli et al. (1993) derived a relation between the abundance ratio $X(CH_2CHCN)/X(CH_3CH_2CN)$ and the evolutionary stage of the core. This ratio has been used by several authors as a chemical clock to estimate the cloud age (Fontani et al. 2008; Müller et al. 2008). Belloche et al. (2009) performed a detailed analysis of the cyanide species detected in Sgr B2, including chemical models based on that of Garrod et al. (2008). Considering the observed relative abundances between these species, they conclude that the main formation mechanism for alkyl cyanides is probably the sequential addition of CH_2 or CH_3 radicals to CN, CH_2CN, and C_2H_4CN on the grain surfaces. Formation of methyl cyanide is dominated by reactions on the grains by addition of CH_3 and CN radicals, but it may also be formed by gas-phase processes after the evaporation of HCN. Vinyl cyanide is predominantly formed in the gas-phase through the reaction of CN with C_2H_4. Then CH_2CHCN accretes onto the grains by being a potential precursor, with HC_3N of ethyl cyanide and *n*-propyl cyanide. After the evaporation of the ice mantles, vinyl cyanide is efficiently formed again in the gas phase.

5.2. Chemical model

We have investigated the observed column densities of CH_2CHCN, CH_3CN, CH_3CH_2CN, HCCCN, and CN using a time and depth dependent gas-grain chemical model, UCL_CHEM. UCL_CHEM is a two-phase model, which follows the collapse of a prestellar core (Phase I), followed by the warming and evaporation of grain mantles (Phase II). In Phase II, we increase the dust and gas temperature up to 300 K to simulate the presence of a nearby infrared source in the core. For the hot core component, we model both a 10 $M_\odot$ and 15 $M_\odot$ star with a final density of 10^7 cm $^{-3}$. During the collapse, atoms and molecules collide with and freeze onto grain surfaces. The depletion efficiency is determined by the fraction of the gas-phase material that is frozen on to the grains, which is dependent on the density, the sticking coefficient and other properties of the species and grains (see Rawlings et al. 1992). In our modeling, we have explored the uncertainty in grain properties and sticking coefficients by varying the depletion percentage. Initial atomic abundances are taken from Sofia & Meyer (2001), as in Viti et al. (2004). Gas-phase reaction rate coefficients are taken from the UMIST database of Woodall et al. (2007), however, some have been updated with those from the KIDA database (Wakelam 2009). We also include some simple grain-surface reactions (mainly hydrogenation) as in Viti et al. (2004). While COMs (complex organic molecules) may also form via surface reactions involving heavier (than hydrogen) species (e.g. Garrod et al. 2008), the mobility of most heavy species on grains has not been experimentally investigated; hence, for this qualitative analysis, we chose to adopt a simpler model where only the most efficient surface reactions occur. In this way we can give a lower limit to the formation of COMs which may be augmented by more complex reactions should they occur. In Phase I, non-thermal desorption is considered as in Roberts et al. (2007).

Within our grid of models, we find that models where we simulate a 10 $M_\odot$ star and 100% of CO frozen onto grain surfaces which most accurately reproduce the observed column densities of CH_2CHCN, CH_3CN, and CH_3CH_2CN. Figure 17 shows the column density as a function of time during phase II for this model. The column density produced by the model for HCCCN is an order of magnitude higher than the observed value. While our models simulate both gas phase and grain surface reactions for all of these species, the grain surface reactions are essential to reproduce the observed column densities. We therefore conclude that we are missing some grain surface destruction routes for HCCCN, and, consequently, overproduced this species in our models. Moreover, the deep decreased of the CN abundance when CH_3CH_2CN appears is observationally confirmed by the lack of the hot core component in the CN lines even at the HIFI frequencies (Crockett et al. 2014). For details of

the same surface chemistry approach, see Viti et al. (2004) and Bell et al. (2014).

5.3. Further issues for CH_2CHCN

Further observations of telescopes with higher sensitivity and spatial resolution, such as Atacama Large Millimeter/submillimeter Array (ALMA), could provide additional detections of other vibrationally excited states above 600 cm^{-1}, such as the outstanding states in the $3v_{11}/2v_{15}/v_{14}$ triad of states near 680 cm^{-1} for which the spectroscopy is presently reported. In this study, we found that the $v_{11} = 3$ (987.9 K or 686.6 cm^{-1}) vibrational mode was near the detection limit, so we could not reliably address other vibrational components of the $3v_{11}/2v_{15}/v_{14}$ triad. We also note that Belloche et al. (2013) have recently detected the combination state $v_{15} = v_{11} = 1$ (809.9 K) but has not yet reported detection of the $v_{10} = 1$ (806.4 K) state toward Sgr B2(N). On the other hand, the $v_{15} = 2$ (960.2 K) excited state detected by these authors might be detected only at the limit in our study.

In the present work, we extended the laboratory coverage of the rotational spectrum of vinyl cyanide and the analysis of its vibrationally excited states to provide ample basis for detection of transitions from further excited vibrational states at even higher vibrational energies. The laboratory basis for detecting states up to as high as $v_9 = 1$ (1250 K) is now available. On the other hand, as implied by Fig. 1 and results for $4v_{11} = 4$, considerable spectroscopic analysis is required for satisfactory understanding of states above $v_9 = 1$.

6. Summary

Vinyl cyanide is one of the most abundant molecules in Orion-KL and a possible precursor of alanine. This study of the vinyl cyanide species improves the knowledge of the physical and chemical conditions of this high-mass star forming region. We have performed an identification of the ground state of CH_2CHCN and of its vibrationally excited states (up to 988 K) in the Orion-KL Nebula thanks to a new spectroscopic laboratory analysis by using Stark modulation and frequency-modulated spectrometers. Our results are based on rotational diagrams, integrated-frequency maps, and Gaussian fits to optimize the physical and chemical parameters that simulate the best synthetic spectrum of CH_2CHCN (using MADEX), which fit the observation conditions of the Orion-KL region in an accurate way. We have found $N(CH_2CHCN) \simeq (6 \pm 2) \times 10^{15}$ cm^{-2} from four cloud components of hot core/plateau nature (320-90 K). A total abundance of $(3.1 \pm 0.9) \times 10^{-8}$ for vinyl cyanide is provided in this work. We have detected the CH_2CHCN $v_{11} = 2$, 3 vibrational modes for the first time in Orion-KL and the CH_2CHCN $v_{10} = 1 \Leftrightarrow (v_{11} = 1, v_{15} = 1)$ excited state for the first time in the space. We have seen that these species with those of the three monosubstituted ^{13}C and the ^{15}N isotopologues and the tentative detection of the three monodeuterated species of vinyl cyanide contribute with more than 1100 observed lines in the 80–280 GHz domain covered by the Orion line survey. We highlight the importance for spectroscopic catalogs to introduce vibrationally excited species in the astronomical detections.

The column density ratios between the vinyl cyanide g.s. and the vibrationally excited states have been used to obtain temperatures at which the vibrational modes are excited and to correct the ground column density from the vibrational partition function. The high vibrational temperature ($T_{vib} > T_{rot}$) for the states $v_{10} = 1 \Leftrightarrow (v_{11} = 1, v_{15} = 1)$ and $v_{11} = 3$ suggests a temperature gradient toward the inner regions of the hot core. To infer the population mechanism of the vibrationally excited states (collisions and/or infrared radiation), collisional rates are needed.

Owing to the importance of isomerism for understanding a more precise way in forming interstellar molecules, we have included the study of ethyl isocyanide, methyl isocyanide, isocyanoacetylene, 3-imino-1, 2-propadienylidene, and isocyanamide in our work. We have provided the detection of methyl isocyanide for the first time in Orion-KL and tentative detections for the rest.

Finally, we have investigated the studied column densities of CH_2CHCN, CH_3CN, CH_3CH_2CN, and HCCCN using a time dependent gas-grain chemical model (UCL_CHEM) which reproduce the observed column densities for these molecules reasonably well, although it overestimates that for HCCCN. This is probably due to the efficiency for its formation on the grains being too high: a detailed investigation of the formation and destruction route for this species in chemical models is beyond the scope of this work. More quantitative models ought to be able to reproduce this molecule by investigating the efficiency of the formation of HCCCN on the grains.

Acknowledgements. We thank the anonymous referee who provided comments that improved this manuscript. We thank INTA-CSIC, and the Spanish MINECO and Junta de Castilla y León for funding support from grants the CONSOLIDER program "ASTROMOL" CSD2009-00038, AYA2009-07304, AYA2012-32032, CTQ2010-19008 and VA175U13. C.B. thanks also the Spanish MINECO for the FPI grant (BES-2011-047695). The IFPAN authors acknowledge a grant from the Polish National Science Centre, decision number DEC/2011/02/A/ST2/00298. Portions of this research were carried out at the Jet Propulsion Laboratory, California Institute of technology, under contract with the National Aeronautics and Space Administration.

References

Adande, G. R., & Ziurys, L. M. 2012, ApJ, 744, 194
Anderson, R. J., & Gwinn, W. D. 1968, J. Chem. Phys., 49, 39, 88
Agúndez, M., Cernicharo, J., Pardo, J. R., et al. 2008, Astron. Space Sci., 313, 229
Anders, E., & Grevesse, N. 1989, Geochim. Cosmochim. Acta, 53, 197
Balucani, N., Asvany, O., Huang, L. C. L., et al. 2000, ApJ, 545, 892
Baskakov, O. I., Dyubko, S. F., Ilyushin, V. V., et al. 1996, J. Mol. Spectr., 179, 94
Bauer, A., & Bogey, M. 1970, C. R. Acad. Sci. Paris, 271B, 892
Bell, T., Cernicharo, J., Viti, S., et al. 2014, A&A, 564, A114
Belloche, A., Garrod, T. D., Müller, H. S. P., et al. 2009, A&A, 499, 215
Belloche, A., Müller, H. S. P., Menten, K. M., Schilke, P., & Comito, C. 2013, A&A, 559, A47
Bera, P. P., Lee, T. J., & Schaefer, H. F. 2009, J. Chem. Phys., 131, 074303
Bestmann, G., & Dreizler, H. 1982, Z. Naturforsch, 37a, 58
Betz, A. L. 1981, ApJ, 244, L103
Beuther, H., & Nissen, H. D. 2008, ApJ, 679, L121
Birk, H. 1988, Ph.D. Thesis, Justus Liebig-Universit Giessen, Germany
Blake, G. A., Sutton, E. C., Masson, C. R., & Philips, T. G. 1987, ApJ, 315, 621
Blake, G. A., Mundy, L. G., Carlstrom, J., et al. 1996, ApJ, 472, L49
Bolton, K., Owen, N. L., & Sheridan, J. 1970, Spectrochim. Acta, 26, 909
Botschwina, P., Horn, M., Seeger, S., & Flgge, J. 1993, Chem. Phys. Lett., 195, 4, 427
Bouchoux, G., Nguyen, M. T., & Longevialle, P. 1992, J. Am. Chem. Soc., 114, 10000
Capone, L. A., Prasad, S. S., Huntress, W. T., et al. 1981, Nature, 293, 45
Carvajal, M., Margulés, L., Tercero, B., et al. 2009, A&A, 500, 1109
Caselli, P. 2005, Ap&SS Library, 324, 47
Caselli, P., Hasegawa, T. I., & Herbst, E. 1993, ApJ, 408, 548
Cazzoli, G., & Kisiel, Z. 1988, J. Mol. Spectr., 130, 303
Cernicharo, J. 1985, Internal IRAM report (Granada: IRAM)
Cernicharo, J. 2012, in ECLA-2011: Proc. of the European Conference on Laboratory Astrophysics, EAS Pub. Ser. 2012, eds. C. Stehl, C. Joblin, & L. d'Hendecourt (Cambridge: Cambridge Univ. Press), 58, 251
Cernicharo, J., Kahane, C., Guelin, M., & Gomez-Gonzalez, J. 1988, A&A, 189, L1
Cernicharo, J., Tercero, B. A., Fuente, A., et al. 2013, ApJ, 771, L10
Charnley, S. B., Tielens, A. G. G. M., & Millar, T. J. 1992, ApJ, 399, L71

Cole, A. R. H., & Green, A. A. 1973, J. Mol. Spectr., 48, 246
Colmont, J. M., Wlodarczak, G., Priem, D., et al. 1997, J. Mol. Spectr., 181, 330
Costain, C. C., & Stoicheff, B. P. 1959, J. Chem. Phys., 1959, 30, 777
Coudert, L. H., Drouin, B. J., Tercero, B., et al. 2013, ApJ, 779, 119
Crockett, N. R., Bergin, E. A., Neill, J. L., et al. 2014, ApJ, 787, 2
Cummins, S. E., Linke, R. A., & Thaddeus, P. 1986, ApJSS, 60, 819
Daly, A. M., Bermúdez, C., López, A., et al. 768, 81, ApJ, 2013
Demaison, J., Cosléou, J., Bocquet, R., & Lesarri, A. G. 1994, J. Mol. Spectr., 167, 400
Demyk, K., Mäder, H., Tercero, B., et al. 2007, A&A, 466, 255
Demyk, K., Wlodarczak, G., & Carvajal, M. 2008, A&A, 489, 589
DeFrees, D. J., McLean, A. D., & Herbst, E. 1985, ApJ, 293, 236
Ervasti, H. K., Jobst, K. J., Gerbaux, P., et al. 2009, Chem. Phys. Lett., 482, 211
Esplugues, G. B., Tercero, B., Cernicharo, J., et al. 2013a, A&A, 556, A143
Esplugues, G. B., Cernicharo, J., Viti, S., et al. 2013b, A&A, 559, A51
Fliege, E., & Dreizler, H. 1985, Z. Naturforsch., 40a, 43
Fontani, F., Caselli, P., Bourke, T. L., Cesaroni, R., & Brand, J. 2008, A&A, 477, L45
Gardner, F. F., & Winnewisser, G. 1975, ApJ, 195, L127
Garrod, R. T., Weaver, S. L. W., & Herbst, E. 2008, ApJ, 682, 283
Gensheimer, P. D. 1997, Ap&SS, 251, 199
Gerry, M. C. L., & Winnewiser, G. 1973, J. Mol. Spectr., 48, 1
Golsmith, P. F., & Langer, W. D. 1999, ApJ, 517, 209
Green, S., & Herbst, E. 1979, ApJ, 229, 121
Gripp, J., Guarnieri, A., Stahl, W., & Lentz, D. 2000, J. Mol. Struc. 526, 81
Guarnieri, A., Hinze, R., Krüger, M., et al. 1992, J. Mol. Spectr., 156, 1, 39
Guélin, M., Brouillet, N., Cernicharo, J., Combes, F., & Wooten, A. 2008, Ap&SS, 313, 45
Halverson, F., Stamm, R. F., & Whalen, J. J. 1948, J. Chem. Phys., 16, 808
Haykal, I., Carvajal, M., Tercero, B., et al. 2014, A&A, 568, A58
Heise, H. M., Lutz, H., & Dreizler, H. 1974, Z. Naturforsch., 29, 1345
Hirahara, Y., Ohshima, Y., & Endo, Y. 1993, ApJ, 403, L83
Hirota, T., Bushimata, T., Choi, Y. K., et al. 2007, PASJ, 59, 897
Ichikawa, K., Hamada, Y., Sugawara, Y., et al. 1982, Chem. Phys., 72, 301
Irvine, W. M., & Schloerb, F. P. 1984, ApJ, 282, 516
Irvine, W. M., Friberg, P., Hjalmarson, A., et al. 1988, ApJ, 334, L107
Johansson, L. B. E., Andersson, C., Elldèr, J., et al. 1984, A&A, 130, 227
Johnson, D. R., Lovas, F. J., Guélin, M., & Thaddeus, P. 1977, ApJ, 218, 370
Kawaguchi, K., Ohishi, M., & Ishikawa, S.-I. 1992a, ApJ, 386, L51
Kawaguchi, K., Takano, S., Ohishi, M., et al. 1992b, ApJ, 396, L49
Khlifi, M., Nollet, M., Paillous, P., et al. 1999, J. Mol. Spectr., 194, 206
Kim, M. K., Hirota, T., Honma, M., et al. 2008, PASJ, 60, 991
Kisiel, Z. 2001, in Spectroscopy from Space, eds. J., Demaison, et al. (Dordrecht: Kluwer Academic Publishers), 91
Kisiel, Z., Pszczolkowski, L., Medvedev, I. R., et al. 2005, J. Mol. Spectr., 233, 231
Kisiel, Z., Pszczolkowski, L., Drouin, B. J., et al. 2009a, J. Mol. Spectr., 258, 26
Kisiel, Z., Bialkowska-Jaworska, E., Butler, R. A. H, et al. 2009b, J. Mol. Spectr., 254, 78
Kisiel, Z., Pszczolkowski, L., Drouin, B. J., et al. 2011, talk MH09, 66th International Symp. on Molecular Spectroscopy, Columbus, Ohio, USA
Kisiel, Z., Pszczolkowski, L., Drouin, B. J., et al. 2012, J. Mol. Spectr., 280, 134
Kolesniková, L., Tercero, B., Cernicharo, J., et al. 2014, ApJ, 784, L7
Krasnicki, A., & Kisiel, Z. 2011, J. Mol. Spectr., 270, 83
Krasnicki, A., Kisiel, Z., Drouin B. J., & Pearson J. C. 2011, J. Mol. Struct., 1006, 20
Krüger, M., & Dreizler, H. 1992, Z. Naturforsch., 47a, 1067
Leonori, F., Petrucci, R., Wang, X., Casavecchia, P., & Balucani, N. 2012, Chem. Phys. Lett., 553, 1
Margulès, L., Motiyenko, R. A., Demyk, K., et al. 2009, A&A, 493, 565
Margulès, L., Huet, T. R., Demaison, J., et al. 2010, ApJ, 714, 1120
Mathews, H. E., & Sears, T. J. 1983, ApJ, 267, L53
Martinez Jr., O., Lattanzi, V., Thorwirth, S., & McCarthy, M. C. 2013, J. Chem. Phys., 138, 094316
Menten, K. M., Reid, M. J., Forbrich, J., & Brunthaler A. 2007, A&A, 474, 515
Mehringer, D. M., & Snyder, L. 1996, ApJ, 471, 897
Minh, Y. C., & Irvine, W. M. 1991, Ap&SS, 175, 165
Morris, M., Turner, B. E., Palmer, P., & Zuckerman, B. 1976, ApJ, 205, 82
Motiyenko, R. A., Tercero, B., Cernicharo, J., & Margulés, L. 2012, A&A, 548, A71
Müller, H. S. P., Thorwirth, S., Roth, D. A., & Winnewisser, G. 2001, A&A, 370, L49
Müller, H. S. P., Schlöder, F., Stutzki, J., & Winnewisser, G. 2005, J. Mol. Struct., 742, 215
Müller, H. S. P., Belloche, A., Menten, Comito, C., & Shilke, P. 2008, J. Mol. Spectr., 251, 319
Neil, J. L., Crockett, N. R., Bergin, E. A., Pearson, J. C., & Li-Hong, Xu 2013, ApJ, 777, 85
Nummelin, A., & Bergman, P. 1999, A&A, 341, L59
Nummelin, A., Bergman, P., Hjalmarson, Å, et al. 2000, ApJSS, 128, 213
Occhiogrosso, A., Viti, S., & Balucani, N. 2013, MNRAS, 432, 3423
Ohisi, M., & Kaifu, N. 1998, J. Chem. Soc. Faraday Discuss., 109, 205
Pardo, J. R., Cernicharo, J., & Serabyn, E. 2001a, IEEE Tras. Antennas and Propagation, 49, 1683
Pardo, J. R., Cernicharo, J., Herpin, F., Kawamura, J., et al. 2001b, ApJ, 562, 799
Persson, C. M., Olofsson, A. O. H., Koning, N., et al. 2007, A&A, 476, 2, 807
Petrie, S. A. H. 1991, Ph.D. Thesis, University of Canterbury, New Zealand (`ir.canterbury.ac.nz`)
Pickett, H. M. 1991, J. Mol. Spectr., 148, 371
Pickett, H. M., Poynter, R. L., Cohen, E. A., et al. 1998, J. Quant. Spectr. Rad. Transf., 60, 883
Pliva, J., Le, L. D., Johns, J. W. C., Lu, Z., & Bernheim, R. A. 1995, J. Mol. Spectr., 173, 2, 423
Pracna, P., Urban, J., Votava, O., et al. 2011, J. Phys. Chem. A., 115, 1063
Rawlings, J. M. C., Hartquist, T. W., Menten, K. M., & Williams, D. A. 1992, MNRAS, 255, 471
Read, W. G., Cohen, E. A., & Pickett, H. M. 1986, J. Mol. Spectr., 115, 316
Remijan, A. J., Hollis, J. M., Lovas, F. J., Plusquellic, D. F., & Jewell, P. R. 2005, ApJ, 632, 333
Roberts, J. F., Rawlings, J. M. C., Viti, S., & Williams, D. A. 2007, MNRAS, 382, 733
Rodgers, S. D., & Charnley, S. B. 2001, ApJ, 546, 324
Rodgers, S. D., & Millar, T. J. 1996, MNRAS, 280, 1046
Roueff, E., Lis, D. C., vanderTak, F. F. S., Gerin, M., & Goldsmith, P. F. 2005, A&A, 438, 585
Sandstrom, K. M., Peek, J. E. G., Bower, G. C., et al. 2007, ApJ, 667, 1161
Savage, C., Apponi, A. J., Ziurys, L. M., & Wyckoff, S. 2002, ApJ, 578, 211
Schäfer, E., & Winnewisser, M. 1982, Ber. Bunsenges. Phys. Chem., 86, 780
Schäfer, E., Winnewisser, M., & Christiansen, J. J. 1981, Chem. Phys. Lett., 81, 380
Schilke, P., Walmsley, C. M., Pineau Des Forets, G., et al. 1992, A&A, 256, 595
Schilke, P., Groesbeck, T. D., Blake, G. A., & Philips, T. G. 1997, ApJSS, 108, 301
Sofia, U. J., & Meyer, D. M. 2001, ApJ, 554, L221
Stolze, M., & Sutter, D. H. 1985, Z. Naturforsch. Teil A, 40a, 998
Sutton, E. C., Blake, G. A., Masson, C. R., & Phillips, T. G. 1985, A&A, 58, 341
Sutton, E. C., Peng, R., Danchi, W. C., et al. 1995, ApJSS, 97, 455
Tercero, B. 2012, Thesis UCM, Spain
Tercero, B., Cernicharo, J., Pardo, J. R., & Goicoechea, J. R. 2010, A&A, 517, A96
Tercero, B., Vincent L., Cernicharo, J., Viti S., & Marcelino, N. 2011, A&A, 528, A26
Tercero, B., Margulès, L., Carvajal, M., et al. 2012, A&A, 538, 119
Tercero, B., Kleiner, I., Cernicharo, J., et al. 2013, ApJ, 770, L13
Tielens, A. G. G. M. 2005, The Physics and Chemistry of the Interstellar Medium (Cambridge University Press)
Turner, B. E. 1991, ApJSS, 76, 617
Turner, B. E., Kyslyakov, A. G., Liszt, H. S., & Kaifu, N. 1975, ApJ, 201, L149
Vigren, E., Hamberg, M., Zhaunerchyk, V., et al. 2009, ApJ, 695, 317
Vincet, M. A., & Dykstra, C. E. 1980, J. Chem. Phys., 73, 3838
Viti, S., Collings, M. P., Dever, J. W., McCoustra, M. R. S., & Williams, D. A., 2004, MNRAS, 354, 1141
Wakelam, V. 2009, BAAS, 41, 665
Widicus Weaver, S. L., & Friedel, D. N. 2012, ApJS, 201, 16
Wilcox, W. S., Goldstein, J. H., & Simmons, J. W. 1954, J. Chem. Phys., 22, 516
Woodall, J., Agúndez, M., MarkwickKemper, A. J., & Millar, T. J. 2007, A&A, 466, 1197
Wyckoff, S., Kleine, M., Peterson, B. A., Wehinger, P. A., & Ziurys, L. M. 2000, ApJ, 535, 991
Yamada, K., & Winnewisser, M. 1975, Z. Naturforsch, A, 30, 672
Ziurys, L. M., & McGonagle, D. 1993, ApJSS, 89, 155

Appendix A

Table A.1. Spectroscopic constants in the diagonal blocks of the Hamiltonian for the $2v_{15} \Leftrightarrow v_{14} \Leftrightarrow 3v_{11}$ triad of vibrational states in vinyl cyanide compared with those for the ground state.

	Ground state	$2v_{15}$	v_{14}	$3v_{11}$
A/MHz	49 850.69655(43)[a]	51 864.336(36)	50 344.872(21)	47 990.329(47)
B/MHz	4971.212565(37)	4977.66513(90)	4974.53973(78)	5028.9277(13)
C/MHz	4513.828516(39)	4532.01579(78)	4519.08450(62)	4537.6921(11)
Δ_J/kHz	2.244058(13)	2.23613(25)	2.26543(26)	2.31540(32)
Δ_{JK}/kHz	−85.6209(35)	−101.725(13)	−81.531(12)	−62.131(12)
Δ_K/kHz	2715.4213(94)	4021.39(65)	2752.53(50)	1416.57(67)
δ_J/kHz	0.4566499(32)	0.44884(16)	0.45991(16)	0.48731(24)
δ_K/kHz	24.4935(22)	26.477(90)	27.126(82)	32.642(96)
Φ_J/Hz	0.0064338(17)	0.006223(44)	0.006097(45)	0.006248(56)
Φ_{JK}/Hz	−0.00425(40)	0.129(16)	0.063(15)	0.094(17)
Φ_{KJ}/Hz	−7.7804(39)	−25.21(11)	−7.03(10)	4.74(10)
Φ_K/Hz	384.762(63)	1391.8(35)	395.8(16)	−317.0(41)
ϕ_J/Hz	0.00236953(79)	0.002184(22)	0.002218(23)	0.002359(33)
ϕ_{JK}/Hz	0.14283(40)	0.126(16)	0.088(16)	0.252(17)
ϕ_K/Hz	37.011(58)	66.2(24)	42.9(21)	27.1(21)
L_J/mHz	−0.000026315(71)	[0.]	[0.]	[0.]
L_{JJK}/mHz	−0.001077(29)	[0.]	[0.]	[0.]
L_{JK}/mHz	0.4279(30)	[0.]	[0.]	[0.]
L_{KKJ}/mHz	0.012(12)	9.07(38)	3.62(38)	3.64(22)
L_K/mHz	−61.41(17)	−658.9(84)	−77.6(88)	161.3(94)
l_J/mHz	−0.000011602(36)	[0.]	[0.]	[0.]
l_{JK}/mHz	−0.000956(20)	[0.]	[0.]	[0.]
l_{KJ}/mHz	−0.1436(46)	[0.]	[0.]	0.988(40)
l_K/mHz	8.91(18)	16.3(10)	8.03(88)	−25.43(69)
P_{KJ}/mHz	−0.0000156(31)	[0.]	[0.]	[0.]
P_{KKJ}/mHz	−0.0001977(57)	[0.]	[0.]	[0.]
P_K/mHz	0.00867(15)	[0.]	[0.]	[0.]
ΔE^b/MHz		0.0	549 163.34(55)	694 443.66(90)
ΔE/cm^{-1}		0.0	18.31812(2)	23.16415(3)
$N_{\rm lines}{}^c$	4490,0	1329,52	1287,53	1250,81
$\sigma_{\rm fit}{}^d$/MHz	0.144	0.265[e]	0.228[e]	0.309[e]
$\sigma_{\rm rms}{}^d$	0.713	1.980	1.467	2.329

Notes. [(a)] Round parentheses enclose standard errors in units of the last quoted digit of the value of the constant; square parentheses enclose assumed values. [(b)] The fitted vibrational energy difference relative to the lowest vibrational state in the triad. [(c)] The number of distinct frequency fitted lines and the number of lines rejected at the 10σ fitting criterion of the SPFIT program. [(d)] Deviations of fit for the different vibrational subsets. [(e)] The coupled fit for the complete triad encompasses 3866 lines, at an overall $\sigma_{\rm fit}$ of 0.269 MHz and requires also the use of constants reported in Table A.3.

Table A.2. Spectroscopic constants in the off-diagonal blocks of the Hamiltonian for the $v_{10} \Leftrightarrow v_{11}v_{15}$ and $v_{11}v_{10} \Leftrightarrow 2v_{11}v_{15}$ dyads of vibrational states in vinyl cyanide.

	$v_{10} \Leftrightarrow v_{11}v_{15}$	$v_{11}v_{10} \Leftrightarrow 2v_{11}v_{15}$		$v_{10} \Leftrightarrow v_{11}v_{15}$	$v_{11}v_{10} \Leftrightarrow 2v_{11}v_{15}$
G_a/MHz	1623.(13)	1557.(34)	G_b/MHz	643.32(46)	929.1(30)
G_a^J/MHz	0.2192(48)	0.4834(45)	G_b^J/MHz	0.01663(17)	0.00766(38)
G_a^K/MHz	6.432(76)	3.67(10)			
G_a^{JK}/MHz	0.0001240(23)				
F_{bc}/MHz	4.151(90)	9.447(88)	F_{ac}/MHz	−27.14(29)	−14.20(69)
			F_{ac}^J/MHz	−0.0001184(26)	

Notes. [(a)] Round parentheses enclose standard errors in units of the last quoted digit of the value of the constant, and only the constants with non-zero values are listed. [(b)] These constants complement those in the diagonal blocks listed in Table 2.

A&A 572, A44 (2014)

Table A.3. Spectroscopic constants in the off-diagonal blocks of the Hamiltonian for the $2v_{15} \Leftrightarrow v_{14} \Leftrightarrow 3v_{11}$ triad of vibrational states in vinyl cyanide.

	$2v_{15} \Leftrightarrow v_{14}$	$v_{14} \Leftrightarrow 3v_{11}$		$2v_{15} \Leftrightarrow 3v_{11}$
G_a/MHz	5852.21(58)	223.63(15)	G_c/MHz	25.8(27)
G_a^J/MHz	0.01958(32)			
G_a^K/MHz	−2.790(18)	−0.1703(17)	F_{ab}/MHz	3.59(22)
G_a^{JJ}/MHz	−0.000000324(61)			
G_a^{JK}/MHz	−0.0000335(23)		W	14179.2(17)
G_a^{KK}/MHz	0.001503(51)			
			$W_{\pm}$/MHz	0.8521(24)
F_{bc}/MHz		0.4557(30)	$W_{\pm}^J$/MHz	0.00000540(82)
			$W_{\pm}^K$/MHz	0.00847(15)
G_b/MHz	−9.50(21)	18.180(61)	$W_{\pm}^{JK}$/kHz	−0.000000700(44)
G_b^K/MHz	−0.4173(94)		$W_{\pm}^{KK}$/kHz	0.00000523(16)

Notes. [(a)] Round parentheses enclose standard errors in units of the last quoted digit of the value of the constant, and only the constants with non-zero values are listed. [(b)] These constants complement those in the diagonal blocks listed in Table A.1.

Table A.4. Spectroscopic constants in the effective rotational Hamiltonian for the v_9 and $4v_{11}$ excited vibrational states of vinyl cyanide.

	v_9	$4v_{11}$
A/MHz	49 828.53(89)[a]	47 495.5(22)
B/MHz	4953.0854(34)	5047.5125(98)
C/MHz	4501.1911(18)	4545.1778(85)
Δ_J/kHz	2.2025(18)	2.3223(66)
Δ_{JK}/kHz	−92.279(81)	−56.27(34)
Δ_K/kHz	2500.(135)	−87.(529)
δ_J/kHz	0.4392(11)	0.4766(46)
δ_K/kHz	11.17(53)	28.9(48)
Φ_J/Hz	0.00469(72)	0.0368(68)
Φ_{JK}/Hz	−2.22(36)	5.3(31)
Φ_{KJ}/Hz	−28.6(17)	−32.(13)
Φ_K/Hz	[0.]	104900.(42879)
ϕ_J/Hz	0.00145(38)	−0.0185(36)
ϕ_{JK}/Hz	−0.93(18)	7.6(18)
ϕ_K/Hz	−159.(48)	1131.(532)
N_{lines}[b]	373, 7	225, 17
σ_{fit}/MHz	0.167	0.250
σ_{rms}	1.665	2.496

Notes. [(a)] Round parentheses enclose standard errors in units of the last quoted digit of the value of the constant; square parentheses enclose assumed values. [(b)] The number of distinct frequency fitted lines and the number of confidently assigned lines rejected at the 10σ fitting criterion of the SPFIT program.

Table A.5. Vibrational changes in rotational constants[a] for the studied excited vibrational states in vinyl cyanide.

	Exp.	Calc. I[b]	Calc. II[c]		Exp.	Estimated[d]
v_{11}	−680.2411(15)[d]	−782	−674.20	$v_{11}v_{15}$	40.02(61)	271
	19.56011(10)[d]	19.14	20.28		21.4597(70)	22.69
	8.13824(10)[d]	8.00	8.51		17.7744(13)	17.31
v_{15}	951.3883(18)	1002	900.77	$2v_{15}$	2013.674(35)	1903
	3.13085(12)	5.94	3.94		6.45356(89)	6.26
	9.16787(11)	10.28	8.95		18.2016(10)	18.34
v_{10}	−300.67(63)	−369	−326.14	$3v_{11}$	−1860.399(47)	−2041.
	−5.5434(98)	−5.49	−5.79		57.7162(12)	58.69
	−4.2057(13)	−3.98	−4.20		23.8494(13)	24.41
v_{14}	494.2055(11)	606	566.66	$v_{10}v_{11}$	−988.98(62)	−981
	3.32747(40)	2.37	3.10		13.766(32)	14.02
	5.25568(31)	4.43	4.88		4.1072(31)	3.93
v_9	−22.17(89)	−37	39.53	$2v_{11}v_{15}$	−725.83(56)	−409
	−18.1272(34)	−17.52	−18.47		40.2814(98)	42.25
	−12.6374(11)	−12.35	−13.27		26.2639(85)	25.44
				$4v_{11}$	−2355.2(22)	−2721
					76.2999(98)	78.24
					31.3493(85)	32.55

Notes. [(a)] The tabulated values for each state are differences relative to the ground state constants: $(A_v - A_0)$, $(B_v - B_0)$, and $(C_v - C_0)$ all in MHz. [(b)] From anharmonic force field calculation at the MP2/6-311++G(d, p) level. [(c)] From anharmonic force field calculation at the CCSD(T)/6-31G(d, p) level. [(d)] Estimated from experimental changes listed in the second column by assuming their additivity.

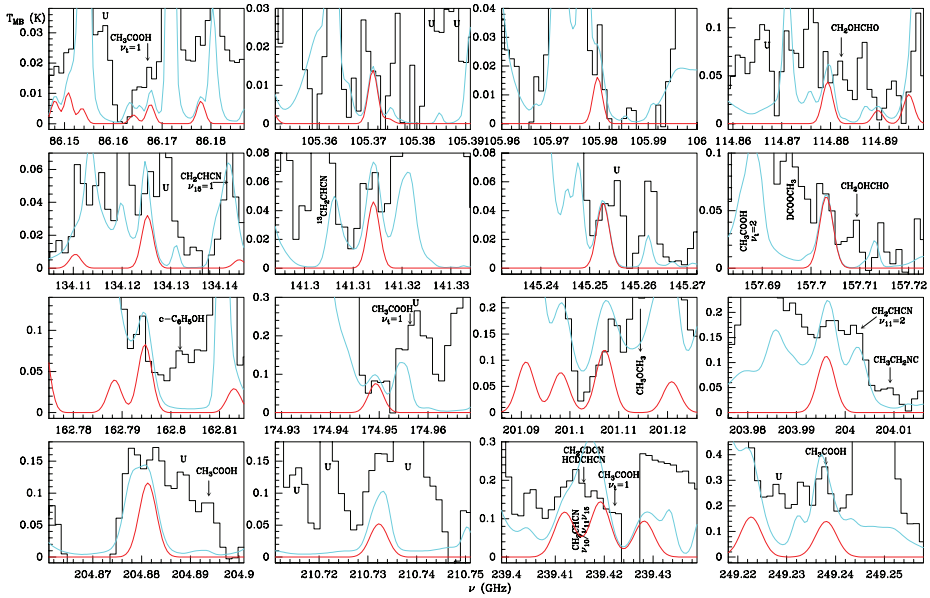

Fig. A.1. Observed lines from Orion-KL (histogram spectra) and model (thin red curves) of CH_2CHCN of $v_{11} = 3$. The cyan line corresponds to the model of the molecules we have already studied in this survey (see text Sect. 4.4.2), including the CH_2CHCN species. A v_{LSR} of 5 km s^{-1} is assumed.

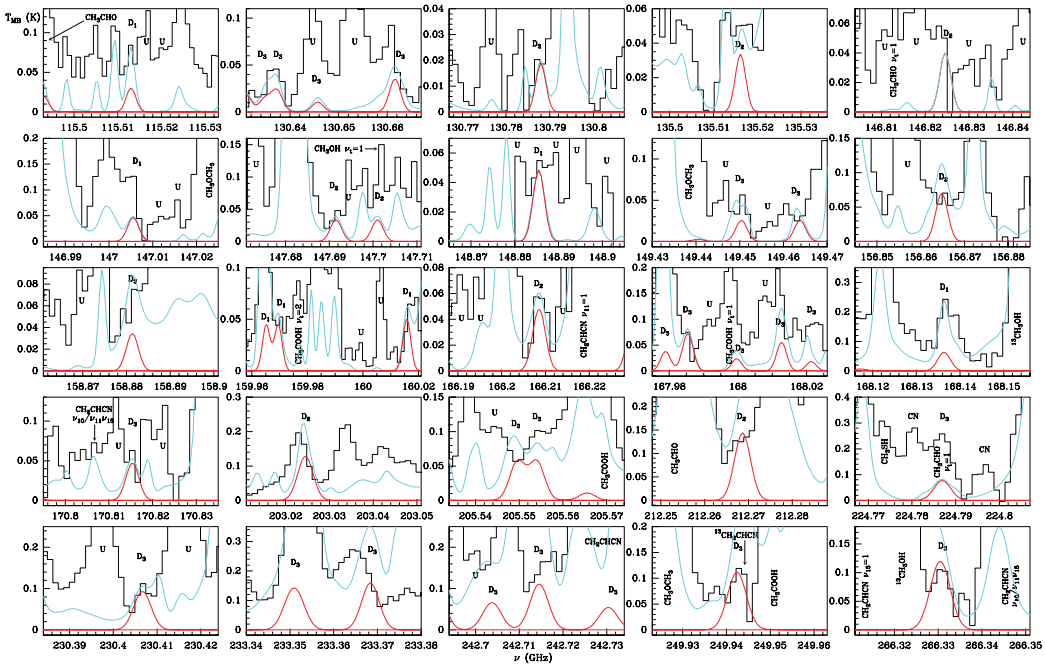

Fig. A.2. Observed lines from Orion-KL (histogram spectra) and model (thin red curves) of deuterated isotopes for CH_2CHCN in the ground state. The subindex of D_i (i = 1, 2, 3) correspond to the position of the isotope in the molecule ($D_1CD_2CD_3CN$). The cyan line corresponds to the model of the molecules we have already studied in this survey (see text Sect. 4.4.2), including the CH_2CHCN species. A v_{LSR} of 5 km s^{-1} is assumed.

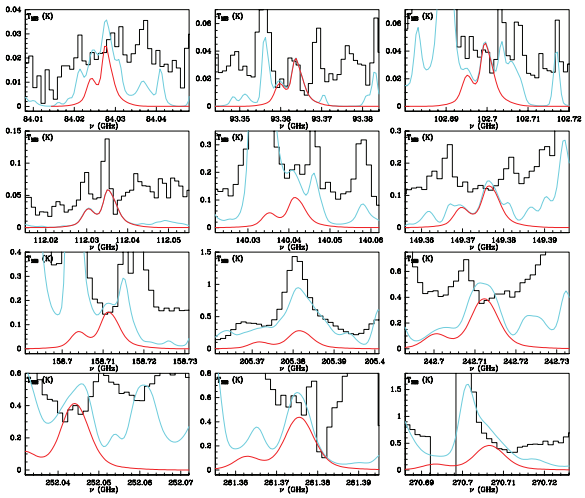

Fig. A.3. Observed lines from Orion-KL (histogram spectra) and model (thin red curves) of 3-imino-1,2-propadienyllidene in its ground state. The cyan line corresponds to the model of the molecules we have already studied in this survey (see text Sect. 4.4.2), including the CH_2CHCN species. A v_{LSR} of 5 km s^{-1} is assumed.

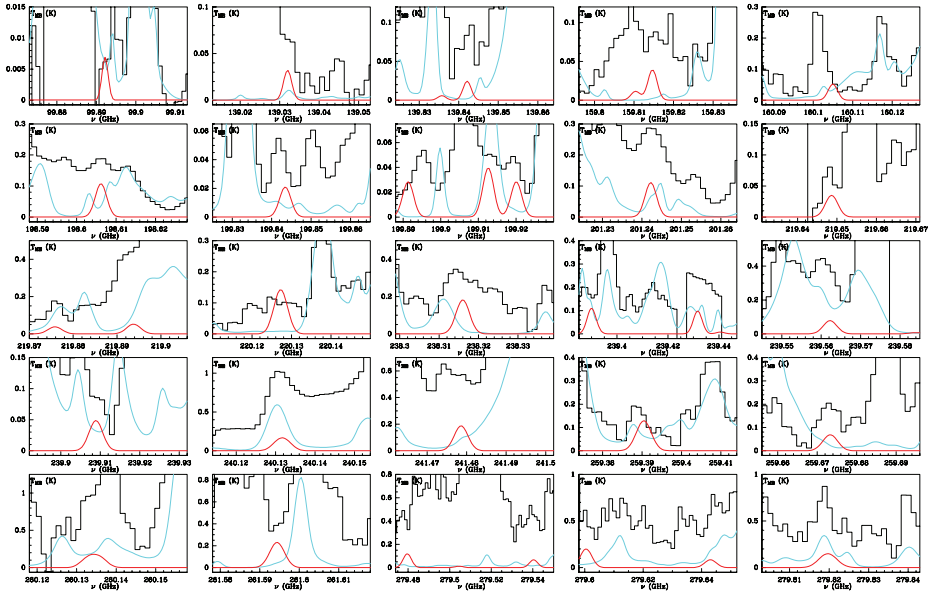

Fig. A.4. Observed lines from Orion-KL (histogram spectra) and model (thin red curves) of cyanamide in its ground state. The cyan line corresponds to the model of the molecules we have already studied in this survey (see text Sect. 4.4.2), including the CH_2CHCN species. A v_{LSR} of 5 km s^{-1} is assumed.

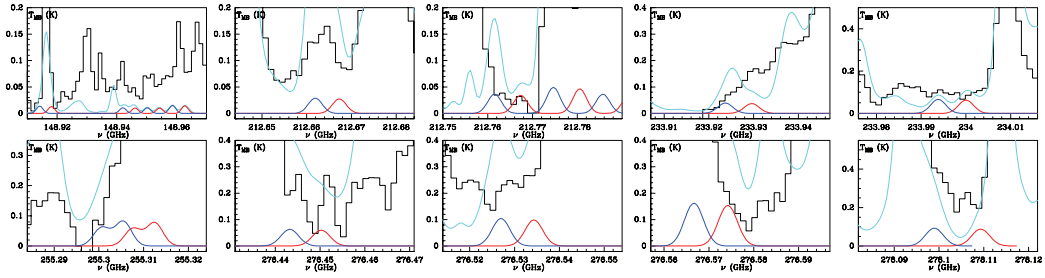

Fig. A.5. Observed lines from Orion-KL (histogram spectra) and model (thin red and blue curves) of isocyanamide in its ground state. The cyan line corresponds to the model of the molecules we have already studied in this survey (see text Sect. 4.4.2), including the CH_2CHCN species. A v_{LSR} of 5 km s^{-1} is assumed.

A&A 572, A44 (2014)

Table A.6. Detected lines of CH_2CHCN g.s.

Transition $J_{K_a,K_c} - J'_{K'_a,K'_c}$	Predicted frequency (MHz)	S_{ij}	E_u (K)	v_{LSR} km s^{-1}	Δv km s^{-1}	T_{MB} (K)	$\int T_{MB} dv$ (K km s^{-1})
$9_{1,9}$–$8_{1,8}$	83 207.507	8.89	22.1	5.0[1]		0.24[2]	
		Wide comp.		3.5 ± 0.4	14 ± 1	0.12	1.8 ± 0.2
		Narrow comp.		5.2 ± 0.3	0.8 ± 0.4	0.12	0.78 ± 0.11
$9_{0,9}$–$8_{0,8}$	84 946.003	9.00	20.4	4.4[1]		0.24[2]	
				4.4 ± 0.4	11 ± 1	0.23	2.7 ± 0.2
$9_{2,8}$–$8_{2,7}$	85 302.649	8.56	29.1	5.2[1]		0.24[2]	
				5.2 ± 0.3	9.5 ± 0.7	0.22	2.26 ± 0.14
⋮	⋮	⋮		⋮		⋮	
$14_{0,14}$–$13_{0,13}$	131 267.475	14.00	47.5	2.5[1]		2.08[2]	
$14_{2,13}$–$13_{2,12}$	132 524.586	13.70	56.4	[14]		...	
$14_{5,10}$–$13_{5,9}$	132 900.001	12.20	101.9	5.7[1]		1.18[2]	
$14_{5,9}$–$13_{5,8}$	132 900.012[†]	12.20	101.9	5.8[1]		”	
				6.1 ± 0.5	7.8 ± 0.9	1.02	8.4 ± 0.9
$14_{6,9}$–$13_{6,8}$	132 905.283	11.40	125.6	5.1[1]		1.02[2]	
$14_{6,8}$–$13_{6,7}$	132 905.283[†]	11.40	125.6	5.1[1]		”	
⋮	⋮	⋮		⋮		⋮	
$21_{2,20}$–$20_{2,19}$	198 258.130	20.80	113.6	2.7[1,12]		6.30[2]	
$21_{6,16}$–$20_{6,15}$	199 396.979	19.30	183.0	4.7[1]		2.25[2]	
$21_{6,15}$–$20_{6,14}$	199 396.985[†]	19.30	183.0	4.7[1]		”	
$21_{7,15}$–$20_{7,14}$	199 401.677	18.70	211.0	5.1[1]		2.45[2]	
$21_{7,14}$–$20_{7,13}$	199 401.677[†]	18.70	211.0	5.1[1]		”	
⋮	⋮	⋮		⋮		⋮	

Notes. Emission lines of CH_2CHCN ground state present in the spectral scan of the Orion-KL from the radio-telescope of IRAM-30 m. Column 1 indicates the line transition, Col. 2 gives the predicted frequency in the laboratory, Col. 3 the line strength, Col. 4 upper level energy, Col. 5 observed radial velocities relative to the local system rest (v_{LSR}), Col. 6 the line width, Col. 7 main beam temperature, and Col. 8 shows the area of the line. The superscripts are as follows: [(†)] Blended with the previous line. [(*)] noise level. [(**)] Hole in the observed spectrum. [(1)] Peak channel line observed velocity. [(2)] Peak channel line intensity. [(3)] Blended with CH_3CCH. [(4)] Blended with $^{34}SO_2$. [(5)] Blended with t-CH_3CH_2OH. [(6)] Blended with $OC^{34}S$. [(7)] Blended with $H^{13}CCCN$. [(8)] Blended with CH_3OH. [(9)] Blended with CH_3COOH $v_t = 0$. [(10)] Blended with $^{13}CH_3OH$. [(11)] Blended with U-line. [(12)] Blended with CH_3CH_2CN. [(13)] Blended with CH_2CHCN $v_{15} = 1$. [(14)] Blended with CH_3OCH_3. [(15)] Blended with $HCOOCH_3$. [(16)] Blended with $H_2C^{34}S$. [(17)] Blended with $CH_3CH_2^{13}CN$. [(18)] Blended with $^{13}CH_3CH_2CN$. [(19)] Blended with CH_3CH_2CN v_{13}/v_{21}. [(20)] Blended with $HCOOCH_3$ $v_t = 1$. [(21)] Blended with $^{13}CH_3CN$. [(22)] Blended with CH_3CH_2CN $v_{20} = 1$. [(23)] Blended with $^{33}SO_2$. [(24)] Blended with CH_2CHCN $v_{11} = 1$. [(25)] Blended with CH_3CHO. [(26)] Blended with $H_{33}\alpha$. [(27)] Blended with $(CH_3)_2CO$. [(28)] Blended with SiS. [(29)] Blended with HCCCN. [(30)] Blended with SO_2. [(31)] Blended with CH_3CN. [(32)] Blended with HCCCN $v_6 = 1$. [(33)] Blended with CH_2CHCN $v_{10}/v_{11}v_{15}$. [(34)] Blended with H_2CO. [(35)] Blended with HCCCN $v_7 = 1$. [(36)] Blended with $HCOO^{13}CH_3$. [(37)] Blended with SO_2 $v_2 = 1$. [(38)] Blended with CO. [(39)] Blended with C_3H_2. [(40)] Blended with $CH_3^{13}CN$. [(41)] Blended with CH_2CHCN $v_{11} = 2$. [(42)] Blended with HDCO. [(43)] Blended with HDCS. [(44)] Blended with $H^{13}COOCH_3$. [(45)] Blended with ^{34}SO. [(46)] Blended with CH_3SH. [(47)] Blended with ^{29}SiO. [(48)] Blended with CH_3CN $v_8 = 1$. [(49)] Blended with SO. [(50)] Blended with HCN. [(51)] Blended with HDO. [(52)] Blended with NO. [(53)] Blended with HCO^+. [(54)] Blended with NH_2CHO. [(55)] Blended with $CH_3^{13}CH_2CN$. [(56)] Blended with CH_3OD. (This table is available in its entirety at the CDS. A portion is shown here for guidance regarding its form and content.)

Table A.7. Detected b-type lines of CH_2CHCN g.s.

Transition $J_{K_a,K_c} - J'_{K'_a,K'_c}$	Predicted frequency (MHz)	S_{ij}	E_u (K)	v_{LSR}[1] km s^{-1}	Observed frequency (MHz)	Observed T_{MB} (K)[2]	Model T_{MB} (K)
$18_{1,17}$–$17_{0,18}$	95 212.208	11.40	81.7	4.95[3]	95212.2	0.03	0.01
$20_{1,19}$–$20_{0,20}$	108 813.600	11.40	99.7	3.74	108814.0	0.02	0.01
$18_{2,16}$–$18_{1,17}$	113 831.149	14.00	87.1	5.48	113831.0	0.02	0.02
⋮	⋮	⋮		⋮		⋮	
$29_{2,27}$–$29_{1,28}$	131 168.734	22.70	209.5	3.88[5]	131169.2	0.04	0.01
$17_{0,17}$–$16_{1,16}$	136 855.602	11.00	69.0	4.75[4]	136855.7	0.05	0.02
⋮	⋮	⋮		⋮		⋮	
$39_{2,37}$–$39_{1,38}$	199 913.795	22.40	369.5	5.41	199913.5	0.02	0.02
$20_{1,20}$–$19_{0,19}$	200 364.538	14.20	95.2	6.62	200363.4	0.08	0.06
$24_{0,24}$–$23_{1,23}$	211 519.057	18.10	134.5	6.62[4]	211518.4	0.12	0.07
⋮	⋮	⋮		⋮		⋮	

Notes. Emission b-type lines of CH_2CHCN ground state present in the spectral scan of the Orion-KL from the radio-telescope of IRAM-30 m. Column 1 indicates the line transition, Col. 2 gives the predicted frequency in the laboratory, Col. 3 the line strength, Col. 4 upper level energy, Col. 5 observed radial velocities relatives (v_{LSR}), Col. 6 observed centroid frequencies assuming a v_{LSR} of 5 km s^{-1}, Col. 7 observed mean beam temperature, and Col. 8 mean beam temperature obtained with the model. [(1)] Peak line observed velocity. [(2)] Peak line intensity. [(3)] Blended with $v_{11} = 1$. [(4)] Blended with U-line. [(5)] Blended with $DCOOCH_3$. (This table is available in its entirety at the CDS. A portion is shown here for guidance regarding its form and content.)

A&A 572, A44 (2014)

Table A.8. Detected lines of CH_2CHCN $v_{11} = 1$.

Transition $J_{K_a,K_c} - J'_{K'_a,K'_c}$	Predicted frequency (MHz)	S_{ij}	E_u (K)	v_{LSR} km s^{-1}	Δv km s^{-1}	T_{MB} (K)	$\int T_{MB} dv$ (K km s^{-1})
$9_{1,9}$–$8_{1,8}$	83 398.992	8.89	350.6	5.4[1,3]		0.08[2]	
$9_{0,9}$–$8_{0,8}$	85 167.948	9.00	349.0	5.3[1]		0.03[2]	
				5.3 ± 0.5	6 ± 1	0.04	0.24 ± 0.04
$9_{2,8}$–$8_{2,7}$	85 547.124	8.56	357.5	6.4[1]		0.04[2]	
				6.6 ± 0.5	8 ± 1	0.03	0.29 ± 0.03
⋮	⋮	⋮		⋮		⋮	
$14_{0,14}$–$13_{0,13}$	131 561.145	14.00	376.1	4.9[1,10]		0.37[2]	
$14_{2,13}$–$13_{2,12}$	132 894.527	13.70	384.9	[11]		...	
⋮	⋮	⋮		⋮		⋮	
$21_{2,20}$–$20_{2,19}$	198 781.116	20.80	442.2	5.0[1]		0.21[2]	
				5.00 ± 0.11	7.5 ± 0.3	0.21	1.70 ± 0.07
$21_{7,15}$–$20_{7,14}$	199 974.194	18.70	538.2	2.9[1]		0.48[2]	
$21_{7,14}$–$20_{7,13}$	199 974.194†	18.70	538.2	2.9[1]		″	
$21_{6,16}$–$20_{6,15}$	199 976.624†	19.30	510.6	6.6[1]		″	
$21_{6,15}$–$20_{6,14}$	199 976.631†	19.30	510.6	6.6[1]		″	
				4.8 ± 0.6	12 ± 1	0.41	5.1 ± 0.5
⋮	⋮	⋮		⋮		⋮	

Notes. Emission lines of CH_2CHCN $v_{11} = 1$ present in the spectral scan of the Orion-KL from the radio-telescope of IRAM-30 m. Column 1 indicates the line transition, Col. 2 gives the predicted frequency in the laboratory, Col. 3 the line strength, Col. 4 upper level energy, Col. 5 observed radial velocities relative to the local system rest (v_{LSR}), Col. 6 the line width, Col. 7 main beam temperature, and Col. 8 shows the area of the line. The superscripts are as follows: (†) Blended with the previous line. (**) Hole in the observed spectrum. (1) Peak channel line observed velocity. (2) Peak channel line intensity. (3) Blended with U-line. (4) Blended with H^+ (H 42α). (5) Blended with $^{13}CH_3OH$. (6) Blended with OCS. (7) Blended with $(CH_3)_2CO$. (8) Blended with H 49β. (9) Blended with CH_3CH_2CN. (10) Blended with $^{33}SO_2$. (11) Blended with CH_3OH. (12) Blended with CH_3OCH_3. (13) Blended with $O^{13}CS$. (14) Blended with CH_3CH_2CN $v_{20} = 1$. (15) Blended with $HCOOCH_3$. (16) Blended with $CH_3^{13}CH_2CN$. (17) Blended with $^{13}CH_3CN$. (18) Blended with CH_3CH_2CN v_{13}/v_{21}. (19) Blended with H_2CO. (20) Blended with CH_2CHCN. (21) Blended with $^{34}SO_2$. (22) Blended with CH_2CHCN $v_{10}/v_{11}v_{15}$. (23) Blended with $HCOO^{13}CH_3$. (24) Blended with $H^{13}COOCH_3$. (25) Blended with CH_2CHCN $v_{15} = 1$. (26) Blended with ^{29}SiO. (27) Blended with HCCCN $\nu = 0$. (28) Blended with H_2CCO. (29) Blended with SO_2. (30) Blended with CH_2CHCN $v_{11} = 2$. (31) Blended with CH_3CN $v_8 = 1$. (32) Blended with $CH_2CH^{13}CN$. (33) Blended with HCCCN $v_6 = 1$. (34) Blended with H_2CCC. (35) Blended with NH_2CHO. (36) Blended with $|g_+$-$g_-|$-CH_3CH_2OH. (37) Blended with $SO^{17}O$. (38) Blended with CCCS. (39) Blended with HNCO. (40) Blended with CH_3CCH. (41) Blended with $HCC^{13}CN$ $v_6 = 1$. (42) Blended with HCCCN $v_7 = 2$. (43) Blended with HDCO. (44) Blended with CH_3OD. (45) Blended with $H_2^{13}CS$. (46) Blended with $CH_3CH_2^{13}CN$. (47) Blended with $^{34}S^{18}O$. (48) Blended with CH_3COOH $v_t = 0$. (49) Blended with HCCCN $v_7 = 3$. (50) Blended with CH_2DCCH. (51) Blended with $SO^{18}O$. (52) Blended with $O^{13}C^{34}S$. (53) Blended with $HNC^{18}O$. (54) Blended with $CH_3C^{15}N$. (55) Blended with CH_3CN. (56) Blended with $CH_3^{13}CN$. (57) Blended with SO. (58) Blended with $^{13}CH_2CHCN$. (59) Blended with HDCS. (60) Blended with $H_2C^{33}S$. (61) Blended with H_2CS. (This table is available in its entirety at the CDS. A portion is shown here for guidance regarding its form and content.)

Table A.9. Detected lines of CH_2CHCN $v_{11} = 2$.

Transition $J_{K_a,K_c} - J'_{K'_a,K'_c}$	Predicted frequency (MHz)	S_{ij}	E_u (K)	v_{LSR} km s^{-1}	Δv km s^{-1}	T_{MB} (K)	$\int T_{MB} dv$ (K km s^{-1})
$9_{1,9}$–$8_{1,8}$	83 586.209	8.89	680.0	[3,4]		...	
$9_{0,9}$–$8_{0,8}$	85 384.841	8.99	678.3	6.8[1]		0.02[2]	
				6.8 ± 1.8	4 ± 2	0.02	0.06 ± 0.04
$9_{2,8}$–$8_{2,7}$	85 787.036	8.56	686.8	[5]		...	
⋮	⋮	⋮		⋮		⋮	
$14_{0,14}$–$13_{0,13}$	131 846.587	14.00	705.5	[7]		...	
$14_{2,13}$–$13_{2,12}$	133 257.141	13.70	714.2	8.0[1]		0.07[2]	
$14_{6,9}$–$13_{6,8}$	133 664.633	11.40	781.4	5.9[1]		0.04[2]	
$14_{6,8}$–$13_{6,7}$	133 664.633[†]	11.40	781.4	5.9[1]		″	
$14_{5,10}$–$13_{5,9}$	133 666.986[†]	12.20	758.4	6.8[1]		″	
$14_{5,9}$–$13_{5,8}$	133 667.002[†]	12.20	758.4	6.8[1]		″	
⋮	⋮	⋮		⋮		⋮	
$21_{2,20}$–$20_{2,19}$	199 292.525	20.80	771.7	[29]		...	
$21_{7,15}$–$20_{7,14}$	200 537.645	18.70	866.4	3.8[1,6]		0.30[2]	
$21_{7,14}$–$20_{7,13}$	200 537.645[†]	18.70	866.4	3.8[1,6]		″	
$21_{6,16}$–$20_{6,15}$	200 546.938	19.30	839.2	0.9[1,30]		0.18[2]	
$21_{6,15}$–$20_{6,14}$	200 546.947[†]	19.30	839.2	0.9[1,30]		″	
$21_{8,14}$–$20_{8,13}$	200 551.088[†]	18.00	897.1	7.1[1,30]		″	
$21_{8,13}$–$20_{8,12}$	200 551.088[†]	18.00	897.1	7.1[1,30]		″	
⋮	⋮	⋮		⋮		⋮	

Notes. Emission lines of CH_2CHCN $v_{11} = 2$ present in the spectral scan of the Orion-KL from the radio-telescope of IRAM-30 m. Column 1 indicates the line transition, Col. 2 gives the predicted frequency in the laboratory, Col. 3 the line strength, Col. 4 upper level energy, Col. 5 observed radial velocities relative to the local system rest (v_{LSR}), Col. 6 the line width, Col. 7 main beam temperature, and Col. 8 shows the area of the line. The superscripts are as follows: [(†)] Blended with the previous line. [(**)] Hole in the observed spectrum. [(1)] Peak channel line observed velocity. [(2)] Peak channel line intensity. [(3)] Blended with H 53β. [(4)] Blended with $Si^{17}O$. [(5)] Blended with $HCOOCH_3$. [(6)] Blended with U-line. [(7)] Blended with HNCO. [(8)] Blended with CH_3CH_2CN. [(9)] Blended with CH_2CHCN $v_{15} = 1$. [(10)] Blended with $CH_2^{13}CHCN$. [(11)] Blended with SO_2. [(12)] Blended with $^{34}SO_2$. [(13)] Blended with $^{13}CH_3OH$. [(14)] Blended with $(CH_3)_2CO$. [(15)] Blended with CH_2CHCN. [(16)] Blended with CH_3OH. [(17)] Blended with CH_3CHO. [(18)] Blended with CH_3CH_2CN v_{13}/v_{21}. [(19)] Blended with CH_3CH_2CN $v_{20} = 1$. [(20)] Blended with H 54δ. [(21)] Blended with NO. [(22)] Blended with $H^{13}COOCH_3$. [(23)] Blended with CH_2CHCN $v_{10}/v_{11}v_{15}$. [(24)] Blended with CH_3OCH_3. [(25)] Blended with $CH_3CH_2^{13}CN$. [(26)] Blended with H_2CCO. [(27)] Blended with c-C_2H_4O. [(28)] Blended with $|g_+$-$g_-|$-CH_3CH_2OH. [(29)] Blended with $HC^{13}CCN$. [(30)] Blended with $HCC^{13}CN$. [(31)] Blended with HCCCN $v_7 = 1$. [(32)] Blended with HCCCN v_4+v_7. [(33)] Blended with $CH_3CH_2C^{15}N$. [(34)] Blended with CH_2CHCN $v_{11} = 1$. [(35)] Blended with $CH_2^{13}CHCN$. [(36)] Blended with NH_2CHO. [(37)] Blended with $^{13}CH_3CH_2CN$. [(38)] Blended with HCCCN $v_7 = 2$. [(39)] Blended with SO. [(40)] Blended with H_2CCO. [(41)] Blended with $SO^{18}O$. [(42)] Blended with HCCCN. [(43)] Blended with $H^{13}CCCN$. [(44)] Blended with $CH_2CH^{13}CN$. [(45)] Blended with SO_2 $v_2 = 1$. [(46)] Blended with $CH_3^{13}CN$. [(47)] Blended with $DCOOCH_3$. [(48)] Blended with CH_3CN. [(49)] Blended with H_2CS. [(50)] Blended with CCCS. [(51)] Blended with CH_3COOH $v_t = 0$. [(52)] Blended with $HNC^{18}O$. [(53)] Blended with $CH_3^{13}CH_2CN$. [(54)] Blended with OCS. [(55)] Blended with H_2CCC. [(56)] Blended with CH_3CN $v_8 = 1$. [(57)] Blended with HDCO. [(58)] Blended with $CH_3C^{15}N$. [(59)] Blended with HCO^+. [(60)] Blended with $^{13}CH_3CN$. [(61)] Blended with $HCOO^{13}CH_3$. [(62)] Blended with t-CH_3CH_2OH. [(63)] Blended with $H^{15}NCO$. [(64)] Blended with $H_2C^{18}O$. (This table is available in its entirety at the CDS. A portion is shown here for guidance regarding its form and content.)

A&A 572, A44 (2014)

Table A.10. Detected lines of CH_2CHCN $v_{11} = 3$.

Transition $J_{K_a,K_c} - J'_{K'_a,K'_c}$	Predicted frequency (MHz)	S_{ij}	E_u (K)	v_{LSR} km s^{-1}	Δv km s^{-1}	T_{MB} (K)	$\int T_{MB} dv$ (K km s^{-1})
$9_{1,9}$–$8_{1,8}$	83 769.181	8.89	1007.6	[3]		...	
$9_{0,9}$–$8_{0,8}$	85 596.639	8.99	1006.1	[3]		...	
$9_{2,8}$–$8_{2,7}$	86 022.191	8.56	1014.4	[4]		...	
$9_{5,5}$–$8_{5,4}$	86 148.048	6.22	1057.9	4.5[1]		0.01[2]	
$9_{5,4}$–$8_{5,3}$	86 148.048†	6.22	1057.9	4.5[1]		″	
⋮	⋮	⋮		⋮		⋮	
$14_{1,14}$–$13_{1,13}$	130 055.036	13.90	1034.4	[11,12]		...	
$14_{0,14}$–$13_{0,13}$	132 123.977	14.00	1033.3	[13]		...	
$14_{2,13}$–$13_{2,12}$	133 612.205	13.70	1041.9	[4]		...	
$14_{6,9}$–$13_{6,8}$	134 034.186	11.40	1108.3	[6]		...	
$14_{6,8}$–$13_{6,7}$	134 034.187†	11.40	1108.3	[6]		...	
⋮	⋮	⋮		⋮		⋮	
$21_{2,20}$–$20_{2,19}$	199 792.621	20.80	1099.5	[19,27,28]		...	
$21_{7,15}$–$20_{7,14}$	201 090.968	18.70	1193.1	[10]		...	
$21_{7,15}$–$20_{7,14}$	201 090.968†	18.70	1193.1	[10]		...	
$21_{8,14}$–$20_{8,13}$	201 098.099†	18.00	1224.1	[10]		...	
$21_{8,13}$–$20_{8,12}$	201 098.099†	18.00	1224.1	[10]		...	
⋮	⋮	⋮		⋮		⋮	

Notes. Emission lines of CH_2CHCN $v_{11} = 3$ present in the spectral scan of the Orion-KL from the radio-telescope of IRAM-30 m. Column 1 indicates the line transition, Col. 2 gives the predicted frequency in the laboratory, Col. 3 the line strength, Col. 4 upper level energy, Col. 5 observed radial velocities relative to the local system rest (v_{LSR}), Col. 6 the line width, Col. 7 main beam temperature, and Col. 8 shows the area of the line. The superscripts are as follows: [(†)] Blended with the previous line. [(*)] Noise level. [(**)] Hole in the observed spectrum. [(1)] Peak channel line observed velocity. [(2)] Peak channel line intensity. [(3)] Blended with U-line. [(4)] Blended with $HCOOCH_3$. [(5)] Blended with CH_3OCH_3. [(6)] Blended with CH_3CH_2CN. [(7)] Blended with $CH_3CH_2C^{15}N$. [(8)] Blended with H 49β. [(9)] Blended with CH_2CHCN $v_{11} = 1$. [(10)] Blended with CH_3OH. [(11)] Blended with $O^{13}C^{34}S$. [(12)] Blended with $CH_3^{13}CH_2CN$. [(13)] Blended with $^{34}SO_2$. [(14)] Blended with $H^{13}CS$. [(15)] Blended with $H^{13}COOCH_3$. [(16)] Blended with CH_2CHOH. [(17)] Blended with $(CH_3)_2CO$. [(18)] Blended with SO_2 $v_2 = 1$. [(19)] Blended with CH_3CH_2CN v_{13}/v_{21}. [(20)] Blended with HDO. [(21)] Blended with CH_3OD. [(22)] Blended with $SO^{17}O$. [(23)] Blended with HCCCN. [(24)] Blended with ^{29}SiO. [(25)] Blended with $CH_3CH_2^{13}CN$. [(26)] Blended with $^{13}CH_2CHCN$. [(27)] Blended with CH_2CHCN $v_{15} = 1$. [(28)] Blended with $HCC^{13}CN$ $v_7 = 1$. [(29)] Blended with CHDCHCN. [(30)] Blended with $CH_2^{13}CHCN$. [(31)] Blended with H_2CCO. [(32)] Blended with SO_2. [(33)] Blended with CH_3CH_2CN $v_{20} = 1$. [(34)] Blended with H_2CS. [(35)] Blended with $^{33}SO_2$. [(36)] Blended with $DCOOCH_3$. [(37)] Blended with c-C_3H_2. [(38)] Blended with CH_2CHCN. [(39)] Blended with $^{13}CH_3OH$. [(40)] Blended with $HN^{13}CO$. [(41)] Blended with $^{13}CH_3CH_2CN$. [(42)] Blended with $HNC^{18}O$. [(43)] Blended with $SO^{18}O$. [(44)] Blended with $H^{13}CCCN$ $v_7 = 1$. [(45)] Blended with $HCOO^{13}CH_3$. [(46)] Blended with $|g_+$-$g_-|$-CH_3CH_2OH. [(47)] Blended with t-CH_3CH_2OH. [(48)] Blended with D_2CO. [(49)] Blended with $CH_3C^{15}N$. [(50)] Blended with NH_2CHO. [(51)] Blended with CH_3CN $v_8 = 1$. [(52)] Blended with ^{34}SO. [(53)] Blended with ^{33}SO. [(54)] Blended with CH_3COOH $v_t = 0$. [(55)] Blended with CH_3OD. [(56)] Blended with $H^{13}CN$. [(57)] Blended with H_2CCS. [(58)] Blended with HDCO. [(59)] Blended with CH_2CHCN $v_{11} = 2$. [(60)] Blended with CH_2DCN. [(61)] Blended with DCCCN. (This table is available in its entirety at the CDS. A portion is shown here for guidance regarding its form and content.)

Table A.11. Detected lines of CH_2CHCN $v_{15} = 1$.

Transition $J_{K_a,K_c} - J'_{K'_a,K'_c}$	Predicted frequency (MHz)	S_{ij}	E_u (K)	v_{LSR} km s^{-1}	Δv km s^{-1}	T_{MB} (K)	$\int T_{MB} dv$ (K km s^{-1})
$9_{1,9}$–$8_{1,8}$	83 349.865	8.89	500.9	[3]		...	
$9_{0,9}$–$8_{0,8}$	85 075.547	9.00	499.1	5.6[1]		0.03[2]	
$9_{2,8}$–$8_{2,7}$	85 416.767	8.56	508.0	[4]		...	
$9_{4,6}$–$8_{4,5}$	85 528.061	7.22	534.5	4.0[1]		0.02[2]	
$9_{4,5}$–$8_{4,4}$	85 528.107†	7.22	534.5	4.2[1]		″	
$9_{5,5}$–$8_{5,4}$	85 532.951	6.22	554.4	4.1[1]		0.02[2]	
$9_{5,4}$–$8_{5,3}$	85 532.951†	6.22	554.4	4.1[1]		″	
				4.3 ± 0.2	7.2 ± 0.7	0.02	0.12 ± 0.01
⋮	⋮	⋮		⋮		⋮	
$14_{0,14}$–$13_{0,13}$	131 504.447	14.00	526.2	6.6[1,13]		0.11[2]	
$14_{2,13}$–$13_{2,12}$	132 709.220	13.70	535.3	6.1[1]		0.08[2]	
$14_{5,10}$–$13_{5,9}$	133 073.970	12.20	581.7	[4]		...	
$14_{5,9}$–$13_{5,8}$	133 073.979†	12.20	581.7	[4]		...	
⋮	⋮	⋮		⋮		⋮	
$21_{2,20}$–$20_{2,19}$	198 556.992	20.80	592.6	5.5[1]		0.16[2]	
				5.60 ± 0.11	5.2 ± 0.4	0.17	0.91 ± 0.08
$21_{6,16}$–$20_{6,15}$	199 658.717	19.30	663.4	[4,32]		...	
$21_{6,15}$–$20_{6,14}$	199 658.722†	19.30	663.4	[4,32]		...	
$21_{7,15}$–$20_{7,14}$	199 669.152	18.70	692.0	[4,32]		...	
$21_{7,14}$–$20_{7,13}$	199 669.152†	18.70	692.0	[4,32]		...	
$21_{5,17}$–$20_{5,16}$	199 683.011	19.80	639.2	[6]		...	
$21_{5,16}$–$20_{5,15}$	199 683.411†	19.80	639.2	[6]		...	
⋮	⋮	⋮		⋮		⋮	

Notes. Emission lines of CH_2CHCN $v_{15} = 1$ present in the spectral scan of the Orion-KL from the radio-telescope of IRAM-30 m. Column 1 indicates the line transition, Col. 2 gives the predicted frequency in the laboratory, Col. 3 the line strength, Col. 4 upper level energy, Col. 5 observed radial velocities relative to the local system rest (v_{LSR}), Col. 6 the line width, Col. 7 main beam temperature, and Col. 8 shows the area of the line. The superscripts are as follows: (†) Blended with the previous line. (**) Hole in the observed spectrum. (1) Peak channel line observed velocity. (2) Peak channel line intensity. (3) Blended with $HCOOCH_3$. (4) Blended with CH_2CHCN. (5) Blended with CH_2CHCN $v_{11} = 1$. (6) Blended with U-line. (7) Blended with CCH. (8) Blended with $^{13}CH_3OH$. (9) Blended with $CH_2^{13}CHCN$. (10) Blended with CH_3OH. (11) Blended with ^{34}SO. (12) Blended with CH_3COOH $v_t = 0$. (13) Blended with t-CH_3CH_2OH. (14) Blended with $(CH_3)_2CO$. (15) Blended with CH_3CH_2CN. (16) Blended with SO_2. (17) Blended with $^{13}CH_3CH_2CN$. (18) Blended with $CH_3C^{15}N$. (19) Blended with DNCO. (20) Blended with CH_3CH_2CN v_{13}/v_{21}. (21) Blended with $HCC^{13}CN$ $v_7 = 1$. (22) Blended with $H^{13}COOCH_3$. (23) Blended with $HCOOCH_3$ $v_t = 1$. (24) Blended with CH_3OCH_3. (25) Blended with CH_3OCOD. (26) Blended with HNCO. (27) Blended with H_2CCO. (28) Blended with NS. (29) Blended with CH_2DCCH. (30) Blended with CH_3CH_2CN $v_{20} = 1$. (31) Blended with ^{18}OCS. (32) Blended with SiS. (33) Blended with HCCCN. (34) Blended with $CH_3CH_2C^{15}N$. (35) Blended with H_2C_3. (36) Blended with |g$_+$-g$_-$ |-CH_3CH_2OH. (37) Blended with $SO^{18}O$. (38) Blended with CH_3CHO. (39) Blended with HCCCN $v_6 = 1$. (40) Blended with H_2CO. (41) Blended with $HN^{13}CO$. (42) Blended with HCCCN $v_7 = 1$. (43) Blended with $^{33}SO_2$. (44) Blended with OCS. (45) Blended with DNCS. (46) Blended with CH_3CN $v_8 = 1$. (47) Blended with HCCCN $v_7 = 2$. (48) Blended with $H^{13}CCCN$ $v_7 = 1$. (49) Blended with $^{13}CH_2CHCN$. (50) Blended with HCCCN v_6+v_7. (51) Blended with $H^{13}CCCN$ $\nu = 0$. (52) Blended with CH_2CHCN $v_{10}/v_{11}v_{15}$. (53) Blended with CH_3CN. (54) Blended with $CH_3^{13}CN$. (55) Blended with $HCOO^{13}CH_3$. (56) Blended with $CH_3^{13}CH_2CN$. (57) Blended with $^{34}SO_2$. (58) Blended with HDCS. (59) Blended with $O^{13}CS$. (60) Blended with CH_2CHCN $v_{11} = 3$. (61) Blended with HCCCN $v_7 = 3$. (62) Blended with $DCOOCH_3$. (63) Blended with $H^{13}COOCH_3$. (64) Blended with NH_2CHO. (65) Blended with CH_3OD. (66) Blended with g$_-$-CH_3CH_2OH. (This table is available in its entirety at the CDS. A portion is shown here for guidance regarding its form and content.)

A&A 572, A44 (2014)

Table A.12. Detected lines of CH_2CHCN $v_{10} = 1 \Leftrightarrow (v_{11} = 1, v_{15} = 1)$.

Transition $J_{K_a,K_c,v} - J'_{K'_a,K'_c,v'}$	Predicted frequency (MHz)	S_{ij}	E_u (K)	v_{LSR}[1] km s^{-1}	Observed frequency (MHz)	Observed T_{MB} (K)[2]	Model T_{MB} (K)
$9_{1,9,0}$–$8_{1,8,0}$	83 116.219	8.89	830.7	4.4	83 116.4	0.02	0.01
$9_{1,9,1}$–$8_{1,8,1}$	83 527.527	8.89	834.3	1.9	83 528.4	0.03	0.01
$9_{0,9,0}$–$8_{0,8,0}$	84 834.239	8.99	829.0	7.4	84 833.6	0.01	0.01
$9_{2,9,0}$–$8_{2,8,0}$	85 222.373	8.55	837.7	[3]	...	...	...
⋮	⋮	⋮		⋮		⋮	
$14_{0,14,0}$–$13_{0,13,0}$	131 110.736	14.00	856.1	[22]	...	...	...
$14_{2,13,0}$–$13_{2,12,0}$	132 389.964	13.70	864.9	3.0	132 390.8	0.04	0.04
$14_{5,10,0}$–$13_{5,9,0}$	132 761.289	12.20	910.1	[5]	...	...	...
$14_{5,9,0}$–$13_{5,8,0}$	132 761.289†	12.20	910.1	[5]	...	...	...
$14_{6,9,0}$–$13_{6,8,0}$	132 767.225	11.40	933.6	[5]	...	...	...
$14_{6,8,0}$–$13_{6,7,0}$	132 767.225†	11.40	933.6	[5]	...	...	...
⋮	⋮	⋮		⋮		⋮	
$21_{2,20,0}$–$20_{2,19,0}$	198 041.306	20.80	922.0	[16]	...	...	...
$21_{2,20,1}$–$20_{2,19,1}$	199 062.857	20.80	926.1	6.0	199 062.2	0.08	0.10
$21_{6,16,0}$–$20_{6,15,0}$	199 190.101	19.30	991.0	7.5[5,16]	199 188.4	0.15	0.15
$21_{6,15,0}$–$20_{6,14,0}$	199 190.107†	19.30	991.0	7.5[5,16]	199188.4	”	0.15
$21_{7,14,0}$–$20_{7,13,0}$	199 196.532	18.70	1018.8	4.0	199 197.1	0.14	0.13
$21_{7,15,0}$–$20_{7,14,0}$	199 196.532†	18.70	1018.8	4.0	199197.1	”	0.13
⋮	⋮	⋮		⋮		⋮	

Notes. Emission lines of CH_2CHCN $v_{10} = 1 \Leftrightarrow (v_{11} = 1, v_{15} = 1)$ present in the spectral scan of the Orion-KL from the radio-telescope of IRAM-30 m. The quantum number v corresponds with the vibrational level and takes the value $v = 0$ and $v = 1$ whether the state is $v_{10} = 1$ or $(v_{11} = 1, v_{15} = 1)$, respectively. Column 1 indicates the line transition, Col. 2 gives the predicted frequency in the laboratory, Col. 3 the line strength, Col. 4 upper level energy, Col. 5 observed radial velocities relative to the local system rest (v_{LSR}), Col. 6 observed centroid frequencies assuming a v_{LSR} of 5 km s^{-1}, Col. 7 observed main beam temperature, and Col. 8 mean beam temperature obtained with the model. The superscripts are as follows: (†) Blended with the last one. (**) Hole in the observed spectrum. (1) Peak channel line observed velocity. (2) Peak channel line intensity. (3) Blended with ^{33}SO. (4) Blended with HCS^+. (5) Blended with U-line. (6) Blended with $HCOOCH_3$. (7) Blended with SO. (8) Blended with $CH_3CH_2C^{15}N$. (9) Blended with $(CH_3)_2CO$. (10) Blended with CH_3OCH_3. (11) Blended with CH_3OH. (12) Blended with HDCS. (13) Blended with $^{13}CH_3OH$. (14) Blended with $CH_2^{13}CHCN$. (15) Blended with CH_2CHCN. (16) Blended with CH_3CH_2CN. (17) Blended with $^{34}SO_2$. (18) Blended with $CH_2CH^{13}CN$. (19) Blended with $CH_3C^{15}N$. (20) Blended with CH_3CN $v_8 = 1$. (21) Blended with c-C_2H_4O. (22) Blended with $CH_3CH_2^{13}CN$. (23) Blended with CH_2CHCN $v_{15} = 1$. (24) Blended with SO_2. (25) Blended with CH_3CH_2CN v_{13}/v_{21}. (26) Blended with $|g_+$-$g_-|$-CH_3CH_2OH. (27) Blended with CH_3OD. (28) Blended with $CH_3^{13}CH_2CN$. (29) Blended with CH_3CH_2CN $v_{20} = 1$. (30) Blended with CH_2CHCN $v_{11} = 2$. (31) Blended with CH_3CHO. (32) Blended with CH_2CHCN $v_{11} = 1$. (33) Blended with $^{13}CH_2CHCN$. (34) Blended with $H^{13}COOCH_3$. (35) Blended with $SO^{17}O$. (36) Blended with $OC^{36}S$. (37) Blended with SO_2 $v_2 = 1$. (38) Blended with HCCCN $v_7 = 2$. (39) Blended with $H_2^{13}CS$. (40) Blended with NH_2CHO. (41) Blended with H_2CS. (42) Blended with $^{33}SO_2$. (43) Blended with $HCOO^{13}CH_3$. (44) Blended with $^{13}CH_3CH_2CN$. (45) Blended with $HCC^{13}CN$ $v_7 = 2$. (46) Blended with CH_3CN. (47) Blended with $DCOOCH_3$. (48) Blended with $HC^{13}CCN$ $v = 0$. (49) Blended with SiS. (50) Blended with $O^{13}CS$. (51) Blended with H_2CO. (52) Blended with HCCCN. (53) Blended with t-CH_3CH_2OH. (54) Blended with $CH_3^{18}OH$. (55) Blended with $C^{18}O$. (56) Blended with $O^{34}S^{18}O$. (57) Blended with HDCO. (58) Blended with HCCCN $v_6 = 1$. (59) Blended with $HNC^{18}O$. (60) Blended with $SO^{18}O$. (61) Blended with CO. (62) Blended with HCCCN $v_6 = 2$. (63) Blended with HCCCN $v_7 = 3$. (64) Blended with CH_3COOH $v_t = 0$. (65) Blended with CH_2CHCN $v_{11} = 3$. (66) Blended with CH_2CDCN. (67) Blended with CH_3CN $v_8 = 1$. (68) Blended with CCCS. (69) Blended with $HCC^{13}CN$. (70) Blended with ^{34}SO. (71) Blended with $H^{13}CCCN$. (72) Blended with HDO. (73) Blended with $^{13}CH_3CN$. (74) Blended with CH_3CCH. (75) Blended with HDCS. (76) Blended with $CH_3^{13}CN$. (77) Blended with HCOOH. (78) Blended with SiO. (79) Blended with SiO $v = 1$. (80) Blended with DCOOH. (81) Blended with HCN. (82) Blended with $H_2C^{34}S$. (83) Blended with NH_2CHO $v_{12} = 1$. (84) Blended with $CH_2CHC^{15}N$. (85) Blended with CH_3OD. (86) Blended with DCHCHCN. (This table is available in its entirety at the CDS. A portion is shown here for guidance regarding its form and content.)

Table A.13. Detected lines of $^{13}C_1$, $^{13}C_2$, and $^{13}C_3$ isotopologues of CH_2CHCN.

Transition $J_{K_a,K_c} - J'_{K'_a,K'_c}$	Predicted frequency (MHz)	S_{ij}	E_u (K)	v_{LSR}[1] km s^{-1}	Observed frequency (MHz)	Observed T_{MB} (K)[3]	Model T_{MB} (K)
Detected lines of $^{13}CH_2CHCN$							
$9_{1,9}$–$8_{1,8}$	81 051.736	8.89	21.6	5.54	81 051.6	0.01	0.01
$9_{2,8}$–$8_{2,7}$	83 064.074	8.56	28.5	5.66[2]	83 063.9	0.01	0.01
$9_{4,6}$–$8_{4,5}$	83 172.144	7.22	54.2	2.66	83 172.8	0.01	0.01
$9_{4,5}$–$8_{4,4}$	83 172.189†	7.22	54.2	2.82	″	″	″
$9_{3,6}$–$8_{3,5}$	83 187.779	8.00	39.2	6.34[2]	83 187.4	0.02	0.01
$9_{6,4}$–$8_{6,3}$	83 188.121†	5.00	96.8	7.57[2]	″	″	″
$9_{6,3}$–$8_{6,2}$	83 188.121†	5.00	96.8	7.57[2]	″	″	″
⋮	⋮	⋮		⋮		⋮	
$14_{1,13}$–$13_{1,12}$	131 955.171	13.90	49.7	8.06[3]	131 953.8	0.13	0.03
$15_{2,14}$–$14_{2,13}$	138 228.563	14.70	61.7	5.78	138 228.3	0.08	0.03
$15_{5,11}$–$14_{5,10}$	138 657.101	13.30	106.6	1.60[2]	138 658.6	0.08	0.05
$15_{5,10}$–$14_{5,9}$	138 657.119†	13.30	106.6	1.64[2]	″	″	″
$15_{4,12}$–$14_{4,11}$	138 678.606	13.90	87.4	3.79	138 679.1	0.08	0.07
$15_{4,11}$–$14_{4,10}$	138 678.418†	13.90	87.4	7.71	″	″	″
$15_{7,9}$–$14_{7,8}$	138 680.928†	11.70	157.8	8.81	″	″	″
$15_{7,8}$–$14_{7,7}$	138 680.928†	11.70	157.8	8.81	″	″	″
⋮	⋮	⋮		⋮		⋮	
$22_{0,22}$–$21_{0,21}$	198 591.415	22.00	110.7	3.79[7]	198 592.3	0.18	0.08
$22_{4,19}$–$21_{4,18}$	203 539.866	21.30	110.7	0.49[2]	203 542.9	0.21	0.08
$22_{10,12}$–$21_{10,11}$	203 542.989†	17.50	325.0	5.09[2]	″	″	″
$22_{10,13}$–$21_{10,12}$	203 542.989†	17.50	325.0	5.09[2]	″	″	″
⋮	⋮	⋮		⋮		⋮	
Detected lines of $CH_2{}^{13}CHCN$							
$9_{4,6}$–$8_{4,5}$	84 961.208	7.22	54.1	0.86	84 962.9	0.01	0.01
$9_{4,5}$–$8_{4,4}$	84 961.208†	7.22	54.1	0.65	″	″	″
$9_{5,5}$–$8_{5,4}$	84 963.011†	6.22	73.0	5.50	″	″	″
$9_{5,4}$–$8_{5,3}$	84 963.011†	6.22	73.0	5.50	″	″	″
$9_{2,7}$–$8_{2,6}$	85 278.270	8.56	28.9	8.17[2]	85 277.4	0.02	0.01
⋮	⋮	⋮		⋮		⋮	
$14_{0,14}$–$13_{0,13}$	130 481.709	14.00	47.2	5.48	130 481.5	0.09	0.03
$14_{5,10}$–$13_{5,9}$	132 191.757	12.20	100.2	4.38[2]	132 192.0	0.13	0.05
$14_{5,9}$–$13_{5,8}$	132 191.770†	12.20	100.2	4.41[2]	″	″	″
$14_{6,9}$–$13_{6,8}$	132 194.320†	11.40	123.3	7.81[2]	″	″	″
$14_{6,8}$–$13_{6,7}$	132 194.320†	11.40	123.3	7.81[2]	″	″	″
⋮	⋮	⋮		⋮		⋮	
$21_{7,15}$–$20_{7,14}$	198 336.172	18.70	207.7	4.26	198 336.7	0.18	0.18
$21_{7,14}$–$20_{7,13}$	198 336.172†	18.70	207.7	4.26	″	″	″
$21_{6,16}$–$20_{6,15}$	198 336.544†	19.30	180.4	4.83	″	″	″
$21_{6,15}$–$20_{6,14}$	198 336.552†	19.30	180.4	4.84	″	″	″
$21_{8,14}$–$20_{8,13}$	198 358.019	18.00	239.1	1.45[2]	198 360.4	0.12	0.07
$21_{8,13}$–$20_{8,12}$	198 358.019†	18.00	239.1	1.45[2]	″	″	″
⋮	⋮	⋮		⋮		⋮	

Notes. Emission lines of of $^{13}CH_2CHCN$, $CH_2^{13}CHCN$ and $CH_2CH^{13}CN$ isotopologues in its ground state present in the spectral scan of the Orion-KL from the radio-telescope of IRAM-30 m. Column 1 indicates the line transition, Col. 2 gives the predicted frequency in the laboratory, Col. 3 the line strength, Col. 4 upper level energy, Col. 5 observed radial velocities relatives (v_{LSR}), Col. 6 observed centroid frequencies assuming a v_{LSR} of 5 km s^{-1}, Col. 7 observed mean beam temperature, and Col. 8 mean beam temperature obtained with the model. The superscripts are as follows: (†) Blended with the last one. (1) Peak line intensity. (2) Blended with U-line. (3) Blended with $HCOOCH_3$. (4) Blended with $CH_2CHC^{15}N$. (5) Blended with $DCOOCH_3$. (6) Blended with $HCOO^{13}CH_3$. (7) Blended with $CH_2CH^{13}CN$. (8) Blended with g_+-CH_3CH_2OH. (9) Blended with H_2CCS. (10) Blended with CH_3CH_2CN v_{13}/v_{21}. (11) Blended with CH_3CCD. (12) Blended with t-CH_3CH_2OH. (13) Blended with CH_3CH_2CN. (14) Blended with CH_2CHCN $v_{11} = 1$. (15) Blended with CH_3COOH $v_t = 0$. (16) Blended with $(CH_3)_2CO$. (17) Blended with CH_2CHCN $v_{10}/v_{11}v_{15}$. (18) Blended with $H^{13}COOCH_3$. (19) Blended with $SO^{18}O$. (20) Blended with CH_3CHO. (21) Blended with $SO^{17}O$. (22) Blended with ^{13}CN. (23) Blended with $CH_2CH^{13}CN$. (24) Blended with $CH_2^{13}CHCN$. (25) Blended with $HCOOCH_3$ $v_t = 1$. (26) Blended with $^{13}CH_2CHCN$. (27) Blended with NH_2D. (28) Blended with $^{13}CH_3OH$. (29) Blended with $^{33}SO_2$. (30) Blended with SO_2 $v_2 = 2$. (This table is available in its entirety at the CDS. A portion is shown here for guidance regarding its form and content.)

Table A.13. continued.

Transition $J_{K_a,K_c} - J'_{K'_a,K'_c}$	Predicted frequency (MHz)	S_{ij}	E_u (K)	v_{LSR}[1] km s^{-1}	Observed frequency (MHz)	Observed T_{MB} (K)[3]	Model T_{MB} (K)
Detected lines of $CH_2CH^{13}CN$							
$9_{5,5}$–$8_{5,4}$	85 041.672	6.22	74.4	2.61[2]	85 042.4	0.02	0.01
$9_{5,4}$–$8_{5,3}$	85 041.672†	6.22	74.4	2.61[2]	″	″	″
$9_{6,4}$–$8_{6,3}$	85 053.074	5.00	98.1	3.16	85 055.4	0.01	0.01
$9_{6,3}$–$8_{6,2}$	85 053.074†	5.00	98.1	3.16	″	″	″
$9_{3,6}$–$8_{3,5}$	85 055.519†	8.00	39.9	5.47	″	″	″
$10_{0,10}$–$9_{0,9}$	93 864.835	9.99	24.8	3.50[2]	93 865.2	0.02	0.01
⋮	⋮	⋮		⋮		⋮	
$21_{9,12}$–$20_{9,11}$	198 588.933	17.10	279.3	7.61[2,26]	198 587.2	0.31	0.11
$21_{9,13}$–$20_{9,12}$	198 588.933†	17.10	279.3	7.61[2,26]	″	″	″
$21_{4,17}$–$20_{4,16}$	198 654.522	20.20	139.4	4.75[27]	198 654.6	0.20	0.07
$21_{13,9}$–$20_{13,8}$	198 864.217	13.00	467.0	6.22[2]	198 863.4	0.10	0.04
$21_{13,8}$–$20_{13,7}$	198 864.217†	13.00	467.0	6.22[2]	″	″	″
$22_{1,22}$–$21_{1,21}$	201 496.193	21.95	113.7	3.60	201 497.1	0.10	0.13
⋮	⋮	⋮		⋮		⋮	

Table A.14. Detected lines of vinyl isocyanide (CH_2CHNC).

Transition $J_{K_a,K_c} - J'_{K'_a,K'_c}$	Predicted frequency (MHz)	S_{ij}	E_u (K)	v_{LSR}[1] km s^{-1}	Observed frequency (MHz)	Observed T_{MB} (K)[2]	Model T_{MB} (K)
$9_{2,8}$–$8_{2,7}$	92 222.557	8.56	31.0	2.74	92 223.3	0.02	0.01
$9_{3,7}$–$8_{3,6}$	92 376.457	8.00	42.2	8.82[3]	92 375.3	0.03	0.01
$9_{6,4}$–$8_{6,3}$	92 379.404	5.00	102.0	5.48[7]	92 379.3	0.01	0.01
$9_{6,3}$–$8_{6,2}$	92 379.404†	5.00	102.0	5.48[7]	92 379.3	0.01	0.01
$9_{3,6}$–$8_{3,5}$	92 386.902	8.00	42.2	6.95	92 386.3	0.02	0.01
⋮	⋮	⋮		⋮		⋮	
$13_{2,12}$–$12_{2,11}$	133 062.524	12.70	53.6	3.41[6]	133 063.2	0.04	0.03
$13_{3,10}$–$12_{3,9}$	133 566.376	12.30	64.8	6.48	133 565.7	0.04	0.03
$13_{2,11}$–$12_{2,10}$	134 563.575	12.70	53.9	4.75[7]	134 563.7	0.08	0.04
$14_{0,14}$–$13_{0,13}$	141 702.008	14.00	51.3	5.82	141 701.6	0.04	0.04
⋮	⋮	⋮		⋮		⋮	
$19_{2,17}$–$18_{2,16}$	198 094.397	18.80	103.3	4.50[10]	198 094.8	0.09	0.10
$19_{1,18}$–$18_{1,17}$	198 245.681	18.90	97.7	8.79	198 242.9	0.10	0.10
$20_{3,18}$–$19_{3,17}$	205 532.002	19.50	123.5	8.41	205 529.7	0.10	0.10
$21_{1,21}$–$20_{1,20}$	208 561.673	20.90	112.7	2.99	208 563.0	0.15	0.12
⋮	⋮	⋮		⋮		⋮	

Notes. Emission lines of vinyl isocyanide (CH_2CHNC) present in the spectral scan of the Orion-KL from the radio-telescope of IRAM-30 m. Column 1 indicates the line transition, Col. 2 gives the predicted frequency in the laboratory, Col. 3 the line strength, Col. 4 upper level energy, Col. 5 observed radial velocities relatives (v_{LSR}), Col. 6 observed centroid frequencies assuming a v_{LSR} of 5 km s^{-1}, Col. 7 observed mean beam temperature, and Col. 8 mean beam temperature obtained with the model. The superscripts are as follows: (†) Blended with the last one. (1) Peak line observed velocity. (2) Peak line intensity. (3) Blended with HCOOCH3 $v_t = 1$. (4) Blended with $HCOOCH_3$. (5) Blended with $H^{13}COOCH_3$. (6) Blended with CH_2CHCN. (7) Blended with U-line. (8) Blended with $SO^{18}O$. (9) Blended with $DCOOCH_3$. (10) Blended with O-H_2CS. (11) Blended with HCDCHCN. (12) Blended with CH_3CH_2CN. (13) Blended with $(CH_3)_2CO$. (14) Blended with $CH_3CH_2C^{15}N$. (15) Blended with $HCOO^{13}CH_3$. (This table is available in its entirety at the CDS. A portion is shown here for guidance regarding its form and content.)

Appendix B: Typographical error in Daly et al. (2013)

Table B.1. Physico-chemical conditions of Orion-KL from CH_3CH_2CN.

	Hot core 1	*Hot core 2*	*Hot core 3*	
d_{sou} (")	4	10	25	
offset (")	5	5	5	
v_{exp} (km s^{-1})	5	13	22	
v_{LSR} (km s^{-1})	5	3	3	
T_{ETL} (K)	275	110	65	N_{TOTAL} (cm^{-2})
$N(CH_3CH_2CN)$ (cm^{-2})	$\mathbf{(6 \pm 2) \times 10^{16}}$	$(8 \pm 2) \times 10^{15}$	$(3.0 \pm 0.9) \times 10^{15}$	$\mathbf{(7 \pm 2) \times 10^{16}}$
$N(CH_3CH_2CN\ v_{13} = 1/v_{21} = 1)$ (cm^{-2})	$\mathbf{(8 \pm 2) \times 10^{15}}$	$(1.1 \pm 0.3) \times 10^{15}$	$(4 \pm 1) \times 10^{14}$	$\mathbf{(1.0 \pm 0.3) \times 10^{16}}$
$N(CH_3CH_2CN\ v_{20})$ (cm^{-2})	$\mathbf{(3 \pm 1) \times 10^{15}}$	$(4 \pm 1) \times 10^{14}$	$(1.7 \pm 0.5) \times 10^{14}$	$\mathbf{(4 \pm 1) \times 10^{15}}$
$N(CH_3CH_2CN\ v_{12})$ (cm^{-2})	$\mathbf{(1.2 \pm 0.6) \times 10^{15}}$	$(1.6 \pm 0.5) \times 10^{14}$	$(6 \pm 3) \times 10^{13}$	$\mathbf{(1.4 \pm 0.7) \times 10^{15}}$
$N(^{13}CH_3CH_2CN)$ (cm^{-2})	$(7 \pm 2) \times 10^{14}$	$(1.9 \pm 0.6) \times 10^{14}$	$(7 \pm 2) \times 10^{13}$	
$N(CH_3{}^{13}CH_2CN)$ (cm^{-2})	$(7 \pm 2) \times 10^{14}$	$(1.9 \pm 0.6) \times 10^{14}$	$(7 \pm 2) \times 10^{13}$	
$N(CH_3CH_2{}^{13}CN)$ (cm^{-2})	$(7 \pm 2) \times 10^{14}$	$(1.9 \pm 0.6) \times 10^{14}$	$(7 \pm 2) \times 10^{13}$	
$N(CH_3CH_2C^{15}N)$ (cm^{-2})	$(2 \pm 1) \times 10^{14}$	$(5 \pm 3) \times 10^{13}$	$(1.7 \pm 0.8) \times 10^{13}$	
N(A-CH_2DCH_2CN) (cm^{-2})	$\leq 6 \times 10^{14}$	$\leq 2 \times 10^{14}$	$\leq 6 \times 10^{13}$	
N(S-CH_2DCH_2CN) (cm^{-2})	$\leq 7 \times 10^{14}$	$\leq 1 \times 10^{14}$	$\leq 6 \times 10^{13}$	
$N(CH_3CHDCN)$ (cm^{-2})	$\leq 6 \times 10^{14}$	$\leq 2 \times 10^{14}$	$\leq 6 \times 10^{13}$	

Notes. Physico-chemical conditions of Orion-KL from the analysis of ethyl cyanide emission lines in the range of 80–280 GHz. In bold type, we display the doubled revised values. The other values are the same. The revised values corresponded to the hot narrow component (1) for the ground and excited states. Vibrational temperatures are not affected, while isotopic ratios have to be changed by the same correction factor.

Table B.2. Isotopic abundances for CH_3CH_2CN in the Orion-KL region.

	$^{12}C/^{13}C$	$^{14}N/^{15}N$	H/D
Isotopic abundance (ratio X)	73 ± 22	256 ± 128	0.012 ± 0.005

Notes. Owing to the error in the column densities of hot narrow component for the ground and excited states, isotopic abundances are increased by a factor less than 2 for $^{12}C/^{13}C$ and $^{14}N/^{15}N$ ratios of ethyl cyanide. On the other hand, the H/D ratio is decreased by half.

5.3 Descubrimiento de acetato de metilo y de *gauche* formiato de etilo en Orión

El artículo que nos ocupa en esta sección fue uno de los resultados más impactantes del barrido espectral sobre Orión-KL: se trata del descubriento, por primera vez en el espacio, de acetato de metilo (CH_3COOCH_3) y de uno de sus isómeros, el confórmero *gauche* de formiato de etilo (*g*-CH_3CH_2OCOH). El trabajo fue publicado en la revista *The Astrophysical Journal Letters* en el año 2013.

El acetato de metilo es una molécula dominada por la doble torsión de los grupos metilo y presenta cinco estados de simetría: AA (A_1 y A_2), EA (E_1), AE (E_2), EE (E_3 y E_4). Debido a esta complejidad en los estados de simetría, el patrón que presentan las líneas de emisión de la molécula puede ser identificado de manera inequívoca en espectros que presenten una alta densidad de líneas, como en el caso de Orión-KL. La detección de esta molécula supuso la primera identificación de una especie que contiene el grupo acetato en el espacio. De esta manera, el trabajo demostró la complejidad química del medio interestelar y abrió el camino para explorar nuevas rutas químicas en este medio. Metil acetato probablemente se forme por medio de múltiples reacciones a partir de especies detectadas en regiones de formación de estrellas como formiato de metilo, ácido acético o metanol. La identificación de la ruta más favorable supone un reto para la comprensión de la formación de especies complejas. Como ya hemos visto, en estas regiones la química detectada es el producto de reacciones en fase gaseosa, reacciones sobre los mantos del polvo y de la evaporación de estos mantos, donde otra vez las especies evaporadas pueden reaccionar en la fase gaseosa.

A pesar de que el objetivo principal del artículo era mostrar esta primera identificación (de ahí su presentación en formato *Letter*) en él se presenta la búsqueda en Orión de diferentes isómeros del metil acetato. Se detectaron los dos confórmeros, *trans* y *gauche* de formiato de etilo. El segundo, también por primera vez en el espacio. Mediante el análisis de todas estas especies se determinó que los isómeros parecían estar relacionados espacialmente en la fuente. De otros tres isómeros de estas especies −ácido propanoico (CH_3CH_2COOH), hidroxiacetona (CH_3COCH_2OH) y metoxiacetaldehído (CH_3OCH_2OH)−, solo pudimos aportar límites superiores para sus densidades de columna pues no fueron identificadas por encima del límite de detección de nuestro barrido espectral.

A continuación presentamos el artículo de esta primera detección de un acetato en el espacio. En el Apéndice C se muestra la tabla que forma parte del contenido *online* del artículo y que se puede encontrar en la base de datos CDS[3].

[3] http://vizier.cfa.harvard.edu/viz-bin/VizieR?-source=J/ApJ/770/L13

The Astrophysical Journal Letters, 770:L13 (6pp), 2013 June 10 doi:10.1088/2041-8205/770/1/L13

DISCOVERY OF METHYL ACETATE AND GAUCHE ETHYL FORMATE IN ORION*

B. Tercero[1], I. Kleiner[2], J. Cernicharo[1], H. V. L. Nguyen[2], A. López[1], and G. M. Muñoz Caro[1]
[1] Department of Astrophysics, CAB, INTA-CSIC, Crta Torrejón-Ajalvir, km. 4, E-28850 Torrejón de Ardoz, Madrid, Spain; terceromb@cab.inta-csic.es, jcernicharo@cab.inta-csic.es, lopezja@cab.inta-csic.es, munozcg@cab.inta-csic.es
[2] Laboratoire Interuniversitaire des Systèmes Atmosphériques, CNRS/IPSL UMR7583 et Universités Paris Diderot et Paris Est, 61 av. Général de Gaulle, F-94010 Créteil, France; isabelle.kleiner@lisa.u-pec.fr, nguyen@pc.rwth-aachen.de
Received 2013 April 18; accepted 2013 May 2; published 2013 May 28

ABSTRACT

We report on the discovery of methyl acetate, CH_3COOCH_3, through the detection of a large number of rotational lines from each one of the spin states of the molecule: AA species (A_1 or A_2), EA species (E_1), AE species (E_2), and EE species (E_3 or E_4). We also report, for the first time in space, the detection of the *gauche* conformer of ethyl formate, CH_3CH_2OCOH, in the same source. The *trans* conformer is also detected for the first time outside the Galactic center source SgrB2. From the derived velocity of the emission of methyl acetate, we conclude that it arises mainly from the compact ridge region with a total column density of $(4.2 \pm 0.5) \times 10^{15}$ cm^{-2}. The derived rotational temperature is 150 K. The column density for each conformer of ethyl formate, *trans* and *gauche*, is $(4.5 \pm 1.0) \times 10^{14}$ cm^{-2}. Their abundance ratio indicates a kinetic temperature of 135 K for the emitting gas and suggests that gas-phase reactions could participate efficiently in the formation of both conformers in addition to cold ice mantle reactions on the surface of dust grains.

Key words: ISM: abundances – ISM: individual objects (Orion KL) – ISM: molecules – line: identification – molecular data

Online-only material: machine-readable table

1. INTRODUCTION

The line survey of Orion carried out by Tercero and collaborators using the IRAM 30 m telescope presents a forest of lines arising from isotopologues and vibrationally excited states of abundant species (see, e.g., Tercero et al. 2010, 2011; Daly et al. 2013). The problem of identifying these features was a real challenge as initially we had more than 8000 unidentified lines. The analysis of the data has been done molecule by molecule (Tercero 2012). For each species we explored the literature for spectroscopic information on the isotopologues and vibrationally excited states, but substantial laboratory work was missing for most of these species. In 2006 we began a close collaboration with different spectroscopic laboratories that allowed us to identify nearly 4000 of these unknown lines (often called *weeds*). The ^{13}C and ^{15}N isotopologues from ethyl cyanide, CH_3CH_2CN, were measured by Demyk et al. (2007) and Margulès et al. (2009). Several vibrationally excited states of the same species were characterized in the laboratory by Daly et al. (2013). The ^{13}C, deuterated, and ^{18}O isotopologues of methyl formate were observed in the laboratory by Carvajal et al. (2009), Margulès et al. (2010), and Tercero et al. (2012), respectively. The vibrationally excited state ν_{12} of formamide was measured in the laboratory by Motiyenko et al. (2012). Finally, A. López et al. (in preparation) have characterized in the laboratory several vibrationally excited states of vinyl cyanide, CH_2CHCN, which have been identified in Orion together with all its isotopologues ^{13}C, ^{15}N, and D. All these isotopologues and vibrationally excited states were detected in space for the first time, thanks to these new laboratory data. In addition, the study of the survey was divided in the analysis of different families of molecules: CS-bearing species (Tercero et al. 2010), silicon-bearing molecules (Tercero et al. 2011), SO and SO_2 (Esplugues et al. 2013). Work on other species, such as HCN, HNC, and HCO^+, CH_3CN, HC_3N, and HC_5N, and organic saturated O-rich species, is in progress (N. Marcelino et al., in preparation; T. A. Bell et al., in preparation; G. B. Esplugues et al., in preparation; A. López et al., in preparation).

Although many of the still 4000 remaining U lines could belong to rare isotopologues of complex organic molecules, we believe that we are ready now to begin the search for new molecular species. The study of a cloud such as Orion could provide important clues on the formation of complex organic molecules on the grain surfaces and/or in the gas phase. A systematic line survey with most *weeds* removed permits us to address the problem of the abundances of isomers and derivates of key species, such as methyl formate, ethyl cyanide, and others. Moreover, it will constitute the best spectral template for future ALMA observations of hot cores.

In this Letter we report the detection for the first time in space of methyl acetate, CH_3COOCH_3, from the detection of many lines from the states AA, AE, EA, and EE (E_3, and E_4) of this molecule at 3, 2, and 1.3 mm. The *gauche* conformer of ethyl formate (an isomer of methyl acetate), for which the *anti* conformer was previously detected in SgrB2 by Belloche et al. (2009), has also been detected in Orion. This detection of ethyl formate outside the Galactic center indicates that this species is also efficiently produced in hot cores.

2. OBSERVATIONS

The observations were carried out using the IRAM 30 m radiotelescope during several periods (see Tercero et al. 2010). System temperatures were in the range 200–800 K for the 1.3 mm receivers, 200–500 K for the 2 mm receivers, and 100–350 K for the 3 mm receivers, depending on the particular frequency, weather conditions, and source elevation. The intensity scale was calibrated using two absorbers at different temperatures and using the Atmospheric Transmission Model (Cernicharo 1985; Pardo et al. 2001). Pointing and focus

* This work was based on observations carried out with the IRAM 30 m telescope. IRAM is supported by INSU/CNRS (France), MPG (Germany), and IGN (Spain).

were regularly checked on the nearby quasars 0420−014 and 0528+134. Observations were made in the balanced wobbler-switching mode. We pointed the observations toward IRc2 at α(J2000) = $5^h35^m14^s.5$, δ(J2000)=−5° 22′ 30″.0. The data were processed using the IRAM GILDAS software[3] (developed by the Institute de Radioastronomie Millimetrique). We considered lines with intensities ⩾0.02 K, covering three or more channels. Figures are shown in units of main beam antenna temperature, $T_{MB} = T_A^\star/\eta_{MB}$, where η_{MB} is the main beam efficiency. A more detailed description of the observations can be found in Tercero et al. (2010).

3. FREQUENCY AND INTENSITY PREDICTIONS FOR METHYL ACETATE

Methyl acetate, [CH_3–O–C(=O)–CH_3], has been studied by Sheridan et al. (1980) using Stark spectrometers in the frequency region from 8 to 40 GHz. In 2011, the investigation was considerably improved with 315 new lines recorded using the molecular beam Fourier transform microwave spectrometer in Aachen and 519 lines recorded using the free jet absorption Stark-modulated millimeterwave (FJASMmm) spectrometer in Bologna (Tudorie et al. 2011). A newly written program BELGI-Cs-2Tops based on the Hamiltonian described by Ohashi et al. (2004) was used to fit the complete data set with 27 molecular parameters, up to $J = 19$ and $K_a = 7$. More than 800 new microwave and millimeter-wave measurements were assigned to the ground-state transitions in methyl acetate and fit, leading to rms deviations of 4 kHz for the microwave lines and of 40 kHz for the millimeter-wave lines, i.e., to residuals essentially equal to the experimental measurement errors. The heights for two internal rotation barriers were determined to be of 102 cm^{-1} for the acetyl CH_3 internal rotor and of 422 cm^{-1} for the ester CH_3. As the theoretical background and code presently used have been extensively described by Tudorie et al. (2011), we will summarize here only the main characteristics.

The BELGI-Cs-2Tops program is restricted to (1) asymmetric top molecules containing two non-equivalent CH_3 internal rotors, and (2) molecules belonging to the Cs point group at equilibrium. This code is most closely related to a code used only once in the literature for a treatment of the microwave spectrum of the molecule N-methylacetamide [CH_3–NH–C(=O)–CH_3] (Ohashi et al. 2004) although some differences exist as detailed in Tudorie et al. (2011).

The torsional and rotational Hamiltonian is diagonalized in separate symmetry blocks, each characterized by one of the five (σ_1, σ_2) pairs, where σ_1 and σ_2 designate the symmetry indicators for each of the A and B tops. We follow the notation used in Table 1 of Ohashi et al. (2004), i.e., we have for the five symmetry species: $\sigma_1 = 0$, $\sigma_2 = 0$, AA species (A_1 or A_2 in the G_{18} permutation-inversion group of the molecule); $\sigma_1 = \pm1$, $\sigma_2 = 0$, EA species (E_1); $\sigma_1 = 0$, $\sigma_2 = \pm1$, AE species (E_2); $\sigma_1 = \pm1$, $\sigma_2 = \mp1$, EE species (E_3); and $\sigma_1 = \pm1$, $\sigma_2 = \pm1$, EE species (E_4). The higher barrier hindering the ester methyl group internal rotation (422 cm^{-1}) corresponds to the smaller splittings between the AA and the E_2 lines, whereas the lower barrier (102 cm^{-1}) hindering the acetyl methyl group is responsible for the larger splittings between the AA and the E_1 lines. The splittings between the E_3 lines and the E_4 lines are due to the coupling between the two tops. Statistical weights for methyl acetate are 16, 16, 16, 8, and 8 for the A_1 or A_2 (AA), E_1 (AE), E_2 (EA), E_3, and E_4, respectively (Ohashi et al. 2004). The zero-point energies for the $J = K = 0$ levels are 99.9450 cm^{-1}, 99.9551 cm^{-1}, 101.0947 cm^{-1}, 101.1047 cm^{-1}, and 101.1049 cm^{-1} for A, E_2, E_1, E_3, and E_4 species, respectively.

The spectroscopic constants determined from the previous fit published in Tudorie et al. (2011) are used in the present study to predict the transition frequencies for the $\nu_t = 0$ torsional ground state up to $J = 30$. Since we did only fit the observed lines in the laboratory up to $J = 19$, $K_a \leqslant 7$, large uncertainties exist for the higher J and K_a values (we estimate 1σ uncertainties of 0.1–0.5 MHz for $J < 25$ and 0.5–2 for $25 \leqslant J \leqslant 30$). For the present Letter we also have implemented in the BELGI-Cs-2Tops the calculation of the intensities using the same method as described in Hougen et al. (1994) and Kleiner (2010) for the one-top codes.[4] The BELGI-Cs-2Tops code is written in a quasi-principal-axis-method (PAM) axis system which can be obtained by a rotation about the c-axis from the principal axis system (PAM) by the angle θ, as shown in Equation (9) of Ohashi et al. (2004). The value of θ in methyl acetate is determined to be −0.0316385(95) radians (Tudorie et al. 2011). Using the values determined by Sheridan et al. (1980) in the PAM axis system, we obtain for the components of the electric dipole moments in the quasi-PAM axis system, $\mu_a = -0.008$ D and $\mu_b = 1.641$ D.

4. RESULTS AND DISCUSSION

The predicted frequencies and intensities, together with the energy of the levels, have been implemented in the MADEX code (Cernicharo 2012). Each one of the five states, AA, AE (E_2), EA (E_1), EE (E_3 and E_4), has been considered as an independent molecular species for the calculation of line intensities. For the kinetic temperature of Orion levels above $J = 30$ could be significantly populated and some lines could also contribute to the Orion spectrum. The predictions from our spectroscopic code have, however, large uncertainties for larger Js (see above). The synthetic spectrum of methyl acetate was calculated assuming LTE conditions (due to the lack of collisional rates for this molecule) for a kinetic temperature of 150 ± 20 K, an LSR velocity of the cloud of 8 km s^{-1}, a line width of 3 km s^{-1}, and a column density for each state AA, EA, and AE of (10.4 ± 1.0) × 10^{14} cm^{-2}, and of (5.2 ± 1.0) × 10^{14} cm^{-2} for the E_1 and E_2 states. Size (15″) and offset (7″) from the pointing position (IRc2) of the compact ridge component (see Favre et al. 2011; Genzel & Stutzki 1989; Blake et al. 1987) are taken into account in our model. Beam dilution is corrected for each line depending on their frequency. Consequently, the total column density of methyl acetate in Orion is 4.2 ± 0.5 × 10^{15} cm^{-2}, which includes a correction factor to the partition function computed for $T_K = 150$ K and $J \leqslant 30$ of 2.6. It includes the torsional excited states (estimated energies) and rotational levels up to $J = 65$. Figures 1–3 show selected lines from the best-fit synthetic spectrum to the Orion data. The full list of detected lines is provided in Table 1 (electronic version), where we list 215 unblended lines as well as 163 lines moderately blended with other species. No unblended lines of CH_3COOCH_3 are missing. The detection is fully secure taking into account that the systematic pattern of the lines arising from the different states is always present. Lines from $\nu_t = 1$ could be also detectable as the vibrational partition function

[3] http://www.iram.fr/IRAMFR/GILDAS

[4] The BELGI-Cs code is publicly available at the PROSPE website, Programs for ROtational SPEctroscopy, managed by Kisiel at http://www.ifpan.edu.pl/~kisiel/prospe.htm.

Table 1
Detected Lines of CH_3COOCH_3

J	K_a	K_c	p	J'	K'_a	K'_c	p'	State	Predicted Freq. (MHz)	Error (MHz)	E_u (K)	$S_{ij}\,\mu^2$	Observed Freq. (MHz)	T_{mb} (K)	Blend
13	0	13		12	1	12		E3	82779.635	.012	28.6	31.30	82780.2	0.03	CH_3CH_2CN $^{33}SO_2$
13	0	13		12	1	12		E4	82779.725	.012	28.6	31.30	[a]		
13	0	13		12	1	12		EA	82780.026	.012	28.6	31.30	[a]		
13	1	13		12	0	12		E4	82808.862	.012	28.6	31.30	82809.2	0.04	$HCOOCH_3$ $v_t = 1$
13	1	13		12	0	12		E3	82808.881	.012	28.6	31.30	[a]		
13	1	13		12	0	12		EA	82809.267	.012	28.6	31.30	[a]		
13	0	13		12	1	12		AE	82823.351	.012	28.6	31.30	82823.2	0.04	
13	0	13	1	12	1	12	1	AA	82823.702	.012	28.6	31.30	[a]		

Notes. Emission lines of CH_3COOCH_3 present in the spectral scan of Orion KL from the IRAM 30 m radiotelescope. Columns 1–8 indicate the line transition, Column 9 the state of the molecule, Column 10 the predicted frequency in the laboratory, Column 11 the uncertainty of frequency predictions, Column 12 the upper level energy, Column 13 the line strength, Column 14 the observed frequency assuming a v_{LSR} of 8 km s^{-1}, Column 15 the mean beam temperature, and Column 16 the blends.

[a] Blended with previous line.

(This table is available in its entirety in a machine-readable form in the online journal. A portion is shown here for guidance regarding its form and content.)

indicates that the population of the $v_t = 1$ levels from the two methyl groups will be a factor 1.5–2 below that of the $v_t = 0$ states. Unfortunately, no accurate predictions are available for the torsionally excited states.

Ethyl formate has two conformers, *trans* (also called *anti*) and *gauche*, with the latter being 65 ± 21 cm^{-1} (94 K) above in energy (Riveros & Wilson 1967). The *gauche* conformer has two possible orientations of the terminal methyl group and, hence, it could be twice as abundant as the *trans* conformer if the energy difference were zero (Belloche et al. 2009). We have used the spectroscopic laboratory data from Riveros & Wilson (1967), Meyer & Wilson (1970), and Demaison et al. (1984) to derive the rotational constants which were incorporated into the MADEX code. The predictions were checked against the corresponding entry in the JPL catalog (Pickett et al. 1998). The *trans* conformer of ethyl formate was detected in SgrB2 by Belloche et al. (2009) but only upper limits were obtained for the *gauche* one. We have identified both conformers in the line survey of Orion through 90 features free of blending (52 *trans* and 38 *gauche*). Selected identified lines are shown in Figure 4. We found that the *gauche* conformer has less intense lines than the *trans* one for transitions at 3 and 2 mm. However, at higher frequencies, there are many multiplet transitions of the *gauche* that coincide in frequency and they become prominent in the Orion data. The best fit to the data (assuming the same physical conditions and source parameter—v_{LSR}, Δv, size, and offset—than those used for methyl acetate corresponding to the compact ridge component of Orion KL) provides a rotational temperature of 150 ± 20 K, and a column density for each conformer of $(4.5 \pm 1.0) \times 10^{14}$ cm^{-2}, i.e., a total column density for ethyl formate $\simeq$5 times below that of methyl acetate. From the observed abundance ratio between the *trans* and *gauche* conformers, $N_{gauche}/N_{trans} \simeq 1 = 2 \times e^{-94/T}$, we derive a kinetic temperature for the emitting gas of 135 ± 30 K. If the lowest energy conformer of ethyl formate, the *trans* one, was formed on the ices before the warm phase of the cloud, isomerization to the *gauche* form will require a high kinetic energy and, perhaps, a long time to overpass the barrier to isomerization of 550 K (Riveros & Wilson 1967). Our result points toward a fast equilibrium between both conformers at 150 K and in a time comparable to the duration of the present warm phase of the cloud. If the molecule is formed in the gas phase, the energy liberated in the process could help in the isomerization process and the observed conformer temperature will reflect the kinetic temperature of the gas. However, no chemical paths are included in the present chemical models to form either ethyl formate or methyl acetate. New laboratory experiments are needed to understand the way these species could be formed in gas phase or in ices and how conformers of the same species can equilibrate at a temperature close to the kinetic temperature of the gas.

Methyl acetate is probably formed via multiple reaction pathways from species detected in hot cores such as methyl formate, acetic acid, and methanol. In icy grain mantles, methanol is one of the common molecular components. Acetic acid is a relatively large molecule that would be difficult to detect in the ice by IR observations and that could be the precursor of methyl acetate and ethyl formate. Only formic acid (HCOOH) has been proposed as a possible carrier of the 7.24 μm band toward high-mass protostars, while the 7.41 μm band could be due to the formate ion ($HCOO^-$) and acetaldehyde (CH_3CHO), according to Schutte et al. (1999). Formation of HCOOH on a surface occurs experimentally at low temperatures, mainly through hydrogenation of the HO–CO complex (Ioppolo et al. 2011). Other possible formation routes in the ice are via precursor cations (Woon 2011) or by reactions of superthermal $O(^3P)$ atoms and CH_4 with an overcoat of CO (Madzunkov et al. 2010). Also photon or electron irradiation of H_2O:CO ice mixtures leads to formation of formic acid among other products, including methanol in the case of photoprocessing (Watanabe et al. 2007; Bennett et al. 2011). HCOOH was found to spontaneously deprotonate when sufficient water is present to stabilize charge transfer complexes. Both ammonia and water can serve as proton acceptors, yielding ammonium (NH_4^+) and hydronium (H_3O^+) counterions (Park & Woon 2006). The so-formed formate ion ($HCOO^-$) might intervene in the formation of species like methyl acetate in the ice matrix, but this was, to our knowledge, not confirmed experimentally. Brouillet et al. (2013) have recently observed with high angular resolution CH_3OCH_3 and CH_3OCOH toward Orion-IRc2 and conclude that the similarity in the spatial distribution of both species points toward a common precursor. The observation of a similar abundance for the two conformers of ethyl formate points to a gas-phase production path rather than to a low-temperature

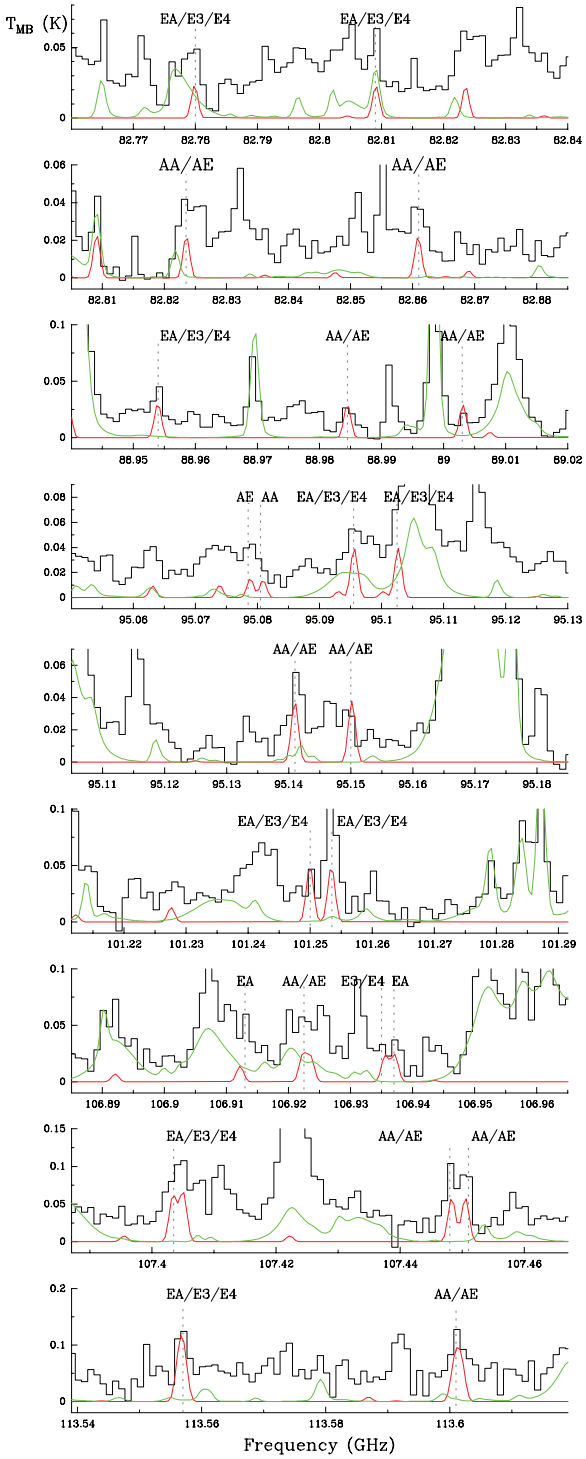

Figure 1. Selected lines of methyl acetate at 3 mm, CH_3COOCH_3, toward Orion-IRc2. The lines from the different states are identified. The continuous green line corresponds to all lines already modeled in our previous papers (see the text).

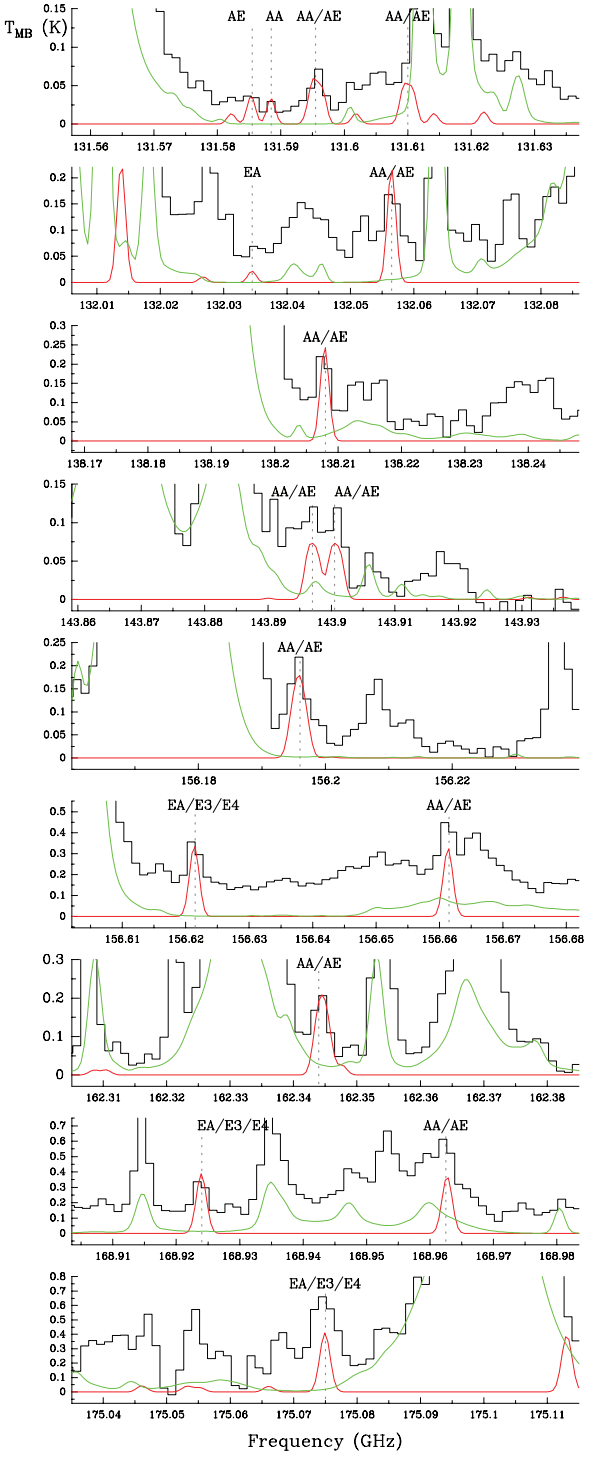

Figure 2. Selected lines of methyl acetate at 2 mm, CH_3COOCH_3, toward Orion-IRc2. The lines from the different states are identified. The continuous green line corresponds to all lines already modeled in our previous papers (see the text).

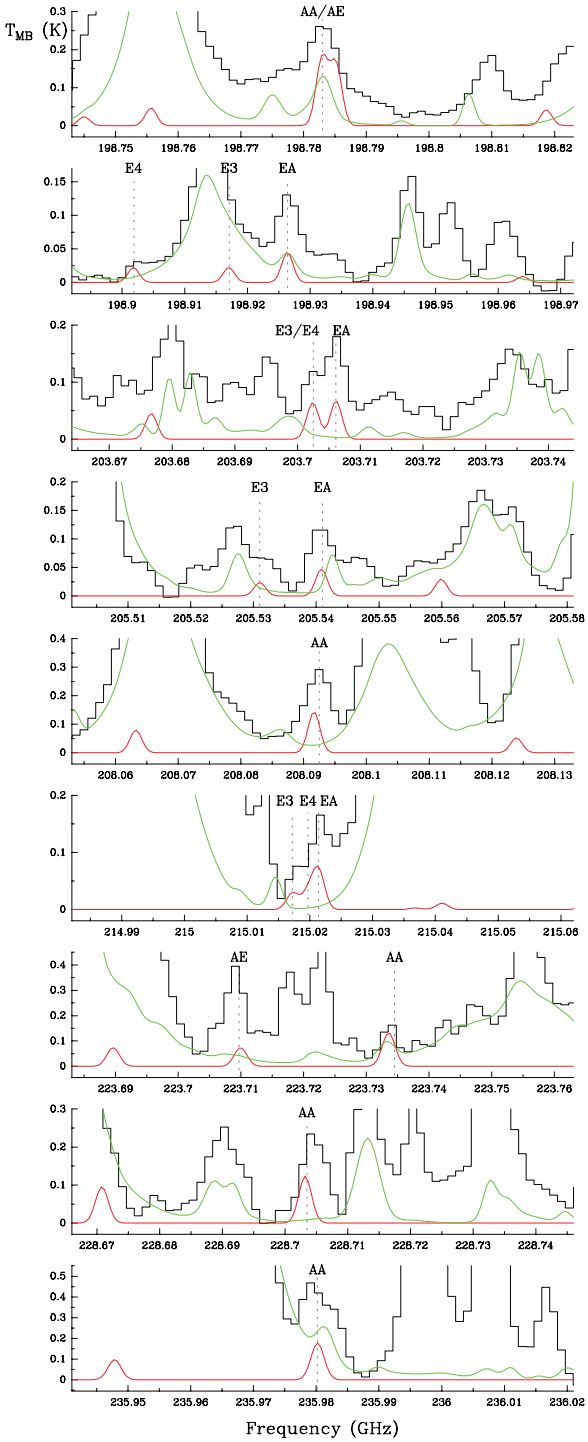

Figure 3. Selected lines of methyl acetate at 1.3 mm, CH_3COOCH_3, toward Orion-IRc2. The lines from the different states are identified. The continuous green line corresponds to all lines already modeled in our previous papers (see the text).

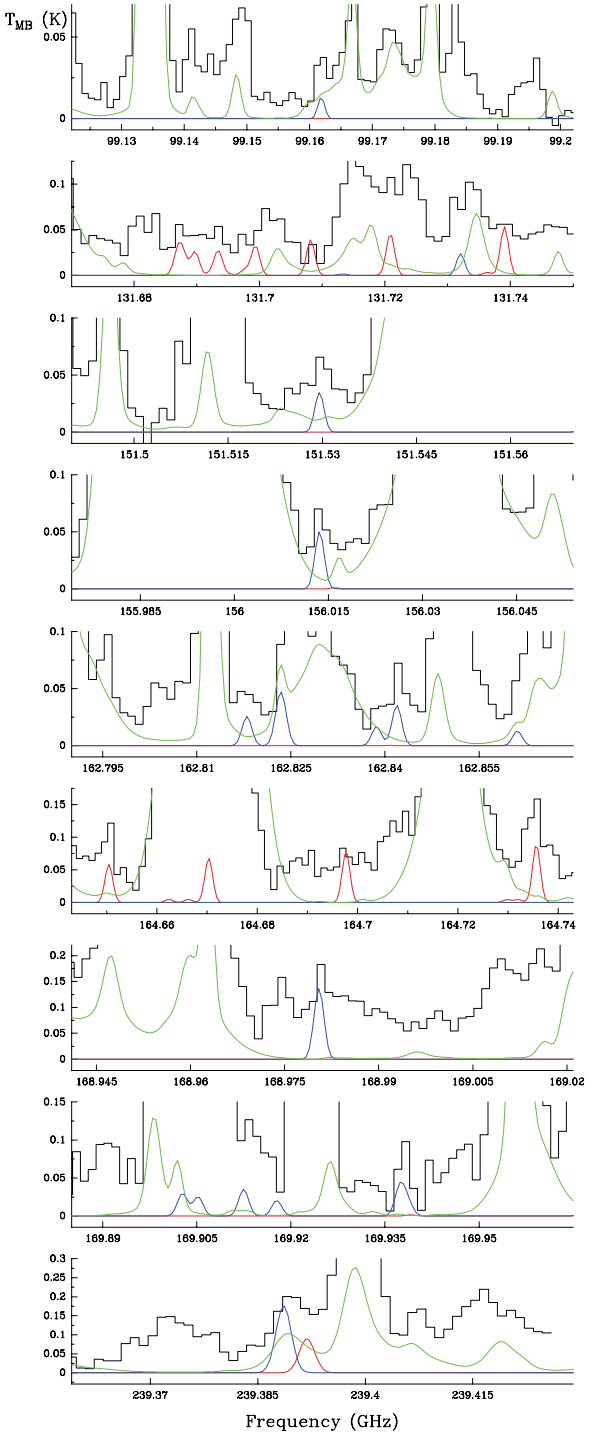

Figure 4. Selected lines of the *trans* (red line) and *gauche* (blue) conformers of ethyl formate, CH_3CH_2OCOH, toward Orion-IRc2. The synthetic spectrum corresponds to the same column density for both conformers (see the text). The continuous green line corresponds to all lines already modeled in our previous papers (see the text).

ice formation mechanism. Radicals such as methoxy (CH_3O; Cernicharo et al. 2012) or CH_3CO could play an important role in the gas-phase chemistry. However, methoxy has been observed only toward cold dark clouds (Cernicharo et al. 2012) and it is not detected in our line survey of Orion; CH_3CO has not yet been detected in the Interstellar Medium (ISM).

The two conformers of ethyl formate and methyl acetate are isomers of the $C_3H_6O_2$. Three additional isomers, propanoic (propionic) acid (CH_3CH_2COOH), hydroxyacetone (CH_3COCH_2OH), and methoxyacetaldehyde (CH_3OCH_2OH), could be also present in Orion. The three species are implemented in MADEX. For hydroxyacetone, the available spectroscopic data have been summarized by Braakman et al. (2010) and cover frequencies up to 431.8 GHz (dipole moments from Kattija-Ari & Harmony 1980). We obtain an upper limit to its column density of 8×10^{13} cm^{-2} (see also Apponi et al. 2006 for an upper limit to its column density toward SgrB2). For propionic acid and methoxyacetaldehyde, we also obtain upper limits to their column densities of 1.6×10^{14} and 2×10^{14} cm^{-2}, respectively. We note, however, that frequency predictions above 40 GHz for these two molecular species are rather uncertain (Stifvater 1975; Ouyang & Howard 2008; Hirano et al. 1987). Hence, of the known possible non-cyclic isomers of $C_3H_6O_2$, methyl acetate appears to be the most abundant one. Laboratory spectroscopic data are needed for propionic acid and methoxyacetaldehyde in order to draw further conclusions on their contribution to the ice mantle and gas-phase chemistry of hot cores, and to the forest of still unknown spectral features in Orion.

J. Cernicharo, B. Tercero, G. Muñoz Caro, and A. López thank the Spanish MICINN for funding support through grants, AYA2009- 07304, AYA2011-29375, and CSD2009-00038. I. Kleiner acknowledges support from the French national PCMI program, and support from the ANR-08-BLAN-0054 contract (France). J. Cernicharo thanks U. Paris Est for an invited professor position associated to this work.

REFERENCES

Apponi, A. J., Hoy, J. J., Halfen, D. T., et al. 2006, ApJ, 652, 1787
Belloche, A., Garrod, R. T., Müller, H. S. P., et al. 2009, A&A, 499, 215
Bennett, C. J., Hama, T., King, Y. S., et al. 2011, ApJ, 727, 27
Blake, G. A., Sutton, E. C., Masson, C. R., & Philips, T. H. 1987, ApJ, 315, 621
Braakman, R., Drouin, B. J., Widicus Weaver, S. L., & Blake, G. A. 2010, JMoSp, 264, 43
Brouillet, N., Despois, D., Baudry, A., et al. 2013, A&A, 550, 46
Carvajal, M., Margulès, L., Tercero, B., et al. 2009, A&A, 500, 1109
Cernicharo, J. 1985, Internal IRAM report (Granada: IRAM)
Cernicharo, J. 2012, in ECLA-2011: Proceedings of the European Conference Laboratory Astrophysics, ed. C. Stehlé, C. Joblin, & L. d'Hendecourt (Cambridge: Cambridge Univ. Press), 251
Cernicharo, J., Marcelino, N., Roueff, E., et al. 2012, ApJL, 759, L43
Daly, A. M., Bermúdez, C., López, A., et al. 2013, ApJ, 768, 81
Demaison, J., Boucher, D., Burie, J., & Dubrulle, A. 1984, ZNatA, 39, 560
Demyk, K., Mäder, H., Tercero, B., et al. 2007, A&A, 466, 255
Esplugues, G. B., Tercero, B., Cernicharo, J., et al. 2013, A&A, submitted
Favre, C., Despois, D., Brouillet, N., et al. 2011, A&A, 532, 32
Genzel, R., & Stutzki, J. 1989, ARA&A, 27, 41
Hirano, H., Shibano, J., Mitani, A., et al. 1987, JMoSt, 162, 359
Hougen, J. T., Kleiner, I., & Godefroid, M. 1994, JMoSp, 163, 559
Ioppolo, S., Cuppen, H. M., van Dishoeck, E. F., & Linnartz, H. 2011, MNRAS, 410, 1089
Kattija-Ari, M., & Harmony, M. D. 1980, Int. J. Quantum Chem. Symp., 14, 443
Kleiner, I. 2010, JMoSp, 260, 1
Madzunkov, S. M., MacAskill, J. A., & Chuthan, A. 2010, ApJ, 712, 194
Margulès, L., Huet, T. R., Demaison, J., et al. 2010, ApJ, 714, 1120
Margulès, L., Motiyenko, R. A., Demyk, K., et al. 2009, A&A, 493, 565
Meyer, R., & Wilson, E. B. 1970, JChPh, 53, 3969
Motiyenko, R. A., Tercero, B., Cernicharo, J., & Margulès, L. 2012, A&A, 548, A71
Ohashi, N., Hougen, J. T., Suenram, R. D., et al. 2004, JMoSp, 227, 28
Ouyang, B., & Howard, B. J. 2008, JPCA, 112, 8208
Pardo, J. R., Cernicharo, J., & Serabyn, E. 2001, ITAP, 49/12, 1683
Park, J-Y., & Woon, D. E. 2006, ApJ, 648, 1285
Pickett, H. M., Poynter, R. L., Cohen, E. A., et al. 1998, JQSRT, 60, 883
Riveros, J. M., & Wilson, E. B. 1967, JChPh, 46, 4605
Schutte, W. A., Boogert, A. C. A., Tielens, A. G. G. M., et al. 1999, A&A, 343, 966
Sheridan, J., Bossert, W., & Bauder, A. 1980, JMoSp, 80, 1
Stifvater, O. L. 1975, JChPh, 62, 233
Tercero, B. 2012, PhD thesis, Univ. Complutense de Madrid
Tercero, B., Cernicharo, J., Pardo, J. R., & Goicoechea, J. R. 2010, A&A, 517, 96
Tercero, B., Margulès, L., Carvajal, M., et al. 2012, A&A, 538, A119
Tercero, B., Vincent, L., Cernicharo, J., Viti, S., & Marcelino, N. 2011, A&A, 528, 26
Tudorie, M., Kleiner, I., Hougen, J. T., et al. 2011, JMoSp, 269, 211
Watanabe, N., Mouri, O., Nagaoka, A., et al. 2007, ApJ, 668, 1001
Woon, D. E. 2011, ApJ, 728, 44

5.4 Buscando *trans* etil metil éter en Orión-KL

El artículo que se presenta a continuación trata sobre la búsqueda de *tran* etil metil éter (tEME, $CH_3CH_2OCH_3$) en Orión-KL. Debido a la relevancia de los resultados obtenidos, el artículo se publicó como *Letter to the Editor* en la revista *Astronomy and Astrophysics* en el año 2015.

Como hemos visto en el artículo anterior, la contrapartida con el grupo etilo (CH_3CH_2-) de una molécula muy abundante en Orión como el formiato de metilo (CH_3OCOH) fue detectada a través de sus dos confórmeros (*trans* y *gauche* formiato de etilo). Esto nos sugería que podríamos hallar nuevas especies saturadas y oxigenadas en Orión si buscábamos la variante con el grupo etilo de aquellas abundantes con el grupo metilo. Considerando que el dimetil éter (CH_3OCH_3) es una de las especies más abundantes de la región y de que diversos estudios demuestran que se correlaciona espacialmente con el formiato de metilo, nos decantamos por la búsqueda de tEME. Además, al contrario que lo que ocurría en los tres artículos presentados anteriormente, las frecuencias de las transiciones de esta especie ya habían sido publicadas y estaban disponibles para la comunidad científica. Esto, nos permitía realizar la búsqueda en Orión sin tener que acudir previamente a los laboratorios de espectroscopía molecular.

En este caso, y también a diferencia de lo que vimos en los artículos ya presentados, una primera búsqueda en el barrido espectral con el telescopio de IRAM de 30 m no aportó resultados concluyentes. No hallábamos líneas ausentes, pero, al tener la especies cinco estados de simetría, el espectro rotacional debía presentar un patrón que no conseguíamos diferenciar en los datos del 30 m. La principal razón era por el alto grado de solapamiento y mezcla de líneas pertenecientes a distintas especies en el espectro de esta fuente. Esto supone un serio límite para detectar especies poco abundantes en la región. Por este motivo, para la búsqueda de este tipo de moléculas debíamos acudir a datos que fueran más sensibles y que pudieran resolver espacialmente las distintas componentes de la fuente.

Afortunadamente, los primeros datos obtenidos con el interferómetro ALMA en Orión-KL ya se encontraban disponibles (datos de la verificación científica de ALMA a 1.3 mm) y nuestra búsqueda de tEME usando estos datos resultó prometedora. Centrándonos en la componente del *compact ridge* encontramos un espectro donde las líneas no presentan un alto grado de solapamiento (la emisión de esta región se caracteriza por líneas estrechas) y conseguimos reproducir los patrones de líneas observados al modelizar la emisión de tEME con las condiciones físicas típicas de esta componente. A pesar de los buenos resultados, no pudimos dar esta detección por definitiva debido, principalmente, a que el limitado rango de frecuencias de los datos de ALMA SV.

Nuestro análisis de esta molécula y de especies relacionadas también apunta a que tEME está presente en la región. En este artículo, además de realizar modelos con MADEX para tEME y algunos de sus isómeros (propanol), creamos mapas con los datos de ALMA para distintas especies oxigenadas encontradas en Orión con grupo metilo y con grupo etilo. Uno de los resultados más relevantes es la diferenciación espacial de especies que parecían pertenecer a una misma ”familia” molecular: las moléculas orgánicas saturadas ricas en oxígeno. Especies como etanol (CH_3CH_2OH) presentan el máximo de emisón en la región del *hot core* mientras que tEME o formiato de etilo presentan este máximo en el *compact ridge*. Este resultado apunta hacia una diferencia en los precursores de estas especies y advierte de la peligrosa simplificación que puede efectuarse al asumir que las especies que presentan ciertas características comunes tengan un origen también común en la región.

En las siguientes páginas mostramos el artículo y remitimos al lector al mismo para que pueda

encontrar las explicaciones detalladas de esta investigación.

Para seguir la misma estructura que en la presentación de las publicaciones anteriores, las Tablas A.1, A.2 y A.3 de este artículo se mostrarán en el Apéndice D.

A&A 582, L1 (2015)
DOI: 10.1051/0004-6361/201526255

Astronomy & Astrophysics

Letter to the Editor

Searching for trans ethyl methyl ether in Orion KL⋆,⋆⋆

B. Tercero[1], J. Cernicharo[1], A. López[1,2], N. Brouillet[3,4], L. Kolesniková[5], R. A. Motiyenko[6], L. Margulès[6], J. L. Alonso[5], and J.-C. Guillemin[7]

[1] Grupo de Astrofísica Molecular. Instituto de CC. de Materiales de Madrid (ICMM-CSIC). Sor Juana Inés de la Cruz, 3, Cantoblanco, 28049 Madrid, Spain
e-mail: b.tercero@icmm.csic.es; jose.cernicharo@csic.es
[2] Dpto. de Astrofísica, CAB, INTA-CSIC, Crta Torrejón-Ajalvir, km 4, 28850 Torrejón de Ardoz, Madrid, Spain
[3] Université Bordeaux, LAB, UMR 5804, 33270 Floirac, France
[4] CNRS, LAB, UMR 5804, 33270 Floirac, France
[5] Grupo de Espectroscopía Molecular (GEM), Edificio Quifima, Área de Química-Física, Laboratorios de Espectroscopía y Bioespectroscopía, Parque Científico UVa, Unidad Asociada CSIC, Universidad de Valladolid, 47011 Valladolid, Spain
[6] Laboratoire de Physique des Lasers, Atomes, et Molécules, UMR CNRS 8523, Université de Lille I, 59655 Villeneuve d'Ascq Cédex, France
[7] Institut des Sciences Chimiques de Rennes, École Nationale Supérieure de Chimie de Rennes, CNRS, UMR 6226, 11 Allée de Beaulieu, CS 50837, 35708 Rennes Cedex 7, France

Received 3 April 2015 / Accepted 16 August 2015

ABSTRACT

We report on the tentative detection of trans ethyl methyl ether (tEME), t-$CH_3CH_2OCH_3$, through the identification of a large number of rotational lines from each one of the spin states of the molecule towards Orion KL. We also search for gauche-trans-n-propanol, Gt-n-$CH_3CH_2CH_2OH$, an isomer of tEME in the same source. We have identified lines of both species in the IRAM 30 m line survey and in the ALMA Science Verification data. We have obtained ALMA maps to establish the spatial distribution of these species. Whereas tEME mainly arises from the compact ridge component of Orion, Gt-n-propanol appears at the emission peak of ethanol (south hot core). The derived column densities of these species at the location of their emission peaks are $\leq(4.0 \pm 0.8) \times 10^{15}$ cm^{-2} and $\leq(1.0 \pm 0.2) \times 10^{15}$ cm^{-2} for tEME and Gt-n-propanol, respectively. The rotational temperature is ~100 K for both molecules. We also provide maps of CH_3OCOH, CH_3CH_2OCOH, CH_3OCH_3, CH_3OH, and CH_3CH_2OH to compare the distribution of these organic saturated O-bearing species containing methyl and ethyl groups in this region. Abundance ratios of related species and upper limits to the abundances of non-detected ethers are provided. We derive an abundance ratio $N(CH_3OCH_3)/N(\text{tEME}) \geq 150$ in the compact ridge of Orion.

Key words. ISM: abundances – ISM: clouds – ISM: individual objects: Orion KL – ISM: molecules – radio lines: ISM – surveys

1. Introduction

The spectral millimeter-wave survey of Orion KL carried out with the IRAM 30 m radio telescope (Tercero et al. 2010; Tercero 2012) shows more than 15 400 spectral features of which about 11 000 have been identified and attributed to 50 molecules (199 different isotopologues and vibrational modes). To date, there have been several works based on these data. As the result of a fruitful collaboration with spectroscopy laboratories, 3000 previously unidentified lines have been assigned to new species in the interstellar medium (ISM). We have detected in space 16 new isotopologues and vibrationally excited states of abundant molecules in Orion for the first time (Demyk et al. 2007; Margulès et al. 2009, 2010; Carvajal et al. 2009; Tercero et al. 2012; Motiyenko et al. 2012; Daly et al. 2013; Coudert et al. 2013; Haykal et al. 2014; López et al. 2014) as well as four new molecules (Tercero et al. 2013; Cernicharo et al. 2013; Kolesniková et al. 2014). These identifications reduce the number of unidentified lines and mitigate line confusion in the spectra. Nevertheless, many features still remain unidentified and correspond to new species that we have to search and identify. Formates, ethers, acetates, alcohols, and cyanides are the best candidates for this purpose in Orion.

The recent search for trans ethyl methyl ether (tEME) in selected hot cores (Sgr B2(N-LMH) and W51 e1/e2) by Carroll et al. (2015) only provides upper limits to tEME. Hence, the results from that work do not confirm the previous tentative identification of this species by Fuchs et al. (2005) towards W51 e1/e2.

A systematic line survey with most weeds removed permits us to address the problem of the abundances of isomers and derivatives of key species, such as methyl formate (A. López et al., in prep.), through combined IRAM and ALMA studies.

In this Letter, we report on the tentative detection of tEME towards the compact ridge (CR) of Orion KL. We have detected emission of features arising from the five spin states at 3, 2, and

⋆ This paper makes use of the following ALMA data: ADS/JAO.ALMA#2011.0.00009.SV. ALMA is a partnership of ESO (representing its member states), NSF (USA), and NINS (Japan) with NRC (Canada), NSC, and ASIAA (Taiwan), and KASI (Republic of Korea), in cooperation with the Republic of Chile. The Joint ALMA Observatory is operated by ESO, AUI/NRAO, and NAOJ. This work was also based on observations carried out with the IRAM 30-m telescope. IRAM is supported by INSU/CNRS (France), MPG (Germany), and IGN (Spain).

⋆⋆ Appendix A is available in electronic form at http://www.aanda.org

A&A 582, L1 (2015)

1 mm with the IRAM 30 m telescope and the ALMA interferometer. In addition, several unidentified lines of these data have been identified as belonging to the gauche-trans conformer of n-propanol (an isomer of tEME). ALMA maps of organic saturated O-bearing species containing methyl, ethyl, and propyl groups, abundance ratios of related species, and upper limits to the column densities of non-detected ethers are presented and discussed in Sect. 4.

2. Observations

IRAM 30 m: new data of the IRAM 30 m telescope, which complement and improve those of Tercero et al. (2010), were collected in August 2013 and March 2014 towards Orion KL (see Tercero et al. 2010 and López et al. 2014, for information about the previous data set). Frequencies in the ranges 80.7−116, 122.7−161.2, 199.7−291.0, 291.4−306.7 GHz, were observed with the EMIR receivers connected to the FFTS (200 kHz of spectral resolution) spectrometers. We pointed towards IRc2 source at $\alpha_{2000.0} = 5^h35^m14^s.5$, $\delta_{2000.0} = -5°22'30''.0$, corresponding to the survey position (see Sect. 4). We observed an additional position to target the CR: $\alpha_{2000.0} = 5^h35^m14^s.3$, $\delta_{2000.0} = -5°22'37''.0$ (see Sect. 4). The observations were performed using the wobbler switching mode with a beam throw in azimuth of ±120″. The intensity scale was calibrated using the atmospheric transmission model (ATM, Cernicharo 1985; Pardo et al. 2001). Focus and pointing were checked every 1−2 h on planets or nearby quasars. System temperatures were in the range of 100−800 K from the lowest to highest frequencies. Half power beam width (HPBW) ranged from 31″ to 8″ from 80 to 307 GHz (*HPBW*[arcsec] = 2460/Freq.[GHz]). The data were reduced using the GILDAS package[1].

ALMA SV: the ALMA Science Verification (SV) data[2] were taken in January 2012 towards the IRc2 region in Orion. The observations were carried out with 16 antennas of 12 m in Band 6 (213.715–246.627 GHz). The primary beam was ≃27″. Spectral resolution was 0.488 MHz corresponding to a velocity resolution of 0.64 km s^{-1}. The observations were centred on coordinates: $\alpha_{J2000} = 05^h35^m14^s.35$, $\delta_{J2000} = -05°22'35''.00$. The CASA software[3] was used for initial processing and then the visibilities were exported to the GILDAS package. The line maps were cleaned using the HOGBOM algorithm (Högbom 1974). The synthesized beam ranged from 2″.00 × 1″.48 with a PA of 176° at 214.0 GHz to 1″.75 × 1″.29 with a PA of 164° at 246.4 GHz. The brightness temperature to flux density conversion factor is 9 K for 1 Jy per beam.

3. Results

3.1. Search for trans ethyl methyl ether

ALMA SV data: frequency predictions from Fuchs et al. (2003) and dipole moments measured by Hayashi & Kuwada (1975) of tEME were implemented in MADEX (Cernicharo 2012) to model the emission of this species and search for it towards Orion KL. Using the ALMA SV data, we extracted the averaged spectrum over 5 × 5 pixels (1″ × 1″) around the CH_3OCH_3 emission peak of the CR component (Position A; see Sect. 4). The advantage of ALMA with respect to single dish telescope data (see below) is the drastic reduction of the confusion limit.

[1] http://www.iram.fr/IRAMFR/GILDAS

[2] http://almascience.eso.org/almadata/sciver/OrionKLBand6/

[3] http://casa.nrao.edu

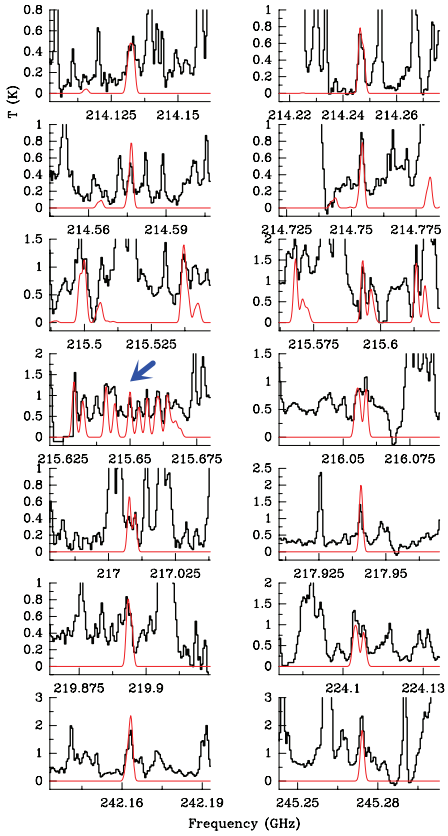

Fig. 1. Selected lines of trans ethyl methyl ether, t-$CH_3CH_2OCH_3$, towards Orion KL detected with the ALMA interferometer in Position A (see text). A v_{LSR} of +7.5 km s^{-1} is assumed.

The ALMA SV data show the presence of tEME as shown in Fig. 1 (selected lines) and Fig. A.1 (all lines favourable for detection (corresponding to *b*-type transitions with upper level energies up to 300 K and large line strenghts, $S_{ij} \geq 1$) present in the ALMA SV frequency range). The model that best fits the data is shown with the red line. The assumed parameters are a source size of 3″, $v_{LSR} = +7.5$ km s^{-1}, $\Delta v = 2.0$ km s^{-1}, and $T_K = 100 \pm 20$ K. Using MADEX and assuming local thermodynamic equilibrium (LTE), we obtain $N_{g.s.}$(tEME) ≤ $(4.0 \pm 0.8) \times 10^{15}$ cm^{-2}. In our models, rotation temperature and column density values are given with their corresponding uncertainty and we obtained them by fitting all available lines by eye. We adopted the source size in agreement with the emission of the maps (see below). In addition, a considerable number of unblended features allows us to fix the radial velocities and line widths. According to our model, in the ALMA frequency range only 33% of the detectable lines of tEME (102 lines) are totally hidden by the emission of stronger lines of other species. At least 46 lines (45% of the detectable lines) shown in Fig. A.1 are free of blending, i.e. these lines are present at the expected radial velocity and there are no other species with significant intensity at the same observed frequency (±3 MHz). Another point to ensure this tentative detection is that the forest of lines emitted by tEME between 215.5 and 215.7 GHz is not covered by lines of abundant molecules in the source allowing the detection

of several lines that follow a straightened pattern (see Fig. 1). Hence, there are several clues that could reveal the presence of this species in the CR of Orion KL, but further analysis exploring new available ALMA data and modelling all the molecular content of the CR is needed to give the definitive detection in space of tEME. Table A.1 gives line parameters and blends of all lines of favourable transitions in the ALMA SV data. The spatial distribution of tEME is shown in Fig. 2. Lines that we found to be unblended at the Position A appear blended with emission from other components in the averaged spectrum (see the case of the 30 m data). We selected a line at 245.274 GHz, which is mixed with some emission from extreme velocities of $^{34}SO_2$ and SO_2. Nevertheless, the emission of tEME at Position A in Fig. 2 is not blended (see Sect. 4).

IRAM 30 m data: to search for tEME in the IRAM data, a synthetic spectra of tEME (red curve in Fig. A.2) was obtained with MADEX assuming LTE and adopting the following physical parameters: source diameter 3″, $T_K = 100 \pm 30$ K, $v_{LSR} = +7.5$ km s^{-1}, $\Delta v = 1.5$ km s^{-1}; and a column density of $(9\pm3)\times10^{15}$ cm^{-2} for the ground state (g.s.) of tEME. According to our model, all favourable lines for detection in the 30 m data were detected or were blended with features from more abundant species. Nevertheless, owing to the weakness of the features ($T_{MB} < 0.1$ K at 3 mm, $T_{MB} < 0.2$ K at 2 mm, and $T_{MB} < 1$ K at 1.3−0.9 mm) and the high level of line confusion at ∼1 mm, only a few lines were mostly free of blending with other species in this domain. Whereas the synthetic beam of the ALMA SV is 1.″90 × 1.″40, in the 30 m the beam diameter ranging from 30″ to 8″. Therefore, in the 30 m data, the spectrum is a mix of all molecules from all source components (average spectrum over the beam) given rise to a high level of line blending and line confusion. Table A.2 shows line parameters, intensity provided by the model, and blends of all lines of favourable transitions in the 30 m data.

3.2. Search for gauche-trans-n-propanol

All lines of Gt-$CH_3CH_2CH_2OH$, an isomer of C_3H_8O (as well as tEME), reported by Maeda et al. (2006) and the dipole moments from Abdurakhmanov et al. (1969) were used to derive its rotational constants and to implement this species in MADEX. We conducted the search for Gt-n-propanol in the ALMA SV data at two different positions: Position A and the position where the emission peak of ethanol is located (Position B; see Sect. 4). We assign several unidentified lines in the source at Position B to this species. According to our model ($d_{sou} = 3''$, $v_{LSR} = +8.0$ km s^{-1}, $\Delta v = 3.0$ km s^{-1}, $T_K = 100 \pm 20$ K, and $N_{g.s} \leq (1.0 \pm 0.2) \times 10^{15}$ cm^{-2}), many of the lines are below the detection limit although the strongest features are detected. Unfortunately, several lines remain blended (see Fig. A.3). A few lines of this species are also detected in the IRAM 30 m data at the survey position (Fig. A.2 bottom panel; model parameters: $d_{sou} = 3''$, $v_{LSR} = +8.0$ km s^{-1}, $\Delta v = 1.5$ km s^{-1}, $T_K = 100 \pm 20$ K, and $N_{g.s} \leq (2.0 \pm 0.4) \times 10^{15}$ cm^{-2}). Table A.3 shows line parameters for the detected lines. The derived upper limit to its column density (assuming the same physical parameters than those of the tEME ALMA model) at Position A is $\leq(3.0 \pm 0.6) \times 10^{14}$ cm^{-2}. The spatial distribution of this species around Position B is shown in Fig. 2. To perform the ALMA map, we averaged the emission between v_{LSR} 6 and 9 km s^{-1} of two lines (lines at 236.138 and 244.765 GHz). Emission around source *I* should be due to other less abundant species in Orion (we did not find Gt-n-propanol at these positions).

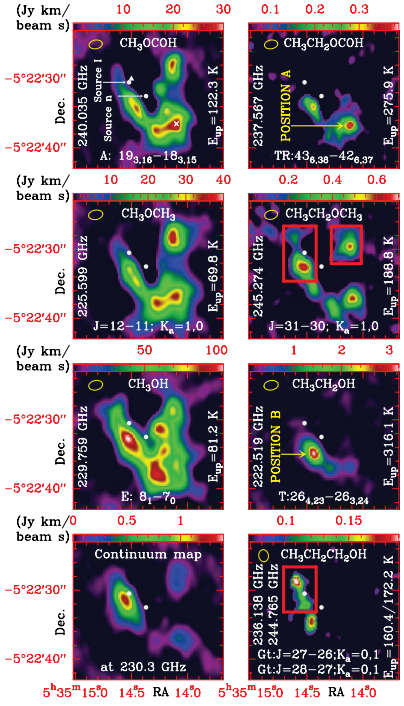

Fig. 2. ALMA maps of organic saturated O-bearing molecules in Orion KL which have been detected containing both the methyl and the ethyl group, as well as a map of Gt-n-propanol and a continuum map at the central frequencies of the ALMA *SV* band (∼230 GHz). Emission that probably arises from blended species in these maps is confined inside red rectangles. The yellow ellipse at the top left corner of the maps represents the ALMA synthetic beam. Triangle symbol: IRAM 30 m "survey position" (see Sect. 2). Cross symbol: IRAM 30 m compact ridge position (see Sect. 2). Position A: compact ridge (coordinates $\alpha_{2000.0} = 5^h35^m14^s.1$, $\delta_{2000.0} = -5°22'37''.9$). Position B: south hot core (coordinates $\alpha_{2000.0} = 5^h35^m14^s.4$, $\delta_{2000.0} = -5°22'34''.9$).

4. Discussion

Species containing the functional groups formate, alcohol, and ether have been detected in Orion with both the methyl and ethyl groups (methyl formate (MF), ethyl formate (EF), methanol, ethanol, dimethyl ether (DME), and tEME). ALMA maps for the spatial distribution of these species as well as Gt-n-propanol are shown in Fig. 2. To address the flux filtered out by ALMA and the accuracy of the maps in a larger energy range, the following discussion is also based on the maps shown in Fig. 5 of Feng et al. (2015; maps performed mixing SMA and IRAM 30 m data) with MF, DME, methanol, and ethanol. For MF, DME, and methanol the spatial distribution and the position of the emission peaks are in agreement with those of the maps presented in this work (note, however, that the ALMA maps provide a more detailed structure at small scales, i.e. ≤5″). For ethanol, we note a more extended spatial distribution in the map of Feng et al. (2015) mostly due to the lower energy of the transition involved. Nevertheless, the emission peak of ethanol is located at the same position.

For the methyl species, we note: i) a rather similar spatial structure: the three species present the V shape distribution of several clumps (at least six) studied by Favre et al. (2011) for the distribution of MF, which was mapped using data from the

Table 1. Column densities and ratios.

Species	$N_{g.s.}$ ($\times 10^{15}$) [cm^{-2}]	N Ratio
CH_3OCH_3 (DME)	$600 \pm 120^{a,b}$	
$CH_3CH_2OCH_3$ (tEME)	$\leq 4.0 \pm 0.8^{a}$	DME/tEME ≥ 150
$CH_3CH_2OCH_2CH_3$ (Tt-DEE)†	$\leq 1.0 \pm 0.2^{a}$	DME/Tt-DEE ≥ 600 tEME/Tt-DEE ≥ 4
CH_3OCHCH_2 (cis-MVE)††	$\leq 0.5 \pm 0.1^{a}$	DME/cis-MVE ≥ 1200 tEME/cis-MVE ≥ 9
CH_3OCOH (MF)	$240 \pm 50^{a,b,c}$	
CH_3CH_2OCOH (EF)	$2.0 \pm 0.4^{a,d}$	MF/EF $\simeq 120$
CH_3OH (MetOH)	$2700 \pm 500^{b,e,f}$	
CH_3CH_2OH (EtOH)	$60 \pm 10^{b,d,e}$	MetOH/EtOH $\simeq 45$
Gt-$CH_3CH_2CH_2OH$ (PropOH)	1.0 ± 0.2^{e}	MetOH/PropOH $\simeq 2700$ EtOH/PropOH $\simeq 60$

Notes. $^{(\dagger)}$ trans-trans diethyl ether. $^{(\dagger\dagger)}$ cis methyl vinyl ether. $^{(a)}$ Position A; same physical parameters of the ALMA tEME model (see Sect. 3.1). $^{(b)}$ Three kinetic temperatures: 50 ± 10, 150 ± 30, and 250 ± 75 K. $^{(c)}$ b type lines fitted (a type lines are optically thick); another component has been included to properly fit the observed line profiles ($v_{LSR} = +9$ km s^{-1}, $\Delta v = 4$ km s^{-1}, $T_K = 150 \pm 30$ K, $N_{g.s} = (1.0 \pm 0.2) \times 10^{17}$ cm^{-2}). $^{(d)}$ trans+gauche. $^{(e)}$ Position B; assuming the same physical parameters of the ALMA Gt-n-propanol model (see Sect. 3.2). $^{(f)}$ $^{12}C/^{13}C = 45$ (Tercero et al. 2010).

Plateau de Bure Interferometer (PdBI); ii) that although Brouillet et al. (2013) probed a striking similarity between the spatial distributions of CH_3OCH_3 and CH_3OCOH, we found some differences in the relative intensities of both species. These differences could be mostly due to different excitation temperatures of the involved transitions; and iii) although methanol also follows this V shape structure, a displacement of the intensity peaks is observed with respect to MF. This behaviour suggests methanol as a possible precursor of MF and DME (see also Neill et al. 2011).

Comparing the methyl and ethyl species, we note: i) a reduced spatial distribution of the three ethyl species with respect to their methyl counterpart; ii) the two emission peaks of EF are correlated with those found in MF; iii) the emission peak of tEME is at the same position as the DME peak at the CR (Position A); and iv) the emission peak of ethanol (Position B) is displaced 2″ south-west from the methanol peak.

Concerning the ethyl and propyl species, we note: i) a close correlation between EF and tEME; and ii) ethanol also presents a "V" shape structure (see Fig. 5 of Feng et al. 2015) with the bulk of the emission located away from the CR and coinciding with that of Gt-n-propanol. The ethanol/propanol peak is displaced 1.″5 south from the ethylene glycol $(CH_2OH)_2$ peak (Brouillet et al. 2015), which is a double alcohol and we could naively expect to have the same spatial distribution. Whereas the ethylene glycol peak corresponds to the $^{13}CH_3OH$ peak, the ethanol/propanol peak is the same as that of deuterated methanol (CH_2DOH; see Peng et al. 2012).

Table 1 shows derived column densities and ratios for related species. The derived ratios and the spatial distribution of these molecules suggest important gas phase processes after the evaporation of the mantles of dust grains in hot cores. Possible reactions of the methoxy radical (CH_3O), detected recently in space (Cernicharo et al. 2012), with other species could lead to the increase of chemical complexity in hot cores and hot corinos (Balucani et al. 2015). The spatial stratification of the different species also suggests the time dependent effects on the chemistry of the gas. The detection of the less stable isomers of some species (Tercero et al. 2013) also points in this direction.

To summarize, a combined IRAM 30 m and ALMA SV data study allows us to provide a solid starting point to assess the identification of tEME in the ISM. In addition, some unidentified lines in the source have been assigned to another C_3H_8O isomer, Gt-n-propanol. ALMA maps show different spatial distributions for these species. Whereas tEME seems to mainly arises from the CR component (as well as EF) (Position A), emission from Gt-n-propanol could be located at the south hot core (at the same position as the emission peak of ethanol) (Position B). The CR is no longer the main host of all organic saturated O-bearing species in Orion (see also Peng et al. 2013, for the spatial distribution of acetone and A. López et al., in prep. for the acetic acid emission).

Acknowledgements. We thank Marcelino Agúndez for carefully reading the paper and providing useful comments and suggestions. B.T., J.C., and A.L. thank the Spanish MINECO for funding support under grants CSD2009-00038, AYA2009-07304, and AYA2012-32032 and also the ERC for funding support under grant ERC-2013-Syg-610256-NANOCOSMOS.

References

Abdurakhmanov, A. A., Ragimova, R. A., & Imanov, L. M. 1969, Opt. Spektrosk., 26, 135 (English transl. in 1969, Opt. Spectrosc., 25, 75)
Balucani, N., Ceccarelli, C., & Taquet, V. 2015, MNRAS, 449, L16
Brouillet, N., Despois, D., Baudry, A., et al. 2013, A&A, 550, A46
Brouillet, N., Despois, D., Lu, X.-H., et al. 2015, A&A, accepted
Carroll, P. B., McGuire, B. A., Blake, G. A., et al. 2015, ApJ, 799, 15
Carvajal, M., Margulès, L., Tercero, B., et al. 2009, A&A, 500, 1109
Cernicharo, J. 1985, Internal IRAM Report (Granada: IRAM)
Cernicharo, J. 2012, in ECLA-2011: Proc. Europ. Conf. on Laboratory Astrophysics, eds. C. Stehl, C. Joblin, & L. d'Hendecourt (Cambridge: Cambridge Univ. Press), EAS PS, 58, 251
Cernicharo, J., Marcelino, N., Roueff, E., et al. 2012, ApJ, 759, L43
Cernicharo, J., Tercero, B., Fuente, A., et al. 2013, ApJ, 771, L10
Coudert, L. H., Drouin, B. J., Tercero, B., et al. 2013, ApJ, 779, 119
Daly, A.M., Bermúdez, C., López, A., et al. 2013, ApJ, 768, 81
Demyk, K., Mäder, H., Tercero, B., et al. 2007, A&A, 466, 255
Favre, C., Despois, D., Brouillet, N., et al. 2011, A&A, 532, A32
Feng, S. Y., Beuther, H., Henning, T. 2015, A&A, accepted
Fuchs, U., Winnewisser, G., Groner, P., De Lucia, F. C., & Herbst, E. 2003, ApJS, 144, 277
Fuchs, G. W., Fuchs, U., Giesen, T. F., & Wyrowski, F. 2005, A&A, 444, 521
Hayashi, M., & Kuwada, K. 1975, J. Mol. Struct., 28, 147
Haykal, I., Carvajal, M., Tercero, B. et al. 2014, A&A, 568, A58
Högbom, J. A. 1974, A&AS, 15, 417
Kolesniková, L., Tercero, B., Cernicharo, J., et al. 2014, ApJ, 784, L7
López, A., Tercero, B., Kisiel, Z. et al. 2014, A&A, 572, A44
Maeda, A., De Lucia, F., C., Herbst, E. et al. 2006, ApJS, 162, 428
Margulès, L., Motiyenko, R. A., Demyk, K., et al. 2009, A&A, 493, 565
Margulès, L., Huet, T. R., Demaison, J., et al. 2010, ApJ, 714, 1120
Motiyenko, R. A., Tercero B., Cernicharo, J., & Margulès, L. 2012, A&A, 548, A71
Neill, J. L., Steber, A. L., Muckle, M. T., et al. 2011, J. Phys. Chem. A, 115, 6472
Pardo, J. R., Cernicharo, & J., Serabyn, E. 2001, IEEE Trans. Antennas and Propagation, 49, 12
Peng, T.-C., Despois, D., Brouillet, N., Parise, B., & Baudry, A. 2012, A&A, 543, A152
Peng, T.-C., Despois, D., Brouillet, N., et al. 2013, A&A, 554, A78
Tercero, B. 2012, Ph.D. Thesis, Univ. Complutense de Madrid
Tercero, B., Cernicharo, J., Pardo, J. R., & Goicoechea, J. R. 2010, A&A, 517, A96
Tercero, B., Margulès, L., Carvajal, M., et al. 2012, A&A, 538, A119
Tercero, B., Kleiner, I., Cernicharo, J., et al. 2013, ApJ, 770, L13

Pages 5 to 43 are available in the electronic edition of the journal at http://www.aanda.org

Appendix A: Online figures and tables

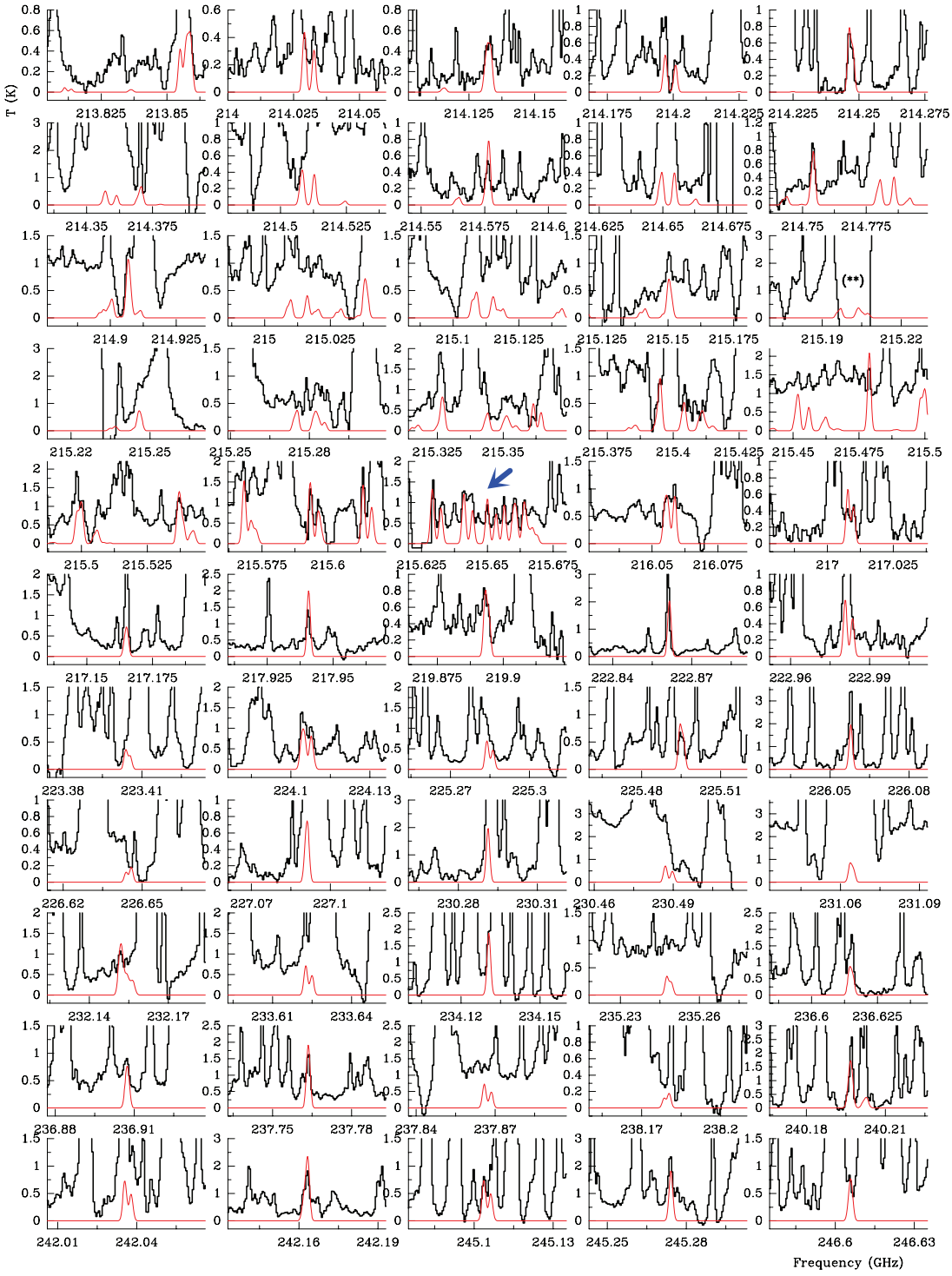

Fig. A.1. Lines of trans ethyl methyl ether, t-$CH_3CH_2OCH_3$, towards Orion KL detected with the ALMA interferometer in Position A (see text). (**): Features blended with SO (see Table A.1; artifacts in the spectrum due to the cleaning process). A v_{LSR} of +7.5 km s^{-1} is assumed.

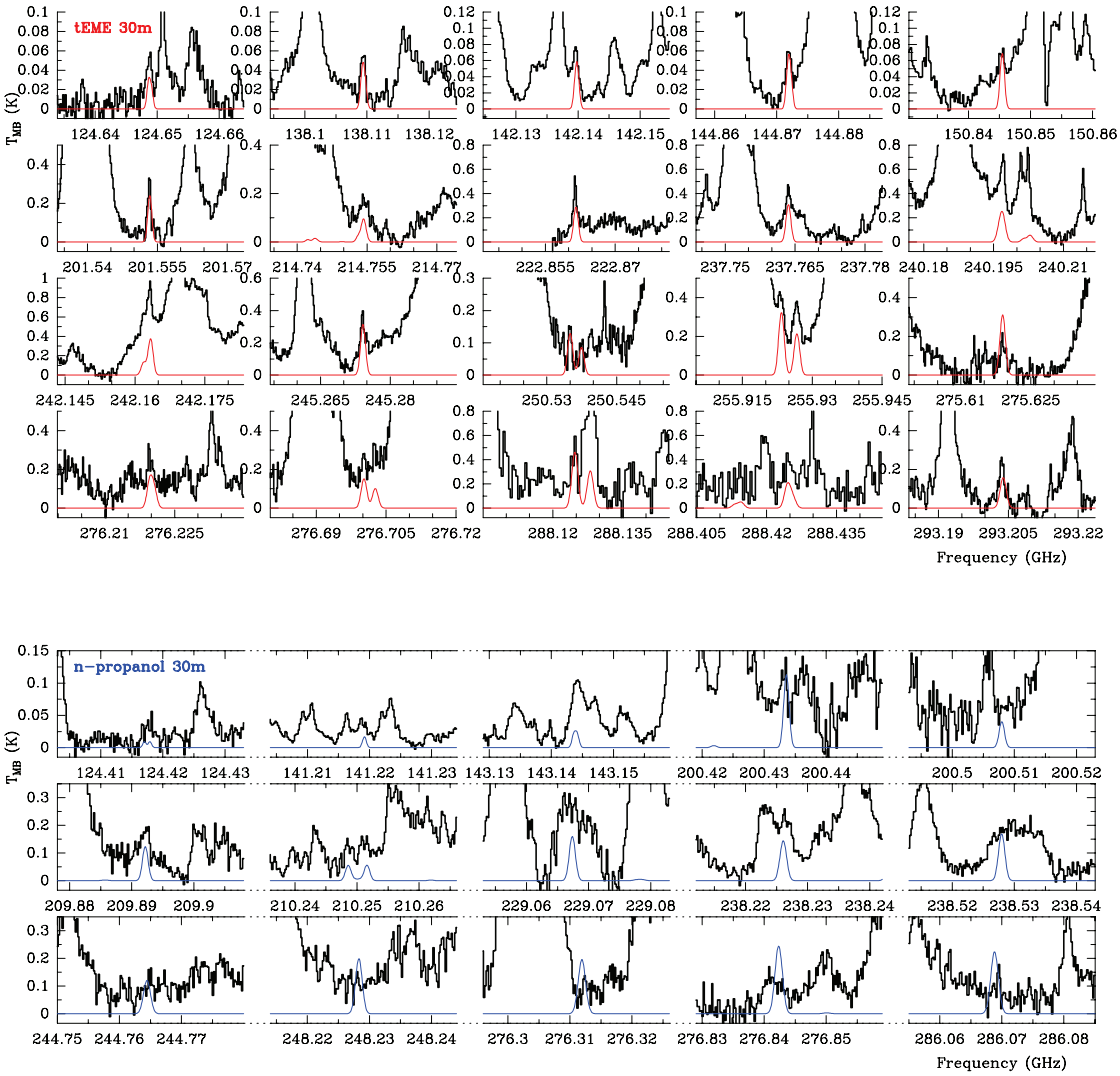

Fig. A.2. *Top panel*: selected lines of trans ethyl methyl ether, t-$CH_3CH_2OCH_3$, towards Orion KL detected with the IRAM 30 m telescope. Data in the frequency range 124−151 GHz are those of the survey position. From 201 to 293.5 GHz the data are those of the CR (see Sect. 2), where the emission peak of organic saturated O-rich species such as dimethyl ether (CH_3OCH_3) and methyl formate (CH_3OCOH) is located (Favre et al. 2011; Brouillet et al. 2013). A v_{LSR} of +7.5 km s^{-1} is assumed. *Bottom panel*: selected lines of gauche-trans-n-Propanol, Gt-n-$CH_3CH_2CH_2OH$, towards Orion KL detected with the IRAM 30 m telescope. A v_{LSR} of +7.5 km s^{-1} is assumed.

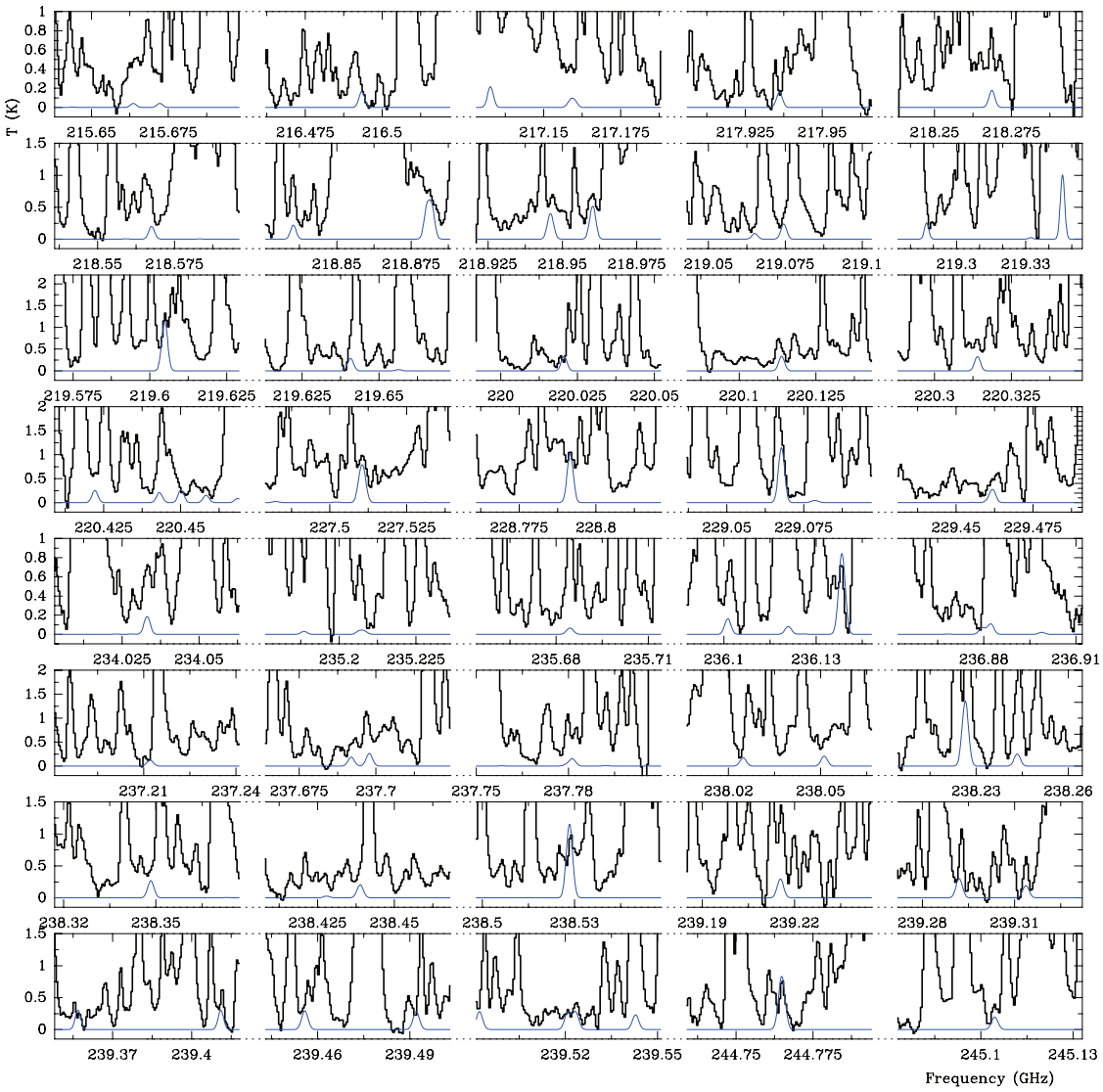

Fig. A.3. Lines of gauche-trans-n-propanol, Gt-n-$CH_3CH_2CH_2OH$, towards Orion KL detected with the ALMA interferometer in Position B (see text). A v_{LSR} of +8 km s^{-1} is assumed.

5.5 Isómeros de C_2H_4O en Orión-KL: Formiato de metilo, Ácido acético y Glicolaldehído. Una visión de conjunto de ALMA y de IRAM 30 m

En esta sección presentamos el borrador de un artículo en el que estoy actualmente trabajando. En los siguientes meses será enviado a la revista *Astronomy and Astrophysics*. Hemos decidido seguir con el formato de publicación pues el trabajo está realmente avanzado. Todos los resultados relevantes están contenidos en el borrador y presentados siguiendo los estándares de las publicaciones que hemos visto ya en esta tesis.

En este trabajo analizamos la emisión en Orión-KL de tres isómeros que siguen la fórmula C_2H_4O usando los datos de ALMA y de IRAM 30 m. Como hemos apuntado ya, estudiar la emisión de distintos isómeros en la región nos proporciona pistas importantes sobre los mecanismos de producción de estas especies.

Uno de estos isómeros es el formiato de metilo (CH_3OCOH), molécula muy abundante en regiones de formación estelar y de la que ya hemos hablado ampliamente. Los otros dos isómeros estudiados son el ácido acético (CH_3COOH) y el glicolaldehído (CH_2OHCHO). Ambas especies habían sido detectadas en otras regiones de formación estelar, por ejemplo, en Sgr B2. Aquí son detectadas por primera vez en Orión-KL. Además, detectamos los dos primeros estados vibracionalmente excitados del ácido acético por primera vez en el espacio. Merece la pena destacar que el formiato de metilo es varios órdenes de magnitud más abundante que los otros dos isómeros aún sin ser la especie energéticamente más estable. Como en los artículos previos, mediante el análisis de toda la emisión en conjunto y con la construcción de modelos adecuados, hemos conseguido determinar de manera precisa las condiciones físicas de las distintas componentes responsables de la emisión.

El resultado más impactante de este estudio es la diferente distribución espacial de estas especies en la región. Mientras que el máximo de emisión de formiato de metilo aparece en la región del *compact ridge*, tal y como hemos visto previamente, sus isómeros presentan emisión casi exclusivamente en el *hot core*. Este resultado puede relacionarse con la diferencia espacial entre distintas especies orgánicas oxigenadas en la región que vimos en el artículo anterior. Esto nos llevó a analizar los trabajos de este tipo de especies que han sido publicados usando datos interferométricos. El estudio conjunto de los resultados de este artículo con el de los trabajos previos, nos llevó a distinguir entre dos grupos de especies oxigenadas saturadas en la región. En principio, la diferencia es simple: aquellas cuyo máximo de emsión se encuentra en el *compact ridge* y aquellas cuyo máximo se encuentra en el *hot core*. Sin embargo, hemos advertido diferencias estructurales significativas entre las moléculas que pertenecen a cada grupo que nos llevan a proponer distintos precursores para estas especies: el radical hidroximetilo ($-CH_2OH$) para las especies presentes en el *hot core* y el radical metoxi (CH_3O-) para las especies con el máximo de emisión en el *compact ridge*.

Es interesante destacar que estos dos radicales son isómeros entre sí. Esto apunta de nuevo a la importancia de estudios donde se analice la emisión de distintas variantes isómeras. En los siguientes meses queremos profundizar en esta investigación. En colaboración con expertos en química del medio interestelar y en astrofísica de laboratorio, trataremos de averiguar las condiciones físicas que puedan favorecer la evaporación de uno u otro radical de los mantos del polvo.

Sin más, pasamos a presentar la actual versión del artículo. Quiero advertir de que aún sin estar

totalmente terminado, los contenidos son consistentes y puede ser leído como un todo.

Las Tablas B.2-B.8 de este artículo serán incluidas en el Apéndice E. Como en los artículos anteriores, se trata de las tablas donde se muestra la identificación de las líneas y los parámetros espectroscópicos y observacionales de las mismas. Téngase en cuenta que la Tabla B.1 y el Apéndice C contenidos en el artículo son mostrados en esta parte de la tesis.

Astronomy & Astrophysics manuscript no. MF˙AC˙GLYC˙tesis
June 14, 2017

$C_2H_4O_2$ isomers in Orion KL: Methyl formate, Acetic acid, and Glycolaldehyde. An overview of ALMA and IRAM 30m.

★,★★,★★★

A. López[1,2], B. Tercero[2], and J. Cernicharo[2]

[1] Centro de Astrobiología (CSIC-INTA). Departamento de Astrofísica Molecular. Ctra. de Ajalvir Km 4, 28850 Torrejón de Ardoz, Madrid, Spain.
[2] Grupo de Astrofísica Molecular. Instituto de CC. de Materiales de Madrid (ICMM-CSIC). Sor Juana Inés de la Cruz, 3, Cantoblanco, 28049 Madrid, Spain.
e-mail: lopezja@cab.inta-csic.es; b.tercero@icmm.csic.es; jose.cernicharo@csic.es;...

Received ; accepted

ABSTRACT

Emission from three functional isomers according to the $C_2H_4O_2$ formula −methyl formate (CH_3OCOH), acetic acid (CH_3COOH), and glycolaldehyde (CH_2OHCHO)− has been studied in Orion KL using the ALMA Science Verification data (213.7−246.7 GHz) and the IRAM 30m data (80−307 GHz). The high spatial resolution provided by the ALMA data allows us to set out the different cloud components involved in the emission of these species. This information is very valuable to model in an accuracy way all lines of these species detected with the 30m in a wide range of frequencies. Thus the physical parameters derived from this model are highly constrained. In addition, we propose that the differences in the spatial distribution of these isomers is due to different precursos ejected from the grain mantles.

Key words. ISM: abundances – ISM: molecules – Line: identification – Radio lines: ISM – Stars: formation

1. Introduction

Many of the lines observed from Orion KL, the nearest region at 418±6 pc (Kim et al. 2008) of on-going high-mass star formation, in the (sub)-millimeter range come from several complex organic molecules (COMs) which have a common feature (internal rotation of the methyl group) that involves spectra with a great number of rotational transitions. This feature is presented in abundant molecules such as methyl formate [hereafter MF] (CH_3OCOH), dimethyl ether (CH_3OCH_3), and methanol (CH_3OH), among others. High-mass star-forming processes (radiation of the newly born stars, outflows, in-fall motions, accretion disks) interact with the surrounding given rise to a large variety of COMs in the region. Molecules as complex as methyl acetate (CH_3COOCH_3) and *trans* ethyl methyl ether (*t*-$CH_3CH_2OCH_3$) have been detected in this source (Tercero et al. 2015; Tercero et al. 2013).

MF is the most abundant between its isomers, acetic acid [hereafter AA] (CH_3COOH) and glycolaldehyde [hereafter GLY] (CH_2OHCHO), in the interstellar medium (ISM), specially in star-forming regions (SFRs) (see e.g. Burke et al. 2015; Mehringer et al. 1997; Hollis et al. 2000). MF (ester functional group), AA (carboxyl and hydroxyl groups), and GLY (hydroxyl and aldehyde groups) represent the diversity of organic functional groups found in the ISM. The simplest aldose, GLY, could be implicated in the formation of a more complex sugar constituent of RNA (ribonucleic acid), i.e. ribose ($C_5H_{10}O_5$) (Hollis et al. 2000). Likewise, AA could be involved in the generation of glycine (NH_2CH_2COOH, aminoacetic acid), the smallest amino acid found in the proteins, through its relationship with glycinal (NH_2CH_2CHO) (Garrod 2013). Although MF has not a direct relation with molecules of biological interest (Burke et al. 2015), the high abundance of MF in SFRs is a matter under discussion, also due to the fact that AA is the most stable species (Dickens et al. 2001) between the three isomers.

MF has been found in a large variety of astrophysical environments, being ubiquitous in SFRs. Since its first detection in 1975 by Brown and collaborators (Brown et al. 1975) until now, CH_3OCOH has been the subject of many studies. For instance, Favre et al. (2011; 2014) have studied the emission of MF and its ^{13}C isotopologues in Orion KL using PdBI (Plateau de Bure Interferometer) and ALMA (Atacama Large Millimeter Array) data. Although many clumps are involved in the emission of these species, these works have demonstrated that the compact ridge (CR) is the main host of MF in the source. In addition, the rotational levels of low-energy torsional states of many COMs are excited under the physical conditions of the source (see e. g. López et al. 2014). Kobayashi et al. (2007) and Takano et al. (2012) reported the first detection of MF in its $v_t = 1$ and $v_t = 2$, respectively, for the first time in space towards Orion KL. Recently, Sakai et al. (2015) have studied the spatial distribution of these species using the ALMA data.

⋆ Appendix A (online Figures) and Appendix B (online Tables) are only available in electronic form at http://www.aanda.org.
⋆⋆ The 3 and 2 mm survey of Orion KL is available at the CDS.
⋆⋆⋆ This paper makes use of the following ALMA data: ADS/JAO.ALMA#2011.0.00009.SV. ALMA is a partnership of ESO (representing its member states), NSF (USA) and NINS (Japan), together with NRC (Canada), NSC and ASIAA (Taiwan), and KASI (Republic of Korea), in cooperation with the Republic of Chile. The Joint ALMA Observatory is operated by ESO, AUI/NRAO and NAOJ. This work is also based on observations carried out with the IRAM 30-meter telescope. IRAM is supported by INSU/CNRS (France), MPG (Germany), and IGN (Spain).

Many of the unidentified lines (U-lines) in spectral line surveys, such as those of Sgr B2 and Orion KL, were due to CH_3OCOH in its torsional excited states and some of its isotopologues (Carvajal et al. 2009; Margulés et al. 2010; Tercero et al. 2012; Coudert et al. 2013; Haykal et al. 2014). Moreover, the study of the isotopologue species provides the isotopic abundances in the astrophysical environment, as well as column densities from the analysis of optically thin lines.

Spectroscopic analysis in the laboratory is essential prior to identification of such COMs in space. The rotational spectrum of MF has been studied by Curl (1959), Bauder (1979), Demaison et al. (1983), Plummer et al. (1984; 1986), Oesterling et al. (1999), Karakawa et al. (2001), Ogata et al. (2004), Carvajal et al. (2007), and Ilyushin et al. (2009). The rotational spectrum of methyl formate in its first torsional excited state ($v_t = 1$) was studied by Odashima et al. (2003), Ogata et al. (2004), Carvajal et al. (2007), and Ilyushin et al. (2009). Maeda et al. (2008) assigned many other lines of MF to the first excited state, and also included the spectroscopic analysis of the second torsional excited state ($v_t = 2$). Later, Kobayashi et al. (2013) extended the number of assignments in the laboratory for both states A and E of v_t=2 MF below 120 GHz.

AA was firstly detected towards the SFR Sgr B2(N-LMH) by Mehringer et al. (1997). After that, this species has been also found in other hot molecular cores (HMCs) (w51e2, Remijan et al. 2002; G34.3+0.15, Remijan et al. 2003; and G19.61−0.23, Shiao et al. 2010), and in the low-mass protostar IRAS16293−2422 (Cazaux et al. 2003).

The rotational spectrum of CH_3COOH has been studied by Tabor (1957), Krishiel & Saegebarth (1971), van Eijck et al. (1981), Demaison et al. (1982), Wlodarczak & Demaison (1988) Ilyushin et al. (2001; 2008; 2013). The A-E substates frequency differences are very large leading to a hard laboratory work in the assignments for the doublet transitions (Krishiel & Saegebarth 1971). The first and second torsional excited states have been studied in the laboratory by van Eijck & van Duijneveldt (1983), and Ilyushin et al. (2001; 2003; 2008; 2013). The energies of these torsional states are only about 110 and 200 K (for $v_t = 1$ and $v_t = 2$, respectively) above the ground state (g.s.) suggesting their feasible detection in hot cores.

The other $C_2H_4O_2$ isomer, GLY, was detected for the first time in Sgr B2(N) by Hollis et al. (2000). After that, this species has also been identified in the hot molecular core G31.41+0.31 (Beltrán et al. 2009), in the surrounding of the young binary sun-like star IRAS 16293−2422 (Jørgensen et al. 2012), and in the solar-type protostar NGC 1333 IRAS2A (Coutens et al. 2015).

Spectroscopic studies of GLY were firstly conducted by Michelsen & Klaboe (1969) and Marstokk & Møllendal (1970). More recently, these works have been carried out by Butler et al. (2001), Widicus Weaver et al. (2005) (including the three first vibrationally excited states), and Carroll et al. (2010).

In this work we have analyzed the molecular emission of three $C_2H_4O_2$ isomers (MF, AA, and GLY) in a combined ALMA and IRAM (Institut de Radioastronomie Millimétrique) 30m telescope study allowing us to address the chemical and physical properties of the different cloud components of Orion KL. We have detected up to the second excited state of MF at about 350 K or 243 cm^{-1} over the g. s. However, states with higher energies could be detected when further spectroscopic analysis would be available. AA has been detected in its g.s. (for the first time in Orion KL) and in its two first torsional excited states for the first time in space and GLY has been detected for the first time in Orion KL.

It was though that organic O-rich molecules emerge mainly from the CR component of Orion KL, but recently, interferometric studies of the spatial distribution of this kind of species point out to different regions for their emission (see e. g. Tercero et al. 2015, Brouillet et al. 2015, Peng et al. 2013 and references therein). In this work, ALMA maps of MF, AA, and GLY have been performed revealing different spatial distributions for these species. These differences suggest different chemical pathways for their formation (see e.g. Burke et al. 2015, Calcutt et al. 2014).

In this paper, our main goal is to provide an accurate physical and chemical model of the source for these three isomers, mapping their emission with ALMA and fitting simultaneously all lines related with these species that appear in the broad frequency band covered by the IRAM 30m survey. We have divided this paper as following: Observation procedures are shown in Sect. 2. Section 3 is focused on the analysis of MF (Sect. 3.1), AA (Sect. 3.2), and GLY (Sect. 3.3). Discussion and summary are given in Sect. 4 and Sect. 5, respectively.

2. Observations

2.1. ALMA Science Verification

The ALMA Science Verification (SV) data[1] were taken on January 2012 towards the IRc2 region in Orion. The observations were carried out with 16 antennas of 12 m in the frequency range from 213.715 to 246.627 GHz (Band 6). The primary beam was ≃27″. Spectral resolution was 0.488 MHz (≃ 0.64 km s^{-1} in the observed frequency range). The observations were centered on coordinates: $\alpha_{J2000} = 05^h35^m14.^s35$, $\delta_{J2000} = 05°22'35.''00$.

The CASA software[2] was used for initial processing, and then the visibilities were exported to the GILDAS package[3] for further analysis. The line maps were cleaned using the HOGBOM algorithm (Högbom 1974). The synthesized beam ranged from 2.″00×1.″48 with a PA of 176° at 214.0 GHz to 1.″75×1.″29 with a PA of 164° at 246.4 GHz. The brightness temperature to flux density conversion factor is 9 K for 1 Jy per beam. The continuum emission was subtracted in the maps by carefully selecting line-free channels.

2.2. IRAM 30m

New data of the IRAM 30m telescope were collected in August 2013 and March 2014 towards Orion KL. Frequencies in the ranges 80.7−116, 122.7−161.2, and 199.7−306.7 GHz, were observed with the Eight MIxer Receivers (EMIR) connected to the Fast Fourier Transform Spectrometers (FFTS, 200 kHz of spectral resolution) allowing us to cover 16 GHz of bandwidth in each frequency setting. We pointed towards IRc2 source at $\alpha_{2000.0} = 5^h35^m14.^s5$, $\delta_{2000.0} = -5°22'30.''0$ corresponding to the 'survey position' (see Fig. **??**). We observed another position to target the CR: $\alpha_{2000.0} = 5^h35^m14.^s3$, $\delta_{2000.0} = -5°22'37.''0$ (see Fig. **??**).

Another set of data using this telescope were observed between September 2004 and January 2007 with the A, B, C, and D receivers[4] (79.6−115.7, 130.0−176 GHz, and 196.7−281 GHz)

[1] http://almascience.eso.org/almadata/sciver/OrionKLBand6/

[2] http://casa.nrao.edu

[3] http://www.iram.fr/IRAMFR/GILDAS

[4] The reduced data at 3 and 2 mm are available at the CDS. The data at 1.3 mm are affected by pointing errors at some frequencies and

and pointing towards the 'survey position'. Backends provided a spectrum of 1−1.25 MHz of spectral resolution. For further information about observations and data reduction of this set of data see Tercero et al. (2010) and López et al. (2014).

For both sets of data, the observations were performed using the wobbler switching mode with a beam throw in azimuth of ±120″. The intensity scale was calibrated using the atmospheric transmission model (ATM, Cernicharo 1985; Pardo et al. 2001a). Focus and pointing were checked every 1−2 hours on planets or nearby quasars. System temperatures were in the range of 100−800 K from the lowest to the highest frequencies. Half power beam width (HPBW) ranged from 31″ to 8″ from 80 to 307 GHz (HPBW[arcsec]=2460/Freq.[GHz]). The data were reduced using the GILDAS package checking for image sideband contamination and fitting and removing 0−1 order baselines. Figures are shown in main beam temperature (T_{MB}) that is related to the antenna temperature (T_A^*) by the equation: T_{MB}=T_A^*/η_{MB}, where η_{MB} is the ratio between the main beam efficiency (B_{eff}) and the forward efficiency (F_{eff}) which depends on the frequency. For the IRAM 30m telescope, η_{MB} is 0.85, 0.80, 0.64, and 0.56 at 86, 145, 230, and 280 GHz, respectively.

3. Results and data analysis

3.1. Methyl formate (A- and E-CH_3OCOH)

The high abundance of CH_3OCOH in Orion KL together with the high values of its electric dipolar moments (μ_a = 1.63 D and μ_b = 0.68 D) and the existence of low-lying vibrational torsional modes lead a very large density of MF lines in the (sub)-millimeter domain.

More than 6000 spectral features between 80−306 GHz have been detected in the IRAM 30m survey of Orion KL caused mainly by MF: 2517 for the g.s., 1593 for the v_t = 1 state, 851 for the v_t = 2, and ∼1050 for the most abundant isotopologues (Carvajal et al. 2009; Margulés et al. 2010; Tercero et al. 2012; Coudert et al. 2013; Haykal et al. 2014).

3.1.1. ALMA SV data: CH_3OCOH maps and source components

To determine the spatial distribution and the cloud components required to model the methyl formate emission in Orion KL, we performed velocity and line integrated maps of CH_3OCOH using the ALMA SV data. Figure **??** shows maps of five CH_3OCOH lines free of blending with other species (only the line at 244.073 GHz is mixed at 9.8 km s^{-1} with the extreme blue velocities of another line of MF v_t=1). Transitions with energies of the upper level from 36.3 K to 449.4 K have been selected which include lines in the torsional excited states v_t = 1 and 2. To address the uncertainty introduced in these maps by the lack of short spacings for these data, we compared our results with the maps shown in Feng et al. (2015) who have analyzed the spatial distribution of MF combining SMA (Sub-Millimeter Array) and IRAM 30m data. Although the ALMA maps provide a higher detail at small scales, we note a similar spatial distribution as well as the emission peak located at the same position (see Fig. 5 of Feng et al. 2015). Maps of Fig. **??** show similar spatial distribution of MF in all these lines at a given velocity. Sakai et al. (2015) have recently studied this three states of methyl formate also with the ALMA SV data obtaining the same result. These maps present the *V* shape distribution of several clumps found with the PdBI by Favre et al. (2011). However, the ALMA maps show a clump at 5 km s^{-1} at the North-East of source *n* that the PdBI maps of Favre et al. (2011) did not present. We also note that the emission at 3-5 km s^{-1} is relatively more intense at the West of source *I* for the lines with larger energies. This could point out to a warmer region at this position.

We distinguish 10 different clumps of MF emission (see Fig. 2) contained in this *V* shape structure mentioned above. We have named them as (between brackets we add the Favre et al. 2011 nomenclature if the emission peak of the clump coincides with one of those found by these authors): North hot core (N-HC), Mid hot core (M-HC) [MF6], South hot core (S-HC) [MF2], South-East compact ridge (SE-CR) [MF3], compact ridge (CR) [MF1], North compact ridge (N-CR), North-East compact ridge (NE-CR) [MF12], Spherical clump (SC), South North-South clump (S-NS) [MF4], and North North-South clump (N-NS) [MF5]. Figure 2 shows the MF lines at the position of the peak intensity of these clumps. We notice the large variety of radial velocities at the peak channel, line widths, and shapes of these lines. In order to characterize the line parameters of each clump, we analyzed, by Gaussian fits, the profiles of the lines corresponding to the five selected MF transitions at each position given above (see Fig. A.1, only available online). Table B.1, only available online, shows the coordinates of the emission peak of these clumps and the observed line parameters.

3.1.2. IRAM 30m data: CH_3OCOH model

According to the cloud components unveiled from the ALMA maps, we performed a model to fit the observed lines with the IRAM 30m telescope in a wide range of frequencies (80-307 GHz). Figs. 3-5 (in the body of the text) and A.2-A.7 (only available online) show a sample of selected MF lines covering a wide range of upper level energies (from 6 to 550 K) as well as both *a* and *b*-type transitions of the ground state (g.s.) and the first and second torsional modes together with our best model. In these Figures, lines between 80 and 178 GHz (3 and 2 mm windows) are those detected at the 'survey position' (at these frequencies the HPBW of the telescope covers all Orion components, see Sect. 2.2), whereas lines between 197 and 306 GHz (1.3 and 0.9 mm windows) are those detected pointing at the CR (see Sect. 2.2), where the emission peak of MF is located (see Sect. 3.1.1). Tables B.2, B.3, and B.4, only available online, list spectroscopic and line parameters for the lines shown in these Figures.

Spectroscopic constants derived from a fit with the MADEX code (Cernicharo 2012) based on the lines reported by Ogata et al. (2004) and dipole moments from Curl (1959), were used to obtain the predicted frequencies and spectroscopic line parameters. Column densities and rotational temperatures were calculated using MADEX and assuming LTE, due to the lack of collisional rates for these species, and a detailed multi-source structure. Table 1 shows the adopted physical parameters for each component that better reproduce the observed lines.

This model fits in a reasonable way all lines found between 80 and 307 GHz. From this final model, we could derive the following insights: i) twelve different components are derived from the ALMA maps and the Gaussian fits to the lines arising from each clump; ii) accurate rotational temperatures are obtained fitting the IRAM 30m observed lines. We notice that two differents temperatures were needed to fit tha lines for the component at 9 km s^{-1}; iii) the model is lacking some intensity for high energy *b*-type g.s. lines (see Fig. A.4) probably due to the *a*-type lines

have to be carefully analyzed so these observations are available under request to B. Tercero.

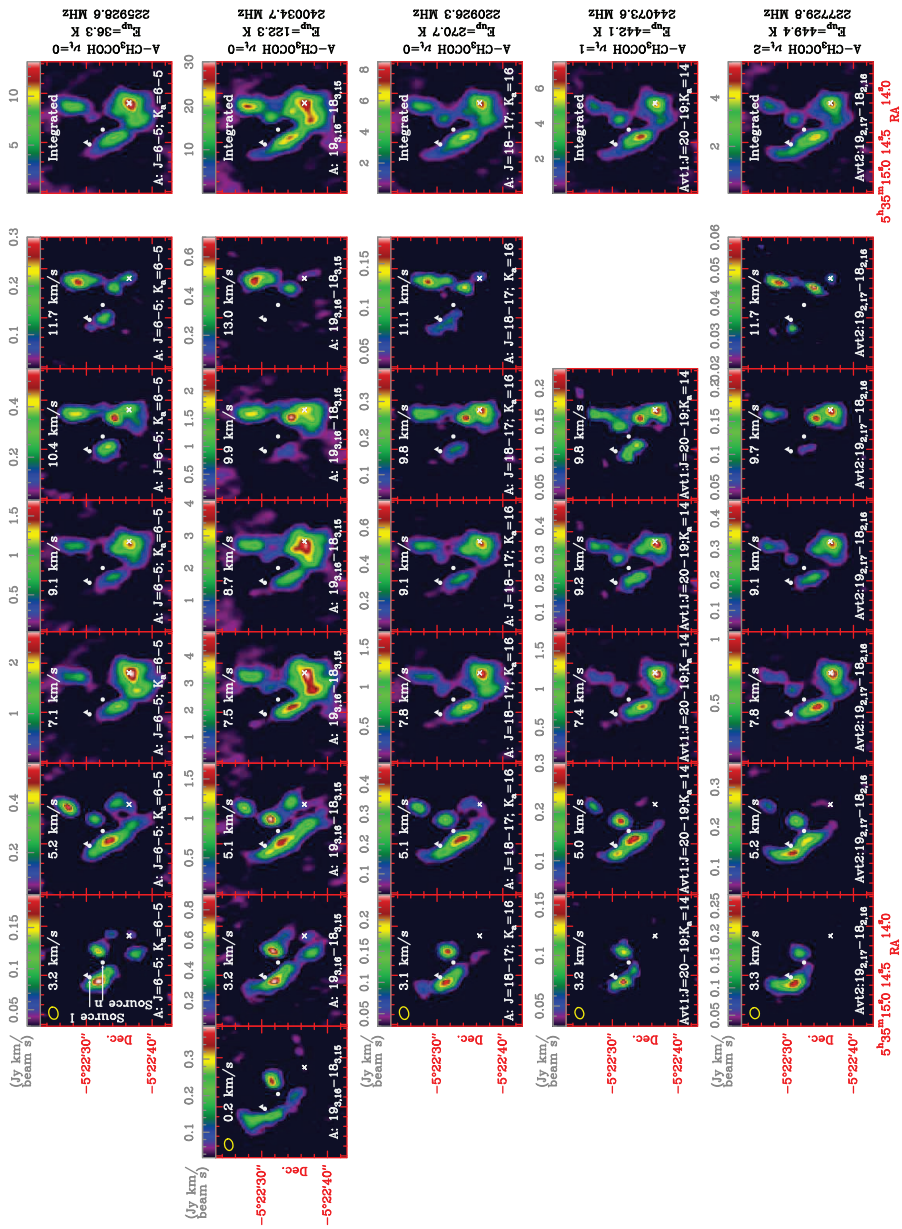

Fig. 1. Maps at different radial velocities and of the integrated line intensity of selected CH_3OCOH lines. Triangle and cross signs mark the pointing positions of the 30m survey at IRc2 ('survey position') and the compact ridge, respectively. Yellow ellipse at the upper left corner of the maps represents the synthetic beam of ALMA.

that emerge from the inner and hotter parts of the CR are optically thick; iv) in the same way, the low energy *a*-type g.s. lines have more intensity than the model (see Fig 3), indicating that a cold (≤ 40 K) and (probably) extended component is emitting this contribution; v) we found a total column density (A+E) of $(1.9\pm0.6)\times10^{18}$, $(2.9\pm0.9)\times10^{17}$, and $(9\pm3)\times10^{16}$ cm^{-2} for MF g.s., v_t=1, and v_t=2, respectively, in Orion KL.

3.1.3. Vibrational temperatures: CH_3OCOH

The vibrational energies for the A and E states of MF are different by a small factor (see Fig. 6). Consequently, we derive vibrational temperatures for each state (A and E) and cloud components following Eq. 1 (see Table 2).

$$\frac{N(\mathrm{CH_3OCOH}\ v_t)}{N(\mathrm{CH_3OCOH})} = \frac{\exp\left(-\frac{E_{v_t}}{T_{\mathrm{vib}}}\right)}{f_v} \qquad (1)$$

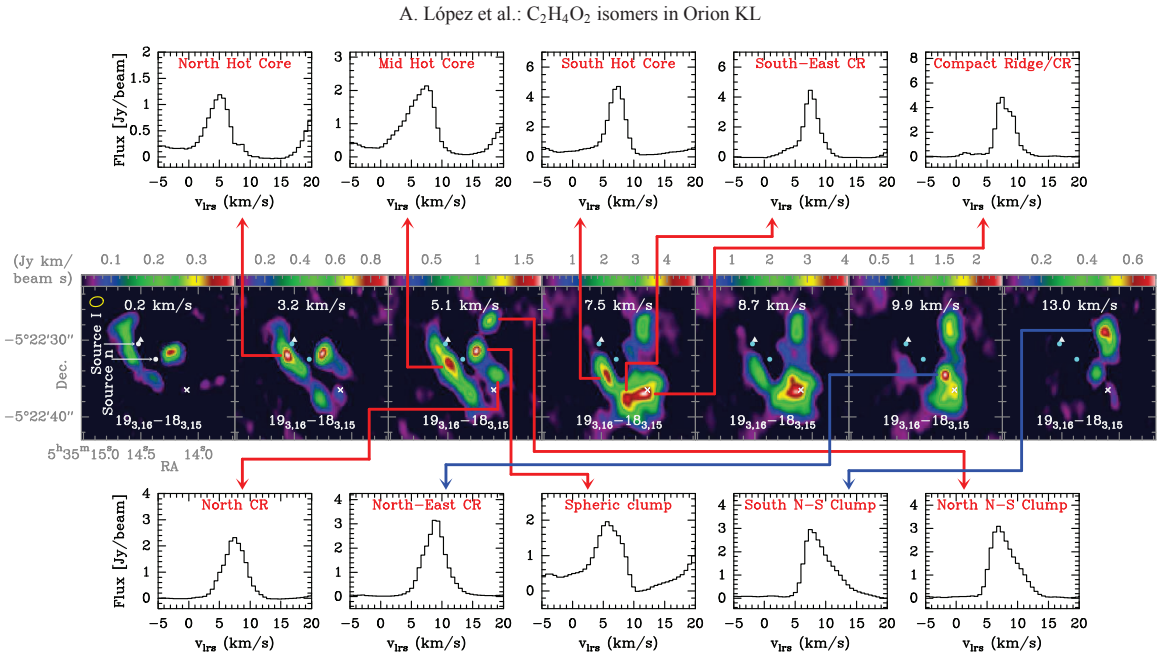

Fig. 2. Lines of CH_3OCOH at different positions. The rest frequency is 240.034 GHz ($19_{3,16}$-$18_{3,15}$ transition of A-CH_3OCOH).

Table 1. Methyl formate: Physical parameters

Parameter	N-HC	M-HC	S-HC	SE-CR	CR	N-CR	Cold NE-CR	Hot NE-CR	Warm SC	Hot SC	S-NS	M-NS	N-NS
d_{sou} (″)	2	2	2	4	2	2	2	2	2	2	2	3	2
offset† (″)	2 (12)	2 (10)	4 (6)	9 (2)	9 (0)	8 (2)	7 (2)	7 (2)	4 (6)	4 (6)	5 (8)	5.5 (9)	6 (10)
v_{LSR} (km s^{-1})	3.0	5.5	7.5	7.5	7.5	5.0	9.0	9.0	5.5	8.0	7.5	9.5	6.5
Δv_{FWHM} (km s^{-1})	6.0	5.0	2.0	1.5	1.5	4.0	2.5	1.5	3.5	2.0	2.0	6.0	2.0
T_{rot} (K)	200±60	250±75	250±75	60±18	250±75	100±30	100±30	250±75	150±45	200±60	150±45	150±45	150±45
$N_{g.s.}\times10^{16}$†† (cm^{-2})	10±3	18±5	10±3	40±12	18±5	10±3	14±4	12±4	14±4	1.4±0.4	4.0±1.2	30±9	6±2
$N_{v_t=1}\times10^{15}$†† (cm^{-2})	16±5	30±9	15±4	40±12	17±5	20±6	20±6	20±6	30±9	1.2±0.4	2.0±0.6	40±12	30±9
$N_{v_t=2}\times10^{15}$†† (cm^{-2})	3.0±0.9	7±2	9±3	9±3	8±2	5±2	10±3	8±2	7±2	0.9±0.3	1.0±0.3	19±6	6±2

†: with respect to IRc2 (CR); ††: A+E.
Acronyms: North hot core (N-HC), Mid hot core (M-HC), South hot core (S-HC), South-East compact ridge (SE-CR), compact ridge (CR), North compact ridge (N-CR), Cold North-East compact ridge (Cold NE-CR), Hot North-East compact ridge (Hot NE-CR), Warm Spherical clump (Warm SC), Hot Spherical clump (Hot SC), South North-South clump (S-NS), Mid North-South clump (M-NS), North North-South clump (N-NS).

where v_t identifies the vibrational mode, E_{v_t} is the energy of the corresponding vibrational state, $T_{\rm vib}$ is the vibrational temperature, f_v is the vibrational partition function, $N(CH_3OCOH\ v_t)$ is the column density of the vibrational state, and $N(CH_3OCOH)$ is the total column density of MF. Taking into account the relation $N(CH_3OCOH)$=$N_{\rm g.s.}\times f_v$ and assuming the same partition function for these species in the ground and in the vibrationally excited states, we only need the energy of each vibrational state and the calculated column density to derive the vibrational temperatures.

Owing to the small differences found in the derived T_{vib} for each state (see Table 2), we will discuss the average value (A+E/2). There is a tendency to a higher vibrational temperature for the second excited torsional mode above the first one, but these differences are not significant.

The highest vibrational temperatures obtained are those of the N-NS component being 272 K and 148 K for $v_t = 1$ and $v_t = 2$, respectively. This high temperature for the first excited state (272 K) is in disagreement with the derived value for $v_t = 2$, so we could suspect that the column density of this component in the $v_t = 1$ state has been overestimated. In contrast, the lowest vibrational temperatures belongs to the S-NS component (63 K for $v_t = 1$ and 91 K for $v_t = 2$) and the Cold SE-CR component (78 K for $v_t = 1$ and 89 K for $v_t = 2$). The corresponding T_{rot} for the S-NS and the Cold SE-CR were 150 and 60 K, respectively; therefore, we found T_{vib}<T_{rot} for the S-NS, and the opposite (T_{vib}>T_{rot}) occurs for Cold SE-CR.

The total averaged vibrational temperatures are 112 K and 114 K for the vibrational torsional mode $v_t = 1$ and $v_t = 2$, respectively. Finally, we do not observe strong differences between $T_{\rm rot}$ and $T_{\rm vib}$ so we cannot distinguish (between collisions and/or far-IR pumping) the excitation mechanisms of the vibrational levels. On the other hand, possible temperature gradients of the components are minimized due to the detailed source model in which the typical size of each component is 2″.

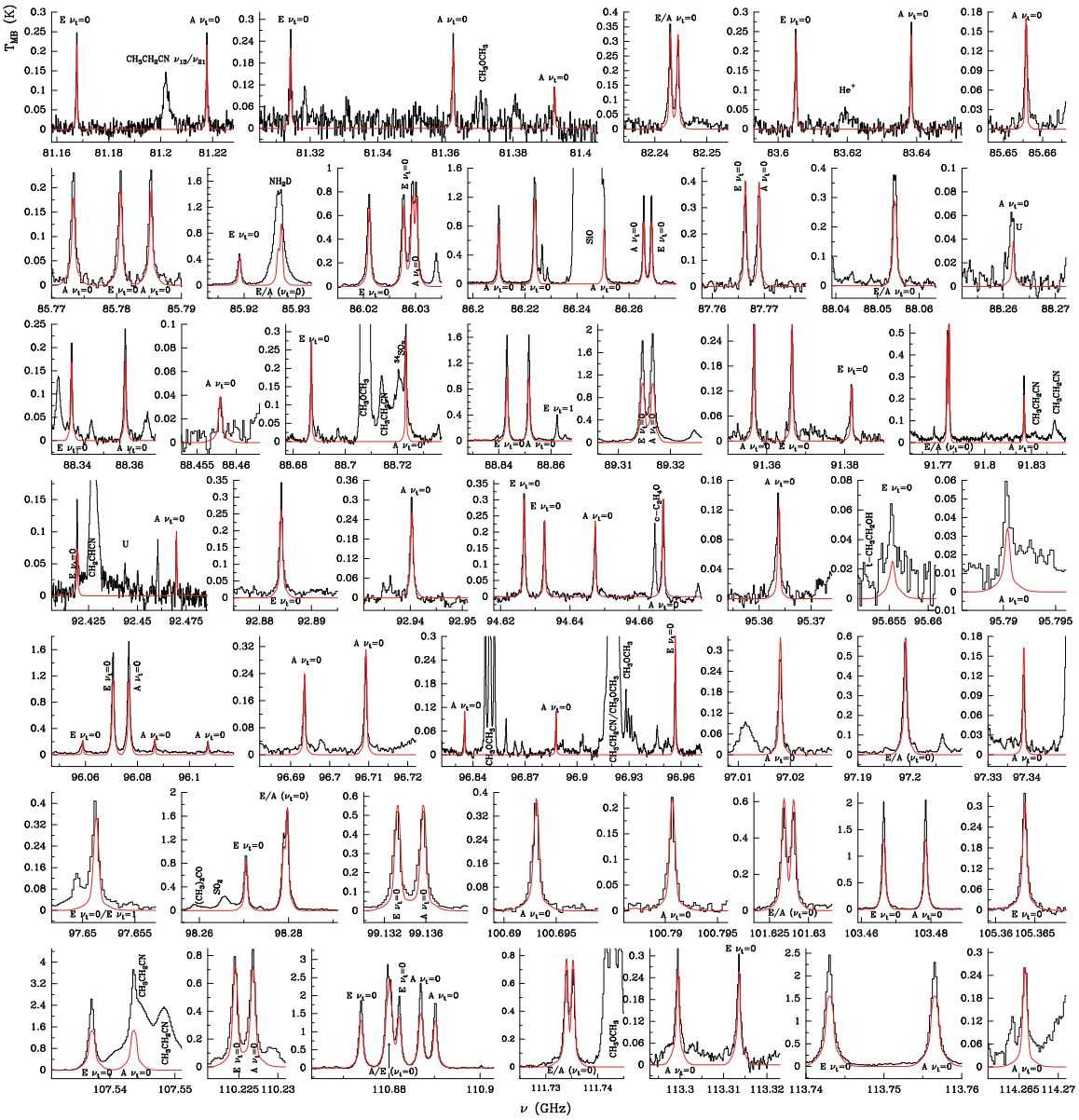

Fig. 3. Observed lines towards Orion KL (histogram spectra) and model (thin red curves) of methyl formate (CH_3OCOH) in the ground state (v_t=0) in the 3 mm window. A v_{LSR} of 7.5 km s^{-1} is assumed.

3.2. Acetic acid (A- and E-CH_3COOH)

In this work, AA has been detected towards Orion KL in its g.s. for the first time in Orion KL and in its two first torsional excited modes for the first time in space.

3.2.1. ALMA SV data: CH_3COOH maps and source components

Acetic acid $v_t = 0$, 1, and 2 have been detected in the ALMA SV data towards the middle of the hot core cumply structure (M-HC) of Orion KL (see Fig 7).

Figure 7 shows maps of three radial velocities (~6.0, ~7.5, and ~9.0 km s^{-1}) and of the integrated line intensity of six CH_3COOH lines practically free of blending. The spatial distribution of the emission is consistent with the detection of these species in the M-HC. We note a slightly displacement of the

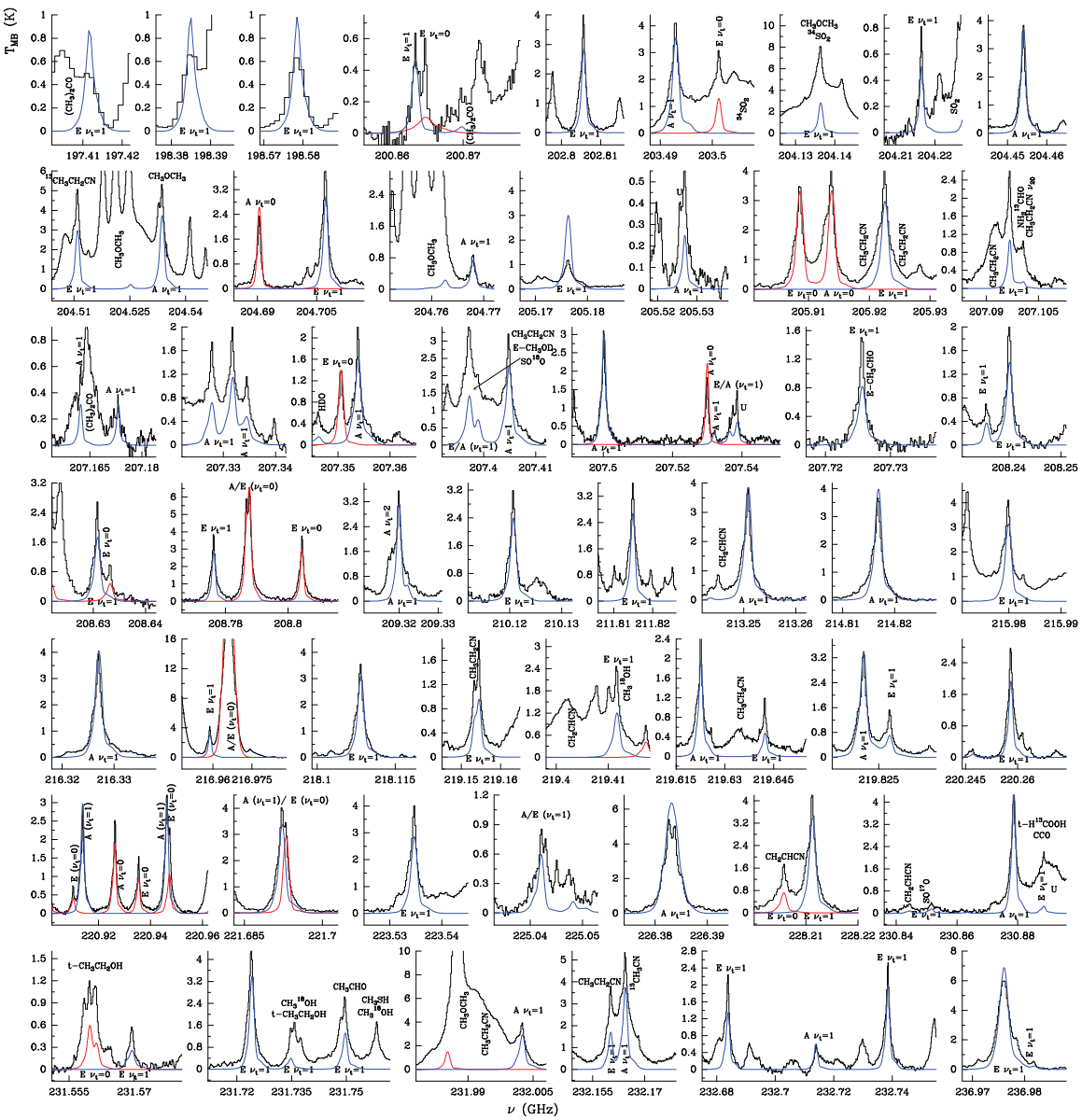

Fig. 4. Observed lines towards Orion KL (histogram spectra) and model (thin blue curves) of methyl formate (CH_3OCOH) in the first torsional state (v_t=1) in the 1.3 mm window.The red line corresponds to the model of methyl formate in its ground state. A v_{LSR} of 7.5 km s^{-1} is assumed.

maximum of the emission with the radial velocity: from South-East to North-West from 6 to 9 km s^{-1}. However, the reduced spectral coverage of the ALMA SV data and possible blending of the lines with less abundant species avoid us to give firmer conclusions about this displacement. The peak emission of the integrated line intensity maps is located at similar positions. In Table 3, spectroscopic parameters of the involved transitions in Fig. 7, blends, and the pixel of the emission peak displayed by the maps in Fig. 7 are shown. We conclude that the emission peak of AA (see Table 3) is around the (118, 141) pixel which corresponds with coordinates: $\alpha_{2000.0}$=05^{h}35^{m}14^s.503, $\delta_{2000.0}$=−05°22′32.″52. Emission in other Orion KL components shown by these maps agrees with the blends given in Table 3.

Figure 8 shows the ALMA 5×5 pixels (~1″×~1″) averaged spectrum around the pixel (118, 141) −emission peak of acetic acid− (histogram black spectra). The thin red, blue, and green curves are the models of CH_3COOH v_t = 0, 1, and 2, respectively, performed using the MADEX code[5], LTE, and as-

[5] Frequencies, energies, and line strengths have been taken from the predictions of Ilyushin et al. (2013).

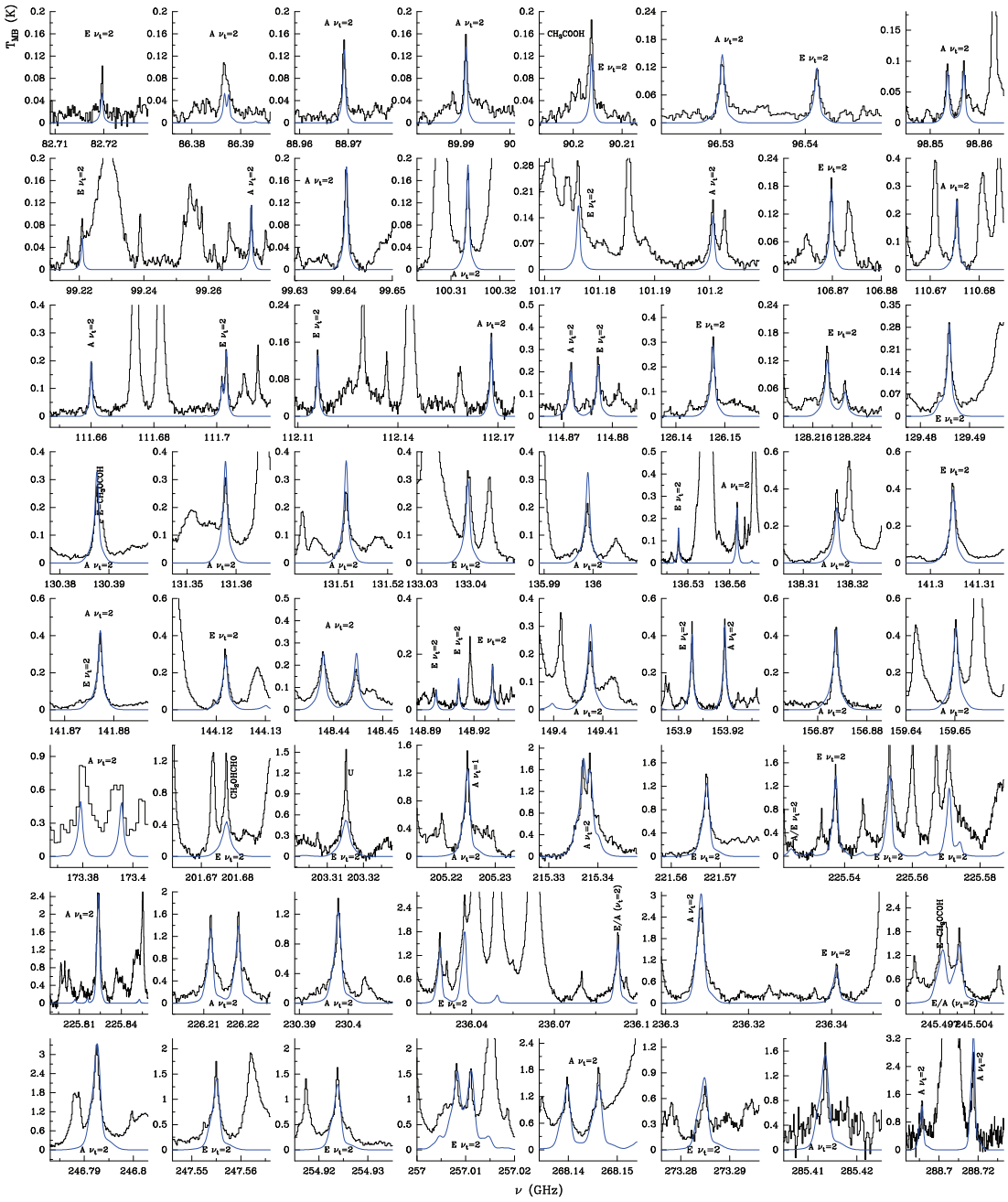

Fig. 5. Observed lines towards Orion KL (histogram spectra) and model (thin blue curves) of methyl formate (CH_3OCOH) in the second torsional state (v_t=2) through the 3, 2, 1.3 and 0.9 mm windows. A v_{LSR} of 7.5 km s^{-1} is assumed.

suming: $d_{sou} = 2''$, $T_K = 110$ K, $\Delta v = 3$ km s^{-1}, $v_{LSR} = 8$ km s^{-1}, $N = 3{\times}10^{15}$ cm^{-2} for $v_t = 0$ (A+E) and $N = 2{\times}10^{15}$ cm^{-2} for each vibrationally excited state (A+E). The column density is similar for the three states. This probes that the difference in energy of these states is low and, in this source, the three levels should have similar population.

Acetic acid g.s. has previously been searched for by Remijan et al. (2003) towards Orion KL using the BIMA (Berkeley Illinois Maryland Association) array (synthetic beam of about 11.″5×7.″5). These authors did not find AA above the detection limit of their observations (~0.15 Jy/beam) at 3 mm either in the

Table 3. Lines of CH_3COOH involved in the ALMA maps.

State	J	K_a	K_c	J'	K'_a	K'_c	Predicted freq. (MHz)	E_u (K)	$S_{ij}\mu^2$ (D^2)	Blend	Pixel Peak int.
E v_t=0	20	0	20	19	0	19	218010.022	112.1	23.9	CH_3CCD	(119, 140)
	20	0	20	19	1	19	218010.022	112.1	32.6		
	20	1	20	19	0	19	218010.022	112.1	32.6		
	20	1	20	19	1	19	218010.022	112.1	23.9		
A v_t=0	20	1	19	19	2	18	228073.754	121.6	15.9	CH_3CHO v_t=2	(119, 142)
	20	1	19	19	1	18	228073.754	121.6	37.4	CH_3OCOH v_t=1, (b type, E_{up}=670.3 K)	
	20	2	19	19	2	18	228073.754	121.6	37.4		
	20	2	19	19	1	18	228073.754	121.6	15.9		
E v_t=0	22	0	22	21	0	21	239305.851	134.6	49.8	...	(119, 139)
	22	0	22	21	1	21	239305.851	134.6	12.4		
	22	1	22	21	0	21	239305.851	134.6	12.4		
	22	1	22	21	1	21	239305.851	134.6	49.8		
A v_t=1	20	0	20	19	0	19	217607.963	225.5	20.8	$CH_3CH_2C^{15}N$	(118, 141)
	20	0	20	19	1	19	217607.963	225.5	35.6	CH_3CH_2CN v_{13}/v_{21} (c type)	
	20	1	20	19	0	19	217607.963	225.5	35.6		
	20	1	20	19	1	19	217607.963	225.5	20.8		
E v_t=1	17	3	14	16	4	13	217875.073	210.9	28.6	...	(119, 139)
	17	4	14	16	4	13	217875.074	210.9	9.32		
	17	3	14	16	3	13	217875.079	210.9	9.32		
	17	4	14	16	3	13	217875.080	210.9	28.6		
A v_t=2	19	3	16	18	4	15	246481.996	309.9	26.9	...	(116, 142)
	19	4	16	18	4	15	246482.478	309.9	15.3		
	19	3	16	18	3	15	246483.288	309.9	15.3		
	19	4	16	18	3	15	246483.770	309.9	26.9		

Note.- Spectroscopic parameters and blends of the CH_3COOH transitions involved in Fig. 7. The pixel of the emission peak at the integrated line intensity maps is displayed in the last column.

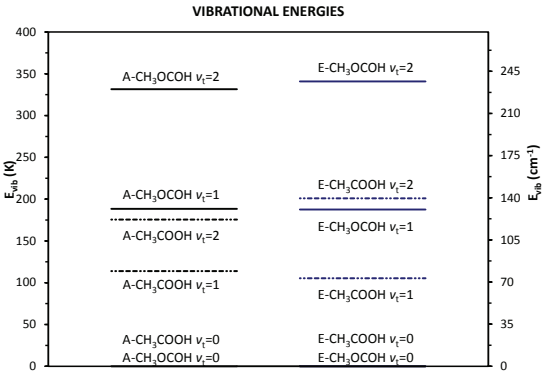

Fig. 6. Vibrational energies (E_{vib}) for the A and E states of CH_3OCOH and CH_3COOH in the first and second torsional modes.

Table 2. Methyl formate: vibrational temperatures

Cloud components	T_{vib}(MF v_t=1) (K) A	E	T_{vib}(MF v_t=2) (K) A	E
N-HC	105	105	97	100
M-HC	103	102	103	106
S-HC	99	99	138	142
SE-CR	78	77	87	90
CR	80	79	106	109
N-CR	136	135	111	114
Cold NE-CR	117	116	128	132
Hot NE-CR	117	116	122	126
Warm SC	117	116	111	114
Hot SC	77	76	105	108
S-NS	63	63	90	92
M-NS	91	90	120	123
N-NS	272	271	144	148

Note.- E_{vib} = 188.40 K (A-v_t=1), 187.57 K (E-v_t=1), 331.56 K (A-v_t=2), 340.88 K (E-v_t=2).

hot core or in the CR. Our model predicts intensities below this limit for the lines searched by Remijan et al. (2003).

3.2.2. IRAM 30m data: CH_3COOH model

Acetic acid has also been detected in the 30m survey of Orion KL. Although the large percentage of blended lines in these data, we did not find missing lines between 80 and 306 GHz. As we have pointed out in previous works (see Kolesniková et al. 2015 and Tercero et al. 2015), the spectrum of the IRAM 30m telescope is a mix of all molecules from all source components (averaged spectrum over the beam) given rise to a high level of blending and line confusion, whereas with ALMA, a drastic reduction of the line confusion allows the detection of a larger number of unblended features, especially for the less abundant species. Table 4 shows the number of lines of AA identified in the IRAM 30m data. Our identifications are based on a whole inspection of the data and the modeled synthetic spectrum of the molecule (see below) where we obtain the total number of detectable lines. Unblended features are those which present the expected radial velocity and there is not another species at the same observed frequency (±3 MHz) with significant intensity (if for the unblended frequencies we do not found the line we are looking for, then we do not claim detection). Partially blended lines are those which present either a mismatch in the peak channel of the line or significant contribution from another species at

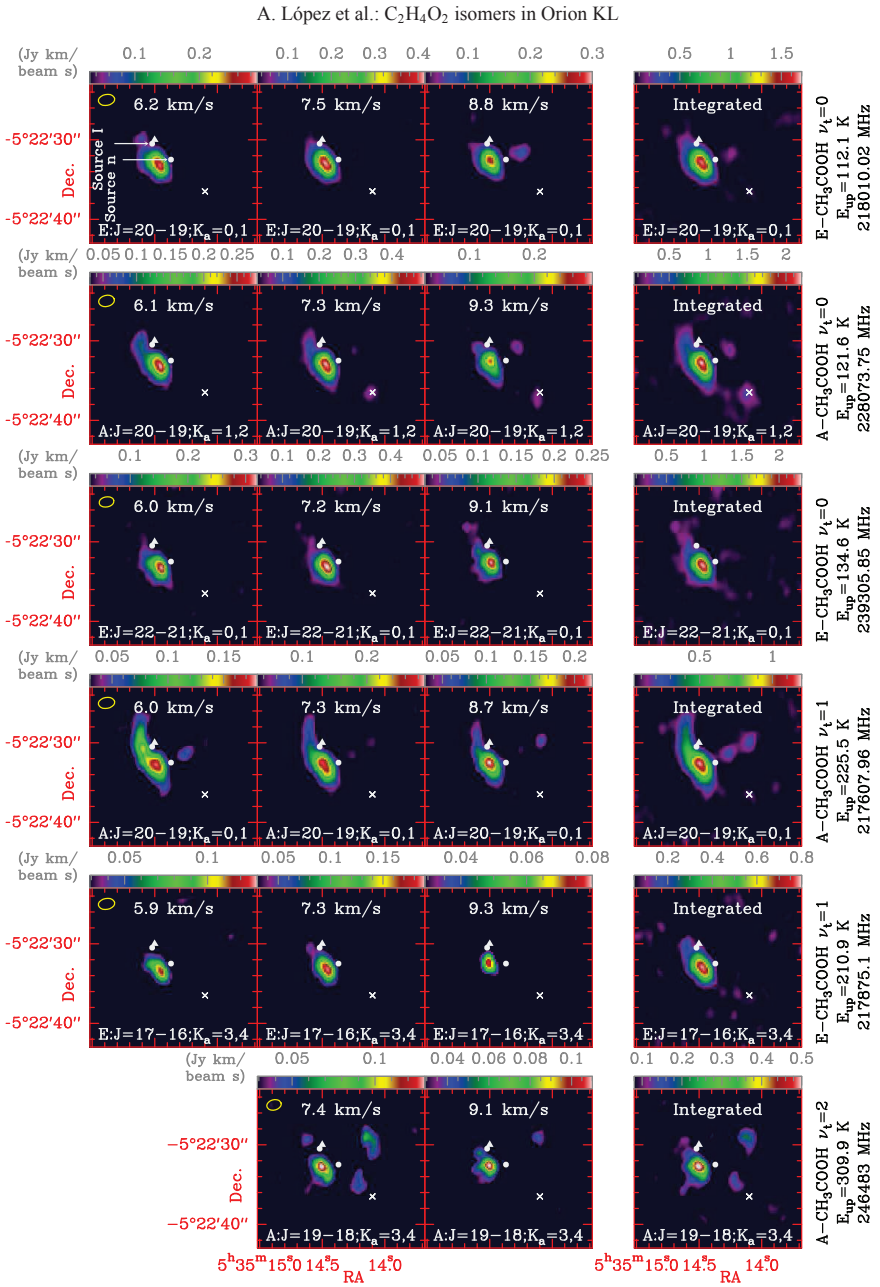

Fig. 7. Maps of three radial velocities (6.0, 7.5, and 9.0 km s^{-1}) and of the integrated line intensity of the less blended CH_3COOH lines. Triangle and cross signs mark the pointing positions of the 30m survey at IRc2 and the Compact Ridge, respectively. Yellow ellipse at the upper left corner of the maps represents the synthetic beam of ALMA.

the peak channel of the feature. Blended lines are those that are close enough to other stronger features.

Figures A.8, A.9, and A.10, only available online, show detected lines of AA $v_t = 0$, 1, and 2, respectively, in the IRAM 30m data (at the 'survey position') together with our best model. Tables B.5, B.6, and B.7, only available online, list line parameters and blends of all detectable lines in the 30m data for AA g.s., AA $v_t = 1$, and AA $v_t = 2$, respectively. A single component (M-HC) has been considered to derive the synthetic spectrum using MADEX and LTE according with the following physical parameters (in agreement with those obtained in Sect. 3.2.1): $d_{sou} = 2''$, offset = $1''.5$ (with respect the 'survey position', see Sect. 2.2), $T_K = 110 \pm 33$ K, $\Delta v = 3$ (2 for $v_t = 1,2$) km s^{-1}, $v_{LSR} = 7.5$ km s^{-1}. We derived column densities of $N = (1.2 \pm 0.4) \times 10^{16}$ cm^{-2}, $N = (5 \pm 2) \times 10^{15}$ cm^{-2}, and

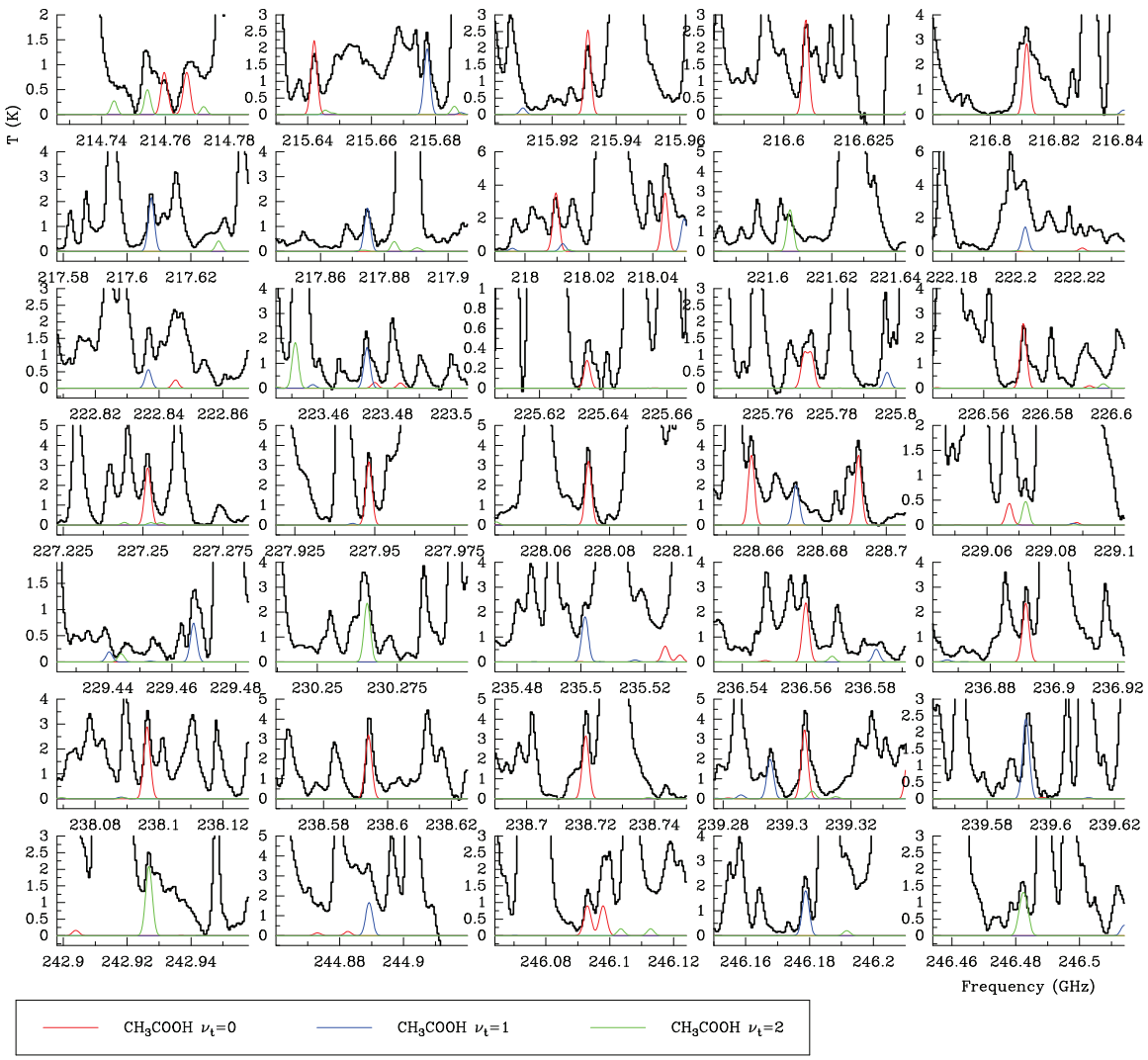

Fig. 8. Lines of CH_3COOH, towards Orion KL. Histogram black spectrum is the averaged spectrum over 5×5 pixel around the acetic acid peak (pixel: 118, 141) of the ALMA SV data (see text for references). Red, blue, and green thin lines are the synthetic spectrum of CH_3COOH v_t=0, 1, and 2, respectively.

$N = (4\pm1)\times10^{15}$ cm^{-2} for $v_t = 0$ (A+E), $v_t = 1$ (A+E) and $v_t = 2$ (A+E), respectively.

Table 4. Acetic acid and glycolaldehyde lines in the IRAM 30m data

Species	Detectable (total)	Unblended	Partially blended	Totally blended
AA g.s.	286	146 (%)	78 (%)	62 (%)
AA v_t=1	145	69 (%)	45 (%)	31 (%)
AA v_t=2	126	69 (%)	34 (%)	23 (%)
GLY g.s.	242	121 (%)	71 (%)	50 (%)

Note.- See Sect. 3.2.2.

3.3. Glycolaldehyde (CH_2OHCHO)

In this work, glycolaldehyde has been detected for the first time in Orion KL.

3.3.1. ALMA SV data: CH_2OHCHO maps and source components

We have search for glycolaldehyde in the ALMA SV data towards two different positions: at the AA peak (M-HC) and at the MF peak (CR). We found this species towards the former position.

Left panel of Fig. 9 shows maps at 7.5 km s^{-1} of some glycolaldehyde lines partially free of blendingIn Table 5, spectroscopic parameters of the involved transitions in Fig. 9, blends,

and the pixel of the emission peak (between SW of source *I* and SE of source *n*) displayed by these maps are shown. The spatial distribution of the emission is consistent with the detection of this species at a similar position of CH_3COOH. We conclude that the emission peak of glycolaldehyde (see Table 5) is around the (121, 135) pixel which corresponds with $\alpha_{2000.0}$=$05^h35^m14.453^s$, $\delta_{2000.0}$=−05°22'33.82" (displaced 1.″5 South-West with respect the AA peak). Emission in other Orion KL components shown by these maps agrees with the blends given in Table 5.

Central and right panels show the ALMA 5×5 pixels (∼1.″×∼1.″) averaged spectrum around the pixels (121, 135) −emission peak of GLY− and (149, 119) −emission peak of MF− (histogram black spectra). The thin red curve is the model for GLY adapted to the ALMA data (using the MADEX code[6], LTE, and assuming: $d_{sou} = 2$", $T_K = 110$ K, $N = 2\times10^{14}$ cm^{-2}, $\Delta v = 2$ km s^{-1}, and $v_{LSR} = 7.5$ km s^{-1}). The radial velocity at 7.5 km s^{-1} with respect to the rest frequency of the CH_2OHCHO transitions is marked with a dashed blue line.

3.3.2. IRAM 30m data: CH_2OHCHO model

Glycolaldehyde has also been detected in the 30m survey of Orion KL. As for AA, we did not find missing lines between 80 and 306 GHz. Table 4 shows the number of GLY lines identified in the IRAM 30m data (see Sect. 3.2.2). Figure 10 shows detected lines of GLY in the IRAM 30m data (at the 'survey position') together with our best model. Table B.8, only available online, list line parameters and blends of all detectable lines in the 30m data of GLY. As well as for AA, a single component (M-HC) has been considered to derive the synthetic spectrum using MADEX and LTE according to the following physical parameters (in agreement with those obtained in Sect. 3.3.1): $d_{sou} = 2$", offset = 1.″5 (with respect the 'survey position', see Sect. 2.2), $T_K = 110\pm33$ K, $\Delta v = 2$ km s^{-1}, $v_{LSR} = 7.5$ km s^{-1}. We derived a column density of $N = (3.5\pm1.1)\times10^{15}$ cm^{-2}.

4. Discussion

Methyl formate is one of the most abundant molecules in the ISM. Its dense rotational spectrum allows us to characterize the physical-chemical conditions of the region in which it resides on. These species is frequently found in molecular condensations associated with massive star forming regions, "hot cores", although it has also been detected in those regions associated with low-mass stars "hot corinos" (Cazaux et al. 2003; Bottinelli et al. 2004a; Sakai et al. 2006, 2007). It should be noted that, although CH_3OCOH is relatively abundant both in hot cores and hot corinos, it is especially abundant in Orion KL (Favre et al. 2011). Moreover, it is suggested that organic molecules may be different along the protostellar evolution in both hot core/corinos. Sakai et al. (2006, 2007) proposed that CH_3OCOH is associated with a very early evolutionary phase of star formation (Class 0 protostars), and, therefore, the emission lines of MF might be an important tracer to the trigger of star formation activity (Kobayashi et al. 2007).

[6] Spectroscopic constants were derived from a fit with the MADEX code to the lines reported by Carroll et al. (2010). The dipole moment was that measured by Marstokk & Møllendal (1970).

4.1. Chemical formation pathways

Calcutt et al. (2014) provided PdBI maps of MF and GLY of four massive star-forming hot cores (G31.41+0.31, G24.78+0.08 A1, G24.78+0.08 A2, and G29.96−0.02). They found MF and GLY tracing similar spatial distribution in these distant sources although GLY cloud be a better tracer of the inner conditions of the hot core closer to the embedded protostar. Nevertheless, the presence of GLY has only been confirmed towards G31.41+0.31 (Beltrán et al. 2009) and the GLY maps of G24.78+0.08 (A1 and A2) and G29.96−0.02 are based on the observation of a single transition of GLY in these sources. We found also GLY associated to the hottest component of the source. Issues such as the evolutionary stage of the different Orion KL's components, the composition of the dust grains previous the collapse phase, the molecules accreted on to the grains and/or the gas phase chemistry should be addressed to explain the evident difference between the molecular content of the CR and the M-HC.

Nowadays, thanks to the recent papers based on interferometric data and related to O-bearing species in Orion KL, we can infer the following chemical differentiation: The compact ridge is the main host of CH_3OCOH, CH_3OCH_3, $CH_3CH_2OCH_3$, CH_3COOCH_3, and CH_3CH_2OCOH (see Favre et al. 2011; Brouillet et al. 2013; Tercero et al. 2015). All these species present a common feature: an oxygen bounded to two carbons by two single bonds (see Fig. 11). The middle of the hot core structure, which also presents emission of CH_3OCOH and CH_3OCH_3, is the main host of CH_3CH_2OH, CH_3COCH_3 (this species also traces a relatively extended emission similar to the spatial distribution found for N-bearing species), CH_3COOH, CH_2OHCHO, and $OHCH_2CH_2OH$ (see Peng et al. 2013; Brouillet et al. 2015; Tercero et al. 2015). These species present a hydroxyl group (−OH) and/or a carboxyl group (−CO) (see Fig. 11).

According to the internal structure of these species, we can propose different precursors for the formation of the species found in each clump.

In the structure of the abundant molecules in the CR, we found CH_3O-, the methoxy radical, (Cernicharo et al. 2012); for ethyl formate a H from CH_3O has been replaced by a $-CH_2$ group. On the other hand, an isomer of methoxy, hydroxymethyl ($-CH_2OH$), is a constituent of molecules found in the M-HC such as ethanol, GLY, and ethylene glycol. In fact, the large abundance of ethylene glycol (two $-CH_2OH$ bounded) in the M-HC (see Brouillet et al. 2015) could be easily explained if $-CH_2OH$ is the main precursor for the O-bearing species in this component. In addition, AA has changed the two H of hydroxymethyl by a methyl group ($-CH_3$) and an Oxygen. The only molecule that not follows this "law" is acetone which seems to be more connected with the N-bearing species in Orion KL (see Peng et al. 2013). We propose methoxy (CH_3O-) and hydroxymethyl ($-CH_2OH$) as the precursors of the O-bearing species in the CR and in the M-HC of Orion KL, respectively. Physical and chemical conditions of the gas and the dust grains under one of these species is favored should be investigated.

5. Summary and conclusions

- A consistent study of the $C_2H_4O_2$ isomers (MF, AA, and GLY) has been carried out based on the ALMA SV and the IRAM 30m data.
- In this work, AA g.s. and GLY g.s. have been detected for the first time in Orion KL. In addition, due to the low energies of the two first vibrational modes of AA, we have identified

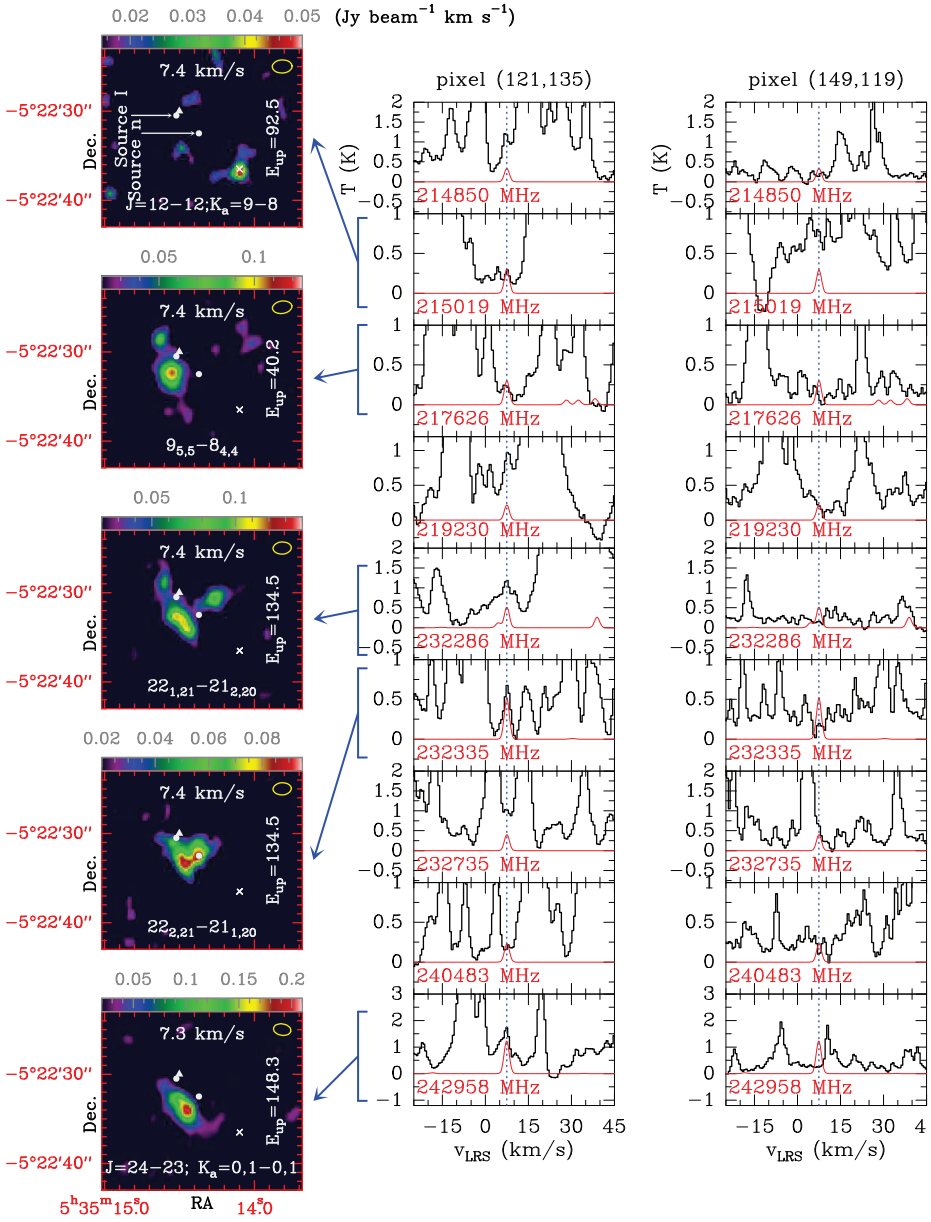

Fig. 9. Mid and right panels depict lines of glycolaldehyde, CH_2OHCHO, towards two different positions in Orion KL. Histogram black spectrum is the averaged spectrum over 5×5 pixel around the glycolaldehyde peak (pixel: 121, 135) and the methyl formate peak (pixel: 149, 119) of the ALMA SV data (see text for references). Red thin line is the synthetic spectrum of glycolaldehyde. Left panel shows maps of this species at a $v_{LSR} \simeq 7.5$ km s^{-1}. Triangle and cross signs mark the pointing positions of the 30m survey at IRc2 and the Compact Ridge, respectively. Yellow ellipse at the upper right corner of the maps represents the synthetic beam of ALMA.

AA v_t=1 and AA v_t=1 in Orion KL and for the first time in space.

– Thanks to the high spatial resolution achieved by the ALMA maps we have determined in a accurate way the different cloud components involved in the emission of MF, AA and GLY.
– Ten different clumps are involved in the MF emission being the CR the main host of this species in Orion KL. Emission of AA and GLY comes from a single clump located at the M-HC.
– Detailed models that reproduce the observed lines of MF, AA and GLY in the IRAM 30m data (from 80 to 307 GHz) have been performed based on the source components un-

Table 5. Lines of CH_2CHCHO in ALMA data.

J	K_a	K_c	J'	K'_a	K'_c	Predicted freq. (MHz)	E_u (K)	S_{ij}	Blend	Pixel Peak int.
13	9	4	13	8	5	214849.576	99.7	4.43	CH_3CHO	...
13	9	5	13	8	6	214849.596	99.7	4.43		
12	9	3	12	8	4	215018.683	92.5	3.64	CH_3COOCH_3/$DCOOCH_3$	(120, 134)
12	9	4	12	8	5	215018.688	92.5	3.64		
9	5	5	8	4	4	217626.097	40.2	4.64	$CH_2CH^{13}CN$/$CH_3CH_2C^{15}N$ CH_3CHO v_t=1 (b type)	(115, 143)
13	4	10	12	3	9	219230.205	60.5	4.02	CH_3CH_2CN ν_{13}/ν_{21} CH_3COCH_3	...
22	1	21	21	2	20	232286.155	134.5	17.4	CH_3CH_2CN (b type, E_u=738.1 K)	(120, 137)
22	2	21	21	1	20	232335.444	134.5	17.4	$CH_3{}^{13}CH_2CN$ (E_u=580.4 K)	(120, 137)
21	3	19	20	2	18	232734.963	131.2	13.1	CH_3COCH_3/$HCOOCH_3$ v_t=1	...
12	10	2	12	9	3	240482.808	104.0	2.84	CH_3COCH3/CH3COOH v_t=1	...
12	10	3	12	9	4	240482.808	104.0	2.84		
24	0	24	23	1	23	242957.816	148.3	22.5		(121, 135)
24	1	24	23	1	23	242957.904	148.3	23.8		
24	0	24	23	0	23	242957.983	148.3	23.8		
24	1	24	23	0	23	242958.072	148.3	22.5		

Note.- Spectroscopic parameters and blends of the CH_2OHCHO lines shown in Fig. 9. The pixel of the emission peak (between SE of source *I* and SW of source *n*) of the maps depicted in Fig. 9 is displayed in the last column.

veiled by the ALMA maps and LTE approximation. These models provide constrained values for the rotational temperatures and the column densities of MF, AA, and GLY in each source component.

– Vibrational temperatures have been derived for the two first low lying vibrationally excited states of MF. In all cases, we have obtained values of T_{vib} in agreement with the rotational temperatures provided by the model. Therefore, the main mechanism that populates the vibrational levels (collisions and/or IR pumping) cannot be distinguished.
– The organic O-bearing species detected in Orion KL can be divided into two groups depending on the main host component, i.e., the CR or the M-HC. A common structural feature has been discerned for each group of species. These differences lead to suggest a different precursor for the species found in each component: in the CR the methoxy radical (CH_3O-) could play the major role in forming the O-bearing species, whereas the hydroxymethyl radical ($-CH_2OH$) may be the main precursor for these species in the M-HC.

References

Balucani, N., Ceccarelli, C., Taquet, V. 2015, MNRAS, 449, L16
Bauder, A., 1979, J. Phys. Chem., 8, 3
Bell, T., Cernicharo, J. , Viti, S. et al., 2014, A&A, 218, 72
Beltrán, M. T., Codella, C., Viti, S., Neri, R., and Cesaroni, R., 2009, Highlights of Astron., 15, XXVIIth IAU General Assembly
Bennett, C. J., and Kaiser, R., 2007, ApJ, 661, 899
Bottinelli, S., Ceccarelli,C., Lefloch, B., et al. 2004a, ApJ, 615, 354
Brouillet, N., Despois, D., Baudry, A. et al. 2013, A&A, 550, 46
Brouillet, N., Despois, D., Lu, X.-H. et al. 2015, A&A, 576, 129
Brown, R. D., Crofts, J. G., Gardner, F. F., et al. 1975, ApJ, 197, L29
Burke, D. J., Puletti, F., Brown, W. A., et al., 2015, MNRAS, 447, 1444
Butler, R. A. H. and De Lucia, F. C., et. al, 2001, ApJS. S., 134, 319
Calcutt, H., Viti, S., Codella, C., et al., 2014, MNRAS, 443, 3157
Carroll, P. B., Drouin, B. J., and Widicus Weaver, S. L., 2010, ApJ, 723, 845
Carvajal, M., Willaert, F., Demaison, J., Kleiner, I., 2007, J. Mol. Spec., 246, 2, 158
Carvajal, M., L. Margulés, L., Tercero, B., Demyk, K., Kleiner, I., et al., 2009, A&A, 500, 1109
Cazaux, S., Tielens, A. G. G. M., Ceccarelli, C., et al., 2003, ApJ, 593, L51
Cernicharo, J., 1985, Internal IRAM report (Granada: IRAM)
Cernicharo, J. 2012, in ECLA-2011: Proceedings of the European Conference on Laboratory Astrophysics, EAS Publications Series, 2012, Editors: C. Stehl, C. Joblin, & L. d'Hendecourt (Cambridge: Cambridge Univ. Press), "Laboratory astrophysics and astrochemistry in the Herschel/ALMA era", 58, 251
Cernicharo, J., Marcelino, N., Roueff, E., et al. 2012, ApJ, 759, L43
Coudert, L. H., Drouin, B. J., Tercero, B., et al. 2013, ApJ, 779, 119
Coutens, A., Persson, M. V., Jørgensen, J. K., Wampfler, S. F., and Lykke, J. M. 2015, A&A, 576, 5
Curl Jr, R. F. 1959, J. Chem. Phhys., 30, 1529
Daly, A. M., Bermúdez, C., López, A., et al., 768, **81**, ApJ, 2013
Demaison, J., Dubrulle, A., Boucher, D., Burie, J., and van Eijck, B. P. 1982, J. Mol. Spec., 94, 211
Demaison, J., Boucher, D., Dubrulle, A., and Van Eijck, B. P. 1983, J. Mol. Spec., 102, 260
Demaison, J., Margulés, L., Kleiner, I., and Császár, A. G. 2010, J. Mol. Spec., 259, 70
Demyk, K., Mäder, H., Tercero, B., et al., 2007, A&A, 466, 255
Dickens, J. E., Irvine, W. M., Nummelin, A., et al. 2001, Spectrochimica Acta Part A: Molecular and Biomolecular Spectroscopy, 57, 643
Esplugues, G. B., Tercero, B., Cernicharo, J., et al., A&A, 2013a, 556, A143
Esplugues, G. B., Cernicharo, J., Viti, S., et al., A&A, 2013b, 559, A51
Favre, C., Despois, D., Brouillet, N., et al. 2011, A&A, 532, 32
Favre, C., Carvajal, M., Field, D. et al. 2014, ApJS. S., 215, 25
Feng, S., Beuther, H., Henning, T. et al. 2015, A&A, accepted
Garrod, R. T. 2013, ApJ, 765, 60
Haykal, I., Carvajal, M., Tercero, B., et al. 2014, A&A, 568, A58
Hollis, J. M., Lovas, F. J., and Jewell, P. R. 2000, ApJ, 540, L107
Hollis, J. M., Vogel, S. N., Snyder, L. E., Jewell, P. R. and Lovas, F. J. 2001, ApJ, 554, L81
Hollis, J. M., Jewell, P. R., Lovas, F. J., and Remijan, A. 2004, ApJ, 613, L45
Ilyushin, V. V., Alekseeva, E. A., Dyubkoa, S. F., et al. 2001, J. Mol. Spec., 205, 286
Ilyushin, V. V., Alekseeva, E. A., Dyubkoa, S. F., and Kleiner, I. 2003, J. Mol. Spec., 220, 170
Ilyushin, V., Kleiner, I., and Lovas, F. J. 2008, J. Phys. Chem. Reference Data, 37, 97
Ilyushin, V., Kryvda, A., AND Alekseev, E. 2009, J. Mol. Spec., 255, 32
Ilyushin, V. V., Endres, C. P., Lewen, F., Schlemmer, S., Drouin, B. J. 2013, J. Mol. Spectrosc., 290, 31
Jørgensen, J. K., Favre, C., Bisschop, S. E., et al. 2012, ApJ, 757, L4
Karakawa, Y., Oka, K., Odashima, H., Takagi, K., and Tsunekawa, S. 2001, J. Mol. Spectrosc., 210, 196
Kim, M. K., Hirota, T., Honma, M., et al. 2008, PASJ, 60, 991
Kobayashi, K., Ogata, K., Tsunekawa, S., and Takano, S. 2007, ApJ, 657, L17
Kobayashi, K., Kazunori Takamura, K., Sakai, Y. 2013, ApJS. S., 205, 9

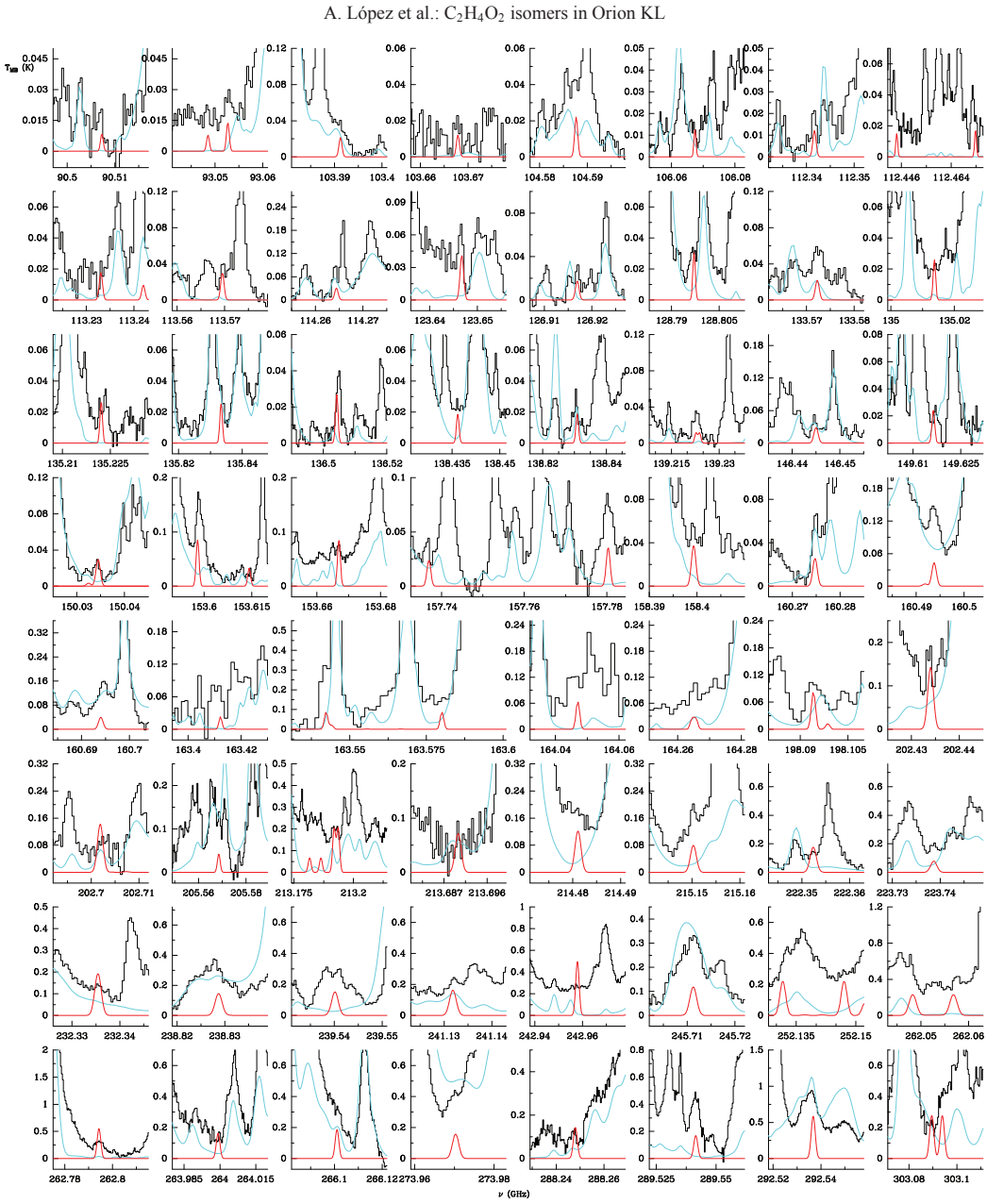

Fig. 10. Observed lines from Orion KL (histogram spectra) and model (thin red curves) of glycolaldehyde (CH_2OHCHO) in the ground state in the 3, 2, 1, and 0.9 millimeter windows. The cyan line corresponds to the model of the molecules we have already studied in this survey (see Appendix C), except for the model of CH_2OHCHO. A v_{LSR} of 7.5 km s^{-1} is assumed.

Kolesniková, L., Tercero, B., Cernicharo, J., et al., 2014, ApJ, 784, L7
Kolesniková, L., Pea, I., Alonso, J. L. et al. 2015, A&A, 577, 91
Krisher, L. C. and Saegebarth, E. 1971, J. Mol. Spec., 54, 4553
López, A., Tercero, B., Kisiel, Z., et al. 2014, A&A, 572, A44
Maeda, A., De Lucia, F. C., and Herbst, E. 2008, J. Mol. Spec., 251, 293
Marcelino, N., Cernicharo, J., Tercero, B., Roueff, E. 2009, ApJ, 690, L27
Margulès, L., Motiyenko, R. A., Demyk, K., et al. 2009, A&A, 493, 565
Margulés, L., Huet, T. R., Demaison, J., et al. 2010, ApJ, 714, 1120
Marstokk, K.-M. and Møllendal, H. 1970, J. Mol. Struc., 5, 205
Mehringer, D. M., Snyder, L. E., Miao, Y., and Lovas, F. J. 1997, ApJ, 480, L71
Michelsen, H. and Klaboe, P. 1969, J. Mol. Struc., 4, 293
Motiyenko, R. A., Tercero, B., Cernicharo, J., and Margulés, L., 2012, A&A, 548, A71
Neill, J. L., Steber, A. L., Muckle, M. T., et al. 2011, JPCA, 115, 6472
H. Odashima, H., Ogata, K., Karakawa, Y., Takagi, K., and Tsunekawa S. 2003, Molecules 8, 139
Oesterling, L. C. , Albert, S., De Lucia, F. C., Sastry, K. V. L. N., and Herbst, E. 1999, ApJ, 521, 255
Ogata, K., Odashima, H., Takagi, K. and Tsunekawa, S. 2004, J. Mol. Spec., 225, 14

Pardo, J. R., Cernicharo, J. and Serabyn, E. 2001a, IEEE Tras. Antennas and Propagation, 49, 1683
Peng, T.-C., Despois, D., Brouillet, N., et al. 2013, A&A, 554, 78
Plummer, G. M., Herbst, E., De Lucia, F. C., and Blake, G. A. 1986, ApJS. S., 55, 633
Plummer, G. M., Herbst, E., De Lucia, F. C., and Blake, G. A. 1986, ApJS. S., 60, 949
Remijan, A., Snyder, L. E., Liu, S.-Y., Mehringer, D., and Kuan, Y.-J. 2002, ApJ, 576, 264
Remijan, A., Snyder, L. E., Friedel, D. N., Liu, S.-Y., and Shah, R. Y. 2003, ApJ, 590, 314
Remijan, A., Shiao, Y.-S., Friedel, D. N., Meier, D. S., and Snyder, L. E. 2004, ApJ, 617, 384
Requena-Torres, M. A., Martn-Pintado, J., Rodrguez-Franco, A., et al. 2006, ApJ, 455, 971
Sakai, N., Sakai, T., and Yamamoto, S. 2006, PASJ, 58, L15
Sakai, N., Sakai, T., and Yamamoto, S. 2007, ApJ, 660, 363
Sakai, Y., Kobayashi, K., and Hirota, T. 2015, ApJ, 803, 97
Shiao, Y.-S. J., Looney, L. W., Remijan, A. J., Snyder, L. E., and Friedel, D. N. 2010, ApJ, 716, 286
Tabor, W. J. 1957, J. Chem. Phys. 27, 974
Takano, S., Sakai, Y., Kakimoto, S., Sasaki, M., and Kobayashi, K. 2012, PASJ, 64, 89
Tercero B., Cernicharo, J., Pardo, J. R., and Goicoechea, J. R. 2010, A&A, 517, 96
Tercero B., Vincent L., Cernicharo, J., Viti S., and Marcelino N., 2011, A&A, 528, 26
Tercero, B., Margulès, L., Carvajal, M., et al. 2012, A&A, 538, 119
Tercero, B., Kleiner, I., Cernicharo, J. et al. 2013, ApJ, 770 L13
Tercero, B., Cernicharo, J., López, A. et al. 2015, A&A Letters, accepted
van Eijck, B. P., van Opheusden, J., van Schaik, M. M. M., and van Zoeren, E. 1981, J. Mol. Spectr., 86, 465
van Eijck, B. P. and van Duijneveldt, F. B. 1983, J. Mol. Spectr., 102, 273
Widicus Weaver, S. L., Butler, R. A. H., Drouin, B. J. et al. 2005, ApJS. S., 158, 188
Wlodarczak, G. and Demaison, J. 1988, A&A, 192, 313

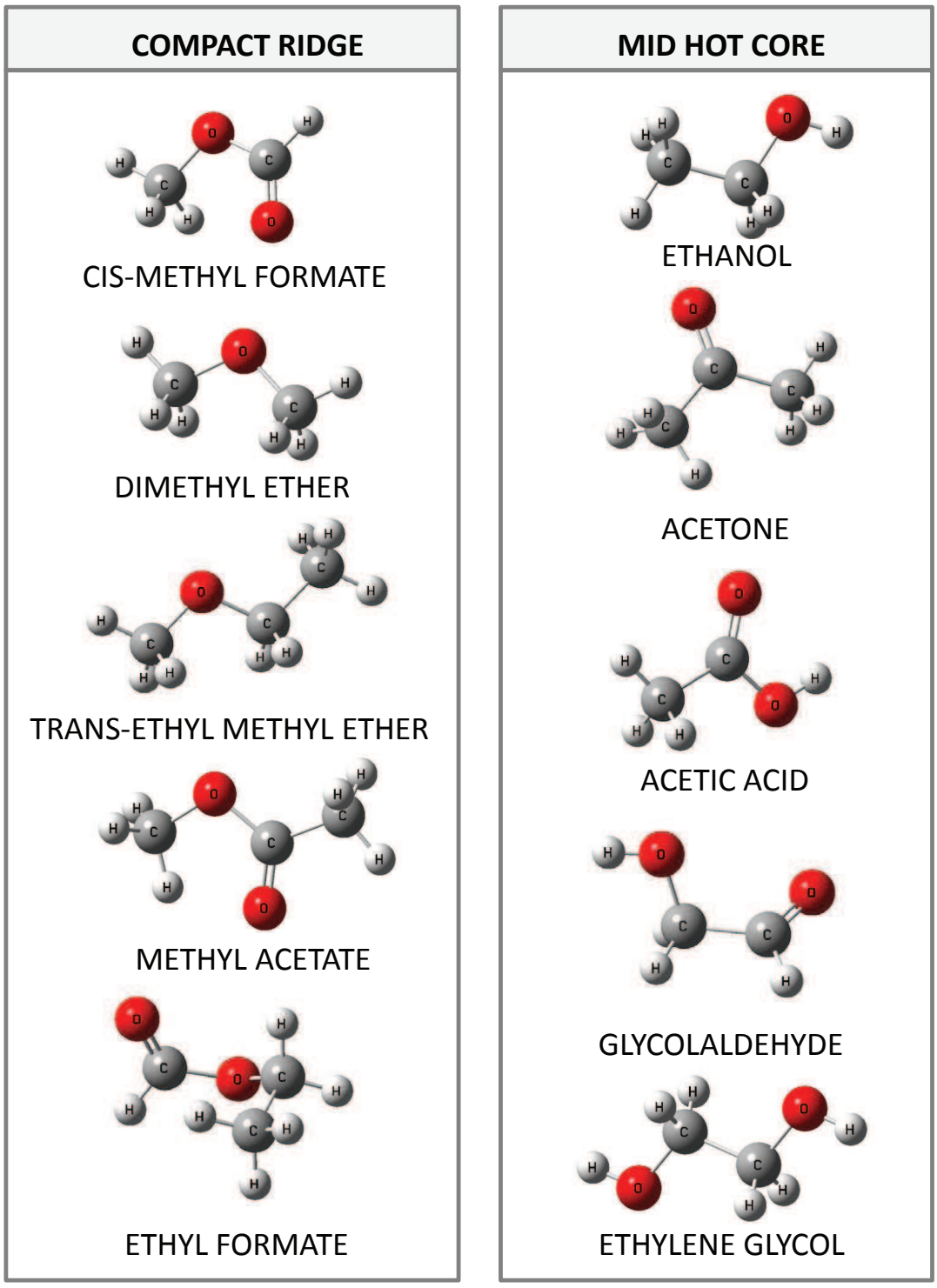

Fig. 11. Structure of the O-bearing molecules found towards the compact ridge and the mid hot core of Orion KL.

Appendix A: Online Figures

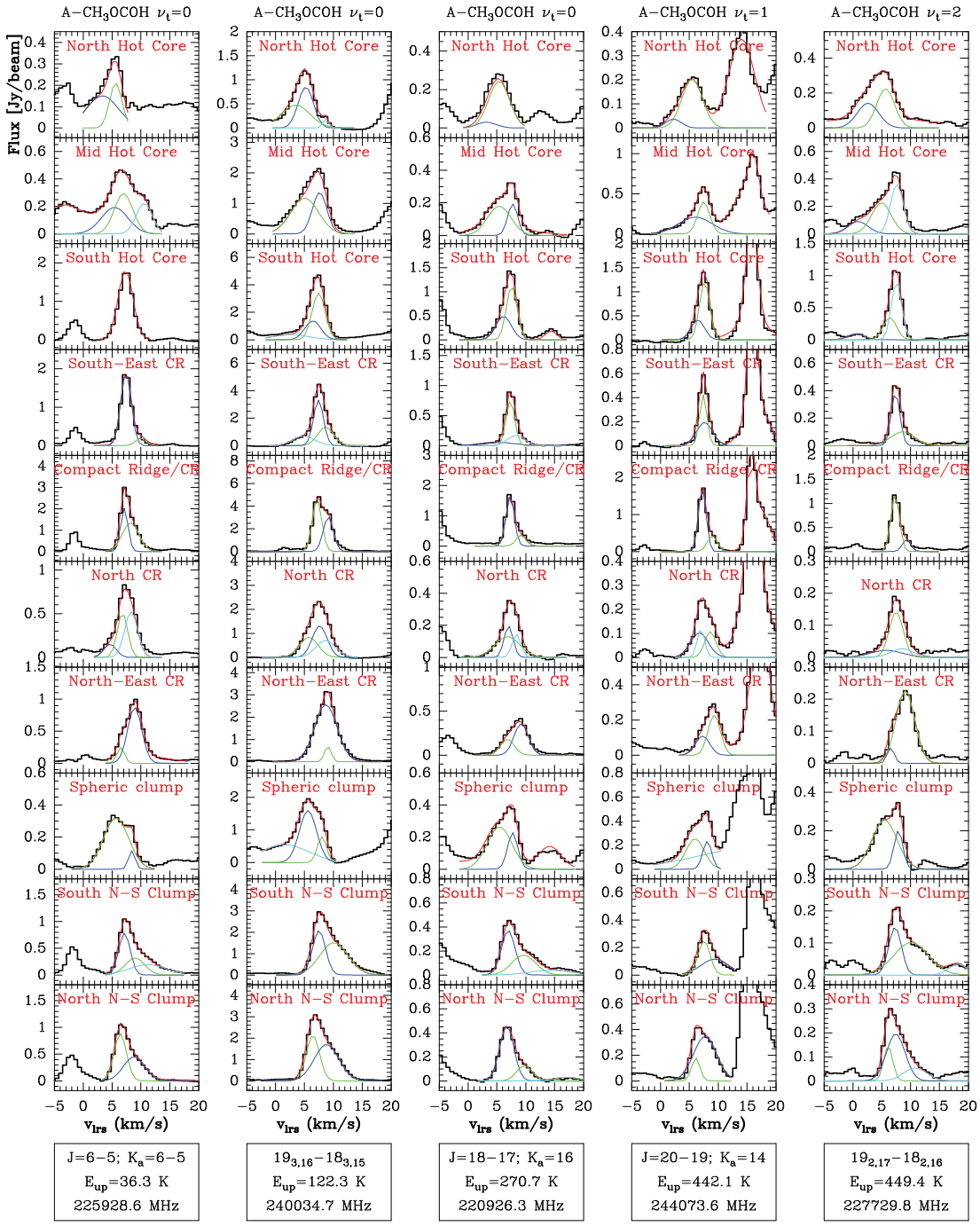

Fig. A.1. Lines of CH_3OCOH and Gaussian fits to the line profiles at different positions.

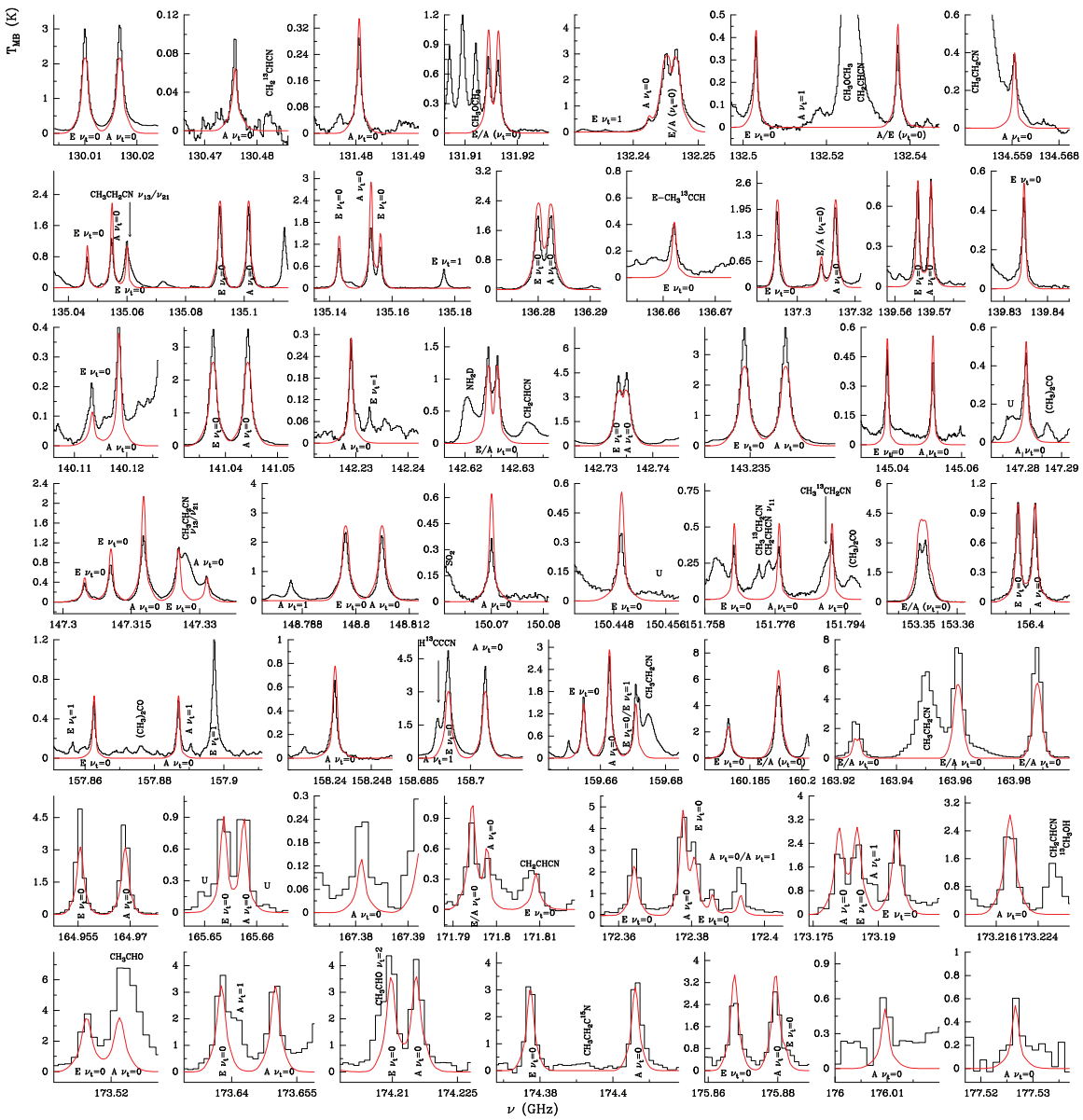

Fig. A.2. Observed lines towards Orion KL (histogram spectra) and model (thin red curves) of methyl formate (CH_3OCOH) in the ground state (v_t=0) in the 2 mm window. A v_{LSR} of 7.5 km s^{-1} is assumed.

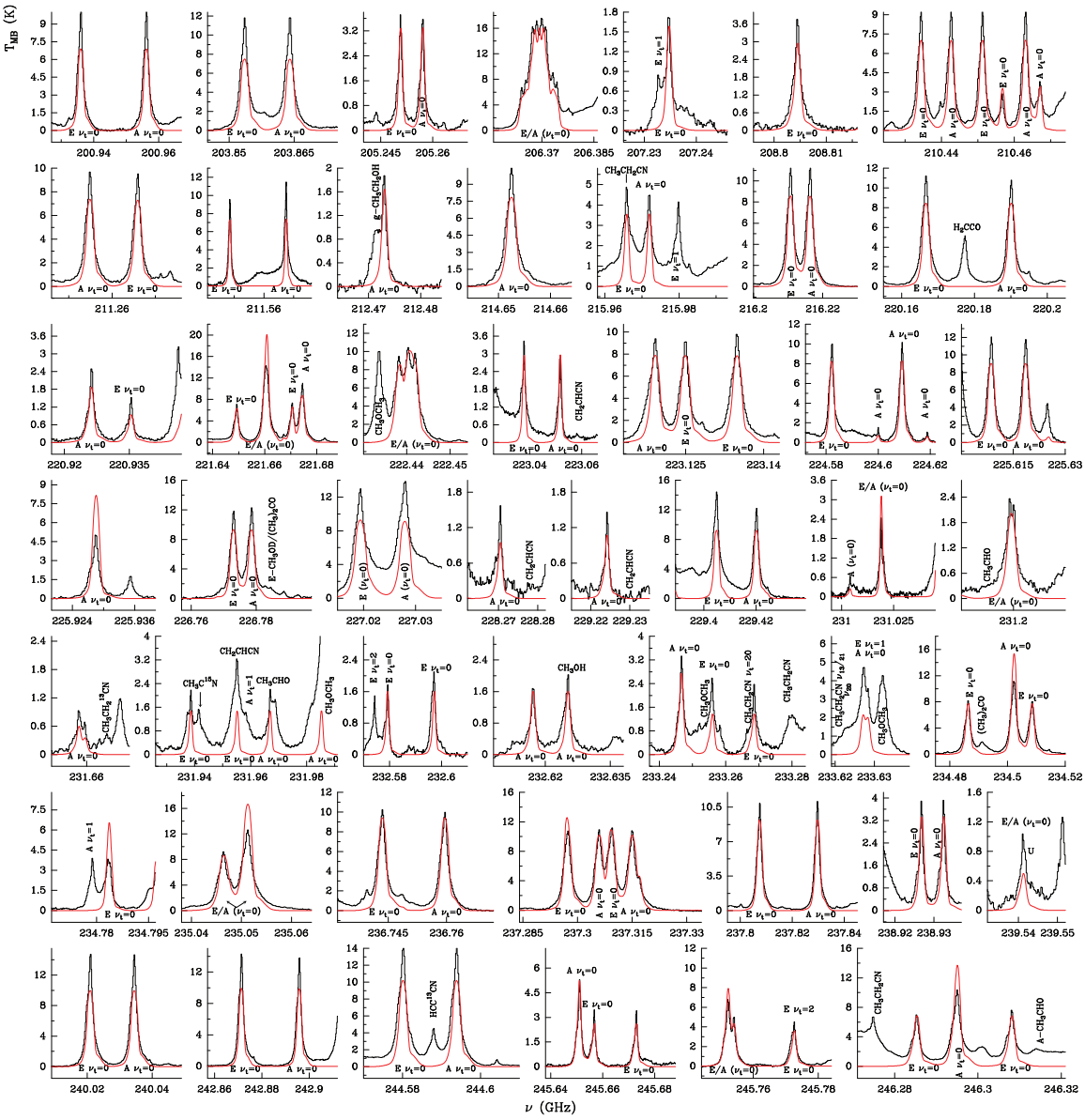

Fig. A.3. Observed lines towards Orion KL (histogram spectra) and model (thin red curves) of methyl formate (CH_3OCOH) in the ground state (v_t=0) in the 1.3 mm window. A v_{LSR} of 7.5 km s^{-1} is assumed.

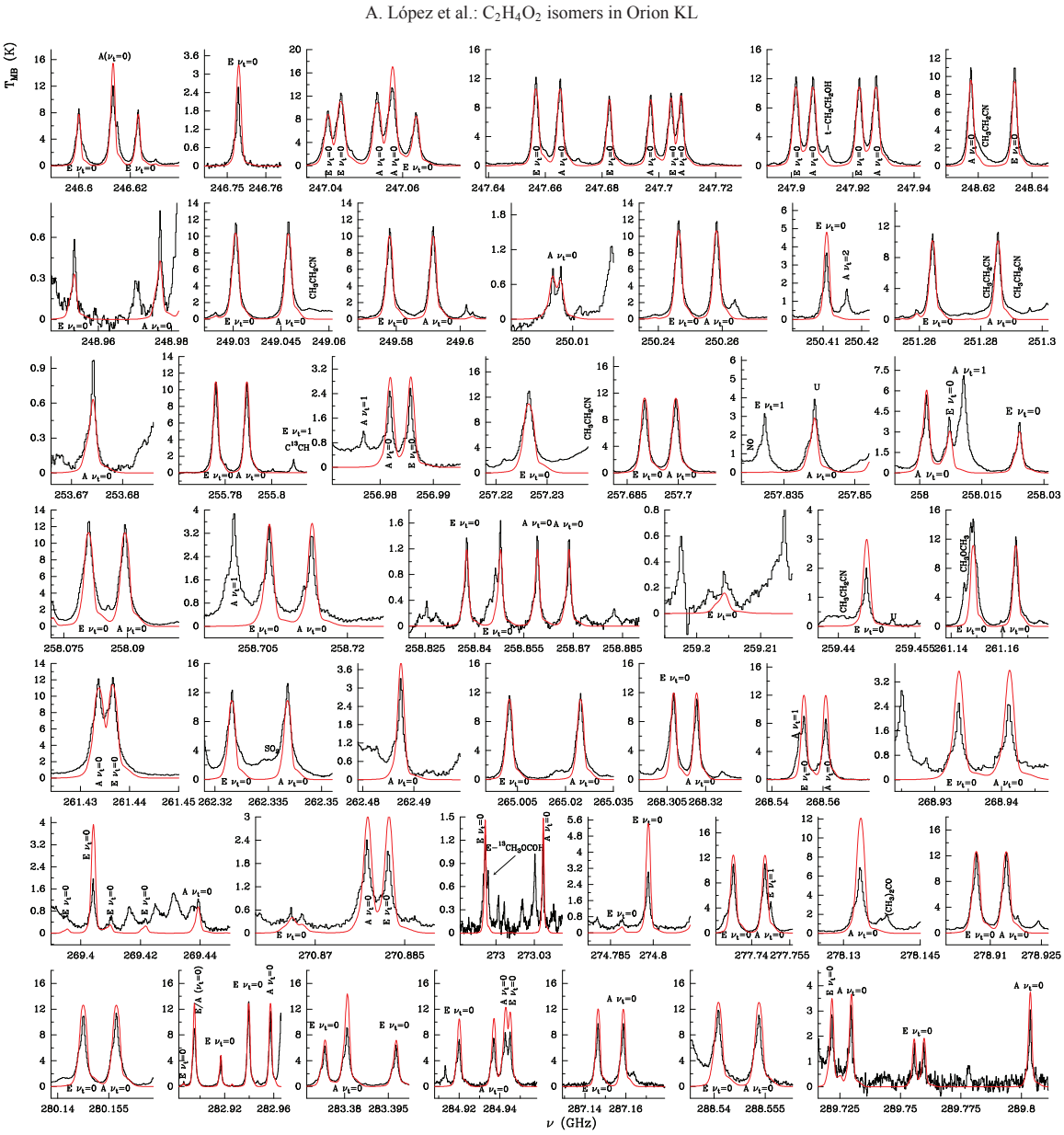

Fig. A.4. Observed lines towards Orion KL (histogram spectra) and model (thin red curves) of methyl formate (CH_3OCOH) in the ground state (v_t=0) in the 1-0.9 mm window. A v_{LSR} of 7.5 km s^{-1} is assumed.

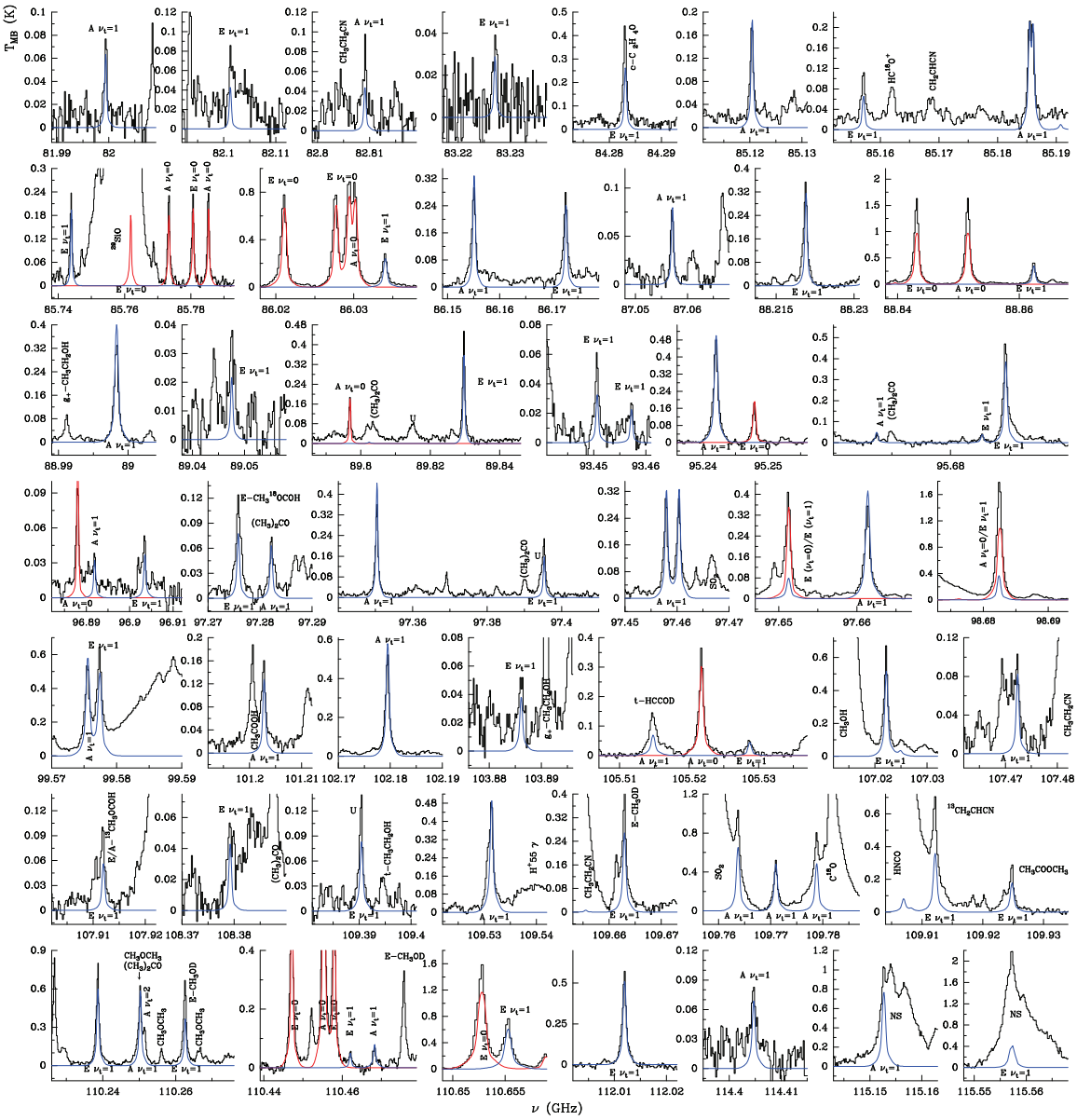

Fig. A.5. Observed lines towards Orion KL (histogram spectra) and model (thin blue curves) of methyl formate (CH_3OCOH) in the first torsional state (v_t=1) in the 3 mm window. The red line corresponds to the model of methyl formate in its ground state. A v_{LSR} of 7.5 km s^{-1} is assumed.

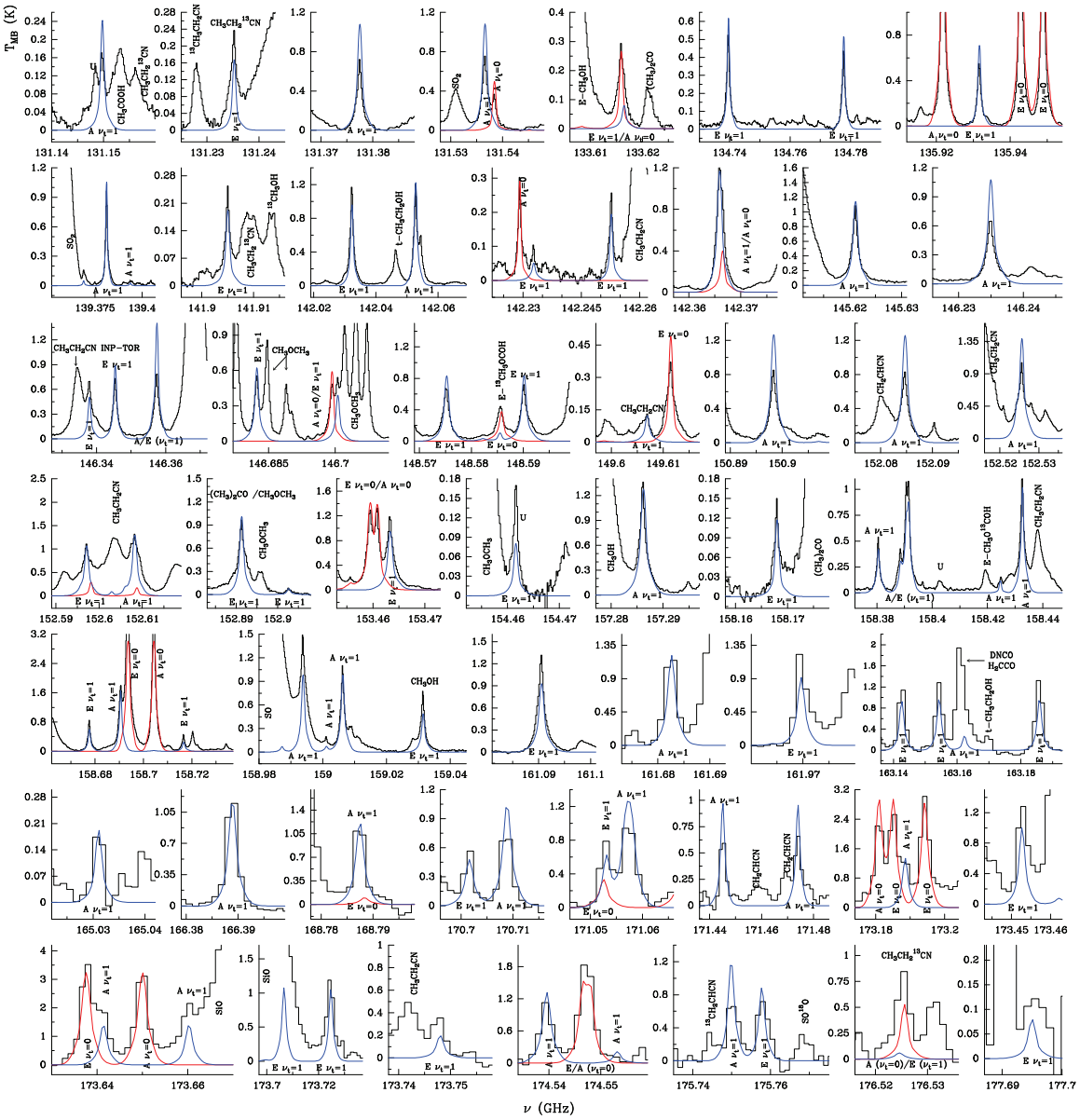

Fig. A.6. Observed lines towards Orion KL (histogram spectra) and model (thin blue curves) of methyl formate (CH_3OCOH) in the first torsional state (v_t=1) in the 2 mm window.The red line corresponds to the model of methyl formate in its ground state. A v_{LSR} of 7.5 km s^{-1} is assumed.

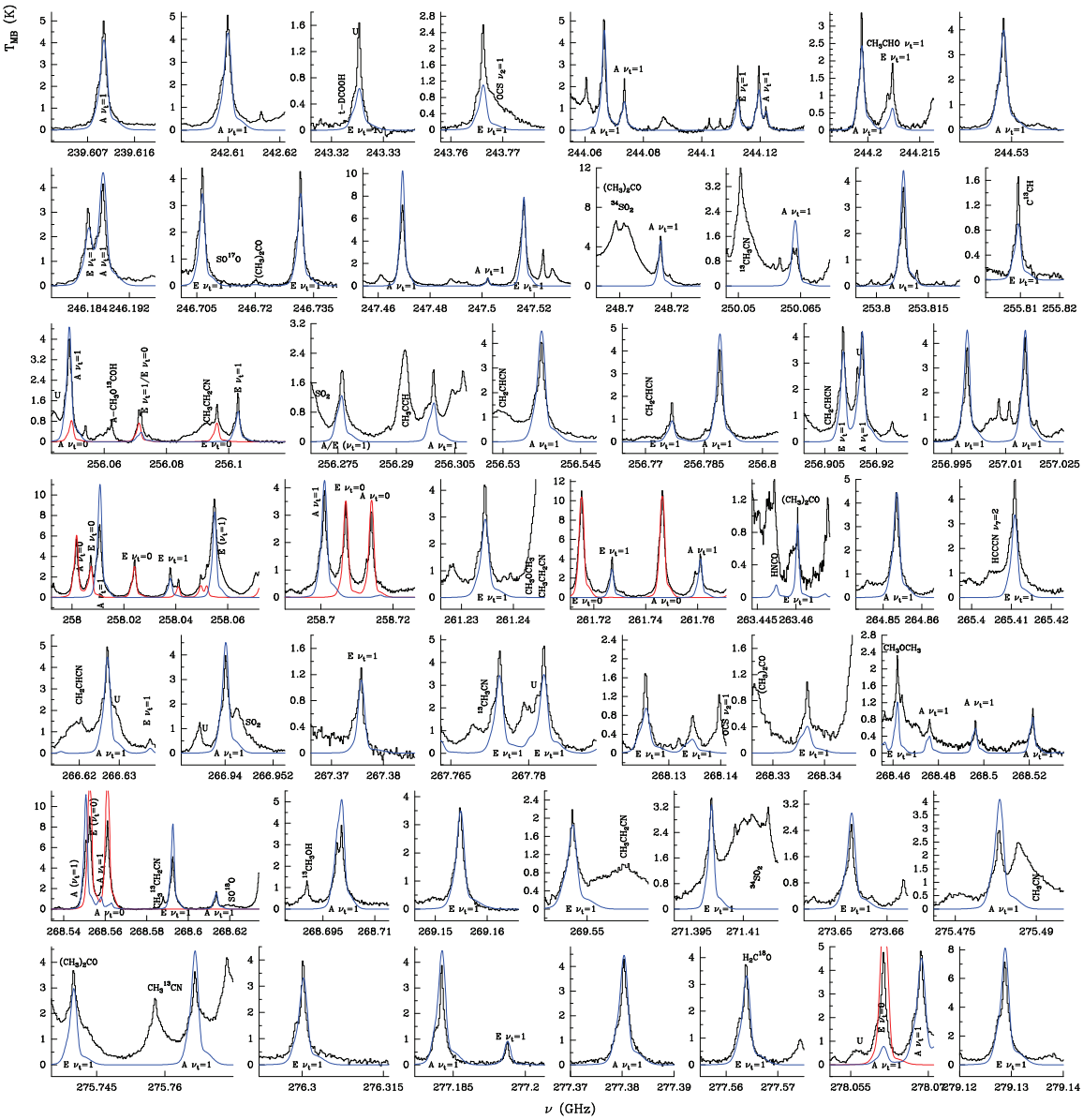

Fig. A.7. Observed lines towards Orion KL (histogram spectra) and model (thin blue curves) of methyl formate (CH_3OCOH) in the first torsional state (v_t=1) in the 1-0.9 mm window. The red line corresponds to the model of methyl formate in its ground state. A v_{LSR} of 7.5 km s^{-1} is assumed.

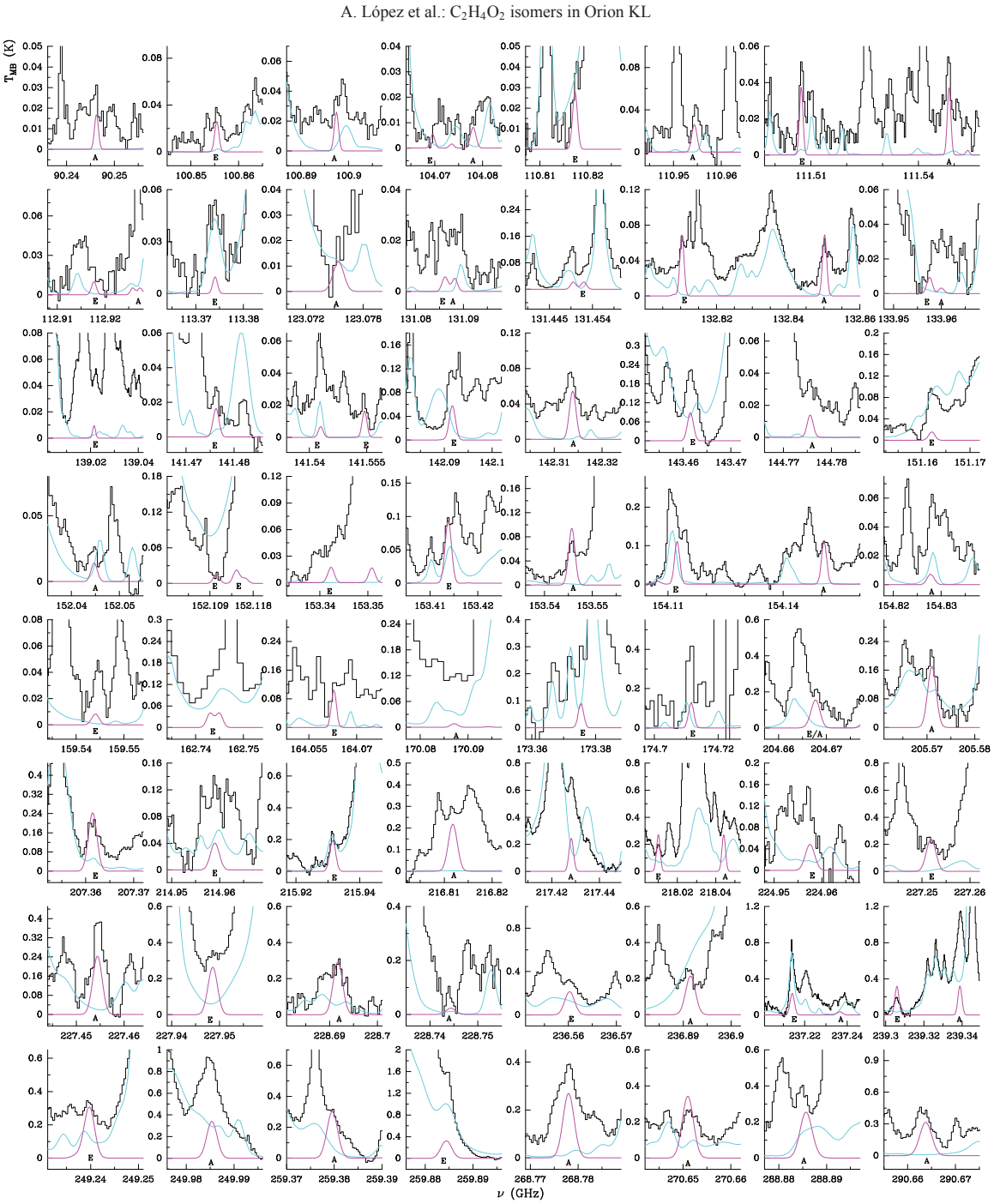

Fig. A.8. Observed lines from Orion KL (histogram spectra) and model (thin fucsia curves) of acetic acid (CH_3COOH) in the ground state between 80 and 306 GHz. The cyan line corresponds to the model of the molecules we have already studied in this survey (see Appendix C), except for the model of CH_3COOH. A v_{LSR} of 7.5 km s^{-1} is assumed.

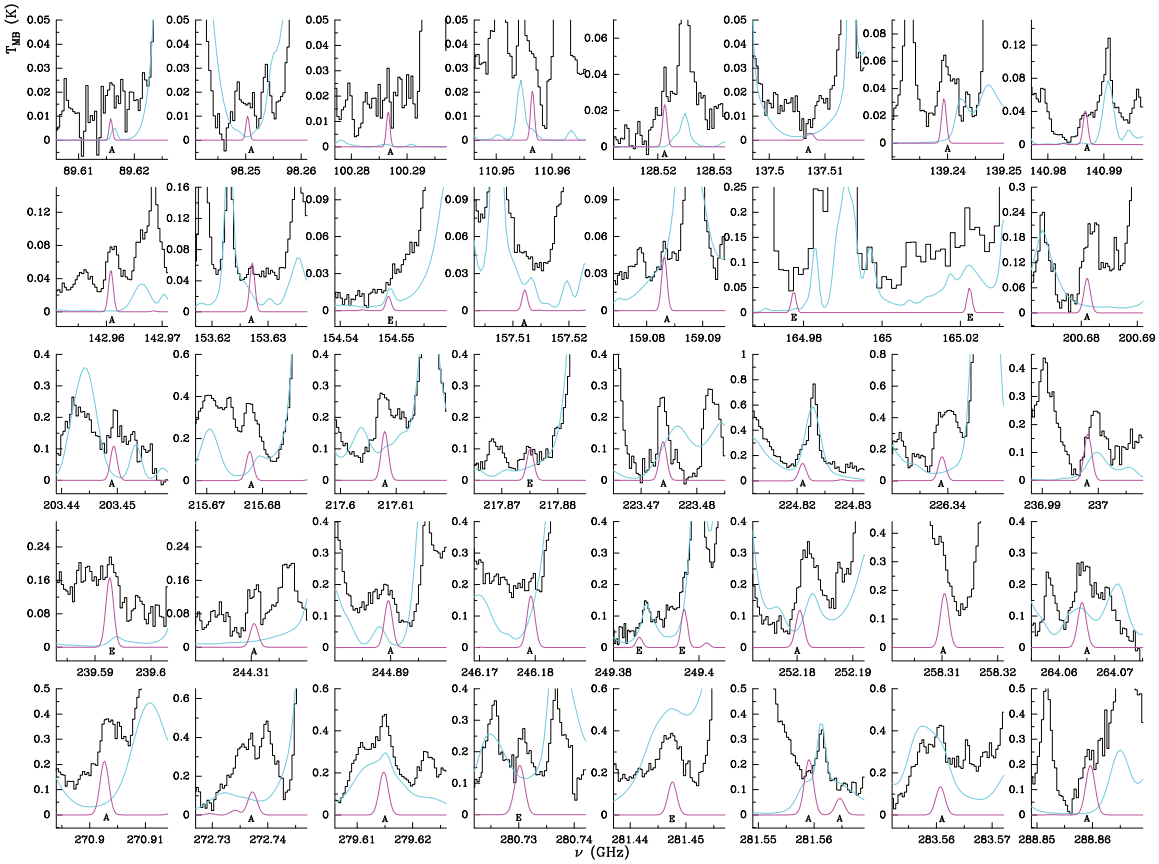

Fig. A.9. Observed lines from Orion KL (histogram spectra) and model (thin fucsia curves) of acetic acid (CH_3COOH) in the first torsional state ($v_t = 1$) between 80 and 306 GHz. The cyan line corresponds to the model of the molecules we have already studied in this survey (see Appendix C), except for the model of CH_3COOH. A v_{LSR} of 7.5 km s^{-1} is assumed.

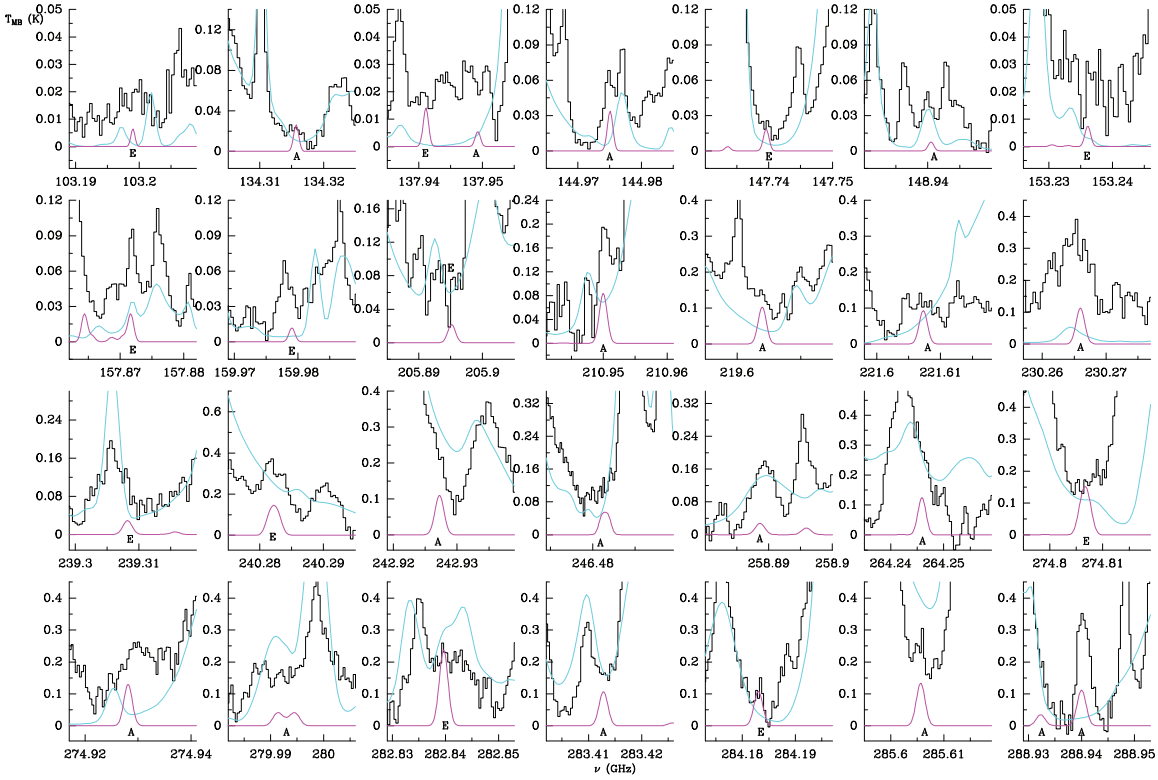

Fig. A.10. Observed lines from Orion KL (histogram spectra) and model (thin fucsia curves) of acetic acid (CH_3COOH) in the second torsional state ($v_t = 2$) between 80 and 306 GHz. The cyan line corresponds to the model of the molecules we have already studied in this survey (see Appendix C), except for the model of CH_3COOH. A v_{LSR} of 7.5 km s^{-1} is assumed.

Table B.1. Methyl formate: components and observed line parameters

Component	Coordinates	Line Parameters	v_t=0;J=6-5;K_a=6-5 *Freq.* = 225.929 GHz E_{up} = 36.3 K	v_t=0;$19_{3,16}$-$18_{3,15}$ *Freq.* = 240.035 GHz E_{up} = 122.3 K	v_t=0;J=18-17;K_a=16 *Freq.* = 220.926 GHz E_{up} = 280.7 K	v_t=1;J=20-19;K_a=14 *Freq.* = 244.074 GHz E_{up} = 442.1 K	v_t=2;$19_{2,17}$-$18_{2,16}$ *Freq.* = 227.730 GHz E_{up} = 449.4 K
N-HC	$\alpha_{2000.0} = 05^h35^m14^s.6$	v_{LSR} (km s^{-1})	3.3 / 5.6	3.5 / 5.2 / 8.7	5.4	2.3 / 5.5	2.6 / 5.7
	$\delta_{2000.0} = -05°22'30''.8$	Δv (km s^{-1})	6.5 / 2.5	5.8 / 3.1 / 1.1	4.2	3.2 / 4.2	4.4 / 3.6
		Flux (Jy/beam)	0.1 / 0.2	0.5 / 0.8 / 0.2	0.2	0.04 / 0.2	0.1 / 0.2
M-HC	$\alpha_{2000.0} = 05^h35^m14^s.5$	v_{LSR} (km s^{-1})	5.4 / 7.0 / 10.6	5.0 / 7.6	5.4 / 7.7	6.0 / 7.5	0.9 / 4.9 / 7.6
	$\delta_{2000.0} = -05°22'32''.3$	Δv (km s^{-1})	5.4 / 3.7 / 3.3	5.6 / 2.9	4.8 / 2.0	6.9 / 2.5	4.1 / 4.0 / 2.6
		Flux (Jy/beam)	0.2 / 0.3 / 0.2	1.2 / 1.4	0.2 / 0.2	0.2 / 0.4	0.1 / 0.2 / 0.4
S-HC	$\alpha_{2000.0} = 05^h35^m14^s.4$	v_{LSR} (km s^{-1})	7.3	2.3 / 6.4 / 7.4	6.2 / 7.5	6.5 / 7.6	0.5 / 6.4 / 7.6
	$\delta_{2000.0} = -05°22'34''.8$	Δv (km s^{-1})	3.1	7.3 / 3.3 / 2.6	3.2 / 2.1	2.7 / 2.1	3.3 / 2.7 / 2.1
		Flux (Jy/beam)	1.8	0.4 / 1.4 / 3.4	0.5 / 1.1	0.4 / 1.2	0.1 / 0.3 / 0.9
SE-CR	$\alpha_{2000.0} = 05^h35^m14^s.3$	v_{LSR} (km s^{-1})	7.4 / 9.9	4.9 / 7.4 / 8.7	5.3 / 7.3 / 8.3	7.4 / 7.6	7.4 / 8.6
	$\delta_{2000.0} = -05°22'37''.8$	Δv (km s^{-1})	2.2 / 2.1	4.5 / 2.0 / 3.3	6.7 / 1.7 / 3.4	1.4 / 3.3	1.8 / 4.8
		Flux (Jy/beam)	1.9 / 0.2	0.7 / 3.3 / 1.3	0.1 / 0.8 / 0.2	0.4 / 0.2	0.4 / 0.1
CR	$\alpha_{2000.0} = 05^h35^m14^s.1$	v_{LSR} (km s^{-1})	7.1 / 8.2	7.2 / 9.1	7.3 / 9.2	7.2 / 9.0	7.3 / 9.3
	$\delta_{2000.0} = -05°22'36''.9$	Δv (km s^{-1})	1.5 / 3.4	1.9 / 2.0	1.7 / 2.0	1.6 / 2.1	1.7 / 1.7
		Flux (Jy/beam)	2.0 / 1.3	4.6 / 3.1	1.6 / 0.4	1.7 / 0.4	1.2 / 0.2
N-CR	$\alpha_{2000.0} = 05^h35^m14^s.1$	v_{LSR} (km s^{-1})	4.5 / 6.8 / 8.3	5.8 / 7.6 / 8.7	6.8 / 7.0 / 8.4	6.7 / 7.0 / 8.6	5.8 / 7.5 / 8.5
	$\delta_{2000.0} = -05°22'34''.3$	Δv (km s^{-1})	2.5 / 2.1 / 2.6	3.8 / 3.0 / 4.0	5.1 / 1.8 / 1.8	3.6 / 1.5 / 2.3	6.6 / 2.8 / 4.7
		Flux (Jy/beam)	0.2 / 0.5 / 0.5	0.8 / 1.3 / 0.7	0.1 / 0.2 / 0.1	0.1 / 0.1 / 0.1	0.02 / 0.1 / 0.03
NE-CR	$\alpha_{2000.0} = 05^h35^m14^s.2$	v_{LSR} (km s^{-1})	6.5 / 8.9	8.7 / 9.0	6.8 / 9.2	7.3 / 9.3	6.5 / 9.1
	$\delta_{2000.0} = -05°22'34''.3$	Δv (km s^{-1})	1.5 / 2.9	4.6 / 1.4	2.9 / 2.9	2.9 / 2.5	1.5 / 3.8
		Flux (Jy/beam)	0.2 / 0.9	2.6 / 0.7	0.2 / 0.4	0.1 / 0.2	0.05 / 0.2
SC	$\alpha_{2000.0} = 05^h35^m14^s.2$	v_{LSR} (km s^{-1})	5.7 / 8.4	1.6 / 5.6 / 8.0	5.5 / 7.7	6.0 / 8.1	5.5 / 7.9
	$\delta_{2000.0} = -05°22'31''.1$	Δv (km s^{-1})	5.1 / 1.3	9.9 / 3.5 / 1.9	5.0 / 2.1	3.7 / 1.8	5.1 / 1.8
		Flux (Jy/beam)	0.3 / 0.1	0.5 / 1.6 / 0.8	0.3 / 0.2	0.3 / 0.2	0.3 / 0.2
S-NS	$\alpha_{2000.0} = 05^h35^m14^s.1$	v_{LSR} (km s^{-1})	7.2 / 9.0 / 11.2	7.5 / 10.1	7.0 / 9.6 / 14.5	7.6 / 9.4	7.3 / 10.1
	$\delta_{2000.0} = -05°22'29''.1$	Δv (km s^{-1})	2.3 / 3.9 / 7.5	2.6 / 5.8	2.8 / 4.9 / 8.7	2.4 / 5.7	2.6 / 7.1
		Flux (Jy/beam)	0.8 / 0.3 / 0.2	2.1 / 1.5	0.4 / 0.2 / 0.04	0.2 / 0.1	0.1 / 0.1
N-NS	$\alpha_{2000.0} = 05^h35^m14^s.1$	v_{LSR} (km s^{-1})	6.4 / 8.8	6.5 / 8.8	6.7 / 9.8 / 17.0	6.1 / 7.7	6.1 / 7.4 / 10.8
	$\delta_{2000.0} = -05°22'27''.3$	Δv (km s^{-1})	2.5 / 4.3	2.7 / 5.0	2.9 / 3.2 / 5.0	1.7 / 4.7	1.8 / 3.8 / 4.8
		Flux (Jy/beam)	0.9 / 0.4	2.1 / 1.7	0.5 / 0.1 / 0.03	0.2 / 0.3	0.1 / 0.2 / 0.05

Appendix C: Total model

In Figs. A.8−A.10 and 10 a model with all already studied species in this survey is included (cyan line). The list of considered molecules in this model and published works containing the detailed analysis for each species are shown in Table C.1:

Table C.1. Species included in the total model

Reference	Studied species	Notes
Tercero et al. (2010)†	OCS, CS, H_2CS, HCS^+, CCS, CCCS	(b) (c)
Tercero et al. (2011)†	SiO, SiS	(b) (c)
Daly et al. (2013)†	CH_3CH_2CN	(a) (b) (c)
Esplugues et al. (2013a)†	SO, SO_2	(b) (c)
Esplugues et al. (2013b)†	HC_3N, HC_5N	(b) (c) (d)
López et al. (2014)†	CH_2CHCN	(a) (b) (c)
Marcelino et al. in prep.†	HCN, HNC, HCO^+	(b) (c) (d) (e)
Demyk et al. (2007)	^{13}C-CH_3CH_2CN	(a) (c)
Margulès et al. (2009)	$CH_3CH_2C^{15}N$, CH_3CHDCN, and CH_2DCH_2CN	(a) (c)
Carvajal et al. (2009)	^{13}C-$HCOOCH_3$	(a) (c)
Marcelino et al. (2009)	HNCO	(c)
Margulés et al. (2010)	$DCOOCH_3$	(a) (c)
Tercero et al. (2012)	^{18}O-$HCOOCH_3$	(a) (c)
Motiyenko et al. (2012)	NH_2CHO, NH_2CHO v_{12}=1	(a) (c)
Coudert et al. (2013)	$HCOOCH_2D$	(a) (c)
Tercero et al. (2013)	CH_3COOCH_3, CH_3CH_2OCOH	(a) (c)
Bell et al. (2014)	CH_3CN	(b) (c)
Kolesniková et al. (2014)	CH_3CH_2SH, CH_3SH, CH_3OH, $^{13}CH_3OH$, CH_3CH_2OH	(a) (c)
Haykal et al. (2014)	^{13}C-$HCOOCH_3$ v_t=1	(a) (c)
Tercero et al. (2015)	$CH_3CH_2OCH_3$	(c) (e)
This work	$HCOOCH_3$ v_t=0,1,2, CH_3COOH v_t=0,1,2, CH_2OHCHO	(c) (e)
In progress	CH_2OCH_2, AG-$OHCH_2CH_2OH$	(c)
In progress	^{13}C-CH_3CN, CH_3CN v_8=1	(c)
In progress	CH_3OCH_3, CH_3COCH_3, $H_2{}^{13}CO$	(c)

†: In these analysis we have include all isotopologues and vibrational excited states of the molecule. (a) - Papers in collaboration with spectroscopists. (b) - Papers dividing the analysis of the Orion's surveys in different families of molecules. (c) - Papers based on the IRAM 30m 1D-survey and/or 2D-survey. (d) - Papers based on Herschel/HIFI data. (e) - Papers based on ALMA SV data.

5.6 Resultados globales

Como hemos visto, uno de los resultados más relevantes de los artículos que hemos presentado, radica en la primera detección de nuevas moléculas y de varios estados excitados vibracionalmente, gracias al trabajo de colaboración con expertos en espectroscopía molecular.

De este modo, respecto a las moléculas que contienen nitrógeno, CH_3CH_2CN y CH_2CHCN, detectamos, por primera en el espacio tres modos vibracionales: CH_3CH_2CN v_{12}=1, CH_3CH_2CN v_{20}=1 y CH_2CHCN v_{10}=1/(v_{11}=1, v_{15}=1).

En conjunto, hemos identificado más de 3000 líneas en el espectro observado pertenecientes a especies de ambas moléculas.

Por otro lado, respecto a las moléculas que contienen oxígeno, hemos estudiado tres isómeros funcionales que siguen la fórmula $C_2H_4O_2$: formiato de metilo (CH_3OCOH); ácido acético (CH_3COOH) y glicolaldehído (CH_2OHCOH). Las moléculas que poseen un rotor interno del grupo funcional $-CH_3$ (metilo) poseen un espectro rotacional muy denso, lo que aumenta la complejidad del análisis. Esto unido a la gran abundancia del formiato de metilo se traduce en que hemos detectado más de 6000 líneas en el barrido espectral de Orión-KL pertenecientes a diferentes especies de esta molécula. La emisión de líneas rotacionales del CH_3OCOH parece proceder principalmente de la nube denominada *compact ridge*. Sin embargo, las líneas de sus isómeros (CH_3COOH y CH_2OHCOH), que son mucho menos abundantes, emergen de una posición diferente de la nube, el *hot core*.

Otro grupo de moléculas con oxígeno que hemos analizado, es el de la molécula de acetato de metilo (CH_3OCOCH_3) y su isómero, el formiato de etilo (CH_3CH_2OCOH). El CH_3OCOCH_3 ha sido detectado por primera vez en el espacio en el presente trabajo, al igual que su isómero, el confórmero *gauche*-CH_3CH_2OCOH. Las líneas de emisión de estas moléculas emergen principalmente de la componente de la nube denominada *compact ridge*, a una temperatura de 150 K.

Además, la compleja molécula interestelar de 12 átomos, el *trans*-etil metil éter ($CH_3CH_2OCH_3$), la hemos detectado tentativamente en nuestra fuente de Orión-KL (Tercero et al. 2015). Previamente, Carroll et al. 2015 (2015) proporcionaron un límite superior a su densidad de columna en otra región de formación de estrellas masivas, Sgr B2, cercana al centro galáctico. Las líneas identificadas de esta molécula provienen de la componente de la nube de Orión-KL *compact ridge* y obtenemos una temperatura rotacional de 100 K. Sin embargo, su isómero, el *gauche-trans-n*-propanol (gt-n-$CH_3CH_2CH_2OH$) presenta el máximo de emisión en el *hot core*. La emisión de esta especie solo detectada tentativamente, coincide espacialmente con la de su posible precursor, etanol (CH_3CH_2OH).

5.6.1 Identificación de líneas

La cantidad de líneas moleculares identificadas en nuestra fuente astrofísica ha permitido reducir considerablemente el número de líneas sin identificar en el barrido espectral de Orión-KL de Tercero et al. (2010). En total, 9 600 líneas espectrales han sido analizadas en los trabajos que hemos presentado. De ellas, cerca de 4000 eran líneas no identificadas previamente (Tabla 5.1). Hasta la fecha, en nuestro barrido espectral hemos detectado unas 50 moléculas diferentes, cerca de 200 especies considerando los distintos modos vibracionales e isotopólogos.

Tabla 5.1: Análisis de las moléculas con N y O que comprenden la tesis.

Molécula (emisión dominante)	datos	líneas detectadas	nueva deteción
CH_3CH_2CN (HC)	IRAM-30 m	>2 000 líneas*,**	v_{12}=1††, v_{20}=1††
CH_2CHCN (HC)	IRAM-30 m	>1 100 líneas*,**	v_{11}=2,3†, (v_{10}=1)⇔(v_{11}=1,v_{15}=1)††
CH_3OCOH (CR)			AA†
CH_3COOH (M-HC)	IRAM-30 m, ALMA SV	>6 000 líneas*,**	AA v_t=1,2††
CH_2OHCHO (M-HC)			GLY†
CH_3OCOCH_3 (CR)	IRAM-30 m	>300 líneas	††-MAc
CH_3CH_2OCOH (CR)			*trans*-EF†, *gauche*-EF††
$CH_3CH_2OCH_3$ (CR)	IRAM-30 m, ALMA SV	≈200 líneas	trans-EME (tentativa)††

Nota. Esta tabla muestra las diferentes moléculas que hemos analizado en este trabajo, la región de la nube dominante de la que proviene la emisión molecular, los datos espectrales de los que dispusimos, la cantidad de líneas detectadas incluyendo los estados excitados e isotopólogos en el caso de considerarlos, así como las especies detectadas por primera vez en Orión-KL y/o en el espacio. ∗incluido los estados excitados;∗∗incluido los isotopólogos; †detectada en Orión-KL; ††detectada en el espacio; AA=Acetic Acid; GLY=Glycolaldehyde; MAc=Methyl Acetate; EF=Ethyl Formate; EME=Ethyl Methyl Ether; CR=*Compact Ridge*; HC=*Hot Core*; M-HC=*mid Hot Core*.

A modo informativo, en la Tabla 5.2 mostramos otras fuentes en las que han sido detectadas las especies estudiadas en trabajo.

5.6.2 Sumario de los resultados

En esta sección vamos a ordenar los resultados de estos artículos en base a diferentes criterios de manera que pueda servir de base para estudios comparativos entre la emisión de las distintas especies en la fuente.

En primer lugar, en la Tabla 5.3 encontramos las densidades de columna de la componente dominante para la emisión de las moléculas estudiadas en esta tesis en el nivel fundamental. En la Tabla 5.4 se muestran estos mismos resultados para todas las especies que hemos visto en este trabajo (incluyendo los niveles vibracionalmente excitados y diferentes isotopólogos). Por otro lado, en la Tabla 5.5 los valores de las densidades de columna de cada molécula se presentan en función de determinados rangos de temperatura rotacional. Debido a las múltiples subcomponentes de la nube, para algunos casos (por ejemplo para el formiato de metilo) se han agrupado varias componentes en las dos componentes principales de la nube que hemos estudiado a lo largo de esta tesis, *hot core* y *compact ridge*. Así, diferenciamos entre: HC(T≥250 K), HC(150<T<250 K), HC(70<T<150 K), HC(T≤70 K), CR(T≥250 K), CR(150<T<250 K), CR(70<T<150 K), y CR(T≤70 K).

Tabla 5.2: Moléculas de la tesis detectadas en otras fuentes.

CH_3CH_2CN	Orión-KL (Johnson et al. 1977), SgrB2 (Miao and Snyder 1997), G34.3+0.2 (Mehringer and Snyder 1996), TMC-1 (Minh and Irvine 1991)*, L134N (Minh and Irvine 1991), IRAS 16293-2422 (Cazaux et al. 2003), NGC7129 FIRS 2 (Fuente et al. 2014)
v_{13}=1/v_{21}=1	Orión-KL (Daly et al. 2013), SgrB2 (Mehringer et al. 2004), NGC7129 FIRS 2 (Fuente et al. 2014)
v_{12}=1	Orión-KL (Daly et al. 2013)
v_{20}=1	Orión-KL (Daly et al. 2013)
^{13}C	Orión-KL (Demyk et al. 2007), SgrB2 (Margulès et al. 2016)
^{15}N	Orión-KL (Margulès et al. 2009), SgrB2 (Belloche et al. 2013)
CH_2CHCN	Orión-KL (Blake et al. 1987), SgrB2 (Gardner and Winnewisser 1975), G34.3+0.2 (Mehringer and Snyder 1996), TMC-1 (Matthews and Sears 1983), IRC+10216 (Agúndez et al. 2008), NGC7129 FIRS 2 (Fuente et al. 2014)
v_{11}=1	Orión-KL (Schilke et al. 1997), SgrB2 (Nummelin and Bergman 1999), NGC7129 FIRS 2 (Fuente et al. 2014)
v_{11}=2	Orión-KL (López et al. 2014), SgrB2 (Nummelin and Bergman 1999)
v_{11}=3	Orión-KL (López et al. 2014), SgrB2 (Belloche et al. 2013)
v_{15}=1	Orión-KL (Schilke et al. 1997), SgrB2 (Nummelin and Bergman 1999)
v_{10}=1/(v_{11}=1,v_{15}=1)	Orión-KL (López et al. 2014)
^{13}C	Orión-KL (López et al. 2014), SgrB2 (Müller et al. 2008)
CH_3OCOH	Orión-KL (Churchwell et al. 1980), SgrB2 (Brown et al. 1975), W51 (Churchwell et al. 1980), G34.3+0.15 (MacDonald et al. 1996), IRAS 16293-2422 (Jørgensen et al. 2016), NGC7129 FIRS 2 (Fuente et al. 2014)
v_t=1	Orión-KL (Kobayashi et al. 2007), W51e2 (Demyk et al. 2008), NGC7129 FIRS 2 (Fuente et al. 2014)
v_t=2	Orión-KL (Takano et al. 2012)
CH_3COOH	Orión-KL (López *in prep.*), SgrB2 (Mehringer et al. 1997), W51e2 (Remijan et al. 2002), G34.3+0.15 (Remijan et al. 2003), G19.61-0.23 (Shiao et al. 2010)
v_t=1,2	Orión-KL (López *in prep.*)
CH_2OHCHO	Orión-KL (López *in prep.*), SgrB2 (Hollis et al. 2000), G31.41+0.31 (Beltrán et al. 2009), IRAS 16293-2422 (Jørgensen et al. 2012), NGC1333 IRAS2A (Coutens et al. 2015), NGC7129 FIRS2 (Fuente et al. 2014)
t-$CH_3CH_2OCH_3$	Orión-KL (Tercero et al. 2015)
gt-n-$CH_3CH_2CH_2OH$	Orión-KL (Tercero et al. 2015)
CH_3OCOCH_3	Orión-KL (Tercero et al. 2013)
CH_3CH_2OCOH	Orión-KL (Belloche et al. 2009)

Nota. Esta tabla muestra las diferentes moléculas que hemos analizado en este trabajo y las fuentes en las que han sido detectadas por primera vez, incluyendo los estados excitados e isotopólogos en el caso de las moléculas que contienen nitrógeno. ∗*no detectado en TMC-1 (se aporta un upper limit)*

Tabla 5.3: Densidad de comlumna y emisión de las moléculas con N y O que comprenden esta tesis.

Molécula	N(cm^{-2})*	T(K)	región de emisión dominante	d_{sou}(")/offset (")†
CH_3CH_2CN	$(6\pm2)\times10^{16}$	275	HC	4/5
CH_2CHCN	$(3.0\pm0.9)\times10^{15}$	320	HC	5/2
CH_3OCOH	$(4.0\pm1.2)\times10^{17}$	60	SE-CR	4/9
	$(1.8\pm0.5)\times10^{17}$	250	CR	2/9
CH_3COOH	$(3.5\pm1.1)\times10^{15}$	110	M-HC	2/1.5
CH_2OHCHO	$(5\pm2)\times10^{15}$	110	M-HC	2/1.5
CH_3OCOCH_3	$(4.0\pm0.5)\times10^{15}$	150	CR	15/7
CH_3CH_2OCOH	$(4.5\pm1.0)\times10^{14}$	150	CR	15/7
$CH_3CH_2OCH_3$	$(9\pm3)\times10^{15}$	100	CR	3/0

Nota. Esta tabla muestra la densidad de columna en la componente principal de emisión de las diferentes moléculas (en su estado fundamental) que hemos analizado en este trabajo, así como la temperatura rotacional obtenido y el tamaño de la fuente considerado (d_{sou}). El $offset$ es la distancia de la componente respecto a la posición de apuntado (IRc2). $*$correspondiente a la región de emisión dominante; †respecto a la posición de IRc2; SE-CR=*South-East Compact Ridge*; CR=*Compact Ridge*; HC=*Hot Core*; M-HC=*mid Hot Core*.

TABLA 5.4: DENSIDAD DE COLUMNA DE TODAS LAS MOLÉCULAS CON N Y O QUE COMPRENDEN LA TESIS.

Molécula	N(cm^{-2})	T(K)	región de emisión dominante	offset (")
CH_3CH_2CN				
v=0 (g.s.)	6×10^{16}	275	HC	5
	8×10^{15}	110	HC	5
	3×10^{15}	65	HC	5
(v_{13}=1)⇔(v_{21}=1)	8×10^{15}	275	HC	5
	1.1×10^{15}	110	HC	5
	4×10^{14}	65	HC	5
v_{20}=1	3×10^{15}	275	HC	5
	4×10^{14}	110	HC	5
	1.7×10^{14}	65	HC	5
v_{12}=1	1.2×10^{15}	275	HC	5
	1.6×10^{14}	110	HC	5
	6×10^{13}	65	HC	5
$^{13}C_1$	7×10^{14}	275	HC	5
	1.9×10^{14}	110	HC	5
	7×10^{13}	65	HC	5
$^{13}C_2$	7×10^{14}	275	HC	5
	1.9×10^{14}	110	HC	5
	7×10^{13}	65	HC	5
$^{13}C_3$	7×10^{14}	275	HC	5
	1.9×10^{14}	110	HC	5
	7×10^{13}	65	HC	5
^{15}N	2×10^{14}	275	HC	5
	5×10^{13}	110	HC	5
	1.7×10^{13}	65	HC	5
A-D_1	$\leq6\times10^{14}$	275	HC	5
	$\leq2\times10^{14}$	110	HC	5
	$\leq6\times10^{13}$	65	HC	5
S-D_1	$\leq6\times10^{14}$	275	HC	5
	$\leq1\times10^{14}$	110	HC	5
	$\leq6\times10^{13}$	65	HC	5
D_2	$\leq6\times10^{14}$	275	HC	5
	$\leq2\times10^{14}$	110	HC	5
	$\leq6\times10^{13}$	65	HC	5
CH_2CHCN				
v=0 (g.s.)	3×10^{15}	320	HC	2
	1×10^{15}	100	HC	2
	9×10^{14}	200	HC	0
	1.3×10^{15}	90	HC	0
v_{11}=1	9×10^{14}	320	HC	2
	2.5×10^{14}	100	HC	2
v_{11}=2	2×10^{14}	320	HC	2

continued.

Molécula	N(cm^{-2})	T(K)	región de emisión dominante	offset (")
	5×10^{13}	100	HC	2
v_{11}=3	$\leq2\times10^{14}$	320	HC	2
	$\leq5\times10^{13}$	100	HC	2
v_{15}=1	4×10^{14}	320	HC	2
	1×10^{14}	100	HC	2
(v_{10}=1)⇔(v_{11}=1,v_{15}=1)	4×10^{14}	320	HC	2
	8×10^{13}	100	HC	2
$^{13}C_1$	4×10^{14}	320	HC	2
	5×10^{13}	100	HC	2
$^{13}C_2$	4×10^{14}	320	HC	2
	5×10^{13}	100	HC	2
$^{13}C_3$	4×10^{14}	320	HC	2
	5×10^{13}	100	HC	2
HCD_1	$\leq4\times10^{14}$	320	HC	2
	$\leq4\times10^{13}$	100	HC	2
D_1CH	$\leq4\times10^{14}$	320	HC	2
	$\leq4\times10^{13}$	100	HC	2
D_2	$\leq3\times10^{14}$	320	HC	2
	$\leq3\times10^{13}$	100	HC	2
CH_3OCOH				
v_t=0 (g.s.)	1.8×10^{17}	250	M-HC	2
	4×10^{17}	60	SE-CR	9
	3×10^{17}	150	M-NS	5.5
v_t=1	3×10^{16}	250	M-HC	2
	4×10^{16}	60	SE-CR	9
	4×10^{16}	150	M-NS	5.5
v_t=2	9×10^{15}	250	M-HC	2
	9×10^{15}	60	SE-CR	9
	1.9×10^{16}	150	M-NS	5.5
CH_3COOH				
v_t=0 (g.s.)	5×10^{15}	110	M-HC	1.5
v_t=1	4×10^{15}	110	M-HC	1.5
v_t=2	4×10^{15}	110	M-HC	1.5
CH_2OHCHO	3.5×10^{15}	110	M-HC	1.5
CH_3CN(*)				
v=0 (g.s.)	1×10^{16}	300	h-CR	3
	6×10^{15}	180	o-HC	3
v_8=1	4×10^{14}	300	h-CR	3
	5.4×10^{14}	400	d-HC	3
CH_3NC	6×10^{13}	265	averaged(HC/CR/plateau)	3
CH_2CHCN	$\leq3\times10^{14}$	320	HC	2
	$\leq5\times10^{13}$	100	HC	2
HCCCN(*)				

continued.

Molécula	N(cm^{-2})	T(K)	región de emisión dominante	offset (")
v=0 (g.s.)	2×10^{14}	110	CR	7
	1×10^{15}	220	o-HC	2
HCCNC	2×10^{12}	110	CR	7
	1×10^{13}	220	o-HC	2
HNCCC	1×10^{11}	110	CR	7
	8×10^{12}	220	o-HC	2
NH_2CN	$\leq3\times10^{13}$	200	HC	2
NH_2NC	$\leq5\times10^{13}$	200	HC	2
t-$CH_3CH_2OCH_3$	9×10^{15}	100	CR	3
gt-$CH_3CH_2CH_2OH$	$\leq2\times10^{14}$	100	CR	3
CH_3OCOCH_3				
(AA, EA, AE, E_1, E_2)	4.2×10^{15}	150	CR	7
CH_3CH_2OCOH				
gauche-	4.5×10^{14}	150	CR	7
trans-	4.5×10^{14}	150	CR	7

Nota. Esta tabla muestra las diferentes moléculas que hemos analizado en este trabajo, las densidades de columna y las temperaturas rotacionales obtenidas en el análisiss, la región de la nube dominante de la que proviene la emisión molecular, y el offset de cada componente con respecto a la posición de apuntado. $*$debido a la gran cantidad de componentes de la nube sólo tenemos en cuenta la región de la nube dominante de la que proviene la emisión molecular (*hot core* y *compact ridge*); CR=*Compact Ridge*; HC=*Hot Core*; M-HC=*mid Hot Core*; SE-CR=*South-East Compact Ridge*; M-NS=*mid north-south clump*; h-CR=*hot Compact Ridge*; o-HC=*outer Hot Core*; d-HC=*dense Hot Core*.

TABLA 5.5: DENSIDAD DE COLUMNA SEGÚN LA TEMPERATURA DE LAS COMPONENTES DE LA NUBE DE TODAS LAS MOLÉCULAS CON N Y O QUE COMPRENDEN LA TESIS.

Molécula/región	HC (T≥250)	HC (150>T>250)	HC (70>T>150)	HC (T≤70)	CR (T≥250)	CR (150>T>250)	CR (70>T>150)	CR (T≤70)
EtCN(g.s.)	6×10^{16}		8×10^{15}	3×10^{15}				
EtCN-v_{13}/v_{21}	8×10^{15}		1.1×10^{15}	4×10^{14}				
EtCN-v_{20}=1	3×10^{15}		4×10^{14}	1.7×10^{14}				
EtCN-v_{12}=1	1.2×10^{15}		1.6×10^{14}	6×10^{13}				
EtCN-$^{13}C_1$	7×10^{14}		1.9×10^{14}	7×10^{13}				
EtCN-$^{13}C_2$	7×10^{14}		1.9×10^{14}	7×10^{13}				
EtCN-$^{13}C_3$	7×10^{14}		1.9×10^{14}	7×10^{13}				
EtCN-^{15}N	2×10^{14}		5×10^{13}	1.7×10^{13}				
EtCN-A-D_1	6×10^{14}		2×10^{14}	6×10^{13}				
EtCN-S-D_1	6×10^{14}		1×10^{14}	6×10^{13}				
EtCN-D_2	6×10^{14}		2×10^{14}	6×10^{13}				
VyCN(g.s.)	3×10^{15}	9×10^{14}	1×10^{15}	1.3×10^{15}				
VyCN-v_{11}=1	9×10^{14}		2.5×10^{14}					
VyCN-v_{11}=2	2×10^{14}		5×10^{13}					
VyCN-v_{11}=3	2×10^{14}		5×10^{13}					
VyCN-v_{15}=1	4×10^{14}		1×10^{14}					
VyCN-$v_{10}/v_{11}v_{15}$	4×10^{14}		8×10^{13}					
VyCN-$^{13}C_1$	4×10^{14}		5×10^{13}					
VyCN-$^{13}C_2$	4×10^{14}		5×10^{13}					
VyCN-$^{13}C_3$	4×10^{14}		5×10^{13}					
VyCN-^{15}N	1×10^{14}		2×10^{13}					
VyCN-HCD_1	4×10^{14}		4×10^{13}					
VyCN-D_1CH	4×10^{14}		4×10^{13}					
VyCN-D_2	3×10^{14}		3×10^{13}					
MF(g.s.)					1.8×10^{17}	3×10^{17}		4×10^{17}
MF-v_t=1					3×10^{16}	4×10^{16}		4×10^{16}
MF-v_t=2					9×10^{15}	1.9×10^{16}		9×10^{15}
AA(g.s.)			5×10^{15}					
AA-v_t=1			4×10^{15}					
AA-v_t=2			4×10^{15}					
GLY			3.5×10^{15}					
MeCN(g.s.)∗		2×10^{16}			1×10^{16}			
MeCN-v_8=1∗	5.4×10^{14}				4×10^{14}			
MeNC	6×10^{13}				6×10^{13}			
VyNC	3×10^{14}		5×10^{13}					
EtNC		2×10^{14}						
HCCCN(g.s.)∗		1×10^{15}					2×10^{14}	
HCCNC		1×10^{13}					2×10^{12}	
HNCCC		8×10^{12}					1×10^{14}	
CNA		3×10^{13}						

continued.

Molécula/región	HC (T≥250)	HC (150<T<250)	HC (70<T<150)	HC (T≤70)	CR (T≥250)	CR (150<T<250)	CR (70<T<150)	CR (T≤70)
NCA		5×10^{13}						
t-EME							9×10^{15}	
gt-propOH							2×10^{14}	
AcMe						4.2×10^{15}		
g-EF						4.5×10^{14}		
t-EF						4.5×10^{14}		

Nota. Esta tabla muestra las diferentes moléculas que hemos analizado en este trabajo, las densidades de columna de cada componente distribuidas según determinados rangos de temperaturas rotacionales. Debido a las múltiples subcomponentes de la nube, en algunos casos se han agrupado varias componentes en las dos componentes principales, *hot core* y *compact ridge* (∗). CR=*Compact Ridge*; HC=*Hot Core*; EtCN=cianuro de etilo; VyCN=cianuro de vinilo; MF=formiato de metilo; AA=Ácido acético; GLY=clicolaldehído; MeNC=isocianuro de metilo; VyNC=isocianuro de vinilo; EtNC=isocianuro de etilo; CNA=cianamida; NCA=isocianamida; t-EME=trans-etil metil éter; gt-PropOH=gauche-trans-Propanol;AcMe=Acetato de metilo; g(t)-EF=gauche(trans)-formiato de etilo.

5.6.3 Moléculas prebióticas

Como ya hemos visto a lo largo de la tesis, las moléculas de nuestro estudio son de naturaleza orgánica. Sus grupos funcionales guardan especial relación con muchas de las moléculas prebióticas como las proteinas. Veamos cómo puede ser esta conexión:

Las moléculas que contienen el grupo −CN (ciano), son de especial importancia, ya que los enlaces carbono-nitrógeno son precursores potenciales de aminoácidos ($NH_2CH(R)COOH$), proteínas, etc. (Balucani 2009). Por otro lado, las moléculas que contienen el grupo −COOH (carboxilo) también pueden intervenir en la formación de aminoácidos y azúcares (Balucani 2009).

El cianuro de etilo o propionitrilo (CH_3CH_2CN) podría ser un intermedio en la formación de aminoácidos, por ejemplo al poder actuar como precursor del 2-aminopropionitrilo ($CH_3CH(NH_2)CN$) y mediante reacciones de hidrogenación, del aminoácido alanina ($NH_2CH(CH_3)COOH$), uno de los 20 aminoácidos que componen las proteínas (Møllendal et al. 2012). Asimismo, el cianuro de vinilo o acrilonitrilo (CH_2CHCN) es también un posible precursor de este aminoácido.

En realción a los isómeros de C_2H_4O, el formiato de metilo (CH_3OCOH) podría tener relación de manera indirecta con moléculas de interés biológico, como el dimetil éter (CH_3OCH_3) debido poseer un precursor común, el metanol (CH_3OH). El ácido acético (CH_3COOH) es un posible precursor de la glicina (NH_2CH_2COOH), otro de los 20 aminácidos que constituyen las proteínas (Bennett and Kaiser 2007). El glicolaldehído (CH_2OHCOH), el azúcar más simple, puede estar implicado en la síntesis de la Ribosa ($C_5H_{10}O_5$), un azúcar implicado en la producción de ARN (Bennett and Kaiser 2007).

Los componentes primigenios que se han detectado hasta el momento en cuerpos del Sistema Solar (especialmente en los cometas) nos han revelado su naturaleza rica en agua y moléculas orgánicas, las cuales parecen tener un vínculo común con el material químico procesado en las nubes moleculares (Ehrenfreund and Charnley 2000; Irvine 1998; Whipple 1950,1951; Cronin and Chang 1993).

Recientemente se han descubierto moléculas orgánicas complejas en el disco proto-planetario de un sistema estelar jóven (Öberg et al. 2015) demostrando que las COMs podrían sobrevivir y desarrollarse en el ambiente altamente energético de un sistema planetario en formación (donde los choques y radiación podrían romper fácilmente los enlaces químicos). Estos autores han observado cianuros como CH_3CN, HC_3N, y HCN, en el disco de una estrella Herbig de tipo espectral Ae[4] de la región de formación estelar de Tauro. Sugieren que los cometas podrían estar actuando como preservadores de moléculas orgánicas en los sistemas planetarios. De hecho, ciertos experimentos de laboratorio han respaldado la producción de azúcares y aminoácidos a partir de cianuros orgánicos en análogos de granos interestelares (Caro et al. 2002, Öberg et al. 2009). Por lo que es probable que las moléculas orgánicas formadas en la nebulosa queden resguardadas en cometas y/o en el manto de hielo del polvo interestelar, pudiendo ser transportadas a entornos donde prospere la química prebiótica.

[4]Es una estrella jóven, embebida en la nube de gas y polvo, que aún no ha entrado en la secuencia principal.

5.6.4 Trabajos publicados

En esta sección presento las referencias de todos los trabajos en los que he participado durante mi periodo de estudiante de doctorado.

- B. Tercero, I. Kleiner, J. Cernicharo, H. V. L. Nguyen, A. López, G. M. Muñoz Caro, ”Discovery of Methyl Acetate and Gauche Ethyl Formate in Orion”, ApJL, 770, L13, 2013. doi:10.1088/2041-8205/770/1/L13

- A. M. Daly, C. Bermúdez, A. López, B. Tercero, J. Pearson, N. Marcelino, J. L. Alonso and J. Cernicharo, ”Laboratory Characterization and Astrophysical Detection of Vibrationally Excited States of Ethyl Cyanide”, ApJ, 768, 81, 2013. doi:10.1088/0004-637X/768/1/81

- A. López, B. Tercero, Z. Kisiel , A. M. Daly, C. Bermúdez, H. Calcutt, N. Marcelino, S. Viti, B.J. Drouin, I.R. Medvedev, C. F. Neese, L. Pszczolkowski, J. L. Alonso, and J. Cernicharo, ”Laboratory Characterization and Astrophysical Detection of Vibrationally Excited States of Vinyl Cyanide in Orion-KL.”, A&A, 572, A44, 2014. doi: 10.1051/0004-6361/201423622

-B. Tercero, J. Cernicharo, A. López, N. Brouillet, L. Kolesniková, R. A. Motiyenko, L. Margulès, J. L. Alonso, J. C. Guillemin, ”Searching for Trans Ethyl Methyl Ether in Orion KL”, A&A, 582, L1, 2015. doi:10.1051/0004-6361/201526255

-A. López, B. Tercero, J. Cernicharo, et al., ”$C_2H_4O_2$ isomers in Orion KL: Methyl formate, Acetic acid, and Glycolaldehyde. An overview of ALMA and IRAM 30m.”, in preparation (2017)

. . . . . .

Otras publicaciones (no incluidas en esa tesis):

- I. Haykal , M. Carvajal , B. Tercero , I. Kleiner , A. López , J. Cernicharo , R. A. Motiyenko , T. R. Huet , J.C. Guillemin , and L. Margulés, ”THz spectroscopy and first ISM detection of excited torsional states of ^{13}C-methyl formate”, A&A, 568A, 58H, 2014, doi: 10.1051/0004-6361/201322937

- A. Fuente, J.Cernicharo, P. Caselli, C. McCoey, D. Johnstone, M. Fich, T. van Kempen, A. Palau, U. Yildiz, B. Tercero, A. López, ”The hot core towards the intermediate mass protostar NGC 7129 FIRS 2. Chemical similarities with Orion KL”, A&A, 568A, 65F, 2014, doi: 10.1051/0004-6361/201323074

- J. Cernicharo, Z. Kisiel, B. Tercero, L. Kolesniková, I. R. Medvedev, A. López, S. Fortman, M. Winnewisser, F. C. de Lucia, J. L. Alonso, and J.-C. Guillemin, ”A rigorous detection of interstellar CH_3NCO: An important missing species in astrochemical networks”, A&A, 587, L4, 2016, DOI: 10.1051/0004-6361/201527531

Capítulo 6

Conclusiones y Perspectivas

6.1 Conclusión de los resultados

El análisis astrofísico de las moléculas que contienen nitrógeno (CH_3CH_2CN y CH_2CHCN) ha sido combinado con el análisis de laboratorio, así como con el cálculo teórico, permitiendo la detección interestelar de nuevos estados excitados (CH_2CHCN v_{11}=2,3; CH_3CH_2CN v_{12}=1 y v_{20}=1; CH_2CHCN (v_{10}=1)⇔(v_{11}=1,v_{15}=1), y reducido de manera significativa el número de líneas sin identificar en el espectro de Orión-KL. Para el caso de las moléculas con oxígeno (CH_3OCOH e isómeros, CH_3OCOCH_3 y CH_3CH_2OCOH; $CH_3CH_2OCH_3$), hemos realizado un análisis exhaustivo de sus distribuciones espaciales y detectado algunas de ellas por primera vez en el espacio (CH_3COOH v_t=1,2; CH_3OCOCH_3; *gauche*-CH_3CH_2OCOH; *trans*-$CH_3CH_2OCH_3$−detección tentativa) y en Orión-KL (CH_3COOH, CH_2OHCHO).

La diferenciación química se manifiesta en la distinta posición de la que emergen las líneas de las moléculas con nitrógeno y aquellas con oxígeno, lo cual puede utilizarse para sugerir posibles rutas químicas de formación de moléculas. Asimismo, puede perfilarse aún mejor tras el estudio de isómeros funcionales de moléculas abundantes (como ocurre en el presente trabajo) y con la mejora de los modelos de química sobre la superficie de los granos de polvo. Esa diferenciación química, primordialmente entre el ”compact ridge” y el ”hot core”, puede tener su origen en las condiciones iniciales anteriores a la formación de las estrellas de la región, caracterizada por una etapa *fría* que posiblemente acabó diferenciando el calentamiento producido en los comienzos de la formación estelar. De este modo, en el ”hot core”, que fue quizá algo más ”caliente” que el ”compact ridge”, la molécula de CO en la fase gas, podría no haber permanecido suficiente tiempo sobre la superficie de los granos de polvo como para ser hidrogenado a metanol (CH_3OH), la molécula precursora de las moléculas orgánicas con oxígeno (Williams & Herbst 2002).

La gran cantidad de líneas detectadas correspondientes a las moléculas de este trabajo, además de reducir el número de líneas sin identificar en nuestro espectro de la nebulosa de Orión-KL, hace más precisa la estimación de las condiciones físicas y químicas de esta región de formación de estrellas masivas, así como de su estructura. Con esto aportamos unos resultados significativos, que servirán como referencia para el estudio espectral de otros *hot cores*.

6.2 Conclusiones globales de la tesis

La variedad de disciplinas científicas, que se necesitan para poder llevar a cabo el análisis de moléculas orgánicas complejas observadas en la nube de Orión-KL, ha implicado un laborioso estudio hacia la comprensión de temas multidisciplinares tratados durante esta tesis. La colaboración con grupos de laboratorio permite la detección de nuevas especies moleculares en el medio interestelar. Haber participado en la caracterización e identificación de líneas espectrales en el laboratorio, como los datos aquí obtenidos para las moléculas de cianuro de etilo y cianuro de vinilo, ha supuesto una gran oportunidad para acercarse aún más al análisis de estas herramientas de diagnóstico de las nubes

moleculares. Del mismo modo en que se le da importancia al hecho de tomar uno mismo los datos espectrales con los radiotelescopios, poder implicarse en el trabajo de laboratorio resulta una experiencia única y completa para el estudio de las moléculas orgánicas complejas interestelares. Gracias a J. Cernicharo y J. L. Alonso, pude involucrarme en un laboratorio de espectroscopía milimétrica de gran interés e impacto científico (GEM-QUIFIMA).

La posibilidad de acceso a los datos de ALMA SV revela la emisión de las moléculas procedentes de subregiones de la nube, ayudando a la modelización de las líneas observadas en los datos del interferómetro y en los datos del telescopio de antena única (30m de IRAM).

Las moléculas orgánicas complejas presentan innumerables líneas rotacionales en su espectro, por ello se requiere un estudio previo exhaustivo de su espectroscopía. Esto unido a la gran cantidad de transiciones moleculares que se emiten en la región de formación de estrellas masivas de Orión-KL, hacen del análisis astrofísico un riguroso trabajo de identificación que refleja la complejidad química que se presenta en la nube molecular de Orión-KL. Gracias al barrido espectral de Orión-KL realizado por B. Tercero se ha podido llevar a cabo la asignación de las nuevas especies moleculares presentes en esta tesis, que estudiadas en familias de moléculas, con N y con O, han aportado una comprensión aún más detallada acerca de sus interrelaciones en la nube molecular.

6.3 Perspectivas futuras

Con el tiempo, se espera poder tener acceso a estados excitados de energías vibracionales cada vez mayores, pertenecientes a moléculas orgánicas complejas ya detectadas (como por ejemplo el estado v_9=1 o el v_{11}=4 del CH_2CHCN, v_t=3 del CH_3OCOH) y aquellas que aún quedan por detectar con la red de radiotelescopios de ALMA, y otros telescopios de sensibilidad y resolución comparables. También se podrán detectar nuevas especies moleculares complejas y de gran interés prebiótico, incluso perfilar las condiciones fisico-químicas de la nube de Orión-KL gracias al diagnóstico molecular con nuevas moléculas, y aportar nuevos resultados que nos ayuden a completar y caracterizar las rutas químicas interestelares, que se desarrollan en regiones de formación de estrellas masivas.

Material Adicional

Apéndice A

Daly et al. 2013, ApJ, 768, 81

Tabla A.1: Detected lines of CH_3CH_2CN ν_{13}=1/ν_{21}=1

Transition $J_{K_a,K_c,\nu} - J'_{K'_a,K'_c,\nu'}$	Predicted freq. (MHz)	S_{ij}	E_u (K)	v_{LSR} km s^{-1}	Δv km s^{-1}	T_{MB}[(2)] (K)	$\int T_{MB} dv$ (K)
$9_{1,9,1}$-$8_{1,8,1}$	80481.139	15.20	330.5	4.3[(1)]		0.13	
$9_{2,8,0}$-$8_{2,7,0}$	80481.228†	15.20	330.5	4.6[(1)]		”	
				4.4±0.5	10.6±1.5	0.12	1.4±0.2
$9_{2,8,1}$-$8_{2,7,1}$	80590.893	14.10	325.7	0.7[(1,3)]		0.09	
$9_{3,7,0}$-$8_{3,6,0}$	80592.859†	14.10	325.7	6.6[(1,3)]		”	
$9_{3,7,1}$-$8_{3,6,1}$	80715.621	14.10	325.6	6.0[(1,4)]		0.13	
$9_{3,6,0}$-$8_{3,5,0}$	80715.791†	14.10	325.6	6.6[(1,4)]		”	
$9_{4,6,0}$-$8_{4,5,0}$	80747.552	12.60	333.0	4.0[(1,4)]		0.22	
$9_{4,5,2}$-$8_{4,4,2}$	80747.778†	12.40	333.0	4.8[(1,4)]		”	
$9_{4,6,1}$-$8_{4,5,1}$	80747.927†	12.40	333.0	5.4[(1,4)]		”	
$9_{4,5,0}$-$8_{4,4,0}$	80748.341†	12.60	332.9	6.9[(1,4)]		”	
$9_{3,6,2}$-$8_{3,5,2}$	81419.780	15.20	320.6	4.8[(1,3)]		0.15	
$9_{2,7,0}$-$8_{2,6,0}$	81419.824†	15.20	320.6	5.0[(1,3)]		”	
$9_{2,7,2}$-$8_{2,6,2}$	82517.689	15.80	317.9	4.2[(1,5)]		0.14	
$9_{1,8,0}$-$8_{1,7,0}$	82517.789†	15.80	317.9	4.6[(1,5)]		”	
$9_{1,8,3}$-$8_{1,7,3}$	82541.641	15.70	327.0	3.9[(1,6)]		0.15	
$10_{1,10,0}$-$9_{1,9,0}$	86978.463	17.60	321.1	4.6[(1)]		0.17	
$10_{1,9,2}$-$9_{1,8,2}$	86978.480†	17.60	321.1	4.6[(1)]		”	
				4.6±0.5	11.6±1.4	0.16	2.0±0.2
$10_{0,10,2}$-$9_{0,9,2}$	88398.478	17.70	320.5	4.4[(1,3)]		0.25	
$10_{0,10,0}$-$9_{0,9,0}$	88398.507†	17.70	320.5	4.5[(1,3)]		”	
$10_{0,10,3}$-$9_{0,9,3}$	88508.838	17.60	329.5	3.2[(1,7)]		0.20	
$10_{0,10,5}$-$9_{0,9,5}$	88509.322†	17.60	329.5	4.8[(1,7)]		”	
$10_{2,9,3}$-$9_{2,8,3}$	89340.217	16.80	334.5	4.8[(1)]		0.17	
$10_{1,9,5}$-$9_{1,8,5}$	89340.770†	16.80	334.5	6.6[(1)]		”	
				5.8±0.2	8.8±0.4	0.16	1.49±0.06
$10_{2,9,1}$-$9_{2,8,1}$	89342.467	15.70	329.9	3.9[(1)]		0.15	
				3.8±0.4	9.4±0.5	0.12	1.22±0.03
$10_{3,8,0}$-$9_{3,7,0}$	89348.007	15.70	329.9	4.7[(1)]		0.09	
				4.7±0.4	14.3±1.2	0.08	1.19±0.08
$10_{1,10,1}$-$9_{1,9,1}$	89368.428	16.90	324.8	5.0[(1,4)]		0.18	
$10_{2,9,0}$-$9_{2,8,0}$	89368.542†	16.90	324.8	5.4[(1,4)]		”	

Tabla A.1: continued.

Transition $J_{K_a,K_c,v} - J'_{K'_a,K'_c,v'}$	Predicted freq. (MHz)	S_{ij}	E_u (K)	v_{LSR} km s^{-1}	Δv km s^{-1}	$T_{MB}{}^{(2)}$ (K)	$\int T_{MB} dv$ (K)
$10_{4,7,3}$-$9_{4,6,3}$	89641.453	14.30	348.9	2.6$^{(1,4)}$		0.29	
$10_{4,7,4}$-$9_{4,6,4}$	89641.998†	14.30	348.9	4.4$^{(1,4)}$		”	
$10_{4,6,3}$-$9_{4,5,3}$	89642.132†	14.30	349.0	4.9$^{(1,4)}$		”	
$10_{4,6,5}$-$9_{4,5,5}$	89642.436†	14.30	348.9	5.9$^{(1,4)}$		”	
$10_{4,7,0}$-$9_{4,6,0}$	89738.630	14.50	337.2	1.6$^{(1)}$		0.26	
$10_{4,6,2}$-$9_{4,5,2}$	89738.894†	13.90	337.2	2.4$^{(1)}$		”	
$10_{4,7,1}$-$9_{4,6,1}$	89739.860†	13.90	337.2	5.7$^{(1)}$		”	
$10_{4,6,0}$-$9_{4,5,0}$	89740.033†	14.50	337.2	6.3$^{(1)}$		”	
$10_{2,8,3}$-$9_{2,7,3}$	90367.017	16.80	334.6	3.1$^{(1,8)}$		0.19	
$10_{2,8,5}$-$9_{2,7,5}$	90367.596†	16.80	334.6	5.1$^{(1,8)}$		”	
$10_{3,7,2}$-$9_{3,6,2}$	90632.644	16.90	325.0	5.1$^{(1)}$		0.17	
$10_{2,8,0}$-$9_{2,7,0}$	90633.814†	16.90	325.0	5.3$^{(1)}$		”	
		Wide comp.		0.8±1.3	17.5±1.8	0.08	1.5±0.2
		Narrow comp.		5.7±0.3	7.1±0.9	0.12	0.9±0.2
$10_{2,8,2}$-$9_{2,7,2}$	91603.442	17.50	322.4	4.1$^{(1,4)}$		0.27	
$10_{1,9,0}$-$9_{1,8,0}$	91603.558†	17.50	322.4	4.4$^{(1,4)}$		”	
$10_{1,9,3}$-$9_{1,8,3}$	91662.328	17.40	331.4	3.5$^{(1)}$		0.24	
$10_{2,9,4}$-$9_{2,8,4}$	91663.226†	17.40	331.4	6.5$^{(1)}$		”	
$11_{1,11,0}$-$10_{1,10,0}$	95611.489	19.20	325.7	4.4$^{(1)}$		0.28	
$11_{1,10,2}$-$10_{1,9,2}$	95611.506†	19.20	325.7	4.5$^{(1)}$		”	
		Wide comp.		0.9±0.5	19.8±0.6	0.10	2.02±0.12
		Narrow comp.		4.67±0.12	6.5±0.3	0.17	1.17±0.06
$11_{0,11,2}$-$10_{0,10,2}$	96991.897	19.30	325.2	4.5$^{(1)}$		0.36	
$11_{0,11,0}$-$10_{0,10,0}$	96991.928†	19.30	325.2	4.6$^{(1)}$		”	
$11_{0,11,3}$-$10_{0,10,3}$	97152.908	19.20	334.1	3.4$^{(1)}$		0.22	
$11_{0,11,5}$-$10_{0,10,5}$	97153.431†	19.20	334.1	5.0$^{(1)}$		”	
$11_{2,10,3}$-$10_{2,9,3}$	98227.206	18.50	339.2	5.9$^{(1)}$		0.25	
$11_{1,10,5}$-$10_{1,9,5}$	98227.798†	18.50	339.2	7.7$^{(1)}$		”	
$11_{1,11,1}$-$10_{1,10,1}$	98238.205	18.60	329.5	3.5$^{(1)}$		0.30	
$11_{2,10,0}$-$10_{2,9,0}$	98238.349†	18.60	329.5	3.9$^{(1)}$		”	
$11_{6,6,1}$-$10_{6,5,1}$	98617.867	12.80	362.9	1.8$^{(1)}$		0.75	
$11_{6,5,2}$-$10_{6,4,2}$	98617.907†	12.80	362.9	1.7$^{(1)}$		”	
$11_{4,8,3}$-$10_{4,7,3}$	98619.451†	16.20	353.6	3.0$^{(1)}$		”	
$11_{5,7,3}$-$10_{5,6,3}$	98620.275†	0.94	364.4	5.5$^{(1)}$		”	
$11_{5,6,3}$-$10_{5,5,3}$	98620.290†	0.94	364.4	5.5$^{(1)}$		”	
$11_{4,8,4}$-$10_{4,7,4}$	98620.377†	16.20	353.6	5.8$^{(1)}$		”	
$11_{5,7,4}$-$10_{5,6,4}$	98620.410†	14.50	364.4	5.9$^{(1)}$		”	

Tabla A.1: continued.

Transition $J_{K_a,K_c,v} - J'_{K'_a,K'_c,v'}$	Predicted freq. (MHz)	S_{ij}	E_u (K)	v_{LSR} km s^{-1}	Δv km s^{-1}	$T_{MB}{}^{(2)}$ (K)	$\int T_{MB} dv$ (K)
$11_{4,7,3}$-$10_{4,6,3}$	98620.805†	16.20	353.6	7.1[1]		”	
$11_{4,7,5}$-$10_{4,6,5}$	98620.821†	16.20	353.6	7.2[1]		”	
$11_{5,6,5}$-$10_{5,5,5}$	98621.018†	14.50	364.4	7.8[1]		”	
$11_{3,9,3}$-$10_{3,8,3}$	98642.029	17.50	345.3	4.6[1]		0.23	
$11_{3,8,5}$-$10_{3,7,5}$	98644.506	17.40	345.3	6.0[1]		0.25	
$11_{4,8,0}$-$10_{4,7,0}$	98735.640	16.40	342.0	4.5[1,5]		0.28	
$11_{4,7,2}$-$10_{4,6,2}$	98735.773†	15.90	342.0	4.9[1,5]		”	
$11_{4,8,1}$-$10_{4,7,1}$	98738.682	15.90	342.0	5.3[1,5]		0.36	
$11_{4,7,0}$-$10_{4,6,0}$	98739.060†	16.40	342.0	6.4[1,5]		”	
$11_{2,9,3}$-$10_{2,8,3}$	99566.134	18.50	339.4	3.1[1]		0.24	
$11_{2,9,5}$-$10_{2,8,5}$	99566.817†	18.50	339.4	5.2[1]		”	
$11_{3,8,2}$-$10_{3,7,2}$	99879.830	18.60	329.7	4.4[1]		0.28	
$11_{2,9,0}$-$10_{2,8,0}$	99879.889†	18.60	329.7	4.6[1]		”	
$11_{2,9,2}$-$10_{2,8,2}$	100659.254	19.20	327.2	5.1[1,10,11]		0.53	
$11_{1,10,0}$-$10_{1,9,0}$	100659.390†	19.20	327.2	5.6[1,10,11]		”	
$11_{1,10,3}$-$10_{1,9,3}$	100764.007	19.00	336.3	3.5[1]		0.24	
$11_{2,10,4}$-$10_{2,9,4}$	100764.998†	19.00	336.3	6.5[1]		”	
$12_{0,12,2}$-$11_{0,11,2}$	105539.535	20.90	330.3	4.6[1]		0.35	
$12_{0,12,0}$-$11_{0,11,0}$	105539.568†	20.90	330.3	4.6[1]		”	
$12_{0,12,3}$-$11_{0,11,3}$	105754.835	20.80	339.2	3.7[1]		0.38	
$12_{0,12,5}$-$11_{0,11,5}$	105755.397†	20.80	339.2	5.3[1]		”	
$12_{1,12,1}$-$11_{1,11,1}$	107088.634	20.30	334.6	4.2[1]		0.38	
$12_{2,11,0}$-$11_{2,10,0}$	107088.813†	20.30	334.6	4.7[1]		”	
$12_{2,11,3}$-$11_{2,10,3}$	107101.610	20.10	344.3	3.7[1]		0.35	
$12_{1,11,5}$-$11_{1,10,5}$	107102.246†	20.10	344.3	5.5[1]		”	
$12_{4,9,3}$-$11_{4,8,3}$	107601.242	17.90	358.8	0.7[1,10]		0.71	
$12_{4,9,4}$-$11_{4,8,4}$	107602.854†	17.90	358.8	3.8[1,10]		”	
$12_{4,8,5}$-$11_{4,7,5}$	107603.199†	17.90	358.8	4.8[1,10]		”	
$12_{4,8,3}$-$11_{4,7,3}$	107603.774†	17.90	358.8	6.4[1,10]		”	
$12_{4,9,1}$-$11_{4,8,1}$	107745.272	18.00	347.2	5.0[1]		0.33	
$12_{4,8,0}$-$11_{4,7,0}$	107745.539†	18.20	347.2	5.7[1]		”	
$12_{2,10,3}$-$11_{2,9,3}$	108794.120	20.10	344.6	3.8[1]		0.33	
$12_{2,10,5}$-$11_{2,9,5}$	108794.907†	20.10	344.6	5.9[1]		”	
$12_{2,10,2}$-$11_{2,9,2}$	109680.271	20.80	332.5	4.1[1,12]		0.42	
$12_{1,11,0}$-$11_{1,10,0}$	109680.429†	20.80	332.5	4.5[1,12]		”	
$12_{1,11,3}$-$11_{1,10,3}$	109843.668	20.60	341.6	3.1[1]		0.36	
$12_{2,11,4}$-$11_{2,10,4}$	109844.749†	20.60	341.6	6.0[1]		”	

Tabla A.1: continued.

Transition $J_{K_a,K_c,v} - J'_{K'_a,K'_c,v'}$	Predicted freq. (MHz)	S_{ij}	E_u (K)	v_{LSR} km s^{-1}	Δv km s^{-1}	$T_{MB}{}^{(2)}$ (K)	$\int T_{MB} dv$ (K)
$13_{1,13,0}$-$12_{1,12,0}$	109833.472	22.40	336.1	5.0[1]		0.30	
$13_{1,12,2}$-$12_{1,11,2}$	109833.486†	22.40	336.1	5.0[1]		”	
				4.4±0.4	13.7±1.1	0.28	4.1±0.3
$13_{0,13,2}$-$12_{0,12,2}$	114048.398	22.50	335.7	4.3[1]		0.44	
$13_{0,13,0}$-$12_{0,12,0}$	114048.432†	22.50	335.7	4.4[1]		”	
$13_{0,13,3}$-$12_{0,12,3}$	114319.470	22.30	344.7	3.4[1,13]		0.43	
$13_{0,13,5}$-$12_{0,12,5}$	114320.071†	22.30	344.7	4.9[1,13]		”	
$15_{1,15,0}$-$14_{1,14,0}$	129998.719	25.40	348.2	4.7[1]		0.43	
$15_{1,14,2}$-$14_{1,13,2}$	129998.731†	25.40	348.2	4.7[1]		”	
		Wide comp.		1.6±0.9	32.3±3.2	0.13	4.6±0.2
		Narrow comp.		4.8±0.12	7.8±0.4	0.31	2.6±0.2
$15_{2,14,1}$-$14_{2,13,1}$	130196.054	25.00	357.2	2.4[1,14]		0.47	
$15_{1,15,3}$-$14_{1,14,3}$	130197.344†	25.00	357.2	5.4[1,14]		”	
$15_{0,15,2}$-$14_{0,14,2}$	130982.537	25.40	347.9	4.8[1]		0.55	
$15_{0,15,0}$-$14_{0,14,0}$	130982.571†	25.40	347.9	4.9[1]		”	
		Wide comp.		5.1±0.4	25.8±1.7	0.22	6.1±0.3
		Narrow comp.		4.8±0.12	6.5±0.5	0.33	2.3±0.2
$15_{0,15,3}$-$14_{0,14,3}$	131364.195	25.20	356.9	3.8[1]		0.48	
$15_{0,15,5}$-$14_{0,14,5}$	131364.889†	25.20	356.9	5.4[1]		”	
		Wide comp.		2.4±0.3	23.4±1.4	0.15	3.78±0.12
		Narrow comp.		5.0±0.08	6.9±0.2	0.33	2.45±0.06
$15_{1,15,1}$-$14_{1,14,1}$	133504.665	24.90	352.6	3.8[1]		0.61	
$15_{2,14,0}$-$14_{2,13,0}$	133504.998†	24.90	352.6	4.6[1]		”	
				3.8±0.2	12.2±0.6	0.57	7.4±0.3
$15_{2,14,3}$-$14_{2,13,3}$	133644.412	24.60	362.3	4.7[1,15]		0.66	
$15_{4,12,1}$-$14_{4,11,1}$	133645.198†	24.60	362.3	6.5[1,15]		”	
$15_{6,10,1}$-$14_{6,9,1}$	134616.201	21.70	374.6	4.5[1,4]		0.82	
$15_{6,9,2}$-$14_{6,8,2}$	134616.380†	21.70	374.6	4.9[1,4]		”	
$15_{5,11,0}$-$14_{5,10,0}$	134616.440†	20.30	374.6	5.1[1,4]		”	
$15_{5,10,0}$-$14_{5,9,0}$	134616.579†	20.30	374.6	5.4[1,4]		”	
$15_{5,10,2}$-$14_{5,9,2}$	134793.384	23.00	365.2	4.4[1,5]		0.51	
$15_{4,12,0}$-$14_{4,11,0}$	134793.532†	23.10	365.2	4.8[1,5]		”	
$15_{3,12,3}$-$14_{3,11,3}$	134920.841	23.80	368.6	5.3[1,16]		0.59	
$15_{2,14,4}$-$14_{2,13,4}$	134921.414†	23.80	368.6	6.6[1,16]		”	
$15_{3,12,2}$-$14_{3,11,2}$	137047.481	24.80	353.4	4.0[1]		0.84	
$15_{2,13,0}$-$14_{2,12,0}$	137047.590†	24.80	353.4	4.2[1]		”	
$16_{1,16,0}$-$15_{1,15,0}$	138561.581	26.80	354.8	4.9[1,5]		0.74	

Tabla A.1: continued.

Transition $J_{K_a,K_c,v} - J'_{K'_a,K'_c,v'}$	Predicted freq. (MHz)	S_{ij}	E_u (K)	v_{LSR} km s^{-1}	Δv km s^{-1}	$T_{MB}{}^{(2)}$ (K)	$\int T_{MB} dv$ (K)
$16_{1,15,2}$-$15_{1,14,2}$	138561.591†	26.80	354.8	4.9[1,5]		”	
$16_{2,15,1}$-$15_{2,14,1}$	138748.846	26.40	363.9	3.6[1]		0.71	
$16_{1,16,3}$-$15_{1,15,3}$	138749.282†	26.40	363.9	4.5[1]		”	
$16_{0,16,2}$-$15_{0,15,2}$	139423.746	26.80	354.6	4.1[1,17]		0.97	
$16_{0,16,0}$-$15_{0,15,0}$	139423.778†	26.80	354.6	4.2[1,17]		”	
$16_{0,16,3}$-$15_{0,15,3}$	139860.184	26.50	363.6	4.0[1]		1.00	
$16_{0,16,5}$-$15_{0,15,5}$	139860.937†	26.50	363.6	5.6[1]		”	
$16_{1,16,1}$-$15_{1,15,1}$	142258.108	26.30	359.4	3.9[1]		0.72	
$16_{2,15,0}$-$15_{2,14,0}$	142258.514†	26.30	359.4	4.8[1]		”	
$16_{2,15,3}$-$15_{2,14,3}$	142464.804	26.00	369.1	2.8[1,4]		0.92	
$16_{6,11,1}$-$15_{6,10,1}$	143615.702	23.20	381.5	5.1[1,4]		1.99	
$16_{6,10,2}$-$15_{6,9,2}$	143615.888†	23.20	381.5	5.5[1,4]		”	
$16_{5,12,0}$-$15_{5,11,0}$	143615.900†	22.70	381.5	5.5[1,4]		”	
$16_{11,6,1}$-$15_{11,5,1}$	143615.931†	11.50	483.5	5.6[1,4]		”	
$16_{11,5,2}$-$15_{11,4,2}$	143616.108†	11.50	483.5	5.9[1,4]		”	
$16_{5,11,0}$-$15_{5,10,0}$	143616.155†	22.70	381.5	6.0[1,4]		”	
$16_{7,10,4}$-$15_{7,9,4}$	143770.696	18.80	422.8	4.2[1]		1.06	
$16_{7,9,5}$-$15_{7,8,5}$	143771.715†	18.80	422.8	6.3[1]		”	
$16_{5,11,2}$-$15_{5,10,2}$	143828.018	24.50	372.1	4.7[1]		0.88	
$16_{4,13,0}$-$15_{4,12,0}$	143828.179†	24.50	372.1	5.1[1]		”	
$16_{3,13,3}$-$15_{3,12,3}$	144027.853	25.30	375.5	4.6[1,10]		0.97	
$16_{2,15,4}$-$15_{3,14,4}$	144028.579†	25.30	375.5	6.1[1,10]		”	
$16_{3,13,0}$-$15_{3,12,0}$	144268.658	25.50	365.0	3.9[1,18]		0.76	
$16_{4,12,2}$-$15_{4,11,2}$	144269.536†	25.50	365.0	5.8[1,18]		”	
$16_{2,14,2}$-$15_{2,13,2}$	145304.881	26.60	357.8	3.9[1,19]		0.90	
$16_{1,15,0}$-$15_{1,14,0}$	145305.196†	26.60	357.8	4.5[1,19]		”	
$16_{2,14,3}$-$15_{2,13,3}$	145834.926	26.00	369.9	3.6[1,3]		0.74	
$16_{3,13,2}$-$15_{3,12,2}$	146333.380	26.30	360.4	5.3[1]		0.64	
$16_{2,14,0}$-$15_{2,13,0}$	146333.506†	26.30	360.4	5.8[1]		”	
$17_{1,17,0}$-$16_{1,16,0}$	147112.367	28.10	361.9	5.6[1,3]		0.89	
$17_{1,16,2}$-$16_{1,15,2}$	147112.376†	28.10	361.9	5.6[1,3]		”	
$17_{0,17,2}$-$16_{0,16,2}$	147856.634	28.20	361.7	4.7[1]		0.92	
$17_{0,17,0}$-$16_{0,16,0}$	147856.665†	28.20	361.7	4.8[1]		”	
				4.7±0.3	10.2±0.8	0.82	8.9±0.5
$17_{1,17,1}$-$16_{1,16,1}$	150981.853	27.60	366.7	4.5[1]		0.71	
$17_{2,16,0}$-$16_{2,15,0}$	150982.348†	27.60	366.7	5.5[1]		”	
$17_{2,16,3}$-$16_{2,15,3}$	151272.117	27.40	376.4	3.4[1]		0.76	

Tabla A.1: continued.

Transition $J_{K_a,K_c,v} - J'_{K'_a,K'_c,v'}$	Predicted freq. (MHz)	S_{ij}	E_u (K)	v_{LSR} km s^{-1}	Δv km s^{-1}	$T_{MB}{}^{(2)}$ (K)	$\int T_{MB} dv$ (K)
$17_{5,12,2}$-$16_{5,11,2}$	152871.989	26.00	379.5	4.4[1]		0.81	
$17_{4,14,0}$-$16_{4,13,0}$	152872.156†	26.00	379.5	4.7[1]		”	
$17_{4,13,0}$-$16_{4,12,0}$	152953.661	26.00	379.5	5.3[1,20]		1.28	
$17_{2,15,2}$-$16_{2,14,2}$	154066.310	27.90	365.1	4.6[1,18]		0.91	
$17_{1,16,0}$-$16_{1,15,0}$	154066.691†	27.90	365.1	5.3[1,18]		”	
$17_{2,15,3}$-$16_{2,14,3}$	155073.918	27.40	374.4	3.3[1,21]		0.98	
$17_{2,15,5}$-$16_{2,14,5}$	155075.312†	27.40	374.4	6.0[1,21]		”	
$17_{3,14,2}$-$16_{3,13,2}$	155597.154	27.60	367.9	4.7[1]		1.09	
$17_{2,15,0}$-$16_{2,14,0}$	155597.302†	27.60	367.9	5.0[1]		”	
$18_{1,18,3}$-$17_{1,17,3}$	155915.641	29.00	378.5	4.4[1]		1.12	
$18_{1,17,5}$-$17_{1,16,5}$	155915.943†	29.00	378.5	5.0[1]		”	
$18_{1,18,1}$-$17_{1,17,1}$	159673.343	28.90	374.3	5.1[1,22]		1.19	
$18_{2,17,0}$-$17_{2,16,0}$	159673.946†	28.90	374.3	6.2[1,22]		”	
$18_{4,14,0}$-$17_{4,13,0}$	162051.232	27.30	387.2	4.8[1]		1.14	
$18_{3,15,3}$-$17_{3,14,3}$	162326.688	27.90	390.6	2.8[1,23,24]		1.12	
$18_{3,16,4}$-$17_{3,15,4}$	162327.647†	27.90	390.6	4.6[1,23,24]		”	
$18_{3,15,0}$-$17_{3,14,0}$	162726.506	28.30	380.3	4.9[1]		1.08	
$18_{4,14,2}$-$17_{4,13,2}$	162726.805†	28.30	380.3	5.4[1]		”	
$18_{2,16,2}$-$17_{2,15,2}$	162758.366	29.20	373.0	5.2[1]		1.22	
$18_{1,17,0}$-$17_{1,16,0}$	162758.831†	29.20	373.0	6.1[1]		”	
$18_{1,17,3}$-$17_{1,16,3}$	163675.769	29.00	382.3	4.0[1]		1.12	
$18_{1,18,4}$-$17_{1,17,4}$	163677.333†	29.00	382.3	6.9[1]		”	
$19_{1,19,0}$-$18_{1,18,0}$	164181.504	30.70	377.2	5.0[1]		0.88	
$19_{1,18,2}$-$18_{1,17,2}$	164181.510†	30.70	377.2	5.0[1]		”	
		Wide comp.		3.2±0.2	17.0±0.3	0.52	9.4±0.2
		Narrow comp.		5.19±0.12	4.7±0.2	0.38	1.89±0.09
$18_{2,16,3}$-$17_{2,15,3}$	164279.531	28.60	385.3	3.7[1,3]		0.86	
$19_{1,19,3}$-$18_{1,18,3}$	164515.941	30.10	386.3	4.4[1]		0.88	
$19_{1,18,5}$-$18_{1,17,5}$	164516.483†	30.10	386.3	4.4[1]		”	
		Wide comp.		3.1±0.5	21.7±1.4	0.40	9.2±0.5
		Narrow comp.		4.8±0.2	5.0±0.5	0.48	2.5±0.4
$19_{0,19,2}$-$18_{0,18,2}$	164715.544	30.70	377.1	4.76[1]		0.87	
$19_{0,19,0}$-$18_{0,18,0}$	164715.571†	30.70	377.1	4.81[1]		”	
				4.81±0.14	10.2±0.4	0.80	8.7±0.2
$18_{3,15,2}$-$17_{3,14,2}$	164830.575	28.90	375.8	4.49[1]		0.87	
$18_{2,16,0}$-$17_{2,15,0}$	164830.748†	28.90	375.8	4.80[1]		”	
		Wide comp.		3.3±0.6	28.8±2.0	0.28	8.4±0.4

Tabla A.1: continued.

Transition $J_{K_a,K_c,v} - J'_{K'_a,K'_c,v'}$	Predicted freq. (MHz)	S_{ij}	E_u (K)	v_{LSR} km s^{-1}	Δv km s^{-1}	$T_{MB}{}^{(2)}$ (K)	$\int T_{MB} dv$ (K)
		Narrow comp.		4.65±0.12	7.0±0.4	0.58	4.3±0.4
$19_{0,19,3}$-$18_{0,18,3}$	165337.926	30.10	386.2	4.7[1]		1.22	
$19_{0,19,5}$-$18_{0,18,5}$	165338.932†	30.10	386.2	4.7[1]		”	
$19_{2,18,3}$-$18_{2,17,3}$	168851.117	29.90	392.2	4.4[1]		1.03	
$19_{2,17,5}$-$18_{2,16,5}$	168852.111†	29.90	392.2	6.2[1]		”	
$19_{5,15,0}$-$18_{5,14,0}$	170645.215	27.40	404.7	4.8[1]		1.62	
$19_{5,14,2}$-$18_{5,13,2}$	170645.387†	27.00	404.7	5.1[1]		”	
$19_{5,15,1}$-$18_{5,14,1}$	170645.757†	27.00	404.7	5.7[1]		”	
$19_{5,14,0}$-$18_{5,13,0}$	170646.470†	27.40	404.7	7.0[1]		”	
$19_{4,16,4}$-$18_{4,15,4}$	170657.214	28.20	407.0	4.8[1]		”	
$19_{3,17,1}$-$18_{3,16,1}$	170991.490	28.60	395.4	5.0[1]		0.90	
$19_{4,16,0}$-$18_{4,15,0}$	170991.654†	28.60	395.4	5.3[1]		”	
$19_{2,17,2}$-$18_{2,16,2}$	171176.428	30.40	381.2	4.7[1,25]		1.04	
$19_{1,18,0}$-$18_{1,17,0}$	171377.001†	30.40	381.2	5.7[1,25]		”	
$19_{3,16,0}$-$18_{3,15,0}$	171997.358	29.50	388.4	4.6[1]		1.19	
$19_{4,15,2}$-$18_{4,14,2}$	171997.537†	29.50	388.4	5.0[1]		”	
$20_{1,20,0}$-$19_{1,19,0}$	172701.813	31.90	385.5	6.0[1]		1.71	
$20_{1,19,2}$-$19_{1,18,2}$	172701.818†	31.90	385.5	6.0[1]		”	
$20_{0,20,2}$-$19_{0,19,2}$	173147.161	31.90	385.4	4.1[1,26]		1.68	
$20_{0,20,0}$-$19_{0,19,0}$	173147.185†	31.90	385.4	4.2[1,26]		”	
$19_{2,17,3}$-$18_{2,18,3}$	173437.820	29.80	393.6	2.8[1]		1.52	
$19_{3,16,5}$-$18_{3,15,5}$	173439.546†	29.80	393.6	5.8[1]		”	
$20_{0,20,3}$-$19_{0,19,3}$	173849.756	31.00	394.5	4.2[1]		1.49	
$20_{0,20,5}$-$19_{0,19,5}$	173850.870†	31.00	394.5	6.2[1]		”	
$19_{3,16,2}$-$18_{3,15,2}$	174026.415	30.20	384.2	5.3[1,5,10]		1.30	
$19_{2,17,0}$-$18_{2,16,0}$	174026.617†	30.20	384.2	5.7[1,5,10]		”	
$23_{1,23,0}$-$22_{1,22,0}$	198216.981	35.10	412.8	4.8[1,10]		1.14	
$23_{1,22,2}$-$22_{1,21,2}$	198216.982†	35.10	412.8	4.8[1,10]		”	
$23_{0,23,2}$-$22_{4,22,2}$	198263.403	35.10	412.8	4.9[1,23]		1.76	
$23_{0,23,0}$-$22_{0,22,0}$	198263.420†	35.10	412.8	4.9[1,23]		”	
$22_{1,21,3}$-$21_{1,20,3}$	198751.960	33.30	417.9	3.6[1,16]		1.79	
$22_{1,22,4}$-$21_{1,21,4}$	198753.752†	33.30	417.9	6.3[1,16]		”	
$22_{4,19,1}$-$21_{4,18,1}$	198836.558	32.00	422.8	4.0[1]		0.76	
$22_{4,18,0}$-$21_{4,17,0}$	198837.498†	32.00	422.8	5.4[1]		”	
				4.8±0.3	8.8±1.0	0.65	6.2±1.4
$23_{1,23,3}$-$22_{1,22,3}$	199226.137	18.80	422.1	1.6[1,27]		0.61	
$23_{1,22,5}$-$22_{1,21,5}$	199226.137†	18.70	422.0	5.8[1,27]		”	

Tabla A.1: continued.

Transition $J_{K_a,K_c,v} - J'_{K'_a,K'_c,v'}$	Predicted freq. (MHz)	S_{ij}	E_u (K)	v_{LSR} km s^{-1}	Δv km s^{-1}	$T_{MB}{}^{(2)}$ (K)	$\int T_{MB} dv$ (K)
$23_{0,23,3}$-$22_{0,22,3}$	199384.894	18.70	422.0	5.3$^{(1,26)}$		1.14	
$23_{0,23,5}$-$22_{0,22,5}$	199385.426†	18.60	422.0	6.1$^{(1,26)}$		”	
$22_{3,19,0}$-$21_{3,18,0}$	199388.153	32.90	415.9	4.6$^{(1)}$		1.01	
$22_{3,20,1}$-$21_{3,19,1}$	199388.153†	32.90	415.9	4.6$^{(1)}$		”	
		Wide comp.		3.0±0.5	15.1±1.0	0.61	9.7±0.8
		Narrow comp.		4.8±0.2	4.5±0.7	0.58	2.1±0.6
$22_{2,20,3}$-$21_{2,19,3}$	200478.063	33.00	421.2	2.5$^{(1,24)}$		1.11	
$22_{3,19,5}$-$21_{3,18,5}$	200480.458†	33.00	421.2	6.0$^{(1,24)}$		”	
$22_{3,19,2}$-$21_{3,15,2}$	201324.899	33.50	411.8	4.5$^{(1)}$		1.18	
$22_{2,20,0}$-$21_{2,19,0}$	201325.225†	33.50	411.8	5.0$^{(1)}$		”	
$23_{2,22,3}$-$22_{2,21,3}$	203914.467	34.10	428.8	3.8$^{(1)}$		1.39	
$23_{2,21,5}$-$22_{2,20,5}$	203915.730†	34.10	428.8	5.7$^{(1)}$		”	
$23_{2,22,1}$-$22_{2,21,1}$	205598.563	34.00	425.0	4.4$^{(1)}$		1.49	
$23_{3,21,0}$-$22_{3,20,0}$	205599.334†	34.00	425.0	4.4$^{(1)}$		”	
$23_{5,18,2}$-$22_{5,17,2}$	206770.332	31.90	441.8	4.3$^{(1)}$		1.01	
$23_{5,19,0}$-$22_{5,18,0}$	206770.542†	32.00	441.8	4.6$^{(1)}$		”	
$23_{5,19,1}$-$22_{5,18,1}$	206777.473	31.90	441.8	5.0$^{(1,23)}$		0.95	
$23_{5,18,0}$-$22_{5,17,0}$	206777.873†	32.00	441.8	5.6$^{(1,23)}$		”	
$24_{0,24,2}$-$23_{0,23,2}$	206909.407	36.00	422.7	4.7$^{(1,10)}$		1.71	
$23_{4,19,3}$-$22_{4,18,3}$	206909.421†	32.60	444.1	4.8$^{(1,10)}$		”	
$24_{0,24,0}$-$23_{0,23,0}$	206909.422†	36.00	422.7	4.8$^{(1,10)}$		”	
$23_{4,20,4}$-$22_{4,19,4}$	206910.309†	32.60	444.1	6.0$^{(1,10)}$		”	
$23_{1,22,3}$-$22_{1,21,3}$	207415.760	34.30	427.9	3.2$^{(1)}$		1.50	
$23_{1,23,4}$-$22_{1,22,4}$	207417.589†	34.30	427.8	5.9$^{(1)}$		”	
$24_{1,24,3}$-$23_{1,23,3}$	208099.627	25.60	432.1	3.3$^{(1,28)}$		1.06	
$24_{1,23,5}$-$23_{1,22,5}$	208101.958†	25.60	432.1	3.6$^{(1,28)}$		”	
$23_{3,21,3}$-$22_{3,20,3}$	209302.450	33.90	431.2	3.7$^{(1)}$		1.88	
$23_{3,20,5}$-$22_{3,19,5}$	209305.066†	33.90	431.2	7.5$^{(1)}$		”	
$23_{3,20,2}$-$22_{3,19,2}$	210307.395	34.40	421.9	4.3$^{(1)}$		1.73	
$23_{3,21,0}$-$22_{3,20,0}$	210307.786†	34.40	421.9	4.8$^{(1)}$		”	
$24_{1,24,1}$-$23_{1,23,1}$	210956.862	35.50	429.0	4.1$^{(1,22)}$		0.85	
$24_{2,23,0}$-$23_{2,22,0}$	210958.763†	35.50	429.0	6.8$^{(1,22)}$		”	
		Wide comp.		5.3±0.2	14.9±0.8	0.48	7.6±0.3
		Narrow comp.		5.71±0.09	4.5±0.4	0.38	1.8±0.3
$24_{2,23,3}$-$23_{2,22,3}$	212676.347	35.00	439.1	4.1$^{(1)}$		1.16	
$24_{2,22,5}$-$23_{2,21,5}$	212677.711†	35.00	439.0	6.0$^{(1)}$		”	
$24_{2,22,2}$-$23_{2,21,2}$	213283.190	35.60	428.4	3.3$^{(1)}$		1.06	

Tabla A.1: continued.

Transition $J_{K_a,K_c,v} - J'_{K'_a,K'_c,v'}$	Predicted freq. (MHz)	S_{ij}	E_u (K)	v_{LSR} km s^{-1}	Δv km s^{-1}	$T_{MB}{}^{(2)}$ (K)	$\int T_{MB} dv$ (K)
$24_{1,23,0}$-$23_{1,22,0}$	213284.910†	35.60	428.4	5.7[1]		”	
$25_{0,25,2}$-$24_{0,24,2}$	215358.416	36.90	433.0	5.2[1]		1.50	
$25_{0,25,0}$-$24_{0,24,0}$	215358.430†	36.90	433.0	5.3[1]		”	
$24_{6,19,1}$-$23_{6,18,1}$	215475.954	31.70	463.6	4.7[1,23]		2.04	
$24_{6,18,2}$-$23_{6,17,2}$	215476.285†	31.70	463.6	5.2[1,23]		”	
$24_{6,19,0}$-$23_{6,18,0}$	215476.528†	22.50	463.6	5.5[1,23]		”	
$24_{6,18,0}$-$23_{6,17,0}$	215476.718†	22.50	463.6	5.8[1,23]		”	
$24_{5,20,4}$-$23_{5,19,4}$	215558.703	32.00	465.1	3.2[1]		1.13	
$24_{5,19,3}$-$23_{5,18,3}$	215560.798†	32.40	465.1	6.1[1]		”	
$24_{4,20,3}$-$23_{4,19,3}$	216012.388	33.60	454.5	4.4[1]		1.30	
$24_{4,21,4}$-$23_{4,20,4}$	216013.429†	33.60	454.5	5.8[1]		”	
$24_{1,23,3}$-$23_{1,22,3}$	216044.679	35.10	438.2	3.6[1]		1.28	
$24_{1,24,4}$-$23_{1,23,4}$	216046.534†	35.10	438.2	6.2[1]		”	
$25_{0,25,3}$-$24_{0,24,3}$	216523.771	33.80	442.5	3.6[1]		1.09	
$25_{0,25,5}$-$24_{0,24,5}$	216526.068†	33.80	442.5	6.8[1]		”	
$25_{4,20,2}$-$24_{1,19,2}$	216543.861	34.00	443.0	4.7[1]		1.08	
$25_{4,21,0}$-$24_{1,20,0}$	216543.957†	34.00	443.0	4.8[1]		”	
$26_{1,25,2}$-$25_{1,24,2}$	223680.347	37.70	443.8	4.7[1]		1.70	
$26_{1,26,0}$-$25_{1,25,0}$	223680.348†	37.70	443.8	4.7[1]		”	
$26_{0,26,2}$-$25_{0,25,2}$	223809.900	37.70	443.8	5.6[1]		1.75	
$26_{0,26,0}$-$25_{0,25,0}$	223809.913†	37.70	443.8	5.7[1]		”	
$25_{4,22,1}$-$24_{4,21,1}$	226989.104	34.90	454.1	4.0[1,7]		2.14	
$25_{4,21,0}$-$24_{4,20,0}$	226990.269†	34.90	454.1	5.5[1,7]		”	
$26_{1,26,1}$-$25_{1,25,1}$	227624.578	37.20	450.4	3.6[1]		2.15	
$26_{2,25,0}$-$25_{2,24,0}$	227627.196†	37.20	450.4	7.1[1]		”	
$26_{2,24,2}$-$25_{2,23,2}$	229502.376	37.20	450.0	4.2[1,5]		1.07	
$26_{1,25,0}$-$25_{1,24,0}$	229504.946†	37.20	450.0	7.5[1,5]		”	
$26_{5,22,1}$-$25_{5,21,1}$	233967.759	34.70	474.2	5.4[1,14]		0.37	
$26_{5,21,0}$-$25_{5,20,0}$	233968.101†	34.70	474.2	5.9[1,14]		”	
$26_{4,22,3}$-$25_{4,21,3}$	234280.549	35.20	476.6	4.8[1,29]		1.57	
$26_{4,23,4}$-$25_{4,22,4}$	234281.823†	35.20	476.6	6.5[1,29]		”	
$27_{0,27,5}$-$26_{0,26,5}$	234362.806	37.40	464.5	7.0[1]		1.44	
$27_{1,27,1}$-$26_{1,26,1}$	235866.279	37.90	461.7	2.3[1]		1.14	
$27_{2,26,0}$-$26_{2,25,0}$	235869.249†	37.90	461.7	6.1[1]		”	
$26_{4,23,1}$-$25_{4,22,1}$	236408.854	35.80	465.5	4.3[1]		1.53	
$26_{4,22,0}$-$25_{4,21,0}$	236409.828†	35.80	465.5	5.5[1]		”	
$26_{3,23,3}$-$25_{3,22,3}$	236648.882	36.10	469.0	4.2[1,25]		1.59	

Tabla A.1: continued.

Transition $J_{K_a,K_c,v} - J'_{K'_a,K'_c,v'}$	Predicted freq. (MHz)	S_{ij}	E_u (K)	v_{LSR} km s^{-1}	Δv km s^{-1}	$T_{MB}{}^{(2)}$ (K)	$\int T_{MB} dv$ (K)
$28_{1,27,2}$-$27_{1,26,2}$	240635.450	39.20	466.5	5.1[1]		1.58	
$28_{1,28,0}$-$27_{1,27,0}$	240635.452†	39.20	466.5	5.1[1]		”	
$27_{3,25,1}$-$26_{3,24,1}$	246800.036	37.20	470.6	4.8[1]		1.97	
$27_{3,24,0}$-$26_{3,23,0}$	246800.149†	37.20	470.6	4.9[1]		”	
$29_{2,28,1}$-$28_{2,27,1}$	252191.246	39.20	485.5	2.0[1]		1.39	
$29_{2,28,0}$-$28_{2,27,0}$	252194.705†	39.20	485.5	6.1[1]		”	
$28_{2,26,3}$-$27_{2,25,3}$	252441.465	37.60	487.7	4.2[1]		1.73	
$28_{3,26,1}$-$27_{3,25,1}$	256090.222	37.80	483.0	4.8[1,30,31]		0.74	
$28_{3,25,0}$-$27_{3,24,0}$	256090.358†	37.80	483.0	5.0[1,30,31]		”	
$30_{1,29,2}$-$29_{1,28,2}$	257578.164	40.30	490.8	5.2[1,32]		0.68	
$30_{1,30,0}$-$29_{1,29,0}$	257578.166†	40.30	490.8	5.2[1,32]		”	
$29_{3,26,2}$-$28_{3,25,2}$	257619.724	38.60	493.0	5.6[1,4]		0.80	
$29_{3,27,0}$-$28_{3,26,0}$	257623.517†	38.60	493.0	5.6[1,4]		”	
$30_{0,30,2}$-$29_{0,29,2}$	257630.349	40.30	490.8	5.4[1]		0.71	
$30_{0,30,0}$-$29_{0,29,0}$	257630.356†	40.30	490.8	5.4[1]		”	
$29_{1,28,3}$-$28_{1,27,3}$	258792.182	35.00	496.2	5.1[1]		0.73	
$29_{2,28,4}$-$28_{2,27,4}$	258792.707†	34.90	496.2	5.7[1]		”	
$29_{6,23,2}$-$28_{6,22,2}$	260594.218	35.00	521.8	4.1[1]		4.30	
$29_{6,24,0}$-$28_{6,23,0}$	260594.282†	35.20	521.8	4.2[1]		”	
$29_{6,24,1}$-$28_{6,23,1}$	260594.716†	35.00	521.8	4.6[1]		”	
$29_{6,23,0}$-$28_{6,22,0}$	260595.697†	35.20	521.8	5.8[1]		”	
$29_{5,24,3}$-$28_{5,23,3}$	260771.847	36.10	523.3	4.7[1]		2.64	
$29_{5,25,4}$-$28_{5,24,4}$	260772.535†	36.10	523.3	5.5[1]		”	
$29_{4,26,3}$-$28_{4,25,3}$	260815.923	37.20	512.7	3.7[1]		2.72	
$29_{3,26,5}$-$28_{3,25,5}$	260817.440†	37.20	512.7	5.5[1]		”	
$29_{5,25,1}$-$28_{5,24,1}$	261207.556	36.70	510.5	4.8[1]		2.23	
$29_{5,25,0}$-$28_{5,24,0}$	261207.787†	36.80	510.5	5.0[1]		”	
$29_{4,25,0}$-$28_{4,24,0}$	264276.041	37.90	502.2	5.8[1]		1.37	
$29_{4,26,1}$-$28_{4,25,1}$	264276.121†	37.90	502.2	5.9[1]		”	
$29_{3,26,3}$-$28_{3,25,3}$	264614.183	38.00	505.7	3.2[1]		1.02	
$29_{4,26,4}$-$28_{4,25,4}$	264616.242†	38.00	505.7	5.5[1]		”	
$29_{3,27,1}$-$28_{3,26,1}$	265331.381	38.40	495.7	4.5[1,22]		0.79	
$29_{3,26,0}$-$28_{3,25,0}$	265331.543†	38.40	495.7	4.6[1,22]		”	
		Wide comp.		3.3±0.6	25.7±1.5	0.31	3.6±0.2
		Narrow comp.		4.59±0.12	7.06±0.05	0.49	8.4±0.3
$30_{4,26,3}$-$29_{4,25,3}$	271124.448	37.70	526.0	4.2[1]		1.31	
$30_{4,26,5}$-$29_{4,25,5}$	271126.104†	37.70	526.0	6.1[1]		”	

Tabla A.1: continued.

Transition $J_{K_a,K_c,v} - J'_{K'_a,K'_c,v'}$	Predicted freq. (MHz)	S_{ij}	E_u (K)	v_{LSR} km s^{-1}	Δv km s^{-1}	$T_{MB}^{(2)}$ (K)	$\int T_{MB} dv$ (K)
$30_{4,27,0}$-$29_{4,26,0}$	272018.523	38.20	514.7	4.7$^{(1)}$		2.06	
$30_{4,26,2}$-$29_{4,25,2}$	272018.539†	38.20	514.7	4.7$^{(1)}$		”	

Tabla A1. Emission lines of CH_3CH_2CN ν_{13}=1/ν_{21}=1 present in the spectral scan of the Orion KL from the radio-telescope of IRAM 30-m. Column 1 indicates the line transition, the v quantum number defines A and E states: v=0 is A for the bend and v=3 is A for the torsion; v=1 and 2 are E for the bend and v=4 and 5 are E for the torsion, Col. 2 gives the predicted frequency in the laboratory, Col. 3 the line strength, Col. 4 upper level energy, Col. 5 observed radial velocities, Col. 6 the line widths derived by gaussian fits, Col. 7 mean beam temperature,and Col. 8 shows the area of the line. For some not blended lines we give line parameters obtained by Gaussian fits. † blended with the last one. (1) peak line observed velocity. (2) peak line intensity. (3) blended with U-line. (4) blended with CH_3CH_2CN ν_{20}. (5) blended with $(CH_3)_2CO$. (6) blended with $HC^{13}CCN$. (7) blended with $HC^{13}CCN$ ν_7=1. (8) blended with E-CH_3OD. (9) blended with $Si^{18}O$ v=0-3. (10) blended with E-$HCOOCH_3$. (11) blended with t-CH_3CH_2OH. (12) blended with $^{33}SO_2$. (13) blended with CH_3CHO ν_t=2. (14) blended with $SO^{18}O$. (15) blended with SO_2 ν_2=1. (16) blended with HCOOH. (17) blended with $CH_3CH_2C^{15}N$. (18) blended with CH_2CHCN ν_{11}=1. (19) blended with CH_2CHCN ν_{15}. (20) blended with $^{34}SO_2$. (21) blended with HCCCN. (22) influence of CH_3CH_2CN ν_{12}. (23) blended with CH_3CH_2CN. (24) blended with A-$HCOOCH_3$. (25) blended with CH_3OH, ν_t=0,1. (26) blended with g-CH_3CH_2OH. (27) blended with $^{13}CH_3OH$, ν_t=0,1. (28) blended with $CH_2{}^{13}CHCN$ ν_t=0. (29) blended with CH_3OCH_3. (30) blended with $SO^{17}O$. (31) blended with A-$HCOO^{13}CH_3$. (32) blended with E-$HCOO^{13}CH_3$.

Tabla A.2: Detected lines of CH_3CH_2CN ν_{20}

Transition $J_{K_a,K_c} - J'_{K'_a,K'_c}$	Predicted freq. (MHz)	S_{ij}	E_u (K)	v_{LSR} km s^{-1}	Δv km s^{-1}	T_{MB}[(2)] (K)	$\int T_{MB} dv$ (K)
$9_{2,8}$-$8_{2,7}$	80470.356	8.55	567.6	4.7[(1)]		0.03	
				5.8±0.7	11.3±1.5	0.03	0.40±0.05
$9_{6,4}$-$8_{6,3}$	80665.506	5.00	602.9	2.0[(1,3)]		0.25	
$9_{6,3}$-$8_{6,2}$	80665.506†	5.00	602.9	2.0[(1,3)]		”	
$9_{5,5}$-$8_{5,4}$	80668.091†	6.22	590.8	7.6[(1,3)]		”	
$9_{5,4}$-$8_{5,3}$	80668.091†	6.22	590.8	7.6[(1,3)]		”	
$9_{7,3}$-$8_{7,2}$	80669.367†	3.56	617.2	5.7[(1,3)]		”	
$9_{7,2}$-$8_{7,1}$	80669.367†	3.56	617.2	5.7[(1,3)]		”	
$9_{2,7}$-$8_{2,6}$	81319.905	8.55	567.7	6.1[(1,4)]		0.07	
$9_{1,8}$-$8_{1,7}$	82506.659	8.88	564.8	6.1[(1)]		0.05	
				6.0±0.3	4.6±0.7	0.04	0.21±0.03
$10_{4,7}$-$9_{4,6}$	89660.494	8.40	585.2	2.3[(1,5)]		0.14	
$10_{4,6}$-$9_{4,5}$	89661.472†	8.40	585.2	5.6[(1,5)]		”	
$10_{3,7}$-$9_{3,6}$	89754.552	9.10	577.5	5.7[(1,5)]		0.07	
$10_{2,8}$-$9_{2,7}$	90516.931	9.60	572.1	5.4[(1)]		0.06	
				5.5±0.4	9.8±1.6	0.05	0.54±0.10
$11_{1,11}$-$10_{1,10}$	95548.551	10.90	572.5	5.5[(1)]		0.06	
$11_{1,11}$-$10_{1,10}$	97010.944	11.00	572.0	6.4[(1)]		0.08	
				6.35±0.13	8.7±0.3	0.09	0.80±0.02
$11_{2,10}$-$10_{2,9}$	98258.296	10.60	576.6	1.6[(1)]		0.06	
				1.7±0.9	7.2±1.5	0.06	0.48±0.11
$11_{6,6}$-$10_{6,5}$	98601.198	7.73	611.9	5.0[(1)]		0.15	
$11_{6,5}$-$10_{6,4}$	98601.198†	7.73	611.9	5.0[(1)]		”	
$11_{7,5}$-$10_{7,4}$	98601.751†	6.55	626.2	6.6[(1)]		”	
$11_{7,4}$-$10_{7,3}$	98601.751†	6.55	626.2	6.6[(1)]		”	
				5.8±0.2	12.4±0.6	0.17	2.20±0.09
$11_{4,8}$-$10_{4,7}$	98642.179	9.55	589.9	5.0[(1)]		0.23	
$11_{4,7}$-$10_{4,6}$	98645.650†	9.55	589.9	4.4[(1)]		0.25	
$11_{3,9}$-$10_{3,8}$	98687.187	10.20	582.2	4.9[(1)]		0.07	
				4.8±1.0	6.8±1.4	0.06	0.37±0.09
$11_{3,8}$-$10_{3,7}$	98777.517	10.20	582.2	3.8[(1)]		0.07	
				3.1±0.4	13.2±0.7	0.06	0.83±0.09
$11_{2,9}$-$10_{2,8}$	99749.866	10.60	576.9	4.8[(1)]		0.08	
				4.8±0.2	9.2±0.4	0.08	0.83±0.09
$11_{1,10}$-$10_{1,9}$	100673.335	10.90	574.0	5.6[(1)]		0.09	
				5.1±0.4	5.2±0.7	0.06	0.25±0.05

Tabla A.2: continued.

Transition $J_{K_a,K_c} - J'_{K'_a,K'_c}$	Predicted freq. (MHz)	S_{ij}	E_u (K)	v_{LSR} km s^{-1}	Δv km s^{-1}	T_{MB}[(2)] (K)	$\int T_{MB} dv$ (K)
$12_{1,12}$-$11_{1,11}$	104166.301	11.90	577.5	4.7[(1)]		0.11	
				4.7±0.2	5.9±0.7	0.10	0.63±0.09
$12_{0,12}$-$11_{0,11}$	105570.959	12.00	577.1	4.3[(1)]		0.11	
				3.8±1.7	9.0±3.2	0.12	0.9±0.3
$12_{2,11}$-$11_{2,10}$	107132.018	11.70	581.8	5.1[(1)]		0.10	
		Wide comp.		4.1±0.8	13.1±1.9	0.09	1.2±0.2
		Narrow comp.		5.4±2.0	2.9±4.2	0.02	0.052±0.10
$12_{7,6}$-$11_{7,5}$	107569.213	7.92	631.4	0.8[(1)]		0.16	
$12_{7,5}$-$11_{7,4}$	107569.213†	7.92	631.4	0.8[(1)]		”	
$12_{6,7}$-$11_{6,6}$	107571.220†	9.00	617.1	6.4[(1)]		”	
$12_{6,6}$-$11_{6,5}$	107571.221†	9.00	617.1	6.4[(1)]		”	
				3.7±0.7	11.7±1.9	0.16	2.0±0.3
$12_{8,5}$-$11_{8,4}$	107575.295	6.67	647.9	4.00[(1)]		0.12	
$12_{8,4}$-$11_{8,3}$	107575.295†	6.67	647.9	4.0[(1)]		”	
				3.8±0.3	8.1±0.9	0.12	1.01±0.10
$12_{3,10}$-$11_{3,9}$	107677.926	11.20	587.4	5.1[(1)]		0.10	
				5.1±0.2	7.8±0.8	0.09	0.60±0.04
$12_{3,9}$-$11_{3,8}$	107817.578	11.20	587.4	5.4[(1)]		0.08	
				5.5±0.5	7.2±1.0	0.08	0.62±0.08
$12_{2,10}$-$11_{2,9}$	107817.578	11.70	582.1	4.8[(1)]		0.10	
				4.88±0.13	7.5±0.3	0.10	0.81±0.03
$12_{1,11}$-$11_{1,10}$	109715.553	11.90	579.3	5.9[(1)]		0.11	
				5.91±0.12	8.3±0.3	0.11	0.98±0.03
$13_{1,13}$-$12_{1,12}$	112771.434	12.90	583.0	4.9[(1)]		0.14	
				4.2±0.2	10.1±0.6	0.13	1.42±0.07
$13_{0,13}$-$12_{0,12}$	114090.739	13.00	582.5	4.3[(1,6)]		0.24	
$15_{0,15}$-$14_{0,14}$	131038.929	15.00	594.7	4.3[(1)]		0.23	
				4.06±0.11	9.4±0.4	0.21	1.57±0.08
$15_{2,14}$-$14_{2,13}$	133659.207	14.70	599.7	4.6[(1)]		0.21	
				4.06±0.11	8.1±0.4	0.20	1.72±0.14
$15_{9,6}$-$14_{9,5}$	134487.418	9.60	684.4	3.0[(1)]		0.19	
$15_{9,7}$-$14_{9,6}$	134487.418†	9.60	684.4	3.0[(1)]		”	
$15_{6,10}$-$14_{6,9}$	134491.599	12.60	635.2	3.9[(1)]		0.28	
$15_{6,9}$-$14_{6,8}$	134491.603†	12.60	635.2	3.9[(1)]		”	
				3.7±0.2	5.3±0.5	0.18	1.00±0.14
$15_{3,12}$-$14_{3,11}$	135071.345	14.40	605.5	4.5[(1)]		0.18	
				4.6±0.2	8.5±0.9	0.15	1.4±0.2

Tabla A.2: continued.

Transition $J_{K_a,K_c} - J'_{K'_a,K'_c}$	Predicted freq. (MHz)	S_{ij}	E_u (K)	v_{LSR} km s^{-1}	Δv km s^{-1}	$T_{MB}{}^{(2)}$ (K)	$\int T_{MB} dv$ (K)
$15_{2,13}$-$14_{2,12}$	136907.490	14.70	600.5	4.7[1,6]		0.41	
$16_{1,16}$-$15_{1,15}$	138507.416	15.90	601.7	2.3[1]		0.24	
				2.4±0.3	13.4±0.4	0.24	3.46±0.02
$16_{9,8}$-$15_{9,7}$	143454.754	10.90	691.5	3.6[1]		0.27	
$16_{9,7}$-$15_{9,6}$	143454.754†	10.90	691.5	3.6[1]		”	
				3.52±0.05	7.49±0.14	0.25	2.02±0.04
$16_{3,14}$-$15_{3,13}$	143640.082	15.40	612.4	3.5[1,7,8]		0.52	
$16_{4,12}$-$15_{4,11}$	143646.142	15.00	620.1	5.1[1]		0.40	
				4.8±0.2	7.0±0.6	0.29	2.2±0.4
$16_{3,13}$-$15_{3,12}$	144211.335	15.40	612.4	5.1[1,9,10]		0.31	
$16_{1,15}$-$15_{1,14}$	145512.937	15.90	604.7	4.9[1,11]		0.40	
$16_{2,14}$-$15_{2,13}$	146209.046	15.80	607.5	5.8[1]		0.25	
				6.0±0.3	7.3±0.8	0.24	1.9±0.2
$17_{1,17}$-$16_{1,16}$	147061.444	16.90	608.7	4.1[1]		0.40	
$17_{0,17}$-$16_{0,16}$	147915.039	16.90	608.7	3.8[1]		0.46	
$17_{2,16}$-$16_{2,15}$	151256.466	16.80	613.8	4.0[1]		0.27	
				4.0±0.3	11.5±1.0	0.26	3.2±0.2
$17_{8,10}$-$16_{8,9}$	152415.995	13.20	680.2	3.4[1]		0.30	
$17_{8,9}$-$16_{8,8}$	152415.995†	13.20	680.2	3.4[1]		”	
$17_{7,11}$-$16_{7,10}$	152422.288	14.10	663.7	2.8[1]		0.60	
$17_{7,10}$-$16_{7,9}$	152422.288†	14.10	663.7	2.8[1]		”	
$17_{9,9}$-$16_{9,8}$	152422.372†	12.20	698.8	3.0[1]		”	
$17_{9,8}$-$16_{9,7}$	152422.372†	12.20	698.8	3.0[1]		”	
$17_{1,16}$-$16_{1,15}$	154345.084	16.90	612.1	4.9[1]		0.28	
				5.0±0.2	8.1±0.5	0.23	1.93±0.11
$18_{1,18}$-$17_{1,17}$	155604.383	17.90	616.2	5.0[1,8]		0.49	
$18_{1,18}$-$17_{1,17}$	155604.383	17.90	616.2	5.0[1,8]		0.49	
$18_{0,18}$-$17_{0,17}$	156341.680	17.90	616.0	5.0[1,12]		0.44	
$18_{2,17}$-$17_{2,16}$	160026.639	17.80	621.5	5.1[1,13]		0.46	
$18_{11,8}$-$17_{11,7}$	161426.944	11.30	750.5	1.4[1]		0.75	
$18_{11,7}$-$17_{11,6}$	161426.944†	11.30	750.5	1.4[1]		”	
$18_{6,13}$-$17_{6,12}$	161430.232†	16.00	657.1	4.8[1]		”	
$18_{6,12}$-$17_{6,11}$	161430.269†	16.00	657.1	4.8[1]		”	
$18_{3,15}$-$17_{3,14}$	162591.902	17.50	627.6	4.2[1]		0.33	
				4.3±0.2	7.9±0.7	0.21	1.8±0.2
$19_{1,19}$-$18_{1,18}$	164137.082	18.90	624.1	3.9[1]		0.33	
				4.1±0.2	6.21±0.48	0.21	1.4±0.2

Tabla A.2: continued.

Transition $J_{K_a,K_c} - J'_{K'_a,K'_c}$	Predicted freq. (MHz)	S_{ij}	E_u (K)	v_{LSR} km s^{-1}	Δv km s^{-1}	$T_{MB}{}^{(2)}$ (K)	$\int T_{MB} dv$ (K)
$18_{2,16}$-$17_{2,15}$	164765.029	17.80	622.9	3.4[1]		0.52	
$19_{0,19}$-$18_{0,18}$	164766.518†	18.90	623.9	6.1[1]		”	
				5.0±0.4	9.7±0.8	0.45	4.7±0.4
$19_{8,12}$-$18_{8,11}$	170356.990	15.60	696.1	2.4[1,14]		0.72	
$19_{8,11}$-$18_{8,10}$	170356.990†	15.60	696.1	2.4[1,14]		”	
$19_{9,11}$-$18_{9,10}$	170358.512†	14.70	714.8	5.1[1,14]		”	
$19_{9,10}$-$18_{9,9}$	170358.512†	14.70	714.8	5.1[1,14]		”	
$19_{3,16}$-$18_{3,15}$	171835.966	18.50	635.9	5.3[1]		0.53	
$22_{10,13}$-$21_{10,12}$	197272.588	17.50	762.7	0.8[1,15]		0.67	
$22_{10,12}$-$21_{10,11}$	197272.588†	17.50	762.7	0.8[1,15]		”	
$22_{8,15}$-$21_{8,14}$	197274.492†	19.10	723.2	3.7[1,15]		”	
$22_{8,14}$-$21_{8,13}$	197274.492†	19.10	723.2	3.7[1,15]		”	
$22_{11,11}$-$21_{11,10}$	197292.236	16.50	785.8	4.0[1,7]		0.51	
$22_{11,12}$-$21_{11,11}$	197292.236†	16.50	785.8	4.0[1,7]		”	
$23_{1,23}$-$22_{1,22}$	198182.913	22.90	659.7	4.1[1]		0.55	
				4.31±0.10	6.5±0.3	0.51	3.5±0.2
$23_{0,23}$-$22_{0,22}$	198488.522	22.90	659.6	4.5[1]		0.59	
				4.51±0.12	6.6±0.3	0.55	5.1±0.2
$22_{3,19}$-$21_{3,18}$	199775.037	21.60	663.3	5.0[1]		0.29	
				5.2±0.2	9.2±0.5	0.29	2.83±0.14
$22_{2,20}$-$21_{3,19}$	201512.520	21.80	658.9	4.6[1]		0.41	
				4.67±0.12	8.2±0.3	0.41	3.52±0.11
$23_{2,22}$-$22_{3,21}$	203579.325	22.80	666.2	7.1[1]		0.46	
				7.8±0.3	17.8±0.4	0.46	8.7±0.3
$23_{5,18}$-$22_{5,17}$	206562.179	21.90	690.3	4.2[1]		0.38	
$23_{3,20}$-$22_{3,19}$	209144.078	22.60	673.3	5.1[1]		0.54	
$23_{2,21}$-$22_{2,20}$	210596.535	22.80	669.0	5.2[1]		0.47	
				5.3±0.2	12.6±0.7	0.44	5.9±0.2
$24_{2,23}$-$23_{2,22}$	212230.463	23.80	676.4	4.3[1,9]		0.33	
$24_{7,18}$-$23_{7,17}$	215274.435	22.00	726.9	2.1[1]		0.47	
$24_{7,17}$-$23_{7,16}$	215274.456†	22.00	726.9	2.1[1]		”	
				2.0±0.2	10.7±0.7	0.45	5.3±0.2
$25_{0,25}$-$24_{0,24}$	215370.956	24.90	679.9	3.6[1]		0.62	
				0.2±0.4	5.2±0.3	0.40	2.3±0.2
$24_{6,19}$-$23_{6,18}$	215376.496	22.50	712.7	2.7[1]		0.77	
$24_{6,18}$-$23_{6,17}$	215377.432†	22.50	712.7	4.0[1]		”	
				3.32±0.05	6.07±0.12	0.78	5.12±0.10

TABLA A.2: CONTINUED.

Transition $J_{K_a,K_c} - J'_{K'_a,K'_c}$	Predicted freq. (MHz)	S_{ij}	E_u (K)	v_{LSR} km s^{-1}	Δv km s^{-1}	$T_{MB}{}^{(2)}$ (K)	$\int T_{MB} dv$ (K)
$24_{4,21}$-$23_{4,20}$	215782.255	23.00	690.8	3.6[1]		0.46	
				3.71±0.08	7.9±0.2	0.44	3.76±0.14
$24_{3,21}$-$23_{3,20}$	218529.971	23.60	683.8	3.7[1]		0.63	
$24_{3,22}$-$23_{3,21}$	219632.027	23.80	679.6	4.4[1]		0.62	
$25_{2,24}$-$24_{2,23}$	220862.669	24.80	687.0	3.5[1,15]		0.55	
$26_{0,26}$-$25_{0,25}$	223816.798	25.90	690.6	5.5[1,7]		0.67	
$25_{3,23}$-$24_{3,22}$	224107.320	24.60	693.7	3.9[1,7]		0.63	
$25_{2,23}$-$24_{2,22}$	228615.634	24.80	690.5	3.5[1]		0.58	
				3.4±0.4	10.2±1.1	0.56	6.1±0.6
$26_{2,25}$-$25_{2,24}$	229476.628	25.80	698.0	4.8[1]		0.46	
$26_{8,19}$-$25_{8,18}$	233177.263	23.50	765.4	2.2[1,15,7]		0.41	
$26_{8,18}$-$25_{8,17}$	233177.264†	23.50	765.4	2.2[1,15,7]		”	
$26_{12,15}$-$25_{12,14}$	233179.289†	20.50	853.2	4.8[1,15,7]		”	
$26_{12,14}$-$25_{12,13}$	233179.289†	20.50	853.2	4.8[1,15,7]		”	
$26_{7,20}$-$25_{7,19}$	233247.719	24.10	748.9	3.4[1,15]		0.35	
$26_{7,19}$-$25_{7,18}$	233247.780†	24.10	748.9	3.5[1,15]		”	
$26_{4,22}$-$25_{4,21}$	234593.014	25.40	712.9	4.4[1]		0.60	
$26_{2,24}$-$25_{2,23}$	237544.142	25.80	701.9	4.4[1,5,16,17]		0.49	
$27_{2,26}$-$26_{2,25}$	238073.154	26.80	709.4	4.2[1]		0.39	
				4.30±0.12	7.0±0.5	0.39	2.9±0.2
$27_{12,16}$-$26_{12,15}$	242142.272	21.70	864.8	2.8[5]		0.28	
$27_{12,15}$-$26_{12,14}$	242142.272†	21.70	864.8	2.8[5]		”	
$27_{8,20}$-$26_{8,19}$	242155.477	24.60	777.0	2.9[1]		0.47	
$27_{8,19}$-$26_{8,18}$	242155.479†	24.60	777.0	2.9[1]		”	
				2.9±0.2	5.8±0.3	0.47	5.2±0.3
$27_{4,24}$-$26_{4,23}$	242845.180	26.40	724.4	4.7[1,18]		0.90	
$28_{1,27}$-$27_{1,26}$	248256.770	27.80	720.8	4.9[1,5]		1.16	
$29_{1,29}$-$28_{1,28}$	249079.493	28.90	725.3	3.8[1,19]		0.74	
$28_{6,23}$-$27_{6,22}$	251409.069	26.70	758.3	1.4[1,20]		0.89	
$28_{6,22}$-$27_{6,21}$	251407.801	26.70	758.3	7.5[1,20]		0.89	
$28_{4,24}$-$27_{4,23}$	253074.062	27.40	736.8	0.4[1]		0.92	
$28_{3,25}$-$27_{3,24}$	256057.617	27.70	730.3	2.8[1,21]		0.38	
$29_{1,28}$-$28_{1,27}$	256622.105	27.70	730.3	4.1[1]		0.46	
				4.2±0.2	6.8±0.7	0.44	3.2±0.4
$30_{1,30}$-$29_{1,29}$	257549.349	29.90	737.6	5.2[1]		0.20	
				5.16±0.06	4.3±0.2	0.21	0.95±0.03
$30_{0,30}$-$29_{0,29}$	257619.312	29.90	737.6	4.1[1,8]		0.80	

Tabla A.2: continued.

Transition $J_{K_a,K_c} - J'_{K'_a,K'_c}$	Predicted freq. (MHz)	S_{ij}	E_u (K)	v_{LSR} km s^{-1}	Δv km s^{-1}	$T_{MB}{}^{(2)}$ (K)	$\int T_{MB} dv$ (K)
$29_{3,27}$-$28_{3,26}$	259436.760	29.90	737.6	3.7$^{(1,22)}$		0.50	
$29_{12,18}$-$28_{12,17}$	260066.278	24.00	889.4	1.9$^{(1)}$		0.91	
$29_{12,17}$-$28_{12,16}$	260066.278†	24.00	889.4	1.9$^{(1)}$		”	
$29_{8,22}$-$28_{8,21}$	260115.183	26.80	801.5	3.36$^{(1)}$		1.12	
$29_{8,21}$-$28_{8,20}$	260115.189†	26.80	801.5	3.4$^{(1)}$		”	
$29_{4,26}$-$28_{4,25}$	260857.503	28.40	749.0	3.7$^{(1,5)}$		1.57	
$29_{4,25}$-$28_{4,24}$	262365.724	28.40	749.4	3.8$^{(1,6)}$		0.49	
$30_{2,29}$-$29_{2,28}$	263767.717	29.80	746.2	7.0$^{(1)}$		0.56	
$29_{2,27}$-$28_{2,26}$	263971.820	28.80	738.7	3.6$^{(1)}$		0.44	
$30_{1,29}$-$29_{1,28}$	264986.039	29.80	745.9	4.0$^{(1)}$		0.32	
				4.0±0.2	4.5±0.4	0.31	1.49±0.10
$29_{3,26}$-$28_{3,25}$	265389.404	28.70	743.0	3.4$^{(1)}$		0.37	
				3.35±0.10	8.2±0.3	0.38	3.22±0.08
$30_{3,28}$-$29_{3,27}$	268214.513	29.70	753.9	2.5$^{(1)}$		0.54	
$30_{8,23}$-$29_{8,22}$	269096.747	27.90	814.4	4.6$^{(1,15)}$		0.13	
$30_{8,22}$-$29_{8,21}$	269096.757†	27.90	814.4	4.6$^{(1,15)}$		”	
$30_{4,26}$-$29_{4,25}$	271692.172	29.50	762.4	3.4$^{(1)}$		0.62	
$31_{2,30}$-$30_{2,29}$	272304.403	30.80	759.2	3.8$^{(1)}$		0.68	
				3.9±0.6	7.7±1.8	0.65	5.3±1.1
$31_{1,30}$-$30_{1,29}$	273352.181	30.80	759.0	3.3$^{(1)}$		0.68	
				3.3±0.4	13.8±1.3	0.64	8.1±0.6
$32_{1,32}$-$31_{1,31}$	274481.096	31.90	763.6	4.0$^{(1)}$		0.59	
				3.76±0.09	4.5±0.2	0.56	2.7±0.2
$30_{3,27}$-$29_{3,26}$	274685.183	29.70	756.2	3.7$^{(1)}$		0.58	
				3.7±0.2	7.5±1.0	0.54	4.3±0.5
$31_{3,29}$-$30_{3,28}$	276969.491	30.70	767.2	4.6$^{(1,10,22,23)}$		0.69	

Tabla A2. Emission lines of CH_3CH_2CN ν_{20} present in the spectral scan of the Orion KL from the radio-telescope of IRAM 30-m. Column 1 indicates the line transition, Col. 2 gives the predicted frequency in the laboratory, Col. 3 the line strength, Col. 4 upper level energy, Col. 5 observed radial velocities, Col. 6 observed line widths, Col. 7 mean beam temperature, and Col. 8 the area of the line. For some not blended lines we give line parameters obtained by Gaussian fits. † blended with the last one.

(1) peak line observed velocity. (2) peak line intensity. (3) blended with CH_3OH, ν_t=0,1. (4) blended with $H_2C^{17}O$. (5) blended with U-line. (6) blended with ^{18}OCS. (7) blended with E-$HCOOCH_3$. (8) blended with CH_3CH_2CN ν_{13}=1/ν_{21}=1. (9) blended with A-$H^{13}COOCH_3$. (10) blended with E-$H^{13}COOCH_3$. (11) blended with $HCC^{13}CN$ ν_7=1. (12) blended with SHD. (13) blended with $CH_3CH_2{}^{13}CN$. (14) influence of CH_3CH_2CN ν_{12}=1. (15) blended with A-$HCOOCH_3$. (16) blended with CH_3OCH_3. (17) blended with $(CH_3)_2CO$. (18) blended with CH_3CHDCN. (19) blended with $HCOO^{13}CH_3$. (20) blended with $^{33}SO_2$. (21) blended with $HC^{13}CCN$ ν_6=1. (22) blended with $CH_3{}^{13}CH_2CN$. (23) blended with $H^{15}NCO$.

TABLA A.3: DETECTED LINES OF CH_3CH_2CN ν_{12}=1

Transition $J_{K_a,K_c} - J'_{K'_a,K'_c}$	Predicted freq. (MHz)	S_{ij}	E_u (K)	Observed freq. (MHz)	v_{LSR}[1] km s^{-1}	Observed T_{MB} (K)	Model T_{MB} (K)
$9_{2,8}$-$8_{2,7}$	80288.056	8.55	799.3	80290.1	1.5	0.01	0.02
$9_{8,1}$-$8_{8,0}$	80495.806	1.89	867.3	80496.5	6.4	0.02	0.01
$9_{8,2}$-$8_{8,1}$	80495.806†	1.89	867.3	”	6.4	”	”
$9_{4,6}$-$8_{4,5}$	80498.676	7.22	813.0	80499.8	4.8	0.02	0.02
$9_{4,5}$-$8_{4,4}$	80499.106†	7.22	813.0	”	6.4	”	”
$9_{3,7}$-$8_{3,6}$	80528.735	8.00	805.0	80530.5	2.4	0.02	0.02
$9_{3,6}$-$8_{3,5}$	80560.434	8.00	805.0	80562.0	3.2	0.02	0.02
$9_{2,7}$-$8_{2,6}$	81129.013	8.55	799.5	81130.5	3.5	0.03	0.02
$10_{1,10}$-$9_{1,9}$	86693.722	9.90	799.6	86694.4[2]	6.8	0.05	0.02
$10_{0,10}$-$9_{0,9}$	88211.372	9.98	799.0	88212.5	5.1	0.01	0.03
$10_{7,4}$-$9_{7,3}$	89432.639	5.10	854.6	89434.7	2.2	0.04	0.04
$10_{7,3}$-$9_{7,2}$	89432.639†	5.10	854.6	”	2.2	”	”
$10_{5,6}$-$9_{5,5}$	89434.665	7.50	827.5	”	9.0	”	”
$10_{5,5}$-$9_{5,4}$	89434.673†	7.50	827.5	”	9.0	”	”
$10_{9,2}$-$9_{9,1}$	89453.471	1.90	890.8	89456.0	0.5	0.05	0.04
$10_{9,1}$-$9_{9,0}$	89453.471†	1.90	890.8	”	0.5	”	”
$10_{4,7}$-$9_{4,6}$	89455.811†	8.40	817.3	”	8.4	”	”
$10_{4,6}$-$9_{4,5}$	89456.740†	8.40	817.3	”	6.5	”	”
$10_{3,7}$-$9_{3,6}$	89547.806	9.10	809.3	89549.5	3.3	0.01	0.02
$10_{1,9}$-$9_{1,8}$	91421.404	9.89	800.8	91423.2	3.1	...	0.03
$11_{1,11}$-$10_{1,10}$	95304.641	10.90	804.2	95306.4	3.5	...	0.03
$11_{6,6}$-$10_{6,5}$	98377.598	7.73	844.6	98379.5	3.2	0.04	0.05
$11_{6,5}$-$10_{6,4}$	98377.598†	7.73	844.6	”	3.2	”	”
$11_{7,5}$-$10_{7,4}$	98378.958†	6.55	859.3	”	7.3	”	”
$11_{7,4}$-$10_{7,3}$	98378.958†	6.55	859.3	”	7.3	”	”
$11_{8,3}$-$10_{8,2}$	98386.910	5.18	876.3	98388.5	4.2	0.07	0.06
$11_{8,4}$-$10_{8,3}$	98386.910†	5.18	876.3	”	4.2	”	”
$11_{5,7}$-$10_{5,6}$	98386.990†	8.73	832.2	”	4.5	”	”
$11_{5,6}$-$10_{5,5}$	98387.009†	8.73	832.2	”	4.5	”	”
$11_{10,1}$-$10_{10,0}$	98415.812	1.91	916.9	98417.7[3]	...	...	0.04
$11_{10,2}$-$10_{10,1}$	98415.812†	1.91	916.9	”	...	”	”
$11_{4,8}$-$10_{4,7}$	98416.866†	9.55	822.0	”	...	”	”
$11_{4,7}$-$10_{4,6}$	98418.721†	9.55	822.0	”	...	”	”
$11_{2,9}$-$10_{2,8}$	99515.201	10.60	808.6	99516.7	4.4	0.04	0.03
$11_{1,10}$-$10_{1,9}$	100475.798	10.90	805.7	100477.5	4.0	0.02	0.04
$12_{1,12}$-$11_{1,11}$	103901.878	11.90	809.1	103903.8	3.5	0.02	0.04

Tabla A.3: continued.

Transition $J_{K_a,K_c} - J'_{K'_a,K'_c}$	Predicted freq. (MHz)	S_{ij}	E_u (K)	Observed freq. (MHz)	v_{LSR}[1] km s^{-1}	Observed T_{MB} (K)	Model T_{MB} (K)
$12_{0,12}$-$11_{0,11}$	105340.456	12.00	808.7	105341.5	6.0	0.03	0.05
$12_{2,12}$-$11_{2,11}$	106890.772	11.70	813.5	106892.4	4.5	0.06	0.04
$12_{7,6}$-$11_{7,5}$	107326.124	7.92	864.5	107328.5	2.4	0.07	0.08
$12_{7,5}$-$11_{7,4}$	107326.124†	7.92	864.5	”	2.4	”	”
$12_{6,7}$-$11_{6,6}$	107327.223†	9.00	849.8	”	5.4	”	”
$12_{6,6}$-$11_{6,5}$	107327.223†	9.00	849.8	”	5.4	”	”
$12_{5,8}$-$11_{5,7}$	107341.835	9.92	837.3	107342.5	7.1	0.05	0.06
$12_{5,7}$-$11_{5,6}$	107341.879†	9.92	837.3	”	7.2	”	”
$12_{9,4}$-$11_{9,3}$	107345.781	5.25	900.6	107345.9	8.7	0.04	0.03
$12_{9,3}$-$11_{9,2}$	107345.781†	5.25	900.6	”	8.7	”	”
$12_{4,9}$-$11_{4,8}$	107382.132	10.70	827.1	107384.0	3.8	0.04	0.04
$12_{11,2}$-$11_{11,1}$	107383.310†	1.92	945.8	”	7.0	”	”
$12_{11,1}$-$11_{11,0}$	107383.310†	1.92	945.8	”	7.0	”	”
$12_{4,8}$-$11_{4,7}$	107385.602†	10.70	827.1	”	4.6	”	”
$12_{3,10}$-$11_{3,9}$	107432.034	11.20	819.2	107433.2	5.8	0.04	0.04
$12_{2,10}$-$11_{2,9}$	108757.664	11.70	813.8	108758.2[4]	7.5	0.03	0.05
$13_{1,13}$-$12_{1,12}$	112485.400	12.90	814.5	112487.6	3.1	0.04	0.06
$13_{0,13}$-$12_{0,12}$	113840.833	13.00	814.1	113841.3	7.7	0.08	0.06
$15_{0,15}$-$14_{0,14}$	130747.416	15.00	826.3	130749.0	5.4	0.08	0.08
$15_{7,9}$-$14_{7,8}$	134173.563	11.70	882.5	134176.9	1.5	0.10	0.13
$15_{7,8}$-$14_{7,7}$	134173.563†	11.70	882.5	”	1.5	”	”
$15_{8,8}$-$14_{8,7}$	134175.060†	10.70	899.5	”	4.9	”	”
$15_{8,7}$-$14_{8,6}$	134175.060†	10.70	899.5	”	4.9	”	”
$15_{4,11}$-$14_{4,10}$	134322.280	13.90	845.2	134322.6	8.3	0.07	0.07
$15_{3,13}$-$14_{3,12}$	134346.381	14.40	837.3	134347.6	6.2	0.05	0.08
$15_{3,12}$-$14_{3,11}$	134753.144	14.40	837.3	134754.6	5.8	0.03	0.08
$15_{1,14}$-$14_{1,13}$	136367.688	14.90	829.3	136370.3	3.2	0.13	0.09
$15_{2,13}$-$14_{2,12}$	136594.777	14.70	832.1	136596.5	5.2	0.09	0.09
$16_{0,16}$-$15_{0,15}$	139168.744	15.90	832.9	139171.3[5]	3.4	0.14	0.10
$16_{8,9}$-$15_{8,8}$	143123.571	12.00	906.3	143126.3	3.3	0.13	0.17
$16_{8,8}$-$15_{8,7}$	143123.571†	12.00	906.3	”	3.3	”	”
$16_{7,10}$-$15_{7,9}$	143124.942†	12.90	889.4	”	6.1	”	”
$16_{7,9}$-$15_{7,8}$	143124.942†	12.90	889.4	”	6.1	”	”
$16_{9,8}$-$15_{9,7}$	143133.124	10.90	925.5	143134.9	5.2	0.06	0.08
$16_{9,7}$-$15_{9,6}$	143133.124†	10.90	925.5	”	5.2	”	”
$16_{6,11}$-$15_{6,10}$	143143.165	13.80	874.7	143145.0	5.1	0.11	0.13
$16_{6,10}$-$15_{6,9}$	143143.174†	13.80	874.7	”	5.1	”	”

Tabla A.3: continued.

Transition $J_{K_a,K_c} - J'_{K'_a,K'_c}$	Predicted freq. (MHz)	S_{ij}	E_u (K)	Observed freq. (MHz)	v_{LSR}[1] km s^{-1}	Observed T_{MB} (K)	Model T_{MB} (K)
$16_{12,5}$-$15_{12,4}$	143202.870	7.00	996.6	143205.0[2]	4.5	0.14	0.03
$16_{12,4}$-$15_{12,3}$	143202.870†	7.00	996.6	”	4.5	”	”
$16_{3,14}$-$15_{3,13}$	143314.370	15.40	844.2	143316.3[6]	4.9	0.19	0.15
$16_{4,12}$-$15_{4,11}$	143315.895†	15.00	852.1	”	8.1	”	”
$16_{1,15}$-$15_{1,14}$	145238.109	15.90	836.2	145239.4	6.2	0.12	0.11
$17_{2,16}$-$16_{2,15}$	150920.075	16.80	845.5	150921.5[7]	6.1	0.11	0.11
$17_{8,10}$-$16_{8,9}$	152072.752	13.20	913.6	152073.8	7.0	0.14	0.12
$17_{8,9}$-$16_{8,8}$	152072.752†	13.20	913.6	”	7.0	”	”
$17_{2,15}$-$16_{2,14}$	155153.262	16.80	846.6	155153.2[2]	8.8	0.12	0.12
$18_{8,11}$-$17_{8,10}$	161022.640	14.40	921.4	161023.8	6.9	0.13	0.13
$18_{8,10}$-$17_{8,9}$	161022.640†	14.40	921.4	”	6.9	”	”
$18_{9,10}$-$17_{9,9}$	161028.416	13.50	940.6	161032.5[8]	1.3	0.31	0.15
$18_{9,9}$-$17_{9,8}$	161028.416†	13.50	940.6	”	1.3	”	”
$18_{7,12}$-$17_{7,11}$	161031.502	15.30	904.4	”	7.1	”	0.18
$18_{7,11}$-$17_{7,10}$	161031.502†	15.30	904.4	”	7.1	”	”
$18_{5,14}$-$17_{5,13}$	161136.123	16.60	877.3	161139.3	3.1	0.16	0.17
$18_{5,13}$-$17_{5,12}$	161138.006†	16.60	877.3	”	6.6	”	”
$18_{1,17}$-$17_{1,16}$	162827.458	17.90	851.4	162830.1	4.2	0.13	0.13
$19_{1,19}$-$18_{1,18}$	163720.308	18.90	855.6	163722.5	4.9	0.17	0.14
$18_{2,16}$-$17_{2,15}$	164407.020	17.80	854.5	164409.0[9]	5.4	0.19	0.13
$19_{7,13}$-$18_{7,12}$	169986.831	16.40	912.6	169989.6[2]	4.1	0.44	0.18
$19_{7,12}$-$18_{7,11}$	169986.832†	16.40	912.6	”	4.1	...	”
$19_{5,15}$-$18_{5,14}$	170114.621	17.70	885.4	170117.5	3.8	0.15	0.15
$19_{5,14}$-$18_{5,13}$	170117.700	17.70	885.4	”	8.7	”	”
$19_{1,18}$-$18_{1,17}$	171540.387	18.90	859.7	171542.7	4.9	0.21	0.15
$22_{2,20}$-$21_{2,19}$	201109.338	21.80	890.4	201111.4	6.0	0.16	0.19
$23_{2,22}$-$22_{2,21}$	203132.611	22.80	897.7	203135.0[10]	5.4	0.11	0.19
$24_{1,23}$-$23_{1,22}$	214290.671	23.90	907.0	214292.6	6.3	0.12	0.21
$24_{3,22}$-$23_{3,21}$	214753.726	23.60	914.6	214756.3	5.4	0.12	0.21
$25_{0,25}$-$24_{0,24}$	214833.410	24.90	911.2	214836.7[4,11]	4.4	0.36	0.21
$24_{6,19}$-$23_{6,18}$	214886.143	22.50	945.1	214889.5	4.3	0.24	0.29
$24_{6,18}$-$23_{6,17}$	214886.999†	22.50	945.1	”	5.5	”	”
$26_{0,26}$-$25_{0,25}$	223254.102	25.90	921.9	223256.1[10]	6.3	0.30	0.22
$25_{3,23}$-$24_{3,22}$	223620.285	24.60	925.4	223623.7[12]	4.5	0.36	0.20
$25_{3,22}$-$24_{3,21}$	227376.660	24.60	926.3	227378.6[2]	6.5	0.33	0.21
$25_{2,23}$-$24_{2,22}$	228187.982	24.80	922.0	228189.8	6.6	0.22	0.22
$26_{1,25}$-$25_{1,24}$	231090.514	25.80	928.8	231092.1	6.9	0.18	0.22

TABLA A.3: CONTINUED.

Transition $J_{K_a,K_c} - J'_{K'_a,K'_c}$	Predicted freq. (MHz)	S_{ij}	E_u (K)	Observed freq. (MHz)	v_{LSR}[(1)] km s^{-1}	Observed T_{MB} (K)	Model T_{MB} (K)
$27_{1,27}$-$26_{1,26}$	231532.301	26.90	933.1	231536.1[(2)]	4.1	0.12	0.02
$27_{0,27}$-$26_{0,26}$	231677.353	26.90	933.0	231679.9	5.6	0.18	0.23
$27_{4,24}$-$26_{4,23}$	242297.460	26.40	956.2	242300.4	5.3	0.13	0.20
$28_{7,22}$-$27_{7,21}$	250659.807	26.30	1005.3	250658.5[(2,13)]	7.4	0.09	0.31
$28_{7,21}$-$27_{7,20}$	250659.951†	26.30	1005.3	”	7.3	”	”
$28_{5,24}$-$27_{5,23}$	251113.452	27.10	978.3	251117.5	4.2	0.15	0.21
$29_{3,27}$-$28_{3,26}$	258887.069	28.70	972.5	258888.5	7.3	0.12	0.23
$30_{2,29}$-$29_{2,28}$	263189.521	29.80	977.5	263192.5	5.6	0.16	0.23
$31_{3,29}$-$30_{3,28}$	276389.827	30.70	998.6	276391.8	6.9	0.31	0.22
$31_{5,26}$-$30_{5,25}$	278417.211	30.20	1017.1	278422.0	3.8	0.38	0.20

Tabla A3. Emission lines of CH_3CH_2CN ν_{12}=1 present in the spectral scan of the Orion KL from the radio-telescope of IRAM 30-m. Column 1 indicates the line transition, Col. 2 gives the predicted frequency in the laboratory, Col. 3 the line strength, Col. 4 upper level energy, Col. 5 observed centroid frequencies, Col. 6 observed radial velocities, Col. 7 observed mean beam temperature, and Col. 8 mean beam temperature obtained with the model.

(1) peak line observed velocity. (2) blended with U-line. (3) blended with ^{33}SO. (4) blended with A-$HCOOCH_3$. (5) blended with C-C_2H_4O. (6) blended with CH_2CHCN ν_{11}=2. (7) blended with CH_3CH_2CN ν_{13}/ν_{21}. (8) blended with NH_2D. (9) blended with H_2CCO. (10) blended with $CH_3{}^{13}CH_2CN$. (11) blended with SO_2 ν_2=1. (12) blended with E-$HCOOCH_3$. (13) blended with $^{13}CH_3CH_2CN$.

Tabla A.4: Measured transitions of ν_{20} of ethyl cyanide.

J'	K'_a	K'_c	J"	K''_a	K''_c	ν(Hz)	e$_\nu$(Hz)	f$_\nu$(Hz)	O-C(Hz)	Blend	f$_{Peak}$(Hz)
3	0	3	2	0	2	26839.519	0.05		-0.007		
4	0	4	3	0	3	35751.461	0.05		0.021		
5	0	5	4	0	4	44633.991	0.05		0.016		
6	0	6	5	0	5	53480.380	0.05		0.012		
7	0	7	6	0	6	62284.613	0.05		0.013		
8	0	8	7	0	7	71041.824	0.05		-0.011		
9	0	9	8	0	8	79748.976	0.05		0.065		
10	0	10	9	0	9	88404.817	0.05		0.023		
11	0	11	10	0	10	97010.865	0.05		0.007		
12	0	12	11	0	11	105570.915	0.05		0.039		
13	0	13	12	0	12	114090.690	0.05		0.028		
14	0	14	13	0	13	122577.470	0.05		0.057		
15	0	15	14	0	14	131038.928	0.05		0.052		
15	0	15	14	0	14	131038.960	0.05		0.084		
16	0	16	15	0	15	139482.530	0.05		-0.013		
16	0	16	15	0	15	139482.562	0.05		0.019		
17	0	17	16	0	16	147915.160	0.05		0.133		
18	0	18	17	0	17	156341.780	0.05		0.085		
19	0	19	18	0	18	164766.650	0.05		0.084		
20	0	20	19	0	19	173192.430	0.05		0.034		
24	0	24	23	0	23	206928.436	0.05		0.081		
25	0	25	24	0	24	215371.401	0.20		0.057		
26	0	26	25	0	25	223817.327	0.20		0.054		
27	0	27	26	0	26	232265.680	0.20		0.052		
28	0	28	27	0	27	240715.942	0.20		0.048		
29	0	29	28	0	28	249167.628	0.20		0.045		
30	0	30	29	0	29	257620.126	0.20		-0.121		
31	0	31	30	0	30	266073.523	0.20		0.039		
33	0	33	32	0	32	282980.327	0.05		0.005		
34	0	34	33	0	33	291433.279	0.05		-0.074		
35	0	35	34	0	34	299885.804	0.05		-0.006		
36	0	36	35	0	35	308337.504	0.05		0.004		
37	0	37	36	0	36	316788.232	0.05		-0.023		
38	0	38	37	0	37	325237.916	0.05		-0.016		
39	0	39	38	0	38	333686.392	0.05		-0.014		
40	0	40	39	0	39	342133.533	0.05		-0.034		
41	0	41	40	0	40	350579.260	0.05		-0.061		
53	0	53	52	0	52	451793.829	0.05		-0.114		
54	0	54	53	0	53	460215.653	0.05		-0.047		
55	0	55	54	0	54	468635.142	0.05		-0.138		
56	0	56	55	0	55	477052.662	0.05		0.018		
57	0	57	56	0	56	485467.706	0.05		-0.044		
58	0	58	57	0	57	493880.609	0.05		0.049		
59	0	59	58	0	58	502291.096	0.05		0.062		
61	0	61	60	0	60	519104.894	0.05		0.072		
62	0	62	61	0	61	527508.107	0.05		0.048		
70	0	70	69	0	69	594641.191	0.05		-0.076		

Tabla A.4: continued.

J'	K'_a	K'_c	J"	K''_a	K''_c	ν(Hz)	e$_\nu$(Hz)	f$_\nu$(Hz)	O-C(Hz)	Blend	f$_{Peak}$(Hz)
3	1	2	2	1	1	27576.759	0.05		-0.067		
4	1	3	3	1	2	36759.880	0.05		-0.050		
4	1	4	3	1	3	34861.170	0.05		-0.083		
5	1	4	4	1	3	45934.935	0.05		-0.028		
5	1	5	4	1	4	43562.815	0.05		-0.009		
6	1	5	5	1	4	55099.600	0.05		-0.039		
6	1	6	5	1	5	52255.420	0.05		-0.205		
7	1	6	6	1	5	64251.447	0.05		-0.049		
7	1	7	6	1	6	60938.322	0.05		0.038		
8	1	7	7	1	6	73387.752	0.05		-0.102		
8	1	8	7	1	7	69609.689	0.05		0.062		
9	1	8	8	1	7	82505.734	0.05		-0.050		
9	1	9	8	1	8	78268.726	0.05		0.029		
10	1	9	9	1	8	91602.028	0.05		-0.051		
10	1	10	9	1	9	86914.841	0.05		0.072		
11	1	10	10	1	9	100673.189	0.05		-0.046		
11	1	11	10	1	10	95547.388	0.05		0.027		
12	1	11	11	1	10	109715.389	0.05		-0.062		
12	1	12	11	1	11	104166.276	0.05		0.045		
13	1	12	12	1	11	118724.500	0.05		-0.148		
13	1	13	12	1	12	112771.445	0.05		0.076		
14	1	13	13	1	12	127696.550	0.05		0.012		
14	1	14	13	1	13	121363.020	0.05		0.039		
15	1	14	14	1	13	136626.740	0.05		0.015		
15	1	15	14	1	14	129941.480	0.05		0.015		
16	1	15	15	1	14	145510.910	0.05		0.021		
16	1	16	15	1	15	138507.458	0.05		0.073		
17	1	16	16	1	15	154344.990	0.05		-0.034		
17	1	17	16	1	16	147061.410	0.05		-0.023		
18	1	17	17	1	16	163125.760	0.05		0.003		
18	1	18	17	1	17	155604.450	0.05		0.054		
19	1	18	18	1	17	171850.740	0.05		0.027		
19	1	19	18	1	18	164137.160	0.05		0.033		
20	1	20	19	1	19	172660.570	0.05		0.068		
24	1	23	23	1	22	214666.271	0.20		0.060		
24	1	24	23	1	23	206677.614	0.05		0.054		
25	1	24	24	1	23	223097.791	0.20		0.161		
25	1	25	24	1	24	215166.664	0.20		0.062		
26	1	25	25	1	24	231501.568	0.20		0.046		
26	1	26	25	1	25	223650.946	0.20		0.056		
27	1	26	26	1	25	239885.804	0.20		0.061		
27	1	27	26	1	26	232131.014	0.20		0.050		
28	1	27	27	1	26	248257.592	0.20		0.082		
28	1	28	27	1	27	240607.336	0.20		0.040		
29	1	28	28	1	27	256623.047	0.20		0.058		
29	1	29	28	1	28	249080.325	0.20		0.037		
30	1	29	29	1	28	264987.157	0.20		0.073		
30	1	30	29	1	29	257550.307	0.20		0.028		

Tabla A.4: continued.

J'	K'_a	K'_c	J"	K''_a	K''_c	ν(Hz)	e$_\nu$(Hz)	f$_\nu$(Hz)	O-C(Hz)	Blend	f$_{peak}$(Hz)
31	1	30	30	1	29	273353.451	0.05		0.047		
31	1	31	30	1	30	266017.580	0.20		0.028		
32	1	31	31	1	30	281724.403	0.05		0.031		
32	1	32	31	1	31	274482.329	0.05		-0.009		
33	1	32	32	1	31	290101.461	0.05		0.056		
33	1	33	32	1	32	282944.834	0.05		0.009		
34	1	33	33	1	32	298485.187	0.05		0.051		
34	1	34	33	1	33	291405.146	0.05		-0.014		
35	1	34	34	1	33	306875.633	0.05		0.016		
35	1	35	34	1	34	299863.505	0.05		0.045		
36	1	35	35	1	34	315272.557	0.05		0.048		
36	1	36	35	1	35	308319.807	0.05		-0.003		
37	1	36	36	1	35	323675.264	0.05		0.036		
37	1	37	36	1	36	316774.264	0.05		-0.012		
38	1	37	37	1	36	332083.030	0.05		-0.025		
38	1	38	37	1	37	325226.875	0.05		-0.025		
39	1	38	38	1	37	340495.269	0.05		0.048		
39	1	39	38	1	38	333677.679	0.05		-0.031		
40	1	39	39	1	38	348910.971	0.05		0.015		
40	1	40	39	1	39	342126.838	0.05		0.116		
41	1	40	40	1	39	357329.520	0.05		-0.010		
41	1	41	40	1	40	350573.910	0.05		-0.028		
42	1	42	41	1	41	359019.250	0.05		-0.104		
46	1	45	45	1	44	399443.568	0.05		-0.015		
47	1	46	46	1	45	407867.183	0.05		-0.077		
47	1	47	46	1	46	401218.719	0.05		-0.098		
48	1	47	47	1	46	416290.361	0.05		-0.012		
48	1	48	47	1	47	409653.215	0.05		0.208		
49	1	48	48	1	47	424712.601	0.05		-0.053		
49	1	49	48	1	48	418085.687	0.05	*	0.463		
50	1	49	49	1	48	433133.780	0.05		-0.089		
51	1	50	50	1	49	441553.762	0.05		-0.057		
51	1	51	50	1	50	434943.777	0.05		0.177		
52	1	51	51	1	50	449972.241	0.05		-0.089		
52	1	52	51	1	51	443369.854	0.05		0.166		
53	1	52	52	1	51	458389.208	0.05		-0.044		
53	1	53	52	1	52	451793.828	0.05		0.168		
54	1	53	53	1	52	466804.420	0.05		-0.034		
54	1	54	53	1	53	460215.617	0.05		0.138		
55	1	55	54	1	54	468635.074	0.05		-0.034		
56	1	55	55	1	54	483629.543	0.05	*	0.296		
56	1	56	55	1	55	477052.661	0.05		0.152		
57	1	56	56	1	55	492038.560	0.05		-0.083		
57	1	57	56	1	56	485467.701	0.05		0.056		
58	1	57	57	1	56	500445.894	0.05		-0.035		
58	1	58	57	1	57	493880.609	0.05		0.131		
59	1	58	58	1	57	508850.954	0.05		-0.075		
60	1	59	59	1	58	517253.801	0.05		-0.075		

Tabla A.4: continued.

J'	K'_a	K'_c	J"	K''_a	K''_c	ν(Hz)	e$_\nu$(Hz)	f$_\nu$(Hz)	O-C(Hz)	Blend	f$_{Peak}$(Hz)
60	1	60	59	1	59	510699.197	0.05		0.112		
61	1	60	60	1	59	525654.333	0.05		-0.072		
61	1	61	60	1	60	519104.906	0.05		0.122		
62	1	61	61	1	60	534052.531	0.05		-0.029		
62	1	62	61	1	61	527508.042	0.05		0.013		
63	1	62	62	1	61	542448.295	0.05		0.011		
63	1	63	62	1	62	535908.882	0.05		0.097		
64	1	64	63	1	63	544307.120	0.05		0.107		
65	1	64	64	1	63	559231.701	0.05	*	-0.537		
65	1	65	64	1	64	552702.768	0.05		0.091		
66	1	65	65	1	64	567619.857	0.05	*	-0.514		
66	1	66	65	1	65	561095.814	0.05		0.073		
67	1	66	66	1	65	576005.443	0.05	*	-0.438		
67	1	67	66	1	66	569486.199	0.05		0.032		
68	1	67	67	1	66	584388.337	0.05	*	-0.385		
68	1	68	67	1	67	577873.921	0.05		0.001		
69	1	68	68	1	67	592768.426	0.05	*	-0.427		
69	1	69	68	1	68	586258.933	0.05		-0.031		
70	1	69	69	1	68	601145.797	0.05	*	-0.434		
70	1	70	69	1	69	594641.191	0.05		-0.072		
71	1	71	70	1	70	603020.638	0.05		-0.144		
4	2	3	3	2	2	35820.625	0.05		-0.089		
5	2	3	4	2	2	44912.697	0.05		-0.091		
5	2	4	4	2	3	44766.282	0.05		0.129		
6	2	4	5	2	3	53960.640	0.05		-0.007		
6	2	5	5	2	4	53705.080	0.05		-0.029		
7	2	5	6	2	4	63042.420	0.05		-0.006		
7	2	6	6	2	5	62636.290	0.05		-0.008		
8	2	6	7	2	5	72161.553	0.05		-0.022		
8	2	7	7	2	6	71558.410	0.05		-0.038		
9	2	7	8	2	6	81319.810	0.05		-0.047		
9	2	8	8	2	7	80470.332	0.05		0.029		
10	2	8	9	2	7	90516.853	0.05		-0.026		
10	2	9	9	2	8	89370.617	0.05		-0.015		
11	2	9	10	2	8	99749.740	0.05		-0.072		
11	2	10	10	2	9	98258.253	0.05		0.018		
12	2	10	11	2	9	109013.350	0.05		-0.024		
12	2	11	11	2	10	107131.971	0.05		0.016		
13	2	11	12	2	10	118300.070	0.05		-0.109		
13	2	12	12	2	11	115990.720	0.05		0.029		
14	2	12	13	2	11	127601.390	0.05		0.017		
14	2	13	13	2	12	124833.410	0.05		0.002		
15	2	13	14	2	12	136907.290	0.05		-0.158		
15	2	14	14	2	13	133659.160	0.05		0.006		
16	2	14	15	2	13	146208.952	0.05		-0.066		
16	2	15	15	2	14	142467.119	0.05		0.042		
17	2	15	16	2	14	155497.290	0.05		-0.128		
17	2	16	16	2	15	151256.440	0.05		0.001		

Tabla A.4: continued.

J'	K'_a	K'_c	J"	K''_a	K''_c	ν(Hz)	e$_\nu$(Hz)	f$_\nu$(Hz)	O-C(Hz)	Blend	f$_{peak}$(Hz)
18	2	16	17	2	15	164764.960	0.05		-0.088		
18	2	17	17	2	16	160026.640	0.05		0.008		
19	2	18	18	2	17	168777.210	0.05		0.017		
24	2	23	23	2	22	212230.804	0.20		0.060		
25	2	24	24	2	23	220863.109	0.20		0.074		
26	2	25	25	2	24	229477.157	0.20		0.065		
27	2	25	26	2	24	246415.407	0.05		-0.028		
27	2	26	26	2	25	238073.797	0.20		0.067		
28	2	26	27	2	25	255225.482	0.05		0.027		
28	2	27	27	2	26	246653.940	0.20		0.070		
29	2	28	28	2	27	255218.582	0.20		0.067		
30	2	28	29	2	27	272657.330	0.05		-0.014		
30	2	29	29	2	28	263768.792	0.20		0.066		
31	2	29	30	2	28	281278.761	0.05		-0.007		
31	2	30	30	2	29	272305.654	0.05		0.063		
32	2	30	31	2	29	289839.285	0.05		0.017		
32	2	31	31	2	30	280830.250	0.05		0.042		
33	2	31	32	2	30	298342.511	0.05		0.042		
33	2	32	32	2	31	289343.719	0.05		0.065		
34	2	32	33	2	31	306793.665	0.05		0.022		
34	2	33	33	2	32	297847.016	0.05		0.045		
35	2	33	34	2	32	315199.573	0.05		0.071		
35	2	34	34	2	33	306341.221	0.05		0.071		
36	2	34	35	2	33	323567.873	0.05		0.073		
36	2	35	35	2	34	314827.141	0.05		0.025		
37	2	36	36	2	35	323305.761	0.05		0.042		
38	2	36	37	2	35	340224.908	0.05		0.117		
38	2	37	37	2	36	331777.849	0.05		0.115		
39	2	37	38	2	36	348529.458	0.05		0.054		
39	2	38	38	2	37	340243.862	0.05		0.010		
40	2	38	39	2	37	356827.439	0.05		0.068		
40	2	39	39	2	38	348704.710	0.05		0.022		
41	2	40	40	2	39	357160.780	0.05		0.004		
45	2	43	44	2	42	398366.827	0.05		-0.014		
46	2	44	45	2	43	406698.869	0.05		0.021		
46	2	45	45	2	44	399383.921	0.05		-0.045		
47	2	45	46	2	44	415039.802	0.05		0.016		
47	2	46	46	2	45	407819.054	0.05		-0.081		
48	2	46	47	2	45	423389.044	0.05		-0.022		
48	2	47	47	2	46	416251.532	0.05		-0.059		
49	2	47	48	2	46	431745.915	0.05		0.032		
49	2	48	48	2	47	424681.396	0.05		-0.053		
50	2	48	49	2	47	440109.311	0.05		-0.011		
50	2	49	49	2	48	433108.765	0.05		-0.032		
51	2	49	50	2	48	448478.311	0.05		-0.120		
51	2	50	50	2	49	441533.650	0.05		-0.052		
52	2	50	51	2	49	456852.260	0.05		-0.015		
52	2	51	51	2	50	449956.165	0.05		-0.044		

Tabla A.4: continued.

J'	K'_a	K'_c	J"	K''_a	K''_c	ν(Hz)	e$_\nu$(Hz)	f$_\nu$(Hz)	O-C(Hz)	Blend	f$_{Peak}$(Hz)
53	2	51	52	2	50	465229.953	0.05		-0.010		
53	2	52	52	2	51	458376.279	0.05		-0.070		
54	2	52	53	2	51	473610.662	0.05		-0.009		
54	2	53	53	2	52	466794.008	0.05		-0.128		
55	2	53	54	2	52	481993.625	0.05		-0.024		
55	2	54	54	2	53	475209.520	0.05		-0.058		
56	2	54	55	2	53	490378.184	0.05		-0.044		
56	2	55	55	2	54	483622.705	0.05		0.035		
57	2	55	56	2	54	498763.811	0.05		0.000		
57	2	56	56	2	55	492033.286	0.05		-0.114		
58	2	56	57	2	55	507149.870	0.05		-0.004		
58	2	57	57	2	56	500441.668	0.05		-0.084		
59	2	57	58	2	56	515535.964	0.05		0.004		
59	2	58	58	2	57	508848.129	0.05	*	0.424		
60	2	58	59	2	57	523921.670	0.05		0.001		
60	2	59	59	2	58	517251.103	0.05		-0.128		
61	2	59	60	2	58	532306.653	0.05		0.000		
61	2	60	60	2	59	525652.138	0.05		-0.165		
62	2	60	61	2	59	540690.616	0.05		0.005		
62	2	61	61	2	60	534050.666	0.05		-0.223		
63	2	61	62	2	60	549073.293	0.05		0.011		
63	2	62	62	2	61	542446.476	0.05	*	-0.482		
64	2	62	63	2	61	557454.563	0.05		0.125		
65	2	63	64	2	62	565833.938	0.05		0.057		
65	2	64	64	2	63	559231.701	0.05	*	0.297		
66	2	64	65	2	63	574211.492	0.05		0.055		
66	2	65	65	2	64	567619.857	0.05		0.147		
67	2	65	66	2	64	582587.027	0.05		0.071		
67	2	66	66	2	65	576005.443	0.05		0.087		
68	2	66	67	2	65	590960.342	0.05		0.040		
68	2	67	67	2	66	584388.337	0.05		0.030		
69	2	67	68	2	66	599331.472	0.05		0.115		
69	2	68	68	2	67	592768.426	0.05		-0.098		
70	2	69	69	2	68	601145.797	0.05		-0.174		
5	3	3	4	3	2	44809.152	0.05		-0.233		
6	3	3	5	3	2	53783.445	0.05		-0.032		
6	3	4	5	3	3	53779.596	0.05		0.106		
7	3	4	6	3	3	62762.328	0.05		-0.082		
7	3	5	6	3	4	62753.458	0.05		0.007		
8	3	5	7	3	4	71749.038	0.05		-0.245		
8	3	6	7	3	5	71731.485	0.05		0.085		
9	3	6	8	3	5	80745.797	0.05		-0.156		
9	3	7	8	3	6	80713.327	0.05		0.072		
10	3	7	9	3	6	89754.402	0.05		-0.154		
10	3	8	9	3	7	89698.756	0.05		0.054		
11	3	8	10	3	7	98777.406	0.05		-0.119		
11	3	9	10	3	8	98687.302	0.05		0.111		
12	3	9	11	3	8	107817.517	0.05		-0.074		

Tabla A.4: continued.

J'	K'_a	K'_c	J"	K''_a	K''_c	ν(Hz)	e$_\nu$(Hz)	f$_\nu$(Hz)	O-C(Hz)	Blend	f$_{peak}$(Hz)
12	3	10	11	3	9	107677.884	0.05		-0.050		
13	3	10	12	3	9	116877.750	0.05		-0.013		
13	3	11	12	3	10	116669.840	0.05		-0.074		
14	3	11	13	3	10	125961.140	0.05		-0.118		
14	3	12	13	3	11	125661.691	0.05		-0.216		
15	3	12	14	3	11	135071.260	0.05		-0.132		
15	3	13	14	3	12	134652.580	0.05		0.080		
16	3	13	15	3	12	144211.350	0.05		-0.052		
16	3	14	15	3	13	143640.037	0.05		-0.091		
17	3	14	16	3	13	153384.130	0.05		-0.063		
17	3	15	16	3	14	152623.144	0.05		0.038		
18	3	15	17	3	14	162592.050	0.05		0.026		
18	3	16	17	3	15	161599.820	0.05		0.151		
19	3	17	18	3	16	170567.660	0.05	*	-0.349		
25	3	23	24	3	22	224107.863	0.20		0.036		
26	3	24	25	3	23	232971.653	0.20		-0.006		
27	3	24	26	3	23	246698.026	0.05		-0.109		
27	3	25	26	3	24	241815.164	0.20		0.000		
28	3	25	27	3	24	256058.825	0.05		-0.076		
28	3	26	27	3	25	250637.498	0.20		0.043		
29	3	26	28	3	25	265390.842	0.05		-0.103		
29	3	27	28	3	26	259437.908	0.20		0.076		
30	3	27	29	3	26	274686.950	0.05		-0.068		
30	3	28	29	3	27	268215.812	0.20		0.032		
31	3	28	30	3	27	283940.886	0.05		-0.067		
31	3	29	30	3	28	276971.032	0.05		0.056		
32	3	29	31	3	28	293147.502	0.05		-0.049		
32	3	30	31	3	29	285703.366	0.05		0.076		
33	3	30	32	3	29	302302.386	0.05		-0.029		
33	3	31	32	3	30	294412.836	0.05		0.055		
34	3	31	33	3	30	311401.727	0.05		-0.028		
34	3	32	33	3	31	303099.760	0.05		0.068		
35	3	32	34	3	31	320442.228	0.05		-0.014		
35	3	33	34	3	32	311764.486	0.05		0.048		
36	3	33	35	3	32	329420.900	0.05		-0.009		
36	3	34	35	3	33	320407.660	0.05		0.061		
37	3	34	36	3	33	338335.187	0.05		0.051		
37	3	35	36	3	34	329029.953	0.05		0.051		
38	3	35	37	3	34	347182.709	0.05		-0.001		
38	3	36	37	3	35	337632.274	0.05		0.071		
39	3	36	38	3	35	355961.976	0.05		0.007		
39	3	37	38	3	36	346215.547	0.05		0.084		
40	3	38	39	3	37	354780.786	0.05		0.055		
44	3	41	43	3	40	398840.739	0.05		0.024		
45	3	42	44	3	41	407232.588	0.05		0.032		
45	3	43	44	3	42	397376.868	0.05		0.009		
46	3	43	45	3	42	415576.368	0.05		0.054		
46	3	44	45	3	43	405858.053	0.05		0.034		

Tabla A.4: continued.

J'	K'_a	K'_c	J"	K''_a	K''_c	ν(Hz)	e$_\nu$(Hz)	f$_\nu$(Hz)	O-C(Hz)	Blend	f$_{Peak}$(Hz)
47	3	44	46	3	43	423880.091	0.05		0.080		
47	3	45	46	3	44	414329.044	0.05		0.040		
48	3	45	47	3	44	432152.114	0.05		-0.068		
48	3	46	47	3	45	422790.815	0.05		0.037		
49	3	46	48	3	45	440401.141	0.05		-0.230		
49	3	47	48	3	46	431244.219	0.05		-0.013		
50	3	47	49	3	46	448635.683	0.05		0.039		
50	3	48	49	3	47	439690.177	0.05		0.001		
51	3	48	50	3	47	456862.217	0.05		0.018		
51	3	49	50	3	48	448129.348	0.05		0.004		
52	3	49	51	3	48	465087.099	0.05		0.001		
52	3	50	51	3	49	456562.392	0.05		0.005		
53	3	50	52	3	49	473315.146	0.05		0.008		
53	3	51	52	3	50	464989.866	0.05		-0.015		
54	3	51	53	3	50	481549.874	0.05		0.015		
54	3	52	53	3	51	473412.282	0.05		-0.047		
55	3	52	54	3	51	489793.564	0.05		-0.075		
55	3	53	54	3	52	481830.158	0.05		-0.006		
56	3	53	55	3	52	498047.890	0.05		0.030		
56	3	54	55	3	53	490243.737	0.05		-0.020		
57	3	54	56	3	53	506313.121	0.05		0.025		
57	3	55	56	3	54	498653.401	0.05		-0.020		
58	3	55	57	3	54	514589.327	0.05		0.026		
58	3	56	57	3	55	507059.436	0.05		0.019		
59	3	56	58	3	55	522876.010	0.05		0.024		
59	3	57	58	3	56	515461.974	0.05		0.013		
60	3	57	59	3	56	531172.396	0.05		0.032		
60	3	58	59	3	57	523861.216	0.05		-0.013		
61	3	58	60	3	57	539477.640	0.05		0.169		
61	3	59	60	3	58	532257.372	0.05		0.012		
62	3	59	61	3	58	547790.286	0.05		0.029		
62	3	60	61	3	59	540650.460	0.05		-0.004		
63	3	60	62	3	59	556109.656	0.05		0.009		
63	3	61	62	3	60	549040.631	0.05		0.005		
64	3	61	63	3	60	564434.426	0.05		-0.170		
64	3	62	63	3	61	557427.644	0.05	*	-0.262		
65	3	62	64	3	61	572764.388	0.05	*	0.279		
65	3	63	64	3	62	565812.398	0.05		0.049		
66	3	63	65	3	62	581096.901	0.05	*	-0.363		
66	3	64	65	3	63	574194.088	0.05		0.106		
67	3	64	66	3	63	589432.161	0.05	*	-1.062		
67	3	65	66	3	64	582572.894	0.05		0.075		
69	3	67	68	3	66	599322.228	0.05		0.119		
5	4	1	4	4	0	44804.792	0.05	*	0.343	Yes	44804.446
5	4	2	4	4	1	44804.792	0.05	*	0.347	Yes	44804.446
6	4	2	5	4	1	53770.065	0.05		0.127		
7	4	3	6	4	2	62737.949	0.05		0.036	Yes	62737.913
7	4	4	6	4	3	62737.949	0.05		0.036	Yes	62737.913

Tabla A.4: continued.

J'	K'_a	K'_c	J"	K''_a	K''_c	ν(Hz)	e$_\nu$(Hz)	f$_\nu$(Hz)	O-C(Hz)	Blend	f$_{peak}$(Hz)
8	4	4	7	4	3	71708.844	0.05		0.026	Yes	71708.818
8	4	5	7	4	4	71708.844	0.05		0.026	Yes	71708.818
9	4	6	8	4	5	80682.711	0.05		-0.124		
10	4	6	9	4	5	89661.002	0.05		-0.060	Yes	89661.062
10	4	7	9	4	6	89661.002	0.05		-0.060	Yes	89661.062
11	4	7	10	4	6	98645.172	0.05	*	0.951		
11	4	8	10	4	7	98642.033	0.05		-0.235		
12	4	8	11	4	7	107631.624	0.05		-0.239		
12	4	9	11	4	8	107629.180	0.05	*	0.967		
13	4	9	12	4	8	116625.813	0.05	*	0.698		
13	4	10	12	4	9	116618.441	0.05		-0.202		
14	4	10	13	4	9	125625.260	0.05	*	0.562		
14	4	11	13	4	10	125613.455	0.05	*	-0.281		
15	4	11	14	4	10	134631.290	0.05		-0.152		
15	4	12	14	4	11	134613.283	0.05	*	-0.300		
16	4	12	15	4	11	143646.060	0.05	*	-0.255		
16	4	13	15	4	12	143618.076	0.05		-0.109		
18	4	15	17	4	14	161641.421	0.05	*	0.350		
19	4	15	18	4	14	170751.857	0.05		-0.042		
19	4	16	18	4	15	170658.810	0.05		0.076		
23	4	19	22	4	18	207098.473	0.05		-0.069		
23	4	20	22	4	19	206756.430	0.05		0.008		
24	4	20	23	4	19	216236.799	0.20		-0.017		
24	4	21	23	4	20	215782.835	0.20		-0.027		
25	4	21	24	4	20	225401.008	0.20		-0.039		
25	4	22	24	4	21	224807.669	0.20		0.025		
26	4	22	25	4	21	234593.873	0.20		-0.082		
26	4	23	25	4	22	233829.321	0.20		0.039		
27	4	23	26	4	22	243818.018	0.20		-0.035		
27	4	24	26	4	23	242846.172	0.20		0.001		
28	4	24	27	4	23	253075.363	0.20		-0.036		
28	4	25	27	4	24	251856.577	0.20		-0.040		
29	4	25	28	4	24	262367.247	0.20		-0.067		
29	4	26	28	4	25	260858.902	0.20		0.040		
30	4	27	29	4	26	269850.922	0.20		-0.191		
31	4	27	30	4	26	281054.448	0.05		-0.070		
31	4	28	30	4	27	278831.571	0.05		-0.007		
32	4	28	31	4	27	290445.889	0.05		-0.053		
32	4	29	31	4	28	287798.654	0.05		0.163		
33	4	29	32	4	28	299863.505	0.05	*	-0.291		
33	4	30	32	4	29	296750.166	0.05		0.017		
34	4	30	33	4	29	309301.698	0.05		-0.079		
34	4	31	33	4	30	305684.933	0.05		0.004		
35	4	31	34	4	30	318751.947	0.05		-0.063		
35	4	32	34	4	31	314601.337	0.05		0.013		
36	4	32	35	4	31	328205.384	0.05		-0.053		
36	4	33	35	4	32	323497.933	0.05		-0.021		
37	4	33	36	4	32	337652.247	0.05		-0.071		

Tabla A.4: continued.

J'	K'_a	K'_c	J"	K''_a	K''_c	ν(Hz)	e$_\nu$(Hz)	f$_\nu$(Hz)	O-C(Hz)	Blend	f$_{Peak}$(Hz)
37	4	34	36	4	33	332373.640	0.05		0.047		
38	4	34	37	4	33	347082.736	0.05		-0.051		
38	4	35	37	4	34	341227.476	0.05	*	0.298		
39	4	35	38	4	34	356487.307	0.05		-0.049		
39	4	36	38	4	35	350057.957	0.05		0.137		
40	4	37	39	4	36	358864.865	0.05		0.044		
44	4	40	43	4	39	402852.748	0.05		0.018		
45	4	41	44	4	40	411954.705	0.05		0.083		
45	4	42	44	4	41	402534.036	0.05		0.050		
46	4	42	45	4	41	420990.564	0.05	*	0.382		
46	4	43	45	4	42	411195.114	0.05		0.067		
47	4	43	46	4	42	429956.721	0.05		0.045		
47	4	44	46	4	43	419832.850	0.05		0.046		
48	4	44	47	4	43	438851.928	0.05		0.064		
48	4	45	47	4	44	428447.990	0.05		0.011		
49	4	45	48	4	44	447674.115	0.05		0.093		
49	4	46	48	4	45	437041.484	0.05		0.063		
50	4	46	49	4	45	456422.047	0.05		-0.001		
50	4	47	49	4	46	445614.155	0.05		0.070		
51	4	47	50	4	46	465095.667	0.05		0.054		
51	4	48	50	4	47	454167.045	0.05		0.028		
52	4	48	51	4	47	473695.382	0.05		0.031		
52	4	49	51	4	48	462701.348	0.05		0.023		
53	4	49	52	4	48	482223.082	0.05		0.026		
53	4	50	52	4	49	471218.306	0.05		0.143		
54	4	50	53	4	49	490681.889	0.05		0.047		
54	4	51	53	4	50	479718.705	0.05		-0.003		
55	4	51	54	4	50	499076.256	0.05		0.028		
55	4	52	54	4	51	488204.166	0.05		0.029		
56	4	52	55	4	51	507412.104	0.05		-0.013		
56	4	53	55	4	52	496675.638	0.05		0.026		
57	4	53	56	4	52	515696.612	0.05		-0.026		
57	4	54	56	4	53	505134.317	0.05		0.054		
58	4	54	57	4	53	523937.871	0.05		0.007		
58	4	55	57	4	54	513581.222	0.05		0.051		
59	4	55	58	4	54	532144.393	0.05		-0.026		
59	4	56	58	4	55	522017.440	0.05		0.078		
60	4	56	59	4	55	540324.815	0.05		-0.209		
60	4	57	59	4	56	530443.849	0.05		0.056		
61	4	57	60	4	56	548487.970	0.05		-0.084		
61	4	58	60	4	57	538861.381	0.05		0.031		
62	4	58	61	4	57	556640.970	0.05		-0.175		
62	4	59	61	4	58	547270.874	0.05		0.030		
63	4	59	62	4	58	564791.013	0.05		0.107		
63	4	60	62	4	59	555673.039	0.05		0.033		
64	4	60	63	4	59	572942.587	0.05		-0.164		
64	4	61	63	4	60	564068.449	0.05		-0.043		
65	4	61	64	4	60	581100.762	0.05		-0.091		

Tabla A.4: continued.

J'	K'_a	K'_c	J"	K''_a	K''_c	ν(Hz)	e$_\nu$(Hz)	f$_\nu$(Hz)	O-C(Hz)	Blend	f$_{peak}$(Hz)
65	4	62	64	4	61	572457.896	0.05		0.011		
66	4	62	65	4	61	589268.164	0.05		-0.027		
66	4	63	65	4	62	580841.354	0.05	*	-0.341		
67	4	63	66	4	62	597447.277	0.05	*	0.596		
67	4	64	66	4	63	589219.255	0.05	*	-1.112		
9	5	4	8	5	3	80668.202	0.05		-0.045		
10	5	6	9	5	5	89638.707	0.05		-0.051		
11	5	7	10	5	6	98611.666	0.05		0.071		
12	5	8	11	5	7	107587.007	0.05		0.025		
13	5	9	12	5	8	116565.110	0.05		-0.035		
14	5	9	13	5	8	125546.368	0.05		-0.140		
15	5	10	14	5	9	134530.759	0.05		-0.121	Yes	134530.880
15	5	11	14	5	10	134530.759	0.05		-0.121	Yes	134530.880
18	5	14	17	5	13	161505.136	0.05		-0.106		
19	5	14	18	5	13	170507.694	0.05		-0.141		
23	5	18	22	5	17	206562.716	0.05		-0.170		
23	5	19	22	5	18	206544.371	0.05		-0.038		
24	5	19	23	5	18	215592.180	0.20		-0.221		
24	5	20	23	5	19	215565.288	0.20		-0.103		
25	5	20	24	5	19	224629.396	0.20		-0.145		
25	5	21	24	5	20	224590.613	0.20		-0.116		
26	5	21	25	5	20	233675.069	0.20		-0.099		
26	5	22	25	5	21	233620.418	0.20		0.140		
27	5	22	26	5	21	242730.226	0.20		-0.064		
27	5	23	26	5	22	242653.852	0.20		0.046		
28	5	23	27	5	22	251796.037	0.20		-0.042		
28	5	24	27	5	23	251691.009	0.20		0.031		
29	5	24	28	5	23	260873.741	0.20		-0.153		
29	5	25	28	5	24	260731.381	0.20		0.029		
30	5	25	29	5	24	269965.267	0.20		-0.028		
30	5	26	29	5	25	269774.399	0.20		0.037		
31	5	26	30	5	25	279072.124	0.05		0.071		
31	5	27	30	5	26	278819.224	0.05		-0.090		
32	5	27	31	5	26	288196.114	0.05		-0.041		
32	5	28	31	5	27	287865.361	0.05		-0.017		
33	5	28	32	5	27	297339.765	0.05		-0.025		
33	5	29	32	5	28	296911.540	0.05		-0.045		
34	5	29	33	5	28	306505.284	0.05		-0.031		
34	5	30	33	5	29	305956.813	0.05		-0.015		
35	5	30	34	5	29	315695.178	0.05		-0.019		
35	5	31	34	5	30	314999.843	0.05		-0.023		
36	5	31	35	5	30	324911.895	0.05		-0.027		
36	5	32	35	5	31	324039.344	0.05		0.008		
37	5	32	36	5	31	334157.821	0.05		-0.035		
37	5	33	36	5	32	333073.761	0.05		-0.001		
38	5	33	37	5	32	343435.049	0.05		-0.021		
38	5	34	37	5	33	342101.526	0.05		-0.046		
39	5	34	38	5	33	352745.102	0.05		-0.011		

Tabla A.4: continued.

J'	K'_a	K'_c	J"	K''_a	K''_c	ν(Hz)	e$_\nu$(Hz)	f$_\nu$(Hz)	O-C(Hz)	Blend	f$_{Peak}$(Hz)
39	5	35	38	5	34	351121.135	0.05		0.011		
44	5	39	43	5	38	399772.063	0.05		-0.032		
44	5	40	43	5	39	396035.406	0.05		0.021		
45	5	40	44	5	39	409250.044	0.05		0.073		
45	5	41	44	5	40	404970.039	0.05		0.176		
46	5	41	45	5	40	418737.092	0.05		0.048		
46	5	42	45	5	41	413884.779	0.05		0.154		
47	5	42	46	5	41	428224.296	0.05		0.069		
47	5	43	46	5	42	422778.332	0.05		-0.012		
48	5	43	47	5	42	437701.844	0.05		0.097		
48	5	44	47	5	43	431649.898	0.05		0.062		
49	5	44	48	5	43	447159.613	0.05		-0.029		
49	5	45	48	5	44	440498.057	0.05		-0.014		
50	5	45	49	5	44	456588.306	0.05		0.072		
50	5	46	49	5	45	449322.239	0.05		0.049		
51	5	46	50	5	45	465978.523	0.05		0.002		
51	5	47	50	5	46	458121.474	0.05		-0.034		
52	5	47	51	5	46	475322.385	0.05		-0.056		
52	5	48	51	5	47	466895.572	0.05		0.046		
53	5	48	52	5	47	484612.061	0.05	*	-0.939		
53	5	49	52	5	48	475643.956	0.05		0.030		
54	5	50	53	5	49	484366.495	0.05		-0.084		
55	5	50	54	5	49	503011.432	0.05		0.064		
55	5	51	54	5	50	493063.553	0.05		0.019		
56	5	51	55	5	50	512110.295	0.05		0.066		
56	5	52	55	5	51	501735.047	0.05		0.030		
57	5	53	56	5	52	510381.447	0.05		0.028		
58	5	53	57	5	52	530090.884	0.05		0.086		
58	5	54	57	5	53	519003.333	0.05		0.044		
59	5	54	58	5	53	538967.790	0.05		-0.050		
59	5	55	58	5	54	527601.355	0.05		0.039		
60	5	55	59	5	54	547767.273	0.05		0.005		
60	5	56	59	5	55	536176.321	0.05		0.009		
61	5	56	60	5	55	556488.371	0.05		0.078		
61	5	57	60	5	56	544729.182	0.05		-0.018		
62	5	57	61	5	56	565131.075	0.05		0.180		
62	5	58	61	5	57	553261.537	0.05	*	0.544		
63	5	58	62	5	57	573695.896	0.05		-0.067		
63	5	59	62	5	58	561772.515	0.05	*	-0.253		
64	5	59	63	5	58	582185.374	0.05		-0.079		
64	5	60	63	5	59	570265.709	0.05		0.049		
65	5	60	64	5	59	590602.411	0.05		-0.116		
65	5	61	64	5	60	578740.895	0.05		0.070		
66	5	61	65	5	60	598951.494	0.05		-0.142		
66	5	62	65	5	61	587199.501	0.05		0.065		
67	5	63	66	5	62	595642.652	0.05		-0.004		
68	5	64	67	5	63	604071.513	0.05		-0.115		
10	6	5	9	6	4	89632.888	0.05		-0.061		

Tabla A.4: continued.

J'	K'_a	K'_c	J"	K''_a	K''_c	ν(Hz)	e$_\nu$(Hz)	f$_\nu$(Hz)	O-C(Hz)	Blend	f$_{peak}$(Hz)
11	6	5	10	6	4	98601.522	0.05		0.018		
12	6	6	11	6	5	107571.583	0.05		0.027		
13	6	7	12	6	6	116543.187	0.05		-0.052		
15	6	9	14	6	8	134492.011	0.05		-0.025		
16	6	10	15	6	9	143469.405	0.05		-0.013		
17	6	11	16	6	10	152448.967	0.05		-0.003		
18	6	13	17	6	12	161430.839	0.05		0.049		
27	6	21	26	6	20	242396.355	0.05	*	0.525		
27	6	22	26	6	21	242393.845	0.05	*	1.438		
29	6	23	28	6	22	260427.277	0.05		-0.006		
29	6	24	28	6	23	260418.783	0.05	*	-1.032		
30	6	24	29	6	23	269449.515	0.05	*	-0.281		
30	6	25	29	6	24	269439.505	0.05	*	0.500		
31	6	25	30	6	24	278477.030	0.05	*	-0.268		
31	6	26	30	6	25	278462.869	0.05	*	0.956		
32	6	26	31	6	25	287510.055	0.05		-0.155		
33	6	27	32	6	26	296548.901	0.05		-0.115		
33	6	28	32	6	27	296518.940	0.05		0.061		
34	6	28	33	6	27	305594.222	0.05		-0.068		
34	6	29	33	6	28	305552.866	0.05		0.029		
35	6	29	34	6	28	314646.630	0.05		-0.069		
35	6	30	34	6	29	314590.318	0.05		0.027		
36	6	30	35	6	29	323706.982	0.05		-0.042		
36	6	31	35	6	30	323631.040	0.05		-0.011		
37	6	31	36	6	30	332776.015	0.05		-0.160		
37	6	32	36	6	31	332674.895	0.05		0.040		
38	6	32	37	6	31	341855.205	0.05		-0.004		
38	6	33	37	6	32	341721.368	0.05		0.011		
39	6	33	38	6	32	350945.314	0.05		-0.030		
39	6	34	38	6	33	350770.122	0.05		0.001		
40	6	35	39	6	34	359820.502	0.05		-0.107		
44	6	38	43	6	37	396617.919	0.05		0.027		
44	6	39	43	6	38	396025.087	0.05		-0.089		
45	6	39	44	6	38	405810.388	0.05		0.041		
45	6	40	44	6	39	405072.336	0.05		0.050		
46	6	40	45	6	39	415027.291	0.05		0.017		
46	6	41	45	6	40	414116.100	0.05	*	0.599		
47	6	41	46	6	40	424270.962	0.05		0.020		
47	6	42	46	6	41	423153.129	0.05	*	-0.355		
48	6	42	47	6	41	433543.399	0.05		-0.057		
48	6	43	47	6	42	432184.762	0.05		-0.049		
49	6	43	48	6	42	442846.679	0.05		0.093		
49	6	44	48	6	43	441208.037	0.05		0.064		
50	6	44	49	6	43	452181.629	0.05		0.066		
50	6	45	49	6	44	450221.427	0.05		0.025		
51	6	45	50	6	44	461547.887	0.05	*	-0.957		
51	6	46	50	6	45	459223.495	0.05		0.007		
52	6	47	51	6	46	468212.633	0.05		0.031		

Tabla A.4: continued.

J'	K'_a	K'_c	J"	K''_a	K''_c	ν(Hz)	e$_\nu$(Hz)	f$_\nu$(Hz)	O-C(Hz)	Blend	f$_{Peak}$(Hz)
53	6	47	52	6	46	480376.872	0.05		0.075		
53	6	48	52	6	47	477187.178	0.05		0.060		
54	6	48	53	6	47	489832.241	0.05		-0.138		
54	6	49	53	6	48	486145.558	0.05		0.120		
55	6	49	54	6	48	499309.848	0.05		0.060		
56	6	50	55	6	49	508802.622	0.05		-0.042		
56	6	51	55	6	50	504007.378	0.05		0.008		
57	6	51	56	6	50	518302.840	0.05	*	-0.406		
57	6	52	56	6	51	512908.145	0.05		0.018		
58	6	53	57	6	52	521787.061	0.05		0.043		
59	6	54	58	6	53	530642.939	0.05		0.032		
60	6	55	59	6	54	539474.760	0.05		-0.041		
61	6	56	60	6	55	548281.968	0.05		0.103		
62	6	56	61	6	55	565594.588	0.05		-0.160		
62	6	57	61	6	56	557063.478	0.05		0.050		
63	6	57	62	6	56	574944.866	0.05		0.153		
63	6	58	62	6	57	565818.986	0.05		-0.004		
64	6	58	63	6	57	584239.404	0.05		0.049		
64	6	59	63	6	58	574548.303	0.05		0.079		
65	6	59	64	6	58	593472.428	0.05		0.036		
65	6	60	64	6	59	583250.883	0.05		-0.096		
66	6	60	65	6	59	602638.601	0.05		0.015		
11	7	5	10	7	4	98602.176	0.05		-0.008		
12	7	6	11	7	5	107569.674	0.05		-0.012		
13	7	7	12	7	6	116538.208	0.05		0.071		
14	7	7	13	7	6	125507.488	0.05		-0.128		
16	7	9	15	7	8	143449.970	0.05		0.008		
18	7	11	17	7	10	161397.352	0.05		0.019		
23	7	16	22	7	15	206291.754	0.05		0.028	Yes	206291.726
23	7	17	22	7	16	206291.754	0.05		0.028	Yes	206291.726
24	7	17	23	7	16	215275.705	0.20		0.039	Yes	215275.666
24	7	18	23	7	17	215275.705	0.20		0.039	Yes	215275.666
25	7	18	24	7	17	224261.496	0.20		0.024	Yes	224261.472
25	7	19	24	7	18	224261.496	0.20		0.024	Yes	224261.472
26	7	19	25	7	18	233249.264	0.20		0.039	Yes	233249.225
26	7	20	25	7	19	233249.264	0.20		0.039	Yes	233249.225
27	7	20	26	7	19	242238.752	0.05	*	-0.302	Yes	242239.004
27	7	21	26	7	20	242238.752	0.05	*	-0.202	Yes	242239.004
28	7	21	27	7	20	251230.932	0.20		0.040	Yes	251230.892
28	7	22	27	7	21	251230.932	0.20		0.040	Yes	251230.892
29	7	22	28	7	21	260224.990	0.20		0.017	Yes	260224.973
29	7	23	28	7	22	260224.990	0.20		0.017	Yes	260224.973
30	7	23	29	7	22	269221.438	0.20		-0.092		
30	7	24	29	7	23	269222.517	0.20	*	1.382		
31	7	24	30	7	23	278220.107	0.05		0.047	Yes	278220.060
31	7	25	30	7	24	278220.107	0.05		0.047	Yes	278220.060
32	7	25	31	7	24	287221.137	0.05		-0.112	Yes	287221.249
32	7	26	31	7	25	287221.137	0.05		-0.112	Yes	287221.249

Tabla A.4: continued.

J'	K'_a	K'_c	J"	K''_a	K''_c	ν(Hz)	e$_\nu$(Hz)	f$_\nu$(Hz)	O-C(Hz)	Blend	f$_{peak}$(Hz)
33	7	26	32	7	25	296225.027	0.05		0.031	Yes	296224.996
33	7	27	32	7	26	296225.027	0.05		0.031	Yes	296224.996
36	7	29	35	7	28	323253.778	0.05	*	-0.911		
36	7	30	35	7	29	323250.824	0.05	*	0.276		
37	7	30	36	7	29	332270.122	0.05	*	-0.475		
37	7	31	36	7	30	332265.056	0.05	*	0.330		
38	7	31	37	7	30	341289.744	0.05		-0.203		
38	7	32	37	7	31	341281.156	0.05	*	-0.552		
39	7	32	38	7	31	350312.908	0.05		-0.067		
39	7	33	38	7	32	350301.603	0.05		0.071		
40	7	33	39	7	32	359339.890	0.05		-0.066		
40	7	34	39	7	33	359324.260	0.05		0.046		
44	7	37	43	7	36	395494.656	0.05		-0.025		
44	7	38	43	7	37	395442.652	0.05	*	-0.388		
45	7	38	44	7	37	404547.377	0.05		-0.076		
46	7	39	45	7	38	413607.063	0.05		-0.048		
47	7	40	46	7	39	422674.423	0.05		-0.039		
47	7	41	46	7	40	422557.998	0.05	*	-0.724		
48	7	41	47	7	40	431750.434	0.05		-0.008		
48	7	42	47	7	41	431600.936	0.05		-0.248		
49	7	42	48	7	41	440836.103	0.05		-0.020		
49	7	43	48	7	42	440644.892	0.05		-0.099		
50	7	43	49	7	42	449932.669	0.05		-0.063		
50	7	44	49	7	43	449689.597	0.05		-0.062		
51	7	44	50	7	43	459041.544	0.05		-0.116		
51	7	45	50	7	44	458734.579	0.05		-0.034		
52	7	45	51	7	44	468163.684	0.05	*	-0.779		
52	7	46	51	7	45	467779.184	0.05		0.002		
53	7	46	52	7	45	477304.103	0.05	*	1.232		
53	7	47	52	7	46	476822.628	0.05		0.035		
54	7	47	53	7	46	486458.599	0.05		-0.164		
54	7	48	53	7	47	485863.932	0.05		-0.038		
55	7	48	54	7	47	495634.021	0.05		-0.140		
55	7	49	54	7	48	494902.362	0.05		0.029		
56	7	49	55	7	48	504831.108	0.05		-0.067		
56	7	50	55	7	49	503936.629	0.05		0.030		
57	7	50	56	7	49	514051.843	0.05		-0.109		
57	7	51	56	7	50	512965.637	0.05		0.051		
58	7	51	57	7	50	523298.380	0.05		-0.196		
58	7	52	57	7	51	521988.054	0.05		0.032		
59	7	52	58	7	51	532572.594	0.05	*	-0.365		
59	7	53	58	7	52	531002.568	0.05		0.014		
60	7	53	59	7	52	541875.985	0.05	*	-0.699		
60	7	54	59	7	53	540007.610	0.05		-0.150		
61	7	55	60	7	54	549002.173	0.05		0.008		
62	7	56	61	7	55	557984.283	0.05		0.026		
63	7	57	62	7	56	566952.557	0.05		0.048		
64	7	58	63	7	57	575905.331	0.05		-0.063		

Tabla A.4: continued.

J'	K'_a	K'_c	J"	K''_a	K''_c	ν(Hz)	e$_\nu$(Hz)	f$_\nu$(Hz)	O-C(Hz)	Blend	f$_{Peak}$(Hz)
65	7	59	64	7	58	584841.525	0.05		0.115		
66	7	60	65	7	59	593759.054	0.05		-0.045		
67	7	61	66	7	60	602657.035	0.05		-0.032		
12	8	4	11	8	3	107575.996	0.05		0.084		
13	8	6	12	8	5	116543.187	0.05	*	0.274		
14	8	6	13	8	5	125510.348	0.05		-0.120		
16	8	8	15	8	7	143447.447	0.05		0.037		
17	8	9	16	8	8	152416.863	0.05		-0.013		
18	8	10	17	8	9	161387.060	0.05		0.002		
19	8	11	18	8	10	170358.044	0.05		0.048		
23	8	15	22	8	14	206250.147	0.05		0.070	Yes	206250.077
23	8	16	22	8	15	206250.147	0.05		0.070	Yes	206250.077
25	8	17	24	8	16	224201.746	0.20		0.093	Yes	224201.653
25	8	18	24	8	17	224201.746	0.20		0.093	Yes	224201.653
26	8	18	25	8	17	233179.066	0.20		0.108	Yes	233178.959
26	8	19	25	8	18	233179.066	0.20		0.108	Yes	233178.959
27	8	19	26	8	18	242157.368	0.20		0.042	Yes	242157.326
27	8	20	26	8	19	242157.368	0.20		0.042	Yes	242157.326
28	8	20	27	8	19	251136.899	0.20		0.104	Yes	251136.795
28	8	21	27	8	20	251136.899	0.20		0.104	Yes	251136.795
29	8	21	28	8	20	260117.497	0.20		0.093	Yes	260117.404
29	8	22	28	8	21	260117.497	0.20		0.093	Yes	260117.404
30	8	22	29	8	21	269099.279	0.20		0.086	Yes	269099.193
30	8	23	29	8	22	269099.279	0.20		0.086	Yes	269099.193
31	8	23	30	8	22	278082.217	0.05		0.017	Yes	278082.200
31	8	24	30	8	23	278082.217	0.05		0.017	Yes	278082.200
33	8	25	32	8	24	296052.045	0.05		0.006	Yes	296052.039
33	8	26	32	8	25	296052.045	0.05		0.006	Yes	296052.039
34	8	26	33	8	25	305038.931	0.05		-0.024	Yes	305038.955
34	8	27	33	8	26	305038.931	0.05		-0.024	Yes	305038.955
35	8	27	34	8	26	314027.307	0.05		0.047	Yes	314027.260
35	8	28	34	8	27	314027.307	0.05		0.047	Yes	314027.260
36	8	28	35	8	27	323017.075	0.05		0.074	Yes	323017.001
36	8	29	35	8	28	323017.075	0.05		0.074	Yes	323017.001
37	8	29	36	8	28	332008.216	0.05		-0.010	Yes	332008.226
37	8	30	36	8	29	332008.216	0.05		-0.010	Yes	332008.226
38	8	30	37	8	29	341001.108	0.05		0.123	Yes	341000.985
38	8	31	37	8	30	341001.108	0.05		0.123	Yes	341000.985
39	8	31	38	8	30	349995.813	0.05		0.225		
39	8	32	38	8	31	349994.812	0.05	*	-0.260		
40	8	32	39	8	31	358991.428	0.05		0.110	Yes	358991.318
40	8	33	39	8	32	358991.428	0.05		0.110	Yes	358991.318
47	8	39	46	8	38	422018.338	0.05	*	-0.318		
47	8	40	46	8	39	422010.778	0.05		0.022		
48	8	40	47	8	39	431031.484	0.05		-0.202		
48	8	41	47	8	40	431020.942	0.05		-0.048		
49	8	41	48	8	40	440047.354	0.05		-0.159		
49	8	42	48	8	41	440033.135	0.05		-0.004		

Tabla A.4: continued.

J'	K'_a	K'_c	J"	K''_a	K''_c	ν(Hz)	e$_\nu$(Hz)	f$_\nu$(Hz)	O-C(Hz)	Blend	f$_{peak}$(Hz)
50	8	42	49	8	41	449066.268	0.05		-0.110		
50	8	43	49	8	42	449047.215	0.05		0.016		
51	8	43	50	8	42	458088.349	0.05		-0.208		
51	8	44	50	8	43	458063.126	0.05		-0.019		
52	8	44	51	8	43	467114.169	0.05		-0.208		
52	8	45	51	8	44	467080.936	0.05		0.005		
53	8	45	52	8	44	476143.925	0.05	*	-0.293		
53	8	46	52	8	45	476100.471	0.05		-0.017		
54	8	46	53	8	45	485178.253	0.05	*	-0.271		
54	8	47	53	8	46	485121.748	0.05		0.037		
55	8	47	54	8	46	494217.536	0.05	*	-0.277		
55	8	48	54	8	47	494144.491	0.05		0.030		
56	8	48	55	8	47	503262.324	0.05	*	-0.362		
56	8	49	55	8	48	503168.579	0.05		0.025		
57	8	49	56	8	48	512313.410	0.05	*	-0.429		
57	8	50	56	8	49	512193.754	0.05		-0.004		
58	8	50	57	8	49	521371.556	0.05	*	-0.520		
58	8	51	57	8	50	521219.816	0.05		0.030		
59	8	51	58	8	50	530437.583	0.05	*	-0.735		
59	8	52	58	8	51	530246.350	0.05		0.063		
60	8	52	59	8	51	539512.542	0.05	*	-1.074		
60	8	53	59	8	52	539272.921	0.05		0.081		
61	8	53	60	8	52	548597.618	0.05	*	-1.545		
61	8	54	60	8	53	548298.976	0.05		0.024		
62	8	54	61	8	53	557693.960	0.05	*	-2.335		
62	8	55	61	8	54	557324.082	0.05		0.036		
63	8	55	62	8	54	566802.544	0.05	*	-3.958		
63	8	56	62	8	55	566347.482	0.05		0.020		
64	8	57	63	8	56	575368.388	0.05		-0.061		
66	8	59	65	8	58	593399.508	0.05		-0.174		
67	8	60	66	8	59	602408.142	0.05		0.166		
13	9	5	12	9	4	116554.425	0.05		0.075		
14	9	5	13	9	4	125521.252	0.05		0.024		
15	9	6	14	9	5	134488.226	0.05		-0.133		
16	9	7	15	9	6	143455.736	0.05		-0.021		
18	9	9	17	9	8	161391.523	0.05		0.103		
19	9	10	18	9	9	170359.789	0.05		0.074		
24	9	15	23	9	14	215206.501	0.20		0.094	Yes	215206.407
24	9	16	23	9	15	215206.501	0.20		0.094	Yes	215206.407
25	9	16	24	9	15	224176.966	0.20		0.081	Yes	224176.885
25	9	17	24	9	16	224176.966	0.20		0.081	Yes	224176.885
26	9	17	25	9	16	233147.872	0.20		0.099	Yes	233147.773
26	9	18	25	9	17	233147.872	0.20		0.099	Yes	233147.773
27	9	18	26	9	17	242119.294	0.05		0.210	Yes	242119.084
27	9	19	26	9	18	242119.294	0.05		0.210	Yes	242119.084
28	9	19	27	9	18	251090.930	0.20		0.098	Yes	251090.832
28	9	20	27	9	19	251090.930	0.20		0.098	Yes	251090.832
29	9	20	28	9	19	260063.123	0.20		0.096	Yes	260063.027

Tabla A.4: continued.

J'	K'_a	K'_c	J"	K''_a	K''_c	ν(Hz)	e$_\nu$(Hz)	f$_\nu$(Hz)	O-C(Hz)	Blend	f$_{Peak}$(Hz)
29	9	21	28	9	20	260063.123	0.20		0.096	Yes	260063.027
33	9	24	32	9	23	295956.546	0.05		0.006	Yes	295956.540
33	9	25	32	9	24	295956.546	0.05		0.006	Yes	295956.540
34	9	25	33	9	24	304931.200	0.05		0.037	Yes	304931.163
34	9	26	33	9	25	304931.200	0.05		0.037	Yes	304931.163
35	9	26	34	9	25	313906.368	0.05		0.058	Yes	313906.310
35	9	27	34	9	26	313906.368	0.05		0.058	Yes	313906.310
36	9	27	35	9	26	322882.001	0.05		0.007	Yes	322881.994
36	9	28	35	9	27	322882.001	0.05		0.007	Yes	322881.994
37	9	28	36	9	27	331858.291	0.05		0.063	Yes	331858.228
37	9	29	36	9	28	331858.291	0.05		0.063	Yes	331858.228
38	9	29	37	9	28	340835.075	0.05		0.047	Yes	340835.028
38	9	30	37	9	29	340835.075	0.05		0.047	Yes	340835.028
39	9	30	38	9	29	349812.473	0.05		0.065	Yes	349812.408
39	9	31	38	9	30	349812.473	0.05		0.065	Yes	349812.408
40	9	31	39	9	30	358790.480	0.05		0.096	Yes	358790.384
40	9	32	39	9	31	358790.480	0.05		0.096	Yes	358790.384
45	9	36	44	9	35	403690.405	0.05	*	0.466	Yes	403689.844
45	9	37	44	9	36	403690.405	0.05	*	0.656	Yes	403689.844
46	9	37	45	9	36	412671.961	0.05		0.163	Yes	412671.798
46	9	38	45	9	37	412671.961	0.05		0.163	Yes	412671.798
47	9	38	46	9	37	421654.653	0.05		0.157	Yes	421654.496
47	9	39	46	9	38	421654.653	0.05		0.157	Yes	421654.496
48	9	39	47	9	38	430638.412	0.05	*	0.166	Yes	430637.968
48	9	40	47	9	39	430638.412	0.05	*	0.721	Yes	430637.968
49	9	40	48	9	39	439623.619	0.05	*	0.984		
49	9	41	48	9	40	439621.784	0.05		-0.071		
50	9	41	49	9	40	448608.271	0.05	*	0.366		
50	9	42	49	9	41	448606.782	0.05		-0.035		
51	9	42	50	9	41	457592.747	0.05	*	-1.360	Yes	457593.354
51	9	43	50	9	42	457592.747	0.05	*	0.145	Yes	457593.354
52	9	44	51	9	43	466579.129	0.05		-0.103		
53	9	44	52	9	43	475570.455	0.05	*	0.900		
53	9	45	52	9	44	475566.827	0.05		0.096		
54	9	46	53	9	45	484555.218	0.05		0.098		
55	9	46	54	9	45	493550.720	0.05	*	1.148		
55	9	47	54	9	46	493544.573	0.05		0.154		
56	9	47	55	9	46	502542.534	0.05	*	1.001		
56	9	48	55	9	47	502534.588	0.05		-0.052		
57	9	48	56	9	47	511535.828	0.05	*	0.869		
57	9	49	56	9	48	511525.773	0.05		-0.022		
58	9	49	57	9	48	520530.838	0.05	*	0.844		
58	9	50	57	9	49	520517.823	0.05		-0.063		
59	9	50	58	9	49	529527.610	0.05	*	0.800		
59	9	51	58	9	50	529510.924	0.05		0.019		
60	9	51	59	9	50	538526.215	0.05	*	0.608		
60	9	52	59	9	51	538504.941	0.05		0.105		
61	9	52	60	9	51	547527.294	0.05	*	0.673		

Tabla A.4: continued.

J'	K'_a	K'_c	J"	K''_a	K''_c	ν(Hz)	e$_\nu$(Hz)	f$_\nu$(Hz)	O-C(Hz)	Blend	f$_{peak}$(Hz)
61	9	53	60	9	52	547499.846	0.05		0.201		
63	9	54	62	9	53	565536.993	0.05	*	0.556		
63	9	55	62	9	54	565490.604	0.05	*	-1.072		
64	9	55	63	9	54	574546.320	0.05	*	0.387		
13	10	3	12	10	2	116570.896	0.05		0.103		
14	10	4	13	10	3	125537.916	0.05		0.088		
15	10	5	14	10	4	134504.871	0.05		0.001		
17	10	7	16	10	6	152439.035	0.05		0.066		
23	10	13	22	10	12	206241.087	0.05		-0.172	Yes	206241.259
23	10	14	22	10	13	206241.087	0.05		-0.172	Yes	206241.259
24	10	14	23	10	13	215208.287	0.20		0.009	Yes	215208.278
24	10	15	23	10	14	215208.287	0.20		0.009	Yes	215208.278
25	10	15	24	10	14	224175.349	0.20		0.069	Yes	224175.280
25	10	16	24	10	15	224175.349	0.20		0.069	Yes	224175.280
26	10	16	25	10	15	233142.334	0.20		0.074	Yes	233142.260
26	10	17	25	10	16	233142.334	0.20		0.074	Yes	233142.260
27	10	17	26	10	16	242109.283	0.20		0.068	Yes	242109.215
27	10	18	26	10	17	242109.283	0.20		0.068	Yes	242109.215
28	10	18	27	10	17	251076.195	0.20		0.056	Yes	251076.139
28	10	19	27	10	18	251076.195	0.20		0.056	Yes	251076.139
29	10	19	28	10	18	260043.085	0.20		0.057	Yes	260043.028
29	10	20	28	10	19	260043.085	0.20		0.057	Yes	260043.028
30	10	20	29	10	19	269009.987	0.20		0.112	Yes	269009.875
30	10	21	29	10	20	269009.987	0.20		0.112	Yes	269009.875
31	10	21	30	10	20	277976.627	0.05		-0.050	Yes	277976.677
31	10	22	30	10	21	277976.627	0.05		-0.050	Yes	277976.677
33	10	23	32	10	22	295909.748	0.05	*	-0.372	Yes	295910.121
33	10	24	32	10	23	295909.748	0.05	*	-0.372	Yes	295910.121
34	10	24	33	10	23	304876.674	0.05		-0.076	Yes	304876.750
34	10	25	33	10	24	304876.674	0.05		-0.076	Yes	304876.750
35	10	25	34	10	24	313843.211	0.05		-0.100	Yes	313843.311
35	10	26	34	10	25	313843.211	0.05		-0.100	Yes	313843.311
36	10	26	35	10	25	322809.719	0.05		-0.078	Yes	322809.797
36	10	27	35	10	26	322809.719	0.05		-0.078	Yes	322809.797
37	10	27	36	10	26	331776.112	0.05		-0.089	Yes	331776.201
37	10	28	36	10	27	331776.112	0.05		-0.089	Yes	331776.201
38	10	28	37	10	27	340742.903	0.05	*	0.384	Yes	340742.518
38	10	29	37	10	28	340742.903	0.05	*	0.384	Yes	340742.518
39	10	29	38	10	28	349708.110	0.05	*	-0.632	Yes	349708.742
39	10	30	38	10	29	349708.110	0.05	*	-0.632	Yes	349708.742
40	10	30	39	10	29	358674.665	0.05		-0.203	Yes	358674.868
40	10	31	39	10	30	358674.665	0.05		-0.203	Yes	358674.868
45	10	35	44	10	34	403503.592	0.05		-0.237	Yes	403503.829
45	10	36	44	10	35	403503.592	0.05		-0.237	Yes	403503.829
46	10	36	45	10	35	412468.974	0.05	*	-0.287	Yes	412469.257
46	10	37	45	10	36	412468.974	0.05	*	-0.277	Yes	412469.257
47	10	37	46	10	36	421434.302	0.05	*	-0.259	Yes	421434.554
47	10	38	46	10	37	421434.302	0.05	*	-0.245	Yes	421434.554

Tabla A.4: continued.

J'	K'_a	K'_c	J"	K''_a	K''_c	ν(Hz)	e$_\nu$(Hz)	f$_\nu$(Hz)	O-C(Hz)	Blend	f$_{peak}$(Hz)
48	10	38	47	10	37	430399.548	0.05		-0.173	Yes	430399.721
48	10	39	47	10	38	430399.548	0.05		-0.173	Yes	430399.721
49	10	39	48	10	38	439364.456	0.05	*	-0.314	Yes	439364.754
49	10	40	48	10	39	439364.456	0.05	*	-0.281	Yes	439364.754
50	10	40	49	10	39	448329.389	0.05	*	-0.288	Yes	448329.654
50	10	41	49	10	40	448329.389	0.05	*	-0.241	Yes	448329.654
51	10	41	50	10	40	457294.194	0.05	*	-0.262		
51	10	42	50	10	41	457294.161	0.05		-0.227		
52	10	42	51	10	41	466258.799	0.05	*	-0.309	Yes	466259.060
52	10	43	51	10	42	466258.799	0.05	*	-0.212	Yes	466259.060
53	10	43	52	10	42	475223.373	0.05		-0.199	Yes	475223.572
53	10	44	52	10	43	475223.373	0.05		-0.199	Yes	475223.572
54	10	44	53	10	43	484187.737	0.05	*	-0.322		
54	10	45	53	10	44	484187.712	0.05		-0.152		
55	10	45	54	10	44	493152.183	0.05		-0.191		
55	10	46	54	10	45	493152.155	0.05		0.054		
56	10	46	55	10	45	502116.512	0.05		0.105	Yes	502116.407
56	10	47	55	10	46	502116.512	0.05		0.105	Yes	502116.407
57	10	47	56	10	46	511081.510	0.05	*	0.765	Yes	511080.482
57	10	48	56	10	47	511081.510	0.05	*	1.290	Yes	511080.482
60	10	50	59	10	49	537973.769	0.05	*	0.821		
60	10	51	59	10	50	537971.946	0.05	*	0.330		
62	10	52	61	10	51	555903.196	0.05	*	2.005		
62	10	53	61	10	52	555899.151	0.05	*	0.364		
63	10	53	62	10	52	564868.977	0.05	*	3.505		
63	10	54	62	10	53	564862.860	0.05	*	0.591		
14	11	3	13	11	2	125559.053	0.05		-0.053		
16	11	5	15	11	4	143494.171	0.05		0.009		
17	11	6	16	11	5	152461.372	0.05		-0.022		
18	11	7	17	11	6	161428.399	0.05		-0.012		
19	11	8	18	11	7	170395.204	0.05		0.007		
23	11	12	22	11	11	206259.757	0.05		0.010	Yes	206259.747
23	11	13	22	11	12	206259.757	0.05		0.010	Yes	206259.747
25	11	14	24	11	13	224190.264	0.20		0.016	Yes	224190.248
25	11	15	24	11	14	224190.264	0.20		0.016	Yes	224190.248
26	11	15	25	11	14	233155.088	0.20		0.089	Yes	233154.999
26	11	16	25	11	15	233155.088	0.20		0.089	Yes	233154.999
27	11	16	26	11	15	242119.294	0.05		-0.102		
28	11	17	27	11	16	251083.496	0.20		0.076	Yes	251083.420
28	11	18	27	11	17	251083.496	0.20		0.076	Yes	251083.420
29	11	18	28	11	17	260047.141	0.20		0.085	Yes	260047.056
29	11	19	28	11	18	260047.141	0.20		0.085	Yes	260047.056
30	11	19	29	11	18	269010.044	0.05		-0.241	Yes	269010.285
30	11	20	29	11	19	269010.044	0.05		-0.241	Yes	269010.285
31	11	20	30	11	19	277973.139	0.05		0.049	Yes	277973.090
31	11	21	30	11	20	277973.139	0.05		0.049	Yes	277973.090
32	11	21	31	11	20	286935.484	0.05		0.031	Yes	286935.453
32	11	22	31	11	21	286935.484	0.05		0.031	Yes	286935.453

Tabla A.4: continued.

J'	K'_a	K'_c	J"	K''_a	K''_c	ν(Hz)	e$_\nu$(Hz)	f$_\nu$(Hz)	O-C(Hz)	Blend	f$_{peak}$(Hz)
33	11	22	32	11	21	295898.040	0.05	*	0.683	Yes	295897.357
33	11	23	32	11	22	295898.040	0.05	*	0.683	Yes	295897.357
34	11	23	33	11	22	304858.841	0.05		0.059	Yes	304858.782
34	11	24	33	11	23	304858.841	0.05		0.059	Yes	304858.782
35	11	24	34	11	23	313819.808	0.05		0.098	Yes	313819.710
35	11	25	34	11	24	313819.808	0.05		0.098	Yes	313819.710
36	11	25	35	11	24	322780.345	0.05		0.223	Yes	322780.122
36	11	26	35	11	25	322780.345	0.05		0.223	Yes	322780.122
37	11	26	36	11	25	331740.178	0.05		0.178	Yes	331740.000
37	11	27	36	11	26	331740.178	0.05		0.178	Yes	331740.000
38	11	27	37	11	26	340699.782	0.05	*	0.458	Yes	340699.323
38	11	28	37	11	27	340699.782	0.05	*	0.458	Yes	340699.323
39	11	28	38	11	27	349658.280	0.05		0.206	Yes	349658.074
39	11	29	38	11	28	349658.280	0.05		0.206	Yes	349658.074
40	11	29	39	11	28	358616.553	0.05	*	0.320	Yes	358616.233
40	11	30	39	11	29	358616.553	0.05	*	0.320	Yes	358616.233
53	11	43	52	11	42	475009.327	0.05	*	-0.290		
54	11	44	53	11	43	483956.891	0.05	*	-0.586		
15	12	3	14	12	2	134553.065	0.05		-0.016		
16	12	4	15	12	3	143521.464	0.05		0.006		
18	12	6	17	12	5	161457.126	0.05		0.010		
19	12	7	18	12	6	170424.286	0.05		-0.063		
25	12	13	24	12	12	224217.951	0.20		0.073	Yes	224217.878
25	12	14	24	12	13	224217.951	0.20		0.073	Yes	224217.878
26	12	14	25	12	13	233181.745	0.20		0.156	Yes	233181.589
26	12	15	25	12	14	233181.745	0.20		0.156	Yes	233181.589
27	12	15	26	12	14	242144.809	0.20		0.112	Yes	242144.697
27	12	16	26	12	15	242144.809	0.20		0.112	Yes	242144.697
28	12	16	27	12	15	251107.306	0.20		0.131	Yes	251107.175
28	12	17	27	12	16	251107.306	0.20		0.131	Yes	251107.175
29	12	17	28	12	16	260069.127	0.20		0.130	Yes	260068.997
29	12	18	28	12	17	260069.127	0.20		0.130	Yes	260068.997
30	12	18	29	12	17	269030.166	0.05		0.029	Yes	269030.137
30	12	19	29	12	18	269030.166	0.05		0.029	Yes	269030.137
32	12	20	31	12	19	286950.309	0.05		0.045	Yes	286950.264
32	12	21	31	12	20	286950.309	0.05		0.045	Yes	286950.264
33	12	21	32	12	20	295909.748	0.05	*	0.551	Yes	295909.196
33	12	22	32	12	21	295909.748	0.05	*	0.551	Yes	295909.196
34	12	22	33	12	21	304867.461	0.05		0.122	Yes	304867.339
34	12	23	33	12	22	304867.461	0.05		0.122	Yes	304867.339
35	12	23	34	12	22	313824.737	0.05		0.074	Yes	313824.663
35	12	24	34	12	23	313824.737	0.05		0.074	Yes	313824.663
36	12	24	35	12	23	322781.318	0.05		0.176	Yes	322781.142
36	12	25	35	12	24	322781.318	0.05		0.176	Yes	322781.142
37	12	25	36	12	24	331737.135	0.05	*	0.387	Yes	331736.747
37	12	26	36	12	25	331737.135	0.05	*	0.387	Yes	331736.747
38	12	26	37	12	25	340691.559	0.05		0.108	Yes	340691.451
38	12	27	37	12	26	340691.559	0.05		0.108	Yes	340691.451

Tabla A.4: continued.

J'	K'_a	K'_c	J"	K''_a	K''_c	ν(Hz)	e$_\nu$(Hz)	f$_\nu$(Hz)	O-C(Hz)	Blend	f$_{Peak}$(Hz)
39	12	27	38	12	26	349645.428	0.05		0.204	Yes	349645.225
39	12	28	38	12	27	349645.428	0.05		0.204	Yes	349645.225
40	12	28	39	12	27	358598.203	0.05		0.164	Yes	358598.039
40	12	29	39	12	28	358598.203	0.05		0.164	Yes	358598.039
51	12	40	50	12	39	457007.952	0.05	*	0.525		
52	12	40	51	12	39	465946.893	0.05	*	0.425	Yes	465946.467
52	12	41	51	12	40	465946.893	0.05	*	0.425	Yes	465946.467
53	12	41	52	12	40	474884.807	0.05	*	0.637	Yes	474884.169
53	12	42	52	12	41	474884.807	0.05	*	0.637	Yes	474884.169
54	12	43	53	12	42	483821.170	0.05	*	0.666		
16	13	3	15	13	2	143553.096	0.05		-0.059		
17	13	4	16	13	3	152522.456	0.05		0.015		
19	13	6	18	13	5	170459.419	0.05		-0.031		
27	13	14	26	13	13	242182.274	0.05		0.238	Yes	242182.037
27	13	15	26	13	14	242182.274	0.05		0.238	Yes	242182.037
28	13	15	27	13	14	251143.950	0.05		-0.017		
29	13	16	28	13	15	260104.960	0.05		-0.075	Yes	260105.035
29	13	17	28	13	16	260104.960	0.05		-0.075	Yes	260105.035
30	13	17	29	13	16	269065.160	0.05		-0.047	Yes	269065.207
30	13	18	29	13	17	269065.160	0.05		-0.047	Yes	269065.207
31	13	18	30	13	17	278024.322	0.05		-0.128	Yes	278024.450
31	13	19	30	13	18	278024.322	0.05		-0.128	Yes	278024.450
33	13	20	32	13	19	295939.955	0.05		-0.056	Yes	295940.011
33	13	21	32	13	20	295939.955	0.05		-0.056	Yes	295940.011
34	13	21	33	13	20	304896.225	0.05		-0.037	Yes	304896.262
34	13	22	33	13	21	304896.225	0.05		-0.037	Yes	304896.262
35	13	22	34	13	21	313851.348	0.05		-0.099	Yes	313851.447
35	13	23	34	13	22	313851.348	0.05		-0.099	Yes	313851.447
36	13	23	35	13	22	322805.592	0.05		0.059	Yes	322805.533
36	13	24	35	13	23	322805.592	0.05		0.059	Yes	322805.533
37	13	24	36	13	23	331758.536	0.05		0.052	Yes	331758.484
37	13	25	36	13	24	331758.536	0.05		0.052	Yes	331758.484
38	13	25	37	13	24	340710.552	0.05	*	0.287	Yes	340710.265
38	13	26	37	13	25	340710.552	0.05	*	0.287	Yes	340710.265
39	13	26	38	13	25	349660.730	0.05		-0.112	Yes	349660.842
39	13	27	38	13	26	349660.730	0.05		-0.112	Yes	349660.842
40	13	27	39	13	26	358610.116	0.05		-0.062	Yes	358610.178
40	13	28	39	13	27	358610.116	0.05		-0.062	Yes	358610.178
18	14	4	17	14	3	161530.060	0.05		-0.043		
19	14	5	18	14	4	170499.753	0.05		-0.035		
27	14	13	26	14	12	242229.195	0.05		-0.205	Yes	242229.400
27	14	14	26	14	13	242229.195	0.05		-0.205	Yes	242229.400
28	14	14	27	14	13	251191.412	0.05		-0.141	Yes	251191.552
28	14	15	27	14	14	251191.412	0.05		-0.141	Yes	251191.552
29	14	15	28	14	14	260152.492	0.05		-0.187	Yes	260152.678
29	14	16	28	14	15	260152.492	0.05		-0.187	Yes	260152.678
31	14	17	30	14	16	278071.505	0.05		-0.190	Yes	278071.695
31	14	18	30	14	17	278071.505	0.05		-0.190	Yes	278071.695

Tabla A.4: continued.

J'	K'_a	K'_c	J"	K''_a	K''_c	ν(Hz)	e$_\nu$(Hz)	f$_\nu$(Hz)	O-C(Hz)	Blend	f$_{peak}$(Hz)
32	14	18	31	14	17	287029.294	0.05		-0.214	Yes	287029.508
32	14	19	31	14	18	287029.294	0.05		-0.214	Yes	287029.508
33	14	19	32	14	18	295985.871	0.05	*	-0.267	Yes	295986.138
33	14	20	32	14	19	295985.871	0.05	*	-0.267	Yes	295986.138
34	14	20	33	14	19	304941.247	0.05	*	-0.300	Yes	304941.547
34	14	21	33	14	20	304941.247	0.05	*	-0.300	Yes	304941.547
35	14	21	34	14	20	313895.401	0.05	*	-0.293	Yes	313895.695
35	14	22	34	14	21	313895.401	0.05	*	-0.293	Yes	313895.695
36	14	22	35	14	21	322848.243	0.05	*	-0.298	Yes	322848.541
36	14	23	35	14	22	322848.243	0.05	*	-0.298	Yes	322848.541
37	14	23	36	14	22	331799.672	0.05	*	-0.375	Yes	331800.047
37	14	24	36	14	23	331799.672	0.05	*	-0.375	Yes	331800.047
38	14	24	37	14	23	340749.808	0.05	*	-0.364	Yes	340750.172
38	14	25	37	14	24	340749.808	0.05	*	-0.364	Yes	340750.172
39	14	25	38	14	24	349698.440	0.05	*	-0.436	Yes	349698.876
39	14	26	38	14	25	349698.440	0.05	*	-0.436	Yes	349698.876
40	14	26	39	14	25	358645.691	0.05	*	-0.428	Yes	358646.119
40	14	27	39	14	26	358645.691	0.05	*	-0.428	Yes	358646.119
57	14	43	56	14	42	510485.299	0.05	*	-0.592		
58	14	44	57	14	43	519399.096	0.05	*	-0.682		
27	15	12	26	15	11	242285.062	0.05	*	-0.356	Yes	242285.418
27	15	13	26	15	12	242285.062	0.05	*	-0.356	Yes	242285.418
29	15	14	28	15	13	260208.811	0.05	*	-1.426		
29	15	15	28	15	14	260213.080	0.05	*	2.842		
30	15	15	29	15	14	269169.257	0.05	*	-1.608		
30	15	16	29	15	15	269173.517	0.05	*	2.651		
31	15	16	30	15	15	278128.455	0.05	*	-1.792	Yes	278130.248
31	15	17	30	15	16	278128.455	0.05	*	-1.792	Yes	278130.248
32	15	17	31	15	16	287086.694	0.05	*	-1.647	Yes	287088.342
32	15	18	31	15	17	287086.694	0.05	*	-1.647	Yes	287088.342
35	15	20	34	15	19	313955.027	0.05	*	0.569	Yes	313954.457
35	15	21	34	15	20	313955.027	0.05	*	0.569	Yes	313954.457
37	15	22	36	15	21	331858.291	0.05	*	0.331	Yes	331857.960
37	15	23	36	15	22	331858.291	0.05	*	0.331	Yes	331857.960
38	15	23	37	15	22	340808.271	0.05	*	0.864	Yes	340807.407
38	15	24	37	15	23	340808.271	0.05	*	0.864	Yes	340807.407
55	15	40	54	15	39	492667.373	0.05		-0.077		
56	15	41	55	15	40	501581.388	0.05		0.077	Yes	501581.311
56	15	42	55	15	41	501581.388	0.05		0.077	Yes	501581.311
57	15	42	56	15	41	510492.734	0.05		-0.028	Yes	510492.762
57	15	43	56	15	42	510492.734	0.05		-0.028	Yes	510492.762
28	16	12	27	16	11	251313.729	0.05	*	0.262	Yes	251313.466
28	16	13	27	16	12	251313.729	0.05	*	0.262	Yes	251313.466
29	16	13	28	16	12	260276.684	0.05		0.153	Yes	260276.531
29	16	14	28	16	13	260276.684	0.05		0.153	Yes	260276.531
31	16	15	30	16	14	278198.872	0.05		0.202	Yes	278198.670
31	16	16	30	16	15	278198.872	0.05		0.202	Yes	278198.670
32	16	16	31	16	15	287157.911	0.05	*	0.260	Yes	287157.651

Tabla A.4: continued.

J'	K'_a	K'_c	J"	K''_a	K''_c	ν(Hz)	e$_\nu$(Hz)	f$_\nu$(Hz)	O-C(Hz)	Blend	f$_{Peak}$(Hz)
32	16	17	31	16	16	287157.911	0.05	*	0.260	Yes	287157.651
33	16	17	32	16	16	296115.466	0.05	*	0.288	Yes	296115.177
33	16	18	32	16	17	296115.466	0.05	*	0.288	Yes	296115.177
34	16	18	33	16	17	305071.702	0.05	*	0.499	Yes	305071.203
34	16	19	33	16	18	305071.702	0.05	*	0.499	Yes	305071.203
35	16	19	34	16	18	314025.943	0.05	*	0.263	Yes	314025.680
35	16	20	34	16	19	314025.943	0.05	*	0.263	Yes	314025.680
37	16	21	36	16	20	331930.232	0.05	*	0.431	Yes	331929.800
37	16	22	36	16	21	331930.232	0.05	*	0.431	Yes	331929.800
38	16	22	37	16	21	340879.858	0.05	*	0.508	Yes	340879.349
38	16	23	37	16	22	340879.858	0.05	*	0.508	Yes	340879.349
39	16	23	38	16	22	349827.708	0.05	*	0.547	Yes	349827.161
39	16	24	38	16	23	349827.708	0.05	*	0.547	Yes	349827.161
40	16	24	39	16	23	358773.797	0.05	*	0.609	Yes	358773.188
40	16	25	39	16	24	358773.797	0.05	*	0.609	Yes	358773.188
53	16	37	52	16	36	474887.962	0.05	*	0.633		
55	16	39	54	16	38	492716.957	0.05		0.140	Yes	492716.817
55	16	40	54	16	39	492716.957	0.05		0.140	Yes	492716.817
25	17	9	24	17	8	224483.891	0.20		0.127		
26	17	10	25	17	9	233452.585	0.20		0.147		
27	17	11	26	17	10	242421.034	0.20	*	1.181		
28	17	11	27	17	10	251386.044	0.05		0.086	Yes	251385.958
28	17	12	27	17	11	251386.044	0.05		0.086	Yes	251385.958
29	17	12	28	17	11	260350.902	0.20		0.197		
29	17	13	28	17	12	260350.819	0.05		0.114		
30	17	13	29	17	12	269313.897	0.05		-0.147	Yes	269314.044
30	17	14	29	17	13	269313.897	0.05		-0.147	Yes	269314.044
31	17	14	30	17	13	278275.988	0.05		0.062	Yes	278275.926
31	17	15	30	17	14	278275.988	0.05		0.062	Yes	278275.926
32	17	15	31	17	14	287236.398	0.05		0.097	Yes	287236.301
32	17	16	31	17	15	287236.398	0.05		0.097	Yes	287236.301
35	17	18	34	17	17	314107.784	0.05		-0.103	Yes	314107.887
35	17	19	34	17	18	314107.784	0.05		-0.103	Yes	314107.887
36	17	19	35	17	18	323061.695	0.05		-0.043	Yes	323061.738
36	17	20	35	17	19	323061.695	0.05		-0.043	Yes	323061.738
38	17	21	37	17	20	340964.200	0.05		0.078	Yes	340964.122
38	17	22	37	17	21	340964.200	0.05		0.078	Yes	340964.122
39	17	22	38	17	21	349912.630	0.05		0.074	Yes	349912.556
39	17	23	38	17	22	349912.630	0.05		0.074	Yes	349912.556
40	17	23	39	17	22	358859.189	0.05		0.105	Yes	358859.084
40	17	24	39	17	23	358859.189	0.05		0.105	Yes	358859.084
52	17	35	51	17	34	466049.655	0.05	*	-0.781		
52	17	36	51	17	35	466050.816	0.05	*	0.379		
24	18	6	23	18	5	215584.294	0.20		0.079		
26	18	8	25	18	7	233527.509	0.20		0.082		
26	18	9	25	18	8	233526.474	0.20		-0.953		
28	18	10	27	18	9	251465.492	0.05		0.179	Yes	251465.313
28	18	11	27	18	10	251465.492	0.05		0.179	Yes	251465.313

Tabla A.4: continued.

J'	K'_a	K'_c	J"	K''_a	K''_c	ν(Hz)	e$_\nu$(Hz)	f$_\nu$(Hz)	O-C(Hz)	Blend	f$_{peak}$(Hz)
29	18	11	28	18	10	260432.223	0.20		0.093		
29	18	12	28	18	11	260432.199	0.05		0.069		
30	18	12	29	18	11	269397.265	0.05		-0.195	Yes	269397.460
30	18	13	29	18	12	269397.265	0.05		-0.195	Yes	269397.460
31	18	13	30	18	12	278360.968	0.05	*	-0.284	Yes	278361.252
31	18	14	30	18	13	278360.968	0.05	*	-0.284	Yes	278361.252
32	18	14	31	18	13	287323.651	0.05		0.198	Yes	287323.453
32	18	15	31	18	14	287323.651	0.05		0.198	Yes	287323.453
33	18	15	32	18	14	296283.990	0.05		-0.022	Yes	296284.012
33	18	16	32	18	15	296283.990	0.05		-0.022	Yes	296284.012
34	18	16	33	18	15	305243.047	0.05		0.170	Yes	305242.877
34	18	17	33	18	16	305243.047	0.05		0.170	Yes	305242.877
35	18	17	34	18	16	314200.096	0.05		0.101	Yes	314199.995
35	18	18	34	18	17	314200.096	0.05		0.101	Yes	314199.995
36	18	18	35	18	17	323155.416	0.05		0.101	Yes	323155.315
36	18	19	35	18	18	323155.416	0.05		0.101	Yes	323155.315
37	18	19	36	18	18	332108.949	0.05		0.165	Yes	332108.784
37	18	20	36	18	19	332108.949	0.05		0.165	Yes	332108.784
39	18	21	38	18	20	350010.374	0.05	*	0.413	Yes	350009.960
39	18	22	38	18	21	350010.374	0.05	*	0.413	Yes	350009.960
25	19	7	24	19	6	224635.090	0.20		0.464		
27	19	8	26	19	7	242580.229	0.20		-0.139	Yes	242580.368
27	19	9	26	19	8	242580.229	0.20		-0.139	Yes	242580.368
28	19	9	27	19	8	251551.039	0.20		-0.058	Yes	251551.097
28	19	10	27	19	9	251551.039	0.20		-0.058	Yes	251551.097
29	19	10	28	19	9	260520.425	0.20		0.099	Yes	260520.327
29	19	11	28	19	10	260520.425	0.20		0.099	Yes	260520.327
30	19	11	29	19	10	269487.950	0.05		-0.052	Yes	269488.002
30	19	12	29	19	11	269487.950	0.05		-0.052	Yes	269488.002
31	19	12	30	19	11	278454.165	0.05		0.095	Yes	278454.070
31	19	13	30	19	12	278454.165	0.05		0.095	Yes	278454.070
32	19	13	31	19	12	287418.411	0.05		-0.065	Yes	287418.476
32	19	14	31	19	13	287418.411	0.05		-0.065	Yes	287418.476
33	19	14	32	19	13	296381.144	0.05		-0.023	Yes	296381.167
33	19	15	32	19	14	296381.144	0.05		-0.023	Yes	296381.167
34	19	15	33	19	14	305342.176	0.05		0.088		
34	19	16	33	19	15	305342.947	0.05	*	0.859		
37	19	18	36	19	17	332213.693	0.05		0.000	Yes	332213.693
37	19	19	36	19	18	332213.693	0.05		0.000	Yes	332213.693
39	19	20	38	19	19	350118.143	0.05		-0.114	Yes	350118.257
39	19	21	38	19	20	350118.143	0.05		-0.114	Yes	350118.257
40	19	21	39	19	20	359067.794	0.05	*	0.368	Yes	359067.425
40	19	22	39	19	21	359067.794	0.05	*	0.368	Yes	359067.425
24	20	4	23	20	3	215739.842	0.20		-0.332		
26	20	6	25	20	5	233694.266	0.20		-0.196		
31	20	11	30	20	10	278553.616	0.05	*	-0.315	Yes	278553.931
31	20	12	30	20	11	278553.616	0.05	*	-0.315	Yes	278553.931
32	20	12	31	20	11	287520.853	0.05		-0.026	Yes	287520.879

Tabla A.4: continued.

J'	K'_a	K'_c	J"	K''_a	K''_c	ν(Hz)	e$_\nu$(Hz)	f$_\nu$(Hz)	O-C(Hz)	Blend	f$_{Peak}$(Hz)
32	20	13	31	20	12	287520.853	0.05		-0.026	Yes	287520.879
40	20	20	39	20	19	359187.807	0.05		0.058	Yes	359187.749
40	20	21	39	20	20	359187.807	0.05		0.058	Yes	359187.749
32	21	11	31	21	10	287629.980	0.05	*	-0.294	Yes	287630.275
32	21	12	31	21	11	287629.980	0.05	*	-0.294	Yes	287630.275
33	21	12	32	21	11	296598.046	0.05		-0.189	Yes	296598.235
33	21	13	32	21	12	296598.046	0.05		-0.189	Yes	296598.235
34	21	13	33	21	12	305564.104	0.05		-0.201	Yes	305564.305
34	21	14	33	21	13	305564.104	0.05		-0.201	Yes	305564.305
35	21	14	34	21	13	314528.291	0.05		-0.136	Yes	314528.427
35	21	15	34	21	14	314528.291	0.05		-0.136	Yes	314528.427
31	22	9	30	22	8	278773.926	0.05	*	0.494	Yes	278773.431
31	22	10	30	22	9	278773.926	0.05	*	0.494	Yes	278773.431
33	22	11	32	22	10	296717.093	0.05	*	-0.295	Yes	296717.389
33	22	12	32	22	11	296717.093	0.05	*	-0.295	Yes	296717.389
33	25	8	32	25	7	297114.394	0.05	*	0.332	Yes	297114.062
33	25	9	32	25	8	297114.394	0.05	*	0.332	Yes	297114.062
13	1	13	12	0	12	122543.000	0.05	*	-0.350		
15	1	15	14	0	14	137179.600	0.05		-0.122		
16	1	16	15	0	15	144648.210	0.05		-0.021		
18	1	18	17	0	17	159916.480	0.05		-0.009		
19	1	19	18	0	18	167711.910	0.05		-0.011		
24	1	24	23	0	23	207969.752	0.05		0.060		
27	1	27	26	0	26	232801.268	0.05		0.091		
28	1	28	27	0	27	241142.845	0.05		-0.001		
29	1	29	28	0	28	249507.250	0.20		0.011		
30	1	30	29	0	29	257889.975	0.20		0.040		
31	1	31	30	0	30	266287.210	0.05		-0.030		
32	1	32	31	0	31	274696.101	0.05		0.007		
33	1	33	32	0	32	283114.059	0.05		0.085		
34	1	34	33	0	33	291538.710	0.05		-0.103		
35	1	35	34	0	34	299968.898	0.05		-0.022		
37	1	37	36	0	36	316839.697	0.05		0.002		
38	1	38	37	0	37	325278.260	0.05		-0.079		
40	1	40	39	0	39	342158.416	0.05		-0.017		
41	1	41	40	0	40	350598.647	0.05		-0.157		
42	1	42	41	0	41	359038.690	0.05		-0.147		
15	2	13	14	1	14	243482.507	0.05	*	-0.372		
19	2	17	18	1	18	312844.684	0.05	*	-0.445		
20	2	18	19	1	19	331920.295	0.05	*	-0.888		
21	2	19	20	1	20	351644.295	0.05		-0.019		
25	2	24	24	1	23	237496.430	0.20		-0.171		
26	2	25	25	1	24	243875.541	0.05	*	-0.521		
27	2	26	26	1	25	250448.188	0.05		-0.083		
29	2	28	28	1	27	264177.414	0.05		0.011		
30	2	29	29	1	28	271323.148	0.05		0.008		
33	2	32	32	1	31	293737.698	0.05		-0.035		
34	2	33	33	1	32	301483.294	0.05		-0.005		

Tabla A.4: continued.

J'	K'_a	K'_c	J"	K''_a	K''_c	ν(Hz)	e$_\nu$(Hz)	f$_\nu$(Hz)	O-C(Hz)	Blend	f$_{peak}$(Hz)
35	2	34	34	1	33	309339.085	0.05		-0.229		
36	2	35	35	1	34	317290.820	0.05		0.007		
37	2	36	36	1	35	325324.004	0.05		-0.019		
38	2	37	37	1	36	333426.572	0.05		0.044		
39	2	38	38	1	37	341587.330	0.05		0.005		
41	2	40	40	1	39	358046.508	0.05		-0.104		
31	3	28	30	2	29	492574.203	0.05	*	-0.964		
56	3	54	55	2	53	490974.285	0.05		-0.058		
58	3	56	57	2	55	507545.059	0.05		-0.084		
59	3	57	58	2	56	515857.164	0.05		-0.066		
6	0	6	5	1	5	33867.010	0.05	*	0.272		
9	0	9	8	1	8	64138.761	0.05		0.214		
10	0	10	9	1	9	74274.871	0.05		0.226		
11	0	11	10	1	10	84370.916	0.05		0.181		
12	0	12	11	1	11	94394.408	0.05		0.159		
13	0	13	12	1	12	104318.832	0.05		0.152		
14	0	14	13	1	13	114124.898	0.05		0.173		
15	0	15	14	1	14	123800.731	0.05		0.111		
15	0	15	14	1	14	123800.770	0.05		0.150		
16	0	16	15	1	15	133341.778	0.05		0.080		
16	0	16	15	1	15	133341.790	0.05		0.092		
17	0	17	16	1	16	142749.430	0.05		0.090		
18	0	18	17	1	17	152029.730	0.05		0.128		
20	0	20	19	1	19	170247.210	0.05		0.169		
26	0	26	25	1	25	222980.712	0.20		0.035		
27	0	27	26	1	26	231595.472	0.20		0.057		
28	0	28	27	1	27	240180.479	0.05		0.134		
29	0	29	28	1	28	248740.677	0.05		0.045		
30	0	30	29	1	29	257280.688	0.05		0.097		
31	0	31	30	1	30	265803.801	0.05		0.005		
32	0	32	31	1	31	274313.220	0.05		0.031		
33	0	33	32	1	32	282811.180	0.05		0.007		
34	0	34	33	1	33	291299.700	0.05		-0.001		
37	0	37	36	1	36	316722.839	0.05		0.003		
38	0	38	37	1	37	325186.427	0.05		-0.066		
39	0	39	38	1	38	333646.019	0.05		0.020		
41	0	41	40	1	40	350554.370	0.05		-0.085		
42	0	42	41	1	41	359004.030	0.05		-0.070		
54	1	53	53	2	52	466753.823	0.05		0.060		
57	1	56	56	2	55	492012.962	0.05		-0.126		
59	1	58	58	2	57	508836.103	0.05	*	1.208		
60	1	59	59	2	58	517241.073	0.05		0.007		
61	1	60	60	2	59	525644.205	0.05		-0.036		
6	1	5	6	0	6	28352.470	0.05		-0.161		
7	1	6	7	0	7	30319.440	0.05		-0.087		
8	1	7	8	0	8	32665.470	0.05		-0.076		
9	1	8	9	0	9	35422.430	0.05		0.011		
10	1	9	10	0	10	38619.800	0.05		0.097		

Tabla A.4: continued.

J'	K'_a	K'_c	J"	K''_a	K''_c	ν(Hz)	e$_\nu$(Hz)	f$_\nu$(Hz)	O-C(Hz)	Blend	f$_{Peak}$(Hz)
13	1	12	13	0	13	51060.720	0.05		0.079		
14	1	13	14	0	14	56179.750	0.05		-0.015		
15	1	14	15	0	15	61767.700	0.05		0.086		
4	2	2	4	1	3	66646.700	0.05		0.002		
5	2	3	5	1	4	65624.716	0.05		0.193		
6	2	4	6	1	5	64485.520	0.05		-0.011		
7	2	5	7	1	6	63276.464	0.05		0.004		
7	2	6	7	1	7	75634.778	0.05		-0.052		
8	2	6	8	1	7	62050.152	0.05		-0.030		
8	2	7	8	1	8	77583.633	0.05		-0.017		
9	2	7	9	1	8	60864.220	0.05		-0.035		
9	2	8	9	1	9	79785.357	0.05		0.101		
10	2	8	10	1	9	59779.072	0.05		0.016		
10	2	9	10	1	10	82241.252	0.05		0.133		
11	2	9	11	1	10	58855.583	0.05		-0.050		
11	2	10	11	1	11	84952.027	0.05		0.034		
12	2	10	12	1	11	58153.496	0.05		-0.060		
12	2	11	12	1	12	87917.771	0.05		0.054		
13	2	11	13	1	12	57729.017	0.05		-0.070		
13	2	12	13	1	13	91137.133	0.05		0.094		
14	2	12	14	1	13	57633.828	0.05		-0.094		
14	2	13	14	1	14	94607.607	0.05		0.141		
15	2	13	15	1	14	57914.501	0.05		-0.144		
15	2	14	15	1	15	98325.298	0.05		0.144		
16	2	14	16	1	15	58612.712	0.05		-0.062		
16	2	15	16	1	16	102284.933	0.05		0.086		
45	2	43	45	1	44	242126.519	0.20		-0.644		
9	3	6	9	2	7	113177.296	0.05	*	0.472		
9	3	7	9	2	8	115482.996	0.05	*	0.427		
10	3	7	10	2	8	112415.130	0.05	*	0.629		
10	3	8	10	2	9	115810.405	0.05		-0.234		
11	3	8	11	2	9	111442.733	0.05	*	0.520		
11	3	9	11	2	10	116239.559	0.05		-0.037		
12	3	9	12	2	10	110246.691	0.05	*	0.260		
13	3	10	13	2	11	108824.190	0.05		0.175		
13	3	11	13	2	12	117465.076	0.05	*	0.278		
14	3	11	14	2	12	107183.991	0.05		0.091		
14	3	12	14	2	13	118293.859	0.05	*	0.562		
15	3	12	15	2	13	105347.912	0.05		0.068		
15	3	13	15	2	14	119286.690	0.05		0.047		
16	3	13	16	2	14	103350.247	0.05		0.019		
16	3	14	16	2	15	120459.646	0.05		-0.047		
12	4	9	12	3	10	160457.770	0.05		-0.058		
13	4	10	13	3	11	160405.953	0.05	*	-0.603		
14	4	11	14	3	12	160357.535	0.05	*	-0.850		
15	4	12	15	3	13	160317.909	0.05	*	-1.560		
16	4	13	16	3	14	160296.591	0.05	*	-0.935		

Tabla A4. Los parámetros de la cabecera de las columnas para las medida de las transiciones de CH_3CH_2CN ν_{20} es la siguiente: Col. 1-3 y 4-6 se corresponde con los números cuánticos del nivel superior e inferior respectivamente. Col. 7 y 8 es la frecuencia observada y el error en la frecuencia, respectivamente. Col. 9 indica con un $*$ aquellas líneas no ajustadas. Col. 10 se corresponde con la diferencia entre las frecuencias observada y calculada. Col. 11 indica con [Yes] si existe solapamiento con otra especie molecular. Col. 12 muestra el pico de frecuencia media ponderada

Tabla A.5: Measured transitions of ν_{12} of ethyl cyanide.

J'	K'_a	K'_c	J"	K''_a	K''_c	ν(Hz)	e$_\nu$(Hz)	f$_\nu$(Hz)	O-C(Hz)	Blend	f$_{Peak}$(Hz)
2	0	2	1	0	1	17864.600	0.05		-0.002		
4	0	4	3	0	3	35670.530	0.05		0.008		
5	0	5	4	0	4	44533.415	0.05		-0.032		
6	0	6	5	0	5	53360.500	0.05		-0.108		
7	0	7	6	0	6	62145.961	0.05		-0.045		
8	0	8	7	0	7	70884.747	0.05		-0.022		
9	0	9	8	0	8	79573.643	0.05		0.009		
10	0	10	9	0	9	88211.405	0.05		0.014		
11	0	11	10	0	10	96799.224	0.05		0.052		
12	0	12	11	0	11	105340.472	0.05		-0.003		
13	0	13	12	0	12	113840.205	0.05	*	-0.646		
14	0	14	13	0	13	122307.260	0.05		-0.031		
15	0	15	14	0	14	130747.370	0.05		-0.061		
16	0	16	15	0	15	139168.740	0.05		-0.016		
17	0	17	16	0	16	147578.040	0.05		0.073		
18	0	18	17	0	17	155980.540	0.05		-0.039		
19	0	19	18	0	18	164380.830	0.05		0.040		
20	0	20	19	0	19	172781.540	0.05		0.001		
21	0	21	20	0	20	181184.626	0.05		-0.057		
22	0	22	21	0	21	189591.210	0.05		-0.025		
24	0	24	23	0	23	206415.694	0.05		-0.025		
25	0	25	24	0	24	214833.350	0.20		0.013		
26	0	26	25	0	25	223253.988	0.20		-0.023		
27	0	27	26	0	26	231677.220	0.20		-0.020		
28	0	28	27	0	27	240102.494	0.20		-0.018		
29	0	29	28	0	28	248529.317	0.20		-0.019		
30	0	30	29	0	29	256957.240	0.20		-0.018		
31	0	31	30	0	30	265385.866	0.20		-0.001		
32	0	32	31	0	31	273814.760	0.05		-0.042		
33	0	33	32	0	32	282243.700	0.05		-0.047		
34	0	34	33	0	33	290672.400	0.05		-0.029		
35	0	35	34	0	34	299100.620	0.05		0.007		
36	0	36	35	0	35	307528.050	0.05		-0.046		
37	0	37	36	0	36	315954.680	0.05		-0.026		
38	0	38	37	0	37	324380.260	0.05		-0.031		
39	0	39	38	0	38	332804.704	0.05		-0.019		
41	0	41	40	0	40	349649.700	0.05		0.011		
42	0	42	41	0	41	358070.040	0.05		0.005		
47	0	47	46	0	46	400147.522	0.05		0.056		
48	0	48	47	0	47	408557.567	0.05		-0.102		
51	0	51	50	0	50	433776.677	0.05		0.156	Yes	433776.521
52	0	52	51	0	51	442178.993	0.05		0.021	Yes	442178.971
53	0	53	52	0	52	450579.248	0.05		-0.098	Yes	450579.346
54	0	54	53	0	53	458977.589	0.05		-0.016	Yes	458977.604
55	0	55	54	0	54	467373.687	0.05		-0.022	Yes	467373.709
56	0	56	55	0	55	475767.684	0.05		0.064	Yes	475767.620
57	0	57	56	0	56	484159.357	0.05		0.058	Yes	484159.299

Tabla A.5: continued.

J'	K'_a	K'_c	J"	K''_a	K''_c	ν(Hz)	e$_\nu$(Hz)	f$_\nu$(Hz)	O-C(Hz)	Blend	f$_{peak}$(Hz)
58	0	58	57	0	57	492548.695	0.05		-0.013	Yes	492548.708
59	0	59	58	0	58	500935.738	0.05		-0.070	Yes	500935.808
60	0	60	59	0	59	509320.546	0.05		-0.015	Yes	509320.561
61	0	61	60	0	60	517702.903	0.05		-0.026	Yes	517702.929
62	0	62	61	0	61	526082.858	0.05		-0.016	Yes	526082.874
63	0	63	62	0	62	534460.338	0.05		-0.021	Yes	534460.359
64	0	64	63	0	63	542835.317	0.05		-0.029	Yes	542835.346
65	0	65	64	0	64	551207.708	0.05		-0.089	Yes	551207.797
66	0	66	65	0	65	559577.635	0.05		-0.041	Yes	559577.676
67	0	67	66	0	66	567944.903	0.05		-0.042	Yes	567944.945
68	0	68	67	0	67	576309.587	0.05		0.020	Yes	576309.567
69	0	69	68	0	68	584671.447	0.05		-0.059	Yes	584671.506
70	0	70	69	0	69	593030.669	0.05		-0.055	Yes	593030.724
71	0	71	70	0	70	601387.042	0.05		-0.144	Yes	601387.186
2	1	1	1	1	0	18350.740	0.05		-0.039		
2	1	2	1	1	1	17393.370	0.05		0.002		
3	1	2	2	1	1	27521.430	0.05		0.065		
3	1	3	2	1	2	26085.360	0.05		-0.038		
4	1	3	3	1	2	36686.140	0.05		0.049		
4	1	4	3	1	3	34772.025	0.05		0.082		
6	1	5	5	1	4	54989.370	0.05		-0.002		
6	1	6	5	1	5	52122.220	0.05		0.174		
7	1	6	6	1	5	64123.120	0.05		-0.133		
7	1	7	6	1	6	60782.560	0.05		-0.149		
8	1	7	7	1	6	73241.870	0.05		0.020		
8	1	8	7	1	7	69432.030	0.05		-0.120		
9	1	8	8	1	7	82342.255	0.05		-0.035		
9	1	9	8	1	8	78069.310	0.05		-0.096		
10	1	9	9	1	8	91421.395	0.05		-0.029		
10	1	10	9	1	9	86693.690	0.05		-0.054		
11	1	10	10	1	9	100475.874	0.05		0.055		
11	1	11	10	1	10	95304.700	0.05		0.036		
12	1	11	11	1	10	109501.744	0.05		-0.001		
12	1	12	11	1	11	103901.874	0.05		-0.028		
13	1	12	12	1	11	118495.280	0.05		0.079		
13	1	13	12	1	12	112485.464	0.05		0.041		
14	1	13	13	1	12	127451.880	0.05		-0.089		
14	1	14	13	1	13	121055.329	0.05		-0.078		
15	1	14	14	1	13	136367.640	0.05		-0.071		
15	1	15	14	1	14	129612.200	0.05		-0.024		
16	1	15	15	1	14	145238.140	0.05		0.007		
16	1	16	15	1	15	138156.370	0.05		-0.039		
17	1	16	16	1	15	154059.170	0.05		-0.042		
17	1	17	16	1	16	146688.830	0.05		0.201		
18	1	17	17	1	16	162827.510	0.05		0.021		
18	1	18	17	1	17	155209.630	0.05		-0.022		
19	1	18	18	1	17	171540.370	0.05		-0.053		
19	1	19	18	1	18	163720.300	0.05		-0.009		

Tabla A.5: continued.

J'	K'_a	K'_c	J"	K''_a	K''_c	ν(Hz)	e$_\nu$(Hz)	f$_\nu$(Hz)	O-C(Hz)	Blend	f$_{Peak}$(Hz)
20	1	19	19	1	18	180196.783	0.05		0.027		
20	1	20	19	1	19	172221.400	0.05		-0.066		
21	1	20	20	1	19	188796.848	0.05		0.004		
21	1	21	20	1	20	180713.974	0.05		-0.020		
22	1	21	21	1	20	197342.831	0.05		-0.049		
22	1	22	21	1	21	189198.692	0.05		-0.052		
23	1	22	22	1	21	205838.918	0.05		-0.014		
24	1	23	23	1	22	214290.747	0.20		-0.013		
24	1	24	23	1	23	206148.079	0.05		-0.026		
25	1	24	24	1	23	222705.404	0.20		-0.003		
25	1	25	24	1	24	214614.146	0.20		-0.023		
26	1	25	25	1	24	231090.633	0.20		-0.001		
26	1	26	25	1	25	223075.350	0.20		0.005		
27	1	26	26	1	25	239454.291	0.20		0.010		
27	1	27	26	1	26	231532.173	0.20		-0.014		
28	1	27	27	1	26	247803.708	0.20		0.014		
28	1	28	27	1	27	239985.159	0.20		-0.020		
29	1	28	28	1	27	256145.293	0.05		0.022		
29	1	29	28	1	28	248434.712	0.20		-0.022		
30	1	29	29	1	28	264484.230	0.20		0.011		
30	1	30	29	1	29	256881.195	0.05		-0.011		
31	1	30	30	1	29	272824.500	0.05		0.034		
31	1	31	30	1	30	265324.871	0.20		-0.019		
32	1	31	31	1	30	281168.780	0.05		0.038		
32	1	32	31	1	31	273765.980	0.05		-0.048		
33	1	32	32	1	31	289518.760	0.05		0.031		
33	1	33	32	1	32	282204.780	0.05		-0.040		
34	1	33	33	1	32	297875.270	0.05		-0.006		
34	1	34	33	1	33	290641.410	0.05		-0.012		
35	1	34	34	1	33	306238.670	0.05		0.069		
35	1	35	34	1	34	299075.910	0.05		-0.050		
36	1	35	35	1	34	314608.530	0.05		0.049		
36	1	36	35	1	35	307508.530	0.05		0.002		
37	1	36	36	1	35	322984.420	0.05		0.011		
37	1	37	36	1	36	315939.070	0.05		-0.127		
38	1	37	37	1	36	331365.734	0.05		0.023		
38	1	38	37	1	37	324367.990	0.05		-0.027		
39	1	38	38	1	37	339751.651	0.05		0.012		
40	1	39	39	1	38	348141.450	0.05		0.024		
40	1	40	39	1	39	341220.210	0.05		-0.020		
40	1	40	39	1	39	341220.220	0.05		-0.010		
41	1	40	40	1	39	356534.370	0.05		0.037		
41	1	41	40	1	40	349643.500	0.05		-0.149		
41	1	41	40	1	40	349643.516	0.05		-0.132		
42	1	42	41	1	41	358065.280	0.05		0.003		
46	1	45	45	1	44	398523.685	0.05		0.031		
47	1	46	46	1	45	406922.970	0.05		0.011		
47	1	47	46	1	46	400145.964	0.05		-0.076		

Tabla A.5: continued.

J'	K'_a	K'_c	J"	K''_a	K''_c	ν(Hz)	e$_\nu$(Hz)	f$_\nu$(Hz)	O-C(Hz)	Blend	f$_{peak}$(Hz)
47	1	47	46	1	46	400145.964	0.05		-0.076		
48	1	47	47	1	46	415321.843	0.05		-0.005		
48	1	48	47	1	47	408556.695	0.05		0.144		
48	1	48	47	1	47	408556.696	0.05		0.145		
49	1	48	48	1	47	423720.075	0.05		0.041		
50	1	49	49	1	48	432117.267	0.05		-0.006		
51	1	51	50	1	50	433776.677	0.05		0.156	Yes	433776.521
52	1	51	51	1	50	448908.048	0.05		-0.039		
52	1	52	51	1	51	442178.993	0.05		0.021	Yes	442178.971
53	1	52	52	1	51	457301.347	0.05		0.029		
53	1	53	52	1	52	450579.248	0.05		-0.098	Yes	450579.346
54	1	53	53	1	52	465692.933	0.05		0.027		
54	1	54	53	1	53	458977.589	0.05		-0.016	Yes	458977.604
55	1	55	54	1	54	467373.687	0.05		-0.022	Yes	467373.709
56	1	55	55	1	54	482470.747	0.05		0.068		
56	1	56	55	1	55	475767.684	0.05		0.064	Yes	475767.620
57	1	56	56	1	55	490856.536	0.05		-0.123		
57	1	57	56	1	56	484159.357	0.05		0.058	Yes	484159.299
58	1	57	57	1	56	499240.694	0.05		0.109		
58	1	58	57	1	57	492548.695	0.05		-0.013	Yes	492548.708
59	1	58	58	1	57	507622.313	0.05		-0.066		
59	1	59	58	1	58	500935.738	0.05		-0.070	Yes	500935.808
60	1	59	59	1	58	516001.979	0.05		0.010		
60	1	60	59	1	59	509320.546	0.05		-0.015	Yes	509320.561
61	1	60	60	1	59	524379.343	0.05		0.052		
61	1	61	60	1	60	517702.903	0.05		-0.026	Yes	517702.929
62	1	61	61	1	60	532754.367	0.05		0.082		
62	1	62	61	1	61	526082.858	0.05		-0.016	Yes	526082.874
63	1	62	62	1	61	541127.003	0.05		0.112		
63	1	63	62	1	62	534460.338	0.05		-0.021	Yes	534460.359
64	1	63	63	1	62	549497.036	0.05		-0.024		
64	1	64	63	1	63	542835.317	0.05		-0.029	Yes	542835.346
65	1	64	64	1	63	557864.289	0.05		0.046	Yes	557864.243
65	1	65	64	1	64	551207.708	0.05		-0.089	Yes	551207.797
66	1	65	65	1	64	566229.332	0.05		-0.152	Yes	566229.484
66	1	66	65	1	65	559577.635	0.05		-0.041	Yes	559577.676
67	1	66	66	1	65	574592.186	0.05		0.067	Yes	574592.120
67	1	67	66	1	66	567944.903	0.05		-0.042	Yes	567944.945
68	1	67	67	1	66	582952.317	0.05		0.209	Yes	582952.108
68	1	68	67	1	67	576309.587	0.05		0.020	Yes	576309.567
69	1	69	68	1	68	584671.447	0.05		-0.059	Yes	584671.506
70	1	69	69	1	68	599664.076	0.05		0.091	Yes	599663.985
70	1	70	69	1	69	593030.669	0.05		-0.055	Yes	593030.724
71	1	71	70	1	70	601387.042	0.05		-0.144	Yes	601387.186
4	2	3	3	2	2	35739.020	0.05		-0.061		
5	2	3	4	2	2	44809.152	0.05		-0.038		
5	2	4	4	2	3	44664.238	0.05		0.014		
6	2	4	5	2	3	53835.700	0.05		0.073		

Tabla A.5: continued.

J'	K'_a	K'_c	J"	K''_a	K''_c	ν(Hz)	e$_\nu$(Hz)	f$_\nu$(Hz)	O-C(Hz)	Blend	f$_{peak}$(Hz)
6	2	5	5	2	4	53582.850	0.05		-0.109		
7	2	5	6	2	4	62895.690	0.05		0.009		
7	2	6	6	2	5	62493.980	0.05		-0.036		
8	2	6	7	2	5	71992.850	0.05		-0.004		
8	2	7	7	2	6	71395.960	0.05		-0.178		
9	2	7	8	2	6	81128.961	0.05		-0.064		
9	2	8	8	2	7	80288.123	0.05		0.043		
10	2	8	9	2	7	90304.007	0.05		0.007		
10	2	9	9	2	8	89168.642	0.05		0.016		
11	2	9	10	2	8	99515.086	0.05		-0.122		
11	2	10	10	2	9	98036.578	0.05		-0.007		
12	2	10	11	2	9	108757.634	0.05		-0.034		
12	2	11	11	2	10	106890.807	0.05		-0.002		
13	2	11	12	2	10	118024.280	0.05		-0.003		
13	2	12	12	2	11	115730.142	0.05		-0.061		
14	2	13	13	2	12	124553.700	0.05		-0.036		
15	2	13	14	2	12	136594.740	0.05		-0.023		
15	2	14	14	2	13	133360.480	0.05		0.023		
16	2	14	15	2	13	145879.980	0.05		0.051		
16	2	15	15	2	14	142149.580	0.05		0.073		
17	2	15	16	2	14	155153.190	0.05		-0.043		
17	2	16	16	2	15	150920.120	0.05		-0.021		
18	2	16	17	2	15	164407.010	0.05		0.029		
18	2	17	17	2	16	159671.613	0.05		-0.122		
19	2	18	18	2	17	168403.770	0.05		-0.037		
20	2	18	19	2	17	182830.478	0.05		-0.070		
20	2	19	19	2	18	177115.968	0.05		-0.059		
21	2	19	20	2	18	191990.113	0.05		-0.020		
21	2	20	20	2	19	185808.194	0.05		-0.031		
22	2	20	21	2	19	201109.222	0.05		-0.039		
22	2	21	21	2	20	194480.422	0.05		0.019		
23	2	21	22	2	20	210184.194	0.05		-0.033		
23	2	22	22	2	21	203132.731	0.05		0.003		
24	2	22	23	2	21	219211.519	0.20		-0.032		
24	2	23	23	2	22	211765.533	0.05		-0.005		
25	2	23	24	2	22	228187.866	0.20		-0.022		
25	2	24	24	2	23	220379.337	0.20		0.007		
26	2	24	25	2	23	237110.011	0.20		-0.013		
26	2	25	25	2	24	228974.766	0.20		0.016		
27	2	25	26	2	24	245974.930	0.05		-0.026		
27	2	26	26	2	25	237552.581	0.20		0.010		
28	2	26	27	2	25	254780.032	0.05		-0.016		
28	2	27	27	2	26	246113.697	0.20		0.016		
29	2	27	28	2	26	263523.254	0.20		-0.013		
29	2	28	28	2	27	254659.061	0.20		0.010		
30	2	28	29	2	27	272203.430	0.05		-0.030		
30	2	29	29	2	28	263189.690	0.05		-0.027		
31	2	29	30	2	28	280820.531	0.05		-0.116		

Tabla A.5: continued.

J'	K'_a	K'_c	J"	K''_a	K''_c	ν(Hz)	e$_\nu$(Hz)	f$_\nu$(Hz)	O-C(Hz)	Blend	f$_{peak}$(Hz)
31	2	30	30	2	29	271706.790	0.05		0.041		
32	2	30	31	2	29	289376.270	0.05		-0.014		
32	2	31	31	2	30	280211.270	0.05		0.039		
33	2	31	32	2	30	297873.510	0.05		0.072		
33	2	32	32	2	31	288704.210	0.05		-0.027		
34	2	32	33	2	31	306316.842	0.05		0.026		
34	2	33	33	2	32	297186.830	0.05		0.021		
35	2	33	34	2	32	314712.485	0.05		-0.130		
35	2	34	34	2	33	305659.919	0.05		-0.027		
36	2	34	35	2	33	323068.223	0.05		0.019		
36	2	35	35	2	34	314124.660	0.05		0.076		
37	2	35	36	2	34	331391.648	0.05		0.004		
37	2	36	36	2	35	322581.620	0.05		0.031		
38	2	36	37	2	35	339691.087	0.05		-0.068		
39	2	37	38	2	36	347974.578	0.05		-0.001		
39	2	38	38	2	37	339475.870	0.05		0.074		
40	2	38	39	2	37	356248.990	0.05		0.038		
40	2	39	39	2	38	347914.350	0.05		0.004		
41	2	40	40	2	39	356348.000	0.05		0.035		
45	2	43	44	2	42	397649.403	0.05		0.014		
46	2	44	45	2	43	405952.081	0.05		-0.042		
46	2	45	45	2	44	398456.819	0.05		0.018		
47	2	45	46	2	44	414263.883	0.05		-0.060		
47	2	46	46	2	45	406868.867	0.05		0.034		
48	2	46	47	2	45	422584.375	0.05		-0.027		
48	2	47	47	2	46	415278.078	0.05		-0.022		
49	2	47	48	2	46	430912.829	0.05		0.038		
49	2	48	48	2	47	423684.783	0.05		0.051		
50	2	48	49	2	47	439248.220	0.05		-0.027		
50	2	49	49	2	48	432088.831	0.05		0.004		
51	2	49	50	2	48	447589.811	0.05		-0.030		
51	2	50	50	2	49	440490.583	0.05		0.121		
52	2	50	51	2	49	455936.622	0.05		-0.013		
53	2	52	52	2	51	457286.501	0.05		-0.049		
54	2	52	53	2	51	472642.218	0.05		-0.041		
54	2	53	53	2	52	465681.223	0.05		0.159		
55	2	53	54	2	52	480999.474	0.05		0.013		
55	2	54	54	2	53	474073.271	0.05		0.027		
56	2	54	55	2	53	489358.519	0.05		-0.105		
56	2	55	55	2	54	482463.127	0.05		0.039		
57	2	55	56	2	54	497718.986	0.05		-0.136		
57	2	56	56	2	55	490850.619	0.05		0.029		
58	2	56	57	2	55	506080.333	0.05		-0.063		
58	2	57	57	2	56	499235.759	0.05		0.022		
59	2	57	58	2	56	514441.916	0.05		-0.044		
59	2	58	58	2	57	507618.543	0.05		0.034		
60	2	58	59	2	57	522803.371	0.05		-0.014		
60	2	59	59	2	58	515998.950	0.05		0.067		

Tabla A.5: continued.

J'	K'_a	K'_c	J"	K''_a	K''_c	ν(Hz)	e$_\nu$(Hz)	f$_\nu$(Hz)	O-C(Hz)	Blend	f$_{Peak}$(Hz)
61	2	59	60	2	58	531164.260	0.05		-0.038		
61	2	60	60	2	59	524376.835	0.05		0.004		
62	2	60	61	2	59	539524.322	0.05		-0.055		
62	2	61	61	2	60	532752.284	0.05		-0.040		
63	2	61	62	2	60	547883.310	0.05		-0.030		
63	2	62	62	2	61	541125.257	0.05		-0.073		
64	2	62	63	2	61	556240.924	0.05		-0.016		
64	2	63	63	2	62	549496.016	0.05		0.199		
65	2	63	64	2	62	564596.857	0.05		-0.107		
65	2	64	64	2	63	557864.289	0.05		0.046	Yes	557864.243
66	2	65	65	2	64	566229.332	0.05		-0.152	Yes	566229.484
67	2	66	66	2	65	574592.186	0.05		0.067	Yes	574592.120
68	2	66	67	2	65	589653.865	0.05		0.032		
68	2	67	67	2	66	582952.317	0.05		0.209	Yes	582952.108
69	2	67	68	2	66	598001.983	0.05		0.079		
70	2	69	69	2	68	599664.076	0.05		0.091	Yes	599663.985
6	3	4	5	3	3	53656.922	0.05	*	0.260		
7	3	4	6	3	3	62618.676	0.05		-0.075		
7	3	5	6	3	4	62610.159	0.05		0.091		
8	3	5	7	3	4	71584.666	0.05		-0.120		
8	3	6	7	3	5	71567.490	0.05		0.038		
9	3	6	8	3	5	80560.359	0.05		-0.088		
9	3	7	8	3	6	80528.819	0.05		0.070		
10	3	7	9	3	6	89547.745	0.05		-0.074		
10	3	8	9	3	7	89493.703	0.05		0.034		
11	3	8	10	3	7	98549.238	0.05		-0.042		
11	3	9	10	3	8	98461.714	0.05		0.026		
12	3	9	11	3	8	107567.469	0.05		-0.033		
12	3	10	11	3	9	107432.075	0.05		0.023		
13	3	10	12	3	9	116605.752	0.05	*	0.324		
13	3	11	12	3	10	116403.809	0.05		0.028		
14	3	12	13	3	11	125375.722	0.05		0.033		
15	3	12	14	3	11	134753.141	0.05		0.000		
15	3	13	14	3	12	134346.367	0.05		-0.035		
16	3	13	15	3	12	143869.389	0.05		-0.036		
16	3	14	15	3	13	143314.437	0.05		0.044		
17	3	14	16	3	13	153018.017	0.05		0.009		
17	3	15	16	3	14	152277.861	0.05		-0.152		
18	3	15	17	3	14	162201.270	0.05		0.021		
18	3	16	17	3	15	161235.519	0.05		-0.008		
19	3	17	18	3	16	170185.184	0.05		0.030		
20	3	17	19	3	16	180676.070	0.05		0.002		
20	3	18	19	3	17	179125.070	0.05		-0.034		
21	3	18	20	3	17	189966.192	0.05		-0.009		
21	3	19	20	3	18	188054.844	0.05	*	1.236		
22	3	20	21	3	19	196968.937	0.05		-0.019		
23	3	20	22	3	19	208634.657	0.05		-0.020		
23	3	21	22	3	20	205869.525	0.05		0.004		

Tabla A.5: continued.

J'	K'_a	K'_c	J"	K''_a	K''_c	ν(Hz)	e$_\nu$(Hz)	f$_\nu$(Hz)	O-C(Hz)	Blend	f$_{peak}$(Hz)
24	3	21	23	3	20	218000.469	0.20		-0.024		
24	3	22	23	3	21	214753.826	0.20		0.042		
25	3	22	24	3	21	227376.435	0.20		-0.015		
25	3	23	24	3	22	223620.370	0.20		0.017		
26	3	23	25	3	22	236753.157	0.20		-0.030		
26	3	24	25	3	23	232467.987	0.20		0.006		
27	3	24	26	3	23	246121.109	0.20		-0.021		
27	3	25	26	3	24	241295.579	0.05		-0.001		
28	3	25	27	3	24	255471.003	0.20		-0.040		
28	3	26	27	3	25	250102.188	0.05		-0.042		
29	3	26	28	3	25	264794.429	0.20		-0.031		
29	3	27	28	3	26	258887.150	0.05		-0.040		
30	3	27	29	3	26	274083.870	0.05		-0.050		
30	3	28	29	3	27	267649.905	0.20		0.006		
31	3	28	30	3	27	283332.846	0.05		-0.183		
31	3	29	30	3	28	276389.960	0.05		-0.026		
32	3	29	31	3	28	292536.219	0.05		-0.163		
32	3	30	31	3	29	285107.300	0.05		0.034		
33	3	30	32	3	29	301689.360	0.05		-0.056		
33	3	31	32	3	30	293801.730	0.05		-0.010		
34	3	31	33	3	30	310788.073	0.05		-0.143		
34	3	32	33	3	31	302473.507	0.05		-0.086		
35	3	32	34	3	31	319829.370	0.05		0.009		
35	3	33	34	3	32	311123.069	0.05		-0.110		
36	3	33	35	3	32	328809.772	0.05		-0.037		
36	3	34	35	3	33	319751.020	0.05		-0.001		
37	3	34	36	3	33	337726.770	0.05		-0.084		
37	3	35	36	3	34	328357.810	0.05		0.022		
38	3	35	37	3	34	346578.105	0.05		-0.053		
38	3	36	37	3	35	336944.280	0.05		-0.003		
39	3	36	38	3	35	355361.850	0.05		-0.013		
39	3	37	38	3	36	345511.370	0.05		-0.051		
40	3	38	39	3	37	354060.230	0.05		0.022		
44	3	41	43	3	40	398259.513	0.05		0.044		
45	3	42	44	3	41	406650.307	0.05		0.050		
45	3	43	44	3	42	396567.596	0.05		-0.070		
46	3	43	45	3	42	414989.878	0.05		0.038		
46	3	44	45	3	43	405029.769	0.05		-0.009		
47	3	44	46	3	43	423285.840	0.05		0.079		
47	3	45	46	3	44	413481.260	0.05		-0.032		
48	3	45	47	3	44	431546.191	0.05		-0.087		
48	3	46	47	3	45	421923.220	0.05		0.027		
49	3	47	48	3	46	430356.330	0.05		-0.064		
50	3	48	49	3	47	438781.742	0.05		0.008		
51	3	48	50	3	47	456198.635	0.05		-0.045		
51	3	49	50	3	48	447199.961	0.05		-0.014		
52	3	49	51	3	48	464398.046	0.05		0.046		
52	3	50	51	3	49	455611.781	0.05		-0.019		

Tabla A.5: continued.

J'	K'_a	K'_c	J"	K''_a	K''_c	ν(Hz)	e$_\nu$(Hz)	f$_\nu$(Hz)	O-C(Hz)	Blend	f$_{Peak}$(Hz)
53	3	50	52	3	49	472598.193	0.05		0.023		
53	3	51	52	3	50	464017.762	0.05		-0.054		
54	3	51	53	3	50	480803.284	0.05		-0.039		
54	3	52	53	3	51	472418.512	0.05		-0.044		
55	3	52	54	3	51	489016.384	0.05		-0.009		
55	3	53	54	3	52	480814.445	0.05		-0.040		
56	3	53	55	3	52	497239.147	0.05		-0.108		
56	3	54	55	3	53	489205.949	0.05		-0.051		
57	3	54	56	3	53	505472.845	0.05		-0.044		
57	3	55	56	3	54	497593.350	0.05		-0.091		
58	3	55	57	3	54	513717.571	0.05		0.002		
58	3	55	57	3	54	513717.863	0.05	*	0.294		
59	3	56	58	3	55	521972.917	0.05		-0.124		
59	3	57	58	3	56	514357.192	0.05		-0.005		
60	3	57	59	3	56	530238.618	0.05		-0.065		
60	3	58	59	3	57	522733.913	0.05		-0.032		
61	3	59	60	3	58	531107.437	0.05		-0.060		
62	3	60	61	3	59	539477.640	0.05	*	-0.339		
63	3	60	62	3	59	555087.359	0.05		-0.071		
63	3	61	62	3	60	547845.424	0.05		-0.064		
64	3	61	63	3	60	563384.174	0.05		0.006		
64	3	62	63	3	61	556210.017	0.05		-0.081		
65	3	62	64	3	61	571686.039	0.05		-0.058		
65	3	63	64	3	62	564571.969	0.05		0.105		
66	3	63	65	3	62	579992.198	0.05		-0.063		
66	3	64	65	3	63	572930.916	0.05		0.096		
67	3	65	66	3	64	581286.972	0.05		-0.018		
68	3	66	67	3	65	589640.440	0.05		0.057		
69	3	67	68	3	66	597991.049	0.05		0.050		
6	4	3	5	4	2	53647.530	0.05		0.168		
7	4	4	6	4	3	62594.861	0.05		0.036		
8	4	5	7	4	4	71545.264	0.05		0.124		
9	4	5	8	4	4	80498.925	0.05		-0.190		
11	4	7	10	4	6	98418.587	0.05		-0.143		
11	4	8	10	4	7	98417.019	0.05		0.144		
12	4	8	11	4	7	107385.550	0.05		-0.060		
12	4	9	11	4	8	107382.377	0.05		0.237		
13	4	9	12	4	8	116358.000	0.05		-0.010		
13	4	10	12	4	9	116351.906	0.05		0.047		
14	4	11	13	4	10	125326.057	0.05		-0.156		
15	4	11	14	4	10	134322.250	0.05		-0.032		
15	4	12	14	4	11	134305.324	0.05		0.020		
16	4	12	15	4	11	143315.951	0.05		0.057		
16	4	13	15	4	12	143289.143	0.05		-0.003		
17	4	13	16	4	12	152318.560	0.05		0.007		
17	4	14	16	4	13	152277.861	0.05		0.216		
19	4	15	18	4	14	170356.248	0.05		-0.019		
20	4	16	19	4	15	179394.447	0.05		-0.030		

Tabla A.5: continued.

J'	K'_a	K'_c	J"	K''_a	K''_c	ν(Hz)	e$_\nu$(Hz)	f$_\nu$(Hz)	O-C(Hz)	Blend	f$_{peak}$(Hz)
20	4	17	19	4	16	179268.261	0.05		0.030		
21	4	17	20	4	16	188448.088	0.05		0.008		
21	4	18	20	4	17	188271.717	0.05		-0.062		
22	4	18	21	4	17	197519.632	0.05	*	0.388		
22	4	19	21	4	18	197277.520	0.05		0.084		
23	4	19	22	4	18	206610.374	0.05		0.008		
23	4	20	22	4	19	206284.252	0.05		0.036		
24	4	20	23	4	19	215724.053	0.20		0.020		
24	4	21	23	4	20	215291.083	0.20		0.113		
25	4	21	24	4	20	224862.991	0.20		0.041		
25	4	22	24	4	21	224296.423	0.20		0.023		
26	4	22	25	4	21	234029.836	0.20		0.007		
26	4	23	25	4	22	233299.109	0.20		0.041		
27	4	23	26	4	22	243227.242	0.20		0.022		
27	4	24	26	4	23	242297.477	0.20		0.065		
28	4	24	27	4	23	252457.301	0.05		0.001		
29	4	25	28	4	24	261721.589	0.20		-0.009		
29	4	26	28	4	25	260274.486	0.20		0.029		
30	4	26	29	4	25	271020.572	0.05		-0.124		
31	4	27	30	4	26	280353.834	0.05		-0.079		
32	4	28	31	4	27	289718.880	0.05		-0.158		
33	4	29	32	4	28	299112.031	0.05		-0.108		
33	4	30	32	4	29	296100.825	0.05		-0.106		
34	4	30	33	4	29	308527.366	0.05		-0.170		
34	4	31	33	4	30	305020.692	0.05		-0.210		
35	4	31	34	4	30	317957.760	0.05		-0.163		
35	4	32	34	4	31	313922.937	0.05		-0.085		
36	4	32	35	4	31	327394.657	0.05		-0.039		
37	4	33	36	4	32	336828.369	0.05		-0.039		
37	4	34	36	4	33	331668.224	0.05		0.000		
38	4	34	37	4	33	346249.275	0.05		-0.023		
39	4	35	38	4	34	355647.777	0.05		-0.026		
39	4	36	38	4	35	349327.082	0.05		0.013		
40	4	37	39	4	36	358121.910	0.05		0.038		
45	4	41	44	4	40	411136.806	0.05		-0.015		
45	4	42	44	4	41	401732.237	0.05		-0.029		
46	4	42	45	4	41	420182.958	0.05		0.046		
46	4	43	45	4	42	410381.437	0.05		-0.049		
47	4	43	46	4	42	429161.333	0.05		0.026		
47	4	44	46	4	43	419007.159	0.05		-0.037		
48	4	44	47	4	43	438069.609	0.05		0.034		
48	4	45	47	4	44	427610.047	0.05		0.002		
49	4	45	48	4	44	446905.789	0.05		0.014		
49	4	46	48	4	45	436190.764	0.05		-0.053		
50	4	46	49	4	45	455668.506	0.05		-0.007		
50	4	47	49	4	46	444750.343	0.05		-0.064		
51	4	47	50	4	46	464357.120	0.05		0.046		
51	4	48	50	4	47	453289.798	0.05		-0.009		

Tabla A.5: continued.

J'	K'_a	K'_c	J"	K''_a	K''_c	ν(Hz)	e$_\nu$(Hz)	f$_\nu$(Hz)	O-C(Hz)	Blend	f$_{peak}$(Hz)
52	4	48	51	4	47	472971.641	0.05		0.049		
52	4	49	51	4	48	461810.042	0.05		-0.043		
53	4	49	52	4	48	481513.247	0.05		0.010		
53	4	50	52	4	49	470312.108	0.05	*	-0.254		
54	4	50	53	4	49	489984.510	0.05		0.118		
54	4	51	53	4	50	478797.749	0.05		-0.041		
55	4	51	54	4	50	498388.833	0.05		0.053		
55	4	52	54	4	51	487267.443	0.05		-0.089		
56	4	52	55	4	51	506731.652	0.05		0.149		
56	4	53	55	4	52	495722.686	0.05		-0.063		
57	4	54	56	4	53	504164.554	0.05		-0.021		
58	4	54	57	4	53	523258.735	0.05		0.098		
58	4	55	57	4	54	512593.973	0.05		-0.132		
59	4	55	58	4	54	531458.844	0.05		0.056		
59	4	56	58	4	55	521012.343	0.05		-0.042		
60	4	56	59	4	55	539628.088	0.05		0.071		
60	4	57	59	4	56	529420.405	0.05		0.004		
61	4	57	60	4	56	547774.865	0.05		0.025		
61	4	58	60	4	57	537819.085	0.05		0.016		
62	4	59	61	4	58	546209.259	0.05		0.026		
63	4	59	62	4	58	564032.368	0.05		-0.110		
64	4	61	63	4	60	562966.962	0.05		-0.095		
65	4	61	64	4	60	580284.366	0.05		-0.002		
65	4	62	64	4	61	571335.917	0.05		-0.113		
66	4	62	65	4	61	588419.727	0.05		0.100		
66	4	63	65	4	62	579699.123	0.05		-0.010		
67	4	63	66	4	62	596564.923	0.05		0.043		
67	4	64	66	4	63	588056.843	0.05		-0.004		
68	4	64	67	4	63	604721.792	0.05		0.094		
68	4	65	67	4	64	596409.557	0.05		-0.031		
69	4	66	68	4	65	604757.745	0.05		0.031		
7	5	2	6	5	1	62590.699	0.05		0.138	Yes	62590.561
7	5	3	6	5	2	62590.699	0.05		0.138	Yes	62590.561
9	5	4	8	5	3	80484.650	0.05		0.007	Yes	80484.643
9	5	5	8	5	4	80484.650	0.05		0.007	Yes	80484.643
10	5	5	9	5	4	89434.690	0.05		0.016	Yes	89434.674
10	5	6	9	5	5	89434.690	0.05		0.016	Yes	89434.674
11	5	6	10	5	5	98387.005	0.05		0.002	Yes	98387.003
11	5	7	10	5	6	98387.005	0.05		0.002	Yes	98387.003
12	5	7	11	5	6	107341.894	0.05		0.034	Yes	107341.860
12	5	8	11	5	7	107341.894	0.05		0.034	Yes	107341.860
13	5	8	12	5	7	116299.553	0.05		0.079	Yes	116299.474
13	5	9	12	5	8	116299.553	0.05		0.079	Yes	116299.474
14	5	9	13	5	8	125260.176	0.05		0.100	Yes	125260.076
14	5	10	13	5	9	125260.176	0.05		0.100	Yes	125260.076
15	5	10	14	5	9	134223.913	0.05		0.015	Yes	134223.898
15	5	11	14	5	10	134223.913	0.05		0.015	Yes	134223.898
17	5	12	16	5	11	152162.707	0.05		0.004		

Tabla A.5: continued.

J'	K'_a	K'_c	J"	K''_a	K''_c	ν(Hz)	e$_\nu$(Hz)	f$_\nu$(Hz)	O-C(Hz)	Blend	f$_{peak}$(Hz)
17	5	13	16	5	12	152161.623	0.05		0.036		
18	5	13	17	5	12	161138.013	0.05		0.022		
18	5	14	17	5	13	161136.151	0.05		0.041		
19	5	14	18	5	13	170117.695	0.05		0.016		
19	5	15	18	5	14	170114.629	0.05		0.027		
20	5	15	19	5	14	179102.074	0.05		-0.046		
20	5	16	19	5	15	179097.295	0.05		0.075		
21	5	16	20	5	15	188091.766	0.05		0.056		
21	5	17	20	5	16	188084.144	0.05		0.048		
22	5	17	21	5	16	197086.928	0.05		0.027		
22	5	18	21	5	17	197075.309	0.05		-0.020		
23	5	18	22	5	17	206088.184	0.05		-0.030		
23	5	19	22	5	18	206071.086	0.05		0.109		
24	5	19	23	5	18	215096.292	0.20		0.044		
24	5	20	23	5	19	215071.113	0.20		0.066		
25	5	20	24	5	19	224111.755	0.20		0.047		
25	5	21	24	5	20	224075.550	0.20		0.065		
26	5	21	25	5	20	233135.459	0.20		0.046		
26	5	22	25	5	21	233084.217	0.20		0.050		
27	5	22	26	5	21	242168.365	0.20		0.046		
27	5	23	26	5	22	242096.938	0.20		0.053		
28	5	24	27	5	23	251113.384	0.05		0.047		
29	5	24	28	5	23	260266.432	0.05		0.065		
29	5	25	28	5	24	260133.177	0.20		0.063		
30	5	25	29	5	24	269334.258	0.05		-0.023		
30	5	26	29	5	25	269155.716	0.20		0.022		
31	5	26	30	5	25	278416.940	0.05		-0.032		
31	5	27	30	5	26	278180.456	0.05		0.030		
32	5	27	31	5	26	287516.394	0.05		0.055		
33	5	29	32	5	28	296233.080	0.05		-0.018		
34	5	29	33	5	28	305773.573	0.05		-0.105		
34	5	30	33	5	29	305258.958	0.05		-0.115		
35	5	31	34	5	30	314283.184	0.05		-0.090		
36	5	31	35	5	30	324125.006	0.05		0.085		
36	5	32	35	5	31	323304.363	0.05		-0.032		
37	5	32	36	5	31	333341.893	0.05		0.072		
37	5	33	36	5	32	332321.119	0.05		0.104		
38	5	33	37	5	32	342589.230	0.05		0.021		
38	5	34	37	5	33	341331.667	0.05		0.053		
39	5	34	38	5	33	351868.832	0.05		0.000		
39	5	35	38	5	34	350334.639	0.05		0.043		
44	5	39	43	5	38	398750.147	0.05		-0.041		
44	5	40	43	5	39	395176.589	0.05		0.005		
45	5	40	44	5	39	408204.808	0.05		0.009		
45	5	41	44	5	40	404098.777	0.05		0.002		
46	5	41	45	5	40	417672.269	0.05		0.019		
47	5	42	46	5	41	427144.131	0.05		0.107		
47	5	43	46	5	42	421884.687	0.05		-0.010		

Tabla A.5: continued.

J'	K'_a	K'_c	J"	K''_a	K''_c	ν(Hz)	e$_\nu$(Hz)	f$_\nu$(Hz)	O-C(Hz)	Blend	f$_{Peak}$(Hz)
48	5	43	47	5	42	436610.728	0.05		0.004		
48	5	44	47	5	43	430746.065	0.05		0.234		
49	5	44	48	5	43	446062.538	0.05		-0.007		
49	5	45	48	5	44	439584.399	0.05		0.152		
50	5	45	49	5	44	455489.694	0.05		-0.050		
51	5	46	50	5	45	464883.128	0.05		0.052		
51	5	47	50	5	46	457189.427	0.05		0.047		
52	5	47	51	5	46	474234.132	0.05		0.036		
52	5	48	51	5	47	465954.809	0.05		0.053		
53	5	48	52	5	47	483535.395	0.05		0.033		
53	5	49	52	5	48	474694.858	0.05		0.115		
54	5	49	53	5	48	492780.622	0.05		0.130		
54	5	50	53	5	49	483409.165	0.05		0.048		
55	5	50	54	5	49	501964.159	0.05		0.026		
55	5	51	54	5	50	492097.863	0.05		0.028		
56	5	52	55	5	51	500761.036	0.05		0.005		
57	5	52	56	5	51	520129.953	0.05		-0.086		
57	5	53	56	5	52	509399.034	0.05		0.031		
58	5	53	57	5	52	529105.539	0.05		-0.204		
58	5	54	57	5	53	518012.110	0.05		-0.100		
59	5	55	58	5	54	526601.233	0.05		-0.023		
60	5	55	59	5	54	546830.760	0.05		-0.209		
60	5	56	59	5	55	535166.847	0.05		-0.028		
61	5	56	60	5	55	555577.368	0.05		-0.203		
61	5	57	60	5	56	543709.817	0.05		-0.100		
62	5	57	61	5	56	564245.968	0.05		0.004		
63	5	58	62	5	57	572836.597	0.05		0.135		
64	5	59	63	5	58	581350.342	0.05		0.011		
64	5	60	63	5	59	569213.282	0.05		-0.170		
65	5	60	64	5	59	589790.119	0.05		0.191		
65	5	61	64	5	60	577676.443	0.05		0.069		
66	5	61	65	5	60	598158.860	0.05		0.037		
66	5	62	65	5	61	586122.026	0.05		-0.039		
67	5	63	66	5	62	594551.675	0.05		-0.006		
68	5	64	67	5	63	602966.359	0.05		-0.006		
10	6	4	9	6	3	89429.588	0.05		0.134	Yes	89429.454
10	6	5	9	6	4	89429.588	0.05		0.134	Yes	89429.454
11	6	5	10	6	4	98377.616	0.05		0.018	Yes	98377.598
11	6	6	10	6	5	98377.616	0.05		0.018	Yes	98377.598
13	6	7	12	6	6	116278.501	0.05		0.044	Yes	116278.457
13	6	8	12	6	7	116278.501	0.05		0.044	Yes	116278.457
14	6	8	13	6	7	125231.513	0.05		0.076	Yes	125231.437
14	6	9	13	6	8	125231.513	0.05		0.076	Yes	125231.437
15	6	9	14	6	8	134186.186	0.05		-0.108	Yes	134186.294
15	6	10	14	6	9	134186.186	0.05		-0.108	Yes	134186.294
16	6	10	15	6	9	143143.225	0.05		0.066	Yes	143143.159
16	6	11	15	6	10	143143.225	0.05		0.066	Yes	143143.159
17	6	11	16	6	10	152102.209	0.05		0.044	Yes	152102.165

Tabla A.5: continued.

J'	K'_a	K'_c	J"	K''_a	K''_c	ν(Hz)	e$_\nu$(Hz)	f$_\nu$(Hz)	O-C(Hz)	Blend	f$_{peak}$(Hz)
17	6	12	16	6	11	152102.209	0.05		0.044	Yes	152102.165
18	6	12	17	6	11	161063.483	0.05		0.037	Yes	161063.446
18	6	13	17	6	12	161063.483	0.05		0.037	Yes	161063.446
19	6	13	18	6	12	170027.214	0.05		0.079	Yes	170027.136
19	6	14	18	6	13	170027.214	0.05		0.079	Yes	170027.136
20	6	14	19	6	13	178993.436	0.05		0.067	Yes	178993.369
20	6	15	19	6	14	178993.436	0.05		0.067	Yes	178993.369
21	6	15	20	6	14	187962.348	0.05		0.066	Yes	187962.282
21	6	16	20	6	15	187962.348	0.05		0.066	Yes	187962.282
22	6	16	21	6	15	196934.081	0.05		0.066	Yes	196934.015
22	6	17	21	6	16	196934.081	0.05		0.066	Yes	196934.015
24	6	18	23	6	17	214887.002	0.20		0.067		
24	6	19	23	6	18	214886.158	0.20		0.079		
25	6	19	24	6	18	223868.287	0.20		0.057		
25	6	20	24	6	19	223866.965	0.20		0.077		
26	6	20	25	6	19	232853.121	0.20		0.068		
26	6	21	25	6	20	232851.068	0.20		0.083		
27	6	21	26	6	20	241841.643	0.05		0.033		
27	6	22	26	6	21	241838.539	0.05		0.060		
28	6	22	27	6	21	250834.195	0.20		0.064		
28	6	23	27	6	22	250829.556	0.20		0.085		
29	6	23	28	6	22	259830.927	0.05		0.048		
29	6	24	28	6	23	259824.106	0.20		0.059		
30	6	24	29	6	23	268832.154	0.20		0.005		
30	6	25	29	6	24	268822.263	0.05		-0.011		
31	6	25	30	6	24	277838.317	0.05		0.033		
31	6	26	30	6	25	277824.264	0.05		0.064		
32	6	26	31	6	25	286849.780	0.05		0.102		
32	6	27	31	6	26	286829.899	0.05		0.057		
33	6	28	32	6	27	295839.173	0.05		-0.012		
34	6	28	33	6	27	304890.072	0.05		-0.085		
34	6	29	33	6	28	304852.172	0.05		0.002		
35	6	29	34	6	28	313920.322	0.05		-0.081		
35	6	30	34	6	29	313868.549	0.05		-0.141		
36	6	30	35	6	29	322958.151	0.05		-0.110		
36	6	31	35	6	30	322888.518	0.05		-0.059		
37	6	32	36	6	31	331911.584	0.05		-0.015		
38	6	32	37	6	31	341060.445	0.05		0.092		
38	6	33	37	6	32	340937.451	0.05		0.006		
39	6	33	38	6	32	350126.942	0.05		0.225		
39	6	34	38	6	33	349965.842	0.05		0.126		
40	6	34	39	6	33	359204.967	0.05		-0.016		
40	6	35	39	6	34	358995.956	0.05		0.034		
44	6	38	43	6	37	395669.710	0.05		0.136		
44	6	39	43	6	38	395122.626	0.05		0.099		
45	6	39	44	6	38	404833.343	0.05		0.076		
45	6	40	44	6	39	404151.302	0.05		0.061		
46	6	40	45	6	39	414020.384	0.05		0.057		

Tabla A.5: continued.

J'	K'_a	K'_c	J"	K''_a	K''_c	ν(Hz)	e$_\nu$(Hz)	f$_\nu$(Hz)	O-C(Hz)	Blend	f$_{Peak}$(Hz)
47	6	41	46	6	40	423232.991	0.05		-0.030		
47	6	42	46	6	41	422197.324	0.05		-0.080		
48	6	42	47	6	41	432473.541	0.05		0.024		
49	6	43	48	6	42	441743.820	0.05		0.083		
50	6	44	49	6	43	451045.215	0.05		0.037		
50	6	45	49	6	44	449218.271	0.05		0.216		
51	6	46	50	6	45	458206.002	0.05		0.009		
52	6	47	51	6	46	467181.779	0.05		-0.040		
53	6	47	52	6	46	479140.723	0.05		0.008		
54	6	48	53	6	47	488565.695	0.05		0.073		
55	6	49	54	6	48	498015.189	0.05		0.158		
55	6	50	54	6	49	494020.656	0.05		0.002		
56	6	50	55	6	49	507483.472	0.05		-0.009		
56	6	51	55	6	50	502932.131	0.05		-0.094		
57	6	51	56	6	50	516964.051	0.05		0.002		
58	6	52	57	6	51	526448.562	0.05		0.003		
58	6	53	57	6	52	520694.769	0.05		0.036		
59	6	53	58	6	52	535927.871	0.05		-0.025		
59	6	54	58	6	53	529543.371	0.05		0.206		
60	6	54	59	6	53	545392.382	0.05		-0.027		
60	6	55	59	6	54	538368.291	0.05		0.035		
61	6	55	60	6	54	554832.273	0.05		-0.081		
61	6	56	60	6	55	547169.364	0.05	*	0.268		
62	6	56	61	6	55	564238.126	0.05		-0.174		
63	6	58	62	6	57	564695.178	0.05		0.033		
64	6	59	63	6	58	573419.389	0.05		0.052		
65	6	60	64	6	59	582117.112	0.05		-0.131		
10	7	3	9	7	2	89432.852	0.05		0.197	Yes	89432.655
10	7	4	9	7	3	89432.852	0.05		0.197	Yes	89432.655
11	7	4	10	7	3	98378.992	0.05		0.035	Yes	98378.957
11	7	5	10	7	4	98378.992	0.05		0.035	Yes	98378.957
12	7	5	11	7	4	107326.120	0.05		-0.001	Yes	107326.121
12	7	6	11	7	5	107326.120	0.05		-0.001	Yes	107326.121
13	7	6	12	7	5	116274.257	0.05		0.032	Yes	116274.225
13	7	7	12	7	6	116274.257	0.05		0.032	Yes	116274.225
14	7	7	13	7	6	125223.399	0.05		0.055	Yes	125223.344
14	7	8	13	7	7	125223.399	0.05		0.055	Yes	125223.344
15	7	8	14	7	7	134173.638	0.05		0.084	Yes	134173.554
15	7	9	14	7	8	134173.638	0.05		0.084	Yes	134173.554
16	7	9	15	7	8	143124.991	0.05		0.061	Yes	143124.930
16	7	10	15	7	9	143124.991	0.05		0.061	Yes	143124.930
17	7	10	16	7	9	152077.621	0.05		0.073	Yes	152077.548
17	7	11	16	7	10	152077.621	0.05		0.073	Yes	152077.548
18	7	11	17	7	10	161031.520	0.05		0.038	Yes	161031.482
18	7	12	17	7	11	161031.520	0.05		0.038	Yes	161031.482
19	7	12	18	7	11	169986.921	0.05		0.114	Yes	169986.807
19	7	13	18	7	12	169986.921	0.05		0.114	Yes	169986.807
20	7	13	19	7	12	178943.686	0.05		0.088	Yes	178943.598

Tabla A.5: continued.

J'	K'_a	K'_c	J"	K''_a	K''_c	ν(Hz)	e$_\nu$(Hz)	f$_\nu$(Hz)	O-C(Hz)	Blend	f$_{peak}$(Hz)
20	7	14	19	7	13	178943.686	0.05		0.088	Yes	178943.598
21	7	14	20	7	13	187902.021	0.05		0.091	Yes	187901.930
21	7	15	20	7	14	187902.021	0.05		0.091	Yes	187901.930
22	7	15	21	7	14	196861.982	0.05		0.105	Yes	196861.877
22	7	16	21	7	15	196861.982	0.05		0.105	Yes	196861.877
23	7	16	22	7	15	205823.579	0.05		0.064	Yes	205823.516
23	7	17	22	7	16	205823.579	0.05		0.064	Yes	205823.516
24	7	17	23	7	16	214787.029	0.05		0.109	Yes	214786.921
24	7	18	23	7	17	214787.029	0.05		0.109	Yes	214786.921
25	7	18	24	7	17	223752.247	0.05		0.078	Yes	223752.170
25	7	19	24	7	18	223752.247	0.05		0.078	Yes	223752.170
26	7	19	25	7	18	232719.422	0.05		0.083	Yes	232719.340
26	7	20	25	7	19	232719.422	0.05		0.083	Yes	232719.340
27	7	20	26	7	19	241688.581	0.05		0.071	Yes	241688.510
27	7	21	26	7	20	241688.581	0.05		0.071	Yes	241688.510
28	7	21	27	7	20	250659.845	0.05		0.085	Yes	250659.760
28	7	22	27	7	21	250659.845	0.05		0.085	Yes	250659.760
29	7	22	28	7	21	259633.251	0.05		0.078	Yes	259633.174
29	7	23	28	7	22	259633.251	0.05		0.078	Yes	259633.174
30	7	23	29	7	22	268608.938	0.05		-0.074	Yes	268609.011
30	7	23	29	7	22	268608.938	0.05		-0.074	Yes	268609.011
32	7	25	31	7	24	286567.282	0.05		0.033	Yes	286567.248
32	7	26	31	7	25	286567.282	0.05		0.033	Yes	286567.248
33	7	26	32	7	25	295550.367	0.05		0.182	Yes	295550.186
33	7	27	32	7	26	295550.367	0.05		0.182	Yes	295550.186
34	7	27	33	7	26	304536.708	0.05		0.074		
34	7	28	33	7	27	304534.914	0.05		0.068		
35	7	28	34	7	27	313525.379	0.05		0.070		
35	7	29	34	7	28	313522.728	0.05		0.011		
36	7	29	35	7	28	322517.026	0.05		0.054		
36	7	30	35	7	29	322513.066	0.05		-0.189		
37	7	30	36	7	29	331511.870	0.05		0.078		
38	7	32	37	7	31	340502.583	0.05		0.018		
39	7	33	38	7	32	349501.485	0.05		0.060		
45	7	39	44	7	38	403553.592	0.05		0.061		
46	7	39	45	7	38	412651.780	0.05		0.076		
46	7	40	45	7	39	412571.453	0.05		0.071		
47	7	40	46	7	39	421695.830	0.05		0.015		
47	7	41	46	7	40	421591.618	0.05		0.202		
48	7	41	47	7	40	430748.292	0.05		0.221		
48	7	42	47	7	41	430613.451	0.05		0.107		
50	7	43	49	7	42	448881.011	0.05		-0.120		
50	7	44	49	7	43	448661.551	0.05		0.185		
51	7	44	50	7	43	457964.406	0.05		0.046		
52	7	45	51	7	44	467060.556	0.05		-0.047		
52	7	46	51	7	45	466711.535	0.05		-0.059		
53	7	47	52	7	46	475735.806	0.05		-0.133		
55	7	48	54	7	47	494444.373	0.05		-0.008		

Tabla A.5: continued.

J'	K'_a	K'_c	J"	K''_a	K''_c	ν(Hz)	e$_\nu$(Hz)	f$_\nu$(Hz)	O-C(Hz)	Blend	f$_{Peak}$(Hz)
56	7	49	55	7	48	503610.470	0.05		0.103		
57	7	50	56	7	49	512798.978	0.05		0.150		
60	7	54	59	7	53	538804.763	0.05		0.032		
61	7	54	60	7	53	549817.169	0.05		0.110		
61	7	55	60	7	54	547785.884	0.05		0.149		
63	7	56	62	7	55	568503.884	0.05		-0.030		
63	7	57	62	7	56	565712.235	0.05		0.029		
64	7	57	63	7	56	577892.069	0.05		-0.087		
64	7	58	63	7	57	574654.666	0.05		-0.005		
65	7	58	64	7	57	587307.611	0.05		-0.179		
65	7	59	64	7	58	583581.347	0.05		0.054		
66	7	59	65	7	58	596746.998	0.05	*	-0.326		
66	7	60	65	7	59	592490.593	0.05		-0.014		
67	7	61	66	7	60	601381.143	0.05		-0.055		
11	8	3	10	8	2	98387.005	0.05		0.098	Yes	98386.907
11	8	4	10	8	3	98387.005	0.05		0.098	Yes	98386.907
12	8	4	11	8	3	107333.138	0.05		-0.001	Yes	107333.139
12	8	5	11	8	4	107333.138	0.05		-0.001	Yes	107333.139
13	8	5	12	8	4	116279.971	0.05		0.091	Yes	116279.880
13	8	6	12	8	5	116279.971	0.05		0.091	Yes	116279.880
14	8	6	13	8	5	125227.242	0.05		0.072	Yes	125227.170
14	8	7	13	8	6	125227.242	0.05		0.072	Yes	125227.170
15	8	7	14	8	6	134175.125	0.05		0.076	Yes	134175.049
15	8	8	14	8	7	134175.125	0.05		0.076	Yes	134175.049
16	8	8	15	8	7	143123.595	0.05		0.037	Yes	143123.558
16	8	9	15	8	8	143123.595	0.05		0.037	Yes	143123.558
17	8	9	16	8	8	152072.818	0.05		0.083	Yes	152072.735
17	8	10	16	8	9	152072.818	0.05		0.083	Yes	152072.735
18	8	10	17	8	9	161022.707	0.05		0.087	Yes	161022.620
18	8	11	17	8	10	161022.707	0.05		0.087	Yes	161022.620
19	8	11	18	8	10	169973.344	0.05		0.093	Yes	169973.251
19	8	12	18	8	11	169973.344	0.05		0.093	Yes	169973.251
20	8	12	19	8	11	178924.835	0.05		0.167	Yes	178924.668
20	8	13	19	8	12	178924.835	0.05		0.167	Yes	178924.668
21	8	13	20	8	12	187876.976	0.05		0.069	Yes	187876.907
21	8	14	20	8	13	187876.976	0.05		0.069	Yes	187876.907
22	8	14	21	8	13	196830.003	0.05		-0.004	Yes	196830.007
22	8	15	21	8	14	196830.003	0.05		-0.004	Yes	196830.007
23	8	15	22	8	14	205784.067	0.05		0.061	Yes	205784.006
23	8	16	22	8	15	205784.067	0.05		0.061	Yes	205784.006
24	8	16	23	8	15	214739.024	0.20		0.083	Yes	214738.941
24	8	17	23	8	16	214739.024	0.20		0.083	Yes	214738.941
25	8	17	24	8	16	223694.933	0.20		0.082	Yes	223694.850
25	8	18	24	8	17	223694.933	0.20		0.082	Yes	223694.850
26	8	18	25	8	17	232651.837	0.20		0.067	Yes	232651.771
26	8	19	25	8	18	232651.837	0.20		0.067	Yes	232651.771
27	8	19	26	8	18	241609.811	0.20		0.072	Yes	241609.740
27	8	20	26	8	19	241609.811	0.20		0.072	Yes	241609.740

Tabla A.5: continued.

J'	K'_a	K'_c	J"	K''_a	K''_c	ν(Hz)	e$_\nu$(Hz)	f$_\nu$(Hz)	O-C(Hz)	Blend	f$_{peak}$(Hz)
28	8	20	27	8	19	250568.864	0.20		0.068	Yes	250568.796
28	8	21	27	8	20	250568.864	0.20		0.068	Yes	250568.796
29	8	21	28	8	20	259529.046	0.20		0.069	Yes	259528.977
29	8	22	28	8	21	259529.046	0.20		0.069	Yes	259528.977
30	8	22	29	8	21	268490.379	0.20		0.058	Yes	268490.322
30	8	23	29	8	22	268490.379	0.20		0.058	Yes	268490.322
31	8	23	30	8	22	277452.901	0.05		0.032	Yes	277452.869
31	8	24	30	8	23	277452.901	0.05		0.032	Yes	277452.869
32	8	24	31	8	23	286416.697	0.05		0.038	Yes	286416.659
32	8	25	31	8	24	286416.697	0.05		0.038	Yes	286416.659
33	8	25	32	8	24	295381.706	0.05		-0.026	Yes	295381.733
33	8	26	32	8	25	295381.706	0.05		-0.026	Yes	295381.733
34	8	26	33	8	25	304348.181	0.05		0.049	Yes	304348.131
34	8	27	33	8	26	304348.181	0.05		0.049	Yes	304348.131
35	8	27	34	8	26	313315.945	0.05		0.046	Yes	313315.898
35	8	28	34	8	27	313315.945	0.05		0.046	Yes	313315.898
36	8	28	35	8	27	322285.115	0.05		0.037	Yes	322285.078
36	8	29	35	8	28	322285.115	0.05		0.037	Yes	322285.078
37	8	29	36	8	28	331255.744	0.05		0.025	Yes	331255.718
37	8	30	36	8	29	331255.744	0.05		0.025	Yes	331255.718
38	8	30	37	8	29	340227.913	0.05		-0.108		
38	8	31	37	8	30	340227.912	0.05		0.201		
39	8	31	38	8	30	349201.562	0.05		-0.238		
39	8	32	38	8	31	349201.561	0.05		0.215		
40	8	32	39	8	31	358176.969	0.05	*	-0.253		
40	8	33	39	8	32	358176.963	0.05	*	0.402		
45	8	37	44	8	36	403081.559	0.05		-0.076		
45	8	38	44	8	37	403077.948	0.05		0.022		
46	8	38	45	8	37	412068.549	0.05		-0.103		
46	8	39	45	8	38	412063.655	0.05		0.107		
47	8	39	46	8	38	421057.757	0.05		-0.242		
47	8	40	46	8	39	421050.995	0.05		-0.039		
48	8	40	47	8	39	430049.958	0.05		0.115		
51	8	43	50	8	42	457042.235	0.05		-0.138		
52	8	44	51	8	43	466046.477	0.05		0.074		
53	8	45	52	8	44	475054.408	0.05		0.177		
54	8	46	53	8	45	484066.462	0.05		0.202		
55	8	47	54	8	46	493082.804	0.05		-0.155		
55	8	48	54	8	47	493018.237	0.05		0.225		
56	8	48	55	8	47	502104.962	0.05		0.087		
58	8	51	57	8	50	520031.710	0.05		-0.136		
60	8	52	59	8	51	538258.993	0.05		0.095		
60	8	53	59	8	52	538044.835	0.05		-0.018		
61	8	53	60	8	52	547318.512	0.05		-0.002		
61	8	54	60	8	53	547051.588	0.05		0.223		
62	8	54	61	8	53	556388.931	0.05		0.103		
63	8	55	62	8	54	565471.048	0.05		-0.170		
63	8	56	62	8	55	565061.953	0.05		0.143		

Tabla A.5: continued.

J'	K'_a	K'_c	J"	K''_a	K''_c	ν(Hz)	e$_\nu$(Hz)	f$_\nu$(Hz)	O-C(Hz)	Blend	f$_{Peak}$(Hz)
64	8	57	63	8	56	574064.620	0.05		0.159		
65	8	57	64	8	56	583678.509	0.05		0.066		
65	8	58	64	8	57	583064.606	0.05		0.205		
66	8	58	65	8	57	592806.585	0.05		-0.142		
67	8	59	66	8	58	601953.539	0.05	*	-0.408		
11	9	2	10	9	1	98399.548	0.05		0.029	Yes	98399.519
11	9	3	10	9	2	98399.548	0.05		0.029	Yes	98399.519
12	9	3	11	9	2	107345.941	0.05		0.169	Yes	107345.772
12	9	4	11	9	3	107345.941	0.05		0.169	Yes	107345.772
13	9	4	12	9	3	116292.366	0.05		0.126	Yes	116292.240
13	9	5	12	9	4	116292.366	0.05		0.126	Yes	116292.240
14	9	5	13	9	4	125239.033	0.05		0.091	Yes	125238.942
14	9	6	13	9	5	125239.033	0.05		0.091	Yes	125238.942
15	9	6	14	9	5	134186.186	0.05	*	0.294	Yes	134185.892
15	9	7	14	9	6	134186.186	0.05	*	0.294	Yes	134185.892
16	9	7	15	9	6	143133.193	0.05		0.086	Yes	143133.107
16	9	8	15	9	7	143133.193	0.05		0.086	Yes	143133.107
17	9	8	16	9	7	152080.642	0.05		0.040	Yes	152080.602
17	9	9	16	9	8	152080.642	0.05		0.040	Yes	152080.602
18	9	9	17	9	8	161028.454	0.05		0.062	Yes	161028.392
18	9	10	17	9	9	161028.454	0.05		0.062	Yes	161028.392
19	9	10	18	9	9	169976.570	0.05		0.078	Yes	169976.492
19	9	11	18	9	10	169976.570	0.05		0.078	Yes	169976.492
20	9	11	19	9	10	178924.835	0.05		-0.082	Yes	178924.917
20	9	12	19	9	11	178924.835	0.05		-0.082	Yes	178924.917
21	9	12	20	9	11	187873.733	0.05		0.052	Yes	187873.681
21	9	13	20	9	12	187873.733	0.05		0.052	Yes	187873.681
22	9	13	21	9	12	196822.774	0.05		-0.024	Yes	196822.798
22	9	14	21	9	13	196822.774	0.05		-0.024	Yes	196822.798
23	9	14	22	9	13	205772.386	0.05		0.106	Yes	205772.280
23	9	15	22	9	14	205772.386	0.05		0.106	Yes	205772.280
24	9	15	23	9	14	214722.182	0.05		0.039	Yes	214722.143
24	9	16	23	9	15	214722.182	0.05		0.039	Yes	214722.143
25	9	16	24	9	15	223672.474	0.05		0.077	Yes	223672.397
25	9	17	24	9	16	223672.474	0.05		0.077	Yes	223672.397
26	9	17	25	9	16	232623.113	0.05		0.056	Yes	232623.057
26	9	18	25	9	17	232623.113	0.05		0.056	Yes	232623.057
27	9	18	26	9	17	241574.175	0.05		0.040	Yes	241574.134
27	9	19	26	9	18	241574.175	0.05		0.040	Yes	241574.134
28	9	19	27	9	18	250525.684	0.05		0.042	Yes	250525.642
28	9	20	27	9	19	250525.684	0.05		0.042	Yes	250525.642
29	9	20	28	9	19	259477.634	0.05		0.043	Yes	259477.591
29	9	21	28	9	20	259477.634	0.05		0.043	Yes	259477.591
30	9	21	29	9	20	268430.031	0.05		0.037	Yes	268429.994
30	9	22	29	9	21	268430.031	0.05		0.037	Yes	268429.994
31	9	22	30	9	21	277382.915	0.05		0.051	Yes	277382.864
31	9	23	30	9	22	277382.915	0.05		0.051	Yes	277382.864
32	9	23	31	9	22	286336.269	0.05		0.057	Yes	286336.212

Tabla A.5: continued.

J'	K'_a	K'_c	J"	K''_a	K''_c	ν(Hz)	e$_\nu$(Hz)	f$_\nu$(Hz)	O-C(Hz)	Blend	f$_{peak}$(Hz)
32	9	24	31	9	23	286336.269	0.05		0.057	Yes	286336.212
33	9	24	32	9	23	295290.020	0.05		-0.030	Yes	295290.050
33	9	25	32	9	24	295290.020	0.05		-0.030	Yes	295290.050
35	9	26	34	9	25	313199.191	0.05		-0.055	Yes	313199.246
35	9	27	34	9	26	313199.191	0.05		-0.055	Yes	313199.246
36	9	27	35	9	26	322154.709	0.05		0.080	Yes	322154.630
36	9	28	35	9	27	322154.709	0.05		0.080	Yes	322154.630
37	9	28	36	9	27	331110.692	0.05		0.138	Yes	331110.555
37	9	29	36	9	28	331110.692	0.05		0.138	Yes	331110.555
38	9	29	37	9	28	340067.391	0.05	*	0.356	Yes	340067.034
38	9	30	37	9	29	340067.391	0.05	*	0.356	Yes	340067.034
39	9	30	38	9	29	349024.599	0.05	*	0.515	Yes	349024.083
39	9	31	38	9	30	349024.599	0.05	*	0.515	Yes	349024.083
47	9	38	46	9	37	420703.397	0.05	*	0.382	Yes	420703.015
47	9	39	46	9	38	420703.397	0.05	*	0.382	Yes	420703.015
48	9	39	47	9	38	429666.398	0.05	*	0.388	Yes	429666.010
48	9	40	47	9	39	429666.398	0.05	*	0.388	Yes	429666.010
49	9	40	48	9	39	438630.093	0.05	*	0.308	Yes	438629.786
49	9	41	48	9	40	438630.093	0.05	*	0.308	Yes	438629.786
50	9	41	49	9	40	447594.518	0.05		0.143	Yes	447594.375
50	9	42	49	9	41	447594.518	0.05		0.143	Yes	447594.375
51	9	42	50	9	41	456559.772	0.05		-0.040	Yes	456559.812
51	9	43	50	9	42	456559.772	0.05		-0.040	Yes	456559.812
52	9	43	51	9	42	465526.940	0.05		-0.092		
52	9	44	51	9	43	465525.503	0.05	*	0.260		
53	9	44	52	9	43	474494.511	0.05		-0.102		
53	9	45	52	9	44	474492.387	0.05		0.215		
54	9	45	53	9	44	483463.247	0.05		-0.033		
56	9	47	55	9	46	501404.148	0.05		-0.067		
56	9	48	55	9	47	501398.504	0.05	*	0.255		
57	9	48	56	9	47	510376.571	0.05		-0.123		
57	9	49	56	9	48	510368.998	0.05		0.239		
59	9	50	58	9	49	528326.300	0.05		-0.036		
59	9	51	58	9	50	528312.963	0.05	*	0.412		
60	9	51	59	9	50	537303.694	0.05		-0.140		
61	9	52	60	9	51	546283.248	0.05		-0.139		
61	9	53	60	9	52	546260.287	0.05	*	0.308		
62	9	53	61	9	52	555265.090	0.05		-0.149		
62	9	54	61	9	53	555235.261	0.05	*	0.272		
63	9	54	62	9	53	564249.753	0.05		0.074		
63	9	55	62	9	54	564211.175	0.05	*	0.383		
64	9	55	63	9	54	573236.887	0.05		-0.152		
64	9	56	63	9	55	573187.568	0.05	*	0.256		
65	9	56	64	9	55	582227.375	0.05	*	-0.333		
66	9	58	65	9	57	591142.364	0.05	*	0.315		
67	9	59	66	9	58	600120.344	0.05	*	0.382		
12	10	2	11	10	1	107362.958	0.05		0.236		
13	10	3	12	10	2	116309.724	0.05		0.063		

Tabla A.5: continued.

J'	K'_a	K'_c	J"	K''_a	K''_c	ν(Hz)	e$_\nu$(Hz)	f$_\nu$(Hz)	O-C(Hz)	Blend	f$_{Peak}$(Hz)
14	10	4	13	10	3	125256.663	0.05		0.056		
15	10	6	14	10	5	134203.587	0.05		0.028		
16	10	6	15	10	5	143150.578	0.05		0.061		
17	10	7	16	10	6	152097.517	0.05		0.039		
18	10	8	17	10	7	161044.452	0.05		0.009		
19	10	9	18	10	8	169991.412	0.05		0.005		
20	10	10	19	10	9	178938.379	0.05		0.009		
21	10	11	20	10	10	187885.376	0.05		0.048		
22	10	12	21	10	11	196832.252	0.05		-0.028		
23	10	13	22	10	12	205779.229	0.05		0.008	Yes	205779.220
23	10	14	22	10	13	205779.229	0.05		0.008	Yes	205779.220
24	10	14	23	10	13	214726.151	0.05		0.004	Yes	214726.147
24	10	15	23	10	14	214726.151	0.05		0.004	Yes	214726.147
25	10	15	24	10	14	223673.021	0.05		-0.035	Yes	223673.056
25	10	16	24	10	15	223673.021	0.05		-0.035	Yes	223673.056
26	10	16	25	10	15	232619.925	0.05		-0.019	Yes	232619.944
26	10	17	25	10	16	232619.925	0.05		-0.019	Yes	232619.944
27	10	17	26	10	16	241566.871	0.05		0.067	Yes	241566.805
27	10	18	26	10	17	241566.871	0.05		0.067	Yes	241566.805
28	10	18	27	10	17	250513.597	0.05		-0.038	Yes	250513.635
28	10	19	27	10	18	250513.597	0.05		-0.038	Yes	250513.635
29	10	19	28	10	18	259460.383	0.05		-0.046	Yes	259460.429
29	10	20	28	10	19	259460.383	0.05		-0.046	Yes	259460.429
30	10	20	29	10	19	268407.141	0.05		-0.042	Yes	268407.183
30	10	21	29	10	20	268407.141	0.05		-0.042	Yes	268407.183
31	10	21	30	10	20	277353.524	0.05	*	-0.365	Yes	277353.889
31	10	22	30	10	21	277353.524	0.05	*	-0.365	Yes	277353.889
32	10	22	31	10	21	286300.439	0.05		-0.105		
32	10	23	31	10	22	286300.442	0.05		-0.103		
33	10	23	32	10	22	295247.049	0.05		-0.092	Yes	295247.141
33	10	24	32	10	23	295247.049	0.05		-0.092	Yes	295247.141
34	10	24	33	10	23	304193.590	0.05		-0.085	Yes	304193.674
34	10	25	33	10	24	304193.590	0.05		-0.085	Yes	304193.674
35	10	25	34	10	24	313140.049	0.05		-0.089	Yes	313140.138
35	10	26	34	10	25	313140.049	0.05		-0.089	Yes	313140.138
36	10	26	35	10	25	322086.462	0.05		-0.063		
36	10	27	35	10	26	322086.463	0.05		-0.062		
37	10	27	36	10	26	331032.834	0.05		0.003	Yes	331032.831
37	10	28	36	10	27	331032.834	0.05		0.003	Yes	331032.831
38	10	28	37	10	27	339979.084	0.05		0.036	Yes	339979.048
38	10	29	37	10	28	339979.084	0.05		0.036	Yes	339979.048
39	10	29	38	10	28	348925.383	0.05		0.212	Yes	348925.171
39	10	30	38	10	29	348925.383	0.05		0.212	Yes	348925.171
40	10	30	39	10	29	357871.983	0.05	*	0.789	Yes	357871.194
40	10	31	39	10	30	357871.983	0.05	*	0.789	Yes	357871.194
12	11	1	11	11	0	107383.604	0.05	*	0.348		
13	11	2	12	11	1	116331.394	0.05		0.184		
14	11	3	13	11	2	125279.019	0.05		0.013		

Tabla A.5: continued.

J'	K'_a	K'_c	J"	K''_a	K''_c	ν(Hz)	e$_\nu$(Hz)	f$_\nu$(Hz)	O-C(Hz)	Blend	f$_{peak}$(Hz)
15	11	5	14	11	4	134226.593	0.05		-0.036		
16	11	5	15	11	4	143174.039	0.05		-0.027		
17	11	6	16	11	5	152121.306	0.05		0.002		
18	11	7	17	11	6	161068.335	0.05		0.006		
19	11	8	18	11	7	170015.136	0.05		0.010		
20	11	9	19	11	8	178961.722	0.05		0.042		
21	11	10	20	11	9	187907.999	0.05		0.021		
22	11	11	21	11	10	196854.027	0.05		0.023		
23	11	12	22	11	11	205799.762	0.05		0.020	Yes	205799.742
23	11	13	22	11	12	205799.762	0.05		0.020	Yes	205799.742
24	11	13	23	11	12	214745.118	0.05		-0.059	Yes	214745.177
24	11	14	23	11	13	214745.118	0.05		-0.059	Yes	214745.177
25	11	14	24	11	13	223690.255	0.05		-0.039	Yes	223690.294
25	11	15	24	11	14	223690.255	0.05		-0.039	Yes	223690.294
26	11	15	25	11	14	232635.033	0.05		-0.043	Yes	232635.076
26	11	16	25	11	15	232635.033	0.05		-0.043	Yes	232635.076
27	11	16	26	11	15	241579.444	0.05		-0.062	Yes	241579.506
27	11	17	26	11	16	241579.444	0.05		-0.062	Yes	241579.506
28	11	17	27	11	16	250523.474	0.05		-0.095	Yes	250523.569
28	11	18	27	11	17	250523.474	0.05		-0.095	Yes	250523.569
29	11	18	28	11	17	259467.168	0.05		-0.078	Yes	259467.246
29	11	19	28	11	18	259467.168	0.05		-0.078	Yes	259467.246
30	11	19	29	11	18	268410.416	0.05		-0.105	Yes	268410.521
30	11	20	29	11	19	268410.416	0.05		-0.105	Yes	268410.521
31	11	20	30	11	19	277353.524	0.05		0.148	Yes	277353.376
31	11	21	30	11	20	277353.524	0.05		0.148	Yes	277353.376
32	11	21	31	11	20	286295.675	0.05		-0.119		
32	11	22	31	11	21	286295.681	0.05		-0.113		
33	11	22	32	11	21	295237.612	0.05		-0.144	Yes	295237.756
33	11	23	32	11	22	295237.612	0.05		-0.144	Yes	295237.756
34	11	23	33	11	22	304179.081	0.05		-0.163	Yes	304179.244
34	11	24	33	11	23	304179.081	0.05		-0.163	Yes	304179.244
35	11	24	34	11	23	313120.083	0.05		-0.157	Yes	313120.240
35	11	25	34	11	24	313120.083	0.05		-0.157	Yes	313120.240
36	11	26	35	11	25	322060.541	0.05		-0.184		
37	11	26	36	11	25	331000.675	0.05		-0.006	Yes	331000.680
37	11	27	36	11	26	331000.675	0.05		-0.006	Yes	331000.680
38	11	27	37	11	26	339939.890	0.05		-0.197		
38	11	28	37	11	27	339939.890	0.05		-0.197		
39	11	28	38	11	27	348878.741	0.05		-0.185	Yes	348878.926
39	11	29	38	11	28	348878.741	0.05		-0.185	Yes	348878.926
40	11	29	39	11	28	357816.981	0.05		-0.197	Yes	357817.178
40	11	30	39	11	29	357816.981	0.05		-0.197	Yes	357817.178
45	11	34	44	11	33	402498.723	0.05		-0.231	Yes	402498.954
45	11	35	44	11	34	402498.723	0.05		-0.231	Yes	402498.954
46	11	35	45	11	34	411433.013	0.05	*	-0.265	Yes	411433.277
46	11	36	45	11	35	411433.013	0.05	*	-0.265	Yes	411433.277
47	11	36	46	11	35	420366.683	0.05		-0.195	Yes	420366.878

Tabla A.5: continued.

J'	K'_a	K'_c	J"	K''_a	K''_c	ν(Hz)	e$_\nu$(Hz)	f$_\nu$(Hz)	O-C(Hz)	Blend	f$_{Peak}$(Hz)
47	11	37	46	11	36	420366.683	0.05		-0.195	Yes	420366.878
48	11	37	47	11	36	429299.525	0.05		-0.213	Yes	429299.738
48	11	38	47	11	37	429299.525	0.05		-0.213	Yes	429299.738
49	11	38	48	11	37	438231.676	0.05		-0.162	Yes	438231.838
49	11	39	48	11	38	438231.676	0.05		-0.162	Yes	438231.838
50	11	39	49	11	38	447163.025	0.05		-0.134	Yes	447163.159
50	11	40	49	11	39	447163.025	0.05		-0.134	Yes	447163.159
51	11	40	50	11	39	456093.608	0.05		-0.076	Yes	456093.684
51	11	41	50	11	40	456093.608	0.05		-0.076	Yes	456093.684
52	11	41	51	11	40	465023.269	0.05		-0.125	Yes	465023.394
52	11	42	51	11	41	465023.269	0.05		-0.125	Yes	465023.394
53	11	42	52	11	41	473952.180	0.05		-0.094	Yes	473952.273
53	11	43	52	11	42	473952.180	0.05		-0.094	Yes	473952.273
54	11	43	53	11	42	482880.227	0.05		-0.076	Yes	482880.303
54	11	44	53	11	43	482880.227	0.05		-0.076	Yes	482880.303
55	11	44	54	11	43	491807.459	0.05		-0.009	Yes	491807.469
55	11	45	54	11	44	491807.459	0.05		-0.009	Yes	491807.469
56	11	45	55	11	44	500733.609	0.05		-0.145	Yes	500733.753
56	11	46	55	11	45	500733.609	0.05		-0.145	Yes	500733.753
57	11	46	56	11	45	509659.315	0.05		0.172	Yes	509659.143
57	11	47	56	11	46	509659.315	0.05		0.172	Yes	509659.143
58	11	47	57	11	46	518583.759	0.05		0.137	Yes	518583.623
58	11	48	57	11	47	518583.759	0.05		0.137	Yes	518583.623
60	11	49	59	11	48	536430.072	0.05	*	0.270	Yes	536429.802
60	11	50	59	11	49	536430.072	0.05	*	0.270	Yes	536429.802
61	11	50	60	11	49	545351.965	0.05	*	0.486	Yes	545351.479
61	11	51	60	11	50	545351.965	0.05	*	0.486	Yes	545351.479
62	11	51	61	11	50	554272.814	0.05	*	0.615	Yes	554272.199
62	11	52	61	11	51	554272.814	0.05	*	0.615	Yes	554272.199
63	11	52	62	11	51	563192.718	0.05	*	0.763	Yes	563191.956
63	11	53	62	11	52	563192.718	0.05	*	0.763	Yes	563191.956
13	12	1	12	12	0	116356.412	0.05		0.091		
14	12	2	13	12	1	125305.466	0.05		0.032		
15	12	4	14	12	3	134254.230	0.05		-0.009		
16	12	4	15	12	3	143202.729	0.05		0.015		
17	12	5	16	12	4	152150.852	0.05		0.018		
18	12	6	17	12	5	161098.565	0.05		-0.013		
19	12	7	18	12	6	170045.791	0.05		-0.129		
20	12	8	19	12	7	178992.686	0.05		-0.152		
21	12	9	20	12	8	187939.212	0.05		-0.096		
22	12	10	21	12	9	196885.243	0.05		-0.062		
23	12	11	22	12	10	205830.804	0.05		-0.001	Yes	205830.804
23	12	12	22	12	11	205830.804	0.05		-0.001	Yes	205830.804
24	12	12	23	12	11	214775.659	0.05		-0.123	Yes	214775.782
24	12	13	23	12	12	214775.659	0.05		-0.123	Yes	214775.782
25	12	13	24	12	12	223720.043	0.05		-0.171	Yes	223720.213
25	12	14	24	12	13	223720.043	0.05		-0.171	Yes	223720.213
26	12	14	25	12	13	232663.917	0.05		-0.156	Yes	232664.072

Tabla A.5: continued.

J'	K'_a	K'_c	J"	K''_a	K''_c	ν(Hz)	e$_\nu$(Hz)	f$_\nu$(Hz)	O-C(Hz)	Blend	f$_{peak}$(Hz)
26	12	15	25	12	14	232663.917	0.05		-0.156	Yes	232664.072
27	12	15	26	12	14	241607.216	0.05		-0.118	Yes	241607.334
27	12	16	26	12	15	241607.216	0.05		-0.118	Yes	241607.334
28	12	16	27	12	15	250549.774	0.05		-0.199	Yes	250549.974
28	12	17	27	12	16	250549.774	0.05		-0.199	Yes	250549.974
29	12	17	28	12	16	259491.743	0.05		-0.221	Yes	259491.964
29	12	18	28	12	17	259491.743	0.05		-0.221	Yes	259491.964
30	12	19	29	12	18	268433.047	0.05		-0.232		
31	12	19	30	12	18	277373.587	0.05	*	-0.307	Yes	277373.894
31	12	20	30	12	19	277373.587	0.05	*	-0.307	Yes	277373.894
32	12	20	31	12	19	286313.445	0.05	*	-0.336		
32	12	21	31	12	20	286313.457	0.05	*	-0.324		
33	12	21	32	12	20	295252.548	0.05	*	-0.364	Yes	295252.912
33	12	22	32	12	21	295252.548	0.05	*	-0.364	Yes	295252.912
34	12	22	33	12	21	304190.883	0.05	*	-0.379	Yes	304191.263
34	12	23	33	12	22	304190.883	0.05	*	-0.379	Yes	304191.263
35	12	23	34	12	22	313128.401	0.05	*	-0.403	Yes	313128.804
35	12	24	34	12	23	313128.401	0.05	*	-0.403	Yes	313128.804
36	12	24	35	12	23	322065.042	0.05	*	-0.467	Yes	322065.508
36	12	25	35	12	24	322065.042	0.05	*	-0.467	Yes	322065.508
37	12	25	36	12	24	331000.676	0.05	*	-0.673	Yes	331001.348
37	12	26	36	12	25	331000.676	0.05	*	-0.673	Yes	331001.348
38	12	26	37	12	25	339935.795	0.05	*	-0.502	Yes	339936.297
38	12	27	37	12	26	339935.795	0.05	*	-0.502	Yes	339936.297
39	12	27	38	12	26	348869.798	0.05	*	-0.526	Yes	348870.324
39	12	28	38	12	27	348869.798	0.05	*	-0.526	Yes	348870.324
40	12	28	39	12	27	357802.803	0.05	*	-0.601	Yes	357803.403
40	12	29	39	12	28	357802.803	0.05	*	-0.601	Yes	357803.403
45	12	33	44	12	32	402452.852	0.05	*	-0.718	Yes	402453.570
45	12	34	44	12	33	402452.852	0.05	*	-0.718	Yes	402453.570
46	12	34	45	12	33	411379.647	0.05	*	-0.709	Yes	411380.355
46	12	35	45	12	34	411379.647	0.05	*	-0.709	Yes	411380.355
47	12	35	46	12	34	420305.219	0.05	*	-0.772	Yes	420305.991
47	12	36	46	12	35	420305.219	0.05	*	-0.772	Yes	420305.991
48	12	36	47	12	35	429229.678	0.05	*	-0.769	Yes	429230.447
48	12	37	47	12	36	429229.678	0.05	*	-0.769	Yes	429230.447
49	12	37	48	12	36	438152.928	0.05	*	-0.766	Yes	438153.694
49	12	38	48	12	37	438152.928	0.05	*	-0.766	Yes	438153.694
50	12	38	49	12	37	447074.690	0.05	*	-1.014	Yes	447075.704
50	12	39	49	12	38	447074.690	0.05	*	-1.014	Yes	447075.704
51	12	39	50	12	38	455995.690	0.05	*	-0.758	Yes	455996.447
51	12	40	50	12	39	455995.690	0.05	*	-0.758	Yes	455996.447
52	12	40	51	12	39	464915.143	0.05	*	-0.752	Yes	464915.895
52	12	41	51	12	40	464915.143	0.05	*	-0.752	Yes	464915.895
53	12	41	52	12	40	473833.234	0.05	*	-0.785	Yes	473834.018
53	12	42	52	12	41	473833.234	0.05	*	-0.785	Yes	473834.018
54	12	42	53	12	41	482749.944	0.05	*	-0.844	Yes	482750.788
54	12	43	53	12	42	482749.944	0.05	*	-0.844	Yes	482750.788

Tabla A.5: continued.

J'	K'_a	K'_c	J"	K''_a	K''_c	ν(Hz)	e$_\nu$(Hz)	f$_\nu$(Hz)	O-C(Hz)	Blend	f$_{Peak}$(Hz)
55	12	43	54	12	42	491665.359	0.05	*	-0.818		
56	12	44	55	12	43	500579.362	0.05	*	-0.793	Yes	500580.155
56	12	45	55	12	44	500579.362	0.05	*	-0.793	Yes	500580.155
57	12	45	56	12	44	509491.878	0.05	*	-0.817	Yes	509492.695
57	12	46	56	12	45	509491.878	0.05	*	-0.817	Yes	509492.695
58	12	46	57	12	45	518403.000	0.05	*	-0.770	Yes	518403.770
58	12	47	57	12	46	518403.000	0.05	*	-0.770	Yes	518403.770
59	12	47	58	12	46	527312.581	0.05	*	-0.770	Yes	527313.351
59	12	48	58	12	47	527312.581	0.05	*	-0.770	Yes	527313.351
60	12	48	59	12	47	536220.673	0.05	*	-0.739	Yes	536221.412
60	12	49	59	12	48	536220.673	0.05	*	-0.739	Yes	536221.412
61	12	49	60	12	48	545127.272	0.05	*	-0.653	Yes	545127.925
61	12	50	60	12	49	545127.272	0.05	*	-0.653	Yes	545127.925
62	12	50	61	12	49	554032.446	0.05	*	-0.420	Yes	554032.866
62	12	51	61	12	50	554032.446	0.05	*	-0.420	Yes	554032.866
63	12	51	62	12	50	562935.970	0.05		-0.238	Yes	562936.208
63	12	52	62	12	51	562935.970	0.05		-0.238	Yes	562936.208
66	12	54	65	12	53	589635.962	0.05	*	-0.442		
67	12	56	66	12	55	598532.037	0.05	*	-1.050		
15	13	2	14	13	1	134285.917	0.05		0.085		
16	13	3	15	13	2	143235.874	0.05		0.087		
17	13	4	16	13	3	152185.390	0.05		0.121		
18	13	5	17	13	4	161134.334	0.05		0.089		
19	13	6	18	13	5	170082.765	0.05		0.078		
20	13	7	19	13	6	179030.729	0.05		0.167		
21	13	8	20	13	7	187978.034	0.05		0.194		
22	13	9	21	13	8	196924.651	0.05		0.163		
24	13	11	23	13	10	214816.086	0.05	*	0.312	Yes	214815.774
24	13	12	23	13	11	214816.086	0.05	*	0.312	Yes	214815.774
25	13	12	24	13	11	223760.701	0.05	*	0.354	Yes	223760.347
25	13	13	24	13	12	223760.701	0.05	*	0.354	Yes	223760.347
26	13	13	25	13	12	232704.614	0.05	*	0.449	Yes	232704.165
26	13	14	25	13	13	232704.614	0.05	*	0.449	Yes	232704.165
27	13	14	26	13	13	241647.717	0.20		0.523	Yes	241647.194
27	13	15	26	13	14	241647.717	0.20		0.523	Yes	241647.194
28	13	15	27	13	14	250589.973	0.05	*	0.570	Yes	250589.403
28	13	16	27	13	15	250589.973	0.05	*	0.570	Yes	250589.403
29	13	16	28	13	15	259531.537	0.05	*	0.778	Yes	259530.759
29	13	17	28	13	16	259531.537	0.05	*	0.778	Yes	259530.759
30	13	17	29	13	16	268472.128	0.20		0.899	Yes	268471.229
30	13	18	29	13	17	268472.128	0.20		0.899	Yes	268471.229
33	13	20	32	13	19	295288.394	0.05	*	1.403	Yes	295286.991
33	13	21	32	13	20	295288.394	0.05	*	1.403	Yes	295286.991
34	13	21	33	13	20	304225.340	0.05	*	1.756	Yes	304223.584
34	13	22	33	13	21	304225.340	0.05	*	1.756	Yes	304223.584
35	13	22	34	13	21	313161.312	0.05	*	2.188	Yes	313159.124
35	13	23	34	13	22	313161.312	0.05	*	2.188	Yes	313159.124
36	13	23	35	13	22	322096.344	0.05	*	2.768	Yes	322093.576

Tabla A.5: continued.

J'	K'_a	K'_c	J"	K''_a	K''_c	ν(Hz)	e$_\nu$(Hz)	f$_\nu$(Hz)	O-C(Hz)	Blend	f$_{peak}$(Hz)
36	13	24	35	13	23	322096.344	0.05	*	2.768	Yes	322093.576
38	13	25	37	13	24	339963.270	0.05	*	4.190	Yes	339959.080
38	13	26	37	13	25	339963.270	0.05	*	4.190	Yes	339959.080
39	13	26	38	13	25	348893.093	0.05	*	3.030	Yes	348890.062
39	13	27	38	13	26	348893.093	0.05	*	3.030	Yes	348890.062
15	14	2	14	14	1	134321.039	0.05		0.020		
16	14	2	15	14	1	143272.862	0.05		0.039		
17	14	3	16	14	2	152224.196	0.05		0.137		
18	14	4	17	14	3	161174.709	0.05		0.021		
19	14	5	18	14	4	170124.638	0.05		-0.037		
20	14	6	19	14	5	179074.075	0.05		0.091		
21	14	7	20	14	6	188022.568	0.05		-0.008		
22	14	8	21	14	7	196970.477	0.05		0.061		
24	14	10	23	14	9	214863.710	0.05		0.019	Yes	214863.691
24	14	11	23	14	10	214863.710	0.05		0.019	Yes	214863.691
25	14	11	24	14	10	223809.047	0.05		-0.004	Yes	223809.051
25	14	12	24	14	11	223809.047	0.05		-0.004	Yes	223809.051
26	14	12	25	14	11	232753.510	0.05		0.001	Yes	232753.509
26	14	13	25	14	12	232753.510	0.05		0.001	Yes	232753.509
27	14	13	26	14	12	241697.044	0.05		0.016	Yes	241697.028
27	14	14	26	14	13	241697.044	0.05		0.016	Yes	241697.028
28	14	14	27	14	13	250639.588	0.05		0.018	Yes	250639.570
28	14	15	27	14	14	250639.588	0.05		0.018	Yes	250639.570
29	14	15	28	14	14	259581.100	0.05		0.003	Yes	259581.097
29	14	16	28	14	15	259581.100	0.05		0.003	Yes	259581.097
30	14	16	29	14	15	268521.575	0.05		0.004	Yes	268521.571
30	14	17	29	14	16	268521.575	0.05		0.004	Yes	268521.571
31	14	17	30	14	16	277460.939	0.05		-0.014	Yes	277460.953
31	14	18	30	14	17	277460.939	0.05		-0.014	Yes	277460.953
32	14	18	31	14	17	286399.255	0.05		0.050	Yes	286399.205
32	14	19	31	14	18	286399.255	0.05		0.050	Yes	286399.205
33	14	19	32	14	18	295336.200	0.05		-0.089	Yes	295336.289
33	14	20	32	14	19	295336.200	0.05		-0.089	Yes	295336.289
34	14	20	33	14	19	304272.101	0.05		-0.064	Yes	304272.165
34	14	21	33	14	20	304272.101	0.05		-0.064	Yes	304272.165
35	14	21	34	14	20	313206.771	0.05		-0.024	Yes	313206.795
35	14	22	34	14	21	313206.771	0.05		-0.024	Yes	313206.795
36	14	22	35	14	21	322140.171	0.05		0.033	Yes	322140.139
36	14	23	35	14	22	322140.171	0.05		0.033	Yes	322140.139
37	14	23	36	14	22	331072.211	0.05		0.053	Yes	331072.158
37	14	24	36	14	23	331072.211	0.05		0.053	Yes	331072.158
38	14	24	37	14	23	340002.857	0.05		0.045	Yes	340002.812
38	14	25	37	14	24	340002.857	0.05		0.045	Yes	340002.812
39	14	25	38	14	24	348932.105	0.05		0.042	Yes	348932.063
39	14	26	38	14	25	348932.105	0.05		0.042	Yes	348932.063
40	14	26	39	14	25	357859.915	0.05		0.046	Yes	357859.869
40	14	27	39	14	26	357859.915	0.05		0.046	Yes	357859.869
18	15	3	17	15	2	161219.570	0.05		0.130		

Tabla A.5: continued.

J'	K'_a	K'_c	J"	K''_a	K''_c	ν(Hz)	e$_\nu$(Hz)	f$_\nu$(Hz)	O-C(Hz)	Blend	f$_{Peak}$(Hz)
19	15	4	18	15	3	170171.398	0.05		0.052		
20	15	5	19	15	4	179122.491	0.05		0.009		
21	15	6	20	15	5	188072.848	0.05		0.041		
22	15	7	21	15	6	197022.292	0.05		0.013		
24	15	9	23	15	8	214918.544	0.05		0.044	Yes	214918.500
24	15	10	23	15	9	214918.544	0.05		0.044	Yes	214918.500
25	15	10	24	15	9	223865.203	0.05		0.038	Yes	223865.165
25	15	11	24	15	10	223865.203	0.05		0.038	Yes	223865.165
26	15	11	25	15	10	232810.841	0.05		0.031	Yes	232810.810
26	15	12	25	15	11	232810.841	0.05		0.031	Yes	232810.810
27	15	12	26	15	11	241755.400	0.05		0.005	Yes	241755.395
27	15	13	26	15	12	241755.400	0.05		0.005	Yes	241755.395
28	15	13	27	15	12	250698.908	0.05		0.033	Yes	250698.875
28	15	14	27	15	13	250698.908	0.05		0.033	Yes	250698.875
29	15	14	28	15	13	259641.240	0.05		0.030	Yes	259641.210
29	15	15	28	15	14	259641.240	0.05		0.030	Yes	259641.210
30	15	15	29	15	14	268582.384	0.05		0.027	Yes	268582.357
30	15	16	29	15	15	268582.384	0.05		0.027	Yes	268582.357
32	15	17	31	15	16	286460.924	0.05		0.008	Yes	286460.916
32	15	18	31	15	17	286460.924	0.05		0.008	Yes	286460.916
33	15	18	32	15	17	295398.157	0.05		-0.087	Yes	295398.243
33	15	19	32	15	18	295398.157	0.05		-0.087	Yes	295398.243
34	15	19	33	15	18	304334.131	0.05		-0.080	Yes	304334.211
34	15	20	33	15	19	304334.131	0.05		-0.080	Yes	304334.211
35	15	20	34	15	19	313268.771	0.05		-0.007	Yes	313268.777
35	15	21	34	15	20	313268.771	0.05		-0.007	Yes	313268.777
36	15	21	35	15	20	322201.897	0.05		-0.001		
36	15	22	35	15	21	322201.894	0.05		-0.004		
37	15	23	36	15	22	331133.510	0.05		-0.021		
38	15	23	37	15	22	340063.599	0.05		-0.033	Yes	340063.632
38	15	24	37	15	23	340063.599	0.05		-0.033	Yes	340063.632
39	15	24	38	15	23	348991.488	0.05	*	-0.670	Yes	348992.157
39	15	25	38	15	24	348991.488	0.05	*	-0.670	Yes	348992.157
40	15	25	39	15	24	357919.049	0.05		-0.016	Yes	357919.064
40	15	26	39	15	25	357919.049	0.05		-0.016	Yes	357919.064
45	15	30	44	15	29	402527.802	0.05		0.025	Yes	402527.777
45	15	31	44	15	30	402527.802	0.05		0.025	Yes	402527.777
46	15	31	45	15	30	411443.633	0.05	*	-0.415	Yes	411444.048
46	15	32	45	15	31	411443.633	0.05	*	-0.415	Yes	411444.048
47	15	32	46	15	31	420358.431	0.05		0.040	Yes	420358.390
47	15	33	46	15	32	420358.431	0.05		0.040	Yes	420358.390
48	15	33	47	15	32	429270.744	0.05		-0.016	Yes	429270.761
48	15	34	47	15	33	429270.744	0.05		-0.016	Yes	429270.761
49	15	34	48	15	33	438181.153	0.05		0.038	Yes	438181.115
49	15	35	48	15	34	438181.153	0.05		0.038	Yes	438181.115
50	15	35	49	15	34	447089.445	0.05		0.037	Yes	447089.408
50	15	36	49	15	35	447089.445	0.05		0.037	Yes	447089.408
52	15	37	51	15	36	464899.610	0.05		-0.022	Yes	464899.632

Tabla A.5: continued.

J'	K'_a	K'_c	J"	K''_a	K''_c	ν(Hz)	e$_\nu$(Hz)	f$_\nu$(Hz)	O-C(Hz)	Blend	f$_{peak}$(Hz)
52	15	38	51	15	37	464899.610	0.05		-0.022	Yes	464899.632
53	15	38	52	15	37	473801.556	0.05		0.083	Yes	473801.473
53	15	39	52	15	38	473801.556	0.05		0.083	Yes	473801.473
54	15	39	53	15	38	482701.110	0.05		0.035	Yes	482701.075
54	15	40	53	15	39	482701.110	0.05		0.035	Yes	482701.075
55	15	40	54	15	39	491598.473	0.05		0.082	Yes	491598.391
55	15	41	54	15	40	491598.473	0.05		0.082	Yes	491598.391
56	15	41	55	15	40	500493.545	0.05		0.166	Yes	500493.378
56	15	42	55	15	41	500493.545	0.05		0.166	Yes	500493.378
57	15	42	56	15	41	509386.049	0.05		0.057	Yes	509385.991
57	15	43	56	15	42	509386.049	0.05		0.057	Yes	509385.991
58	15	43	57	15	42	518276.297	0.05		0.113	Yes	518276.184
58	15	44	57	15	43	518276.297	0.05		0.113	Yes	518276.184
59	15	44	58	15	43	527164.080	0.05		0.166	Yes	527163.914
59	15	45	58	15	44	527164.080	0.05		0.166	Yes	527163.914
60	15	45	59	15	44	536049.313	0.05		0.179	Yes	536049.134
60	15	46	59	15	45	536049.313	0.05		0.179	Yes	536049.134
61	15	46	60	15	45	544932.127	0.05	*	0.326	Yes	544931.801
61	15	47	60	15	46	544932.127	0.05	*	0.326	Yes	544931.801
62	15	47	61	15	46	553812.295	0.05	*	0.424	Yes	553811.870
62	15	48	61	15	47	553812.295	0.05	*	0.424	Yes	553811.870
63	15	48	62	15	47	562689.872	0.05	*	0.575	Yes	562689.297
63	15	49	62	15	48	562689.872	0.05	*	0.575	Yes	562689.297
64	15	49	63	15	48	571564.884	0.05	*	0.848	Yes	571564.036
64	15	50	63	15	49	571564.884	0.05	*	0.848	Yes	571564.036
17	16	2	16	16	1	152313.243	0.05		0.047		
20	16	4	19	16	3	179175.571	0.05		-0.013		
21	16	5	20	16	4	188127.945	0.05		-0.049		
22	16	6	21	16	5	197079.360	0.05		-0.109		
24	16	8	23	16	7	214979.382	0.05		-0.050	Yes	214979.432
24	16	9	23	16	8	214979.382	0.05		-0.050	Yes	214979.432
25	16	9	24	16	8	223927.809	0.05		-0.020	Yes	223927.830
25	16	10	24	16	9	223927.809	0.05		-0.020	Yes	223927.830
26	16	10	25	16	9	232875.114	0.05		0.002	Yes	232875.111
26	16	11	25	16	10	232875.114	0.05		0.002	Yes	232875.111
27	16	11	26	16	10	241821.283	0.05		0.052	Yes	241821.231
27	16	12	26	16	11	241821.283	0.05		0.052	Yes	241821.231
28	16	12	27	16	11	250766.165	0.05		0.022	Yes	250766.144
28	16	13	27	16	12	250766.165	0.05		0.022	Yes	250766.144
29	16	13	28	16	12	259709.786	0.05		-0.017	Yes	259709.803
29	16	14	28	16	13	259709.786	0.05		-0.017	Yes	259709.803
30	16	14	29	16	13	268652.177	0.05		0.014	Yes	268652.163
30	16	15	29	16	14	268652.177	0.05		0.014	Yes	268652.163
31	16	15	30	16	14	277593.154	0.05		-0.025	Yes	277593.179
31	16	16	30	16	15	277593.154	0.05		-0.025	Yes	277593.179
32	16	16	31	16	15	286532.814	0.05		0.011	Yes	286532.803
32	16	17	31	16	16	286532.814	0.05		0.011	Yes	286532.803
33	16	17	32	16	16	295470.977	0.05		-0.013	Yes	295470.990

Tabla A.5: continued.

J'	K'_a	K'_c	J"	K''_a	K''_c	ν(Hz)	e$_\nu$(Hz)	f$_\nu$(Hz)	O-C(Hz)	Blend	f$_{Peak}$(Hz)
33	16	18	32	16	17	295470.977	0.05		-0.013	Yes	295470.990
34	16	18	33	16	17	304407.682	0.05		-0.013	Yes	304407.695
34	16	19	33	16	18	304407.682	0.05		-0.013	Yes	304407.695
35	16	19	34	16	18	313342.811	0.05		-0.059	Yes	313342.870
35	16	20	34	16	19	313342.811	0.05		-0.059	Yes	313342.870
36	16	20	35	16	19	322276.470	0.05		0.001	Yes	322276.469
36	16	21	35	16	20	322276.470	0.05		0.001	Yes	322276.469
37	16	21	36	16	20	331208.452	0.05		0.006	Yes	331208.446
37	16	22	36	16	21	331208.452	0.05		0.006	Yes	331208.446
38	16	22	37	16	21	340138.768	0.05		0.014	Yes	340138.754
38	16	23	37	16	22	340138.768	0.05		0.014	Yes	340138.754
39	16	23	38	16	22	349067.353	0.05		0.006	Yes	349067.347
39	16	24	38	16	23	349067.353	0.05		0.006	Yes	349067.347
40	16	24	39	16	23	357994.199	0.05		0.022	Yes	357994.178
40	16	25	39	16	24	357994.199	0.05		0.022	Yes	357994.178
46	16	30	45	16	29	411515.638	0.05		0.104	Yes	411515.534
46	16	31	45	16	30	411515.638	0.05		0.104	Yes	411515.534
47	16	31	46	16	30	420428.682	0.05		-0.034	Yes	420428.716
47	16	32	46	16	31	420428.682	0.05		-0.034	Yes	420428.716
48	16	32	47	16	31	429339.784	0.05		0.024	Yes	429339.760
48	16	33	47	16	32	429339.784	0.05		0.024	Yes	429339.760
49	16	33	48	16	32	438248.652	0.05		0.033	Yes	438248.618
49	16	34	48	16	33	438248.652	0.05		0.033	Yes	438248.618
50	16	34	49	16	33	447155.274	0.05		0.030	Yes	447155.244
50	16	35	49	16	34	447155.274	0.05		0.030	Yes	447155.244
51	16	35	50	16	34	456059.624	0.05		0.035	Yes	456059.589
51	16	36	50	16	35	456059.624	0.05		0.035	Yes	456059.589
52	16	36	51	16	35	464961.631	0.05		0.024	Yes	464961.607
52	16	37	51	16	36	464961.631	0.05		0.024	Yes	464961.607
53	16	37	52	16	36	473861.264	0.05		0.014	Yes	473861.250
53	16	38	52	16	37	473861.264	0.05		0.014	Yes	473861.250
54	16	38	53	16	37	482758.428	0.05		-0.043	Yes	482758.471
54	16	39	53	16	38	482758.428	0.05		-0.043	Yes	482758.471
55	16	39	54	16	38	491653.292	0.05		0.070	Yes	491653.222
55	16	40	54	16	39	491653.292	0.05		0.070	Yes	491653.222
56	16	40	55	16	39	500545.398	0.05		-0.058	Yes	500545.456
56	16	41	55	16	40	500545.398	0.05		-0.058	Yes	500545.456
57	16	41	56	16	40	509435.086	0.05		-0.040	Yes	509435.125
57	16	42	56	16	41	509435.086	0.05		-0.040	Yes	509435.125
58	16	42	57	16	41	518322.050	0.05		-0.133	Yes	518322.183
58	16	43	57	16	42	518322.050	0.05		-0.133	Yes	518322.183
60	16	44	59	16	43	536088.057	0.05		-0.216	Yes	536088.274
60	16	45	59	16	44	536088.057	0.05		-0.216	Yes	536088.274
61	16	45	60	16	44	544966.930	0.05	*	-0.282	Yes	544967.212
61	16	46	60	16	45	544966.930	0.05	*	-0.282	Yes	544967.212
62	16	46	61	16	45	553843.019	0.05	*	-0.331	Yes	553843.350
62	16	47	61	16	46	553843.019	0.05	*	-0.331	Yes	553843.350
63	16	47	62	16	46	562716.222	0.05	*	-0.419	Yes	562716.640

Tabla A.5: continued.

J'	K'_a	K'_c	J"	K''_a	K''_c	ν(Hz)	e$_\nu$(Hz)	f$_\nu$(Hz)	O-C(Hz)	Blend	f$_{peak}$(Hz)
63	16	48	62	16	47	562716.222	0.05	*	-0.419	Yes	562716.640
64	16	48	63	16	47	571586.529	0.05	*	-0.507	Yes	571587.036
64	16	49	63	16	48	571586.529	0.05	*	-0.507	Yes	571587.036
65	16	49	64	16	48	580453.916	0.05	*	-0.574	Yes	580454.490
65	16	50	64	16	49	580453.916	0.05	*	-0.574	Yes	580454.490
66	16	50	65	16	49	589318.251	0.05	*	-0.705	Yes	589318.956
66	16	51	65	16	50	589318.251	0.05	*	-0.705	Yes	589318.956
67	16	51	66	16	50	598179.567	0.05	*	-0.820	Yes	598180.388
67	16	52	66	16	51	598179.567	0.05	*	-0.820	Yes	598180.388
24	17	7	23	17	6	215045.350	0.05	*	-0.529	Yes	215045.880
24	17	8	23	17	7	215045.350	0.05	*	-0.529	Yes	215045.880
25	17	8	24	17	7	223995.681	0.05	*	-0.689	Yes	223996.370
25	17	9	24	17	8	223995.681	0.05	*	-0.689	Yes	223996.370
26	17	9	25	17	8	232944.974	0.05	*	-0.689	Yes	232945.663
26	17	10	25	17	9	232944.974	0.05	*	-0.689	Yes	232945.663
27	17	10	26	17	9	241892.968	0.05	*	-0.742	Yes	241893.709
27	17	11	26	17	10	241892.968	0.05	*	-0.742	Yes	241893.709
28	17	11	27	17	10	250839.827	0.05	*	-0.635	Yes	250840.462
28	17	12	27	17	11	250839.827	0.05	*	-0.635	Yes	250840.462
29	17	12	28	17	11	259785.148	0.05	*	-0.723	Yes	259785.871
29	17	13	28	17	12	259785.148	0.05	*	-0.723	Yes	259785.871
30	17	13	29	17	12	268730.809	0.05	*	0.921	Yes	268729.888
30	17	14	29	17	13	268730.809	0.05	*	0.921	Yes	268729.888
32	17	15	31	17	14	286612.910	0.05	*	-0.642	Yes	286613.552
32	17	16	31	17	15	286612.910	0.05	*	-0.642	Yes	286613.552
33	17	16	32	17	15	295552.583	0.05	*	-0.518	Yes	295553.101
33	17	17	32	17	16	295552.583	0.05	*	-0.518	Yes	295553.101
35	17	18	34	17	17	313426.882	0.05	*	-0.507	Yes	313427.389
35	17	19	34	17	18	313426.882	0.05	*	-0.507	Yes	313427.389
36	17	19	35	17	18	322361.492	0.05	*	-0.538	Yes	322362.031
36	17	20	35	17	19	322361.492	0.05	*	-0.538	Yes	322362.031
37	17	20	36	17	19	331294.583	0.05	*	-0.355	Yes	331294.938
37	17	21	36	17	20	331294.583	0.05	*	-0.355	Yes	331294.938
38	17	21	37	17	20	340224.907	0.05	*	-1.156	Yes	340226.062
38	17	22	37	17	21	340224.907	0.05	*	-1.156	Yes	340226.062
39	17	22	38	17	21	349154.823	0.05	*	-0.531	Yes	349155.354
39	17	23	38	17	22	349154.823	0.05	*	-0.531	Yes	349155.354
40	17	23	39	17	22	358082.304	0.05	*	-0.462	Yes	358082.765
40	17	24	39	17	23	358082.304	0.05	*	-0.462	Yes	358082.765
45	17	28	44	17	27	402689.522	0.05	*	-0.353	Yes	402689.875
45	17	29	44	17	28	402689.522	0.05	*	-0.353	Yes	402689.875
46	17	29	45	17	28	411604.648	0.05	*	-0.315	Yes	411604.963
46	17	30	45	17	29	411604.648	0.05	*	-0.315	Yes	411604.963
47	17	30	46	17	29	420517.456	0.05	*	-0.368	Yes	420517.824
47	17	31	46	17	30	420517.456	0.05	*	-0.368	Yes	420517.824
48	17	31	47	17	30	429427.909	0.05	*	-0.501	Yes	429428.410
48	17	32	47	17	31	429427.909	0.05	*	-0.501	Yes	429428.410
50	17	33	49	17	32	447242.442	0.05		-0.114	Yes	447242.556

Tabla A.5: continued.

J'	K'_a	K'_c	J"	K''_a	K''_c	ν(Hz)	e$_\nu$(Hz)	f$_\nu$(Hz)	O-C(Hz)	Blend	f$_{peak}$(Hz)
50	17	34	49	17	33	447242.442	0.05		-0.114	Yes	447242.556
51	17	34	50	17	33	456145.942	0.05		-0.075	Yes	456146.017
51	17	35	50	17	34	456145.942	0.05		-0.075	Yes	456146.017
52	17	35	51	17	34	465046.919	0.05		-0.087	Yes	465047.006
52	17	36	51	17	35	465046.919	0.05		-0.087	Yes	465047.006
53	17	36	52	17	35	473945.458	0.05		-0.013	Yes	473945.471
53	17	37	52	17	36	473945.458	0.05		-0.013	Yes	473945.471
54	17	37	53	17	36	482841.341	0.05		-0.023	Yes	482841.364
54	17	38	53	17	37	482841.341	0.05		-0.023	Yes	482841.364
55	17	38	54	17	37	491734.641	0.05		0.005	Yes	491734.636
55	17	39	54	17	38	491734.641	0.05		0.005	Yes	491734.636
56	17	39	55	17	38	500625.281	0.05		0.044	Yes	500625.237
56	17	40	55	17	39	500625.281	0.05		0.044	Yes	500625.237
57	17	40	56	17	39	509513.135	0.05		0.016	Yes	509513.118
57	17	41	56	17	40	509513.135	0.05		0.016	Yes	509513.118
58	17	41	57	17	40	518398.342	0.05		0.111	Yes	518398.231
58	17	42	57	17	41	518398.342	0.05		0.111	Yes	518398.231
59	17	42	58	17	41	527280.623	0.05		0.098	Yes	527280.525
59	17	43	58	17	42	527280.623	0.05		0.098	Yes	527280.525
60	17	43	59	17	42	536159.964	0.05		0.012	Yes	536159.952
60	17	44	59	17	43	536159.964	0.05		0.012	Yes	536159.952
61	17	44	60	17	43	545036.513	0.05		0.050	Yes	545036.463
61	17	45	60	17	44	545036.513	0.05		0.050	Yes	545036.463
62	17	45	61	17	44	553910.068	0.05		0.059	Yes	553910.009
62	17	46	61	17	45	553910.068	0.05		0.059	Yes	553910.009
63	17	46	62	17	45	562780.575	0.05		0.033	Yes	562780.542
63	17	47	62	17	46	562780.575	0.05		0.033	Yes	562780.542
64	17	47	63	17	46	571647.976	0.05		-0.037	Yes	571648.013
64	17	48	63	17	47	571647.976	0.05		-0.037	Yes	571648.013
65	17	48	64	17	47	580512.186	0.05		-0.187	Yes	580512.373
65	17	49	64	17	48	580512.186	0.05		-0.187	Yes	580512.373
6	0	6	5	1	5	33131.490	0.05		-0.042		
8	0	8	7	1	7	53257.520	0.05		-0.031		
9	0	9	8	1	8	63398.981	0.05		-0.055		
10	0	10	9	1	9	73540.974	0.05		-0.047		
11	0	11	10	1	10	83646.387	0.05		-0.062		
12	0	12	11	1	11	93682.174	0.05		-0.086		
15	0	15	14	1	14	123134.798	0.05	*	-0.303		
16	0	16	15	1	15	132691.540	0.05		-0.094		
17	0	17	16	1	16	142113.141	0.05		-0.051		
18	0	18	17	1	17	151405.073	0.05		-0.068		
19	0	19	18	1	18	160576.307	0.05		0.028		
20	0	20	19	1	19	169637.430	0.05		-0.079		
21	0	21	20	1	20	178600.533	0.05		-0.193		
22	0	22	21	1	21	187477.850	0.05		-0.117		
24	0	24	23	1	23	205019.930	0.05		-0.073		
25	0	25	24	1	24	213705.163	0.05		-0.073		
29	0	29	28	1	28	248061.426	0.05		-0.026		

Tabla A.5: continued.

J'	K'_a	K'_c	J"	K''_a	K''_c	ν(Hz)	e$_\nu$(Hz)	f$_\nu$(Hz)	O-C(Hz)	Blend	f$_{peak}$(Hz)
31	0	31	30	1	30	265088.590	0.05		-0.046		
32	0	32	31	1	31	273578.418	0.05		-0.130		
33	0	33	32	1	32	282056.262	0.05		-0.005		
34	0	34	33	1	33	290523.800	0.05		-0.075		
35	0	35	34	1	34	298983.042	0.05		-0.023		
37	0	37	36	1	36	315881.125	0.05	*	-0.255		
38	0	38	37	1	37	324322.872	0.05	*	0.397		
41	0	41	40	1	40	349621.583	0.05		0.076		
59	0	59	58	1	58	500935.738	0.05		0.233		
61	0	61	60	1	60	517702.903	0.05		0.159		
13	1	12	12	2	11	65455.917	0.05		-0.032		
14	1	13	13	2	12	77177.746	0.05		0.031		
15	1	14	14	2	13	88991.696	0.05		0.007		
17	1	16	16	2	15	112779.057	0.05		-0.014		
6	1	6	5	0	5	72351.122	0.05		0.000		
7	1	7	6	0	6	79773.253	0.05		0.030		
8	1	8	7	0	7	87059.376	0.05		0.009		
9	1	9	8	0	8	94244.009	0.05		0.004		
10	1	10	9	0	9	101364.150	0.05		0.035		
11	1	11	10	0	10	108457.458	0.05		0.071		
12	1	12	11	0	11	115560.110	0.05		-0.007		
13	1	13	12	0	12	122705.089	0.05		0.024		
14	1	14	13	0	13	129919.653	0.05		0.033		
15	1	15	14	0	14	137224.578	0.05		0.025		
16	1	16	15	0	15	144633.553	0.05		0.022		
17	1	17	16	0	16	152153.368	0.05		-0.036		
24	1	24	23	0	23	207543.826	0.05		0.006		
29	1	29	28	0	28	248902.652	0.05		0.033		
30	1	30	29	0	29	257254.427	0.05		-0.062		
33	1	33	32	0	32	282392.286	0.05		-0.014		
34	1	34	33	0	33	290789.969	0.05		-0.007		
35	1	35	34	0	34	299193.525	0.05		0.018		
36	1	36	35	0	35	307601.675	0.05	*	0.253		
37	1	37	36	0	36	316012.500	0.05		-0.023		
38	1	38	37	0	37	324426.050	0.05		0.216		
39	1	39	38	0	38	332840.610	0.05		0.045		
41	1	41	40	0	40	349671.825	0.05		-0.006		
42	1	42	41	0	41	358087.349	0.05		-0.070		
3	2	1	2	1	2	98397.978	0.05	*	0.688		
4	2	3	3	1	2	105142.541	0.05		0.040		
5	2	3	4	1	4	118160.592	0.05	*	-0.276		
7	2	6	6	1	5	128365.400	0.05		0.005		
8	2	6	7	1	7	150529.492	0.05	*	0.553		
9	2	8	8	1	7	142684.863	0.05	*	0.353		
10	2	9	9	1	8	149510.788	0.05		-0.058		
12	2	11	11	1	10	162540.293	0.05	*	-0.704		
17	2	15	16	1	16	278482.865	0.05	*	0.709		
18	2	16	17	1	17	296201.863	0.05	*	1.354		

Tabla A.5: continued.

J'	K'_a	K'_c	J"	K''_a	K''_c	ν(Hz)	e$_\nu$(Hz)	f$_\nu$(Hz)	O-C(Hz)	Blend	f$_{Peak}$(Hz)
29	2	28	28	1	27	264310.838	0.05		0.025		
30	2	29	29	1	28	271355.388	0.05		0.129		
33	2	32	32	1	31	293500.129	0.05		0.081		
34	2	33	33	1	32	301168.215	0.05		0.087		
36	2	35	35	1	34	316839.697	0.05	*	0.915		
37	2	36	36	1	35	324811.931	0.05		0.040		
38	2	37	37	1	36	332859.244	0.05		0.006		
4	1	3	4	0	4	26097.404	0.05		-0.031		
5	1	4	5	0	5	27406.956	0.05		0.125		
6	1	5	6	0	6	29035.680	0.05		0.085		
7	1	6	7	0	7	31012.870	0.05		0.027		
8	1	7	8	0	8	33370.070	0.05		0.146		
9	1	8	9	0	9	36138.570	0.05		-0.010		
10	1	9	10	0	10	39348.696	0.05		0.083		
13	1	12	13	0	13	51840.860	0.05		-0.019		
14	1	13	14	0	14	56985.650	0.05		0.093		
19	1	18	19	0	19	89163.127	0.05		0.123		
20	1	19	20	0	20	96578.349	0.05		0.128		
21	1	20	21	0	21	104190.566	0.05		0.183		
23	1	22	23	0	23	119779.475	0.05		0.104		
24	1	23	24	0	24	127654.330	0.05		-0.082		
25	1	24	25	0	25	135525.678	0.05	*	-0.804		
26	1	25	26	0	26	143362.743	0.05	*	-0.363		
28	1	27	28	0	28	158841.186	0.05		-0.144		
6	2	4	6	1	5	66377.959	0.05		-0.073		
6	2	5	6	1	6	75916.445	0.05		-0.015		
7	2	6	7	1	7	77627.729	0.05		-0.038		
8	2	7	8	1	8	79591.707	0.05		-0.048		
9	2	8	9	1	9	81810.357	0.05		-0.072		
10	2	9	10	1	10	84285.225	0.05		-0.086		
11	2	10	11	1	11	87017.176	0.05		-0.056		
12	2	11	12	1	12	90006.073	0.05		-0.066		
14	2	12	14	1	13	59249.603	0.05		-0.033		
14	2	13	14	1	14	96749.299	0.05		0.050		
15	2	13	15	1	14	59476.656	0.05		-0.032		
15	2	14	15	1	15	100497.530	0.05		0.048		
16	2	14	16	1	15	60118.423	0.05		-0.061		
16	2	15	16	1	16	104490.640	0.05		0.059		
17	2	15	17	1	16	61212.453	0.05		-0.052		
17	2	16	17	1	17	108722.176	0.05		0.084		
18	2	16	18	1	17	62791.983	0.05		-0.013		
18	2	17	18	1	18	113184.276	0.05		0.101		
19	2	17	19	1	18	64886.126	0.05		-0.045		
19	2	18	19	1	19	117867.935	0.05	*	0.263		
20	2	18	20	1	19	67519.891	0.05		-0.073		
21	2	19	21	1	20	70713.661	0.05	*	0.408		
22	2	20	22	1	21	74479.556	0.05		-0.078		
23	2	21	23	1	22	78824.823	0.05		-0.107		

Tabla A.5: continued.

J'	K'_a	K'_c	J"	K''_a	K''_c	ν(Hz)	e$_\nu$(Hz)	f$_\nu$(Hz)	O-C(Hz)	Blend	f$_{Peak}$(Hz)
24	2	22	24	1	23	83745.573	0.05		-0.148		
25	2	23	25	1	24	89228.066	0.05		-0.136		

Tabla A5. Los parámetros de la cabecera de las columnas para las medida de las transiciones de CH_3CH_2CN ν_{12} es la siguiente: Col. 1-3 y 4-6 se corresponde con los números cuánticos del nivel superior e inferior respectivamente. Col. 7 y 8 es la frecuencia observada y el error en la frecuencia, respectivamente. Col. 9 indica con un $*$ aquellas líneas no ajustadas. Col. 10 se corresponde con la diferencia entre las frecuencias observada y calculada. Col. 11 indica con [Yes] si existe solapamiento con otra especie molecular. Col. 12 muestra el pico de frecuencia media ponderada.

Apéndice B

López et al. 2014, A&A, 572, A44

Tabla B.1: Detected lines of CH_2CHCN g.s. .

Transition $J_{K_a,K_c} - J'_{K'_a,K'_c}$	Predicted frequency (MHz)	S_{ij}	E_u (K)	v_{LSR} km s^{-1}	Δv km s^{-1}	T_{MB} (K)	$\int T_{MB} dv$ (K km s^{-1})
$9_{1,9}$-$8_{1,8}$	83207.507	8.89	22.1	5.0[1]		0.24[2]	
		Wide comp.		3.5±0.4	14±1	0.12	1.8±0.2
		Narrow comp.		5.2±0.3	0.8±0.4	0.12	0.78±0.11
$9_{0,9}$-$8_{0,8}$	84946.003	9.00	20.4	4.4[1]		0.24[2]	
				4.4±0.4	11±1	0.23	2.7±0.2
$9_{2,8}$-$8_{2,7}$	85302.649	8.56	29.1	5.2[1]		0.24[2]	
				5.2±0.3	9.5±0.7	0.22	2.26±0.14
$9_{4,6}$-$8_{4,5}$	85416.746	7.22	55.1	5.3[1]		0.32[2]	
$9_{4,5}$-$8_{4,4}$	85416.797†	7.22	55.1	5.4[1]		”	
				5.45±0.06	7.4±0.3	0.31	2.46±0.08
$9_{5,5}$-$8_{5,4}$	85419.956	6.22	74.5	5.2[1]		0.31[2]	
$9_{5,4}$-$8_{5,3}$	85419.956†	6.22	74.5	5.2[1]		”	
				5.7±0.4	10±1	0.31	3.4±0.4
$9_{3,7}$-$8_{3,6}$	85426.922	8.00	40.0	5.3[1]		0.20[2]	
				5.3±0.4	11±1	0.20	2.4±0.2
$9_{6,4}$-$8_{6,3}$	85431.192	5.00	98.3	6.7[1,3]		0.21[2]	
$9_{6,3}$-$8_{6,2}$	85431.192†	5.00	98.3	6.7[1,3]		”	
				6.9±0.3	8.8±0.8	0.22	2.0±0.2
$9_{3,6}$-$8_{3,5}$	85434.528	8.00	40.0	5.5[1]		0.24[2]	
				5.7±0.3	11.8±0.9	0.22	2.8±0.2
$9_{7,3}$-$8_{7,2}$	85447.698	3.56	126.3	6.3[1]		0.13[2]	
$9_{7,2}$-$8_{7,1}$	85447.698†	3.56	126.3	6.3[1]		”	
$9_{8,1}$-$8_{8,0}$	85468.367	1.89	158.5	5.1[1]		0.05[2]	
$9_{8,2}$-$8_{8,1}$	85468.367†	1.89	158.5	5.1[1]		”	
				5.1±0.5	7±1	0.05	0.39±0.05
$9_{2,7}$-$8_{2,6}$	85715.426	8.56	29.2	5.1[1]		0.23[2]	
		Wide comp.		3.7±0.2	16.4±0.6	0.09	1.62±0.06
		Narrow comp.		5.18±0.07	5.5±0.2	0.14	0.80±0.06
$9_{1,8}$-$8_{1,7}$	87312.818	8.89	23.1	5.0[1]		0.30[2]	
				4.89±0.14	8.6±0.4	0.32	2.96±0.14
$10_{1,10}$-$9_{1,9}$	92426.251	9.90	26.6	5.2[1,4]		0.40[2]	
		Wide comp.		2.9±0.4	16±1	0.21	3.5±0.2

Tabla B.1: continued.

Transition $J_{K_a,K_c} - J'_{K'_a,K'_c}$	Predicted frequency (MHz)	S_{ij}	E_u (K)	v_{LSR} km s^{-1}	Δv km s^{-1}	T_{MB} (K)	$\int T_{MB} dv$ (K km s^{-1})
		Narrow comp.		5.4±0.3	5.2±0.6	0.20	1.1±0.2
$10_{0,10}$-$9_{0,9}$	94276.637	9.99	25.0	4.2[1,5]		0.38[2]	
				4.16±0.15	9.6±0.4	0.38	3.94±0.13
$10_{2,9}$-$9_{2,8}$	94760.783	9.60	33.7	5.6[1]		0.29[2]	
		Wide comp.		4.4±0.5	14±1	0.16	2.4±0.3
		Narrow comp.		5.6±0.3	4±1	0.16	0.8±0.3
$10_{4,7}$-$9_{4,6}$	94913.117	8.40	59.7	3.6[1]		0.79[2]	
$10_{4,6}$-$9_{4,5}$	94913.229†	8.40	59.7	3.9[1]		”	
$10_{5,6}$-$9_{5,5}$	94913.960†	7.50	79.1	6.2[1]		”	
$10_{5,5}$-$9_{5,4}$	94913.961†	7.50	79.1	6.2[1]		”	
		Wide comp.		2.0±0.2	19±1	0.26	5.3±0.2
		Narrow comp.		5.23±0.09	7.3±0.3	0.57	4.4±0.3
$10_{6,5}$-$9_{6,4}$	94925.004	6.40	102.8	5.9[1,6]		0.31[2]	
$10_{6,4}$-$9_{6,3}$	94925.004†	6.40	102.8	5.9[1,6]		”	
$10_{3,8}$-$9_{3,7}$	94928.608	9.10	44.5	5.4[1]		0.41[2]	
				5.4±0.6	9±1	0.39	3.8±0.51
$10_{3,7}$-$9_{3,6}$	94941.632	9.10	44.5	4.1[1]		0.46[2]	
$10_{7,4}$-$9_{7,3}$	94942.491†	5.10	130.8	6.8[1]		”	
$10_{7,3}$-$9_{7,2}$	94942.491†	5.10	130.8	6.8[1]		”	
		Wide comp.		2.9±0.6	15±1	0.17	2.8±0.4
		Narrow comp.		6.1±0.2	7.0±0.7	0.33	2.4±0.5
$10_{8,3}$-$9_{8,2}$	94964.909	3.60	163.1	4.6[1]		0.12[2]	
$10_{8,2}$-$9_{8,1}$	94964.909†	3.60	163.1	4.6[1]		”	
$10_{9,2}$-$9_{9,1}$	94991.513	1.90	199.6	5.3[1]		0.04[2]	
$10_{9,1}$-$9_{9,0}$	94991.513†	1.90	199.6	5.3[1]		”	
				5.3±0.3	7.1±0.7	0.04	0.33±0.03
$10_{2,8}$-$9_{2,7}$	95325.476	9.60	33.8	4.9[1]		0.37[2]	
		Wide comp.		1.4±0.8	22±1	0.12	2.9±0.2
		Narrow comp.		5.1±0.2	6.1±0.4	0.25	1.7±0.2
$10_{1,9}$-$9_{1,8}$	96982.440	9.60	27.8	4.8[1,7]		0.66[2]	
$11_{1,11}$-$10_{1,10}$	101637.233	10.90	31.5	5.1[1]		0.52[2]	
		Wide comp.		3.5±0.5	15±1	0.24	3.8±0.4
		Narrow comp.		5.3±0.2	5.6±0.6	0.30	1.8±0.4
$11_{0,11}$-$10_{0,10}$	103575.398	11.00	29.9	5.1[1]		0.52[2]	
		Wide comp.		2.0±0.5	14.7±0.7	0.19	3.0±0.2
		Narrow comp.		5.36±0.12	5.6±0.3	0.36	2.2±0.2
$11_{2,10}$-$10_{2,9}$	104212.649	10.60	38.7	5.1[1]		0.48[2]	

Tabla B.1: continued.

Transition $J_{K_a,K_c} - J'_{K'_a,K'_c}$	Predicted frequency (MHz)	S_{ij}	E_u (K)	v_{LSR} km s^{-1}	Δv km s^{-1}	T_{MB} (K)	$\int T_{MB} dv$ (K km s^{-1})
		Wide comp.		3.3±0.3	15±1	0.21	3.5±0.2
		Narrow comp.		5.22±0.11	5.2±0.4	0.34	1.8±0.2
$11_{5,7}$-$10_{5,6}$	104408.877	8.73	84.1	2.9[1,8]		3.45[2]	
$11_{5,6}$-$10_{5,5}$	104408.878†	8.73	84.1	2.9[1,8]		”	
$11_{4,8}$-$10_{4,7}$	104411.244†	9.55	64.7	8.3[1,8]		”	
$11_{4,7}$-$10_{4,6}$	104411.467†	9.55	64.7	7.6[1,8]		”	
$11_{6,6}$-$10_{6,5}$	104419.274	7.73	107.8	4.0[1,9]		0.54[2]	
$11_{6,5}$-$10_{6,4}$	104419.274†	7.73	107.8	4.0[1,9]		”	
$11_{3,9}$-$10_{3,8}$	104432.782	10.20	49.5	5.1[1]		0.49[2]	
$11_{7,5}$-$10_{7,4}$	104437.474	6.55	135.8	5.1[1]		0.44[2]	
$11_{7,4}$-$10_{7,3}$	104437.474†	6.55	135.8	5.1[1]		”	
$11_{3,8}$-$10_{3,7}$	104453.916	10.20	49.5	5.9[1,10]		0.56[2]	
$11_{8,3}$-$10_{8,2}$	104461.467	5.18	168.1	4.6[1]		0.24[2]	
$11_{8,4}$-$10_{8,3}$	104461.467†	5.18	168.1	4.6[1]		”	
$11_{9,3}$-$10_{9,2}$	104490.310	3.64	204.6	5.5[1]		0.14[2]	
$11_{9,2}$-$10_{9,1}$	104490.310†	3.64	204.6	5.5[1]		”	
$11_{10,1}$-$10_{10,0}$	104523.501	19.10	245.3	4.9[1,11]		0.07[2]	
$11_{10,2}$-$10_{10,1}$	104523.501†	19.10	245.3	4.9[1,11]		”	
$11_{2,9}$-$10_{2,8}$	104960.542	10.60	38.8	5.0[1]		0.51[2]	
		Wide comp.		2.4±0.3	17±1	0.25	4.5±0.3
		Narrow comp.		5.1±0.2	5.5±0.6	0.33	2.0±0.3
$11_{1,10}$-$10_{1,9}$	106641.391	10.90	32.9	4.9[1]		0.64[2]	
$12_{1,12}$-$11_{1,11}$	110839.977	11.90	36.8	5.0[1]		0.66[2]	
		Wide comp.		2.4±0.3	17±1	0.26	4.0±0.4
		Narrow comp.		5.1±0.2	5.5±0.6	0.42	2.5±0.4
$12_{0,12}$-$11_{0,11}$	112840.646	12.00	35.3	5.6[1]		0.42[2]	
		Wide comp.		4.2±0.3	17.1±1	0.27	4.9±0.1
		Narrow comp.		5.7±0.2	4.6±0.3	0.19	0.95±0.01
$12_{2,11}$-$11_{2,10}$	113657.637	11.70	44.1	5.3[1]		0.36[2]	
$12_{5,8}$-$11_{5,7}$	113904.796	9.92	89.6	4.9[1]		0.83[2]	
$12_{5,7}$-$11_{5,6}$	113904.799†	9.92	89.6	4.9[1]		”	
$12_{4,9}$-$11_{4,8}$	113911.289	10.70	70.1	0.7[1,12]		1.18[2]	
$12_{4,8}$-$11_{4,7}$	113911.706†	10.70	70.1	0.4[1,12]		”	
$12_{6,7}$-$11_{6,6}$	113914.047†	9.00	113.3	6.6[1,12]		”	
$12_{6,6}$-$11_{6,5}$	113914.047†	9.00	113.3	6.6[1,12]		”	
$12_{7,6}$-$11_{7,5}$	113932.664	7.92	141.3	4.6[1]		0.49[2]	
$12_{7,5}$-$11_{7,4}$	113932.664†	7.92	141.3	4.6[1]		”	

Tabla B.1: continued.

Transition $J_{K_a,K_c} - J'_{K'_a,K'_c}$	Predicted frequency (MHz)	S_{ij}	E_u (K)	v_{LSR} km s^{-1}	Δv km s^{-1}	T_{MB} (K)	$\int T_{MB} dv$ (K km s^{-1})
$12_{3,10}$-$11_{3,9}$	113939.399	11.20	55.0	5.3[(1)]		0.60[(2)]	
$12_{8,5}$-$11_{8,4}$	113958.043	6.67	173.6	4.8[(1)]		0.39[(2)]	
$12_{8,4}$-$11_{8,3}$	113958.043†	6.67	173.6	4.8[(1)]		”	
$12_{3,9}$-$11_{3,8}$	113972.216	11.20	55.0	4.3[(1)]		0.76[(2)]	
$12_{9,4}$-$11_{9,3}$	113988.965	5.25	210.1	5.0[(1)]		0.26[(2)]	
$12_{9,3}$-$11_{9,2}$	113988.965†	5.25	210.1	5.0[(1)]		”	
$12_{10,2}$-$11_{10,1}$	114024.785	3.67	250.8	4.7[(1)]		0.13[(2)]	
$12_{10,3}$-$11_{10,2}$	114024.785†	3.67	250.8	4.7[(1)]		”	
$12_{11,2}$-$11_{11,1}$	114065.125	1.92	295.7	[(5,13)]		...	
$12_{11,1}$-$11_{11,0}$	114065.125†	1.92	295.7	[(5,13)]		...	
$12_{2,10}$-$11_{2,9}$	114621.568	11.70	44.3	5.4[(1)]		0.59[(2)]	
		Wide comp.		5.4±0.2	12.7±0.9	0.38	5.1±0.3
		Narrow comp.		5.41±0.06	2.6±0.2	0.34	0.96±0.12
$14_{0,14}$-$13_{0,13}$	131267.475	14.00	47.5	2.5[(1)]		2.08[(2)]	
$14_{2,13}$-$13_{2,12}$	132524.586	13.70	56.4	[(14)]		...	
$14_{5,10}$-$13_{5,9}$	132900.001	12.20	101.9	5.7[(1)]		1.18[(2)]	
$14_{5,9}$-$13_{5,8}$	132900.012†	12.20	101.9	5.8[(1)]		”	
				6.1±0.5	7.8±0.9	1.02	8.4±0.9
$14_{6,9}$-$13_{6,8}$	132905.283	11.40	125.6	5.1[(1)]		1.02[(2)]	
$14_{6,8}$-$13_{6,7}$	132905.283†	11.40	125.6	5.1[(1)]		”	
$14_{4,11}$-$13_{4,10}$	132917.744	12.90	82.4	5.7[(1,15)]		3.96[(2)]	
$14_{4,10}$-$13_{4,9}$	132919.000†	12.90	82.4	5.7[(1,15)]		”	
$14_{7,8}$-$13_{7,7}$	132923.742†	10.50	153.6	5.7[(1,15)]		”	
$14_{7,7}$-$13_{7,6}$	132923.742†	10.50	153.6	5.7[(1,15)]		”	
$14_{8,7}$-$13_{8,6}$	132951.255	9.43	185.9	4.9[(1)]		0.51[(2)]	
$14_{8,6}$-$13_{8,5}$	132951.255†	9.43	185.9	4.9[(1)]		”	
				4.9±0.2	6.1±0.4	0.40	2.6±0.2
$14_{3,12}$-$13_{3,11}$	132959.413	13.40	67.3	5.1[(1)]		0.68[(2)]	
		Wide comp.		3.8±0.4	19±1	0.29	6.0±0.3
		Narrow comp.		5.15±0.11	4.7±0.4	0.44	2.2±0.2
$14_{9,6}$-$13_{9,5}$	132985.900	8.21	222.4	5.0[(1)]		0.38[(2)]	
$14_{9,5}$-$13_{9,4}$	132985.900†	8.21	222.4	5.0[(1)]		”	
				4.9±0.3	7.6±0.7	0.36	2.9±0.2
$14_{10,4}$-$13_{10,3}$	133026.666	6.86	263.1	5.9[(1,16)]		0.42[(2)]	
$14_{10,5}$-$13_{10,4}$	133026.666†	6.86	263.1	5.9[(1,16)]		”	
$14_{3,11}$-$13_{3,10}$	133030.668	13.40	67.3	4.8[(1)]		0.77[(2)]	
				4.8±0.3	8.9±0.6	0.73	6.9±0.4

Tabla B.1: continued.

Transition $J_{K_a,K_c} - J'_{K'_a,K'_c}$	Predicted frequency (MHz)	S_{ij}	E_u (K)	v_{LSR} km s^{-1}	Δv km s^{-1}	T_{MB} (K)	$\int T_{MB} dv$ (K km s^{-1})
$14_{11,4}$-$13_{11,3}$	133072.968	5.36	308.0	4.4[1,13]		0.28[2]	
$14_{11,3}$-$13_{11,2}$	133072.968†	5.36	308.0	4.4[1,13]		”	
$14_{12,2}$-$13_{12,1}$	133124.438	3.71	357.0	[12,13]		...	
$14_{12,3}$-$13_{12,2}$	133124.438†	3.71	357.0	[12,13]		...	
$14_{13,2}$-$13_{13,1}$	133180.824	1.93	410.2	[15]		...	
$14_{13,1}$-$13_{13,0}$	133180.824†	1.93	410.2	[15]		...	
$14_{2,12}$-$13_{2,11}$	134021.823	13.70	56.7	6.0[1]		0.85[2]	
				6.2±0.5	8±1	0.80	7.1±0.7
$14_{1,13}$-$13_{1,12}$	135539.953	13.90	51.0	8.2[1,15]		2.80[2]	
$15_{1,15}$-$14_{1,14}$	138395.146	14.90	55.4	4.2[1]		0.95[2]	
				4.2±0.2	11.1±0.7	0.92	10.9 ±0.6
$15_{0,15}$-$14_{0,14}$	140429.436	15.00	54.2	4.9[1]		0.94[2]	
		Wide comp.		3.1±0.2	17.2±0.9	0.45	8.2±0.3
		Narrow comp.		5.12±0.15	5.8±0.4	0.51	3.2±0.4
$15_{2,14}$-$14_{2,13}$	141947.301	14.70	63.2	4.9[1]		1.24[2]	
		Wide comp.		1.8±0.6	16±2	0.67	8.2±0.3
		Narrow comp.		5.3±0.3	6.0±0.5	0.64	3.2±0.4
$15_{5,11}$-$14_{5,10}$	142399.465	13.30	108.7	1.6[1,14]		2.00[2]	
$15_{5,10}$-$14_{5,9}$	142399.486†	13.30	108.7	1.5[1,14]		”	
$15_{6,10}$-$14_{6,9}$	142401.835†	12.60	132.4	3.4[1,14]		”	
$15_{6,9}$-$14_{6,8}$	142401.835†	12.60	132.4	3.4[1,14]		”	
$15_{7,9}$-$14_{7,8}$	142419.665	11.70	160.5	4.9[1]		1.04[2]	
$15_{7,8}$-$14_{7,7}$	142419.665†	11.70	160.5	4.9[1]		”	
$15_{4,12}$-$14_{4,11}$	142424.437	13.90	89.3	2.7[1]		1.47[2]	
$15_{4,11}$-$14_{4,10}$	142426.489†	13.90	89.3	7.1[1]		”	
$15_{8,8}$-$14_{8,7}$	142447.892	10.70	192.7	5.1[1]		0.84[2]	
$15_{8,7}$-$14_{8,6}$	142447.892†	10.70	192.7	5.1[1]		”	
				5.0±0.3	8±1	0.80	7.2±0.8
$15_{3,13}$-$14_{3,12}$	142472.339	14.40	74.2	5.3[1]		1.05[2]	
$15_{9,6}$-$14_{9,5}$	142484.158	9.60	229.2	5.1[1]		0.57[2]	
$15_{9,7}$-$14_{9,6}$	142484.158†	9.60	229.2	5.1[1]		”	
				5.0±0.3	8±1	0.53	4.3±0.3
$15_{10,6}$-$14_{10,5}$	142527.225	8.33	269.9	5.2[1]		0.47[2]	
$15_{10,5}$-$14_{10,4}$	142527.225†	8.33	269.9	5.2[1]		”	
$15_{3,12}$-$14_{3,11}$	142572.959	14.40	74.2	5.2[1]		1.06[2]	
$15_{11,5}$-$14_{11,4}$	142576.381†	6.93	314.8	5.5[1]		”	
$15_{11,4}$-$14_{11,3}$	142576.381†	6.93	314.8	5.5[1]		”	

Tabla B.1: continued.

Transition $J_{K_a,K_c} - J'_{K'_a,K'_c}$	Predicted frequency (MHz)	S_{ij}	E_u (K)	v_{LSR} km s^{-1}	Δv km s^{-1}	T_{MB} (K)	$\int T_{MB} dv$ (K km s^{-1})
		Wide comp.		2.0±0.5	15±1	0.69	10.9±0.8
		Narrow comp.		5.6±0.3	4.4±0.6	0.48	2.2±0.6
$15_{12,3}$-$14_{12,2}$	142631.178	5.40	363.9	5.8[1,17]		0.29[2]	
$15_{12,4}$-$14_{12,3}$	142631.178†	5.40	363.9	5.8[1,17]		”	
$15_{13,3}$-$14_{13,2}$	142691.318	3.73	417.0	[11,18]		...	
$15_{13,2}$-$14_{13,1}$	142691.318†	3.73	417.0	[11,18]		...	
$15_{14,1}$-$14_{14,0}$	142756.580	1.93	474.3	[14]		...	
$15_{14,2}$-$14_{14,1}$	142756.580†	1.93	474.3	[14]		...	
$15_{2,13}$-$14_{2,12}$	143759.241	14.70	63.6	5.3[1]		1.37[2]	
				4.6±0.3	9±1	1.31	13.1±1.1
$15_{1,14}$-$14_{1,13}$	145141.495	14.90	58.0	5.5[1]		1.27[2]	
				5.1±0.7	15±2	1.18	19.4±1.9
$16_{1,16}$-$15_{1,15}$	147561.704	15.90	62.5	5.1[1]		1.08[2]	
		Wide comp.		2.8±0.5	18±2	0.56	10.9±0.4
		Narrow comp.		5.2±0.1	4.9±0.4	0.56	2.9±0.4
$16_{0,16}$-$15_{0,15}$	149558.700	16.00	61.4	4.6[1]		1.33[2]	
				4.6±0.2	11.0±0.7	1.18	13.8±0.6
$16_{2,15}$-$15_{2,14}$	151356.950	15.70	70.5	4.4[1]		1.30[2]	
				5.0±0.3	9.9±0.8	1.15	12.2±1.0
$16_{6,11}$-$15_{6,10}$	151899.067	13.80	139.7	3.4[1]		2.54[2]	
$16_{6,10}$-$15_{6,9}$	151899.068†	13.80	139.7	3.4[1]		”	
$16_{5,12}$-$15_{5,11}$	151900.287†	14.40	116.0	5.8[1]		”	
$16_{5,11}$-$15_{5,10}$	151900.325†	14.40	116.0	5.9[1]		”	
		Wide comp.		2.8±0.4	22.8±1.5	0.92	22.3±1.1
		Narrow comp.		5.2±0.1	6.8±0.4	1.65	12.0±1.3
$16_{7,10}$-$15_{7,9}$	151915.867	12.90	167.7	4.7[1,4]		1.39[2]	
$16_{7,9}$-$15_{7,8}$	151915.867†	12.90	167.7	4.7[1,4]		”	
				3.4±0.2	11.2±0.7	1.32	15.8±2.0
$16_{4,13}$-$15_{4,12}$	151933.610	15.00	96.6	5.2[1]		1.32[2]	
$16_{4,12}$-$15_{4,11}$	151936.853	15.00	96.6	5.6[1,15]		1.86[2]	
$16_{8,9}$-$15_{8,8}$	151944.551	12.00	200.0	4.6[1]		1.17[2]	
$16_{8,8}$-$15_{8,7}$	151944.551†	12.00	200.0	4.6[1]		”	
				4.5±0.4	8±1	1.16	9.4±1.3
$16_{9,8}$-$15_{9,7}$	151982.261	10.90	236.5	5.4[1]		0.78[2]	
$16_{9,7}$-$15_{9,6}$	151982.261†	10.90	236.5	5.4[1]		”	
$16_{3,14}$-$15_{3,13}$	151986.766	15.40	81.4	6.4[1,15]		1.55[2]	
$16_{10,7}$-$15_{10,6}$	152027.504	9.75	277.2	5.2[1]		0.42[2]	

Tabla B.1: continued.

Transition $J_{K_a,K_c} - J'_{K'_a,K'_c}$	Predicted frequency (MHz)	S_{ij}	E_u (K)	v_{LSR} km s^{-1}	Δv km s^{-1}	T_{MB} (K)	$\int T_{MB} dv$ (K km s^{-1})
$16_{10,6}$-$15_{10,5}$	152027.504†	9.75	277.2	5.2[1]		”	
		Wide comp.		4.6±0.3	13.7±0.6	0.30	4.3±0.2
		Narrow comp.		5.4±0.2	3.4±2.9	0.21	0.77±0.08
$16_{11,6}$-$15_{11,5}$	152079.419	8.44	322.1	6.1[1,15]		0.52[2]	
$16_{11,5}$-$15_{11,4}$	152079.419†	8.44	322.1	6.1[1,15]		”	
$16_{3,13}$-$15_{3,12}$	152125.551	15.40	81.5	4.3[1]		0.76[2]	
				4.3±0.6	8±2	0.71	5.8±1.0
$16_{12,4}$-$15_{12,3}$	152137.474	7.00	371.2	[19]		...	
$16_{12,5}$-$15_{12,4}$	152137.474†	7.00	371.2	[19]		...	
$16_{13,4}$-$15_{13,3}$	152201.310	5.44	424.3	7.7[1]		0.10[2]	
$16_{13,3}$-$15_{13,2}$	152201.310†	5.44	424.3	7.7[1]		”	
$16_{14,2}$-$15_{14,1}$	152270.670	3.75	481.6	7.6[1,20]		0.19[2]	
$16_{14,3}$-$15_{14,2}$	152270.670†	3.75	481.6	7.6[1,20]		”	
$16_{2,14}$-$15_{2,13}$	153518.939	15.70	71.0	7.9[1,15]		5.21[2]	
$16_{1,15}$-$15_{1,14}$	154724.532	15.90	65.4	4.4[1]		1.49[2]	
		Wide comp.		2.6±0.4	20±2	0.51	10.80±0.09
		Narrow comp.		4.52±0.15	7.0±0.3	0.71	7.7±0.5
$17_{1,17}$-$16_{1,16}$	156718.805	16.90	70.0	5.2[1]		1.78[2]	
		Wide comp.		2.4±0.2	16.2±5	1.01	17.3±0.5
		Narrow comp.		5.42±0.10	4.6±0.3	1.42	4.3±0.4
$17_{0,17}$-$16_{0,16}$	158657.430	17.00	69.0	5.2[1]		1.58[2]	
		Wide comp.		3.69±0.11	15.8±0.3	0.81	13.7±0.2
		Narrow comp.		5.31±0.05	4.76±0.15	1.15	4.1±0.2
$17_{2,16}$-$16_{2,15}$	160758.759	16.80	78.2	2.5[1,14,21]		2.86[2]	
$17_{6,12}$-$16_{6,11}$	161397.025	14.90	147.5	3.9[1,22]		3.35[2]	
$17_{6,11}$-$16_{6,10}$	161397.026†	14.90	147.5	3.9[1,22]		”	
$17_{5,13}$-$16_{5,12}$	161402.555	15.50	123.7	4.7[1,12,19]		4.02[2]	
$17_{5,12}$-$16_{5,11}$	161402.622†	15.50	123.7	4.8[1,12,19]		”	
$17_{7,11}$-$16_{7,10}$	161412.366	14.10	175.5	1.7[1,15]		4.33[2]	
$17_{7,10}$-$16_{7,9}$	161412.366†	14.10	175.5	1.7[1,15]		”	
$17_{8,10}$-$16_{8,9}$	161441.232	13.20	207.8	2.0[1]		2.84[2]	
$17_{8,9}$-$16_{8,8}$	161441.232†	13.20	207.8	2.0[1]		”	
$17_{4,14}$-$16_{4,13}$	161445.370†	16.10	104.3	5.7[1]		”	
$17_{4,13}$-$16_{4,12}$	161450.349	16.10	104.3	4.9[1,12,19,23]		3.57[2]	
$17_{9,8}$-$16_{9,7}$	161480.200	12.20	244.3	[12,19]		...	
$17_{9,9}$-$16_{9,8}$	161480.200†	12.20	244.3	[12,19]		...	
$17_{3,15}$-$16_{3,14}$	161502.266	16.50	89.2	4.6[1,12,19]		2.44[2]	

Tabla B.1: continued.

Transition $J_{K_a,K_c} - J'_{K'_a,K'_c}$	Predicted frequency (MHz)	S_{ij}	E_u (K)	v_{LSR} km s^{-1}	Δv km s^{-1}	T_{MB} (K)	$\int T_{MB} dv$ (K km s^{-1})
$17_{10,7}$-$16_{10,6}$	161527.483	11.10	285.0	5.8[1]		1.05[2]	
$17_{10,8}$-$16_{10,7}$	161527.483†	11.10	285.0	5.8[1]		”	
$17_{11,6}$-$16_{11,5}$	161582.059	9.88	329.9	[12,19]		...	
$17_{11,7}$-$16_{11,6}$	161582.059†	9.88	329.9	[12,19]		...	
$17_{12,5}$-$16_{12,4}$	161643.294	8.53	378.9	6.7[1,15,22]		1.04[2]	
$17_{12,6}$-$16_{12,5}$	161643.294†	8.53	378.9	6.7[1,15,22]		”	
$17_{3,14}$-$16_{3,13}$	161689.756	16.50	89.2	5.8[1]		2.42[2]	
$17_{13,5}$-$16_{13,4}$	161710.767	7.06	432.1	[19]		...	
$17_{13,4}$-$16_{13,3}$	161710.767†	7.06	432.1	[19]		...	
$17_{14,3}$-$16_{14,2}$	161784.177	5.47	489.3	[10,15]		...	
$17_{14,4}$-$16_{14,3}$	161784.177†	5.47	489.3	[10,15]		...	
$17_{15,3}$-$16_{15,2}$	161863.300	3.76	550.6	[12,24]		...	
$17_{15,2}$-$16_{15,1}$	161863.300†	3.76	550.6	[12,24]		...	
$17_{16,1}$-$16_{16,0}$	161947.954	1.94	615.9	[12]		...	
$17_{16,2}$-$16_{16,1}$	161947.954†	1.94	615.9	[12]		...	
$17_{2,15}$-$16_{2,14}$	163298.003	16.80	78.8	4.72[1]		1.67[2]	
		Wide comp.		1.5±0.6	23±2	0.49	11.7±0.7
		Narrow comp.		4.87±0.11	6.4±0.3	0.68	8.3±0.6
$17_{1,16}$-$16_{1,15}$	164287.213	16.90	73.3	4.9[1]		1.15[2]	
				4.3±0.4	14±1	1.05	15.7±1.1
$18_{1,18}$-$17_{1,17}$	165866.442	17.90	77.9	4.8[1]		1.67[2]	
		Wide comp.		0.6±0.4	14.2±0.7	0.58	8.7±0.5
		Narrow comp.		5.09±0.09	5.8±0.2	1.12	7.0±0.4
$18_{0,18}$-$17_{0,17}$	167728.433	18.00	77.1	4.4[1]		1.89[2]	
		Wide comp.		3.8±0.6	30±2	0.77	24.5±1.1
		Narrow comp.		4.44±0.14	5.8±0.4	1.18	7.2±0.7
$18_{2,17}$-$17_{2,16}$	170150.275	17.80	86.4	4.9[1]		1.49[2]	
$18_{6,13}$-$17_{6,12}$	170895.752	16.00	155.7	5.2[1]		1.80[2]	
$18_{6,12}$-$17_{6,11}$	170895.752†	16.00	155.7	5.2[1]		”	
$18_{5,14}$-$17_{5,13}$	170906.356	16.60	131.9	5.2[1]		2.29[2]	
$18_{5,13}$-$17_{5,12}$	170906.470†	16.60	131.9	5.4[1]		”	
$18_{7,12}$-$17_{7,11}$	170909.180†	15.30	183.7	6.5[1]		”	
$18_{7,11}$-$17_{7,10}$	170909.180†	15.30	183.7	6.5[1]		”	
$18_{8,11}$-$17_{8,10}$	170937.936	14.40	216.0	5.2[1]		1.06[2]	
$18_{8,10}$-$17_{8,9}$	170937.936†	14.40	216.0	5.2[1]		”	
		Wide comp.		3.1±0.4	11.3±0.9	0.60	7.2±0.6
		Narrow comp.		5.4±0.2	3.8±0.6	0.61	2.4±0.6

Tabla B.1: continued.

Transition $J_{K_a,K_c} - J'_{K'_a,K'_c}$	Predicted frequency (MHz)	S_{ij}	E_u (K)	v_{LSR} km s^{-1}	Δv km s^{-1}	T_{MB} (K)	$\int T_{MB} dv$ (K km s^{-1})
$18_{4,15}$-$17_{4,14}$	170959.809	17.10	112.5	5.5[1]		1.25[2]	
		Wide comp.		4.7±0.4	9.34±0.9	0.94	9.3±0.8
		Narrow comp.		5.8±0.4	3.0±0.6	0.36	1.1±0.9
$18_{4,14}$-$17_{8,13}$	170967.260	17.10	112.5	5.7[1]		1.25[2]	
		Wide comp.		4.2±0.2	11.9±0.7	1.00	12.7±0.5
		Narrow comp.		5.87±0.10	2.1±0.9	0.43	0.9±0.2
$18_{9,9}$-$17_{9,8}$	170977.963	13.50	252.5	5.1[1]		0.83[2]	
$18_{9,10}$-$17_{9,9}$	170977.963†	13.50	252.5	5.1[1]		”	
		Wide comp.		5.2±0.6	20±3	0.43	9.0±0.5
		Narrow comp.		5.1±0.3	5.0±0.6	0.44	2.3±0.4
$18_{3,16}$-$17_{3,15}$	171018.334	17.50	97.4	5.1[1]		1.33[2]	
		Wide comp.		2.3±0.4	19.2±0.4	0.57	11.67±0.05
		Narrow comp.		5.27±0.12	4.9±0.2	0.80	4.16±0.13
$18_{10,8}$-$17_{10,7}$	171027.145	12.40	293.2	5.8[1,15,20]		1.03[2]	
$18_{10,9}$-$17_{10,8}$	171027.145†	12.40	293.2	5.8[1,15,20]		”	
$18_{11,7}$-$17_{11,6}$	171084.275	11.30	338.1	5.5[1]		0.61[2]	
$18_{11,8}$-$17_{11,7}$	171084.275†	11.30	338.1	5.5[1]		”	
$18_{12,6}$-$17_{12,5}$	171148.610	10.00	387.1	5.4[1]		0.41[2]	
$18_{12,7}$-$17_{12,6}$	171148.610†	10.00	387.1	5.4[1]		”	
				5.34±0.14	6.7±0.4	0.37	1.80±0.13
$18_{13,6}$-$17_{13,5}$	171219.655	8.61	440.3	6.1[1]		0.30[2]	
$18_{13,5}$-$17_{13,4}$	171219.655†	8.61	440.3	6.1[1]		”	
$18_{3,15}$-$17_{3,14}$	171266.971	17.50	97.4	4.7[1]		1.73[2]	
$18_{14,4}$-$17_{14,3}$	171297.064	7.11	497.6	[25]		0.59[2]	
$18_{14,5}$-$17_{14,4}$	171297.064†	7.11	497.6	[25]		”	
$18_{2,16}$-$17_{2,15}$	173092.853	17.80	87.1	4.3[1,14]		3.22[2]	
$18_{1,17}$-$17_{1,16}$	173827.600	17.90	87.1	4.8[1]		2.04[2]	
				4.88±0.15	8.9±0.4	1.96	18.6±0.6
$19_{1,19}$-$18_{1,18}$	175004.679	18.90	86.3	5.2[1,26]		2.82[2]	
$19_{0,19}$-$18_{0,18}$	176774.998	19.00	85.6	4.9[1]		2.66[2]	
		Wide comp.		2.6±0.7	29±2	0.74	23.1±1.3
		Narrow comp.		4.91±0.12	5.7±0.4	1.96	11.9±1.0
$21_{2,20}$-$20_{2,19}$	198258.130	20.80	113.6	2.7[1,12]		6.30[2]	
$21_{6,16}$-$20_{6,15}$	199396.979	19.30	183.0	4.7[1]		2.25[2]	
$21_{6,15}$-$20_{6,14}$	199396.985†	19.30	183.0	4.7[1]		”	
$21_{7,15}$-$20_{7,14}$	199401.677	18.70	211.0	5.1[1]		2.45[2]	
$21_{7,14}$-$20_{7,13}$	199401.677†	18.70	211.0	5.1[1]		”	

Tabla B.1: continued.

Transition $J_{K_a,K_c} - J'_{K'_a,K'_c}$	Predicted frequency (MHz)	S_{ij}	E_u (K)	v_{LSR} km s^{-1}	Δv km s^{-1}	T_{MB} (K)	$\int T_{MB} dv$ (K km s^{-1})
$21_{5,17}$-$20_{5,16}$	199427.807	19.80	159.3	4.3[1]		3.12[2]	
$21_{8,14}$-$20_{8,13}$	199428.187†	18.00	243.3	4.8[1]		”	
$21_{8,13}$-$20_{8,12}$	199428.187†	18.00	243.3	4.8[1]		”	
$21_{5,16}$-$20_{5,15}$	199428.271†	19.80	159.3	5.0[1]		”	
		Wide comp.		6.9±0.6	28±1	0.84	25.2±0.9
		Narrow comp.		4.61±0.09	6±2	2.34	16.9±0.3
$21_{9,12}$-$20_{9,11}$	199470.082	17.10	279.8	5.4[1]		1.43[2]	
$21_{9,13}$-$20_{9,12}$	199470.082†	17.10	279.8	5.4[1]		”	
		Wide comp.		6.5±0.8	16±2	0.48	8.1±1.2
		Narrow comp.		5.3±0.3	5.9±0.5	0.94	5.9±0.4
$21_{4,18}$-$20_{4,17}$	199519.754	20.20	139.9	5.1[1]		1.78[2]	
$21_{10,11}$-$20_{10,10}$	199524.026†	16.20	320.6	5.9[1]		1.45[2]	
$21_{10,12}$-$20_{10,11}$	199524.026†	16.20	320.6	5.9[1]		”	
$21_{4,17}$-$20_{4,16}$	199541.735	20.20	139.9	4.49[1]		1.57[2]	
				4.8±0.5	7±1	1.61	12.3±1.8
$21_{3,19}$-$20_{3,18}$	199563.913	20.60	124.8	3.0[1,12]		2.15[2]	
$21_{11,10}$-$20_{11,9}$	199588.127	15.20	365.5	4.4[1,27]		1.11[2]	
$21_{11,11}$-$20_{11,10}$	199588.127†	15.20	365.5	4.4[1,27]		”	
$21_{12,9}$-$20_{12,8}$	199661.227	14.10	414.5	[28]		...	
$21_{12,10}$-$20_{12,9}$	199661.227†	14.10	414.5	[28]		...	
$21_{13,9}$-$20_{13,8}$	199742.571	13.00	467.7	5.6[1]		0.31[2]	
$21_{13,8}$-$20_{13,7}$	199742.571†	13.00	467.7	5.6[1]		”	
				5.1±0.11	4.9±0.2	0.30	1.60±0.08
$21_{14,7}$-$20_{14,6}$	199831.637	11.70	525.0	3.3[1]		0.17[2]	
$21_{14,8}$-$20_{14,7}$	199831.637†	11.70	525.0	3.3[1]		”	
				3.2±0.3	6.0±0.8	0.17	1.11±0.12
$21_{15,7}$-$20_{15,6}$	199928.042	10.30	586.3	[14]		...	
$21_{15,6}$-$20_{15,5}$	199928.042†	10.30	586.3	[14]		...	
$21_{16,5}$-$20_{16,4}$	200031.489	8.81	651.6	8.9[1,24]		0.26[2]	
$21_{16,6}$-$20_{16,5}$	200031.489†	8.81	651.6	8.9[1,24]		”	
$21_{3,18}$-$20_{3,17}$	200091.591	20.60	124.9	4.4[1]		1.28[2]	
				4.8±0.5	4.6±0.3	1.25	12.3±1.8
$21_{17,5}$-$20_{17,4}$	200141.740	7.24	720.9	[29]		...	
$21_{17,4}$-$20_{17,3}$	200141.740†	7.24	720.9	[29]		...	
$21_{18,3}$-$20_{18,2}$	200258.593	5.57	794.1	[30]		...	
$21_{18,4}$-$20_{18,3}$	200258.593†	5.57	794.1	[30]		...	
$21_{19,3}$-$20_{19,2}$	200381.872	3.81	871.2	[18]		...	

Tabla B.1: continued.

Transition $J_{K_a,K_c} - J'_{K'_a,K'_c}$	Predicted frequency (MHz)	S_{ij}	E_u (K)	v_{LSR} km s^{-1}	Δv km s^{-1}	T_{MB} (K)	$\int T_{MB} dv$ (K km s^{-1})
$21_{19,2}$-$20_{19,1}$	200381.872†	3.81	871.2	[18]		...	
$21_{1,20}$-$20_{1,19}$	202294.697	20.90	109.4	8.9[1,12,31]		8.05[2]	
$21_{1,22}$-$20_{1,21}$	202364.585	21.90	114.2	[15,31]		...	
$21_{2,19}$-$20_{2,18}$	202529.816	20.80	114.9	5.1[1,19]		2.00[2]	
$22_{0,22}$-$21_{0,21}$	203804.119	22.00	113.6	4.5[1]		1.34[2]	
$22_{2,21}$-$21_{2,20}$	207603.687	21.80	123.5	5.0[1]		1.44[2]	
		Wide comp.		2.1±0.5	14.1±0.9	0.56	8.4±0.8
		Narrow comp.		5.16±0.10	5.1±0.3	0.96	5.2±0.5
$22_{6,17}$-$21_{6,16}$	208899.214	20.40	193.0	4.5[1]		3.54[2]	
$22_{6,16}$-$21_{6,15}$	208899.224†	20.40	193.0	4.5[1]		”	
$22_{7,16}$-$21_{7,15}$	208899.917†	19.80	221.1	5.5[1]		”	
$22_{7,15}$-$21_{7,14}$	208899.917†	19.80	221.1	5.5[1]		”	
$22_{8,15}$-$21_{8,14}$	208924.983	19.10	253.3	4.7[1]		1.76[2]	
$22_{8,14}$-$21_{8,13}$	208924.983†	19.10	253.3	4.7[1]		”	
				4.6±0.3	8.2±0.7	1.66	14.4±1.0
$22_{5,18}$-$21_{5,17}$	208938.580	20.90	169.3	4.2[1]		2.84[2]	
$22_{5,17}$-$21_{5,16}$	208939.288†	20.90	169.3	5.2[1]		”	
		Wide comp.		4.3±0.4	28±1	0.86	25.8±0.9
		Narrow comp.		4.72±0.06	6.68±0.11	2.06	14.64±0.12
$22_{9,14}$-$21_{9,13}$	208967.027	18.30	289.9	5.0[1]		1.82[2]	
$22_{9,13}$-$21_{9,12}$	208967.027†	18.30	289.9	5.0[1]		”	
$22_{10,13}$-$21_{10,12}$	209022.220	17.50	330.6	6.5[1,15]		2.53[2]	
$22_{10,12}$-$21_{10,11}$	209022.220†	17.50	330.6	6.5[1,15]		”	
$22_{4,19}$-$21_{4,18}$	209045.330	21.30	149.9	5.3[1]		1.81[2]	
$22_{4,18}$-$21_{4,17}$	209075.744	21.30	149.9	4.2[1]		3.06[2]	
$22_{3,20}$-$21_{3,19}$	209075.924†	21.60	134.8	4.5[1]		”	
				4.5±0.2	8.3±0.7	2.90	25.73±3.2
$22_{11,11}$-$21_{11,10}$	209088.393	16.50	375.5	5.6[1]		0.82[2]	
$22_{11,12}$-$21_{11,11}$	209088.393†	16.50	375.5	5.6[1]		”	
				5.5±0.2	6.6±0.6	0.71	5.0±0.5
$22_{12,11}$-$21_{12,10}$	209164.223	15.50	424.6	5.4[1]		0.68[2]	
$22_{12,10}$-$21_{12,9}$	209164.223†	15.50	424.6	5.4[1]		”	
				5±2	7±2	0.68	5.3±0.6
$22_{13,9}$-$21_{13,8}$	209248.848	14.30	477.7	[15,29]		...	
$22_{13,10}$-$21_{13,9}$	209248.848†	14.30	477.7	[15,29]		...	
$22_{14,8}$-$21_{14,7}$	209341.677	13.10	535.0	5.3[1]		0.33[2]	
$22_{14,9}$-$21_{14,8}$	209341.677†	13.10	535.0	5.3[1]		”	

Tabla B.1: continued.

Transition $J_{K_a,K_c} - J'_{K'_a,K'_c}$	Predicted frequency (MHz)	S_{ij}	E_u (K)	v_{LSR} km s^{-1}	Δv km s^{-1}	T_{MB} (K)	$\int T_{MB} dv$ (K km s^{-1})
				5.5±0.3	7.0±0.8	0.35	2.6±0.3
$22_{15,8}$-$21_{15,7}$	209442.278	11.80	596.3	6.4[1]		0.44[2]	
$22_{15,7}$-$21_{15,6}$	209442.278†	11.80	596.3	6.4[1]		”	
$22_{16,6}$-$21_{16,5}$	209550.319	10.40	661.7	[24]		...	
$22_{16,7}$-$21_{16,6}$	209550.319†	10.40	661.7	[24]		...	
$22_{17,6}$-$21_{17,5}$	209665.534	8.86	730.9	2.9[1]		0.15[2]	
$22_{17,5}$-$21_{17,4}$	209665.534†	8.86	730.9	2.9[1]		”	
$22_{3,19}$-$21_{3,18}$	209735.857	21.60	134.9	3.3[1,32]		4.25[2]	
$22_{18,4}$-$21_{18,3}$	209787.701	7.27	804.2	4.9[1,33]		0.10[2]	
$22_{18,5}$-$21_{18,4}$	209787.701†	7.27	804.2	4.9[1,33]		”	
$23_{1,23}$-$22_{1,22}$	211467.095	22.90	124.3	4.9[1]		1.65[2]	
		Wide comp.		3.3±0.4	13±1	0.77	5.0±1.0
		Narrow comp.		5.14±0.12	5.1±0.5	0.92	10.6±1.0
$22_{1,21}$-$21_{1,20}$	211725.503	21.90	119.6	5.0[1]		1.61[2]	
$22_{2,20}$-$21_{2,19}$	212344.665	21.80	125.1	5.0[1]		1.81[2]	
		Wide comp.		1.7±0.3	16.4±0.7	0.61	10.7±0.5
		Narrow comp.		5.14±0.06	5.3±0.2	1.29	7.3±0.4
$23_{0,23}$-$22_{0,22}$	212788.735	23.00	123.8	7.9[1]		1.89[2]	
		Wide comp.		3.5±0.2	21.1±0.7	0.73	16.4±0.4
		Narrow comp.		5.00±0.04	5.5±0.2	1.20	7.1±0.3
$23_{2,22}$-$22_{2,21}$	216936.717	22.80	133.9	4.9[1]		2.60[2]	
				4.8±0.3	6.6±0.8	2.63	18.4±2.0
$23_{7,17}$-$22_{7,16}$	218398.555	20.90	231.5	5.5[1]		4.02[2]	
$23_{7,16}$-$22_{7,15}$	218398.555†	20.90	231.5	5.5[1]		”	
$23_{6,18}$-$22_{6,17}$	218402.434†	21.40	203.5	5.7[1]		3.97[2]	
$23_{6,17}$-$22_{6,16}$	218402.450†	21.40	203.5	5.7[1]		”	
$23_{8,16}$-$22_{8,15}$	218421.801	20.20	263.8	4.6[1]		2.20[2]	
$23_{8,15}$-$22_{8,14}$	218421.801†	20.20	263.8	4.6[1]		”	
				4.5±0.2	8.1±0.6	2.07	17.7±1.0
$23_{5,19}$-$22_{5,18}$	218451.297	21.90	179.8	4.1[1]		4.18[2]	
$23_{5,18}$-$22_{5,17}$	218452.356†	21.90	179.8	5.6[1]		”	
$23_{9,15}$-$22_{9,14}$	218463.739	19.50	300.3	5.7[1,15]		3.67[2]	
$23_{9,14}$-$22_{9,13}$	218463.739†	19.50	300.3	5.7[1,15]		”	
$23_{10,14}$-$22_{10,13}$	218519.999	18.70	341.1	5.2[1]		1.59[2]	
$23_{10,13}$-$22_{10,12}$	218519.999†	18.70	341.1	5.2[1]		”	
				5.22±0.14	6.6±0.4	1.52	10.6±0.6
$23_{4,20}$-$22_{4,19}$	218573.646	22.30	160.4	4.7[1]		2.46[2]	

Tabla B.1: continued.

Transition $J_{K_a,K_c} - J'_{K'_a,K'_c}$	Predicted frequency (MHz)	S_{ij}	E_u (K)	v_{LSR} km s^{-1}	Δv km s^{-1}	T_{MB} (K)	$\int T_{MB} dv$ (K km s^{-1})
				4.4±0.1	7.6±0.3	2.83	19.8±0.8
$23_{3,21}$-$22_{3,20}$	218585.071	22.60	145.3	3.8[1,15]		2.95[2]	
$23_{11,13}$-$22_{11,12}$	218588.108†	17.70	386.0	8.0[1,15]		”	
$23_{11,12}$-$22_{11,11}$	218588.108†	17.70	386.0	8.0[1,15]		”	
$23_{4,19}$-$22_{4,18}$	218615.091	22.30	160.4	5.1[1]		2.32[2]	
		Wide comp.		1.3±0.5	17.6±0.9	0.62	11.6±0.6
		Narrow comp.		5.14±0.06	5.6±0.2	1.86	11.0±0.6
$23_{12,11}$-$22_{12,10}$	218666.563	16.70	435.1	5.2[1]		0.68[2]	
$23_{12,12}$-$22_{12,11}$	218666.563†	16.70	435.1	5.2[1]		”	
				5.35±0.08	5.1±0.2	0.64	3.5±0.2
$23_{13,11}$-$22_{13,10}$	218754.388	15.70	488.2	[34]		...	
$23_{13,10}$-$22_{13,9}$	218754.388†	15.70	488.2	[34]		...	
$23_{14,9}$-$22_{14,8}$	218850.914	14.50	545.5	[35]		...	
$23_{14,10}$-$22_{14,9}$	218850.914†	14.50	545.5	[35]		...	
$23_{15,9}$-$22_{15,8}$	218955.656	13.20	606.8	7.7[1,36]		0.49[2]	
$23_{15,8}$-$22_{15,7}$	218955.656†	13.20	606.8	7.7[1,36]		”	
$23_{16,7}$-$22_{16,6}$	219068.245	11.90	672.2	6.8[1]		0.20[2]	
$23_{16,8}$-$22_{16,7}$	219068.245†	11.90	672.2	6.8[1]		”	
$23_{17,7}$-$22_{17,6}$	219188.385	10.40	741.5	[35]		...	
$23_{17,6}$-$22_{17,5}$	219188.385†	10.40	741.5	[35]		...	
$23_{18,5}$-$22_{18,4}$	219315.831	8.91	814.7	[19]		...	
$23_{18,6}$-$22_{18,5}$	219315.831†	8.91	814.7	[19]		...	
$23_{3,20}$-$22_{3,19}$	219400.584	22.60	145.5	4.9[1]		2.70[2]	
$23_{19,5}$-$22_{19,4}$	219450.372	7.30	891.8	[12,14,37]		...	
$23_{19,4}$-$22_{19,3}$	219450.372†	7.30	891.8	[12,14,37]		...	
$23_{20,3}$-$22_{20,2}$	219591.822	5.61	972.7	[15,18]		...	
$23_{20,4}$-$22_{20,3}$	219591.822†	5.61	972.7	[12,22]		...	
$24_{1,24}$-$23_{1,23}$	220561.393	23.90	134.9	4.7[1]		2.52[2]	
				4.84±0.12	6.4±0.2	2.41	16.5±1.0
$23_{1,22}$-$22_{1,21}$	221123.857	22.90	130.2	5.1[1]		2.10[2]	
				5.25±0.07	6.7±0.2	1.73	12.3±0.2
$24_{0,24}$-$23_{0,23}$	221766.034	24.00	134.5	5.5[1]		2.73[2]	
$23_{2,21}$-$22_{2,20}$	222153.496	22.80	135.7	4.9[1]		2.78	
				4.84±0.11	7.3±0.1	2.82	22.0±0.5
$24_{2,23}$-$23_{2,22}$	226256.880	23.80	144.8	5.0[1]		3.04[2]	
$24_{7,18}$-$23_{7,17}$	227897.606	22.00	242.5	4.8[1]		2.91[2]	
$24_{7,17}$-$23_{7,16}$	227897.607†	22.00	242.5	4.8[1]		”	

Tabla B.1: continued.

Transition $J_{K_a,K_c} - J'_{K'_a,K'_c}$	Predicted frequency (MHz)	S_{ij}	E_u (K)	v_{LSR} km s^{-1}	Δv km s^{-1}	T_{MB} (K)	$\int T_{MB} dv$ (K km s^{-1})
				4.8±0.2	7.7±0.6	2.87	23.5±1.5
$24_{6,19}$-$23_{6,18}$	227906.682	22.50	214.5	5.1[(1)]		3.47[(2)]	
$24_{6,18}$-$23_{6,17}$	227906.708†	22.50	214.5	5.1[(1)]		”	
				5.0±0.2	8.6±0.5	3.32	30.3±1.5
$24_{8,17}$-$23_{8,16}$	227918.642	21.30	274.8	5.2[(1)]		2.53[(2)]	
$24_{8,16}$-$23_{8,15}$	227918.642†	21.30	274.8	5.2[(1)]		”	
				5.2±0.2	6.6±0.5	2.48	17.5±1.1
$24_{9,15}$-$23_{9,14}$	227960.206	20.60	311.3	5.3[(1)]		2.33[(2)]	
$24_{9,16}$-$23_{9,15}$	227960.206†	20.60	311.3	5.3[(1)]		”	
				5.9±0.4	7±1	2.06	14.7±2.5
$24_{5,20}$-$23_{5,19}$	227966.030	23.00	190.7	3.2[(1,32)]		4.68[(2)]	
$24_{5,19}$-$23_{5,18}$	227967.587†	23.00	190.7	5.2[(1,32)]		”	
$24_{10,15}$-$23_{10,14}$	228017.342	19.80	352.0	4.9[(1)]		1.71[(2)]	
$24_{10,14}$-$23_{10,13}$	228017.342†	19.80	352.0	4.9[(1)]		”	
				5.1±0.1	6.5±0.3	1.63	13.3±0.4
$24_{11,13}$-$23_{11,12}$	228087.246	19.00	396.9	1.3[(1)]		3.14[(2)]	
$24_{11,14}$-$23_{11,13}$	228087.246†	19.00	396.9	1.3[(1)]		”	
$24_{3,22}$-$23_{3,21}$	228090.536†	23.60	156.2	5.7[(1)]		”	
		Wide comp.		3.5±0.4	17±1	1.36	24.7±0.6
		Narrow comp.		6.2±0.2	6.8±0.3	1.90	13.8±0.6
$24_{4,21}$-$23_{4,20}$	228104.613	23.30	171.3	5.1[(1)]		2.69[(2)]	
				5.02±0.12	6.6±0.3	2.61	18.4±0.9
$24_{4,20}$-$23_{4,19}$	228160.304	23.30	171.4	5.2[(1)]		2.71[(2)]	
				5.12±0.06	6.4±0.2	2.62	17.8±0.7
$24_{12,13}$-$23_{12,12}$	228168.218	18.00	446.0	6.1[(1)]		1.39[(2)]	
$24_{12,12}$-$23_{12,11}$	228168.218†	18.00	446.0	6.1[(1)]		”	
				6.0±0.2	8.1±0.4	1.38	11.9±0.6
$24_{13,11}$-$23_{13,10}$	228259.158	17.00	499.2	7.0[(1,13)]		0.51[(2)]	
$24_{13,12}$-$23_{13,11}$	228259.158†	17.00	499.2	7.0[(1,13)]		”	
$24_{14,10}$-$23_{14,9}$	228359.312	15.80	556.5	6.5[(1,15)]		0.55[(2)]	
$24_{14,11}$-$23_{14,10}$	228359.312†	15.80	556.5	6.5[(1,15)]		”	
$24_{15,10}$-$23_{15,9}$	228468.138	14.60	617.8	6.8[(1,8)]		0.59[(2)]	
$24_{15,9}$-$23_{15,8}$	228468.138†	14.60	617.8	6.8[(1,8)]		”	
$24_{16,8}$-$23_{16,7}$	228585.226	13.30	683.1	5.3[(1)]		0.18[(2)]	
$24_{16,9}$-$23_{16,8}$	228585.226†	13.30	683.1	5.3[(1)]		”	
				5.5±0.6	6±1	0.17	1.1±0.2
$24_{17,8}$-$23_{17,7}$	228710.250	12.00	752.4	4.6[(1,13,24)]		0.29[(2)]	

Tabla B.1: continued.

Transition $J_{K_a,K_c} - J'_{K'_a,K'_c}$	Predicted frequency (MHz)	S_{ij}	E_u (K)	v_{LSR} km s^{-1}	Δv km s^{-1}	T_{MB} (K)	$\int T_{MB} dv$ (K km s^{-1})
$24_{17,7}$-$23_{17,6}$	228710.250†	12.00	752.4	4.6[1,13,24]		”	
$24_{18,6}$-$23_{18,5}$	228842.939	10.50	825.7	7.6[1]		0.14[2]	
$24_{18,7}$-$23_{18,6}$	228842.939†	10.50	825.7	7.6[1]		”	
$24_{19,6}$-$23_{19,5}$	228983.064	8.96	902.8	[14,27]		...	
$24_{19,5}$-$23_{19,4}$	228983.064†	8.96	902.8	[14,27]		...	
$24_{3,21}$-$23_{3,20}$	229087.047	23.60	156.5	5.0[1]		2.64[2]	
		Wide comp.		2.7±0.2	17.4±0.4	0.94	17.5±0.4
		Narrow comp.		5.02±0.05	5.2±0.05	1.79	10.0±0.4
$24_{20,4}$-$23_{20,3}$	229130.421	7.33	983.7	[11]		...	
$24_{20,5}$-$23_{20,4}$	229130.421†	7.33	983.7	[11]		...	
$24_{21,4}$-$23_{21,3}$	229284.829	5.63	1068.5	[12]		...	
$24_{21,3}$-$23_{21,2}$	229284.829†	5.63	1068.5	[12]		...	
$25_{1,25}$-$24_{1,24}$	229647.837	24.90	145.9	4.7[1]		1.21[2]	
				5.15±0.07	7.3±0.2	1.10	8.6±0.2
$24_{1,23}$-$23_{1,22}$	230487.936	23.90	141.3	[38]		...	
$25_{0,25}$-$24_{0,24}$	230738.555	25.00	145.5	4.8[1]		1.35[2]	
		Wide comp.		2.0±0.6	21±2	0.48	10.5±0.4
		Narrow comp.		4.88±0.15	5.4±0.4	0.94	5.4±0.6
$24_{2,22}$-$23_{2,21}$	231952.330	23.80	146.8	4.5[1]		0.55[2]	
				4.5±0.2	5.7±0.5	0.57	3.5±0.3
$25_{2,24}$-$24_{2,23}$	235563.881	24.80	156.1	5.1[1]		1.96[2]	
		Wide comp.		3.8±0.4	16.84±0.13	0.12	9.6±0.6
		Narrow comp.		5.22±0.07	5.4±0.2	1.39	7.9±0.4
$25_{7,19}$-$24_{7,18}$	237397.088	23.00	253.9	5.0[1,15]		1.88[2]	
$25_{7,18}$-$24_{7,17}$	237397.088†	23.00	253.9	5.0[1,15]		”	
				4.51±0.13	6.8±0.2	1.77	12.8±0.2
$25_{6,20}$-$24_{6,20}$	237411.999	23.60	225.9	5.0[1]		2.28[2]	
$25_{6,19}$-$24_{6,18}$	237412.040†	23.60	225.9	5.0[1]		”	
$25_{8,18}$-$24_{8,17}$	237415.503†	22.40	286.2	8.6[1]		”	
$25_{8,17}$-$24_{8,16}$	237415.503†	22.40	286.2	8.6[1]		”	
$25_{9,17}$-$24_{9,16}$	237456.417	21.80	322.7	5.2[1]		1.14[2]	
$25_{9,16}$-$24_{9,15}$	237456.417†	21.80	322.7	5.2[1]		”	
				4.9±0.2	7.5±0.7	1.05	8.4±0.8
$25_{5,21}$-$24_{5,20}$	237482.851	24.00	202.1	3.7[1]		1.96[2]	
$25_{5,20}$-$24_{5,19}$	237485.102†	24.00	202.1	6.6[1]		”	
$25_{10,15}$-$24_{10,14}$	237514.230	21.00	363.4	6.4[1,23]		1.07[2]	
$25_{10,16}$-$24_{10,15}$	237514.230†	21.00	363.4	6.4[1,23]		”	

Tabla B.1: continued.

Transition $J_{K_a,K_c} - J'_{K'_a,K'_c}$	Predicted frequency (MHz)	S_{ij}	E_u (K)	v_{LSR} km s^{-1}	Δv km s^{-1}	T_{MB} (K)	$\int T_{MB} dv$ (K km s^{-1})
$25_{11,15}$-$24_{11,14}$	237585.782	20.20	408.3	5.7[1]		0.76[2]	
$25_{11,14}$-$24_{11,13}$	237585.782†	20.20	408.3	5.7[1]		”	
				5.91±0.07	4.8±0.2	0.58	3.0±0.2
$25_{3,23}$-$24_{3,22}$	237591.475	24.60	167.6	6.0[1]		1.49[2]	
$25_{4,22}$-$24_{4,21}$	237638.100	24.40	182.8	5.2[1]		1.30[2]	
$25_{12,13}$-$24_{12,12}$	237669.158	19.20	457.4	5.5[1]		0.47[2]	
$25_{12,14}$-$24_{12,13}$	237669.158†	19.20	457.4	5.5[1]		”	
				5.55±0.09	5.6±0.3	0.45	2.72±0.12
$25_{4,21}$-$24_{4,20}$	237711.970	24.40	182.8	5.0[1,13,27]		1.47[2]	
$25_{13,12}$-$24_{13,11}$	237763.122	18.20	510.6	6.7[1]		0.81[2]	
$25_{13,13}$-$24_{13,12}$	237763.122†	18.20	510.6	6.7[1]		”	
				5.2±0.2	9.16±0.12	0.74	7.1±0.2
$25_{14,12}$-$24_{14,11}$	237866.833	17.20	567.9	5.7[1]		0.39[2]	
$25_{14,11}$-$24_{14,10}$	237866.833†	17.20	567.9	5.7[1]		”	
				5.7±0.4	10±1	”	3.8±0.4
$25_{15,11}$-$24_{15,10}$	237979.684	16.00	629.2	[10]		...	
$25_{15,10}$-$24_{15,9}$	237979.684†	16.00	629.2	[10]		...	
$25_{16,9}$-$24_{16,8}$	238101.222	14.80	694.6	6.2[1]		0.16[2]	
$25_{16,10}$-$24_{16,9}$	238101.222†	14.80	694.6	6.2[1]		”	
$25_{17,9}$-$24_{17,8}$	238231.086	13.40	763.9	[24]		...	
$25_{17,8}$-$24_{17,7}$	238231.086†	13.40	763.9	[24]		...	
$25_{18,7}$-$24_{18,6}$	238368.981	12.00	837.1	[20]		...	
$25_{18,8}$-$24_{18,7}$	238368.981†	12.00	837.1	[20]		...	
$25_{19,7}$-$24_{19,6}$	238514.655	10.60	914.2	[39]		...	
$25_{19,6}$-$24_{19,5}$	238514.655†	10.60	914.2	[39]		...	
$25_{20,5}$-$24_{20,4}$	238667.890	9.00	995.2	[5]		...	
$25_{20,6}$-$24_{20,5}$	238667.890†	9.00	995.2	[5]		...	
$26_{1,26}$-$25_{1,25}$	238726.808	25.90	157.4	4.9[1]		3.04[2]	
		Wide comp.		3.0±0.3	15.4±0.8	1.25	20.5±1.1
		Narrow comp.		5.05±0.08	4.8±0.2	1.85	9.5±0.8
$25_{3,22}$-$24_{3,22}$	238796.291	24.60	167.4	5.5[1,40]		2.59[2]	
$25_{21,5}$-$24_{21,4}$	238828.488	7.36	1079.9	[24,41]		...	
$25_{21,4}$-$24_{21,3}$	238828.488†	7.36	1079.9	[24,41]		...	
$26_{0,26}$-$25_{0,25}$	239708.391	26.00	157.1	5.3[1]		2.75[2]	
$25_{1,24}$-$24_{1,23}$	239816.141	24.90	152.8	5.4[1]		3.53[2]	
				5.4±0.2	6.5±0.5	3.43	23.6±2.1
$25_{2,23}$-$24_{2,22}$	241737.559	24.80	158.5	5.0[1]		3.64[2]	

Tabla B.1: continued.

Transition $J_{K_a,K_c} - J'_{K'_a,K'_c}$	Predicted frequency (MHz)	S_{ij}	E_u (K)	v_{LSR} km s^{-1}	Δv km s^{-1}	T_{MB} (K)	$\int T_{MB} dv$ (K km s^{-1})
		Wide comp.		0.7±0.5	18±2	1.35	25.9±1.3
		Narrow comp.		5.15±0.09	5.4±0.2	2.52	14.6±1.1
$26_{2,25}$-$25_{2,24}$	244857.473	25.80	167.9	5.0[1]		3.40[2]	
		Wide comp.		2.7±0.2	19.2±0.8	1.16	23.7±0.8
		Narrow comp.		5.11±0.06	5.3±0.2	2.31	13.0±0.6
$26_{7,20}$-$25_{7,19}$	246897.015	24.10	265.7	5.1[1]		3.11[2]	
$26_{7,19}$-$25_{7,18}$	246897.016†	24.10	265.7	5.1[1]		”	
				5.0±0.3	11±1	2.84	33.8±2.8
$26_{8,19}$-$25_{8,18}$	246912.384	23.50	298.0	5.2[1,15]		9.52[2]	
$26_{8,18}$-$25_{8,17}$	246912.384†	23.50	298.0	5.2[1,15]		”	
$26_{6,21}$-$25_{6,20}$	246918.428	24.60	237.7	0.9[1,42]		6.42[2]	
$26_{6,20}$-$25_{6,19}$	246918.491†	24.60	237.7	1.0[1,42]		”	
$26_{9,18}$-$25_{9,17}$	246952.358	22.90	334.5	4.8[1]		1.86[2]	
$26_{9,17}$-$25_{9,16}$	246952.358†	22.90	334.5	4.8[1]		”	
		Wide comp.		4.19±0.15	9.0±0.4	1.11	11.0±0.5
		Narrow comp.		5.32±0.14	4.2±0.2	0.84	3.7±0.2
$26_{5,22}$-$25_{5,21}$	247001.823	25.00	214.0	2.1[1]		3.54[2]	
$26_{5,21}$-$25_{5,20}$	247005.027†	25.00	214.0	6.0[1]		3.54[2]	
				5.0±0.3	11±1	3.31	32.7±0.6
$26_{10,17}$-$25_{10,16}$	247010.642	22.20	375.3	6.7[1]		2.64[2]	
$26_{10,16}$-$25_{10,15}$	247010.642†	22.20	375.3	6.7[1]		”	
$26_{11,16}$-$25_{11,15}$	247083.689	21.30	420.2	1.3[1,10]		1.72[2]	
$26_{11,15}$-$25_{11,14}$	247083.689†	21.30	420.2	1.3[1,10]		”	
$26_{3,24}$-$25_{3,23}$	247087.032†	25.70	179.5	5.4[1,10]		”	
$26_{12,15}$-$25_{12,14}$	247169.351	20.50	469.9	4.6[1,8]		0.96[2]	
$26_{12,14}$-$25_{12,13}$	247169.351†	20.50	469.9	4.6[1,8]		”	
$26_{4,23}$-$25_{4,22}$	247173.930†	25.40	194.6	4.6[1,8]		1.68[2]	
$26_{13,14}$-$25_{13,13}$	247266.248	19.50	522.5	0.2[1,14]		1.54[2]	
$26_{13,13}$-$25_{13,12}$	247266.248†	19.50	522.5	0.2[1,14]		”	
$26_{4,22}$-$25_{4,21}$	247270.744†	25.40	194.6	5.3[1,14]		”	
$26_{14,12}$-$25_{14,11}$	247373.441	18.50	579.8	6.2[1]		0.38[2]	
$26_{14,13}$-$25_{14,12}$	247373.441†	18.50	579.8	6.2[1]		”	
				5.20±0.2	7.9±0.5	0.37	3.2±0.2
$26_{15,12}$-$25_{15,11}$	247490.256	17.30	641.1	8.4[1,43]		0.52[2]	
$26_{15,11}$-$25_{15,10}$	247490.256†	17.30	641.1	8.4[1,43]		”	
$26_{16,10}$-$25_{16,9}$	247616.191	16.20	706.5	[8]		...	
$26_{16,11}$-$25_{16,10}$	247616.191†	16.20	706.5	[8]		...	

Tabla B.1: continued.

Transition $J_{K_a,K_c} - J'_{K'_a,K'_c}$	Predicted frequency (MHz)	S_{ij}	E_u (K)	v_{LSR} km s^{-1}	Δv km s^{-1}	T_{MB} (K)	$\int T_{MB} dv$ (K km s^{-1})
$26_{17,10}$-$25_{17,9}$	247750.851	14.90	775.8	5.8[1,43,44]		0.53[2]	
$26_{17,9}$-$25_{17,8}$	247750.851†	14.90	775.8	5.8[1,43,44]		”	
$27_{1,27}$-$26_{1,26}$	247798.704	27.00	169.3	5.0[1]		1.44[2]	
		Wide comp.		3.0±0.2	14.8±0.5	0.89	14.0±0.5
		Narrow comp.		5.18±0.12	4.3±0.4	0.61	2.8±0.4
$26_{18,8}$-$25_{18,7}$	247893.912	13.50	849.0	7.6[1,43]		0.42[2]	
$26_{18,9}$-$25_{18,8}$	247893.912†	13.50	849.0	7.6[1,43]		”	
$26_{19,8}$-$25_{19,7}$	248045.102	12.10	926.1	[12]		...	
$26_{19,7}$-$25_{19,6}$	248045.102†	12.10	926.1	[12]		...	
$26_{20,6}$-$25_{20,5}$	248204.182	10.60	1007.1	4.9[1]		0.11[2]	
$26_{20,7}$-$25_{20,6}$	248204.182†	10.60	1007.1	4.9[1]		”	
$26_{3,23}$-$25_{3,22}$	248529.049	25.70	179.9	4.8[1,9]		3.21[2]	
$27_{0,27}$-$26_{0,26}$	248677.191	27.00	169.0	3.8[1,15,27]		6.29[2]	
$26_{1,25}$-$25_{1,24}$	249107.178	25.90	164.7	4.1[1,19,24]		4.29[2]	
$26_{2,24}$-$25_{2,23}$	251505.957	25.90	170.5	[1,11,12,23]		...	
$27_{2,26}$-$26_{2,25}$	254137.458	26.80	180.1	5.2[1]		1.57[2]	
$27_{7,21}$-$26_{7,20}$	256397.404	25.20	278.0	5.9[1,12]		3.67[2]	
$27_{7,20}$-$26_{7,19}$	256397.406†	25.20	278.0	5.9[1,12]		”	
$27_{8,20}$-$26_{8,19}$	256409.285	24.60	310.3	5.9[1]		1.17[2]	
$27_{8,19}$-$26_{8,18}$	256409.285†	24.60	310.3	5.9[1]		”	
				5.2±0.4	6±1	0.96	6.7±1.7
$27_{6,22}$-$26_{6,21}$	256426.012	13.40	250.0	4.9[1]		1.23[2]	
$27_{6,21}$-$26_{6,20}$	256426.109†	13.40	250.0	5.1[1]		”	
		Wide comp.		2.41±0.13	12±1	0.51	6.3±0.2
		Narrow comp.		5.4±0.2	5.4±0.3	0.83	4.8±0.4
$27_{9,19}$-$26_{9,18}$	256448.017	24.00	346.8	6.2[1,11]		1.33[2]	
$27_{9,18}$-$26_{9,17}$	256448.017†	24.00	346.8	6.2[1,11]		”	
$27_{10,17}$-$26_{10,16}$	256506.558	23.30	387.6	6.1[1,11]		1.28[2]	
$27_{10,18}$-$26_{10,17}$	256506.558†	23.30	387.6	6.1[1,11]		”	
$27_{5,23}$-$26_{5,22}$	256523.004	26.10	226.3	0.7[1]		0.99[2]	
$27_{5,22}$-$26_{5,21}$	256527.502†	26.10	226.3	6.0[1]		”	
				4.13±0.14	11.1±0.4	1.03	12.3±0.3
$27_{3,25}$-$26_{3,24}$	256576.342	26.70	191.8	4.3[1]		1.53[2]	
$27_{11,16}$-$26_{11,15}$	256580.941†	22.50	432.5	8.3[1]		”	
$27_{11,17}$-$26_{11,16}$	256580.941†	22.50	432.5	8.3[1]		”	
				4.3±0.4	7.2±0.9	1.54	11.9±1.4
$27_{12,15}$-$26_{12,14}$	256668.769	21.70	481.6	4.7[1,10]		1.74[2]	

Tabla B.1: continued.

Transition $J_{K_a,K_c} - J'_{K'_a,K'_c}$	Predicted frequency (MHz)	S_{ij}	E_u (K)	v_{LSR} km s^{-1}	Δv km s^{-1}	T_{MB} (K)	$\int T_{MB} dv$ (K km s^{-1})
$27_{12,16}$-$26_{12,15}$	256668.769†	21.70	481.6	4.7[1,10]		”	
$27_{4,24}$-$26_{4,23}$	256711.878	26.40	206.9	5.3[1]		1.16[2]	
		Wide comp.		3.6±0.2	10.0±0.3	0.64	6.8±0.4
		Narrow comp.		5.64±0.07	4.2±0.2	0.51	2.2±0.3
$27_{13,15}$-$26_{13,14}$	256768.502	20.70	534.8	5.5[1]		0.42[2]	
$27_{13,14}$-$26_{13,13}$	256768.502†	20.70	534.8	5.5[1]		”	
$27_{4,23}$-$26_{4,22}$	256837.352	26.40	207.0	5.1[1]		1.14[2]	
				4.5±0.4	11±1	1.09	12.9±1.2
$28_{1,28}$-$27_{1,27}$	256863.926	28.00	181.6	[45]		...	
$27_{14,13}$-$26_{14,12}$	256879.099†	19.70	592.1	[45]		...	
$27_{14,14}$-$26_{14,13}$	256879.099†	19.70	592.1	[45]		...	
$27_{15,13}$-$26_{15,12}$	256999.814	18.70	653.4	[46]		...	
$27_{15,12}$-$26_{15,11}$	256999.814†	18.70	653.4	[46]		...	
$27_{16,11}$-$26_{16,10}$	257130.093	17.50	718.8	[15,31]		...	
$27_{16,12}$-$26_{16,11}$	257130.093†	17.50	718.8	[15,31]		...	
$27_{17,11}$-$26_{17,10}$	257269.502	16.30	788.1	[15,47]		...	
$27_{17,10}$-$26_{17,9}$	257269.502†	16.30	788.1	[15,47]		...	
$27_{18,9}$-$26_{18,8}$	257417.690	15.00	861.4	[10,37]		...	
$27_{18,10}$-$26_{18,9}$	257417.690†	15.00	861.4	[10,37]		...	
$27_{19,9}$-$26_{19,8}$	257574.358	13.60	938.5	[48]		...	
$27_{19,8}$-$26_{19,7}$	257574.358†	13.60	938.5	[48]		...	
$28_{0,28}$-$27_{0,27}$	257646.199	28.00	181.4	5.2[1]		0.87[2]	
		Wide comp.		3.31±0.14	12.8±0.5	0.46	6.24±0.12
		Narrow comp.		5.19±0.08	4.2±0.2	0.40	1.8±0.2
$27_{3,24}$-$26_{3,23}$	258285.654	26.70	192.2	[49]		...	
$27_{1,26}$-$26_{1,25}$	258360.147	26.90	177.1	5.0[1]		1.11[2]	
				5.06±0.12	7.9±0.3	1.01	8.5±0.3
$27_{2,25}$-$26_{2,24}$	261254.670	26.90	183.1	5.0[1]		5.18[2]	
$28_{2,27}$-$27_{2,26}$	263403.693	27.80	192.7	4.0[1,14]		4.18[2]	
$28_{7,22}$-$27_{7,21}$	265898.270	26.30	290.8	[50]		...	
$28_{7,21}$-$27_{7,20}$	265898.272†	26.30	290.8	[50]		...	
$28_{8,21}$-$27_{8,20}$	265906.203†	25.70	323.1	[50]		...	
$28_{8,20}$-$27_{8,19}$	265906.203†	25.70	323.1	[50]		...	
$29_{1,29}$-$28_{1,28}$	265922.880	29.00	194.4	6.5[1]		2.41[2]	
$28_{6,23}$-$27_{6,22}$	265934.792	26.70	262.8	6.1[1]		1.97[2]	
$28_{6,22}$-$27_{6,21}$	265934.936†	26.70	262.8	6.2[1]		”	
$28_{9,20}$-$27_{9,19}$	265943.383	25.10	359.6	5.7[1]		1.11[2]	

Tabla B.1: continued.

Transition $J_{K_a,K_c} - J'_{K'_a,K'_c}$	Predicted frequency (MHz)	S_{ij}	E_u (K)	v_{LSR} km s^{-1}	Δv km s^{-1}	T_{MB} (K)	$\int T_{MB} dv$ (K km s^{-1})
$28_{9,19}$-$27_{9,18}$	265943.383†	25.10	359.6	5.7[1]		”	
$28_{10,19}$-$27_{10,18}$	266001.959	24.40	400.3	5.7[1]		0.71[2]	
$28_{10,18}$-$27_{10,17}$	266001.959†	24.40	400.3	5.7[1]		”	
		Wide comp.		2.8±0.4	11.9±0.6	0.44	5.6±0.4
		Narrow comp.		6.03±0.13	3.6±0.3	0.32	1.3±0.2
$28_{5,24}$-$27_{5,23}$	266046.445	27.10	239.1	5.0[1,19]		2.49[2]	
$28_{5,23}$-$27_{5,22}$	266052.678	24.10	239.1	5.0[1]		2.49[2]	
$28_{3,26}$-$27_{3,25}$	266058.547	27.70	204.6	6.0[1,19]		2.35[2]	
$28_{11,18}$-$27_{11,17}$	266077.512	23.70	445.3	6.2[1,5,22]		0.82[2]	
$28_{11,17}$-$27_{11,16}$	266077.512†	23.70	445.3	6.2[1,5,22]		”	
$28_{12,17}$-$27_{12,16}$	266167.379	22.90	494.4	[8,51]		...	
$28_{12,16}$-$27_{12,15}$	266167.379†	22.90	494.4	[8,51]		...	
$28_{4,25}$-$27_{4,24}$	266251.665	27.40	219.7	5.2[1,5]		1.85[2]	
$28_{13,16}$-$27_{13,15}$	266269.851	22.00	547.6	7.3[1,52]		1.77[2]	
$28_{13,15}$-$27_{13,14}$	266269.851†	22.00	547.6	7.3[1,52]		”	
$28_{14,14}$-$27_{14,13}$	266383.771	21.00	604.9	6.3[1,13]		0.55[2]	
$28_{14,15}$-$27_{14,14}$	266383.771†	21.00	604.9	6.3[1,13]		”	
$28_{4,24}$-$27_{4,23}$	266412.597	27.40	219.7	4.9[1,14]		1.86[2]	
$28_{15,14}$-$27_{15,13}$	266508.320	20.00	666.2	6.6[1]		0.25[2]	
$28_{15,13}$-$27_{15,12}$	266508.320†	20.00	666.2	6.6[1]		”	
$29_{0,29}$-$28_{0,28}$	266616.301	29.00	194.1	4.7[1]		2.10[2]	
				4.8±0.2	6.4±0.5	1.96	13.4±2.1
$28_{16,12}$-$27_{16,11}$	266642.887	18.90	731.6	5.0[1]		0.28[2]	
$28_{16,13}$-$27_{16,12}$	266642.887†	18.90	731.6	5.0[1]		”	
$28_{17,12}$-$27_{17,11}$	266786.998	17.70	800.9	4.1[1]		0.20[2]	
$28_{17,11}$-$27_{17,10}$	266786.998†	17.70	800.9	4.1[1]		”	
$28_{18,10}$-$27_{18,9}$	266940.269	16.40	874.2	[30]		...	
$28_{18,11}$-$27_{18,10}$	266940.269†	16.40	874.2	[30]		...	
$28_{19,10}$-$27_{19,9}$	267102.379	15.10	951.3	[11]		...	
$28_{19,9}$-$27_{19,8}$	267102.379†	15.10	951.3	[11]		...	
$28_{20,8}$-$27_{20,7}$	267273.050	13.70	1032.3	[9]**		...	
$28_{20,9}$-$27_{20,8}$	267273.050†	13.70	1032.3	[9]**		...	
$28_{21,8}$-$27_{21,7}$	267452.036	12.30	1117.0	[11]		...	
$28_{21,7}$-$27_{21,6}$	267452.036†	12.30	1117.0	[11]		...	
$28_{1,27}$-$27_{1,26}$	267574.631	27.90	190.0	[53]		...	
$28_{22,6}$-$27_{22,5}$	267639.118	10.70	1205.5	6.1[1,11,13]		0.12[2]	
$28_{22,7}$-$27_{22,6}$	267639.118†	10.70	1205.5	6.1[1,11,13]		”	

Tabla B.1: continued.

Transition $J_{K_a,K_c} - J'_{K'_a,K'_c}$	Predicted frequency (MHz)	S_{ij}	E_u (K)	v_{LSR} km s^{-1}	Δv km s^{-1}	T_{MB} (K)	$\int T_{MB} dv$ (K km s^{-1})
$28_{23,6}$-$27_{23,5}$	267834.094	9.11	1297.7	(11)		...	
$28_{23,5}$-$27_{23,4}$	267834.094†	9.11	1297.7	(11)		...	
$28_{24,4}$-$27_{24,3}$	268036.784	7.43	1393.6	(11)		...	
$28_{24,5}$-$27_{24,4}$	268036.784†	7.43	1393.6	(11)		...	
$28_{3,25}$-$27_{3,24}$	268065.943	27.70	205.1	5.1(1)		1.58(2)	
				5.20±0.08	6.2±0.3	1.68	11.1±0.8
$28_{2,26}$-$27_{2,25}$	270981.175	27.90	196.1	5.3(1)		3.13(2)	
		Wide comp.		5.5±1.1	15±1	1.36	22.1±1.6
		Narrow comp.		5.0±1.1	4±1	1.74	8.2±1.6
$29_{2,28}$-$28_{2,27}$	272656.087	28.80	205.8	4.8(1,22)		3.45(2)	
$30_{1,30}$-$29_{1,29}$	274975.961	30.00	207.6	5.1(1)		1.54(2)	
				5.15±0.12	5.8±0.4	1.42	8.7±1.2
$29_{7,23}$-$28_{7,22}$	275399.629	27.30	304.0	3.1(1)		3.07(2)	
$29_{7,22}$-$28_{7,21}$	275399.629†	27.30	304.0	3.1(1)		”	
$29_{8,22}$-$28_{8,21}$	275403.137†	26.80	336.3	6.9(1)		”	
$29_{8,21}$-$28_{8,20}$	275403.137†	26.80	336.3	6.9(1)		”	
		Wide comp.		3.8±0.3	14.4±0.2	1.06	16.2±0.2
		Narrow comp.		5.30±0.09	8.4±0.07	1.95	17.44±0.11
$29_{9,21}$-$28_{9,20}$	275438.443	26.20	372.8	5.8(1)		1.85(2)	
$29_{9,20}$-$28_{9,19}$	275438.443†	26.20	372.8	5.8(1)		”	
$29_{6,24}$-$28_{6,23}$	275444.809	27.80	276.0	5.2(1)		2.21(2)	
$29_{6,23}$-$28_{6,22}$	275445.022†	27.80	276.0	5.2(1)		”	
$29_{10,19}$-$28_{10,18}$	275496.823	25.60	413.6	6.1(1)		1.58(2)	
$29_{10,20}$-$28_{10,19}$	275496.823†	25.60	413.6	6.1(1)		”	
				5.9±0.2	7.3±0.6	1.49	7.2±0.5
$29_{3,27}$-$28_{3,26}$	275532.794	28.70	217.8	5.3(1)		2.01(2)	
		Wide comp.		3.3±0.4	15.1±0.8	0.82	13.2±0.8
		Narrow comp.		5.49±0.08	5.6±0.2	1.20	7.2±0.5
$29_{5,25}$-$28_{5,24}$	275572.188	28.10	252.3	2.1(1,31)		4.35(2)	
$29_{11,19}$-$28_{11,18}$	275573.378†	24.80	458.5	3.4(1,31)		”	
$29_{11,18}$-$28_{11,17}$	275573.378†	24.80	458.5	3.4(1,31)		”	
$29_{5,24}$-$28_{5,23}$	275580.720	28.10	252.3	5.4(31)		2.80(2)	
$30_{0,30}$-$29_{0,29}$	275588.085	30.00	207.4	4.7(1)		3.26(2)	
				4.8±0.2	6.9±0.6	3.06	22.6±2.4
$29_{12,17}$-$28_{12,16}$	275665.153	24.00	507.6	(31)		...	
$29_{12,18}$-$28_{12,17}$	275665.153†	24.00	507.6	(31)		...	
$29_{13,16}$-$28_{13,15}$	275770.258	23.20	560.8	(24,31)		...	

Tabla B.1: continued.

Transition $J_{K_a,K_c} - J'_{K'_a,K'_c}$	Predicted frequency (MHz)	S_{ij}	E_u (K)	v_{LSR} km s^{-1}	Δv km s^{-1}	T_{MB} (K)	$\int T_{MB} dv$ (K km s^{-1})
$29_{13,17}$-$28_{13,16}$	275770.258†	23.20	560.8	(24,31)		...	
$29_{4,26}$-$28_{4,25}$	275792.965	28.40	232.9	5.7(1)		2.69(2)	
				5.3±0.13	8.1±0.4	2.39	20.5±0.8
$29_{14,15}$-$28_{14,14}$	275887.420	22.20	618.1	(31)		...	
$29_{14,16}$-$28_{14,15}$	275887.420†	22.20	618.1	(31)		...	
$29_{4,25}$-$28_{4,24}$	275997.358	28.40	233.0	5.5(1,27,54)		1.99(2)	
$29_{15,14}$-$28_{15,13}$	276015.734	21.20	679.5	3.8(1)		0.49(2)	
$29_{15,15}$-$28_{15,14}$	276015.734†	21.20	679.5	3.8(1)		”	
$29_{16,13}$-$28_{16,12}$	276154.531	20.20	744.8	4.4(1)		0.34(2)	
$29_{16,14}$-$28_{16,13}$	276154.531†	20.20	744.8	4.4(1)		”	
$29_{17,13}$-$28_{17,12}$	276303.294	19.00	814.2	5.7(1,13)		0.74(2)	
$29_{17,12}$-$28_{17,11}$	276303.294†	19.00	814.2	5.7(1,13)		”	
$29_{18,11}$-$28_{18,10}$	276461.606	17.80	887.4	4.7(1,55)		0.23(2)	
$29_{18,12}$-$28_{18,11}$	276461.606†	17.80	887.4	4.7(1,55)		”	
$29_{19,11}$-$28_{19,10}$	276629.118	16.60	964.6	(11)		...	
$29_{19,10}$-$28_{19,9}$	276629.118†	16.60	964.6	(11)		...	
$29_{1,28}$-$28_{1,27}$	276750.763	28.90	203.2	6.0(1,12,56)		5.73(2)	
$29_{20,9}$-$28_{20,8}$	276805.531	15.20	1045.6	(14,17)		...	
$29_{20,10}$-$28_{20,9}$	276805.531†	15.20	1045.6	(14,17)		...	
$29_{3,26}$-$28_{3,25}$	277869.189	28.70	218.4	5.4(1,12)		9.36(2)	

Tabla A6. Emission lines of CH_2CHCN ground state present in the spectral scan of the Orion-KL from the radio-telescope of IRAM 30-m. Column 1 indicates the line transition, Col. 2 gives the predicted frequency in the laboratory, Col. 3 the line strength, Col. 4 upper level energy, Col. 5 observed radial velocities relative to the local system rest (v_{LSR}), Col. 6 the line width, Col. 7 main beam temperature, and Col. 8 shows the area of the line. † blended with the previous line. ∗ noise level. ∗∗ hole in the observed spectrum.

(1) peak channel line observed velocity. (2) peak channel line intensity. (3) blended with CH_3CCH. (4) blended with $^{34}SO_2$. (5) blended with t-CH_3CH_2OH. (6) blended with $OC^{34}S$. (7) blended with $H^{13}CCCN$. (8) blended with CH_3OH. (9) blended with CH_3COOH v_t=0. (10) blended with $^{13}CH_3OH$. (11) blended with U-line. (12) blended with CH_3CH_2CN. (13) blended with CH_2CHCN v_{15}=1. (14) blended with CH_3OCH_3. (15) blended with $HCOOCH_3$. (16) blended with $H_2C^{34}S$. (17) blended with $CH_3CH_2{}^{13}CN$. (18) blended with $^{13}CH_3CH_2CN$. (19) blended with CH_3CH_2CN v_{13}/v_{21}. (20) blended with $HCOOCH_3$ v_t=1. (21) blended with $^{13}CH_3CN$. (22) blended with CH_3CH_2CN v_{20}=1. (23) blended with $^{33}SO_2$. (24) blended with CH_2CHCN v_{11}=1. (25) blended with CH_3CHO. (26) blended with $H_{33}\alpha$. (27) blended with $(CH_3)_2CO$. (28) blended with SiS. (28) blended with HCCCN. (30) blended with SO_2. (31) blended with CH_3CN. (32) blended with HCCCN v_6=1. (33) blended with CH_2CHCN

$v_{10}/v_{11}v_{15}$. (34) blended with H_2CO. (35) blended with HCCCN v_7=1. (36) blended with $HCOO^{13}CH_3$. (37) blended with SO_2 v_2=1. (38) blended with CO. (39) blended with C_3H_2. (40) blended with $CH_3{}^{13}CN$. (41) blended with CH_2CHCN v_{11}=2. (42) blended with HDCO. (43) blended with HDCS. (44) blended with $H^{13}COOCH_3$. (45) blended with ^{34}SO. (46) blended with CH_3SH. (47) blended with ^{29}SiO. (48) blended with CH_3CN v_8=1. (49) blended with SO. (50) blended with HCN. (51) blended with HDO. (52) blended with NO. (53) blended with HCO^+. (54) blended with NH_2CHO. (55) blended with $CH_3{}^{13}CH_2CN$. (56) blended with CH_3OD.

Tabla B.2: Detected b-type lines of CH_2CHCN g.s. .

Transition $J_{K_a,K_c} - J'_{K'_a,K'_c}$	Predicted frequency (MHz)	S_{ij}	E_u (K)	v_{LSR}[(1)] km s^{-1}	Observed frequency (MHz)	Observed T_{MB} (K)[(2)]	Model T_{MB} (K)
$18_{1,17}$-$17_{0,18}$	95212.208	11.40	81.7	4.95[(3)]	95212.2	0.03	0.01
$20_{1,19}$-$20_{0,20}$	108813.600	11.40	99.7	3.74	108814.0	0.02	0.01
$18_{2,16}$-$18_{1,17}$	113831.149	14.00	87.1	5.48	113831.0	0.02	0.02
$22_{2,20}$-$22_{1,21}$	114120.970	18.10	125.1	7.75	114019.0	0.04	0.02
$15_{0,15}$-$14_{1,14}$	114596.321	9.22	54.2	5.82[(4)]	114596.0	0.03	0.01
$29_{2,27}$-$29_{1,28}$	131168.734	22.70	209.5	3.88[(5)]	131169.2	0.04	0.01
$17_{0,17}$-$16_{1,16}$	136855.602	11.00	69.0	4.75[(4)]	136855.7	0.05	0.02
$13_{1,13}$-$12_{0,12}$	149952.784	8.11	42.5	5.15[(4)]	149952.7	0.09	0.03
$19_{0,19}$-$18_{1,18}$	158773.785	13.00	85.6	4.21[(4)]	158771.7	0.08	0.04
$39_{2,37}$-$39_{1,38}$	199913.795	22.40	369.5	5.41	199913.5	0.02	0.02
$20_{1,20}$-$19_{0,19}$	200364.538	14.20	95.2	6.62	200363.4	0.08	0.06
$24_{0,24}$-$23_{1,23}$	211519.057	18.10	134.5	6.62[(4)]	211518.4	0.12	0.07
$9_{2,8}$-$8_{1,7}$	212451.692	3.14	29.1	2.94	212453.2	0.05	0.03
$29_{1,28}$-$28_{2,27}$	219722.155	12.00	203.2	5.28[(4)]	219722.0	0.08	0.03
$7_{3,4}$-$7_{2,5}$	225075.522	3.40	32.2	4.88[(4)]	225075.6	0.13	0.03
$26_{0,26}$-$25_{1,25}$	231756.775	20.20	157.1	6.55[(4)]	231755.6	0.23	0.08
$20_{3,18}$-$20_{2,19}$	232100.843	10.60	115.2	5.75	232100.3	0.08	0.06
$21_{3,19}$-$21_{2,20}$	233406.626	11.10	124.8	6.22	233405.7	0.05	0.06
$12_{2,11}$-$11_{1,10}$	234146.112	4.02	44.1	3.41	234147.4	0.05	0.04
$27_{3,25}$-$27_{2,26}$	245056.911	14.10	191.8	6.75[(4)]	245055.4	0.09	0.05
$36_{1,35}$-$36_{0,36}$	263133.842	10.00	308.4	6.15[(4)]	263132.8	0.05	0.02
$33_{3,31}$-$33_{2,32}$	264402.882	16.40	275.2	5.15[(4)]	264402.8	0.10	0.04
$30_{1,30}$-$29_{0,29}$	279591.813	24.40	207.6	5.94[(4)]	279591.0	0.32	0.10

Tabla A6. Emission b-type lines of CH_2CHCN ground state present in the spectral scan of the Orion-KL from the radio-telescope of IRAM 30-m. Column 1 indicates the line transition, Col. 2 gives the predicted frequency in the laboratory, Col. 3 the line strength, Col. 4 upper level energy, Col. 5 observed centroid frequencies, Col. 6 observed radial velocities relatives (v_{LSR}), Col. 7 observed mean beam temperature, y Col. 8 mean beam temperature obtained with the model. The observed parameters are shown when the line is not blended with other molecule, moreover, when only calculated parameters are given means the line can not be fitted like a gaussian or there is some contribution from other molecule. † blended with the last one.

(1) peak line observed velocity. (2) peak line intensity. (3) blended with v_{11}=1. (4) blended with U-line. (5) blended with $DCOOCH_3$.

Tabla B.3: Detected lines of CH_2CHCN v_{11}=1 .

Transition $J_{K_a,K_c} - J'_{K'_a,K'_c}$	Predicted frequency (MHz)	S_{ij}	E_u (K)	v_{LSR} km s^{-1}	Δv km s^{-1}	T_{MB} (K)	$\int T_{MB} dv$ (K km s^{-1})
$9_{1,9}$-$8_{1,8}$	83398.992	8.89	350.6	5.4[1,3]		0.08[2]	
$9_{0,9}$-$8_{0,8}$	85167.948	9.00	349.0	5.3[1]		0.03[2]	
				5.3±0.5	6±1	0.04	0.24±0.04
$9_{2,8}$-$8_{2,7}$	85547.124	8.56	357.5	6.4[1]		0.04[2]	
				6.6±0.5	8±1	0.03	0.29±0.03
$9_{4,6}$-$8_{4,5}$	85665.793	7.22	383.1	2.8[1]		0.07[2]	
$9_{4,5}$-$8_{4,4}$	85665.852†	7.22	383.1	3.0[1]		”	
$9_{5,5}$-$8_{5,4}$	85666.957†	6.22	402.3	6.9[1]		”	
$9_{5,4}$-$8_{5,3}$	85666.958†	6.22	402.3	6.9[1]		”	
				4.9±0.5	13±2	0.05	0.73±0.07
$9_{6,4}$-$8_{6,3}$	85676.209	5.00	425.6	2.7[1]		0.03[2]	
$9_{6,3}$-$8_{6,2}$	85676.209†	5.00	425.6	2.7[1]		”	
$9_{3,7}$-$8_{3,6}$	85678.266†	8.00	368.2	8.1[1]		”	
$9_{3,6}$-$8_{3,5}$	85686.710	8.00	368.2	[1,4]		...	
$9_{7,3}$-$8_{7,2}$	85690.626†	3.56	453.2	[1,4]		...	
$9_{7,2}$-$8_{7,1}$	85690.626†	3.56	453.2	[1,4]		...	
$9_{8,2}$-$8_{8,1}$	85709.046	1.89	485.0	3.9[1]		0.02[2]	
$9_{8,1}$-$8_{8,0}$	85709.046†	1.89	485.0	3.9[1]		”	
$9_{2,7}$-$8_{2,6}$	85987.171	8.56	357.6	4.2[1]		0.04[2]	
				4.3±0.4	8±1	0.04	0.30±0.03
$9_{1,8}$-$8_{1,7}$	87606.097	8.89	351.6	5.7[1]		0.04[2]	
				5.6±0.4	7±1	0.04	0.29±0.04
$10_{1,10}$-$9_{1,9}$	92637.415	9.90	335.1	4.3[1]		0.07[2]	
$10_{0,10}$-$9_{0,9}$	94516.441	9.99	353.5	4.3[1]		0.05[2]	
				4.3±0.8	6±2	0.04	0.27±0.06
$10_{2,9}$-$9_{2,8}$	95031.193	9.60	362.1	5.0[1]		0.04[2]	
				5.0±0.2	6.0±0.3	0.04	0.28±0.02
$10_{5,6}$-$9_{5,5}$	95188.702	7.50	406.8	1.7[1]		0.11[2]	
$10_{5,5}$-$9_{5,4}$	95188.703†	7.50	406.8	1.7[1]		”	
$10_{4,7}$-$9_{4,6}$	95190.312†	8.40	387.7	6.8[1]		”	
$10_{4,6}$-$9_{4,5}$	95190.441†	8.40	387.7	7.2[1]		”	
$10_{6,5}$-$9_{6,4}$	95197.445	6.40	430.2	5.2[1]		0.09[2]	
$10_{6,4}$-$9_{6,3}$	95197.445†	6.40	430.2	5.2[1]		”	
$10_{3,8}$-$9_{3,7}$	95208.542	9.10	372.8	[1,5]		...	
$10_{7,4}$-$9_{7,3}$	95212.555	5.10	457.8	6.1[1]		0.04[2]	
$10_{7,3}$-$9_{7,2}$	95212.555†	5.10	457.8	6.1[1]		”	

Tabla B.3: continued.

Transition $J_{K_a,K_c} - J'_{K'_a,K'_c}$	Predicted frequency (MHz)	S_{ij}	E_u (K)	v_{LSR} km s^{-1}	Δv km s^{-1}	T_{MB} (K)	$\int T_{MB} dv$ (K km s^{-1})
$10_{3,7}$-$9_{3,6}$	95223.001	9.10	372.8	5.8[1]		0.06[2]	
$10_{8,3}$-$9_{8,2}$	95232.437	3.60	489.6	5.8[1,3]		0.04[2]	
$10_{8,2}$-$9_{8,1}$	95232.437†	3.60	489.6	5.8[1,3]		”	
$10_{9,2}$-$9_{9,1}$	95256.353	1.90	525.6	5.4[1]		0.01[2]	
$10_{9,1}$-$9_{9,0}$	95256.353†	1.90	525.6	5.4[1]		”	
$10_{2,8}$-$9_{2,7}$	95632.961	9.60	362.2	5.4[1]		0.04[2]	
				5.4±0.9	6.0±0.3	0.04	0.28±0.07
$10_{1,9}$-$9_{1,8}$	97306.190	9.90	356.3	[6]		...	
$11_{1,11}$-$10_{1,10}$	101867.640	10.90	360.0	5.0[1]		0.11[2]	
$11_{0,11}$-$10_{0,10}$	103831.228	11.00	358.5	3.2[1,3]		0.16[2]	
$11_{2,10}$-$10_{2,9}$	104509.878	10.60	367.1	5.4[1]		0.12[2]	
$11_{5,7}$-$10_{5,6}$	104711.453	8.73	411.9	4.8[1]		0.13[2]	
$11_{5,6}$-$10_{5,5}$	104711.453†	8.73	411.9	4.8[1]		”	
$11_{4,8}$-$10_{4,7}$	104716.735	9.55	392.7	0.3[1,7]		0.18[2]	
$11_{4,7}$-$10_{4,6}$	104716.992†	9.55	392.7	0.4[1,7]		”	
$11_{6,6}$-$10_{6,5}$	104719.202†	7.73	435.2	6.8[1,7]		”	
$11_{6,5}$-$10_{6,4}$	104719.202†	7.73	435.2	6.8[1,7]		”	
$11_{7,5}$-$10_{7,4}$	104734.718	6.55	462.8	5.6[1]		0.05[2]	
$11_{7,4}$-$10_{7,3}$	104734.718†	6.55	462.8	5.6[1]		”	
				5.6±0.3	3±1	0.05	0.18±0.05
$11_{3,9}$-$10_{3,8}$	104741.451	10.20	377.8	5.0[1]		0.07[2]	
				4.9±0.6	5±1	0.06	0.36±0.07
$11_{8,3}$-$10_{8,2}$	104755.879	5.18	494.6	4.4[1]		0.05[2]	
$11_{8,4}$-$10_{8,3}$	104755.879†	5.18	494.6	4.4[1]		”	
$11_{3,8}$-$10_{3,7}$	104764.911	10.20	377.8	6.3[1]		0.07[2]	
$11_{9,3}$-$10_{9,2}$	104781.702	3.64	530.6	6.8[1]		0.04[2]	
$11_{9,2}$-$10_{9,1}$	104781.702†	3.64	530.6	6.8[1]		”	
$11_{2,9}$-$10_{2,8}$	105305.199	10.60	367.3	[8]		...	
$11_{1,10}$-$10_{1,9}$	106994.873	10.90	361.5	5.8[1]		0.08[2]	
$12_{1,12}$-$11_{1,11}$	111089.174	11.90	365.3	4.5[1]		0.14[2]	
$12_{0,12}$-$11_{0,11}$	113110.705	12.00	363.9	5.5[1,3]		0.14[2]	
$12_{2,11}$-$11_{2,10}$	113978.725	11.70	372.6	[9]		...	
$12_{5,8}$-$11_{5,7}$	114235.309	9.92	417.3	5.9[1]		0.16[2]	
$12_{5,7}$-$11_{5,6}$	114235.313†	9.92	417.3	5.9[1]		”	
$12_{6,7}$-$11_{6,6}$	114241.532	9.00	440.7	6.4[1]		0.14[2]	
$12_{6,6}$-$11_{6,5}$	114241.532†	9.00	440.7	6.4[1]		”	
$12_{4,9}$-$11_{4,8}$	114245.237	10.70	398.2	5.2[1]		0.21[2]	

Tabla B.3: continued.

Transition $J_{K_a,K_c} - J'_{K'_a,K'_c}$	Predicted frequency (MHz)	S_{ij}	E_u (K)	v_{LSR} km s^{-1}	Δv km s^{-1}	T_{MB} (K)	$\int T_{MB} dv$ (K km s^{-1})
$12_{4,8}$-$11_{4,7}$	114245.718†	10.70	398.2	6.4[1]		”	
$12_{7,6}$-$11_{7,5}$	114257.139	7.92	468.3	6.3[1]		0.10[2]	
$12_{7,5}$-$11_{7,4}$	114257.139†	7.92	468.3	6.3[1]		”	
$12_{3,10}$-$11_{3,9}$	114276.932	11.20	383.3	3.7[1,3]		0.18[2]	
$12_{8,5}$-$11_{8,4}$	114279.375†	6.67	500.1	7.9[1,3]		”	
$12_{8,4}$-$11_{8,3}$	114279.375†	6.67	500.1	7.9[1,3]		”	
$12_{9,3}$-$11_{9,2}$	114306.968	5.25	536.1	[3]		...	
$12_{9,4}$-$11_{9,3}$	114306.968†	5.25	536.1	[3]		...	
$12_{3,9}$-$11_{3,8}$	114313.356	11.20	383.3	4.4[1]		0.14[2]	
$12_{10,2}$-$11_{10,1}$	114339.256	3.67	576.3	[3]		...	
$12_{10,3}$-$11_{10,2}$	114339.256†	3.67	576.3	[3]		...	
$12_{2,10}$-$11_{2,9}$	115004.755	11.70	372.8	4.5[1]		0.04[2]	
$14_{0,14}$-$13_{0,13}$	131561.145	14.00	376.1	4.9[1,10]		0.37[2]	
$14_{2,13}$-$13_{2,12}$	132894.527	13.70	384.9	[11]		...	
$14_{5,10}$-$13_{5,9}$	133286.733	12.20	429.7	3.6[1]		0.28[2]	
$14_{5,9}$-$13_{5,8}$	133286.746†	12.20	429.7	3.6[1]		”	
$14_{6,9}$-$13_{6,8}$	133288.114†	11.40	453.1	6.7[1]		”	
$14_{6,8}$-$13_{6,7}$	133288.114†	11.40	453.1	6.7[1]		”	
				5.6±0.3	7.6±0.7	0.28	2.25±0.42
$14_{7,8}$-$13_{7,7}$	133302.844	12.90	480.7	5.6[1]		0.17[2]	
$14_{7,7}$-$13_{7,6}$	133302.844†	12.90	480.7	5.6[1]		”	
$14_{4,11}$-$13_{4,10}$	133309.134	12.90	410.5	[12]		...	
$14_{4,10}$-$13_{4,9}$	133310.584†	12.90	410.5	[12]		...	
$14_{8,7}$-$13_{8,6}$	133326.552	9.43	512.5	3.9[1]		0.17[2]	
$14_{8,6}$-$13_{8,5}$	133326.552†	9.43	512.5	3.9[1]		”	
$14_{3,12}$-$13_{3,11}$	133354.956	13.40	395.6	[13]		...	
$14_{9,5}$-$13_{9,4}$	133357.219†	8.21	548.5	[13]		...	
$14_{9,6}$-$13_{9,5}$	133357.219†	8.21	548.5	[13]		...	
$14_{10,5}$-$13_{10,4}$	133393.800	6.86	588.6	6.0[1,3]		0.06[2]	
$14_{10,4}$-$13_{10,3}$	133393.800†	6.86	588.6	6.0[1,3]		”	
$14_{3,11}$-$13_{3,10}$	133434.021	13.40	395.6	5.0[1]		0.19[2]	
$14_{11,4}$-$13_{11,3}$	133435.705†	5.36	632.9	8.8[1]		”	
$14_{11,3}$-$13_{11,2}$	133435.705†	5.36	632.9	8.8[1]		”	
$14_{2,12}$-$13_{2,11}$	134485.416	13.70	385.2	[9,14]		...	
$14_{1,13}$-$13_{1,12}$	135977.055	13.90	379.6	[15]		...	
$15_{1,15}$-$14_{1,14}$	138697.984	14.90	384.0	5.0[1]		0.22[2]	
$15_{0,15}$-$14_{0,14}$	140732.970	15.00	382.9	5.3[1,9]		0.27[2]	

Tabla B.3: continued.

Transition $J_{K_a,K_c} - J'_{K'_a,K'_c}$	Predicted frequency (MHz)	S_{ij}	E_u (K)	v_{LSR} km s^{-1}	Δv km s^{-1}	T_{MB} (K)	$\int T_{MB} dv$ (K km s^{-1})
$15_{2,14}$-$14_{2,13}$	142338.971	14.70	391.7	(9)		...	
$15_{6,10}$-$14_{6,9}$	142812.468	12.60	459.9	(15)		...	
$15_{6,9}$-$14_{6,8}$	142812.468†	12.60	459.9	(15)		...	
$15_{5,11}$-$14_{5,10}$	142814.497†	13.30	436.5	(15)		...	
$15_{5,10}$-$14_{5,9}$	142814.522†	13.30	436.5	(15)		...	
$15_{7,9}$-$14_{7,8}$	142826.172	11.70	487.5	6.5(1,16)		0.32(2)	
$15_{7,8}$-$14_{7,7}$	142826.172†	11.70	487.5	6.5(1,16)		”	
$15_{4,12}$-$14_{4,11}$	142844.832	13.90	417.4	3.3(1)		0.25(2)	
$15_{4,11}$-$14_{4,10}$	142847.202†	13.90	417.4	8.2(1)		”	
$15_{8,7}$-$14_{8,6}$	142850.241†	10.70	519.3	6.3(1)		”	
$15_{8,8}$-$14_{8,7}$	142850.241†	10.70	519.3	6.3(1)		”	
$15_{9,7}$-$14_{9,6}$	142882.189	9.60	555.3	(17)		...	
$15_{9,6}$-$14_{9,5}$	142882.189†	9.60	555.3	(17)		...	
$15_{3,13}$-$14_{3,12}$	142896.960	14.40	402.5	(5,15)		...	
$15_{10,6}$-$14_{10,5}$	142920.732	8.33	595.5	(5,15)		...	
$15_{10,5}$-$14_{10,4}$	142920.732†	8.33	595.5	(5,15)		...	
$15_{11,4}$-$14_{11,3}$	142965.148	6.93	639.8	(15)		...	
$15_{11,5}$-$14_{11,4}$	142965.148†	6.93	639.8	(15)		...	
$15_{3,12}$-$14_{3,11}$	143008.586	1.44	402.5	3.7(1,7)		0.37(2)	
$15_{2,13}$-$14_{2,12}$	144264.138	14.70	392.1	(18)		...	
$15_{1,14}$-$14_{1,13}$	145604.185	14.90	386.6	(19)		...	
$16_{1,16}$-$15_{1,15}$	147881.541	15.90	391.0	4.9(1)		0.34(2)	
$16_{0,16}$-$15_{0,15}$	149871.238	16.00	390.1	6.4(1)		0.48(2)	
$16_{2,15}$-$15_{2,14}$	151773.646	15.70	399.0	(15)		...	
$16_{6,11}$-$15_{6,10}$	152337.597	13.80	467.2	(9)		...	
$16_{6,10}$-$15_{6,9}$	152337.597†	13.80	467.2	(9)		...	
$16_{5,12}$-$15_{5,11}$	152343.759	14.40	443.8	(9,18)		...	
$16_{5,11}$-$15_{5,10}$	152343.805†	14.40	443.8	(9,18)		...	
$16_{7,10}$-$15_{7,9}$	152349.848†	12.90	494.8	(9,18)		...	
$16_{7,9}$-$15_{7,8}$	152349.848†	12.90	494.8	(9,18)		...	
$16_{8,8}$-$15_{8,7}$	152374.002	12.00	526.6	(9)		...	
$16_{8,9}$-$15_{8,8}$	152374.002†	12.00	526.6	(9)		...	
$16_{4,13}$-$15_{4,12}$	152383.211	15.00	424.7	(9)		...	
$16_{4,12}$-$15_{4,11}$	152386.956†	15.00	424.7	(9)		...	
$16_{9,8}$-$15_{9,7}$	152407.043	10.90	562.6	(9,18)		...	
$16_{9,7}$-$15_{9,6}$	152407.043†	10.90	562.6	(9,18)		...	
$16_{3,14}$-$15_{3,13}$	152440.458	15.40	409.8	(9)		...	

Tabla B.3: continued.

Transition $J_{K_a,K_c} - J'_{K'_a,K'_c}$	Predicted frequency (MHz)	S_{ij}	E_u (K)	v_{LSR} km s^{-1}	Δv km s^{-1}	T_{MB} (K)	$\int T_{MB} dv$ (K km s^{-1})
$16_{10,6}$-$15_{10,5}$	152447.416†	9.75	602.8	[9]		...	
$16_{10,7}$-$15_{10,6}$	152447.416†	9.75	602.8	[9]		...	
$16_{3,13}$-$15_{3,12}$	152594.382	15.40	409.8	[15]		...	
$16_{2,14}$-$15_{2,13}$	154065.377	15.70	899.5	[18]		...	
$16_{1,15}$-$15_{1,14}$	155211.430	15.90	394.1	6.9[1,3]		0.29[2]	
$17_{1,17}$-$16_{1,16}$	157055.233	16.90	398.6	[11]		...	
$17_{0,17}$-$16_{0,16}$	158978.488	17.00	397.7	[11]		...	
$17_{2,16}$-$16_{2,15}$	161197.973	16.80	406.7	6.7[1]		0.42[2]	
$16_{6,12}$-$15_{6,11}$	161863.551	14.90	475.0	5.4[1,9,20]		0.86[2]	
$16_{6,11}$-$15_{6,10}$	161863.551†	14.90	475.0	5.4[1,9,20]		”	
$17_{7,11}$-$16_{7,10}$	161873.893	14.10	502.6	3.9[1,3]		0.91[2]	
$17_{7,10}$-$16_{7,9}$	161873.893†	14.10	502.6	3.9[1,3]		”	
$17_{5,13}$-$16_{5,12}$	161874.616†	15.50	451.6	5.2[1,3]		”	
$17_{5,12}$-$16_{5,11}$	161874.696†	15.50	451.6	5.4[1,3]		”	
$17_{8,10}$-$16_{8,9}$	161897.839	13.20	534.4	3.2[1,3]		0.36[2]	
$17_{8,9}$-$16_{8,8}$	161897.839†	13.20	534.4	3.2[1,3]		”	
$17_{4,14}$-$16_{4,13}$	161924.382	16.10	432.5	[18]		...	
$17_{4,13}$-$16_{4,12}$	161930.132†	16.10	432.5	[18]		...	
$17_{9,9}$-$16_{9,8}$	161931.774†	12.20	570.4	[18]		...	
$17_{9,8}$-$16_{9,7}$	161931.774†	12.20	570.4	[18]		...	
$17_{10,8}$-$16_{10,7}$	161973.833	11.10	610.6	[9]		...	
$17_{10,7}$-$16_{10,6}$	161973.833†	11.10	610.6	[9]		...	
$17_{3,15}$-$16_{3,14}$	161984.970	16.50	417.6	6.1[1]		0.46[2]	
$17_{11,7}$-$16_{11,6}$	162022.966	9.88	654.9	[21]		...	
$17_{11,6}$-$16_{11,5}$	162022.966†	9.88	654.9	[21]		...	
$17_{12,6}$-$16_{12,5}$	162078.538	8.53	703.3	[3,22]		...	
$17_{12,5}$-$16_{12,4}$	162078.538†	8.53	703.3	[3,22]		...	
$17_{3,14}$-$16_{3,13}$	162192.845	16.50	417.6	[9]		...	
$17_{2,15}$-$16_{2,14}$	163885.788	16.80	407.4	4.9[1]		0.28[2]	
$17_{1,16}$-$16_{1,15}$	164796.787	16.90	402.0	5.2[1]		0.33[2]	
$18_{1,18}$-$17_{1,17}$	166219.078	17.90	406.6	5.0[1]		0.26[2]	
$18_{0,18}$-$17_{0,17}$	168057.908	18.00	405.7	5.2[1,23]		0.34[2]	
$18_{2,17}$-$17_{2,16}$	170611.398	17.80	414.9	[18]		...	
$18_{6,13}$-$17_{6,12}$	171390.382	16.00	483.2	5.1[1]		0.37[2]	
$18_{6,12}$-$17_{6,11}$	171390.383†	16.00	483.2	5.1[1]		”	
$18_{7,12}$-$17_{7,11}$	171398.329	15.30	510.8	3.8[1,24]		0.25[2]	
$18_{7,11}$-$17_{7,10}$	171398.329†	15.30	510.8	3.8[1,24]		”	

Tabla B.3: continued.

Transition $J_{K_a,K_c} - J'_{K'_a,K'_c}$	Predicted frequency (MHz)	S_{ij}	E_u (K)	v_{LSR} km s^{-1}	Δv km s^{-1}	T_{MB} (K)	$\int T_{MB} dv$ (K km s^{-1})
$18_{5,14}$-$17_{5,13}$	171407.163	16.60	459.8	6.0[1]		0.45[2]	
$18_{5,13}$-$17_{5,12}$	171407.300†	16.60	459.8	6.2[1]		”	
$18_{8,11}$-$17_{8,10}$	171421.756	14.40	542.6	6.4[1]		0.24[2]	
$18_{8,10}$-$17_{8,9}$	171421.756†	14.40	542.6	6.4[1]		”	
$18_{9,9}$-$17_{9,8}$	171456.373	13.50	578.6	4.7[1,25]		0.26[2]	
$18_{9,10}$-$17_{9,9}$	171456.373†	13.50	578.6	4.7[1,25]		”	
$18_{4,15}$-$17_{4,14}$	171468.439	17.10	440.7	6.0[1,20]		0.39[2]	
$18_{4,14}$-$17_{4,13}$	171477.043	17.10	440.7	5.7[1]		0.28[2]	
$18_{10,9}$-$17_{10,8}$	171499.967	12.40	618.8	[3,26]		...	
$18_{10,8}$-$17_{10,7}$	171499.967†	12.40	618.8	[3,26]		...	
$18_{3,16}$-$17_{3,15}$	171529.936	17.50	425.8	6.2[1]		0.48[2]	
$18_{11,7}$-$17_{11,6}$	171551.293	11.30	663.1	[7]		...	
$18_{11,8}$-$17_{11,7}$	171551.293†	11.30	663.1	[7]		...	
$18_{12,6}$-$17_{12,5}$	171609.602	10.00	696.1	7.1[1]		0.13[2]	
$18_{12,7}$-$17_{12,6}$	171609.602†	10.00	696.1	7.1[1]		”	
$18_{13,6}$-$17_{13,5}$	171674.410	8.61	764.0	[3,22]		...	
$18_{13,5}$-$17_{13,4}$	171674.410†	8.61	764.0	[3,22]		...	
$18_{14,4}$-$17_{14,3}$	171745.387	7.11	820.6	[9]		...	
$18_{14,5}$-$17_{14,4}$	171745.387†	7.11	820.6	[9]		...	
$18_{3,15}$-$17_{3,14}$	171805.498	17.50	425.9	1.9[1,3,15]		0.40[2]	
$18_{2,16}$-$17_{2,15}$	173721.353	17.80	415.7	[27]		...	
$18_{1,17}$-$17_{1,16}$	174358.161	17.90	410.4	5.8[1]		0.54[2]	
$19_{1,19}$-$18_{1,18}$	175373.171	18.90	415.0	2.4[1]		0.39[2]	
$19_{0,19}$-$18_{0,18}$	177113.143	19.00	414.3	[3]		...	
$21_{2,20}$-$20_{2,19}$	198781.116	20.80	442.2	5.0[1]		0.21[2]	
				5.00±0.11	7.5±0.3	0.21	1.70±0.07
$21_{7,15}$-$20_{7,14}$	199974.194	18.70	538.2	2.9[1]		0.48[2]	
$21_{7,14}$-$20_{7,13}$	199974.194†	18.70	538.2	2.9[1]		”	
$21_{6,16}$-$20_{6,15}$	199976.624†	19.30	510.6	6.6[1]		”	
$21_{6,15}$-$20_{6,14}$	199976.631†	19.30	510.6	6.6[1]		”	
				4.8±0.6	12±1	0.41	5.1±0.5
$21_{8,14}$-$20_{8,13}$	199994.020	18.00	570.1	[18]		...	
$21_{8,13}$-$20_{8,12}$	199994.020†	18.00	570.1	[18]		...	
$21_{5,17}$-$20_{5,16}$	200015.883	19.80	487.3	4.3[1]		0.30[2]	
$21_{5,16}$-$20_{5,15}$	200016.441†	19.80	487.3	5.2[1]		”	
				4.8±0.6	7.4±0.3	0.33	2.63±0.09
$21_{9,13}$-$20_{9,12}$	200029.290	17.10	606.1	5.6[1,9]		0.23[2]	

Tabla B.3: continued.

Transition $J_{K_a,K_c} - J'_{K'_a,K'_c}$	Predicted frequency (MHz)	S_{ij}	E_u (K)	v_{LSR} km s^{-1}	Δv km s^{-1}	T_{MB} (K)	$\int T_{MB} dv$ (K km s^{-1})
$21_{9,12}$-$20_{9,11}$	200029.290†	17.10	606.1	5.6[1,9]		”	
$21_{10,12}$-$20_{10,11}$	200076.495	16.20	646.2	4.9[1]		0.14[2]	
$21_{10,11}$-$20_{10,12}$	200076.495†	16.20	646.2	4.9[1]		”	
				4.2±1.9	8±2	0.15	1.3±0.2
$21_{4,18}$-$20_{4,17}$	200118.463	20.20	468.1	[27]		...	
$21_{11,11}$-$20_{11,10}$	200133.665†	15.20	690.6	[27]		...	
$21_{11,10}$-$20_{11,9}$	200133.665†	15.20	690.6	[27]		...	
$21_{4,17}$-$20_{4,16}$	200143.832†	20.20	468.1	[27]		...	
$21_{3,19}$-$20_{3,18}$	200160.904	20.60	453.3	[28]		...	
$21_{12,10}$-$20_{12,9}$	200199.618	14.10	739.0	[12]		...	
$21_{12,9}$-$20_{12,8}$	200199.618†	14.10	739.0	[12]		...	
$21_{13,8}$-$20_{13,7}$	200273.599	13.00	791.5	[29]		...	
$21_{13,9}$-$20_{13,8}$	200273.599†	13.00	791.5	[29]		...	
$21_{14,7}$-$20_{14,6}$	200355.096	11.70	848.1	4.6[1,22]		0.07[2]	
$21_{14,8}$-$20_{14,7}$	200355.096†	11.70	848.1	4.6[1,22]		”	
$21_{15,7}$-$20_{15,6}$	200443.743	10.30	908.7	3.6[1]		0.10[2]	
$21_{15,6}$-$20_{15,5}$	200443.743†	10.30	908.7	3.6[1]		”	
$21_{16,5}$-$20_{16,4}$	200539.257	8.81	973.3	[3,30]		...	
$21_{16,6}$-$20_{16,5}$	200539.257†	8.81	973.3	[3,30]		...	
$21_{3,18}$-$20_{3,17}$	200744.718	20.60	453.4	5.1[1,30]		0.34[2]	
				5.0±0.8	6±2	0.30	1.2±0.8
$22_{1,22}$-$21_{1,21}$	202778.912	21.90	442.9	6.5[1,31]		0.45[2]	
$21_{1,20}$-$20_{1,19}$	202876.912	21.90	442.9	[31]		...	
$21_{2,19}$-$20_{2,18}$	203272.786	20.80	443.6	6.4[1,10]		0.58[2]	
$22_{0,22}$-$21_{0,21}$	204172.450	22.00	442.3	4.8[1]		0.54[2]	
$22_{2,21}$-$21_{2,20}$	208145.956	21.80	452.2	5.2[1,32]		0.63[2]	
$22_{7,16}$-$21_{7,15}$	209500.406	19.80	548.3	5.1[1]		0.66[2]	
$22_{7,15}$-$21_{7,14}$	209500.406†	19.80	548.3	5.1[1]		”	
$22_{6,17}$-$21_{6,16}$	209507.453	20.40	547.7	5.5[1]		0.70[2]	
$22_{6,16}$-$21_{6,15}$	209507.465†	20.40	547.7	5.6[1]		”	
$22_{8,15}$-$21_{8,14}$	209518.290	19.10	580.1	[11]		...	
$22_{8,14}$-$21_{8,13}$	209518.290†	19.10	580.1	[11]		...	
$22_{9,14}$-$21_{9,13}$	209553.274	18.30	616.1	1.5[1,20]		1.11[2]	
$22_{9,13}$-$21_{9,12}$	209553.274†	18.30	616.1	1.5[1,20]		”	
$22_{5,18}$-$21_{5,17}$	209556.118†	20.90	497.3	5.6[1,20]		”	
$22_{5,17}$-$21_{5,16}$	209556.969†	20.90	497.3	6.8[1,20]		”	
$22_{10,12}$-$21_{10,11}$	209601.321	17.50	656.3	5.7[1]		0.26[2]	

Tabla B.3: continued.

Transition $J_{K_a,K_c} - J'_{K'_a,K'_c}$	Predicted frequency (MHz)	S_{ij}	E_u (K)	v_{LSR} km s^{-1}	Δv km s^{-1}	T_{MB} (K)	$\int T_{MB} dv$ (K km s^{-1})
$22_{10,13}$-$21_{10,12}$	209601.321†	17.50	656.3	5.7[1]		”	
$22_{11,11}$-$21_{11,10}$	209660.173	16.50	685.2	7.5[1,3]		0.38[2]	
$22_{11,12}$-$21_{11,11}$	209660.173†	16.50	685.2	7.5[1,3]		”	
$22_{4,19}$-$21_{4,18}$	209674.444	21.30	478.2	5.8[1,3]		0.76[2]	
$22_{3,20}$-$21_{3,19}$	209700.725	21.60	463.3	3.3[1,7]		0.78[2]	
$22_{4,18}$-$21_{4,17}$	209709.541	21.30	478.2	4.9[1,3]		0.71[2]	
$22_{12,10}$-$21_{12,9}$	209728.470	15.50	749.0	[20,33]		...	
$22_{12,11}$-$21_{12,10}$	209728.470†	15.50	749.0	[20,33]		...	
$22_{13,10}$-$21_{13,9}$	209805.348	14.30	801.6	[34]		...	
$22_{13,9}$-$21_{13,8}$	209805.348†	14.30	801.6	[34]		...	
$22_{14,8}$-$21_{14,7}$	209890.223	13.10	858.1	[3]		...	
$22_{14,9}$-$21_{14,8}$	209890.223†	13.10	858.1	[3]		...	
$22_{15,8}$-$21_{15,7}$	209982.678	11.80	918.8	[12]		...	
$22_{15,7}$-$21_{15,6}$	209982.678†	11.80	918.8	[12]		...	
$22_{16,6}$-$21_{16,5}$	210082.396	10.40	983.4	[3]		...	
$22_{16,7}$-$21_{16,6}$	210082.396†	10.40	983.4	[3]		...	
$22_{17,6}$-$21_{17,5}$	210189.118	8.86	1051.9	[3]		...	
$22_{17,5}$-$21_{17,4}$	210189.118†	8.86	1051.9	[3]		...	
$22_{3,19}$-$21_{3,18}$	210430.281	21.60	463.5	[15]		...	
$23_{1,23}$-$22_{1,22}$	211896.252	22.90	453.0	5.6[1]		0.25[2]	
$22_{1,21}$-$21_{1,20}$	212320.150	21.90	448.4	[35]		...	
$22_{2,20}$-$21_{2,19}$	213122.236	21.80	453.8	6.2[1,24]		0.63[2]	
$23_{0,23}$-$22_{0,22}$	213169.019	23.00	452.6	5.2[1]		0.57[2]	
$23_{2,22}$-$22_{2,21}$	217497.586	22.80	462.6	6.1[1,36]		0.80[2]	
$23_{7,17}$-$22_{7,16}$	219027.114	20.90	558.8	5.2[1]		0.52[2]	
$23_{7,16}$-$22_{7,15}$	219027.114†	20.90	558.8	5.2[1]		”	
				5.2±0.2	6.5±0.5	0.51	3.6±0.2
$23_{6,18}$-$22_{6,17}$	219039.405	21.40	531.2	5.8[1,3]		0.98[2]	
$23_{6,17}$-$22_{6,16}$	219039.426†	21.40	531.2	5.8[1,3]		”	
$23_{8,16}$-$22_{8,15}$	219042.656†	20.20	590.6	7.7[1,3]		”	
$23_{8,15}$-$22_{8,14}$	219042.656†	20.20	590.6	7.7[1,3]		”	
$23_{9,15}$-$22_{9,14}$	219077.080	19.50	626.6	6.9[1,3]		0.61[2]	
$23_{9,14}$-$22_{9,13}$	219077.080†	19.50	626.6	6.9[1,3]		”	
$23_{5,19}$-$22_{5,18}$	219098.494	21.90	507.8	4.3[1]		0.72[2]	
$23_{5,18}$-$22_{5,17}$	219099.767†	21.90	666.8	6.0[1]		”	
$23_{10,14}$-$22_{10,13}$	219125.777	18.70	666.8	5.9[1]		0.36[2]	
$23_{10,13}$-$22_{10,12}$	219125.777†	18.70	711.1	5.9[1]		”	

Tabla B.3: continued.

Transition $J_{K_a,K_c} - J'_{K'_a,K'_c}$	Predicted frequency (MHz)	S_{ij}	E_u (K)	v_{LSR} km s^{-1}	Δv km s^{-1}	T_{MB} (K)	$\int T_{MB} dv$ (K km s^{-1})
$23_{11,13}$-$22_{11,12}$	219186.165	17.70	711.1	[20]		...	
$23_{11,12}$-$22_{11,11}$	219186.165†	17.70	711.1	[20]		...	
$23_{4,20}$-$22_{4,19}$	219233.332	22.30	488.7	[7,37]		...	
$23_{3,21}$-$22_{3,20}$	219237.245†	22.60	473.9	[7,37]		...	
$23_{12,11}$-$22_{12,10}$	219256.697	16.70	759.6	[7,15]		...	
$23_{12,12}$-$22_{12,11}$	219256.697†	16.70	759.6	[7,15]		...	
$23_{4,19}$-$22_{4,18}$	219281.147	22.30	488.7	[29]		...	
$23_{13,10}$-$22_{13,9}$	219336.385	15.70	812.1	[36]		...	
$23_{13,11}$-$22_{13,10}$	219336.385†	15.70	812.1	[36]		...	
$23_{14,10}$-$22_{14,9}$	219424.569	14.50	868.7	6.8[1]		0.10[2]	
$23_{14,9}$-$22_{14,8}$	219424.569†	14.50	868.7	6.8[1]		”	
$23_{15,9}$-$22_{15,8}$	219520.776	13.20	929.3	[9]		...	
$23_{15,8}$-$22_{15,7}$	219520.776†	13.20	929.3	[9]		...	
$23_{16,7}$-$22_{16,6}$	219624.649	11.90	993.9	[24,38]		...	
$23_{16,8}$-$22_{16,7}$	219624.649†	11.90	993.9	[24,38]		...	
$23_{17,7}$-$22_{17,6}$	219735.902	10.40	1062.5	[39]		...	
$23_{17,6}$-$22_{17,5}$	219735.902†	10.40	1062.5	[39]		...	
$23_{18,5}$-$22_{18,4}$	219854.286	8.91	1134.9	[3]		...	
$23_{18,6}$-$22_{18,5}$	219854.286†	8.91	1134.9	[3]		...	
$23_{19,5}$-$22_{19,4}$	219979.574	7.30	1211.3	[11,24]		...	
$23_{19,4}$-$22_{19,3}$	219979.574†	7.30	1211.3	[11,24]		...	
$23_{20,3}$-$22_{20,2}$	220111.544	5.61	1291.5	4.6[1]		0.02[2]	
$23_{20,4}$-$22_{20,3}$	220111.544†	5.61	1291.5	4.6[1]		”	
$23_{3,20}$-$22_{3,19}$	220137.954	22.60	474.0	6.4[1]		0.35[2]	
				5.63±0.08	5.6±0.2	0.35	2.05±0.13
$24_{1,24}$-$23_{1,23}$	221005.220	23.90	463.6	4.4[1]		0.54[2]	
$23_{1,22}$-$22_{1,21}$	221728.966	22.90	459.0	[21]		...	
$24_{0,24}$-$23_{0,23}$	222159.276	24.00	463.2	[40]		...	
$23_{2,21}$-$22_{2,20}$	222963.571	22.80	464.5	6.4[1,3]		0.86[2]	
$24_{2,23}$-$23_{2,22}$	226835.665	23.80	473.5	6.6[1,41]		0.96[2]	
$24_{7,18}$-$23_{7,17}$	228554.339	22.00	569.8	5.0[1]		0.46[2]	
$24_{7,17}$-$23_{7,16}$	228554.339†	22.00	569.8	5.0[1]		”	
				4.6±0.2	7.8±0.5	0.47	3.9±0.2
$24_{8,17}$-$23_{8,16}$	228567.121	21.30	601.6	5.4[1]		0.40[2]	
$24_{8,16}$-$23_{8,15}$	228567.121†	21.30	601.6	5.4[1]		”	
$24_{6,19}$-$23_{6,18}$	228572.529	22.50	542.2	4.3[1,27]		0.78[2]	
$24_{6,18}$-$23_{6,17}$	228572.562†	22.50	542.2	4.3[1,27]		”	

Tabla B.3: continued.

Transition $J_{K_a,K_c} - J'_{K'_a,K'_c}$	Predicted frequency (MHz)	S_{ij}	E_u (K)	v_{LSR} km s^{-1}	Δv km s^{-1}	T_{MB} (K)	$\int T_{MB} dv$ (K km s^{-1})
$24_{9,16}$-$23_{9,15}$	228600.701	20.60	637.6	5.2[1]		0.26[2]	
$24_{9,15}$-$23_{9,14}$	228600.701†	20.60	637.6	5.2[1]		”	
				4.73±0.06	6.0±0.2	0.27	1.75±0.05
$24_{5,20}$-$23_{5,19}$	228643.093	23.00	518.8	[15]		...	
$24_{5,19}$-$23_{5,18}$	228644.963†	23.00	518.8	[15]		...	
$24_{10,15}$-$23_{10,14}$	228649.844†	19.80	677.8	[15]		...	
$24_{10,14}$-$23_{10,13}$	228649.844†	19.80	677.8	[15]		...	
$24_{11,13}$-$23_{11,12}$	228711.619	19.00	706.7	6.4[1,20,25]		0.30[2]	
$24_{11,14}$-$23_{11,13}$	228711.619†	19.00	706.7	6.4[1,20,25]		”	
$24_{3,22}$-$23_{3,21}$	228769.580	23.60	484.8	5.4[1]		0.46[2]	
				5.14±0.12	7.9±0.3	0.45	3.78±0.13
$24_{12,13}$-$23_{12,12}$	228784.270	18.00	755.2	4.1[1]		0.25[2]	
$24_{12,12}$-$23_{12,11}$	228784.270†	18.00	755.2	4.1[1]		”	
$24_{4,21}$-$23_{4,20}$	228795.015	23.30	499.7	2.6[1,9]		0.79[2]	
$24_{4,20}$-$23_{4,19}$	228859.248	23.30	499.7	[42,43]		...	
$24_{13,12}$-$23_{13,11}$	228866.679	17.00	823.1	[42,43]		...	
$24_{13,11}$-$23_{13,10}$	228866.679†	17.00	823.1	[42,43]		...	
$24_{14,10}$-$23_{14,9}$	228958.097	15.80	879.7	6.7[1]		0.10[2]	
$24_{14,11}$-$23_{14,10}$	228958.097†	15.80	879.7	6.7[1]		”	
				6.4±0.3	3.3±0.5	0.08	0.28±0.04
$24_{15,10}$-$23_{15,9}$	229057.997	14.60	940.3	[7]		...	
$24_{15,9}$-$23_{15,8}$	229057.997†	14.60	940.3	[7]		...	
$24_{16,8}$-$23_{16,7}$	229165.977	13.30	1004.9	[3]		...	
$24_{16,9}$-$23_{16,8}$	229165.977†	13.30	1004.9	[3]		...	
$24_{17,8}$-$23_{17,7}$	229281.717	12.00	1073.5	[9]		...	
$24_{17,7}$-$23_{17,6}$	229281.717†	12.00	1073.5	[9]		...	
$24_{3,21}$-$23_{3,20}$	229869.001	23.60	485.1	[13]		...	
$25_{1,25}$-$24_{1,24}$	230106.215	24.90	474.7	1.7[1,3,44]		0.28[2]	
$24_{1,23}$-$23_{1,22}$	231101.166	23.30	470.1	4.4[1]		0.62[2]	
$25_{0,25}$-$24_{0,24}$	231145.708	25.00	474.3	6.1[1,45]		1.10[2]	
$24_{2,22}$-$23_{2,21}$	232792.721	23.80	475.7	[9]		...	
$25_{2,24}$-$24_{2,23}$	236159.904	24.80	484.9	6.2[1,46]		1.09[2]	
$25_{7,19}$-$24_{7,18}$	238082.101	23.00	581.2	6.0[1,47]		0.78[2]	
$25_{7,18}$-$24_{7,17}$	238082.102†	23.00	581.2	6.0[1,47]		”	
$25_{8,18}$-$24_{8,17}$	238091.686	22.40	613.0	5.4[1]		0.67[2]	
$25_{8,17}$-$24_{8,16}$	238091.686†	22.40	613.0	5.4[1]		”	
$25_{6,20}$-$24_{6,19}$	238106.874	23.60	553.6	5.7[1]		0.80[2]	

Tabla B.3: continued.

Transition $J_{K_a,K_c} - J'_{K'_a,K'_c}$	Predicted frequency (MHz)	S_{ij}	E_u (K)	v_{LSR} km s^{-1}	Δv km s^{-1}	T_{MB} (K)	$\int T_{MB} dv$ (K km s^{-1})
$25_{6,19}$-$24_{6,18}$	238106.926†	23.60	553.6	5.7[1]		”	
$25_{9,17}$-$24_{9,16}$	238124.127	21.80	649.0	6.5[1]		0.36[2]	
$25_{9,16}$-$24_{9,15}$	238124.127†	21.80	649.0	6.5[1]		”	
$25_{10,15}$-$24_{10,14}$	238173.505	21.00	689.2	6.4[1,16,24]		0.28[2]	
$25_{10,16}$-$24_{10,15}$	238173.505†	21.00	689.2	6.4[1,16,24]		”	
$25_{5,21}$-$24_{5,20}$	238189.989	24.00	530.2	6.6[1,15]		0.86[2]	
$25_{5,20}$-$24_{5,19}$	238192.692†	24.00	530.2	8.0[1,15]		”	
$25_{11,14}$-$24_{11,13}$	238236.510	20.20	718.1	6.4[1,20]		0.51[2]	
$25_{11,15}$-$24_{11,14}$	238236.510†	20.20	718.1	6.4[1,20]		”	
$25_{3,23}$-$24_{3,22}$	238296.823	24.60	496.3	4.9[1]		0.49[2]	
				4.5±0.2	7.1±0.4	0.52	4.0±0.2
$25_{12,13}$-$24_{12,12}$	238311.160	19.20	782.0	[3]		...	
$25_{12,14}$-$24_{12,13}$	238311.160†	19.20	782.0	[3]		...	
$25_{4,22}$-$24_{4,21}$	238359.333	24.40	511.1	4.2[1,37]		0.51[2]	
$25_{13,13}$-$24_{13,12}$	238396.196	18.20	834.5	[3,48]		...	
$25_{13,12}$-$24_{13,11}$	238396.196†	18.20	834.5	[3,48]		...	
$25_{4,21}$-$24_{4,20}$	238444.506	24.40	511.1	5.2[1]		0.54[2]	
				5.2±0.2	6.3±0.6	0.54	3.6±0.4
$25_{14,11}$-$24_{14,10}$	238490.776	17.20	891.1	**		...	
$25_{14,12}$-$24_{14,11}$	238490.776†	17.20	891.1	**		...	
$25_{15,11}$-$24_{15,10}$	238594.305	16.00	951.7	4.9[1,20,49]		0.17[2]	
$25_{15,10}$-$24_{15,9}$	238594.305†	16.00	951.7	4.9[1,20,49]		”	
$25_{16,9}$-$24_{16,8}$	238706.338	14.80	1016.4	[3]		...	
$25_{16,10}$-$24_{16,9}$	238706.338†	14.80	1016.4	[3]		...	
$25_{17,9}$-$24_{17,8}$	238826.522	13.40	1084.9	[3,22]		...	
$25_{17,8}$-$24_{17,7}$	238826.522†	13.40	1084.9	[3,22]		...	
$26_{1,26}$-$25_{1,25}$	239199.654	25.90	486.2	4.1[1]		0.87[2]	
$25_{3,22}$-$24_{3,21}$	239624.398	24.60	496.6	[31]		...	
$26_{0,26}$-$25_{0,25}$	240130.312	26.00	485.9	5.4[1,18]		0.87[2]	
$25_{1,24}$-$24_{1,23}$	240435.183	24.90	481.7	[9]		...	
$25_{2,23}$-$24_{2,22}$	242606.029	24.80	487.3	[50]		...	
$26_{2,25}$-$25_{2,24}$	245470.066	25.80	496.6	[15]		...	
$26_{7,20}$-$25_{7,19}$	247610.422	24.10	593.1	[11]		...	
$26_{7,19}$-$25_{7,18}$	247610.423†	24.10	593.1	[11]		...	
$26_{8,19}$-$25_{8,18}$	247616.355†	23.50	624.9	[11]		...	
$26_{8,18}$-$25_{8,17}$	247616.355†	23.50	624.9	[11]		...	
$26_{6,21}$-$25_{6,20}$	247642.489	24.60	565.5	3.8[1]		0.46[2]	

Tabla B.3: continued.

Transition $J_{K_a,K_c} - J'_{K'_a,K'_c}$	Predicted frequency (MHz)	S_{ij}	E_u (K)	v_{LSR} km s^{-1}	Δv km s^{-1}	T_{MB} (K)	$\int T_{MB} dv$ (K km s^{-1})
$26_{6,20}$-$25_{6,19}$	247642.568†	24.60	565.5	3.9[1]		”	
				3.8±0.4	5±2	0.47	2.6±0.5
$26_{9,18}$-$25_{9,17}$	247647.348	22.90	660.9	4.0[1]		0.30[2]	
$26_{9,17}$-$25_{9,16}$	247647.348†	22.90	660.9	4.0[1]		”	
$26_{10,17}$-$25_{10,16}$	247696.741	22.20	701.1	[15,51]		...	
$26_{10,16}$-$25_{10,15}$	247696.741†	22.20	701.1	[15,51]		...	
$26_{5,22}$-$25_{5,21}$	247739.253	25.00	542.1	2.6[1]		0.46[2]	
$26_{5,21}$-$25_{5,20}$	247743.100†	25.00	542.1	7.3[1]		”	
$26_{11,16}$-$25_{11,15}$	247760.814	21.30	730.0	3.3[1]		0.22[2]	
$26_{11,15}$-$25_{11,14}$	247760.814†	21.30	730.0	3.3[1]		”	
$26_{3,24}$-$25_{3,23}$	247818.057	25.70	508.2	6.1[1]		0.29[2]	
$26_{12,15}$-$25_{12,14}$	247837.339	20.50	793.9	[11]		...	
$26_{12,14}$-$25_{12,13}$	247837.339†	20.50	793.9	[11]		...	
$26_{13,13}$-$25_{13,12}$	247924.904	19.50	846.4	[15]		...	
$26_{13,14}$-$25_{13,13}$	247924.904†	19.50	846.4	[15]		...	
$26_{4,23}$-$25_{4,22}$	247926.076†	25.40	523.0	[15]		...	
$26_{14,13}$-$25_{14,12}$	248022.566	18.50	903.0	[46]		...	
$26_{14,12}$-$25_{14,11}$	248022.566†	18.50	903.0	[46]		...	
$26_{4,22}$-$25_{4,21}$	248037.665	25.40	523.1	[9]		...	
$26_{15,11}$-$25_{15,10}$	248129.661	17.30	963.6	[3]		...	
$26_{15,12}$-$25_{15,11}$	248129.661†	17.30	963.6	[3]		...	
$26_{16,10}$-$25_{16,9}$	248245.694	16.20	1028.3	[7,52]		...	
$26_{16,11}$-$25_{16,10}$	248245.694†	16.20	1028.3	[7,52]		...	
$27_{1,27}$-$26_{1,26}$	248285.965	26.90	498.1	[11]		...	
$27_{0,27}$-$26_{0,26}$	249114.622	27.00	497.8	[18,20]		...	
$26_{3,23}$-$25_{3,22}$	249404.734	25.70	508.6	2.7[1,53]		1.44[2]	
$26_{1,25}$-$25_{1,24}$	249729.833	25.90	493.7	[5,54]		...	
$26_{2,24}$-$25_{2,23}$	252400.254	25.90	499.4	6.3[1]		0.51[2]	
				5.1±0.2	9.2±0.6	0.48	4.7±0.4
$27_{2,26}$-$26_{2,25}$	254765.969	26.80	508.9	5.4[1,20]		0.72[2]	
$27_{7,21}$-$26_{7,20}$	257139.320	25.20	605.4	**		...	
$27_{7,20}$-$26_{7,19}$	257139.322†	25.20	605.4	**		...	
$27_{8,20}$-$26_{8,19}$	257141.130†	24.60	637.3	**		...	
$27_{8,19}$-$26_{8,18}$	257141.130†	24.60	637.3	**		...	
$27_{9,19}$-$26_{9,18}$	257170.354	24.00	673.3	5.7[1]		0.36[2]	
$27_{9,18}$-$26_{9,17}$	257170.354†	24.00	673.3	5.7[1]		”	
				6.1±0.2	5.5±0.4	0.21	1.21±0.12

Tabla B.3: continued.

Transition $J_{K_a,K_c} - J'_{K'_a,K'_c}$	Predicted frequency (MHz)	S_{ij}	E_u (K)	v_{LSR} km s^{-1}	Δv km s^{-1}	T_{MB} (K)	$\int T_{MB} dv$ (K km s^{-1})
$27_{6,22}$-$26_{6,21}$	257179.420	25.70	577.8	3.2[1]		0.42[2]	
$27_{6,21}$-$26_{6,20}$	257179.541†	25.70	577.8	3.2[1]		”	
$27_{10,17}$-$26_{10,16}$	257219.534	23.30	713.5	[15]		...	
$27_{10,18}$-$26_{10,17}$	257219.534†	23.30	713.5	[15]		...	
$27_{11,17}$-$26_{11,16}$	257284.506	22.50	757.8	[55]		...	
$27_{11,16}$-$26_{11,15}$	257284.506†	22.50	757.8	[55]		...	
$27_{5,23}$-$26_{5,22}$	257290.945†	26.10	554.5	[55]		...	
$27_{5,22}$-$26_{5,21}$	257296.345†	26.10	554.5	[55]		...	
$27_{3,25}$-$26_{3,24}$	257332.363	26.70	520.5	[10,56]		...	
$27_{12,15}$-$26_{12,14}$	257362.777	21.70	806.2	[10,56]		...	
$27_{12,16}$-$26_{12,15}$	257362.777†	21.70	806.2	[10,56]		...	
$28_{1,28}$-$27_{1,27}$	257365.583†	28.00	510.4	[10,56]		...	
$27_{13,14}$-$26_{13,13}$	257452.770	20.70	858.8	[31,55]		...	
$27_{13,15}$-$26_{13,14}$	257452.770†	20.70	858.8	[31,55]		...	
$27_{4,24}$-$26_{4,23}$	257494.978	26.40	535.4	[3]		...	
$27_{14,13}$-$26_{14,12}$	257553.432	19.70	915.4	5.6[1]		0.24[2]	
$27_{14,14}$-$26_{14,13}$	257553.432†	19.70	915.4	5.6[1]		”	
$27_{4,23}$-$26_{4,22}$	257639.544	26.40	535.4	5.5[1]		0.70[2]	
$27_{15,13}$-$26_{15,12}$	257664.026	18.70	976.0	5.0[1,20]		0.31[2]	
$27_{15,12}$-$26_{15,11}$	257664.026†	18.70	976.0	5.0[1,20]		”	
$28_{0,28}$-$27_{0,27}$	258099.756	28.00	510.2	5.8[1]		0.31[2]	
				5.8±0.3	8±1	0.32	2.7±0.3
$27_{19,9}$-$26_{19,8}$	258196.275	13.60	1258.1	[12,25]		...	
$27_{19,8}$-$26_{19,7}$	258196.275†	13.60	1258.1	[12,25]		...	
$27_{1,26}$-$26_{1,25}$	258984.408	26.90	506.1	5.0[1]		1.00[2]	
$27_{3,24}$-$26_{3,23}$	259210.108	26.70	521.0	5.4[1]		0.39[2]	
$27_{2,25}$-$26_{2,24}$	262172.537	26.90	512.0	6.1[1]		0.87[2]	
$28_{2,27}$-$27_{2,26}$	264047.491	27.80	521.5	5.4[1]		0.53[2]	
				5.2±0.14	8.6±0.3	0.54	4.90±0.15
$29_{1,29}$-$28_{1,28}$	266438.936	29.00	523.2	4.9[1,24]		0.51[2]	
$28_{8,21}$-$27_{8,20}$	266666.012	25.70	650.0	4.0[1,13]		1.50[2]	
$28_{8,20}$-$27_{8,19}$	266666.012†	25.70	650.0	4.0[1,13]		”	
$28_{7,22}$-$27_{7,21}$	266666.816†	26.30	618.2	7.1[1,13]		”	
$28_{7,21}$-$27_{7,20}$	266666.819†	26.30	618.2	7.1[1,13]		”	
$28_{9,20}$-$27_{9,19}$	266693.135	25.10	686.1	5.2[1,9]		1.17[2]	
$28_{9,19}$-$27_{9,18}$	266693.135†	25.10	686.1	5.2[1,9]		”	
$28_{6,23}$-$27_{6,22}$	266717.718	26.70	590.6	5.9[1,10]		0.74[2]	

Tabla B.3: continued.

Transition $J_{K_a,K_c} - J'_{K'_a,K'_c}$	Predicted frequency (MHz)	S_{ij}	E_u (K)	v_{LSR} km s^{-1}	Δv km s^{-1}	T_{MB} (K)	$\int T_{MB} dv$ (K km s^{-1})
$28_{6,22}$-$27_{6,21}$	266717.898†	26.70	590.6	6.1[(1,10)]		”	
$28_{10,18}$-$27_{10,17}$	266741.867	24.40	726.3	6.1[(1)]		0.35[(2)]	
$28_{10,19}$-$27_{10,18}$	266741.867†	24.40	726.3	6.1[(1)]		”	
$28_{11,18}$-$27_{11,17}$	266807.562	23.70	755.2	5.7[(1,3)]		0.56[(2)]	
$28_{11,17}$-$27_{11,16}$	266807.562†	23.70	755.2	5.7[(1,3)]		”	
$28_{3,26}$-$27_{3,25}$	266838.828	27.70	533.3	[(11)]		...	
$28_{5,24}$-$27_{5,23}$	266845.120†	27.10	567.3	[(11)]		...	
$28_{5,23}$-$27_{5,22}$	266852.601†	27.10	567.3	[(11)]		...	
$28_{12,17}$-$27_{12,16}$	266887.445	22.90	803.6	6.6[(1)]		0.16[(2)]	
$28_{12,16}$-$27_{12,15}$	266887.445†	22.90	803.6	6.6[(1)]		”	
$28_{13,16}$-$27_{13,15}$	266979.761	22.00	871.6	4.7[(1,51)]		0.51[(2)]	
$28_{13,15}$-$27_{13,14}$	266979.761†	22.00	871.6	4.7[(1,51)]		0.51[(2)]	
$28_{4,25}$-$27_{4,24}$	267065.719	27.40	548.2	[(35)]		...	
$28_{14,15}$-$27_{14,14}$	267083.340	21.00	928.2	1.5[(1,3)]		0.38[(2)]	
$28_{14,14}$-$27_{14,13}$	267083.340†	21.00	928.2	1.5[(1,3)]		”	
$29_{0,29}$-$28_{0,28}$	267086.476†	29.00	523.0	5.0[(1)]		0.44[(2)]	
$28_{15,13}$-$27_{15,12}$	267197.364	20.00	988.8	[(57)]		...	
$28_{15,14}$-$27_{15,13}$	267197.364†	20.00	988.8	[(57)]		...	
$28_{4,24}$-$27_{4,23}$	267251.050	27.40	548.3	6.0[(1)]		0.39[(2)]	
$28_{16,12}$-$27_{16,11}$	267321.228	18.90	1053.5	**		...	
$28_{16,13}$-$27_{16,12}$	267321.228†	18.90	1053.5	**		...	
$28_{17,12}$-$27_{17,11}$	267454.462	17.70	1122.1	[(3,20,22)]		...	
$28_{17,11}$-$27_{17,10}$	267454.462†	17.70	1122.1	[(3,18,41)]		...	
$28_{1,27}$-$27_{1,26}$	268198.768	27.90	519.0	6.2[(1,58)]		0.55[(2)]	
$28_{3,25}$-$27_{3,24}$	269040.038	27.70	533.9	[(9,14)]		...	
$28_{2,26}$-$27_{2,25}$	271920.354	27.90	525.1	[(3)]		...	
$29_{2,28}$-$28_{2,27}$	273314.573	28.80	534.7	7.2[(1,59)]		0.39[(2)]	
$30_{1,30}$-$29_{1,29}$	275506.446	30.00	536.4	3.5[(1,3)]		1.03[(2)]	
$30_{0,30}$-$29_{0,29}$	276075.253	30.00	536.3	6.5[(1)]		1.03[(2)]	
$29_{8,22}$-$28_{8,21}$	276191.004	26.80	663.3	5.3[(1)]		0.54[(2)]	
$29_{8,21}$-$28_{8,20}$	276191.004†	26.80	663.3	5.3[(1)]		”	
				5.8±0.2	6.4±0.3	0.26	3.8±0.2
$29_{7,23}$-$28_{7,22}$	276198.931	27.30	631.5	7.8[(1)]		0.50[(2)]	
$29_{7,22}$-$28_{7,21}$	276198.935†	27.30	631.5	7.8[(1)]		”	
$29_{9,21}$-$28_{9,20}$	276215.682	26.20	699.3	6.2[(1)]		0.51[(2)]	
$29_{9,20}$-$28_{9,19}$	276215.682†	26.20	699.3	6.2[(1)]		”	
				5.8±0.2	8.1±0.4	0.38	3.31±0.15

Tabla B.3: continued.

Transition $J_{K_a,K_c} - J'_{K'_a,K'_c}$	Predicted frequency (MHz)	S_{ij}	E_u (K)	v_{LSR} km s^{-1}	Δv km s^{-1}	T_{MB} (K)	$\int T_{MB} dv$ (K km s^{-1})
$29_{6,24}$-$28_{6,23}$	276257.429	27.80	603.9	9.0[1,29]		0.75[2]	
$29_{6,23}$-$28_{6,22}$	276257.429†	27.80	603.9	9.0[1,29]		”	
$29_{10,20}$-$28_{10,19}$	276263.719	25.60	739.5	3.5[1]		0.26[2]	
$29_{10,19}$-$28_{10,18}$	276263.719†	25.60	739.5	3.5[1]		”	
$29_{11,19}$-$28_{11,18}$	276329.957	24.80	783.9	[3]		...	
$29_{11,18}$-$28_{11,17}$	276329.957†	24.80	783.9	[3]		...	
$29_{3,27}$-$28_{3,26}$	276336.557	28.70	546.6	6.5[1]		0.86[2]	
$29_{5,25}$-$28_{5,24}$	276401.818	28.10	580.6	[31,35,60]		...	
$29_{12,17}$-$28_{12,16}$	276411.314	24.00	816.9	3.4[1,31]		0.77[2]	
$29_{12,18}$-$28_{12,17}$	276411.314†	24.00	816.9	3.4[1,31]		”	
$29_{5,24}$-$28_{5,23}$	276412.057†	28.10	580.6	4.0[1,31]		”	
$29_{13,16}$-$28_{13,15}$	276505.844	23.20	884.9	[9,18]		...	
$29_{13,17}$-$28_{13,16}$	276505.844†	23.20	884.9	[9,18]		...	
$29_{14,16}$-$28_{14,15}$	276612.253	22.20	941.5	[23]		...	
$29_{14,15}$-$28_{14,14}$	276612.253†	22.20	941.5	[23]		...	
$29_{4,26}$-$28_{4,25}$	276637.919	28.40	561.5	5.1[1]		0.40[2]	
$29_{15,15}$-$28_{15,14}$	276729.635	21.20	1002.1	[22,24]		...	
$29_{15,14}$-$28_{15,13}$	276729.635†	21.20	1002.1	[22,24]		...	
$29_{16,13}$-$28_{16,12}$	276857.327	20.20	1066.8	[29,36,46]		...	
$29_{16,14}$-$28_{16,13}$	276857.327†	20.20	1066.8	[29,36,46]		...	
$29_{4,25}$-$28_{4,24}$	276873.178	28.40	561.5	6.4[1,46]		0.58[2]	
$29_{17,13}$-$28_{17,12}$	276994.811	19.00	1135.4	[7]		...	
$29_{17,12}$-$28_{17,11}$	276994.811†	19.00	1135.4	[7]		...	
$29_{18,11}$-$28_{18,10}$	277141.663	17.80	1207.9	[3]		...	
$29_{18,12}$-$28_{18,11}$	277141.663†	17.80	1207.9	[3]		...	
$29_{19,11}$-$28_{19,10}$	277297.513	16.60	1284.3	[3]		...	
$29_{19,10}$-$28_{19,9}$	277297.513†	16.60	1284.3	[3]		...	
$29_{1,28}$-$28_{1,27}$	277373.414	28.90	532.3	5.9[1]		0.91[2]	
$29_{3,26}$-$28_{3,25}$	278893.388	28.70	547.3	[61]		...	

Tabla A6. Emission lines of CH_2CHCN v_{11}=1 present in the spectral scan of the Orion-KL from the radio-telescope of IRAM 30-m. Column 1 indicates the line transition, Col. 2 gives the predicted frequency in the laboratory, Col. 3 the line strength, Col. 4 upper level energy, Col. 5 observed radial velocities relative to the local system rest (v_{LSR}), Col. 6 the line width, Col. 7 main beam temperature, and Col. 8 shows the area of the line. † blended with the previous line. ∗∗ hole in the observed spectrum.

(1) peak channel line observed velocity. (2) peak channel line intensity. (3) blended with U-line. (4) blended with H^+ (H 42α). (5) blended with $^{13}CH_3OH$. (6) blended with OCS. (7) blended with $(CH_3)_2CO$. (8) blended with H 49β. (9) blended with CH_3CH_2CN. (10) blended with $^{33}SO_2$. (11) blended with CH_3OH. (12) blended with CH_3OCH_3. (13) blended with $O^{13}CS$. (14) blended with CH_3CH_2CN v_{20}=1. (15) blended with $HCOOCH_3$. (16) blended with $CH_3{}^{13}CH_2CN$. (17) blended with $^{13}CH_3CN$. (18) blended with CH_3CH_2CN v_{13}/v_{21}. (19) blended with H_2CO. (20) blended with CH_2CHCN. (21) blended with $^{34}SO_2$. (22) blended with CH_2CHCN $v_{10}/v_{11}v_{15}$. (23) blended with $HCOO^{13}CH_3$. (24) blended with $H^{13}COOCH_3$. (25) blended with CH_2CHCN v_{15}=1. (26) blended with ^{29}SiO. (27) blended with HCCCN ν=0. (28) blended with H_2CCO. (29) blended with SO_2. (30) blended with CH_2CHCN v_{11}=2. (31) blended with CH_3CN v_8=1. (32) blended with $CH_2CH^{13}CN$. (33) blended with HCCCN v_6=1. (34) blended with H_2CCC. (35) blended with NH_2CHO. (36) blended with $|g_+$-$g_-|$-CH_3CH_2OH. (37) blended with $SO^{17}O$. (38) blended with CCCS. (39) blended with HNCO. (40) blended with CH_3CCH. (41) blended with $HCC^{13}CN$ v_6=1. (42) blended with HCCCN v_7=2. (43) blended with HDCO. (44) blended with CH_3OD. (45) blended with $H_2{}^{13}CS$. (46) blended with $CH_3CH_2{}^{13}CN$. (47) blended with $^{34}S^{18}O$. (48) blended with CH_3COOH v_t=0. (49) blended with HCCCN v_7=3. (50) blended with CH_2DCCH. (51) blended with $SO^{18}O$. (52) blended with $O^{13}C^{34}S$. (53) blended with $HNC^{18}O$. (54) blended with $CH_3C^{15}N$. (55) blended with CH_3CN. (56) blended with $CH_3{}^{13}CN$. (57) blended with SO. (58) blended with $^{13}CH_2CHCN$. (59) blended with HDCS. (60) blended with $H_2C^{33}S$. (61) blended with H_2CS.

Tabla B.4: Detected lines of CH_2CHCN v_{11}=2 .

Transition $J_{K_a,K_c} - J'_{K'_a,K'_c}$	Predicted frequency (MHz)	S_{ij}	E_u (K)	v_{LSR} km s^{-1}	Δv km s^{-1}	T_{MB} (K)	$\int T_{MB} dv$ (K km s^{-1})
$9_{1,9}$-$8_{1,8}$	83586.209	8.89	680.0	(3,4)		...	
$9_{0,9}$-$8_{0,8}$	85384.841	8.99	678.3	6.8(1)		0.02(2)	
				6.8±1.8	4±2	0.02	0.06±0.04
$9_{2,8}$-$8_{2,7}$	85787.036	8.56	686.8	(5)		...	
$9_{5,5}$-$8_{5,4}$	85909.768	6.22	730.9	8.4(1,6)		0.02(2)	
$9_{5,4}$-$8_{5,3}$	85909.769†	6.22	730.9	8.4(1,6)		”	
$9_{4,6}$-$8_{4,5}$	85910.556†	7.22	712.0	6.9(1,6)		”	
$9_{4,5}$-$8_{4,4}$	85910.556†	7.22	712.0	6.9(1,6)		”	
$9_{3,7}$-$8_{3,6}$	85925.250	8.00	697.3	(5)		...	
$9_{3,6}$-$8_{3,5}$	85934.580	8.00	697.3	(6)		...	
$9_{2,7}$-$8_{2,6}$	86254.865	8.56	686.9	(6)		...	
$9_{1,8}$-$8_{1,7}$	87894.325	8.89	681.0	(7)		...	
$10_{1,10}$-$9_{1,9}$	92843.810	9.90	684.4	3.7(1)		0.02(2)	
$10_{0,10}$-$9_{0,9}$	94750.528	9.99	682.9	2.8(1)		0.02(2)	
$10_{2,9}$-$9_{2,8}$	95296.506	9.60	691.4	7.9(1)		0.01(2)	
				7.9±0.2	7.2±0.5	0.01	0.07±0.01
$10_{5,6}$-$9_{5,5}$	95458.792	7.50	735.5	(6)		...	
$10_{5,5}$-$9_{5,4}$	95458.793†	7.50	735.5	(6)		...	
$10_{4,7}$-$9_{4,6}$	95462.755†	8.40	716.6	(6)		...	
$10_{4,6}$-$9_{4,5}$	95462.903†	8.40	716.6	(6)		...	
$10_{6,5}$-$9_{6,4}$	95465.362	6.40	758.5	(6)		...	
$10_{6,4}$-$9_{6,3}$	95465.362†	6.40	758.5	(6)		...	
$10_{7,4}$-$9_{7,3}$	95478.241	5.10	785.8	4.6(1)		0.02(2)	
$10_{7,3}$-$9_{7,2}$	95478.241†	5.10	785.8	4.6(1)		”	
				4.6±1.0	3.1±0.8	0.02	0.06±0.02
$10_{3,8}$-$9_{3,7}$	95483.635	9.10	701.9	3.1(1)		0.01(2)	
$10_{3,7}$-$9_{3,6}$	95499.610	9.10	701.9	(8)		...	
$10_{2,8}$-$9_{2,7}$	95936.014	9.60	691.5	7.5(1)		0.02(2)	
$10_{1,9}$-$9_{1,8}$	97624.273	9.90	685.7	5.3(1)		0.02(2)	
$11_{1,11}$-$10_{1,10}$	102092.769	10.90	689.3	6.4(1)		0.03(2)	
				6.4±0.4	3.9±0.6	0.02	0.10±0.02
$11_{0,11}$-$10_{0,10}$	104080.675	11.00	687.9	8.2(1)		0.03(2)	
$11_{2,10}$-$10_{2,9}$	104798.928	10.60	696.4	1.7(1,6)		0.04(2)	
$11_{5,7}$-$10_{5,6}$	105008.918	8.73	740.5	5.7(1)		0.01(2)	
$11_{5,6}$-$10_{5,5}$	105008.919†	8.73	740.5	5.7(1)		”	
$11_{6,6}$-$10_{6,5}$	105014.157	7.73	763.6	5.2(1)		0.01(2)	

Tabla B.4: continued.

Transition $J_{K_a,K_c} - J'_{K'_a,K'_c}$	Predicted frequency (MHz)	S_{ij}	E_u (K)	v_{LSR} km s^{-1}	Δv km s^{-1}	T_{MB} (K)	$\int T_{MB} dv$ (K km s^{-1})
$11_{6,5}$-$10_{6,4}$	105014.157†	7.73	763.6	5.2[1]		”	
$11_{4,8}$-$10_{4,7}$	105017.008	9.55	721.6	1.8[1]		0.03[2]	
$11_{4,7}$-$10_{4,6}$	105017.303†	9.55	721.6	2.6[1]		”	
				2.26±1.2	5±1	0.02	0.11±0.04
$11_{7,5}$-$10_{7,4}$	105027.149	6.55	790.8	[6]		...	
$11_{7,4}$-$10_{7,3}$	105027.149†	6.55	790.8	[6]		...	
$11_{3,9}$-$10_{3,8}$	105044.795	10.20	706.9	[5]		...	
$11_{8,3}$-$10_{8,2}$	105045.651†	5.18	822.2	[5]		...	
$11_{8,4}$-$10_{8,3}$	105045.651†	5.18	822.2	[5]		...	
$11_{3,8}$-$10_{3,7}$	105070.713	10.20	706.9	[6,9]		...	
$11_{2,9}$-$10_{2,8}$	105645.039	10.60	696.5	7.5[1]		0.02[2]	
$11_{1,10}$-$10_{1,9}$	107342.050	10.90	690.8	7.8[1,6]		0.06[2]	
$12_{1,12}$-$11_{1,11}$	111332.582	11.90	694.7	[6]		...	
$12_{0,12}$-$11_{0,11}$	113373.723	12.00	693.3	7.1[1,10]		0.04[2]	
$12_{2,11}$-$11_{2,10}$	114293.622	11.70	701.9	4.1[1]		0.04[2]	
$12_{5,8}$-$11_{5,7}$	114560.253	9.92	746.0	[11]		...	
$12_{5,7}$-$11_{5,6}$	114560.257†	9.92	746.0	[11]		...	
$12_{6,7}$-$11_{6,6}$	114563.596†	9.00	769.1	[11]		...	
$12_{6,6}$-$11_{6,5}$	114563.596†	9.00	769.1	[11]		...	
$12_{4,9}$-$11_{4,8}$	114573.503	10.70	727.1	[12,13,14]		...	
$12_{4,8}$-$11_{4,7}$	114574.055†	10.70	727.1	[12,13,14]		...	
$12_{7,6}$-$11_{7,5}$	114576.365†	7.92	796.3	[12,13,14]		...	
$12_{7,5}$-$11_{7,4}$	114576.365†	7.92	796.3	[12,13,14]		...	
$12_{8,5}$-$11_{8,4}$	114595.648	6.67	827.7	4.1[1,15]		0.03[2]	
$12_{8,4}$-$11_{8,3}$	114595.648†	6.67	827.7	4.1[1,15]		”	
$12_{3,10}$-$11_{3,9}$	114608.650	11.20	712.4	[6]		...	
$12_{3,9}$-$11_{3,8}$	114648.889	11.20	712.4	[16]		...	
$12_{2,10}$-$11_{2,9}$	115382.717	11.70	702.1	[6]		...	
$14_{0,14}$-$13_{0,13}$	131846.587	14.00	705.5	[7]		...	
$14_{2,13}$-$13_{2,12}$	133257.141	13.70	714.2	8.0[1]		0.07[2]	
$14_{6,9}$-$13_{6,8}$	133664.633	11.40	781.4	5.9[1]		0.04[2]	
$14_{6,8}$-$13_{6,7}$	133664.633†	11.40	781.4	5.9[1]		”	
$14_{5,10}$-$13_{5,9}$	133666.986†	12.20	758.4	6.8[1]		”	
$14_{5,9}$-$13_{5,8}$	133667.002†	12.20	758.4	6.8[1]		”	
$14_{7,8}$-$13_{7,7}$	133675.831	10.50	808.7	3.0[1,6]		0.03[2]	
$14_{7,7}$-$13_{7,6}$	133675.831†	10.50	808.7	3.0[1,6]		”	
$14_{4,11}$-$13_{4,10}$	133693.924	12.90	739.5	2.5[1]		0.07[2]	

Tabla B.4: continued.

Transition $J_{K_a,K_c} - J'_{K'_a,K'_c}$	Predicted frequency (MHz)	S_{ij}	E_u (K)	v_{LSR} km s^{-1}	Δv km s^{-1}	T_{MB} (K)	$\int T_{MB} dv$ (K km s^{-1})
$14_{4,10}$-$13_{4,9}$	133695.587†	12.90	739.5	6.2[1]		”	
				5.8±0.4	5±1	0.08	0.38±0.12
$14_{3,12}$-$13_{3,11}$	133743.689	13.40	724.8	3.7[1,6]		0.08[2]	
$14_{3,11}$-$13_{3,10}$	133831.007	13.40	724.8	[17]		...	
$14_{2,12}$-$13_{2,11}$	134942.808	13.70	714.6	[11]		...	
$14_{1,13}$-$13_{1,12}$	136405.766	13.90	709.1	6.6[1,6]		0.05[2]	
$15_{1,15}$-$14_{1,14}$	138993.496	14.90	713.4	6.6[1]		0.07[2]	
$15_{0,15}$-$14_{0,14}$	141027.791	15.00	712.3	6.9[1]		0.07[2]	
$15_{2,14}$-$14_{2,13}$	142724.661	14.70	721.1	[8]		...	
$15_{6,10}$-$14_{6,9}$	143216.346	12.60	788.3	[5]		...	
$15_{6,9}$-$14_{6,8}$	143216.346†	12.60	788.3	[5]		...	
$15_{5,11}$-$14_{5,10}$	143222.601	13.30	765.3	5.4[1,6]		0.09[2]	
$15_{5,10}$-$14_{5,9}$	143222.631†	13.30	765.3	5.4[1,6]		”	
$15_{7,9}$-$14_{7,8}$	143226.135	11.70	815.6	8.6[1,6]		0.11[2]	
$15_{7,8}$-$14_{7,7}$	143226.135†	11.70	815.6	8.6[1,6]		”	
$15_{8,7}$-$14_{8,6}$	143246.274	10.70	846.9	[5]		...	
$15_{8,8}$-$14_{8,7}$	143246.274†	10.70	846.9	[5]		...	
$15_{4,12}$-$14_{4,11}$	143258.173	13.90	746.4	[14,18]		...	
$15_{4,11}$-$14_{4,10}$	143260.891†	13.90	746.4	[14,18]		...	
$15_{9,6}$-$14_{9,5}$	143274.146	9.60	882.5	7.1[1]		0.03[2]	
$15_{9,7}$-$14_{9,6}$	143274.146†	9.60	882.5	7.1[1]		”	
$15_{10,5}$-$14_{10,4}$	143308.410	8.33	922.1	[6]		...	
$15_{10,6}$-$14_{10,5}$	143308.410†	8.33	922.1	[6]		...	
$15_{3,13}$-$14_{3,12}$	143314.260	14.40	731.7	[6]		...	
$15_{3,12}$-$14_{3,11}$	143437.511	14.40	731.7	[8,19]		...	
$15_{2,13}$-$14_{2,12}$	144762.219	14.70	721.5	8.4[1,6]		0.09[2]	
$15_{1,14}$-$14_{1,13}$	146057.714	14.90	716.1	[13]		...	
$16_{1,16}$-$15_{1,15}$	148193.547	15.90	720.5	[13]		...	
$16_{0,16}$-$15_{0,15}$	150174.678	16.00	719.5	[20,21]		...	
$16_{2,15}$-$15_{2,14}$	152181.846	15.70	728.4	[5,9,14,22]		...	
$16_{6,11}$-$15_{6,10}$	152768.932	13.80	795.7	6.6[1,6,23]		0.19[2]	
$16_{6,10}$-$15_{6,9}$	152768.932†	13.80	795.7	6.6[1,6,23]		”	
$16_{7,10}$-$15_{7,9}$	152776.855	12.90	822.9	[5]		...	
$16_{7,9}$-$15_{7,8}$	152776.855†	12.90	822.9	[5]		...	
$16_{5,12}$-$15_{5,11}$	152779.856†	14.40	772.6	[5]		...	
$16_{5,11}$-$15_{5,10}$	152779.856†	14.40	772.6	[5]		...	
$16_{8,9}$-$15_{8,8}$	152796.722	12.00	854.3	[5]		...	

Tabla B.4: continued.

Transition $J_{K_a,K_c} - J'_{K'_a,K'_c}$	Predicted frequency (MHz)	S_{ij}	E_u (K)	v_{LSR} km s^{-1}	Δv km s^{-1}	T_{MB} (K)	$\int T_{MB} dv$ (K km s^{-1})
$16_{8,8}$-$15_{8,7}$	152796.722†	12.00	854.3	(5)		...	
$16_{4,13}$-$15_{4,12}$	152825.305	15.00	753.7	(24)		...	
$16_{9,8}$-$15_{9,7}$	152825.349†	10.90	889.8	(24)		...	
$16_{9,7}$-$15_{9,6}$	152825.349†	10.90	889.8	(24)		...	
$16_{4,12}$-$15_{4,11}$	152829.601	15.00	753.7	(24)		...	
$16_{10,7}$-$15_{10,6}$	152861.109	9.75	929.4	(24)		...	
$16_{10,6}$-$15_{10,5}$	152861.109†	9.75	929.4	(24)		...	
$16_{3,14}$-$15_{3,13}$	152886.304	15.40	739.0	(14,24)		...	
$16_{11,6}$-$15_{11,5}$	152903.099	8.44	973.2	(6)		...	
$16_{11,5}$-$15_{11,4}$	152903.099†	8.44	973.2	(6)		...	
$16_{3,13}$-$15_{3,12}$	153056.213	15.40	739.1	(24)		...	
$16_{2,14}$-$15_{2,13}$	154604.267	15.70	728.9	7.2(1)		0.04(2)	
				7.2±0.7	3±2	0.05	0.14±0.07
$16_{1,15}$-$15_{1,14}$	155688.353	15.90	723.6	6.8(1)		0.10(2)	
$17_{1,17}$-$16_{1,16}$	157383.332	16.90	728.0	(25)		...	
$17_{0,17}$-$16_{0,16}$	159290.174	17.00	727.2	(14)		...	
$17_{2,16}$-$16_{2,15}$	161628.091	16.80	736.1	(18,26)		...	
$17_{6,12}$-$16_{6,11}$	162322.447	14.90	803.4	(5,8,18)		...	
$17_{6,11}$-$16_{6,10}$	162322.448†	14.90	803.4	(5,8,18)		...	
$17_{7,11}$-$16_{7,10}$	162328.020†	14.10	830.7	(5,8,18)		...	
$17_{7,10}$-$16_{7,9}$	162328.020†	14.10	830.7	(5,8,18)		...	
$17_{5,13}$-$16_{5,12}$	162338.860	15.50	780.4	(6)		...	
$17_{5,12}$-$16_{5,11}$	162338.956†	15.50	780.4	(6)		...	
$17_{8,10}$-$16_{8,9}$	162347.301	13.20	862.1	5.0(1)		0.06(2)	
$17_{8,9}$-$16_{8,8}$	162347.301†	13.20	862.1	5.0(1)		”	
				4.9±0.2	4±1	0.11	0.29±0.05
$17_{9,9}$-$16_{9,8}$	162376.472	12.20	897.6	4.8(1)		0.08(2)	
$17_{9,8}$-$16_{9,7}$	162376.472†	12.20	897.6	4.8(1)		”	
$17_{4,14}$-$16_{4,13}$	162395.438	16.10	761.5	6.1(1)		0.10(2)	
$17_{4,13}$-$16_{4,12}$	162402.032	16.10	761.5	5.7(1)		0.10(2)	
$17_{10,8}$-$16_{10,7}$	162413.576	11.10	937.2	(24)		...	
$17_{10,7}$-$16_{10,6}$	162413.576†	11.10	937.2	(24)		...	
$17_{11,7}$-$16_{11,6}$	162457.527	9.88	951.0	1.9(1)		0.05(2)	
$17_{11,6}$-$16_{11,5}$	162457.527†	9.88	951.0	1.9(1)		”	
$17_{3,15}$-$16_{3,14}$	162459.288†	16.50	746.8	5.2(1)		”	
$17_{12,6}$-$16_{12,5}$	162507.689	8.53	1028.8	3.8(1,27)		0.04(2)	
$17_{12,5}$-$16_{12,4}$	162507.689†	8.53	1028.8	3.8(1,27)		”	

Tabla B.4: continued.

Transition $J_{K_a,K_c} - J'_{K'_a,K'_c}$	Predicted frequency (MHz)	S_{ij}	E_u (K)	v_{LSR} km s^{-1}	Δv km s^{-1}	T_{MB} (K)	$\int T_{MB} dv$ (K km s^{-1})
$17_{3,14}$-$16_{3,13}$	162688.675	16.50	746.9	(8,22)		...	
$17_{2,15}$-$16_{2,14}$	164465.169	16.80	736.8	4.5(1,6)		0.14(2)	
$17_{1,16}$-$16_{1,15}$	165295.521	16.90	731.5	(5)		...	
$18_{1,18}$-$17_{1,17}$	166562.900	17.90	736.0	(13)		...	
$18_{0,18}$-$17_{0,17}$	168377.853	18.00	735.2	(6)		...	
$18_{2,17}$-$17_{2,16}$	171062.814	18.00	735.2	(5)		...	
$18_{6,13}$-$17_{6,12}$	171876.949	16.00	811.7	(5)		...	
$18_{6,12}$-$17_{6,11}$	171876.951†	16.00	811.7	(5)		...	
$18_{7,12}$-$17_{7,11}$	171879.655†	15.30	838.9	(5)		...	
$18_{7,11}$-$17_{7,10}$	171879.655†	15.30	838.9	(5)		...	
$18_{8,11}$-$17_{8,10}$	171898.020	14.40	870.3	7.2(1,6)		0.17(2)	
$18_{8,10}$-$17_{8,9}$	171898.020†	14.40	870.3	7.2(1,6)		”	
$18_{5,14}$-$17_{5,13}$	171899.715†	16.60	788.6	7.9(1,6)		”	
$18_{5,13}$-$17_{5,12}$	171899.878†	16.60	788.6	7.6(1,6)		0.17(2)	
$18_{9,9}$-$17_{9,8}$	171927.509	13.50	905.8	(6)		...	
$18_{9,10}$-$17_{9,9}$	171927.509†	13.50	905.8	(6)		...	
$18_{10,8}$-$17_{10,7}$	171965.795	12.40	945.5	(28)		...	
$18_{10,9}$-$17_{10,8}$	171965.795†	12.40	945.5	(28)		...	
$18_{4,15}$-$17_{4,14}$	171968.666	17.10	769.8	(14)		...	
$18_{4,14}$-$17_{4,13}$	171978.533	17.10	769.8	5.4(1)		0.10(2)	
$18_{3,16}$-$17_{3,15}$	172032.594	17.50	755.1	(5,16)		...	
$18_{3,15}$-$17_{3,14}$	172336.550	17.50	755.1	5.4(1)		0.16(2)	
$18_{1,17}$-$17_{1,16}$	174876.963	17.90	739.9	8.2(1)		0.20(2)	
$19_{1,19}$-$18_{1,18}$	175732.381	18.90	744.5	(7)		...	
$19_{0,19}$-$18_{0,18}$	177441.706	19.00	743.8	(6)		...	
$21_{2,20}$-$20_{2,19}$	199292.525	20.80	771.7	(29)		...	
$21_{7,15}$-$20_{7,14}$	200537.645	18.70	866.4	3.8(1,6)		0.30(2)	
$21_{7,14}$-$20_{7,13}$	200537.645†	18.70	866.4	3.8(1,6)		”	
$21_{6,16}$-$20_{6,15}$	200546.938	19.30	839.2	0.9(1,30)		0.18(2)	
$21_{6,15}$-$20_{6,14}$	200546.947†	19.30	839.2	0.9(1,30)		”	
$21_{8,14}$-$20_{8,13}$	200551.088†	18.00	897.1	7.1(1,30)		”	
$21_{8,13}$-$20_{8,12}$	200551.088†	18.00	897.1	7.1(1,30)		”	
$21_{9,12}$-$20_{9,11}$	200580.048	17.10	933.3	(30)		...	
$21_{9,13}$-$20_{9,12}$	200580.048†	17.10	933.3	(30)		...	
$21_{5,17}$-$20_{5,16}$	200594.427	19.80	816.1	3.5(1)		0.14(2)	
$21_{5,16}$-$20_{5,15}$	200595.091†	19.80	816.1	4.5(1)		”	
				3.9±0.2	8.9±0.8	0.12	1.12±0.08

Tabla B.4: continued.

Transition $J_{K_a,K_c} - J'_{K'_a,K'_c}$	Predicted frequency (MHz)	S_{ij}	E_u (K)	v_{LSR} km s^{-1}	Δv km s^{-1}	T_{MB} (K)	$\int T_{MB} dv$ (K km s^{-1})
$21_{10,12}$-$20_{10,11}$	200620.823	16.20	973.0	(31)		...	
$21_{10,11}$-$20_{10,10}$	200620.823†	16.20	973.0	(31)		...	
$21_{11,10}$-$20_{11,9}$	200671.355	15.20	1016.8	5.3(1,14,32,33)		0.12(2)	
$21_{11,11}$-$20_{11,10}$	200671.355†	15.20	1016.8	5.3(1,14,32,33)		”	
$21_{4,18}$-$20_{4,17}$	200707.431	20.20	797.3	(6)		...	
$21_{12,10}$-$20_{12,9}$	200730.424	14.10	1064.6	(14)		...	
$21_{12,9}$-$20_{12,8}$	200730.424†	14.10	1064.6	(14)		...	
$21_{4,17}$-$20_{4,16}$	200736.514	20.20	797.3	(14)		...	
$21_{3,19}$-$20_{3,18}$	200747.157	20.60	782.6	(34)		...	
$21_{13,9}$-$20_{13,8}$	200797.267	13.00	1116.5	(11)		...	
$21_{13,8}$-$20_{13,7}$	200797.267†	13.00	1116.5	(11)		...	
$21_{14,7}$-$20_{14,6}$	200871.382	11.70	1172.4	(8)		...	
$21_{14,8}$-$20_{14,7}$	200871.382†	11.70	1172.4	(8)		...	
$21_{3,18}$-$20_{3,17}$	201389.985	20.60	782.7	(8)		...	
$22_{1,22}$-$21_{1,21}$	203182.670	21.90	772.4	5.5(1)		0.12(2)	
$21_{1,20}$-$20_{1,19}$	203443.597	20.90	767.8	9.8(1)		0.06(2)	
$21_{2,19}$-$20_{2,18}$	204002.725	20.80	773.1	6.6(1)		0.16(2)	
$22_{0,22}$-$21_{0,21}$	204531.482	22.00	771.9	(24)		...	
$22_{2,21}$-$21_{2,20}$	208676.017	21.80	781.7	(6)		...	
$22_{7,16}$-$21_{7,15}$	210091.424	19.80	876.5	5.9(1,8)		0.21(2)	
$22_{7,15}$-$21_{7,14}$	210091.425†	19.80	876.5	5.9(1,8)		”	
$22_{8,15}$-$21_{8,14}$	210102.438	19.10	907.9	2.0(1)		0.14(2)	
$22_{8,14}$-$21_{8,13}$	210102.438†	19.10	907.9	2.0(1)		”	
$22_{6,17}$-$21_{6,16}$	210105.950†	20.40	849.3	7.0(1)		”	
$22_{6,16}$-$21_{6,15}$	210105.966†	20.40	849.3	7.0(1)		”	
$22_{9,14}$-$21_{9,13}$	210130.685	18.30	943.4	6.6(1)		0.03(2)	
$22_{9,13}$-$21_{9,12}$	210130.685†	18.30	943.4	6.6(1)		”	
$22_{5,18}$-$21_{5,17}$	210163.710	20.90	826.2	4.6(1)		0.21(2)	
$22_{5,17}$-$21_{5,16}$	210164.723†	20.90	826.2	6.1(1)		”	
$22_{10,12}$-$21_{10,11}$	210171.906	17.50	983.1	(6,35)		...	
$22_{10,13}$-$21_{10,12}$	210171.906†	17.50	983.1	(6,35)		...	
$22_{11,12}$-$21_{11,11}$	210223.733	16.50	1026.8	(22)		...	
$22_{11,11}$-$21_{11,10}$	210223.733†	16.50	1026.8	(22)		...	
$22_{12,10}$-$21_{12,9}$	210284.760	15.50	1074.7	(6)		...	
$22_{12,11}$-$21_{12,10}$	210284.760†	15.50	1074.7	(6)		...	
$22_{4,19}$-$21_{4,18}$	210293.371	21.30	807.4	5.1(1)		0.14(2)	
$22_{3,20}$-$21_{3,19}$	210314.141	21.60	792.7	(18)		...	

Tabla B.4: continued.

Transition $J_{K_a,K_c} - J'_{K'_a,K'_c}$	Predicted frequency (MHz)	S_{ij}	E_u (K)	v_{LSR} km s^{-1}	Δv km s^{-1}	T_{MB} (K)	$\int T_{MB} dv$ (K km s^{-1})
$22_{4,18}$-$21_{4,17}$	210333.598	21.30	807.4	(8)		...	
$22_{3,19}$-$21_{3,18}$	211116.785	21.60	792.9	5.4(1)		0.06(2)	
				5.3±0.6	4±1	0.06	0.29±0.07
$23_{1,23}$-$22_{1,22}$	212314.463	22.90	782.6	(36)		...	
$22_{1,21}$-$21_{1,20}$	212898.845	21.90	778.0	**		...	
$23_{0,23}$-$22_{0,22}$	213540.159	23.00	782.2	5.9(1)		0.13(2)	
$22_{2,20}$-$21_{2,19}$	213885.405	21.80	783.4	(37)		...	
$23_{2,22}$-$22_{2,21}$	218045.616	22.80	792.2	(6)		...	
$23_{7,17}$-$22_{7,16}$	219645.805	20.90	887.0	2.6(1)		0.08(2)	
$23_{7,16}$-$22_{7,15}$	219645.806†	20.90	887.0	2.6(1)		”	
$23_{8,16}$-$22_{8,15}$	219653.963	20.20	918.4	(7)		...	
$23_{8,15}$-$22_{8,14}$	219653.963†	20.20	918.4	(7)		...	
$23_{6,18}$-$22_{6,17}$	219666.231	21.40	859.8	6.6(1)		0.09(2)	
$23_{6,17}$-$22_{6,16}$	219666.256†	21.40	859.8	6.7(1)		”	
$23_{9,15}$-$22_{9,14}$	219681.207	19.50	954.0	(38)		...	
$23_{9,14}$-$22_{9,13}$	219681.207†	19.50	954.0	(38)		...	
$23_{10,14}$-$22_{10,13}$	219722.668	18.70	993.6	6.0(1,15)		0.14(2)	
$23_{10,13}$-$22_{10,12}$	219722.668†	18.70	993.6	6.0(1,15)		”	
$23_{5,19}$-$22_{5,18}$	219735.341	21.90	836.8	(7)		...	
$23_{5,18}$-$22_{5,17}$	219736.856†	21.90	836.8	(7)		...	
$23_{11,12}$-$22_{11,11}$	219775.635	17.70	1037.4	(7)		...	
$23_{11,13}$-$22_{11,12}$	219775.635†	17.70	1037.4	(7)		...	
$23_{12,11}$-$22_{12,10}$	219838.502	16.70	1085.2	2.9(1,6)		0.08(2)	
$23_{12,12}$-$22_{12,11}$	219838.502†	16.70	1085.2	2.9(1,6)		”	
$23_{3,21}$-$22_{3,20}$	219877.364	22.60	803.3	6.9(1)		0.12(2)	
$23_{4,20}$-$22_{4,19}$	219882.378	22.30	817.9	5.0(1)		0.10(2)	
$23_{4,19}$-$22_{4,18}$	219937.172	22.30	817.9	(39)		...	
$23_{3,20}$-$22_{3,19}$	220867.345	22.60	803.5	(5,19)		...	
$24_{1,24}$-$23_{1,23}$	221437.757	23.90	793.2	(5,18)		...	
$23_{1,22}$-$22_{1,21}$	222316.991	22.90	788.7	(40)		...	
$24_{0,24}$-$23_{0,23}$	222543.520	24.00	792.8	5.6(1)		0.13(2)	
$23_{2,21}$-$22_{2,20}$	223757.838	22.80	794.1	(28,41)		...	
$24_{2,23}$-$23_{2,22}$	227400.984	23.80	803.1	(42)		...	
$24_{7,18}$-$23_{7,17}$	229200.814	22.00	898.0	(43)		...	
$24_{7,17}$-$23_{7,16}$	229200.814†	22.00	898.0	(43)		...	
$24_{8,17}$-$23_{8,16}$	229205.670†	21.30	929.4	(43)		...	
$24_{8,16}$-$23_{8,15}$	229205.670†	21.30	929.4	(43)		...	

Tabla B.4: continued.

Transition $J_{K_a,K_c} - J'_{K'_a,K'_c}$	Predicted frequency (MHz)	S_{ij}	E_u (K)	v_{LSR} km s^{-1}	Δv km s^{-1}	T_{MB} (K)	$\int T_{MB} dv$ (K km s^{-1})
$24_{6,19}$-$23_{6,18}$	229227.837	22.50	870.8	6.3[1]		0.15[2]	
$24_{6,18}$-$23_{6,17}$	229227.878†	22.50	870.8	6.4[1]		”	
$24_{9,16}$-$23_{9,15}$	229231.609†	20.60	965.0	6.8[1]		”	
$24_{9,15}$-$23_{9,14}$	229231.609†	20.60	965.0	6.8[1]		”	
$24_{10,15}$-$23_{10,14}$	229273.092	19.80	1004.6	[8]		...	
$24_{10,14}$-$23_{10,13}$	229273.092†	19.80	1004.6	[8]		...	
$24_{5,20}$-$23_{5,19}$	229309.408	23.00	847.8	5.6[1]		0.22[2]	
$24_{5,19}$-$23_{5,18}$	229311.633†	23.00	847.8	8.5[1]		”	
$24_{11,14}$-$23_{11,13}$	229327.040	19.00	1048.4	[11]		...	
$24_{11,13}$-$23_{11,12}$	229327.040†	19.00	1048.4	[11]		...	
$24_{12,13}$-$23_{12,12}$	229391.623	18.00	1096.2	[6]		...	
$24_{12,12}$-$23_{12,11}$	229391.623†	18.00	1096.2	[6]		...	
$24_{3,22}$-$23_{3,21}$	229435.873	23.60	814.3	7.1[1]		0.18[2]	
$24_{13,12}$-$23_{13,11}$	229465.695	17.00	1148.1	[8]		...	
$24_{13,11}$-$23_{13,10}$	229465.695†	17.00	1148.1	[8]		...	
$24_{4,21}$-$23_{4,20}$	229474.318	23.30	828.9	[19,44]		...	
$24_{4,20}$-$23_{4,19}$	229547.905	23.30	829.0	[45]		...	
$24_{14,10}$-$23_{14,9}$	229548.502†	15.80	1204.1	[45]		...	
$24_{14,11}$-$23_{14,10}$	229548.502†	15.80	1204.1	[45]		...	
$25_{1,25}$-$24_{1,24}$	230552.991	24.90	804.3	[6]		...	
$24_{3,21}$-$23_{3,20}$	230642.911	23.60	814.5	5.2[1]		0.17[2]	
				5.14±0.14	5.2±0.3	0.20	1.11±0.06
$25_{0,25}$-$24_{0,24}$	231543.979	25.00	803.9	7.9[1]		0.16[2]	
$24_{1,23}$-$23_{1,22}$	231696.184	23.90	799.8	7.4[1]		0.16[2]	
$24_{2,22}$-$23_{2,21}$	233615.877	23.80	805.4	5.2[1,8]		0.19[2]	
$25_{2,24}$-$24_{2,23}$	236741.841	24.80	814.4	[5]		...	
$25_{7,19}$-$24_{7,18}$	238756.476	23.00	909.5	7.8[1]		0.21[2]	
$25_{7,18}$-$24_{7,17}$	238756.477†	23.00	909.5	7.8[1]		”	
$25_{8,18}$-$24_{8,17}$	238757.566†	22.40	940.9	6.1[1]		”	
$25_{8,17}$-$24_{8,16}$	238757.566†	22.40	940.9	6.1[1]		”	
$25_{9,17}$-$24_{9,16}$	238781.884	21.80	976.4	[6]		...	
$25_{9,16}$-$24_{9,15}$	238781.884†	21.80	976.4	[6]		...	
$25_{6,20}$-$24_{6,19}$	238790.824	23.60	882.3	[15,46]		...	
$25_{6,19}$-$24_{6,18}$	238790.887†	23.60	882.3	[15,46]		...	
$25_{10,15}$-$24_{10,14}$	238823.165	21.00	1016.1	8.6[1,15]		0.17[2]	
$25_{10,16}$-$24_{10,15}$	238823.165†	21.00	1016.1	8.6[1,15]		”	
$25_{11,15}$-$24_{11,14}$	238877.927	20.20	1059.9	5.7[1]		0.11[2]	

Tabla B.4: continued.

Transition $J_{K_a,K_c} - J'_{K'_a,K'_c}$	Predicted frequency (MHz)	S_{ij}	E_u (K)	v_{LSR} km s^{-1}	Δv km s^{-1}	T_{MB} (K)	$\int T_{MB} dv$ (K km s^{-1})
$25_{11,14}$-$24_{11,13}$	238877.927†	20.20	1059.9	5.7[1]		"	
$25_{5,21}$-$24_{5,20}$	238885.992	24.00	859.2	[6,47]		...	
$25_{5,20}$-$24_{5,19}$	238885.992†	24.00	859.2	[6,47]		...	
$25_{3,23}$-$24_{3,22}$	238988.701	24.60	825.7	[11]		...	
$25_{4,22}$-$24_{4,21}$	239068.999	24.40	840.4	[48]		...	
$25_{4,21}$-$24_{4,20}$	239166.548	24.40	840.4	[18,37]		...	
$26_{1,26}$-$25_{1,25}$	239660.622	25.90	815.8	5.0[1]		0.20[2]	
$26_{3,22}$-$25_{3,21}$	240444.342	24.60	826.1	[18]		...	
$26_{0,26}$-$25_{0,25}$	240543.432	26.00	815.5	[49]		...	
$25_{1,24}$-$24_{1,23}$	241034.927	24.90	811.4	[5,13]		...	
$25_{2,23}$-$24_{2,22}$	243455.835	24.80	817.0	[18]		...	
$26_{2,25}$-$25_{2,24}$	246067.964	25.80	826.3	[5,16]		...	
$26_{8,19}$-$25_{8,18}$	248309.658	23.50	952.8	2.3[1]		0.31[2]	
$26_{8,18}$-$25_{8,17}$	248309.658†	23.50	952.8	2.3[1]		"	
$26_{7,20}$-$25_{7,19}$	248312.817†	24.10	921.4	6.1[1]		"	
$26_{7,19}$-$25_{7,18}$	248312.818†	24.10	921.4	6.1[1]		"	
$26_{9,18}$-$25_{9,17}$	248332.027	22.90	988.4	[6]		...	
$26_{9,17}$-$25_{9,16}$	248332.027†	22.90	988.4	[6]		...	
$26_{6,21}$-$25_{6,20}$	248355.248	24.60	894.2	[12]		...	
$26_{6,20}$-$25_{6,19}$	248355.248†	24.60	894.2	[12]		...	
$26_{10,17}$-$25_{10,16}$	248372.872	22.20	1028.0	[12]		...	
$26_{10,16}$-$25_{10,15}$	248372.872†	22.20	1028.0	[12]		...	
$26_{11,15}$-$25_{11,14}$	248428.273	21.30	1071.8	[8,11,41]		...	
$26_{11,16}$-$25_{11,15}$	248428.273†	21.30	1071.8	[8,11,41]		...	
$26_{5,22}$-$25_{5,21}$	248465.168	25.00	871.2	[14,28]		...	
$26_{5,21}$-$25_{5,20}$	248469.746	25.00	871.2	[6]		...	
$26_{12,14}$-$25_{12,13}$	248495.899	20.50	1119.6	[50]		...	
$26_{12,15}$-$25_{12,14}$	248495.899†	20.50	1119.6	[50]		...	
$26_{3,24}$-$25_{3,23}$	248534.871	25.70	837.7	[15,51]		...	
$26_{13,13}$-$25_{13,12}$	248574.288	19.50	1171.6	[28]		...	
$26_{13,14}$-$25_{13,13}$	248574.288†	19.50	1171.6	[28]		...	
$26_{14,13}$-$25_{14,12}$	248662.480	18.50	1227.5	[5,52]		...	
$26_{14,12}$-$25_{14,11}$	248662.480†	18.50	1227.5	[5,52]		...	
$26_{4,23}$-$25_{4,22}$	248666.176†	25.40	852.4	[5,52]		...	
$26_{15,11}$-$25_{15,10}$	248759.810	17.30	1287.4	5.7[1]		0.26[2]	
$26_{15,12}$-$25_{15,11}$	248759.810†	17.30	1287.4	5.7[1]		"	
$27_{1,27}$-$26_{1,26}$	248761.116†	26.90	827.7	7.3[1]		"	

Tabla B.4: continued.

Transition $J_{K_a,K_c} - J'_{K'_a,K'_c}$	Predicted frequency (MHz)	S_{ij}	E_u (K)	v_{LSR} km s^{-1}	Δv km s^{-1}	T_{MB} (K)	$\int T_{MB} dv$ (K km s^{-1})
$26_{4,22}$-$25_{4,21}$	248793.933	25.40	852.4	(5)		...	
$27_{0,27}$-$26_{0,26}$	249543.291	27.00	827.5	(14)		...	
$26_{3,23}$-$25_{3,22}$	250272.043	25.70	838.1	4.5(1,53)		0.24(2)	
$26_{1,25}$-$25_{1,24}$	250332.187	25.90	823.4	(18,25)		...	
$26_{2,24}$-$25_{2,23}$	253274.461	25.90	829.2	(18)		...	
$27_{2,26}$-$26_{2,25}$	255379.193	26.80	838.5	(44,54)		...	
$28_{1,28}$-$27_{1,27}$	257854.937	27.90	840.1	(53,5,21)		...	
$27_{8,20}$-$26_{8,19}$	257861.951	24.60	965.2	(5)		...	
$27_{8,19}$-$26_{8,18}$	257861.951†	24.60	965.2	(5)		...	
$27_{7,21}$-$26_{7,20}$	257869.863	25.20	933.8	(21,55)		...	
$27_{7,20}$-$26_{7,19}$	257869.865†	25.20	933.8	(21,55)		...	
$27_{9,19}$-$26_{9,18}$	257882.029	24.00	1000.7	7.3(1,23)		0.14(2)	
$27_{9,18}$-$26_{9,17}$	257882.029†	24.00	1000.7	7.3(1,23)		”	
$27_{6,22}$-$26_{6,21}$	257921.164	25.70	906.6	8.7(1)		0.27(2)	
$27_{6,21}$-$26_{6,20}$	257921.313†	25.70	906.6	8.6(1)		”	
$27_{10,18}$-$26_{10,17}$	257922.196†	23.30	1040.4	7.5(1)		”	
$27_{10,17}$-$26_{10,16}$	257922.196†	23.30	1040.4	7.5(1)		0.27(2)	
				9.6±1.2	4±1	0.54	2.0±0.9
$27_{11,17}$-$26_{11,16}$	257978.056	22.50	1084.2	7.8(1,56)		0.53(2)	
$27_{11,16}$-$26_{11,15}$	257978.056†	22.50	1084.2	7.8(1,56)		”	
$27_{12,15}$-$26_{12,14}$	258046.999	21.70	1132.0	(5,56)		...	
$27_{12,16}$-$26_{12,15}$	258046.999†	21.70	1132.0	(5,56)		...	
$27_{5,23}$-$26_{5,22}$	258047.003†	26.10	883.6	(5,56)		...	
$27_{5,22}$-$26_{5,21}$	258053.427†	26.10	883.6	(5,56)		...	
$27_{3,25}$-$26_{3,24}$	258073.408	26.70	850.1	(5,56,57)		...	
$27_{4,24}$-$26_{4,23}$	258265.541	26.40	864.7	(39)		...	
$27_{4,23}$-$26_{4,22}$	258430.985	26.40	864.8	5.6(1,6)		”	
$28_{0,28}$-$27_{0,27}$	258544.554	28.00	839.9	(24,56)		...	
$27_{1,26}$-$26_{1,25}$	259587.496	26.90	835.9	(11)		...	
$27_{3,24}$-$26_{3,23}$	260125.831	26.70	850.6	5.6(1,5)		0.36(2)	
$27_{2,25}$-$26_{2,24}$	263068.892	26.90	841.8	7.8(1,6)		0.25(2)	
$28_{2,27}$-$27_{2,26}$	264675.434	27.80	851.2	(28)		...	
$29_{1,29}$-$28_{1,28}$	266942.547	28.90	852.9	(11,15)		...	
$28_{8,21}$-$27_{8,20}$	267414.453	25.70	978.0	(16)		...	
$28_{8,20}$-$27_{8,19}$	267414.453†	25.70	978.0	(16)		...	
$28_{7,22}$-$27_{7,21}$	267427.640	26.30	946.6	2.7(1,58)		0.21(2)	
$28_{7,21}$-$27_{7,20}$	267427.644†	26.30	946.6	2.7(1,58)		”	

Tabla B.4: continued.

Transition $J_{K_a,K_c} - J'_{K'_a,K'_c}$	Predicted frequency (MHz)	S_{ij}	E_u (K)	v_{LSR} km s^{-1}	Δv km s^{-1}	T_{MB} (K)	$\int T_{MB} dv$ (K km s^{-1})
$28_{9,20}$-$27_{9,19}$	267431.887†	25.10	1013.6	7.5[1,58]		”	
$28_{9,19}$-$27_{9,18}$	267431.887†	25.10	1013.6	7.5[1,58]		”	
$28_{10,18}$-$27_{10,17}$	267471.123	24.40	1053.2	[37]		...	
$28_{10,19}$-$27_{10,18}$	267471.123†	24.40	1053.2	[37]		...	
$28_{6,23}$-$27_{6,22}$	267488.629	26.70	919.4	[13,24,58]		...	
$28_{6,22}$-$27_{6,21}$	267488.851†	26.70	919.4	[13,24,58]		...	
$28_{11,18}$-$27_{11,17}$	267527.256	23.70	1097.0	[54,58]		...	
$28_{11,17}$-$27_{11,16}$	267527.256†	23.70	1097.0	[54,58]		...	
$29_{0,29}$-$27_{0,28}$	267547.864	29.00	852.7	[59]		...	
$28_{12,16}$-$27_{12,15}$	267597.372	22.90	1144.9	[5,25]		...	
$28_{12,17}$-$27_{12,16}$	267597.372†	22.90	1144.9	[5,25]		...	
$28_{3,26}$-$27_{3,25}$	267603.351	27.70	862.9	[58]		...	
$28_{5,24}$-$27_{5,23}$	267631.551	27.10	896.4	[6]		...	
$28_{5,23}$-$27_{5,22}$	267640.450	27.10	896.4	7.8[1,15]		0.10[2]	
$28_{13,16}$-$27_{13,15}$	267679.641	22.20	1196.8	2.0[1,15]		0.06[2]	
$28_{13,15}$-$27_{13,14}$	267679.641†	22.20	1196.8	2.0[1,15]		”	
$28_{4,25}$-$27_{4,24}$	267866.724	27.40	877.6	[12,60]		...	
$28_{4,24}$-$27_{4,23}$	268078.722	27.40	877.6	[6,61]		...	
$28_{1,27}$-$27_{1,26}$	268801.046	27.90	848.8	[8]		...	
$28_{3,25}$-$27_{3,24}$	270004.852	27.70	863.5	5.9[1]		0.24[2]	
				5.8±1.4	3±1	0.34	1.1±0.4
$28_{2,26}$-$27_{2,25}$	272836.596	27.90	854.9	[6]		...	
$29_{2,28}$-$28_{2,27}$	273956.661	28.80	864.4	[6]		...	
$30_{1,30}$-$29_{1,29}$	276024.393	30.00	866.1	4.2[1]		0.16[2]	
$30_{0,30}$-$29_{0,29}$	276553.589	30.00	866.0	[36,62]		...	
$29_{8,22}$-$28_{8,21}$	276967.169	26.80	991.3	[54,61,63]		...	
$29_{8,21}$-$28_{8,20}$	276967.169†	26.80	991.3	[54,61,63]		...	
$29_{9,21}$-$28_{9,20}$	276981.593	26.20	1026.9	[6,14]		...	
$29_{9,20}$-$28_{9,19}$	276981.593†	26.20	1026.9	[6,14]		...	
$29_{7,23}$-$28_{7,22}$	276986.174†	27.30	959.9	[6,14]		...	
$29_{7,22}$-$28_{7,21}$	276986.180†	27.30	959.9	[6,14]		...	
$29_{10,20}$-$28_{10,19}$	277019.638	25.60	1066.5	[56]		...	
$29_{10,19}$-$28_{10,18}$	277019.638†	25.60	1066.5	[56]		...	
$29_{6,24}$-$28_{6,23}$	277057.697	27.80	932.7	[18,64]		...	
$29_{6,23}$-$28_{6,22}$	277058.025†	27.80	932.7	[18,64]		...	
$29_{11,18}$-$28_{11,17}$	277075.850	24.80	1110.3	[28]		...	
$29_{11,19}$-$28_{11,18}$	277075.850†	24.80	1110.3	[28]		...	

Tabla B.4: continued.

Transition $J_{K_a,K_c} - J'_{K'_a,K'_c}$	Predicted frequency (MHz)	S_{ij}	E_u (K)	v_{LSR} km s^{-1}	Δv km s^{-1}	T_{MB} (K)	$\int T_{MB} dv$ (K km s^{-1})
$29_{3,27}$-$28_{3,26}$	277123.761	28.70	876.2	(18,22)		...	
$29_{12,17}$-$28_{12,16}$	277146.990	24.00	1158.2	(6)		...	
$29_{12,18}$-$28_{12,17}$	277146.990†	24.00	1158.2	(6)		...	
$29_{5,25}$-$28_{5,24}$	277218.855	28.10	909.7	6.6(1,5)		0.38(2)	
$29_{13,17}$-$28_{13,16}$	277231.025	23.20	1210.1	3.9(1,37)		0.47(2)	
$29_{13,16}$-$28_{13,15}$	277231.025†	23.20	1210.1	3.9(1,37)		”	
$29_{5,24}$-$28_{5,23}$	277231.033†	28.10	909.7	3.9(1,37)		”	
$29_{14,15}$-$28_{14,14}$	277326.614	22.20	1266.0	(5)		...	
$29_{14,16}$-$28_{14,15}$	277326.614†	22.20	1266.0	(5)		...	
$29_{15,15}$-$28_{15,14}$	277432.833	21.20	1326.0	(8,51,61)		...	
$29_{15,14}$-$28_{15,13}$	277432.833†	21.20	1326.0	(8,51,61)		...	
$29_{4,26}$-$28_{4,25}$	277469.292	28.40	890.9	(12,19,22)		...	
$29_{4,25}$-$28_{4,24}$	277738.255	28.40	891.0	(5)		...	
$29_{1,28}$-$28_{1,27}$	277973.756	28.90	862.1	(5,19)		...	
$29_{3,26}$-$28_{3,25}$	279907.508	28.70	877.0	6.6(1,6)		0.45(2)	

Tabla A7. Emission lines of CH_2CHCN v_{11}=2 present in the spectral scan of the Orion-KL from the radio-telescope of IRAM 30-m. Column 1 indicates the line transition, Col. 2 gives the predicted frequency in the laboratory, Col. 3 the line strength, Col. 4 upper level energy, Col. 5 observed radial velocities relative to the local system rest (v_{LSR}), Col. 6 the line width, Col. 7 main beam temperature, and Col. 8 shows the area of the line. † blended with the previous line. ∗∗ hole in the observed spectrum.

(1) peak channel line observed velocity. (2) peak channel line intensity. (3) blended with H 53β. (4) blended with $Si^{17}O$. (5) blended with $HCOOCH_3$. (6) blended with U-line. (7) blended with HNCO. (8) blended with CH_3CH_2CN. (9) blended with CH_2CHCN v_{15}=1. (10) blended with $CH_2{}^{13}CHCN$. (11) blended with SO_2. (12) blended with $^{34}SO_2$. (13) blended with $^{13}CH_3OH$. (14) blended with $(CH_3)_2CO$. (15) blended with CH_2CHCN. (16) blended with CH_3OH. (17) blended with CH_3CHO. (18) blended with CH_3CH_2CN v_{13}/v_{21}. (19) blended with CH_3CH_2CN v_{20}=1. (20) blended with H 54δ. (21) blended with NO. (22) blended with $H^{13}COOCH_3$. (23) blended with CH_2CHCN $v_{10}/v_{11}v_{15}$. (24) blended with CH_3OCH_3. (25) blended with $CH_3CH_2{}^{13}CN$. (26) blended with H_2CCO. (27) blended with c-C_2H_4O. (28) blended with $|g_+$-$g_-|$-CH_3CH_2OH. (29) blended with $HC^{13}CCN$. (30) blended with $HCC^{13}CN$. (31) blended with HCCCN v_7=1. (32) blended with HCCCN v_4+v_7. (33) blended with $CH_3CH_2C^{15}N$. (34) blended with CH_2CHCN v_{11}=1. (35) blended with $CH_2{}^{13}CHCN$. (36) blended with NH_2CHO. (37) blended with $^{13}CH_3CH_2CN$. (38) blended with HCCCN v_7=2. (39) blended with SO. (40) blended with H_2CCO. (41) blended with $SO^{18}O$. (42) blended with HCCCN. (43) blended with $H^{13}CCCN$. (44) blended with $CH_2CH^{13}CN$. (45) blended with SO_2 v_2=1. (46) blended with $CH_3{}^{13}CN$. (47) blended with $DCOOCH_3$. (48) blended with CH_3CN. (49) blended with H_2CS. (50) blended with CCCS. (51) blended with CH_3COOH v_t=0. (52) blended with $HNC^{18}O$. (53) blended with $CH_3{}^{13}CH_2CN$. (54) blended with OCS. (55) blended with H_2CCC. (56) blended with CH_3CN v_8=1. (57) blended with HDCO. (58) blended with $CH_3C^{15}N$. (59) blended with HCO^+. (60) blended with $^{13}CH_3CN$. (61) blended with $HCOO^{13}CH_3$. (62) blended with t-CH_3CH_2OH (63) blended with $H^{15}NCO$. (64) blended with $H_2C^{18}O$.

Tabla B.5: Detected lines of CH_2CHCN v_{11}=3 .

Transition $J_{K_a,K_c} - J'_{K'_a,K'_c}$	Predicted frequency (MHz)	S_{ij}	E_u (K)	v_{LSR} km s^{-1}	Δv km s^{-1}	T_{MB} (K)	$\int T_{MB} dv$ (K km s^{-1})
$9_{1,9}$-$8_{1,8}$	83769.181	8.89	1007.6	(3)		...	
$9_{0,9}$-$8_{0,8}$	85596.639	8.99	1006.1	(3)		...	
$9_{2,8}$-$8_{2,7}$	86022.191	8.56	1014.4	(4)		...	
$9_{5,5}$-$8_{5,4}$	86148.048	6.22	1057.9	4.5(1)		0.01(2)	
$9_{5,4}$-$8_{5,3}$	86148.048†	6.22	1057.9	4.5(1)		”	
$9_{4,6}$-$8_{4,5}$	86150.753	7.22	1039.3	6.9(1)		0.02(2)	
$9_{4,5}$-$8_{4,4}$	86150.830†	7.22	1039.3	7.2(1)		”	
$9_{6,4}$-$8_{6,3}$	86153.607	5.00	1080.7	(3)		...	
$9_{6,3}$-$8_{6,2}$	86153.607†	5.00	1080.7	(3)		...	
$9_{3,7}$-$8_{3,6}$	86167.628	8.00	1024.8	6.5(1)		0.01(2)	
$9_{3,6}$-$8_{3,5}$	86177.892	8.00	1024.8	7.4(1,3)		0.02(2)	
$9_{2,7}$-$8_{2,6}$	86518.215	8.56	1014.5	(3)		...	
$9_{1,8}$-$8_{1,7}$	88177.186	8.89	1008.7	(4)		...	
$10_{1,10}$-$9_{1,9}$	93045.462	9.90	1012.1	(3)		...	
$10_{0,10}$-$9_{0,9}$	94978.886	9.99	1010.6	(4)		...	
$10_{2,9}$-$9_{2,8}$	95556.511	9.60	1019.0	(5)		...	
$10_{5,6}$-$9_{5,5}$	95723.850	7.50	1062.5	(5,6,7)		...	
$10_{5,5}$-$9_{5,4}$	95723.850†	7.50	1062.5	(5,6,7)		...	
$10_{6,5}$-$9_{6,4}$	95728.292†	6.40	1085.3	(5,6,7)		...	
$10_{6,4}$-$9_{6,3}$	95728.292†	6.40	1085.3	(5,6,7)		...	
$10_{4,7}$-$9_{4,6}$	95730.128†	8.40	1043.9	(5,6,7)		...	
$10_{4,6}$-$9_{4,5}$	95730.296†	8.40	1043.9	(5,6,7)		...	
$10_{7,4}$-$9_{7,3}$	95738.985	5.10	1112.2	(6)		...	
$10_{7,3}$-$9_{7,2}$	95738.985	5.10	1112.2	(6)		...	
$10_{3,8}$-$9_{3,7}$	95753.609	9.10	1029.4	(4)		...	
$10_{8,2}$-$9_{8,1}$	95754.157†	3.60	1143.2	(4)		...	
$10_{8,3}$-$9_{8,2}$	95754.157†	3.60	1143.2	(4)		...	
$10_{3,7}$-$9_{3,6}$	95771.182	9.10	1029.4	(3)		...	
$10_{9,2}$-$9_{9,1}$	95773.005†	1.90	1178.3	(3)		...	
$10_{9,1}$-$9_{9,0}$	95773.005†	1.90	1178.3	(3)		...	
$10_{2,8}$-$9_{2,7}$	96234.286	9.60	1019.1	6.0(1)		0.02(2)	
				6.0±1.6	4±2	0.01	0.05±0.10
$10_{1,9}$-$9_{1,8}$	97936.352	9.90	1013.4	(3)		...	
$11_{1,11}$-$10_{1,10}$	102312.653	10.90	1017.0	(3)		...	
$11_{0,11}$-$10_{0,10}$	104323.759	11.00	1015.6	(3)		...	
$11_{2,10}$-$10_{2,9}$	105083.385	10.90	1024.0	8.8(1,3)		0.05(2)	

Tabla B.5: continued.

Transition $J_{K_a,K_c} - J'_{K'_a,K'_c}$	Predicted frequency (MHz)	S_{ij}	E_u (K)	v_{LSR} km s^{-1}	Δv km s^{-1}	T_{MB} (K)	$\int T_{MB} dv$ (K km s^{-1})
$11_{5,7}$-$10_{5,6}$	105300.849	8.73	1067.6	(8,9)		...	
$11_{5,6}$-$10_{5,5}$	105300.849†	8.73	1067.6	(8,9)		...	
$11_{6,6}$-$10_{6,5}$	105303.627†	7.73	1090.3	(8,9)		...	
$11_{6,5}$-$10_{6,4}$	105303.627†	7.73	1090.3	(8,9)		...	
$11_{4,8}$-$10_{4,7}$	105311.710	9.55	1048.9	(8,9)		...	
$11_{4,7}$-$10_{4,6}$	105312.046†	9.55	1048.9	(8,9)		...	
$11_{7,5}$-$10_{7,4}$	105314.144	6.55	1117.2	5.1(1,3)		0.04(2)	
$11_{7,4}$-$10_{7,3}$	105314.144†	6.55	1117.2	5.1(1,3)		”	
$11_{3,9}$-$10_{3,8}$	105342.504	10.20	1034.4	(3)		...	
$11_{3,8}$-$10_{3,7}$	105371.013	10.20	1034.4	(3)		...	
$11_{2,9}$-$10_{5,8}$	105979.648	10.60	1024.2	3.7(1)		0.04(2)	
$11_{1,10}$-$10_{1,9}$	107682.571	10.90	1018.6	(3)		...	
$12_{1,12}$-$11_{1,11}$	111570.238	11.90	1022.4	5.7(1)		0.05(2)	
$12_{0,12}$-$11_{0,11}$	113629.769	12.00	1021.1	4.4(1,3)		0.07(2)	
$12_{2,11}$-$11_{2,10}$	114602.094	11.70	1029.5	(3)		...	
$12_{5,8}$-$11_{5,7}$	114879.166	9.92	1073.1	5.6(1)		0.05(2)	
$12_{5,7}$-$11_{5,6}$	114879.170†	9.92	1073.1	5.6(1)		”	
$12_{6,7}$-$11_{6,6}$	114879.678†	9.00	1095.9	7.0(1)		”	
$12_{6,6}$-$11_{6,5}$	114879.678†	9.00	1095.9	7.0(1)		”	
$12_{7,6}$-$11_{7,5}$	114889.662	7.92	1122.7	(4)		...	
$12_{7,5}$-$11_{7,4}$	114889.662†	7.92	1122.7	(4)		...	
$12_{4,9}$-$11_{4,8}$	114895.701	10.70	1054.5	(10)		...	
$12_{4,8}$-$11_{4,7}$	114896.331†	10.70	1054.5	(10)		...	
$12_{8,4}$-$11_{8,3}$	114906.039	6.67	1153.7	(3)		...	
$12_{8,5}$-$11_{8,4}$	114906.039†	6.67	1153.7	(3)		...	
$12_{3,10}$-$11_{3,9}$	114934.217	11.20	1040.0	5.7(1,11)		0.04(2)	
$12_{3,9}$-$11_{3,8}$	114978.471	11.20	1040.0	(4)		...	
$14_{1,14}$-$13_{1,13}$	130055.036	13.90	1034.4	(11,12)		...	
$14_{0,14}$-$13_{0,13}$	132123.977	14.00	1033.3	(13)		...	
$14_{2,13}$-$13_{2,12}$	133612.205	13.70	1041.9	(4)		...	
$14_{6,9}$-$13_{6,8}$	134034.186	11.40	1108.3	(6)		...	
$14_{6,8}$-$13_{6,7}$	134034.187†	11.40	1108.3	(6)		...	
$14_{5,10}$-$13_{5,9}$	134040.225	12.20	1085.5	(14)		...	
$14_{5,9}$-$13_{5,8}$	134040.244†	12.20	1085.5	(14)		...	
$14_{7,8}$-$13_{7,7}$	134041.909†	10.50	1135.2	(14)		...	
$14_{7,7}$-$13_{7,6}$	134041.909†	10.50	1135.2	(14)		...	
$14_{8,6}$-$13_{8,5}$	134058.498	9.43	1166.2	(5)		...	

Tabla B.5: continued.

Transition $J_{K_a,K_c} - J'_{K'_a,K'_c}$	Predicted frequency (MHz)	S_{ij}	E_u (K)	v_{LSR} km s^{-1}	Δv km s^{-1}	T_{MB} (K)	$\int T_{MB} dv$ (K km s^{-1})
$14_{8,7}$-$13_{8,6}$	134058.498†	9.43	1166.2	(5)		...	
$14_{4,11}$-$13_{4,10}$	134071.663	12.90	1066.9	(15)		...	
$14_{4,10}$-$13_{4,9}$	134073.561†	12.90	1066.9	(15)		...	
$14_{9,5}$-$13_{9,4}$	134081.715	8.21	1201.2	(15)		...	
$14_{9,6}$-$13_{9,5}$	134081.715†	8.21	1201.2	(15)		...	
$14_{10,4}$-$13_{10,3}$	134110.432	6.86	1240.4	(3)		...	
$14_{10,5}$-$13_{10,4}$	134110.432†	6.86	1240.4	(3)		...	
$14_{3,12}$-$13_{3,11}$	134125.220	13.40	1052.4	3.9(1)		0.05(2)	
$14_{3,11}$-$13_{3,10}$	134221.217	13.40	1052.4	(16)		...	
$14_{2,12}$-$13_{2,11}$	135393.362	13.70	1042.3	2.4(1)		0.06(2)	
$14_{1,13}$-$13_{1,12}$	136825.744	13.90	1036.9	(6)		...	
$15_{1,15}$-$14_{1,14}$	139281.724	14.90	1041.1	(6,17)		...	
$15_{0,15}$-$14_{0,14}$	141314.132	15.00	1040.1	4.3(1)		0.06(2)	
$15_{2,14}$-$14_{2,13}$	143102.237	14.70	1048.8	(10)		...	
$15_{4,12}$-$14_{4,11}$	143663.980	13.90	1073.8	(18)		...	
$15_{4,11}$-$14_{4,10}$	143667.079†	13.90	1073.8	(19)		...	
$15_{3,13}$-$14_{3,12}$	143723.824	14.40	1059.3	(20)		...	
$15_{3,12}$-$14_{3,11}$	143859.291	14.40	1059.3	(10)		...	
$15_{2,13}$-$14_{2,12}$	145252.769	14.70	1049.2	4.4(1)		0.03(2)	
$15_{1,14}$-$14_{1,13}$	146501.767	14.90	1043.9	(3)		...	
$16_{1,16}$-$15_{1,15}$	148497.759	15.90	1048.2	(5)		...	
$16_{0,16}$-$15_{0,15}$	150469.302	16.00	1047.3	(5)		...	
$16_{2,15}$-$15_{2,14}$	152581.372	15.70	1056.1	(3)		...	
$16_{6,11}$-$15_{6,10}$	153192.337	13.80	1122.5	7.6(1,3)		0.06(2)	
$16_{6,10}$-$15_{6,9}$	153192.337†	13.80	1122.5	7.6(1,3)		”	
$16_{7,10}$-$15_{7,9}$	153195.992	12.90	1149.4	3.2(1,3)		0.10(2)	
$16_{7,9}$-$15_{7,8}$	153195.992†	12.90	1149.4	3.2(1,3)		”	
$16_{5,12}$-$15_{5,11}$	153207.977	14.40	1099.7	8.1(1,3)		0.07(2)	
$16_{5,11}$-$15_{5,10}$	153208.042†	14.40	1099.7	8.0(1,3)		”	
$16_{8,9}$-$15_{8,8}$	153211.633	12.00	1180.4	2.3(1,3)		0.08(2)	
$16_{8,8}$-$15_{8,7}$	153211.633†	12.00	1180.4	2.3(1,3)		”	
$16_{9,8}$-$15_{9,7}$	153235.906	10.90	1215.5	3.4(1)		0.04(2)	
$16_{9,7}$-$15_{9,6}$	153235.906†	10.90	1215.5	3.4(1)		”	
$16_{4,13}$-$15_{4,12}$	153259.388	15.00	1081.1	(6)		...	
$16_{4,12}$-$15_{4,11}$	153264.285†	15.00	1081.1	(6)		...	
$16_{3,14}$-$15_{3,13}$	153323.874	15.40	1066.6	(21)		...	
$16_{3,13}$-$15_{3,12}$	153510.566	15.40	1066.7	(4)		...	

Tabla B.5: continued.

Transition $J_{K_a,K_c} - J'_{K'_a,K'_c}$	Predicted frequency (MHz)	S_{ij}	E_u (K)	v_{LSR} km s^{-1}	Δv km s^{-1}	T_{MB} (K)	$\int T_{MB} dv$ (K km s^{-1})
$16_{2,14}$-$15_{2,13}$	155134.829	15.70	1056.7	(5)		...	
$16_{1,15}$-$15_{1,14}$	156155.026	15.90	1051.4	(22)		...	
$17_{1,17}$-$16_{1,16}$	157703.128	19.60	1055.8	6.3(1)		0.06(2)	
$17_{0,17}$-$16_{0,16}$	159592.809	17.00	1055.0	(4)		...	
$17_{2,16}$-$16_{2,15}$	162048.978	16.80	1063.9	(6,19)		...	
$17_{5,13}$-$16_{5,12}$	162794.657	15.50	1107.6	5.5(1,22)		0.07(2)	
$17_{5,12}$-$16_{5,11}$	162794.771†	15.50	1107.6	5.7(1,22)		”	
$17_{4,14}$-$16_{4,13}$	162858.012	16.10	1088.9	(3)		...	
$17_{4,13}$-$16_{4,12}$	162865.529	16.10	1088.9	(3)		...	
$17_{3,15}$-$16_{3,14}$	162924.784	16.50	1074.4	(4)		...	
$17_{3,14}$-$16_{3,13}$	163176.735	16.50	1074.5	(3)		...	
$17_{2,15}$-$16_{2,14}$	165035.307	16.80	1064.6	7.3(1)		0.12(2)	
$17_{1,16}$-$16_{1,15}$	165783.200	16.90	1059.4	4.0(1,23)		0.13(2)	
$18_{1,18}$-$17_{1,17}$	166897.911	17.90	1063.8	(10)		...	
$18_{0,18}$-$17_{0,17}$	168688.606	18.00	1063.1	3.9(1)		0.04(2)	
$18_{2,17}$-$17_{2,16}$	171504.456	17.80	1072.1	(24)		...	
$18_{7,12}$-$17_{7,11}$	172352.174	15.30	1165.5	0.4(1,3)		0.16(2)	
$18_{7,11}$-$17_{7,10}$	172352.174†	15.30	1165.5	0.4(1,3)		”	
$18_{6,13}$-$17_{6,12}$	172354.651†	16.00	1138.6	3.9(1,3)		”	
$18_{6,12}$-$17_{6,11}$	172354.653†	16.00	1138.6	3.9(1,3)		”	
$18_{5,14}$-$17_{5,13}$	172383.362	16.60	1115.8	(4)		...	
$18_{5,13}$-$17_{5,12}$	172383.362†	16.60	1115.8	(4)		...	
$18_{4,15}$-$17_{4,14}$	172459.950	17.10	1097.2	(6)		...	
$18_{4,14}$-$17_{4,13}$	172471.195	17.10	1097.2	(3)		...	
$18_{3,16}$-$17_{3,15}$	172525.880	17.50	1082.7	(3)		...	
$18_{3,15}$-$17_{3,14}$	172859.584	17.50	1082.8	(23)		...	
$18_{2,16}$-$17_{2,15}$	174949.306	17.80	1073.0	5.2(1)		0.06(2)	
$18_{1,17}$-$17_{1,16}$	175383.875	17.90	1067.8	(4)		...	
$19_{1,19}$-$18_{1,18}$	176082.273	18.90	1072.3	(5,25,26)		...	
$19_{0,19}$-$18_{0,18}$	177761.017	19.00	1071.6	(3)		...	
$21_{2,20}$-$20_{2,19}$	199792.621	20.80	1099.5	(19,27,28)		...	
$21_{7,15}$-$20_{7,14}$	201090.968	18.70	1193.1	(10)		...	
$21_{7,15}$-$20_{7,14}$	201090.968†	18.70	1193.1	(10)		...	
$21_{8,14}$-$20_{8,13}$	201098.099†	18.00	1224.1	(10)		...	
$21_{8,13}$-$20_{8,12}$	201098.099†	18.00	1224.1	(10)		...	
$21_{6,16}$-$20_{6,15}$	201107.072	19.30	1166.2	3.9(1,3)		0.15(2)	
$21_{6,15}$-$20_{6,14}$	201107.083†	19.30	1166.2	3.9(1,3)		”	

Tabla B.5: continued.

Transition $J_{K_a,K_c} - J'_{K'_a,K'_c}$	Predicted frequency (MHz)	S_{ij}	E_u (K)	v_{LSR} km s^{-1}	Δv km s^{-1}	T_{MB} (K)	$\int T_{MB} dv$ (K km s^{-1})
$21_{9,13}$-$20_{9,12}$	201120.834	17.10	1259.2	[25,29]		...	
$21_{9,12}$-$20_{9,11}$	201120.834†	17.10	1259.2	[25,29]		...	
$21_{10,12}$-$20_{10,11}$	201155.287	16.20	1298.4	[3,25]		...	
$21_{10,11}$-$20_{10,10}$	201155.287†	16.20	1298.4	[3,25]		...	
$21_{5,17}$-$20_{5,16}$	201162.771†	19.80	1143.4	[3,25]		...	
$21_{5,16}$-$20_{5,15}$	201163.554†	19.80	1143.4	[3,25]		...	
$21_{11,11}$-$20_{11,10}$	201199.328	15.20	1341.6	[25,30]		...	
$21_{11,10}$-$20_{11,9}$	201199.328†	15.20	1341.6	[25,30]		...	
$21_{12,9}$-$20_{12,8}$	201251.727	14.10	1388.9	[3]		...	
$21_{12,10}$-$20_{12,9}$	201251.727†	14.10	1388.9	[3]		...	
$21_{4,18}$-$20_{4,17}$	201286.131	20.20	1124.8	3.4[1]		0.08[2]	
				3.2±1.9	5±2	0.07	0.4±0.2
$21_{4,17}$-$20_{4,16}$	201319.250	20.20	1124.8	[19]		...	
$21_{3,19}$-$20_{3,18}$	201322.367†	20.60	1110.3	[19]		...	
$21_{3,18}$-$20_{3,17}$	202026.731	20.60	1110.5	[31]		...	
$22_{1,22}$-$21_{1,21}$	203575.591	21.90	1100.3	[5,32,33]		...	
$21_{1,20}$-$20_{1,19}$	203996.095	20.90	1095.8	3.3[1,6]		0.17[2]	
$21_{2,19}$-$20_{2,18}$	204718.826	20.80	1101.0	[5]		...	
$22_{0,22}$-$21_{0,21}$	204881.283	22.00	1099.8	2.0[1,3]		0.17[2]	
$22_{2,21}$-$21_{2,20}$	209194.302	21.80	1109.6	[34]		...	
$22_{7,16}$-$21_{7,15}$	210671.906	19.80	1203.2	7.9[1,4,35]		0.16[2]	
$22_{7,15}$-$21_{7,14}$	210671.907†	19.80	1203.2	7.9[1,4,35]		”	
$22_{8,15}$-$21_{8,14}$	210676.120	19.10	1234.2	9.0[1,36]		0.21[2]	
$22_{8,14}$-$21_{8,13}$	210676.120†	19.10	1234.2	9.0[1,36]		”	
$22_{6,17}$-$21_{6,16}$	210693.863	20.40	1176.3	*		...	
$22_{6,16}$-$21_{6,15}$	210693.882†	20.40	1176.3	*		...	
$22_{9,13}$-$21_{9,12}$	210697.720	18.30	1269.3	[37]		...	
$22_{9,14}$-$21_{9,13}$	210697.720†	18.30	1269.3	[37]		...	
$22_{10,12}$-$21_{10,11}$	210732.233	17.50	1308.5	5.0[1,3]		0.14[2]	
$22_{10,13}$-$21_{10,12}$	210732.233†	17.50	1308.5	5.0[1,3]		”	
$22_{5,18}$-$21_{5,17}$	210760.707	20.90	1153.5	[17]		...	
$22_{5,17}$-$21_{5,16}$	210761.902†	20.90	1153.5	[17]		...	
$22_{11,11}$-$21_{11,10}$	210777.201	16.50	1351.7	[25]		...	
$22_{11,12}$-$21_{11,11}$	210777.201†	16.50	1351.7	[25]		...	
$22_{12,10}$-$21_{12,9}$	210831.203	15.50	1399.0	3.8[1]		0.08[2]	
$22_{12,11}$-$21_{12,10}$	210831.203†	15.50	1399.0	3.8[1]		”	
$22_{13,9}$-$21_{13,8}$	210893.392	14.30	1450.4	[3]		...	

Tabla B.5: continued.

Transition $J_{K_a,K_c} - J'_{K'_a,K'_c}$	Predicted frequency (MHz)	S_{ij}	E_u (K)	v_{LSR} km s^{-1}	Δv km s^{-1}	T_{MB} (K)	$\int T_{MB} dv$ (K km s^{-1})
$22_{13,10}$-$21_{13,9}$	210893.392†	14.30	1450.4	(3)		...	
$22_{4,19}$-$21_{4,18}$	210901.613	21.30	1134.9	(3)		...	
$22_{3,20}$-$21_{3,19}$	210915.970	21.60	1120.5	5.3(1)		0.07(2)	
$22_{4,18}$-$21_{4,17}$	210947.407	21.30	1134.9	5.6(1,3)		0.21(2)	
$22_{3,19}$-$21_{3,18}$	211794.656	21.60	1120.6	(3)		...	
$23_{1,23}$-$22_{1,22}$	212721.323	22.90	1110.5	(17,18)		...	
$22_{1,21}$-$21_{1,20}$	213462.118	21.90	1106.0	1.6(1)		0.14(2)	
$23_{0,23}$-$22_{0,22}$	213902.041	23.00	1110.1	(3)		...	
$22_{2,20}$-$21_{2,19}$	214633.469	21.80	1111.3	(4)		...	
$23_{2,22}$-$22_{2,21}$	218581.442	22.80	1120.0	(38)		...	
$23_{7,17}$-$22_{7,16}$	220253.571	20.90	1213.7	(3)		...	
$23_{7,16}$-$22_{7,15}$	220253.572†	20.90	1213.7	(3)		...	
$23_{8,16}$-$22_{8,15}$	220254.414†	20.20	1244.7	(3)		...	
$23_{8,15}$-$22_{8,14}$	220254.414†	20.20	1244.7	(3)		...	
$23_{9,15}$-$22_{9,14}$	220274.573	19.50	1279.8	*		...	
$23_{9,14}$-$22_{9,13}$	220274.573†	19.50	1279.8	*		...	
$23_{6,18}$-$22_{6,17}$	220282.090	21.40	1186.9	5.3(1)		0.12(2)	
$23_{6,17}$-$22_{6,16}$	220282.090†	21.40	1186.9	5.3(1)		"	
				4.5±0.4	4±1	0.10	0.47±0.09
$23_{10,14}$-$22_{10,13}$	220308.926	18.70	1319.0	(3)		...	
$23_{10,13}$-$22_{10,12}$	220308.926†	18.70	1319.0	(3)		...	
$23_{5,19}$-$22_{5,18}$	220361.220	21.90	1164.1	(17,39)		...	
$23_{5,18}$-$22_{5,17}$	220363.008†	21.90	1164.1	(17,39)		...	
$23_{3,21}$-$22_{3,20}$	220505.360	22.60	1131.0	(3)		...	
$23_{4,20}$-$22_{4,19}$	220520.338	22.30	1145.5	6.3(1)		0.10(2)	
$23_{4,19}$-$22_{4,18}$	220582.692	22.30	1145.5	(40)		...	
$23_{3,20}$-$22_{3,19}$	221588.004	22.60	1131.3	6.5(1)		0.14(2)	
$24_{1,24}$-$23_{1,23}$	221858.419	23.90	1121.1	(17,41)		...	
$23_{1,22}$-$22_{1,21}$	222888.734	22.90	1116.7	(41)		...	
$24_{0,24}$-$23_{0,23}$	222918.414	24.00	1120.8	(6)		...	
$23_{2,21}$-$22_{2,20}$	224535.735	22.80	1122.1	5.9(1,3)		0.31(2)	
$24_{2,23}$-$23_{2,22}$	227953.715	23.80	1131.0	6.0(1,4,42)		0.33(2)	
$24_{8,17}$-$23_{8,16}$	229832.997	21.30	1255.8	(3)		...	
$24_{8,16}$-$23_{8,15}$	229832.997†	21.30	1255.8	(3)		...	
$24_{7,18}$-$23_{7,17}$	229835.998	22.00	1224.8	5.7(1,3)		0.24(2)	
$24_{7,17}$-$23_{7,16}$	229835.998†	22.00	1224.8	5.7(1,3)		"	
$24_{9,16}$-$23_{9,15}$	229851.392	20.60	1290.9	(6,13,43)		...	

Tabla B.5: continued.

Transition $J_{K_a,K_c} - J'_{K'_a,K'_c}$	Predicted frequency (MHz)	S_{ij}	E_u (K)	v_{LSR} km s^{-1}	Δv km s^{-1}	T_{MB} (K)	$\int T_{MB} dv$ (K km s^{-1})
$24_{9,15}$-$23_{9,14}$	229851.392†	20.60	1290.9	(6,13,43)		...	
$24_{6,19}$-$23_{6,18}$	229871.820	22.50	1197.9	(9,10)		...	
$24_{6,18}$-$23_{6,17}$	229871.869†	22.50	1197.9	(9,10)		...	
$24_{10,14}$-$23_{10,13}$	229885.357	19.80	1330.1	6.4(1,3)		0.09(2)	
$24_{10,15}$-$23_{10,14}$	229885.357†	19.80	1330.1	6.4(1,3)		”	
$24_{11,13}$-$23_{11,12}$	229931.686	19.00	1373.3	(17)		...	
$24_{11,14}$-$23_{11,13}$	229931.686†	19.00	1373.3	(17)		...	
$24_{5,20}$-$23_{5,19}$	229964.408	23.00	1175.1	5.2(1,23)		0.16(2)	
$24_{5,19}$-$23_{5,18}$	229967.033†	23.00	1175.1	8.6(1,23)		”	
$24_{12,13}$-$23_{12,12}$	229988.519	18.00	1420.7	(3)		...	
$24_{12,12}$-$23_{12,11}$	229988.519†	18.00	1420.7	(3)		...	
$24_{13,11}$-$23_{13,10}$	230054.734	17.00	1472.0	(3)		...	
$24_{13,12}$-$23_{13,11}$	230054.734†	17.00	1472.0	(3)		...	
$24_{3,22}$-$23_{3,21}$	230089.526	23.60	1142.1	(27,44)		...	
$24_{14,10}$-$23_{14,9}$	230129.649	15.80	1527.4	(3)		...	
$24_{14,11}$-$23_{14,10}$	230129.649†	15.80	1527.4	(3)		...	
$24_{4,21}$-$23_{4,20}$	230142.149	23.30	1156.6	(5,45)		...	
$24_{4,20}$-$23_{4,19}$	230225.856	23.30	1156.6	(19,22,46)		...	
$25_{1,25}$-$24_{1,24}$	230987.354	24.90	1132.2	(17,46,47)		...	
$24_{3,21}$-$23_{3,20}$	231407.947	23.60	1142.4	4.9(1,48)		0.29(2)	
$25_{0,25}$-$24_{0,24}$	231932.726	25.00	1131.9	(15,45,49)		...	
$24_{1,23}$-$23_{1,22}$	232274.126	23.90	1127.9	(50)		...	
$24_{2,22}$-$23_{2,21}$	234421.430	23.80	1133.4	(6,32)		...	
$25_{2,24}$-$24_{2,23}$	237310.854	24.80	1142.4	(4,33)		...	
$25_{8,18}$-$24_{8,17}$	239411.881	22.40	1267.3	5.0(1)		0.15(2)	
$25_{8,17}$-$24_{8,16}$	239411.881†	22.40	1267.3	5.0(1)		”	
$25_{7,19}$-$24_{7,18}$	239419.220	23.00	1236.3	6.4(1)		0.14(2)	
$25_{7,18}$-$24_{7,17}$	239419.221†	23.00	1236.3	6.4(1)		”	
$25_{9,17}$-$24_{9,16}$	239428.178	21.80	1302.4	**		...	
$25_{9,16}$-$24_{9,15}$	239428.178†	21.80	1302.4	**		...	
$25_{10,15}$-$24_{10,14}$	239461.516	21.00	1341.6	**		...	
$25_{10,16}$-$24_{10,15}$	239461.516†	21.00	1341.6	**		...	
$25_{6,20}$-$24_{6,19}$	239463.119†	23.60	1209.4	**		...	
$25_{6,19}$-$24_{6,18}$	239463.197†	23.60	1209.4	**		...	
$25_{11,14}$-$24_{11,13}$	239508.265	20.20	1384.8	6.8(1)		0.11(2)	
$25_{11,15}$-$24_{11,14}$	239508.265†	20.20	1384.8	6.8(1)		”	
$25_{5,21}$-$24_{5,20}$	239570.362	24.00	1186.6	(51)		...	

Tabla B.5: continued.

Transition $J_{K_a,K_c} - J'_{K'_a,K'_c}$	Predicted frequency (MHz)	S_{ij}	E_u (K)	v_{LSR} km s^{-1}	Δv km s^{-1}	T_{MB} (K)	$\int T_{MB} dv$ (K km s^{-1})
$25_{5,20}$-$24_{5,19}$	239574.154†	24.00	1186.6	(3)		...	
$25_{3,23}$-$24_{3,22}$	239667.447	24.60	1153.6	(6,51)		...	
$25_{4,22}$-$24_{4,21}$	239766.828	24.40	1168.1	5.6(1)		0.15(2)	
$25_{4,21}$-$24_{4,20}$	239877.741	24.40	1168.1	(51)		...	
$26_{1,26}$-$25_{1,25}$	240108.619	25.90	1143.7	5.3(1,47)		0.37(2)	
$26_{0,26}$-$25_{0,25}$	240946.754	26.00	1143.5	(32)		...	
$25_{3,22}$-$24_{3,21}$	241255.217	24.60	1154.0	(4,41)		...	
$25_{1,24}$-$24_{1,23}$	241616.905	24.90	1139.5	(32)		...	
$25_{2,23}$-$24_{2,22}$	244286.846	24.80	1145.1	(17)		...	
$26_{2,25}$-$25_{2,24}$	246652.659	25.80	1154.2	(52)		...	
$26_{8,19}$-$25_{8,18}$	248991.083	23.50	1279.2	(4)		...	
$26_{8,18}$-$25_{8,17}$	248991.083†	23.50	1279.2	(4)		...	
$26_{7,20}$-$25_{7,19}$	249003.274	24.10	1248.2	(3)		...	
$26_{7,19}$-$25_{7,18}$	249003.275†	24.10	1248.2	(3)		...	
$26_{9,18}$-$25_{9,17}$	249004.933†	22.90	1314.3	(3)		...	
$26_{9,17}$-$25_{9,16}$	249004.933†	22.90	1314.3	(3)		...	
$26_{10,17}$-$25_{10,16}$	249037.396	22.20	1353.5	(4)		...	
$26_{10,16}$-$25_{10,15}$	249037.396†	22.20	1353.5	(4)		...	
$26_{6,21}$-$25_{6,20}$	249056.055	24.60	1221.3	(19)		...	
$26_{6,20}$-$25_{6,19}$	249056.175†	24.60	1221.3	(19)		...	
$26_{11,15}$-$25_{11,14}$	249084.381	21.30	1396.8	(33,36)		...	
$26_{11,16}$-$25_{11,15}$	249084.381†	21.30	1396.8	(33,36)		...	
$26_{5,22}$-$25_{5,21}$	249179.168	25.00	1198.6	(6,33,53)		...	
$26_{5,21}$-$25_{5,20}$	249184.563†	25.00	1198.6	(6,33,53)		...	
$27_{1,27}$-$26_{1,26}$	249222.708	26.90	1155.7	(6,27)		...	
$26_{3,24}$-$25_{3,23}$	249238.095	25.70	1165.5	5.4(1,54)		0.36(2)	
$26_{4,23}$-$25_{4,22}$	249394.094	25.40	1180.0	(17)		...	
$26_{4,22}$-$25_{4,21}$	249394.280	25.40	1180.1	(3,17)		...	
$27_{0,27}$-$26_{0,26}$	249961.782	27.00	1155.5	(3)		...	
$26_{1,25}$-$25_{1,24}$	250916.235	25.90	1151.5	(19,38)		...	
$26_{3,23}$-$25_{3,22}$	251129.984	25.70	1166.0	(33,38)		...	
$26_{2,24}$-$25_{2,23}$	254128.735	25.90	1157.3	(38)		...	
$27_{2,26}$-$26_{2,25}$	255979.000	26.80	1166.5	(39)		...	
$28_{1,28}$-$27_{1,27}$	258330.112	27.90	1168.1	(51,55)		...	
$27_{8,20}$-$26_{8,19}$	258570.615	24.60	1291.6	8.5(1)		0.19(2)	
$27_{8,19}$-$26_{8,18}$	258570.615†	24.60	1291.6	8.5(1)		”	
$27_{9,19}$-$26_{9,18}$	258581.656	24.00	1326.7	(3,12,17,41)		...	

Tabla B.5: continued.

Transition $J_{K_a,K_c} - J'_{K'_a,K'_c}$	Predicted frequency (MHz)	S_{ij}	E_u (K)	v_{LSR} km s^{-1}	Δv km s^{-1}	T_{MB} (K)	$\int T_{MB} dv$ (K km s^{-1})
$27_{9,18}$-$26_{9,17}$	258581.656†	24.00	1326.7	(3,12,17,41)		...	
$27_{7,21}$-$26_{7,20}$	258588.194	25.20	1260.6	(3)		...	
$27_{7,20}$-$26_{7,19}$	258588.196†	25.20	1260.6	(3)		...	
$27_{10,18}$-$26_{10,17}$	258612.986	23.30	1365.9	(3)		...	
$27_{10,17}$-$26_{10,16}$	258612.986†	23.30	1365.9	(3)		...	
$27_{6,22}$-$26_{6,21}$	258650.696	25.70	1233.7	(3,32)		...	
$27_{6,21}$-$26_{6,20}$	258650.877†	25.70	1233.7	(3,32)		...	
$27_{11,16}$-$26_{11,15}$	258660.016	22.50	1409.2	(3,32)		...	
$27_{11,17}$-$26_{11,16}$	258660.016†	22.50	1409.2	(3,32)		...	
$27_{12,15}$-$26_{12,14}$	258720.070	21.70	1456.5	(3)		...	
$27_{12,16}$-$26_{12,15}$	258720.070†	21.70	1456.5	(3)		...	
$27_{5,23}$-$26_{5,22}$	258790.897	26.10	1211.0	(19)		...	
$27_{13,15}$-$26_{13,14}$	258791.526†	20.70	1507.9	(19)		...	
$27_{13,14}$-$26_{13,13}$	258791.526†	20.70	1507.9	(19)		...	
$27_{5,22}$-$26_{5,21}$	258798.466	26.10	1211.0	(12)		...	
$27_{3,25}$-$26_{3,24}$	258800.452†	26.70	1178.0	(3)		...	
$27_{14,14}$-$26_{14,13}$	258873.377	19.70	1563.3	(3)		...	
$27_{14,13}$-$26_{14,12}$	258873.377†	19.70	1563.3	(3)		...	
$27_{15,13}$-$26_{15,12}$	258964.997	18.70	1622.6	(32)		...	
$27_{15,12}$-$26_{15,11}$	258964.997†	18.70	1622.6	(32)		...	
$28_{0,28}$-$27_{0,27}$	258978.678	28.00	1167.9	(3)		...	
$27_{4,24}$-$26_{4,23}$	259023.601	26.40	1192.5	(56)		...	
$27_{16,11}$-$26_{16,10}$	259066.002	17.50	1685.9	(3)		...	
$27_{16,12}$-$26_{16,11}$	259066.002†	17.50	1685.9	(3)		...	
$27_{17,11}$-$26_{17,10}$	259176.172	16.30	1753.2	(3)		...	
$27_{17,10}$-$26_{17,9}$	259176.172†	16.30	1753.2	(3)		...	
$27_{4,23}$-$26_{4,22}$	259211.508	26.40	1192.5	(5,9,35)		...	
$27_{1,26}$-$26_{1,25}$	260171.944	26.90	1164.0	(19)		...	
$27_{3,24}$-$26_{3,23}$	261031.741	26.70	1178.5	(4)		...	
$27_{2,25}$-$26_{2,24}$	263944.237	26.90	1170.0	(17)		...	
$28_{2,27}$-$27_{2,26}$	265289.819	27.80	1179.2	(10)		...	
$29_{1,29}$-$28_{1,28}$	267431.312	28.90	1180.9	(32,49,57)		...	
$29_{0,29}$-$28_{0,28}$	267997.969	29.00	1180.8	(6)		...	
$28_{8,21}$-$27_{8,20}$	268150.495	25.70	1304.5	(18,32)		...	
$28_{8,20}$-$27_{8,19}$	268150.495†	25.70	1304.5	(18,32)		...	
$28_{9,20}$-$27_{9,19}$	268158.350†	25.10	1339.6	(18,32)		...	
$28_{9,19}$-$27_{9,18}$	268158.350†	25.10	1339.6	(18,32)		...	

Tabla B.5: continued.

Transition $J_{K_a,K_c} - J'_{K'_a,K'_c}$	Predicted frequency (MHz)	S_{ij}	E_u (K)	v_{LSR} km s^{-1}	Δv km s^{-1}	T_{MB} (K)	$\int T_{MB} dv$ (K km s^{-1})
$28_{7,22}$-$27_{7,21}$	268174.016†	26.30	1273.5	(18,32)		...	
$28_{7,21}$-$27_{7,20}$	268174.021†	26.30	1273.5	(18,32)		...	
$28_{10,19}$-$27_{10,18}$	268188.279†	24.40	1378.8	(18,32		...	
$28_{10,18}$-$27_{10,17}$	268188.279†	24.40	1378.8	(18,32)		...	
$28_{11,18}$-$27_{11,17}$	268235.157	23.70	1422.1	(3)		...	
$28_{11,17}$-$27_{11,16}$	268235.157†	23.70	1422.1	(3)		...	
$28_{6,23}$-$27_{6,22}$	268247.108	26.70	1246.6	(3)		...	
$28_{6,22}$-$27_{6,21}$	268247.379†	26.70	1246.6	(3)		...	
$28_{12,17}$-$27_{12,16}$	268295.990	22.90	1469.4	(58)		...	
$28_{12,16}$-$27_{12,15}$	268295.990†	22.90	1469.4	(58)		...	
$28_{3,26}$-$27_{3,25}$	268353.520	27.70	1190.8	(3,15)		...	
$28_{13,15}$-$27_{13,14}$	268368.962	22.20	1520.8	(10)		...	
$28_{13,16}$-$27_{13,15}$	268368.962†	22.20	1520.8	(10)		...	
$28_{5,24}$-$27_{5,23}$	268405.613	27.10	1223.9	(19)		...	
$28_{5,23}$-$27_{5,22}$	268416.093	27.10	1223.9	(3)		...	
$28_{4,25}$-$27_{4,24}$	268654.936	27.40	1205.4	7.8(1)		0.16(2)	
$28_{4,24}$-$27_{4,23}$	268895.561	27.40	1205.4	(6,19)		...	
$28_{1,27}$-$27_{1,26}$	269384.606	27.90	1176.9	(6,19)		...	
$28_{3,25}$-$27_{3,24}$	270959.213	27.70	1191.5	(3)		...	
$28_{2,26}$-$27_{2,25}$	273730.812	27.90	1183.1	(3)		...	
$29_{2,28}$-$28_{2,27}$	274585.129	28.80	1192.4	6.4(1,26)		0.31(2)	
$30_{1,30}$-$29_{1,29}$	276526.774	29.90	1194.2	5.0(1,5,21)		0.25(2)	
$30_{0,30}$-$29_{0,29}$	277019.914	30.00	1194.0	(51,59)		...	
$29_{8,22}$-$28_{8,21}$	277730.736	26.80	1317.8	(5,46)		...	
$29_{8,21}$-$28_{8,20}$	277730.736†	26.80	1317.8	(5,46)		...	
$29_{9,21}$-$28_{9,20}$	277735.015†	26.20	1352.9	(5,46)		...	
$29_{9,20}$-$28_{9,19}$	277735.015†	26.20	1352.9	(5,46)		...	
$29_{7,23}$-$28_{7,22}$	277760.778	27.30	1286.8	(6,15)		...	
$29_{7,22}$-$28_{7,21}$	277760.785†	27.30	1286.8	(6,15)		...	
$29_{10,19}$-$28_{10,18}$	277763.268†	25.60	1392.1	(6,15)		...	
$29_{10,20}$-$28_{10,19}$	277763.268†	25.60	1392.1	(6,15)		...	
$29_{11,19}$-$28_{11,18}$	277809.788	24.80	1435.4	(6,19)		...	
$29_{11,18}$-$28_{11,17}$	277809.788†	24.80	1435.4	(6,19)		...	
$29_{6,24}$-$28_{6,23}$	277845.360	27.80	1260.0	6.6(1)		0.16(2)	
$29_{6,23}$-$28_{6,22}$	277845.759†	27.80	1260.0	7.1(1)		”	
$29_{12,17}$-$28_{12,16}$	277871.244	24.00	1482.7	(6,38)		...	
$29_{12,18}$-$28_{12,17}$	277871.244†	24.00	1482.7	(6,38)		...	

Tabla B.5: continued.

Transition $J_{K_a,K_c} - J'_{K'_a,K'_c}$	Predicted frequency (MHz)	S_{ij}	E_u (K)	v_{LSR} km s^{-1}	Δv km s^{-1}	T_{MB} (K)	$\int T_{MB} dv$ (K km s^{-1})
$29_{3,27}$-$28_{3,26}$	277896.328	28.70	1204.2	(60)		...	
$29_{13,17}$-$28_{13,16}$	277945.609	23.20	1534.1	(3)		...	
$29_{13,16}$-$28_{13,15}$	277945.609†	23.20	1534.1	(3)		...	
$29_{5,25}$-$28_{5,24}$	278023.363	28.10	1237.2	(6)		...	
$29_{5,24}$-$28_{5,23}$	278037.697	28.10	1237.2	(26,46)		...	
$29_{4,26}$-$28_{4,25}$	278287.616	28.40	1218.7	(10)		...	
$29_{1,28}$-$28_{1,27}$	278555.606	28.90	1190.3	(61)		...	
$29_{4,25}$-$28_{4,24}$	278592.679	28.40	1218.8	(10)		...	

Tabla A8. Emission lines of CH_2CHCN v_{11}=3 present in the spectral scan of the Orion-KL from the radio-telescope of IRAM 30-m. Column 1 indicates the line transition, Col. 2 gives the predicted frequency in the laboratory, Col. 3 the line strength, Col. 4 upper level energy, Col. 5 observed radial velocities relative to the local system rest (v_{LSR}), Col. 6 the line width, Col. 7 main beam temperature, and Col. 8 shows the area of the line. † blended with the previous line. $*$ noise level. $**$ hole in the observed spectrum.

(1) peak channel line observed velocity. (2) peak channel line intensity. (3) blended with U-line. (4) blended with $HCOOCH_3$. (5) blended with CH_3OCH_3. (6) blended with CH_3CH_2CN. (7) blended with $CH_3CH_2C^{15}N$. (8) blended with H 49β. (9) blended with CH_2CHCN v_{11}=1. (10) blended with CH_3OH. (11) blended with $O^{13}C^{34}S$. (12) blended with $CH_3{}^{13}CH_2CN$. (13) blended with $^{34}SO_2$. (14) blended with $H^{13}CS$. (15) blended with $H^{13}COOCH_3$. (16) blended with CH_2CHOH. (17) blended with $(CH_3)_2CO$. (18) blended with SO_2 v_2=1. (19) blended with CH_3CH_2CN v_{13}/v_{21}. (20) blended with HDO. (21) blended with CH_3OD. (22) blended with $SO^{17}O$. (23) blended with HCCCN. (24) blended with ^{29}SiO. (25) blended with $CH_3CH_2{}^{13}CN$. (26) blended with $^{13}CH_2CHCN$. (27) blended with CH_2CHCN v_{15}=1. (28) blended with $HCC^{13}CN$ v_7=1. (29) blended with CHDCHCN. (30) blended with $CH_2{}^{13}CHCN$. (31) blended with H_2CCO. (32) blended with SO_2. (33) blended with CH_3CH_2CN v_{20}=1. (34) blended with H_2CS. (35) blended with $^{33}SO_2$. (36) blended with $DCOOCH_3$. (37) blended with c-C_3H_2. (38) blended with CH_2CHCN. (39) blended with $^{13}CH_3OH$. (40) blended with $HN^{13}CO$. (41) blended with $^{13}CH_3CH_2CN$. (42) blended with $HNC^{18}O$. (43) blended with $SO^{18}O$. (44) blended with $H^{13}CCCN$ v_7=1. (45) blended with $HCOO^{13}CH_3$. (46) blended with |g_+-g_-|-CH_3CH_2OH. (47) blended with t-CH_3CH_2OH. (48) blended with D_2CO. (49) blended with $CH_3C^{15}N$. (50) blended with NH_2CHO. (51) blended with CH_3CN v_8=1. (52) blended with ^{34}SO. (53) blended with ^{33}SO. (54) blended with CH_3COOH v_t=0. (55) blended with CH_3OD. (56) blended with $H^{13}CN$. (57) blended with H_2CCS. (58) blended with HDCO. (59) blended with CH_2CHCN v_{11}=2. (60) blended with CH_2DCN. (61) blended with DCCCN.

Tabla B.6: Detected lines of CH_2CHCN v_{15}=1 .

Transition $J_{K_a,K_c} - J'_{K'_a,K'_c}$	Predicted frequency (MHz)	S_{ij}	E_u (K)	v_{LSR} km s^{-1}	Δv km s^{-1}	T_{MB} (K)	$\int T_{MB} dv$ (K km s^{-1})
$9_{1,9}$-$8_{1,8}$	83349.865	8.89	500.9	(3)		...	
$9_{0,9}$-$8_{0,8}$	85075.547	9.00	499.1	5.6(1)		0.03(2)	
$9_{2,8}$-$8_{2,7}$	85416.767	8.56	508.0	(4)		...	
$9_{4,6}$-$8_{4,5}$	85528.061	7.22	534.5	4.0(1)		0.02(2)	
$9_{4,5}$-$8_{4,4}$	85528.107†	7.22	534.5	4.2(1)		”	
$9_{5,5}$-$8_{5,4}$	85532.951	6.22	554.4	4.1(1)		0.02(2)	
$9_{5,4}$-$8_{5,3}$	85532.951†	6.22	554.4	4.1(1)		”	
				4.3±0.2	7.2±0.7	0.02	0.12±0.01
$9_{3,7}$-$8_{3,6}$	85536.445	8.00	519.1	1.8(1)		0.01(2)	
$9_{3,6}$-$8_{3,5}$	85543.458	8.00	519.1	6.5(1)		0.02(2)	
				6.5±0.4	3.5±0.5	0.01	0.05±0.01
$9_{6,4}$-$8_{6,3}$	85545.876	5.00	578.6	3.4(1,5)		0.04(2)	
$9_{6,3}$-$8_{6,2}$	85545.876†	5.00	578.6	3.4(1,5)		”	
$9_{2,7}$-$8_{2,6}$	85810.690	8.56	508.1	(6)		...	
$9_{1,8}$-$8_{1,7}$	87401.383	8.89	501.9	(7)		...	
$10_{1,10}$-$9_{1,9}$	92585.520	9.90	505.3	(3,8)		...	
$10_{0,10}$-$9_{0,9}$	94425.263	9.99	503.7	6.7(1,9)		0.05(2)	
				6.40±0.08	6.8±0.2	0.04	0.27±0.01
$10_{2,9}$-$9_{2,8}$	94888.425	9.60	512.6	6.1(1)		0.03(2)	
				6.1±0.6	10±1	0.03	0.30±0.04
$10_{4,7}$-$9_{4,6}$	95036.464	8.40	539.1	5.4(1)		0.05(2)	
$10_{4,6}$-$9_{4,5}$	95036.563†	8.40	539.1	5.7(1)		”	
$10_{5,6}$-$9_{5,5}$	95039.298	7.50	558.9	5.6(1)		0.04(2)	
$10_{5,5}$-$9_{5,4}$	95039.298†	7.50	558.9	5.6(1)		”	
				5.6±0.2	5.6±0.4	0.03	0.17±0.01
$10_{3,8}$-$9_{3,7}$	95049.840	9.10	523.6	7.8(1)		0.03(2)	
$10_{6,5}$-$9_{6,4}$	95052.284†	6.40	583.1	3.2(1)		”	
$10_{6,4}$-$9_{6,3}$	95052.284†	6.40	583.1	6.4(1)		”	
$10_{3,7}$-$9_{3,6}$	95061.849	9.10	523.6	4.8(1)		0.03(2)	
				4.8±0.8	6±2	0.02	0.16±0.04
$10_{7,4}$-$9_{7,3}$	95071.819	5.10	611.7	4.9(1,6)		0.03(2)	
$10_{7,3}$-$9_{7,2}$	95071.819†	5.10	611.7	4.9(1,6)		”	
$10_{8,2}$-$9_{8,1}$	95096.440	3.60	644.6	(6)		...	
$10_{8,3}$-$9_{8,2}$	95096.440†	3.60	644.6	(6)		...	
$10_{2,8}$-$9_{2,7}$	95427.491	9.60	512.6	5.8(1,6)		0.04(2)	
$10_{1,9}$-$9_{1,8}$	97082.304	9.90	506.5	5.9(1)		0.03(2)	

Tabla B.6: continued.

Transition $J_{K_a,K_c} - J'_{K'_a,K'_c}$	Predicted frequency (MHz)	S_{ij}	E_u (K)	v_{LSR} km s^{-1}	Δv km s^{-1}	T_{MB} (K)	$\int T_{MB} dv$ (K km s^{-1})
				5.9±0.8	6±2	0.03	0.20±0.04
$11_{1,11}$-$10_{1,10}$	101813.714	10.90	510.2	4.8[1]		0.04[2]	
				4.8±0.8	5±2	0.03	0.16±0.05
$11_{0,11}$-$10_{0,10}$	103744.365	11.00	508.6	5.9[1]		0.04[2]	
$11_{2,10}$-$10_{2,9}$	104354.080	10.60	517.6	[10]		...	
$11_{5,7}$-$10_{5,6}$	104546.490	8.73	563.9	4.7[1]		0.07[2]	
$11_{5,6}$-$10_{5,5}$	104546.491†	8.73	563.9	4.7[1]		”	
$11_{4,8}$-$10_{4,7}$	104546.519†	9.55	544.1	4.8[1]		”	
$11_{4,7}$-$10_{4,6}$	104546.717†	9.55	544.1	5.3[1]		”	
				4.8±0.4	6.0±0.9	0.07	0.46±0.06
$11_{6,6}$-$10_{6,5}$	104559.103	7.73	588.1	3.9[1]		0.04[2]	
$11_{6,5}$-$10_{6,4}$	104559.103†	7.73	588.1	3.9[1]		”	
				3.8±0.7	7±1	0.03	0.26±0.05
$11_{3,9}$-$10_{3,8}$	104565.623	10.20	528.7	5.0[1]		0.04[2]	
				4.3±0.4	8±1	0.04	0.32±0.05
$11_{7,5}$-$10_{7,4}$	104579.602	6.55	616.7	3.4[1]		0.03[2]	
$11_{7,4}$-$10_{7,3}$	104579.602†	6.55	616.7	3.4[1]		”	
				3.3±0.5	12.9±0.7	0.02	0.33±0.03
$11_{3,8}$-$10_{3,7}$	104585.110	10.20	528.7	3.6[1,6]		0.05[2]	
$11_{8,3}$-$10_{8,2}$	104606.047	5.18	649.6	4.9[1]		0.02[2]	
$11_{8,4}$-$10_{8,3}$	104606.047†	5.18	649.6	4.9[1]		”	
$11_{2,9}$-$10_{2,8}$	105068.319	10.60	517.7	2.8[1,5,6]		0.12[2]	
$11_{1,10}$-$10_{1,9}$	106753.065	10.90	511.6	[11]		...	
$12_{1,12}$-$11_{1,11}$	111033.976	11.90	515.6	7.6[1]		0.08[2]	
$12_{0,12}$-$11_{0,11}$	113031.186	12.00	514.1	5.3[1,4,12]		0.05[2]	
$12_{2,11}$-$11_{2,10}$	113813.147	11.70	523.0	8.2[1]		0.03[2]	
$12_{5,8}$-$11_{5,7}$	114054.610	9.92	569.4	4.2[1,6]		0.10[2]	
$12_{5,7}$-$11_{5,6}$	114054.613†	9.92	569.4	4.2[1,6]		”	
$12_{4,9}$-$11_{4,8}$	114058.378	10.70	549.6	6.2[1]		0.06[2]	
$12_{4,8}$-$11_{4,7}$	114058.749†	10.70	549.6	7.1[1]		”	
$12_{6,7}$-$11_{6,6}$	114066.374	9.00	593.6	[9,13]		...	
$12_{6,6}$-$11_{6,5}$	114066.374†	9.00	593.6	[9,13]		...	
$12_{3,10}$-$11_{3,9}$	114083.762	11.20	534.1	[6]		...	
$12_{7,6}$-$11_{7,5}$	114087.555	7.92	622.2	[6]		...	
$12_{7,5}$-$11_{7,4}$	114087.555†	7.92	622.2	[6]		...	
$12_{3,9}$-$11_{3,8}$	114114.024	11.20	534.1	2.5[1,6]		0.12[2]	
$12_{2,10}$-$11_{2,9}$	114734.177	11.70	523.2	5.4[1,6]		0.07[2]	

Tabla B.6: continued.

Transition $J_{K_a,K_c} - J'_{K'_a,K'_c}$	Predicted frequency (MHz)	S_{ij}	E_u (K)	v_{LSR} km s^{-1}	Δv km s^{-1}	T_{MB} (K)	$\int T_{MB} dv$ (K km s^{-1})
$14_{0,14}$-$13_{0,13}$	131504.447	14.00	526.2	6.6[1,13]		0.11[2]	
$14_{2,13}$-$13_{2,12}$	132709.220	13.70	535.3	6.1[1]		0.08[2]	
$14_{5,10}$-$13_{5,9}$	133073.970	12.20	581.7	[4]		...	
$14_{5,9}$-$13_{5,8}$	133073.979†	12.20	581.7	[4]		...	
$14_{6,9}$-$13_{6,8}$	133082.435	11.40	605.9	[3]		...	
$14_{6,8}$-$13_{6,7}$	133082.435†	11.40	605.9	[3]		...	
$14_{4,11}$-$13_{4,10}$	133088.086	12.90	561.9	4.7[1]		0.07[2]	
$14_{4,10}$-$13_{4,9}$	133089.205†	12.90	561.9	4.7[1]		”	
$14_{7,8}$-$13_{7,7}$	133104.030	10.50	634.5	[14]		...	
$14_{7,7}$-$13_{7,6}$	133104.030†	10.50	634.5	[14]		...	
$14_{3,12}$-$13_{3,11}$	133126.628	13.40	546.4	[4,15]		...	
$14_{8,7}$-$13_{8,6}$	133134.796	9.43	667.4	[4,15]		...	
$14_{8,6}$-$13_{8,5}$	133134.796†	9.43	667.4	[4,15]		...	
$14_{9,6}$-$13_{9,5}$	133172.869	8.21	704.6	4.0[1]		0.05[2]	
$14_{9,5}$-$13_{9,4}$	133172.869†	8.21	704.6	4.0[1]		”	
$14_{3,11}$-$13_{3,10}$	133192.350	13.40	546.5	7.7[1,6,12]		0.09[2]	
$14_{2,12}$-$13_{2,11}$	134141.825	13.70	535.6	4.8[1]		0.07[2]	
				4.9±0.2	6.7±0.5	0.07	0.48±0.03
$14_{1,13}$-$13_{1,12}$	135690.914	1.39	529.8	[16]		...	
$15_{1,15}$-$14_{1,14}$	138643.548	14.90	534.2	5.8[1]		0.09[2]	
$15_{0,15}$-$14_{0,14}$	140690.913	15.00	533.0	[14]		...	
$15_{2,14}$-$14_{2,13}$	142145.099	14.70	542.1	6.5[1]		0.09[2]	
$15_{5,11}$-$14_{5,10}$	142585.373	13.30	588.6	4.9[1]		0.09[2]	
$15_{5,10}$-$14_{5,9}$	142585.391†	13.30	588.6	4.8[1]		”	
				4.6±0.4	8±1	0.09	0.76±0.09
$15_{6,10}$-$14_{6,9}$	142591.303	12.60	612.8	4.7[1]		0.10[2]	
$15_{6,9}$-$14_{6,8}$	142591.303†	12.60	612.8	4.7[1]		”	
				4.7±0.3	5.7±0.8	0.13	0.82±0.09
$15_{4,12}$-$14_{4,11}$	142606.205	13.90	568.7	1.3[1]		0.10[2]	
$15_{4,11}$-$14_{4,10}$	142608.034†	13.90	568.7	5.2[1]		”	
				3.3±0.2	6.0±0.8	0.10	0.64±0.07
$15_{7,9}$-$14_{7,8}$	142612.580	11.70	641.4	5.7[1]		0.04[2]	
$15_{7,8}$-$14_{7,7}$	142612.580†	11.70	641.4	5.7[1]		”	
				6.3±0.3	4.5±0.5	0.03	0.14±0.02
$15_{8,8}$-$14_{8,7}$	142644.348	10.70	674.3	[17]		...	
$15_{8,7}$-$14_{8,6}$	142644.348†	10.70	674.3	[17]		...	
$15_{3,13}$-$14_{3,12}$	142650.933	14.40	553.3	[6]		...	

Tabla B.6: continued.

Transition $J_{K_a,K_c} - J'_{K'_a,K'_c}$	Predicted frequency (MHz)	S_{ij}	E_u (K)	v_{LSR} km s^{-1}	Δv km s^{-1}	T_{MB} (K)	$\int T_{MB} dv$ (K km s^{-1})
$15_{3,12}$-$14_{3,11}$	142743.756	14.40	553.3	(18,19)		...	
$15_{2,13}$-$14_{2,12}$	143882.222	14.70	542.5	(20)		...	
$15_{1,14}$-$14_{1,13}$	145307.136	14.90	536.8	(20,21)		...	
$16_{1,16}$-$15_{1,15}$	147828.832	15.90	541.3	3.6(1)		0.10(2)	
$16_{0,16}$-$15_{0,15}$	149845.222	16.00	540.2	5.4(1,6)		0.20(2)	
$16_{2,15}$-$15_{2,14}$	151572.144	15.70	549.4	(8)		...	
$16_{5,12}$-$15_{5,11}$	152098.034	14.40	595.9	1.4(1,6)		0.26(2)	
$16_{5,11}$-$15_{5,10}$	152098.067†	14.40	595.9	1.4(1,6)		”	
$16_{6,11}$-$15_{6,10}$	152100.782†	13.80	620.1	6.8(1,6)		”	
$16_{6,10}$-$15_{6,9}$	152100.783†	13.80	620.1	6.8(1,6)		”	
$16_{7,10}$-$15_{7,9}$	152121.359	12.90	648.7	(4,6)		...	
$16_{7,9}$-$15_{7,8}$	152121.359†	12.90	648.7	(4,6)		...	
$16_{4,13}$-$15_{4,12}$	152126.661	15.00	576.0	(4)		...	
$16_{4,12}$-$15_{4,11}$	152129.552†	15.00	576.0	(4)		...	
$16_{8,9}$-$15_{8,8}$	152153.881	12.00	681.6	5.4(1)		0.06(2)	
$16_{8,8}$-$15_{8,7}$	152153.881†	12.00	681.6	5.4(1)		”	
				5.3±0.4	8±1	0.07	0.62±0.06
$16_{3,14}$-$15_{3,13}$	152176.751	15.40	560.6	(4,14,22)		...	
$16_{9,8}$-$15_{9,7}$	152195.588	10.90	718.8	(3)		...	
$16_{9,7}$-$15_{9,6}$	152195.588†	10.90	718.8	(3)		...	
$16_{10,7}$-$15_{10,6}$	152245.017	9.75	760.3	5.7(1,6)		0.16(2)	
$16_{10,6}$-$15_{10,5}$	152245.017†	9.75	760.3	5.7(1,6)		”	
$16_{3,13}$-$15_{3,12}$	152304.807	15.40	560.6	(15,20)		...	
$16_{2,14}$-$15_{2,13}$	153644.786	15.70	549.9	6.6(1,6,23)		0.29(2)	
$16_{1,15}$-$15_{1,14}$	154905.812	15.90	544.2	6.4(1)		0.25(2)	
$17_{1,17}$-$16_{1,16}$	157004.932	16.90	548.8	4.1(1,24,25)		0.28(2)	
$17_{0,17}$-$16_{0,16}$	158969.257	17.00	547.8	(6)		...	
$17_{2,16}$-$16_{2,15}$	160989.824	16.80	557.1	5.8(1)		0.19(2)	
$17_{6,12}$-$16_{6,11}$	161610.913	14.90	627.8	4.2(1)		0.35(2)	
$17_{6,11}$-$16_{6,10}$	161610.913†	14.90	627.8	4.2(1)		”	
$17_{5,13}$-$16_{5,12}$	161612.034†	15.50	603.6	6.3(1)		”	
$17_{5,12}$-$16_{5,11}$	161612.092†	15.50	603.6	6.4(1)		”	
$17_{7,11}$-$16_{7,10}$	161630.380	14.10	656.4	(3,26)		...	
$17_{7,10}$-$16_{7,9}$	161630.380†	14.10	656.4	(3,26)		...	
$17_{4,14}$-$16_{4,13}$	161649.560	16.10	583.8	(20)		...	
$17_{4,13}$-$16_{4,12}$	161653.998†	16.10	583.8	(20)		...	
$17_{8,10}$-$16_{8,9}$	161663.393	13.20	689.3	(27)		...	

Tabla B.6: continued.

Transition $J_{K_a,K_c} - J'_{K'_a,K'_c}$	Predicted frequency (MHz)	S_{ij}	E_u (K)	v_{LSR} km s^{-1}	Δv km s^{-1}	T_{MB} (K)	$\int T_{MB} dv$ (K km s^{-1})
$17_{8,9}$-$16_{8,8}$	161663.393†	13.20	689.3	(27)		...	
$17_{3,15}$-$16_{3,14}$	161703.686	16.50	568.4	(28)		...	
$17_{9,8}$-$16_{9,7}$	161706.653†	12.20	726.5	(28)		...	
$17_{9,9}$-$16_{9,8}$	161706.653†	12.20	726.5	(28)		...	
$17_{10,7}$-$16_{10,6}$	161758.416	11.10	768.0	(29)		...	
$17_{10,8}$-$16_{10,7}$	161758.416†	11.10	768.0	(29)		...	
$17_{11,7}$-$16_{11,6}$	161817.666	9.88	813.8	(6)		...	
$17_{11,6}$-$16_{11,5}$	161817.666†	9.88	813.8	(6)		...	
$17_{3,14}$-$16_{3,13}$	161876.727	16.50	568.4	(5)		...	
$17_{2,15}$-$16_{2,14}$	163426.916	16.80	557.7	5.0(1)		0.13(2)	
				5.1±0.9	9±2	0.14	1.3±0.3
$17_{1,16}$-$16_{1,15}$	164485.197	16.90	552.1	(10)		...	
$18_{1,18}$-$17_{1,17}$	166171.819	17.90	556.8	(10)		...	
$18_{0,18}$-$17_{0,17}$	168065.536	18.00	555.9	7.5(1,6)		0.29(2)	
$18_{2,17}$-$17_{2,16}$	170397.627	17.80	565.3	6.9(1,30)		0.20(2)	
$18_{6,13}$-$17_{6,12}$	171121.733	16.00	636.1	5.5(1,6,23)		0.28(2)	
$18_{6,12}$-$17_{6,11}$	171121.734†	16.00	636.1	5.5(1,6,23)		”	
$18_{5,14}$-$17_{5,13}$	171127.453	16.60	611.8	4.5(1,31)		0.20(2)	
$18_{5,13}$-$17_{5,12}$	171127.551†	16.60	611.8	4.7(1,31)		”	
$18_{7,12}$-$17_{7,11}$	171139.656	15.30	664.6	(6,12)		...	
$18_{7,11}$-$17_{7,10}$	171139.656†	15.30	664.6	(6,12)		...	
$18_{8,11}$-$17_{8,10}$	171172.882	14.40	697.5	(10,20)		...	
$18_{8,10}$-$17_{8,9}$	171172.882†	14.40	697.5	(10,20)		...	
$18_{4,15}$-$17_{4,14}$	171174.989†	17.10	592.0	(10,20)		...	
$18_{4,14}$-$17_{4,13}$	171181.632†	17.10	592.0	(10,20)		...	
$18_{9,9}$-$17_{9,8}$	171217.504	13.50	734.8	(4,6)		...	
$18_{9,10}$-$17_{9,9}$	171217.504†	13.50	734.8	(4,6)		...	
$18_{3,16}$-$17_{3,15}$	171231.278	17.50	576.6	(15)		...	
$18_{10,8}$-$17_{10,7}$	171271.464	12.40	776.3	(14)		...	
$18_{10,9}$-$17_{10,8}$	171271.464†	12.40	776.3	(14)		...	
$18_{11,7}$-$17_{11,6}$	171333.567	11.30	822.0	(6)		...	
$18_{11,8}$-$17_{11,7}$	171333.567†	11.30	822.0	(6)		...	
$18_{12,6}$-$17_{12,5}$	171403.059	10.00	872.0	(5,22)		...	
$18_{2,16}$-$17_{2,15}$	173225.360	17.80	566.0	(8)		...	
$18_{1,17}$-$17_{1,16}$	174043.465	17.90	560.5	(6)		...	
$19_{1,19}$-$18_{1,18}$	175329.534	18.90	565.2	(6,11)		...	
$19_{0,19}$-$18_{0,18}$	177137.079	19.00	564.4	(6)		...	

Tabla B.6: continued.

Transition $J_{K_a,K_c} - J'_{K'_a,K'_c}$	Predicted frequency (MHz)	S_{ij}	E_u (K)	v_{LSR} km s^{-1}	Δv km s^{-1}	T_{MB} (K)	$\int T_{MB} dv$ (K km s^{-1})
$21_{2,20}$-$20_{2,19}$	198556.992	20.80	592.6	5.5[1]		0.16[2]	
				5.60±0.11	5.2±0.4	0.17	0.91±0.08
$21_{6,16}$-$20_{6,15}$	199658.717	19.30	663.4	[4,32]		...	
$21_{6,15}$-$20_{6,14}$	199658.722†	19.30	663.4	[4,32]		...	
$21_{7,15}$-$20_{7,14}$	199669.152	18.70	692.0	[4,32]		...	
$21_{7,14}$-$20_{7,13}$	199669.152†	18.70	692.0	[4,32]		...	
$21_{5,17}$-$20_{5,16}$	199683.011	19.80	639.2	[6]		...	
$21_{5,16}$-$20_{5,15}$	199683.411†	19.80	639.2	[6]		...	
$21_{8,14}$-$20_{8,13}$	199701.185	18.00	724.9	4.8[1]		0.12[2]	
$21_{8,13}$-$20_{8,12}$	199701.185†	18.00	724.9	4.8[1]		”	
				4.6±0.4	6±1	0.15	0.9±0.2
$21_{9,12}$-$20_{9,11}$	199748.641	17.10	762.1	[15]		...	
$21_{9,13}$-$20_{9,12}$	199748.641†	17.10	762.1	[15]		...	
$21_{4,18}$-$20_{4,17}$	199767.036	20.20	619.4	7.6[1]		0.16[2]	
$21_{4,17}$-$20_{4,16}$	199786.638	20.20	619.4	[20,21]		...	
$21_{10,12}$-$20_{10,11}$	199808.293	16.20	803.7	4.8[1]		0.10[2]	
$21_{10,11}$-$20_{10,10}$	199808.293†	16.20	803.7	4.8[1]		”	
$21_{3,19}$-$20_{3,18}$	199812.383†	20.60	604.0	7.1[1]		”	
$21_{11,10}$-$20_{11,9}$	199878.285	15.20	849.4	4.8[1]		0.07[2]	
$21_{11,11}$-$20_{11,10}$	199878.285†	15.20	849.4	4.8[1]		”	
				4.91±0.05	4.8±0.1	0.07	0.35±0.01
$21_{12,10}$-$20_{12,9}$	199957.463	14.10	899.4	6.9[1]		0.07[2]	
$21_{12,9}$-$20_{12,8}$	199957.463†	14.10	899.4	6.9[1]		”	
$21_{13,9}$-$20_{13,8}$	200045.057	13.00	953.5	[21,24]		...	
$21_{13,8}$-$20_{13,7}$	200045.057†	13.00	953.5	[21,24]		...	
$21_{14,7}$-$20_{14,6}$	200140.523	11.70	1011.8	[5,33]		...	
$21_{14,8}$-$20_{14,7}$	200140.523†	11.70	1011.8	[5,33]		...	
$21_{15,7}$-$20_{15,6}$	200243.454	10.30	1074.2	[34]		...	
$21_{15,6}$-$20_{15,5}$	200243.454†	10.30	1074.2	[34]		...	
$21_{3,18}$-$20_{3,17}$	200300.201	20.60	604.1	[16]		...	
$21_{16,5}$-$20_{16,4}$	200353.532	8.81	1140.6	[5]		...	
$21_{16,6}$-$20_{16,5}$	200353.532†	8.81	1140.6	[5]		...	
$21_{1,20}$-$20_{1,19}$	202572.347	20.90	588.3	7.6[1,3]		0.61[2]	
$21_{2,19}$-$20_{2,18}$	202679.195	20.80	593.8	4.9[1,6]		0.41[2]	
$22_{1,22}$-$21_{1,21}$	202748.974	21.90	593.1	[19]		...	
$22_{0,22}$-$21_{0,21}$	204237.302	22.00	592.5	[16]		...	
$22_{2,21}$-$21_{2,20}$	207920.633	21.80	602.5	[22,35]		...	

Tabla B.6: continued.

Transition $J_{K_a,K_c} - J'_{K'_a,K'_c}$	Predicted frequency (MHz)	S_{ij}	E_u (K)	v_{LSR} km s^{-1}	Δv km s^{-1}	T_{MB} (K)	$\int T_{MB} dv$ (K km s^{-1})
$22_{6,17}$-$21_{6,16}$	209172.681	20.40	673.5	3.2[1]		0.38[2]	
$22_{6,16}$-$21_{6,15}$	209172.690†	20.40	673.5	3.2[1]		”	
$22_{7,16}$-$21_{7,15}$	209179.585	19.80	702.0	6.8[1,6]		0.42[2]	
$22_{7,15}$-$21_{7,14}$	209179.585†	19.80	702.0	6.8[1,6]		”	
$22_{5,18}$-$21_{5,17}$	209204.884	20.90	649.3	[3]		...	
$22_{5,17}$-$21_{5,16}$	209205.495†	20.90	649.3	[3]		...	
$22_{8,15}$-$21_{8,14}$	209210.554†	19.10	735.0	[3]		...	
$22_{8,14}$-$21_{8,13}$	209210.554†	19.10	735.0	[3]		...	
$22_{9,14}$-$21_{9,13}$	209258.502	18.30	772.2	5.3[1]		0.36[2]	
$22_{9,13}$-$21_{9,12}$	209258.502†	18.30	772.2	5.3[1]		”	
$22_{4,19}$-$21_{4,18}$	209303.039	21.30	629.4	[20]		...	
$22_{10,13}$-$21_{10,12}$	209319.726	17.50	813.7	[6]		...	
$22_{10,12}$-$21_{10,11}$	209319.726†	17.50	813.7	[6]		...	
$22_{4,18}$-$21_{4,17}$	209330.166	21.30	629.4	5.0[1,6]		0.41[2]	
$22_{3,20}$-$21_{3,19}$	209336.713	21.60	614.0	6.4[1]		0.32[2]	
$22_{11,11}$-$21_{11,10}$	209392.105	16.50	859.5	5.1[1,36]		0.30[2]	
$22_{11,12}$-$21_{11,11}$	209392.105†	16.50	859.5	5.1[1,36]		”	
$22_{12,10}$-$21_{12,9}$	209474.325	15.50	909.4	[3]		...	
$22_{12,11}$-$21_{12,10}$	209474.325†	15.50	909.4	[3]		...	
$22_{13,9}$-$21_{13,8}$	209565.512	14.30	963.6	[6]		...	
$22_{13,10}$-$21_{13,9}$	209565.512†	14.30	963.6	[6]		...	
$22_{14,8}$-$21_{14,7}$	209665.054	13.10	1021.9	[4]		...	
$22_{14,9}$-$21_{14,8}$	209665.054†	13.10	1021.9	[4]		...	
$22_{15,8}$-$21_{15,7}$	209772.494	11.80	1084.2	[6]		...	
$22_{15,7}$-$21_{15,6}$	209772.494†	11.80	1084.2	[6]		...	
$22_{16,6}$-$21_{16,5}$	209887.480	10.40	1150.7	[6]		...	
$22_{16,7}$-$21_{16,6}$	209887.480†	10.40	1150.7	[6]		...	
$22_{3,19}$-$21_{3,18}$	209947.176	21.60	614.1	[16]		...	
$23_{1,23}$-$22_{1,22}$	211871.600	22.90	603.3	[6,37]		...	
$22_{1,21}$-$21_{1,20}$	212026.781	21.90	598.4	3.6[1,38]		0.54[2]	
$22_{2,20}$-$21_{2,19}$	212502.450	21.80	604.0	3.8[1]		0.43[2]	
$23_{0,23}$-$22_{0,22}$	213243.952	23.00	602.7	5.5[1,6]		0.53[2]	
$23_{2,22}$-$22_{2,21}$	217272.213	22.80	613.0	5.4[1]		0.32[2]	
$23_{6,18}$-$21_{6,17}$	218687.527	21.40	684.0	[39]		...	
$23_{6,17}$-$21_{6,16}$	218687.540†	21.40	684.0	[39]		...	
$23_{7,17}$-$21_{7,16}$	218690.338†	20.90	712.5	[39]		...	
$23_{7,16}$-$21_{7,15}$	218690.338†	20.90	712.5	[39]		...	

Tabla B.6: continued.

Transition $J_{K_a,K_c} - J'_{K'_a,K'_c}$	Predicted frequency (MHz)	S_{ij}	E_u (K)	v_{LSR} km s^{-1}	Δv km s^{-1}	T_{MB} (K)	$\int T_{MB} dv$ (K km s^{-1})
$23_{8,16}$-$22_{8,15}$	218719.886	20.20	745.5	4.6[1]		0.24[2]	
$23_{8,15}$-$22_{8,14}$	218719.886†	20.20	745.5	4.6[1]		”	
				4.5±0.2	5.3±0.4	0.22	1.25±0.11
$23_{5,19}$-$22_{5,18}$	218728.556	21.90	659.8	4.4[1]		0.60[2]	
$23_{5,18}$-$22_{5,17}$	218729.470†	21.90	659.8	5.6[1]		”	
$23_{9,15}$-$21_{9,14}$	218768.080	19.50	782.7	[40]		...	
$23_{9,14}$-$21_{9,13}$	218768.080†	19.50	782.7	[40]		...	
$23_{10,14}$-$22_{10,13}$	218830.701	18.70	824.2	5.9[1,36]		0.41[2]	
$23_{10,13}$-$22_{10,12}$	218830.701†	18.70	824.2	5.9[1,36]		”	
$23_{4,20}$-$22_{4,19}$	218841.664	22.30	639.9	4.8[1,41]		0.36[2]	
$23_{3,21}$-$22_{3,20}$	218858.495	22.60	624.5	[42]		...	
$23_{3,19}$-$22_{3,18}$	218878.637	22.30	640.0	[43]		...	
$23_{11,13}$-$22_{11,12}$	218905.337	17.70	870.0	[44]		...	
$23_{11,12}$-$22_{11,11}$	218905.337†	17.70	870.0	[44]		...	
$23_{12,11}$-$22_{12,10}$	218990.497	16.70	919.9	[26]		...	
$23_{12,12}$-$22_{12,11}$	218990.497†	16.70	919.9	[26]		...	
$23_{13,10}$-$22_{13,9}$	219085.198	15.70	974.1	[6]		...	
$23_{13,11}$-$22_{13,10}$	219085.198†	15.70	974.1	[6]		...	
$23_{14,9}$-$22_{14,8}$	219188.751	14.50	1032.4	[42]		...	
$23_{14,10}$-$22_{14,9}$	219188.751†	14.50	1032.4	[42]		...	
$23_{15,9}$-$22_{15,8}$	219300.647	13.20	1094.8	[24,45]		...	
$23_{15,8}$-$22_{15,7}$	219300.647†	13.20	1094.8	[24,45]		...	
$23_{16,7}$-$22_{16,6}$	219420.494	11.90	1161.2	[5,6]		...	
$23_{16,8}$-$22_{16,7}$	219420.494†	11.90	1161.2	[5,6]		...	
$23_{3,20}$-$22_{3,19}$	219613.427	22.60	624.7	5.2[1]		0.33[2]	
$24_{1,24}$-$23_{1,23}$	220986.100	23.90	613.9	[3,43,46]		...	
$23_{1,22}$-$22_{1,21}$	221450.396	22.90	609.1	[3,20]		...	
$24_{0,24}$-$23_{0,23}$	222242.403	24.00	613.4	[24]		...	
$23_{2,21}$-$22_{2,20}$	222321.314	22.80	614.7	3.8[1,24]		0.52[2]	
$24_{2,23}$-$23_{2,22}$	226611.392	23.80	623.8	6.1[1,6]		0.31[2]	
$24_{7,18}$-$23_{7,17}$	228201.426	22.00	723.5	3.5[1,3]		0.74[2]	
$24_{7,17}$-$23_{7,16}$	228201.426†	22.00	723.5	3.5[1,3]		”	
$24_{6,19}$-$23_{6,18}$	228203.292†	22.50	694.9	6.0[1,3]		”	
$24_{6,18}$-$23_{6,17}$	228203.314†	22.50	694.9	6.0[1,3]		”	
$24_{8,17}$-$23_{8,16}$	228229.177	21.30	756.4	[6,9]		...	
$24_{8,16}$-$23_{8,15}$	228229.177†	21.30	756.4	[6,9]		...	
$24_{5,20}$-$23_{5,19}$	228254.096	23.00	670.7	[4]		...	

Tabla B.6: continued.

Transition $J_{K_a,K_c} - J'_{K'_a,K'_c}$	Predicted frequency (MHz)	S_{ij}	E_u (K)	v_{LSR} km s^{-1}	Δv km s^{-1}	T_{MB} (K)	$\int T_{MB} dv$ (K km s^{-1})
$24_{5,19}$-$23_{5,18}$	228255.438†	23.00	670.7	(4)		...	
$24_{9,16}$-$23_{9,15}$	228277.362	20.60	793.6	7.5(1)		0.16(2)	
$24_{9,15}$-$23_{9,14}$	228277.362†	20.60	793.6	7.5(1)		”	
$24_{10,14}$-$23_{10,13}$	228341.197	19.80	835.2	(6)		...	
$24_{10,15}$-$23_{10,14}$	228341.197†	19.80	835.2	(6)		...	
$24_{3,22}$-$23_{3,21}$	228376.959	23.60	635.5	3.4(1,6)		0.34(2)	
$24_{4,21}$-$23_{4,20}$	228382.837	23.30	650.9	5.1(1,35)		0.39(2)	
$24_{11,13}$-$23_{11,12}$	228417.952	19.00	880.9	(3,24)		...	
$24_{11,14}$-$23_{11,13}$	228417.952†	19.00	880.9	(3,24)		...	
$24_{4,20}$-$23_{4,19}$	228432.529	23.30	650.9	7.4(1,6)		0.43(2)	
$24_{12,13}$-$23_{12,12}$	228505.949	18.00	930.9	3.8(1)		0.19(2)	
$24_{12,12}$-$23_{12,11}$	228505.949†	18.00	930.9	3.8(1)		”	
$24_{13,12}$-$23_{13,11}$	228604.080	17.00	985.1	3.0(1,5)		0.10(2)	
$24_{13,11}$-$23_{13,10}$	228604.080†	17.00	985.1	3.0(1,5)		”	
$24_{14,10}$-$23_{14,9}$	228711.576	15.80	1043.4	(4,5)		...	
$24_{14,11}$-$23_{14,10}$	228711.576†	15.80	1043.4	(4,5)		...	
$24_{15,10}$-$23_{15,9}$	228827.870	14.60	1105.8	(47)		...	
$24_{15,9}$-$23_{15,8}$	228827.870†	14.60	1105.8	(47)		...	
$24_{16,8}$-$23_{16,7}$	228952.532	13.30	1172.2	(5,6)		...	
$24_{16,9}$-$23_{16,8}$	228952.532†	13.30	1172.2	(5,6)		...	
$24_{3,21}$-$23_{3,20}$	229300.226	23.60	635.7	4.6(1)		0.32(2)	
$25_{1,25}$-$24_{1,24}$	230092.805	24.90	624.9	5.4(1,48)		0.24(2)	
				4.4±0.2	6.8±0.5	0.28	2.01±0.11
$24_{1,23}$-$23_{1,22}$	230841.395	23.90	620.1	5.3(1)		0.25(2)	
$25_{0,25}$-$24_{0,24}$	231235.244	25.00	624.5	2.9(1,3,49)		0.27(2)	
$24_{2,22}$-$23_{2,21}$	232131.874	23.80	625.8	5.1(1,22,30)		0.21(2)	
$25_{2,24}$-$24_{2,23}$	235937.871	24.80	635.2	(8)		...	
$25_{7,19}$-$24_{7,18}$	237712.859	23.00	734.9	(4,14,50)		...	
$25_{7,18}$-$24_{7,17}$	237712.860†	23.00	734.9	(4,50)		...	
$25_{6,20}$-$24_{6,19}$	237720.014†	23.60	706.3	(4,14,50)		...	
$25_{6,19}$-$24_{6,18}$	237720.048†	23.60	706.3	(4,14,50)		...	
$25_{8,18}$-$24_{8,17}$	237738.424	22.40	767.8	5.3(1)		0.21(2)	
$25_{8,17}$-$24_{8,16}$	237738.424†	22.40	767.8	5.3(1)		”	
$25_{5,21}$-$24_{5,20}$	237781.568	24.00	682.1	1.6(1,14,33)		1.45(2)	
$25_{5,20}$-$24_{5,19}$	237783.508†	24.00	682.1	4.0(1,14,33)		”	
$25_{9,17}$-$24_{9,16}$	237786.333†	21.80	805.1	7.6(1,14,33)		”	
$25_{9,16}$-$24_{9,15}$	237786.333†	21.80	805.1	7.6(1,14,33)		”	

Tabla B.6: continued.

Transition $J_{K_a,K_c} - J'_{K'_a,K'_c}$	Predicted frequency (MHz)	S_{ij}	E_u (K)	v_{LSR} km s^{-1}	Δv km s^{-1}	T_{MB} (K)	$\int T_{MB} dv$ (K km s^{-1})
$25_{10,16}$-$24_{10,15}$	237851.191	21.00	846.6	(15)		...	
$25_{10,15}$-$24_{10,14}$	237851.191†	21.00	846.6	(15)		...	
$25_{3,23}$-$24_{3,22}$	237891.307	24.60	646.9	(6)		...	
$25_{4,22}$-$24_{4,21}$	237926.446	24.40	662.3	**		...	
$25_{11,14}$-$24_{11,13}$	237929.924†	20.20	892.3	**		...	
$25_{11,15}$-$24_{11,14}$	237929.924†	20.20	892.3	**		...	
$25_{4,21}$-$24_{4,20}$	237992.374	24.40	662.3	5.1(1)		0.40(2)	
$25_{12,13}$-$24_{12,12}$	238020.647	19.20	942.3	(24,51)		...	
$25_{12,14}$-$24_{12,13}$	238020.647†	19.20	942.3	(24,51)		...	
$25_{13,12}$-$24_{13,11}$	238122.122	18.20	996.5	(5)		...	
$25_{13,13}$-$24_{13,12}$	238122.122†	18.20	996.5	(5)		...	
$25_{14,11}$-$24_{14,10}$	238233.490	17.20	1054.8	(4,5)		...	
$25_{14,12}$-$24_{14,11}$	238233.490†	17.20	1054.8	(4,5)		...	
$25_{15,11}$-$24_{15,10}$	238354.125	16.00	1117.2	(14)		...	
$25_{15,10}$-$24_{15,9}$	238354.125†	16.00	1117.2	(14)		...	
$25_{16,9}$-$24_{16,8}$	238483.550	14.80	1183.6	(6,52)		...	
$25_{16,10}$-$24_{16,9}$	238483.550†	14.80	1183.6	(6,52)		...	
$25_{3,22}$-$24_{3,21}$	239008.661	24.60	647.2	(53,54)		...	
$26_{1,26}$-$25_{1,25}$	239192.072	26.00	636.4	5.9(1,53)		0.49(2)	
$25_{1,24}$-$24_{1,23}$	240198.159	24.90	631.7	4.1(1,22,55)		0.57(2)	
$26_{0,26}$-$25_{0,25}$	240224.647	26.00	636.0	(6)		...	
$25_{2,23}$-$24_{2,22}$	241930.544	24.80	637.4	(15)		...	
$26_{2,25}$-$25_{2,24}$	245251.394	25.80	646.9	3.7(1)		0.44(2)	
$26_{7,20}$-$25_{7,19}$	247224.651	24.10	764.8	(10)		...	
$26_{7,19}$-$25_{7,18}$	247224.652†	24.10	764.8	(10)		...	
$26_{6,21}$-$25_{6,20}$	247237.730	24.60	718.2	1.7(1,3)		0.64(2)	
$26_{6,20}$-$25_{6,19}$	247237.783†	24.60	718.2	1.7(1,3)		”	
$26_{8,19}$-$25_{8,18}$	247247.622	23.50	779.7	(56)		...	
$26_{8,18}$-$25_{8,17}$	247247.622†	23.50	779.7	(56)		...	
$26_{9,18}$-$25_{9,17}$	247294.980	22.90	816.9	**		...	
$26_{9,17}$-$25_{9,16}$	247294.980†	22.90	816.9	**		...	
$26_{5,22}$-$25_{5,21}$	247311.034	25.00	694.0	2.9(1)		0.40(2)	
$26_{5,21}$-$25_{5,20}$	247313.796†	25.00	694.0	6.3(1)		”	
$26_{10,16}$-$25_{10,15}$	247360.661	22.20	858.1	2.8(1,3,9)		0.29(2)	
$26_{10,17}$-$25_{10,16}$	247360.661†	22.20	858.1	2.8(1,3,9)		”	
$26_{3,24}$-$25_{3,23}$	247400.726	25.70	658.8	5.2(1)		0.47(2)	
$26_{11,16}$-$25_{11,15}$	247441.225	21.30	904.2	(57)		...	

Tabla B.6: continued.

Transition $J_{K_a,K_c} - J'_{K'_a,K'_c}$	Predicted frequency (MHz)	S_{ij}	E_u (K)	v_{LSR} km s^{-1}	Δv km s^{-1}	T_{MB} (K)	$\int T_{MB} dv$ (K km s^{-1})
$26_{11,15}$-$25_{11,14}$	247441.225†	21.30	904.2	(57)		...	
$26_{4,23}$-$25_{4,22}$	247472.336	25.40	674.2	(6)		...	
$26_{12,15}$-$25_{12,14}$	247534.560	20.50	954.2	3.1(1,49)		0.28(2)	
$26_{12,14}$-$25_{12,13}$	247534.560†	20.50	954.2	3.1(1,49)		”	
$26_{4,22}$-$25_{4,21}$	247558.766	25.40	674.2	(14)		...	
$26_{13,14}$-$25_{13,13}$	247639.288	19.50	1008.4	(6)		...	
$26_{13,13}$-$25_{13,12}$	247639.288†	19.50	1008.4	(6)		...	
$26_{14,13}$-$25_{14,12}$	247754.455	18.50	1066.7	(4,5,12)		...	
$26_{14,12}$-$25_{14,11}$	247754.455†	18.50	1066.7	(4,5,12)		...	
$26_{15,12}$-$25_{15,11}$	247879.369	17.30	1129.1	(3)		...	
$26_{15,11}$-$25_{15,10}$	247879.369†	17.30	1129.1	(3)		...	
$26_{16,10}$-$25_{16,9}$	248013.505	16.20	1195.6	(58)		...	
$26_{16,11}$-$25_{16,10}$	248013.505†	16.20	1195.6	(58)		...	
$27_{1,27}$-$26_{1,26}$	248284.273	27.00	648.3	(10)		...	
$26_{3,23}$-$25_{3,22}$	248739.558	25.70	659.1	(3)		...	
$27_{0,27}$-$26_{0,26}$	249212.360	27.00	648.0	(15)		...	
$26_{1,25}$-$25_{1,24}$	249519.327	25.90	643.6	(15)		...	
$26_{2,24}$-$25_{2,23}$	251714.095	25.90	649.5	(20)		...	
$27_{2,26}$-$26_{2,25}$	254551.752	26.80	659.2	(59)		...	
$27_{7,21}$-$26_{7,20}$	256736.814	25.20	759.1	3.7(1,6)		0.19(2)	
$27_{7,20}$-$26_{7,19}$	256736.815†	25.20	759.1	3.7(1,6)		”	
$27_{6,22}$-$26_{6,21}$	256756.477	25.70	730.5	3.1(1)		0.60(2)	
$27_{6,21}$-$26_{6,20}$	256756.557†	25.70	730.5	3.2(1)		”	
$27_{8,20}$-$26_{8,19}$	256756.768†	24.60	792.0	3.4(1)		”	
$27_{8,19}$-$26_{8,18}$	256756.768†	24.60	792.0	3.4(1)		”	
$27_{9,19}$-$26_{9,18}$	256803.285	24.00	829.3	(20)		...	
$27_{9,18}$-$26_{9,17}$	256803.285†	24.00	829.3	(20)		...	
$27_{5,23}$-$26_{5,22}$	256842.547	26.10	706.3	(60)		...	
$27_{5,22}$-$26_{5,21}$	256846.425†	26.10	706.3	(60)		...	
$27_{10,18}$-$26_{10,17}$	256869.586	23.30	870.8	(11)		...	
$27_{10,17}$-$26_{10,16}$	256869.586†	23.30	870.8	(11)		...	
$27_{3,25}$-$26_{3,24}$	256904.390	26.70	671.1	(6)		...	
$27_{11,16}$-$26_{11,15}$	256951.826	22.50	916.6	(6)		...	
$27_{11,17}$-$26_{11,16}$	256951.826†	22.50	916.6	(6)		...	
$27_{4,24}$-$26_{4,23}$	257020.309	26.40	686.5	7.5(1)		0.24(2)	
$27_{12,16}$-$26_{12,15}$	257047.656	21.70	966.5	(24)		...	
$27_{12,15}$-$26_{12,14}$	257047.656†	21.70	966.5	(24)		...	

Tabla B.6: continued.

Transition $J_{K_a,K_c} - J'_{K'_a,K'_c}$	Predicted frequency (MHz)	S_{ij}	E_u (K)	v_{LSR} km s^{-1}	Δv km s^{-1}	T_{MB} (K)	$\int T_{MB} dv$ (K km s^{-1})
$27_{4,23}$-$26_{4,22}$	257132.364	26.40	686.6	**		...	
$27_{13,14}$-$26_{13,13}$	257155.544	20.70	1020.7	(54)		...	
$27_{13,15}$-$26_{13,14}$	257155.544†	20.70	1020.7	(54)		...	
$28_{1,28}$-$27_{1,27}$	257369.790	28.00	660.7	(14)		...	
$28_{0,28}$-$27_{0,27}$	258199.737	28.00	660.4	(46,60)		...	
$27_{3,24}$-$26_{3,23}$	258493.402	26.70	671.5	(3)		...	
$27_{1,26}$-$26_{1,25}$	258803.871	26.90	656.1	5.9(1,60)		0.21(2)	
$27_{2,25}$-$26_{2,24}$	261479.659	26.90	662.1	(6)		...	
$28_{2,27}$-$27_{2,26}$	263838.783	27.80	671.8	5.9(1)		0.14(2)	
$28_{7,22}$-$27_{7,21}$	266249.359	26.30	771.9	(4,13)		...	
$28_{7,21}$-$27_{7,20}$	266249.360†	26.30	771.9	(4,13)		...	
$28_{8,21}$-$27_{8,20}$	266265.858	25.70	804.8	(4,6)		...	
$28_{8,20}$-$27_{8,19}$	266265.858†	25.70	804.8	(4,6)		...	
$28_{6,23}$-$27_{6,22}$	266276.292†	26.70	743.3	(4,6)		...	
$28_{6,22}$-$27_{6,21}$	266276.412†	26.70	743.3	(4,6)		...	
$28_{9,20}$-$27_{9,19}$	266311.236	25.10	842.0	(61,62)		...	
$28_{9,19}$-$27_{9,18}$	266311.236†	25.10	842.0	(61,62)		...	
$28_{5,24}$-$27_{5,23}$	266376.157	27.10	719.1	3.9(1)		0.47(2)	
$28_{10,18}$-$27_{10,17}$	266377.942†	24.40	883.6	5.9(1)		”	
$28_{10,19}$-$27_{10,18}$	266377.942†	24.40	883.6	5.9(1)		”	
$28_{5,23}$-$27_{5,22}$	266381.531†	27.10	719.1	8.6(1,4)		”	
$28_{3,26}$-$27_{3,25}$	266401.477	27.70	683.9	5.0(1)		0.41(2)	
				4.6±0.3	7.4±0.2	0.34	2.71±0.15
$29_{1,29}$-$28_{1,28}$	266449.007	29.00	673.4	4.1(1,63)		0.35(2)	
$28_{11,18}$-$27_{11,17}$	266461.701	23.70	929.3	5.1(1,34)		0.24(2)	
$28_{11,17}$-$27_{11,16}$	266461.701†	23.70	929.3	5.1(1,34)		”	
$28_{12,16}$-$27_{12,15}$	266559.903	22.90	979.3	4.5(1,55)		0.26(2)	
$28_{12,17}$-$27_{12,16}$	266559.903†	22.90	979.3	4.5(1,55)		”	
$28_{4,25}$-$27_{4,24}$	266570.122	27.40	699.3	5.8(1)		0.32(2)	
$28_{13,15}$-$27_{13,14}$	266670.853	22.00	1033.5	(5,59)		...	
$28_{13,16}$-$27_{13,15}$	266670.853†	22.00	1033.5	(5,59)		...	
$28_{4,7}$-$27_{4,23}$	266713.893	27.40	699.4	(22,43)		...	
$28_{14,15}$-$27_{14,14}$	266793.387	21.00	1091.8	8.8(1,4)		0.12(2)	
$28_{14,14}$-$27_{14,13}$	266793.387†	21.00	1091.8	8.8(1,4)		”	
$28_{15,13}$-$27_{15,12}$	266926.666	20.00	1154.3	5.7(1)		0.06(2)	
$28_{15,14}$-$27_{15,13}$	266926.666†	20.00	1154.3	5.7(1)		”	
$28_{16,12}$-$27_{16,11}$	267070.061	18.90	1220.7	(3,5,64)		...	

Tabla B.6: continued.

Transition $J_{K_a,K_c} - J'_{K'_a,K'_c}$	Predicted frequency (MHz)	S_{ij}	E_u (K)	v_{LSR} km s^{-1}	Δv km s^{-1}	T_{MB} (K)	$\int T_{MB} dv$ (K km s^{-1})
$28_{16,13}$-$27_{16,12}$	267070.061†	18.90	1220.7	(3,5,64)		...	
$29_{0,29}$-$28_{0,28}$	267187.774	29.00	673.2	(6)		...	
$28_{1,27}$-$27_{1,26}$	268051.179	27.90	668.9	5.5(1,55)		0.30(2)	
$28_{3,25}$-$27_{3,24}$	268270.254	27.70	684.4	(49)		...	
$28_{2,26}$-$27_{2,25}$	271224.695	27.90	675.1	(3)		...	
$29_{2,28}$-$28_{2,27}$	273112.379	28.80	684.9	(15,24)		...	
$30_{1,30}$-$29_{1,29}$	275522.307	30.00	686.7	(4,54)		...	
$29_{7,23}$-$28_{7,22}$	275762.298	27.30	785.1	(14)		...	
$29_{7,22}$-$28_{7,21}$	275762.301†	27.30	785.1	(14)		...	
$29_{8,22}$-$28_{8,21}$	275774.887	26.80	818.0	(4,53,54)		...	
$29_{8,21}$-$28_{8,20}$	275774.887†	26.80	818.0	(4,53,54)		...	
$29_{6,24}$-$28_{6,23}$	275797.212	27.80	756.5	(4)		...	
$29_{6,23}$-$28_{6,22}$	275797.389†	27.80	756.5	(4)		...	
$29_{9,21}$-$28_{9,20}$	275818.817	26.20	855.3	(14,46,53)		...	
$29_{9,20}$-$28_{9,19}$	275818.817†	26.20	855.3	(14,46,53)		...	
$29_{10,19}$-$28_{10,18}$	275885.708	25.60	896.8	(53)		...	
$29_{10,20}$-$28_{10,19}$	275885.708†	25.60	896.8	(53)		...	
$29_{3,27}$-$28_{3,26}$	275891.168†	28.70	697.1	(53)		...	
$29_{5,25}$-$28_{5,24}$	275911.903	28.10	732.3	(14,53)		...	
$29_{5,24}$-$28_{5,23}$	275919.261†	28.10	732.3	(14,53)		...	
$29_{11,19}$-$28_{11,18}$	275970.821	24.80	942.6	(64)		...	
$29_{11,18}$-$28_{11,17}$	275970.821†	24.80	942.6	(64)		...	
$29_{12,17}$-$28_{12,16}$	276071.268	24.00	992.6	(65)		...	
$29_{12,18}$-$28_{12,17}$	276071.268†	24.00	992.6	(65)		...	
$29_{4,26}$-$28_{4,25}$	276121.480	28.40	712.6	5.8(1,24)		0.31(2)	
$30_{0,30}$-$29_{0,29}$	276177.161	30.00	686.5	(64)		...	
$29_{13,17}$-$28_{13,16}$	276185.181	23.20	1046.8	(5,64)		...	
$29_{13,16}$-$28_{13,15}$	276185.181†	23.20	1046.8	(5,64)		...	
$29_{4,25}$-$28_{4,24}$	276304.154	28.40	712.6	(4,46)		...	
$29_{14,15}$-$28_{14,14}$	276311.277	22.20	1105.1	(7)		...	
$29_{14,16}$-$28_{14,15}$	276311.277†	22.20	1105.1	(7)		...	
$29_{15,15}$-$28_{15,14}$	276448.638	21.20	1167.5	(66)		...	
$29_{15,14}$-$28_{15,13}$	276448.638†	21.20	1167.5	(66)		...	
$29_{16,14}$-$28_{16,13}$	276596.576	20.20	1234.0	(9)		...	
$29_{16,13}$-$28_{16,12}$	276596.576†	20.20	1234.0	(9)		...	
$29_{1,28}$-$28_{1,27}$	277261.129	28.90	682.2	4.0(1)		0.38(2)	
$29_{3,26}$-$28_{3,25}$	278069.674	28.70	697.7	(15,36,55)		...	

Tabla A9. Emission lines of CH_2CHCN v_{15} =1 present in the spectral scan of the Orion-KL from the radio-telescope of IRAM 30-m. Column 1 indicates the line transition, Col. 2 gives the predicted frequency in the laboratory, Col. 3 the line strength, Col. 4 upper level energy, Col. 5 observed radial velocities relative to the local system rest (v_{LSR}), Col. 6 the line width, Col. 7 main beam temperature, and Col. 8 shows the area of the line. † blended with the previous line. ∗∗ hole in the observed spectrum.

(1) peak channel line observed velocity. (2) peak channel line intensity. (3) blended with $HCOOCH_3$. (4) blended with CH_2CHCN. (5) blended with CH_2CHCN v_{11}=1. (6) blended with U-line. (7) blended with CCH. (8) blended with $^{13}CH_3OH$. (9) blended with $CH_2{}^{13}CHCN$. (10) blended with CH_3OH. (11) blended with ^{34}SO. (12) blended with CH_3COOH v_t=0. (13) blended with t-CH_3CH_2OH. (14) blended with $(CH_3)_2CO$. (15) blended with CH_3CH_2CN. (16) blended with SO_2. (17) blended with $^{13}CH_3CH_2CN$. (18) blended with $CH_3C^{15}N$. (19) blended with DNCO. (20) blended with CH_3CH_2CN v_{13}/v_{21}. (21) blended with $HCC^{13}CN$ v_7=1. (22) blended with $H^{13}COOCH_3$. (23) blended with $HCOOCH_3$ v_t=1. (24) blended with CH_3OCH_3. (25) blended with CH_3OCOD. (26) blended with HNCO. (27) blended with H_2CCO. (28) blended with NS. (29) blended with CH_2DCCH. (30) blended with CH_3CH_2CN v_{20}=1. (31) blended with ^{18}OCS. (32) blended with SiS. (33) blended with HCCCN. (34) blended with $CH_3CH_2C^{15}N$. (35) blended with H_2C_3. (36) blended with $|g_+$-$g_-|$-CH_3CH_2OH. (37) blended with $SO^{18}O$. (38) blended with CH_3CHO. (39) blended with HCCCN v_6=1. (40) blended with H_2CO. (41) blended with $HN^{13}CO$. (42) blended with HCCCN v_7=1. (43) blended with $^{33}SO_2$. (44) blended with OCS. (45) blended with DNCS. (46) blended with CH_3CN v_8=1. (47) blended with HCCCN v_7=2. (48) blended with $H^{13}CCCN$ v_7=1. (49) blended with $^{13}CH_2CHCN$. (50) blended with HCCCN v_6+v_7. (51) blended with $H^{13}CCCN$ ν=0. (52) blended with CH_2CHCN $v_{10}/v_{11}v_{15}$. (53) blended with CH_3CN. (54) blended with $CH_3{}^{13}CN$. (55) blended with $HCOO^{13}CH_3$. (56) blended with $CH_3{}^{13}CH_2CN$. (57) blended with $^{34}SO_2$. (58) blended with HDCS. (59) blended with $O^{13}CS$. (60) blended with CH_2CHCN v_{11}=3. (61) blended with HCCCN v_7=3. (62) blended with $DCOOCH_3$. (63) blended with $H^{13}COOCH_3$. (64) blended with NH_2CHO. (65) blended with CH_3OD. (66) blended with g_--CH_3CH_2OH.

Tabla B.7: Detected lines of CH_2CHCN v_{10}=1⇔(v_{11}=1,v_{15}=1) .

Transition $J_{K_a,K_c,v} - J'_{K'_a,K'_c,v'}$	Predicted frequency (MHz)	S_{ij}	E_u (K)	v_{LSR}[(1)] km s^{-1}	Observed frequency (MHz)	Observed T_{MB} (K)[(2)]	Model T_{MB} (K)
$9_{1,9,0}$-$8_{1,8,0}$	83116.219	8.89	830.7	4.4	83116.4	0.02	0.01
$9_{1,9,1}$-$8_{1,8,1}$	83527.527	8.89	834.3	1.9	83528.4	0.03	0.01
$9_{0,9,0}$-$8_{0,8,0}$	84834.239	8.99	829.0	7.4	84833.6	0.01	0.01
$9_{2,9,0}$-$8_{2,8,0}$	85222.373	8.55	837.7	[(3)]	...	...	...
$9_{3,7,0}$-$8_{3,6,0}$	85340.554	8.00	848.4	[(4)]	...	...	...
$9_{3,6,0}$-$8_{3,5,0}$	85348.444	8.00	848.4	[(5)]	...	...	...
$9_{0,9,1}$-$8_{0,8,1}$	85486.459	8.99	832.6	[(5)]	...	...	...
$9_{2,8,1}$-$8_{2,7,1}$	85655.927	8.55	841.3	[(6)]	...	...	...
$9_{2,7,0}$-$8_{2,6,0}$	85661.661	8.55	837.7	6.9	85661.1	0.02	0.01
$9_{3,7,1}$-$8_{3,6,1}$	85784.891	8.00	852.1	[(6)]	...	...	...
$9_{3,6,1}$-$8_{3,5,1}$	85792.783	8.00	852.1	[(5)]	...	...	...
$9_{2,7,1}$-$8_{2,6,1}$	86079.867	8.56	841.4	[(7)]	...	...	...
$9_{1,8,0}$-$8_{1,7,0}$	87008.941	8.88	831.7	[(8)]	...	...	...
$9_{1,8,1}$-$8_{1,7,1}$	87661.428	8.89	835.3	[(9)]	...	...	...
$10_{1,10,0}$-$9_{1,9,0}$	92325.160	9.90	835.2	4.7	92325.3	0.03	0.01
$10_{1,10,1}$-$9_{1,9,1}$	92783.148	9.90	838.7	7.8	92782.3	0.01	0.01
$10_{0,10,0}$-$9_{0,9,0}$	94154.846	9.99	833.5	[(10)]	...	...	...
$10_{2,9,0}$-$9_{2,8,0}$	94670.177	9.60	842.2	[(5)]	...	...	...
$10_{4,7,0}$-$9_{4,6,0}$	94814.331	8.40	868.0	[(11)]	...	...	...
$10_{4,6,0}$-$9_{4,5,0}$	94814.446†	8.40	868.0	[(11)]	...	...	...
$10_{5,6,0}$-$9_{5,5,0}$	94814.769†	7.50	887.3	[(11)]	...	...	...
$10_{5,5,0}$-$9_{5,4,0}$	94814.770†	7.50	887.3	[(11)]	...	...	...
$10_{6,4,0}$-$9_{6,3,0}$	94826.374	6.40	910.9	3.8[(12)]	94826.7	0.04	0.01
$10_{6,5,0}$-$9_{6,4,0}$	94826.374†	6.40	910.9	3.8[(12)]	94826.7	”	0.01
$10_{3,8,0}$-$9_{3,7,0}$	94832.745	9.10	853.0	[(13)]	...	...	...
$10_{7,3,0}$-$9_{7,2,0}$	94844.899	5.10	938.7	2.3[(14)]	94847.2	0.03	0.02
$10_{7,4,0}$-$9_{7,3,0}$	94844.899†	5.10	938.7	2.3[(14)]	94847.2	”	0.02
$10_{3,7,0}$-$9_{3,6,0}$	94846.260†	9.10	853.0	2.0[(5)]	94847.2	”	0.02
$10_{0,10,1}$-$9_{0,9,1}$	94912.300	9.98	837.2	[(15)]	...		...
$10_{2,9,1}$-$9_{2,8,1}$	95152.572	9.60	845.9	6.1	95152.2	0.02	0.01
$10_{2,8,0}$-$9_{2,7,0}$	95271.845	9.60	842.3	[(13)]	...		...
$10_{5,6,1}$-$9_{5,5,1}$	95310.019	7.50	891.3	8.5	95308.9	0.02	0.03
$10_{5,5,1}$-$9_{5,4,1}$	95310.019†	7.50	891.3	8.5	95308.9	”	0.03
$10_{4,7,1}$-$9_{4,6,1}$	95310.299†	8.40	871.9	8.6	95308.9	”	0.03
$10_{4,6,1}$-$9_{4,5,1}$	95310.415†	8.40	871.9	8.2	95308.9	”	0.03
$10_{3,8,1}$-$9_{3,7,1}$	95326.489	9.10	856.7	[(15)]	...		...

Tabla B.7: continued.

Transition $J_{K_a,K_c,v} - J'_{K'_a,K'_c,v'}$	Predicted frequency (MHz)	S_{ij}	E_u (K)	v_{LSR}[1] km s^{-1}	Observed frequency (MHz)	Observed T_{MB} (K)[2]	Model T_{MB} (K)
$10_{3,7,1}$-$9_{3,6,1}$	95340.001	9.10	856.7	[5]	...		...
$10_{2,8,1}$-$9_{2,7,1}$	95732.327	9.60	845.9	[8,10,16]	...		...
$10_{1,9,0}$-$9_{1,8,0}$	96606.793	9.89	836.3	[9]	...		...
$10_{1,9,1}$-$9_{1,8,1}$	97360.687	9.90	840.0	6.6	97359.4	0.02	0.02
$11_{1,11,0}$-$10_{1,10,0}$	101526.437	10.90	840.0	5.8	101526.1	0.02	0.01
$11_{1,11,1}$-$10_{1,10,1}$	102031.365	10.90	843.6	[17]	...		...
$11_{0,11,0}$-$10_{0,10,0}$	103444.142	11.00	838.5	[5]	...		...
$11_{2,10,0}$-$10_{2,9,0}$	104111.416	10.60	847.2	[16]	...		...
$11_{3,9,0}$-$10_{3,8,0}$	104327.440	10.20	858.0	1.6[5]	104328.6	0.04	0.02
$11_{0,11,1}$-$10_{0,10,1}$	104336.175	11.00	842.2	[11]	...		...
$11_{3,8,0}$-$10_{3,7,0}$	104349.379	10.20	858.0	5.7	104349.1	0.04	0.01
$11_{2,10,1}$-$10_{2,9,1}$	104642.751	10.60	850.9	[5]	...	...	...
$11_{5,7,1}$-$10_{5,6,1}$	104844.640	8.73	896.4	3.7	104845.1	0.02	0.02
$11_{5,6,1}$-$10_{5,5,1}$	104844.640†	8.73	896.4	3.7	104845.1	”	0.02
$11_{4,8,1}$-$10_{4,7,1}$	104848.285	9.54	876.9	1.2[5]	104849.6	0.05	0.03
$11_{4,7,1}$-$10_{4,6,1}$	104848.518†	9.54	876.9	1.9[5]	104849.6	”	0.03
$11_{6,5,1}$-$10_{6,4,1}$	104853.585	7.73	920.1	[5]	...	...	...
$11_{6,6,1}$-$10_{6,5,1}$	104853.585†	7.73	920.1	[5]	...	...	...
$11_{3,9,1}$-$10_{3,8,1}$	104870.596	10.20	861.8	8.6	104869.1	”	0.03
$11_{3,8,1}$-$10_{3,7,1}$	104892.520	10.20	861.8	6.2[5]	104892.1	”	0.02
$11_{2,9,0}$-$10_{2,8,0}$	104909.295	10.60	847.3	[5]	...	...	...
$11_{2,9,1}$-$10_{2,8,1}$	105410.258	10.60	851.0	[5]	...	...	...
$11_{1,10,0}$-$10_{1,9,0}$	106163.213	10.90	841.4	4.2[18]	106163.5	0.03	0.02
$11_{1,10,1}$-$10_{1,9,1}$	107046.236	10.90	845.1	[16,19]	...	...	...
$12_{1,12,0}$-$11_{1,11,0}$	110719.577	11.90	845.3	[20]	...	...	...
$12_{1,12,1}$-$11_{1,11,1}$	111271.769	11.90	849.0	7.0	111271.0	0.02	0.02
$12_{0,12,0}$-$11_{0,11,0}$	112700.451	12.00	843.9	[5]	...	...	...
$12_{2,11,0}$-$11_{2,10,0}$	113545.506	11.70	852.7	5.2	113545.4	0.04	0.02
$12_{0,12,1}$-$11_{0,11,1}$	113781.503	11.90	847.6	[5]	...	...	...
$12_{5,8,0}$-$11_{5,7,0}$	113785.826	9.92	897.8	7.4	113784.9	0.06	0.04
$12_{5,7,0}$-$11_{5,6,0}$	113785.826†	9.92	897.8	7.4	113784.9	”	0.04
$12_{4,9,0}$-$11_{4,8,0}$	113792.904	10.70	878.5	[10]	...	...	...
$12_{4,8,0}$-$11_{4,7,0}$	113793.334†	10.70	878.5	[10]	...	...	...
$12_{6,7,0}$-$11_{6,6,0}$	113795.698†	9.00	921.3	[10]	...	...	...
$12_{6,6,0}$-$11_{6,5,0}$	113795.699†	9.00	921.3	[10]	...	...	...
$12_{7,5,0}$-$11_{7,4,0}$	113815.528	7.92	949.1	[5]	...	...	...
$12_{7,6,0}$-$11_{7,5,0}$	113815.528†	7.92	949.1	[5]	...	...	...

Tabla B.7: continued.

Transition $J_{K_a,K_c,v} - J'_{K'_a,K'_c,v'}$	Predicted frequency (MHz)	S_{ij}	E_u (K)	v_{LSR}[(1)] km s^{-1}	Observed frequency (MHz)	Observed T_{MB} (K)[(2)]	Model T_{MB} (K)
$12_{3,10,0}$-$11_{3,9,0}$	113824.589	11.20	863.5	4.1[(5)]	113824.9	0.05	0.02
$12_{8,4,0}$-$11_{8,3,0}$	113842.462	6.67	981.1	[(6)]	...	...	...
$12_{8,5,0}$-$11_{8,4,0}$	113842.462†	6.67	981.1	[(6)]	...	...	...
$12_{3,9,0}$-$11_{3,8,0}$	113858.669	11.20	863.5	[(9)]	...	...	...
$12_{2,11,1}$-$11_{2,10,1}$	114125.856	11.70	856.4	4.8	114126.0	0.05	0.02
$12_{5,8,1}$-$11_{5,7,1}$	114380.292	9.92	901.9	7.2[(5)]	114379.5	0.06	0.03
$12_{5,7,1}$-$11_{5,6,1}$	114380.295†	9.92	901.9	7.2[(5)]	114379.5	”	0.03
$12_{6,6,1}$-$11_{6,5,1}$	114387.936	9.00	925.6	5.1	114387.9	0.05	0.06
$12_{6,7,1}$-$11_{6,6,1}$	114387.936†	9.00	925.6	5.1	114387.9	”	0.06
$12_{4,9,1}$-$11_{4,8,1}$	114388.228†	10.70	882.4	5.8	114387.9	”	0.06
$12_{4,8,1}$-$11_{4,7,1}$	114388.664†	10.70	882.4	7.0	114387.9	”	0.06
$12_{7,5,1}$-$11_{7,4,1}$	114404.814	7.92	953.7	[(5)]	...	...	...
$12_{7,6,1}$-$11_{7,5,1}$	114404.814†	7.92	953.7	[(5)]	...	...	...
$12_{3,10,1}$-$11_{3,9,1}$	114417.159	11.30	867.2	[(5)]	...	...	...
$12_{8,4,1}$-$11_{8,3,1}$	114428.365	6.67	986.0	[(5)]	...	...	...
$12_{8,5,1}$-$11_{8,4,1}$	114428.365†	6.67	986.0	[(5)]	...	...	...
$12_{3,9,1}$-$11_{3,8,1}$	114451.201	11.20	867.3	5.7[(21)]	114451.0	0.05	0.02
$12_{9,3,1}$-$11_{9,2,1}$	114457.414	5.25	1022.6	[(5)]	...	...	...
$12_{9,4,1}$-$11_{9,3,1}$	114457.414†	5.25	1022.6	[(5)]	...	...	...
$12_{2,10,0}$-$11_{2,9,0}$	114575.211	11.70	852.8	[(9,13,17)]	...	...	...
$12_{2,10,1}$-$11_{2,9,1}$	115114.546	11.70	852.8	[(9)]	...	...	...
$14_{0,14,0}$-$13_{0,13,0}$	131110.736	14.00	856.1	[(22)]	...	...	...
$14_{2,13,0}$-$13_{2,12,0}$	132389.964	13.70	864.9	3.0	132390.8	0.04	0.04
$14_{5,10,0}$-$13_{5,9,0}$	132761.289	12.20	910.1	[(5)]	...	...	...
$14_{5,9,0}$-$13_{5,8,0}$	132761.289†	12.20	910.1	[(5)]	...	...	...
$14_{6,9,0}$-$13_{6,8,0}$	132767.225	11.40	933.6	[(5)]	...	...	...
$14_{6,8,0}$-$13_{6,7,0}$	132767.225†	11.40	933.6	[(5)]	...	...	...
$14_{4,11,0}$-$13_{4,10,0}$	132779.853	12.90	890.8	[(5)]	...	...	...
$14_{4,10,0}$-$13_{4,9,0}$	132781.150†	12.90	890.8	[(5)]	...	...	...
$14_{7,7,0}$-$13_{7,6,0}$	132787.052	10.50	961.4	[(5)]	...	...	...
$14_{7,8,0}$-$13_{7,7,0}$	132787.052†	10.50	961.4	[(5)]	...	...	...
$14_{8,6,0}$-$13_{8,5,0}$	132816.346	9.43	993.4	[(6)]	...	...	...
$14_{8,7,0}$-$13_{8,6,0}$	132816.346†	9.43	993.4	[(6)]	...	...	...
$14_{3,12,0}$-$13_{3,11,0}$	132825.660	13.40	875.7	[(5)]	...	...	...
$14_{9,5,0}$-$13_{9,4,0}$	132853.033	8.21	1029.7	5.7	132852.7	0.03	0.02
$14_{9,6,0}$-$13_{9,5,0}$	132853.033†	8.21	1029.7	5.7	132852.7	”	0.02
$14_{3,11,0}$-$13_{3,10,0}$	132899.724	13.40	875.8	[(15)]	...	...	...

Tabla B.7: continued.

Transition $J_{K_a,K_c,v} - J'_{K'_a,K'_c,v'}$	Predicted frequency (MHz)	S_{ij}	E_u (K)	v_{LSR}[(1)] km s^{-1}	Observed frequency (MHz)	Observed T_{MB} (K)[(2)]	Model T_{MB} (K)
$14_{0,14,1}$-$13_{0,13,1}$	132961.899	13.70	859.9	[(15)]	...	...	...
$14_{2,13,1}$-$13_{2,12,1}$	133068.465	13.70	868.7	[(15,23)]	...	...	...
$14_{4,11,1}$-$13_{4,10,1}$	133474.605	12.90	894.8	[(17)]	...	...	...
$14_{4,10,1}$-$13_{4,9,1}$	133475.918†	12.90	894.8	[(17)]	...	...	...
$14_{3,12,1}$-$13_{3,11,1}$	133517.060	13.40	879.6	5.5	133517.7	0.06	0.04
$14_{3,11,1}$-$13_{3,10,1}$	133590.958	13.40	879.6	5.5[(1,5)]	133590.7	0.09	0.04
$14_{2,12,0}$-$13_{2,11,0}$	133993.089	13.70	865.2	[(24)]	...	...	...
$14_{1,13,0}$-$13_{1,12,0}$	134189.516	13.70	859.4	[(25)]	...	...	...
$14_{2,12,1}$-$13_{2,11,1}$	134602.064	13.70	869.0	5.8	134601.7	0.05	0.04
$14_{1,13,1}$-$13_{1,12,1}$	136004.544	13.90	863.3	5.5[(5)]	136004.3	0.07	0.04
$15_{1,15,0}$-$14_{1,14,0}$	138246.549	14.90	863.9	[(5)]	...	...	...
$15_{1,15,1}$-$14_{1,14,1}$	138945.734	14.90	867.7	[(5)]	...	...	...
$15_{0,15,0}$-$14_{0,14,0}$	140264.937	15.00	862.8	[(5)]	...	...	...
$15_{2,14,0}$-$14_{2,13,0}$	141799.230	14.70	871.7	4.1[(14)]	141799.6	0.06	0.05
$15_{5,11,0}$-$14_{5,10,0}$	142250.898	13.30	916.9	3.5[(26)]	142251.6	0.22	0.08
$15_{5,10,0}$-$14_{5,9,0}$	142250.920†	13.30	916.9	3.5[(26)]	142251.6	”	0.08
$15_{6,10,0}$-$14_{6,9,0}$	142253.927	12.60	940.4	[(26)]	...	...	...
$15_{6,9,0}$-$14_{6,8,0}$	142253.927†	12.60	940.4	[(26)]	...	...	...
$15_{7,8,0}$-$14_{7,7,0}$	142273.196	11.70	968.2	[(16)]	...	...	...
$15_{7,9,0}$-$14_{7,8,0}$	142273.196†	11.70	968.2	[(16)]	...	...	...
$15_{4,12,0}$-$14_{4,11,0}$	142276.833	13.90	897.6	[(11)]	...	...	...
$15_{4,11,0}$-$14_{4,10,0}$	142278.953†	13.90	897.6	[(11)]	...	...	...
$15_{8,7,0}$-$14_{8,6,0}$	142303.312	10.70	1000.3	[(5)]	...	...	...
$15_{8,8,0}$-$14_{8,7,0}$	142303.312†	10.70	1000.3	[(5)]	...	...	...
$15_{3,13,0}$-$14_{3,12,0}$	142329.090	14.40	882.6	[(6)]	...	...	...
$15_{3,12,0}$-$14_{3,11,0}$	142433.732	14.40	882.6	[(5)]	...	...	...
$15_{2,14,1}$-$14_{2,13,1}$	142526.819	14.70	875.5	[(15)]	...	...	...
$15_{1,14,0}$-$14_{0,14,1}$	142865.530	14.60	866.8	[(5)]	...	...	...
$15_{5,11,1}$-$14_{5,10,1}$	142994.345	13.30	921.1	4.4	142994.7	0.12	0.11
$15_{5,10,1}$-$14_{5,9,1}$	142994.367†	13.30	921.1	4.4	142994.7	”	0.11
$15_{6,10,1}$-$14_{6,9,1}$	142994.609†	12.60	944.9	4.9	142994.7	”	0.11
$15_{6,9,1}$-$14_{6,8,1}$	142994.609†	12.60	944.9	4.9	142994.7	”	0.11
$15_{4,12,1}$-$14_{4,11,1}$	143021.325	13.90	901.6	[(10)]	...	...	...
$15_{4,11,1}$-$14_{4,10,1}$	143023.471†	13.90	901.6	[(10)]	...	...	...
$15_{3,13,1}$-$14_{3,12,1}$	143069.898	14.40	886.5	[(24)]	...	...	...
$15_{3,12,1}$-$14_{3,11,1}$	143174.237	14.40	886.5	[(11,25)]	...	...	...
$15_{2,13,0}$-$14_{2,12,0}$	143742.742	14.70	872.1	[(27)]	...	...	...

Tabla B.7: continued.

Transition $J_{K_a,K_c,v} - J'_{K'_a,K'_c,v'}$	Predicted frequency (MHz)	S_{ij}	E_u (K)	v_{LSR}[1] km s^{-1}	Observed frequency (MHz)	Observed T_{MB} (K)[2]	Model T_{MB} (K)
$15_{2,13,1}$-$14_{2,12,1}$	144383.139	14.70	875.9	[5]	...	...	...
$15_{1,14,1}$-$14_{1,13,1}$	145619.786	14.90	870.3	[5]	...	...	...
$16_{1,16,0}$-$15_{1,15,0}$	147403.907	15.90	871.0	[6]	...	...	...
$16_{1,16,1}$-$15_{1,15,1}$	148159.353	16.00	874.8	[5]	...	...	...
$16_{0,16,0}$-$15_{0,15,0}$	149386.665	16.00	870.0	[5]	...	...	...
$16_{2,15,0}$-$15_{2,14,0}$	151199.144	15.70	879.0	[5]	...	...	...
$16_{0,16,1}$-$15_{0,15,1}$	151701.771	15.50	873.5	[9]	...	...	...
$16_{6,11,0}$-$15_{6,10,0}$	151741.314	13.70	947.7	[5]	...	...	...
$16_{6,10,0}$-$15_{6,9,0}$	151741.314†	13.70	947.7	[5]	...	...	...
$16_{5,12,0}$-$15_{5,11,0}$	151741.881†	14.40	924.2	[5]	...	...	...
$16_{5,11,0}$-$15_{5,10,0}$	151741.920†	14.40	924.2	[5]	...	...	...
$16_{7,9,0}$-$15_{7,8,0}$	151759.617	12.90	975.5	[5]	...	...	...
$16_{7,10,0}$-$15_{7,9,0}$	151759.617†	12.90	975.5	[5]	...	...	...
$16_{4,13,0}$-$15_{4,12,0}$	151776.321	15.00	904.9	[8,14]	...	...	...
$16_{4,12,0}$-$15_{4,11,0}$	151779.673†	15.00	904.9	[8,14]	...	...	...
$16_{8,8,0}$-$15_{8,7,0}$	151790.294	12.00	1007.6	[6,28]	...	...	...
$16_{8,9,0}$-$15_{8,8,0}$	151790.294†	12.00	1007.6	[6,28]	...	...	...
$16_{9,7,0}$-$15_{9,6,0}$	151830.306	10.90	1043.8	[5]	...	...	...
$16_{9,8,0}$-$15_{9,7,0}$	151830.306†	10.90	1043.8	[5]	...	...	...
$16_{3,14,0}$-$15_{3,13,0}$	151833.987	15.40	889.9	[5]	...	...	...
$16_{10,6,0}$-$15_{10,5,0}$	151878.053	9.75	1084.2	[5]	...	...	...
$16_{10,7,0}$-$15_{10,6,0}$	151878.053†	9.75	1084.2	[5]	...	...	...
$16_{2,15,1}$-$15_{2,14,1}$	151975.804	15.70	882.8	[5,15]	...	...	...
$16_{3,13,0}$-$15_{3,12,0}$	151978.400†	15.40	889.9	[15]	...	...	...
$16_{6,11,1}$-$15_{6,10,1}$	152531.524	13.80	952.2	[6,16]	...	...	...
$16_{6,10,1}$-$15_{6,9,1}$	152531.525†	13.80	952.2	[6,16]	...	...	...
$16_{5,12,1}$-$15_{5,11,1}$	152535.030†	14.40	928.4	[6,16]	...	...	...
$16_{5,11,1}$-$15_{5,10,1}$	152535.030†	14.40	928.4	[6,16]	...	...	...
$16_{7,9,1}$-$15_{7,8,1}$	152545.943	12.90	980.2	[16,25]	...	...	...
$16_{7,10,1}$-$15_{7,9,1}$	152545.943†	12.90	980.2	[16,25]	...	...	...
$16_{4,13,1}$-$15_{1,12,1}$	152570.571	15.00	908.9	[25]	...	...	...
$16_{8,8,1}$-$15_{8,7,1}$	152572.162†	12.00	1012.6	[25]	...	...	...
$16_{8,9,1}$-$15_{8,8,1}$	152572.162†	12.00	1012.6	[25]	...	...	...
$16_{4,12,1}$-$15_{4,11,1}$	152573.963†	15.00	908.9	[25]	...	...	...
$16_{3,14,1}$-$15_{3,13,1}$	152624.196	15.40	893.8	[25,29]	...	...	...
$16_{3,13,1}$-$15_{3,12,1}$	152768.087	15.40	893.8	[5,30]	...	...	...
$16_{1,15,0}$-$15_{1,14,0}$	152953.043	15.60	874.1	[17]	...	...	...

Tabla B.7: continued.

Transition $J_{K_a,K_c,v} - J'_{K'_a,K'_c,v'}$	Predicted frequency (MHz)	S_{ij}	E_u (K)	v_{LSR}[(1)] km s^{-1}	Observed frequency (MHz)	Observed T_{MB} (K)[(2)]	Model T_{MB} (K)
$16_{2,14,0}$-$15_{2,13,0}$	153515.926	15.70	879.5	(6,15)	...	...	...
$16_{2,14,1}$-$15_{2,13,1}$	154186.204	15.70	883.3	(31)	...	...	...
$16_{1,15,1}$-$15_{1,14,1}$	155214.581	15.90	877.7	(5,32)	...	...	...
$17_{1,17,0}$-$16_{1,16,0}$	156551.903	16.90	878.5	5.3[(6,33)]	156551.7	0.21	0.07
$17_{1,17,1}$-$16_{1,16,1}$	157388.716	17.00	882.3	(9,22)	...	...	...
$17_{0,17,0}$-$16_{0,16,0}$	158477.998	17.00	877.3	5.0[(22,34)]	158478.0	0.16	0.07
$17_{0,17,1}$-$16_{0,16,1}$	160318.641	16.60	881.2	(5)	...	...	...
$17_{2,16,0}$-$16_{2,15,0}$	160589.194	16.80	886.7	(6)	...	...	...
$17_{6,12,0}$-$16_{6,11,0}$	161229.432	14.90	955.5	(5)	...	...	...
$17_{6,11,0}$-$16_{6,10,0}$	161229.432†	14.90	955.5	(5)	...	...	...
$17_{5,13,0}$-$16_{5,12,0}$	161234.324	15.50	931.9	(5)	...	...	...
$17_{5,12,0}$-$16_{5,11,0}$	161234.393†	15.50	931.9	(5)	...	...	...
$17_{7,10,0}$-$16_{7,9,0}$	161246.336	14.10	983.3	4.4	161246.6	0.08	0.06
$17_{7,11,0}$-$16_{7,10,0}$	161246.336†	14.10	983.3	4.4	161246.6	”	0.06
$17_{4,14,0}$-$16_{4,13,0}$	161278.428	16.10	912.6	(10)	...	...	...
$17_{4,13,0}$-$16_{4,12,0}$	161283.577†	16.10	912.6	(10)	...	...	...
$17_{3,15,0}$-$16_{3,14,0}$	161339.906	16.50	897.6	(26)	...	...	...
$17_{2,16,1}$-$16_{2,15,1}$	161414. 896	16.80	890.6	(6,15)	...	...	...
$17_{3,14,0}$-$16_{3,13,0}$	161535.119	16.50	897.6	(25,35)	...	...	...
$17_{6,12,1}$-$16_{6,11,1}$	162069.195	14.90	959.9	(16)	...	...	...
$17_{6,11,1}$-$16_{6,10,1}$	162069.196†	14.90	959.9	(16)	...	...	...
$17_{5,13,1}$-$16_{5,12,1}$	162077.201	15.50	936.2	(16,32)	...	...	...
$17_{5,12,1}$-$16_{5,11,1}$	162077.272†	15.50	936.2	(16,32)	...	...	...
$17_{7,10,1}$-$16_{7,9,1}$	162081.986	14.10	988.0	(6)	...	...	...
$17_{7,11,1}$-$16_{7,10,1}$	162081.986†	14.10	988.0	(6)	...	...	...
$17_{8,9,1}$-$16_{8,8,1}$	162108.225	13.20	1020.3	5.6	162107.9	0.07	0.05
$17_{8,10,1}$-$16_{8,9,1}$	162108.225†	13.20	1020.3	5.6	162107.9	”	0.05
$17_{4,14,1}$-$16_{4,13,1}$	162122.451	16.10	916.7	(6)	...	...	...
$17_{4,13,1}$-$16_{4,12,1}$	162127.658†	16.10	916.7	(6)	...	...	...
$17_{3,15,1}$-$16_{3,14,1}$	162179.504	16.50	901.6	(16)	...	...	...
$17_{3,14,1}$-$16_{3,13,1}$	162373.856	16.50	901.6	(5,36)	...	...	...
$17_{1,16,0}$-$16_{1,15,0}$	162983.178	16.80	882.0	(5,37)	...	...	...
$17_{2,15,0}$-$16_{2,14,0}$	163308.243	16.80	887.3	(6)	...	...	...
$17_{2,15,1}$-$16_{2,14,1}$	164008.063	16.80	891.2	(5)	...	...	...
$17_{1,16,1}$-$16_{1,15,1}$	164788.583	16.90	885.6	(38)	...	...	...
$18_{1,18,0}$-$17_{1,17,0}$	165690.522	17.90	886.5	(13)	...	...	...
$18_{1,18,1}$-$17_{1,17,1}$	167014.982	15.50	890.3	4.4[(18)]	167015.4	0.08	0.07

Tabla B.7: continued.

Transition $J_{K_a,K_c,v} - J'_{K'_a,K'_c,v'}$	Predicted frequency (MHz)	S_{ij}	E_u (K)	v_{LSR}[(1)] km s^{-1}	Observed frequency (MHz)	Observed T_{MB} (K)[(2)]	Model T_{MB} (K)
$18_{0,18,0}$-$17_{0,17,0}$	167541.662	18.00	885.6	[(39)]	...	...	...
$18_{0,18,1}$-$17_{0,17,1}$	169061.834	17.80	889.4	[(9)]	...	...	...
$18_{2,17,0}$-$17_{2,16,0}$	169968.890	17.80	894.9	6.1	169968.3	0.12	0.07
$18_{6,13,0}$-$17_{6,12,0}$	170718.325	16.00	963.7	1.7 [(25)]	170720.2	0.12	0.09
$18_{6,12,0}$-$17_{6,11,0}$	170718.326†	16.00	963.7	1.7[(25)]	170720.2	”	0.09
$18_{5,14,0}$-$17_{5,13,0}$	170728.317	16.60	940.1	5.2	170728.2	0.17	0.10
$18_{5,13,0}$-$17_{5,12,0}$	170728.435†	16.60	940.1	5.2	170728.2	”	0.10
$18_{7,11,0}$-$17_{7,10,0}$	170733.369	15.30	991.5	[(5)]	...	...	...
$18_{7,12,0}$-$17_{7,11,0}$	170733.369†	15.30	991.5	[(5)]	...	...	...
$18_{8,10,0}$-$17_{8,9,0}$	170764.312	14.40	1023.5	[(24)]	...	...	...
$18_{8,11,0}$-$17_{8,10,0}$	170764.312†	14.40	1023.5	[(24)]	...	...	...
$18_{4,15,0}$-$17_{4,14,0}$	170783.246	17.10	920.8	[(5)]	...	...	...
$18_{4,14,0}$-$17_{4,13,0}$	170790.954†	17.10	920.8	[(5)]	...	...	...
$18_{9,9,0}$-$17_{9,8,0}$	170806.886	13.50	1059.7	6.1	170806.2	0.09	0.04
$18_{9,10,0}$-$17_{9,9,0}$	170806.886†	13.50	1059.7	6.1	170806.2	”	0.04
$18_{2,17,1}$-$17_{2,16,1}$	170843.596	17.80	898.8	2.6	170844.9	0.06	0.12
$18_{3,16,0}$-$17_{3,15,0}$	170846.327†	17.50	905.8	7.4	170844.9	”	0.12
$18_{10,8,0}$-$17_{10,7,0}$	170858.856	12.40	1100.2	7.2	170857.6	0.07	0.03
$18_{10,9,0}$-$17_{10,8,0}$	170858.856†	12.40	1100.2	7.2	170857.6	”	0.03
$18_{11,7,0}$-$17_{11,6,0}$	170918.936	11.30	1144.7	5.8[(15)]	170918.4	0.07	0.03
$18_{11,8,0}$-$17_{11,7,0}$	170918.936†	11.30	1144.7	5.8[(15)]	170918.4	”	0.03
$18_{3,15,0}$-$17_{3,14,0}$	171105.377	17.50	905.9	[(5,34)]	...	...	...
$18_{6,13,1}$-$17_{6,12,1}$	171607.666	16.00	968.2	4.1[(32)]	171608.2	0.12	0.09
$18_{6,12,1}$-$17_{6,11,1}$	171607.667†	16.00	968.2	4.1[(32)]	171608.2	”	0.09
$18_{7,12,1}$-$17_{7,11,1}$	171618.371	15.30	996.2	[(40)]	...	...	...
$18_{7,11,1}$-$17_{7,10,1}$	171618.371†	15.30	996.2	[(40)]	...	...	...
$18_{5,14,1}$-$17_{5,13,1}$	171620.943†	16.60	944.4	[(40)]	...	...	...
$18_{5,13,1}$-$17_{5,12,1}$	171621.063†	16.60	944.4	[(40)]	...	...	...
$18_{8,10,1}$-$17_{8,9,1}$	171644.336	14.40	1028.6	[(11)]	...	...	...
$18_{8,11,1}$-$17_{8,10,1}$	171644.336†	14.40	1028.6	[(11)]	...	...	...
$18_{4,15,1}$-$17_{4,14,1}$	171677.053	17.10	925.0	[(5,32)]	...	...	...
$18_{9,9,1}$-$17_{9,8,1}$	171681.532	13.50	1065.2	[(41)]	...	...	...
$18_{9,10,1}$-$17_{9,9,1}$	171681.532†	13.50	1065.2	[(41)]	...	...	...
$18_{4,14,1}$-$17_{4,13,1}$	171684.845†	17.10	925.0	[(41)]	...	...	...
$18_{3,16,1}$-$17_{3,15,1}$	171735.300	17.50	909.8	[(16)]	...	...	...
$18_{3,15,1}$-$17_{3,14,1}$	171992.981	17.50	909.9	[(6)]	...	...	...
$18_{1,17,0}$-$17_{1,16,0}$	172430.747	15.70	890.2	[(42)]	...	...	...

Tabla B.7: continued.

Transition $J_{K_a,K_c,v} - J'_{K'_a,K'_c,v'}$	Predicted frequency (MHz)	S_{ij}	E_u (K)	v_{LSR}[(1)] km s^{-1}	Observed frequency (MHz)	Observed T_{MB} (K)[(2)]	Model T_{MB} (K)
$18_{2,16,0}$-$17_{2,15,0}$	173114.009	17.80	895.7	[(6)]	...	...	...
$18_{2,16,1}$-$17_{2,15,1}$	173844.831	17.80	899.5	[(25)]	...	...	...
$18_{1,17,1}$-$17_{1,16,1}$	174341.970	17.90	894.0	[(30,41)]	...	...	...
$18_{1,18,1}$-$17_{1,17,1}$	174555.409	22.30	890.3	[(5)]	...	...	...
$19_{1,19,0}$-$18_{1,18,0}$	174819.822	18.90	894.9	6.0[(5)]	174819.3	0.17	0.07
$19_{1,19,1}$-$18_{1,18,1}$	174921.452	9.50	898.7	[(7)]	...	...	...
$19_{0,19,0}$-$18_{0,18,0}$	176580.881	19.00	894.1	[(6)]	...	...	...
$19_{1,19,1}$-$18_{1,17,0}$	177046.114	9.60	898.7	[(5)]	...	...	...
$19_{0,19,1}$-$18_{0,18,1}$	177921.209	18.90	897.9	[(5,27)]	...	...	...
$21_{2,20,0}$-$20_{2,19,0}$	198041.306	20.80	922.0	[(16)]	...	...	...
$21_{2,20,1}$-$20_{2,19,1}$	199062.857	20.80	926.1	6.0	199062.2	0.08	0.10
$21_{6,16,0}$-$20_{6,15,0}$	199190.101	19.30	991.0	7.5[(5,16)]	199188.4	0.15	0.15
$21_{6,15,0}$-$20_{6,14,0}$	199190.107†	19.30	991.0	7.5[(5,16)]	199188.4	”	0.15
$21_{7,14,0}$-$20_{7,13,0}$	199196.532	18.70	1018.8	4.0	199197.1	0.14	0.13
$21_{7,15,0}$-$20_{7,14,0}$	199196.532†	18.70	1018.8	4.0	199197.1	”	0.13
$21_{5,17,0}$-$20_{5,16,0}$	199220.464	19.80	967.4	6.2	199219.6	0.28	0.16
$21_{5,16,0}$-$20_{5,15,0}$	199220.944†	19.80	967.4	6.9	199219.6	”	0.16
$21_{8,13,0}$-$20_{8,12,0}$	199225.484	18.00	1050.8	[(13,25)]	...	...	...
$21_{8,14,0}$-$20_{8,13,0}$	199225.484†	18.00	1050.8	[(13,25)]	...	...	...
$21_{9,12,0}$-$20_{9,11,0}$	199270.271	17.10	1087.1	[(31)]	...	...	...
$21_{9,13,0}$-$20_{9,12,0}$	199270.271†	17.10	1087.1	[(31)]	...	...	...
$21_{4,18,0}$-$20_{4,17,0}$	199314.525	20.20	948.1	[(26)]	...	...	...
$21_{10,11,0}$-$20_{10,10,0}$	199327.407	16.20	1127.5	[(43)]	...	...	...
$21_{10,12,0}$-$20_{10,11,0}$	199327.407†	16.20	1127.5	[(43)]	...	...	...
$21_{4,17,0}$-$20_{4,16,0}$	199337.294	20.20	948.1	[(5)]	...	...	...
$21_{3,19,0}$-$20_{3,18,0}$	199362.384	20.60	933.1	[(6)]	...	...	...
$21_{3,18,0}$-$20_{3,17,0}$	199913.409	20.60	933.3	5.0[(15)]	199913.4	0.04	0.10
$21_{6,16,1}$-$20_{6,15,1}$	200228.409	19.30	995.6	3.0	200229.6	0.22	0.21
$21_{6,15,1}$-$20_{6,14,1}$	200228.329†	19.30	995.6	3.0	200229.6	”	0.21
$21_{7,15,1}$-$20_{7,14,1}$	200229.751†	18.70	1023.7	5.2	200229.6	”	0.21
$21_{7,14,1}$-$20_{7,13,1}$	200229.751†	18.70	1023.7	5.2	200229.6	”	0.21
$21_{8,13,1}$-$20_{8,12,1}$	200252.965	18.00	1056.0	[(5)]	...	...	...
$21_{8,14,1}$-$20_{8,13,1}$	200252.965†	18.00	1056.0	[(5)]	...	...	...
$21_{5,17,1}$-$20_{5,16,1}$	200262.469	19.80	971.9	[(6,26)]	...	...	...
$21_{5,16,1}$-$20_{5,15,1}$	200262.959†	19.80	971.9	[(6,26)]	...	...	...
$21_{9,12,1}$-$20_{9,11,1}$	200291.540	17.10	1092.6	[(24)]	...	...	...
$21_{9,13,1}$-$20_{9,12,1}$	200291.540†	17.10	1092.6	[(24)]	...	...	...

Tabla B.7: continued.

Transition $J_{K_a,K_c,v} - J'_{K'_a,K'_c,v'}$	Predicted frequency (MHz)	S_{ij}	E_u (K)	v_{LSR}[(1)] km s^{-1}	Observed frequency (MHz)	Observed T_{MB} (K)[(2)]	Model T_{MB} (K)
$21_{10,11,1}$-$20_{10,10,1}$	200342.178	16.20	1133.4	[(26,35)]	...	...	...
$21_{10,12,1}$-$20_{10,11,1}$	200342.178†	16.20	1133.4	[(26,35)]	...	...	...
$21_{4,18,1}$-$20_{4,17,1}$	200357.737	20.20	952.4	7.7[(32)]	200355.9	0.09	0.09
$21_{4,17,1}$-$20_{4,16,1}$	200380.722	20.20	952.4	[(15,44)]	...	...	...
$21_{3,19,1}$-$20_{3,18,1}$	200399.365	20.60	937.3	6.4[(5)]	200398.4	0.13	0.10
$21_{11,10,1}$-$20_{11,9,1}$	200403.025†	15.20	1178.5	6.1[(5)]	200398.4	”	0.10
$21_{11,11,1}$-$20_{11,10,1}$	200403.025†	15.20	1178.5	6.1[(5)]	200398.4	”	0.10
$21_{12,9,1}$-$20_{12,8,1}$	200472.962	14.10	1227.6	[(6,25)]	...	...	...
$21_{12,10,1}$-$20_{12,9,1}$	200472.962†	14.10	1227.6	[(6,25)]	...	...	...
$21_{13,8,1}$-$20_{13,7,1}$	200551.259	13.00	1281.0	[(30,45)]	...	...	...
$21_{13,9,1}$-$20_{13,8,1}$	200551.259†	13.00	1281.0	[(30,45)]	...	...	...
$21_{3,18,1}$-$20_{3,17,1}$	200945.742	20.60	937.4	4.9	200945.8	0.06	0.10
$21_{1,20,0}$-$20_{1,19,0}$	201771.285	20.90	917.9	[(5)]	...	...	...
$22_{1,22,0}$-$21_{1,21,0}$	202153.351	21.90	922.7	[(46)]	...	...	...
$21_{2,19,0}$-$20_{2,18,0}$	202542.789	20.80	923.4	[(15,25)]	...	...	...
$21_{1,20,1}$-$20_{1,19,1}$	202884.847	20.90	921.8	[(20,32)]	...	...	...
$22_{1,22,1}$-$21_{1,21,1}$	203176.295	22.00	926.7	[(47)]	...	...	...
$21_{2,19,1}$-$20_{2,18,1}$	203399.100	20.80	927.4	[(16,24)]	...	...	...
$22_{0,22,0}$-$21_{3,21,0}$	203587.506	22.00	922.1	4.4	203584.8	0.10	0.12
$22_{0,22,1}$-$21_{0,21,1}$	204780.110	22.00	926.1	[(10)]	...	...	...
$22_{2,21,0}$-$21_{2,20,0}$	207375.176	21.80	932.0	[(6)]	...	...	...
$22_{2,21,1}$-$21_{2,20,1}$	208445.721	21.80	936.1	[(16,21)]	...	...	...
$22_{6,17,0}$-$21_{6,16,0}$	208682.541	20.40	1001.0	[(5)]	...	...	...
$22_{6,16,0}$-$21_{6,15,0}$	208682.551†	20.40	1001.0	[(5)]	...	...	...
$22_{7,16,0}$-$21_{7,15,0}$	208684.999†	19.80	1028.8	[(5)]	...	...	...
$22_{7,15,0}$-$21_{7,14,0}$	208685.000†	19.80	1028.8	[(5)]	...	...	...
$22_{8,14,0}$-$21_{8,13,0}$	208712.583	19.10	1060.8	[(24)]	...	...	...
$22_{8,15,0}$-$21_{8,14,0}$	208712.583†	19.10	1060.8	[(24)]	...	...	...
$22_{5,18,0}$-$21_{5,17,0}$	208721.517	20.90	977.4	[(24)]	...	...	...
$22_{5,17,0}$-$21_{5,16,0}$	208722.249†	20.90	977.4	[(24)]	...	...	...
$22_{9,13,0}$-$21_{9,12,0}$	208757.625	18.30	1097.1	[(5)]	...	...	...
$22_{9,14,0}$-$21_{9,13,0}$	208757.625†	18.30	1097.1	[(5)]	...	...	...
$22_{10,12,0}$-$21_{10,11,0}$	208816.140	17.50	1137.5	5.4	208815.8	0.06	0.05
$22_{10,13,0}$-$21_{10,12,0}$	208816.140†	17.50	1137.5	5.4	208815.8	”	0.05
$22_{4,19,0}$-$21_{4,18,0}$	208830.610	21.30	958.2	5.5[(48)]	208830.2	0.11	0.09
$22_{4,18,0}$-$21_{4,17,0}$	208862.131	21.30	958.2	3.3[(48)]	208863.3	0.22	0.18
$22_{3,20,0}$-$21_{3,19,0}$	208864.301†	21.60	943.2	6.5[(48)]	208863.3	”	0.18

Tabla B.7: continued.

Transition $J_{K_a,K_c,v} - J'_{K'_a,K'_c,v'}$	Predicted frequency (MHz)	S_{ij}	E_u (K)	v_{LSR}[(1)] km s^{-1}	Observed frequency (MHz)	Observed T_{MB} (K)[(2)]	Model T_{MB} (K)
$22_{3,19,0}$-$21_{3,18,0}$	209554.019	21.60	943.3	[(15,32)]	...	...	...
$22_{7,16,1}$-$21_{7,15,1}$	209767.678	19.80	1033.8	4.1	209768.3	0.26	0.20
$22_{7,15,1}$-$21_{7,14,1}$	209767.678†	19.80	1033.8	4.1	209768.3	”	0.20
$22_{6,17,1}$-$21_{6,16,1}$	209770.437†	20.40	1005.7	8.1	209768.3	”	0.20
$22_{6,16,1}$-$21_{6,15,1}$	209770.447†	20.40	1005.7	8.1	209768.3	”	0.20
$22_{8,14,1}$-$21_{8,13,1}$	209789.275	19.10	1066.1	6.8[(15)]	...	0.09	0.08
$22_{8,15,1}$-$21_{8,14,1}$	209789.275†	19.10	1066.1	6.8[(15)]	...	”	0.08
$22_{5,18,1}$-$21_{5,17,1}$	209813.357	20.90	981.9	[(10)]	...	...	...
$22_{5,17,1}$-$21_{5,16,1}$	209814.103†	20.90	981.9	[(10)]	...	...	...
$22_{9,13,1}$-$21_{9,12,1}$	209827.835	18.30	1102.7	[(22)]	...	...	...
$22_{9,14,1}$-$21_{9,13,1}$	209827.835†	18.30	1102.7	[(22)]	...	...	...
$22_{10,12,1}$-$21_{10,11,1}$	209879.560	17.50	1143.5	[(16)]	...	...	...
$22_{10,13,1}$-$21_{10,12,1}$	209879.560†	17.50	1143.5	[(16)]	...	...	...
$22_{4,19,1}$-$21_{4,18,1}$	209923.627	21.30	962.5	[(6)]	...	...	...
$22_{11,11,1}$-$21_{11,10,1}$	209942.321	16.50	1188.5	[(24)]	...	...	...
$22_{11,12,1}$-$21_{11,11,1}$	209942.321†	16.50	1188.5	[(24)]	...	...	...
$22_{3,20,1}$-$21_{3,19,1}$	209950.571	21.60	947.4	[(24)]	...	...	...
$22_{4,18,1}$-$21_{4,17,1}$	209955.430†	21.30	962.5	[(24)]	...	...	...
$22_{12,10,1}$-$21_{12,9,1}$	210014.831	15.50	1237.7	[(5)]	...	...	...
$22_{12,11,1}$-$21_{12,10,1}$	210014.831†	15.50	1237.7	[(5)]	...	...	...
$22_{13,9,1}$-$21_{13,8,1}$	210096.258	14.30	1291.1	[(42)]	...	...	...
$22_{13,10,1}$-$21_{13,9,1}$	210096.258†	14.30	1291.1	[(42)]	...	...	...
$22_{14,8,1}$-$21_{14,7,1}$	210186.019	13.10	1348.5	[(5,32)]	...	...	...
$22_{14,9,1}$-$21_{14,8,1}$	210186.019†	13.10	1348.5	[(5,32)]	...	...	...
$22_{3,19,1}$-$21_{3,18,1}$	210633.613	21.60	947.5	[(5)]	...	...	...
$23_{1,23,0}$-$22_{1,22,0}$	211247.191	22.90	932.8	[(5,6)]	...	...	...
$22_{1,21,0}$-$21_{1,22,0}$	211259.490	21.90	928.1	[(6)]	...	...	...
$23_{1,23,1}$-$22_{1,22,1}$	212310.380	23.00	936.9	[(5)]	...	...	...
$22_{2,20,0}$-$21_{2,19,0}$	212333.066	21.80	933.6	4.7	212333.3	0.26	0.12
$22_{1,21,1}$-$21_{1,20,1}$	212361.176	21.90	932.0	4.6	212361.4	0.22	0.12
$23_{0,23,0}$-$22_{0,22,0}$	212564.406	23.00	932.3	[(9)]	...	...	...
$22_{2,20,1}$-$21_{2,19,1}$	213249.226	21.80	937.6	[(5)]	...	...	...
$23_{0,23,1}$-$22_{0,22,1}$	213760.970	23.00	936.3	7.9[(5)]	213758.8	0.17	0.14
$23_{2,22,0}$-$22_{2,21,0}$	216696.636	22.80	942.4	[(5)]	...	...	...
$23_{2,22,1}$-$22_{2,21,1}$	217816.324	22.80	946.5	[(5,49)]	...	...	...
$23_{7,17,0}$-$22_{7,16,0}$	218173.870	20.90	1039.3	4.25	218174.4	0.24	0.24
$23_{7,16,0}$-$22_{7,15,0}$	218173.870†	20.90	1039.3	4.25	218174.4	”	0.24

Tabla B.7: continued.

Transition $J_{K_a,K_c,v} - J'_{K'_a,K'_c,v'}$	Predicted frequency (MHz)	S_{ij}	E_u (K)	v_{LSR}[(1)] km s^{-1}	Observed frequency (MHz)	Observed T_{MB} (K)[(2)]	Model T_{MB} (K)
$23_{6,18,0}$-$22_{6,17,0}$	218175.978†	21.40	1011.5	7.14	218174.4	”	0.24
$23_{6,17,0}$-$22_{6,16,0}$	218175.995†	21.40	1011.5	7.17	218174.4	”	0.24
$23_{8,15,0}$-$22_{8,14,0}$	218199.703	20.20	1071.3	[(50)]	...	...	...
$23_{8,16,0}$-$22_{8,15,0}$	218199.703†	20.20	1071.3	[(50)]	...	...	...
$23_{5,19,0}$-$22_{5,18,0}$	218224.540	21.90	987.9	[(51)]	...	...	...
$23_{5,18,0}$-$22_{5,17,0}$	218225.636†	21.90	987.9	[(51)]	...	...	...
$23_{9,14,0}$-$22_{9,13,0}$	218244.742	19.50	1107.6	7.2[(35)]	...	0.12	0.07
$23_{9,15,0}$-$22_{9,14,0}$	218244.742†	19.50	1107.6	7.2[(35)]	...	”	0.07
$23_{10,13,0}$-$22_{10,12,0}$	218304.448	18.70	1148.0	[(52)]	...	...	...
$23_{10,14,0}$-$22_{10,13,0}$	218304.448†	18.70	1148.0	[(52)]	...	...	...
$23_{4,20,0}$-$22_{4,19,0}$	218349.466	22.30	968.6	[(52)]	...	...	...
$23_{3,21,0}$-$22_{3,20,0}$	218363.200	22.60	953.6	3.8	218364.1	0.13	0.11
$23_{11,12,0}$-$22_{11,11,0}$	218376.242	17.70	1192.6	[(5)]	...	...	...
$23_{11,13,0}$-$22_{11,12,0}$	218376.242†	17.70	1192.6	[(5)]	...	...	...
$23_{4,19,0}$-$22_{4,18,0}$	218392.442	22.30	968.6	[(16)]	...	...	...
$23_{12,11,0}$-$22_{12,10,0}$	218458.547	16.70	1241.3	[(53)]	...	...	...
$23_{12,12,0}$-$22_{12,11,0}$	218458.547†	16.70	1241.3	[(53)]	...	...	...
$23_{13,10,0}$-$22_{13,9,0}$	218550.334	15.70	1294.1	[(5)]	...	...	...
$23_{13,11,0}$-$22_{13,10,0}$	218550.334†	15.70	1294.1	[(5)]	...	...	...
$23_{3,20,0}$-$22_{3,19,0}$	219216.278	22.60	953.8	[(25)]	...	...	...
$23_{7,17,1}$-$22_{7,16,1}$	219306.033	20.90	1044.3	[(9)]	...	...	...
$23_{7,16,1}$-$22_{7,15,1}$	219306.034†	20.90	1044.3	[(9)]	...	...	...
$23_{6,18,1}$-$22_{6,17,1}$	219313.572	21.40	1016.2	[(25)]	...	...	...
$23_{6,17,1}$-$22_{6,16,1}$	219313.590†	21.40	1016.2	[(25)]	...	...	...
$23_{8,15,1}$-$22_{8,14,1}$	219325.635	20.20	1076.6	[(25)]	...	...	...
$23_{8,16,1}$-$22_{8,15,1}$	219325.635†	20.20	1076.6	[(25)]	...	...	...
$23_{9,14,1}$-$22_{9,13,1}$	219363.922	19.50	1113.2	[(17)]	...	...	...
$23_{9,15,1}$-$22_{9,14,1}$	219363.922†	19.50	1113.2	[(17)]	...	...	...
$23_{5,19,1}$-$22_{5,18,1}$	219366.234†	21.90	992.5	[(17)]	...	...	...
$23_{5,18,1}$-$22_{5,17,1}$	219367.350†	21.90	992.5	[(17)]	...	...	...
$23_{10,13,1}$-$22_{10,12,1}$	219416.552	18.70	1154.0	[(54)]	...	...	...
$23_{10,14,1}$-$22_{10,13,1}$	219416.552†	18.70	1154.0	[(54)]	...	...	...
$23_{11,12,1}$-$22_{11,11,1}$	219481.091	17.70	1199.1	3.90[(6)]	219481.9	0.15	0.04
$23_{11,13,1}$-$22_{11,12,1}$	219481.091†	17.70	1199.1	3.90[(6)]	219481.9	”	0.04
$23_{4,20,1}$-$22_{4,19,1}$	219492.282	22.30	973.0	[(16)]	...	...	...
$23_{3,21,1}$-$22_{3,20,1}$	219498.733†	22.60	957.9	[(16)]	...	...	...
$23_{4,19,1}$-$22_{4,18,1}$	219535.617	22.30	973.0	[(55)]	...	...	...

Tabla B.7: continued.

Transition $J_{K_a,K_c,v} - J'_{K'_a,K'_c,v'}$	Predicted frequency (MHz)	S_{ij}	E_u (K)	v_{LSR}[(1)] km s^{-1}	Observed frequency (MHz)	Observed T_{MB} (K)[(2)]	Model T_{MB} (K)
$24_{1,24,0}$-$23_{1,23,0}$	220332.868	23.90	943.4	6.3	220331.9	0.13	0.13
$23_{3,20,1}$-$22_{3,19,1}$	220342.405	22.60	958.1	[(5)]	...	...	...
$23_{1,22,0}$-$22_{1,21,0}$	220690.867	22.90	938.7	[(46)]	...	...	...
$24_{1,24,1}$-$23_{1,23,1}$	221438.698	24.00	947.5	[(6,23,25)]	...	...	...
$24_{0,24,0}$-$23_{0,23,0}$	221533.880	24.00	942.9	6.0	221533.1	0.15	0.14
$23_{1,22,1}$-$22_{1,21,1}$	221817.025	22.90	942.7	2.2[(5)]	221819.1	0.11	0.14
$23_{2,21,0}$-$22_{2,20,0}$	222104.379	22.80	944.3	[(56)]	...	...	...
$24_{0,24,1}$-$23_{0,23,1}$	222745.388	24.00	947.0	[(26)]	...	...	...
$23_{2,21,1}$-$22_{2,20,1}$	223090.983	22.80	948.3	[(25,29)]	...	...	...
$24_{2,23,0}$-$23_{2,22,0}$	226005.372	23.80	953.2	[(5)]	...	...	...
$24_{2,23,1}$-$23_{2,22,1}$	227174.530	23.80	957.4	[(16)]	...	...	...
$24_{7,18,0}$-$23_{7,17,0}$	227663.160	22.00	1050.2	[(6)]	...	...	...
$24_{7,17,0}$-$23_{7,16,0}$	227663.160†	22.00	1050.2	[(6)]	...	...	...
$24_{6,19,0}$-$23_{6,18,0}$	227670.458	22.50	1022.4	[(57)]	...	...	...
$24_{6,18,0}$-$23_{6,17,0}$	227670.485†	22.50	1022.4	[(57)]	...	...	...
$24_{8,16,0}$-$23_{8,15,0}$	227686.845	21.30	1082.2	3.9[(5)]	227687.7	0.07	0.10
$24_{8,17,0}$-$23_{8,16,0}$	227686.845†	21.30	1082.2	3.9[(5)]	227687.7	”	0.10
$24_{5,20,0}$-$23_{5,19,0}$	227729.610	23.00	998.8	[(5)]	...	...	...
$24_{5,19,0}$-$23_{5,18,0}$	227731.221†	23.00	998.8	[(5)]	...	...	...
$24_{5,15,0}$-$23_{5,14,0}$	227731.609†	20.60	1118.5	[(5)]	...	...	...
$24_{5,16,0}$-$23_{5,15,0}$	227731.609†	20.60	1118.5	[(5)]	...	...	...
$24_{10,14,0}$-$23_{10,13,0}$	227792.313	19.80	1158.9	[(58)]	...	...	...
$24_{10,15,0}$-$23_{10,14,0}$	227792.313†	19.80	1158.9	[(58)]	...	...	...
$24_{3,22,0}$-$23_{3,21,0}$	227858.249	23.60	964.6	4.2	227858.9	0.18	0.12
$24_{11,13,0}$-$23_{11,12,0}$	227866.043	19.00	1203.5	[(5)]	...	...	...
$24_{11,14,0}$-$23_{11,13,0}$	227866.043†	19.00	1203.5	[(5)]	...	...	...
$24_{4,21,0}$-$23_{4,20,0}$	227871.000	23.30	979.6	5.8	227870.4	0.14	0.12
$24_{4,20,0}$-$23_{4,19,0}$	227928.779	23.30	979.6	[(29)]	...	...	...
$24_{12,12,0}$-$23_{12,11,0}$	227951.017	18.00	1252.2	[(6,59)]	...	...	...
$24_{12,13,0}$-$23_{12,12,0}$	227951.017†	18.00	1252.2	[(6,59)]	...	...	...
$24_{13,11,0}$-$23_{13,10,0}$	228046.082	17.00	1305.0	[(25)]	...	...	...
$24_{13,12,0}$-$23_{13,11,0}$	228046.082†	17.00	1305.0	[(25)]	...	...	...
$24_{7,18,1}$-$23_{7,17,1}$	228844.834	22.00	1055.3	[(15,26)]	...	...	...
$24_{7,17,1}$-$23_{7,16,1}$	228844.834†	22.00	1055.3	[(15,26)]	...	...	...
$24_{6,19,1}$-$23_{6,18,1}$	228857.772	22.50	1027.2	[(32,38,57)]	...	...	...
$24_{6,18,1}$-$23_{6,17,1}$	228857.800†	22.50	1027.2	[(32,38,57)]	...	...	...
$24_{8,16,1}$-$23_{8,15,1}$	228862.045†	21.30	1087.6	[(32,38,57)]	...	...	...

Tabla B.7: continued.

Transition $J_{K_a,K_c,v} - J'_{K'_a,K'_c,v'}$	Predicted frequency (MHz)	S_{ij}	E_u (K)	v_{LSR}[1] km s^{-1}	Observed frequency (MHz)	Observed T_{MB} (K)[2]	Model T_{MB} (K)
$24_{8,17,1}$-$23_{8,16,1}$	228862.045†	21.30	1087.6	(32,38,57)	...	...	...
$24_{9,15,1}$-$23_{9,14,1}$	228899.792	20.60	1124.2	(37,43,60)	...	...	...
$24_{9,16,1}$-$23_{9,15,1}$	228899.792†	20.60	1124.2	(37,43,60)	...	...	...
$24_{3,21,0}$-$23_{3,20,0}$	228901.619†	23.60	964.8	(37,43,60)	...	...	...
$24_{5,20,1}$-$23_{5,19,1}$	228921.174	23.00	1003.5	4.2	228921.7	0.08	0.17
$24_{5,19,1}$-$23_{5,18,1}$	228922.815†	23.00	1003.5	6.3	228921.7	”	0.17
$24_{10,14,1}$-$23_{10,13,1}$	228953.135	19.80	1165.0	7.0(32)	228951.5	0.12	0.10
$24_{10,15,1}$-$23_{10,14,1}$	228953.135†	19.80	1165.0	7.0(32)	228951.5	”	0.10
$24_{11,13,1}$-$23_{11,12,1}$	229019.310	19.00	1210.1	5.8	229018.6	0.08	0.08
$24_{11,14,1}$-$23_{11,13,1}$	229019.310†	19.00	1210.1	5.8	229018.6	”	0.08
$24_{3,22,1}$-$23_{3,21,1}$	229043.016	23.60	968.9	(9)	...	...	...
$24_{4,21,1}$-$23_{4,20,1}$	229063.602	23.30	984.0	2.4(5)	229065.3	0.18	0.09
$24_{12,12,1}$-$23_{12,11,1}$	229096.650	18.00	1259.3	(15)	...	...	...
$24_{12,13,1}$-$23_{12,12,1}$	229096.650†	18.00	1259.3	(15)	...	...	...
$24_{4,20,1}$-$23_{4,19,1}$	229121.828	23.30	984.0	(9,40)	...	...	...
$24_{13,11,1}$-$23_{13,10,1}$	229184.084	17.00	1312.6	3.1(5,14)	229185.5	0.10	0.04
$24_{13,12,1}$-$23_{13,11,1}$	229184.084†	17.00	1312.6	3.1(5,14)	229185.5	”	0.04
$25_{1,25,0}$-$24_{1,24,0}$	229410.738	24.90	954.4	(6,16)	...	...	...
$24_{3,21,1}$-$23_{3,20,1}$	230073.374	23.60	969.1	0.6(47)	230076.7	0.19	0.23
$24_{1,23,0}$-$23_{1,22,0}$	230075.401†	23.90	949.7	3.2(47)	230076.7	”	0.23
$25_{0,25,0}$-$24_{0,24,0}$	230498.478	25.00	954.0	(61)	...	...	...
$25_{1,25,1}$-$24_{1,24,1}$	230560.110	25.00	958.6	(5)	...	...	...
$24_{1,23,1}$-$23_{1,22,1}$	231249.645	23.90	953.8	1.4(6,31)	231251.2	0.08	0.12
$25_{0,25,1}$-$24_{0,24,1}$	231732.233	25.00	958.2	(53,54)	...	...	...
$24_{2,22,0}$-$23_{2,21,0}$	231853.475	23.80	955.4	(16)	...	...	...
$24_{2,22,1}$-$23_{2,21,1}$	232920.186	23.80	959.5	4.8	232917.1	0.12	0.11
$25_{2,24,0}$-$24_{2,23,0}$	235301.112	24.80	964.5	5.6(5)	235300.7	0.26	0.13
$25_{2,24,1}$-$24_{2,23,1}$	236520.937	24.80	968.8	(52)	...	...	...
$25_{7,19,0}$-$24_{7,18,0}$	237152.887	23.00	1061.6	3.8	237153.8	0.22	0.19
$25_{7,18,0}$-$24_{7,17,0}$	237152.888†	23.00	1061.6	3.8	237153.8	”	0.19
$25_{6,20,0}$-$24_{6,19,0}$	237166.024	23.60	1033.8	(16,17)	...	...	...
$25_{6,19,0}$-$24_{6,18,0}$	237166.066†	23.60	1033.8	(16,17)	...	...	...
$25_{8,17,0}$-$24_{8,16,0}$	237174.010†	22.40	1093.6	(16,17)	...	...	...
$25_{8,18,0}$-$24_{8,17,0}$	237174.010†	22.40	1093.6	(16,17)	...	...	...
$25_{9,16,0}$-$24_{9,15,0}$	237218.216	21.80	1129.9	(5)	...	...	...
$25_{9,17,0}$-$24_{9,16,0}$	237218.216†	21.80	1129.9	(5)	...	...	...
$25_{5,21,0}$-$24_{5,20,0}$	237236.799	24.00	1010.2	(5)	...	...	...

Tabla B.7: continued.

Transition $J_{K_a,K_c,v} - J'_{K'_a,K'_c,v'}$	Predicted frequency (MHz)	S_{ij}	E_u (K)	v_{LSR}[(1)] km s^{-1}	Observed frequency (MHz)	Observed T_{MB} (K)[(2)]	Model T_{MB} (K)
$25_{5,20,0}$-$24_{5,19,0}$	237239.127†	24.00	1010.2	(5)	...	...	...
$25_{3,23,0}$-$24_{3,22,0}$	237348.592	24.60	976.0	(6)	...	...	...
$25_{4,22,0}$-$24_{4,21,0}$	237395.075	24.40	991.0	(6,15)	...	...	...
$25_{4,21,0}$-$24_{4,20,0}$	237471.759	24.40	991.0	(15,25,62)	...	...	...
$25_{7,19,1}$-$24_{7,18,1}$	238384.095	23.00	1066.7	4.7	238384.3	0.20	0.19
$25_{7,18,1}$-$24_{7,17,1}$	238384.096†	23.00	1066.7	4.7	238384.3	”	0.19
$25_{8,17,1}$-$24_{8,16,1}$	238398.505	22.40	1099.1	(63)	...	...	...
$25_{8,18,1}$-$24_{8,17,1}$	238398.505†	22.40	1099.1	(63)	...	...	...
$25_{6,20,1}$-$24_{6,19,1}$	238403.080†	23.60	1038.7	(63)	...	...	...
$25_{6,19,1}$-$24_{6,18,1}$	238403.123†	23.60	1038.7	(63	...	...	...
$25_{9,16,1}$-$24_{9,15,1}$	238435.431	21.80	1135.7	(5)	...	...	...
$25_{9,17,1}$-$24_{9,16,1}$	238435.431†	21.80	1135.7	(5)	...	...	...
$25_{5,21,1}$-$24_{5,20,1}$	238478.249	24.00	1014.9	5.1[(46)]	238479.4	0.26	0.33
$25_{5,20,1}$-$24_{5,19,1}$	238480.621†	24.00	1014.9	5.1[(46)]	238479.4	”	0.33
$26_{1,26,0}$-$25_{1,25,0}$	238481.176†	26.00	965.8	7.3[(46)]	238479.4	”	0.33
$25_{10,15,1}$-$24_{10,14,1}$	238489.289	21.00	1176.5	**	...	...	...
$25_{10,16,1}$-$24_{10,15,1}$	238489.289†	21.00	1176.5	**	...	...	...
$25_{11,14,1}$-$24_{11,13,1}$	238556.952	20.20	1221.5	(5)	...	...	...
$25_{11,15,1}$-$24_{11,14,1}$	238556.952†	20.20	1221.5	(5)	...	...	...
$25_{3,23,1}$-$24_{3,24,1}$	238582.564	24.60	980.4	(5)	...	...	...
$25_{3,22,0}$-$24_{3,21,0}$	238611.238	24.60	976.3	(6,9,57)	...	...	...
$25_{12,13,1}$-$24_{12,12,1}$	238636.540	19.20	1270.7	(5)	...	...	...
$25_{12,14,1}$-$24_{12,13,1}$	238636.540†	19.20	1270.7	(5)	...	...	...
$25_{4,22,1}$-$24_{4,21,1}$	238637.447†	24.40	995.5	(5)	...	...	...
$25_{4,21,1}$-$24_{4,20,1}$	238714.672	24.40	995.5	(32,64)	...	...	...
$25_{13,12,1}$-$24_{13,11,1}$	238726.845	18.20	1324.1	(11,15)	...	...	...
$25_{13,13,1}$-$24_{13,12,1}$	238726.845†	18.20	1324.1	(11,15)	...	...	...
$25_{14,11,1}$-$24_{14,10,1}$	238827.038	17.20	1381.5	(5,32)	...	...	...
$25_{14,12,1}$-$24_{14,11,1}$	238827.038†	17.20	1381.5	(5,32)	...	...	...
$25_{1,24,0}$-$24_{1,23,0}$	239416.632	24.90	961.2	3.1[(65,66)]	239418.1	0.14	0.14
$26_{0,26,0}$-$25_{0,25,0}$	239460.306	26.00	965.5	**	...	...	...
$26_{1,26,1}$-$25_{1,25,1}$	239674.450	26.00	970.1	(16,67)	...	...	...
$25_{3,22,1}$-$24_{3,21,1}$	239827.521	24.60	980.6	(67)	...	...	...
$25_{1,24,1}$-$24_{1,23,1}$	240665.147	24.90	965.3	8.9[(26,33)]	240652.0	0.22	0.16
$26_{0,26,1}$-$25_{0,25,1}$	240721.369	26.00	969.7	(26,33)	...	...	...
$25_{2,23,0}$-$24_{2,22,0}$	241578.697	24.90	967.0	(11)	...	...	...
$25_{2,23,1}$-$24_{2,22,1}$	242733.064	24.80	971.2	(29,43,68)	...	...	...

Tabla B.7: continued.

Transition $J_{K_a,K_c,v} - J'_{K'_a,K'_c,v'}$	Predicted frequency (MHz)	S_{ij}	E_u (K)	v_{LSR}[1] km s^{-1}	Observed frequency (MHz)	Observed T_{MB} (K)[2]	Model T_{MB} (K)
$26_{2,25,0}$-$25_{2,24,0}$	244583.625	25.80	976.3	[69]	...	...	...
$26_{2,25,1}$-$25_{2,24,1}$	245854.366	25.80	980.6	3.3	245855.8	0.17	0.12
$26_{7,20,0}$-$25_{7,19,0}$	246643.069	24.10	1073.4	[70]	...	...	...
$26_{7,19,0}$-$25_{7,18,0}$	246643.070†	24.10	1073.4	[70]	...	...	...
$26_{8,18,0}$-$25_{8,17,0}$	246661.197†	23.50	1105.5	[70]	...	...	...
$26_{8,19,0}$-$25_{8,18,0}$	246661.197†	23.50	1105.5	[70]	...	...	...
$26_{6,21,0}$-$25_{6,20,0}$	246662.720†	24.60	1045.6	[70]	...	...	...
$26_{6,20,0}$-$25_{6,19,0}$	246662.786†	24.60	1045.6	[70]	...	...	...
$26_{9,17,0}$-$25_{9,16,0}$	246704.552	22.90	1141.7	[5]	...	...	...
$26_{9,18,0}$-$25_{9,17,0}$	246704.552†	22.90	1141.7	[5]	...	...	...
$26_{5,22,0}$-$25_{5,21,0}$	246746.173	25.00	1022.1	[6]	...	...	...
$26_{5,21,0}$-$25_{5,20,0}$	246749.490†	25.00	1022.1	[6]	...	...	...
$26_{10,16,0}$-$25_{10,15,0}$	246766.638	22.20	1182.2	[5]	...	...	...
$26_{10,17,0}$-$25_{10,16,0}$	246766.638†	22.20	1182.2	[5]	...	...	...
$26_{3,24,0}$-$25_{3,23,0}$	246833.365	25.70	987.8	[71]	...	...	...
$26_{11,15,0}$-$25_{11,14,0}$	246843.781	21.30	1226.7	[5]	...	...	...
$26_{11,16,0}$-$25_{11,15,0}$	246843.781†	21.30	1226.7	[5]	...	...	...
$26_{4,23,0}$-$25_{4,22,0}$	246921.510	25.40	1002.8	[16,72]	...	...	...
$26_{4,22,0}$-$25_{4,21,0}$	247022.074	25.40	1002.8	3.9[15,16]	247023.0	0.19	0.11
$27_{1,27,0}$-$26_{1,26,0}$	247544.574	26.90	977.7	4.5[16]	247545.0	0.17	0.14
$26_{7,20,1}$-$25_{7,19,1}$	247923.834	24.10	1078.6	[6,32]	...	...	...
$26_{7,19,1}$-$25_{7,18,1}$	247923.835†	24.10	1078.6	[6,32]	...	...	...
$26_{8,18,1}$-$25_{8,17,1}$	247935.013	23.50	1111.0	[5]	...	...	...
$26_{8,19,1}$-$25_{8,18,1}$	247935.013†	23.50	1111.0	[5]	...	...	...
$26_{6,21,1}$-$25_{6,20,1}$	247949.538	24.60	1050.6	[6]	...	...	...
$26_{6,20,1}$-$25_{6,19,1}$	247949.605†	24.60	1050.6	[6]	...	...	...
$26_{9,17,1}$-$25_{9,16,1}$	247970.829	22.90	1147.6	[11]	...	...	...
$26_{9,18,1}$-$25_{9,17,1}$	247970.829†	22.90	1147.6	[11]	...	...	...
$26_{10,16,1}$-$25_{10,15,1}$	248024.994	22.20	1188.4	[5,18,32]	...	...	...
$26_{10,17,1}$-$25_{10,16,1}$	248024.994†	22.20	1188.4	[5,18,32]	...	...	...
$26_{5,22,1}$-$25_{5,21,1}$	248037.522	25.00	1026.8	[16,32]	...	...	...
$26_{5,21,1}$-$25_{5,20,1}$	248040.898†	25.00	1026.8	[16,32]	...	...	...
$26_{11,15,1}$-$25_{11,14,1}$	248093.991	21.30	1233.4	[13]	...	...	...
$26_{11,16,1}$-$25_{11,15,1}$	248093.991†	21.30	1233.4	[13]	...	...	...
$26_{3,24,1}$-$25_{3,23,1}$	248116.512	25.70	992.3	5.9[64]	248115.7	0.26	0.12
$26_{12,14,1}$-$25_{12,13,1}$	248175.709	20.50	1282.6	[26]	...	...	...
$26_{12,15,1}$-$25_{12,14,1}$	248175.709†	20.50	1282.6	[26]	...	...	...

Tabla B.7: continued.

Transition $J_{K_a,K_c,v} - J'_{K'_a,K'_c,v'}$	Predicted frequency (MHz)	S_{ij}	E_u (K)	v_{LSR}[(1)] km s^{-1}	Observed frequency (MHz)	Observed T_{MB} (K)[(2)]	Model T_{MB} (K)
$26_{4,23,1}$-$25_{4,22,1}$	248213.627	25.40	1007.4	(5)	...	...	...
$26_{13,13,1}$-$25_{13,12,1}$	248268.793	19.50	1336.0	(9,16)	...	...	...
$26_{13,14,1}$-$25_{13,13,1}$	248268.793†	19.50	1336.0	(9,16)	...	...	...
$26_{4,22,1}$-$25_{4,21,1}$	248314.826	25.40	1007.4	(5,30)	...	...	...
$26_{3,23,0}$-$25_{3,22,0}$	248345.994	25.60	988.2	(17)	...	...	...
$26_{14,12,1}$-$25_{14,11,1}$	248372.316	18.50	1393.4	(17)	...	...	...
$26_{14,13,1}$-$25_{14,12,1}$	248372.316†	18.50	1393.4	(17)	...	...	...
$27_{0,27,0}$-$26_{0,26,0}$	248421.029	27.00	977.4	(16)	...	...	...
$26_{15,11,1}$-$25_{15,10,1}$	248485.601	17.30	1455.0	(5)	...	...	...
$26_{15,12,1}$-$25_{15,11,1}$	248485.601†	17.30	1455.0	(5)	...	...	...
$26_{1,25,0}$-$25_{1,24,0}$	248715.973	25.90	973.1	(5)	...	...	...
$27_{1,27,1}$-$26_{1,26,1}$	248781.879	27.00	982.0	(16)	...	...	...
$26_{3,23,1}$-$25_{3,22,1}$	249605.498	25.70	992.6	3.9[(6,53)]	249606.4	0.27	0.12
$27_{0,27,1}$-$26_{0,26,1}$	249713.036	27.00	981.7	(6,28,73)	...	...	...
$26_{1,25,1}$-$25_{1,24,1}$	250028.952	25.90	977.3	(5)	...	...	...
$26_{2,24,0}$-$25_{2,23,0}$	251279.453	25.90	979.0	(6,16,25)	...	...	...
$26_{2,24,1}$-$25_{2,23,1}$	252526.293	25.80	983.3	(5)	...	...	...
$27_{2,26,0}$-$26_{2,25,0}$	253852.724	26.80	988.4	3.4	253854.1	0.22	0.14
$27_{2,26,1}$-$26_{2,25,1}$	255177.777	26.90	992.8	(14)	...	...	...
$27_{7,21,0}$-$26_{7,20,0}$	256133.723	25.20	1085.7	(6,10)	...	...	...
$27_{7,20,0}$-$26_{7,19,0}$	256133.724†	25.20	1085.7	(6,10)	...	...	...
$27_{8,19,0}$-$26_{8,18,0}$	256148.406	24.60	1117.7	(5)	...	...	...
$27_{8,20,0}$-$26_{8,19,0}$	256148.406†	24.60	1117.7	(5)	...	...	...
$27_{6,22,0}$-$26_{6,21,0}$	256160.590	25.70	1057.9	(5)	...	...	...
$27_{6,21,0}$-$26_{6,20,0}$	256160.690†	25.70	1057.9	(5)	...	...	...
$27_{9,18,0}$-$26_{9,17,0}$	256190.604	24.00	1154.0	(10)	...	...	...
$27_{9,19,0}$-$26_{9,18,0}$	256190.604†	24.00	1154.0	(10)	...	...	...
$27_{10,17,0}$-$26_{10,16,0}$	256253.059	23.30	1194.4	(24)	...	...	...
$27_{10,18,0}$-$26_{10,17,0}$	256253.059†	23.30	1194.4	(24)	...	...	...
$27_{5,23,0}$-$26_{5,22,0}$	256257.793†	26.10	1034.4	(24)	...	...	...
$27_{5,22,0}$-$26_{5,21,0}$	256262.451†	26.10	1034.4	(24)	...	...	...
$27_{3,25,0}$-$26_{3,24,0}$	256311.699	26.70	1000.1	(74)	...	...	...
$27_{11,16,0}$-$26_{11,15,0}$	256331.669	22.50	1239.1	(74)	...	...	...
$27_{11,17,0}$-$26_{11,16,0}$	256331.669†	22.50	1239.1	(74)	...	...	...
$27_{12,15,0}$-$26_{12,14,0}$	256423.946	21.70	1287.8	(15)	...	...	...
$27_{12,16,0}$-$26_{12,15,0}$	256423.946†	21.70	1287.8	(15)	...	...	...
$27_{4,24,0}$-$26_{4,23,0}$	256450.072	26.40	1015.1	(15)	...	...	...

Tabla B.7: continued.

Transition $J_{K_a,K_c,v} - J'_{K'_a,K'_c,v'}$	Predicted frequency (MHz)	S_{ij}	E_u (K)	v_{LSR}[1] km s^{-1}	Observed frequency (MHz)	Observed T_{MB} (K)[2]	Model T_{MB} (K)
$27_{13,14,0}$-$26_{13,13,0}$	256528.285	20.70	1340.6	(15)	...	...	...
$27_{13,15,0}$-$26_{13,14,0}$	256528.285†	20.70	1340.6	(15)	...	...	...
$27_{4,23,0}$-$26_{4,22,0}$	256580.491	26.40	1015.2	(15,72)	...	...	...
$28_{1,28,0}$-$27_{1,27,0}$	256601.331	27.90	990.0	(75)	...	...	...
$27_{14,13,0}$-$26_{14,12,0}$	256643.595	19.70	1397.5	(5)	...	...	...
$27_{14,14,0}$-$26_{14,13,0}$	256643.595†	19.70	1397.5	(5)	...	...	...
$28_{0,28,0}$-$27_{0,27,0}$	257381.906	28.00	989.8	(76)	...	...	...
$27_{7,21,1}$-$26_{7,20,1}$	257464.067	25.20	1091.0	(46)	...	...	...
$27_{7,20,1}$-$26_{7,19,1}$	257464.069†	25.20	1091.0	(46)	...	...	...
$27_{8,19,1}$-$26_{8,18,1}$	257471.569†	24.60	1123.3	(46)	...	...	...
$27_{8,20,1}$-$26_{8,19,1}$	257471.569†	24.60	1123.3	(46)	...	...	...
$27_{6,22,1}$-$26_{6,21,1}$	257497.189	25.70	1062.9	(5,32)	...	...	...
$27_{6,21,1}$-$26_{6,20,1}$	257497.292†	25.70	1062.9	(5,32)	...	...	...
$27_{9,18,1}$-$26_{9,17,1}$	257505.972	24.00	1159.9	(46)	...	...	...
$27_{9,19,1}$-$26_{9,18,1}$	257505.972†	24.00	1159.9	(46)	...	...	...
$27_{10,17,1}$-$26_{10,16,1}$	257560.229	23.30	1200.7	8.2[5]	257556.1	0.17	0.12
$27_{10,18,1}$-$26_{10,17,1}$	257560.229†	23.30	1200.7	8.2[5]	257556.1	”	0.12
$27_{5,23,1}$-$26_{5,22,1}$	257599.051	26.10	1039.2	(19,21,34)	...	...	...
$27_{5,22,1}$-$26_{5,21,1}$	257603.791	26.10	1039.2	5.8	257603.1	0.08	0.15
$27_{11,16,1}$-$26_{11,15,1}$	257630.402	22.50	1245.8	(25)	...	...	...
$27_{11,17,1}$-$26_{11,16,1}$	257630.402†	22.50	1245.8	(25)	...	...	...
$27_{3,25,1}$-$26_{3,24,1}$	257643.992	26.70	1004.6	(16)	...	...	...
$27_{12,15,1}$-$26_{12,14,1}$	257714.128	21.70	1295.0	(5)	...	...	...
$27_{12,16,1}$-$26_{12,15,1}$	257714.128†	21.70	1295.0	(5)	...	...	...
$27_{4,24,1}$-$26_{4,23,1}$	257791.902	26.40	1019.8	(6,19)	...	...	...
$28_{1,28,1}$-$27_{1,27,1}$	257882.687	28.00	994.4	5.7[30]	257882.1	0.09	0.14
$27_{4,23,1}$-$26_{4,22,1}$	257923.042	26.40	1019.8	4.9[30]	257923.2	0.20	0.12
$27_{1,26,0}$-$26_{1,25,0}$	257974.080	26.90	985.5	(77)	...	...	...
$27_{3,24,0}$-$26_{3,23,0}$	258106.295	26.70	1000.6	3.2[32]	258107.8	0.15	0.13
$28_{0,28,1}$-$27_{0,27,1}$	258707.545	28.00	994.1	(6,78,79)	...	...	...
$27_{1,26,1}$-$26_{1,25,1}$	259366.408	26.90	989.8	8.4[44]	259363.5	0.21	0.18
$27_{3,24,1}$-$26_{3,23,1}$	259407.521	26.70	1005.1	4.5[22]	259407.9	0.30	0.12
$27_{2,25,0}$-$26_{2,24,0}$	260955.173	26.90	991.6	5.6	260954.6	0.33	0.14
$27_{2,25,1}$-$26_{2,24,1}$	262296.990	26.90	995.9	(22)	...	...	...
$28_{2,27,0}$-$27_{2,26,0}$	263108.275	27.80	1001.1	(10,13,31)	...	...	...
$28_{2,27,1}$-$27_{2,26,1}$	264494.554	27.90	1005.5	4.8	264494.8	0.23	0.14
$28_{7,22,0}$-$27_{7,21,0}$	265624.865	26.20	1098.4	8.3[5]	265622.0	0.21	0.23

Tabla B.7: continued.

Transition $J_{K_a,K_c,v} - J'_{K'_a,K'_c,v'}$	Predicted frequency (MHz)	S_{ij}	E_u (K)	v_{LSR}[(1)] km s^{-1}	Observed frequency (MHz)	Observed T_{MB} (K)[(2)]	Model T_{MB} (K)
$28_{7,21,0}$-$27_{7,20,0}$	265624.868†	26.20	1098.4	8.3[(5)]	265622.0	”	0.23
$28_{8,20,0}$-$27_{8,19,0}$	265635.639	25.70	1130.5	6.5	265634.3	0.18	0.14
$28_{8,21,0}$-$27_{8,20,0}$	265635.639†	25.70	1130.5	6.5	265634.3	”	0.14
$29_{1,29,0}$-$28_{1,28,0}$	265651.847	29.00	1002.8	4.7[(5)]	265652.1	0.21	0.19
$28_{6,23,0}$-$27_{6,22,0}$	265659.680	26.70	1070.6	6.7	265658.2	0.04	0.19
$28_{6,22,0}$-$27_{6,21,0}$	265659.829†	26.70	1070.6	6.9	265658.2	”	0.19
$28_{9,19,0}$-$27_{9,18,0}$	265676.363	25.10	1166.8	4.4[(80)]	265677.0	0.16	0.11
$28_{9,20,0}$-$27_{9,19,0}$	265676.363†	25.10	1166.8	4.4[(80)]	265677.0	”	0.11
$28_{10,18,0}$-$27_{10,17,0}$	265738.959	24.40	1207.2	[(5)]	...	...	...
$28_{10,19,0}$-$27_{10,18,0}$	265738.959†	24.40	1207.2	[(5)]	...	...	...
$28_{5,24,0}$-$27_{5,23,0}$	265771.712	27.10	1047.1	4.7	265772.0	0.06	0.14
$28_{5,23,0}$-$27_{5,22,0}$	265778.170	27.10	1047.1	4.1[(10)]	265779.0	0.22	0.18
$28_{3,26,0}$-$27_{3,25,0}$	265782.735	27.70	1012.9	5.2[(5)]	265782.6	0.21	0.19
$28_{11,17,0}$-$27_{11,16,0}$	265818.868	23.70	1251.8	[(5)]	...	...	...
$28_{11,18,0}$-$27_{11,17,0}$	265818.868†	23.70	1251.8	[(5)]	...	...	...
$28_{12,16,0}$-$27_{12,15,0}$	265913.329	22.90	1300.5	[(15,81)]	...	...	...
$28_{12,17,0}$-$27_{12,16,0}$	265913.329†	22.90	1300.5	[(15,81)]	...	...	...
$28_{4,25,0}$-$27_{4,24,0}$	265980.475	27.40	1027.9	[(82)]	...	...	...
$28_{13,15,0}$-$27_{13,14,0}$	266020.561	22.00	1353.4	[(9,26)]	...	...	...
$28_{13,16,0}$-$27_{13,15,0}$	266020.561†	22.00	1353.4	[(9,26)]	...	...	...
$28_{14,14,0}$-$27_{14,13,0}$	266139.361	21.00	1410.2	[(25)]	...	...	...
$28_{14,15,0}$-$27_{14,14,0}$	266139.361†	21.00	1410.2	[(25)]	...	...	...
$28_{4,24,0}$-$27_{4,23,0}$	266147.862†	27.40	1027.9	[(25)]	...	...	...
$29_{0,29,0}$-$28_{0,28,0}$	266343.838	29.00	1002.6	4.8	266344.0	0.16	0.15
$29_{1,29,1}$-$28_{1,28,1}$	266977.223	29.00	1007.2	1.9[(32)]	266980.0	0.42	0.18
$28_{7,22,1}$-$27_{7,21,1}$	267004.809	26.30	1103.8	2.4[(83)]	267007.1	0.36	0.30
$28_{7,21,1}$-$27_{7,20,1}$	267004.812†	26.30	1103.8	2.4[(83)]	267007.1	”	0.30
$28_{8,20,1}$-$27_{8,19,1}$	267008.171†	25.70	1136.1	6.2[(83)]	267007.1	”	0.30
$28_{8,21,1}$-$27_{8,19,1}$	267008.171†	25.70	1136.1	6.2[(83)]	267007.1	”	0.30
$28_{9,19,1}$-$27_{9,18,1}$	267040.848	25.10	1172.7	1.5[(5)]	267043.9	0.20	0.17
$28_{9,20,1}$-$27_{9,19,1}$	267040.848†	25.10	1172.7	1.5[(5)]	267043.9	”	0.17
$28_{6,23,1}$-$27_{6,22,1}$	267046.077†	26.70	1075.7	3.2[(35)]	267047.6	0.28	0.21
$28_{6,22,1}$-$27_{6,21,1}$	267046.230†	26.70	1075.7	3.4[(35)]	267047.6	”	0.21
$28_{10,18,1}$-$27_{10,17,1}$	267094.974	24.40	1213.6	6.2[(17)]	267093.9	0.20	0.08
$28_{10,19,1}$-$27_{10,18,1}$	267094.974†	24.40	1213.6	6.2[(17)]	267093.9	”	0.08
$28_{5,24,1}$-$27_{5,23,1}$	267162.885	27.10	1052.0	[(10)]	...	...	...
$28_{3,26,1}$-$27_{3,25,1}$	267164.143†	27.70	1017.5	[(10)]	...	...	...

Tabla B.7: continued.

Transition $J_{K_a,K_c,v} - J'_{K'_a,K'_c,v'}$	Predicted frequency (MHz)	S_{ij}	E_u (K)	v_{LSR}[(1)] km s^{-1}	Observed frequency (MHz)	Observed T_{MB} (K)[(2)]	Model T_{MB} (K)
$28_{11,17,1}$-$27_{11,16,1}$	267166.158†	23.70	1258.6	(10)	...	...	...
$28_{11,18,1}$-$27_{11,17,1}$	267166.158†	23.70	1258.6	(10)	...	...	...
$28_{5,23,1}$-$27_{5,22,1}$	267169.454	27.10	1052.0	(10)	...	...	...
$28_{1,27,0}$-$27_{1,26,0}$	267191.468	27.90	998.4	(7)	...	...	...
$28_{12,16,1}$-$27_{12,15,1}$	267251.765	22.90	1307.8	(5,32)	...	...	...
$28_{12,17,1}$-$27_{12,16,1}$	267251.765†	22.90	1307.8	(5,32)	...	...	...
$28_{13,15,1}$-$27_{13,14,1}$	267350.113	22.00	1361.2	6.2[(84)]	267349.0	0.10	0.05
$28_{13,16,1}$-$27_{13,15,1}$	267350.113†	22.00	1361.2	6.2[(84)]	267349.0	”	0.05
$28_{4,25,1}$-$27_{4,24,1}$	267371.981	27.40	1032.6	(5)	...	...	...
$28_{14,14,1}$-$27_{14,13,1}$	267460.059	21.00	1418.6	(11)	...	...	...
$28_{14,15,1}$-$27_{14,14,1}$	267460.059†	21.00	1418.6	(11)	...	...	...
$28_{4,24,1}$-$27_{4,23,1}$	267540.150	27.40	1032.6	(24)	...	...	...
$29_{0,29,1}$-$28_{0,28,1}$	267705.139	29.00	1007.0	(5)	...	...	...
$28_{3,25,0}$-$27_{3,24,0}$	267891.981	27.70	1013.4	(5)	...	...	...
$28_{1,27,1}$-$27_{1,26,1}$	268663.438	27.90	1002.7	7.8[(13)]	268660.9	0.09	0.18
$28_{3,25,1}$-$27_{3,24,1}$	269233.266	27.70	1018.0	(16,25)	...	...	...
$28_{2,26,0}$-$27_{2,25,0}$	270603.020	27.90	1004.5	3.1[(5)]	270604.8	0.42	0.18
$28_{2,26,1}$-$27_{2,25,1}$	272042.698	27.90	1008.9	(16)	...	...	...
$28_{2,28,0}$-$27_{2,27,0}$	272350.189	28.80	1014.1	(11,85)	...	...	...
$29_{2,28,1}$-$28_{2,27,1}$	273818.703	28.90	1018.7	4.8[(83)]	273818.8	0.22	0.14
$30_{1,30,0}$-$29_{1,29,0}$	274696.519	29.90	1016.0	(41)	...	...	...
$29_{7,23,0}$-$28_{7,22,0}$	275116.514	27.30	1111.7	3.8	275117.5	0.15	0.18
$29_{7,22,0}$-$28_{7,21,0}$	275116.517†	27.30	1111.7	3.8	275117.5	”	0.18
$29_{8,21,0}$-$28_{8,20,0}$	275122.893	26.80	1143.7	(5)	...	...	...
$29_{8,22,0}$-$28_{8,21,0}$	275122.893†	26.80	1143.7	(5)	...	...	...
$29_{6,24,0}$-$28_{6,23,0}$	275160.030	27.80	1083.8	(5)	...	...	...
$29_{6,23,0}$-$28_{6,22,0}$	275160.251†	27.80	1083.8	(5)	...	...	...
$29_{9,20,0}$-$28_{9,19,0}$	275161.817†	26.20	1180.0	(5)	...	...	...
$29_{9,21,0}$-$28_{9,20,0}$	275161.817†	26.20	1180.0	(5)	...	...	...
$29_{10,19,0}$-$28_{10,18,0}$	275224.321	25.60	1220.4	(24)	...	...	...
$29_{10,20,0}$-$28_{10,19,0}$	275224.321†	25.60	1220.4	(24)	...	...	...
$29_{3,27,0}$-$28_{3,26,0}$	275245.625	28.70	1026.1	(24)	...	...	...
$29_{5,25,0}$-$28_{5,24,0}$	275287.974	28.10	1060.3	(5)	...	...	...
$29_{5,24,0}$-$28_{5,23,0}$	275296.818	28.10	1060.3	(5)	...	...	...
$29_{11,18,0}$-$28_{11,17,0}$	275305.355	24.80	1265.0	(5)	...	...	...
$29_{11,19,0}$-$28_{11,18,0}$	275305.355†	24.80	1265.0	(5)	...	...	...
$30_{0,30,0}$-$29_{0,29,0}$	275307.423†	30.00	1015.8	(5)	...	...	...

Tabla B.7: continued.

Transition $J_{K_a,K_c,v} - J'_{K'_a,K'_c,v'}$	Predicted frequency (MHz)	S_{ij}	E_u (K)	v_{LSR}[(1)] km s^{-1}	Observed frequency (MHz)	Observed T_{MB} (K)[(2)]	Model T_{MB} (K)
$29_{12,17,0}$-$28_{12,16,0}$	275401.865	24.00	1313.8	(15)	...	...	...
$29_{12,18,0}$-$28_{12,17,0}$	275401.865†	24.00	1313.8	(15)	...	...	...
$29_{13,16,0}$-$28_{13,15,0}$	275511.887	23.20	1366.6	(6,86)	...	...	...
$29_{13,17,0}$-$28_{13,16,0}$	275511.887†	23.20	1366.6	(6,86)	...	...	...
$29_{4,26,0}$-$28_{4,25,0}$	275512.381†	28.40	1041.1	(6,86)	...	...	...
$29_{14,15,0}$-$28_{14,14,0}$	275634.091	22.20	1423.5	(5)	...	...	...
$29_{14,16,0}$-$28_{14,15,0}$	275634.091†	22.20	1423.5	(5)	...	...	...
$29_{4,25,0}$-$28_{4,24,0}$	275725.124	28.40	1041.2	(46,76)	...	...	...
$30_{1,30,0}$-$29_{1,29,1}$	276065.857	30.00	1020.4	(27)	...	...	...
$29_{1,28,0}$-$28_{1,27,0}$	276368.853	28.90	1011.6	3.6	276370.1	0.21	0.19
$29_{8,21,1}$-$28_{8,20,1}$	276544.817	26.80	1149.4	(67)	...	...	...
$29_{8,22,1}$-$28_{8,21,1}$	276544.817†	26.80	1149.4	(67)	...	...	...
$29_{7,23,1}$-$28_{7,22,1}$	276546.077†	27.30	1117.1	(67)	...	...	...
$29_{7,22,1}$-$28_{7,21,1}$	276546.080†	27.30	1117.1	(67)	...	...	...
$29_{9,20,1}$-$28_{9,19,1}$	276575.444	26.20	1186.0	4.6	276575.8	0.15	0.17
$29_{9,21,1}$-$28_{9,20,1}$	276575.444†	26.20	1186.0	4.6	276575.8	”	0.17
$29_{6,24,1}$-$28_{6,23,1}$	276596.242	27.80	1089.0	(14)	...	...	...
$29_{6,23,1}$-$28_{6,22,1}$	276596.467†	27.80	1089.0	(14)	...	...	...
$29_{10,19,1}$-$28_{10,18,1}$	276629.209	25.60	1226.8	(15,32,43)	...	...	...
$29_{10,20,1}$-$28_{10,19,1}$	276629.209†	25.60	1226.8	(15,32,43)	...	...	...
$29_{3,27,1}$-$28_{3,26,1}$	276676.119	28.70	1030.7	(67)	...	...	...
$29_{11,18,1}$-$28_{11,17,1}$	276701.232	24.80	1271.9	(11,67)	...	...	...
$29_{11,19,1}$-$28_{11,18,1}$	276701.232†	24.80	1271.9	(11,67)	...	...	...
$30_{0,30,1}$-$29_{0,29,1}$	276705.948†	30.00	1020.2	(11,67)	...	...	...
$29_{5,25,1}$-$28_{5,24,1}$	276729.066	28.10	1065.3	(5,33)	...	...	...
$29_{5,24,1}$-$28_{5,23,1}$	276738.058	28.10	1065.3	(67)	...	...	...
$29_{12,17,1}$-$28_{12,16,1}$	276788.590	24.00	1321.1	(5)	...	...	...
$29_{12,18,1}$-$28_{12,17,1}$	276788.590†	24.00	1321.1	(5)	...	...	...
$29_{4,26,1}$-$28_{4,25,1}$	276953.517	28.50	1045.9	(9,43)	...	...	...
$29_{4,25,1}$-$28_{4,24,1}$	277167.061	28.50	1045.9	(6,11,26)	...	...	...
$29_{3,26,0}$-$28_{3,25,0}$	277702.204	28.70	1026.8	(5)	...	...	...
$29_{1,28,1}$-$28_{1,27,1}$	277917.094	28.90	1016.0	(16,26)	...	...	...
$29_{3,26,1}$-$28_{3,25,1}$	279081.801	28.70	1031.4	(6,17)	...	...	...

Tabla A10. Emission lines of CH_2CHCN v_{10}=1⇔(v_{11}=1,v_{15}=1) present in the spectral scan of the Orion-KL from the radio-telescope of IRAM 30-m. The quantum number v is corresponded with the

vibrational level, and take the value ν=0 and ν=1 whether the state is v_{10}=1 or (v_{11}=1,v_{15}=1), respectively. Column 1 indicates the line transition, Col. 2 gives the predicted frequency in the laboratory, Col. 3 the line strength, Col. 4 upper level energy, Col. 5 observed radial velocities relative to the local system rest (v_{LSR}), Col. 6 observed centroid frequencies assuming a v_{LSR} of 5 km s^{-1}, Col. 7 observed main beam temperature, y Col. 8 mean beam temperature obtained with the model. † blended with the last one. ∗∗ hole in the observed spectrum.

(1) peak channel line observed velocity. (2) peak channel line intensity. (3) blended with ^{33}SO. (4) blended with HCS^+. (5) blended with U-line. (6) blended with $HCOOCH_3$. (7) blended with SO. (8) blended with $CH_3CH_2C^{15}N$. (9) blended with $(CH_3)_2CO$. (10) blended with CH_3OCH_3. (11) blended with CH_3OH. (12) blended with HDCS. (13) blended with $^{13}CH_3OH$. (14) blended with $CH_2{}^{13}CHCN$. (15) blended with CH_2CHCN. (16) blended with CH_3CH_2CN. (17) blended with $^{34}SO_2$. (18) blended with $CH_2CH^{13}CN$. (19) blended with $CH_3C^{15}N$. (20) blended with CH_3CN v_8=1. (21) blended with c-C_2H_4O. (22) blended with $CH_3CH_2{}^{13}CN$. (23) blended with CH_2CHCN v_{15}=1. (24) blended with SO_2. (25) blended with CH_3CH_2CN v_{13}/v_{21}. (26) blended with $|g_+$-$g_-|$-CH_3CH_2OH. (27) blended with CH_3OD. (28) blended with $CH_3{}^{13}CH_2CN$. (29) blended with CH_3CH_2CN v_{20}=1. (30) blended with CH_2CHCN v_{11}=2. (31) blended with CH_3CHO. (32) blended with CH_2CHCN v_{11}=1. (33) blended with $^{13}CH_2CHCN$. (34) blended with $H^{13}COOCH_3$. (35) blended with $SO^{17}O$. (36) blended with $OC^{36}S$. (37) blended with SO_2 v_2=1. (38) blended with HCCCN v_7=2. (39) blended with $H_2{}^{13}CS$. (40) blended with NH_2CHO. (41) blended with H_2CS. (42) blended with $^{33}SO_2$. (43) blended with $HCOO^{13}CH_3$. (44) blended with $^{13}CH_3CH_2CN$. (45) blended with $HCC^{13}CN$ v_7=2. (46) blended with CH_3CN. (47) blended with $DCOOCH_3$. (48) blended with $HC^{13}CCN$ ν=0. (49) blended with SiS. (50) blended with $O^{13}CS$. (51) blended with H_2CO. (52) blended with HCCCN. (53) blended with t-CH_3CH_2OH. (54) blended with $CH_3{}^{18}OH$. (55) blended with $C^{18}O$. (56) blended with $O^{34}S^{18}O$. (57) blended with HDCO. (58) blended with HCCCN v_6=1. (59) blended with $HNC^{18}O$. (60) blended with $SO^{18}O$. (61) blended with CO. (62) blended with HCCCN v_6=2. (63) blended with HCCCN v_7=3. (64) blended with CH_3COOH v_t=0. (65) blended with CH_2CHCN v_{11}=3. (66) blended with CH_2CDCN. (67) blended with CH_3CN v_8=1. (68) blended with CCCS. (69) blended with $HCC^{13}CN$. (70) blended with ^{34}SO. (71) blended with $H^{13}CCCN$. (72) blended with HDO. (73) blended with $^{13}CH_3CN$. (74) blended with CH_3CCH. (75) blended with HDCS. (76) blended with $CH_3{}^{13}CN$. (77) blended with HCOOH. (78) blended with SiO. (79) blended with SiO ν=1. (80) blended with DCOOH. (81) blended with HCN. (82) blended with $H_2C^{34}S$. (83) blended with NH_2CHO v_{12}=1. (84) blended with $CH_2CHC^{15}N$. (85) blended with CH_3OD. (86) blended with DCHCHCN.

Tabla B.8: Detected lines of $^{13}C_1$, $^{13}C_2$, and $^{13}C_3$ isotopologues of CH_2CHCN. .

Transition $J_{K_a,K_c} - J'_{K'_a,K'_c}$	Predicted frequency (MHz)	S_{ij}	E_u (K)	v_{LSR}[1] km s^{-1}	Observed frequency (MHz)	Observed T_{MB} (K)[3]	Model T_{MB} (K)
Detected lines of $^{13}CH_2CHCN$							
$9_{1,9}$-$8_{1,8}$	81051.736	8.89	21.6	5.54	81051.6	0.01	0.01
$9_{2,8}$-$8_{2,7}$	83064.074	8.56	28.5	5.66[2]	83063.9	0.01	0.01
$9_{4,6}$-$8_{4,5}$	83172.144	7.22	54.2	2.66	83172.8	0.01	0.01
$9_{4,5}$-$8_{4,4}$	83172.189†	7.22	54.2	2.82	”	”	”
$9_{3,6}$-$8_{3,5}$	83187.779	8.00	39.2	6.34[2]	83187.4	0.02	0.01
$9_{6,4}$-$8_{6,3}$	83188.121†	5.00	96.8	7.57[2]	”	”	”
$9_{6,3}$-$8_{6,2}$	83188.121†	5.00	96.8	7.57[2]	”	”	”
$9_{2,7}$-$8_{2,6}$	83449.819	8.56	28.5	6.59	83449.4	0.01	0.01
$10_{4,7}$-$9_{4,6}$	92418.684	8.40	58.6	6.26[3]	92418.3	0.08	0.02
$10_{4,6}$-$9_{4,5}$	92418.782†	8.40	58.6	6.58[3]	”	”	”
$10_{3,8}$-$9_{3,7}$	92432.345	9.10	43.6	5.28	92432.3	0.04	0.01
$10_{6,5}$-$9_{6,4}$	92432.545†	6.40	101.3	5.92	”	”	”
$10_{6,4}$-$9_{6,3}$	92432.545†	6.40	101.3	5.92	”	”	”
$10_{2,8}$-$9_{2,7}$	92802.577	9.60	33.0	3.54[2,4]	92803.1	0.02	0.01
$11_{1,11}$-$10_{1,10}$	99006.148	10.90	30.7	3.49[2]	99006.7	0.04	0.01
$11_{5,7}$-$10_{5,6}$	101665.997	8.73	82.7	1.28	101667.6	0.03	0.03
$11_{5,6}$-$10_{5,5}$	101665.998†	8.73	82.7	1.28	”	”	”
$11_{4,8}$-$10_{4,7}$	101666.845†	9.55	63.5	3.78	”	”	”
$11_{4,7}$-$10_{4,6}$	101667.041†	9.55	63.5	4.36	”	”	”
$11_{6,6}$-$10_{6,5}$	101677.377	7.73	106.1	5.78	101677.1	0.01	0.01
$11_{6,5}$-$10_{6,4}$	101677.377†	7.73	106.1	5.78	”	”	”
$11_{3,8}$-$10_{3,7}$	101705.350	10.20	48.5	5.62	101705.1	0.02	0.01
$11_{1,10}$-$10_{1,9}$	103814.998	10.91	32.1	7.55	103814.1	0.03	0.02
$12_{1,12}$-$11_{1,11}$	107971.949	11.90	35.9	4.48[5]	107972.2	0.04	0.02
$12_{5,8}$-$11_{5,7}$	110912.196	9.92	88.0	5.55[6]	110912.0	0.010	0.03
$12_{5,7}$-$11_{5,6}$	110912.199†	9.92	88.0	5.55[6]	”	”	”
$12_{7,6}$-$11_{7,5}$	110942.195	7.92	139.1	6.90	110941.5	0.03	0.03
$12_{7,5}$-$11_{7,4}$	110942.195†	7.92	139.1	6.90	”	”	”
$12_{3,10}$-$11_{3,9}$	110942.268†	11.20	53.8	7.10	”	”	”
$12_{8,5}$-$11_{8,4}$	110968.372	6.67	171.0	2.09	110971.0	0.01	0.01
$12_{8,4}$-$11_{8,3}$	110968.372†	6.67	171.0	2.09	”	”	”
$12_{3,9}$-$11_{3,8}$	110972.076†	11.20	53.8	7.91	”	”	”
$12_{1,11}$-$11_{1,10}$	113208.132	11.90	37.5	6.48	113207.6	0.05	0.02
$14_{1,13}$-$13_{1,12}$	131955.171	13.90	49.7	8.06[3]	131953.8	0.13	0.03

Tabla B.8: continued.

Transition $J_{K_a,K_c} - J'_{K'_a,K'_c}$	Predicted frequency (MHz)	S_{ij}	E_u (K)	v_{LSR}[(1)] km s^{-1}	Observed frequency (MHz)	Observed T_{MB} (K)[(3)]	Model T_{MB} (K)
$15_{2,14}$-$14_{2,13}$	138228.563	14.70	61.7	5.78	138228.3	0.08	0.03
$15_{5,11}$-$14_{5,10}$	138657.101	13.30	106.6	1.60[(2)]	138658.6	0.08	0.05
$15_{5,10}$-$14_{5,9}$	138657.119†	13.30	106.6	1.64[(2)]	”	”	”
$15_{4,12}$-$14_{4,11}$	138678.606	13.90	87.4	3.79	138679.1	0.08	0.07
$15_{4,11}$-$14_{4,10}$	138678.418†	13.90	87.4	7.71	”	”	”
$15_{7,9}$-$14_{7,8}$	138680.928†	11.70	157.8	8.81	”	”	”
$15_{7,8}$-$14_{7,7}$	138680.928†	11.70	157.8	8.81	”	”	”
$16_{0,16}$-$15_{0,15}$	145706.594	16.00	59.8	5.07	145706.6	0.05	0.04
$16_{7,10}$-$15_{7,9}$	147927.617	12.90	164.9	5.08[(2)]	147927.5	0.14	0.06
$16_{7,9}$-$15_{7,8}$	147927.617†	12.90	164.9	5.08[(2)]	”	”	”
$16_{2,14}$-$15_{2,13}$	149423.658	15.70	69.2	6.18[(2)]	149423.1	0.18	0.04
$17_{0,17}$-$16_{0,16}$	154577.622	17.00	67.2	1.56[(2)]	154579.3	0.10	0.05
$17_{2,16}$-$16_{2,15}$	156553.396	16.80	76.3	8.64[(3)]	156551.3	0.24	0.05
$17_{1,16}$-$16_{1,15}$	159954.627	16.90	71.4	4.96	159954.7	0.07	0.05
$18_{0,18}$-$17_{0,17}$	163421.683	18.00	75.1	7.18	163420.5	0.07	0.06
$18_{6,13}$-$17_{6,12}$	166405.983	16.00	152.7	6.13	166405.4	0.10	0.07
$18_{6,12}$-$17_{6,11}$	166405.984†	16.00	152.7	6.13	”	”	”
$18_{5,14}$-$17_{5,13}$	166413.159	16.60	129.3	7.79	166411.6	0.07	0.09
$18_{5,13}$-$17_{5,12}$	166413.256†	16.60	129.3	7.97	”	”	”
$18_{7,12}$-$17_{7,11}$	166421.746	15.30	180.4	5.19	166421.7	0.08	0.06
$18_{7,11}$-$17_{7,10}$	166421.746†	15.30	180.4	5.19	”	”	”
$18_{8,11}$-$17_{8,10}$	166452.312	14.40	212.3	7.71[(2)]	166450.8	0.11	0.04
$18_{8,10}$-$17_{8,9}$	166452.312†	14.40	212.3	7.71[(2)]	”	”	”
$18_{4,15}$-$17_{4,14}$	166461.008	17.10	110.1	6.18	166460.4	0.10	0.05
$18_{4,14}$-$17_{4,13}$	166467.589	17.10	110.1	4.49	166467.9	0.11	0.05
$18_{3,15}$-$17_{3,14}$	166742.703	17.50	95.2	3.96[(2)]	166743.3	0.07	0.05
$18_{2,16}$-$17_{2,15}$	168467.430	17.80	84.9	6.48[(2)]	168466.6	0.18	0.05
$18_{1,17}$-$17_{1,16}$	169248.732	17.90	79.5	8.82[(2)]	169246.5	0.20	0.06
$22_{0,22}$-$21_{0,21}$	198591.415	22.00	110.7	3.79[(7)]	198592.3	0.18	0.08
$22_{4,19}$-$21_{4,18}$	203539.866	21.30	110.7	0.49[(2)]	203542.9	0.21	0.08
$22_{10,12}$-$21_{10,11}$	203542.989†	17.50	325.0	5.09[(2)]	”	”	”
$22_{10,13}$-$21_{10,12}$	203542.989†	17.50	325.0	5.09[(2)]	”	”	”
$22_{12,11}$-$21_{12,10}$	203688.767	15.50	417.9	6.24	203687.9	0.07	0.02
$22_{12,10}$-$21_{12,9}$	203688.767†	15.50	417.9	6.24	”	”	”
$22_{2,20}$-$21_{2,19}$	206665.745	21.80	121.9	6.75	206664.5	0.10	0.08
$23_{2,22}$-$22_{2,21}$	211281.591	22.80	130.6	6.13	211280.8	0.05	0.09
$23_{6,18}$-$22_{6,17}$	212661.615	21.43	199.3	5.35	212661.4	0.13	0.21

Tabla B.8: continued.

Transition $J_{K_a,K_c} - J'_{K'_a,K'_c}$	Predicted frequency (MHz)	S_{ij}	E_u (K)	v_{LSR}[1] km s^{-1}	Observed frequency (MHz)	Observed T_{MB} (K)[3]	Model T_{MB} (K)
$23_{6,17}$-$22_{6,16}$	212661.628†	21.43	199.3	5.37	”	”	”
$23_{7,17}$-$22_{7,16}$	212662.107†	20.90	227.0	6.01	”	”	”
$23_{7,16}$-$22_{7,15}$	212662.108†	20.90	227.0	6.01	”	”	”
$23_{8,16}$-$22_{8,15}$	212688.554	20.20	258.9	5.42	212688.3	0.15	0.08
$23_{8,15}$-$22_{8,14}$	212688.554†	20.20	258.9	5.42	”	”	”
$23_{5,19}$-$22_{5,18}$	212703.782	21.90	175.9	7.47	212702.1	0.06	0.13
$23_{5,18}$-$22_{5,17}$	212704.692†	21.90	175.9	8.76	”	”	”
$23_{9,15}$-$22_{9,14}$	212733.075	19.50	295.0	4.68[8]	212733.3	0.23	0.12
$23_{9,14}$-$22_{9,13}$	212733.075†	19.50	295.0	4.68[8]	”	”	”
$23_{4,19}$-$22_{4,18}$	212852.690	22.30	156.7	5.95[9]	212852.0	0.19	0.08
$23_{12,12}$-$22_{12,11}$	212942.218	16.70	428.1	2.27[2]	212944.2	0.09	0.06
$23_{12,11}$-$22_{12,10}$	212942.218†	16.70	428.1	2.27[2]	”	”	”
$24_{1,24}$-$23_{1,23}$	214886.764	23.90	131.5	5.54[2]	214886.3	0.26	0.10
$23_{1,22}$-$22_{1,21}$	215342.365	22.94	126.8	3.70	215343.3	0.12	0.15
$24_{0,24}$-$23_{0,23}$	216098.566	24.00	131.0	1.97[2]	216100.7	0.13	0.10
$24_{7,18}$-$23_{7,17}$	221911.151	22.00	237.6	4.02[10]	221911.8	0.27	0.14
$24_{7,17}$-$23_{7,16}$	221911.151†	22.00	237.6	4.02[10]	”	”	”
$24_{11,13}$-$23_{11,12}$	222111.873	19.00	390.3	5.01	222111.8	0.07	0.08
$24_{11,14}$-$23_{11,13}$	222111.873†	19.00	390.3	5.01	”	”	”
$24_{3,21}$-$23_{3,20}$	222997.260	23.60	152.6	5.48	222996.9	0.12	0.09
$25_{1,25}$-$24_{1,24}$	223741.761	24.90	142.2	6.54[2]	223740.6	0.20	0.10
$25_{4,22}$-$24_{4,21}$	231375.833	24.40	178.4	5.41	231375.5	0.11	0.13
$26_{1,26}$-$25_{1,25}$	232589.519	26.00	153.4	6.71	232588.2	0.09	0.11
$25_{1,24}$-$24_{1,23}$	233569.104	24.90	148.8	6.22[11,12]	233568.2	0.20	0.16
$26_{5,22}$-$25_{5,21}$	240499.668	25.00	209.2	4.88[2]	240499.8	0.28	0.11
$26_{5,21}$-$25_{5,20}$	240502.420†	25.00	209.2	8.31[2]	”	”	”
$26_{10,17}$-$25_{10,16}$	240534.575	22.20	368.5	5.54	240534.2	0.11	0.06
$26_{10,16}$-$25_{10,15}$	240534.575†	22.20	368.5	5.54	”	”	”
$27_{2,26}$-$26_{2,25}$	247530.387	26.80	175.5	4.08	247531.1	0.33	0.11
$27_{4,24}$-$26_{4,23}$	249944.482	26.40	202.0	5.31[2]	249944.3	0.15	0.10
$29_{0,29}$-$28_{0,28}$	259803.026	29.00	189.2	6.28	259801.9	0.19	0.19
$28_{1,27}$-$27_{1,26}$	260646.346	27.90	185.0	5.37[2]	260646.0	0.12	0.68
$28_{3,25}$-$27_{3,24}$	260902.720	27.70	200.0	5.78[2]	260902.0	0.91	0.11
$29_{2,28}$-$28_{2,27}$	265577.461	28.80	200.5	6.71	265576.0	0.18	0.12
$29_{6,24}$-$28_{6,23}$	268198.935	27.80	269.9	6.32[13,14,15]	268197.7	0.57	0.16
$29_{6,23}$-$28_{6,22}$	268199.113†	27.80	269.9	6.52[13,14,15]	”	”	”
$30_{8,23}$-$29_{8,22}$	277418.158	27.90	342.8	5.55[6,13]	277417.7	0.34	0.23

Tabla B.8: continued.

Transition $J_{K_a,K_c} - J'_{K'_a,K'_c}$	Predicted frequency (MHz)	S_{ij}	E_u (K)	v_{LSR}[(1)] km s^{-1}	Observed frequency (MHz)	Observed T_{MB} (K)[(3)]	Model T_{MB} (K)
$30_{8,22}$-$29_{8,21}$	277418.158†	27.90	342.8	5.55[(6,13)]	”	”	”
$30_{1,29}$-$29_{1,28}$	278516.492	29.90	211.3	6.32	278514.8	0.57	0.12
Detected lines of $CH_2{}^{13}CHCN$							
$9_{4,6}$-$8_{4,5}$	84961.208	7.22	54.1	0.86	84962.9	0.01	0.01
$9_{4,5}$-$8_{4,4}$	84961.208†	7.22	54.1	0.65	”	”	”
$9_{5,5}$-$8_{5,4}$	84963.011†	6.22	73.0	5.50	”	”	”
$9_{5,4}$-$8_{5,3}$	84963.011†	6.22	73.0	5.50	”	”	”
$9_{2,7}$-$8_{2,6}$	85278.270	8.56	28.9	8.17[(2)]	85277.4	0.02	0.01
$10_{1,10}$-$9_{1,9}$	91880.967	9.90	26.4	7.35[(16)]	91880.3	0.01	0.01
$10_{0,10}$-$9_{0,9}$	93739.396	9.99	24.8	2.44[(2)]	93740.1	0.02	0.01
$10_{2,8}$-$9_{2,7}$	94844.358	9.60	33.4	5.42[(17)]	94844.2	0.01	0.01
$11_{2,10}$-$10_{2,9}$	103648.488	10.60	38.3	6.19[(16)]	103648.1	0.04	0.01
$11_{5,7}$-$10_{5,6}$	103851.088	8.73	82.5	4.94	103851.1	0.01	0.02
$11_{5,6}$-$10_{5,5}$	103851.088†	8.73	82.5	4.95	”	”	”
$11_{4,8}$-$10_{4,7}$	103855.518	9.55	63.6	4.65	103855.6	0.01	0.02
$11_{4,7}$-$10_{4,6}$	103855.773†	9.55	63.6	5.38	”	”	”
$11_{6,6}$-$10_{6,5}$	103859.695	7.73	105.6	6.71	103859.1	0.01	0.02
$11_{6,5}$-$10_{6,4}$	103859.695†	7.73	105.6	6.71	”	”	”
$11_{3,9}$-$10_{3,8}$	103879.329	10.20	48.9	5.72	103879.1	0.01	0.01
$11_{8,4}$-$10_{8,3}$	103898.217	5.18	164.3	5.28	103898.1	0.01	0.01
$11_{8,3}$-$10_{8,2}$	103898.217†	5.18	164.3	5.28	”	”	”
$11_{3,8}$-$10_{3,7}$	103902.551	10.20	48.9	6.18	103902.1	0.03	0.01
$12_{0,12}$-$11_{0,11}$	112181.663	12.00	35.1	1.51[(2)]	112183.0	0.03	0.02
$12_{6,7}$-$11_{6,6}$	113303.920	9.00	111.1	2.29	113304.9	0.08	0.04
$12_{6,6}$-$11_{6,5}$	113303.920†	9.00	111.1	2.29	”	”	”
$12_{4,9}$-$11_{4,8}$	113305.692†	10.70	69.0	6.98	”	”	”
$12_{4,8}$-$11_{4,7}$	113306.168†	10.70	69.0	8.24	”	”	”
$12_{3,9}$-$11_{3,8}$	113372.402	11.20	54.3	3.59[(2,15)]	113372.9	0.04	0.03
$12_{9,4}$-$11_{9,3}$	113372.466†	5.25	205.3	3.76[(2,15)]	”	”	”
$12_{9,3}$-$11_{9,2}$	113372.466†	5.25	205.3	3.76[(2,15)]	”	”	”
$14_{0,14}$-$13_{0,13}$	130481.709	14.00	47.2	5.48	130481.5	0.09	0.03
$14_{5,10}$-$13_{5,9}$	132191.757	12.20	100.2	4.38[(2)]	132192.0	0.13	0.05
$14_{5,9}$-$13_{5,8}$	132191.770†	12.20	100.2	4.41[(2)]	”	”	”
$14_{6,9}$-$13_{6,8}$	132194.320†	11.40	123.3	7.81[(2)]	”	”	”
$14_{6,8}$-$13_{6,7}$	132194.320†	11.40	123.3	7.81[(2)]	”	”	”
$14_{7,8}$-$13_{7,7}$	132210.248	10.50	150.6	6.59	132209.5	0.03	0.05
$14_{7,7}$-$13_{7,6}$	132210.248†	10.50	150.6	6.59	132209.5	0.03	0.05

Tabla B.8: continued.

Transition $J_{K_a,K_c} - J'_{K'_a,K'_c}$	Predicted frequency (MHz)	S_{ij}	E_u (K)	v_{LSR}[1] km s^{-1}	Observed frequency (MHz)	Observed T_{MB} (K)[3]	Model T_{MB} (K)
$14_{4,11}$-$13_{4,10}$	132212.906	12.90	81.3	1.40	132214.4	0.05	0.05
$14_{4,10}$-$13_{4,9}$	132214.343†	12.90	81.3	4.66	”	”	”
$14_{9,6}$-$13_{9,5}$	132267.130	8.21	217.6	3.32	132267.8	0.03	0.01
$14_{9,5}$-$13_{9,4}$	132267.130†	8.21	217.6	3.32	”	”	”
$14_{3,11}$-$13_{3,10}$	132335.676	13.40	66.6	1.92[7,18]	132337.0	0.05	0.05
$15_{1,15}$-$14_{1,14}$	137566.400	14.90	55.0	5.42[2]	137566.2	0.08	0.03
$15_{4,12}$-$14_{4,11}$	141670.249	13.90	88.1	0.02[3,7,16]	141672.6	0.19	0.04
$15_{4,11}$-$14_{4,10}$	141672.597†	13.90	88.1	4.98[3,7,16]	”	”	”
$15_{8,8}$-$14_{8,7}$	141681.016	10.70	188.8	4.66	141681.2	0.10	0.03
$15_{8,7}$-$14_{8,6}$	141681.016†	10.70	188.8	4.66	”	”	”
$15_{9,7}$-$14_{9,6}$	141714.333	9.60	224.4	5.89	141713.9	0.08	0.02
$15_{9,6}$-$14_{9,5}$	141714.333†	9.60	224.4	5.89	”	”	”
$15_{1,14}$-$14_{1,13}$	144397.619	14.90	57.7	3.90[2]	144398.2	0.11	0.04
$16_{6,11}$-$15_{6,10}$	151087.659	13.80	137.4	4.25[2]	151088.1	0.08	0.06
$16_{6,10}$-$15_{6,9}$	151087.660†	13.80	137.4	4.26[2]	”	”	”
$16_{5,12}$-$15_{5,11}$	151092.389	14.40	114.2	3.80	151093.0	0.07	0.07
$16_{5,11}$-$15_{5,10}$	151092.435†	14.40	114.2	3.89	”	”	”
$16_{7,10}$-$15_{7,9}$	151101.329	12.90	164.6	7.18[2]	151100.2	0.05	0.04
$16_{7,9}$-$15_{7,8}$	151101.329†	12.90	164.6	7.18[2]	”	”	”
$16_{3,14}$-$15_{3,13}$	151185.941	15.40	80.6	5.83[2]	151185.5	0.14	0.04
$16_{3,13}$-$15_{3,12}$	151338.305	15.40	80.6	5.48[3]	151338.1	0.16	0.04
$16_{2,14}$-$15_{2,13}$	152792.900	15.70	70.4	5.78	152792.5	0.07	0.04
$16_{1,15}$-$15_{1,14}$	153925.602	15.90	65.0	3.55	153926.3	0.10	0.04
$17_{1,17}$-$16_{1,16}$	155774.417	16.90	69.5	4.90	155774.4	0.08	0.05
$17_{0,17}$-$16_{0,16}$	157676.383	17.00	68.6	3.96[19]	157676.9	0.15	0.05
$17_{2,16}$-$16_{2,15}$	159872.600	16.80	77.6	3.88[2]	159873.2	0.14	0.05
$17_{3,15}$-$16_{3,14}$	160651.973	16.50	88.3	4.28	160652.4	0.11	0.07
$17_{10,8}$-$16_{10,7}$	160652.085†	11.10	279.0	4.48	”	”	”
$17_{10,7}$-$16_{10,6}$	160652.085†	11.10	279.0	4.48	”	”	”
$17_{3,14}$-$16_{3,13}$	160857.742	16.50	88.3	0.98[2]	160859.9	0.15	0.05
$18_{1,18}$-$17_{1,17}$	164863.832	17.90	77.4	3.03[2]	164864.9	0.10	0.06
$18_{5,14}$-$17_{5,13}$	169999.413	16.60	130.1	5.25	169999.2	0.13	0.09
$18_{5,13}$-$17_{5,12}$	169999.549†	16.60	130.1	5.49	”	”	”
$21_{7,15}$-$20_{7,14}$	198336.172	18.70	207.7	4.26	198336.7	0.18	0.18
$21_{7,14}$-$20_{7,13}$	198336.172†	18.70	207.7	4.26	”	”	”
$21_{6,16}$-$20_{6,15}$	198336.544†	19.30	180.4	4.83	”	”	”
$21_{6,15}$-$20_{6,14}$	198336.552†	19.30	180.4	4.84	”	”	”

Tabla B.8: continued.

Transition $J_{K_a,K_c} - J'_{K'_a,K'_c}$	Predicted frequency (MHz)	S_{ij}	E_u (K)	v_{LSR}[(1)] km s^{-1}	Observed frequency (MHz)	Observed T_{MB} (K)[(3)]	Model T_{MB} (K)
$21_{8,14}$-$20_{8,13}$	198358.019	18.00	239.1	1.45[(2)]	198360.4	0.12	0.07
$21_{8,13}$-$20_{8,12}$	198358.019†	18.00	239.1	1.45[(2)]	”	”	”
$21_{5,17}$-$20_{5,16}$	198373.594	19.80	157.3	7.06	198372.3	0.08	0.12
$21_{5,16}$-$20_{5,15}$	198374.147†	19.80	157.3	7.90	”	”	”
$21_{3,18}$-$20_{3,17}$	199092.108	20.60	123.8	8.64[(20)]	199089.6	0.15	0.08
$21_{1,20}$-$20_{1,19}$	201198.679	20.90	108.8	5.42[(21)]	201198.4	0.32	0.08
$21_{2,19}$-$20_{2,18}$	201592.022	20.80	114.1	2.97[(12)]	201593.4	0.13	0.08
$22_{0,22}$-$21_{0,21}$	202505.143	20.00	112.9	5.04	202505.1	0.12	0.12
$22_{2,20}$-$21_{2,19}$	211359.784	21.80	124.3	7.08[(3)]	211358.3	0.18	0.13
$23_{0,23}$-$22_{0,22}$	211429.215	23.00	123.1	6.22[(2)]	211428.4	0.28	0.14
$23_{2,22}$-$22_{2,21}$	215711.803	22.80	133.0	6.48	215710.7	0.19	0.09
$23_{10,13}$-$22_{10,12}$	217338.842	18.70	334.8	6.02[(2)]	217338.1	0.11	0.10
$23_{10,14}$-$22_{10,13}$	217338.842†	18.70	334.8	6.02[(2)]	”	”	”
$23_{4,19}$-$22_{4,18}$	217478.958	22.30	158.8	2.97[(7,22)]	217480.4	0.18	0.18
$23_{13,11}$-$22_{13,10}$	217555.655	15.70	478.1	5.21[(23)]	217555.5	0.07	0.05
$23_{13,10}$-$22_{13,9}$	217555.655†	15.70	478.1	5.21[(23)]	”	”	”
$24_{4,21}$-$23_{4,20}$	226914.854	23.30	169.7	8.17[(2,8)]	226912.5	0.34	0.11
$24_{1,23}$-$23_{1,22}$	229192.300	23.90	140.5	4.84[(2)]	229192.4	0.31	0.11
$24_{2,22}$-$23_{2,21}$	230867.264	23.80	146.0	4.96	230867.3	0.15	0.10
$25_{8,18}$-$24_{8,17}$	236144.993	22.40	281.7	5.75[(12)]	236144.3	0.23	0.18
$25_{8,17}$-$24_{8,16}$	236144.993†	22.40	281.7	5.75[(12)]	”	”	”
$25_{4,21}$-$24_{4,20}$	236485.130	24.40	181.1	4.43[(16)]	236485.5	0.21	0.09
$26_{12,15}$-$25_{12,14}$	245823.098	20.50	460.3	4.84[(7)]	245823.2	0.25	0.04
$26_{12,14}$-$25_{12,13}$	245823.098†	20.50	460.3	4.84[(7)]	”	”	”
$27_{7,21}$-$26_{7,20}$	255034.614	25.20	274.3	6.01	255033.8	0.13	0.15
$27_{7,20}$-$26_{7,19}$	255034.616†	25.20	274.3	6.01	”	”	”
$28_{0,28}$-$27_{0,27}$	255998.483	28.00	180.2	3.03[(2)]	256000.2	0.09	0.12
$28_{7,22}$-$27_{7,21}$	264486.421	26.30	287.0	6.95[(2)]	264484.7	0.39	0.20
$28_{7,21}$-$27_{7,20}$	264486.424†	26.30	287.0	6.96[(2)]	”	”	”
$28_{8,21}$-$27_{8,20}$	264486.614†	25.70	318.5	7.17[(2)]	”	”	”
$28_{8,20}$-$27_{8,19}$	264486.614†	25.70	318.5	7.17[(2)]	”	”	”
$28_{6,23}$-$27_{6,22}$	264532.104	26.70	259.8	7.06	264532.5	0.08	0.15
$28_{6,22}$-$27_{6,21}$	264532.282†	26.70	259.8	7.06	”	”	”
$28_{10,19}$-$27_{10,18}$	264568.160	24.40	393.7	4.56	264566.5	0.13	0.07
$28_{10,18}$-$27_{10,17}$	264568.160†	24.40	393.7	4.56	”	”	”
$28_{11,17}$-$27_{11,16}$	264636.565	23.70	437.5	4.75	264636.8	0.12	0.12
$28_{11,18}$-$27_{11,17}$	264636.565†	23.70	437.5	4.75	”	”	”

Tabla B.8: continued.

Transition $J_{K_a,K_c} - J'_{K'_a,K'_c}$	Predicted frequency (MHz)	S_{ij}	E_u (K)	v_{LSR}[(1)] km s^{-1}	Observed frequency (MHz)	Observed T_{MB} (K)[(3)]	Model T_{MB} (K)
$28_{3,26}$-$27_{3,25}$	264645.465	27.70	203.1	5.60[(2)]	264645.0	0.37	0.12
$28_{4,25}$-$27_{4,24}$	264871.923	27.40	217.8	6.01[(7)]	264871.1	0.17	0.07
$29_{4,25}$-$28_{4,24}$	274598.803	28.40	231.0	6.07	274597.8	0.16	0.11
$29_{1,28}$-$28_{1,27}$	275088.323	28.90	202.1	6.54	275086.9	0.29	0.12
Detected lines of $CH_2CH^{13}CN$							
$9_{5,5}$-$8_{5,4}$	85041.672	6.22	74.4	2.61[(2)]	85042.4	0.02	0.01
$9_{5,4}$-$8_{5,3}$	85041.672†	6.22	74.4	2.61[(2)]	”	”	”
$9_{6,4}$-$8_{6,3}$	85053.074	5.00	98.1	3.16	85055.4	0.01	0.01
$9_{6,3}$-$8_{6,2}$	85053.074†	5.00	98.1	3.16	”	”	”
$9_{3,6}$-$8_{3,5}$	85055.519†	8.00	39.9	5.47	”	”	”
$10_{0,10}$-$9_{0,9}$	93864.835	9.99	24.8	3.50[(2)]	93865.2	0.02	0.01
$10_{4,7}$-$9_{4,6}$	94492.465	8.40	59.5	4.19	94492.7	0.01	0.02
$10_{4,6}$-$9_{4,5}$	94492.573†	8.40	59.5	4.53	”	”	”
$10_{5,6}$-$9_{5,5}$	94493.595†	7.50	78.9	7.78	”	”	”
$10_{5,5}$-$9_{5,4}$	94493.596†	7.50	78.9	7.78	”	”	”
$10_{6,5}$-$9_{6,4}$	94504.845	6.40	102.7	6.95	94504.2	0.01	0.01
$10_{6,4}$-$9_{6,3}$	94504.845†	6.40	102.7	6.95	”	”	”
$10_{1,9}$-$9_{1,8}$	96546.691	9.90	27.7	6.55	96546.2	0.02	0.01
$11_{5,7}$-$10_{5,6}$	103946.416	8.73	83.9	5.81	103946.1	0.01	0.02
$11_{5,6}$-$10_{5,5}$	103946.417†	8.73	83.9	5.82	”	”	”
$11_{4,8}$-$10_{4,7}$	103948.418	9.55	64.5	3.41	103949.1	0.01	0.03
$11_{4,7}$-$10_{4,6}$	103948.418†	9.55	64.5	3.41	”	”	”
$11_{3,9}$-$10_{3,8}$	103969.448	10.20	49.4	7.01[(2)]	103973.6	0.01	0.01
$11_{7,5}$-$10_{7,4}$	103975.484	6.55	135.6	3.20	103976.1	0.01	0.01
$11_{7,4}$-$10_{7,3}$	103975.484†	6.55	135.6	3.20	”	”	”
$11_{3,8}$-$10_{3,7}$	103990.119	10.18	49.4	7.62	103989.2	0.03	0.02
$11_{1,10}$-$10_{1,9}$	106162.668	10.90	32.8	3.90	106163.1	0.03	0.01
$12_{5,8}$-$11_{5,7}$	113400.222	9.92	89.4	3.07	113401.0	0.05	0.03
$12_{5,7}$-$11_{5,6}$	113400.225†	9.92	89.4	3.07	”	”	”
$14_{5,10}$-$13_{5,9}$	132311.141	12.20	101.6	2.72	132312.1	0.03	0.04
$14_{5,9}$-$13_{5,8}$	132311.152†	12.20	101.6	2.75	”	”	”
$14_{6,9}$-$13_{6,8}$	132316.868	11.40	125.3	5.75	132316.5	0.05	0.04
$14_{6,8}$-$13_{6,7}$	132316.868†	11.40	125.3	5.75	”	”	”
$14_{4,11}$-$13_{4,10}$	132328.201	12.90	82.2	4.70	132328.3	0.01	0.05
$14_{4,10}$-$13_{4,9}$	132328.201†	12.90	82.2	7.47	”	”	”
$14_{7,8}$-$13_{7,7}$	132335.677	10.50	153.3	3.20[(18,24)]	132336.4	0.05	0.05
$14_{7,7}$-$13_{7,6}$	132335.677†	10.50	153.3	3.20[(18,24)]	”	”	”

Tabla B.8: continued.

Transition $J_{K_a,K_c} - J'_{K'_a,K'_c}$	Predicted frequency (MHz)	S_{ij}	E_u (K)	v_{LSR}[(1)] km s^{-1}	Observed frequency (MHz)	Observed T_{MB} (K)[(3)]	Model T_{MB} (K)
$14_{9,5}$-$13_{9,4}$	132398.474	8.21	222.1	3.14[(2)]	132399.3	0.04	0.02
$14_{9,6}$-$13_{9,5}$	132398.474†	8.21	222.1	3.14[(2)]	”	”	”
$15_{1,15}$-$14_{1,14}$	137797.972	14.90	55.2	2.29[(5)]	137799.3	0.05	0.04
$15_{5,11}$-$14_{5,10}$	141768.428	13.30	108.4	6.69[(3,16,24)]	141767.6	0.10	0.06
$15_{5,10}$-$14_{5,9}$	141768.448†	13.30	108.4	6.73[(3,16,24)]	”	”	”
$15_{6,10}$-$14_{6,9}$	141771.326	12.60	132.1	6.40	141770.6	0.05	0.06
$15_{6,9}$-$14_{6,8}$	141771.326†	12.60	132.1	6.40	”	”	”
$15_{4,12}$-$14_{4,11}$	141792.584	13.90	89.0	4.85[(18)]	141792.7	0.18	0.06
$15_{4,11}$-$14_{4,10}$	141794.576†	13.90	89.0	9.06[(18)]	”	”	”
$16_{2,15}$-$15_{2,14}$	150690.654	15.70	70.2	7.11[(2)]	150689.6	0.11	0.04
$16_{6,11}$-$15_{6,10}$	151226.450	13.80	139.4	5.74	151226.1	0.19	0.11
$16_{6,10}$-$15_{6,9}$	151226.450†	13.80	139.4	5.74	”	”	”
$16_{5,12}$-$15_{5,11}$	151227.049†	14.40	115.7	6.93	”	”	”
$16_{5,11}$-$15_{5,10}$	151227.086†	14.40	115.7	7.00	”	”	”
$16_{7,10}$-$15_{7,9}$	151243.718	12.90	167.4	7.71[(2)]	151242.4	0.15	0.04
$16_{7,9}$-$15_{7,8}$	151243.718†	12.90	167.4	7.71[(2)]	”	”	”
$16_{9,8}$-$15_{9,7}$	151310.922	10.90	236.1	3.26[(25)]	151311.8	0.14	0.06
$16_{9,7}$-$15_{9,6}$	151310.922†	10.90	236.1	3.26[(25)]	”	”	”
$16_{3,14}$-$15_{3,13}$	151311.820†	15.40	81.2	5.04[(25)]	”	”	”
$16_{3,13}$-$15_{3,12}$	151447.586	15.40	81.2	4.02	151448.1	0.04	0.04
$16_{1,15}$-$15_{1,14}$	154034.309	15.90	65.1	7.66[(2)]	154032.9	0.07	0.05
$17_{0,17}$-$16_{0,16}$	157978.097	17.00	68.7	6.25[(2)]	157977.4	0.18	0.05
$17_{5,13}$-$16_{5,12}$	160687.089	15.50	123.4	1.63[(2)]	160688.9	0.11	0.09
$17_{5,12}$-$16_{5,11}$	160687.154†	15.50	123.4	1.75[(2)]	”	”	”
$17_{8,10}$-$16_{8,9}$	160727.492	13.20	207.4	3.29	160728.4	0.06	0.08
$17_{8,9}$-$16_{8,8}$	160727.492†	13.20	207.4	3.29	”	”	”
$17_{4,14}$-$16_{4,13}$	160728.776†	13.20	207.4	5.69	”	”	”
$17_{4,13}$-$16_{4,12}$	160733.611	16.10	104.0	9.16	160731.4	0.06	0.06
$17_{1,16}$-$16_{1,15}$	163555.565	16.90	73.0	7.36[(2)]	163554.3	0.15	0.05
$18_{0,18}$-$17_{0,17}$	167011.915	18.00	76.7	4.25	167012.3	0.10	0.06
$21_{9,12}$-$20_{9,11}$	198588.933	17.10	279.3	7.61[(2,26)]	198587.2	0.31	0.11
$21_{9,13}$-$20_{9,12}$	198588.933†	17.10	279.3	7.61[(2,26)]	”	”	”
$21_{4,17}$-$20_{4,16}$	198654.522	20.20	139.4	4.75[(27)]	198654.6	0.20	0.07
$21_{13,9}$-$20_{13,8}$	198864.217	13.00	467.0	6.22[(2)]	198863.4	0.10	0.04
$21_{13,8}$-$20_{13,7}$	198864.217†	13.00	467.0	6.22[(2)]	”	”	”
$22_{1,22}$-$21_{1,21}$	201496.193	21.95	113.7	3.60	201497.1	0.10	0.13
$22_{5,18}$-$21_{5,17}$	208011.503	20.90	168.8	5.06	208011.4	0.14	0.13

Tabla B.8: continued.

Transition $J_{K_a,K_c} - J'_{K'_a,K'_c}$	Predicted frequency (MHz)	S_{ij}	E_u (K)	v_{LSR}[1] km s^{-1}	Observed frequency (MHz)	Observed T_{MB} (K)[3]	Model T_{MB} (K)
$22_{5,17}$-$21_{5,16}$	208012.186†	20.90	168.8	6.04	”	”	”
$22_{4,18}$-$21_{4,17}$	208145.690	21.30	149.4	4.84[14]	208145.8	0.60	0.14
$22_{3,20}$-$21_{3,19}$	208147.515†	21.60	134.3	7.47[14]	”	”	”
$22_{3,19}$-$21_{3,18}$	208793.453	21.60	134.4	3.38[13]	208794.6	0.16	0.08
$22_{1,21}$-$21_{1,20}$	210792.865	21.90	119.1	7.06	210791.4	0.05	0.09
$23_{8,16}$-$22_{8,15}$	217455.913	20.20	263.2	5.08[20]	217455.9	0.23	0.15
$23_{8,15}$-$22_{8,14}$	217455.913†	20.20	263.2	5.08[20]	”	”	”
$23_{5,19}$-$22_{5,18}$	217481.788	21.90	179.2	6.81[22,24]	217480.5	0.18	0.18
$23_{5,18}$-$22_{5,17}$	217482.809†	21.90	179.2	6.81[22,24]	”	”	”
$23_{10,14}$-$22_{10,13}$	217555.669	18.70	340.4	5.47[24]	217555.3	0.11	0.07
$23_{10,13}$-$22_{10,12}$	217555.669†	18.70	340.4	5.47[24]	”	”	”
$23_{1,22}$-$22_{1,21}$	220152.450	22.90	129.6	5.55[13]	220152.1	0.29	0.15
$23_{8,17}$-$22_{8,16}$	226910.697	21.30	274.1	3.47[8,28]	226912.0	0.20	0.16
$23_{8,16}$-$22_{8,15}$	226910.697†	21.30	274.1	3.47[8,28]	”	”	”
$24_{9,16}$-$23_{9,15}$	226953.129	20.60	310.6	3.41	226954.4	0.24	0.20
$24_{9,15}$-$23_{9,14}$	226953.129†	20.60	310.6	3.41	”	”	”
$24_{5,20}$-$23_{5,19}$	226954.048†	23.00	190.1	4.63	”	”	”
$24_{5,19}$-$23_{5,18}$	226955.550†	23.00	190.1	6.61	”	”	”
$24_{3,22}$-$23_{3,21}$	227078.166	23.60	155.6	3.54[2]	227079.3	0.23	0.15
$24_{11,14}$-$23_{11,13}$	227078.166†	19.00	396.2	8.29[2]	”	”	”
$24_{11,13}$-$23_{11,12}$	227078.166†	19.00	396.2	8.29[2]	”	”	”
$24_{4,20}$-$23_{4,19}$	227144.220	23.30	170.7	4.84	227144.4	0.22	0.08
$25_{5,21}$-$24_{5,20}$	236428.352	24.00	201.5	3.99	236429.1	0.33	0.14
$25_{5,20}$-$24_{5,19}$	236430.522†	24.00	201.5	6.76	”	”	”
$25_{4,22}$-$24_{4,21}$	236580.913	24.40	182.1	3.74	236581.9	0.17	0.14
$26_{7,20}$-$25_{7,19}$	245803.734	24.10	265.0	6.76[2]	245802.3	0.43	0.12
$26_{7,19}$-$25_{7,18}$	245803.734†	24.10	265.0	6.76[2]	”	”	”
$26_{8,19}$-$25_{8,18}$	245820.291	23.50	297.2	1.42[24]	245823.2	0.25	0.23
$26_{8,18}$-$25_{8,17}$	245820.291†	23.50	297.2	1.42[24]	”	”	”
$26_{6,21}$-$25_{6,20}$	245823.610†	24.60	237.0	5.47[24]	”	”	”
$26_{6,20}$-$25_{6,19}$	245823.671†	24.60	237.0	5.55[24]	”	”	”
$26_{4,22}$-$25_{4,21}$	246168.061	25.40	193.9	6.60	246166.7	0.05	0.10
$27_{0,27}$-$26_{0,26}$	247623.100	27.00	168.3	4.95[2]	247623.1	0.27	0.18
$27_{6,22}$-$26_{6,21}$	255288.823	25.70	249.2	3.79	255289.8	0.07	0.16
$27_{6,21}$-$26_{6,20}$	255288.952†	25.70	249.2	3.90	”	”	”
$27_{3,25}$-$26_{3,24}$	255438.888	26.70	191.0	7.55[2]	255436.7	0.16	0.18
$28_{1,28}$-$27_{1,27}$	255765.736	28.00	180.8	5.72	255765.1	0.17	0.12

Tabla B.8: continued.

Transition $J_{K_a,K_c} - J'_{K'_a,K'_c}$	Predicted frequency (MHz)	S_{ij}	E_u (K)	v_{LSR}[(1)] km s^{-1}	Observed frequency (MHz)	Observed T_{MB} (K)[(3)]	Model T_{MB} (K)
$28_{7,22}$-$27_{7,21}$	264720.544	26.30	289.9	3.34	264722.0	0.18	0.17
$28_{7,21}$-$27_{7,20}$	264720.546†	26.30	289.9	3.35	”	”	”
$29_{1,29}$-$28_{1,28}$	264786.504	29.00	193.5	4.48[(2)]	264787.0	0.32	0.20
$28_{5,23}$-$27_{5,22}$	264870.124	27.10	238.2	4.00[(24)]	264871.0	0.18	0.21
$28_{3,26}$-$27_{3,25}$	264879.672	27.70	203.8	4.63[(2)]	264880.0	0.12	0.15
$28_{4,25}$-$27_{4,24}$	265066.247	27.40	218.9	7.35[(2,29)]	265064.2	0.25	0.17
$29_{2,28}$-$28_{2,27}$	271471.236	28.85	204.9	4.81[(2)]	271471.4	0.29	0.20
$30_{1,30}$-$30_{1,29}$	273801.416	30.00	206.7	3.42[(4,16)]	273802.8	0.41	0.12
$29_{9,21}$-$28_{9,20}$	274221.324	26.20	371.8	6.93[(2)]	274219.5	0.24	0.21
$29_{9,20}$-$28_{9,19}$	274221.324†	26.20	371.8	6.93[(2)]	”	”	”
$29_{6,24}$-$28_{6,23}$	274222.768†	27.80	275.1	8.51[(2)]	”	”	”
$29_{6,23}$-$28_{6,22}$	274222.971†	27.80	275.1	8.73[(2)]	”	”	”
$29_{3,27}$-$28_{3,26}$	274312.655	28.70	216.9	5.05	274312.6	0.20	0.11
$29_{5,25}$-$28_{5,24}$	274347.147	28.10	251.4	4.46[(30)]	274347.6	0.22	0.10
$30_{0,30}$-$29_{0,29}$	274419.275	30.00	206.5	6.75	274417.6	0.14	0.12

Tabla A11. Emission lines of of $^{13}CH_2CHCN$, $CH_2{}^{13}CHCN$ and $CH_2CH^{13}CN$ isotopologues in its ground state present in the spectral scan of the Orion-KL from the radio-telescope of IRAM 30-m. Column 1 indicates the line transition, Col. 2 gives the predicted frequency in the laboratory, Col. 3 the line strength, Col. 4 upper level energy, Col. 5 observed radial velocities relatives (v_{LSR}), Col. 6 observed centroid frequencies assuming a v_{LSR} of 5 km s^{-1}, Col. 7 observed mean beam temperature, and Col. 8 mean beam temperature obtained with the model. † blended with the last one.
(1) peak line intensity. (2) blended with U-line. (3) blended with $HCOOCH_3$. (4) blended with $CH_2CHC^{15}N$. (5) blended with $DCOOCH_3$. (6) blended with $HCOO^{13}CH_3$. (7) blended with $CH_2CH^{13}CN$. (8) blended with g_+-CH_3CH_2OH. (9) blended with H_2CCS. (10) blended with CH_3CH_2CN v_{13}/v_{21} (11) blended with CH_3CCD. (12) blended with t-CH_3CH_2OH. (13) blended with CH_3CH_2CN. (14) blended with CH_2CHCN v_{11}=1. (15) blended with CH_3COOH v_t=0. (16) blended with $(CH_3)_2CO$. (17) blended with CH_2CHCN $v_{10}/v_{11}v_{15}$. (18) blended with $H^{13}COOCH_3$. (19) blended with $SO^{18}O$. (20) blended with CH_3CHO. (21) blended with $SO^{17}O$. (22) blended with ^{13}CN. (23) blended with $CH_2CH^{13}CN$. (24) blended with $CH_2{}^{13}CHCN$. (25) blended with $HCOOCH_3$ v_t=1. (26) blended with $^{13}CH_2CHCN$. (27) blended with NH_2D. (28) blended with $^{13}CH_3OH$. (29) blended with $^{33}SO_2$. (30) blended with SO_2 v_2=2.

Tabla B.9: Detected lines of vinyl isocyanide (CH_2CHNC) .

Transition $J_{K_a,K_c} - J'_{K'_a,K'_c}$	Predicted frequency (MHz)	S_{ij}	E_u (K)	v_{LSR}[(1)] km s^{-1}	Observed frequency (MHz)	Observed T_{MB} (K)[(2)]	Model T_{MB} (K)
$9_{2,8}$-$8_{2,7}$	92222.557	8.56	31.0	2.74	92223.3	0.02	0.01
$9_{3,7}$-$8_{3,6}$	92376.457	8.00	42.2	8.82[(3)]	92375.3	0.03	0.01
$9_{6,4}$-$8_{6,3}$	92379.404	5.00	102.0	5.48[(7)]	92379.3	0.01	0.01
$9_{6,3}$-$8_{6,2}$	92379.404†	5.00	102.0	5.48[(7)]	92379.3	0.01	0.01
$9_{3,6}$-$8_{3,5}$	92386.902	8.00	42.2	6.95	92386.3	0.02	0.01
$9_{1,8}$-$8_{1,7}$	94492.306	8.89	24.9	5.01[(3)]	94492.3	0.03	0.01
$10_{2,9}$-$9_{3,8}$	102444.894	9.60	36.0	4.21	102445.1	0.03	0.01
$10_{5,6}$-$9_{5,5}$	102633.298	7.50	82.6	2.57	102634.1	0.03	0.03
$10_{5,5}$-$9_{5,4}$	102633.299†	7.50	82.6	2.57	102634.1	0.03	0.03
$10_{4,7}$-$9_{4,6}$	102633.302†	8.40	62.6	2.58	102634.1	0.03	0.03
$10_{4,6}$-$9_{4,5}$	102633.470†	8.40	62.6	3.07	102634.1	0.03	0.03
$10_{6,5}$-$9_{6,4}$	102645.824	6.40	107.0	1.27	102647.1	0.03	0.01
$10_{6,4}$-$9_{6,3}$	102645.824†	6.40	107.0	1.27	102647.1	0.03	0.01
$10_{7,4}$-$9_{7,3}$	102666.246	5.10	135.7	2.47	102667.1	0.02	0.01
$10_{7,3}$-$9_{7,2}$	102666.246†	5.10	135.7	2.47	102667.1	0.02	0.01
$10_{1,9}$-$9_{1,8}$	104951.762	9.90	30.0	1.74	104952.9	0.04	0.02
$11_{1,11}$-$10_{1,10}$	109739.072	10.90	33.9	2.54[(7)]	109739.9	0.05	0.02
$11_{0,11}$-$10_{0,10}$	111869.523	11.00	32.3	5.88	111869.2	0.02	0.02
$11_{5,7}$-$10_{5,6}$	112901.295	8.73	88.0	0.95[(7)]	112902.8	0.06	0.02
$11_{5,6}$-$10_{5,5}$	112901.297†	8.73	88.0	0.96[(7)]	112902.8	0.06	0.02
$11_{4,8}$-$10_{4,7}$	112905.398	9.55	68.1	6.20[(4)]	112904.9	0.08	0.03
$11_{4,7}$-$10_{4,6}$	112905.735†	9.55	68.1	7.10[(4)]	112904.9	0.08	0.03
$11_{3,9}$-$10_{3,8}$	112931.938	10.20	52.5	0.07[(5)]	112933.8	0.03	0.02
$11_{7,5}$-$10_{7,4}$	112934.052†	6.55	141.1	5.68[(5)]	112933.8	0.03	0.02
$11_{7,4}$-$10_{7,3}$	112934.052†	6.55	141.1	5.68[(5)]	112933.8	0.03	0.02
$11_{3,8}$-$10_{3,7}$	112960.948	10.20	52.5	2.10[(7)]	112962.0	0.05	0.02
$11_{8,3}$-$10_{8,2}$	112962.337†	5.18	174.2	5.79[(7)]	112962.0	0.05	0.02
$11_{8,4}$-$10_{8,3}$	112962.337†	5.18	174.2	5.79[(7)]	112962.0	0.05	0.02
$13_{2,12}$-$12_{2,11}$	133062.524	12.70	53.6	3.41[(6)]	133063.2	0.04	0.03
$13_{3,10}$-$12_{3,9}$	133566.376	12.30	64.8	6.48	133565.7	0.04	0.03
$13_{2,11}$-$12_{2,10}$	134563.575	12.70	53.9	4.75[(7)]	134563.7	0.08	0.04
$14_{0,14}$-$13_{0,13}$	141702.008	14.00	51.3	5.82	141701.6	0.04	0.04
$14_{2,13}$-$13_{2,12}$	143249.491	13.70	60.5	7.69	143248.2	0.06	0.04
$14_{5,10}$-$13_{5,9}$	143713.735	12.20	107.2	5.20[(8)]	143713.6	0.08	0.06
$14_{5,9}$-$13_{5,8}$	143713.754†	12.20	107.2	5.23[(8)]	143713.6	0.08	0.06
$15_{5,11}$-$14_{5,10}$	153987.760	13.30	114.6	2.25[(7)]	153989.1	0.04	0.12

Tabla B.9: continued.

Transition $J_{K_a,K_c} - J'_{K'_a,K'_c}$	Predicted frequency (MHz)	S_{ij}	E_u (K)	v_{LSR}[(1)] km s^{-1}	Observed frequency (MHz)	Observed T_{MB} (K)[(2)]	Model T_{MB} (K)
$15_{5,10}$-$14_{5,9}$	153987.760†	13.30	114.6	2.25[(7)]	153989.1	0.04	0.12
$15_{6,10}$-$14_{6,9}$	153988.814†	12.60	139.0	4.30[(7)]	153989.1	0.04	0.12
$15_{6,9}$-$14_{6,8}$	153988.814†	12.60	139.0	4.30[(7)]	153989.1	0.04	0.12
$15_{1,14}$-$14_{1,13}$	157010.812	14.90	62.6	3.35[(9)]	157011.7	0.12	0.06
$16_{6,11}$-$15_{6,10}$	164260.029	13.80	146.9	4.75	164260.2	0.08	0.08
$16_{6,10}$-$15_{6,9}$	164260.029†	13.80	146.9	4.75	164260.2	0.08	0.08
$16_{5,12}$-$15_{5,11}$	164263.585†	14.40	122.5	4.19	164264.0	0.10	0.09
$16_{5,11}$-$15_{5,10}$	164263.649†	14.40	122.5	4.31	164264.0	0.10	0.09
$16_{1,15}$-$15_{1,14}$	167360.847	15.90	70.7	8.16	167359.1	0.11	0.07
$17_{6,12}$-$16_{6,11}$	174532.261	14.90	155.3	3.65[(7)]	174533.1	0.14	0.08
$17_{6,11}$-$16_{6,10}$	174532.262†	14.90	155.3	3.65[(7)]	174533.1	0.14	0.08
$19_{2,17}$-$18_{2,16}$	198094.397	18.80	103.3	4.50[(10)]	198094.8	0.09	0.10
$19_{1,18}$-$18_{1,17}$	198245.681	18.90	97.7	8.79	198242.9	0.10	0.10
$20_{3,18}$-$19_{3,17}$	205532.002	19.50	123.5	8.41	205529.7	0.10	0.10
$21_{1,21}$-$20_{1,20}$	208561.673	20.90	112.7	2.99	208563.0	0.15	0.12
$21_{0,21}$-$20_{0,20}$	210109.177	21.00	112.1	6.30[(11)]	210108.3	0.17	0.12
$21_{9,13}$-$20_{9,12}$	215713.949	17.10	293.0	4.28	215714.4	0.07	0.08
$21_{9,12}$-$20_{9,11}$	215713.949†	17.10	293.0	4.28	215714.4	0.07	0.08
$22_{7,16}$-$21_{7,15}$	225908.459	19.80	233.3	0.49[(7)]	225911.9	0.29	0.25
$22_{7,15}$-$21_{7,14}$	225908.459†	19.80	233.3	0.49[(7)]	225911.9	0.29	0.25
$22_{6,17}$-$21_{6,16}$	225910.824†	20.40	204.5	3.63[(7)]	225911.9	0.29	0.25
$22_{6,16}$-$21_{6,15}$	225910.824†	20.40	204.5	3.63[(7)]	225911.9	0.29	0.25
$22_{5,18}$-$21_{5,17}$	225962.718	20.90	180.2	2.81	225964.4	0.14	0.18
$22_{5,17}$-$21_{5,16}$	225963.898†	20.90	180.2	4.38	225964.4	0.14	0.18
$23_{0,23}$-$22_{0,22}$	229481.234	23.00	133.7	4.25	229481.8	0.17	0.14
$22_{2,20}$-$21_{2,19}$	229980.848	21.80	134.9	3.77[(8)]	229981.8	0.17	0.14
$23_{5,19}$-$22_{5,18}$	236254.284	21.90	191.5	3.58[(7)]	236255.3	0.44	0.30
$23_{9,15}$-$22_{9,14}$	236255.997†	19.50	315.2	5.75[(7)]	236255.3	0.44	0.30
$23_{9,14}$-$22_{9,13}$	236255.997†	19.50	315.2	5.75[(7)]	236255.3	0.44	0.30
$23_{5,18}$-$22_{5,17}$	236256.048†	21.90	191.5	5.82[(7)]	236255.3	0.44	0.30
$23_{3,21}$-$22_{3,20}$	236384.511	22.60	156.1	2.19	236386.7	0.12	0.13
$24_{0,24}$-$23_{0,23}$	239157.986	24.00	145.1	4.55	239158.3	0.12	0.15
$24_{2,23}$-$23_{2,22}$	244431.193	23.80	156.0	7.21[(12)]	244429.3	0.28	0.15
$24_{4,21}$-$23_{4,20}$	246718.016	23.30	183.4	4.81[(13)]	246718.2	0.22	0.13
$25_{2,24}$-$24_{2,23}$	254469.066	24.80	168.2	5.05[(14)]	254469.0	0.28	0.16
$25_{9,17}$-$24_{9,16}$	256797.427	21.80	339.4	5.40	256797.1	0.13	0.13
$25_{9,16}$-$24_{9,15}$	256797.427†	21.80	339.4	5.40	256797.1	0.13	0.13

Tabla B.9: continued.

Transition $J_{K_a,K_c} - J'_{K'_a,K'_c}$	Predicted frequency (MHz)	S_{ij}	E_u (K)	v_{LSR}[(1)] km s^{-1}	Observed frequency (MHz)	Observed T_{MB} (K)[(2)]	Model T_{MB} (K)
$25_{3,23}$-$24_{3,22}$	256927.817	24.60	180.2	4.81	256928.0	0.17	0.15
$26_{2,25}$-$25_{2,24}$	264490.900	25.80	180.9	7.03	264489.1	0.34	0.17
$26_{7,20}$-$25_{7,19}$	267007.551	24.10	281.6	4.87[(4)]	267007.6	0.37	0.20
$26_{7,19}$-$25_{7,18}$	267007.552†	24.10	281.6	4.87[(4)]	267007.6	0.37	0.20
$26_{6,21}$-$25_{6,20}$	267038.205	24.60	252.8	2.94[(8)]	267040.0	0.26	0.23
$26_{6,20}$-$25_{6,19}$	267038.322†	24.60	252.8	3.07[(8)]	267040.0	0.26	0.23
$26_{4,23}$-$25_{4,22}$	267352.714	25.40	208.6	3.70[(7)]	267353.8	0.15	0.15
$27_{1,27}$-$26_{1,26}$	267369.330	26.90	182.6	6.76	267367.7	0.20	0.18
$26_{13,13}$-$25_{13,12}$	267442.899	19.50	544.7	5.15	267442.7	0.16	0.06
$26_{13,14}$-$25_{13,13}$	267442.899†	19.50	544.7	5.15	267442.7	0.16	0.06
$27_{2,26}$-$26_{2,25}$	274496.540	26.80	194.1	5.30	274496.2	0.18	0.18
$27_{6,22}$-$26_{6,21}$	277323.960	25.70	266.1	5.15	277323.8	0.27	0.24
$27_{6,21}$-$26_{6,20}$	277324.137†	25.70	266.1	5.34	277323.8	0.27	0.24
$27_{10,17}$-$26_{10,16}$	277406.493	23.30	407.2	5.15[(15)]	277406.4	0.21	0.12
$27_{10,18}$-$26_{10,17}$	277406.493†	23.30	407.2	5.15[(15)]	277406.4	0.21	0.12

Tabla A12. Emission lines of vinyl isocyanide (CH_2CHNC) present in the spectral scan of the Orion-KL from the radio-telescope of IRAM 30-m. Column 1 indicates the line transition, Col. 2 gives the predicted frequency in the laboratory, Col. 3 the line strength, Col. 4 upper level energy, Col. 5 observed radial velocities relatives (v_{LSR}), Col. 6 observed centroid frequencies assuming a v_{LSR} of 5 km s^{-1}, Col. 7 observed mean beam temperature, and Col. 8 mean beam temperature obtained with the model. † blended with the last one.

(1) peak line observed velocity. (2) peak line intensity. (3) blended with HCOOCH3 v_t=1. (4) blended with $HCOOCH_3$. (5) blended with $H^{13}COOCH_3$. (6) blended with CH_2CHCN. (7) blended with U-line. (8) blended with $SO^{18}O$. (9) blended with $DCOOCH_3$. (10) blended with O-H_2CS. (11) blended with HCDCHCN. (12) blended with CH_3CH_2CN. (13) blended with $(CH_3)_2CO$. (14) blended with $CH_3CH_2C^{15}N$. (15) blended with $HCOO^{13}CH_3$.

Apéndice C

Tercero et al. 2013, ApJ, 770, L13

Tabla C.1: Líneas de CH_3OCOCH_3 en Orión-KL con los datos de IRAM-30m.

J	K_a	K_c	p	J'	K'_a	K'_c	p'	State	ν_{lab}(MHz)	$e_{\nu_{lab}}$(MHz)	E_{upp}(K)	$S_{ij}\mu^2(D^2)$	ν_{obs}(MHz)	$f_{\nu_{obs}}$(MHz)	T_{MB}(K)	Blend
13	0	13		12	1	12		E3	82779.635	0.012	28.6	31.30	82780.2	b	0.03	CH_3CH_2CN, $^{33}SO_2$
13	0	13		12	1	12		E4	82779.725	0.012	28.6	31.30	82780.2	d		
13	0	13		12	1	12		EA	82780.026	0.012	28.6	31.30	82780.2	d		
13	1	13		12	0	12		E4	82808.862	0.012	28.6	31.30	82809.2	b	0.04	$HCOOCH_3$ ν_t=1
13	1	13		12	0	12		E3	82808.881	0.012	28.6	31.30	82809.2	d		
13	1	13		12	0	12		EA	82809.267	0.012	28.6	31.30	82809.2	d		
13	0	13		12	1	12		AE	82823.351	0.012	28.6	31.30	82823.2	b	0.04	
13	0	13	1	12	1	12	1	AA	82823.702	0.012	28.6	31.30	82823.2	d		
13	1	13		12	0	12		AE	82860.672	0.012	28.6	31.30	82860.3	b	0.04	
13	1	13	1	12	0	12	1	AA	82861.088	0.012	28.6	31.30	82860.3	d		
13	-1	12		12	2	11		AE	88005.836	0.013	31.8	23.80	88004.3	b	0.04	U-line,CH_3CH_2OCOH
13	1	12	-1	12	2	11	-1	AA	88006.476	0.012	31.8	23.80	88004.3	d		
14	0	14		13	1	13		E3	88939.251	0.015	32.8	34.00	88004.3	b		CH_3OH
14	0	14		13	1	13		E4	88939.307	0.015	32.8	34.00	88004.3	d		
14	0	14		13	1	13		EA	88939.623	0.015	32.8	34.00	88004.3	d		
14	1	14		13	0	13		E3	88953.729	0.015	32.8	34.00	88954.2	b	0.05	
14	1	14		13	0	13		E4	88953.732	0.015	32.8	34.00	88954.2	d		
14	1	14		13	0	13		EA	88954.100	0.015	32.8	34.00	88954.2	d		
14	0	14		13	1	13		AE	88984.328	0.015	32.9	34.00	88984.2	b	0.03	
14	0	14	1	13	1	13	1	AA	88984.680	0.015	32.9	34.00	88984.2	d		
14	1	14		13	0	13		AE	89002.931	0.015	32.9	34.00	89003.1	b	0.02	
14	1	14	1	13	0	13	1	AA	89003.318	0.015	32.9	34.00	89003.1	d		
14	-1	13		13	2	12		E3	94313.817	0.014	36.3	26.70	94315.2	b	0.03	
14	-1	13		13	2	12		E4	94314.988	0.014	36.3	26.70	94315.2	d		
14	-1	13		13	2	12		EA	94315.443	0.014	36.3	26.70	94315.2	d		
14	-1	13		13	2	12		AE	94406.395	0.016	36.4	26.60	94315.2	b		$^{13}CH_3OH$
14	1	13	-1	13	2	12	-1	AA	94407.359	0.016	36.4	26.60	94315.2	d		
14	2	13		13	-1	12		E4	94846.362	0.015	36.3	26.70	94845.2	b	0.03	$CH_2{}^{13}CHCN$
14	2	13		13	-1	12		E3	94847.147	0.015	36.3	26.70	94845.2	d		
14	2	13		13	-1	12		EA	94848.625	0.015	36.3	26.70	94848.3		0.04	
14	2	13		13	-1	12		AE	95078.847	0.016	36.4	26.60	95079.2	b	0.04	
14	2	13	-1	13	1	12	-1	AA	95080.895	0.016	36.4	26.60	95079.2	d		
15	0	15		14	1	14		E3	95095.381	0.018	37.4	36.70	95095.2	b	0.05	
15	0	15		14	1	14		E4	95095.417	0.018	37.4	36.70	95095.2	d		
15	0	15		14	1	14		EA	95095.735	0.018	37.4	36.70	95095.2	d		
15	1	15		14	0	14		E3	95102.484	0.018	37.4	36.70	95095.2	b		CH_3CH_2CN
15	1	15		14	0	14		E4	95102.496	0.018	37.4	36.70	95095.2	d		
15	1	15		14	0	14		EA	95102.840	0.018	37.4	36.70	95095.2	d		

Tabla C.1: continued.

J	K_a	K_c	p	J'	K'_a	K'_c	p'	State	ν_{lab}(MHz)	$e_{\nu_{lab}}$(MHz)	E_{upp}(K)	$S_{ij}\mu^2(D^2)$	ν_{obs}(MHz)	$f_{\nu_{obs}}$(MHz)	$T_{\rm MB}$(K)	Blend
15	0	15		14	1	14		AE	95140.843	0.019	37.4	36.70	95141.2	b	0.07	
15	0	15	1	14	1	14	1	AA	95141.189	0.019	37.4	36.70	95141.2	d		
15	1	15		14	0	14		AE	95150.031	0.019	37.4	36.70	95149.6	b	0.05	
15	1	15	1	14	0	14	1	AA	95150.395	0.019	37.4	36.70	95149.6	d		
15	8	8		15	7	9		AE	99453.375	0.037	62.9	18.40	99453.2		0.03	
24	5	20		24	4	21		AE	99760.840	0.062	114.0	27.30	99761.2	b	0.04	
19	-1	18		19	0	19		E4	99761.002	0.045	63.4	6.79	99761.2	d		
19	-1	18		19	0	19		E3	99761.069	0.045	63.4	6.79	99761.2	d		
14	8	7		14	7	8		AE	99855.500	0.037	57.6	16.30	99856.1	b	0.04	
25	9	17		25	8	18		EA	99856.333	0.092	139.5	38.40	99856.1	d		
26	6	21		26	5	22		AE	100260.011	0.087	136.3	34.10	100265.1		0.05	U-line
26	6	21	-1	26	5	22	1	AA	100272.131	0.086	136.3	34.10	100272.1		0.04	
15	-1	14		14	2	13		E3	100573.374	0.018	41.1	29.50	100576.2	b	0.06	$HCOOCH_3$
15	-1	14		14	2	13		E4	100574.039	0.018	41.1	29.50	100576.2	d		
15	-1	14		14	2	13		EA	100574.893	0.018	41.1	29.50	100576.2	d		
15	-1	14		14	2	13		AE	100696.502	0.020	41.2	29.40	100697.1	b	0.04	
15	1	14	-1	14	2	13	-1	AA	100697.661	0.019	41.2	29.40	100697.1	d		
15	2	14		14	-1	13		E4	100861.610	0.018	41.1	29.50	100862.1	b	0.03	
15	2	14		14	-1	13		E3	100861.974	0.018	41.1	29.50	100862.1	d		
15	2	14		14	-1	13		EA	100863.464	0.018	41.1	29.50	100862.1	d		
15	2	14		14	-1	13		AE	101062.832	0.020	41.2	29.40	101064.1	b	0.04	
15	2	14	-1	14	1	13	-1	AA	101064.631	0.020	41.2	29.40	101064.1	d		
16	0	16		15	1	15		E3	101249.746	0.022	42.3	39.40	101250.2	b	0.05	
16	0	16		15	1	15		E4	101249.772	0.022	42.3	39.40	101250.2	d		
16	0	16		15	1	15		EA	101250.085	0.022	42.3	39.40	101250.2	d		
16	1	16		15	0	15		E3	101253.205	0.022	42.3	39.40	101253.2	b	0.11	U-line
16	1	16		15	0	15		E4	101253.219	0.022	42.3	39.40	101253.2	d		
16	1	16		15	0	15		EA	101253.545	0.022	42.3	39.40	101253.2	d		
16	0	16		15	1	15		AE	101295.082	0.023	42.3	39.40	101253.2	b		CH_3OH
16	0	16	1	15	1	15	1	AA	101295.419	0.023	42.3	39.40	101253.2	d		
16	1	16		15	0	15		AE	101299.584	0.023	42.3	39.40	101253.2	b		$HCOOCH_3$
16	1	16	1	15	0	15	1	AA	101299.931	0.023	42.3	39.40	101253.2	d		
15	2	13	1	14	3	12	1	AA	104119.419	0.020	44.5	21.00	101253.2	b		U-line
15	-2	13		14	3	12		AE	104120.596	0.020	44.5	21.00	101253.2	d		
15	-2	13		14	3	12		EA	104405.034	0.018	44.3	21.10	101253.2			CH_2CHCN, CH_3OH
6	5	2	1	5	4	1	1	AA	104537.910	0.007	15.5	11.90	104536.1	b	0.05	$(CH_3)_2CO$
6	-5	1		5	-4	1		AE	104538.527	0.007	15.5	11.90	104536.1	d		
14	3	12		13	-2	11		AE	105075.447	0.019	39.5	18.50	105076.1		0.07	$(CH_3)_2CO$, $^{13}CH_3OH$

Tabla C.1: continued.

J	K_a	K_c	p	J'	K'_a	K'_c	p'	State	ν_{lab}(MHz)	$e_{\nu_{lab}}$(MHz)	E_{upp}(K)	$S_{ij}\mu^2(D^2)$	ν_{obs}(MHz)	$f_{\nu_{obs}}$(MHz)	$T_{\rm MB}$(K)	Blend
14	3	12	1	13	2	11	1	AA	105083.505	0.019	39.5	18.50	105083.2		0.06	U-line
20	9	12		20	8	13		EA	106187.860	0.066	98.5	27.30	106188.2		0.03	
16	-1	15		15	2	14		E3	106782.100	0.022	46.2	32.20	106188.2	b		$OC^{34}S$
16	-1	15		15	2	14		E4	106782.490	0.022	46.2	32.20	106188.2	d		
16	-1	15		15	2	14		EA	106783.563	0.022	46.2	32.20	106188.2	d		
19	9	11		19	8	12		EA	106912.198	0.063	91.4	25.10	106913.1		0.06	
16	-1	15		15	2	14		AE	106922.295	0.024	46.4	32.10	106922.2	b	0.06	
16	1	15	-1	15	2	14	-1	AA	106923.567	0.024	46.4	32.10	106922.2	d		
16	2	15		15	-1	14		E4	106935.506	0.022	46.2	32.20	106935.1	b	0.04	
16	2	15		15	-1	14		E3	106935.648	0.022	46.2	32.20	106935.1	d		
16	2	15		15	-1	14		EA	106937.122	0.022	46.2	32.20	106937.2		0.04	
22	-9	13		22	-8	14		EA	107385.629	0.087	115.3	31.40	107386.1		0.07	
17	0	17		16	1	16		E3	107403.208	0.027	47.4	42.10	107405.1	b	0.10	
17	0	17		16	1	16		E4	107403.228	0.027	47.4	42.10	107405.1	d		
17	0	17		16	1	16		EA	107403.533	0.027	47.4	42.10	107405.1	d		
22	3	20		22	2	21		E4	107404.477	0.047	88.4	13.50	107405.1	d		
22	3	20		22	2	21		E3	107404.615	0.048	88.4	13.50	107405.1	d		
17	1	17		16	0	16		E3	107404.882	0.027	47.4	42.10	107405.1	d		
17	1	17		16	0	16		E4	107404.896	0.027	47.4	42.10	107405.1	d		
17	1	17		16	0	16		EA	107405.207	0.027	47.4	42.10	107405.1	d		
17	0	17		16	1	16		AE	107448.155	0.028	47.5	42.10	107448.1	b	0.10	$^{13}CH_3OH$
17	0	17	1	16	1	16	1	AA	107448.480	0.028	47.5	42.10	107448.1	d		
17	1	17		16	0	16		AE	107450.346	0.028	47.5	42.10	107450.1	b	0.09	
17	1	17	1	16	0	16	1	AA	107450.676	0.028	47.5	42.10	107450.1	d		
24	9	16	1	24	8	17	-1	AA	107615.928	0.077	132.2	35.90	107617.1	b	0.08	U-line
7	5	3		6	4	3		E3	107616.306	0.007	17.1	11.90	107617.1	d		
7	5	3		6	4	3		EA	107617.208	0.008	17.1	11.90	107617.1	d		
23	-9	14		23	-8	15		AE	107619.664	0.081	123.6	25.70	107617.1	d		
9	4	6		8	3	6		EA	108248.757	0.006	20.4	8.36	108250.1	b	0.04	
21	-9	12		21	-8	13		E3	108248.942	0.086	107.5	29.20	108250.1	d		
30	10	21		30	9	22		E4	108250.054	0.185	195.3	47.10	108250.1	d		
15	9	7		15	8	8		EA	108775.910	0.056	66.6	16.60	108776.1		0.04	
22	-9	13		22	-8	14		AE	109007.584	0.073	115.4	24.50	109008.1	b	0.04	
21	-5	16		20	-6	14		E3	109008.491	0.083	91.8	3.25	109008.1	d		
14	9	6		14	8	7		E4	109008.582	0.063	61.3	14.50	109008.1	d		
14	9	6		14	8	7		EA	109053.373	0.055	61.3	14.50	109053.1		0.03	
20	-9	11		20	-8	12		EA	109056.265	0.074	100.0	27.00	109057.1		0.06	U-line
26	-4	22		26	-3	23		E3	109063.330	0.074	131.0	27.00	109063.2	b	0.02	

Tabla C.1: continued.

J	K_a	K_c	p	J'	K'_a	K'_c	p'	State	ν_{lab}(MHz)	$e_{\nu_{lab}}$(MHz)	E_{upp}(K)	$S_{ij}\mu^2(D^2)$	ν_{obs}(MHz)	$f_{\nu_{obs}}$(MHz)	T_{MB}(K)	Blend
26	-4	22		26	-3	23		E4	109063.340	0.074	131.0	27.00	109063.2	d		
26	-4	22		26	-3	23		EA	109075.997	0.073	131.0	27.00	109074.2		0.03	U-line
22	9	14		22	8	15		AE	109330.660	0.073	115.4	24.50	109330.2		0.03	
11	9	3		11	8	4		EA	109590.655	0.055	47.6	7.78	109591.1	b	0.06	
15	3	13		14	-2	12		AE	109590.717	0.022	44.6	21.30	109591.1	d		
19	-9	10		19	-8	11		EA	109696.803	0.069	93.0	24.90	109698.1		0.04	
30	-10	20		30	-9	21		AE	110026.919	0.200	197.1	47.40	110029.2		0.02	U-line
21	-9	12		21	-8	13		AE	110085.566	0.066	107.6	25.60	110085.2		0.05	
18	-9	9		18	-8	10		EA	110234.012	0.065	86.3	22.80	110234.1		0.02	
18	-4	14		17	5	13		AE	110904.546	0.054	67.7	10.70	110905.1		0.03	
20	-9	11		20	-8	12		AE	110937.388	0.062	100.1	26.00	110938.1		0.04	
20	9	12		20	8	13		AE	110941.055	0.063	100.1	26.00	110940.1		0.05	U-line
20	9	12	1	20	8	13	-1	AA	111033.563	0.057	100.1	27.10	111034.2	b	0.09	CH_2CHCN ν_{15}=1
16	-9	7		16	-8	8		E4	111034.289	0.066	73.9	18.60	111034.2	d		
16	-9	7		16	-8	8		EA	111055.718	0.061	73.9	18.60	111057.1		0.02	
16	-2	14		15	3	13		EA	111354.431	0.022	49.7	24.20	111356.1		0.05	U-line
15	-9	6		15	-8	7		EA	111363.251	0.061	68.3	16.50	111363.1		0.03	
28	6	23		28	5	24		AE	111519.002	0.108	155.6	34.20	111519.0		0.06	
19	9	11		19	8	12		AE	111612.106	0.060	93.0	24.70	111609.1		0.06	$HCOOCH_3$
14	-9	5		14	-8	6		EA	111614.595	0.061	63.0	14.40	111616.1		0.06	U-line
7	5	3		6	4	3		AE	111771.264	0.008	17.9	11.90	111772.1		0.03	
7	-5	2		6	-4	2		EA	111862.793	0.009	18.2	12.00	111862.2		0.04	U-line
18	9	10		18	8	11		AE	112183.502	0.058	86.3	22.80	112184.1	b	0.04	
10	-9	1		10	-8	2		E4	112183.146	0.067	45.5	5.34	112184.1	d		
10	-9	1		10	-8	2		EA	112205.111	0.066	45.5	5.34	112207.2	b	0.04	U-line
18	-9	9		18	-8	10		AE	112205.762	0.057	86.3	22.80	112207.2	d		
18	9	9	-1	18	8	10	1	AA	112217.030	0.052	86.3	22.80	112218.1		0.03	
28	10	19		28	9	20		E4	112239.081	0.150	174.1	43.10	112240.1	b	0.02	
18	9	10	1	18	8	11	-1	AA	112239.887	0.052	86.3	22.80	112240.1	d		
9	3	6	-1	8	2	7	-1	AA	112662.557	0.006	19.1	3.88	112662.6	b	0.05	
17	9	9		17	8	10		AE	112663.797	0.057	79.9	20.70	112662.6	d		
9	-4	5		8	-3	5		EA	112668.697	0.006	21.3	9.08	112668.1		0.05	
17	-9	8		17	-8	9		AE	112686.396	0.055	79.9	20.70	112685.2		0.09	U-line
17	9	8	-1	17	8	9	1	AA	112704.356	0.050	79.9	20.70	112704.2		0.04	U-line
17	9	9	1	17	8	10	-1	AA	112713.429	0.050	79.9	20.70	112715.1	b	0.03	
12	4	9		11	-3	8		E3	112715.215	0.017	32.3	4.68	112715.1	d		
17	-1	16		16	2	15		E3	112962.494	0.027	51.7	35.00	112963.2	b	0.07	
17	-1	16		16	2	15		E4	112962.734	0.027	51.7	35.00	112963.2	d		

Tabla C.1: continued.

J	K_a	K_c	p	J'	K'_a	K'_c	p'	State	ν_{lab}(MHz)	$e_{\nu_{lab}}$(MHz)	E_{upp}(K)	$S_{ij}\mu^2(D^2)$	ν_{obs}(MHz)	$f_{\nu_{obs}}$(MHz)	T_{MB}(K)	Blend
17	-1	16		16	2	15		EA	112963.922	0.027	51.7	35.00	112963.2	d		
17	2	16		16	-1	15		E4	113043.010	0.027	51.7	35.00	113045.2	b	0.07	
17	2	16		16	-1	15		E3	113043.040	0.027	51.7	35.00	113045.2	d		
17	2	16		16	-1	15		EA	113044.489	0.027	51.7	35.00	113045.2	d		
16	-9	7		16	-8	8		AE	113086.712	0.055	74.0	18.60	113086.1		0.02	
16	9	8	1	16	8	9	-1	AA	113111.015	0.049	74.0	18.60	113111.1	b	0.13	CH_2CHCN ν_{11}=1
17	-1	16		16	2	15		AE	113111.910	0.029	51.8	34.90	113111.1	d		
17	1	16	-1	16	2	15	-1	AA	113113.240	0.029	51.8	34.90	113111.1	d		
17	2	16		16	-1	15		AE	113215.444	0.029	51.8	34.90	113215.2		0.08	
17	2	16	-1	16	1	15	-1	AA	113216.981	0.029	51.8	34.90	113217.1		0.10	U-line
15	9	6	-1	15	8	7	1	AA	113440.271	0.048	68.3	16.50	113442.1	b	0.05	
15	9	7	1	15	8	8	-1	AA	113441.415	0.048	68.3	16.50	113442.1	d		
18	0	18		17	1	17		E3	113556.187	0.033	52.9	44.80	113557.1	b	0.12	
18	0	18		17	1	17		E4	113556.203	0.033	52.9	44.80	113557.1	d		
18	0	18		17	1	17		EA	113556.497	0.033	52.9	44.80	113557.1	d		
18	1	18		17	0	17		E3	113556.992	0.033	52.9	44.80	113557.1	d		
18	1	18		17	0	17		E4	113557.005	0.033	52.9	44.80	113557.1	d		
18	1	18		17	0	17		EA	113557.302	0.033	52.9	44.80	113557.1	d		
18	0	18		17	1	17		AE	113600.610	0.033	52.9	44.80	113601.1	b	0.12	
18	0	18	1	17	1	17	1	AA	113600.922	0.033	52.9	44.80	113601.1	d		
18	1	18		17	0	17		AE	113601.669	0.033	52.9	44.80	113601.1	d		
18	1	18	1	17	0	17	1	AA	113601.984	0.033	52.9	44.80	113601.1	d		
6	6	1		5	5	1		EA	113627.823	0.014	18.0	14.60	113628.1		0.08	
14	9	6		14	8	7		AE	113668.291	0.057	63.0	14.40	113669.1		0.05	
14	-9	5		14	-8	6		AE	113690.032	0.055	63.0	14.40	113691.1		0.07	$HCOOCH_3$ ν_t=1
14	9	5	-1	14	8	6	1	AA	113712.785	0.048	63.0	14.40	113713.1	b	0.11	$(CH_3)_2CO$
14	9	6	1	14	8	7	-1	AA	113713.139	0.048	63.0	14.40	113713.1	d		
18	15	4		17	-15	2		E3	113888.908	1.155	122.7	44.30	113890.9	b	0.06	
18	15	4		17	-15	2		E4	113888.937	1.158	122.7	44.30	113890.9	d		
18	15	4		17	-15	2		EA	113889.151	1.152	122.7	44.30	113890.9	d		
13	9	5		13	8	6		AE	113889.470	0.058	58.1	12.30	113890.9	d		
18	-15	3		17	15	3		E3	113895.721	1.148	122.7	44.30	113894.1	b	0.06	
18	-15	3		17	15	3		E4	113895.732	1.151	122.7	44.30	113894.1	d		
18	-15	3		17	15	3		EA	113895.967	1.145	122.7	44.30	113894.1	d		
11	9	2	-1	11	8	3	1	AA	114251.912	0.050	49.3	7.75	114253.1	b	0.06	
11	9	3	1	11	8	4	-1	AA	114251.916	0.050	49.3	7.75	114253.1	d		
25	4	22		25	3	23		E4	114541.651	0.058	117.1	20.20	114542.1	b	0.06	
9	-4	5		8	3	6		AE	114542.356	0.006	21.1	8.79	114542.1	d		

Tabla C.1: continued.

J	K_a	K_c	p	J'	K'_a	K'_c	p'	State	ν_{lab}(MHz)	$e_{\nu_{lab}}$(MHz)	E_{upp}(K)	$S_{ij}\mu^2(D^2)$	ν_{obs}(MHz)	$f_{\nu_{obs}}$(MHz)	$T_{\rm MB}$(K)	Blend
10	4	7		9	-3	6		AE	114744.789	0.009	24.6	9.49	114745.1		0.06	
8	5	4		7	4	4		E3	114832.229	0.007	19.9	11.90	114833.1	b	0.06	
8	5	4		7	4	4		EA	114832.962	0.008	19.9	11.90	114833.1	d		
27	-4	23		27	-3	24		E4	115090.851	0.079	140.2	27.00	115090.2	b	0.04	
27	-4	23		27	-3	24		E3	115090.935	0.079	140.2	27.00	115090.2	d		
27	-4	23		27	-3	24		EA	115104.888	0.078	140.2	27.00	115105.1		0.05	
29	-11	18		29	-10	19		EA	130121.829	0.212	192.2	42.70	130120.7		0.03	
27	11	17		27	10	18		EA	130339.772	0.166	170.3	38.50	130339.8		0.03	
12	-4	8		11	-3	8		EA	130530.429	0.013	33.1	5.55	130532.2		0.05	
19	-2	17		18	3	16		E3	130746.166	0.038	67.7	32.90	130748.1	b	0.09	
19	-2	17		18	3	16		E4	130747.190	0.038	67.7	32.90	130748.1	d		
19	-2	17		18	3	16		EA	130748.640	0.038	67.7	32.90	130748.1	d		
19	-2	17		18	3	16		AE	130952.352	0.042	68.0	32.70	130952.1		0.03	
19	2	17	1	18	3	16	1	AA	130954.246	0.042	68.0	32.70	130954.1		0.05	
20	-1	19		19	2	18		E3	131437.724	0.045	69.7	43.10	131442.2	b	0.09	CH_3CH_2OH
20	-1	19		19	2	18		E4	131437.814	0.045	69.7	43.10	131442.2	d		
20	-1	19		19	2	18		EA	131439.088	0.045	69.7	43.10	131442.2	d		
20	2	19		19	-1	18		E3	131448.610	0.045	69.7	43.10	131449.7	b	0.07	
20	2	19		19	-1	18		E4	131448.667	0.045	69.7	43.10	131449.7	d		
20	2	19		19	-1	18		EA	131449.982	0.045	69.7	43.10	131449.7	d		
19	3	17		18	-2	16		AE	131585.302	0.043	68.0	32.70	131585.1		0.04	
19	3	17	1	18	2	16	1	AA	131588.440	0.042	68.0	32.70	131588.1		0.03	
20	-1	19		19	2	18		AE	131595.148	0.047	69.9	43.00	131596.0	b	0.07	
20	1	19	-1	19	2	18	-1	AA	131596.508	0.047	69.9	43.00	131596.0	d		
20	2	19		19	-1	18		AE	131609.368	0.047	69.9	43.10	131596.0	b		$HCOOCH_3$ ν_t=1
20	2	19	-1	19	1	18	-1	AA	131610.762	0.047	69.9	43.00	131596.0	d		
17	4	14		16	-3	13		EA	131794.702	0.037	58.8	18.20	131796.0	b	0.13	$HCOO^{13}CH_3$
17	4	14		16	-3	13		E3	131794.837	0.038	58.8	18.20	131796.0	d		
21	0	21		20	1	20		E3	132013.676	0.053	71.0	52.90	131796.0	b		$(CH_3)_2CO$, $HCOOCH_3$
21	0	21		20	1	20		E4	132013.684	0.053	71.0	52.90	131796.0	d		
21	1	21		20	0	20		E3	132013.763	0.053	71.0	52.90	131796.0	d		
21	1	21		20	0	20		E4	132013.771	0.053	71.0	52.90	131796.0	d		
21	0	21		20	1	20		EA	132013.944	0.053	71.0	52.90	131796.0	d		
21	1	21		20	0	20		EA	132014.031	0.053	71.0	52.90	131796.0	d		
8	-6	2		7	-5	2		EA	132034.434	0.015	24.5	14.60	132034.7		0.05	
21	0	21		20	1	20		AE	132056.252	0.054	71.0	52.90	132056.0	b	0.15	
21	1	21		20	0	20		AE	132056.368	0.054	71.0	52.90	132056.0	d		
21	0	21	1	20	1	20	1	AA	132056.525	0.054	71.0	52.90	132056.0	d		

Tabla C.1: continued.

J	K_a	K_c	p	J'	K'_a	K'_c	p'	State	ν_{lab}(MHz)	$e_{\nu_{lab}}$(MHz)	E_{upp}(K)	$S_{ij}\mu^2(D^2)$	ν_{obs}(MHz)	$f_{\nu_{obs}}$(MHz)	T_{MB}(K)	Blend
21	1	21	1	20	0	20	1	AA	132056.641	0.054	71.0	52.90	132056.0	d		
8	6	3		7	5	3		AE	132541.848	0.014	24.3	14.60	132542.0		0.04	
8	-6	2		7	-5	2		AE	132575.643	0.012	24.3	14.60	132576.1		0.09	$(CH_3)_2CO$
29	11	19		29	10	20		AE	132801.262	0.187	192.7	34.10	132801.0		0.07	$CH_3CH_2C^{15}N$
26	-11	15		26	-10	16		EA	133150.220	0.171	162.3	36.00	133149.6		0.06	
17	4	14	-1	16	3	13	-1	AA	133744.371	0.039	59.1	18.40	133746.0	b	0.13	CH_2CHCN ν_{11}=2
10	5	5	-1	9	4	6	-1	AA	133746.469	0.009	27.5	12.00	133746.0	d		
19	-3	16		18	4	15		E3	134121.235	0.039	71.5	24.00	134122.1		0.08	U-line
19	-3	16		18	4	15		EA	134125.996	0.039	71.5	24.00	134127.2		0.05	U-line
19	-3	16		18	4	15		E4	134132.389	0.040	71.5	24.00	134129.7		0.07	U-line
7	7	1		6	6	1		E3	134207.734	0.022	24.4	17.30	134204.7		0.08	SO_2
7	7	1		6	6	1		EA	134219.761	0.023	24.4	17.30	134219.7		0.17	CH_3CH_2OH
30	-4	26		30	-3	27		AE	134771.606	0.119	170.2	27.30	134772.1		0.02	
19	11	9		19	10	10		E4	135202.471	0.141	103.7	21.30	135202.0		0.02	
18	4	15		17	-3	14		E4	135602.074	0.042	65.1	21.20	135602.1	b	0.07	
22	-11	11		22	-10	12		E4	135603.832	0.157	127.6	27.50	135602.1	d		
18	4	15		17	-3	14		E3	135616.458	0.041	65.1	21.30	135617.0		0.02	
18	4	15		17	-3	14		EA	135619.345	0.041	65.1	21.20	135620.1		0.07	
26	11	16		26	10	17		AE	135839.145	0.160	162.7	35.60	135839.1		0.11	U-line
18	4	15		17	-3	14		AE	137061.720	0.043	65.4	21.20	137063.4		0.10	U-line
20	-2	18		19	3	17		AE	137217.385	0.049	74.6	35.50	137222.1	b	0.09	U-line
20	2	18	1	19	3	17	1	AA	137219.492	0.049	74.6	35.50	137222.1	d		
20	3	18		19	-2	17		E4	137256.036	0.045	74.3	35.70	137255.9	b	0.08	$HC^{18}OOCH_3$
20	3	18		19	-2	17		E3	137256.257	0.045	74.3	35.70	137255.9	d		
29	4	26		29	3	27		E3	137256.716	0.099	153.4	20.30	137255.9	d		
29	4	26		29	3	27		E4	137256.865	0.099	153.4	20.30	137255.9	d		
20	3	18		19	-2	17		EA	137258.820	0.045	74.3	35.70	137259.7		0.13	
20	3	18		19	-2	17		AE	137567.585	0.049	74.6	35.50	137568.0		0.12	$CH2^{13}CHCN$
20	3	18	1	19	2	17	1	AA	137570.425	0.049	74.6	35.50	137571.0		0.06	
21	-1	20		20	2	19		E3	137588.761	0.052	76.3	45.80	137571.0	b		CH_3OCH_3
21	-1	20		20	2	19		E4	137588.836	0.052	76.3	45.80	137571.0	d		
21	-1	20		20	2	19		EA	137590.107	0.052	76.3	45.80	137571.0	d		
7	-7	0		6	-6	0		E3	137590.134	0.026	25.9	17.30	137571.0	d		
21	2	20		20	-1	19		E3	137594.251	0.052	76.3	45.80	137593.0	b	0.11	
21	2	20		20	-1	19		E4	137594.310	0.052	76.3	45.80	137593.0	d		
21	2	20		20	-1	19		EA	137595.602	0.052	76.3	45.80	137593.0	d		
21	-1	20		20	2	19		AE	137746.422	0.055	76.5	45.80	137749.1	b	0.17	CH_3CH_2OH
21	1	20	-1	20	2	19	-1	AA	137747.773	0.055	76.5	45.80	137749.1	d		

Tabla C.1: continued.

J	K_a	K_c	p	J'	K'_a	K'_c	p'	State	ν_{lab}(MHz)	$e_{\nu_{lab}}$(MHz)	E_{upp}(K)	$S_{ij}\mu^2(D^2)$	ν_{obs}(MHz)	$f_{\nu_{obs}}$(MHz)	T_{MB}(K)	Blend
21	2	20		20	-1	19		AE	137753.627	0.055	76.5	45.80	137755.0	b	0.13	DCOOH
21	2	20	-1	20	1	19	-1	AA	137754.996	0.055	76.5	45.80	137755.0	d		
22	0	22		21	1	21		E3	138165.826	0.062	77.6	55.60	137755.0	b		SO
22	0	22		21	1	21		E4	138165.833	0.062	77.6	55.60	137755.0	d		
22	1	22		21	0	21		E3	138165.867	0.062	77.6	55.60	137755.0	d		
22	1	22		21	0	21		E4	138165.874	0.062	77.6	55.60	137755.0	d		
22	0	22		21	1	21		EA	138166.080	0.062	77.6	55.60	137755.0	d		
22	1	22		21	0	21		EA	138166.122	0.062	77.6	55.60	137755.0	d		
22	0	22		21	1	21		AE	138207.762	0.062	77.7	55.60	138207.2	b	0.21	
22	1	22		21	0	21		AE	138207.817	0.062	77.7	55.60	138207.2	d		
22	0	22	1	21	1	21	1	AA	138208.022	0.062	77.7	55.60	138207.2	d		
22	1	22	1	21	0	21	1	AA	138208.077	0.062	77.7	55.60	138207.2	d		
7	7	1		6	6	1		AE	138714.983	0.026	25.7	17.40	138715.1		0.04	
7	-7	0		6	-6	0		AE	138744.841	0.022	25.7	17.40	138715.1			^{13}CS
7	7	1	1	6	6	0	1	AA	138758.409	0.022	25.7	17.40	138758.1	b	0.10	
7	7	0	-1	6	6	1	-1	AA	138758.411	0.022	25.7	17.40	138758.1	d		
11	5	7		10	-4	6		AE	139261.407	0.012	31.3	10.50	139261.9		0.06	
11	5	7	1	10	4	6	1	AA	139320.452	0.012	31.3	12.10	139318.4		0.05	CH_2DCH_2CN
9	6	3	1	8	5	4	1	AA	139846.770	0.013	27.5	14.70	139847.0		0.07	
19	4	16		18	-3	15		E4	139991.036	0.045	71.6	24.30	139991.1		0.07	
11	-5	6		10	-4	6		E4	140354.201	0.012	31.6	12.00	140349.7	b	0.15	$^{33}SO_2$
11	-5	6		10	-4	6		EA	140355.798	0.012	31.6	12.00	140349.7	d		
16	11	5	-1	16	10	6	1	AA	140513.483	0.105	86.8	14.70	140514.2	b	0.08	
16	11	6	1	16	10	7	-1	AA	140513.486	0.105	86.8	14.70	140514.2	d		
19	4	16		18	-3	15		AE	141090.948	0.048	71.9	24.20	141092.1	b	0.12	U-line
28	-2	26		28	-1	27		EA	141091.471	0.118	137.6	13.50	141092.1	d		
28	3	26		28	2	27		EA	141091.982	0.118	137.6	13.50	141092.1	d		
20	3	17	-1	19	4	16	-1	AA	141210.979	0.050	78.7	26.90	141210.8	b	0.08	
20	-3	17		19	4	16		AE	141211.188	0.050	78.7	26.90	141210.8	d		
11	5	6	-1	10	4	7	-1	AA	141266.398	0.011	31.4	11.90	141267.2		0.15	$HCOOCH_3$
11	-5	6		10	4	7		AE	141282.900	0.012	31.4	10.40	141281.9	b	0.04	
20	-3	17		19	4	16		E3	141284.050	0.045	78.4	27.20	141281.9	d		
20	-3	17		19	4	16		EA	141287.892	0.045	78.4	27.20	141289.7	b	0.13	H_2CCO
20	-3	17		19	4	16		E4	141290.577	0.045	78.4	27.20	141289.7	d		
8	7	2		7	6	2		E4	141471.045	0.024	27.2	17.20	141472.2		0.11	$SO^{17}O$
8	7	2		7	6	2		E3	141501.728	0.022	27.2	17.20	141503.0		0.13	U-line
8	7	2		7	6	2		EA	141513.769	0.022	27.2	17.20	141515.0		0.17	$^{34}SO_2$
21	-2	19		20	3	18		E3	143175.933	0.052	81.2	38.40	143178.4	b	0.16	CH_3OH

Tabla C.1: continued.

J	K_a	K_c	p	J'	K'_a	K'_c	p'	State	ν_{lab}(MHz)	$e_{\nu_{lab}}$(MHz)	E_{upp}(K)	$S_{ij}\mu^2(D^2)$	ν_{obs}(MHz)	$f_{\nu_{obs}}$(MHz)	T_{MB}(K)	Blend
21	-2	19		20	3	18		E4	143176.319	0.052	81.2	38.40	143178.4	d		
21	-2	19		20	3	18		EA	143178.327	0.052	81.2	38.40	143178.4	d		
21	-2	19		20	3	18		AE	143426.261	0.057	81.5	38.30	143425.9	b	0.19	U-line
21	2	19	1	20	3	18	1	AA	143428.486	0.057	81.5	38.30	143425.9	d		
22	-1	21		21	2	20		AE	143896.382	0.063	83.4	48.50	143897.1	b	0.10	$HCOO^{13}CH_3$
22	1	21	-1	21	2	20	-1	AA	143897.721	0.063	83.4	48.50	143897.1	d		
22	2	21		21	-1	20		AE	143900.006	0.063	83.4	48.50	143901.0	b	0.10	
22	2	21	-1	21	1	20	-1	AA	143901.354	0.063	83.4	48.50	143901.0	d		
23	0	23		22	1	22		E3	144317.808	0.071	84.5	58.30	144318.4	b	0.41	$^{13}CH_3OH$
23	0	23		22	1	22		E4	144317.813	0.071	84.5	58.30	144318.4	d		
23	1	23		22	0	22		E3	144317.828	0.071	84.5	58.30	144318.4	d		
23	1	23		22	0	22		E4	144317.832	0.071	84.5	58.30	144318.4	d		
23	0	23		22	1	22		EA	144318.049	0.071	84.5	58.30	144318.4	d		
23	1	23		22	0	22		EA	144318.068	0.071	84.5	58.30	144318.4	d		
23	0	23		22	1	22		AE	144359.105	0.072	84.6	58.30	144358.4	b	0.20	
23	1	23		22	0	22		AE	144359.131	0.072	84.6	58.30	144358.4	d		
23	0	23	1	22	1	22	1	AA	144359.352	0.071	84.6	58.30	144358.4	d		
23	1	23	1	22	0	22	1	AA	144359.378	0.071	84.6	58.30	144358.4	d		
23	14	10		22	-14	8		E3	144660.625	1.563	154.4	57.90	144660.1	b	0.18	U-line
23	14	10		22	-14	8		E4	144660.689	1.566	154.4	57.90	144660.1	d		
23	-14	9		22	14	9		E3	144660.838	1.562	154.4	57.90	144660.1	d		
23	-14	9		22	14	9		E4	144660.901	1.566	154.4	57.90	144660.1	d		
8	-7	1		7	-6	1		EA	144909.215	0.027	28.7	17.30	144909.0	b	0.12	$DCOOCH_3$
20	4	17		19	-3	16		E3	144910.426	0.049	78.4	27.40	144909.0	d		
20	4	17		19	-3	16		EA	144914.704	0.049	78.4	27.30	144916.1		0.11	U-line
29	-12	17		29	-11	18		EA	145190.238	0.249	199.2	40.50	145189.6		0.06	
28	-12	16		28	-11	17		EA	145995.179	0.234	188.9	38.30	145996.1		0.06	
8	7	2		7	6	2		AE	146003.431	0.025	28.5	17.30	146003.6		0.08	$HCO^{18}OCH_3$
8	-7	1		7	-6	1		AE	146033.235	0.022	28.5	17.30	146003.6			$^{34}SO_2$
8	7	2	1	7	6	1	1	AA	146046.808	0.021	28.5	17.30	146047.2	b	0.15	
8	7	1	-1	7	6	2	-1	AA	146046.835	0.021	28.5	17.30	146047.2	d		
10	-6	4		9	-5	4		E3	146465.090	0.015	31.2	14.80	146465.8		0.08	
10	-6	4		9	-5	4		EA	146505.489	0.016	31.2	14.80	146506.1		0.07	
25	-12	13		25	-11	14		E4	147841.813	0.230	160.2	31.90	147842.1		0.05	
21	-3	18		20	4	17		EA	148070.269	0.052	85.6	30.20	148073.2	b	0.11	U-line
21	-3	18		20	4	17		E4	148070.600	0.052	85.6	30.20	148073.2	d		
21	-3	18		20	4	17		AE	148172.541	0.058	85.9	30.00	148173.4	b	0.16	CH_3OCH_3, CH_3CH_2OCOH
21	3	18	-1	20	4	17	-1	AA	148173.628	0.058	85.9	30.00	148173.4	d		

Tabla C.1: continued.

J	K_a	K_c	p	J'	K'_a	K'_c	p'	State	ν_{lab}(MHz)	$e_{\nu_{lab}}$(MHz)	E_{upp}(K)	$S_{ij}\mu^2(D^2)$	ν_{obs}(MHz)	$f_{\nu_{obs}}$(MHz)	$T_{\rm MB}$(K)	Blend
12	-5	7		11	4	8		AE	149110.905	0.013	35.6	11.30	149112.1		0.10	
12	5	7	-1	11	4	8	-1	AA	149113.837	0.014	35.6	11.60	149114.6		0.11	
22	-12	10		22	-11	11		EA	149135.460	0.176	134.8	25.60	149134.6		0.08	U-line
22	-2	20		21	3	19		E3	149344.862	0.060	88.4	41.20	149345.9	b	0.08	
22	-2	20		21	3	19		E4	149345.122	0.060	88.4	41.20	149345.9	d		
22	-2	20		21	3	19		EA	149347.232	0.060	88.4	41.20	149345.9	d		
22	3	20		21	-2	19		E3	149424.304	0.061	88.4	41.20	149424.6	b	0.12	$^{13}CH_2CHCN$
22	3	20		21	-2	19		E4	149424.342	0.061	88.4	41.20	149424.6	d		
22	3	20		21	-2	19		EA	149426.744	0.060	88.4	41.20	149424.6	d		
21	-12	9		21	-11	10		EA	149450.572	0.171	127.1	23.50	149452.1	b	0.09	
29	-2	27		29	-1	28		AE	149452.869	0.177	147.2	13.70	149452.1	d		
29	3	27		29	2	28		AE	149453.210	0.177	147.2	13.70	149452.1	d		
22	-2	20		21	3	19		AE	149603.623	0.065	88.6	41.00	149603.0	b	0.13	
22	2	20	1	21	3	19	1	AA	149605.907	0.065	88.6	41.00	149603.0	d		
13	5	9		12	4	9		E4	149627.986	0.015	39.4	10.10	149631.0		0.08	U-line
13	5	9		12	4	9		EA	149677.002	0.015	39.4	10.10	149677.0		0.20	U-line
22	3	20		21	-2	19		AE	149706.385	0.066	88.6	41.00	149706.1		0.09	
11	6	6		10	5	6		E3	149818.522	0.014	33.8	14.60	149818.1		0.10	
11	6	6		10	5	6		EA	149824.670	0.014	33.8	14.60	149824.7		0.09	
27	12	15	1	27	11	16	-1	AA	149831.013	0.217	179.5	36.20	149832.0		0.05	
23	-1	22		22	2	21		E3	149888.500	0.069	90.4	51.20	149890.0	b	0.27	$HCOOCH_3$ ν_t=1
23	-1	22		22	2	21		E4	149888.558	0.069	90.4	51.20	149890.0	d		
23	-1	22		22	2	21		EA	149889.812	0.069	90.4	51.20	149890.0	d		
23	2	22		22	-1	21		E3	149889.868	0.069	90.4	51.20	149890.0	d		
23	2	22		22	-1	21		E4	149889.923	0.069	90.4	51.20	149890.0	d		
28	-1	27		28	0	28		E3	149890.168	0.169	130.8	6.80	149890.0	d		
28	2	27		28	1	28		E3	149890.181	0.169	130.8	6.80	149890.0	d		
28	-1	27		28	0	28		E4	149890.545	0.168	130.8	6.80	149890.0	d		
28	2	27		28	1	28		E4	149890.558	0.168	130.8	6.80	149890.0	d		
23	2	22		22	-1	21		EA	149891.182	0.069	90.4	51.20	149890.0	d		
23	-1	22		22	2	21		AE	150045.724	0.072	90.6	51.20	150047.1	b	0.19	
23	1	22	-1	22	2	21	-1	AA	150047.049	0.072	90.6	51.20	150047.1	d		
23	2	22		22	-1	21		AE	150047.534	0.072	90.6	51.20	150047.1	d		
23	2	22	-1	22	1	21	-1	AA	150048.864	0.072	90.6	51.20	150047.1	d		
18	-12	6		18	-11	7		E4	150118.880	0.192	106.0	17.10	150119.5		0.03	
13	5	9	1	12	4	8	1	AA	150132.821	0.020	40.2	11.90	150132.0		0.12	CH_3OH
21	4	18		20	-3	17		E4	150236.161	0.055	85.6	30.30	150235.8		0.09	NO
21	4	18		20	-3	17		E3	150238.860	0.055	85.6	30.30	150239.6		0.06	

Tabla C.1: continued.

J	K_a	K_c	p	J'	K'_a	K'_c	p'	State	ν_{lab}(MHz)	$e_{\nu_{lab}}$(MHz)	E_{upp}(K)	$S_{ij}\mu^2(D^2)$	ν_{obs}(MHz)	$f_{\nu_{obs}}$(MHz)	T_{MB}(K)	Blend
24	0	24		23	1	23		E3	150469.613	0.081	91.8	61.00	150469.6	b	0.51	CH_3OCH_3
24	0	24		23	1	23		E4	150469.617	0.081	91.8	61.00	150469.6	d		
24	1	24		23	0	23		E3	150469.622	0.081	91.8	61.00	150469.6	d		
24	1	24		23	0	23		E4	150469.626	0.081	91.8	61.00	150469.6	d		
24	0	24		23	1	23		EA	150469.840	0.081	91.8	61.00	150469.6	d		
24	1	24		23	0	23		EA	150469.849	0.081	91.8	61.00	150469.6	d		
21	4	18		20	-3	17		AE	150906.290	0.061	85.9	30.10	150906.0		0.11	
25	12	13	1	25	11	14	-1	AA	151102.217	0.197	160.8	31.90	151102.1	b	0.06	$CH_2{}^{13}CHCN$
24	16	9		23	-16	0		AE	150102.503	3.339	181.0	60.90	151102.1	d		
24	-16	0		23	16	8		AE	150102.527	3.339	181.0	60.90	151102.1	d		
25	12	14	-1	25	11	15	1	AA	151103.962	0.197	160.8	31.90	151102.1	d		
9	-7	2		8	-6	2		E4	152167.113	0.025	31.8	17.30	152167.1		0.05	
20	12	8	1	20	11	9	-1	AA	153149.165	0.162	120.2	21.40	153149.5	b	0.05	
20	12	9	-1	20	11	10	1	AA	153149.175	0.162	120.2	21.40	153149.5	d		
11	-6	5		10	-5	5		E3	153645.796	0.017	35.1	14.80	153646.0		0.30	CH_2CHCN ν_{15}=1, $HCOOCH_3$ ν_t=1, CH_3CH_2OCOH
11	6	6		10	5	6		AE	154217.288	0.016	34.8	13.80	154215.9		0.23	CH_3CHO
11	-6	5		10	-5	5		AE	154226.609	0.014	34.8	13.80	154229.6		0.29	CH_3CHO
22	-3	19		21	4	18		E3	154593.202	0.060	93.0	33.20	154595.9	b	0.17	
22	-3	19		21	4	18		E4	154595.412	0.060	93.0	33.20	154595.9	d		
22	-3	19		21	4	18		EA	154596.529	0.060	93.0	33.20	154595.9	d		
22	-3	19		21	4	18		AE	154809.972	0.067	93.4	32.90	154810.0	b	0.17	CH_3CH_2CN ν_{13}/ν_2
22	3	19	-1	21	4	18	-1	AA	154811.924	0.067	93.4	32.90	154810.0	d		
8	8	1		7	7	1		E3	154828.599	0.036	31.8	20.00	154829.1		0.07	
8	8	1		7	7	1		EA	154845.969	0.035	31.8	20.00	154846.0		0.08	
23	3	21		22	-2	20		E3	155542.985	0.069	95.8	43.90	155543.4	b	0.18	CH_3OH
23	3	21		22	-2	20		E4	155543.063	0.069	95.8	43.90	155543.4	d		
23	3	21		22	-2	20		EA	155545.377	0.069	95.8	43.90	155543.4	d		
22	4	19		21	-3	18		E4	155862.246	0.062	93.0	33.20	155865.0	b	0.09	$HCOO^{13}CH_3$
22	4	19		21	-3	18		E3	155863.656	0.062	93.0	33.20	155865.0	d		
24	-1	23		23	2	22		E3	156037.940	0.079	97.9	54.00	155865.0	b		$^{34}SO_2$
24	-1	23		23	2	22		E4	156037.994	0.079	97.9	54.00	155865.0	d		
24	2	23		23	-1	22		E3	156038.617	0.079	97.9	54.00	155865.0	d		
24	2	23		23	-1	22		E4	156038.669	0.079	97.9	54.00	155865.0	d		
24	-1	23		23	2	22		EA	156039.236	0.079	97.9	54.00	155865.0	d		
24	2	23		23	-1	22		EA	156039.914	0.079	97.9	54.00	155865.0	d		
10	7	4		9	6	4		E3	156057.921	0.022	33.9	17.20	156058.4		0.13	U-line
10	7	4		9	6	4		EA	156069.933	0.022	33.9	17.20	156069.6		0.09	
24	-1	23		23	2	22		AE	156194.775	0.082	98.1	53.90	156195.8	b	0.20	

Tabla C.1: continued.

J	K_a	K_c	p	J'	K'_a	K'_c	p'	State	ν_{lab}(MHz)	$e_{\nu_{lab}}$(MHz)	E_{upp}(K)	$S_{ij}\mu^2(D^2)$	ν_{obs}(MHz)	$f_{\nu_{obs}}$(MHz)	$T_{\rm MB}$(K)	Blend
24	2	23		23	-1	22		AE	156195.674	0.082	98.1	53.90	156195.8	d		
24	1	23	-1	23	2	22	-1	AA	156196.086	0.082	98.1	53.90	156195.8	d		
24	2	23	-1	23	1	22	-1	AA	156196.987	0.082	98.1	53.90	156195.8	d		
22	4	19		21	-3	18		AE	156417.644	0.069	93.4	33.00	156417.1		0.11	U-line
22	4	19	-1	21	3	18	-1	AA	156422.842	0.069	93.4	33.00	156422.1		0.05	
25	0	25		24	1	24		E3	156621.231	0.092	99.3	63.70	156520.9	b	0.35	
25	0	25		24	1	24		E4	156621.233	0.092	99.3	63.70	156520.9	d		
25	1	25		24	0	24		E3	156621.235	0.092	99.3	63.70	156520.9	d		
25	1	25		24	0	24		E4	156621.238	0.092	99.3	63.70	156520.9	d		
25	0	25		24	1	24		EA	156621.445	0.092	99.3	63.70	156520.9	d		
25	1	25		24	0	24		EA	156621.449	0.092	99.3	63.70	156520.9	d		
25	0	25		24	1	24		AE	156661.260	0.093	99.4	63.70	156660.9	b	0.42	$CH_3CH_2C^{15}N$
25	1	25		24	0	24		AE	156661.266	0.093	99.4	63.70	156660.9	d		
25	0	25	1	24	1	24	1	AA	156661.480	0.092	99.4	63.70	156660.9	d		
25	1	25	1	24	0	24	1	AA	156661.486	0.092	99.4	63.70	156660.9	d		
12	6	7		11	5	7		EA	156905.001	0.016	38.0	14.60	156906.1		0.08	
8	-8	0		7	-7	0		E3	157714.720	0.042	33.5	20.00	157714.0		0.05	
8	-8	0		7	-7	0		E4	157739.624	0.042	33.5	20.00	157714.0			U-line
8	-8	0		7	-7	0		EA	157757.374	0.043	33.5	20.00	157758.1		0.12	
19	5	15		18	-4	14		E4	158632.587	0.064	75.0	14.80	158632.0	b	0.04	
29	-1	28		29	0	29		AE	158633.066	0.256	140.0	6.90	158632.0	d		
29	2	28		29	1	29		AE	158633.074	0.256	140.0	6.90	158632.0	d		
30	-14	16		30	-12	18		E3	158802.750	0.331	217.4	40.60	158803.0		0.06	
30	-14	16		30	-12	18		E4	158806.521	0.362	217.4	40.60	158809.0	b	0.11	U-line
29	14	16		29	12	18		E4	158806.849	0.310	205.2	38.70	158809.0	d		
16	5	12		15	-4	11		AE	159264.661	0.039	56.3	12.30	159264.5		0.03	
14	-5	9		13	-4	9		E4	159372.899	0.023	45.5	10.00	159372.0		0.03	
10	-7	3		9	-6	3		E3	159397.218	0.025	35.3	17.30	159394.5		0.11	$H^{13}COOCH_3$
23	-3	20		22	4	19		AE	161239.742	0.076	101.1	35.80	161237.1	b	0.19	CH_3CH_2CN, ν_{13}/ν_{21}
23	3	20	-1	22	4	19	-1	AA	161242.243	0.076	101.1	35.80	161237.1	d		
24	3	22		23	-2	21		AE	161944.043	0.085	103.9	46.50	161944.0	b	0.12	
24	3	22	1	23	2	21	1	AA	161946.427	0.085	103.9	46.50	161944.0	d		
25	-1	24		24	2	23		E3	162187.260	0.090	105.7	56.70	162187.0	b	0.45	CH_3OD, NH_2D
25	-1	24		24	2	23		E4	162187.310	0.090	105.7	56.70	162187.0	d		
25	2	24		24	-1	23		E3	162187.594	0.090	105.7	56.70	162187.0	d		
25	2	24		24	-1	23		E4	162187.643	0.090	105.7	56.70	162187.0	d		
25	-1	24		24	2	23		EA	162188.540	0.090	105.7	56.70	162187.0	d		
25	2	24		24	-1	23		EA	162188.874	0.090	105.7	56.70	162187.0	d		

Tabla C.1: continued.

J	K_a	K_c	p	J'	K'_a	K'_c	p'	State	ν_{lab}(MHz)	$e_{\nu_{lab}}$(MHz)	E_{upp}(K)	$S_{ij}\mu^2(D^2)$	ν_{obs}(MHz)	$f_{\nu_{obs}}$(MHz)	T_{MB}(K)	Blend
25	-1	24		24	2	23		AE	162343.678	0.093	105.9	56.60	162344.6	b	0.20	
25	2	24		24	-1	23		AE	162344.122	0.093	105.9	56.60	162344.6	d		
25	1	24	-1	24	2	23	-1	AA	162344.975	0.093	105.9	56.60	162344.6	d		
25	2	24	-1	24	1	23	-1	AA	162345.420	0.093	105.9	56.60	162344.6	d		
22	-13	9		22	-12	10		E3	162419.747	0.246	142.6	23.70	162420.8	b	0.06	
22	-13	9		22	-12	10		E4	162421.227	0.273	142.6	23.70	162420.8	d		
22	-13	9		22	-12	10		EA	162457.207	0.231	142.6	23.70	162457.1		0.07	
26	0	26		25	1	25		E3	162772.651	0.104	107.1	66.30	162457.1	b		$HCOOCH_3$, $^{34}SO_2$
26	0	26		25	1	25		E4	162772.652	0.104	107.1	66.30	162457.1	d		
26	1	26		25	0	25		E3	162772.653	0.104	107.1	66.30	162457.1	d		
26	1	26		25	0	25		E4	162772.654	0.104	107.1	66.30	162457.1	d		
26	0	26		25	1	25		EA	162772.851	0.104	107.1	66.30	162457.1	d		
26	1	26		25	0	25		EA	162772.853	0.104	107.1	66.30	162457.1	d		
26	0	26		25	1	25		AE	162812.053	0.105	107.2	66.40	162457.1	b		$HCOOCH_3$
26	1	26		25	0	25		AE	162812.056	0.105	107.2	66.40	162457.1	d		
26	0	26	1	25	1	25	1	AA	162812.260	0.104	107.2	66.40	162457.1	d		
26	1	26	1	25	0	25	1	AA	162812.263	0.104	107.2	66.40	162457.1	d		
19	5	15		18	-4	14		AE	162971.153	0.064	75.5	16.10	162971.0		0.12	NH_2CHO
19	5	15	1	18	4	14	1	AA	162995.644	0.065	75.5	16.00	162995.6		0.03	
11	7	5		10	6	5		E4	163274.565	0.025	37.7	17.30	163273.3		0.07	U-line
11	7	5		10	6	5		EA	163317.333	0.023	37.7	17.30	163322.0		0.22	$HC^{13}CCN$ ν_6=1$^-$
28	-13	15		28	-12	16		AE	163532.304	0.337	197.3	36.30	163531.9		0.07	
23	-4	19		22	5	18		E3	163901.231	0.072	105.1	26.80	163900.9		0.06	
23	-4	19		22	5	18		EA	163905.815	0.072	105.1	26.80	163907.0		0.06	
23	-4	19		22	5	18		E4	163913.347	0.073	105.1	26.80	163913.0	b	0.07	
21	5	17		20	-4	16		E4	163913.399	0.078	89.5	20.80	163913.0	d		
27	13	15		27	12	16		AE	164108.988	0.303	187.4	34.20	164109.5	b	0.09	
27	-13	14		27	-12	15		AE	164110.989	0.326	187.4	34.20	164109.5	d		
20	5	16		19	-4	15		AE	164344.951	0.071	82.5	18.30	164345.8		0.08	
9	-8	1		8	-7	1		E4	165017.679	0.041	36.6	19.90	165018.0		0.14	$H_2C^{17}O$
9	-8	1		8	-7	1		EA	165035.453	0.042	36.6	19.90	165035.8		0.12	
21	13	8	-1	21	12	9	1	AA	166479.113	0.233	135.6	21.60	166478.3	b	0.20	U-line
21	13	9	1	21	12	10	-1	AA	166479.114	0.233	135.6	21.60	166478.3	d		
11	-7	4		10	-6	4		E3	166637.991	0.026	39.2	17.40	166637.9		0.11	
11	-7	4		10	-6	4		E4	166666.867	0.026	39.2	17.40	166667.0		0.16	CH_3CH_2CN, CCS
11	-7	4		10	-6	4		EA	166679.722	0.026	39.2	17.40	166679.0		0.23	$CH_3CH_2C^{15}N$
9	8	2		8	7	2		AE	166715.991	0.038	36.5	19.90	166716.0		0.12	
20	13	7	-1	20	12	8	1	AA	166721.194	0.227	128.2	19.40	166723.0	b	0.12	U-line

Tabla C.1: continued.

J	K_a	K_c	p	J'	K'_a	K'_c	p'	State	ν_{lab}(MHz)	e$_{\nu_{lab}}$(MHz)	E_{upp}(K)	$S_{ij}\mu^2(D^2)$	ν_{obs}(MHz)	f$_{\nu_{obs}}$(MHz)	$T_{\rm MB}$(K)	Blend
20	13	8	1	20	12	9	-1	AA	166721.194	0.227	128.2	19.40	166723.0	d		
9	-8	1		8	-7	1		AE	166741.311	0.035	36.5	19.90	166742.0		0.12	
9	8	2	-1	8	7	1	-1	AA	166760.171	0.033	36.5	19.90	166742.0	b		CH_3CH_2OH
9	8	1	1	8	7	2	1	AA	166760.173	0.033	36.5	19.90	166742.0	d		
18	13	5	-1	18	12	6	1	AA	167113.474	0.217	114.5	14.90	167114.4	b	0.06	
18	13	6	1	18	12	7	-1	AA	167113.474	0.217	114.5	14.90	167114.4	d		
24	-3	21		23	4	20		E3	167218.928	0.079	108.8	38.90	167219.5	b	0.13	
24	-3	21		23	4	20		E4	167219.720	0.079	108.8	38.90	167219.5	d		
24	4	21		23	-3	20		E4	167629.802	0.080	108.8	39.00	167629.0	b	0.13	
24	4	21		23	-3	20		E3	167630.069	0.080	108.8	39.00	167629.0	d		
24	4	21		23	-3	20		EA	167633.720	0.080	108.8	39.00	167634.0		0.24	U-line
25	-2	23		24	3	22		E3	167796.590	0.090	111.6	49.40	167800.9	b	0.25	U-line
25	-2	23		24	3	22		E4	167796.717	0.090	111.6	49.40	167800.9	d		
11	7	5		10	6	5		AE	167798.415	0.024	39.0	17.40	167800.9	d		
25	-2	23		24	3	22		EA	167798.891	0.089	111.6	49.40	167800.9	d		
25	3	23		24	-2	22		E3	167808.088	0.090	111.6	49.40	167807.0	b	0.34	$^{13}CH_3CH_2CN$
25	3	23		24	-2	22		E4	167808.187	0.090	111.6	49.40	167807.0	d		
13	-6	7		12	-5	7		E3	167809.142	0.023	43.9	14.80	167807.0	d		
25	3	23		24	-2	22		EA	167810.405	0.089	111.6	49.40	167807.0	d		
11	7	5	1	10	6	4	1	AA	167839.861	0.021	39.0	17.40	167841.0		0.17	U-line
13	-6	7		12	-5	7		E4	167842.874	0.023	43.9	14.80	167843.9	b	0.20	U-line
11	7	4	-1	10	6	5	-1	AA	167843.656	0.021	39.0	17.40	167843.9	d		
25	3	23		24	-2	22		AE	168077.180	0.096	112.0	49.30	168078.3	b	0.22	$HCOO^{13}CH_3$, $HCOOCH_3$
25	3	23	1	24	2	22	1	AA	168079.522	0.096	112.0	49.30	168078.3	d		
26	-1	25		25	2	24		E3	168336.483	0.102	113.8	59.40	168078.3	b		CH_3CH_2CN ν_{13}/ν_{21}
26	-1	25		25	2	24		E4	168336.530	0.102	113.8	59.40	168078.3	d		
26	2	25		25	-1	24		E3	168336.647	0.102	113.8	59.40	168078.3	d		
26	2	25		25	-1	24		E4	168336.693	0.102	113.8	59.40	168078.3	d		
26	-1	25		25	2	24		EA	168337.747	0.101	113.8	59.40	168078.3	d		
26	2	25		25	-1	24		EA	168337.911	0.101	113.8	59.40	168078.3	d		
26	-1	25		25	2	24		AE	168492.483	0.105	114.0	59.30	168078.3	b		$HCOOCH_3$
26	2	25		25	-1	24		AE	168492.701	0.105	114.0	59.30	168078.3	d		
26	1	25	-1	25	2	24	-1	AA	168493.765	0.105	114.0	59.30	168078.3	d		
26	2	25	-1	25	1	24	-1	AA	168493.984	0.105	114.0	59.30	168078.3	d		
27	0	27		26	1	26		E3	168923.862	0.117	115.2	69.00	168923.9	b	0.32	
27	0	27		26	1	26		E4	168923.862	0.117	115.2	69.00	168923.9	d		
27	1	27		26	0	26		E3	168923.863	0.117	115.2	69.00	168923.9	d		
27	1	27		26	0	26		E4	168923.863	0.117	115.2	69.00	168923.9	d		

Tabla C.1: continued.

J	K_a	K_c	p	J'	K'_a	K'_c	p'	State	ν_{lab}(MHz)	$e_{\nu_{lab}}$(MHz)	E_{upp}(K)	$S_{ij}\mu^2(D^2)$	ν_{obs}(MHz)	$f_{\nu_{obs}}$(MHz)	T_{MB}(K)	Blend
27	0	27		26	1	26		EA	168924.049	0.116	115.2	69.00	168923.9	d		
27	1	27		26	0	26		EA	168924.050	0.116	115.2	69.00	168923.9	d		
27	0	27		26	1	26		AE	168962.642	0.118	115.3	69.10	168962.9	b	0.61	CH_3CH_2CN
27	1	27		26	0	26		AE	168962.644	0.118	115.3	69.10	168962.9	d		
27	0	27	1	26	1	26	1	AA	168962.836	0.117	115.3	69.10	168962.9	d		
27	1	27	1	26	0	26	1	AA	168962.838	0.117	115.3	69.10	168962.9	d		
23	5	19		22	-4	18		E4	171239.933	0.083	105.2	27.10	171239.5		0.08	$HCO^{18}OCH_3$
23	5	19		22	-4	18		EA	171255.472	0.082	105.2	27.10	171254.4		0.13	U-line
10	-8	2		9	-7	2		EA	172308.774	0.041	40.1	19.90	172307.0		0.29	$CH_2CH^{13}CN$
10	8	3	-1	9	7	2	-1	AA	174041.551	0.032	40.0	19.90	174040.8	b	0.41	CH_3CH_2CN ν_{13}/ν_{21}
10	8	2	1	9	7	3	1	AA	174041.564	0.032	40.0	19.90	174040.8	d		
27	-1	26		26	2	25		E3	174485.602	0.114	122.1	62.10	174487.1	b	0.56	
27	-1	26		26	2	25		E4	174485.645	0.114	122.1	62.10	174487.1	d		
27	2	26		26	-1	25		E3	174485.681	0.114	122.1	62.10	174487.1	d		
27	2	26		26	-1	25		E4	174485.725	0.114	122.1	62.10	174487.1	d		
27	-1	26		26	2	25		EA	174486.851	0.114	122.1	62.10	174487.1	d		
27	2	26		26	-1	25		EA	174486.930	0.114	122.1	62.10	174487.1	d		
27	-1	26		26	2	25		AE	174641.195	0.118	122.3	62.00	174642.0	b	0.49	
27	2	26		26	-1	25		AE	174641.302	0.118	122.3	62.00	174642.0	d		
27	1	26	-1	26	2	25	-1	AA	174642.463	0.118	122.3	62.00	174642.0	d		
27	2	26	-1	26	1	25	-1	AA	174642.570	0.118	122.3	62.00	174642.0	d		
28	1	28		27	0	27		E4	175074.852	0.131	123.6	71.70	175074.5	b	0.68	
28	0	28		27	1	27		E4	175074.852	0.131	123.6	71.70	175074.5	d		
28	1	28		27	0	27		E3	175074.853	0.131	123.6	71.70	175074.5	d		
28	0	28		27	1	27		E3	175074.853	0.131	123.6	71.70	175074.5	d		
28	1	28		27	0	27		EA	175075.027	0.130	123.6	71.70	175074.5	d		
28	0	28		27	1	27		EA	175075.027	0.130	123.6	71.70	175074.5	d		
28	0	28		27	1	27		AE	175113.018	0.132	123.7	71.80	175074.5	b		SO_2
28	1	28		27	0	27		AE	175113.019	0.132	123.7	71.80	175074.5	d		
28	0	28	1	27	1	27	1	AA	175113.199	0.131	123.7	71.80	175074.5	d		
28	1	28	1	27	0	27	1	AA	175113.200	0.131	123.7	71.80	175074.5	d		
28	13	16		27	14	14		E3	175430.540	1.973	193.6	71.40	175428.3	b	0.32	
28	-13	15		27	-13	14		E3	175430.546	1.973	193.6	71.40	175428.3	d		
28	13	16		27	14	14		E4	175430.630	1.978	193.6	71.40	175428.3	d		
28	-13	15		27	-13	14		E4	175430.636	1.978	193.6	71.40	175428.3	d		
28	13	16		27	14	14		EA	175430.676	1.970	193.6	71.40	175428.3	d		
28	-13	15		27	-13	14		EA	175430.682	1.970	193.6	71.40	175428.3	d		
9	9	1		8	8	1		EA	175503.343	0.053	40.3	22.70	175503.4		0.30	

Tabla C.1: continued.

J	K_a	K_c	p	J'	K'_a	K'_c	p'	State	ν_{lab}(MHz)	$e_{\nu_{lab}}$(MHz)	E_{upp}(K)	$S_{ij}\mu^2(D^2)$	ν_{obs}(MHz)	$f_{\nu_{obs}}$(MHz)	T_{MB}(K)	Blend
23	6	18		22	-5	17		AE	196983.379	0.120	109.8	18.20	196981.7		0.08	
12	9	4		11	8	4		E3	197355.526	0.061	51.8	22.50	197354.2	b	0.12	$(CH_3)_2CO$
28	5	24		27	-4	23		E4	198049.912	0.129	149.7	42.10	197354.2	d		
29	4	26		28	-3	25		E3	198049.956	0.142	153.4	52.90	198047.9	b	0.26	CH_3CH_2CN
29	4	26		28	-3	25		E4	198050.094	0.142	153.4	52.90	198047.9	d		
28	5	24		27	-4	23		E3	198050.170	0.129	149.7	42.10	198047.9	d		
29	4	26		28	-3	25		EA	198053.160	0.142	153.4	52.90	198055.4	b	0.15	$DCOOCH_3$
28	5	24		27	-4	23		EA	198054.887	0.128	149.7	42.10	198055.4	d		
30	-2	28		29	3	27		E3	198519.079	0.157	156.3	63.00	198055.4	b		$HCOOCH_3$
30	-2	28		29	3	27		E4	198519.164	0.158	156.3	63.00	198055.4	d		
30	3	28		29	-2	27		E3	198519.476	0.158	156.3	63.00	198055.4	d		
30	3	28		29	-2	27		E4	198519.560	0.158	156.3	63.00	198055.4	d		
30	-2	28		29	3	27		EA	198521.270	0.157	156.3	63.00	198055.4	d		
30	3	28		29	-2	27		EA	198521.668	0.157	156.3	63.00	198055.4	d		
28	5	24		27	-4	23		AE	198605.087	0.140	150.3	41.80	198608.0	b	0.18	
28	5	24	1	27	4	23	1	AA	198610.246	0.140	150.3	41.80	198608.0	d		
30	-2	28		29	3	27		AE	198782.672	0.165	156.7	62.90	198783.0	b	0.23	$CH_2CHCN\ \nu_{11}$=1
30	3	28		29	-2	27		AE	198783.197	0.165	156.7	62.90	198783.0	d		
30	2	28	1	29	3	27	1	AA	198784.883	0.165	156.7	62.90	198783.0	d		
30	3	28	1	29	2	27	1	AA	198785.409	0.165	156.7	62.90	198783.0	d		
26	6	21		25	-5	20		E4	198901.855	0.139	135.7	26.50	198901.7		0.03	
26	6	21		25	-5	20		E3	198917.069	0.139	135.7	26.50	198901.7			$^{13}CH_3OH$
26	6	21		25	-5	20		EA	198926.400	0.137	135.8	26.50	198926.7		0.12	$HCOOCH_3$
12	-9	3		11	-8	3		EA	199697.897	0.061	53.6	22.60	199695.5		0.28	$HCOOCH_3$
10	10	1		9	9	1		AE	200764.948	0.083	51.6	25.40	200764.1		0.21	CH_3CH_2OH
28	-5	23		27	6	22		EA	201288.774	0.128	154.9	32.80	201289.3		0.08	
28	-5	23		27	6	22		E4	201292.286	0.128	154.9	32.80	201294.2		0.05	
14	-8	6		13	-7	6		AE	202998.796	0.038	57.6	20.10	202999.1		0.26	U-line
14	8	7	-1	13	7	6	-1	AA	203015.453	0.036	57.6	20.10	203016.6		0.15	U-line
14	8	6	1	13	7	7	1	AA	203019.565	0.036	57.6	20.10	203016.6			U-line
29	-4	25		28	5	24		E3	203702.147	0.142	159.5	45.00	203702.5	b	0.11	
29	-4	25		28	5	24		E4	203702.732	0.142	159.5	45.00	203702.5	d		
29	-4	25		28	5	24		EA	203706.149	0.141	159.5	45.00	203706.2		0.17	U-line
17	7	11		16	6	11		E3	205530.988	0.040	68.6	16.80	205526.7		0.12	$HCOOCH_3\ \nu_t$=1
17	7	11		16	6	11		EA	205540.816	0.038	68.6	16.80	205540.4		0.12	$HCOO^{13}CH_3\ \nu_t$=1
29	-6	23		28	7	22		EA	205620.978	0.201	169.6	24.50	205620.4		0.06	
25	16	10	-1	25	15	11	1	AA	205901.510	0.646	196.4	24.20	205901.7	b	0.14	$^{13}CH_3CH_2CN$
25	16	9	1	25	15	10	-1	AA	205901.510	0.646	196.4	24.20	205901.7	d		

Tabla C.1: continued.

J	K_a	K_c	p	J'	K'_a	K'_c	p'	State	ν_{lab}(MHz)	$e_{\nu_{lab}}$(MHz)	E_{upp}(K)	$S_{ij}\mu^2(D^2)$	ν_{obs}(MHz)	$f_{\nu_{obs}}$(MHz)	T_{MB}(K)	Blend
28	6	23		27	-5	22		E3	206866.750	0.144	155.0	33.00	206868.0		0.05	
11	10	2	-1	10	9	1	-1	AA	208091.622	0.070	55.5	25.30	208092.9	b	0.30	
11	10	1	1	10	9	2	1	AA	208091.622	0.070	55.5	25.30	208092.9	d		
15	8	8		14	7	8		AE	210149.079	0.042	62.9	20.20	210150.4		0.22	$CH_3CH_2{}^{13}CN$
30	4	26	1	29	5	25	1	AA	210323.322	0.170	170.2	47.50	210323.0		0.36	$SO^{17}O$
12	10	3		11	9	3		E3	210752.521	0.093	57.7	25.20	210751.7		0.08	
12	10	3		11	9	3		EA	210779.717	0.080	57.7	25.20	210780.4		0.13	$CH_3CH_2{}^{13}CN$
17	7	10	-1	16	6	11	-1	AA	210850.135	0.041	69.8	17.20	210850.4		0.09	
18	7	12		17	6	12		E4	212120.720	0.046	75.0	16.40	212121.7		0.06	
12	-10	2		11	-9	2		EA	212547.338	0.087	59.6	25.20	212549.1		0.12	CH_3CH_2OCOH
16	8	9		15	7	9		E3	212711.042	0.049	67.1	20.00	212709.1		0.04	U-line
16	8	9		15	7	9		EA	212727.898	0.045	67.1	20.00	212727.9		0.18	SO_2 ν_2=1, $(CH_3)_2CO$
14	-9	5		13	-8	5		EA	214203.534	0.063	63.0	22.70	214204.1		0.07	
30	-5	25		29	6	24		E3	215017.224	0.156	175.4	39.20	215017.9		0.07	
30	-5	25		29	6	24		E4	215019.707	0.156	175.4	39.20	215021.7	b	0.16	
30	-5	25		29	6	24		EA	215021.349	0.155	175.4	39.20	215021.7	d		
22	-17	0		22	-16	0		E4	215021.410	0.811	180.1	15.40	215021.7	d		
14	9	6		13	8	6		AE	216462.024	0.058	63.0	22.70	216462.9		0.11	U-line
14	-9	5		13	-8	5		AE	216482.322	0.056	63.0	22.70	216481.6		0.05	
14	9	6	1	13	8	5	1	AA	216505.961	0.050	63.0	22.70	216506.6	b	0.28	
14	9	5	-1	13	8	6	-1	AA	216506.069	0.050	63.0	22.70	216506.6	d		
11	11	1		10	10	1		E3	216865.997	0.139	60.1	28.10	216864.1		0.07	
11	11	1		10	10	1		EA	216897.591	0.116	60.1	28.10	216896.7		0.16	
19	17	2	-1	19	16	3	1	AA	220112.547	0.769	159.6	8.14	220114.1	b	0.03	
19	17	3	1	19	16	4	-1	AA	220112.547	0.769	159.6	8.14	220114.1	d		
19	7	13	1	18	6	12	1	AA	221234.597	0.058	83.0	16.80	221234.2		0.09	
13	10	4		12	9	4		AE	222600.300	0.083	64.2	25.30	222600.3		0.22	U-line
13	10	4	-1	12	9	3	-1	AA	222643.709	0.070	64.2	25.30	222645.3	b	0.14	
13	10	3	1	12	9	4	1	AA	222643.709	0.070	64.2	25.30	222645.3	d		
15	-9	6		14	-8	6		AE	223709.957	0.058	68.3	22.80	222645.3			U-line
15	9	7	1	14	8	6	1	AA	223733.390	0.053	68.3	22.80	223734.1	b	0.15	$(CH_3)_2CO$
15	9	6	-1	14	8	7	-1	AA	223733.785	0.053	68.3	22.80	223734.1	d		
14	10	5		13	9	5		EA	225347.534	0.083	67.2	25.20	225347.9	b	0.04	
12	-11	1		11	-10	1		E3	225350.418	0.129	66.2	28.00	225347.9	d		
12	-11	1		11	-10	1		EA	225391.693	0.121	66.2	28.00	225391.7		0.10	
20	7	14		19	-6	13		AE	225797.538	0.068	90.2	16.30	225796.6		0.21	CH_3CH_2OH
20	-7	13		19	-6	13		EA	228415.576	0.075	90.3	15.80	228415.4		0.17	
12	11	2		11	10	2		AE	228661.035	0.117	66.4	28.00	228661.6		0.37	$CH_3CH_2{}^{13}CN$

Tabla C.1: continued.

J	K_a	K_c	p	J'	K'_a	K'_c	p'	State	ν_{lab}(MHz)	$e_{\nu_{lab}}$(MHz)	E_{upp}(K)	$S_{ij}\mu^2(D^2)$	ν_{obs}(MHz)	$f_{\nu_{obs}}$(MHz)	$T_{\rm MB}$(K)	Blend
12	11	1	-1	11	10	2	-1	AA	228703.247	0.101	66.5	19.70	228704.1	b	0.24	
12	11	2	1	11	10	1	1	AA	228703.247	0.101	66.5	19.70	228704.1	d		
18	-8	10		17	-7	10		EA	229691.854	0.066	81.0	20.20	229692.8		0.20	
14	-10	4		13	-9	4		AE	229879.711	0.085	69.2	25.30	229879.1		0.22	
14	10	5	-1	13	9	4	-1	AA	229907.958	0.072	69.2	25.30	229909.2	b	0.19	$^{33}SO_2$
14	10	4	1	13	9	5	1	AA	229907.960	0.072	69.2	25.30	229909.2	d		
18	-8	10		17	-7	10		AE	231364.498	0.055	80.9	17.90	231365.3		0.19	CH_3CHO
18	8	11		17	7	11		AE	231389.148	0.055	80.9	17.90	231387.9		0.12	$^{13}CH_3OH$
13	11	3		12	10	3		EA	231489.317	0.118	68.9	27.90	231487.9		0.17	
21	7	15		20	6	15		EA	232021.092	0.066	96.6	12.80	232020.4		0.17	
15	10	6		14	9	6		EA	232615.250	0.085	72.5	25.30	232615.7		0.18	$HCOOCH_3$
24	18	7	-1	24	17	8	1	AA	232650.423	1.082	209.3	17.80	232651.8	b	0.12	
24	18	6	1	24	17	7	-1	AA	232650.423	1.082	209.3	17.80	232651.8	d		
13	-11	2		12	-10	2		EA	232671.558	0.121	70.7	27.90	232673.1		0.20	$HCO^{18}OCH_3$
24	7	18		23	-6	17		AE	232888.090	0.148	122.5	16.30	232887.7		0.21	$HCOO^{13}CH_3$ ν_t=1
30	7	24		29	-6	23		AE	232914.864	0.217	181.4	28.70	232914.8		0.08	
24	7	18	1	23	6	17	1	AA	232930.284	0.151	122.5	16.30	232914.8			$HCOO^{13}CH_3$
17	-9	8		16	-8	8		E3	235771.740	0.080	79.9	22.90	235771.6		0.22	
17	-9	8		16	-8	8		EA	235814.224	0.075	79.9	22.90	235811.7		0.29	U-line
13	11	2	-1	12	10	3	-1	AA	235980.196	0.101	71.0	27.90	235978.7	b	0.45	$^{13}CH_3OH$, $(CH_3)_2CO$, CH_3CH_2OH
13	11	3	1	12	10	2	1	AA	235980.196	0.101	71.0	27.90	235978.7	d		
19	8	12		18	7	12		AE	238380.387	0.062	87.7	13.80	238379.4		0.17	
14	-11	3		13	-10	3		E3	239906.447	0.130	75.6	27.90	239906.7		0.17	CH_2DCH_2CN
18	-9	9		17	-8	9		EA	242955.602	0.081	86.3	22.90	242956.8		0.11	
19	9	11		18	8	11		E3	247728.612	0.085	91.4	22.70	247729.6		0.21	
19	9	11		18	8	11		EA	247750.293	0.077	91.4	22.70	247749.7		0.46	CH2CHCN ν=0. ν_{11}=1
13	12	2		12	11	2		AE	249234.743	0.164	78.4	30.70	249235.6		0.34	
13	-12	1		12	-11	1		AE	249238.947	0.179	78.4	30.70	249240.5		0.38	
14	12	3		13	11	3		EA	252218.086	0.170	81.0	30.60	252216.7		0.14	
19	9	11		18	8	11		AE	252284.292	0.075	93.0	22.90	252284.3		0.21	CH_3OCH_3
19	-9	10		18	-8	10		AE	252304.217	0.075	93.0	22.90	252305.4		0.16	U-line
22	-7	15		21	6	16		AE	252690.865	0.085	105.8	13.90	252690.7		0.20	
21	8	13	1	20	7	14	1	AA	252703.657	0.075	102.3	19.60	252705.7	b	0.16	
22	7	15	-1	21	6	16	-1	AA	252706.499	0.085	105.8	13.90	252705.7	d		
16	11	6		15	10	6		EA	253336.155	0.124	84.7	27.90	253335.5		0.30	$HCOOCH_3$
22	8	15		21	7	15		EA	253435.302	0.083	108.8	18.50	253435.5		0.32	
14	12	3	-1	13	11	2	-1	AA	256549.257	0.147	83.3	20.10	256549.7	b	0.20	
14	12	2	1	13	11	3	1	AA	256549.257	0.147	83.3	20.10	256549.7	d		

Tabla C.1: continued.

J	K_a	K_c	p	J'	K'_a	K'_c	p'	State	ν_{lab}(MHz)	$e_{\nu_{lab}}$(MHz)	E_{upp}(K)	$S_{ij}\mu^2(D^2)$	ν_{obs}(MHz)	$f_{\nu_{obs}}$(MHz)	T_{MB}(K)	Blend
16	11	6		15	10	6		AE	257729.747	0.123	86.8	28.00	257729.6		0.18	$H^{13}COOCH_3$ ν_t=1
16	11	6	1	15	10	5	1	AA	257771.550	0.108	86.8	28.00	257771.7	b	0.26	$HCOOCH_3$
16	11	5	-1	15	10	6	-1	AA	257771.551	0.108	86.8	28.00	257771.7	d		
18	10	9	-1	17	9	8	-1	AA	258811.393	0.086	92.4	25.50	257810.6	b	0.26	
18	10	8	1	17	9	9	1	AA	258811.791	0.086	92.4	25.50	257810.6	d		
20	9	11	-1	19	8	12	-1	AA	259390.307	0.079	100.1	22.90	259390.5		0.20	
23	8	16		22	7	16		E4	259703.268	0.097	117.0	17.60	259703.6		0.19	$H^{13}COOCH_3$ ν_t=1
19	-10	9		18	-9	9		E3	263143.961	0.118	98.9	25.60	263142.9		0.05	
19	-10	9		18	-9	9		EA	263185.765	0.110	98.9	25.60	263185.6		0.06	
21	-9	12		20	-8	12		EA	264079.056	0.108	107.5	22.80	264079.2		0.18	CH_2DCH_2CN
17	-11	6		16	-10	6		AE	264982.355	0.133	92.8	28.10	264982.7		0.16	
24	8	17		23	-7	16		AE	265583.168	0.121	127.0	18.50	265583.7		0.24	$HCOOCH_3$
14	13	2		13	12	2		E3	265629.760	0.287	88.8	33.30	265630.6	b	0.37	
14	13	2		13	12	2		E4	265629.808	0.262	88.8	33.30	265630.6	d		
24	8	17	-1	23	7	16	-1	AA	265631.355	0.123	127.0	18.60	265630.6	d		
14	-13	1		13	-12	1		E4	265640.813	0.260	90.7	33.30	265641.7	b	0.16	
14	-13	1		13	-12	1		E3	265640.952	0.235	90.7	33.30	265641.7	d		
14	-13	1		13	-12	1		EA	265678.203	0.221	90.7	33.30	265679.5		0.19	
19	10	10	-1	18	9	9	-1	AA	265977.878	0.092	99.1	25.60	265977.6	b	0.45	$^{13}CH_3CCH$
19	10	9	1	18	9	10	1	AA	265979.061	0.092	99.1	25.60	265977.6	d		
16	-12	4		15	-11	4		EA	267361.480	0.166	93.7	30.60	267361.8		0.13	
18	11	8		17	10	8		E3	267813.105	0.155	97.0	28.00	267813.5		0.15	$HCO^{18}OCH_3$
18	11	8		17	10	8		EA	267844.232	0.132	97.0	28.00	267843.6		0.23	
25	8	18		24	-7	17		AE	268369.325	0.146	136.0	18.10	268369.2		0.15	CH_3OH
22	9	14		21	8	14		E3	268537.447	0.107	113.8	22.30	268537.6	b	0.18	
24	-8	16		23	-7	16		E4	268538.832	0.143	127.0	17.40	268537.6	d		
24	-8	16		23	-7	16		EA	268548.999	0.137	127.0	17.40	268537.6			$HCOOCH_3$
20	-10	10		19	-9	10		E3	270289.062	0.126	105.9	25.60	270286.7		0.13	U-line
16	12	5	-1	15	11	4	-1	AA	271082.774	0.153	94.2	30.60	271079.2	b	0.57	CH_3OD
16	12	4	1	15	11	5	1	AA	271082.774	0.153	94.2	30.60	271079.2	d		
15	13	3		14	12	3		EA	272962.236	0.240	94.1	33.20	272960.5	b	0.33	$DCOOCH_3$
15	-13	2		14	-12	2		EA	272962.827	0.221	96.0	33.20	272960.5	d		
20	10	11		19	9	11		AE	273068.344	0.105	106.1	25.60	273068.0		0.20	
22	9	14		21	8	14		AE	273208.155	0.098	115.4	18.10	273209.3		0.26	U-line
17	12	6		16	11	6		E4	274030.731	0.198	97.8	30.60	274030.4		0.18	U-line
17	12	6		16	11	6		E3	274036.240	0.212	97.8	30.60	274036.7		0.12	
17	12	6		16	11	6		EA	274071.315	0.178	97.8	30.60	274070.4		0.28	$(CH_3)_2CO$
17	-12	5		16	-11	5		E3	274590.253	0.183	99.6	30.60	274590.5		0.18	

Tabla C.1: continued.

J	K_a	K_c	p	J'	K'_a	K'_c	p'	State	ν_{lab}(MHz)	e$_{\nu_{lab}}$(MHz)	E_{upp}(K)	$S_{ij}\mu^2(D^2)$	ν_{obs}(MHz)	f$_{\nu_{obs}}$(MHz)	$T_{\rm MB}$(K)	Blend
17	-12	5		16	-11	5		E4	274595.198	0.199	99.7	30.60	274594.6		0.28	U-line
19	11	9		18	10	9		EA	275071.798	0.137	103.7	28.10	275070.4		0.25	
23	9	15		22	8	15		E3	275266.308	0.116	122.0	22.00	275070.4			$HCOOCH_3$
23	9	15		22	8	15		EA	275286.530	0.108	122.0	22.00	275287.3		0.12	
21	10	12		20	9	12		E4	275679.368	0.125	111.7	25.40	275679.6		0.14	
15	-13	2		14	-12	2		AE	277036.762	0.256	96.6	33.30	277037.9	b	0.35	CH_3OCH_3
15	13	3		14	12	3		AE	277038.234	0.230	96.6	33.30	277037.9	d		
26	-8	18		25	-7	18		E3	277628.312	0.192	145.4	12.60	277628.6		0.10	

Tabla A13. Parámetros de la cabecera de las columnas: Col. 1-3 y 5-7 se corresponde con los números cuánticos del nivel superior e inferior respectivamente. Col. 4 y 8 indican la paridad del nivel superior e inferior, respectivamente (sólo cuando el valor es no nulo). Col. 9 muestra el estado de simetría de la molécula: AA (A_1/A_2), EA (E_1), AE (E_2), E_3 o E_4. Col. 10 y 14 son las frecuencias de laboratorio y aquellas observadas asumiendo una v_{LSR}=8 km s^{-}1. Col. 11 es el error en la frecuencia de laboratorio. Col. 12 es la energía del nivel superior. Col. 13 es la fuerza de línea en unidades de D^2. Col. 15 india la línea solapada con la anterior (d) y solapada con la siguiente (b). Col. 16 es la temperatura del haz principal. Col. 17 muestra la especie molecular con la que solapan la línea.

Apéndice D

Tercero et al. 2015, A&A, 582, L1

A&A 582, L1 (2015)

Table A.1. Lines of trans-$CH_3CH_2OCH_3$ in ALMA SV data.

Species	Transition $J_{K_a,K_c} - J'_{K'_a,K'_c}$	Predicted frequency (MHz)	E_{upp} (K)	S_{ij}	Observed frequency (MHz)	T (K)	Blends
tEME-EE'	$31_{5,27}$–$31_{4,28}$	213 854.674	220.5	16.34	...	...	CH_3CH_2OH
tEME-EE	$31_{5,27}$–$31_{4,28}$	213 854.982	220.5	16.44	...	...	″
tEME-AE	$31_{5,27}$–$31_{4,28}$	213 855.220	220.5	16.40	...	...	″
tEME-EE	$28_{5,23}$–$28_{4,24}$	213 856.708	185.7	14.17	...	...	″
tEME-AE	$28_{5,23}$–$28_{4,24}$	213 857.473	185.7	13.94	...	...	″
tEME-EE'	$28_{5,23}$–$28_{4,24}$	213 857.509	185.7	13.69	...	...	″
tEME-EA	$31_{5,27}$–$31_{4,28}$	213 858.239	220.5	16.52	...	...	″
tEME-AA	$31_{5,27}$–$31_{4,28}$	213 858.632	220.5	16.53	...	...	″
tEME-EA	$28_{5,23}$–$28_{4,24}$	213 859.015	185.7	14.70	...	...	″
tEME-AA	$28_{5,23}$–$28_{4,24}$	213 859.367	185.7	14.73	...	...	″
tEME-EE'	$30_{5,26}$–$30_{4,27}$	214 028.729	208.6	15.58	...	...	CH_3COCH_3
tEME-EE	$30_{5,26}$–$30_{4,27}$	214 029.157	208.6	15.76	...	...	″
tEME-AE	$30_{5,26}$–$30_{4,27}$	214 029.345	208.6	15.68	...	...	″
tEME-EA	$30_{5,26}$–$30_{4,27}$	214 032.539	208.6	15.91	214 032.3†	0.50	
tEME-AA	$30_{5,26}$–$30_{4,27}$	214 032.539	208.6	15.91	†		
tEME-EE	$27_{5,22}$–$27_{4,23}$	214 131.118	174.9	13.15	214 132.6	0.58	
tEME-AE	$27_{5,22}$–$27_{4,23}$	214 132.010	174.9	12.80	†		
tEME-EE'	$27_{5,22}$–$27_{4,23}$	214 132.166	174.9	12.46	†		
tEME-EA	$27_{5,22}$–$27_{4,23}$	214 133.150	174.9	14.07	†		
tEME-AA	$27_{5,22}$–$27_{4,23}$	214 133.486	174.9	14.14	†		
tEME-EE'	$29_{5,25}$–$29_{4,26}$	214 196.531	196.9	14.73	214 196.8	0.94	
tEME-EE	$29_{5,25}$–$29_{4,26}$	214 197.122	196.9	15.01	†		
tEME-AE	$29_{5,25}$–$29_{4,26}$	214 197.239	196.9	14.88	†		
tEME-EA	$29_{5,25}$–$29_{4,26}$	214 200.673	196.9	15.31	214 201.4	0.41	
tEME-AA	$29_{5,25}$–$29_{4,26}$	214 201.091	196.9	15.31	†		
tEME-EE'	$21_{2,20}$–$20_{1,19}$	214 246.202	93.7	7.76	214 246.5	0.72	
tEME-EE	$21_{2,20}$–$20_{1,19}$	214 246.202	93.7	7.76	†		
tEME-AE	$21_{2,20}$–$20_{1,19}$	214 246.332	93.7	7.76	†		
tEME-EA	$21_{2,20}$–$20_{1,19}$	214 247.602	93.7	7.76	†		
tEME-AA	$21_{2,20}$–$20_{1,19}$	214 247.732	93.7	7.76	†		
tEME-EE'	$26_{5,22}$–$26_{4,22}$	214 355.828	164.4	2.47	...	...	CH_3CH_2OH; SO
tEME-EE'	$28_{5,24}$–$28_{4,25}$	214 356.510	185.7	13.69	...	...	″
tEME-AE	$26_{5,22}$–$26_{4,22}$	214 356.963	164.4	2.08	...	...	″
tEME-EE	$26_{5,22}$–$26_{4,22}$	214 357.232	164.4	1.63	...	...	″
tEME-EE	$28_{5,24}$–$28_{4,25}$	214 357.312	185.7	14.17	...	...	″
tEME-AE	$28_{5,24}$–$28_{4,25}$	214 357.333	185.7	13.93	...	...	″
tEME-EA	$28_{5,24}$–$28_{4,25}$	214 361.091	185.7	14.69	...	...	CH_3OCH_3
tEME-AA	$28_{5,24}$–$28_{4,25}$	214 361.527	185.7	14.72	...	...	″
tEME-EE	$26_{5,21}$–$26_{4,22}$	214 369.161	164.4	11.92	...	...	CH_3COOCH_3
tEME-AE	$26_{5,21}$–$26_{4,22}$	214 370.185	164.4	11.47	...	...	″
tEME-EE'	$26_{5,21}$–$26_{4,22}$	214 370.456	164.4	11.08	...	...	″
tEME-EA	$26_{5,21}$–$26_{4,22}$	214 370.843	164.4	13.42	...	...	″
tEME-AA	$26_{5,21}$–$26_{4,22}$	214 371.154	164.4	13.55	...	...	″
tEME-EE'	$27_{5,23}$–$27_{4,24}$	214 507.462	174.9	12.45	214 508.5	0.61	
tEME-AE	$27_{5,23}$–$27_{4,24}$	214 508.414	174.9	12.79	†		
tEME-EE	$27_{5,23}$–$27_{4,24}$	214 508.510	174.9	13.14	†		
tEME-EA	$27_{5,23}$–$27_{4,24}$	214 512.591	174.9	14.06	...	...	CH_3OCOH $v_t = 1$
tEME-AA	$27_{5,23}$–$27_{4,24}$	214 513.051	174.9	14.13	...	...	″
tEME-EE	$25_{5,20}$–$25_{4,21}$	214 575.213	154.4	10.56	214 576.5	0.58	
tEME-AE	$25_{5,20}$–$25_{4,21}$	214 576.349	154.4	10.10	†		
tEME-EA	$25_{5,20}$–$25_{4,21}$	214 576.498	154.4	12.69	†		
tEME-EE'	$25_{5,20}$–$25_{4,21}$	214 576.706	154.4	9.74	†		
tEME-AA	$25_{5,20}$–$25_{4,21}$	214 576.769	154.4	12.96	†		
tEME-EE'	$26_{5,22}$–$26_{4,23}$	214 648.535	164.4	11.08	...	...	CH_3OCOH
tEME-AE	$26_{5,22}$–$26_{4,23}$	214 649.611	164.4	11.47	...	...	″
tEME-EE	$26_{5,22}$–$26_{4,23}$	214 649.829	164.4	11.92	...	...	″
tEME-EA	$26_{5,22}$–$26_{4,23}$	214 654.288	164.5	13.41	...	...	″
tEME-AA	$26_{5,22}$–$26_{4,23}$	214 654.781	164.5	13.54	...	...	″
tEME-EE	$24_{5,19}$–$24_{4,20}$	214 753.118	144.7	9.23	214 754.0	0.94	
tEME-EA	$24_{5,19}$–$24_{4,20}$	214 754.023	144.7	11.84	†		
tEME-AA	$24_{5,19}$–$24_{4,20}$	214 754.233	144.7	12.38	†		
tEME-AE	$24_{5,19}$–$24_{4,20}$	214 754.329	144.7	8.86	†		
tEME-EE'	$24_{5,19}$–$24_{4,20}$	214 754.733	144.7	8.60	†		
tEME-EE'	$25_{5,21}$–$25_{4,22}$	214 779.208	154.4	9.73	...	...	CH_3OCOH
tEME-AE	$25_{5,21}$–$25_{4,22}$	214 780.378	154.4	10.10	...	...	″
tEME-EE	$25_{5,21}$–$25_{4,22}$	214 780.701	154.4	10.56	...	...	″
tEME-EA	$25_{5,21}$–$25_{4,22}$	214 785.581	154.4	12.69	...	...	″

Notes. Lines of trans-$CH_3CH_2OCH_3$ (tEME) ground state present in the spectral scan of Orion KL from the ALMA interferometer. Column 1 indicates the species, Col. 2 gives the transition, Col. 3 the predicted frequency, Col. 4 upper level energy, Col. 5 the line strength, Col. 6 observed frequency at the peak channel of the line (relative to a v_{LSR} of +7.5 km s^{-1}), Col. 7 brightness temperature at the peak channel of the line, and Col. 8 shows blends with other molecular species. (†) Blended with previous line.

Table A.1. continued.

Species	Transition $J_{K_a,K_c} - J'_{K'_a,K'_c}$	Predicted frequency (MHz)	E_{upp} (K)	S_{ij}	Observed frequency (MHz)	T (K)	Blends
tEME-AA	$25_{5,21}$–$25_{4,22}$	214 786.123	154.4	12.96	...	...	″
tEME-EE'	$23_{5,19}$–$23_{4,19}$	214 895.777	135.4	4.03	...	...	CH_3OCOH $v_t = 1$
tEME-AE	$23_{5,19}$–$23_{4,19}$	214 897.184	135.4	3.90	...	...	″
tEME-EE	$23_{5,19}$–$23_{4,19}$	214 897.739	135.4	3.67	...	...	″
tEME-EE'	$24_{5,20}$–$24_{4,21}$	214 899.228	144.7	8.61	...	...	″
tEME-AE	$24_{5,20}$–$24_{4,21}$	214 900.454	144.7	8.87	...	...	″
tEME-EE	$24_{5,20}$–$24_{4,21}$	214 900.844	144.7	9.23	...	...	″
tEME-EA	$23_{5,19}$–$23_{4,19}$	214 903.639	144.7	1.05	...	...	″
tEME-EA	$24_{5,20}$–$24_{4,21}$	214 906.128	144.7	11.83	214 906.7	1.30	
tEME-EE	$23_{5,18}$–$23_{4,19}$	214 906.260	135.4	8.13	†		
tEME-AA	$24_{5,20}$–$24_{4,21}$	214 906.739	144.7	12.38	†		
tEME-EA	$23_{5,18}$–$23_{4,19}$	214 906.872	135.4	10.76	†		
tEME-AA	$23_{5,18}$–$23_{4,19}$	214 906.992	135.4	11.80	†		
tEME-AE	$23_{5,18}$–$23_{4,19}$	214 907.507	135.4	7.91	†		
tEME-EE'	$23_{5,18}$–$23_{4,19}$	214 907.507	135.4	7.77	†		
tEME-EE	$24_{5,19}$–$24_{4,21}$	214 909.858	144.7	11.83	...	...	CH_3CH_2CN
tEME-EA	$24_{5,19}$–$24_{4,21}$	214 910.548	144.7	0.55	...	...	″
tEME-AE	$24_{5,19}$–$24_{4,21}$	214 911.166	144.7	3.51	...	...	″
tEME-EE'	$24_{5,19}$–$24_{4,21}$	214 911.685	144.7	3.77	...	...	″
tEME-EE'	$23_{5,19}$–$23_{4,20}$	215 008.545	135.4	7.77	...	...	CH_3OCOH $v_t = 2$
tEME-AE	$23_{5,19}$–$23_{4,20}$	215 009.791	135.4	7.91	...	...	″
tEME-EE	$23_{5,19}$–$23_{4,20}$	215 010.209	135.4	8.13	...	...	″
tEME-EA	$23_{5,19}$–$23_{4,20}$	215 015.810	135.4	10.75	215 016.5	1.16	
tEME-AA	$23_{5,19}$–$23_{4,20}$	215 016.519	135.4	11.80	†		
tEME-EE	$23_{5,18}$–$23_{4,20}$	215 018.730	135.4	3.67	...	...	CH_3OCOD
tEME-EA	$23_{5,18}$–$23_{4,20}$	215 019.043	135.4	1.05	...	...	″
tEME-AE	$23_{5,18}$–$23_{4,20}$	215 020.114	135.4	3.90	...	...	″
tEME-EE'	$23_{5,18}$–$23_{4,20}$	215 020.693	135.4	4.03	...	...	″
tEME-EE'	$22_{5,18}$–$22_{4,18}$	215 027.250	126.6	4.02	...	...	U-line
tEME-AE	$22_{5,18}$–$22_{4,18}$	215 028.719	126.6	3.99	...	...	″
tEME-EE	$22_{5,18}$–$22_{4,18}$	215 029.330	126.6	4.00	...	...	″
tEME-EA	$22_{5,18}$–$22_{4,18}$	215 035.544	126.6	1.78	...	...	CH_3OCOD, CH_3COOCH_3
tEME-EE	$22_{5,17}$–$22_{4,18}$	215 037.639	126.6	7.33	...	...	″
tEME-EA	$22_{5,17}$–$22_{4,18}$	215 038.085	126.6	9.45	...	...	″
tEME-AA	$22_{5,17}$–$22_{4,18}$	215 038.089	126.6	11.23	...	...	CH_3CH_2CN
tEME-AE	$22_{5,17}$–$22_{4,18}$	215 038.890	126.6	7.24	...	...	″
tEME-EE'	$22_{5,17}$–$22_{4,18}$	215 039.292	126.6	7.21	...	...	″
tEME-AA	$35_{2,33}$–$34_{3,32}$	215 107.148	250.8	9.27	...	...	CH_3COOCH_3, CH_3OCOH $v_t = 2$
tEME-EA	$35_{2,33}$–$34_{3,32}$	215 107.270	250.8	9.27	...	...	″
tEME-EE'	$22_{5,18}$–$22_{4,19}$	215 107.270	126.6	7.21	...	...	″
tEME-AE	$22_{5,18}$–$22_{4,19}$	215 108.508	126.6	7.24	...	...	″
tEME-EE	$22_{5,18}$–$22_{4,19}$	215 108.923	126.6	7.33	...	...	″
tEME-AE	$35_{2,33}$–$34_{3,32}$	215 109.184	250.8	9.27	...	...	″
tEME-EE	$35_{2,33}$–$34_{3,32}$	215 109.306	250.8	9.27	...	...	″
tEME-EE'	$35_{2,33}$–$34_{3,32}$	215 109.306	250.8	9.27	...	...	″
tEME-EA	$22_{5,18}$–$22_{4,19}$	215 114.713	126.6	9.44	...	...	$CH_3O^{13}COH$
tEME-AA	$22_{5,18}$–$22_{4,19}$	215 115.545	126.6	11.22	...	...	″
tEME-EE	$22_{5,17}$–$22_{4,19}$	215 117.232	126.6	3.90	...	...	CH_3CH_2CN
tEME-EA	$22_{5,17}$–$22_{4,19}$	215 117.254	126.6	1.78	...	...	″
tEME-AE	$22_{5,17}$–$22_{4,19}$	215 118.679	126.6	3.99	...	...	″
tEME-EE'	$22_{5,17}$–$22_{4,19}$	215 119.312	126.6	4.02	...	...	″
tEME-EE'	$21_{5,17}$–$21_{4,17}$	215 139.474	118.0	3.75	...	...	$CH_3O^{13}COH$ $v_t = 1$
tEME-AE	$21_{5,17}$–$21_{4,17}$	215 141.013	118.0	3.82	215 141.0	0.59	$CH_3O^{13}COH$ $v_t = 1$
tEME-EE	$21_{5,17}$–$21_{4,17}$	215 141.682	118.0	3.85	†		
tEME-EA	$21_{5,17}$–$21_{4,17}$	215 148.139	118.0	2.58	215 150.7	1.28	
tEME-EE	$21_{5,16}$–$21_{4,17}$	215 149.914	118.0	6.81	†		
tEME-AA	$21_{5,16}$–$21_{4,17}$	215 150.202	118.0	10.66	†		
tEME-EA	$21_{5,16}$–$21_{4,17}$	215 150.327	118.0	8.07	†		
tEME-AE	$21_{5,16}$–$21_{4,17}$	215 151.142	118.0	6.84	215 150.7†	1.28	
tEME-EE'	$21_{5,16}$–$21_{4,17}$	215 151.503	118.0	6.91	†		
tEME-EE'	$22_{5,17}$–$22_{4,18}$	215 195.665	118.0	6.91	...	...	SO
tEME-AE	$22_{5,17}$–$22_{4,18}$	215 196.869	118.0	6.84	...	...	″
tEME-EE	$22_{5,17}$–$22_{4,18}$	215 197.254	118.0	6.81	...	...	″
tEME-EA	$22_{5,17}$–$22_{4,18}$	215 203.100	118.0	8.07	...	...	″
tEME-AA	$22_{5,17}$–$22_{4,18}$	215 204.068	118.0	10.66	...	...	″
tEME-EA	$22_{5,16}$–$22_{4,18}$	215 205.287	118.0	2.58	...	...	″
tEME-EE	$22_{5,16}$–$22_{4,18}$	215 205.486	118.0	3.84	...	...	″
tEME-AE	$22_{5,16}$–$22_{4,18}$	215 206.998	118.0	3.82	...	...	″
tEME-EE'	$22_{5,16}$–$22_{4,18}$	215 207.694	118.0	3.75	...	...	″
tEME-EE'	$20_{5,16}$–$20_{4,16}$	215 234.851	109.9	3.26	...	...	″
tEME-AE	$20_{5,16}$–$20_{4,16}$	215 236.480	109.9	3.41	...	...	″
tEME-EE	$20_{5,16}$–$20_{4,16}$	215 237.223	109.9	3.55	...	...	″
tEME-EA	$20_{5,16}$–$20_{4,16}$	215 243.901	109.9	3.19	...	...	CH_3COOCH_3

Table A.1. continued.

Species	Transition $J_{K_a,K_c} - J'_{K'_a,K'_c}$	Predicted frequency (MHz)	E_{upp} (K)	S_{ij}	Observed frequency (MHz)	T (K)	Blends
							$CH_3O^{13}COH$, CH_3CH_2CN v_{13}/v_{21}
tEME-EE	$20_{5,15}$–$20_{4,16}$	215 245.438	109.9	6.54	...	...	″
tEME-AA	$20_{5,15}$–$20_{4,16}$	215 245.691	109.9	10.09	...	...	″
tEME-EA	$20_{5,15}$–$20_{4,16}$	215 245.934	109.9	6.89	...	...	″
tEME-AE	$20_{5,15}$–$20_{4,16}$	215 246.615	109.9	6.67	...	...	″
tEME-EE'	$20_{5,15}$–$20_{4,16}$	215 246.907	109.9	6.83	...	...	″
tEME-EE'	$20_{5,16}$–$20_{4,17}$	215 274.126	109.9	6.83	...	...	CH_3COOCH_3, U-line
tEME-AE	$20_{5,16}$–$20_{4,17}$	215 275.268	109.9	6.67	...	...	″
tEME-EE	$20_{5,16}$–$20_{4,17}$	215 275.595	109.9	6.54	...	...	″
tEME-EA	$20_{5,16}$–$20_{4,17}$	215 281.378	109.9	6.89	...	...	U-line
tEME-AA	$20_{5,16}$–$20_{4,17}$	215 282.470	109.9	10.09	...	...	″
tEME-EA	$20_{5,15}$–$20_{4,17}$	215 283.411	109.9	3.19	...	...	″
tEME-EE	$20_{5,15}$–$20_{4,17}$	215 283.810	109.9	3.55	...	...	″
tEME-AE	$20_{5,15}$–$20_{4,17}$	215 285.403	109.9	3.41	...	...	″
tEME-EE'	$20_{5,15}$–$20_{4,17}$	215 286.182	109.9	3.26	...	...	″
tEME-EE'	$19_{5,15}$–$19_{4,15}$	215 315.464	102.2	2.57	...	...	U-line
tEME-AE	$19_{5,15}$–$19_{4,15}$	215 317.213	102.2	2.79	215 317.4	0.54	U-line
tEME-EE	$19_{5,15}$–$19_{4,15}$	215 318.057	102.2	3.02	†		
tEME-EA	$19_{5,15}$–$19_{4,15}$	215 324.992	102.2	3.49	215 327.2	1.96	$^{13}CH_3OCOH$ $v_t = 1$
tEME-EE	$19_{5,14}$–$19_{4,15}$	215 326.280	102.2	6.50	†		
tEME-AA	$19_{5,14}$–$19_{4,15}$	215 326.637	102.2	9.52	†		
tEME-EA	$19_{5,14}$–$19_{4,15}$	215 326.971	102.2	6.03	†		
tEME-AE	$19_{5,14}$–$19_{4,15}$	215 327.373	102.2	6.72	†		
tEME-EE'	$19_{5,14}$–$19_{4,15}$	215 327.561	102.2	6.95	†		
tEME-EE'	$19_{5,15}$–$19_{4,16}$	215 343.169	102.2	6.95	...	...	CH_3OCOH
tEME-AE	$19_{5,15}$–$19_{4,16}$	215 344.214	102.2	6.72	...	...	″
tEME-EE	$19_{5,15}$–$19_{4,16}$	215 344.450	102.2	6.50	...	....	″
tEME-EA	$19_{5,15}$–$19_{4,16}$	215 350.059	102.2	6.03	215 351.2	0.91	CH_3CH_2CN ($v = 0$, v_{13}/v_{21})
tEME-AA	$19_{5,15}$–$19_{4,16}$	215 351.248	102.2	9.52	†		
tEME-EA	$19_{5,14}$–$19_{4,16}$	215 352.037	102.2	3.49	†		
tEME-EE	$19_{5,14}$–$19_{4,16}$	215 352.674	102.2	3.02	†		
tEME-AE	$19_{5,14}$–$19_{4,16}$	215 354.374	102.2	2.79	...	...	CH_3CH_2CN ($v = 0$, v_{13}/v_{21})
tEME-EE'	$19_{5,14}$–$19_{4,16}$	215 355.266	102.2	2.57	...	...	″
tEME-EE'	$12_{3,10}$–$11_{2,9}$	215 361.252	40.5	4.16	215 361.7	0.43	
tEME-EE	$12_{3,10}$–$11_{2,9}$	215 361.484	40.5	4.18	†		
tEME-AE	$12_{3,10}$–$11_{2,9}$	215 361.676	40.5	4.17	†		
tEME-EA	$12_{3,10}$–$11_{2,9}$	215 364.224	40.5	4.19	...	...	CH_3CH_2OH
tEME-AA	$12_{3,10}$–$11_{2,9}$	215 364.533	40.5	4.20	...	...	″
tEME-EA	$18_{5,14}$–$18_{4,14}$	215 393.299	94.8	3.48	215 395.5	1.01	
tEME-EE	$18_{5,13}$–$18_{4,14}$	215 394.256	94.8	6.65	†		
tEME-AA	$18_{5,13}$–$18_{4,14}$	215 394.875	94.8	8.95	†		
tEME-AE	$18_{5,13}$–$18_{4,14}$	215 395.227	94.8	6.94	†		
tEME-EA	$18_{5,13}$–$18_{4,14}$	215 395.264	94.8	5.47	†		
tEME-EE'	$18_{5,13}$–$18_{4,14}$	215 395.280	94.8	7.19	†		
tEME-EE'	$18_{5,14}$–$18_{4,15}$	215 403.394	94.8	7.19	215 404.5	0.91	
tEME-AE	$18_{5,14}$–$18_{4,15}$	215 404.308	94.8	6.94	†		
tEME-EE	$18_{5,14}$–$18_{4,15}$	215 404.417	94.8	6.65	†		
tEME-EA	$18_{5,14}$–$18_{4,15}$	215 409.728	94.8	5.47	215 411.2	0.59	
tEME-AA	$18_{5,14}$–$18_{4,15}$	215 410.979	94.8	8.95	†		
tEME-EA	$18_{5,14}$–$18_{4,15}$	215 411.693	94.8	3.48	†		
tEME-EE	$18_{5,14}$–$18_{4,15}$	215 412.657	94.8	2.31	†		
tEME-EA	$17_{5,13}$–$17_{4,13}$	215 450.467	87.9	3.22	215 451.7	1.65	
tEME-EE	$17_{5,12}$–$17_{4,13}$	215 450.974	87.9	6.90	†		
tEME-EE'	$17_{5,12}$–$17_{4,13}$	215 451.703	87.9	7.39	†		
tEME-AE	$17_{5,12}$–$17_{4,13}$	215 451.799	87.9	7.18	†		
tEME-AA	$17_{5,12}$–$17_{4,13}$	215 452.025	87.9	8.39	†		
tEME-EA	$17_{5,12}$–$17_{4,13}$	215 452.436	87.9	5.17	†		
tEME-EE'	$17_{5,13}$–$17_{4,13}$	215 455.422	87.9	7.39	215 456.2	1.60	$^{13}CH_3OCOH$ $v_t = 1$
tEME-EE	$17_{5,13}$–$17_{4,13}$	215 456.151	87.9	6.90	†		
tEME-AE	$17_{5,13}$–$17_{4,13}$	215 456.193	87.9	7.18	†		
tEME-EA	$17_{5,13}$–$17_{4,14}$	215 461.025	87.9	5.17	215 462.2	1.81	U-line
tEME-AA	$17_{5,13}$–$17_{4,14}$	215 462.304	87.9	8.39	†		
tEME-EA	$17_{5,12}$–$17_{4,14}$	215 462.994	87.9	3.22	†		
tEME-EE'	$27_{1,27}$–$26_{0,26}$	215 478.840	144.2	21.60	215 479.5	1.81	
tEME-EE	$27_{1,27}$–$26_{0,26}$	215 478.840	144.2	21.60	†		
tEME-AE	$27_{1,27}$–$26_{0,26}$	215 478.854	144.2	21.60	†		
tEME-EA	$27_{1,27}$–$26_{0,26}$	215 479.025	144.2	21.60	†		
tEME-AA	$27_{1,27}$–$26_{0,26}$	215 479.039	144.2	21.60	†		
tEME-EE	$16_{5,11}$–$16_{4,12}$	215 497.897	81.3	7.05	215 498.7	1.96	CH_3CH_2CN v_{13}/v_{21}
tEME-EA	$16_{5,12}$–$16_{4,12}$	215 497.943	81.3	2.74	†		
tEME-EE'	$16_{5,11}$–$16_{4,12}$	215 498.372	81.3	7.37	†		
tEME-AE	$16_{5,11}$–$16_{4,12}$	215 498.590	81.3	7.23	†		
tEME-AA	$16_{5,11}$–$16_{4,12}$	215 499.524	81.3	7.82	215 500.2†	1.22	

Table A.1. continued.

Species	Transition $J_{K_a,K_c} - J'_{K'_a,K'_c}$	Predicted frequency (MHz)	E_{upp} (K)	S_{ij}	Observed frequency (MHz)	T (K)	Blends
tEME-EE'	$16_{5,12}$–$16_{4,13}$	215 499.830	81.3	7.37	†		
tEME-EA	$16_{5,11}$–$16_{4,12}$	215 499.921	81.3	5.08	†		
tEME-EE	$16_{5,12}$–$16_{4,13}$	215 500.305	81.3	7.05	†		
tEME-AE	$16_{5,12}$–$16_{4,13}$	215 500.485	81.3	7.24	†		
tEME-EA	$16_{5,12}$–$16_{4,13}$	215 504.636	81.3	5.08	215 506.2	1.22	$CH_3C^{13}CH$
tEME-AA	$16_{5,12}$–$16_{4,13}$	215 505.905	81.3	7.82	†		
tEME-EA	$16_{5,11}$–$16_{4,13}$	215 506.613	81.3	2.74	†		
tEME-EE	$15_{5,10}$–$15_{4,11}$	215 536.404	75.1	6.94	215 537.7	1.33	
tEME-EE'	$15_{5,10}$–$15_{4,11}$	215 536.720	75.1	7.08	†		
tEME-EA	$15_{5,11}$–$15_{4,11}$	215 537.002	75.1	2.05	†		
tEME-AE	$15_{5,10}$–$15_{4,11}$	215 537.010	75.1	7.03	†		
tEME-EE'	$15_{5,11}$–$15_{4,12}$	215 537.169	75.1	7.08	†		
tEME-EE	$15_{5,11}$–$15_{4,12}$	215 537.485	75.1	6.94	†		
tEME-AE	$15_{5,11}$–$15_{4,12}$	215 537.757	75.1	7.08	†		
tEME-AA	$15_{5,10}$–$15_{4,11}$	215 538.650	75.1	7.25	†		
tEME-EA	$15_{5,10}$–$15_{4,11}$	215 538.990	75.1	5.21	†		
tEME-EA	$15_{5,11}$–$15_{4,12}$	215 541.270	75.1	5.21	215 541.5†	1.06	CH_3COOCH_3
tEME-AA	$15_{5,11}$–$15_{4,12}$	215 542.488	75.1	7.25	†		
tEME-EA	$15_{5,10}$–$15_{4,12}$	215 543.258	75.1	2.05	†		
tEME-EE	$14_{5,9}$–$14_{4,10}$	215 567.750	69.3	6.58	215 567.9	2.13	
tEME-EE'	$14_{5,9}$–$14_{4,10}$	215 567.993	69.3	6.63	†		
tEME-EE'	$14_{5,10}$–$14_{4,11}$	215 568.043	69.3	6.63	†		
tEME-EE	$14_{5,10}$–$14_{4,11}$	215 568.286	69.3	6.58	†		
tEME-AE	$14_{5,9}$–$14_{4,10}$	215 568.316	69.3	6.61	†		
tEME-AE	$14_{5,10}$–$14_{4,11}$	215 568.602	69.3	6.61	215 571.7	1.89	CH_3OCOH $v_t = 1$
tEME-AE	$14_{5,10}$–$14_{4,10}$	215 568.774	69.3	1.23	†		
tEME-AA	$14_{5,9}$–$14_{4,10}$	215 570.539	69.3	6.68	†		
tEME-EA	$14_{5,9}$–$14_{4,10}$	215 570.772	69.3	5.45	†		
tEME-EA	$14_{5,10}$–$14_{4,11}$	215 571.650	69.3	5.45	†		
tEME-AA	$14_{5,10}$–$14_{4,11}$	215 572.766	69.3	6.68	†		
tEME-EA	$14_{5,9}$–$14_{4,11}$	215 573.648	69.3	1.23	†		
tEME-EE	$13_{5,8}$–$13_{4,9}$	215 593.014	63.9	6.08	215 593.5	1.41	
tEME-EE'	$13_{5,9}$–$13_{4,10}$	215 593.138	63.9	6.09	†		
tEME-EE'	$13_{5,8}$–$13_{4,9}$	215 593.228	63.9	6.09	†		
tEME-EE	$13_{5,9}$–$13_{4,10}$	215 593.353	63.9	6.08	†		
tEME-AE	$13_{5,8}$–$13_{4,9}$	215 593.566	63.9	6.09	†		
tEME-AE	$13_{5,9}$–$13_{4,10}$	215 593.687	63.9	6.09	†		
tEME-EA	$13_{5,9}$–$13_{4,9}$	215 594.282	63.9	0.53	†		
tEME-AA	$13_{5,8}$–$13_{4,9}$	215 596.207	63.9	6.11	215 596.5	1.12	
tEME-EA	$13_{5,8}$–$13_{4,9}$	215 596.289	63.9	5.58	†		
tEME-EA	$13_{5,9}$–$13_{4,10}$	215 596.478	63.9	5.58	†		
tEME-AA	$13_{5,9}$–$13_{4,10}$	215 597.447	63.9	6.11	†		
tEME-EA	$13_{5,8}$–$13_{4,10}$	215 598.486	63.9	0.53	†		
tEME-EE	$12_{5,7}$–$12_{4,8}$	215 613.102	58.9	5.52	215 613.7	1.89	
tEME-EE'	$12_{5,8}$–$12_{4,9}$	215 613.172	58.9	5.53	†		
tEME-EE'	$12_{5,7}$–$12_{4,8}$	215 613.308	58.9	5.53	†		
tEME-EE	$12_{5,8}$–$12_{4,9}$	215 613.378	58.9	5.52	†		
tEME-AE	$12_{5,7}$–$12_{4,8}$	215 613.651	58.9	5.52	†		
tEME-AE	$12_{5,8}$–$12_{4,9}$	215 613.720	58.9	5.52	†		
tEME-EA	$12_{5,8}$–$12_{4,9}$	215 616.405	58.9	5.37	...	...	$^{13}CH_3OCOH$ $v_t = 1$, CH_3CH_2CN
tEME-EA	$12_{5,7}$–$12_{4,8}$	215 616.490	58.9	5.37	...	...	″
tEME-AA	$12_{5,7}$–$12_{4,8}$	215 616.564	58.9	5.53	...	...	″
tEME-AA	$12_{5,8}$–$12_{4,9}$	215 617.221	58.9	5.53	...	...	″
tEME-EE	$11_{5,6}$–$11_{4,7}$	215 628.800	54.3	4.94	215 629.7	1.60	
tEME-EE'	$11_{5,7}$–$11_{4,8}$	215 628.855	54.3	4.94	†		
tEME-EE'	$11_{5,6}$–$11_{4,7}$	215 629.003	54.3	4.94	†		
tEME-EE	$11_{5,7}$–$11_{4,8}$	215 629.058	54.3	4.94	†		
tEME-AE	$11_{5,6}$–$11_{4,7}$	215 629.349	54.3	4.94	†		
tEME-AE	$11_{5,7}$–$11_{4,8}$	215 629.404	54.3	4.94	†		
tEME-EA	$11_{5,7}$–$11_{4,8}$	215 632.056	54.3	4.91	215 632.7	1.06	
tEME-EA	$11_{5,6}$–$11_{4,7}$	215 632.229	54.3	4.91	†		
tEME-AA	$11_{5,6}$–$11_{4,7}$	215 632.425	54.3	4.94	†		
tEME-AA	$11_{5,7}$–$11_{4,8}$	215 632.754	54.3	4.94	†		
tEME-EE	$10_{5,5}$–$10_{4,6}$	215 640.803	50.0	4.35	215 641.1	1.31	
tEME-EE'	$10_{5,6}$–$10_{4,7}$	215 640.854	50.0	4.35	†		
tEME-EE'	$10_{5,5}$–$10_{4,6}$	215 641.007	50.0	4.35	†		
tEME-EE	$10_{5,6}$–$10_{4,7}$	215 641.058	50.0	4.35	†		
tEME-AE	$10_{5,5}$–$10_{4,6}$	215 641.354	50.0	4.35	†		
tEME-AE	$10_{5,6}$–$10_{4,7}$	215 641.405	50.0	4.35	†		
tEME-EA	$10_{5,6}$–$10_{4,7}$	215 644.051	50.0	4.34	215 644.1	1.26	$^{13}CH_3OCOH$ $v_t = 1$
tEME-EA	$10_{5,5}$–$10_{4,6}$	215 644.248	50.0	4.34	†		
tEME-AA	$10_{5,5}$–$10_{4,6}$	215 644.522	50.0	4.35	†		
tEME-AA	$10_{5,6}$–$10_{4,7}$	215 644.676	50.0	4.35	†		

Table A.1. continued.

Species	Transition $J_{K_a,K_c} - J'_{K'_a,K'_c}$	Predicted frequency (MHz)	E_{upp} (K)	S_{ij}	Observed frequency (MHz)	T (K)	Blends
tEME-EE	$9_{5,4}$–$9_{4,5}$	215 649.740	46.1	3.73	215 650.2	1.02	
tEME-EE'	$9_{5,5}$–$9_{4,6}$	215 649.791	46.1	3.73	†		
tEME-EE'	$9_{5,4}$–$9_{4,5}$	215 649.944	46.1	3.73	†		
tEME-EE	$9_{5,5}$–$9_{4,6}$	215 649.995	46.1	3.73	†		
tEME-AE	$9_{5,4}$–$9_{4,5}$	215 650.292	46.1	3.73	†		
tEME-AE	$9_{5,5}$–$9_{4,6}$	215 650.343	46.1	3.73	†		
tEME-EA	$9_{5,5}$–$9_{4,6}$	215 652.990	46.1	3.73	215 653.2	0.92	
tEME-EA	$9_{5,4}$–$9_{4,5}$	215 653.193	46.1	3.73	†		
tEME-AA	$9_{5,4}$–$9_{4,5}$	215 653.509	46.1	3.73	†		
tEME-AA	$9_{5,5}$–$9_{4,6}$	215 653.575	46.1	3.73	†		
tEME-EE	$8_{5,3}$–$8_{4,4}$	215 656.176	42.7	3.10	215 656.2	1.16	
tEME-EE'	$8_{5,4}$–$8_{4,5}$	215 656.227	42.7	3.10	†		
tEME-EE'	$8_{5,3}$–$8_{4,4}$	215 656.380	42.7	3.10	†		
tEME-EE	$8_{5,4}$–$8_{4,5}$	215 656.432	42.7	3.10	†		
tEME-AE	$8_{5,3}$–$8_{4,4}$	215 656.730	42.7	3.10	†		
tEME-AE	$8_{5,4}$–$8_{4,5}$	215 656.781	42.7	3.10	†		
tEME-EA	$8_{5,4}$–$8_{4,5}$	215 659.431	42.7	3.10	215 660.8	1.16	
tEME-EA	$8_{5,3}$–$8_{4,4}$	215 659.635	42.7	3.10	†		
tEME-AA	$8_{5,3}$–$8_{4,4}$	215 659.972	42.7	3.10	†		
tEME-AA	$8_{5,4}$–$8_{4,5}$	215 659.998	42.7	3.10	†		
tEME-EE	$7_{5,2}$–$7_{4,3}$	215 660.620	39.6	2.43	†		
tEME-EE'	$7_{5,3}$–$7_{4,4}$	215 660.672	39.6	2.43	†		
tEME-EE'	$7_{5,2}$–$7_{4,3}$	215 660.825	39.6	2.43	†		
tEME-EE	$7_{5,3}$–$7_{4,4}$	215 660.877	39.6	2.43	†		
tEME-AE	$7_{5,2}$–$7_{4,3}$	215 661.175	39.6	2.43	†		
tEME-AE	$7_{5,3}$–$7_{4,4}$	215 661.227	39.6	2.43	†		
tEME-EE	$6_{5,1}$–$6_{4,2}$	215 663.523	36.9	1.72	215 664.6	1.11	
tEME-EE'	$6_{5,2}$–$6_{4,3}$	215 663.575	36.9	1.72	†		
tEME-EE'	$6_{5,1}$–$6_{4,2}$	215 663.728	36.9	1.72	†		
tEME-EE	$6_{5,2}$–$6_{4,3}$	215 663.780	36.9	1.72	†		
tEME-EA	$7_{5,3}$–$7_{4,4}$	215 663.879	39.6	2.43	†		
tEME-AE	$6_{5,1}$–$6_{4,2}$	215 664.080	36.9	1.72	†		
tEME-EA	$7_{5,2}$–$7_{4,3}$	215 664.084	39.6	2.43	†		
tEME-AE	$6_{5,2}$–$6_{4,3}$	215 664.131	36.9	1.72	†		
tEME-AA	$7_{5,2}$–$7_{4,3}$	215 664.430	39.6	2.43	†		
tEME-AA	$7_{5,3}$–$7_{4,4}$	215 664.439	39.6	2.43	†		
tEME-EE	$5_{5,0}$–$5_{4,1}$	215 665.279	34.6	0.92	†		
tEME-EE'	$5_{5,1}$–$5_{4,2}$	215 665.331	34.6	0.92	†		
tEME-EE'	$5_{5,0}$–$5_{4,1}$	215 665.485	34.6	0.92	†		
tEME-EE	$5_{5,1}$–$5_{4,2}$	215 665.537	34.6	0.92	†		
tEME-AE	$5_{5,0}$–$5_{4,1}$	215 665.837	34.6	0.92	†		
tEME-AE	$5_{5,1}$–$5_{4,2}$	215 665.889	34.6	0.92	†		
tEME-EA	$6_{5,2}$–$6_{4,3}$	215 666.786	36.9	1.72	215 667.6	0.97	CH_3CH_2CN
tEME-AE	$6_{5,1}$–$6_{4,2}$	215 666.991	36.9	1.72	†		
tEME-AE	$6_{5,1}$–$6_{4,2}$	215 667.342	36.9	1.72	†		
tEME-EA	$6_{5,2}$–$6_{4,3}$	215 667.344	36.9	1.72	†		
tEME-AE	$5_{5,1}$–$5_{4,2}$	215 668.545	34.6	0.92	†		
tEME-AA	$5_{5,0}$–$5_{4,1}$	215 668.751	34.6	0.92	†		
tEME-AA	$5_{5,0}$–$5_{4,1}$	215 669.103	34.6	0.92	†		
tEME-AE	$5_{5,1}$–$5_{4,2}$	215 669.103	34.6	0.92	†		
tEME-EE'	$6_{4,3}$–$5_{3,3}$	216 054.535	26.5	3.73	216 056.4	0.95	
tEME-EE	$6_{4,3}$–$5_{3,3}$	216 054.868	26.5	3.73	†		
tEME-AE	$6_{4,3}$–$5_{3,3}$	216 055.095	26.5	3.73	†		
tEME-EE	$6_{4,2}$–$5_{3,2}$	216 055.759	26.5	3.73	†		
tEME-EE'	$6_{4,2}$–$5_{3,2}$	216 056.093	26.5	3.73	†		
tEME-AE	$6_{4,2}$–$5_{3,2}$	216 056.319	26.5	3.73	†		
tEME-EA	$6_{4,3}$–$5_{3,3}$	216 058.222	26.5	3.69	216 059.3†	1.14	
tEME-EA	$6_{4,2}$–$5_{3,2}$	216 058.519	26.5	3.69	†		
tEME-AA	$6_{4,3}$–$5_{3,2}$	216 058.597	26.5	3.73	†		
tEME-AA	$6_{4,2}$–$5_{3,3}$	216 058.930	26.5	3.73	†		
tEME-EE	$12_{3,9}$–$11_{2,10}$	217 007.530	40.5	4.14	217 007.6	0.49	
tEME-EE'	$12_{3,9}$–$11_{2,10}$	217 007.763	40.5	4.12	†		
tEME-AE	$12_{3,9}$–$11_{2,10}$	217 007.939	40.5	4.13	†		
tEME-EA	$12_{3,9}$–$11_{2,10}$	217 009.762	40.5	4.16	217 010.6	0.54	
tEME-AA	$12_{3,9}$–$11_{2,10}$	217 010.054	40.5	4.16	†		
tEME-AA	$30_{1,29}$–$29_{2,28}$	217 164.465	182.5	13.55	217 165.1	2.68	CH_3OCOH
tEME-EA	$30_{1,29}$–$29_{2,28}$	217 164.508	182.5	13.55	†		
tEME-AE	$30_{1,29}$–$29_{2,28}$	217 165.360	182.5	13.55	†		
tEME-EE	$30_{1,29}$–$29_{2,28}$	217 165.402	182.5	13.55	†		
tEME-EE'	$30_{1,29}$–$29_{2,28}$	217 165.402	182.5	13.55	†		
tEME-AA	$28_{0,28}$–$27_{1,27}$	217 940.650	154.7	22.59	217 940.7	1.46	
tEME-EA	$28_{0,28}$–$27_{1,27}$	217 940.651	154.7	22.59	†		
tEME-AE	$28_{0,28}$–$27_{1,27}$	217 940.758	154.7	22.59	†		

Table A.1. continued.

Species	Transition $J_{K_a,K_c} - J'_{K'_a,K'_c}$	Predicted frequency (MHz)	E_{upp} (K)	S_{ij}	Observed frequency (MHz)	T (K)	Blends
tEME-EE	$28_{0,28}$–$27_{1,27}$	217 940.759	154.7	22.59	†		
tEME-EE'	$28_{0,28}$–$27_{1,27}$	217 940.759	154.7	22.59	†		
tEME-EE'	$22_{2,21}$–$21_{1,20}$	219 893.140	102.2	8.31	219 893.0	0.86	
tEME-EE	$22_{2,21}$–$21_{1,20}$	219 893.140	102.2	8.31	†		
tEME-AE	$22_{2,21}$–$21_{1,20}$	219 893.263	102.2	8.31	†		
tEME-EA	$22_{2,21}$–$21_{1,20}$	219 894.511	102.2	8.31	219 894.5†	0.66	
tEME-AA	$22_{2,21}$–$21_{1,20}$	219 894.635	102.2	8.31	†		
tEME-EE'	$28_{1,28}$–$27_{0,27}$	222 861.487	154.8	22.63	222 861.2	3.06	CH_3OCHO
tEME-EE	$28_{1,28}$–$27_{0,27}$	222 861.487	154.8	22.63	†		
tEME-AE	$28_{1,28}$–$27_{0,27}$	222 861.500	154.8	22.63	†		
tEME-EA	$28_{1,28}$–$27_{0,27}$	222 861.655	154.8	22.63	†		
tEME-AA	$28_{1,28}$–$27_{0,27}$	222 861.668	154.8	22.63	†		
tEME-EE'	$13_{3,11}$–$12_{2,10}$	222 980.574	45.5	4.38	...	...	$CH_3O^{13}COH$
tEME-EE	$13_{3,11}$–$12_{2,10}$	222 980.720	45.5	4.39	...	...	″
tEME-AE	$13_{3,11}$–$12_{2,10}$	222 980.951	45.5	4.39	...	...	″
tEME-EA	$13_{3,11}$–$12_{2,10}$	222 983.368	45.5	4.40	...	...	″
tEME-AA	$13_{3,11}$–$12_{2,10}$	222 983.672	45.5	4.40	...	...	″
tEME-EE	$16_{2,14}$–$15_{1,15}$	223 403.761	57.4	2.48	223 403.5	0.82	CH_3OCH_3
tEME-EE'	$16_{2,14}$–$15_{1,15}$	223 403.762	57.4	2.48	†		
tEME-AE	$16_{2,14}$–$15_{1,15}$	223 404.001	57.4	2.48	†		
tEME-EA	$16_{2,14}$–$15_{1,15}$	223 405.432	57.4	2.48	...	...	CH_3OCH_3
tEME-AA	$16_{2,14}$–$15_{1,15}$	223 405.671	57.4	2.48	...	...	
tEME-EE'	$7_{4,4}$–$6_{3,4}$	224 103.753	29.2	3.89	224 104.2	1.49	
tEME-EE	$7_{4,4}$–$6_{3,4}$	224 104.093	29.2	3.88	†		
tEME-AE	$7_{4,4}$–$6_{3,4}$	224 104.315	29.2	3.89	†		
tEME-EE	$7_{4,3}$–$6_{3,3}$	224 104.926	29.2	3.88	†		
tEME-EE'	$7_{4,3}$–$6_{3,3}$	224 105.266	29.2	3.89	†		
tEME-AE	$7_{4,3}$–$6_{3,3}$	224 105.490	29.2	3.89	†		
tEME-AA	$7_{4,4}$–$6_{3,3}$	224 107.456	29.2	3.90	224 108.0†	1.12	
tEME-EA	$7_{4,4}$–$6_{3,4}$	224 107.546	29.2	3.58	†		
tEME-EA	$7_{4,3}$–$6_{3,3}$	224 107.581	29.2	3.58	†		
tEME-AA	$7_{4,3}$–$6_{3,4}$	224 108.457	29.2	3.90	†		
tEME-EE	$13_{3,10}$–$12_{2,11}$	225 283.674	45.5	4.33	225 283.2	1.41	CH_3CH_2OH
tEME-EE'	$13_{3,10}$–$12_{2,11}$	225 283.820	45.5	4.33	†		
tEME-AE	$13_{3,10}$–$12_{2,11}$	225 284.043	45.5	4.33	†		
tEME-EA	$13_{3,10}$–$12_{2,11}$	225 285.990	45.5	4.34	†		
tEME-AA	$13_{3,10}$–$12_{2,11}$	225 286.286	45.5	4.34	†		
tEME-EE'	$23_{2,22}$–$22_{1,21}$	225 494.508	111.0	8.90	225 494.6	0.72	
tEME-EE	$23_{2,22}$–$22_{1,21}$	225 494.508	111.0	8.90	†		
tEME-AE	$23_{2,22}$–$22_{1,21}$	225 494.625	111.0	8.90	†		
tEME-EA	$23_{2,22}$–$22_{1,21}$	225 495.848	111.0	8.90	†		
tEME-AA	$23_{2,22}$–$22_{1,21}$	225 495.965	111.0	8.90	†		
tEME-EA	$29_{0,29}$–$28_{1,28}$	226 057.836	165.7	23.62	226 058.4	3.50	CH_3CH_2OH
tEME-AA	$29_{0,29}$–$28_{1,28}$	226 057.836	165.7	23.62	†		
tEME-EE	$29_{0,29}$–$28_{1,28}$	226 057.928	165.7	23.62	†		
tEME-EE'	$29_{0,29}$–$28_{1,28}$	226 057.928	165.7	23.62	†		
tEME-AE	$29_{0,29}$–$28_{1,28}$	226 057.928	165.7	23.62	†		
tEME-AA	$31_{1,30}$–$30_{2,29}$	227 090.552	194.5	14.51	...	...	CH_3OH
tEME-EA	$31_{1,30}$–$30_{2,29}$	227 090.589	194.5	14.51	...	...	″
tEME-AE	$31_{1,30}$–$30_{2,29}$	227 091.390	194.5	14.51	...	...	″
tEME-EE	$31_{1,30}$–$30_{2,29}$	227 091.426	194.5	14.51	...	...	″
tEME-EE'	$31_{1,30}$–$30_{2,29}$	227 091.426	194.5	14.51	...	...	″
tEME-EE'	$29_{1,29}$–$28_{0,28}$	230 291.194	165.8	23.66	...	...	CH_3OH, CH_3OCOH
tEME-EE	$29_{1,29}$–$28_{0,28}$	230 291.194	165.8	23.66	...	...	″
tEME-AE	$29_{1,29}$–$28_{0,28}$	230 291.205	165.8	23.66	...	...	″
tEME-EA	$29_{1,29}$–$28_{0,28}$	230 291.345	165.8	23.66	...	...	″
tEME-AA	$29_{1,29}$–$28_{0,28}$	230 291.357	165.8	23.66	...	...	″
tEME-EE'	$14_{3,12}$–$13_{2,11}$	230 486.881	50.9	4.59	230 487.1	0.58	CO
tEME-EE	$14_{3,12}$–$13_{2,11}$	230 486.975	50.9	4.59	†		
tEME-AE	$14_{3,12}$–$13_{2,11}$	230 487.227	50.9	4.59	†		
tEME-EA	$14_{3,12}$–$13_{2,11}$	230 489.569	50.9	4.59	...	...	CO
tEME-AA	$14_{3,12}$–$13_{2,11}$	230 489.869	50.9	4.59	...	...	″
tEME-EE'	$24_{2,23}$–$23_{1,22}$	231 063.540	120.2	9.52	...	...	OCS
tEME-EE	$24_{2,23}$–$23_{1,22}$	231 063.540	120.2	9.52	...	...	″
tEME-AE	$24_{2,23}$–$23_{1,22}$	231 063.652	120.2	9.52	...	...	″
tEME-EA	$24_{2,23}$–$23_{1,22}$	231 064.846	120.2	9.52	...	...	″
tEME-EA	$24_{2,23}$–$23_{1,22}$	231 064.958	120.2	9.52	...	...	″
tEME-EE'	$8_{4,5}$–$7_{3,5}$	232 151.207	32.3	4.03	232 151.8	1.16	
tEME-EE	$8_{4,5}$–$7_{3,5}$	232 151.590	32.3	3.98	†		
tEME-AE	$8_{4,5}$–$7_{3,5}$	232 151.787	32.3	4.01	†		
tEME-EE	$8_{4,4}$–$7_{3,4}$	232 152.098	32.3	3.98	†		
tEME-EE'	$8_{4,4}$–$7_{3,4}$	232 152.480	32.3	4.03	†		
tEME-EA	$8_{4,5}$–$7_{3,4}$	232 152.521	32.3	1.00	†		

Table A.1. continued.

Species	Transition $J_{K_a,K_c} - J'_{K'_a,K'_c}$	Predicted frequency (MHz)	E_{upp} (K)	S_{ij}	Observed frequency (MHz)	T (K)	Blends
tEME-AE	$8_{4,4}$–$7_{3,4}$	232 152.685	32.3	4.01	†		
tEME-AA	$8_{4,5}$–$7_{3,4}$	232 154.033	32.3	4.08	†		
tEME-EA	$8_{4,4}$–$7_{3,4}$	232 154.362	32.3	3.08	†		
tEME-EA	$8_{4,5}$–$7_{3,5}$	232 155.426	32.3	3.08	†		
tEME-AA	$8_{4,4}$–$7_{3,5}$	232 156.540	32.3	4.08	...	...	CH_3OCOH $v_t = 1$
tEME-EA	$8_{4,4}$–$7_{3,5}$	232 157.268	32.3	1.00	...	...	″
tEME-EE	$14_{3,11}$–$13_{2,12}$	233 622.462	51.0	4.51	233 622.5	2.10	CH_3CH_2CN v_{13}/v_{21}
tEME-EE'	$14_{3,11}$–$13_{2,12}$	233 622.556	51.0	4.51	†		
tEME-AE	$14_{3,11}$–$13_{2,12}$	233 622.806	51.0	4.51	†		
tEME-EA	$14_{3,11}$–$13_{2,12}$	233 624.824	51.0	4.51	...	...	CH_3OCOH $v_t = 0,1$
tEME-AA	$14_{3,11}$–$13_{2,12}$	233 625.121	51.0	4.51	...	...	″
tEME-EA	$30_{0,30}$–$29_{1,29}$	234 130.523	177.0	24.66	...	...	CH_3OCOH
tEME-AA	$30_{0,30}$–$29_{1,29}$	234 130.524	177.0	24.66	...	...	″
tEME-EE	$30_{0,30}$–$29_{1,29}$	234 130.601	177.0	24.66	...	...	″
tEME-EE'	$30_{0,30}$–$29_{1,29}$	234 130.601	177.0	24.66	...	...	″
tEME-AE	$30_{0,30}$–$29_{1,29}$	234 130.602	177.0	24.66	...	...	″
tEME-EE	$17_{2,15}$–$16_{1,16}$	235 247.484	64.0	2.37	235 247.5	0.49	U-line
tEME-EE'	$17_{2,15}$–$16_{1,16}$	235 247.485	64.0	2.37	†		
tEME-AE	$17_{2,15}$–$16_{1,16}$	235 247.731	64.0	2.37	†		
tEME-EA	$17_{2,15}$–$16_{1,16}$	235 249.156	64.0	2.37	235 249.6	0.41	U-line
tEME-AA	$17_{2,15}$–$16_{1,16}$	235 249.403	64.0	2.37	†		
tEME-EE'	$25_{2,24}$–$24_{1,23}$	236 614.358	129.8	10.19	236 614.8	1.89	$CH_3O^{13}COH$ $v_t = 1$
tEME-EE	$25_{2,24}$–$24_{1,23}$	236 614.358	129.8	10.19	†		
tEME-AE	$25_{2,24}$–$24_{1,23}$	236 614.464	129.8	10.19	†		
tEME-EA	$25_{2,24}$–$24_{1,23}$	236 615.628	129.8	10.19	†		
tEME-AA	$25_{2,24}$–$24_{1,23}$	236 615.733	129.8	10.19	†		
tEME-AA	$32_{1,31}$–$31_{2,30}$	236 906.877	206.9	15.50	236 907.6	0.99	
tEME-EA	$32_{1,31}$–$31_{2,30}$	236 906.908	206.9	15.50	†		
tEME-AE	$32_{1,31}$–$31_{2,30}$	236 907.656	206.9	15.50	†		
tEME-EE	$32_{1,31}$–$31_{2,30}$	236 907.687	206.9	15.50	†		
tEME-EE'	$32_{1,31}$–$31_{2,30}$	236 907.687	206.9	15.50	†		
tEME-EE'	$30_{1,30}$–$29_{0,29}$	237 763.517	177.1	24.69	237 763.2	1.76	
tEME-EE	$30_{1,30}$–$29_{0,29}$	237 763.517	177.1	24.69	†		
tEME-AE	$30_{1,30}$–$29_{0,29}$	237 763.527	177.1	24.69	†		
tEME-EA	$30_{1,30}$–$29_{0,29}$	237 763.653	177.1	24.69	†		
tEME-AA	$30_{1,30}$–$29_{0,29}$	237 763.664	177.1	24.69	†		
tEME-EE'	$15_{3,13}$–$14_{2,12}$	237 865.715	56.7	4.79	237 866.1	1.40	
tEME-EE	$15_{3,13}$–$14_{2,12}$	237 865.778	56.7	4.80	†		
tEME-AE	$15_{3,13}$–$14_{2,12}$	237 866.042	56.7	4.80	†		
tEME-EA	$15_{3,13}$–$14_{2,12}$	237 868.339	56.7	4.80	...	...	U-line
tEME-AA	$15_{3,13}$–$14_{2,12}$	237 868.635	56.7	4.80	...	...	″
tEME-EA	$9_{4,6}$–$8_{3,5}$	240 195.817	35.8	1.64	240 196.7	2.66	$^{13}CH_3OCOH$
tEME-EE	$9_{4,5}$–$8_{3,5}$	240 196.101	35.8	3.88	†		
tEME-EE'	$9_{4,6}$–$8_{3,6}$	240 196.396	35.8	3.88	†		
tEME-EE'	$9_{4,5}$–$8_{3,5}$	240 196.642	35.8	3.88	†		
tEME-AE	$9_{4,5}$–$8_{3,5}$	240 196.777	35.8	3.88	†		
tEME-EE	$9_{4,6}$–$8_{3,6}$	240 196.937	35.8	3.88	†		
tEME-AE	$9_{4,6}$–$8_{3,6}$	240 197.045	35.8	3.88	†		
tEME-AA	$9_{4,6}$–$8_{3,5}$	240 197.196	35.8	3.88	†		
tEME-EA	$9_{4,5}$–$8_{3,5}$	240 197.654	35.8	3.88	†		
tEME-EA	$9_{4,6}$–$8_{3,6}$	240 201.478	35.8	2.63	...	...	CH_3OCOH $v_t = 1$
tEME-AA	$9_{4,5}$–$8_{3,6}$	240 202.719	35.8	4.28	...	...	″
tEME-EA	$9_{4,5}$–$8_{3,6}$	240 203.315	35.8	1.64	...	...	″
tEME-EE	$15_{3,12}$–$14_{2,13}$	242 035.318	56.8	4.68	...	...	CH_2DOH; CH_2DCN
tEME-EE'	$15_{3,12}$–$14_{2,13}$	242 035.380	56.8	4.68	...	...	″
tEME-AE	$15_{3,12}$–$14_{2,13}$	242 035.647	56.8	4.68	...	...	″
tEME-EA	$15_{3,12}$–$14_{2,13}$	242 037.704	56.8	4.68	...	...	CH_2DOCOH
tEME-AA	$15_{3,12}$–$14_{2,13}$	242 038.002	56.8	4.68	...	...	″
tEME-EE'	$26_{2,25}$–$25_{1,24}$	242 161.785	139.8	10.89	242 163.3	1.86	
tEME-EE	$26_{2,25}$–$25_{1,24}$	242 161.785	139.8	10.89	†		
tEME-AE	$26_{2,25}$–$25_{1,24}$	242 161.884	139.8	10.89	†		
tEME-EA	$26_{2,25}$–$25_{1,24}$	242 163.015	139.8	10.89	†		
tEME-AA	$26_{2,25}$–$25_{1,24}$	242 163.114	139.8	10.89	†		
tEME-EA	$31_{0,31}$–$30_{1,30}$	242 163.369	188.7	25.69	†		
tEME-AA	$31_{0,31}$–$30_{1,30}$	242 163.371	188.7	25.69	†		
tEME-EE	$31_{0,31}$–$30_{1,30}$	242 163.434	188.7	25.69	†		
tEME-EE'	$31_{0,31}$–$30_{1,30}$	242 163.434	188.7	25.69	†		
tEME-AE	$31_{0,31}$–$30_{1,30}$	242 163.436	188.7	25.69	†		
tEME-EE'	$16_{3,14}$–$15_{2,13}$	245 103.550	62.9	4.99	245 103.4	0.92	
tEME-EE	$16_{3,14}$–$15_{2,13}$	245 103.592	62.9	4.99	†		
tEME-AE	$16_{3,14}$–$15_{2,13}$	245 103.864	62.9	4.99	†		
tEME-EA	$16_{3,14}$–$15_{2,13}$	245 106.133	62.9	4.99	245 106.4†	1.13	CH_3OCOH $v_t = 2$
tEME-EA	$16_{3,14}$–$15_{2,13}$	245 106.426	62.9	5.00	†		

Table A.1. continued.

Species	Transition $J_{K_a,K_c} - J'_{K'_a,K'_c}$	Predicted frequency (MHz)	E_{upp} (K)	S_{ij}	Observed frequency (MHz)	T (K)	Blends
tEME-EE'	$31_{1,31}$–$30_{0,30}$	245 274.088	188.8	25.71	245 274.0	2.44	
tEME-EE	$31_{1,31}$–$30_{0,30}$	245 274.088	188.8	25.71	†		
tEME-AE	$31_{1,31}$–$30_{0,30}$	245 274.098	188.8	25.71	†		
tEME-EA	$31_{1,31}$–$30_{0,30}$	245 274.211	188.8	25.71	†		
tEME-AA	$31_{1,31}$–$30_{0,30}$	245 274.221	188.8	25.71	†		
tEME-AA	$33_{1,32}$–$32_{2,31}$	246 605.346	219.6	16.51	246 605.6	0.92	
tEME-EA	$33_{1,32}$–$32_{2,31}$	246 605.372	219.6	16.51	†		
tEME-AE	$33_{1,32}$–$32_{2,31}$	246 606.066	219.6	16.51	†		
tEME-EE	$33_{1,32}$–$32_{2,31}$	246 606.092	219.6	16.51	†		
tEME-EE'	$33_{1,32}$–$32_{2,31}$	246 606.092	219.6	16.51	†		

Table A.2. Lines of trans-$CH_3CH_2OCH_3$ in 30 m data.

Species	Transition $J_{K_a,K_c} - J'_{K'_a,K'_c}$	Predicted frequency (MHz)	E_{upp} (K)	S_{ij}	Observed[1] frequency (MHz)	Observed[1] T_{MB} (K)	Model[2] T_{MB} (K)	Blends
tEME-AA	$13_{0,13}$–$12_{1,12}$	88 665.592	35.0	7.66	88 665.8	0.05	0.01	U-line
tEME-EA	$13_{0,13}$–$12_{1,12}$	88 665.628	35.0	7.66	†			
tEME-AE	$13_{0,13}$–$12_{1,12}$	88 666.042	35.0	7.66	†			
tEME-EE	$13_{0,13}$–$12_{1,12}$	88 666.078	35.0	7.66	†			
tEME-EE'	$13_{0,13}$–$12_{1,12}$	88 666.078	35.0	7.66	†			
tEME-EE'	$10_{1,10}$–$9_{0,9}$	97 575.502	22.0	6.04	...	...	0.01	CH_3OH
tEME-EE	$10_{1,10}$–$9_{0,9}$	97 575.502	22.0	6.04	†			
tEME-AE	$10_{1,10}$–$9_{0,9}$	97 575.556	22.0	6.04	†			
tEME-EA	$10_{1,10}$–$9_{0,9}$	97 576.027	22.0	6.04	†			
tEME-AA	$10_{1,10}$–$9_{0,9}$	97 576.081	22.0	6.04	†			
tEME-AA	$14_{0,14}$–$13_{1,13}$	97 678.316	40.4	8.52	...	...	0.01	CH_3OH, CH_3CH_2CN v_{13}/v_{21}
tEME-EA	$14_{0,14}$–$13_{1,13}$	97 678.350	40.4	8.52	†			
tEME-AE	$14_{0,14}$–$13_{1,13}$	97 678.746	40.4	8.52	†			
tEME-EE	$14_{0,14}$–$13_{1,13}$	97 678.779	40.4	8.52	†			
tEME-EE'	$14_{0,14}$–$13_{1,13}$	97 678.779	40.4	8.52	†			
tEME-EE	$26_{3,23}$–$26_{2,24}$	101 017.882	146.4	17.08	...	...	0.01	U-line
tEME-EE'	$26_{3,23}$–$26_{2,24}$	101 017.884	146.4	17.08	†			
tEME-AE	$26_{3,23}$–$26_{2,24}$	101 018.111	146.4	17.08	†			
tEME-EE	$25_{3,22}$–$25_{2,23}$	102 684.892	136.2	16.03	102 684.6	0.07	0.01	^{18}OCS
tEME-EE'	$25_{3,22}$–$25_{2,23}$	102 684.894	136.2	16.03	†			
tEME-AE	$25_{3,22}$–$25_{2,23}$	102 685.127	136.2	16.03	†			
tEME-EE	$24_{3,21}$–$24_{2,22}$	104 364.955	126.5	15.03	...	...	0.01	CH_3CH_2CN
tEME-EE'	$24_{3,21}$–$24_{2,22}$	104 364.959	126.5	15.03	†			
tEME-AE	$24_{3,21}$–$24_{2,22}$	104 365.198	126.5	15.03	†			
tEME-EE'	$11_{1,11}$–$10_{0,10}$	104 401.631	26.2	6.73	...	...	0.02	CH_2CHCN
tEME-EE	$11_{1,11}$–$10_{0,10}$	104 401.631	26.2	6.73	†			
tEME-AE	$11_{1,11}$–$10_{0,10}$	104 401.683	26.2	6.73	†			
tEME-EA	$11_{1,11}$–$10_{0,10}$	104 402.145	26.2	6.73	†			
tEME-AA	$11_{1,11}$–$10_{0,10}$	104 402.196	26.2	6.73	†			
tEME-EE	$23_{3,20}$–$23_{2,21}$	106 030.362	117.2	14.09	...	...	0.01	CH_3OCOH
tEME-EE'	$23_{3,20}$–$23_{2,21}$	106 030.367	117.2	14.09	†			
tEME-AE	$23_{3,20}$–$23_{2,21}$	106 030.611	117.2	14.09	†			
tEME-AA	$15_{0,15}$–$14_{1,14}$	106 666.950	46.1	9.41	...	...	0.02	CH_3OCOH
tEME-EA	$15_{0,15}$–$14_{1,14}$	106 666.980	46.1	9.41	†			
tEME-AE	$15_{0,15}$–$14_{1,14}$	106 667.358	46.1	9.41	†			
tEME-EE	$15_{0,15}$–$14_{1,14}$	106 667.388	46.1	9.41	†			
tEME-EE'	$15_{0,15}$–$14_{1,14}$	106 667.388	46.1	9.41	†			
tEME-EE	$21_{3,18}$–$21_{2,19}$	109 216.897	99.8	12.35	109 215.1	0.02	0.01	U-line
tEME-EE'	$21_{3,18}$–$21_{2,19}$	109 216.904	99.8	12.35	†			
tEME-AE	$21_{3,18}$–$21_{2,19}$	109 217.159	99.8	12.35	†			
tEME-EA	$21_{3,18}$–$21_{2,19}$	109 219.323	99.8	12.35	109 219.6	0.01	0.01	
tEME-AA	$21_{3,18}$–$21_{2,19}$	109 219.581	99.8	12.35	†			
tEME-EE	$20_{3,17}$–$20_{2,18}$	110 694.695	91.6	11.56	...	...	0.02	CH_3CN $v_8 = 1$
tEME-EE'	$20_{3,17}$–$20_{2,18}$	110 694.705	91.6	11.56	†			
tEME-AE	$20_{3,17}$–$20_{2,18}$	110 694.963	91.6	11.56	†			
tEME-EA	$20_{3,17}$–$20_{2,18}$	110 697.132	91.6	11.56	...	...	0.01	CH_3CN $v_8 = 1$
tEME-AA	$20_{3,17}$–$20_{2,18}$	110 697.395	91.6	11.56	†			
tEME-EE'	$12_{1,12}$–$11_{0,11}$	111 178.747	30.8	7.46	111 178.7	0.03	0.02	
tEME-EE	$12_{1,12}$–$11_{0,11}$	111 178.747	30.8	7.46	†			
tEME-AE	$12_{1,12}$–$11_{0,11}$	111 178.796	30.8	7.46	†			
tEME-EA	$12_{1,12}$–$11_{0,11}$	111 179.248	30.8	7.46	†			
tEME-AA	$12_{1,12}$–$11_{0,11}$	111 179.297	30.8	7.46	†			
tEME-EE	$19_{3,16}$–$19_{2,17}$	112 072.074	83.9	10.80	112 072.3	0.03	0.02	
tEME-EE'	$19_{3,16}$–$19_{2,17}$	112 072.088	83.9	10.80	†			
tEME-AE	$19_{3,16}$–$19_{2,17}$	112 072.349	83.9	10.80	†			
tEME-EA	$19_{3,16}$–$19_{2,17}$	112 074.518	83.9	10.80	112 074.5	0.03	0.01	
tEME-AA	$19_{3,16}$–$19_{2,17}$	112 074.786	83.9	10.80	†			
tEME-EE	$18_{3,15}$–$18_{2,16}$	113 336.061	76.5	10.08	113 336.2	0.02	0.02	
tEME-EE'	$18_{3,15}$–$18_{2,16}$	113 336.081	76.5	10.08	†			
tEME-AE	$18_{3,15}$–$18_{2,16}$	113 336.343	76.5	10.08	†			
tEME-EA	$18_{3,15}$–$18_{2,16}$	113 338.507	76.5	10.08	113 338.7	0.03	0.01	$CH_2^{13}CHCN$
tEME-AA	$18_{3,15}$–$18_{2,16}$	113 338.779	76.5	10.08	†			
tEME-EE	$17_{3,14}$–$17_{2,15}$	114 477.615	69.5	9.39	114 477.9	0.05	0.02	U-line
tEME-EE'	$17_{3,14}$–$17_{2,15}$	114 477.643	69.5	9.39	†			
tEME-AE	$17_{3,14}$–$17_{2,15}$	114 477.905	69.5	9.39	†			

Notes. Lines of trans-$CH_3CH_2OCH_3$ (tEME) ground state present in the spectral scan of Orion KL from the 30 m telescope. Column 1 indicates the species, Col. 2 gives the transition, Col. 3 the predicted frequency, Col. 4 upper level energy, Col. 5 the line strength, Col. 6 observed frequency at the peak channel of the line (relative to a v_{LSR} of +7.5 km s^{-1}), Col. 7 main beam temperature at the peak channel of the line, and Col. 8 shows blends with other molecular species. [(1)] Observed frequencies and intensities are not provided for features that appear totally blended with lines from other species. [(2)] We address all features provided by our model with $T_{MB} > 0.01$ K, $T_{MB} > 0.02$ K, and $T_{MB} > 0.03$ K in the frequency ranges between 80.7−116, 122.7−150, and 150−306.7 GHz, respectively. [(†)] Blended with previous line.

Table A.2. continued.

Species	Transition $J_{K_a,K_c} - J'_{K'_a,K'_c}$	Predicted frequency (MHz)	E_{upp} (K)	S_{ij}	Observed[1] frequency (MHz)	Observed[1] T_{MB} (K)	Model[2] T_{MB} (K)	Blends
tEME-EA	$17_{3,14}-17_{2,15}$	114 480.057	69.5	9.39	...	...	0.01	CH_3COOCH_3
tEME-AA	$17_{3,14}-17_{2,15}$	114 480.333	69.5	9.39	†			
tEME-AE	$20_{1,19}-19_{2,18}$	114 717.852	83.4	6.11	114 718.0	0.06	0.01	CH_3CHO $v_t = 1$
tEME-EE	$20_{1,19}-19_{2,18}$	114 717.961	83.4	6.11	†			
tEME-EE'	$20_{1,19}-19_{2,18}$	114 717.962	83.4	6.11	†			
tEME-EE	$16_{3,13}-16_{2,14}$	115 491.673	62.9	8.73	...	...	0.02	CH_3CHO
tEME-EE'	$16_{3,13}-16_{2,14}$	115 491.713	62.9	8.73	†			
tEME-AE	$16_{3,13}-16_{2,14}$	115 491.972	62.9	8.73	†			
tEME-EA	$16_{3,13}-16_{2,14}$	115 494.106	62.9	8.73	...	...	0.02	CH_3CHO
tEME-AA	$16_{3,13}-16_{2,14}$	115 494.385	62.9	8.73	†			
tEME-AA	$16_{0,16}-15_{1,15}$	115 618.006	52.2	10.34	115 618.4	0.07	0.04	
tEME-EA	$16_{0,16}-15_{1,15}$	115 618.033	52.2	10.34	†			
tEME-AE	$16_{0,16}-15_{1,15}$	115 618.391	52.2	10.34	†			
tEME-EE	$16_{0,16}-15_{1,15}$	115 618.417	52.2	10.34	†			
tEME-EE'	$16_{0,16}-15_{1,15}$	115 618.417	52.2	10.34	†			
tEME-EE'	$19_{3,17}-19_{2,18}$	123 318.746	83.8	10.04	123 318.8	0.02	0.02	
tEME-EE	$19_{3,17}-19_{2,18}$	123 318.760	83.8	10.04	†			
tEME-AE	$19_{3,17}-19_{2,18}$	123 319.043	83.8	10.04	†			
tEME-EA	$19_{3,17}-19_{2,18}$	123 321.168	83.8	10.04	123 321.3	0.04	0.01	$CH_3O^{13}COH$
tEME-AA	$19_{3,17}-19_{2,18}$	123 321.458	83.8	10.04	†			
tEME-EE'	$20_{3,18}-20_{2,19}$	124 043.337	91.6	10.58	124 043.5	0.03	0.02	$CH_3COOH v_t = 1$
tEME-EE	$20_{3,18}-20_{2,19}$	124 043.347	91.6	10.58	†			
tEME-AE	$20_{3,18}-20_{2,19}$	124 043.631	91.6	10.58	†			
tEME-EA	$20_{3,18}-20_{2,19}$	124 045.738	91.6	10.58	124 046.0	0.02	0.01	
tEME-AA	$20_{3,18}-20_{2,19}$	124 046.027	91.6	10.58	†			
tEME-AA	$17_{0,17}-16_{1,16}$	124 519.803	58.7	11.29	124 519.5	0.19	0.05	U-line
tEME-EA	$17_{0,17}-16_{1,16}$	124 519.826	58.7	11.29	†			
tEME-AE	$17_{0,17}-16_{1,16}$	124 520.163	58.7	11.29	†			
tEME-EE	$17_{0,17}-16_{1,16}$	124 520.186	58.7	11.29	†			
tEME-EE'	$17_{0,17}-16_{1,16}$	124 520.186	58.7	11.29	†			
tEME-EE'	$14_{1,14}-13_{0,13}$	124 648.594	41.0	9.02	124 649.0	0.06	0.04	
tEME-EE	$14_{1,14}-13_{0,13}$	124 648.594	41.0	9.02	†			
tEME-AE	$14_{1,14}-13_{0,13}$	124 648.637	41.0	9.02	†			
tEME-EA	$14_{1,14}-13_{0,13}$	124 649.062	41.0	9.02	†			
tEME-AA	$14_{1,14}-13_{0,13}$	124 649.106	41.0	9.02	†			
tEME-EE'	$21_{3,19}-21_{2,20}$	124 866.195	99.7	11.10	...	...	0.02	SO_2
tEME-EE	$21_{3,19}-21_{2,20}$	124 866.202	99.7	11.10	†			
tEME-AE	$21_{3,19}-21_{2,20}$	124 866.487	99.7	11.10	†			
tEME-EA	$21_{3,19}-21_{2,20}$	124 868.576	99.7	11.10	...	...	0.01	SO_2
tEME-AA	$21_{3,19}-21_{2,20}$	124 868.864	99.7	11.10	†			
tEME-AA	$21_{1,20}-20_{2,19}$	125 001.226	91.6	6.68	...	...	0.01	CH_3OCOH
tEME-EA	$21_{1,20}-20_{2,19}$	125 001.329	91.6	6.68	†			
tEME-AE	$21_{1,20}-20_{2,19}$	125 002.535	91.6	6.68	...	...	0.02	CH_3OCOH
tEME-EE	$21_{1,20}-20_{2,19}$	125 002.638	91.6	6.68	†			
tEME-EE'	$21_{1,20}-20_{2,19}$	125 002.638	91.6	6.68	†			
tEME-EE'	$7_{2,6}-6_{1,5}$	125 433.445	15.4	2.61	...	...	0.01	CH_3CH_2CN, SO_2
tEME-EE	$7_{2,6}-6_{1,5}$	125 433.472	15.4	2.61	†			
tEME-AE	$7_{2,6}-6_{1,5}$	125 433.646	15.4	2.61	†			
tEME-EE'	$22_{3,20}-22_{2,21}$	125 793.386	108.2	11.61	...	...	0.02	CH_3CH_2CN v_{13}/v_{21}
tEME-EE	$22_{3,20}-22_{2,21}$	125 793.392	108.2	11.61	†			
tEME-AE	$22_{3,20}-22_{2,21}$	125 793.677	108.2	11.61	†			
tEME-EA	$22_{3,20}-22_{2,21}$	125 795.748	108.2	11.61	...	...	0.01	CH_3CH_2CN v_{13}/v_{21}
tEME-AA	$22_{3,20}-22_{2,21}$	125 796.036	108.2	11.61	†			
tEME-EE'	$23_{3,21}-23_{2,22}$	126 830.671	117.1	12.11	...	...	0.02	$HC^{13}CCN$
tEME-EE	$23_{3,21}-23_{2,22}$	126 830.675	117.1	12.11	†			
tEME-AE	$23_{3,21}-23_{2,22}$	126 830.960	117.1	12.11	†			
tEME-EA	$23_{3,21}-23_{2,22}$	126 833.013	117.1	12.11	...	...	0.01	$HC^{13}CCN$
tEME-AA	$23_{3,21}-23_{2,22}$	126 833.301	117.1	12.11	†			
tEME-EE'	$24_{3,22}-24_{2,23}$	127 983.452	126.4	12.59	127 983.6	0.07	0.02	U-line
tEME-EE	$24_{3,22}-24_{2,23}$	127 983.456	126.4	12.59	†			
tEME-AE	$24_{3,22}-24_{2,23}$	127 983.741	126.4	12.59	†			
tEME-EA	$24_{3,22}-24_{2,23}$	127 985.776	126.4	12.59	127 986.1	0.06	0.01	NH_2CHO $v_{12} = 1$
tEME-AA	$24_{3,22}-24_{2,23}$	127 986.063	126.4	12.59	†			
tEME-EE'	$25_{3,23}-25_{2,24}$	129 256.739	136.1	13.06	129 256.8	0.04	0.02	
tEME-EE	$25_{3,23}-25_{2,24}$	129 256.741	136.1	13.06	†			
tEME-AE	$25_{3,23}-25_{2,24}$	129 257.027	136.1	13.06	†			
tEME-EA	$25_{3,23}-25_{2,24}$	129 259.044	136.1	13.06	129 259.3	0.04	0.01	
tEME-AA	$25_{3,23}-25_{2,24}$	129 259.331	136.0	13.06	†			
tEME-EE'	$26_{3,24}-26_{2,25}$	130 655.101	146.1	13.52	...	...	0.02	U-line
tEME-EE	$26_{3,24}-26_{2,25}$	130 655.103	146.1	13.52	†			
tEME-AE	$26_{3,24}-26_{2,25}$	130 655.389	146.1	13.52	†			
tEME-EA	$26_{3,24}-26_{2,25}$	130 657.388	146.1	13.52	...	...	0.01	U-line
tEME-AA	$26_{3,24}-26_{2,25}$	130 657.674	146.1	13.52	†			

Table A.2. continued.

Species	Transition $J_{K_a,K_c} - J'_{K'_a,K'_c}$	Predicted frequency (MHz)	E_{upp} (K)	S_{ij}	Observed[1] frequency (MHz)	Observed[1] T_{MB} (K)	Model[2] T_{MB} (K)	Blends
tEME-EE'	$15_{1,15}-14_{0,14}$	131 372.619	46.7	9.86	131 372.7	0.05	0.05	
tEME-EE	$15_{1,15}-14_{0,14}$	131 372.619	46.7	9.86	†			
tEME-AE	$15_{1,15}-14_{0,14}$	131 372.660	46.7	9.86	†			
tEME-EA	$15_{1,15}-14_{0,14}$	131 373.069	46.7	9.86	†			
tEME-AA	$15_{1,15}-14_{0,14}$	131 373.110	46.7	9.86	†			
tEME-EE'	$27_{3,25}-27_{2,26}$	132 182.639	156.6	13.95	132 182.8	0.04	0.02	
tEME-EE	$27_{3,25}-27_{2,26}$	132 182.640	156.6	13.95	†			
tEME-AE	$27_{3,25}-27_{2,26}$	132 182.927	156.6	13.95	†			
tEME-EA	$27_{3,25}-27_{2,26}$	132 184.906	156.6	13.95	132 185.5	0.01	0.01	
tEME-AA	$27_{3,25}-27_{2,26}$	132 185.194	156.6	13.95	†			
tEME-EE'	$8_{2,7}-7_{1,6}$	132 547.336	18.5	2.87	132 547.2	0.02	0.02	
tEME-EE	$8_{2,7}-7_{1,6}$	132 547.352	18.5	2.87	†			
tEME-AE	$8_{2,7}-7_{1,6}$	132 547.529	18.5	2.87	†			
tEME-EA	$8_{2,7}-7_{1,6}$	132 548.982	18.5	2.87	132 549.0	0.02	0.01	
tEME-AA	$8_{2,7}-7_{1,6}$	132 549.167	18.5	2.87	†			
tEME-AA	$18_{0,18}-17_{1,17}$	133 362.763	65.6	12.27	...	...	0.06	$O^{13}CS$, CH_2CHCN $v_{11}=1$
tEME-EA	$18_{0,18}-17_{1,17}$	133 362.784	65.6	12.27	†			
tEME-AE	$18_{0,18}-17_{1,17}$	133 363.098	65.6	12.27	†			
tEME-EE	$18_{0,18}-17_{1,17}$	133 363.118	65.6	12.27	†			
tEME-EE'	$18_{0,18}-17_{1,17}$	133 363.118	65.6	12.27	†			
tEME-EE'	$28_{3,26}-28_{2,27}$	133 842.950	167.4	14.37	...	...	0.02	CH_2DOH
tEME-EE	$28_{3,26}-28_{2,27}$	133 842.951	167.4	14.37	†			
tEME-AE	$28_{3,26}-28_{2,27}$	133 843.238	167.4	14.37	†			
tEME-EA	$28_{3,26}-28_{2,27}$	133 845.198	167.4	14.37	...	...	0.01	CH_2DOH
tEME-AA	$28_{3,26}-28_{2,27}$	133 845.486	167.4	14.37	†			
tEME-AA	$22_{1,21}-21_{2,20}$	135 315.986	100.2	7.28	135 316.0	0.07	0.01	U-line
tEME-EA	$22_{1,21}-21_{2,20}$	135 316.082	100.2	7.28	†			
tEME-AE	$22_{1,21}-21_{2,20}$	135 317.259	100.2	7.28	135 317.5	0.05	0.02	CH_3CHO $v_t=1$
tEME-EE	$22_{1,21}-21_{2,20}$	135 317.355	100.2	7.28	†			
tEME-EE'	$22_{1,21}-21_{2,20}$	135 317.355	100.2	7.28	†			
tEME-EE'	$29_{3,27}-29_{2,28}$	135 639.103	178.6	14.77	...	...	0.02	CH_3OCOH $v_t=1$
tEME-EE	$29_{3,27}-29_{2,28}$	135 639.104	178.6	14.77	†			
tEME-AE	$29_{3,27}-29_{2,28}$	135 639.392	178.6	14.77	†			
tEME-EA	$29_{3,27}-29_{2,28}$	135 641.333	178.6	14.77	...	...	0.01	CH_3OCOH $v_t=1$
tEME-AA	$29_{3,27}-29_{2,28}$	135 641.621	178.6	14.77	†			
tEME-EE'	$30_{3,28}-30_{2,29}$	137 573.618	190.2	15.14	137 573.7	0.04	0.02	
tEME-EE	$30_{3,28}-30_{2,29}$	137 573.618	190.2	15.14	†			
tEME-AE	$30_{3,28}-30_{2,29}$	137 573.907	190.2	15.14	†			
tEME-EA	$30_{3,28}-30_{2,29}$	137 575.829	190.2	15.14	137 575.9	0.05	0.02	CH_3COOCH_3
tEME-AA	$30_{3,28}-30_{2,29}$	137 576.118	190.2	15.14	†			
tEME-EE'	$16_{1,16}-15_{0,15}$	138 109.231	52.7	10.73	138 109.7	0.06	0.06	
tEME-EE	$16_{1,16}-15_{0,15}$	138 109.231	52.7	10.73	†			
tEME-AE	$16_{1,16}-15_{0,15}$	138 109.269	52.7	10.73	†			
tEME-EA	$16_{1,16}-15_{0,15}$	138 109.661	52.7	10.73	†			
tEME-AA	$16_{1,16}-15_{0,15}$	138 109.699	52.7	10.73	†			
tEME-EE'	$9_{2,8}-8_{1,7}$	139 530.181	22.0	3.15	...	...	0.02	CH_2DCN
tEME-EE	$9_{2,8}-8_{1,7}$	139 530.191	22.0	3.15	†			
tEME-AE	$9_{2,8}-8_{1,7}$	139 530.369	22.0	3.15	†			
tEME-EA	$9_{2,8}-8_{1,7}$	139 531.807	22.0	3.15	...	...	0.01	CH_2DCN
tEME-AA	$9_{2,8}-8_{1,7}$	139 531.989	22.0	3.15	†			
tEME-EE'	$31_{3,29}-31_{2,30}$	139 648.445	202.2	15.50	...	...	0.02	CH_3COCH_3
tEME-EE	$31_{3,29}-31_{2,30}$	139 648.445	202.2	15.50	†			
tEME-AE	$31_{3,29}-31_{2,30}$	139 648.735	202.2	15.50	†			
tEME-EA	$31_{3,29}-31_{2,30}$	139 650.637	202.2	15.50	...	...	0.01	CH_3COCH_3
tEME-AA	$31_{3,29}-31_{2,30}$	139 650.927	202.2	15.50	†			
tEME-EE	$8_{2,6}-7_{1,7}$	140 527.950	18.5	2.43	140 528.1	0.02	0.02	
tEME-EE'	$8_{2,6}-7_{1,7}$	140 527.966	18.5	2.43	†			
tEME-AE	$8_{2,6}-7_{1,7}$	140 528.160	18.5	2.43	†			
tEME-EA	$8_{2,6}-7_{1,7}$	140 529.589	18.5	2.43	140 529.6	0.03	0.01	U-line
tEME-AA	$8_{2,6}-7_{1,7}$	140 529.791	18.5	2.43	†			
tEME-EE'	$32_{3,30}-32_{2,31}$	141 864.954	214.6	15.83	...	...	0.02	CH_3COOH $v_t=1$
tEME-EE	$32_{3,30}-32_{2,31}$	141 864.954	214.6	15.83	†			
tEME-AE	$32_{3,30}-32_{2,31}$	141 865.246	214.6	15.83	†			
tEME-EA	$32_{3,30}-32_{2,31}$	141 867.127	214.6	15.83	...	...	0.01	CH_3COOH $v_t=1$
tEME-AA	$32_{3,30}-32_{2,31}$	141 867.419	214.6	15.83	†			
tEME-AA	$19_{0,19}-18_{1,18}$	142 139.587	72.8	13.27	142 139.7	0.08	0.06	
tEME-EA	$19_{0,19}-18_{1,18}$	142 139.605	72.8	13.27	†			
tEME-AE	$19_{0,19}-18_{1,18}$	142 139.896	72.8	13.27	†			
tEME-EE	$19_{0,19}-18_{1,18}$	142 139.914	72.8	13.27	†			
tEME-EE'	$19_{0,19}-18_{1,18}$	142 139.914	72.8	13.27	†			
tEME-EE'	$3_{3,1}-2_{2,1}$	143 977.261	12.7	2.45	143 977.8	0.06	0.02	U-line
tEME-EE	$3_{3,1}-2_{2,1}$	143 977.759	12.7	2.41	†			
tEME-AE	$3_{3,1}-2_{2,1}$	143 977.810	12.7	2.44	†			

Table A.2. continued.

Species	Transition $J_{K_a,K_c} - J'_{K'_a,K'_c}$	Predicted frequency (MHz)	E_{upp} (K)	S_{ij}	Observed[1] frequency (MHz)	Observed[1] T_{MB} (K)	Model[2] T_{MB} (K)	Blends
tEME-EA	$3_{3,1}-2_{2,0}$	143 979.010	12.7	.72	143 980.0	0.05	0.02	CH_3COCH_3
tEME-EE	$3_{3,0}-2_{2,0}$	143 979.276	12.7	2.41	†			
tEME-EE'	$3_{3,0}-2_{2,0}$	143 979.774	12.7	2.45	†			
tEME-AE	$3_{3,0}-2_{2,0}$	143 979.832	12.7	2.44	†			
tEME-AA	$3_{3,1}-2_{2,0}$	143 980.192	12.7	2.50	†			
tEME-EA	$3_{3,0}-2_{2,0}$	143 980.533	12.7	1.78	†			
tEME-EE'	$33_{3,31}-33_{2,32}$	144 223.924	227.3	16.14	144 224.0	0.02	0.01	
tEME-EE	$33_{3,31}-33_{2,32}$	144 223.925	227.3	16.14	†			
tEME-AE	$33_{3,31}-33_{2,32}$	144 224.218	227.3	16.14	†			
tEME-EE'	$17_{1,17}-16_{0,16}$	144 871.829	59.2	11.63	144 872.1	0.06	0.06	
tEME-EE	$17_{1,17}-16_{0,16}$	144 871.829	59.2	11.63	†			
tEME-AE	$17_{1,17}-16_{0,16}$	144 871.864	59.2	11.63	†			
tEME-EA	$17_{1,17}-16_{0,16}$	144 872.238	59.2	11.63	†			
tEME-AA	$17_{1,17}-16_{0,16}$	144 872.273	59.2	11.63	†			
tEME-AA	$23_{1,22}-22_{2,21}$	145 647.137	109.2	7.92	145 647.4	0.03	0.01	
tEME-EA	$23_{1,22}-22_{2,21}$	145 647.226	109.2	7.92	†			
tEME-AE	$23_{1,22}-22_{2,21}$	145 648.372	109.2	7.92	145 648.6	0.03	0.02	
tEME-EE	$23_{1,22}-22_{2,21}$	145 648.461	109.2	7.92	†			
tEME-EE'	$23_{1,22}-22_{2,21}$	145 648.462	109.2	7.92	†			
tEME-EE'	$10_{2,9}-9_{1,8}$	146 383.619	25.8	3.44	146 384.0	0.03	0.02	
tEME-EE	$10_{2,9}-9_{1,8}$	146 383.626	25.8	3.44	†			
tEME-AE	$10_{2,9}-9_{1,8}$	146 383.802	25.8	3.44	†			
tEME-EA	$10_{2,9}-9_{1,8}$	146 385.228	25.8	3.44	146 385.5	0.03	0.02	
tEME-AA	$10_{2,9}-9_{1,8}$	146 385.408	25.8	3.44	†			
tEME-EE	$36_{4,32}-36_{3,33}$	146 397.039	276.3	21.88	...	...	0.01	SO_2, CH_3OCH_3
tEME-EE'	$36_{4,32}-36_{3,33}$	146 397.042	276.3	21.88	†			
tEME-AE	$36_{4,32}-36_{3,33}$	146 397.310	276.3	21.88	†			
tEME-EE'	$34_{3,32}-34_{2,33}$	146 725.545	240.5	16.44	146 725.6	0.03	0.01	$SO^{18}O$
tEME-EE	$34_{3,32}-34_{2,33}$	146 725.545	240.5	16.44	†			
tEME-AE	$34_{3,32}-34_{2,33}$	146 725.840	240.5	16.44	†			
tEME-AE	$29_{2,27}-28_{3,26}$	146 736.865	174.4	6.43	...	...	0.01	U-line
tEME-EE	$29_{2,27}-28_{3,26}$	146 737.046	174.4	6.43	†			
tEME-EE'	$29_{2,27}-28_{3,26}$	146 737.048	174.4	6.43	†			
tEME-EE	$35_{4,31}-35_{3,32}$	148 578.427	262.3	20.95	...	...	0.01	CH_3OCOH $v_t = 1$
tEME-EE'	$35_{4,31}-35_{3,32}$	148 578.431	262.3	20.95	†			
tEME-AE	$35_{4,31}-35_{3,32}$	148 578.707	262.3	20.95	†			
tEME-EE'	$35_{3,33}-35_{2,34}$	149 369.412	254.0	16.71	...	...	0.01	CH_3OCOH $v_t = 1$
tEME-EE	$35_{3,33}-35_{2,34}$	149 369.412	254.0	16.71	†			
tEME-AE	$35_{3,33}-35_{2,34}$	149 369.709	254.0	16.71	†			
tEME-EE	$9_{2,7}-8_{1,8}$	149 921.139	22.0	2.54	...	...	0.02	CH_3OCOH
tEME-EE'	$9_{2,7}-8_{1,8}$	149 921.149	22.0	2.54	†			
tEME-AE	$9_{2,7}-8_{1,8}$	149 921.348	22.0	2.54	†			
tEME-EA	$9_{2,7}-8_{1,8}$	149 922.787	22.0	2.54	...	...	0.01	CH_3OCOH
tEME-AA	$9_{2,7}-8_{1,8}$	149 922.992	22.0	2.54	†			
tEME-EE	$34_{4,30}-34_{3,31}$	150 661.347	248.7	20.06	150 661.4	0.04	0.02	U-line
tEME-EE'	$34_{4,30}-34_{3,31}$	150 661.353	248.7	20.06	†			
tEME-AE	$34_{4,30}-34_{3,31}$	150 661.636	248.7	20.06	†			
tEME-EA	$34_{4,30}-34_{3,31}$	150 664.261	248.7	20.06	150 664.4	0.03	0.02	U-line
tEME-AA	$34_{4,30}-34_{3,31}$	150 664.547	248.7	20.06	†			
tEME-AA	$20_{0,20}-19_{1,19}$	150 845.281	80.4	14.28	150 845.4	0.08	0.09	
tEME-EA	$20_{0,20}-19_{1,19}$	150 845.296	80.4	14.28	†			
tEME-AE	$20_{0,20}-19_{1,19}$	150 845.565	80.4	14.28	†			
tEME-EE	$20_{0,20}-19_{1,19}$	150 845.580	80.4	14.28	†			
tEME-EE'	$20_{0,20}-19_{1,19}$	150 845.580	80.4	14.28	†			
tEME-EE'	$18_{1,18}-17_{0,17}$	151 672.109	66.0	12.56	151 672.4	0.06	0.09	
tEME-EE	$18_{1,18}-17_{0,17}$	151 672.109	66.0	12.56	†			
tEME-AE	$18_{1,18}-17_{0,17}$	151 672.141	66.0	12.56	†			
tEME-EA	$18_{1,18}-17_{0,17}$	151 672.495	66.0	12.56	†			
tEME-AA	$18_{1,18}-17_{0,17}$	151 672.527	66.0	12.56	†			
tEME-EE'	$11_{2,10}-10_{1,9}$	153 109.700	30.1	3.73	153 109.7	0.05	0.03	
tEME-EE	$11_{2,10}-10_{1,9}$	153 109.705	30.1	3.73	†			
tEME-AE	$11_{2,10}-10_{1,9}$	153 109.879	30.1	3.73	†			
tEME-EA	$11_{2,10}-10_{1,9}$	153 111.294	30.1	3.73	153 111.4	0.05	0.02	U-line
tEME-AA	$11_{2,10}-10_{1,9}$	153 111.471	30.1	3.73	†			
tEME-EE	$32_{4,28}-32_{3,29}$	154 467.850	222.8	18.42	154 468.1	0.02	0.02	
tEME-EE'	$32_{4,28}-32_{3,29}$	154 467.860	222.8	18.42	†			
tEME-AE	$32_{4,28}-32_{3,29}$	154 468.157	222.8	18.42	†			
tEME-AA	$24_{1,23}-23_{2,22}$	155 980.202	118.5	8.61	...	...	0.03	CH_3CH_2CN $v_{12} = 1$
tEME-EA	$24_{1,23}-23_{2,22}$	155 980.284	118.5	8.61	†			
tEME-AE	$24_{1,23}-23_{2,22}$	155 981.396	118.5	8.61	...	...	0.03	CH_3CH_2CN $v_{12} = 1$
tEME-EE	$24_{1,23}-23_{2,22}$	155 981.478	118.5	8.61	†			
tEME-EE'	$24_{1,23}-23_{2,22}$	155 981.479	118.5	8.61	†			
tEME-EE	$31_{4,27}-31_{3,28}$	156 169.103	210.3	17.65	...	...	0.02	CH_3CH_2CN

Table A.2. continued.

Species	Transition $J_{K_a,K_c} - J'_{K'_a,K'_c}$	Predicted frequency (MHz)	E_{upp} (K)	S_{ij}	Observed[1] frequency (MHz)	Observed[1] T_{MB} (K)	Model[2] T_{MB} (K)	Blends
tEME-EE'	$31_{4,27}-31_{3,28}$	156 169.114	210.3	17.65	†			
tEME-AE	$31_{4,27}-31_{3,28}$	156 169.418	210.3	17.65	†			
tEME-EE	$30_{4,26}-31_{3,27}$	157 727.158	198.3	16.91	157 727.3	0.03	0.02	
tEME-EE'	$30_{4,26}-31_{3,27}$	157 727.174	198.3	16.91	†			
tEME-AE	$30_{4,26}-31_{3,27}$	157 727.482	198.3	16.91	†			
tEME-EE'	$19_{1,19}-18_{0,18}$	158 519.756	73.2	13.52	...	...	0.10	CH_3OCOH $v_t = 1$, CH_3COCH_3
tEME-EE	$19_{1,19}-18_{0,18}$	158 519.756	73.2	13.52	†			
tEME-AE	$19_{1,19}-18_{0,18}$	158 519.786	73.2	13.52	†			
tEME-EA	$19_{1,19}-18_{0,18}$	158 520.119	73.2	13.52	†			
tEME-AA	$19_{1,19}-18_{0,18}$	158 520.149	73.2	13.52	†			
tEME-EE	$29_{4,25}-29_{3,26}$	159 140.100	186.7	16.20	...	...	0.03	U-line
tEME-EE'	$29_{4,25}-29_{3,26}$	159 140.121	186.7	16.19	†			
tEME-AE	$29_{4,25}-29_{3,26}$	159 140.432	186.7	16.20	†			
tEME-EA	$29_{4,25}-29_{3,26}$	159 143.035	186.7	16.20	...	...	0.02	U-line
tEME-AA	$29_{4,25}-29_{3,26}$	159 143.357	186.7	16.20	†			
tEME-AA	$21_{0,21}-20_{1,20}$	159 477.061	88.4	15.31	159 477.1	0.15	0.10	CH_2CN
tEME-EA	$21_{0,21}-20_{1,20}$	159 477.074	88.4	15.31	†			
tEME-AE	$21_{0,21}-20_{1,20}$	159 477.319	88.4	15.31	†			
tEME-EE	$21_{0,21}-20_{1,20}$	159 477.332	88.4	15.31	†			
tEME-EE'	$21_{0,21}-20_{1,20}$	159 477.332	88.4	15.31	†			
tEME-EE	$10_{2,8}-9_{1,9}$	159 548.654	25.9	2.61	159 548.8	0.09	0.02	CH_3COOH $v_t = 2$
tEME-EE'	$10_{2,8}-9_{1,9}$	159 548.661	25.9	2.61	†	〃	〃	
tEME-AE	$10_{2,8}-9_{1,9}$	159 548.866	25.9	2.61	†	〃	〃	
tEME-EE'	$12_{2,11}-11_{1,10}$	159 710.946	34.7	4.05	...	...	0.03	CH_3CH_2CN v_{12}/v_{21}
tEME-EE	$12_{2,11}-11_{1,10}$	159 710.950	34.7	4.05	†			
tEME-AE	$12_{2,11}-11_{1,10}$	159 711.121	34.7	4.05	†			
tEME-EA	$12_{2,11}-11_{1,10}$	159 712.526	34.7	4.05	...	...	0.02	CH_3CH_2CN v_{12}/v_{21}
tEME-AA	$12_{2,11}-11_{1,10}$	159 712.699	34.7	4.05	†			
tEME-EE	$28_{4,24}-28_{3,25}$	160 409.193	175.5	15.50	...	...	0.03	CH_3COCH_3
tEME-EE'	$28_{4,24}-28_{3,25}$	160 409.221	175.5	15.50	†			
tEME-AE	$28_{4,24}-28_{3,25}$	160 409.535	175.5	15.50	†			
tEME-EA	$28_{4,24}-28_{3,25}$	160 412.123	175.5	15.50	...	...	0.02	CH_3OCOH $v_t = 1$
tEME-AA	$28_{4,24}-28_{3,25}$	160 412.450	175.5	15.50	†			
tEME-EE'	$10_{3,8}-9_{2,7}$	199 842.884	31.6	3.55	199 843.5	...	0.05	CH_3OCOH $v_t = 2$
tEME-EE	$10_{3,8}-9_{2,7}$	199 843.513	31.6	3.65	†			
tEME-AE	$10_{3,8}-9_{2,7}$	199 843.521	31.6	3.61	†			
tEME-EA	$10_{3,8}-9_{2,7}$	199 846.703	31.6	3.78	...	...	0.04	CH_3OCOH $v_t = 1$
tEME-AA	$10_{3,8}-9_{2,7}$	199 847.033	31.6	3.78	†			
tEME-EE'	$4_{4,1}-3_{3,1}$	199 953.072	22.3	3.50	199 953.5	0.18	0.06	CH_3CH_2OH
tEME-EE	$4_{4,1}-3_{3,1}$	199 953.406	22.3	3.50	†			
tEME-AE	$4_{4,1}-3_{3,1}$	199 953.633	22.3	3.50	†			
tEME-EE	$4_{4,0}-3_{3,0}$	199 954.307	22.3	3.50	199 954.7	0.12	0.06	CH_3CH_2OH
tEME-EE'	$4_{4,0}-3_{3,0}$	199 954.642	22.3	3.50	†			
tEME-AE	$4_{4,0}-3_{3,0}$	199 954.869	22.3	3.50	†			
tEME-EA	$4_{4,1}-3_{3,1}$	199 956.750	22.3	3.50	199 957.2	0.19	0.08	CH_2CHCN $v_{15} = 1$
tEME-EA	$4_{4,0}-3_{3,0}$	199 957.085	22.3	3.50	†			
tEME-AA	$4_{4,1}-3_{3,0}$	199 957.305	22.3	3.50	†			
tEME-AA	$4_{4,0}-3_{3,1}$	199 957.317	22.3	3.50	†			
tEME-EE	$10_{3,7}-9_{2,8}$	200 603.336	31.6	3.64	...	...	0.05	U-line
tEME-AE	$10_{3,7}-9_{2,8}$	200 603.932	31.6	3.59	†			
tEME-EE'	$10_{3,7}-9_{2,8}$	200 603.965	31.6	3.54	†			
tEME-EA	$10_{3,7}-9_{2,8}$	200 605.130	31.6	3.76	...	...	0.04	CH_3OCOH
tEME-AA	$10_{3,7}-9_{2,8}$	200 605.404	31.6	3.77	†			
tEME-EE	$14_{2,12}-13_{1,13}$	200 820.096	45.3	2.62	...	...	0.04	CH_3OH
tEME-EE'	$14_{2,12}-13_{1,13}$	200 820.098	45.3	2.62	†			
tEME-AE	$14_{2,12}-13_{1,13}$	200 820.324	45.3	2.62	†			
tEME-EA	$14_{2,12}-13_{1,13}$	200 821.765	45.3	2.62	...	...	0.03	CH_3OH
tEME-AA	$14_{2,12}-13_{1,13}$	200 821.991	45.3	2.62	†			
tEME-EE'	$25_{1,25}-24_{0,24}$	200 871.974	124.2	19.55	200 872.2	0.59	0.20	CH_2CHCN $v_{11} = 2$
tEME-EE	$25_{1,25}-24_{0,24}$	200 871.975	124.2	19.55	†			
tEME-AE	$25_{1,25}-24_{0,24}$	200 871.991	124.2	19.55	†			
tEME-EA	$25_{1,25}-24_{0,24}$	200 872.199	124.2	19.55	†			
tEME-AA	$25_{1,25}-24_{0,24}$	200 872.216	124.2	19.55	†			
tEME-AA	$26_{0,26}-25_{1,25}$	201 553.272	133.9	20.51	201 553.4	0.32	0.21	
tEME-EA	$26_{0,26}-25_{1,25}$	201 553.275	133.9	20.51	†			
tEME-AE	$26_{0,26}-25_{1,25}$	201 553.416	133.9	20.51	†			
tEME-EE	$26_{0,26}-25_{1,25}$	201 553.419	133.9	20.51	†			
tEME-EE'	$26_{0,26}-25_{1,25}$	201 553.419	133.9	20.51	†			
tEME-EE'	$19_{2,18}-18_{1,17}$	202 767.815	77.9	6.76	...	...	0.08	$H^{13}CCCN$, CH_3CN $v_8 = 1$
tEME-EE	$19_{2,18}-18_{1,17}$	202 767.815	77.9	6.76	†			
tEME-AE	$19_{2,18}-18_{1,17}$	202 767.956	77.9	6.76	†			
tEME-EA	$19_{2,18}-18_{1,17}$	202 769.267	77.9	6.76	...	...	0.05	$H^{13}CCCN$, CH_3CN $v_8 = 1$
tEME-AA	$19_{2,18}-18_{1,17}$	202 769.407	77.9	6.76	†			

Table A.2. continued.

Species	Transition $J_{K_a,K_c} - J'_{K'_a,K'_c}$	Predicted frequency (MHz)	E_{upp} (K)	S_{ij}	Observed[1] frequency (MHz)	Observed[1] T_{MB} (K)	Model[2] T_{MB} (K)	Blends
tEME-AA	$29_{1,28}-28_{2,27}$	207 138.789	170.9	12.63	207 139.6	0.07	0.07	
tEME-EA	$29_{1,28}-28_{2,27}$	207 138.838	170.9	12.63	†			
tEME-AE	$29_{1,28}-28_{2,27}$	207 139.740	170.9	12.63	†			
tEME-EE	$29_{1,28}-28_{2,27}$	207 139.789	170.9	12.63	†			
tEME-EE'	$29_{1,28}-28_{2,27}$	207 139.789	170.9	12.63	†			
tEME-EE'	$11_{3,9}-10_{2,8}$	207 643.771	35.9	3.90	...	...	0.07	CH_3CH_2CN
tEME-EE	$11_{3,9}-10_{2,8}$	207 644.152	35.9	3.94	†			
tEME-AE	$11_{3,9}-10_{2,8}$	207 644.276	35.9	3.92	†			
tEME-EA	$11_{3,9}-10_{2,8}$	207 647.053	35.9	3.99	207 647.4	0.20	0.05	CH_3CH_2CN
tEME-AA	$11_{3,9}-10_{2,8}$	207 647.369	35.9	3.99	†			
tEME-EE'	$5_{4,2}-4_{3,2}$	208 004.136	24.2	3.60	...	...	0.07	CH_3CH_2CN, CH_3CH_2OH
tEME-EE	$5_{4,2}-4_{3,2}$	208 004.469	24.2	3.60	†			
tEME-AE	$5_{4,2}-4_{3,2}$	208 004.696	24.2	3.60	†			
tEME-EE	$5_{4,1}-4_{3,1}$	208 005.368	24.2	3.60	†			
tEME-EE'	$5_{4,1}-4_{3,1}$	208 005.702	24.2	3.60	†			
tEME-AE	$5_{4,1}-4_{3,1}$	208 005.929	24.2	3.60	†			
tEME-EA	$5_{4,2}-4_{3,2}$	208 007.812	24.2	3.60	...	...	0.09	CH_3CH_2CN, CH_3CH_2OH
tEME-EA	$5_{4,1}-4_{3,1}$	208 008.143	24.2	3.60	†			
tEME-AA	$5_{4,2}-4_{3,1}$	208 008.330	24.2	3.60	†			
tEME-AA	$5_{4,1}-4_{3,2}$	208 008.413	24.2	3.60	†			
tEME-EE'	$26_{1,26}-25_{0,25}$	208 147.627	134.1	20.57	208 147.7	0.58	0.22	CH_2CHCN $v_{11} = 1$
tEME-EE	$26_{1,26}-25_{0,25}$	208 147.627	134.1	20.57	†			
tEME-AE	$26_{1,26}-25_{0,25}$	208 147.642	134.1	20.57	†			
tEME-EA	$26_{1,26}-25_{0,25}$	208 147.831	134.1	20.57	†			
tEME-AA	$26_{1,26}-25_{0,25}$	208 147.846	134.1	20.57	†			
tEME-EE'	$20_{2,19}-19_{1,18}$	208 541.474	85.6	7.24	208 541.5	0.19	0.08	
tEME-EE	$20_{2,19}-19_{1,18}$	208 541.474	85.6	7.24	†			
tEME-AE	$20_{2,19}-19_{1,18}$	208 541.609	85.6	7.24	†			
tEME-EA	$20_{2,19}-19_{1,18}$	208 542.901	85.6	7.24	208 543.0	0.16	0.05	
tEME-AA	$20_{2,19}-19_{1,18}$	208 543.036	85.6	7.24	†			
tEME-EE	$11_{3,8}-10_{2,9}$	208 783.787	35.9	3.92	...	...	0.07	CH_3OCOH
tEME-EE'	$11_{3,8}-10_{2,9}$	208 784.168	35.9	3.88	†			
tEME-AE	$11_{3,8}-10_{2,9}$	208 784.265	35.9	3.90	†			
tEME-EA	$11_{3,8}-10_{2,9}$	208 785.864	35.9	3.96	...	...	0.05	CH_3OCOH
tEME-AA	$11_{3,8}-10_{2,9}$	208 786.150	35.9	3.96	†			
tEME-AA	$27_{0,27}-26_{1,26}$	209 774.111	144.1	21.55	209 774.0	0.35	0.22	CH_2CHCN $v_{15} = 1$
tEME-EA	$27_{0,27}-26_{1,26}$	209 774.113	144.1	21.55	†			
tEME-AE	$27_{0,27}-26_{1,26}$	209 774.236	144.1	21.55	†			
tEME-EE	$27_{0,27}-26_{1,26}$	209 774.238	144.1	21.55	†			
tEME-EE'	$27_{0,27}-26_{1,26}$	209 774.238	144.1	21.55	†			
tEME-EE	$15_{2,13}-14_{1,14}$	211 933.388	51.2	2.56	...	...	0.04	CH_3OCOH
tEME-EE'	$15_{2,13}-14_{1,14}$	211 933.389	51.2	2.56	†			
tEME-AE	$15_{2,13}-14_{1,14}$	211 933.621	51.2	2.56	†			
tEME-EA	$15_{2,13}-14_{1,14}$	211 935.057	51.2	2.56	...	...	0.03	CH_3OCOH
tEME-AA	$15_{2,13}-14_{1,14}$	211 935.290	51.2	2.56	†			
tEME-EE	$32_{5,27}-32_{4,28}$	212 287.353	232.9	17.12	...	...	0.04	CH_3COCH_3
tEME-EE'	$32_{5,27}-32_{4,28}$	212 287.576	232.9	17.07	†			
tEME-AE	$32_{5,27}-32_{4,28}$	212 287.827	232.9	17.10	†			
tEME-EA	$32_{5,27}-32_{4,28}$	212 290.165	232.9	17.17	...	...	0.03	CH_3COCH_3
tEME-AA	$32_{5,27}-32_{4,28}$	212 290.528	232.9	17.17	†			
tEME-EE	$31_{5,26}-31_{4,27}$	212 762.787	220.6	16.46	...	...	0.03	CH_3OCH_3
tEME-EE'	$31_{5,26}-31_{4,27}$	212 763.095	220.6	16.37	†			
tEME-AE	$31_{5,26}-31_{4,27}$	212 763.306	220.6	16.42	†			
tEME-EA	$31_{5,26}-31_{4,27}$	212 765.533	220.6	16.55	212 766.9	0.14	0.03	CH_3OCH_3
tEME-AA	$31_{5,26}-31_{4,27}$	212 765.897	220.6	16.55	†			
tEME-EE	$30_{5,25}-30_{4,26}$	213 178.397	208.6	15.77	...	...	0.04	U-line
tEME-EE'	$30_{5,25}-30_{4,26}$	213 178.825	208.6	15.61	†			
tEME-AE	$30_{5,25}-30_{4,26}$	213 178.976	208.6	15.70	†			
tEME-EA	$30_{5,25}-30_{4,26}$	213 181.046	208.6	15.93	213 181.4	0.21	0.03	CH_2OHCHO
tEME-AA	$30_{5,25}-30_{4,26}$	213 181.410	208.6	15.94	†			
tEME-EE'	$33_{5,29}-33_{4,30}$	213 495.962	245.7	17.69	213 495.8	0.09	0.04	U-line
tEME-EE	$33_{5,29}-33_{4,30}$	213 496.124	245.7	17.72	†			
tEME-AE	$33_{5,29}-33_{4,30}$	213 496.418	245.7	17.71	†			
tEME-EA	$33_{5,29}-33_{4,30}$	213 499.211	245.7	17.75	213 499.3	0.10	0.03	U-line
tEME-AA	$33_{5,29}-33_{4,30}$	213 499.587	245.7	17.75	†			
tEME-EE	$29_{5,24}-29_{4,25}$	213 540.983	196.9	15.03	213 541.4	0.16	0.05	CH_2CHCN $v_{11} = 2$
tEME-EE'	$29_{5,24}-29_{4,25}$	213 541.573	196.9	14.74	†			
tEME-AE	$29_{5,24}-29_{4,25}$	213 541.643	196.9	14.89	†			
tEME-EA	$29_{5,24}-29_{4,25}$	213 543.491	196.9	15.32	...	...	0.04	CH_2CHCN $v_{11} = 2$
tEME-AA	$29_{5,24}-29_{4,25}$	213 543.850	196.9	15.33	†			
tEME-EE'	$32_{5,28}-32_{4,29}$	213 676.308	232.9	17.03	213 676.5	0.20	0.04	CH_3CH_2OH
tEME-EE	$32_{5,28}-32_{4,29}$	213 676.530	232.9	17.09	†			
tEME-AE	$32_{5,28}-32_{4,29}$	213 676.802	232.9	17.06	†			

Table A.2. continued.

Species	Transition $J_{K_a,K_c} - J'_{K'_a,K'_c}$	Predicted frequency (MHz)	E_{upp} (K)	S_{ij}	Observed[1] frequency (MHz)	Observed[1] T_{MB} (K)	Model[2] T_{MB} (K)	Blends
tEME-EA	$32_{5,28}-32_{4,29}$	213 679.692	232.9	17.13	213 680.0	0.14	0.03	CH_3COOCH_3
tEME-AA	$32_{5,28}-32_{4,29}$	213 680.076	232.9	17.14	†			
tEME-EE'	$31_{5,27}-31_{4,28}$	213 854.674	220.5	16.34	...	...	0.05	CH_3CH_2OH
tEME-EE	$31_{5,27}-31_{4,28}$	213 854.982	220.5	16.44	†			
tEME-AE	$31_{5,27}-31_{4,28}$	213 855.220	220.5	16.39	†			
tEME-EE	$28_{5,23}-28_{4,24}$	213 856.708	185.7	14.18	...	...	0.05	CH_3CH_2OH
tEME-AE	$28_{5,23}-28_{4,24}$	213 857.473	185.7	13.94	†			
tEME-EE'	$28_{5,23}-28_{4,24}$	213 857.509	185.7	13.70	†			
tEME-EA	$31_{5,27}-31_{4,28}$	213 858.239	220.5	16.52	...	...	0.05	CH_3CH_2OH
tEME-AA	$31_{5,27}-31_{4,28}$	213 858.632	220.5	16.53	†			
tEME-EA	$28_{5,23}-28_{4,24}$	213 859.015	185.7	14.70	†			
tEME-AA	$28_{5,23}-28_{4,24}$	213 859.367	185.7	14.73	†			
tEME-EE'	$30_{5,26}-30_{4,27}$	214 028.729	208.6	15.59	...	...	0.05	CH_3COCH_3
tEME-EE	$30_{5,26}-30_{4,27}$	214 029.157	208.6	15.76	†			
tEME-AE	$30_{5,26}-30_{4,27}$	214 029.345	208.6	15.68	†			
tEME-EA	$30_{5,26}-30_{4,27}$	214 032.539	208.6	15.91	...	...	0.04	
tEME-AA	$30_{5,26}-30_{4,27}$	214 032.943	208.6	15.92	†			
tEME-EE	$27_{5,22}-27_{4,23}$	214 131.118	174.9	13.15	...	...	0.04	$CH_3CH_2{}^{13}CN$, CH_3COOH $v_t = 1$
tEME-AE	$27_{5,22}-27_{4,23}$	214 132.010	174.9	12.80	†			
tEME-EE'	$27_{5,22}-27_{4,23}$	214 132.166	174.9	12.45	†			
tEME-EA	$27_{5,22}-27_{4,23}$	214 133.150	174.9	14.07	...	...	0.04	$CH_3CH_2{}^{13}CN$, CH_3COOH $v_t = 1$
tEME-AA	$27_{5,22}-27_{4,23}$	214 133.486	174.9	14.14	†			
tEME-EE'	$29_{5,25}-29_{4,25}$	214 196.531	196.9	14.72	...	...	0.05	$CH_3{}^{13}CH_2CN$, $CH_3O{}^{13}COH$ $v_t = 1$
tEME-EE	$29_{5,25}-29_{4,25}$	214 197.122	196.9	15.02	†			
tEME-AE	$29_{5,25}-29_{4,25}$	214 197.239	196.9	14.88	†			
tEME-EA	$29_{5,25}-29_{4,25}$	214 200.673	196.9	15.30	...	...	0.04	$CH_3{}^{13}CH_2CN$, $CH_3O{}^{13}COH$ $v_t = 1$
tEME-AA	$29_{5,25}-29_{4,25}$	214 201.091	196.9	15.32	†			
tEME-EE'	$21_{2,20}-20_{1,19}$	214 246.202	93.7	7.76	214 246.2	0.15	0.09	$^{13}CH_3CN$
tEME-EE	$21_{2,20}-20_{1,19}$	214 246.202	93.7	7.76	†			
tEME-AE	$21_{2,20}-20_{1,19}$	214 246.332	93.7	7.76	†			
tEME-EA	$21_{2,20}-20_{1,19}$	214 247.602	93.7	7.76	214 247.7	0.11	0.06	$^{13}CH_3CN$
tEME-AA	$21_{2,20}-20_{1,19}$	214 247.732	93.7	7.76	†			
tEME-EE'	$26_{5,22}-26_{4,22}$	214 355.828	164.4	2.47	...	...	0.05	SO, $^{13}CH_3CN$
tEME-EE'	$28_{5,24}-28_{4,25}$	214 356.510	185.7	13.69	†			
tEME-AE	$26_{5,22}-26_{4,22}$	214 356.963	164.4	2.08	†			
tEME-EE	$26_{5,22}-26_{4,22}$	214 357.232	164.4	1.63	†			
tEME-EE	$28_{5,24}-28_{4,25}$	214 357.312	185.7	14.17	†			
tEME-AE	$28_{5,24}-28_{4,25}$	214 357.333	185.7	13.93	†			
tEME-EA	$28_{5,24}-28_{4,25}$	214 361.091	185.7	14.69	...	...	0.04	SO, $^{13}CH_3CN$
tEME-AA	$28_{5,24}-28_{4,25}$	214 361.527	185.7	14.72	†			
tEME-EE	$26_{5,21}-26_{4,22}$	214 369.161	164.4	11.92	...	...	0.07	SO, $^{13}CH_3CN$
tEME-AE	$26_{5,21}-26_{4,22}$	214 370.185	164.4	11.47	†			
tEME-EE'	$26_{5,21}-26_{4,22}$	214 370.456	164.4	11.08	†			
tEME-EA	$26_{5,21}-26_{4,22}$	214 370.843	164.4	13.42	†			
tEME-AA	$26_{5,21}-26_{4,22}$	214 371.154	164.4	13.55	†			
tEME-EE'	$27_{5,23}-27_{4,24}$	214 507.462	174.9	12.45	...	...	0.04	CH_3CH_2CN
tEME-AE	$27_{5,23}-27_{4,24}$	214 508.414	174.9	12.79	†			
tEME-EE	$27_{5,23}-27_{4,24}$	214 508.510	174.9	13.15	†			
tEME-EA	$27_{5,23}-27_{4,24}$	214 512.591	174.9	14.07	...	...	0.04	CH_3CH_2CN
tEME-AA	$27_{5,23}-27_{4,24}$	214 513.051	174.9	14.13	†			
tEME-EE	$25_{5,20}-25_{4,21}$	214 575.213	154.4	10.55	...	...	0.09	$^{13}C^{17}O$
tEME-AE	$25_{5,20}-25_{4,21}$	214 576.349	154.4	10.10	†			
tEME-EA	$25_{5,20}-25_{4,21}$	214 576.498	154.4	12.69	†			
tEME-EE'	$25_{5,20}-25_{4,21}$	214 576.706	154.4	9.74	†			
tEME-AA	$25_{5,20}-25_{4,21}$	214 576.769	154.4	12.96	†			
tEME-EE'	$26_{5,22}-26_{4,23}$	214 648.535	164.4	11.08	...	...	0.04	CH_3OCOH
tEME-AE	$26_{5,22}-26_{4,23}$	214 649.611	164.4	11.47	†			
tEME-EE	$26_{5,22}-26_{4,23}$	214 649.829	164.4	11.92	†			
tEME-EA	$26_{5,22}-26_{4,23}$	214 654.288	164.5	13.41	...	...	0.04	CH_3OCOH
tEME-AA	$26_{5,22}-26_{4,23}$	214 654.781	164.5	13.54	†			
tEME-EE	$24_{5,19}-24_{4,20}$	214 753.118	144.7	9.23	214 754.3	0.20	0.09	
tEME-EA	$24_{5,19}-24_{4,20}$	214 754.023	144.7	11.84	†			
tEME-AA	$24_{5,19}-24_{4,20}$	214 754.233	144.7	12.38	†			
tEME-AE	$24_{5,19}-24_{4,20}$	214 754.329	144.7	8.86	†			
tEME-EE'	$24_{5,19}-24_{4,20}$	214 754.733	144.7	8.60	†			
tEME-EE'	$25_{5,21}-25_{4,22}$	214 779.208	154.4	9.74	...	...	0.04	CH_3OCOH
tEME-AE	$25_{5,21}-25_{4,22}$	214 780.378	154.4	10.10	†			
tEME-EE	$25_{5,21}-25_{4,22}$	214 780.701	154.4	10.55	†			
tEME-EA	$25_{5,21}-25_{4,22}$	214 785.581	154.4	12.69	...	...	0.04	CH_3OCOH
tEME-AA	$25_{5,21}-25_{4,22}$	214 786.123	154.4	12.96	†			
tEME-EE'	$24_{5,20}-24_{4,21}$	214 899.228	144.7	8.61	...	...	0.04	CH_3OCOH $v_t = 1$
tEME-AE	$24_{5,20}-24_{4,21}$	214 900.454	144.7	8.87	†			
tEME-EE	$24_{5,20}-24_{4,21}$	214 900.844	144.7	9.23	†			

Table A.2. continued.

Species	Transition $J_{K_a,K_c} - J'_{K'_a,K'_c}$	Predicted frequency (MHz)	E_{upp} (K)	S_{ij}	Observed[1] frequency (MHz)	Observed[1] T_{MB} (K)	Model[2] T_{MB} (K)	Blends
tEME-EA	$24_{5,20}-24_{4,21}$	214 906.128	144.7	11.83	...	...	0.11	CH_3CH_2CN
tEME-EE	$23_{5,18}-23_{4,19}$	214 906.260	135.4	8.13	†			
tEME-AA	$24_{5,20}-24_{4,21}$	214 906.739	144.7	12.38	†			
tEME-EA	$23_{5,18}-23_{4,19}$	214 906.872	135.4	10.76	†			
tEME-AA	$23_{5,18}-23_{4,19}$	214 906.992	135.4	11.80	†			
tEME-AE	$23_{5,18}-23_{4,19}$	214 907.507	135.4	7.91	†			
tEME-EE'	$23_{5,18}-23_{4,19}$	214 907.924	135.4	7.77	†			
tEME-EE	$24_{5,19}-24_{4,21}$	214 909.858	144.7	3.15	†			
tEME-EA	$24_{5,19}-24_{4,21}$	214 910.548	144.7	0.55	†			
tEME-AE	$24_{5,19}-24_{4,21}$	214 911.166	144.7	3.51	†			
tEME-EE'	$24_{5,19}-24_{4,21}$	214 911.685	144.7	3.77	†			
tEME-EE'	$23_{5,19}-23_{4,20}$	215 008.545	135.4	7.77	...	...	0.02	CH_3CH_2CN v_{13}/v_{21}
tEME-AE	$23_{5,19}-23_{4,20}$	215 009.791	135.4	7.91	...	...	0.04	CH_3CH_2CN v_{13}/v_{21}
tEME-EE	$23_{5,19}-23_{4,20}$	215 010.209	135.4	8.13	†			
tEME-EA	$23_{5,19}-23_{4,20}$	215 015.810	135.4	10.75	215 016.7	0.05	0.04	
tEME-AA	$23_{5,19}-23_{4,20}$	215 016.519	135.4	11.80	†			
tEME-EA	$22_{5,18}-22_{4,18}$	215 035.544	126.6	1.78	...	...	0.07	CH_3CH_2CN
tEME-EE	$22_{5,17}-22_{4,18}$	215 037.639	126.6	7.33	†			
tEME-EA	$22_{5,17}-22_{4,18}$	215 038.085	126.6	9.45	†			
tEME-AA	$22_{5,17}-22_{4,18}$	215 038.089	126.6	11.23	†			
tEME-AE	$22_{5,17}-22_{4,18}$	215 038.890	126.6	7.24	†			
tEME-EE'	$22_{5,17}-22_{4,18}$	215 039.292	126.6	7.21	†			
tEME-AA	$35_{2,33}-34_{3,32}$	215 107.148	250.8	9.27	...	...	0.03	CH_3CH_2CN
tEME-EA	$35_{2,33}-34_{3,32}$	215 107.270	250.8	9.27	†			
tEME-EE'	$22_{5,18}-22_{4,19}$	215 107.270	126.6	7.21	†			
tEME-AE	$22_{5,18}-22_{4,19}$	215 108.508	126.6	7.24	†			
tEME-EE	$22_{5,18}-22_{4,19}$	215 108.923	126.6	7.33	...	...	0.05	CH_3CH_2CN
tEME-AE	$35_{2,33}-34_{3,32}$	215 109.184	250.8	9.27	†			
tEME-EE	$35_{2,33}-34_{3,32}$	215 109.306	250.8	9.27	†			
tEME-EE'	$35_{2,33}-34_{3,32}$	215 109.306	250.8	9.27	†			
tEME-EA	$22_{5,18}-22_{4,19}$	215 114.713	126.6	9.45	...	...	0.04	CH_3CH_2CN
tEME-AA	$22_{5,18}-22_{4,19}$	215 115.545	126.6	11.23	†			
tEME-EE	$22_{5,17}-22_{4,19}$	215 117.232	126.6	3.90	†			
tEME-EA	$22_{5,17}-22_{4,19}$	215 117.254	126.6	1.78	†			
tEME-AE	$22_{5,17}-22_{4,19}$	215 118.679	126.6	3.99	†			
tEME-EE'	$22_{5,17}-22_{4,19}$	215 119.312	126.6	4.02	†			
tEME-EA	$21_{5,17}-21_{4,17}$	215 148.139	118.0	2.58	215 150.3	0.25	0.07	CH_3COCH_3
tEME-EE	$21_{5,16}-21_{4,17}$	215 149.914	118.0	6.81	†			
tEME-AA	$21_{5,16}-21_{4,17}$	215 150.202	118.0	10.66	†			
tEME-EA	$21_{5,16}-21_{4,17}$	215 150.327	118.0	8.07	†			
tEME-AE	$21_{5,16}-21_{4,17}$	215 151.142	118.0	6.84	†			
tEME-EE'	$21_{5,16}-21_{4,17}$	215 151.503	118.0	6.91	†			
tEME-EE'	$21_{5,17}-21_{4,18}$	215 195.665	118.0	6.91	...	...	0.04	SO
tEME-AE	$21_{5,17}-21_{4,18}$	215 196.869	118.0	6.84	†			
tEME-EE	$21_{5,17}-21_{4,18}$	215 197.254	118.0	6.81	†			
tEME-EA	$21_{5,17}-21_{4,18}$	215 203.100	118.0	8.07	...	...	0.04	SO
tEME-AA	$21_{5,17}-21_{4,18}$	215 204.068	118.0	10.66	†			
tEME-EA	$21_{5,16}-21_{4,18}$	215 205.287	118.0	2.58	†			
tEME-EE	$21_{5,16}-21_{4,18}$	215 205.486	118.0	3.85	†			
tEME-EA	$20_{5,16}-20_{4,16}$	215 243.901	109.9	3.19	...	...	0.07	SO
tEME-EE	$20_{5,15}-20_{4,16}$	215 245.438	109.9	6.54	†			
tEME-AA	$20_{5,15}-20_{4,16}$	215 245.691	109.9	10.09	†			
tEME-EA	$20_{5,15}-20_{4,16}$	215 245.934	109.9	6.89	†			
tEME-AE	$20_{5,15}-20_{4,16}$	215 246.615	109.9	6.68	†			
tEME-EE'	$20_{5,15}-20_{4,16}$	215 246.907	109.9	6.83	†			
tEME-EE'	$20_{5,16}-20_{4,17}$	215 274.126	109.9	6.83	...	...	0.04	CH_3CH_2CN $v_{20} = 1$
tEME-AE	$20_{5,16}-20_{4,17}$	215 275.268	109.9	6.68	†			
tEME-EE	$20_{5,16}-20_{4,17}$	215 275.595	109.9	6.54	†			
tEME-EA	$20_{5,16}-20_{4,17}$	215 281.378	109.9	6.89	...	...	0.04	CH_3CH_2CN v_{13}/v_{21}
tEME-AA	$20_{5,16}-20_{4,17}$	215 282.470	109.9	10.09	†			
tEME-EA	$20_{5,15}-20_{4,17}$	215 283.411	109.9	3.19	†			
tEME-EE	$20_{5,15}-20_{4,17}$	215 283.810	109.9	3.55	†			
tEME-EA	$19_{5,15}-19_{4,15}$	215 324.992	102.2	3.49	215 326.9	0.20	0.08	CH_3OCOH
tEME-EE	$19_{5,14}-19_{4,15}$	215 326.280	102.2	6.50	†			
tEME-AA	$19_{5,14}-19_{4,15}$	215 326.637	102.2	9.52	†			
tEME-EA	$19_{5,14}-19_{4,15}$	215 326.971	102.2	6.03	†			
tEME-AE	$19_{5,14}-19_{4,15}$	215 327.373	102.2	6.72	†			
tEME-EE'	$19_{5,14}-19_{4,15}$	215 327.561	102.2	6.95	†			
tEME-EE'	$19_{5,15}-19_{4,16}$	215 343.169	102.2	6.95	215 344.3	0.20	0.05	CH_3OCOH $v_t = 1$
tEME-AE	$19_{5,15}-19_{4,16}$	215 344.214	102.2	6.72	†			
tEME-EE	$19_{5,15}-19_{4,16}$	215 344.450	102.2	6.50	†			
tEME-EA	$19_{5,15}-19_{4,16}$	215 350.059	102.2	6.03	...	...	0.05	CH_3CH_2CN
tEME-AA	$19_{5,15}-19_{4,16}$	215 351.248	102.2	9.52	†			

Table A.2. continued.

Species	Transition $J_{K_a,K_c} - J'_{K'_a,K'_c}$	Predicted frequency (MHz)	E_{upp} (K)	S_{ij}	Observed[1] frequency (MHz)	Observed[1] T_{MB} (K)	Model[2] T_{MB} (K)	Blends
tEME-EE'	$12_{3,10}-11_{2,9}$	215 361.252	40.5	4.16	...	...	0.07	CH_3CH_2CN v_{13}/v_{21}
tEME-EE	$12_{3,10}-11_{2,9}$	215 361.484	40.5	4.18	†			
tEME-AE	$12_{3,10}-11_{2,9}$	215 361.676	40.5	4.17	†			
tEME-EA	$12_{3,10}-11_{2,9}$	215 364.224	40.5	4.19	...	...	0.05	CH_3CH_2CN v_{13}/v_{21}
tEME-AA	$12_{3,10}-11_{2,9}$	215 364.533	40.5	4.20	†			
tEME-EE	$18_{5,13}-18_{4,14}$	215 394.256	94.8	6.65	...	...	0.11	CH_3CH_2CN
tEME-AA	$18_{5,13}-18_{4,14}$	215 394.875	94.8	8.95	†			
tEME-AE	$18_{5,13}-18_{4,14}$	215 395.227	94.8	6.94	†			
tEME-EA	$18_{5,13}-18_{4,14}$	215 395.264	94.8	5.47	†			
tEME-EE'	$18_{5,13}-18_{4,14}$	215 395.280	94.8	7.19	†			
tEME-EE'	$18_{5,14}-18_{4,15}$	215 403.394	94.8	7.19	...	...	0.06	CH_3CH_2CN
tEME-AE	$18_{5,14}-18_{4,15}$	215 404.308	94.8	6.94	†			
tEME-EE	$18_{5,14}-18_{4,15}$	215 404.417	94.8	6.65	†			
tEME-EA	$18_{5,14}-18_{4,15}$	215 409.728	94.8	5.47	...	...	0.09	CH_3CH_2CN $v = 0$; v_{13}/v_{21}
tEME-AA	$18_{5,14}-18_{4,15}$	215 410.979	94.8	8.95	†			
tEME-EA	$17_{5,13}-17_{4,13}$	215 450.467	87.9	3.22	215 451.8	0.47	0.11	CH_3CH_2CN $v_{20} = 1$, NH_2CHO $v_{12} = 1$
tEME-EE	$17_{5,13}-17_{4,13}$	215 450.974	87.9	6.90	†			
tEME-EE'	$17_{5,13}-17_{4,13}$	215 451.703	87.9	7.39	†			
tEME-AE	$17_{5,13}-17_{4,13}$	215 451.799	87.9	7.18	†			
tEME-AA	$17_{5,13}-17_{4,13}$	215 452.025	87.9	8.39	†			
tEME-EA	$17_{5,13}-17_{4,13}$	215 452.436	87.9	5.17	†			
tEME-EE'	$17_{5,13}-17_{4,13}$	215 455.422	87.9	7.39	...	...	0.07	CH_3CH_2CN v_{13}/v_{21}, CH_3CH_2OH
tEME-EE	$17_{5,13}-17_{4,13}$	215 456.151	87.9	6.90	†			
tEME-AE	$17_{5,13}-17_{4,13}$	215 456.193	87.9	7.18	†			
tEME-EA	$17_{5,13}-17_{4,14}$	215 461.025	87.9	5.17	...	...	0.04	CH_3CH_2CN v_{13}/v_{21}, CH_3CH_2OH
tEME-AA	$17_{5,13}-17_{4,14}$	215 462.304	87.9	8.39	†			
tEME-EA	$17_{5,12}-17_{4,14}$	215 462.994	87.9	3.22	†			
tEME-EE'	$27_{1,27}-26_{0,26}$	215 478.840	144.2	21.60	...	...	0.24	CH_3CH_2CN v_{13}/v_{21}
tEME-EE	$27_{1,27}-26_{0,26}$	215 478.840	144.2	21.60	†			
tEME-AE	$27_{1,27}-26_{0,26}$	215 478.854	144.2	21.60	†			
tEME-EA	$27_{1,27}-26_{0,26}$	215 479.025	144.2	21.60	†			
tEME-AA	$27_{1,27}-26_{0,26}$	215 479.039	144.2	21.60	†			
tEME-EE	$16_{5,11}-16_{4,12}$	215 497.897	81.3	7.05	...	...	0.09	CH_3OCH_3, CH_3CH_2CN v_{13}/v_{21}
tEME-EA	$16_{5,12}-16_{4,12}$	215 497.943	81.3	2.74	†			
tEME-EE'	$16_{5,11}-16_{4,12}$	215 498.372	81.3	7.37	†			
tEME-AE	$16_{5,11}-16_{4,12}$	215 498.590	81.3	7.24	†			
tEME-AA	$16_{5,11}-16_{4,12}$	215 499.524	81.3	7.82	...	...	0.11	CH_3OCH_3, CH_3CH_2CN v_{13}/v_{21}
tEME-EE'	$16_{5,12}-16_{4,13}$	215 499.830	81.3	7.37	†			
tEME-EA	$16_{5,11}-16_{4,12}$	215 499.921	81.3	5.08	†			
tEME-EE	$16_{5,12}-16_{4,13}$	215 500.305	81.3	7.05	†			
tEME-AE	$16_{5,12}-16_{4,13}$	215 500.485	81.3	7.24	†			
tEME-EA	$16_{5,11}-16_{4,12}$	215 504.636	81.3	5.08	...	...	0.05	CH_3OCH_3, CH_3CH_2CN v_{13}/v_{21}, $^{33}SH_2$
tEME-AA	$16_{5,12}-16_{4,13}$	215 505.905	81.3	7.82	†			
tEME-EA	$16_{5,12}-16_{4,13}$	215 506.613	81.3	2.74	†			
tEME-EE	$15_{5,10}-15_{4,11}$	215 536.404	75.1	6.94	215 536.9	0.25	0.15	CH_3OCOH $v_t = 1$
tEME-EE'	$15_{5,10}-15_{4,11}$	215 536.720	75.1	7.08	†			
tEME-EA	$15_{5,11}-15_{4,11}$	215 537.002	75.1	2.05	†			
tEME-AE	$15_{5,10}-15_{4,11}$	215 537.010	75.1	7.03	†			
tEME-EE'	$15_{5,11}-15_{4,12}$	215 537.169	75.1	7.08	†			
tEME-EE	$15_{5,11}-15_{4,12}$	215 537.485	75.1	6.94	†			
tEME-AE	$15_{5,11}-15_{4,12}$	215 537.757	75.1	7.03	†			
tEME-AA	$15_{5,10}-15_{4,11}$	215 538.650	75.1	7.25	...	...	0.04	CH_3OCOH $v_t = 1$, CH_3CH_2CN v_{13}/v_{21}
tEME-EA	$15_{5,10}-15_{4,11}$	215 538.990	75.1	5.21	†			
tEME-AA	$15_{5,10}-15_{4,11}$	215 538.650	75.1	7.25	†			
tEME-EA	$15_{5,10}-15_{4,11}$	215 538.990	75.1	5.21	†			
tEME-EA	$15_{5,11}-15_{4,12}$	215 541.270	75.1	5.21	†			
tEME-AA	$15_{5,11}-15_{4,12}$	215 542.488	75.1	7.25	†			
tEME-EE	$14_{5,9}-14_{4,10}$	215 567.750	69.3	6.58	...	...	0.17	CH_3CH_2CN $v_{20} = 1$
tEME-EE'	$14_{5,9}-14_{4,10}$	215 567.993	69.3	6.63	†			
tEME-EE'	$14_{5,10}-14_{4,11}$	215 568.043	69.3	6.63	†			
tEME-EE	$14_{5,10}-14_{4,11}$	215 568.286	69.3	6.58	†			
tEME-AE	$14_{5,9}-14_{4,10}$	215 568.316	69.3	6.61	†			
tEME-AE	$14_{5,10}-14_{4,11}$	215 568.602	69.3	6.61	†			
tEME-EA	$14_{5,10}-14_{4,10}$	215 568.774	69.3	1.23	†			
tEME-AA	$14_{5,9}-14_{4,10}$	215 570.539	69.3	6.68	...	...	0.06	CH_3CH_2CN v_{13}/v_{21}
tEME-EA	$14_{5,9}-14_{4,10}$	215 570.772	69.3	5.45	†			
tEME-EA	$14_{5,10}-14_{4,11}$	215 571.650	69.3	5.45	†			
tEME-AA	$14_{5,10}-14_{4,11}$	215 572.766	69.3	6.68	...	...	0.04	CH_3CH_2CN v_{13}/v_{21}
tEME-EA	$14_{5,9}-14_{4,11}$	215 573.648	69.3	1.23	†			
tEME-EE	$13_{5,8}-13_{4,9}$	215 593.014	63.9	6.08	...	...	0.17	CH_3CH_2CN $v_{20} = 1$, SiO $v = 1$
tEME-EE'	$13_{5,9}-13_{4,10}$	215 593.138	63.9	6.09	†			
tEME-EE'	$13_{5,8}-13_{4,9}$	215 593.228	63.9	6.09	†			
tEME-EE	$13_{5,9}-13_{4,10}$	215 593.353	63.9	6.08	†			

Table A.2. continued.

Species	Transition $J_{K_a,K_c} - J'_{K'_a,K'_c}$	Predicted frequency (MHz)	E_{upp} (K)	S_{ij}	Observed[1] frequency (MHz)	Observed[1] T_{MB} (K)	Model[2] T_{MB} (K)	Blends
tEME-AE	$13_{5,8}-13_{4,9}$	215 593.566	63.9	6.09	†			
tEME-AE	$13_{5,9}-13_{4,10}$	215 593.687	63.9	6.09	†			
tEME-AA	$13_{5,8}-13_{4,9}$	215 596.207	63.9	6.11	...	...	0.09	$CH_3CH_2{}^{13}CN$, SiO $v = 1$
tEME-EA	$13_{5,8}-13_{4,9}$	215 596.289	63.9	5.58	†			
tEME-EA	$13_{5,9}-13_{4,10}$	215 596.478	63.9	5.58	†			
tEME-EE	$12_{5,7}-12_{4,8}$	215 613.102	58.9	5.52	...	...	0.18	CH_3CH_2OH, CH_3OCOH $v_t = 1$, CH_3CH_2CN
tEME-EE'	$12_{5,8}-12_{4,9}$	215 613.172	58.9	5.53	†			
tEME-EE'	$12_{5,7}-12_{4,8}$	215 613.308	58.9	5.53	†			
tEME-EE	$12_{5,8}-12_{4,9}$	215 613.378	58.9	5.52	†			
tEME-AE	$12_{5,7}-12_{4,8}$	215 613.651	58.9	5.52	†			
tEME-AE	$12_{5,8}-12_{4,9}$	215 613.720	58.9	5.52	†			
tEME-EA	$12_{5,8}-12_{4,9}$	215 616.405	58.9	5.37	...	...	0.10	CH_3CH_2CN
tEME-EA	$12_{5,7}-12_{4,8}$	215 616.490	58.9	5.37	†			
tEME-AA	$12_{5,7}-12_{4,8}$	215 616.564	58.9	5.53	†			
tEME-AA	$12_{5,8}-12_{4,9}$	215 617.221	58.9	5.53	†			
tEME-EE	$11_{5,6}-11_{4,7}$	215 628.800	54.3	4.94	...	...	0.16	CH_3CH_2CN
tEME-EE'	$11_{5,7}-11_{4,8}$	215 628.855	54.3	4.94	†			
tEME-EE'	$11_{5,6}-11_{4,7}$	215 629.003	54.3	4.94	†			
tEME-EE	$11_{5,7}-11_{4,8}$	215 629.058	54.3	4.94	†			
tEME-AE	$11_{5,6}-11_{4,7}$	215 629.349	54.3	4.94	†			
tEME-AE	$11_{5,7}-11_{4,8}$	215 629.404	54.3	4.94	...	...	0.10	CH_3CH_2CN
tEME-EA	$11_{5,7}-11_{4,8}$	215 632.056	54.3	4.91	†			
tEME-EA	$11_{5,6}-11_{4,7}$	215 632.229	54.3	4.91	†			
tEME-AA	$11_{5,6}-11_{4,7}$	215 632.425	54.3	4.94	†			
tEME-AA	$11_{5,7}-11_{4,8}$	215 632.754	54.3	4.94	†			
tEME-EE	$10_{5,5}-10_{4,6}$	215 640.803	50.0	4.35	215 641.1	0.18	0.13	CH_3COOH
tEME-EE'	$10_{5,6}-10_{4,7}$	215 640.854	50.0	4.35	†			
tEME-EE'	$10_{5,5}-10_{4,6}$	215 641.007	50.0	4.35	†			
tEME-EE	$10_{5,6}-10_{4,7}$	215 641.058	50.0	4.35	†			
tEME-AE	$10_{5,5}-10_{4,6}$	215 641.354	50.0	4.35	†			
tEME-AE	$10_{5,6}-10_{4,7}$	215 641.405	50.0	4.35	†			
tEME-EA	$10_{5,6}-10_{4,7}$	215 644.051	50.0	4.34	215 644.4	0.21	0.10	CH_3COOH
tEME-EA	$10_{5,5}-10_{4,6}$	215 644.248	50.0	4.34	†			
tEME-AA	$10_{5,5}-10_{4,6}$	215 644.522	50.0	4.35	†			
tEME-AA	$10_{5,6}-10_{4,7}$	215 644.676	50.0	4.35	†			
tEME-EE	$9_{5,4}-9_{4,5}$	215 649.740	46.1	3.73	215 650.1	0.42	0.12	CH_3CH_2CN $v_{20} = 1$
tEME-EE'	$9_{5,5}-9_{4,6}$	215 649.791	46.1	3.73	†			
tEME-EE'	$9_{5,4}-9_{4,5}$	215 649.944	46.1	3.73	†			
tEME-EE	$9_{5,5}-9_{4,6}$	215 649.995	46.1	3.73	†			
tEME-AE	$9_{5,4}-9_{4,5}$	215 650.292	46.1	3.73	†			
tEME-AE	$9_{5,5}-9_{4,6}$	215 650.343	46.1	3.73	†			
tEME-EA	$9_{5,5}-9_{4,6}$	215 652.990	46.1	3.73	215 653.4	0.42	0.08	CH_3CH_2CN $v_{20} = 1$
tEME-EA	$9_{5,4}-9_{4,5}$	215 653.193	46.1	3.73	†			
tEME-AA	$9_{5,4}-9_{4,5}$	215 653.509	46.1	3.73	†			
tEME-AA	$9_{5,5}-9_{4,6}$	215 653.575	46.1	3.73	†			
tEME-EE	$8_{5,3}-8_{4,4}$	215 656.176	42.7	3.10	215 656.4	0.43	0.11	CH_3CH_2CN $v_{20} = 1$
tEME-EE'	$8_{5,4}-8_{4,5}$	215 656.227	42.7	3.10	†			
tEME-EE'	$8_{5,3}-8_{4,4}$	215 656.380	42.7	3.10	†			
tEME-EE	$8_{5,4}-8_{4,5}$	215 656.432	42.7	3.10	†			
tEME-AE	$8_{5,3}-8_{4,4}$	215 656.730	42.7	3.10	†			
tEME-AE	$8_{5,4}-8_{4,5}$	215 656.781	42.7	3.10	†			
tEME-EA	$8_{5,4}-8_{4,5}$	215 659.431	42.7	3.10	215 659.8	0.36	0.09	CH_3CH_2CN $v_{20} = 1$
tEME-EA	$8_{5,3}-8_{4,4}$	215 659.635	42.7	3.10	†			
tEME-AA	$8_{5,3}-8_{4,4}$	215 659.972	42.7	3.10	†			
tEME-AA	$8_{5,4}-8_{4,5}$	215 659.998	42.7	3.10	†			
tEME-EE	$7_{5,2}-7_{4,3}$	215 660.620	39.6	2.43	215 660.8	0.34	0.11	CH_3CH_2CN $v_{20} = 1$
tEME-EE'	$7_{5,3}-7_{4,4}$	215 660.672	39.6	2.43	†			
tEME-EE'	$7_{5,2}-7_{4,3}$	215 660.825	39.6	2.43	†			
tEME-EE	$7_{5,3}-7_{4,4}$	215 660.877	39.6	2.43	†			
tEME-AE	$7_{5,2}-7_{4,3}$	215 661.175	39.6	2.43	†			
tEME-AE	$7_{5,3}-7_{4,4}$	215 661.227	39.6	2.43	†			
tEME-EE	$6_{5,1}-6_{4,2}$	215 663.523	36.9	1.72	215 663.9	0.30	0.11	CH_3CH_2CN $v_{20} = 1$
tEME-EE'	$6_{5,2}-6_{4,3}$	215 663.575	36.9	1.72	†			
tEME-EE'	$6_{5,1}-6_{4,2}$	215 663.728	36.9	1.72	†			
tEME-EE	$6_{5,2}-6_{4,3}$	215 663.780	36.9	1.72	†			
tEME-EA	$7_{5,3}-7_{4,4}$	215 663.879	39.6	2.43	†			
tEME-AE	$6_{5,1}-6_{4,2}$	215 664.080	36.9	1.72	†			
tEME-EA	$7_{5,2}-7_{4,3}$	215 664.084	39.6	2.43	†			
tEME-AE	$6_{5,2}-6_{4,3}$	215 664.131	36.9	1.72	†			
tEME-AA	$7_{5,2}-7_{4,3}$	215 664.430	39.6	2.43	†			
tEME-AA	$7_{5,3}-7_{4,4}$	215 664.439	39.6	2.43	†			
tEME-EE	$5_{5,0}-5_{4,1}$	215 665.279	34.6	0.92	†			
tEME-EE'	$5_{5,1}-5_{4,2}$	215 665.331	34.6	0.92	†			

Table A.2. continued.

Species	Transition $J_{K_a,K_c} - J'_{K'_a,K'_c}$	Predicted frequency (MHz)	E_{upp} (K)	S_{ij}	Observed[1] frequency (MHz)	Observed[1] T_{MB} (K)	Model[2] T_{MB} (K)	Blends
tEME-EE'	$5_{5,0}-5_{4,1}$	215 665.485	34.6	0.92	†			
tEME-EE	$5_{5,1}-5_{4,2}$	215 665.537	34.6	0.92	†			
tEME-AE	$5_{5,0}-5_{4,1}$	215 665.837	34.6	0.92	†			
tEME-AE	$5_{5,1}-5_{4,2}$	215 665.889	34.6	0.92	†			
tEME-EA	$6_{5,2}-6_{4,2}$	215 666.786	36.9	1.72	...	...	0.05	CH_3CH_2CN $v = 0$, $v_{20} = 1$
tEME-EA	$6_{5,1}-6_{4,2}$	215 666.991	36.9	1.72	†			
tEME-EA	$5_{5,1}-5_{4,2}$	215 668.545	34.6	0.92	†			
tEME-EA	$5_{5,0}-5_{4,1}$	215 668.751	34.6	0.92	†			
tEME-AA	$5_{5,0}-5_{4,1}$	215 669.103	34.6	0.92	†			
tEME-AA	$5_{5,1}-5_{4,2}$	215 669.103	34.6	0.92	†			
tEME-EE'	$6_{4,3}-5_{3,3}$	216 054.535	26.5	3.73	216 054.9	0.30	0.08	CH_3CH_2CN v_{13}/v_{21}
tEME-EE	$6_{4,3}-5_{3,3}$	216 054.868	26.5	3.73	†			
tEME-AE	$6_{4,3}-5_{3,3}$	216 055.095	26.5	3.73	†			
tEME-EE	$6_{4,2}-5_{3,2}$	216 055.759	26.5	3.73	†			
tEME-EE'	$6_{4,2}-5_{3,2}$	216 056.093	26.5	3.73	216 056.4	0.26	0.08	CH_3CH_2CN v_{13}/v_{21}
tEME-AE	$6_{4,2}-5_{3,2}$	216 056.319	26.5	3.73	†			
tEME-EA	$6_{4,3}-5_{3,3}$	216 058.222	26.5	3.69	216 058.4	0.25	0.10	CH_3CH_2CN v_{13}/v_{21}
tEME-EA	$6_{4,2}-5_{3,2}$	216 058.519	26.5	3.69	†			
tEME-AA	$6_{4,3}-5_{3,2}$	216 058.597	26.5	3.73	†			
tEME-AA	$6_{4,2}-5_{3,3}$	216 058.930	26.5	3.73	†			
tEME-EE	$12_{3,9}-11_{2,10}$	217 007.530	40.5	4.14	217 007.7	0.13	0.08	HDCS, CH_3OCOH
tEME-EE'	$12_{3,9}-11_{2,10}$	217 007.763	40.5	4.12	†			
tEME-AE	$12_{3,9}-11_{2,10}$	217 007.939	40.5	4.13	†			
tEME-EA	$12_{3,9}-11_{2,10}$	217 009.762	40.5	4.16	217 010.0	0.13	0.05	HDCS, CH_3OCOH
tEME-AA	$12_{3,9}-11_{2,10}$	217 010.054	40.5	4.16	†			
tEME-AA	$30_{1,29}-29_{2,28}$	217 164.465	182.5	13.55	...	...	0.07	CH_3OCOH
tEME-EA	$30_{1,29}-29_{2,28}$	217 164.508	182.5	13.55	†			
tEME-AE	$30_{1,29}-29_{2,28}$	217 165.360	182.5	13.55	†			
tEME-EE	$30_{1,29}-29_{2,28}$	217 165.402	182.5	13.55	†			
tEME-EE'	$30_{1,29}-29_{2,28}$	217 165.402	182.5	13.55	†			
tEME-AA	$28_{0,28}-27_{1,27}$	217 940.650	154.7	22.59	217 940.7	0.44	0.25	c-C_3H_2, $HCC^{13}CN$ $v_7 = 1$, CH_3COOCH_3
tEME-EA	$28_{0,28}-27_{1,27}$	217 940.651	154.7	22.59	†			
tEME-AE	$28_{0,28}-27_{1,27}$	217 940.758	154.7	22.59	†			
tEME-EE	$28_{0,28}-27_{1,27}$	217 940.759	154.7	22.59	†			
tEME-EE'	$28_{0,28}-27_{1,27}$	217 940.759	154.7	22.59	†			
tEME-EE'	$22_{2,21}-21_{1,20}$	219 893.140	102.2	8.31	...	...	0.09	SO
tEME-EE	$22_{2,21}-21_{1,20}$	219 893.140	102.2	8.31	†			
tEME-AE	$22_{2,21}-21_{1,20}$	219 893.263	102.2	8.31	†			
tEME-EA	$22_{2,21}-21_{1,20}$	219 894.511	102.2	8.31	...		0.06	SO
tEME-AA	$22_{2,21}-21_{1,20}$	219 894.635	102.2	8.31	†			
tEME-EE'	$28_{1,28}-27_{0,27}$	222 861.487	154.8	22.63	222 861.3	0.55	0.26	CH_3OCOH
tEME-EE	$28_{1,28}-27_{0,27}$	222 861.487	154.8	22.63	†			
tEME-AE	$28_{1,28}-27_{0,27}$	222 861.500	154.8	22.63	†			
tEME-EA	$28_{1,28}-27_{0,27}$	222 861.655	154.8	22.63	†			
tEME-AA	$28_{1,28}-27_{0,27}$	222 861.668	154.8	22.63	†			
tEME-EE'	$13_{3,11}-12_{2,10}$	222 980.574	45.5	4.38	222 980.7	0.22	0.09	$CH_3O^{13}COH$
tEME-EE	$13_{3,11}-12_{2,10}$	222 980.720	45.5	4.39	†			
tEME-AE	$13_{3,11}-12_{2,10}$	222 980.951	45.5	4.39	†			
tEME-EA	$13_{3,11}-12_{2,10}$	222 983.368	45.5	4.40	222 983.7	0.16	0.06	$CH_3O^{13}COH$
tEME-AA	$13_{3,11}-12_{2,10}$	222 983.672	45.5	4.40	†			
tEME-EE	$16_{2,14}-15_{1,15}$	223 403.761	57.4	2.48	...	...	0.04	CH_3OCH_3, CH_3OCOH $v_t = 1$
tEME-EE'	$16_{2,14}-15_{1,15}$	223 403.762	57.4	2.48	†			
tEME-AE	$16_{2,14}-15_{1,15}$	223 404.001	57.4	2.48	†			
tEME-EA	$16_{2,14}-15_{1,15}$	223 405.432	57.4	2.48	...	...	0.03	CH_3OCH_3
tEME-AA	$16_{2,14}-15_{1,15}$	223 405.671	57.4	2.48	†			
tEME-EE'	$7_{4,4}-6_{3,4}$	224 103.753	29.2	3.89	224 103.98	0.63	0.10	CH_3CH_2CN v_{13}/v_{21}
tEME-EE	$7_{4,4}-6_{3,4}$	224 104.093	29.2	3.88	†			
tEME-AE	$7_{4,4}-6_{3,4}$	224 104.315	29.2	3.89	†			
tEME-EE	$7_{4,3}-6_{3,3}$	224 104.926	29.2	3.88	†			
tEME-EE'	$7_{4,3}-6_{3,3}$	224 105.266	29.2	3.89	224 105.2	0.47	0.10	CH_3CH_2CN $v_{20} = 1$
tEME-AE	$7_{4,3}-6_{3,3}$	224 105.490	29.2	3.89	†			
tEME-AA	$7_{4,4}-6_{3,3}$	224 107.456	29.2	3.90	224 107.7	0.52	0.10	CH_3CH_2CN $v_{20} = 1$
tEME-EA	$7_{4,4}-6_{3,4}$	224 107.546	29.2	3.58	†			
tEME-EA	$7_{4,3}-6_{3,3}$	224 107.581	29.2	3.58	†			
tEME-AA	$7_{4,3}-6_{3,4}$	224 108.457	29.2	3.90	†			
tEME-EE	$13_{3,10}-12_{2,11}$	225 283.674	45.5	4.33	...	...	0.09	CH_3CH_2OH
tEME-EE'	$13_{3,10}-12_{2,11}$	225 283.820	45.5	4.33	†			
tEME-AE	$13_{3,10}-12_{2,11}$	225 284.043	45.5	4.33	†			
tEME-EA	$13_{3,10}-12_{2,11}$	225 285.990	45.5	4.34	225 286.28	0.29	0.06	CH_3CH_2OH
tEME-AA	$13_{3,10}-12_{2,11}$	225 286.286	45.5	4.34	†			
tEME-EE'	$23_{2,22}-22_{1,21}$	225 494.508	111.0	8.90	225 494.4	0.12	0.10	
tEME-EE	$23_{2,22}-22_{1,21}$	225 494.508	111.0	8.90	†			
tEME-AE	$23_{2,22}-22_{1,21}$	225 494.625	111.0	8.90	†			

Table A.2. continued.

Species	Transition $J_{K_a,K_c} - J'_{K'_a,K'_c}$	Predicted frequency (MHz)	E_{upp} (K)	S_{ij}	Observed[1] frequency (MHz)	Observed[1] T_{MB} (K)	Model[2] T_{MB} (K)	Blends
tEME-EA	$23_{2,22}-22_{1,21}$	225 495.848	111.0	8.90	225 495.9	0.12	0.07	
tEME-AA	$23_{2,22}-22_{1,21}$	225 495.965	111.0	8.90	†			
tEME-EA	$29_{0,29}-28_{1,28}$	226 057.836	165.7	23.62	226 057.9	0.65	0.26	CH_3CH_2OH
tEME-AA	$29_{0,29}-28_{1,28}$	226 057.836	165.7	23.62	†			
tEME-EE	$29_{0,29}-28_{1,28}$	226 057.928	165.7	23.62	†			
tEME-EE'	$29_{0,29}-28_{1,28}$	226 057.928	165.7	23.62	†			
tEME-AE	$29_{0,29}-28_{1,28}$	226 057.928	165.7	23.62	†			
tEME-AA	$31_{1,30}-30_{2,29}$	227 090.552	194.5	14.51	...	...	0.09	CH_3OH
tEME-EA	$31_{1,30}-30_{2,29}$	227 090.589	194.5	14.51	†			
tEME-AE	$31_{1,30}-30_{2,29}$	227 091.390	194.5	14.51	†			
tEME-EE	$31_{1,30}-30_{2,29}$	227 091.426	194.5	14.51	†			
tEME-EE'	$31_{1,30}-30_{2,29}$	227 091.426	194.5	14.51	†			
tEME-EE'	$29_{1,29}-28_{0,28}$	230 291.194	165.8	23.66	...	...	0.27	CH_3OH
tEME-EE	$29_{1,29}-28_{0,28}$	230 291.194	165.8	23.66	†			
tEME-AE	$29_{1,29}-28_{0,28}$	230 291.205	165.8	23.66	†			
tEME-EA	$29_{1,29}-28_{0,28}$	230 291.345	165.8	23.66	†			
tEME-AA	$29_{1,29}-28_{0,28}$	230 291.357	165.8	23.66	†			
tEME-EE'	$14_{3,12}-13_{2,11}$	230 486.881	50.9	4.59	...	...	0.09	CO
tEME-EE	$14_{3,12}-13_{2,11}$	230 486.975	50.9	4.60	†			
tEME-AE	$14_{3,12}-13_{2,11}$	230 487.227	50.9	4.59	†			
tEME-EA	$14_{3,12}-13_{2,11}$	230 489.569	50.9	4.60	...	...	0.07	CO
tEME-AA	$14_{3,12}-13_{2,11}$	230 489.869	50.9	4.60	†			
tEME-EE'	$24_{2,23}-23_{1,22}$	231 063.540	120.2	9.52	...	...	0.11	OCS
tEME-EE	$24_{2,23}-23_{1,22}$	231 063.540	120.2	9.52	†			
tEME-AE	$24_{2,23}-23_{1,22}$	231 063.652	120.2	9.52	†			
tEME-EA	$24_{2,23}-23_{1,22}$	231 064.846	120.2	9.52	...	...	0.08	OCS
tEME-AA	$24_{2,23}-23_{1,22}$	231 064.958	120.2	9.52	†			
tEME-EE'	$8_{4,5}-7_{3,5}$	232 151.207	32.3	4.03	232 152.1	0.47	0.11	$^{13}CH_3CN$, CH_3OCOH $v_t = 1$
tEME-EE	$8_{4,5}-7_{3,5}$	232 151.590	32.3	3.98	†			
tEME-AE	$8_{4,5}-7_{3,5}$	232 151.787	32.3	4.01	†			
tEME-EE	$8_{4,4}-7_{3,4}$	232 152.098	32.3	3.98	†			
tEME-EE'	$8_{4,4}-7_{3,4}$	232 152.480	32.3	4.03	†			
tEME-EA	$8_{4,5}-7_{3,4}$	232 152.521	32.3	1.00	†			
tEME-AE	$8_{4,4}-7_{3,4}$	232 152.685	32.3	4.01	†			
tEME-AA	$8_{4,5}-7_{3,4}$	232 154.033	32.3	4.08	...	...	0.06	$^{13}CH_3CN$, CH_3OCOH $v_t = 1$
tEME-EA	$8_{4,4}-7_{3,4}$	232 154.362	32.3	3.08	†			
tEME-EA	$8_{4,5}-7_{3,5}$	232 155.426	32.3	3.08	†			
tEME-AA	$8_{4,4}-7_{3,5}$	232 156.540	32.3	4.08	...	...	0.04	$^{13}CH_3CN$, CH_3OCOH $v_t = 1$
tEME-EA	$8_{4,4}-7_{3,5}$	232 157.268	32.3	1.00	†			
tEME-EE	$14_{3,11}-13_{2,12}$	233 622.462	51.0	4.51	...	...	0.10	CH_3OCOH $v_t = 0,1$
tEME-EE'	$14_{3,11}-13_{2,12}$	233 622.556	51.0	4.51	†			
tEME-AE	$14_{3,11}-13_{2,12}$	233 622.806	51.0	4.51	†			
tEME-EA	$14_{3,11}-13_{2,12}$	233 624.824	51.0	4.52	...	...	0.06	CH_3OCOH $v_t = 0,1$
tEME-AA	$14_{3,11}-13_{2,12}$	233 625.121	51.0	4.52	†			
tEME-EA	$30_{0,30}-29_{1,29}$	234 130.523	177.0	24.66	...	...	0.27	CH_3CH_2CN v_{13}/v_{21}
tEME-AA	$30_{0,30}-29_{1,29}$	234 130.524	177.0	24.66	†			
tEME-EE	$30_{0,30}-29_{1,29}$	234 130.601	177.0	24.66	†			
tEME-EE'	$30_{0,30}-29_{1,29}$	234 130.601	177.0	24.66	†			
tEME-AE	$30_{0,30}-29_{1,29}$	234 130.602	177.0	24.66	†			
tEME-EE	$17_{2,15}-16_{1,16}$	235 247.484	64.0	2.37	235 247.6	0.09	0.05	
tEME-EE'	$17_{2,15}-16_{1,16}$	235 247.485	64.0	2.37	†			
tEME-AE	$17_{2,15}-16_{1,16}$	235 247.731	64.0	2.37	†			
tEME-EA	$17_{2,15}-16_{1,16}$	235 249.156	64.0	2.37	235 249.6	0.14	0.03	U-line
tEME-AA	$17_{2,15}-16_{1,16}$	235 249.403	64.0	2.37	†			
tEME-EE'	$25_{2,24}-24_{1,23}$	236 614.358	129.8	10.19	236 614.4	0.30	0.11	CH_3COOCH_3
tEME-EE	$25_{2,24}-24_{1,23}$	236 614.358	129.8	10.19	†			
tEME-AE	$25_{2,24}-24_{1,23}$	236 614.464	129.8	10.19	†			
tEME-EA	$25_{2,24}-24_{1,23}$	236 615.628	129.8	10.19	†		0.08	CH_3COOCH_3
tEME-AA	$25_{2,24}-24_{1,23}$	236 615.733	129.8	10.19	†			
tEME-AA	$32_{1,31}-31_{2,30}$	236 906.877	206.9	15.50	236 907.2	0.30	0.10	CH_3SH, HC_3N $v_6 = 1$
tEME-EA	$32_{1,31}-31_{2,30}$	236 906.908	206.9	15.50	†			
tEME-AE	$32_{1,31}-31_{2,30}$	236 907.656	206.9	15.50	†			
tEME-EE	$32_{1,31}-31_{2,30}$	236 907.687	206.9	15.50	†			
tEME-EE'	$32_{1,31}-31_{2,30}$	236 907.687	206.9	15.50	†			
tEME-EE'	$30_{1,30}-29_{0,29}$	237 763.517	177.1	24.69	237 763.6	0.48	0.28	CH_2CHCN
tEME-EE	$30_{1,30}-29_{0,29}$	237 763.517	177.1	24.69	†			
tEME-AE	$30_{1,30}-29_{0,29}$	237 763.527	177.1	24.69	†			
tEME-EA	$30_{1,30}-29_{0,29}$	237 763.653	177.1	24.69	†			
tEME-AA	$30_{1,30}-29_{0,29}$	237 763.664	177.1	24.69	†			
tEME-EE'	$15_{3,13}-14_{2,12}$	237 865.715	56.7	4.79	...	...	0.10	CH_2CHCN
tEME-EE	$15_{3,13}-14_{2,12}$	237 865.778	56.7	4.80	†			
tEME-AE	$15_{3,13}-14_{2,12}$	237 866.042	56.7	4.80	†			
tEME-EA	$15_{3,13}-14_{2,12}$	237 868.339	56.7	4.80	...	...	0.08	CH_2CHCN

Table A.2. continued.

Species	Transition $J_{K_a,K_c} - J'_{K'_a,K'_c}$	Predicted frequency (MHz)	E_{upp} (K)	S_{ij}	Observed[1] frequency (MHz)	Observed[1] T_{MB} (K)	Model[2] T_{MB} (K)	Blends
tEME-AA	$15_{3,13}-14_{2,12}$	237 868.635	56.7	4.80	†			
tEME-EA	$9_{4,6}-8_{3,5}$	240 195.817	35.8	1.64	...	...	0.10	CH_2CHCN $v_{15}=1$
tEME-EE	$9_{4,5}-8_{3,5}$	240 196.101	35.8	3.88	†			
tEME-EE'	$9_{4,6}-8_{3,6}$	240 196.396	35.8	3.88	†			
tEME-EE'	$9_{4,5}-8_{3,5}$	240 196.642	35.8	3.88	†			
tEME-AE	$9_{4,5}-8_{3,5}$	240 196.777	35.8	3.88	†			
tEME-EE	$9_{4,6}-8_{3,6}$	240 196.937	35.8	3.88	†			
tEME-AE	$9_{4,6}-8_{3,6}$	240 197.045	35.8	3.88	†			
tEME-AA	$9_{4,6}-8_{3,5}$	240 197.196	35.8	3.88	†			
tEME-EA	$9_{4,5}-8_{3,5}$	240 197.654	35.8	3.88	†			
tEME-EA	$9_{4,6}-8_{3,6}$	240 201.478	35.8	2.63	...	...	0.05	CH_2CHCN $v_{15}=1$
tEME-AA	$9_{4,5}-8_{3,6}$	240 202.719	35.8	4.28	†			
tEME-EA	$9_{4,5}-8_{3,6}$	240 203.315	35.8	1.64	†			
tEME-EE	$15_{3,12}-14_{2,13}$	242 035.318	56.8	4.68	...	...	0.10	CH_2DCN
tEME-EE'	$15_{3,12}-14_{2,13}$	242 035.380	56.8	4.68	†			
tEME-AE	$15_{3,12}-14_{2,13}$	242 035.647	56.8	4.68	†			
tEME-EA	$15_{3,12}-14_{2,13}$	242 037.704	56.8	4.68	...	...	0.07	CH_2DCN
tEME-EA	$15_{3,12}-14_{2,13}$	242 038.002	56.8	4.68	†			
tEME-EE'	$26_{2,25}-25_{1,24}$	242 161.785	139.8	10.89	...	...	0.32	CH_3CH_2CN $v_{20}=1$
tEME-EE	$26_{2,25}-25_{1,24}$	242 161.785	139.8	10.89	†			
tEME-AE	$26_{2,25}-25_{1,24}$	242 161.884	139.8	10.89	†			
tEME-EA	$26_{2,25}-25_{1,24}$	242 163.015	139.8	10.89	†			
tEME-AA	$26_{2,25}-25_{1,24}$	242 163.114	139.8	10.89	†			
tEME-EA	$31_{0,31}-30_{1,30}$	242 163.369	188.7	25.69	†			
tEME-AA	$31_{0,31}-30_{1,30}$	242 163.371	188.7	25.69	†			
tEME-EE	$31_{0,31}-30_{1,30}$	242 163.434	188.7	25.69	†			
tEME-EE'	$31_{0,31}-30_{1,30}$	242 163.434	188.7	25.69	†			
tEME-AE	$31_{0,31}-30_{1,30}$	242 163.436	188.7	25.69	†			
tEME-EE'	$16_{3,14}-15_{2,13}$	245 103.550	62.9	4.99	...	...	0.10	$CH_3CH_2{}^{13}CN$
tEME-EE	$16_{3,14}-15_{2,13}$	245 103.592	62.9	4.99	†			
tEME-AE	$16_{3,14}-15_{2,13}$	245 103.864	62.9	4.99	†			
tEME-EA	$16_{3,14}-15_{2,13}$	245 106.133	62.9	4.99	245 106.4	0.32	0.07	CH_2OHCHO
tEME-AA	$16_{3,14}-15_{2,13}$	245 106.426	62.9	5.00	†			
tEME-EE'	$31_{1,31}-30_{0,30}$	245 274.088	188.8	25.71	245 274.3	0.40	0.29	$^{34}SO_2$
tEME-EE	$31_{1,31}-30_{0,30}$	245 274.088	188.8	25.71	†			
tEME-AE	$31_{1,31}-30_{0,30}$	245 274.098	188.8	25.71	†			
tEME-EA	$31_{1,31}-30_{0,30}$	245 274.211	188.8	25.71	†			
tEME-AA	$31_{1,31}-30_{0,30}$	245 274.221	188.8	25.71	†			
tEME-AA	$33_{1,32}-32_{2,31}$	246 605.346	219.6	16.51	246 606.0	0.36	0.11	CH_3OCH_3
tEME-EA	$33_{1,32}-32_{2,31}$	246 605.372	219.6	16.51	†			
tEME-AE	$33_{1,32}-32_{2,31}$	246 606.066	219.6	16.51	†			
tEME-EE	$33_{1,32}-32_{2,31}$	246 606.092	219.6	16.51	†			
tEME-EE'	$33_{1,32}-32_{2,31}$	246 606.092	219.6	16.51	†			
tEME-EE	$18_{2,16}-17_{1,17}$	247 478.246	71.1	2.26	247 478.0	0.16	0.05	CH_3OCOH $v_t=1$
tEME-EE'	$18_{2,16}-17_{1,17}$	247 478.247	71.1	2.26	†			
tEME-AE	$18_{2,16}-17_{1,17}$	247 478.501	71.1	2.26	†			
tEME-EA	$18_{2,16}-17_{1,17}$	247 479.920	71.1	2.26	247 480.0	0.16	0.03	CH_3OCOH $v_t=1$
tEME-AA	$18_{2,16}-17_{1,17}$	247 480.175	71.1	2.26	†			
tEME-EE'	$27_{2,26}-26_{1,25}$	247 721.097	150.2	11.63	247 721.2	0.23	0.11	
tEME-EE	$27_{2,26}-26_{1,25}$	247 721.097	150.2	11.63	†			
tEME-AE	$27_{2,26}-26_{1,25}$	247 721.190	150.2	11.63	†			
tEME-EA	$27_{2,26}-26_{1,25}$	247 722.285	150.2	11.63	†			
tEME-AA	$27_{2,26}-26_{1,25}$	247 722.378	150.2	11.63	†			
tEME-EA	$10_{4,7}-9_{3,6}$	248 234.223	39.7	2.12	248 235.7	0.31	0.15	U-line
tEME-EE	$10_{4,6}-9_{3,6}$	248 235.232	39.7	3.50	†			
tEME-AA	$10_{4,7}-9_{3,6}$	248 235.506	39.7	4.48	†			
tEME-EA	$10_{4,6}-9_{3,6}$	248 236.059	39.7	2.36	†			
tEME-AE	$10_{4,6}-9_{3,6}$	248 236.076	39.7	3.66	†			
tEME-EE'	$10_{4,6}-9_{3,6}$	248 236.093	39.7	3.79	†			
tEME-EE'	$10_{4,7}-9_{3,7}$	248 239.115	39.7	3.79	248 239.8	0.07	0.09	U-line
tEME-AE	$10_{4,7}-9_{3,7}$	248 239.913	39.7	3.66	†			
tEME-EE	$10_{4,7}-9_{3,7}$	248 239.977	39.7	3.50	†			
tEME-EA	$10_{4,7}-9_{3,7}$	248 245.234	39.7	2.36	...	...	0.06	CH_3COCH_3
tEME-AA	$10_{4,6}-9_{3,7}$	248 246.569	39.7	4.48	†			
tEME-EA	$10_{4,6}-9_{3,7}$	248 247.070	39.7	2.12	†			
tEME-EE	$10_{4,6}-9_{3,7}$	248 248.602	39.7	0.98	†			
tEME-AE	$10_{4,6}-9_{3,7}$	248 250.368	39.7	0.82	†			
tEME-EE'	$10_{4,6}-9_{3,7}$	248 251.399	39.7	0.69	†			
tEME-EA	$32_{0,32}-31_{1,31}$	250 160.753	200.8	26.72	...	...	0.29	$^{34}SO_2$
tEME-AA	$32_{0,32}-31_{1,31}$	250 160.756	200.8	26.72	†			
tEME-EE	$32_{0,32}-31_{1,31}$	250 160.807	200.8	26.72	†			
tEME-EE'	$32_{0,32}-31_{1,31}$	250 160.807	200.8	26.72	†			
tEME-AE	$32_{0,32}-31_{1,31}$	250 160.810	200.8	26.72	†			

Table A.2. continued.

Species	Transition $J_{K_a,K_c} - J'_{K'_a,K'_c}$	Predicted frequency (MHz)	E_{upp} (K)	S_{ij}	Observed[1] frequency (MHz)	Observed[1] T_{MB} (K)	Model[2] T_{MB} (K)	Blends
tEME-EE	$16_{3,13}-15_{2,14}$	250 534.903	62.9	4.83	250 535.0	0.16	0.11	
tEME-EE'	$16_{3,13}-15_{2,14}$	250 534.946	62.9	4.83	†			
tEME-AE	$16_{3,13}-15_{2,14}$	250 535.223	62.9	4.83	†			
tEME-EA	$16_{3,13}-15_{2,14}$	250 537.299	62.9	4.83	250 537.5	0.11	0.08	
tEME-AA	$16_{3,13}-15_{2,14}$	250 537.598	62.9	4.83	†			
tEME-EE'	$17_{3,15}-16_{2,14}$	252 188.288	69.5	5.19	252 188.5	0.59	0.11	CH_3CH_2CN v_{13}/v_{21}
tEME-EE	$17_{3,15}-16_{2,14}$	252 188.318	69.5	5.19	†			
tEME-AE	$17_{3,15}-16_{2,14}$	252 188.592	69.5	5.19	†			
tEME-EA	$17_{3,15}-16_{2,14}$	252 190.846	69.5	5.19	...	...	0.08	CH_3CH_2CN v_{13}/v_{21}
tEME-AA	$17_{3,15}-16_{2,14}$	252 191.135	69.5	5.19	†			
tEME-EE'	$32_{1,32}-31_{0,31}$	252 818.715	200.8	26.74	...	...	0.29	CH_3OH
tEME-EE	$32_{1,32}-31_{0,31}$	252 818.715	200.8	26.74	†			
tEME-AE	$32_{1,32}-31_{0,31}$	252 818.724	200.8	26.74	†			
tEME-EA	$32_{1,32}-31_{0,31}$	252 818.826	200.8	26.74	†			
tEME-AA	$32_{1,32}-31_{0,31}$	252 818.835	200.8	26.74	†			
tEME-EE'	$28_{2,27}-27_{1,26}$	253 307.713	161.0	12.42	...	...	0.12	$^{13}CH_3OH$
tEME-EE	$28_{2,27}-27_{1,26}$	253 307.713	161.0	12.42	†			
tEME-AE	$28_{2,27}-27_{1,26}$	253 307.800	161.0	12.42	†			
tEME-EA	$28_{2,27}-27_{1,26}$	253 308.856	161.0	12.42	†			
tEME-AA	$28_{2,27}-27_{1,26}$	253 308.943	161.0	12.42	†			
tEME-EE	$5_{5,0}-4_{4,0}$	255 923.090	34.6	4.50	255 923.1	0.42	0.29	CH_3CH_2CN
tEME-EE'	$5_{5,1}-4_{4,1}$	255 923.151	34.6	4.50	†			
tEME-EE'	$5_{5,0}-4_{4,0}$	255 923.293	34.6	4.50	†			
tEME-EE	$5_{5,1}-4_{4,1}$	255 923.354	34.6	4.50	†			
tEME-AE	$5_{5,0}-4_{4,0}$	255 923.648	34.6	4.50	†			
tEME-AE	$5_{5,1}-4_{4,1}$	255 923.709	34.6	4.50	†			
tEME-EA	$5_{5,1}-4_{4,1}$	255 926.362	34.6	4.50	255 926.5	0.37	0.20	SO_2
tEME-EA	$5_{5,0}-4_{4,0}$	255 926.565	34.6	4.50	†			
tEME-AA	$5_{5,1}-4_{4,0}$	255 926.920	34.6	4.50	†			
tEME-AA	$5_{5,0}-4_{4,1}$	255 926.920	34.6	4.50	†			
tEME-AA	$34_{1,33}-33_{2,32}$	256 180.110	232.7	17.54	256 180.5	0.28	0.11	CH_3OCOH $v_t = 1$
tEME-EA	$34_{1,33}-33_{2,32}$	256 180.131	232.7	17.54	†			
tEME-AE	$34_{1,33}-33_{2,32}$	256 180.771	232.7	17.54	†			
tEME-EE	$34_{1,33}-33_{2,32}$	256 180.792	232.7	17.54	†			
tEME-EE'	$34_{1,33}-33_{2,32}$	256 180.792	232.7	17.54	†			
tEME-EA	$11_{4,8}-10_{3,7}$	256 265.991	43.9	2.59	...	...	0.10	SO_2
tEME-AA	$11_{4,8}-10_{3,7}$	256 267.169	43.9	4.68	†			
tEME-EE	$11_{4,7}-10_{3,7}$	256 267.504	43.9	3.09	†			
tEME-EA	$11_{4,7}-10_{3,7}$	256 267.843	43.9	2.09	†			
tEME-AE	$11_{4,8}-10_{3,8}$	256 280.321	43.9	3.24	...	...	0.07	CH_3OCOH $v_t = 1$
tEME-EE	$11_{4,8}-10_{3,8}$	256 280.554	43.9	3.09	†			
tEME-AE	$11_{4,7}-10_{3,8}$	256 290.759	43.9	1.44	...	...	0.07	CH_3CCH
tEME-EE'	$11_{4,7}-10_{3,8}$	256 291.611	43.9	1.30	†			
tEME-EA	$33_{0,33}-32_{1,32}$	258 126.741	213.2	27.74	...	...	0.29	CH_3CN $v_8 = 1$, CH_3OCOH
tEME-AA	$33_{0,33}-32_{1,32}$	258 126.744	213.2	27.74	†			
tEME-EE	$33_{0,33}-32_{1,32}$	258 126.784	213.2	27.74	†			
tEME-EE'	$33_{0,33}-32_{1,32}$	258 126.784	213.2	27.74	†			
tEME-AE	$33_{0,33}-32_{1,32}$	258 126.787	213.2	27.74	†			
tEME-EE'	$29_{2,28}-28_{1,27}$	258 936.835	172.1	13.24	...	...	0.12	SO_2
tEME-EE	$29_{2,28}-28_{1,27}$	258 936.835	172.1	13.24	†			
tEME-AE	$29_{2,28}-28_{1,27}$	258 936.915	172.1	13.24	†			
tEME-EA	$29_{2,28}-28_{1,27}$	258 937.931	172.1	13.24	†			
tEME-AA	$29_{2,28}-28_{1,27}$	258 938.012	172.1	13.24	†			
tEME-EE'	$18_{3,16}-17_{2,15}$	259 109.696	76.5	5.39	...	...	0.11	CH_3OCOH
tEME-EE	$18_{3,16}-17_{2,15}$	259 109.717	76.5	5.39	†			
tEME-AE	$18_{3,16}-17_{2,15}$	259 109.992	76.5	5.39	†			
tEME-EA	$18_{3,16}-17_{2,15}$	259 112.236	76.5	5.39	...	...	0.08	CH_3OCOH
tEME-AA	$18_{3,16}-17_{2,15}$	259 112.522	76.5	5.39	†			
tEME-EE	$17_{3,14}-16_{2,15}$	259 135.164	69.5	4.97	...	...	0.11	CH_3OCOH
tEME-EE'	$17_{3,14}-16_{2,15}$	259 135.193	69.5	4.97	†			
tEME-AE	$17_{3,14}-16_{2,15}$	259 135.477	69.5	4.97	†			
tEME-EA	$17_{3,14}-16_{2,15}$	259 137.561	69.5	4.97	...	...	0.08	CH_3OCOH
tEME-AA	$17_{3,14}-16_{2,15}$	259 137.860	69.5	4.97	†			
tEME-EE	$19_{2,17}-18_{1,18}$	260 106.865	78.5	2.13	...	...	0.05	CH_3CH_2OH
tEME-EE'	$19_{2,17}-18_{1,18}$	260 106.865	78.5	2.13	†			
tEME-AE	$19_{2,17}-18_{1,18}$	260 107.129	78.5	2.13	†			
tEME-EA	$19_{2,17}-18_{1,18}$	260 108.541	78.5	2.13	...	...	0.05	CH_3CH_2OH
tEME-AA	$19_{2,17}-18_{1,18}$	260 108.805	78.5	2.13	†			
tEME-EE'	$33_{1,33}-32_{0,32}$	260 393.451	213.3	27.76	...	...	0.29	CH_3OCOH
tEME-EE	$33_{1,33}-32_{0,32}$	260 393.451	213.3	27.76	†			
tEME-AE	$33_{1,33}-32_{0,32}$	260 393.460	213.3	27.76	†			
tEME-EA	$33_{1,33}-32_{0,32}$	260 393.552	213.3	27.76	†			
tEME-AA	$33_{1,33}-32_{0,32}$	260 393.560	213.3	27.76	†			

Table A.2. continued.

Species	Transition $J_{K_a,K_c} - J'_{K'_a,K'_c}$	Predicted frequency (MHz)	E_{upp} (K)	S_{ij}	Observed[1] frequency (MHz)	Observed[1] T_{MB} (K)	Model[2] T_{MB} (K)	Blends
tEME-EE'	$40_{6,35}$–$40_{5,36}$	260 504.644	358.5	20.96	...	...		SiO
tEME-EE	$40_{6,35}$–$40_{5,36}$	260 505.033	358.5	21.22	†			
tEME-AE	$40_{6,35}$–$40_{5,36}$	260 505.210	358.5	21.10	†			
tEME-EA	$40_{6,35}$–$40_{5,36}$	260 507.959	358.5	21.43	†			
tEME-AA	$40_{6,35}$–$40_{5,36}$	260 508.333	358.5	21.45	†			
tEME-EE	$38_{6,32}$–$38_{5,33}$	260 681.821	327.9	19.53	...	...	0.03	CH_3CH_2CN
tEME-AE	$38_{6,32}$–$38_{5,33}$	260 682.506	327.9	19.20	†			
tEME-EE'	$38_{6,32}$–$38_{5,33}$	260 682.515	327.9	18.84	†			
tEME-EA	$38_{6,32}$–$38_{5,33}$	260 683.965	327.9	20.17	†			
tEME-AA	$38_{6,32}$–$38_{5,33}$	260 684.291	327.9	20.22	†			
tEME-EE	$37_{6,31}$–$37_{5,32}$	261 001.915	313.2	18.45	...	...	0.03	$OC^{34}S$, CH_3OCOH
tEME-AE	$37_{6,31}$–$37_{5,32}$	261 002.704	313.2	17.96	†			
tEME-EE'	$37_{6,31}$–$37_{5,32}$	261 002.807	313.2	17.46	†			
tEME-EE'	$38_{6,33}$–$38_{5,34}$	261 029.561	327.9	18.84	261 030.4	0.27	0.03	CH_3OCOH $v_t = 1$
tEME-EE	$38_{6,33}$–$38_{5,34}$	261 030.255	327.9	19.53	†			
tEME-AE	$38_{6,33}$–$38_{5,34}$	261 030.302	327.9	19.20	†			
tEME-EA	$38_{6,33}$–$38_{5,34}$	261 033.470	327.9	20.16	...	...	0.03	CH_3OCOH
tEME-AA	$38_{6,33}$–$38_{5,34}$	261 033.876	327.9	20.22	†			
tEME-EE'	$37_{6,32}$–$37_{5,33}$	261 270.008	313.2	17.46	...	...	0.03	CH_3CH_2CN v_{13}/v_{21}
tEME-AE	$37_{6,32}$–$37_{5,33}$	261 270.856	313.2	17.95	†			
tEME-EE	$37_{6,32}$–$37_{5,33}$	261 270.899	313.2	18.45	†			
tEME-AE	$36_{6,30}$–$36_{5,31}$	261 291.812	298.9	16.50	...	...	0.04	CH_3CH_2OH
tEME-EE'	$36_{6,30}$–$36_{5,31}$	261 292.008	298.9	15.92	†			
tEME-EA	$36_{6,30}$–$36_{5,31}$	261 292.672	298.9	18.82	†			
tEME-AA	$36_{6,30}$–$36_{5,31}$	261 292.970	298.9	19.00	†			
tEME-AE	$36_{6,31}$–$36_{5,32}$	261 496.448	298.9	16.50	...	...	0.03	CH_2CN
tEME-EE	$36_{6,31}$–$36_{5,32}$	261 496.589	298.9	17.15	†			
tEME-EA	$36_{6,31}$–$36_{5,32}$	261 500.259	298.9	18.82	...	...	0.03	CH_3OCOH, CH_2CN
tEME-AA	$36_{6,31}$–$36_{5,32}$	261 500.719	298.9	19.00	†			
tEME-EE'	$35_{6,29}$–$35_{5,30}$	261 553.036	285.0	14.38	261 553.2	0.15	0.06	$CH_3O^{13}COH$ $v_t = 1$
tEME-EA	$35_{6,29}$–$35_{5,30}$	261 553.277	285.0	18.06	†			
tEME-AA	$35_{6,29}$–$35_{5,30}$	261 553.546	285.0	18.40	†			
tEME-AE	$35_{6,30}$–$35_{5,31}$	261 707.095	285.0	14.94	...	...	0.03	CH_3OH
tEME-EE	$35_{6,30}$–$35_{5,31}$	261 707.325	285.0	15.65	†			
tEME-EA	$35_{6,30}$–$35_{5,31}$	261 711.277	285.0	18.06	...	...	0.03	CH_3OCOH
tEME-AA	$35_{6,30}$–$35_{5,31}$	261 711.778	285.0	18.40	†			
tEME-EE	$34_{6,28}$–$34_{5,29}$	261 787.091	271.4	14.12	...	...	0.07	CH_3OCOH, CH_3OH, SO
tEME-AE	$34_{6,28}$–$34_{5,29}$	261 788.168	271.4	13.47	†			
tEME-EA	$34_{6,28}$–$34_{5,29}$	261 788.351	271.4	17.16	†			
tEME-EE'	$34_{6,28}$–$34_{5,29}$	261 788.486	271.4	13.02	†			
tEME-AA	$34_{6,28}$–$34_{5,29}$	261 788.577	271.4	17.80	†			
tEME-EE'	$34_{6,29}$–$34_{5,30}$	261 901.878	271.4	13.02	...	...	0.03	CH_3OCH_3, CH_3COCH_3
tEME-AE	$34_{6,29}$–$34_{5,30}$	261 902.977	271.4	13.47	†			
tEME-EE	$34_{6,29}$–$34_{5,30}$	261 903.273	271.4	14.12	†			
tEME-EA	$34_{6,29}$–$34_{5,30}$	261 907.508	271.4	17.16	...	...	0.03	CH_3OCH_3, CH_3COCH_3
tEME-AA	$34_{6,29}$–$34_{5,30}$	261 908.064	271.4	17.80	†			
tEME-EA	$33_{6,27}$–$33_{5,29}$	262 000.261	258.3	16.05	...	...	0.08	CCH
tEME-AE	$33_{6,27}$–$33_{5,29}$	262 000.337	258.3	12.24	†			
tEME-AA	$33_{6,27}$–$33_{5,29}$	262 000.424	258.3	17.21	†			
tEME-EE'	$33_{6,27}$–$33_{5,29}$	262 000.673	258.3	11.95	†			
tEME-AE	$33_{6,27}$–$33_{5,29}$	262 084.400	258.3	12.24	...	...	0.03	CH_3OCOH
tEME-EE	$33_{6,27}$–$33_{5,29}$	262 084.731	258.3	12.72	†			
tEME-EA	$33_{6,27}$–$33_{5,29}$	262 089.211	258.3	16.05	...	...	0.03	CH_3OCOH
tEME-AA	$33_{6,27}$–$33_{5,29}$	262 089.841	258.3	17.21	†			
tEME-EA	$32_{6,27}$–$32_{5,28}$	262 191.119	245.5	14.67	...	...	0.08	CH_3CH_2CN
tEME-AA	$32_{6,26}$–$32_{5,28}$	262 191.200	245.5	16.62	†			
tEME-AE	$32_{6,26}$–$32_{5,28}$	262 191.354	245.5	11.34	†			
tEME-EE'	$32_{6,26}$–$32_{5,28}$	262 191.682	245.5	11.22	†			
tEME-AE	$32_{6,27}$–$32_{5,28}$	262 251.766	245.5	11.34	...	...	0.04	SO_2
tEME-EE	$32_{6,27}$–$32_{5,28}$	262 252.104	245.5	11.61	†			
tEME-EA	$32_{6,27}$–$32_{5,28}$	262 256.756	245.5	14.67	...	...	0.04	SO_2
tEME-AA	$32_{6,27}$–$32_{5,28}$	262 257.479	245.5	16.62	†			
tEME-AE	$32_{6,26}$–$32_{5,28}$	262 260.269	245.5	5.28	†			
tEME-EE'	$32_{6,26}$–$32_{5,28}$	262 260.849	245.5	5.41	†			
tEME-AA	$31_{6,25}$–$31_{5,26}$	262 362.797	233.1	16.04	...	...	0.08	$CH_3{}^{13}CH_2CN$
tEME-EA	$31_{6,25}$–$31_{5,26}$	262 362.814	233.1	13.11	†			
tEME-AE	$31_{6,25}$–$31_{5,26}$	262 363.092	233.1	10.77	†			
tEME-EE'	$31_{6,25}$–$31_{5,26}$	262 363.388	233.1	10.80	†			
tEME-EE'	$31_{6,26}$–$31_{5,27}$	262 404.436	233.1	10.80	...	...	0.04	$^{13}CH_3OCOH$ $v_t = 1$
tEME-AE	$31_{6,26}$–$31_{5,27}$	262 405.547	233.1	10.77	†			
tEME-EE	$31_{6,25}$–$31_{5,27}$	262 405.867	233.1	10.84	†			
tEME-EA	$31_{6,26}$–$31_{5,27}$	262 410.601	233.1	13.11	...	...	0.04	$^{13}CH_3OCOH$ $v_t = 1$
tEME-AA	$31_{6,26}$–$31_{5,27}$	262 411.432	233.1	16.04	†			

Table A.2. continued.

Species	Transition $J_{K_a,K_c} - J'_{K'_a,K'_c}$	Predicted frequency (MHz)	E_{upp} (K)	S_{ij}	Observed[1] frequency (MHz)	Observed[1] T_{MB} (K)	Model[2] T_{MB} (K)	Blends
tEME-EA	$30_{6,25}-30_{5,25}$	262 515.014	221.2	3.88	...	...	0.09	U-line
tEME-EE	$30_{6,24}-30_{5,25}$	262 516.140	221.2	10.39	†			
tEME-AA	$30_{6,24}-30_{5,25}$	262 516.918	221.2	15.45	†			
tEME-EA	$30_{6,24}-30_{5,25}$	262 517.034	221.2	11.57	†			
tEME-AE	$30_{6,24}-30_{5,25}$	262 517.242	221.2	10.51	†			
tEME-EE'	$30_{6,24}-30_{5,25}$	262 517.483	221.2	10.68	†			
tEME-EE'	$30_{6,25}-30_{5,26}$	262 545.215	221.2	10.68	...	...	0.04	H_2CCO
tEME-AE	$30_{6,25}-30_{5,26}$	262 546.281	221.2	10.51	†			
tEME-EE	$30_{6,25}-30_{5,26}$	262 546.558	221.2	10.39	†			
tEME-EA	$30_{6,25}-30_{5,26}$	262 551.283	221.2	11.57	...	...	0.04	H_2CCO
tEME-AA	$30_{6,25}-30_{5,26}$	262 552.224	221.2	15.45	†			
tEME-EE	$30_{6,24}-30_{5,26}$	262 553.207	221.2	5.06	†			
tEME-EA	$30_{6,24}-30_{5,26}$	262 553.303	221.2	3.88	†			
tEME-EE	$29_{6,23}-29_{5,24}$	262 654.283	209.6	10.25	...	...	0.10	CH_3COCH_3
tEME-AA	$29_{6,23}-29_{5,24}$	262 655.095	209.6	14.87	†			
tEME-EA	$29_{6,23}-29_{5,24}$	262 655.300	209.6	10.29	†			
tEME-AE	$29_{6,23}-29_{5,24}$	262 655.326	209.6	10.53	†			
tEME-EE'	$29_{6,23}-29_{5,24}$	262 655.485	209.6	10.83	†			
tEME-EE'	$29_{6,24}-29_{5,25}$	262 673.561	209.6	10.83	...	...	0.05	$HC^{13}CCN$
tEME-AE	$29_{6,24}-29_{5,25}$	262 674.556	209.6	10.53	†			
tEME-EE	$29_{6,24}-29_{5,25}$	262 674.763	209.6	10.25	†			
tEME-EA	$29_{6,24}-29_{5,25}$	262 679.394	209.6	10.29	...	...	0.04	$HC^{13}CCN$
tEME-AA	$29_{6,24}-29_{5,25}$	262 680.434	209.6	14.87	†			
tEME-EA	$29_{6,23}-29_{5,25}$	262 681.315	209.6	4.58	†			
tEME-EE	$29_{6,23}-29_{5,25}$	262 681.410	209.6	4.63	†			
tEME-EA	$28_{6,23}-28_{5,23}$	262 777.103	198.3	4.94	...	...	0.10	CH_3OCH_3
tEME-EE	$28_{6,22}-28_{5,23}$	262 777.763	198.3	10.37	†			
tEME-AA	$28_{6,22}-28_{5,23}$	262 778.714	198.3	14.30	†			
tEME-AE	$28_{6,22}-28_{5,23}$	262 778.719	198.3	10.78	†			
tEME-EE'	$28_{6,22}-28_{5,23}$	262 778.771	198.3	11.17	†			
tEME-EA	$28_{6,22}-28_{5,23}$	262 778.988	198.3	9.35	†			
tEME-EE'	$28_{6,23}-28_{5,24}$	262 790.103	198.3	11.17	262 791.0	0.25	0.05	U-line
tEME-AE	$28_{6,23}-28_{5,24}$	262 791.000	198.3	10.78	†			
tEME-EE	$28_{6,23}-28_{5,24}$	262 791.111	198.3	10.37	†			
tEME-EA	$28_{6,23}-28_{5,24}$	262 795.561	198.3	9.35	...	...	0.04	CH_2OHCHO
tEME-AA	$28_{6,23}-28_{5,24}$	262 796.681	198.3	14.30	†			
tEME-EA	$28_{6,22}-28_{5,24}$	262 797.446	198.3	4.94	†			
tEME-EE	$28_{6,22}-28_{5,24}$	262 797.772	198.3	3.92	†			
tEME-EA	$27_{6,22}-27_{5,22}$	262 887.474	187.5	4.97	...	...	0.10	CH_3COOH, CH_3OCH_3
tEME-EE	$27_{6,21}-27_{5,22}$	262 887.831	187.5	10.70	†			
tEME-EE'	$27_{6,21}-27_{5,22}$	262 888.603	187.5	11.58	†			
tEME-AE	$27_{6,21}-27_{5,22}$	262 888.676	187.5	11.18	†			
tEME-AA	$27_{6,21}-27_{5,22}$	262 889.035	187.5	13.72	†			
tEME-EA	$27_{6,21}-27_{5,22}$	262 889.353	187.5	8.75	†			
tEME-EE'	$27_{6,22}-27_{5,23}$	262 895.483	187.5	11.58	...	...	0.07	CH_3OCH_3
tEME-EE	$27_{6,22}-27_{5,23}$	262 896.256	187.5	10.70	†			
tEME-AE	$27_{6,22}-27_{5,23}$	262 896.265	187.5	11.18	†			
tEME-EA	$27_{6,22}-27_{5,23}$	262 900.436	187.5	8.75	...	...	0.05	CH_3COOH
tEME-AA	$27_{6,22}-27_{5,23}$	262 901.609	187.5	13.72	†			
tEME-EA	$27_{6,21}-27_{5,23}$	262 902.316	187.5	4.97	†			
tEME-EE	$27_{6,21}-27_{5,23}$	262 902.939	187.5	3.02	†			
tEME-EE	$26_{6,20}-26_{5,21}$	262 985.638	177.1	11.11	...	...	0.10	$CH_3{}^{18}OH$
tEME-EA	$26_{6,21}-26_{5,21}$	262 985.653	177.1	4.68	†			
tEME-EE'	$26_{6,20}-26_{5,21}$	262 986.169	177.1	11.87	†			
tEME-AE	$26_{6,20}-26_{5,21}$	262 986.363	177.1	11.54	†			
tEME-AA	$26_{6,20}-26_{5,21}$	262 987.205	177.1	13.15	†			
tEME-EA	$26_{6,20}-26_{5,21}$	262 987.541	177.1	8.47	†			
tEME-EE'	$26_{6,21}-26_{5,22}$	262 990.328	177.1	11.87	...	...	0.09	$CH_3{}^{18}OH$
tEME-EE	$26_{6,21}-26_{5,22}$	262 990.859	177.1	11.11	†			
tEME-AE	$26_{6,21}-26_{5,22}$	262 990.997	177.1	11.54	†			
tEME-EA	$26_{6,21}-26_{5,22}$	262 994.684	177.1	8.47	...	...	0.05	SO_2 $v_2 = 1$
tEME-AA	$26_{6,21}-26_{5,22}$	262 995.883	177.1	13.15	†			
tEME-EA	$26_{6,20}-26_{5,22}$	262 996.572	177.1	4.68	†			
tEME-EE	$26_{6,20}-26_{5,22}$	262 997.567	177.1	2.04	†			
tEME-EE	$25_{6,19}-25_{5,20}$	263 072.263	167.0	11.39	...	...	0.11	U-line
tEME-EE'	$25_{6,19}-25_{5,20}$	263 072.594	167.0	11.92	†			
tEME-EA	$25_{6,20}-25_{5,20}$	263 072.699	167.0	4.12	†			
tEME-AE	$25_{6,19}-25_{5,20}$	263 072.885	167.0	11.70	†			
tEME-AA	$25_{6,19}-25_{5,20}$	263 074.277	167.0	12.58	...	...	0.11	U-line
tEME-EA	$25_{6,19}-25_{5,20}$	263 074.602	167.0	8.46	†			
tEME-EE'	$25_{6,20}-25_{5,21}$	263 075.234	167.0	11.92	†			
tEME-EE	$25_{6,20}-25_{5,21}$	263 075.564	167.0	11.39	†			
tEME-AE	$25_{6,20}-25_{5,21}$	263 075.815	167.0	11.70	†			

Table A.2. continued.

Species	Transition $J_{K_a,K_c} - J'_{K'_a,K'_c}$	Predicted frequency (MHz)	E_{upp} (K)	S_{ij}	Observed[1] frequency (MHz)	Observed[1] T_{MB} (K)	Model[2] T_{MB} (K)	Blends
tEME-EA	$25_{6,20}-25_{5,21}$	263 078.980	167.0	8.46	...	...	0.05	U-line
tEME-AA	$25_{6,20}-25_{5,21}$	263 080.176	167.0	12.58	†			
tEME-EE	$24_{6,19}-24_{5,19}$	263 141.974	157.4	0.60	263 149.1	0.44	0.11	$CH_3O^{13}COH$,CH_3OCOD
tEME-EE	$24_{6,18}-24_{5,19}$	263 148.731	157.4	11.41	†			
tEME-EE'	$24_{6,18}-24_{5,19}$	263 148.928	157.4	11.70	†			
tEME-AE	$24_{6,18}-24_{5,19}$	263 149.281	157.4	11.59	†			
tEME-EA	$24_{6,19}-24_{5,19}$	263 149.579	157.4	3.30	†			
tEME-EE'	$24_{6,19}-24_{5,20}$	263 150.791	157.4	11.70	263 151.0	0.58	0.20	$CH_3O^{13}COH$,CH_3OCOD
tEME-EE	$24_{6,19}-24_{5,20}$	263 150.988	157.4	11.41	†			
tEME-AA	$24_{6,18}-24_{5,19}$	263 151.216	157.4	12.01	†			
tEME-AE	$24_{6,19}-24_{5,20}$	263 151.318	157.4	11.59	†			
tEME-EA	$24_{6,18}-24_{5,19}$	263 151.498	157.4	8.71	†			
tEME-EA	$24_{6,19}-24_{5,20}$	263 153.999	157.4	8.71	†			
tEME-AA	$24_{6,19}-24_{5,20}$	263 155.161	157.4	12.01	263 155.2	0.25	0.05	CH_3OCOD
tEME-EA	$24_{6,18}-24_{5,20}$	263 155.918	157.4	3.30	†			
tEME-EE	$23_{6,17}-23_{5,18}$	263 215.996	148.1	11.17	263 216.3	0.58	0.14	SO_2
tEME-EE'	$23_{6,17}-23_{5,18}$	263 216.118	148.1	11.31	†			
tEME-AE	$23_{6,17}-23_{5,18}$	263 216.506	148.1	11.26	†			
tEME-EA	$23_{6,18}-23_{5,18}$	263 217.183	148.1	2.31	263 217.8	0.59	0.14	SO_2
tEME-EE'	$23_{6,18}-23_{5,19}$	263 217.615	148.1	11.31	†			
tEME-EE	$23_{6,18}-23_{5,19}$	263 217.736	148.1	11.17	†			
tEME-AE	$23_{6,18}-23_{5,19}$	263 218.114	148.1	11.26	†			
tEME-AA	$23_{6,17}-23_{5,18}$	263 218.914	148.1	11.44	†			
tEME-EA	$23_{6,17}-23_{5,18}$	263 219.118	148.1	9.14	†			
tEME-EA	$23_{6,18}-23_{5,19}$	263 220.415	148.1	9.14	...	...	0.05	SO_2
tEME-AA	$23_{6,18}-23_{5,19}$	263 221.507	148.1	11.44	†			
tEME-EA	$23_{6,17}-23_{5,19}$	263 222.351	148.1	2.31	†			
tEME-EE	$22_{6,16}-22_{5,17}$	263 274.922	139.2	10.76	...	...	0.14	CH_3OCH_3
tEME-EE'	$22_{6,16}-22_{5,17}$	263 275.007	139.2	10.82	†			
tEME-AE	$22_{6,16}-22_{5,17}$	263 275.415	139.2	10.80	†			
tEME-EA	$22_{6,17}-22_{5,17}$	263 276.341	139.2	1.34	†			
tEME-EE'	$22_{6,17}-22_{5,18}$	263 276.343	139.2	10.82	†			
tEME-EE	$22_{6,17}-22_{5,18}$	263 276.429	139.2	10.76	†			
tEME-AE	$22_{6,17}-22_{5,18}$	263 276.831	139.2	10.80	†			
tEME-AA	$22_{6,16}-22_{5,17}$	263 278.199	139.2	10.88	...	...	0.11	CH_3OCH_3
tEME-EA	$22_{6,16}-22_{5,17}$	263 278.292	139.2	9.53	†			
tEME-EA	$22_{6,17}-22_{5,18}$	263 278.882	139.2	9.53	†			
tEME-AA	$22_{6,17}-22_{5,18}$	263 279.871	139.2	10.88	†			
tEME-EE	$21_{6,15}-21_{5,16}$	263 326.288	130.7	10.27	263 326.7	0.42	0.14	$HC_3N\ v_7 = 1$, CH_3COCH_3
tEME-EE'	$21_{6,15}-21_{5,16}$	263 326.357	130.7	10.29	†			
tEME-AE	$21_{6,15}-21_{5,16}$	263 326.775	130.7	10.28	†			
tEME-EE'	$21_{6,16}-21_{5,17}$	263 327.628	130.7	10.29	263 327.4	0.51	0.14	$HC_3N\ v_7 = 1$, CH_3COCH_3
tEME-EE	$21_{6,16}-21_{5,17}$	263 327.697	130.7	10.27	†			
tEME-EA	$21_{6,16}-21_{5,16}$	263 327.838	130.7	.64	†			
tEME-AE	$21_{6,16}-21_{5,17}$	263 328.113	130.7	10.28	†			
tEME-EA	$21_{6,15}-21_{5,16}$	263 329.805	130.7	9.67	263 329.9	0.74	0.30	$HC_3N\ v_7 = 1$, CH_3COCH_3
tEME-AA	$21_{6,15}-21_{5,16}$	263 329.839	130.7	10.31	†			
tEME-EA	$21_{6,16}-21_{5,17}$	263 330.025	130.7	9.67	†			
tEME-AA	$21_{6,16}-21_{5,17}$	263 330.894	130.7	10.31	†			
tEME-EE	$20_{6,14}-20_{5,15}$	263 370.802	122.6	9.73	263 370.7	0.51	0.16	$SO^{18}O$, CH_3OCOH
tEME-EE'	$20_{6,14}-20_{5,15}$	263 370.865	122.6	9.74	†			
tEME-AE	$20_{6,14}-20_{5,15}$	263 371.289	122.6	9.73	†			
tEME-EE'	$20_{6,15}-20_{5,16}$	263 372.112	122.6	9.74	263 372.2	0.37	0.16	$SO^{18}O$, CH_3OCOH
tEME-EE	$20_{6,15}-20_{5,16}$	263 372.174	122.6	9.73	†			
tEME-AE	$20_{6,15}-20_{5,16}$	263 372.598	122.6	9.73	†			
tEME-EA	$20_{6,14}-20_{5,15}$	263 374.395	122.6	9.49	...	...	0.17	$SO^{18}O$, CH_3OCOH
tEME-EA	$20_{6,15}-20_{5,16}$	263 374.447	122.6	9.49	†			
tEME-AA	$20_{6,14}-20_{5,15}$	263 374.550	122.6	9.74	†			
tEME-AA	$20_{6,15}-20_{5,16}$	263 375.201	122.6	9.74	†			
tEME-EE	$19_{6,13}-20_{5,14}$	263 409.117	114.8	9.17	...	...	0.17	CH_3OCH_3
tEME-EE'	$19_{6,13}-20_{5,14}$	263 409.177	114.8	9.17	†			
tEME-AE	$19_{6,13}-20_{5,14}$	263 409.605	114.8	9.17	†			
tEME-EE'	$19_{6,14}-20_{5,15}$	263 410.419	114.8	9.17	†			
tEME-EE	$19_{6,14}-20_{5,15}$	263 410.479	114.8	9.17	†			
tEME-AE	$19_{6,14}-20_{5,15}$	263 410.907	114.8	9.17	†			
tEME-EA	$19_{6,14}-20_{5,15}$	263 412.731	114.8	9.09	...	...	0.19	CH_3OCH_3
tEME-EA	$19_{6,13}-20_{5,14}$	263 412.749	114.8	9.09	†			
tEME-AA	$19_{6,13}-20_{5,14}$	263 413.003	114.8	9.18	†			
tEME-EE	$18_{6,12}-18_{5,13}$	263 441.843	107.5	8.61	...	...	0.17	$^{34}SO_2$, $^{33}SO_2$
tEME-EE'	$18_{6,12}-18_{5,13}$	263 441.902	107.5	8.61	†			
tEME-AE	$18_{6,12}-18_{5,13}$	263 442.334	107.5	8.61	†			
tEME-EE'	$18_{6,13}-18_{5,14}$	263 443.145	107.5	8.61	†			
tEME-EE	$18_{6,13}-18_{5,14}$	263 443.204	107.5	8.61	†			

Table A.2. continued.

Species	Transition $J_{K_a,K_c} - J'_{K'_a,K'_c}$	Predicted frequency (MHz)	E_{upp} (K)	S_{ij}	Observed[1] frequency (MHz)	Observed[1] T_{MB} (K)	Model[2] T_{MB} (K)	Blends
tEME-AE	$18_{6,13}-18_{5,14}$	263 443.636	107.5	8.61	†			
tEME-EA	$18_{6,13}-18_{5,14}$	263 445.453	107.5	8.58	...	...	0.19	$^{34}SO_2$, $^{33}SO_2$
tEME-EA	$18_{6,12}-18_{5,13}$	263 445.498	107.5	8.58	†			
tEME-AA	$18_{6,12}-18_{5,13}$	263 445.822	107.5	8.61	†			
tEME-AA	$18_{6,13}-18_{5,14}$	263 446.051	107.5	8.61	†			
tEME-EE	$17_{6,11}-17_{5,12}$	263 469.553	100.5	8.04	263 469.7	0.43	0.17	CH_3CH_2OH
tEME-EE'	$17_{6,11}-17_{5,12}$	263 469.612	100.5	8.04	†			
tEME-AE	$17_{6,11}-17_{5,12}$	263 470.047	100.5	8.04	†			
tEME-EE'	$17_{6,12}-17_{5,13}$	263 470.859	100.5	8.04	†			
tEME-EE	$17_{6,12}-17_{5,13}$	263 470.917	100.5	8.04	†			
tEME-AE	$17_{6,12}-17_{5,13}$	263 471.352	100.5	8.04	†			
tEME-EA	$17_{6,12}-17_{5,13}$	263 473.169	100.5	8.03	263 473.9	0.41	0.19	CH_3CH_2OH
tEME-EA	$17_{6,11}-17_{5,12}$	263 473.223	100.5	8.03	†			
tEME-AA	$17_{6,11}-17_{5,12}$	263 473.595	100.5	8.04	†			
tEME-AA	$17_{6,12}-17_{5,13}$	263 473.725	100.5	8.04	†			
tEME-EE	$16_{6,10}-16_{5,11}$	263 492.786	94.0	7.46	263 492.9	0.26	0.17	CH_3OCH_3
tEME-EE'	$16_{6,10}-16_{5,11}$	263 492.845	94.0	7.46	†			
tEME-AE	$16_{6,10}-16_{5,11}$	263 493.283	94.0	7.46	†			
tEME-EE'	$16_{6,11}-16_{5,12}$	263 494.096	94.0	7.46	263 494.2	0.33	0.17	CH_3OCH_3
tEME-EE	$16_{6,11}-16_{5,12}$	263 494.155	94.0	7.46	†			
tEME-AE	$16_{6,11}-16_{5,12}$	263 494.592	94.0	7.46	†			
tEME-EA	$16_{6,11}-16_{5,12}$	263 496.411	94.0	7.46	263 496.6	0.55	0.19	CH_3OCH_3
tEME-EA	$16_{6,10}-16_{5,11}$	263 496.468	94.0	7.46	†			
tEME-AA	$16_{6,10}-16_{5,11}$	263 496.871	94.0	7.46	†			
tEME-AA	$16_{6,11}-16_{5,12}$	263 496.942	94.0	7.46	†			
tEME-EE	$15_{6,9}-15_{5,10}$	263 512.049	87.8	6.89	...	...	0.17	CH_3OCH_3
tEME-EE'	$15_{6,9}-15_{5,10}$	263 512.108	87.8	6.89	†			
tEME-AE	$15_{6,9}-15_{5,10}$	263 512.548	87.8	6.89	†			
tEME-EE'	$15_{6,10}-15_{5,11}$	263 513.363	87.8	6.89	...	...	0.17	CH_3OCH_3
tEME-EE	$15_{6,10}-15_{5,11}$	263 513.422	87.8	6.89	†			
tEME-AE	$15_{6,10}-15_{5,10}$	263 513.862	87.8	6.89	†			
tEME-EA	$15_{6,10}-15_{5,11}$	263 515.683	87.8	6.88	...	...	0.19	CH_3CH_2CN
tEME-EA	$15_{6,9}-15_{5,10}$	263 515.742	87.8	6.88	†			
tEME-AA	$15_{6,9}-15_{5,10}$	263 516.163	87.8	6.89	†			
tEME-AA	$15_{6,10}-15_{5,11}$	263 516.200	87.8	6.89	†			
tEME-EE	$14_{6,8}-14_{5,9}$	263 527.818	82.0	6.30	...	...	0.16	CH_3OCH_3, CH_3CH_2CN
tEME-EE'	$14_{6,8}-14_{5,9}$	263 527.877	82.0	6.30	†			
tEME-AE	$14_{6,8}-14_{5,9}$	263 528.319	82.0	6.30	†			
tEME-EE'	$14_{6,9}-14_{5,10}$	263 529.136	82.0	6.30	†			
tEME-EE	$14_{6,9}-14_{5,10}$	263 529.195	82.0	6.30	†			
tEME-AE	$14_{6,9}-14_{5,10}$	263 529.637	82.0	6.30	†			
tEME-EA	$14_{6,9}-14_{5,10}$	263 531.461	82.0	6.30	...	...	0.18	CH_3OCH_3
tEME-EA	$14_{6,8}-14_{5,9}$	263 531.520	82.0	6.30	†			
tEME-AA	$14_{6,8}-14_{5,9}$	263 531.953	82.0	6.30	†			
tEME-AA	$14_{6,9}-14_{5,10}$	263 531.971	82.0	6.30	†			
tEME-EE	$13_{6,7}-13_{5,8}$	263 540.536	76.6	5.71	...	...	0.15	NH_2CHO, SO_2
tEME-EE'	$13_{6,7}-13_{5,8}$	263 540.595	76.6	5.71	†			
tEME-AE	$13_{6,7}-13_{5,8}$	263 541.040	76.6	5.71	†			
tEME-EE'	$13_{6,8}-13_{5,9}$	263 541.858	76.6	5.71	†			
tEME-EE	$13_{6,8}-13_{5,9}$	263 541.917	76.6	5.71	†			
tEME-AE	$13_{6,8}-13_{5,9}$	263 542.362	76.6	5.71	†			
tEME-EA	$13_{6,8}-13_{5,9}$	263 544.188	76.6	5.71	...	...	0.18	NH_2CHO, SO_2
tEME-EA	$13_{6,7}-13_{5,8}$	263 544.247	76.6	5.71	†			
tEME-AA	$13_{6,7}-13_{5,8}$	263 544.687	76.6	5.71	†			
tEME-AA	$13_{6,8}-13_{5,9}$	263 544.696	76.6	5.71	†			
tEME-EE	$12_{6,6}-12_{5,7}$	263 550.619	71.5	5.11	...	...	0.14	SO_2
tEME-EE'	$12_{6,6}-12_{5,7}$	263 550.679	71.5	5.11	†			
tEME-AE	$12_{6,6}-12_{5,7}$	263 551.125	71.5	5.11	†			
tEME-EE'	$12_{6,7}-12_{5,8}$	263 551.945	71.5	5.11	†			
tEME-EE	$12_{6,7}-12_{5,8}$	263 552.004	71.5	5.11	†			
tEME-AE	$12_{6,7}-12_{5,8}$	263 552.451	71.5	5.11	†			
tEME-EA	$12_{6,7}-12_{5,8}$	263 554.279	71.5	5.11	...	...	0.16	SO_2
tEME-EA	$12_{6,6}-12_{5,7}$	263 554.338	71.5	5.11	†			
tEME-AA	$12_{6,6}-12_{5,7}$	263 554.783	71.5	5.11	†			
tEME-AA	$12_{6,7}-12_{5,8}$	263 554.787	71.5	5.11	†			
tEME-EE	$11_{6,5}-11_{5,6}$	263 558.451	66.9	4.49	...	...	0.13	SO_2
tEME-EE'	$11_{6,5}-11_{5,6}$	263 558.511	66.9	4.49	†			
tEME-AE	$11_{6,5}-11_{5,6}$	263 558.959	66.9	4.49	†			
tEME-EE'	$11_{6,6}-11_{5,7}$	263 559.780	66.9	4.49	...	...	0.13	SO_2
tEME-EE	$11_{6,6}-11_{5,7}$	263 559.839	66.9	4.49	†			
tEME-AE	$11_{6,6}-11_{5,7}$	263 560.288	66.9	4.49	†			
tEME-EA	$11_{6,6}-11_{5,7}$	263 562.118	66.9	4.49	...	...	0.15	SO_2
tEME-EA	$11_{6,5}-11_{5,6}$	263 562.178	66.9	4.49	†			

Table A.2. continued.

Species	Transition $J_{K_a,K_c} - J'_{K'_a,K'_c}$	Predicted frequency (MHz)	E_{upp} (K)	S_{ij}	Observed[1] frequency (MHz)	Observed[1] T_{MB} (K)	Model[2] T_{MB} (K)	Blends
tEME-AA	$11_{6,5}-11_{5,6}$	263 562.626	66.9	4.49	†			
tEME-AA	$11_{6,6}-11_{5,7}$	263 562.627	66.9	4.49	†			
tEME-EE	$10_{6,4}-10_{5,5}$	263 564.386	62.7	3.85	...	...	0.11	SO_2
tEME-EE'	$10_{6,4}-10_{5,5}$	263 564.446	62.7	3.85	†			
tEME-AE	$10_{6,4}-10_{5,5}$	263 564.897	62.7	3.85	†			
tEME-EE'	$10_{6,5}-10_{5,6}$	263 565.718	62.7	3.85	...	...	0.11	SO_2
tEME-EE	$10_{6,5}-10_{5,6}$	263 565.777	62.7	3.85	†			
tEME-AE	$10_{6,5}-10_{5,6}$	263 566.228	62.7	3.85	†			
tEME-EA	$10_{6,5}-10_{5,6}$	263 568.061	62.7	3.85	...	...	0.21	SO_2
tEME-EA	$10_{6,4}-10_{5,5}$	263 568.120	62.7	3.85	†			
tEME-AA	$10_{6,4}-10_{5,5}$	263 568.570	62.7	3.85	†			
tEME-AA	$10_{6,5}-10_{5,6}$	263 568.571	62.7	3.85	†			
tEME-EE	$9_{6,3}-9_{5,4}$	263 568.750	58.8	3.19	†			
tEME-EE'	$9_{6,3}-9_{5,4}$	263 568.810	58.8	3.19	†			
tEME-AE	$9_{6,3}-9_{5,4}$	263 569.262	58.8	3.19	†			
tEME-EE'	$9_{6,4}-9_{5,5}$	263 570.083	58.8	3.19	†			
tEME-EE	$9_{6,4}-9_{5,5}$	263 570.143	58.8	3.19	†			
tEME-AE	$9_{6,4}-9_{5,5}$	263 570.595	58.8	3.19	†			
tEME-AE	$8_{6,2}-8_{5,3}$	263 572.350	55.3	2.50	263 572.9	0.47	0.20	CH_3OCH_3, HNCO
tEME-EA	$9_{6,4}-9_{5,5}$	263 572.430	58.8	3.19	†			
tEME-EA	$9_{6,3}-9_{5,4}$	263 572.490	58.8	3.19	†			
tEME-AA	$9_{6,3}-9_{5,4}$	263 572.942	58.8	3.19	†			
tEME-AA	$9_{6,4}-9_{5,5}$	263 572.942	58.8	3.19	†			
tEME-EE'	$8_{6,3}-8_{5,4}$	263 573.172	55.3	2.50	†			
tEME-EE	$8_{6,3}-8_{5,4}$	263 573.232	55.3	2.50	†			
tEME-AE	$8_{6,3}-8_{5,4}$	263 573.685	55.3	2.50	†			
tEME-EE	$7_{6,1}-7_{5,2}$	263 573.911	52.2	1.75	†			
tEME-EE'	$7_{6,1}-7_{5,2}$	263 573.972	52.2	1.75	†			
tEME-AE	$7_{6,1}-7_{5,2}$	263 574.426	52.2	1.75	†			
tEME-EE	$6_{6,0}-6_{5,1}$	263 575.211	49.5	0.93	...	...	0.17	CH_3OCH_3, HNCO
tEME-EE'	$7_{6,2}-7_{5,3}$	263 575.249	52.2	1.75	†			
tEME-EE'	$6_{6,0}-6_{5,1}$	263 575.271	49.5	0.93	†			
tEME-EE	$7_{6,2}-7_{5,3}$	263 575.309	52.2	1.75	†			
tEME-EA	$8_{6,3}-8_{5,4}$	263 575.522	55.3	2.50	†			
tEME-EA	$8_{6,2}-8_{5,3}$	263 575.582	55.3	2.50	†			
tEME-AE	$6_{6,0}-6_{5,1}$	263 575.727	49.5	0.93	†			
tEME-AE	$7_{6,2}-7_{5,3}$	263 575.764	52.2	1.75	†			
tEME-AE	$6_{6,1}-6_{5,2}$	263 577.066	49.5	0.93	...	...	0.08	CH_3OCH_3, HNCO
tEME-EA	$7_{6,2}-7_{5,3}$	263 577.602	52.2	1.75	†			
tEME-EA	$7_{6,1}-7_{5,2}$	263 577.662	52.2	1.75	†			
tEME-AA	$7_{6,1}-7_{5,2}$	263 578.117	52.2	1.75	†			
tEME-AA	$7_{6,2}-7_{5,3}$	263 578.117	52.2	1.75	†			
tEME-EA	$6_{6,1}-6_{5,2}$	263 578.906	49.5	0.93	†			
tEME-EA	$6_{6,0}-6_{5,1}$	263 578.966	49.5	0.93	†			
tEME-AA	$6_{6,0}-6_{5,1}$	263 579.422	49.5	0.93	†			
tEME-AA	$6_{6,1}-6_{5,2}$	263 579.422	49.5	0.93	†			
tEME-EE	$6_{5,1}-5_{4,1}$	263 974.290	36.9	4.57	263 974.6	0.84	0.32	CH_3CH_2CN $v_{20}=1$, $CH_3{}^{13}CH_2CN$
tEME-EE'	$6_{5,2}-5_{4,2}$	263 974.352	36.9	4.57	†			
tEME-EE'	$6_{5,1}-5_{4,1}$	263 974.491	36.9	4.57	†			
tEME-EE	$6_{5,2}-5_{4,2}$	263 974.554	36.9	4.57	†			
tEME-AE	$6_{5,1}-5_{4,1}$	263 974.847	36.9	4.57	†			
tEME-AE	$6_{5,2}-5_{4,2}$	263 974.909	36.9	4.57	†			
tEME-EA	$6_{5,2}-5_{4,2}$	263 977.560	36.9	4.57	263 977.9	1.19	0.21	CH_3CH_2CN $v_{20}=1$, $CH_3{}^{13}CH_2CN$, CH_3OCOH $v_t=1$
tEME-EA	$6_{5,1}-5_{4,1}$	263 977.761	36.9	4.57	†			
tEME-AA	$6_{5,2}-5_{4,1}$	263 978.116	36.9	4.57	†			
tEME-AA	$6_{5,1}-5_{4,2}$	263 978.117	36.9	4.57	†			
tEME-EE'	$12_{4,9}-11_{3,8}$	264 279.974	48.6	1.86	...	...	0.04	CH_3CH_2CN v_{13}/v_{21}
tEME-AE	$12_{4,9}-11_{3,8}$	264 281.470	48.6	1.98	†			
tEME-EE	$12_{4,8}-11_{3,8}$	264 282.160	48.6	2.11	†			
tEME-EA	$12_{4,9}-11_{3,8}$	264 288.936	48.6	3.18	264 290.1	0.32	0.08	CH_3CH_2CN v_{13}/v_{21}
tEME-AA	$12_{4,9}-11_{3,8}$	264 289.975	48.6	4.89	†			
tEME-EE	$12_{4,8}-11_{3,8}$	264 290.781	48.6	2.78	†			
tEME-EA	$12_{4,8}-11_{3,8}$	264 290.868	48.6	1.70	†			
tEME-AE	$12_{4,8}-11_{3,8}$	264 291.901	48.6	2.91	264 292.2	0.33	0.07	CH_3CH_2CN v_{13}/v_{21}
tEME-EE'	$12_{4,8}-11_{3,8}$	264 292.217	48.6	3.02	†			
tEME-EE'	$12_{4,9}-11_{3,9}$	264 316.948	48.6	3.02	...	...	0.06	CH_3OH
tEME-AE	$12_{4,9}-11_{3,9}$	264 318.041	48.6	2.91	†			
tEME-EE	$12_{4,9}-11_{3,9}$	264 318.385	48.6	2.78	†			
tEME-EA	$12_{4,9}-11_{3,9}$	264 324.363	48.6	1.70	...	...	0.10	CH_3OH
tEME-AA	$12_{4,8}-11_{3,9}$	264 326.032	48.6	4.89	†			
tEME-EA	$12_{4,8}-11_{3,9}$	264 326.294	48.6	3.18	†			
tEME-EE	$12_{4,8}-11_{3,9}$	264 327.005	48.6	2.11	†			
tEME-AE	$12_{4,8}-11_{3,9}$	264 328.472	48.6	1.98	...	...	0.04	CH_3OH

Table A.2. continued.

Species	Transition $J_{K_a,K_c} - J'_{K'_a,K'_c}$	Predicted frequency (MHz)	E_{upp} (K)	S_{ij}	Observed[1] frequency (MHz)	Observed[1] T_{MB} (K)	Model[2] T_{MB} (K)	Blends
tEME-EE'	$12_{4,8}-11_{3,9}$	264 329.191	48.6	1.86	†			
tEME-EE'	$30_{2,29}-29_{1,28}$	264 623.050	183.6	14.10	...	...	0.14	CH_3CH_2CN v_{13}/v_{21}
tEME-EE	$30_{2,29}-29_{1,28}$	264 623.050	183.6	14.10	†			
tEME-AE	$30_{2,29}-29_{1,28}$	264 623.125	183.6	14.10	†			
tEME-EA	$30_{2,29}-29_{1,28}$	264 624.097	183.6	14.10	†			
tEME-AA	$30_{2,29}-29_{1,28}$	264 624.172	183.6	14.10	†			
tEME-AA	$35_{1,34}-34_{2,33}$	265 627.614	246.2	18.59	...	...	0.13	CH_3COOCH_3
tEME-EA	$35_{1,34}-34_{2,33}$	265 627.630	246.2	18.59	†			
tEME-AE	$35_{1,34}-34_{2,33}$	265 628.218	246.2	18.59	†			
tEME-EE	$35_{1,34}-34_{2,33}$	265 628.234	246.2	18.59	†			
tEME-EE'	$35_{1,34}-34_{2,33}$	265 628.234	246.2	18.59	†			
tEME-EE'	$19_{3,17}-18_{2,16}$	265 859.733	83.8	5.59	...	...	0.13	HCN
tEME-EE	$19_{3,17}-18_{2,16}$	265 859.748	83.8	5.59	†			
tEME-AE	$19_{3,17}-18_{2,16}$	265 860.022	83.8	5.59	†			
tEME-EA	$19_{3,17}-18_{2,16}$	265 862.261	83.8	5.59	...	...	0.09	HCN
tEME-AA	$19_{3,17}-18_{2,16}$	265 862.543	83.8	5.59	†			
tEME-EA	$34_{0,34}-33_{1,33}$	266 065.053	226.0	28.77	...	...	0.28	CH_3COCH_3
tEME-AA	$34_{0,34}-33_{1,33}$	266 065.056	226.0	28.77	†			
tEME-EE	$34_{0,34}-33_{1,33}$	266 065.087	226.0	28.77	†			
tEME-EE'	$34_{0,34}-33_{1,33}$	266 065.087	226.0	28.77	†			
tEME-AE	$34_{0,34}-33_{1,33}$	266 065.091	226.0	28.77	†			
tEME-EE	$18_{3,15}-17_{2,16}$	267 851.372	76.5	5.09	267 851.6	0.71	0.13	CH_3OCOH $v_t = 2$
tEME-EE'	$18_{3,15}-17_{2,16}$	267 851.394	76.5	5.09	†			
tEME-AE	$18_{3,15}-17_{2,16}$	267 851.682	76.5	5.09	†			
tEME-EA	$18_{3,15}-17_{2,16}$	267 853.764	76.5	5.09	...	...	0.09	CH_3OCOH $v_t = 2$
tEME-AA	$18_{3,15}-17_{2,16}$	267 854.063	76.5	5.09	†			
tEME-EE'	$34_{1,34}-33_{0,33}$	267 994.638	226.1	28.78	267 994.7	0.95	0.28	CH_3OCOH $v_t = 2$, CH_3CH_2CN
tEME-EE	$34_{1,34}-33_{0,33}$	267 994.638	226.1	28.78	†			
tEME-AE	$34_{1,34}-33_{0,33}$	267 994.646	226.1	28.78	†			
tEME-EA	$34_{1,34}-33_{0,33}$	267 994.729	226.1	28.78	†			
tEME-AA	$34_{1,34}-33_{0,33}$	267 994.737	226.1	28.78	†			
tEME-EE'	$31_{2,30}-30_{1,29}$	270 379.929	195.5	14.99	270 380.3	0.21	0.15	
tEME-EE	$31_{2,30}-30_{1,29}$	270 379.929	195.5	14.99	†			
tEME-AE	$31_{2,30}-30_{1,29}$	270 379.998	195.5	14.99	†			
tEME-EA	$31_{2,30}-30_{1,29}$	270 380.924	195.5	14.99	†			
tEME-AA	$31_{2,30}-30_{1,29}$	270 380.993	195.5	14.99	†			
tEME-EE	$7_{5,2}-6_{4,2}$	272 025.103	39.6	4.70	272 025.5	1.10	0.35	CH_3CH_2CN v_{13}/v_{21}
tEME-EE'	$7_{5,3}-6_{4,3}$	272 025.167	39.6	4.70	†			
tEME-EE'	$7_{5,2}-6_{4,2}$	272 025.304	39.6	4.70	†			
tEME-EE	$7_{5,3}-6_{4,3}$	272 025.368	39.6	4.70	†			
tEME-AE	$7_{5,2}-6_{4,2}$	272 025.659	39.6	4.70	†			
tEME-AE	$7_{5,3}-6_{4,3}$	272 025.723	39.6	4.70	†			
tEME-EA	$7_{5,3}-6_{4,3}$	272 028.370	39.6	4.70	272 028.6	0.59	0.23	CH_3CH_2CN v_{13}/v_{21}
tEME-EA	$7_{5,2}-6_{4,2}$	272 028.571	39.6	4.70	†			
tEME-AA	$7_{5,3}-6_{4,2}$	272 028.925	39.6	4.70	†			
tEME-AA	$7_{5,2}-6_{4,3}$	272 028.927	39.6	4.70	†			
tEME-EE'	$13_{4,10}-12_{3,9}$	272 291.842	53.6	2.35	272 292.1	0.21	0.03	U-line
tEME-AE	$13_{4,10}-12_{3,9}$	272 293.250	53.6	2.46	272 293.6	0.26	0.05	U-line
tEME-EE	$13_{4,10}-12_{3,9}$	272 293.863	53.6	2.58	†			
tEME-EA	$13_{4,10}-12_{3,9}$	272 300.368	53.6	3.94	272 301.0	0.18	0.08	CH_3OCOH
tEME-AA	$13_{4,10}-12_{3,9}$	272 301.238	53.6	5.09	†			
tEME-EE	$13_{4,9}-12_{3,9}$	272 302.533	53.6	2.51	†			
tEME-EA	$13_{4,9}-12_{3,9}$	272 302.564	53.6	1.15	†			
tEME-AE	$13_{4,9}-12_{3,9}$	272 303.710	53.6	2.64	272 303.9	0.24	0.07	CH_3CH_2CN $v_{20} = 1$
tEME-EE'	$13_{4,9}-12_{3,9}$	272 304.098	53.6	2.74	†			
tEME-EE'	$13_{4,10}-12_{3,10}$	272 351.722	53.6	2.74	...	...	0.06	CH_3OH, CH_3OD
tEME-AE	$13_{4,10}-12_{3,10}$	272 352.884	53.6	2.63	†			
tEME-EE	$13_{4,10}-12_{3,10}$	272 353.288	53.6	2.51	†			
tEME-EA	$13_{4,10}-12_{3,10}$	272 359.310	53.6	1.15	...	...	0.13	CH_3OH, CH_3OD
tEME-AA	$13_{4,9}-12_{3,10}$	272 361.410	53.6	5.09	†			
tEME-EA	$13_{4,9}-12_{3,10}$	272 361.506	53.6	3.94	†			
tEME-EE	$13_{4,9}-12_{3,10}$	272 361.957	53.6	2.58	†			
tEME-AE	$13_{4,9}-12_{3,10}$	272 363.344	53.6	2.46	...	...	0.05	CH_3OH, CH_3OD
tEME-EE'	$13_{4,9}-12_{3,10}$	272 363.978	53.6	2.35	†			
tEME-EE'	$20_{3,18}-19_{2,17}$	272 432.754	91.6	5.79	272 433.0	0.33	0.14	U-line
tEME-EE	$20_{3,18}-19_{2,17}$	272 432.765	91.6	5.79	†			
tEME-AE	$20_{3,18}-19_{2,17}$	272 433.037	91.6	5.79	†			
tEME-EA	$20_{3,18}-19_{2,17}$	272 435.273	91.6	5.79	272 435.7	0.35	0.09	U-line
tEME-AA	$20_{3,18}-19_{2,17}$	272 435.550	91.6	5.79	†			
tEME-AA	$40_{2,38}-39_{3,37}$	272 596.983	325.0	12.66	...	...	0.03	U-line
tEME-EA	$40_{2,38}-39_{3,37}$	272 597.055	325.0	12.66	†			
tEME-AE	$40_{2,38}-39_{3,37}$	272 598.688	325.0	12.66	†			
tEME-EE	$40_{2,38}-39_{3,37}$	272 598.760	325.0	12.66	†			

Table A.2. continued.

Species	Transition $J_{K_a,K_c} - J'_{K'_a,K'_c}$	Predicted frequency (MHz)	E_{upp} (K)	S_{ij}	Observed[1] frequency (MHz)	Observed[1] T_{MB} (K)	Model[2] T_{MB} (K)	Blends
tEME-EE'	$40_{2,38}-39_{3,37}$	272 598.760	325.0	12.66	†			
tEME-EE	$20_{2,18}-19_{1,19}$	273 141.137	86.3	2.00	...	...	0.05	CH_3OCOH
tEME-EE'	$20_{2,18}-19_{1,19}$	273 141.138	86.3	2.00	†			
tEME-AE	$20_{2,18}-19_{1,19}$	273 141.411	86.3	2.00	†			
tEME-EA	$20_{2,18}-19_{1,19}$	273 142.818	86.3	2.00	...	...	0.03	CH_3OCOH
tEME-AA	$20_{2,18}-19_{1,19}$	273 143.092	86.3	2.00	†			
tEME-EA	$35_{0,35}-34_{1,34}$	273 979.063	239.2	29.79	273 979.1	0.73	0.28	CH_3CH_2CN, SO_2
tEME-AA	$35_{0,35}-34_{1,34}$	273 979.067	239.2	29.79	†			
tEME-EE	$35_{0,35}-34_{1,34}$	273 979.089	239.2	29.79	†			
tEME-EE'	$35_{0,35}-34_{1,34}$	273 979.089	239.2	29.79	†			
tEME-AE	$35_{0,35}-34_{1,34}$	273 979.093	239.2	29.79	†			
tEME-AA	$36_{1,35}-35_{2,34}$	274 946.543	260.0	19.65	274 946.9	0.57	0.14	CH_3OCOH $v_t = 1$, H_2CS
tEME-EA	$36_{1,35}-35_{2,34}$	274 946.555	260.0	19.65	†			
tEME-AE	$36_{1,35}-35_{2,34}$	274 947.090	260.0	19.65	†			
tEME-EE	$36_{1,35}-35_{2,34}$	274 947.102	260.0	19.65	†			
tEME-EE'	$36_{1,35}-35_{2,34}$	274 947.102	260.0	19.65	†			
tEME-EE'	$35_{1,35}-34_{0,34}$	275 618.927	239.3	29.80	275 618.9	0.22	0.28	
tEME-EE	$35_{1,35}-34_{0,34}$	275 618.927	239.3	29.80	†			
tEME-AE	$35_{1,35}-34_{0,34}$	275 618.934	239.3	29.80	†			
tEME-EA	$35_{1,35}-34_{0,34}$	275 619.009	239.3	29.80	†			
tEME-AA	$35_{1,35}-34_{0,34}$	275 619.016	239.3	29.80	†			
tEME-EE'	$32_{2,31}-31_{1,30}$	276 219.631	207.8	15.92	276 219.6	0.34	0.15	$^{13}CH_3OCOH$
tEME-EE	$32_{2,31}-31_{1,30}$	276 219.631	207.8	15.92	†			
tEME-AE	$32_{2,31}-31_{1,30}$	276 219.695	207.8	15.92	†			
tEME-EA	$32_{2,31}-31_{1,30}$	276 220.573	207.8	15.92	†			
tEME-AA	$32_{2,31}-31_{1,30}$	276 220.637	207.8	15.92	†			
tEME-EE	$19_{3,16}-18_{2,17}$	276 700.152	83.9	5.20	276 700.3	0.29	0.13	CH_3CN $v_8 = 1$, CH_3OH
tEME-EE'	$19_{3,16}-18_{2,17}$	276 700.167	83.9	5.20	†			
tEME-AE	$19_{3,16}-18_{2,17}$	276 700.458	83.9	5.20	†			
tEME-EA	$19_{3,16}-18_{2,17}$	276 702.533	83.9	5.20	276 702.5	0.34	0.08	CH_3CN $v_8 = 1$, CH_3OH
tEME-AA	$19_{3,16}-18_{2,17}$	276 702.832	83.9	5.20	†			
tEME-EE'	$21_{3,19}-20_{2,18}$	278 825.580	99.7	6.00	278 825.7	0.39	0.14	CH_3CH_2CN, CH_3CH_2CN $v_{20} = 1$, $CH_3{}^{13}CH_2CN$
tEME-EE	$21_{3,19}-20_{2,18}$	278 825.588	99.7	6.00	†			
tEME-AE	$21_{3,19}-20_{2,18}$	278 825.856	99.7	6.00	†			
tEME-EA	$21_{3,19}-20_{2,18}$	278 828.090	99.7	6.00	278 828.4	0.33	0.09	CH_3CH_2CN, CH_3CH_2CN $v_{20} = 1$, $CH_3{}^{13}CH_2CN$
tEME-AA	$21_{3,19}-20_{2,18}$	278 828.362	99.7	6.00	†			
tEME-EE	$8_{5,3}-7_{4,3}$	280 075.262	42.7	4.85	280 075.6	0.40	0.38	
tEME-EE'	$8_{5,4}-7_{4,4}$	280 075.328	42.7	4.85	†			
tEME-EE'	$8_{5,3}-7_{4,3}$	280 075.462	42.7	4.85	†			
tEME-EE	$8_{5,4}-7_{4,4}$	280 075.527	42.7	4.85	†			
tEME-AE	$8_{5,3}-7_{4,3}$	280 075.816	42.7	4.85	†			
tEME-AE	$8_{5,4}-7_{4,4}$	280 075.882	42.7	4.85	†			
tEME-EA	$8_{5,4}-7_{4,4}$	280 078.526	42.7	4.85	280 078.5	0.31	0.25	
tEME-EA	$8_{5,3}-7_{4,3}$	280 078.726	42.7	4.85	†			
tEME-AA	$8_{5,4}-7_{4,3}$	280 079.076	42.7	4.85	†			
tEME-AA	$8_{5,3}-7_{4,4}$	280 079.084	42.7	4.85	†			
tEME-EE'	$14_{4,11}-13_{3,10}$	280 288.955	59.0	2.84	...	...	0.07	CH_3COOH $v_t = 1$
tEME-AE	$14_{4,11}-13_{3,10}$	280 290.299	59.0	2.96	†			
tEME-EE	$14_{4,11}-13_{3,10}$	280 290.853	59.0	3.11	†			
tEME-EA	$14_{4,11}-13_{3,10}$	280 297.013	59.0	4.69	280 297.7	0.12	0.10	
tEME-AA	$14_{4,11}-13_{3,10}$	280 297.720	59.0	5.30	†			
tEME-EE	$14_{4,10}-13_{3,10}$	280 299.704	59.0	2.19	280 301.1	0.10	0.06	U-line
tEME-EA	$14_{4,10}-13_{3,10}$	280 299.889	59.0	0.61	†			
tEME-AE	$14_{4,10}-13_{3,10}$	280 300.898	59.0	2.34	†			
tEME-EE'	$14_{4,10}-13_{3,10}$	280 301.316	59.0	2.46	†			
tEME-EE'	$14_{4,11}-13_{3,11}$	280 383.694	59.0	2.46	280 385.0	0.11	0.06	CH_3OCOH $v_t = 1$
tEME-AE	$14_{4,11}-13_{3,11}$	280 384.884	59.0	2.34	†			
tEME-EE	$14_{4,11}-13_{3,11}$	280 385.307	59.0	2.19	†			
tEME-EA	$14_{4,10}-13_{3,11}$	280 394.040	59.0	4.69	...	...	0.16	CH_3OCOH
tEME-AA	$14_{4,10}-13_{3,11}$	280 394.104	59.0	5.30	†			
tEME-EE	$14_{4,10}-13_{3,11}$	280 394.157	59.0	3.11	†			
tEME-AE	$14_{4,10}-13_{3,11}$	280 395.482	59.0	2.96	†			
tEME-EE'	$14_{4,10}-13_{3,11}$	280 396.055	59.0	2.83	†			
tEME-EA	$36_{0,36}-35_{1,35}$	281 871.802	252.8	30.81	281 871.7	0.25	0.27	U-line
tEME-AA	$36_{0,36}-35_{1,35}$	281 871.806	252.8	30.81	†			
tEME-EE	$36_{0,36}-35_{1,35}$	281 871.822	252.8	30.81	†			
tEME-EE'	$36_{0,36}-35_{1,35}$	281 871.822	252.8	30.81	†			
tEME-AE	$36_{0,36}-35_{1,35}$	281 871.826	252.8	30.81	†			
tEME-EE'	$33_{2,32}-32_{1,31}$	282 152.573	220.4	16.88	282 153.2	0.56	0.16	HC_3N $v_5 = 1$
tEME-EE	$33_{2,32}-32_{1,31}$	282 152.573	220.4	16.88	†			
tEME-AE	$33_{2,32}-32_{1,31}$	282 152.631	220.4	16.88	†			
tEME-EA	$33_{2,32}-32_{1,31}$	282 153.461	220.4	16.88	†			
tEME-AA	$33_{2,32}-32_{1,31}$	282 153.519	220.4	16.88	†			

Table A.2. continued.

Species	Transition $J_{K_a,K_c} - J'_{K'_a,K'_c}$	Predicted frequency (MHz)	E_{upp} (K)	S_{ij}	Observed[1] frequency (MHz)	Observed[1] T_{MB} (K)	Model[2] T_{MB} (K)	Blends
tEME-EE'	$36_{1,36}-35_{0,35}$	283 263.283	252.8	30.82	283 263.4	0.44	0.27	$^{13}CH_3OH$
tEME-EE	$36_{1,36}-35_{0,35}$	283 263.283	252.8	30.82	†			
tEME-AE	$36_{1,36}-35_{0,35}$	283 263.290	252.8	30.82	†			
tEME-EA	$36_{1,36}-35_{0,35}$	283 263.357	252.8	30.82	†			
tEME-AA	$36_{1,36}-35_{0,35}$	283 263.364	252.8	30.82	†			
tEME-AE	$41_{2,39}-40_{3,38}$	283 951.422	341.0	13.47	...	...	0.03	CH_3OCH_3
tEME-EE	$41_{2,39}-40_{3,38}$	283 951.485	341.0	13.47	†			
tEME-EE'	$41_{2,39}-40_{3,38}$	283 951.485	341.0	13.47	†			
tEME-AA	$37_{1,36}-36_{2,35}$	284 137.669	274.2	20.72	288 138.3	0.34	0.14	CH_3OCOH $v_t = 1$
tEME-EA	$37_{1,36}-36_{2,35}$	284 137.677	274.2	20.72	†			
tEME-AE	$37_{1,36}-36_{2,35}$	284 138.161	274.2	20.72	†			
tEME-EE	$37_{1,36}-36_{2,35}$	284 138.169	274.2	20.72	†			
tEME-EE'	$37_{1,36}-36_{2,35}$	284 138.169	274.2	20.72	†			
tEME-EE'	$22_{3,20}-21_{2,19}$	285 037.438	108.2	6.21	...	...	0.14	CH_3CH_2CN v_{13}/v_{21}
tEME-EE	$22_{3,20}-21_{2,19}$	285 037.444	108.2	6.21	†			
tEME-AE	$22_{3,20}-21_{2,19}$	285 037.708	108.2	6.21	†			
tEME-EA	$22_{3,20}-21_{2,19}$	285 039.939	108.2	6.21	...	...	0.09	CH_3CH_2CN v_{13}/v_{21}
tEME-AA	$22_{3,20}-21_{2,19}$	285 040.206	108.2	6.21	†			
tEME-EE	$20_{3,17}-19_{2,18}$	285 699.473	91.6	5.28	...	...	0.14	SO_2
tEME-EE'	$20_{3,17}-19_{2,18}$	285 699.484	91.6	5.28	†			
tEME-AE	$20_{3,17}-19_{2,18}$	285 699.777	91.6	5.28	†			
tEME-EA	$20_{3,17}-19_{2,18}$	285 701.840	91.6	5.28	...	...	0.10	SO_2
tEME-AA	$20_{3,17}-19_{2,18}$	285 702.139	91.6	5.28	†			
tEME-EE	$21_{2,19}-20_{1,20}$	286 585.825	94.5	1.86	...	...	0.05	CH_3COOH $v_t = 1$
tEME-EE'	$21_{2,19}-20_{1,20}$	286 585.825	94.5	1.86	†			
tEME-AE	$21_{2,19}-20_{1,20}$	286 586.110	94.5	1.86	†			
tEME-EA	$21_{2,19}-20_{1,20}$	286 587.511	94.5	1.86	...	...	0.03	U-line
tEME-AA	$21_{2,19}-20_{1,20}$	286 587.796	94.5	1.86	†			
tEME-EE	$9_{5,4}-8_{4,4}$	288 124.443	46.1	5.02	288 124.8	0.59	0.41	
tEME-EE'	$9_{5,5}-8_{4,5}$	288 124.510	46.1	5.02	†			
tEME-EE'	$9_{5,4}-8_{4,4}$	288 124.641	46.1	5.02	†			
tEME-EE	$9_{5,5}-8_{4,5}$	288 124.708	46.1	5.02	†			
tEME-AE	$9_{5,4}-8_{4,4}$	288 124.995	46.1	5.02	†			
tEME-AE	$9_{5,5}-8_{4,5}$	288 125.062	46.1	5.02	†			
tEME-EA	$9_{5,5}-8_{4,5}$	288 127.703	46.1	5.02	...	...	0.27	CH_3OCOH
tEME-EA	$9_{5,4}-8_{4,4}$	288 127.901	46.1	5.02	†			
tEME-AA	$9_{5,5}-8_{4,4}$	288 128.242	46.1	5.02	†			
tEME-AA	$9_{5,4}-8_{4,5}$	288 128.268	46.1	5.02	†			
tEME-EE'	$34_{2,33}-33_{1,32}$	288 187.160	233.4	17.86	288 187.5	0.54	0.17	CH_3OCOH
tEME-EE	$34_{2,33}-33_{1,32}$	288 187.160	233.4	17.86	†			
tEME-AE	$34_{2,33}-33_{1,32}$	288 187.214	233.4	17.86	†			
tEME-EA	$34_{2,33}-33_{1,32}$	288 187.993	233.4	17.86	†			
tEME-AA	$34_{2,33}-33_{1,32}$	288 188.047	233.4	17.86	†			
tEME-EE'	$15_{4,12}-14_{3,11}$	288 267.539	64.8	3.40	...	...	0.09	$SO^{18}O$, CH_3COCH_3
tEME-AE	$15_{4,12}-14_{3,11}$	288 268.817	64.8	3.55	†			
tEME-EE	$15_{4,12}-14_{3,11}$	288 269.302	64.8	3.75	†			
tEME-EA	$15_{4,12}-14_{3,11}$	288 274.971	64.8	5.24	288 275.12	0.14	0.12	$SO^{18}O$
tEME-AA	$15_{4,12}-14_{3,11}$	288 275.555	64.8	5.50	†			
tEME-EE	$15_{4,11}-14_{3,11}$	288 278.681	64.8	1.75	...	...	0.05	U-line
tEME-AE	$15_{4,11}-14_{3,11}$	288 279.849	64.8	1.95	†			
tEME-EE'	$15_{4,11}-14_{3,11}$	288 280.260	64.8	2.11	†			
tEME-EE'	$15_{4,12}-14_{3,12}$	288 413.150	64.8	2.11	...	...	0.05	U-line
tEME-AE	$15_{4,12}-14_{3,12}$	288 414.329	64.8	1.95	†			
tEME-EE	$15_{4,12}-14_{3,12}$	288 414.729	64.8	1.75	†			
tEME-EE	$15_{4,11}-14_{3,12}$	288 424.108	64.8	3.75	288 424.7	0.50	0.20	$CH_3OC^{18}OH$
tEME-EA	$15_{4,11}-14_{3,12}$	288 424.469	64.8	5.24	†			
tEME-AA	$15_{4,11}-14_{3,12}$	288 424.653	64.8	5.50	†			
tEME-AE	$15_{4,11}-14_{3,12}$	288 425.361	64.8	3.55	†			
tEME-EE'	$15_{4,11}-14_{3,12}$	288 425.871	64.8	3.40	†			
tEME-EA	$37_{0,37}-36_{1,36}$	289 745.973	266.7	31.83	289 745.8	0.49	0.26	U-line
tEME-AA	$37_{0,37}-36_{1,36}$	289 745.977	266.7	31.83	†			
tEME-EE	$37_{0,37}-36_{1,36}$	289 745.986	266.7	31.83	†			
tEME-EE'	$37_{0,37}-36_{1,36}$	289 745.986	266.7	31.83	†			
tEME-AE	$37_{0,37}-36_{1,36}$	289 745.991	266.7	31.83	†			
tEME-EE'	$37_{1,37}-36_{0,36}$	290 924.982	266.8	31.83	290 925.0	0.71	0.27	$^{33}SO_2$
tEME-EE	$37_{1,37}-36_{0,36}$	290 924.982	266.8	31.83	†			
tEME-AE	$37_{1,37}-36_{0,36}$	290 924.989	266.8	31.83	†			
tEME-EA	$37_{1,37}-36_{0,36}$	290 925.049	266.8	31.83	†			
tEME-AA	$37_{1,37}-36_{0,36}$	290 925.056	266.8	31.83	†			
tEME-AA	$38_{1,37}-37_{2,36}$	293 203.620	288.8	21.79	293 203.7	0.28	0.14	
tEME-EA	$38_{1,37}-37_{2,36}$	293 203.624	288.8	21.79	†			
tEME-AE	$38_{1,37}-37_{2,36}$	293 204.059	288.8	21.79	†			
tEME-EE	$38_{1,37}-37_{2,36}$	293 204.064	288.8	21.79	†			

Table A.2. continued.

Species	Transition $J_{K_a,K_c} - J'_{K'_a,K'_c}$	Predicted frequency (MHz)	E_{upp} (K)	S_{ij}	Observed[1] frequency (MHz)	Observed[1] T_{MB} (K)	Model[2] T_{MB} (K)	Blends
tEME-EE'	$38_{1,37}-37_{2,36}$	293 204.064	288.8	21.79	†			
tEME-EE'	$35_{2,34}-34_{1,33}$	294 329.625	246.8	18.86	294 330.0	0.28	0.17	
tEME-EE	$35_{2,34}-34_{1,33}$	294 329.625	246.8	18.86	†			
tEME-AE	$35_{2,34}-34_{1,33}$	294 329.673	246.8	18.86	†			
tEME-EA	$35_{2,34}-34_{1,33}$	294 330.403	246.8	18.86	†			
tEME-AA	$35_{2,34}-34_{1,33}$	294 330.451	246.8	18.86	†			
tEME-EE	$21_{3,18}-20_{2,19}$	294 868.623	99.8	5.34	...	...	0.15	CH_3OCOH
tEME-EE'	$21_{3,18}-20_{2,19}$	294 868.631	99.8	5.34	†			
tEME-AE	$21_{3,18}-20_{2,19}$	294 868.926	99.8	5.34	†			
tEME-EE	$37_{2,36}-36_{2,35}$	294 869.441	274.8	36.86	†			
tEME-EE'	$37_{2,36}-36_{2,35}$	294 869.441	274.8	36.86	†			
tEME-AE	$37_{2,36}-36_{2,35}$	294 869.456	274.8	36.86	†			
tEME-EA	$37_{2,36}-36_{2,35}$	294 869.504	274.8	36.86	†			
tEME-AA	$37_{2,36}-36_{2,35}$	294 869.519	274.8	36.86	†			
tEME-EA	$21_{3,18}-20_{2,19}$	294 870.971	99.8	5.34	...	...	0.10	CH_3OCOH
tEME-AA	$21_{3,18}-20_{2,19}$	294 871.271	99.8	5.34	†			
tEME-AA	$42_{2,40}-41_{3,39}$	295 213.922	357.4	14.32	...	...	0.03	CH_3CN $v_8 = 1$
tEME-EA	$42_{2,40}-41_{3,39}$	295 213.976	357.4	14.32	†			
tEME-AE	$42_{2,40}-41_{3,39}$	295 215.469	357.4	14.32	†			
tEME-EE	$42_{2,40}-41_{3,39}$	295 215.522	357.4	14.32	†			
tEME-EE'	$42_{2,40}-41_{3,39}$	295 215.522	357.4	14.32	†			
tEME-EE	$10_{5,5}-9_{4,5}$	296 172.265	50.0	5.20	...	...	0.45	SO_2
tEME-EE'	$10_{5,6}-9_{4,6}$	296 172.333	50.0	5.20	†			
tEME-EE'	$10_{5,5}-9_{4,5}$	296 172.462	50.0	5.20	†			
tEME-EE	$10_{5,6}-9_{4,6}$	296 172.530	50.0	5.20	†			
tEME-AE	$10_{5,5}-9_{4,5}$	296 172.815	50.0	5.20	†			
tEME-AE	$10_{5,6}-9_{4,6}$	296 172.884	50.0	5.20	†			
tEME-EA	$10_{5,6}-9_{4,6}$	296 175.521	50.0	5.20	...	...	0.30	SO_2
tEME-EA	$10_{5,5}-9_{4,5}$	296 175.717	50.0	5.20	†			
tEME-AA	$10_{5,6}-9_{4,5}$	296 176.037	50.0	5.20	†			
tEME-AA	$10_{5,5}-9_{4,6}$	296 176.104	50.0	5.20	†			
tEME-EE'	$16_{4,13}-15_{3,12}$	296 223.035	71.0	4.07	296 224.2	0.49	0.11	CH_3OCOH
tEME-AE	$16_{4,13}-15_{3,12}$	296 224.220	71.0	4.26	†			
tEME-EE	$16_{4,13}-15_{3,12}$	296 224.598	71.0	4.49	†			
tEME-EA	$16_{4,13}-15_{3,12}$	296 229.670	71.0	5.60	296 230.0	0.30	0.13	CH_3OCOH
tEME-AA	$16_{4,13}-15_{3,12}$	296 230.175	71.0	5.70	†			
tEME-EE	$16_{4,12}-15_{3,12}$	296 235.284	71.0	1.21	...	...	0.04	CH_3CH_2CN $v_{12} = 1$
tEME-AE	$16_{4,12}-15_{3,12}$	296 236.371	71.0	1.44	†			
tEME-EE'	$16_{4,12}-15_{3,12}$	296 236.725	71.0	1.63	†			
tEME-EE'	$16_{4,13}-15_{3,13}$	296 440.645	71.0	1.63	...	...	0.04	CH_3CH_2CN
tEME-AE	$16_{4,13}-15_{3,13}$	296 441.764	71.0	1.44	†			
tEME-EE	$16_{4,13}-15_{3,13}$	296 442.086	71.0	1.21	†			
tEME-EE	$16_{4,12}-15_{3,13}$	296 452.772	71.0	4.49	...	...	0.24	CH_3CH_2CN
tEME-EA	$16_{4,12}-15_{3,13}$	296 453.716	71.0	5.59	†			
tEME-AE	$16_{4,12}-15_{3,13}$	296 453.915	71.0	4.26	†			
tEME-AA	$16_{4,12}-15_{3,13}$	296 453.976	71.0	5.70	†			
tEME-EE'	$16_{4,12}-15_{3,13}$	296 454.335	71.0	4.07	†			
tEME-EE'	$24_{3,22}-23_{2,21}$	296 926.193	126.4	6.66	296 926.5	0.17	0.14	
tEME-EE	$24_{3,22}-23_{2,21}$	296 926.197	126.4	6.66	†			
tEME-AE	$24_{3,22}-23_{2,21}$	296 926.450	126.4	6.66	†			
tEME-EA	$24_{3,22}-23_{2,21}$	296 928.675	126.4	6.66	296 928.7	0.42	0.09	CH_3OCOH $v_t = 2$
tEME-AA	$24_{3,22}-23_{2,21}$	296 928.931	126.4	6.66	†			
tEME-EA	$38_{0,38}-37_{1,37}$	297 603.969	281.1	32.84	...	...	0.25	CH_3OCOH $v_t = 2$
tEME-AA	$38_{0,38}-37_{1,37}$	297 603.974	281.1	32.84	†			
tEME-EE	$38_{0,38}-37_{1,37}$	297 603.978	281.1	32.84	†			
tEME-EE'	$38_{0,38}-37_{1,37}$	297 603.978	281.1	32.84	†			
tEME-AE	$38_{0,38}-37_{1,37}$	297 603.982	281.1	32.84	†			
tEME-EE'	$38_{1,38}-37_{0,37}$	298 601.597	281.1	32.85	...	...	0.26	SO_2
tEME-EE	$38_{1,38}-37_{0,37}$	298 601.597	281.1	32.85	†			
tEME-AE	$38_{1,38}-37_{0,37}$	298 601.604	281.1	32.85	†			
tEME-EA	$38_{1,38}-37_{0,37}$	298 601.658	281.1	32.85	†			
tEME-AA	$38_{1,38}-37_{0,37}$	298 601.665	281.1	32.85	†			
tEME-EE	$22_{2,20}-21_{1,21}$	300 442.750	103.1	1.73	...	...	0.05	$H^{13}CCCN$ $v_7 = 1$, CH_3OCOH
tEME-EE'	$22_{2,20}-21_{1,21}$	300 442.750	103.1	1.73	†			
tEME-AE	$22_{2,20}-21_{1,21}$	300 443.046	103.1	1.73	†			
tEME-EA	$22_{2,20}-21_{1,21}$	300 444.445	103.1	1.73	...	...	0.03	$H^{13}CCCN$ $v_7 = 1$, CH_3OCOH
tEME-AA	$22_{2,20}-21_{1,21}$	300 444.741	103.1	1.73	†			
tEME-EE'	$36_{2,35}-35_{1,34}$	300 583.963	260.6	19.88	300 584.4	0.25	0.17	
tEME-EE	$36_{2,35}-35_{1,34}$	300 583.963	260.6	19.88	†			
tEME-AE	$36_{2,35}-35_{1,34}$	300 584.008	260.6	19.88	†			
tEME-EA	$36_{2,35}-35_{1,34}$	300 584.687	260.6	19.88	†			
tEME-AA	$36_{2,35}-35_{1,34}$	300 584.731	260.6	19.88	†			
tEME-AA	$39_{1,38}-38_{2,37}$	302 148.596	303.8	22.87	...	...	0.14	SO_2

Table A.2. continued.

Species	Transition $J_{K_a,K_c} - J'_{K'_a,K'_c}$	Predicted frequency (MHz)	E_{upp} (K)	S_{ij}	Observed[1] frequency (MHz)	Observed[1] T_{MB} (K)	Model[2] T_{MB} (K)	Blends
tEME-EA	$39_{1,38}-38_{2,37}$	302 148.597	303.8	22.87	†			
tEME-AE	$39_{1,38}-38_{2,37}$	302 148.985	303.8	22.87	†			
tEME-EE	$39_{1,38}-38_{2,37}$	302 148.986	303.8	22.87	†			
tEME-EE'	$39_{1,38}-38_{2,37}$	302 148.986	303.8	22.87	†			
tEME-EE'	$25_{3,23}-24_{2,22}$	302 611.864	136.1	6.91	...	...	0.14	CH_3COCH_3
tEME-EE	$25_{3,23}-24_{2,22}$	302 611.867	136.1	6.91	†			
tEME-AE	$25_{3,23}-24_{2,22}$	302 612.114	136.1	6.91	†			
tEME-EA	$25_{3,23}-24_{2,22}$	302 614.334	136.1	6.91	...	...	0.09	CH_3COCH_3
tEME-AA	$25_{3,23}-24_{2,22}$	302 614.582	136.0	6.91	†			
tEME-EE'	$17_{4,14}-16_{3,13}$	304 150.005	77.5	4.81	...	...	0.14	CH_2CHCN
tEME-AE	$17_{4,14}-16_{3,13}$	304 151.052	77.5	4.99	†			
tEME-EE	$17_{4,14}-16_{3,13}$	304 151.281	77.5	5.19	†			
tEME-EA	$17_{4,14}-16_{3,13}$	304 155.769	77.5	5.86	...	...	0.14	CH_2CHCN
tEME-AA	$17_{4,14}-16_{3,13}$	304 156.225	77.5	5.90	†			
tEME-EE	$11_{5,6}-10_{4,6}$	304 218.289	54.3	5.39	...	...	0.48	CH_3OH
tEME-EE'	$11_{5,7}-10_{4,7}$	304 218.360	54.3	5.39	†			
tEME-EE'	$11_{5,6}-10_{4,6}$	304 218.485	54.3	5.39	†			
tEME-EE	$11_{5,7}-10_{4,7}$	304 218.556	54.3	5.39	†			
tEME-AE	$11_{5,6}-10_{4,6}$	304 218.838	54.3	5.39	†			
tEME-AE	$11_{5,7}-10_{4,7}$	304 218.909	54.3	5.39	†			
tEME-EA	$11_{5,7}-10_{4,7}$	304 221.544	54.3	5.38	...	...	0.32	CH_3OH
tEME-EA	$11_{5,6}-10_{4,6}$	304 221.733	54.3	5.38	†			
tEME-AA	$11_{5,7}-10_{4,6}$	304 222.011	54.3	5.39	†			
tEME-AA	$11_{5,6}-10_{4,7}$	304 222.167	54.3	5.39	†			
tEME-EE	$22_{3,19}-21_{2,20}$	304 228.127	108.3	5.38	...	...	0.14	CH_3COCH_3
tEME-EE'	$22_{3,19}-21_{2,20}$	304 228.133	108.3	5.38	†			
tEME-AE	$22_{3,19}-21_{2,20}$	304 228.430	108.3	5.38	†			
tEME-EA	$22_{3,19}-21_{2,20}$	304 230.454	108.3	5.38	...	...	0.10	CH_3COCH_3
tEME-AA	$22_{3,19}-21_{2,20}$	304 230.754	108.3	5.38	†			
tEME-EE	$17_{4,13}-16_{3,14}$	304 481.623	77.5	5.19	...	...	0.25	CH_3OCOH $v_t = 1$
tEME-AE	$17_{4,13}-16_{3,14}$	304 482.613	77.5	4.99	†			
tEME-EE'	$17_{4,13}-16_{3,14}$	304 482.900	77.5	4.81	†			
tEME-EA	$17_{4,13}-16_{3,14}$	304 483.137	77.5	5.85	†			
tEME-AA	$17_{4,13}-16_{3,14}$	304 483.441	77.5	5.90	†			
tEME-EA	$39_{0,39}-38_{1,38}$	305 447.899	295.7	33.86	305 448.1	0.96	0.24	CH_3CH_2CN v_{13}/v_{21}
tEME-EE	$39_{0,39}-38_{1,38}$	305 447.903	295.7	33.86	†			
tEME-EE'	$39_{0,39}-38_{1,38}$	305 447.903	295.7	33.86	†			
tEME-AA	$39_{0,39}-38_{1,38}$	305 447.904	295.7	33.86	†			
tEME-AE	$39_{0,39}-38_{1,38}$	305 447.908	295.7	33.86	†			
tEME-EE	$39_{1,39}-38_{0,38}$	306 290.978	295.7	33.86	...	...	0.24	CH_3OH
tEME-EE'	$39_{1,39}-38_{0,38}$	306 290.978	295.7	33.86	†			
tEME-AE	$39_{1,39}-38_{0,38}$	306 290.985	295.7	33.86	†			
tEME-EA	$39_{1,39}-38_{0,38}$	306 291.035	295.7	33.86	†			
tEME-AA	$39_{1,39}-38_{0,38}$	306 291.041	295.7	33.86	†			
tEME-AA	$43_{2,41}-42_{3,40}$	306 373.059	374.1	15.22	...	...	0.03	CH_3OCH_3
tEME-EA	$43_{2,41}-42_{3,40}$	306 373.104	374.1	15.22	†			
tEME-AE	$43_{2,41}-42_{3,40}$	306 374.522	374.1	15.22	†			
tEME-EE	$43_{2,41}-42_{3,40}$	306 374.567	374.1	15.22	†			
tEME-EE'	$43_{2,41}-42_{3,40}$	306 374.567	374.1	15.22	†			

A&A 582, L1 (2015)

Table A.3. Detected lines of gauche-trans-n-$CH_3CH_2CH_2OH$.

Species	Transition $J_{Ka,Kc} - J'_{K'a,K'c}$	Predicted frequency (MHz)	E_{upp} (K)	S_{ij}	Observed frequency (MHz)	T (K)	Blends/ Comments
Gt-n-propanol	$12_{7,6}$–$12_{6,6}$	124 417.241	58.0	4.25	124 417.1	0.04	30 m; U-line
Gt-n-propanol	$12_{7,5}$–$12_{6,6}$	124 417.256	58.0	4.89	†		
Gt-n-propanol	$12_{7,6}$–$12_{6,7}$	124 418.125	58.0	4.89	124 418.2†	0.06	30 m; U-line
Gt-n-propanol	$12_{7,5}$–$12_{6,7}$	124 418.139	58.0	4.25	†		
Gt-n-propanol	$15_{2,14}$–$14_{1,13}$	141 219.413	55.4	9.14	141 219.8	0.04	30 m
Gt-n-propanol	$6_{5,2}$–$5_{4,1}$	143 143.854	21.1	4.51	143 144.6	0.10	30 m; CH_3CH_2CN $v_{12} = 1$
Gt-n-propanol	$6_{5,1}$–$5_{4,1}$	143 143.873	21.1	4.65	†		
Gt-n-propanol	$6_{5,2}$–$5_{4,2}$	143 144.406	21.1	4.65	†		
Gt-n-propanol	$6_{5,1}$–$5_{4,2}$	143 144.426	21.1	4.51	†		
Gt-n-propanol	$8_{7,2}$–$7_{6,1}$	200 433.919	38.9	6.49	200 434.4	0.13	30 m
Gt-n-propanol	$8_{7,1}$–$7_{6,1}$	200 433.919	38.9	6.63	†		
Gt-n-propanol	$8_{7,2}$–$7_{6,2}$	200 433.920	38.9	6.63	†		
Gt-n-propanol	$8_{7,1}$–$7_{6,2}$	200 433.920	38.9	6.49	†		
Gt-n-propanol	$23_{11,13}$–$23_{10,13}$	200 508.301	181.2	8.64	200 508.8	0.07	30 m
Gt-n-propanol	$23_{11,12}$–$23_{10,13}$	200 508.302	181.2	10.20	†		
Gt-n-propanol	$23_{11,13}$–$23_{10,14}$	200 508.311	181.2	10.20	†		
Gt-n-propanol	$23_{11,12}$–$23_{10,14}$	200 508.312	181.2	8.64	†		
Gt-n-propanol	$9_{7,3}$–$8_{6,2}$	209 892.537	43.0	6.54	209 892.5	0.19	30 m; CH_2CHCN $v_{11} = 1$
Gt-n-propanol	$9_{7,2}$–$8_{6,2}$	209 892.538	43.0	6.78	†		
Gt-n-propanol	$9_{7,3}$–$8_{6,3}$	209 892.542	43.0	6.78	†		
Gt-n-propanol	$9_{7,2}$–$8_{6,3}$	209 892.542	43.0	6.54	†		
Gt-n-propanol	$24_{0,24}$–$23_{1,23}$	210 248.928	127.7	22.15	210 249.1	0.17	30 m
Gt-n-propanol	$24_{1,24}$–$23_{1,23}$	210 250.060	127.7	23.86	†		
Gt-n-propanol	$24_{0,24}$–$23_{0,23}$	210 250.810	127.7	23.86	210 252.8	0.16	30 m
Gt-n-propanol	$24_{1,24}$–$23_{0,23}$	210 251.942	127.7	22.15	†		
Gt-n-propanol	$44_{12,32}$–$44_{11,34}$	210 252.224	517.3	16.71	†		
Gt-n-propanol	$37_{12,26}$–$37_{11,26}$	215 663.302	386.2	14.57	...	...	ALMA; CH_3CH_2CN v_{13}/v_{21}
Gt-n-propanol	$37_{12,25}$–$37_{11,26}$	215 663.793	386.2	19.40	...	...	″
Gt-n-propanol	$37_{12,26}$–$37_{11,27}$	215 663.793	386.2	19.40	...	...	″
Gt-n-propanol	$37_{12,25}$–$37_{11,27}$	215 663.793	386.2	19.40	...	...	″
Gt-n-propanol	$37_{12,26}$–$37_{11,27}$	215 672.076	386.2	19.40	...	...	ALMA; CH_3COOH $v_t = 1$
Gt-n-propanol	$37_{12,25}$–$37_{11,27}$	215 672.568	386.2	14.57	...	...	″
Gt-n-propanol	$24_{3,21}$–$23_{4,20}$	216 493.373	143.6	9.36	...	...	ALMA; CH_3OCOH
Gt-n-propanol	$14_{5,10}$–$13_{4,9}$	217 132.672	59.3	5.22	...	...	ALMA; $CH_3O^{13}COH$ $v_t = 1$, CH_3OD
Gt-n-propanol	$34_{12,23}$–$34_{11,23}$	217 158.546	337.0	13.43	217 159.0	0.48	ALMA; CH_3COOCH_3
Gt-n-propanol	$34_{12,22}$–$34_{11,23}$	217 158.612	337.0	17.25	†		
Gt-n-propanol	$34_{12,23}$–$34_{11,24}$	217 159.977	337.0	17.25	†		
Gt-n-propanol	$34_{12,22}$–$34_{11,24}$	217 160.043	337.0	13.43	†		
Gt-n-propanol	$32_{12,21}$–$32_{11,21}$	217 935.916	306.4	12.61	...	...	ALMA;CH_3OCH_3, $CH_3O^{13}COH$ $v_t = 1$
Gt-n-propanol	$32_{12,20}$–$32_{11,21}$	217 935.931	306.4	15.85	...	...	″
Gt-n-propanol	$32_{12,21}$–$32_{11,22}$	217 936.298	306.4	15.85	...	...	″
Gt-n-propanol	$32_{12,20}$–$32_{11,22}$	217 936.314	306.4	12.61	...	...	″
Gt-n-propanol	$31_{12,20}$–$31_{11,20}$	218 268.548	291.9	12.18	218 269.0	0.84	ALMA; U-line
Gt-n-propanol	$31_{12,19}$–$31_{11,20}$	218 268.555	291.9	12.15	†		
Gt-n-propanol	$31_{12,20}$–$31_{11,21}$	218 268.739	291.9	12.15	†		
Gt-n-propanol	$31_{12,19}$–$31_{11,21}$	218 268.746	291.9	12.18	†		
Gt-n-propanol	$30_{12,19}$–$30_{11,19}$	218 567.524	277.7	11.74	...	...	ALMA; $CH_3O^{13}COH$ $v_t = 1$
Gt-n-propanol	$30_{12,18}$–$30_{11,19}$	218 567.527	277.7	14.45	...	...	″
Gt-n-propanol	$30_{12,19}$–$30_{11,20}$	218 567.616	277.7	14.45	...	...	″
Gt-n-propanol	$30_{12,18}$–$30_{11,20}$	218 567.619	277.7	11.74	...	...	″
Gt-n-propanol	$29_{12,18}$–$29_{11,18}$	218 835.376	264.1	11.28	218 835.5	1.05	ALMA; $CH_3^{18}OCOH$
Gt-n-propanol	$29_{12,17}$–$29_{11,18}$	218 835.377	264.1	13.76	†		
Gt-n-propanol	$29_{12,18}$–$29_{11,19}$	218 835.419	264.1	13.76	†		
Gt-n-propanol	$29_{12,17}$–$29_{11,19}$	218 835.421	264.1	11.28	†		
Gt-n-propanol	$25_{0,25}$–$24_{1,24}$	218 880.233	138.2	23.15	218 881.2	0.80	ALMA
Gt-n-propanol	$25_{1,25}$–$24_{1,24}$	218 880.912	138.2	24.86	†		
Gt-n-propanol	$25_{0,25}$–$24_{0,24}$	218 881.365	138.2	24.86	†		
Gt-n-propanol	$25_{1,25}$–$24_{0,24}$	218 882.044	138.2	23.15	†		
Gt-n-propanol	$12_{6,7}$–$11_{5,6}$	218 945.655	52.0	5.95	218 946.4	0.73	ALMA
Gt-n-propanol	$12_{6,6}$–$11_{5,6}$	218 946.539	52.0	6.77	†		
Gt-n-propanol	$12_{6,7}$–$11_{5,7}$	218 959.585	52.0	6.77	218 960.4	0.76	ALMA
Gt-n-propanol	$16_{3,14}$–$15_{2,14}$	218 960.392	65.9	5.29	†		
Gt-n-propanol	$12_{6,6}$–$11_{5,7}$	218 960.468	52.0	5.95	†		
Gt-n-propanol	$26_{4,22}$–$25_{5,21}$	219 065.066	170.6	6.54	...	...	ALMA; CH_3OCOH $v_t = 1$
Gt-n-propanol	$28_{12,17}$–$28_{11,17}$	219 074.469	250.9	10.82	...	...	ALMA; CH_3OCOH $v_t = 1$
Gt-n-propanol	$28_{12,16}$–$28_{11,17}$	219 074.470	250.9	13.07	...	...	″

Notes. Lines of gauche-trans-n-$CH_3CH_2CH_2OH$ (Gt–n–propanol) ground state present in the spectral scan of Orion KL from the IRAM-30 m telescope and the ALMA interferometer. Col. 1 indicates the species, Col. 2 gives the transition, Col. 3 the predicted frequency, Col. 4 upper level energy, Col. 5 the line strength, Col. 6 observed frequency at the peak channel of the line (relative to a v_{LSR} of +8.0 km s^{-1}), Col. 7 temperature at the peak channel of the line (main beam temperature for the IRAM data), and Col. 8 shows blends with other molecular species and comments. (†) Blended with previous line.

Table A.3. continued.

Species	Transition $J_{K_a,K_c} - J'_{K'_a,K'_c}$	Predicted frequency (MHz)	E_{upp} (K)	S_{ij}	Observed frequency (MHz)	T (K)	Blends/ Comments
Gt-n-propanol	$28_{12,17}-28_{11,18}$	219 074.489	250.9	13.07	...	...	″
Gt-n-propanol	$28_{12,16}-28_{11,18}$	219 074.490	250.9	10.82	...	...	″
Gt-n-propanol	$27_{12,16}-27_{11,16}$	219 287.021	238.1	10.34	...	...	ALMA; CH_3OCOH $v_t = 2$
Gt-n-propanol	$27_{12,15}-27_{11,16}$	219 287.021	238.1	12.38	...	...	″
Gt-n-propanol	$27_{12,16}-27_{11,17}$	219 287.030	238.1	12.38	...	...	″
Gt-n-propanol	$27_{12,15}-27_{11,17}$	219 287.030	238.1	10.34	...	...	″
Gt-n-propanol	$10_{7,4}-9_{6,3}$	219 345.954	47.6	6.62	...	...	ALMA; $CH_3O^{13}COH$
Gt-n-propanol	$10_{7,3}-9_{6,3}$	219 345.955	47.6	6.97	...	...	″
Gt-n-propanol	$10_{7,4}-9_{6,4}$	219 345.976	47.6	6.97	...	...	″
Gt-n-propanol	$10_{7,3}-9_{6,4}$	219 345.977	47.6	6.62	...	...	″
Gt-n-propanol	$8_{8,1}-7_{7,0}$	219 604.840	45.8	7.48	219 604.8	1.39	ALMA
Gt-n-propanol	$8_{8,1}-7_{7,0}$	219 604.840	45.8	7.52	†		
Gt-n-propanol	$8_{8,1}-7_{7,0}$	219 604.840	45.8	7.52	†		
Gt-n-propanol	$8_{8,1}-7_{7,0}$	219 604.840	45.8	7.48	†		
Gt-n-propanol	$25_{12,14}-25_{11,14}$	219 640.715	214.0	9.34	...	...	ALMA; CH_3OCOH $v_t = 1$
Gt-n-propanol	$25_{12,13}-25_{11,14}$	219 640.715	214.0	11.00	...	...	″
Gt-n-propanol	$25_{12,14}-25_{11,15}$	219 640.717	214.0	11.00	...	...	″
Gt-n-propanol	$25_{12,13}-25_{11,15}$	219 640.717	214.0	9.34	...	...	″
Gt-n-propanol	$22_{12,11}-22_{11,11}$	220 020.607	181.3	7.74	...	...	ALMA; U-line
Gt-n-propanol	$22_{12,10}-22_{11,11}$	220 020.607	181.3	8.91	...	...	″
Gt-n-propanol	$22_{12,11}-22_{11,12}$	220 020.607	181.3	8.91	...	...	″
Gt-n-propanol	$22_{12,10}-22_{11,12}$	220 020.607	181.3	7.74	...	...	″
Gt-n-propanol	$21_{12,10}-21_{11,10}$	220 113.805	171.3	7.17	220 113.2	0.81	ALMA; U-line, CH_2CHCN $v_{11} = 1$
Gt-n-propanol	$21_{12,9}-21_{11,10}$	220 113.805	171.3	7.17	†		
Gt-n-propanol	$21_{12,10}-21_{11,11}$	220 113.805	171.3	7.17	†		
Gt-n-propanol	$21_{12,9}-21_{11,11}$	220 113.805	171.3	7.17	†		
Gt-n-propanol	$18_{12,7}-18_{11,7}$	220 313.948	144.0	5.36	220 314.2	0.76	ALMA
Gt-n-propanol	$18_{12,6}-18_{11,7}$	220 313.948	144.0	6.01	†		
Gt-n-propanol	$18_{12,7}-18_{11,8}$	220 313.948	144.0	6.01	†		
Gt-n-propanol	$18_{12,6}-18_{11,8}$	220 313.948	144.0	5.36	†		
Gt-n-propanol	$15_{12,4}-15_{11,4}$	220 422.125	120.8	3.32	220 422.3	0.65	ALMA; $^{13}CH_3OCOH$, $CH_3OC^{18}OH$
Gt-n-propanol	$15_{12,3}-15_{11,4}$	220 422.125	120.8	3.66	†		
Gt-n-propanol	$15_{12,4}-15_{11,5}$	220 422.125	120.8	3.66	†		
Gt-n-propanol	$15_{12,3}-15_{11,5}$	220 422.125	120.8	3.32	†		
Gt-n-propanol	$14_{12,2}-14_{11,3}$	220 443.126	114.0	2.82	...	...	ALMA; CH_3CH_2OH
Gt-n-propanol	$14_{12,3}-14_{11,3}$	220 443.126	114.0	2.57	...	...	″
Gt-n-propanol	$14_{12,2}-14_{11,4}$	220 443.126	114.0	2.57	...	...	″
Gt-n-propanol	$14_{12,3}-14_{11,4}$	220 443.126	114.0	2.82	...	...	″
Gt-n-propanol	$24_{2,22}-23_{3,21}$	220 450.169	139.1	14.32	...	...	ALMA; CH_3CH_2OCOH
Gt-n-propanol	$13_{12,1}-13_{11,3}$	220 458.292	107.6	1.77	220 458.3	0.36	ALMA
Gt-n-propanol	$13_{12,1}-13_{11,2}$	220 458.292	107.6	1.94	†		
Gt-n-propanol	$13_{12,2}-13_{11,3}$	220 458.292	107.6	1.94	†		
Gt-n-propanol	$13_{12,2}-13_{11,2}$	220 458.292	107.6	1.77	†		
Gt-n-propanol	$26_{0,26}-25_{1,25}$	227 509.942	149.1	24.15	227 510.7	1.03	ALMA
Gt-n-propanol	$26_{1,26}-25_{1,25}$	227 510.348	149.1	25.86	†		
Gt-n-propanol	$26_{0,26}-25_{0,25}$	227 510.621	149.1	25.86	†		
Gt-n-propanol	$26_{1,26}-25_{0,25}$	227 511.028	149.1	24.15	†		
Gt-n-propanol	$11_{7,5}-10_{6,4}$	228 791.566	52.6	6.71	228 791.6	1.08	ALMA
Gt-n-propanol	$11_{7,4}-10_{6,4}$	228 791.570	52.6	7.18	†		
Gt-n-propanol	$11_{7,5}-10_{6,5}$	228 791.564	52.6	7.18	†		
Gt-n-propanol	$11_{7,4}-10_{6,5}$	228 791.658	52.6	6.71	†		
Gt-n-propanol	$9_{8,2}-8_{7,1}$	229 067.766	49.9	7.49	229 066.5	2.40	ALMA; U-line
″	″	″	″	″	229 068.4	0.30	30 m
Gt-n-propanol	$9_{8,1}-8_{7,1}$	229 067.766	49.9	7.62	†		
Gt-n-propanol	$9_{8,2}-8_{7,2}$	229 067.766	49.9	7.62	†		
Gt-n-propanol	$9_{8,1}-8_{7,2}$	229 067.766	49.9	7.49	†		
Gt-n-propanol	$24_{3,21}-23_{3,20}$	229 460.087	143.6	23.32	229 462.0	0.55	ALMA
Gt-n-propanol	$25_{2,23}-24_{3,22}$	229 461.862	150.2	15.38	†		
Gt-n-propanol	$23_{4,20}-22_{3,19}$	234 033.112	133.2	8.73	234 033.2	0.74	ALMA; U-line
Gt-n-propanol	$39_{13,27}-39_{12,27}$	235 206.448	432.7	15.38	...	...	ALMA; CH_3OCOH $v_t = 1$
Gt-n-propanol	$39_{13,26}-39_{12,27}$	235 206.535	432.7	20.18	...	...	″
Gt-n-propanol	$39_{13,27}-39_{12,28}$	235 208.140	432.7	20.18	...	...	″
Gt-n-propanol	$39_{13,26}-39_{12,28}$	235 208.227	432.7	15.38	...	...	″
Gt-n-propanol	$38_{13,26}-38_{12,26}$	235 684.048	414.9	15.00	...	...	ALMA; DCOOH
Gt-n-propanol	$38_{13,25}-38_{12,26}$	235 684.093	414.9	19.46	...	...	″
Gt-n-propanol	$38_{13,26}-38_{12,27}$	235 684.969	414.9	19.46	...	...	″
Gt-n-propanol	$38_{13,25}-38_{12,27}$	235 685.014	414.9	15.00	...	...	″
Gt-n-propanol	$19_{3,16}-18_{2,16}$	236 101.301	92.6	8.67	...	...	ALMA; D_2CO, $CH_3^{18}OCOH$
Gt-n-propanol	$37_{13,25}-37_{12,25}$	236 120.704	397.6	14.60	...	...	ALMA; $CH_3O^{13}COH$, CH_3OCOH $v_t = 2$
Gt-n-propanol	$37_{13,24}-37_{12,25}$	236 120.726	397.6	18.75	...	...	″
Gt-n-propanol	$37_{13,25}-37_{12,26}$	236 121.195	397.6	18.75	...	...	″
Gt-n-propanol	$37_{13,24}-37_{12,26}$	236 121.218	397.6	14.60	...	...	″
Gt-n-propanol	$27_{0,27}-26_{1,26}$	236 138.084	160.4	25.15	236 138.5	0.74	ALMA

Table A.3. continued.

Species	Transition $J_{K_a,K_c} - J'_{K'_a,K'_c}$	Predicted frequency (MHz)	E_{upp} (K)	S_{ij}	Observed frequency (MHz)	T (K)	Blends/ Comments
Gt-n-propanol	$27_{1,27}-26_{1,26}$	236 138.327	160.4	26.86	†		
Gt-n-propanol	$27_{0,27}-26_{0,26}$	236 138.490	160.4	26.86	†		
Gt-n-propanol	$27_{1,27}-26_{0,26}$	236 138.733	160.4	25.15	†		
Gt-n-propanol	$17_{2,16}-16_{1,16}$	236 879.561	69.9	2.82	...	...	ALMA; CH_3OCOH
Gt-n-propanol	$35_{13,23}-35_{12,23}$	236 882.213	364.3	13.78	...	...	″
Gt-n-propanol	$35_{13,22}-35_{12,23}$	236 882.218	364.3	17.34	...	...	″
Gt-n-propanol	$35_{13,23}-35_{12,24}$	236 882.345	364.3	17.34	...	...	″
Gt-n-propanol	$35_{13,22}-35_{12,24}$	236 882.350	364.3	13.78	...	...	″
Gt-n-propanol	$34_{13,22}-34_{12,22}$	237 212.075	348.4	13.36	...	...	ALMA; CH_3OCOH $v_t = 2$
Gt-n-propanol	$34_{13,21}-34_{12,22}$	237 212.077	348.4	16.65	...	...	″
Gt-n-propanol	$34_{13,22}-34_{12,23}$	237 212.141	348.4	16.65	...	...	″
Gt-n-propanol	$34_{13,21}-34_{12,23}$	237 212.143	348.4	13.36	...	...	″
Gt-n-propanol	$14_{6,9}-13_{5,9}$	237 691.949	64.3	7.37	237 692.7	0.62	ALMA; $^{13}CH_3OCOH$
Gt-n-propanol	$14_{6,8}-13_{5,9}$	237 697.842	64.3	6.15	237 697.2	1.20	ALMA; $^{13}CH_3OCOH$ $v_t = 1$
Gt-n-propanol	$25_{3,22}-24_{3,21}$	237 779.216	155.0	24.29	...	...	ALMA; $^{13}CH_3OCOH$ $v_t = 1$
Gt-n-propanol	$32_{13,20}-32_{12,20}$	237 781.304	317.9	12.47	...	...	″
Gt-n-propanol	$32_{13,19}-32_{12,20}$	237 781.304	317.9	15.26	...	...	″
Gt-n-propanol	$32_{13,20}-32_{12,21}$	237 781.319	317.9	15.26	...	...	″
Gt-n-propanol	$32_{13,19}-32_{12,21}$	237 781.319	317.9	12.47	...	...	″
Gt-n-propanol	$31_{13,19}-31_{12,19}$	238 024.778	303.3	12.01	...	...	ALMA; CH_3OCOH $v_t = 1$
Gt-n-propanol	$31_{13,18}-31_{12,19}$	238 024.778	303.3	14.57	...	...	″
Gt-n-propanol	$31_{13,19}-31_{12,20}$	238 024.785	303.3	14.57	...	...	″
Gt-n-propanol	$31_{13,18}-31_{12,20}$	238 024.785	303.3	12.01	...	...	″
Gt-n-propanol	$16_{5,11}-15_{4,12}$	238 051.137	73.5	5.21	238 051.4	0.64	ALMA
Gt-n-propanol	$37_{6,31}-37_{5,33}$	238 051.929	342.5	1.83	†	″	″
Gt-n-propanol	$12_{7,6}-11_{6,5}$	238 226.322	58.0	6.81	...	...	ALMA; CH_3OCOH $v_t = 1$
″	″	″	″	″	238 226.8	0.25	30 m; CH_3OCOH $v_t = 1$
Gt-n-propanol	$12_{7,5}-11_{6,5}$	238 226.337	58.0	7.42	†		
Gt-n-propanol	$12_{7,6}-11_{6,6}$	238 226.619	58.0	7.42	†		
Gt-n-propanol	$12_{7,5}-11_{6,6}$	238 226.633	58.0	6.81	†		
Gt-n-propanol	$30_{13,18}-30_{12,18}$	238 243.369	289.2	11.53	...	...	ALMA; U-line
Gt-n-propanol	$30_{13,17}-30_{12,18}$	238 243.369	289.2	13.88	...	...	″
Gt-n-propanol	$30_{13,18}-30_{12,19}$	238 243.372	289.2	13.88	...	...	″
Gt-n-propanol	$30_{13,17}-30_{12,19}$	238 243.372	289.2	11.53	...	...	″
Gt-n-propanol	$26_{6,24}-25_{3,23}$	238 348.325	161.7	16.44	...	...	ALMA; CH_3OCOH
Gt-n-propanol	$29_{13,17}-29_{12,17}$	238 438.858	275.5	11.05	...	...	ALMA; CH_3OH $v_t = 1$
Gt-n-propanol	$29_{13,16}-29_{12,17}$	238 438.858	275.5	13.19	...	...	″
Gt-n-propanol	$29_{13,17}-29_{12,18}$	238 438.859	275.5	13.19	...	...	″
Gt-n-propanol	$29_{13,16}-29_{12,18}$	238 438.859	275.5	11.05	...	...	″
Gt-n-propanol	$10_{8,3}-9_{7,2}$	238 528.368	54.5	7.53	238 528.6	1.01	ALMA
″	″	″	″	″	238 528.8	0.18	30 m
Gt-n-propanol	$10_{8,2}-9_{7,2}$	238 528.368	54.5	7.76	†		
Gt-n-propanol	$10_{8,3}-9_{7,3}$	238 528.368	54.5	7.76	†		
Gt-n-propanol	$10_{8,2}-9_{7,3}$	238 528.368	54.5	7.53	†		
Gt-n-propanol	$23_{13,11}-23_{12,11}$	239 215.407	203.2	7.87	...	...	ALMA; $CH_3{}^{18}OCOH$
Gt-n-propanol	$23_{13,10}-23_{12,11}$	239 215.407	203.2	9.01	...	...	″
Gt-n-propanol	$23_{13,11}-23_{12,12}$	239 215.407	203.2	9.01	...	...	″
Gt-n-propanol	$23_{13,10}-23_{12,12}$	239 215.407	203.2	7.87	...	...	″
Gt-n-propanol	$22_{13,10}-22_{12,10}$	239 291.987	192.7	7.29	...	...	ALMA; CH_3OCOH $v_t = 1$
Gt-n-propanol	$22_{13,9}-22_{12,10}$	239 291.987	192.7	8.29	...	...	″
Gt-n-propanol	$22_{13,10}-22_{12,11}$	239 291.987	192.7	8.29	...	...	″
Gt-n-propanol	$22_{13,9}-22_{12,11}$	239 291.987	192.7	7.29	...	...	″
Gt-n-propanol	$24_{4,21}-23_{3,20}$	239 313.697	144.1	9.74	239 313.9	0.68	ALMA; CH_3OCOH $v_t = 2$
Gt-n-propanol	$21_{13,9}-21_{12,9}$	239 356.844	182.7	6.69	239 357.4	0.26	ALMA
Gt-n-propanol	$21_{13,8}-21_{12,9}$	239 356.844	182.7	7.56	†		
Gt-n-propanol	$21_{13,9}-21_{12,10}$	239 356.844	182.7	7.56	†		
Gt-n-propanol	$21_{13,8}-21_{12,10}$	239 356.844	182.7	6.69	†		
Gt-n-propanol	$20_{13,8}-20_{12,8}$	239 411.108	173.2	6.07	239 411.6	0.65	ALMA; U-line
Gt-n-propanol	$20_{13,7}-20_{12,8}$	239 411.108	173.2	6.83	†		
Gt-n-propanol	$20_{13,8}-20_{12,9}$	239 411.108	173.2	6.83	†		
Gt-n-propanol	$20_{13,7}-20_{12,9}$	239 411.108	173.2	6.07	†		
Gt-n-propanol	$19_{13,6}-19_{12,7}$	239 455.850	164.1	6.07	...	...	ALMA; U-line
Gt-n-propanol	$19_{13,7}-19_{12,7}$	239 455.850	164.1	5.43	...	...	″
Gt-n-propanol	$19_{13,6}-19_{12,8}$	239 455.850	164.1	5.43	...	...	″
Gt-n-propanol	$19_{13,7}-19_{12,8}$	239 455.850	164.1	6.07	...	...	″
Gt-n-propanol	$18_{13,5}-18_{12,6}$	239 492.090	155.5	5.30	...	...	ALMA; CH_3OCOH
Gt-n-propanol	$18_{13,6}-18_{12,6}$	239 492.090	155.5	4.77	...	...	″
Gt-n-propanol	$18_{13,5}-18_{12,7}$	239 492.090	155.5	4.77	...	...	″
Gt-n-propanol	$18_{13,6}-18_{12,7}$	239 492.090	155.5	5.30	...	...	″
Gt-n-propanol	$17_{13,4}-17_{12,5}$	239 520.792	147.3	4.51	239 520.8	0.37	ALMA
Gt-n-propanol	$17_{13,4}-17_{12,6}$	239 520.792	147.3	4.07	†		
Gt-n-propanol	$17_{13,5}-17_{12,5}$	239 520.792	147.3	4.07	†		
Gt-n-propanol	$17_{13,5}-17_{12,6}$	239 520.792	147.3	4.51	†		

Table A.3. continued.

Species	Transition $J_{K_a,K_c} - J'_{K'_a,K'_c}$	Predicted frequency (MHz)	E_{upp} (K)	S_{ij}	Observed frequency (MHz)	T (K)	Blends/ Comments
Gt-n-propanol	$26_{3,24}$–$25_{2,23}$	239 523.360	161.7	16.45	239 523.8	0.44	ALMA
Gt-n-propanol	$16_{13,4}$–$16_{12,5}$	239 542.869	139.6	3.69	...	...	ALMA; CH_3OCOH
Gt-n-propanol	$16_{13,3}$–$16_{12,5}$	239 542.869	139.6	3.35	...	...	″
Gt-n-propanol	$16_{13,3}$–$16_{12,4}$	239 542.869	139.6	3.69	...	...	″
Gt-n-propanol	$16_{13,4}$–$16_{12,4}$	239 542.869	139.6	3.35	...	...	″
Gt-n-propanol	$28_{0,28}$–$27_{1,27}$	244 764.654	172.2	26.16	244 765.0	0.80	ALMA
″	″	″	″	″	244 765.0	0.08	30 m
Gt-n-propanol	$28_{1,28}$–$27_{1,27}$	244 764.799	172.2	27.86	†		
Gt-n-propanol	$28_{0,28}$–$27_{0,27}$	244 764.897	172.2	27.86	†		
Gt-n-propanol	$28_{1,28}$–$27_{0,27}$	244 765.042	172.2	26.16	†		
Gt-n-propanol	$25_{4,22}$–$24_{3,21}$	245 104.539	155.3	10.81	245 104.4	0.44	ALMA
Gt-n-propanol	$9_{9,1}$–$8_{8,0}$	248 228.722	57.7	8.48	248 228.5	0.14	30 m
Gt-n-propanol	$9_{9,0}$–$8_{8,0}$	248 228.722	57.7	8.52	†		
Gt-n-propanol	$9_{9,1}$–$8_{8,1}$	248 228.722	57.7	8.52	†		
Gt-n-propanol	$9_{9,0}$–$8_{8,1}$	248 228.722	57.7	8.48	†		
Gt-n-propanol	$14_{8,7}$–$13_{7,6}$	276 312.369	77.2	7.88	276 312.8	0.15	30 m
Gt-n-propanol	$14_{8,6}$–$13_{7,6}$	276 312.370	77.2	8.60	†		
Gt-n-propanol	$14_{8,7}$–$13_{7,7}$	276 312.417	77.2	8.60	†		
Gt-n-propanol	$14_{8,6}$–$13_{7,7}$	276 312.419	77.2	7.88	†		
Gt-n-propanol	$10_{10,1}$–$9_{9,0}$	276 842.794	71.0	9.48	276 842.8	0.10	30 m
Gt-n-propanol	$10_{10,0}$–$9_{9,0}$	276 842.794	71.0	9.52	†		
Gt-n-propanol	$10_{10,1}$–$9_{9,1}$	276 842.794	71.0	9.52	†		
Gt-n-propanol	$10_{10,0}$–$9_{9,1}$	276 842.794	71.0	9.48	†		
Gt-n-propanol	$13_{9,5}$–$12_{8,4}$	286 069.306	78.6	8.66	286 069.5	0.10	30 m
Gt-n-propanol	$13_{9,4}$–$12_{8,4}$	286 069.306	78.6	9.10	†		
Gt-n-propanol	$13_{9,5}$–$12_{8,5}$	286 069.306	78.6	9.10	†		
Gt-n-propanol	$13_{9,4}$–$12_{8,5}$	286 069.306	78.6	8.66	†		

Apéndice E

Lopez et al. 2017, en preparación

Table B.2. Lines of A-CH_3OCOH and E-CH_3OCOH in its ground state (v_t=0).

Torsional substate	Transition $J_{K_a,K_c} - J'_{K'_a,K'_c}$	Predicted frequency (MHz)	E_{upp} (K)	S_{ij}	Observed frequency (MHz)	T_{MB} (K)	Blends
E	$13_{2,11}$-$13_{1,12}$	81167.785	57.9	6.27	81167.6	0.25	
A	$13_{2,11}$-$13_{1,12}$	81217.801	58.5	6.26	81217.6	0.25	
E	$16_{3,13}$-$16_{2,14}$	81314.214	88.7	10.01	81314.3	0.33	
A	$16_{3,13}$-$16_{2,14}$	81362.350	88.7	10.02	81362.3	0.32	
A	$3_{2,1}$-$2_{1,2}$	81392.257	6.2	1.38	81392.3	0.16	
E	$7_{1,7}$-$6_{0,6}$	82242.986	15.3	5.31	82242.9	0.37	
A	$7_{1,7}$-$6_{0,6}$	82244.451	15.8	5.31	82244.5†	0.31	
E	$10_{3,8}$-$10_{2,9}$	83605.170	37.9	4.97	83605.0	0.28	
A	$10_{3,8}$-$10_{2,9}$	83638.429	38.5	4.98	83638.6	0.30	
A	$4_{2,3}$-$3_{1,2}$	85655.780	8.5	1.90	85655.6	0.30	
A	$21_{5,16}$-$21_{4,17}$	85773.401	155.8	16.88	85773.6	0.24	
E	$20_{5,15}$-$20_{4,16}$	85780.681	142.2	15.72	85780.8	0.24	
A	$20_{5,15}$-$20_{4,16}$	85785.346	142.8	15.76	85785.3	0.24	
E	$7_{6,1}$-$6_{6,0}$	85919.210	39.8	1.86	85919.0	0.49	
E	$7_{6,2}$-$6_{6,1}$	85926.564	39.8	1.86	85926.6	1.47	NH_2D
A	$7_{6,2}$-$6_{6,1}$	85927.206	40.4	1.86	85927.2†	1.48	”
A	$7_{6,1}$-$6_{6,0}$	85927.213	40.4	1.86	85927.2†	”	”
E	$7_{5,2}$-$6_{5,1}$	86021.126	32.5	3.43	86021.0	0.78	
E	$7_{5,3}$-$6_{5,2}$	86027.734	32.5	3.43	86027.6	0.78	
A	$7_{5,3}$-$6_{5,2}$	86029.413	33.1	3.43	86029.2†	0.89	
A	$7_{5,2}$-$6_{5,1}$	86029.413	33.1	3.43	86029.8†	”	
A	$7_{4,4}$-$6_{4,3}$	86210.037	27.2	4.72	86210.0	1.10	
E	$7_{4,3}$-$6_{4,2}$	86223.658	26.6	4.69	86223.9	1.49	
E	$7_{4,4}$-$6_{4,3}$	86224.171	26.6	4.69	” †	”	
A	$7_{4,3}$-$6_{4,2}$	86250.535	27.2	4.72	...	...	SiO
A	$7_{3,5}$-$6_{3,4}$	86265.778	22.5	5.71	86265.6	1.24	
E	$7_{3,5}$-$6_{3,4}$	86268.746	21.9	5.66	86268.8	1.24	
E	$8_{0,8}$-$7_{1,7}$	87766.385	19.5	6.23	87766.6	0.34	
A	$8_{0,8}$-$7_{1,7}$	87769.016	20.1	6.23	87769.1	0.37	
E	$19_{5,14}$-$19_{4,15}$	88053.982	129.8	14.31	88054.3	0.38	
A	$19_{5,14}$-$19_{4,15}$	88054.464	130.4	14.35	” †	”	
A	$19_{5,15}$-$18_{6,12}$	88261.893	129.6	2.19	88261.6	0.08	U-line
E	$22_{5,17}$-$22_{4,18}$	88337.815	168.9	17.49	88337.8	0.22	
A	$22_{5,17}$-$22_{4,18}$	88358.486	169.5	17.54	88358.3	0.25	
A	$18_{4,15}$-$17_{5,12}$	88457.999	112.1	1.75	88457.9	0.04	
E	$11_{3,9}$-$11_{2,10}$	88686.893	44.4	5.28	88686.9	0.28	
A	$11_{3,9}$-$11_{2,10}$	88723.264	45.0	5.28	88723.0	0.37	$^{34}SO_2$
E	$7_{1,6}$-$6_{1,5}$	88843.193	17.4	6.79	88843.3	1.65	
A	$7_{1,6}$-$6_{1,5}$	88851.586	17.9	6.79	88851.5	1.66	
E	$8_{1,8}$-$7_{1,7}$	89314.662	19.5	7.84	89314.6	1.83	
A	$8_{1,8}$-$7_{1,7}$	89316.623	20.1	7.84	89316.8	1.96	
A	$9_{4,5}$-$9_{3,6}$	91356.759	37.2	4.80	91356.6	0.30	
E	$9_{4,5}$-$9_{3,6}$	91366.496	36.7	4.51	91366.6	0.28	
E	$14_{2,12}$-$14_{2,13}$	91381.757	66.4	2.89	91381.6	0.14	
E	$8_{1,8}$-$7_{0,7}$	91775.938	19.5	6.31	91775.9	0.51	
E	$20_{4,16}$-$20_{3,17}$	91776.877	138.1	13.68	91777.2†	0.62	
A	$8_{1,8}$-$7_{0,7}$	91777.210	20.1	6.31	” †	”	
A	$20_{4,16}$-$20_{3,17}$	91825.245	138.7	13.71	91825.2	0.31	
E	$21_{4,17}$-$21_{4,18}$	92419.207	151.1	5.18	92419.0	0.17	
A	$13_{3,10}$-$12_{4,9}$	92470.051	61.3	1.94	92469.9	0.14	
E	$17_{3,14}$-$17_{2,15}$	92884.234	99.1	9.65	92884.0	0.35	
A	$17_{3,14}$-$17_{2,15}$	92940.325	99.7	9.66	92940.2	0.36	
E	$12_{3,10}$-$12_{2,11}$	94626.869	51.4	5.50	94626.9	0.32	
E	$5_{2,4}$-$4_{1,3}$	94632.707	10.9	2.20	94632.6	0.24	
A	$5_{2,4}$-$4_{1,3}$	94647.292	11.4	2.20	94647.4	0.22	
A	$12_{3,10}$-$12_{2,11}$	94666.958	52.0	5.50	94666.8	0.28	
A	$11_{3,9}$-$11_{1,10}$	95363.816	45.0	0.30	95363.6	0.15	
E	$29_{6,23}$-$29_{6,24}$	95655.473	207.3	7.48	95655.3	0.06	
A	$21_{6,15}$-$20_{7,14}$	95790.395	161.6	2.45	95790.7	0.05	
E	$11_{2,10}$-$11_{1,11}$	96059.043	40.1	2.93	96059.9	0.22	
E	$8_{2,7}$-$7_{2,6}$	96070.730	23.0	7.46	96070.7	1.50	
A	$8_{2,7}$-$7_{2,6}$	96076.825	23.6	7.46	96076.7	1.74	
A	$6_{4,2}$-$6_{3,3}$	96086.687	23.0	2.54	96086.7	0.22	
A	$11_{2,10}$-$11_{1,11}$	96107.162	40.7	2.93	96107.3	0.20	
A	$6_{4,3}$-$6_{3,4}$	96693.544	23.0	2.53	96693.3	0.22	
A	$8_{4,5}$-$8_{3,6}$	96709.252	31.9	3.97	96709.1	0.30	

Table B.2. continued.

Torsional substate	Transition $J_{K_a,K_c} - J'_{K'_a,K'_c}$	Predicted frequency (MHz)	E_{upp} (K)	S_{ij}	Observed frequency (MHz)	T_{MB} (K)	Blends
A	$4_{4,0}$-$4_{3,1}$	96835.291	16.5	0.96	96835.3	0.10	
A	$4_{4,1}$-$4_{3,2}$	96888.039	16.5	0.96	96888.0	0.11	
E	$9_{4,6}$-$9_{3,7}$	96956.753	36.6	4.38	96956.5	0.30	
A	$9_{4,6}$-$9_{3,7}$	97018.123	37.2	4.66	97018.2	0.30	
E	$17_{5,12}$-$17_{4,13}$	97199.123	107.2	11.34	97199.0	0.58	
A	$17_{5,12}$-$17_{4,13}$	97199.227	107.8	11.36	” †	”	
A	$4_{2,2}$-$3_{1,3}$	97339.228	8.6	1.28	97339.5	0.13	
E	$10_{4,7}$-$10_{3,8}$	97651.300	42.6	5.27	97651.0	0.41	
E	$8_{6,2}$-$7_{6,1}$	98270.501	44.5	3.50	98270.4	0.94	
E	$8_{6,3}$-$7_{6,2}$	98278.931	44.5	3.50	98279.3	1.71	
A	$8_{6,3}$-$7_{6,2}$	98279.723	45.1	3.50	” †	”	
A	$8_{6,2}$-$7_{6,1}$	98279.764	45.1	3.50	” †	”	
E	$9_{0,9}$-$8_{1,8}$	99133.271	24.3	7.28	99133.3	0.52	
A	$9_{0,9}$-$8_{1,8}$	99135.743	24.9	7.29	99135.5	0.52	
A	$12_{4,9}$-$12_{3,10}$	100693.124	56.8	6.57	100693.3	0.37	
A	$12_{1,11}$-$12_{0,12}$	100790.683	47.3	2.98	100791.0	0.22	
E	$9_{1,9}$-$8_{0,8}$	101626.886	24.4	7.32	101626.9	0.57	
A	$9_{1,9}$-$8_{0,8}$	101628.130	24.9	7.32	101628.2†	0.55	
E	$8_{2,6}$-$7_{2,5}$	103466.577	24.0	7.52	103466.3	2.04	
A	$8_{2,6}$-$7_{2,5}$	103478.642	24.6	7.52	103478.6	2.06	
E	$15_{2,13}$-$15_{1,14}$	105363.731	75.3	6.02	105363.6	0.34	
E	$9_{2,8}$-$8_{2,7}$	107537.264	28.2	8.50	107537.0	2.75	
A	$9_{2,8}$-$8_{2,7}$	107543.693	28.8	8.50	107543.9	3.76	CH_3CH_2CN
E	$10_{0,10}$-$9_{1,9}$	110224.568	29.6	8.31	110224.6	0.80	
A	$10_{0,10}$-$9_{1,9}$	110226.840	30.2	8.32	110226.8	0.85	
E	$9_{5,4}$-$8_{5,3}$	110873.957	42.6	6.22	110873.9	1.89	
E	$9_{3,7}$-$8_{3,6}$	110879.772	32.0	7.99	110879.9	2.92	
A	$9_{5,5}$-$8_{5,4}$	110880.432	43.2	6.23	” †	”	
E	$9_{5,5}$-$8_{5,4}$	110882.343	42.6	6.22	110882.5	2.01	
A	$9_{3,7}$-$8_{3,6}$	110887.076	32.6	7.99	110887.2	2.33	
A	$9_{5,4}$-$8_{5,3}$	110890.242	43.2	6.23	110890.4	1.81	
E	$10_{1,10}$-$9_{0,9}$	111734.006	29.7	8.33	111734.0	0.70	
A	$10_{1,10}$-$9_{0,9}$	111735.294	30.3	8.34	111735.2†	0.71	
A	$22_{6,16}$-$22_{5,17}$	113299.506	175.0	15.13	113299.6	0.36	
E	$22_{6,16}$-$22_{5,17}$	113313.643	174.4	15.08	113313.5	0.31	
E	$9_{3,6}$-$8_{3,5}$	113743.115	32.3	8.00	113743.0	2.45	
A	$9_{3,6}$-$8_{3,5}$	113756.595	32.9	8.00	113756.6	2.31	
A	$13_{2,12}$-$13_{1,13}$	114265.779	54.8	2.97	114265.9	0.26	
E	$11_{2,10}$-$10_{2,9}$	130010.109	40.1	10.55	130010.3	3.00	
A	$11_{2,10}$-$10_{2,9}$	130016.780	40.7	10.54	130016.9	3.06	
A	$27_{5,22}$-$27_{5,23}$	130475.886	247.3	1.05	130475.9	0.09	
A	$20_{3,17}$-$20_{2,18}$	131480.692	134.3	9.08	131480.7	0.29	
E	$12_{0,12}$-$11_{1,11}$	131914.521	41.8	10.33	131914.4	0.78	
A	$12_{0,12}$-$11_{1,11}$	131916.426	42.4	10.37	131916.3†	0.74	
A	$19_{6,13}$-$19_{5,14}$	132242.429	136.8	11.29	132245.0	3.01	
E	$19_{6,13}$-$19_{5,14}$	132244.196	136.2	11.25	132246.9	3.21	
E	$12_{0,12}$-$11_{0,11}$	132245.126	41.8	11.85	” †	”	
A	$12_{0,12}$-$11_{0,11}$	132246.725	42.4	11.84	” †	”	
E	$19_{5,15}$-$19_{4,16}$	132503.096	129.0	10.62	132503.0	0.41	
E	$23_{6,17}$-$22_{7,16}$	132537.765	188.4	2.77	132537.1	0.37	
A	$19_{5,15}$-$19_{4,16}$	132537.121	129.6	10.65	” †	”	
A	$17_{3,15}$-$17_{2,16}$	134559.514	95.6	5.93	134560.5	0.50	
E	$11_{9,2}$-$10_{9,1}$	135046.508	92.1	3.64	135046.5	0.80	
A	$11_{9,3}$-$10_{9,2}$	135054.927	92.7	3.64	135054.8	1.28	
A	$11_{9,2}$-$10_{9,1}$	135054.927	92.7	3.64	” †	”	
E	$11_{9,3}$-$10_{9,2}$	135060.089	92.1	3.64	135060.1	1.20	CH_3CH_2CN v_{13}/v_{21}
E	$11_{3,9}$-$10_{3,8}$	135091.833	44.4	10.16	135091.8	2.10	
A	$11_{3,9}$-$10_{3,8}$	135101.615	45.0	10.15	135101.5	2.10	
E	$11_{8,3}$-$10_{8,2}$	135143.065	80.8	5.18	135143.0	1.10	
A	$11_{8,4}$-$10_{8,3}$	135153.250	81.4	5.19	135153.4	1.65	
A	$11_{8,3}$-$10_{8,2}$	135153.250	81.4	5.19	” †	”	
E	$11_{8,4}$-$10_{8,3}$	135156.261	80.8	5.18	135156.3	1.14	
E	$11_{4,8}$-$10_{4,7}$	136280.063	49.1	9.51	136280.0	2.02	
A	$11_{4,8}$-$10_{4,7}$	136282.586	49.7	9.55	136282.2	2.02	
E	$19_{4,16}$-$19_{3,17}$	136662.174	122.7	8.76	136662.1	0.39	
E	$11_{4,7}$-$10_{4,6}$	137293.189	49.2	9.51	137293.3	1.90	

Table B.2. continued.

Torsional substate	Transition $J_{K_a,K_c} - J'_{K'_a,K'_c}$	Predicted frequency (MHz)	E_{upp} (K)	S_{ij}	Observed frequency (MHz)	T_{MB} (K)	Blends
E	$18_{6,12}$-$18_{5,13}$	137308.136	124.8	10.25	137308.4	0.59	
A	$18_{6,12}$-$18_{5,13}$	137308.623	125.4	10.34	” †	”	
A	$11_{4,7}$-$10_{4,6}$	137313.323	49.8	9.55	137313.2	1.98	
E	$11_{2,10}$-$10_{1,9}$	139565.913	40.1	6.02	139565.9	0.72	
A	$11_{2,10}$-$10_{1,9}$	139569.278	40.7	6.03	139569.4	0.81	
E	$6_{3,4}$-$5_{2,3}$	139834.615	17.8	2.61	139834.8	0.48	
E	$24_{4,20}$-$24_{4,21}$	140113.390	193.4	5.11	140113.3	0.20	
A	$18_{2,16}$-$18_{1,17}$	140118.559	105.7	5.97	140118.7	0.43	
E	$12_{2,11}$-$11_{2,10}$	141037.704	46.9	12.85	141037.3	3.53	
A	$12_{2,11}$-$11_{2,10}$	141044.345	47.5	11.55	141044.3	3.53	
A	$16_{1,15}$-$16_{0,16}$	142229.130	79.7	3.00	142229.3	0.29	
E	$13_{0,13}$-$12_{1,12}$	142624.486	48.7	11.33	142624.4	1.56	
A	$13_{0,13}$-$12_{1,12}$	142626.247	49.3	11.38	142626.3†	1.42	
E	$13_{1,13}$-$12_{1,12}$	142733.520	48.7	12.85	142733.5	4.28	
A	$13_{1,13}$-$12_{1,12}$	142735.139	49.3	12.84	142734.8	4.52	
E	$12_{1,11}$-$11_{1,10}$	143234.203	46.7	11.61	143234.4	3.84	
A	$12_{1,11}$-$11_{1,10}$	143240.499	47.3	11.61	143240.4	3.84	
E	$6_{3,3}$-$5_{2,4}$	145038.618	17.8	2.46	145038.6	0.49	
A	$6_{3,3}$-$5_{2,2}$	145051.762	18.4	2.54	145051.9	0.42	
A	$18_{6,13}$-$18_{5,14}$	147280.989	125.3	10.10	147280.9	0.47	
E	$19_{6,14}$-$19_{5,15}$	147304.797	136.1	10.79	147304.6	0.39	
E	$12_{10,2}$-$11_{10,1}$	147310.574	111.8	3.67	147310.6	0.75	
A	$12_{10,3}$-$11_{10,2}$	147317.738	112.4	3.67	147317.9	1.34	
A	$12_{10,3}$-$11_{10,2}$	147317.738	112.4	3.67	” †	”	
E	$12_{10,3}$-$11_{10,2}$	147325.405	111.8	3.67	147325.2	1.09	
A	$19_{6,14}$-$19_{5,15}$	147331.633	136.7	10.83	147331.5	0.92	
E	$12_{4,9}$-$11_{4,8}$	148797.792	56.3	10.66	148797.8	2.35	
A	$12_{4,9}$-$11_{4,8}$	148805.936	56.8	10.66	148806.0	2.24	
A	$13_{6,8}$-$13_{5,9}$	150070.106	77.7	6.39	150070.3	0.44	
E	$12_{6,6}$-$12_{5,7}$	150449.243	69.4	4.95	150449.3	0.35	
E	$9_{6,3}$-$9_{5,4}$	151765.582	49.9	3.45	151765.6	0.38	
A	$9_{6,3}$-$9_{5,4}$	151777.073	50.4	3.45	151777.0	0.37	
A	$9_{6,4}$-$9_{5,5}$	151790.609	50.4	3.45	151790.8	0.46	
E	$14_{1,14}$-$13_{1,13}$	153350.456	56.0	13.85	153350.6	2.99	
A	$19_{3,17}$-$19_{2,18}$	153353.607	116.7	5.96	153351.9†	3.18	
A	$24_{6,18}$-$23_{7,17}$	153354.019	203.8	3.04	” †	”	
E	$13_{2,12}$-$12_{1,11}$	156397.528	54.2	8.02	156397.6	1.00	
A	$13_{2,12}$-$12_{1,11}$	156401.008	54.8	8.05	156401.1	1.00	
E	$8_{3,6}$-$7_{2,5}$	157862.660	26.7	2.94	157862.7	0.58	
A	$8_{3,6}$-$7_{2,5}$	157886.961	27.2	2.95	157886.9	0.59	
A	$5_{4,2}$-$4_{3,1}$	158241.019	19.5	3.49	158241.0	0.67	
E	$13_{3,11}$-$12_{3,10}$	158693.703	59.0	12.25	158693.8	4.90	
A	$13_{3,11}$-$12_{3,10}$	158704.394	59.6	12.25	158704.5	4.21	
E	$13_{10,3}$-$12_{10,2}$	159654.887	119.4	5.31	159654.9	1.69	
A	$13_{10,4}$-$12_{10,3}$	159662.762	120.0	5.31	159662.8	2.77	
A	$13_{10,3}$-$12_{10,2}$	159662.762	120.0	5.31	” †	”	
E	$13_{10,4}$-$12_{10,3}$	159670.881	119.4	5.31	159671.0	2.01	E-CH_3OCOH v_t=1
E	$13_{7,6}$-$12_{7,5}$	160178.907	85.7	9.24	160178.9	3.03	
E	$13_{7,7}$-$12_{7,6}$	160193.649	85.6	9.24	160193.3	5.53	
A	$13_{7,7}$-$12_{7,6}$	160192.867	86.2	9.24	” †	”	
A	$13_{7,6}$-$12_{7,5}$	160193.385	86.2	9.24	” †	”	
E	$15_{0,15}$-$14_{1,14}$	163925.811	63.9	13.32	163925.6	2.45	
A	$15_{0,15}$-$14_{1,14}$	163927.353	64.5	13.40	” †	”	
E	$15_{1,15}$-$14_{1,14}$	163960.366	63.9	14.86	163960.8	7.44	
A	$15_{1,15}$-$14_{1,14}$	163961.849	64.5	14.84	” †	”	
E	$15_{0,15}$-$14_{0,14}$	163987.449	63.9	14.86	163988.0	7.44	
A	$15_{0,15}$-$14_{0,14}$	163988.898	64.5	14.84	” †	”	
E	$13_{2,11}$-$12_{2,10}$	164955.701	57.9	12.55	164955.6	4.87	
A	$13_{2,11}$-$12_{2,10}$	164968.626	58.5	12.55	164968.3	4.17	
E	$14_{2,13}$-$13_{1,12}$	165653.645	62.0	9.05	165653.6	0.97	
A	$14_{2,13}$-$13_{1,12}$	165657.558	62.6	9.09	165657.4	0.97	
A	$23_{3,20}$-$23_{3,21}$	167381.088	173.2	0.75	167381.3	0.22	
E	$14_{13,1}$-$13_{13,0}$	171794.234	173.5	1.93	171794.3	0.93	
A	$14_{13,1}$-$13_{13,0}$	171794.545	174.1	1.93	” †	”	
A	$14_{13,2}$-$13_{13,1}$	171794.545	174.1	1.93	” †	”	
A	$10_{3,8}$-$9_{2,7}$	171797.885	38.5	3.43	171798.1	0.59	

Table B.2. continued.

Torsional substate	Transition $J_{K_a,K_c} - J'_{K'_a,K'_c}$	Predicted frequency (MHz)	E_{upp} (K)	S_{ij}	Observed frequency (MHz)	T_{MB} (K)	Blends
E	$14_{13,2}$-$13_{13,1}$	171809.143	173.5	1.93	171809.2	0.46	CH_2CHCN
E	$14_{8,6}$-$13_{8,5}$	172364.349	103.8	9.44	172364.3	3.09	
A	$14_{8,7}$-$13_{8,6}$	172377.704	104.4	9.44	172377.9	4.58	
A	$14_{8,6}$-$13_{8,5}$	172377.704	104.4	9.44	” †	”	
E	$14_{8,7}$-$13_{8,6}$	172380.938	103.8	9.44	172380.7	3.44	
E	$15_{1,14}$-$14_{2,13}$	172385.791	70.3	10.05	172385.5	1.24	
A	$15_{1,14}$-$14_{2,13}$	172393.503	70.8	10.11	172393.4	2.26	A-CH_3OCOH v_t=1
A	$14_{6,9}$-$13_{6,8}$	173180.999	86.0	11.44	173180.8	2.35	
E	$14_{6,8}$-$13_{6,7}$	173185.193	85.4	11.39	173185.2	2.63	A-CH_3OCOH v_t=1
E	$14_{6,9}$-$13_{6,8}$	173194.272	85.4	11.39	173194.4	3.16	
A	$14_{6,8}$-$13_{6,7}$	173218.678	86.0	11.44	173218.8	2.43	
E	$15_{2,14}$-$14_{2,13}$	173515.402	70.3	14.57	173515.2	4.05	
A	$15_{2,14}$-$14_{2,13}$	173521.699	70.9	14.56	...	...	CH_3CHO
E	$14_{4,11}$-$13_{4,10}$	173637.672	72.3	12.85	173637.6	3.68	A-CH_3OCOH v_t=1
A	$14_{4,11}$-$13_{4,10}$	173650.125	72.9	12.84	173649.9	3.27	
E	$15_{1,14}$-$14_{1,13}$	174209.781	70.3	14.58	174209.6	4.41	CH_3CHO v_t=2
A	$15_{1,14}$-$14_{1,13}$	174215.560	70.8	11.44	174215.6	4.29	
A	$27_{6,22}$-$27_{5,23}$	174217.996	249.4	14.66	” †	”	
E	$14_{5,9}$-$13_{5,8}$	174377.400	78.3	12.07	174377.3	3.16	
A	$14_{5,9}$-$13_{5,8}$	174406.175	78.9	12.22	174406.4	3.32	
E	$14_{2,12}$-$13_{2,11}$	175867.617	66.4	13.50	175867.9	2.63	
A	$14_{2,12}$-$13_{2,11}$	175879.446	67.0	13.50	175879.3	3.08	
E	$17_{7,11}$-$17_{6,12}$	175882.512	122.4	6.39	... †	...	
A	$17_{7,17}$-$17_{6,12}$	176009.688	123.0	8.69	176009.5	0.76	
A	$15_{7,9}$-$15_{6,10}$	177526.689	103.4	7.22	177526.6	0.92	
E	$16_{5,11}$-$15_{5,10}$	200936.146	96.9	14.44	200936.0	10.36	
A	$16_{5,11}$-$15_{5,10}$	200956.376	97.5	14.44	200956.2	10.60	
E	$17_{3,15}$-$16_{3,14}$	203853.722	95.0	16.32	203853.6	11.93	
A	$17_{3,15}$-$16_{3,14}$	203864.193	95.6	16.30	203864.0	11.93	
E	$18_{1,17}$-$17_{2,16}$	205250.777	98.4	13.10	205250.6	3.72	
A	$18_{1,17}$-$17_{2,16}$	205257.161	98.9	13.22	205257.2	3.60	
E	$19_{0,19}$-$18_{1,18}$	206364.154	100.5	17.23	206364.3	6.86	
A	$19_{0,19}$-$18_{1,18}$	206365.396	101.1	17.42	206365.5†	8.08	
E	$19_{1,19}$-$18_{1,18}$	206367.361	100.5	18.88	206367.4†	16.48	
A	$19_{1,19}$-$18_{1,18}$	206368.594	101.1	18.84	206368.4†	17.25	
E	$19_{0,19}$-$18_{0,18}$	206370.009	100.5	18.88	206370.0†	17.71	
A	$19_{0,19}$-$18_{0,18}$	206371.237	101.1	18.84	206370.9†	16.33	
E	$19_{1,19}$-$18_{0,18}$	206373.215	100.5	17.23	206373.1†	9.15	
A	$19_{1,19}$-$18_{0,18}$	206374.435	101.1	17.42	206374.1†	7.77	
E	$11_{8,3}$-$11_{7,4}$	207234.806	80.8	3.58	207234.9	1.76	
E	$17_{13,5}$-$16_{13,4}$	208804.575	201.7	7.06	208804.6	3.79	
E	$17_{7,10}$-$16_{7,9}$	210434.475	122.4	14.11	210434.3	9.63	
A	$17_{7,11}$-$16_{7,10}$	210442.753	123.0	14.13	210442.5	9.63	
E	$17_{7,11}$-$16_{7,10}$	210451.372	122.4	14.11	210451.4	9.39	
E	$7_{5,2}$-$6_{4,2}$	210456.755	32.5	4.53	210456.7	2.99	
A	$17_{7,10}$-$16_{7,9}$	210463.197	123.0	14.13	210463.1	9.51	
A	$7_{5,3}$-$6_{4,2}$	210467.102	33.1	4.53	210467.2	3.96	
A	$17_{6,12}$-$16_{6,11}$	211255.027	114.6	14.89	211255.0	9.87	
E	$17_{6,12}$-$16_{6,11}$	211266.039	114.0	14.50	211266.0	9.63	
E	$17_{6,11}$-$16_{6,10}$	211537.299	114.0	14.50	211537.0	9.63	
A	$17_{6,11}$-$16_{6,10}$	211575.108	114.6	14.89	211574.9	11.56	
A	$19_{3,16}$-$18_{4,15}$	212473.089	122.3	6.38	212473.0	1.91	g−CH_3CH_2OH
A	$17_{5,12}$-$16_{5,11}$	214652.625	107.8	15.54	214652.6	10.84	
E	$19_{1,18}$-$18_{2,17}$	215965.938	108.7	14.09	215965.9	5.41	CH_3CH_2CN
A	$19_{1,18}$-$18_{2,17}$	215972.062	109.3	14.24	215971.9	4.92	
E	$19_{1,18}$-$18_{1,17}$	216210.862	108.7	18.58	216210.9	11.56	
A	$19_{1,18}$-$18_{1,17}$	216216.524	109.3	18.55	216216.6	11.44	
E	$17_{4,13}$-$16_{4,12}$	220166.852	102.6	16.14	220166.9	11.32	
A	$17_{4,13}$-$16_{4,12}$	220190.267	103.1	16.14	220190.3	10.96	
A	$18_{16,3}$-$17_{16,2}$	220926.304	270.7	3.78	220926.3	2.55	
A	$18_{16,2}$-$17_{16,1}$	220926.304	270.7	3.78	” †	”	
E	$18_{16,2}$-$17_{16,1}$	220935.480	270.1	10.04	220935.3	1.58	
E	$18_{10,8}$-$17_{10,7}$	221649.374	166.7	12.46	221649.3	7.13	
E	$18_{4,15}$-$17_{4,14}$	221660.479	111.5	17.04	221660.7	14.40	
A	$18_{10,9}$-$17_{10,8}$	221661.112	167.3	12.45	” †	”	
A	$18_{10,8}$-$17_{10,7}$	221661.114	167.3	12.45	” †	”	

Table B.2. continued.

Torsional substate	Transition $J_{K_a,K_c} - J'_{K'_a,K'_c}$	Predicted frequency (MHz)	E_{upp} (K)	S_{ij}	Observed frequency (MHz)	T_{MB} (K)	Blends
E	$18_{10,9}$-$17_{10,8}$	221670.738	166.7	12.46	221670.8	7.44	
A	$18_{4,15}$-$17_{4,14}$	221674.677	112.1	17.03	221674.6	11.18	
A	$18_{8,11}$-$17_{8,10}$	222438.272	143.5	14.45	222438.3	9.54	
A	$18_{8,10}$-$17_{8,9}$	222440.383	143.5	14.45	222440.5†	10.31	
E	$18_{8,11}$-$17_{8,10}$	222442.053	142.9	14.46	222441.8†	9.92	
E	$19_{2,17}$-$18_{3,16}$	223037.864	116.0	10.60	223037.9	3.51	
A	$19_{2,17}$-$18_{3,16}$	223051.784	116.0	10.70	223051.7	2.90	
A	$18_{7,12}$-$17_{7,11}$	223119.254	133.7	15.29	223119.3	9.38	
E	$18_{7,11}$-$17_{7,10}$	223125.041	133.1	15.18	223125.0	9.09	
E	$18_{7,12}$-$17_{7,11}$	223134.996	133.1	15.18	223134.8	9.36	
E	$18_{6,12}$-$17_{6,11}$	224582.321	124.8	15.89	224582.3	10.12	
A	$26_{9,17}$-$26_{8,18}$	224600.055	261.7	14.15	224600.0	1.57	
A	$18_{6,12}$-$17_{6,11}$	224609.370	125.4	16.01	224609.2	10.31	
E	$26_{9,17}$-$26_{8,18}$	224618.955	261.1	12.15	224618.7	1.28	
E	$19_{3,17}$-$18_{3,16}$	225608.790	116.1	18.33	225609.1	12.38	
A	$19_{3,17}$-$18_{3,16}$	225618.728	116.7	18.30	225618.6	11.86	
A	$6_{6,1}$-$5_{5,0}$	225928.585	36.3	5.47	225928.6	5.09	
A	$6_{6,0}$-$5_{5,1}$	225928.599	36.3	5.47	” †	”	
E	$20_{1,19}$-$19_{1,18}$	226773.161	119.6	19.58	226773.0	12.03	
A	$20_{1,19}$-$19_{1,18}$	226778.781	120.2	19.55	226778.7	12.48	
E	$19_{2,17}$-$18_{2,16}$	227019.519	116.0	18.35	227019.3	13.11	
A	$19_{2,17}$-$18_{2,16}$	227028.120	116.6	18.32	227027.8	14.01	
A	$24_{9,16}$-$24_{8,17}$	228270.484	231.3	12.59	228270.3	1.62	
A	$23_{9,14}$-$23_{8,15}$	229224.187	217.0	11.83	229224.3	1.50	
E	$18_{3,15}$-$17_{3,14}$	229404.993	110.1	17.35	229404.9	14.52	
A	$18_{3,15}$-$17_{3,14}$	229420.352	110.7	17.34	229420.4	12.34	
E	$12_{4,9}$-$11_{3,8}$	231019.016	56.3	3.89	231019.0	2.43	
A	$29_{3,26}$-$29_{2,27}$	231020.262	264.2	8.99	” †	”	
A	$21_{9,12}$-$21_{8,13}$	231199.324	190.3	10.34	231199.3	2.40	
E	$21_{9,12}$-$21_{8,13}$	231200.172	189.7	10.23	231199.9†	2.25	
A	$27_{3,25}$-$27_{2,26}$	231658.051	221.7	6.00	231658.1	1.03	
A	$27_{3,25}$-$27_{1,26}$	231659.626	221.7	0.58	” †	”	
E	$20_{9,12}$-$20_{8,13}$	231938.642	177.2	9.58	231938.6	2.13	
E	$20_{9,11}$-$20_{8,12}$	231955.204	177.2	9.57	231955.1	2.79	CH_2CHCN
A	$20_{9,11}$-$20_{8,12}$	231966.969	177.8	9.61	231967.1	2.13	CH_3CHO
A	$20_{9,12}$-$20_{8,13}$	231985.319	177.8	9.61	...	...	CH_3OCH_3
E	$19_{9,11}$-$19_{8,12}$	232579.367	165.4	8.86	232579.3	1.81	
E	$19_{9,10}$-$19_{8,11}$	232597.251	165.4	8.86	232597.3	2.16	
A	$19_{9,10}$-$19_{8,11}$	232617.198	166.0	8.87	232617.2	1.72	
A	$19_{9,11}$-$19_{8,12}$	232625.258	166.0	8.87	232625.5	2.08	CH_3OH
A	$19_{16,3}$-$18_{16,2}$	233246.736	281.9	5.53	233246.6	3.35	
A	$19_{16,4}$-$18_{16,3}$	233246.736	281.9	5.53	” †	”	
E	$19_{16,3}$-$18_{16,2}$	233256.045	281.2	5.52	233255.8	2.60	CH_3OCH_3
E	$19_{16,4}$-$18_{16,3}$	233268.622	281.2	5.52	233268.4	2.40	CH_3CH_2CN v_{20}=1
A	$17_{9,8}$-$17_{8,9}$	233627.125	144.1	7.41	233627.3	4.70	E-CH_3COCH_3 v_t=1
A	$17_{9,9}$-$17_{8,10}$	233627.125	144.1	7.41	” †	”	”
E	$19_{9,10}$-$18_{9,9}$	234486.458	165.4	14.75	234486.3	8.24	
A	$19_{9,11}$-$18_{8,10}$	234502.261	166.0	14.75	234502.1	11.20	
A	$19_{9,11}$-$18_{8,10}$	234502.261	166.0	14.75	” †	”	
E	$19_{9,11}$-$18_{9,10}$	234508.612	165.4	14.76	234508.7	8.11	
E	$9_{5,4}$-$8_{4,4}$	234783.353	42.6	4.23	234783.3	3.89	
E	$9_{5,5}$-$8_{4,5}$	234784.000	42.6	4.23	234783.9†	3.64	
A	$19_{8,12}$-$18_{8,11}$	235046.513	154.8	15.64	235046.4	9.14	
E	$11_{9,2}$-$11_{8,3}$	235047.845	92.1	2.81	” †	”	
E	$19_{8,12}$-$18_{8,11}$	235051.353	154.2	15.65	235051.4	12.59	
A	$19_{8,11}$-$18_{8,10}$	235051.409	154.8	15.64	” †	”	
E	$19_{5,15}$-$18_{5,14}$	236743.666	129.0	17.68	236743.6	10.40	
A	$19_{5,15}$-$18_{5,14}$	236759.687	129.6	17.67	236759.4	10.15	
E	$20_{2,18}$-$19_{2,17}$	237297.479	127.4	19.34	237297.3	10.92	
A	$20_{2,18}$-$19_{2,17}$	237306.044	128.0	19.31	237306.1	11.05	
E	$21_{2,20}$-$20_{2,19}$	237309.514	131.0	20.59	237309.3	11.31	
A	$21_{2,20}$-$20_{2,19}$	237315.155	131.6	20.55	237315.0	10.92	
A	$13_{4,10}$-$12_{3,9}$	237317.043	64.6	4.03	” †	”	
E	$19_{6,13}$-$18_{6,12}$	237807.605	136.2	17.10	237807.3	11.05	
A	$19_{6,13}$-$18_{6,12}$	237829.835	136.8	17.12	237829.7	11.31	
E	$20_{3,18}$-$19_{2,17}$	238926.844	127.4	11.69	238926.6	3.94	

Table B.2. continued.

Torsional substate	Transition $J_{K_a,K_c} - J'_{K'_a,K'_c}$	Predicted frequency (MHz)	E_{upp} (K)	S_{ij}	Observed frequency (MHz)	T_{MB} (K)	Blends
A	$20_{3,18}$-$19_{2,17}$	238932.529	128.0	11.82	238932.3	3.99	
E	$32_{5,28}$-$32_{3,29}$	239541.734	327.3	5.88	239541.3	1.07	U-line
A	$32_{5,28}$-$32_{4,29}$	239541.215	327.9	12.01	” †	”	”
E	$19_{3,16}$-$18_{3,15}$	240021.111	121.7	18.29	240021.0	14.91	
A	$19_{3,16}$-$18_{3,15}$	240034.655	122.3	18.27	240034.6	14.78	
E	$19_{5,14}$-$18_{5,13}$	242871.545	129.8	17.73	242871.3	14.40	
A	$19_{5,14}$-$18_{5,13}$	242896.030	130.4	17.72	242896.0	13.88	
E	$20_{4,17}$-$19_{4,16}$	244580.316	134.4	19.08	244580.0	14.52	
A	$20_{4,17}$-$19_{4,16}$	244594.053	135.0	19.06	244593.9	14.40	
A	$20_{15,6}$-$19_{15,5}$	245651.193	273.1	8.76	245651.0	5.35	
A	$20_{15,5}$-$19_{15,4}$	245651.193	273.1	8.76	” †	”	
E	$20_{15,5}$-$19_{15,4}$	245656.884	272.5	8.75	245656.7	3.55	
E	$20_{15,6}$-$19_{15,5}$	245673.007	272.5	8.75	245672.8	3.45	
A	$20_{14,7}$-$19_{14,6}$	245752.248	253.9	10.21	245752.3	6.87	
A	$20_{14,6}$-$19_{14,5}$	245752.248	253.9	10.21	” †	”	
E	$20_{14,6}$-$19_{14,5}$	245754.098	253.3	10.21	245753.9†	5.06	
E	$20_{14,7}$-$19_{14,6}$	245772.672	253.3	10.20	245772.5	4.60	E-CH_3COCH_3 v_t=2
E	$20_{11,9}$-$19_{11,8}$	246285.383	203.6	13.96	246285.3	7.06	
A	$20_{11,10}$-$19_{11,9}$	246295.120	204.2	13.96	246294.8	10.51	
A	$20_{11,9}$-$19_{11,8}$	246295.120	204.2	13.96	” †	”	
E	$20_{11,10}$-$19_{11,9}$	246308.252	203.6	13.97	246308.1	7.70	
E	$20_{10,10}$-$19_{10,9}$	246600.003	189.7	15.02	246600.0	8.67	
A	$20_{10,11}$-$19_{10,10}$	246613.394	190.3	15.01	246613.2	8.48	
A	$20_{10,10}$-$19_{10,9}$	246613.410	190.3	15.01	” †	”	
E	$20_{10,11}$-$19_{10,10}$	246623.215	189.7	15.02	246623.1	8.54	
E	$10_{5,5}$-$9_{4,5}$	246752.946	48.5	3.26	246752.9	2.63	
E	$20_{9,11}$-$19_{9,10}$	247040.622	177.2	15.97	247040.6	9.37	
E	$21_{3,19}$-$20_{3,18}$	247044.110	139.3	20.33	247044.1	12.46	
A	$21_{3,19}$-$20_{3,18}$	247053.522	139.9	20.29	247053.6	12.72	
A	$20_{9,12}$-$19_{9,11}$	247057.279	177.8	15.96	247057.4	13.62	
A	$20_{9,11}$-$19_{9,10}$	247057.757	177.8	15.96	” †	”	
E	$20_{9,12}$-$19_{9,11}$	247063.641	177.2	15.97	247063.7	9.24	
E	$42_{9,34}$-$42_{8,35}$	247655.258	593.2	23.75	247656.9	12.34	
E	$21_{2,19}$-$20_{2,18}$	247656.860	139.2	20.33	” †	”	
A	$21_{2,19}$-$20_{2,18}$	247665.418	139.8	20.30	247665.3	12.08	
E	$20_{8,12}$-$19_{8,11}$	247682.669	166.1	16.80	247682.5	9.76	
A	$20_{8,13}$-$19_{8,12}$	247697.218	166.7	16.81	247697.1	9.89	
E	$20_{8,13}$-$19_{8,12}$	247704.366	166.1	16.82	247704.4	10.15	
A	$20_{8,12}$-$19_{8,11}$	247707.986	166.7	16.81	247707.8	10.15	
E	$22_{2,21}$-$21_{2,20}$	247901.619	142.9	21.60	247901.6	12.34	
A	$22_{2,21}$-$21_{2,20}$	247907.181	143.5	21.54	247907.0	12.34	
E	$22_{1,21}$-$21_{1,20}$	247922.229	142.9	21.59	247922.2	12.21	
A	$22_{1,21}$-$21_{1,20}$	247927.745	143.5	21.54	247927.8	12.59	
A	$20_{7,14}$-$19_{7,13}$	248617.444	157.0	17.56	248617.3	11.18	
E	$20_{7,14}$-$19_{7,13}$	248633.678	156.4	16.92	248633.7	11.05	
E	$33_{4,29}$-$33_{3,30}$	248953.453	346.2	11.87	248953.6	0.60	
A	$31_{10,22}$-$31_{9,23}$	248976.908	360.5	17.32	248977.0	0.81	
E	$20_{5,16}$-$19_{5,15}$	249030.990	141.0	18.74	249030.6	11.69	
A	$20_{5,16}$-$19_{5,15}$	249047.443	141.6	18.72	249047.1	11.82	
E	$20_{6,15}$-$19_{6,14}$	249578.121	148.1	18.22	249578.0	11.05	
A	$20_{6,15}$-$19_{6,14}$	249591.736	148.7	18.21	249591.6	11.31	
A	$27_{1,26}$-$27_{1,27}$	250006.048	210.6	0.31	250006.3	0.94	
A	$27_{1,26}$-$27_{0,27}$	250006.071	210.6	3.01	” †	”	
A	$27_{2,26}$-$27_{1,27}$	250007.624	210.6	3.01	250007.5†	0.97	
A	$27_{2,26}$-$27_{0,27}$	250007.647	210.6	0.31	” †	”	
E	$20_{3,17}$-$19_{3,16}$	250246.500	133.7	19.23	250246.3	11.95	
A	$20_{3,17}$-$19_{3,16}$	250258.416	134.3	19.21	250258.3	11.95	
E	$8_{6,2}$-$7_{5,2}$	250410.931	44.5	5.51	250410.9	3.64	
E	$20_{6,14}$-$19_{6,13}$	251264.464	148.3	18.22	251264.3	10.95	
A	$20_{6,14}$-$19_{6,13}$	251285.739	148.9	18.21	251285.8	10.20	CH_3CH_2CN
A	$28_{10,19}$-$28_{9,20}$	253674.284	306.8	14.94	253674.3	0.98	
E	$21_{4,18}$-$20_{4,17}$	255776.133	146.7	20.09	255776.0	11.05	
A	$21_{4,18}$-$20_{4,17}$	255789.466	147.3	20.06	255789.2	11.05	
A	$18_{4,15}$-$17_{3,14}$	256981.918	112.1	6.18	256981.9	2.52	
E	$18_{4,15}$-$17_{3,14}$	256985.789	111.5	6.14	256985.7	2.59	
E	$20_{5,15}$-$19_{5,14}$	257226.591	142.2	18.82	257226.6	13.11	

Table B.2. continued.

Torsional substate	Transition $J_{K_a,K_c} - J'_{K'_a,K'_c}$	Predicted frequency (MHz)	E_{upp} (K)	S_{ij}	Observed frequency (MHz)	T_{MB} (K)	Blends
E	$22_{3,20}$-$21_{3,19}$	257690.311	151.7	21.33	257690.3	11.05	
A	$22_{3,20}$-$21_{3,19}$	257699.492	152.3	21.29	257699.5	11.31	
A	$21_{17,5}$-$20_{17,4}$	257841.540	327.9	7.24	257841.6	4.21	U-line
A	$21_{17,4}$-$20_{17,3}$	257841.540	327.9	7.24	” †	”	”
A	$21_{15,7}$-$20_{15,6}$	258001.723	285.5	10.29	258001.6	5.77	
A	$21_{15,6}$-$20_{15,5}$	258001.723	285.5	10.29	” †	”	
E	$21_{15,6}$-$20_{15,5}$	258007.304	284.9	10.29	258007.3	4.16	
E	$21_{15,7}$-$20_{15,6}$	258024.149	284.9	10.29	258024.1	3.75	
E	$22_{2,20}$-$21_{2,19}$	258081.006	151.6	21.34	258081.0	12.72	
A	$22_{2,20}$-$21_{2,19}$	258089.554	152.2	21.29	258089.5	12.21	
E	$22_{3,20}$-$21_{2,19}$	258706.927	151.7	13.73	258706.9	3.50	
A	$22_{3,20}$-$21_{2,19}$	258714.082	152.3	13.93	258714.2	3.16	
E	$23_{10,14}$-$23_{9,15}$	258837.623	228.9	11.13	258837.6	1.35	
E	$23_{10,13}$-$23_{9,14}$	258847.918	228.9	11.13	258847.7	1.63	
A	$23_{10,13}$-$23_{9,14}$	258859.141	229.5	11.17	258859.1	1.35	
A	$23_{10,14}$-$23_{9,15}$	258868.737	229.5	11.17	258868.6	1.33	
E	$34_{4,30}$-$34_{4,31}$	259204.388	365.6	6.02	259204.3	0.33	
E	$11_{5,6}$-$10_{4,7}$	259445.553	55.0	2.66	259445.6	1.97	
E	$21_{5,17}$-$20_{5,16}$	261148.888	153.5	19.78	261148.9	14.20	CH_3OCH_3
A	$21_{5,17}$-$20_{5,16}$	261165.463	154.1	19.76	261165.4	12.23	
A	$21_{7,15}$-$20_{7,14}$	261433.787	169.5	18.68	261433.6	12.10	
E	$21_{7,15}$-$20_{7,14}$	261436.736	168.9	18.34	261436.8	12.34	
E	$21_{6,16}$-$20_{6,15}$	262324.885	160.7	19.31	262324.9	12.23	
A	$21_{6,16}$-$20_{6,15}$	262340.574	161.3	19.29	262340.4	13.13	
A	$14_{10,4}$-$14_{9,5}$	262487.467	128.3	4.47	262487.3	3.74	
A	$14_{10,5}$-$14_{9,6}$	262487.468	128.3	4.47	” †	”	
E	$21_{6,15}$-$20_{6,14}$	265002.619	161.0	19.32	265002.6	11.59	
A	$21_{6,15}$-$20_{6,14}$	265024.856	161.6	19.30	265024.7	11.72	
E	$23_{3,21}$-$22_{3,20}$	268307.724	164.5	22.33	268307.6	11.85	
A	$23_{3,21}$-$22_{3,20}$	268316.698	165.1	22.28	268316.5	10.94	
E	$23_{2,21}$-$22_{2,20}$	268552.668	164.5	22.34	268552.6	9.12	A-CH_3OCOH v_t=1
A	$23_{2,21}$-$22_{2,20}$	268561.189	165.1	22.29	268561.1	8.73	
E	$23_{3,21}$-$22_{2,20}$	268933.644	164.5	14.73	268933.6	2.48	
A	$23_{3,21}$-$22_{2,20}$	268941.225	165.1	14.97	268941.2	2.38	
E	$12_{5,8}$-$11_{4,7}$	269404.240	62.1	3.84	269404.4	2.00	
E	$35_{4,31}$-$35_{4,32}$	269409.949	385.5	11.85	269409.8	0.57	
E	$36_{11,25}$-$36_{10,26}$	269421.789	475.0	19.24	269421.8	0.57	
A	$29_{1,28}$-$29_{0,29}$	269439.182	241.0	3.01	269439.4	1.22	
A	$29_{2,28}$-$29_{1,29}$	269439.662	241.0	3.01	” †	”	
E	$33_{4,30}$-$33_{3,31}$	270866.078	334.2	8.89	270866.0	0.63	
E	$33_{4,30}$-$33_{2,31}$	270867.848	334.2	4.85	270867.9†	0.47	
A	$21_{4,18}$-$20_{3,17}$	270878.806	147.3	9.02	270878.6	2.36	
E	$21_{4,18}$-$20_{3,17}$	270882.386	146.7	8.91	270882.4	2.08	
E	$24_{4,20}$-$23_{5,19}$	272991.748	193.4	7.56	272991.6	1.28	E-$^{13}CH_3OCOH$
A	$24_{4,20}$-$23_{5,19}$	273037.128	194.0	7.69	273037.0	1.30	
E	$34_{11,23}$-$34_{10,24}$	274789.061	432.5	15.87	274789.4	0.65	
E	$10_{6,5}$-$9_{5,5}$	274798.303	55.7	5.64	274798.3	3.06	
E	$23_{4,20}$-$22_{4,19}$	277733.003	172.8	22.10	277733.0	11.05	
A	$23_{4,20}$-$22_{4,19}$	277745.386	173.4	22.06	277745.3	11.18	E-CH_3OCOH v_t=1
A	$8_{7,2}$-$7_{6,1}$	278133.374	53.8	6.46	278133.3	6.93	
A	$8_{7,1}$-$7_{6,2}$	278133.381	53.8	6.46	” †	”	
E	$24_{3,22}$-$23_{3,21}$	278906.080	177.9	23.34	278906.0	12.36	
A	$24_{3,22}$-$23_{3,21}$	278914.870	178.5	23.28	278914.8	12.11	
E	$23_{3,20}$-$22_{3,19}$	280147.664	172.6	22.14	280147.6	11.05	
A	$23_{3,20}$-$22_{3,19}$	280157.369	173.2	22.10	280157.1	11.56	
E	$29_{11,19}$-$29_{10,20}$	282886.664	337.0	11.62	282886.6	0.82	
E	$23_{14,9}$-$22_{14,8}$	282896.140	292.2	14.49	282895.1	9.12	
A	$23_{14,10}$-$22_{14,9}$	282895.162	292.8	14.49	” †	”	
A	$23_{14,9}$-$22_{14,8}$	282895.162	292.8	14.49	” †	”	
A	$29_{11,19}$-$29_{10,20}$	282895.162	337.7	14.97	” †	”	
E	$23_{14,10}$-$22_{14,9}$	282916.953	292.2	14.49	282917.0	4.87	
E	$22_{4,18}$-$21_{4,17}$	282939.770	164.7	21.21	282939.7	12.59	
A	$22_{4,18}$-$21_{4,17}$	282957.566	165.3	21.18	282957.4	11.82	
E	$23_{12,11}$-$22_{12,10}$	283373.369	257.8	16.76	283373.3	6.41	
A	$23_{12,12}$-$22_{12,11}$	283381.002	258.4	16.75	283380.9	9.24	
A	$23_{12,11}$-$22_{12,10}$	283381.002	258.4	16.75	” †	”	

Table B.2. continued.

Torsional substate	Transition $J_{K_a,K_c} - J'_{K'_a,K'_c}$	Predicted frequency (MHz)	E_{upp} (K)	S_{ij}	Observed frequency (MHz)	T_{MB} (K)	Blends
E	$23_{12,12}$-$22_{12,11}$	283397.730	257.8	16.76	283397.6	6.54	
E	$23_{9,14}$-$22_{9,13}$	284920.183	216.4	19.51	284920.3	7.44	
A	$23_{9,15}$-$22_{9,14}$	284937.187	217.0	19.49	284937.1	7.70	
A	$23_{9,14}$-$22_{9,13}$	284942.734	217.0	19.49	284942.7	8.47	
E	$23_{9,15}$-$22_{9,14}$	284945.113	216.4	19.51	284945.0	8.60	
E	$23_{7,17}$-$22_{7,16}$	287146.603	195.9	20.88	287146.6	9.89	
A	$23_{7,17}$-$22_{7,16}$	287158.943	196.5	20.88	287158.9	9.89	
E	$24_{4,21}$-$23_{4,20}$	288541.454	186.7	20.11	288541.3	11.95	
A	$24_{4,21}$-$23_{4,20}$	288553.359	187.3	23.06	288553.3	11.18	
E	$25_{3,23}$-$24_{2,22}$	289721.778	191.8	16.71	289721.6	2.92	
A	$25_{3,23}$-$24_{2,22}$	289729.779	192.4	17.03	289729.8	3.26	
E	$17_{11,7}$-$17_{10,8}$	289755.716	169.9	6.09	289755.8	1.80	
E	$17_{11,6}$-$17_{10,7}$	289759.818	169.9	6.09	289759.9	1.80	
A	$17_{11,6}$-$17_{10,7}$	289803.642	170.5	6.09	289803.6	3.11	
A	$17_{11,7}$-$17_{10,8}$	289803.643	170.5	6.09	” †	”	

Note.- Emission lines of CH_3OCOH ground state shown in Figs. 3, A.2, A.3, and A.4. Column 1 indicates the symmetry substate of the torsional mode, Col. 2 gives the quantic numbers of the line transition, Col. 3 the predicted frequency in the laboratory, Col. 4 upper level energy, Col. 5 the line strength, Col. 6 observed frequency at the peak channel of the line (relative to a v_{LSR} of 7.5 kms^{-1}) , Col. 7 main beam temperature at the peak channel of the line, and Col. 8 shows the blending with other molecular species.
† blended with the previous line.

Table B.3. Lines of A-CH_3OCOH and E-CH_3OCOH in its first excited state v_t=1.

Torsional substate	Transition $J_{K_a,K_c} - J'_{K'_a,K'_c}$	Predicted frequency (MHz)	E_{upp} (K)	S_{ij}	Observed frequency (MHz)	T_{MB} (K)	Blends
A	$7_{1,7}$-$6_{0,6}$	81999.401	204.1	5.38	81999.3	0.09	
E	$7_{1,7}$-$6_{0,6}$	82101.315	203.3	5.18	82101.6	0.10	
A	$10_{3,8}$-$10_{2,9}$	82809.138	226.5	5.12	82809.3	0.10	
E	$10_{3,8}$-$10_{2,9}$	83227.097	225.9	4.66	83227.0	0.04	
E	$7_{2,6}$-$6_{2,5}$	84283.109	206.5	6.35	84283.0	0.44	c-C_2H_4O
A	$7_{6,2}$-$6_{6,1}$	85120.437	228.7	1.85	85120.3	0.17	
A	$7_{6,1}$-$6_{6,0}$	85120.437	228.7	1.85	” †	”	
E	$7_{6,1}$-$6_{6,0}$	85157.135	228.6	1.86	85157.3	0.11	
A	$7_{5,3}$-$6_{5,2}$	85185.466	221.4	3.42	85185.7	0.21	
A	$7_{5,2}$-$6_{5,1}$	85185.466	221.4	3.42	” †	”	
E	$7_{4,4}$-$6_{4,3}$	85743.976	214.5	4.72	85743.9	0.24	
E	$7_{3,4}$-$6_{3,3}$	86034.013	210.3	5.74	86033.6	0.28	
A	$7_{3,4}$-$6_{3,3}$	86155.078	210.8	5.70	86155.0	0.30	
E	$7_{3,5}$-$6_{3,4}$	86172.706	209.9	5.69	86172.7	0.28	
A	$8_{0,8}$-$7_{1,7}$	87057.122	208.3	6.30	87057.0	0.07	
E	$7_{1,6}$-$6_{1,5}$	88220.753	205.4	6.80	88220.6	0.35	
E	$8_{1,8}$-$7_{1,7}$	88862.414	207.6	7.85	88862.6	0.41	
A	$7_{2,5}$-$6_{2,4}$	88998.365	207.9	6.42	88998.3	0.32	
E	$8_{0,8}$-$7_{0,7}$	89829.704	207.5	7.88	89829.6	0.45	
E	$10_{4,6}$-$10_{3,7}$	93450.699	230.9	4.22	93450.6	0.06	
E	$5_{2,4}$-$4_{1,3}$	93457.280	198.9	1.80	93457.2	0.02	
A	$8_{2,7}$-$7_{2,6}$	95242.005	211.8	7.44	95242.0	0.48	
A	$7_{4,3}$-$7_{3,4}$	95667.399	215.4	3.33	95667.6	0.05	
E	$10_{4,7}$-$10_{3,8}$	95685.406	230.5	4.58	95685.3	0.04	
E	$8_{2,7}$-$7_{2,6}$	95689.399	211.1	7.46	95689.4	0.48	
A	$5_{4,1}$-$5_{3,2}$	96891.929	207.8	1.82	96891.6	0.04	
E	$11_{4,8}$-$11_{3,9}$	96903.487	237.0	4.79	96903.3	0.06	
E	$8_{7,1}$-$7_{7,0}$	97275.818	242.1	1.88	97275.9	0.12	E-$CH_3{}^{18}OCOH$
A	$9_{4,6}$-$9_{3,7}$	97282.148	225.4	4.73	97282.2	0.08	$(CH_3)_2CO$
A	$8_{6,3}$-$7_{6,2}$	97350.417	233.4	3.50	97350.3	0.35	
A	$8_{6,2}$-$7_{6,1}$	97350.417	233.4	3.50	” †	”	
E	$8_{6,2}$-$7_{6,1}$	97395.342	233.3	3.51	97395.5	0.23	U-line
A	$8_{5,4}$-$7_{5,3}$	97457.967	226.1	4.87	97457.9	0.29	
A	$8_{5,3}$-$7_{5,2}$	97460.395	226.1	4.87	97460.4†	0.30	
E	$8_{7,2}$-$7_{7,1}$	97651.270	241.3	1.88	...	...	E-CH_3OCOH
A	$8_{4,5}$-$7_{4,4}$	97661.401	220.1	5.99	97661.3	0.35	
E	$8_{3,6}$-$7_{3,5}$	98682.421	214.6	6.81	...	...	A-CH_3OCOH
A	$8_{1,7}$-$7_{1,6}$	99575.548	210.9	7.75	99575.6	0.54	
E	$9_{1,9}$-$8_{1,8}$	99577.419	212.4	8.87	99577.4	0.66	
A	$9_{1,9}$-$8_{0,8}$	101202.806	213.2	7.42	101202.6	0.02	
A	$8_{2,6}$-$7_{2,5}$	102179.510	212.8	7.50	102179.3	0.51	
E	$15_{2,13}$-$15_{1,14}$	103886.114	263.1	6.04	103886.0	0.04	
A	$16_{5,11}$-$16_{4,12}$	105514.812	285.1	9.99	105514.9	0.15	t-HCCOD
E	$3_{3,1}$-$2_{2,1}$	105528.729	197.0	2.55	105528.5	0.05	
E	$9_{2,8}$-$8_{2,7}$	107022.159	216.2	8.52	107022.0	0.68	
A	$10_{1,9}$-$9_{2,8}$	107472.344	222.1	4.61	107472.3	0.10	
E	$10_{1,9}$-$9_{2,8}$	107911.928	221.4	4.46	107911.9	0.10	E/A-$^{13}CH_3OCOH$
E	$3_{3,0}$-$2_{2,0}$	108379.260	197.4	2.31	108379.3	0.06	
E	$9_{8,1}$-$8_{8,0}$	109390.436	257.5	1.89	109390.3	0.14	U-line
A	$9_{7,3}$-$8_{7,2}$	109531.413	247.3	3.55	109531.5	0.47	
A	$9_{7,2}$-$8_{7,1}$	109531.413	247.3	3.55	” †	”	
E	$9_{6,3}$-$8_{6,2}$	109662.944	238.6	5.02	109662.9	0.41	E-CH_3OD
A	$9_{3,7}$-$8_{3,6}$	109763.737	220.7	7.97	109763.6	1.05	SO_2
A	$9_{5,5}$-$8_{5,4}$	109770.995	231.3	6.21	109770.8	0.52	
A	$9_{5,4}$-$8_{5,3}$	109778.835	231.3	6.21	109778.8	0.81	$C^{18}O$
E	$9_{5,4}$-$8_{5,3}$	109912.168	231.1	6.25	109912.0	0.72	$^{13}CH_2CHCN$
E	$9_{7,3}$-$8_{7,2}$	109924.817	246.6	3.57	109924.6	0.29	CH_3COOCH_3
E	$10_{1,10}$-$9_{1,9}$	110238.713	217.7	9.88	110238.6	0.81	
A	$9_{4,5}$-$8_{4,4}$	110250.337	225.4	7.21	110250.3	0.62	CH_3OCH_3, $(CH_3)_2CO$, A-CH_3OCOH v_t=2
E	$9_{5,5}$-$8_{5,4}$	110262.642	230.5	6.24	110262.6	0.68	E-CH_3OD
E	$7_{2,6}$-$6_{1,5}$	110462.101	206.5	2.95	110462.0	0.06	
A	$15_{5,10}$-$15_{4,11}$	110468.307	275.6	8.93	110468.3	0.07	
E	$10_{0,10}$-$9_{0,9}$	110655.310	217.6	9.88	110655.0	0.77	
E	$9_{3,6}$-$8_{3,5}$	112011.966	220.4	7.91	110684.1	0.60	
A	$15_{3,13}$-$15_{2,14}$	114404.728	264.3	6.07	114404.9	0.09	
A	$9_{2,7}$-$8_{2,6}$	115152.691	218.3	8.55	115154.2	1.06	NS

Table B.3. continued.

Torsional substate	Transition $J_{K_a,K_c} - J'_{K'_a,K'_c}$	Predicted frequency (MHz)	E_{upp} (K)	S_{ij}	Observed frequency (MHz)	T_{MB} (K)	Blends
E	$9_{2,7}$-$8_{2,6}$	115557.296	217.7	8.60	...	...	NS
A	$12_{0,12}$-$11_{1,11}$	131149.812	230.6	10.48	131149.9	0.14	
E	$12_{0,12}$-$11_{1,11}$	131235.255	229.8	10.13	131235.3	0.24	$CH_3CH_2{}^{13}CN$
A	$12_{1,12}$-$11_{1,11}$	131377.495	230.6	11.82	131377.3	0.73	
A	$12_{0,12}$-$11_{0,11}$	131536.653	230.6	11.82	131536.6	0.76	
E	$11_{10,1}$-$10_{10,0}$	133616.483	294.1	1.91	...	...	A-CH_3OCOH
E	$11_{5,6}$-$10_{5,5}$	134739.627	243.5	8.76	134739.6	0.62	
E	$11_{6,6}$-$10_{6,5}$	134777.758	250.2	7.75	134777.5	0.52	
E	$11_{4,8}$-$10_{4,7}$	135931.664	237.0	9.53	135931.6	0.54	
A	$11_{3,8}$-$10_{3,7}$	139381.193	233.7	10.18	139381.3	0.95	
A	$16_{2,15}$-$16_{0,16}$	139393.776	267.5	1.64	139393.6	0.05	
E	$13_{0,13}$-$12_{1,12}$	141905.019	236.6	11.12	141905.0	0.25	
E	$13_{1,13}$-$12_{1,12}$	142032.295	236.6	12.89	142032.3	1.17	
A	$13_{0,13}$-$12_{0,12}$	142052.774	237.4	12.82	142052.8	1.20	
E	$21_{5,17}$-$21_{4,18}$	142232.708	341.0	11.20	142232.6	0.10	
E	$13_{1,13}$-$12_{0,12}$	142252.685	236.6	11.13	142252.5	0.28	
A	$12_{1,11}$-$11_{1,10}$	142365.919	235.2	11.60	142365.9	1.25	A-CH_3OCOH
A	$12_{3,10}$-$11_{3,9}$	145621.125	240.0	11.19	145621.3	1.03	
A	$12_{8,5}$-$11_{8,4}$	146234.988	276.6	6.67	146234.9	0.64	
A	$12_{8,4}$-$11_{8,3}$	146234.988	276.6	6.67	” †	”	
E	$12_{7,5}$-$11_{7,4}$	146337.965	266.7	7.94	146337.9	0.66	
E	$12_{3,10}$-$11_{3,9}$	146345.423	239.4	11.19	146345.2	0.71	
E	$12_{11,2}$-$11_{11,1}$	146356.286	314.4	1.93	146357.5	0.75	
A	$12_{7,6}$-$11_{7,5}$	146357.492	266.6	7.92	” †	”	
A	$12_{7,5}$-$11_{7,4}$	146357.492	266.6	7.92	” †	”	
E	$12_{6,6}$-$11_{6,5}$	146682.383	257.9	9.03	146682.3	0.56	
E	$12_{8,5}$-$11_{8,4}$	146700.601	276.0	6.70	146700.6	0.54	A-CH_3OCOH
E	$12_{4,8}$-$11_{4,7}$	148575.217	244.6	10.64	148575.3	0.65	
E	$12_{4,9}$-$11_{4,8}$	148590.157	244.1	10.59	148590.2	0.71	
A	$14_{6,8}$-$14_{5,9}$	149606.932	273.8	7.19	149606.9	0.13	CH_3CH_2CN
A	$13_{2,12}$-$12_{2,11}$	150898.356	242.7	12.54	150898.3	0.85	
A	$12_{2,10}$-$11_{2,9}$	152084.700	238.5	11.57	152084.6	0.82	
A	$14_{1,14}$-$13_{1,13}$	152525.637	244.7	13.82	152525.6	1.04	
A	$32_{6,26}$-$32_{5,27}$	152528.049	530.6	19.89	” †	”	
E	$19_{3,17}$-$19_{2,18}$	152595.656	303.7	5.94	152597.1	1.08	
E	$14_{1,14}$-$13_{1,13}$	152597.126	243.9	13.90	” †	”	
A	$8_{6,2}$-$8_{5,3}$	152602.909	233.4	2.72	152608.1	1.29	
A	$8_{6,3}$-$8_{5,4}$	152606.026	233.4	2.72	” †	”	
A	$13_{1,12}$-$12_{1,11}$	152608.268	242.6	12.58	” †	”	
E	$13_{1,12}$-$12_{1,11}$	152891.340	241.9	12.64	152891.3	0.97	$(CH_3)2CO$, CH_3OCH_3
E	$10_{6,5}$-$10_{5,6}$	152902.698	243.7	4.20	152902.6	0.08	
E	$12_{3,9}$-$11_{3,8}$	153463.342	240.5	11.30	153463.3	1.20	
E	$11_{6,5}$-$11_{5,6}$	154461.588	250.9	4.74	154461.6	0.15	U-line
A	$13_{3,11}$-$12_{3,10}$	157286.188	247.5	12.23	157286.3	1.37	
E	$5_{4,2}$-$4_{3,2}$	158167.991	206.9	3.56	158167.9	0.15	
A	$13_{11,2}$-$12_{11,1}$	158380.526	322.3	3.70	158380.6	0.49	
A	$13_{11,3}$-$12_{11,2}$	158380.526	322.3	3.70	†	”	
A	$13_{12,1}$-$12_{12,0}$	158388.509	337.6	1.93	158388.5	0.44	
A	$13_{12,2}$-$12_{12,1}$	158388.509	337.6	1.93	” †	”	
A	$19_{4,15}$-$18_{5,14}$	158388.849	313.2	3.12	” †	”	
E	$13_{8,5}$-$12_{8,4}$	158390.648	284.4	8.10	158390.7†	1.09	
A	$13_{10,3}$-$12_{10,2}$	158391.526	308.2	5.32	158391.7†	”	
A	$13_{10,3}$-$12_{10,2}$	158391.526	308.2	5.32	” †	”	
A	$7_{3,4}$-$6_{2,5}$	158424.671	210.8	2.57	158424.9	0.16	
A	$13_{9,5}$-$12_{9,4}$	158432.673	295.6	6.78	158432.8	1.18	
A	$13_{9,4}$-$12_{9,3}$	158432.673	295.6	6.78	” †	”	
E	$13_{7,6}$-$12_{7,5}$	158677.623	274.3	9.26	158677.6	0.84	
A	$13_{7,7}$-$12_{7,6}$	158690.583	274.2	9.23	158690.6	1.81	
A	$13_{7,6}$-$12_{7,5}$	158690.583	274.2	9.23	” †	”	
E	$13_{10,4}$-$12_{10,3}$	158716.616	307.9	5.34	158716.5	0.46	
A	$13_{6,8}$-$12_{6,7}$	158993.849	265.6	10.22	158993.9	1.50	SO
A	$22_{4,19}$-$22_{3,20}$	159001.155	347.1	9.25	159001.2	0.20	
A	$13_{6,7}$-$12_{6,6}$	159006.303	265.6	10.22	159006.2	1.12	
E	$13_{8,6}$-$12_{8,5}$	159031.511	283.7	8.11	159031.5	0.79	CH_3OH
E	$13_{4,10}$-$12_{4,9}$	161090.565	251.9	11.58	161090.6	1.32	
A	$14_{2,13}$-$13_{2,12}$	161682.634	250.5	13.54	161682.6	1.41	

Table B.3. continued.

Torsional substate	Transition $J_{K_a,K_c} - J'_{K'_a,K'_c}$	Predicted frequency (MHz)	E_{upp} (K)	S_{ij}	Observed frequency (MHz)	T_{MB} (K)	Blends
E	$14_{2,13}$-$13_{2,12}$	161969.656	249.9	13.61	161969.6	1.39	
E	$14_{1,13}$-$13_{1,12}$	163142.587	249.8	13.63	163142.6	1.27	
E	$15_{1,15}$-$14_{1,14}$	163154.325	251.8	14.90	163154.3	1.41	
A	$15_{1,15}$-$14_{0,14}$	163162.333	252.5	13.51	...	...	H_2CCO, DNCO
E	$15_{0,15}$-$14_{0,14}$	163185.864	251.8	14.90	163185.9	1.44	
A	$14_{2,13}$-$13_{1,12}$	165031.078	250.5	9.06	165031.0	0.28	
A	$13_{3,10}$-$12_{3,9}$	166388.878	249.0	12.33	166388.9	1.23	
A	$14_{3,12}$-$13_{3,11}$	168787.455	255.6	13.26	168787.3	1.63	E-CH_3OCOH
E	$14_{8,6}$-$13_{8,5}$	170701.600	292.6	9.45	170701.6	0.66	
A	$14_{9,6}$-$13_{9,5}$	170708.842	303.7	8.23	170708.9	0.78	
A	$14_{9,5}$-$13_{9,4}$	170708.842	303.7	8.23	” †	”	
E	$14_{7,7}$-$13_{7,6}$	171053.094	282.5	10.53	171053.3	0.89	E-CH_3OCOH
A	$14_{7,8}$-$13_{7,7}$	171056.818	282.4	10.50	171057.1	1.04	
A	$14_{7,7}$-$13_{7,6}$	171057.883	282.4	10.50	” †	”	
A	$14_{6,9}$-$13_{6,8}$	171444.983	273.8	11.42	171444.9	0.69	
A	$14_{6,8}$-$13_{6,7}$	171474.023	273.8	11.42	171474.0	0.75	
A	$15_{1,14}$-$14_{1,13}$	173188.580	258.7	14.55	173185.1	2.66	E-CH_3OCOH
E	$15_{1,14}$-$14_{1,13}$	173452.699	258.1	14.63	173452.9	1.38	
A	$16_{1,16}$-$15_{1,15}$	173641.411	260.9	15.82	173638.1	3.66	E-CH_3OCOH
A	$16_{0,16}$-$15_{0,15}$	173660.281	260.9	15.82	173660.3	2.30	
E	$16_{1,16}$-$15_{1,15}$	173706.683	260.1	15.90	...	...	SiO
E	$16_{0,16}$-$15_{0,15}$	173724.731	260.1	15.90	173724.4	1.58	
E	$16_{1,16}$-$15_{0,15}$	173747.990	260.1	14.07	173747.9	0.65	
A	$14_{2,12}$-$13_{2,11}$	174539.547	254.7	13.50	174539.6	1.42	
A	$15_{2,14}$-$14_{1,13}$	174553.136	258.8	10.10	...	...	E/A-CH_3OCOH
A	$14_{4,10}$-$13_{4,9}$	175749.843	261.2	12.84	175749.9	1.05	
E	$14_{4,10}$-$13_{4,9}$	175757.729	260.8	12.69	175757.8	1.13	
E	$19_{7,12}$-$19_{6,13}$	176524.557	332.5	9.69	...	...	A-CH_3OCOH, $CH_3CH_2{}^{13}CN$
E	$11_{3,9}$-$10_{2,8}$	177694.995	232.3	3.66	177695.2	0.21	
E	$16_{6,11}$-$15_{6,10}$	197411.655	291.5	13.79	197411.6	0.68	
E	$16_{5,11}$-$15_{5,10}$	198384.885	284.9	14.40	198384.9	0.66	
E	$16_{5,12}$-$15_{5,11}$	198578.563	284.4	14.35	198578.6	0.76	
E	$6_{5,1}$-$5_{4,1}$	200863.284	217.1	4.32	200863.3	0.63	
E	$17_{3,15}$-$16_{3,14}$	202805.731	282.7	16.37	202805.6	4.05	?
A	$16_{4,12}$-$15_{4,11}$	203493.009	280.0	15.02	203493.0	4.15	?
E	$16_{4,12}$-$15_{4,11}$	204136.446	279.7	15.04	204136.6	8.53	CH_3OCH_3, $^{34}SO_2$
E	$18_{1,17}$-$17_{2,16}$	204216.635	286.0	12.84	204216.6	0.81	
A	$18_{1,17}$-$17_{1,16}$	204454.106	286.6	17.55	204454.3	4.01	
E	$18_{2,17}$-$17_{2,16}$	204510.955	286.1	17.62	204510.9	5.12	$^{13}CH_3CH_2CN$
A	$16_{3,13}$-$15_{3,12}$	204533.737	276.7	15.41	204533.6	5.40	CH_3OCH_3
E	$18_{1,17}$-$17_{1,16}$	204707.365	286.0	17.62	204707.3	4.23	?
A	$18_{2,17}$-$17_{1,16}$	204768.053	286.6	13.15	204768.0	0.89	
E	$16_{3,13}$-$15_{3,12}$	205176.300	276.3	15.46	205176.3	4.18	
A	$19_{8,12}$-$19_{7,13}$	205526.937	342.3	9.54	205526.9	0.59	U-line
E	$17_{2,15}$-$16_{2,14}$	205922.616	282.3	16.43	205922.6	4.09	CH_3CH_2CN
E	$17_{10,7}$-$16_{10,6}$	207096.767	344.9	11.14	207096.6	2.75	CH_3CH_2CN v_{20}=1, $NH_2{}^{13}CHO$
A	$16_{8,8}$-$16_{7,9}$	207162.350	310.6	7.36	207162.4	0.61	$(CH_3)_2CO$
A	$16_{8,9}$-$16_{7,10}$	207173.223	310.6	7.36	207173.1	0.39	
A	$17_{14,3}$-$16_{14,2}$	207327.805	408.7	5.50	207327.6	2.23	?
A	$17_{14,4}$-$16_{14,3}$	207327.805	408.7	5.50	” †	”	?
A	$17_{13,4}$-$16_{13,3}$	207331.815	390.6	7.09	207331.7	2.59	
A	$17_{13,5}$-$16_{13,4}$	207331.815	390.6	7.09	” †	”	
A	$17_{15,2}$-$16_{15,1}$	207334.532	428.1	3.79	207334.2	1.64	?
A	$17_{15,3}$-$16_{15,2}$	207334.532	428.1	3.79	” †	”	?
A	$17_{12,5}$-$16_{12,4}$	207353.952	373.9	8.56	207353.9	2.20	
A	$17_{12,6}$-$16_{12,5}$	207353.952	373.9	8.56	” †	”	
E	$17_{9,8}$-$16_{9,7}$	207397.275	332.1	12.26	207397.2	3.80	CH_3CH_2CN, E-CH_3OD, $SO^{18}O$
A	$9_{4,5}$-$8_{3,6}$	207398.957	225.4	3.77	207398.8†	2.08	”
A	$17_{11,6}$-$16_{11,5}$	207404.959	358.6	9.91	207404.8	3.25	
A	$17_{11,7}$-$16_{11,6}$	207404.959	358.6	9.91	” †	”	
A	$17_{10,8}$-$16_{10,7}$	207500.283	344.5	11.14	207500.3	3.01	
A	$17_{10,7}$-$16_{10,6}$	207500.283	344.5	11.14	” †	”	
A	$15_{8,7}$-$15_{7,8}$	207532.111	301.2	6.63	207532.2	0.26	
A	$15_{8,8}$-$15_{7,9}$	207536.436	301.2	6.63	207536.3	0.61	U-line
E	$17_{12,6}$-$16_{12,5}$	207538.657	373.8	8.58	207538.5†	1.35	”
E	$17_{11,7}$-$16_{11,6}$	207725.686	358.3	9.94	207725.6	1.48	E-CH_3CHO

Table B.3. continued.

Torsional substate	Transition $J_{K_a,K_c} - J'_{K'_a,K'_c}$	Predicted frequency (MHz)	E_{upp} (K)	S_{ij}	Observed frequency (MHz)	T_{MB} (K)	Blends
E	$9_{4,5}$-$8_{3,5}$	208235.678	225.0	3.36	208235.6	0.71	
E	$17_{9,9}$-$16_{9,8}$	208240.132	331.5	12.30	208240.0	2.21	
E	$17_{8,10}$-$16_{8,9}$	208630.811	320.1	13.29	208630.6	2.72	
E	$17_{4,14}$-$16_{4,13}$	208776.279	288.5	16.03	208776.3	3.89	
A	$17_{6,11}$-$16_{6,10}$	209320.067	302.2	14.88	209320.0	3.60	A-CH_3OCOH v_t=2
E	$17_{6,12}$-$16_{6,11}$	210120.757	301.6	14.93	210120.6	3.24	
E	$17_{5,12}$-$16_{5,11}$	211814.973	295.1	15.35	211814.9	3.76	
A	$18_{3,16}$-$17_{3,15}$	213250.919	293.4	17.30	213250.9	3.85	
A	$19_{2,18}$-$18_{2,17}$	214816.945	297.0	17.04	214816.9	3.69	
E	$18_{2,16}$-$17_{2,15}$	215979.944	292.7	17.41	215979.9	4.34	
A	$17_{3,14}$-$16_{3,13}$	216327.065	287.1	16.39	216327.0	3.92	
E	$17_{3,14}$-$16_{3,13}$	216958.834	286.7	16.44	216958.6	4.19	
E	$17_{4,13}$-$16_{4,12}$	218108.438	290.2	16.16	218108.3	3.57	
E	$18_{11,7}$-$17_{11,6}$	219154.534	369.5	11.30	219154.6	1.96	CH_3CH_2CN
E	$18_{10,8}$-$17_{10,7}$	219411.703	355.4	12.47	219411.6	2.50	$CH_3{}^{18}OH$
A	$18_{12,6}$-$17_{12,5}$	219622.694	384.5	10.04	219622.6	2.60	
A	$18_{12,7}$-$17_{12,6}$	219622.694	384.5	10.04	” †	”	
E	$18_{13,6}$-$17_{13,5}$	219642.403	401.2	8.66	219642.2	1.22	
A	$18_{10,9}$-$17_{10,8}$	219822.126	355.1	12.47	219822.3	3.32	
A	$18_{10,8}$-$17_{10,7}$	219822.126	355.1	12.47	” †	”	
E	$18_{12,7}$-$17_{12,6}$	219827.149	384.3	10.05	219827.0	1.55	
E	$18_{8,10}$-$17_{8,9}$	220258.096	331.3	14.48	220258.0	2.80	
A	$18_{7,12}$-$17_{7,11}$	220913.955	321.3	15.29	220913.9	2.94	
A	$18_{7,11}$-$17_{7,10}$	220946.352	321.3	15.29	220946.2	3.29	E-CH_3OCOH
A	$18_{6,13}$-$17_{6,12}$	221692.344	312.8	16.00	221692.3	4.04	E-CH_3OCOH
E	$18_{5,14}$-$17_{5,13}$	223534.727	305.3	16.30	223534.6	4.04	?
A	$25_{1,24}$-$25_{1,25}$	225040.758	369.4	1.70	225040.9	0.39	?
A	$25_{1,24}$-$25_{0,25}$	225040.758	369.4	4.42	” †	”	?
E	$8_{5,3}$-$7_{4,3}$	225042.127	225.9	4.42	225042.2†	0.86	?
A	$21_{0,21}$-$20_{1,20}$	226381.356	310.1	19.38	226382.9	5.48	
A	$21_{1,21}$-$20_{1,20}$	226382.719	310.1	20.85	” †	”	
A	$21_{0,21}$-$20_{0,20}$	226383.864	310.1	20.85	226383.8†	5.06	
A	$21_{1,21}$-$20_{0,20}$	226385.154	310.1	19.38	” †	”	
E	$18_{3,15}$-$17_{3,14}$	228211.291	297.7	17.41	228211.3	4.27	
E	$19_{16,3}$-$18_{16,2}$	230851.687	471.2	5.54	230844.3	0.34	$SO^{17}O$
A	$18_{4,14}$-$17_{4,13}$	230878.810	301.5	17.17	230851.6	0.39	
E	$19_{15,4}$-$18_{15,3}$	230888.681	450.4	7.18	...	...	t-$H^{13}COOH$, CCO
E	$19_{15,5}$-$18_{15,4}$	231569.546	450.0	7.20	231569.29	0.58	
E	$18_{4,14}$-$17_{4,13}$	231724.157	301.3	17.24	231724.0	4.45	
E	$19_{14,6}$-$18_{14,5}$	231734.860	430.5	8.73	231738.2	1.52	$CH_3{}^{18}OH$, t-CH_3CH_2OH
E	$19_{10,9}$-$18_{10,8}$	231749.757	366.5	13.77	231749.6	2.94	CH_3CHO
A	$19_{11,9}$-$18_{11,8}$	232002.595	380.2	12.67	232002.5	4.04	
A	$19_{11,8}$-$18_{11,7}$	232002.595	380.2	12.67	” †	”	
E	$19_{9,10}$-$18_{9,9}$	232160.193	353.8	14.77	232160.0	3.90	CH_3CH_2CN
A	$19_{10,10}$-$18_{10,9}$	232164.437	366.2	13.77	232164.4	5.42	$^{13}CH_3CN$
A	$19_{10,9}$-$18_{10,8}$	232164.437	366.2	13.77	” †	”	”
E	$19_{10,10}$-$18_{10,9}$	232683.931	366.0	13.81	232683.9	2.26	
A	$20_{2,18}$-$19_{3,17}$	232713.990	315.3	11.53	232713.9	0.59	
E	$19_{8,11}$-$18_{8,10}$	232738.618	342.5	15.67	232738.6	2.55	
E	$22_{0,22}$-$21_{1,21}$	236975.184	320.7	19.86	236975.9	6.05	
E	$22_{1,22}$-$21_{1,21}$	236975.844	320.7	21.94	” †	”	
E	$22_{0,22}$-$21_{0,21}$	236976.390	320.7	21.94	236978.1†	2.16	
E	$22_{1,22}$-$21_{0,21}$	236977.050	320.7	19.86	” †	”	
E	$18_{9,9}$-$18_{8,10}$	236981.886	342.7	7.92	236981.9	0.55	
A	$19_{5,14}$-$18_{5,13}$	239610.154	317.6	17.70	239610.0	4.99	
A	$20_{4,17}$-$19_{4,16}$	242610.072	322.2	19.07	242610.0	5.10	
E	$20_{13,7}$-$19_{13,6}$	243325.371	424.5	11.58	243325.3	1.66	U-line
E	$20_{11,9}$-$19_{11,8}$	243766.260	392.3	13.98	243766.3	2.62	OCS v_2=1
A	$27_{1,26}$-$27_{1,27}$	244061.909	397.7	1.71	244066.7	5.12	
A	$27_{1,26}$-$27_{0,27}$	244061.946	397.7	3.14	” †	”	
A	$27_{2,26}$-$27_{1,27}$	244064.350	397.7	3.14	” †	”	
A	$27_{2,26}$-$27_{0,27}$	244064.387	397.7	1.71	” †	”	
A	$19_{4,15}$-$18_{4,14}$	244066.670	313.2	18.22	” †	”	
A	$20_{14,6}$-$19_{14,5}$	244073.580	442.1	10.25	244073.6	2.41	
A	$20_{14,7}$-$19_{14,6}$	244073.580	442.1	10.25	” †	”	
E	$20_{10,10}$-$19_{10,9}$	244112.419	378.3	15.04	244112.5	3.03	

Table B.3. continued.

Torsional substate	Transition $J_{K_a,K_c} - J'_{K'_a,K'_c}$	Predicted frequency (MHz)	E_{upp} (K)	S_{ij}	Observed frequency (MHz)	T_{MB} (K)	Blends
A	$20_{13,7}$-$19_{13,6}$	244119.662	424.0	11.60	244119.8	3.00	
A	$20_{13,8}$-$19_{13,7}$	244119.662	424.0	11.60	” †	”	
A	$21_{2,19}$-$20_{3,18}$	244122.133	327.1	12.58	244122.0	1.10	
A	$20_{12,8}$-$19_{12,7}$	244198.300	407.3	12.85	244198.3	3.43	
A	$20_{12,9}$-$19_{12,8}$	244198.300	407.3	12.85	” †	”	
E	$20_{13,8}$-$19_{13,7}$	244207.136	424.0	11.61	244207.1	1.97	CH_3CHO v_t=1
A	$20_{10,11}$-$19_{10,10}$	244528.537	378.0	15.04	244528.6	4.50	
A	$20_{10,10}$-$19_{10,9}$	244528.537	378.0	15.04	” †	”	
E	$20_{8,13}$-$19_{8,12}$	246184.177	353.8	16.87	246184.0	3.20	
A	$21_{2,19}$-$20_{2,18}$	246187.016	327.1	20.32	246187.1	4.17	
E	$22_{2,21}$-$21_{2,20}$	246706.504	330.4	21.64	246706.3	4.66	
E	$22_{1,21}$-$21_{1,20}$	246731.729	330.4	21.64	246731.6	4.29	
A	$23_{0,23}$-$22_{1,22}$	247468.835	333.4	21.28	247469.5	7.30	
A	$23_{1,23}$-$22_{1,22}$	247469.249	333.4	22.86	” †	”	
A	$23_{0,23}$-$22_{0,22}$	247469.585	333.4	22.86	” †	”	
A	$23_{1,23}$-$22_{0,22}$	247469.999	333.4	21.28	” †	”	
A	$21_{3,19}$-$20_{2,18}$	247502.219	327.2	12.61	247502.3	0.73	
E	$23_{0,23}$-$22_{1,22}$	247515.653	332.6	20.79	247516.2	7.73	
E	$23_{1,23}$-$22_{1,22}$	247516.012	332.6	22.95	” †	”	
E	$23_{0,23}$-$22_{0,22}$	247516.312	332.6	22.95	” †	”	
E	$23_{1,23}$-$22_{0,22}$	247516.671	332.6	20.79	” †	”	
A	$20_{3,17}$-$19_{3,16}$	248715.840	321.4	19.24	248715.9	5.03	
A	$8_{6,3}$-$7_{5,2}$	250063.404	233.4	5.61	250063.0	1.25	
A	$8_{6,2}$-$7_{5,3}$	250063.998	233.4	5.61	250063.9†	1.24	
A	$21_{4,18}$-$20_{4,17}$	253807.849	334.4	20.08	253807.9	3.79	
E	$21_{12,9}$-$20_{12,8}$	255809.484	420.0	14.18	255809.3	1.68	$C^{13}CH$
A	$22_{3,20}$-$21_{3,19}$	256048.804	339.5	21.31	256048.9	4.04	A-CH_3OCOH
E	$21_{15,7}$-$20_{15,6}$	256071.907	474.0	10.34	256071.7	1.16	E-CH_3OCOH
E	$21_{11,10}$-$20_{11,9}$	256103.021	404.6	15.27	256103.0	1.93	
E	$21_{14,8}$-$20_{14,7}$	256275.972	454.5	11.73	256275.9	1.86	
A	$21_{16,5}$-$20_{16,4}$	256275.972	454.5	8.86	” †	”	
A	$21_{16,6}$-$20_{16,5}$	256275.972	454.5	8.86	” †	”	
A	$21_{15,6}$-$20_{15,5}$	256299.660	473.8	10.35	256299.6	1.90	
A	$21_{15,7}$-$20_{15,6}$	256299.660	473.8	10.35	” †	”	
A	$22_{2,20}$-$21_{2,19}$	256537.497	339.4	21.32	256537.6	4.08	
E	$21_{12,10}$-$20_{12,9}$	256776.839	419.5	14.22	256776.6	1.74	
A	$20_{4,16}$-$19_{4,15}$	256789.148	325.6	19.24	256789.2	4.08	
E	$22_{2,20}$-$21_{2,19}$	256910.443	339.1	21.39	256910.3	4.41	
A	$21_{10,12}$-$20_{10,11}$	256915.926	390.3	16.28	256916.0	4.12	
A	$21_{10,11}$-$20_{10,10}$	256915.926	390.3	16.28	” †	”	
A	$23_{2,22}$-$22_{2,21}$	256999.358	343.3	22.57	256999.3	3.86	
A	$23_{1,22}$-$22_{1,21}$	257015.472	343.3	22.57	257015.4	4.30	
A	$24_{0,24}$-$23_{1,23}$	258010.378	345.8	22.23	258010.6	7.20	
A	$24_{1,24}$-$23_{1,23}$	258010.754	345.8	23.87	” †	”	
A	$24_{0,24}$-$23_{0,23}$	258010.754	345.8	23.87	” †	”	
A	$24_{1,24}$-$23_{0,23}$	258011.019	345.8	22.23	” †	”	
E	$21_{9,13}$-$20_{9,12}$	258037.974	377.4	17.23	258037.8	2.93	
E	$24_{0,24}$-$23_{1,23}$	258054.742	345.0	21.70	258054.9	9.64	
E	$24_{1,24}$-$23_{1,23}$	258055.043	345.0	23.97	” †	”	
E	$24_{0,24}$-$23_{0,23}$	258055.043	345.0	23.97	” †	”	
E	$24_{1,24}$-$23_{0,23}$	258055.296	345.0	21.70	” †	”	
A	$21_{5,17}$-$20_{5,16}$	258701.047	341.1	19.77	258701.0	3.93	
E	$21_{6,16}$-$20_{6,15}$	261234.608	348.1	18.96	261234.6	4.09	
E	$21_{6,15}$-$20_{6,14}$	261727.149	348.5	18.99	261727.0	4.05	
A	$21_{6,15}$-$20_{6,14}$	261761.225	348.6	19.30	261761.1	4.37	
E	$9_{6,4}$-$8_{5,4}$	263460.641	237.9	5.58	263460.6	1.12	$(CH_3)_2CO$
A	$22_{4,19}$-$21_{4,18}$	264853.567	347.1	21.09	264853.3	4.47	
E	$22_{4,19}$-$21_{4,18}$	265410.861	346.9	21.15	265410.9	4.90	
A	$23_{3,21}$-$22_{3,20}$	266627.118	352.3	22.32	266627.0	4.98	U-line
A	$23_{2,21}$-$22_{2,20}$	266940.218	352.2	22.32	266940.3	4.05	
E	$7_{7,1}$-$6_{6,1}$	267375.738	236.6	6.44	267375.6	1.54	
E	$24_{2,23}$-$23_{2,22}$	267774.438	355.6	23.65	267774.3	4.45	$^{13}CH_3CN$
E	$23_{3,21}$-$22_{2,20}$	267780.164	351.9	14.46	267783.1	4.69	U-line
E	$24_{1,23}$-$23_{1,22}$	267782.994	355.6	23.65	” †	”	”
E	$22_{18,5}$-$21_{18,4}$	267785.665	553.4	7.32	267785.4†	0.82	”
E	$22_{12,10}$-$21_{12,9}$	268125.641	432.9	15.49	268125.6	2.02	

Table B.3. continued.

Torsional substate	Transition $J_{K_a,K_c} - J'_{K'_a,K'_c}$	Predicted frequency (MHz)	E_{upp} (K)	S_{ij}	Observed frequency (MHz)	T_{MB} (K)	Blends
E	$22_{16,7}$-$21_{16,6}$	268134.591	507.7	10.42	268134.5	1.14	
E	$22_{15,8}$-$21_{15,7}$	268336.710	486.8	11.84	268336.6	1.08	
E	$22_{11,11}$-$21_{11,10}$	268461.963	417.5	16.54	268461.9	2.35	CH_3OCH_3
A	$22_{18,4}$-$21_{18,3}$	268476.140	552.9	7.33	268476.2	0.84	
A	$22_{18,5}$-$21_{18,4}$	268476.140	552.9	7.33	” †	”	
A	$22_{17,5}$-$21_{17,4}$	268496.385	529.5	8.92	268496.4	0.79	
A	$22_{17,6}$-$21_{17,5}$	268496.385	529.5	8.92	” †	”	
A	$22_{16,6}$-$21_{16,5}$	268521.688	507.4	10.43	268521.7	1.10	
A	$22_{16,7}$-$21_{16,6}$	268521.688	507.4	10.43	” †	”	
A	$25_{0,25}$-$24_{1,24}$	268550.512	358.6	23.16	268550.8	6.83	A-CH_3OCOH
A	$25_{1,25}$-$24_{1,24}$	268550.714	358.6	24.88	” †	”	”
A	$25_{0,25}$-$24_{0,24}$	268550.714	358.6	24.88	” †	”	”
A	$25_{1,25}$-$24_{0,24}$	268550.865	358.6	23.16	” †	”	”
E	$25_{0,25}$-$24_{1,24}$	268592.469	357.9	22.74	268592.6	5.19	
E	$25_{1,25}$-$24_{1,24}$	268592.604	357.9	24.96	” †	”	
E	$25_{0,25}$-$24_{0,24}$	268592.604	357.9	24.96	” †	”	
E	$25_{1,25}$-$24_{0,24}$	268592.769	357.9	22.74	” †	”	
A	$22_{14,8}$-$21_{14,7}$	268613.561	467.3	13.16	268613.5	1.78	
A	$22_{14,9}$-$21_{14,8}$	268613.561	467.3	13.16	” †	”	
A	$22_{13,9}$-$21_{13,8}$	268699.137	449.2	14.38	268699.3	3.12	
A	$22_{13,10}$-$21_{13,9}$	268699.137	449.2	14.38	” †	”	
A	$22_{3,19}$-$21_{3,18}$	268700.539	346.7	21.16	268700.5†	3.97	
E	$22_{3,19}$-$21_{3,18}$	269154.933	346.5	21.22	269154.6	3.64	
E	$22_{9,13}$-$21_{9,12}$	269547.693	361.8	7.67	269547.6	2.11	
E	$22_{5,18}$-$21_{5,17}$	271400.844	354.0	20.86	271400.9	3.36	
E	$22_{6,17}$-$21_{6,16}$	273653.253	361.2	19.96	273653.3	2.63	
A	$22_{6,16}$-$21_{6,15}$	275483.282	361.8	20.38	275483.3	2.94	
E	$22_{6,16}$-$21_{6,15}$	275739.989	361.8	20.00	275739.9	4.01	$(CH_3)_2CO$
A	$23_{4,20}$-$22_{4,19}$	275766.695	360.3	22.10	275766.5	4.05	
E	$23_{4,20}$-$22_{4,19}$	276300.275	360.1	22.16	276300.3	4.01	
A	$24_{3,22}$-$23_{3,21}$	277182.741	365.6	23.32	277182.6	3.83	
E	$10_{6,4}$-$9_{5,4}$	277196.342	244.4	5.47	277196.2	0.84	
A	$24_{2,22}$-$23_{2,21}$	277380.387	365.6	23.32	277380.3	4.37	
E	$24_{3,22}$-$23_{3,21}$	277563.993	365.2	23.38	277563.9	3.79	$H_2C^{18}O$
A	$25_{1,24}$-$24_{2,23}$	278061.390	369.4	19.95	...	...	E-CH_3OCOH
A	$25_{2,24}$-$24_{2,23}$	278068.761	369.4	24.58	278068.5	4.85	
E	$26_{0,26}$-$25_{1,25}$	279128.814	371.3	24.27	279128.9	7.09	
E	$26_{1,26}$-$25_{1,25}$	279128.852	371.3	25.87	” †	”	
E	$26_{0,26}$-$25_{0,25}$	279128.852	371.3	25.87	” †	”	
E	$26_{1,26}$-$25_{0,25}$	279128.975	371.3	24.27	” †	”	

Note.- Emission lines of CH_3OCOH in its first torsional state (v_t=1) shown in Figs. 4, A.5, A.6, and A.7. Column 1 indicates the symmetry substate of the torsional mode, Col. 2 gives the quantic numbers of the line transition, Col. 3 the predicted frequency in the laboratory, Col. 4 upper level energy, Col. 5 the line strength, Col. 6 observed frequency at the peak channel of the line (relative to a v_{LSR} of 7.5 kms^{-1}) , Col. 7 main beam temperature at the peak channel of the line, and Col. 8 shows the blending with other molecular species.
† blended with the previous line.

Table B.4. Lines of A-CH_3OCOH and E-CH_3OCOH in its second excited state v_t=2.

Torsional substate	Transition $J_{K_a,K_c} - J'_{K'_a,K'_c}$	Predicted frequency (MHz)	E_{upp} (K)	S_{ij}	Observed frequency (MHz)	T_{MB} (K)	Blends
E	$7_{5,3}$-$6_{5,2}$	82719.621	370.9	4.82	82719.5	0.09	
A	$7_{5,3}$-$6_{5,2}$	86386.663	366.7	3.62	86386.6	0.10	
A	$7_{5,2}$-$6_{5,1}$	86387.492	366.7	3.62	” †	”	
A	$8_{1,8}$-$7_{1,7}$	88969.135	351.7	8.32	88969.3	0.15	
A	$8_{0,8}$-$7_{0,7}$	89991.032	351.6	8.35	89991.0	0.16	
E	$8_{0,8}$-$7_{0,7}$	90203.744	359.1	7.68	90203.6	0.20	E-CH_3COOH
A	$8_{2,7}$-$7_{2,6}$	96530.207	355.6	7.90	96530.3	0.13	
E	$8_{4,5}$-$7_{4,4}$	96541.385	370.4	7.23	96541.4	0.10	
A	$8_{5,4}$-$7_{5,3}$	98853.561	371.5	5.16	98853.5	0.10	
A	$8_{5,3}$-$7_{5,2}$	98856.860	371.5	5.16	98857.0	0.10	
E	$8_{5,3}$-$7_{5,2}$	99220.919	380.6	3.56	99220.9	0.09	
A	$8_{4,5}$-$7_{4,4}$	99273.219	364.9	6.36	99273.4	0.12	
A	$9_{1,9}$-$8_{1,8}$	99640.582	365.5	9.37	99640.6	0.18	
A	$9_{0,9}$-$8_{0,8}$	100313.473	356.5	9.41	100313.3	0.18	
E	$9_{0,9}$-$8_{0,8}$	101176.155	364.0	8.73	101176.0	0.29	
A	$8_{3,5}$-$7_{3,4}$	101200.619	359.8	7.30	101200.6	0.19	
E	$9_{2,7}$-$8_{2,6}$	106869.804	370.6	8.35	106869.9	0.20	
A	$10_{0,10}$-$9_{0,9}$	110675.449	361.8	10.46	110675.6	0.29	
A	$9_{3,7}$-$8_{3,6}$	111660.126	365.0	8.47	111660.0	0.18	
E	$9_{5,4}$-$8_{5,3}$	111701.673	385.9	5.08	111701.6	0.12	
E	$10_{0,10}$-$9_{0,9}$	111703.096	369.3	9.78	111702.9†	0.23	
E	$9_{4,5}$-$8_{4,4}$	112115.985	379.5	6.25	112115.9	0.14	
A	$9_{4,5}$-$8_{4,4}$	112168.025	370.2	7.64	112168.0	0.17	
A	$9_{3,6}$-$8_{3,5}$	114871.546	365.4	8.47	114871.6	0.27	
E	$10_{2,9}$-$9_{2,8}$	114877.105	374.0	9.64	114877.0	0.29	
E	$11_{2,10}$-$10_{2,9}$	126147.591	380.0	10.69	126147.6	0.34	
E	$11_{7,4}$-$10_{8,3}$	128218.926	415.4	6.51	128218.9	0.16	
E	$11_{9,2}$-$10_{9,1}$	128222.610	436.9	3.59	128222.7	0.08	
E	$20_{5,16}$-$20_{4,17}$	129483.779	478.7	12.26	129483.9	0.06	
E	$11_{2,9}$-$10_{2,8}$	129485.906	382.5	10.54	129485.8†	0.28	
A	$11_{2,10}$-$10_{2,9}$	130387.606	372.8	11.18	130387.6	0.24	
A	$12_{1,12}$-$11_{1,11}$	131357.893	373.9	12.57	131357.9	0.30	
A	$12_{0,12}$-$11_{0,11}$	131511.578	373.9	12.57	131511.6	0.24	
E	$11_{3,9}$-$10_{3,8}$	133039.459	384.6	10.58	133039.6	0.32	
A	$11_{3,9}$-$10_{3,8}$	135998.978	377.5	10.76	135998.9	0.22	
E	$11_{6,5}$-$10_{6,4}$	136523.344	406.4	6.70	136523.3	0.11	
A	$11_{5,7}$-$10_{5,6}$	136565.345	389.3	9.22	136565.3	0.28	
A	$11_{4,7}$-$10_{4,6}$	138316.884	382.9	10.09	138316.9	0.40	
E	$13_{1,13}$-$12_{1,12}$	141304.634	388.4	13.14	141304.6	0.43	
E	$20_{2,18}$-$20_{1,19}$	141874.617	465.2	6.85	141874.6	0.06	
A	$13_{1,13}$-$12_{1,12}$	141877.293	380.7	13.62	141877.1†	0.41	
E	$12_{5,8}$-$11_{5,7}$	144121.885	399.5	10.31	144121.9	0.33	
A	$12_{6,7}$-$11_{6,6}$	148437.884	404.5	9.48	148437.9	0.23	
A	$12_{6,6}$-$11_{6,5}$	148444.645	404.5	9.48	148444.6	0.15	
E	$12_{10,3}$-$11_{10,2}$	148896.826	446.1	3.80	148896.6	0.06	
E	$12_{9,4}$-$11_{9,3}$	148910.629	433.7	5.42	148910.8	0.09	
E	$12_{8,5}$-$11_{8,4}$	148931.478	422.9	6.85	148931.4	0.16	
A	$12_{5,7}$-$11_{5,6}$	149407.509	396.5	10.46	149407.3	0.26	
E	$13_{2,11}$-$12_{2,10}$	153905.568	396.7	12.61	153905.6	0.48	
A	$13_{1,12}$-$12_{1,11}$	153918.954	386.7	13.32	153918.9	0.49	
A	$12_{3,9}$-$11_{3,8}$	156873.735	385.9	11.97	156873.6	0.44	
A	$13_{3,11}$-$12_{3,10}$	159650.250	392.3	12.95	159650.3	0.48	
A	$16_{1,16}$-$15_{1,15}$	173379.246	404.2	16.79	173379.3	0.84	
A	$16_{0,16}$-$15_{0,15}$	173395.520	404.2	16.79	173395.4	0.66	
E	$16_{5,12}$-$15_{5,11}$	201677.008	434.4	14.68	201677.0	1.30	CH_2OHCHO
E	$18_{2,17}$-$17_{2,16}$	203315.226	437.4	18.22	203315.3	1.51	U-line
A	$18_{2,17}$-$17_{2,16}$	205224.393	431.0	18.59	205224.3	1.53	A-CH_3OCOH v_t=1
A	$20_{0,20}$-$19_{1,19}$	215335.365	442.5	15.79	215336.9	1.76	
A	$20_{1,20}$-$19_{1,19}$	215337.015	442.5	21.04	” †	”	
A	$20_{0,20}$-$19_{0,19}$	215338.467	442.5	21.04	215338.4†	1.91	
A	$20_{1,20}$-$19_{0,19}$	215340.117	442.5	15.79	” †	”	
E	$19_{3,17}$-$18_{3,16}$	221567.335	454.6	19.01	221567.3	1.40	
A	$15_{8,7}$-$15_{7,8}$	225524.144	449.7	5.84	225524.6	0.28	
E	$23_{9,15}$-$23_{8,16}$	225524.751	551.8	15.01	” †	”	
E	$21_{1,21}$-$20_{1,20}$	225537.464	460.9	21.79	225537.2	1.60	
E	$21_{0,21}$-$20_{0,20}$	225553.397	460.9	21.79	225553.4	2.20	

Table B.4. continued.

Torsional substate	Transition $J_{K_a,K_c} - J'_{K'_a,K'_c}$	Predicted frequency (MHz)	E_{upp} (K)	S_{ij}	Observed frequency (MHz)	T_{MB} (K)	Blends
E	$18_{5,14}$-$17_{5,13}$	225570.961	455.5	16.94	225570.8	2.22	
E	$21_{1,21}$-$20_{0,20}$	225574.143	460.9	16.80	225573.9†	0.90	
A	$21_{0,21}$-$20_{1,20}$	225822.369	453.3	16.63	225822.9	2.50	
A	$21_{1,21}$-$20_{1,20}$	225823.241	453.3	22.09	” †	”	
A	$21_{0,21}$-$20_{0,20}$	225824.019	453.3	22.09	225823.9†	2.50	
A	$21_{1,21}$-$20_{0,20}$	225824.891	453.3	16.63	” †	”	
A	$19_{3,17}$-$18_{3,16}$	226211.859	449.6	19.34	226211.9	1.54	
A	$20_{2,19}$-$19_{2,18}$	226218.904	452.2	20.66	226218.9	1.61	
A	$18_{5,13}$-$17_{5,12}$	230398.004	452.9	17.54	230398.0	1.40	
E	$22_{1,22}$-$21_{1,21}$	236028.499	472.2	22.88	236028.3	1.79	
E	$20_{10,10}$-$19_{10,9}$	236037.055	530.7	15.02	236037.5	2.74	
E	$22_{0,22}$-$21_{0,21}$	236037.568	472.2	22.88	” †	”	
E	$19_{10,10}$-$18_{10,9}$	236093.086	512.8	14.23	236093.1	1.79	
A	$19_{7,12}$-$18_{7,11}$	236093.172	480.5	17.24	” †	”	
A	$22_{0,22}$-$21_{1,21}$	236307.969	464.7	17.47	236308.5	2.69	
A	$22_{1,22}$-$21_{1,21}$	236308.427	464.7	23.18	” †	”	
A	$22_{0,22}$-$21_{0,21}$	236308.841	464.7	23.18	” †	”	
A	$22_{1,22}$-$21_{0,21}$	236309.299	464.7	17.47	” †	”	
E	$19_{7,13}$-$18_{7,12}$	236341.227	480.4	16.75	236341.1	1.10	
A	$20_{9,12}$-$19_{9,11}$	245497.407	514.9	16.60	245497.9	2.03	E-CH_3OCOH v_t=0
A	$20_{9,11}$-$19_{9,10}$	245497.832	514.9	16.60	” †	”	”
E	$22_{2,21}$-$21_{2,20}$	245501.019	481.5	22.54	245500.8†	1.89	
A	$23_{0,23}$-$22_{1,22}$	246792.322	476.5	18.30	246792.6	3.23	
A	$23_{1,23}$-$22_{1,22}$	246792.561	476.5	24.24	” †	”	
A	$23_{0,23}$-$22_{0,22}$	246792.780	476.5	24.24	” †	”	
A	$23_{1,23}$-$22_{0,22}$	246793.019	476.5	18.30	” †	”	
E	$21_{2,19}$-$20_{2,18}$	247555.062	477.1	20.96	247555.0	1.73	
E	$21_{4,17}$-$20_{4,16}$	254923.867	488.1	20.55	254923.9	1.60	
E	$24_{0,24}$-$23_{1,23}$	257004.621	496.4	19.16	257008.1	1.78	
E	$24_{1,24}$-$23_{1,23}$	257008.274	496.4	25.07	” †	”	
E	$24_{0,24}$-$23_{0,23}$	257011.166	496.4	25.07	257010.9†	1.69	
E	$24_{1,24}$-$23_{0,23}$	257014.819	496.4	19.16	” †	”	
A	$24_{1,23}$-$23_{2,22}$	268131.980	500.7	16.91	268139.8	1.66	
A	$24_{2,23}$-$23_{2,22}$	268139.815	500.7	24.88	” †	”	
A	$24_{1,23}$-$23_{1,22}$	268146.274	500.7	24.88	268146.1	1.89	
A	$24_{2,23}$-$23_{1,22}$	268154.110	500.7	16.91	” †	”	
E	$23_{8,15}$-$22_{8,14}$	273284.896	544.2	20.36	273284.9	0.75	
A	$22_{4,18}$-$21_{4,17}$	285413.574	499.5	22.28	285413.6	1.72	
A	$23_{6,18}$-$22_{6,17}$	288691.334	523.2	22.47	288691.3	1.39	
A	$27_{0,27}$-$26_{1,26}$	288717.679	528.9	21.47	288717.5	2.78	
A	$27_{1,27}$-$26_{1,26}$	288717.696	528.9	28.53	” †	”	
A	$27_{0,27}$-$26_{0,26}$	288717.712	528.9	28.53	” †	”	
A	$27_{1,27}$-$26_{0,26}$	288717.728	528.9	21.47	” †	”	

Note.- Emission lines of CH_3OCOH in its second torsional state (v_t=2) shown in Fig. 5. Column 1 indicates the symmetry substate of the torsional mode, Col. 2 gives the quantic numbers of the line transition, Col. 3 the predicted frequency in the laboratory, Col. 4 upper level energy, Col. 5 the line strength, Col. 6 observed frequency at the peak channel of the line (relative to a v_{LSR} of 7.5 kms^{-1}) , Col. 7 main beam temperature at the peak channel of the line, and and Col. 8 shows the blending with other molecular species.
† blended with the previous line.

A. López et al.: $C_2H_4O_2$ isomers in Orion KL

Table B.5. Lines of A-CH_3COOH and E-CH_3COOH in its ground state v_t=0.

Torsional substate	Transition $J_{K_a,K_c} - J'_{K'_a,K'_c}$	Predicted frequency (MHz)	E_{upp} (K)	$S_{ij}\mu^2$ (D^2)	Observed frequency (MHz)	T_{MB} (K)	Blends
E	$8_{0,8}$-$7_{1,7}$	90203.436	20.3	16.30	...	...	U-line
E	$8_{1,8}$-$7_{1,7}$	90203.438	20.3	5.29	... †	...	”
E	$8_{0,8}$-$7_{0,7}$	90203.454	20.3	5.29	... †	...	”
E	$8_{1,8}$-$7_{0,7}$	90203.456	20.3	16.30	... †	...	”
A	$8_{0,8}$-$7_{1,7}$	90246.236	20.3	16.10	90246.4	0.03	
A	$8_{1,8}$-$7_{1,7}$	90246.239	20.3	5.52	” †	”	
A	$8_{0,8}$-$7_{0,7}$	90246.266	20.3	5.52	” †	”	
A	$8_{1,8}$-$7_{0,7}$	90246.270	20.3	16.10	” †	”	
E	$8_{1,7}$-$7_{2,6}$	100168.704	23.9	13.70	100169.1	0.02	
E	$8_{2,7}$-$7_{2,6}$	100168.964	23.9	4.80	” †	”	
E	$8_{1,7}$-$7_{1,6}$	100170.698	23.9	4.80	” †	”	
E	$8_{2,7}$-$7_{1,6}$	100170.957	23.9	13.70	” †	”	
E	$9_{0,9}$-$8_{1,8}$	100855.427	25.2	18.50	100855.4	0.04	
E	$9_{1,9}$-$8_{1,8}$	100855.427	25.2	5.94	” †	”	
E	$9_{0,9}$-$8_{0,8}$	100855.429	25.2	5.94	” †	”	
E	$9_{1,9}$-$8_{0,8}$	100855.429	25.2	18.50	” †	”	
A	$9_{0,9}$-$8_{1,8}$	100897.454	25.2	18.20	100897.3	0.03	
A	$9_{1,9}$-$8_{1,8}$	100897.455	25.2	6.25	” †	”	
A	$9_{0,9}$-$8_{0,8}$	100897.458	25.2	6.25	” †	”	
A	$9_{1,9}$-$8_{0,8}$	100897.458	25.2	18.20	” †	”	
E	$14_{4,10}$-$14_{4,11}$	103356.454	79.8	1.83	103357.1	0.02	
E	$14_{4,10}$-$14_{3,11}$	103356.459	79.8	9.53	” †	”	
E	$14_{5,10}$-$14_{4,11}$	103356.671	79.8	9.53	” †	”	
E	$14_{5,10}$-$14_{3,11}$	103356.676	79.8	1.83	” †	”	
E	$12_{2,10}$-$12_{1,11}$	104069.573	53.2	5.00	...	...	U-line
E	$12_{2,10}$-$12_{2,11}$	104069.573	53.2	0.99	... †	...	”
E	$12_{3,10}$-$12_{2,11}$	104069.578	53.2	5.00	... †	...	”
E	$12_{3,10}$-$12_{1,11}$	104069.578	53.2	0.99	... †	...	”
A	$14_{4,10}$-$14_{4,11}$	104077.734	80.1	1.99	104077.9	0.13	
A	$14_{4,10}$-$14_{3,11}$	104077.745	80.1	9.42	” †	”	
A	$14_{5,10}$-$14_{4,11}$	104078.173	80.1	9.42	” †	”	
A	$14_{5,10}$-$14_{3,11}$	104078.184	80.1	1.99	” †	”	
A	$24_{14,11}$-$24_{13,12}$	104078.588	266.3	29.00	” †	”	
A	$13_{3,10}$-$13_{3,11}$	104574.956	66.2	1.56	...	...	A-CH_3OCOH, U-line
A	$13_{3,10}$-$13_{2,11}$	104574.957	66.2	7.21	... †	...	”
A	$13_{4,10}$-$13_{3,11}$	104575.032	66.2	7.21	... †	...	”
A	$13_{4,10}$-$13_{2,11}$	104575.034	66.2	1.56	... †	...	”
E	$5_{5,1}$-$4_{4,1}$	108912.992	15.3	8.68	...	...	E-CH_3OCOH, SiS
A	$5_{5,1}$-$4_{4,0}$	110179.735	15.6	8.81	110179.7	0.03	U-line
A	$8_{3,6}$-$7_{2,5}$	110499.979	27.0	11.00	110499.8	0.02	U-line
E	$9_{1,8}$-$8_{2,7}$	110817.244	29.2	15.90	110817.5	0.04	
E	$9_{2,8}$-$8_{2,7}$	110817.276	29.2	5.47	” †	”	
E	$9_{1,8}$-$8_{1,7}$	110817.503	29.2	5.47	” †	”	
E	$9_{2,8}$-$8_{1,7}$	110817.535	29.2	15.90	” †	”	
A	$9_{1,8}$-$8_{2,7}$	110954.111	29.3	15.70	110954.6	0.05	
A	$9_{2,8}$-$8_{2,7}$	110954.171	29.3	5.69	” †	”	
A	$9_{1,8}$-$8_{1,7}$	110954.555	29.3	5.69	” †	”	
A	$9_{2,8}$-$8_{1,7}$	110954.615	29.3	15.70	” †	”	
E	$10_{0,10}$-$9_{1,9}$	111507.280	30.5	20.80	111507.3	0.05	
E	$10_{1,10}$-$9_{1,9}$	111507.280	30.5	6.57	” †	”	
E	$10_{1,10}$-$9_{0,9}$	111507.280	32.8	20.80	” †	”	
E	$10_{0,10}$-$9_{0,9}$	111507.280	32.8	6.57	” †	”	
A	$10_{0,10}$-$9_{1,9}$	111548.535	30.5	20.40	111548.4	0.05	
A	$10_{1,10}$-$9_{1,9}$	111548.535	30.5	6.98	” †	”	
A	$10_{1,10}$-$9_{0,9}$	111548.536	30.5	20.40	” †	”	
A	$10_{0,10}$-$9_{0,9}$	111548.536	30.5	6.98	” †	”	
E	$16_{5,11}$-$16_{5,12}$	112917.632	105.4	2.20	112917.9	0.02	
E	$16_{5,11}$-$16_{4,12}$	112917.636	105.4	11.80	” †	”	
E	$16_{6,11}$-$16_{5,12}$	112917.799	105.4	11.80	” †	”	
E	$16_{6,11}$-$16_{4,12}$	112917.803	105.4	2.20	” †	”	
E	$15_{4,11}$-$16_{4,12}$	113374.050	89.7	1.81	113374.0	0.05	$CH_2{}^{13}CHCN$
E	$15_{4,11}$-$16_{3,12}$	113374.051	89.7	9.64	” †	”	”
E	$15_{5,11}$-$16_{4,12}$	113374.081	89.7	9.64	” †	”	”
E	$15_{5,11}$-$16_{3,12}$	113374.082	89.7	9.64	” †	”	”
E	$17_{5,12}$-$17_{5,13}$	122958.695	116.7	2.16	...	...	U-line

Table B.5. continued.

Torsional substate	Transition $J_{K_a,K_c} - J'_{K'_a,K'_c}$	Predicted frequency (MHz)	E_{upp} (K)	$S_{ij}\mu^2$ (D^2)	Observed frequency (MHz)	T_{MB} (K)	Blends
E	$17_{5,12}$-$17_{4,13}$	122958.696	116.7	12.00	... †	...	”
E	$17_{6,12}$-$17_{5,13}$	122958.720	116.7	12.00	... †	...	”
E	$17_{6,12}$-$17_{4,13}$	122958.721	116.7	2.16	... †	...	”
A	$18_{6,12}$-$18_{6,13}$	123075.281	134.8	2.88	123075.6	0.02	
A	$18_{6,12}$-$18_{5,13}$	123075.291	134.8	13.90	” †	”	
A	$18_{7,12}$-$18_{6,13}$	123075.558	134.8	13.90	” †	”	
A	$18_{7,12}$-$18_{5,13}$	123075.568	134.8	2.88	” †	”	
A	$17_{5,12}$-$17_{5,13}$	123702.870	117.0	2.49	123703.1	0.06	CH_2CHCN v_{15}= 1, $CH_2{}^{13}CN$
A	$17_{5,12}$-$17_{4,13}$	123702.872	117.0	11.70	” †	”	
A	$17_{6,12}$-$17_{5,13}$	123702.929	117.0	11.70	” †	”	
A	$17_{6,12}$-$17_{4,13}$	123702.930	117.0	2.49	” †	”	
E	$15_{3,12}$-$15_{3,13}$	123721.516	84.2	1.35	123721.5	0.05	U-line
E	$15_{3,12}$-$15_{2,13}$	123721.516	84.2	7.50	” †	”	”
E	$15_{4,12}$-$15_{2,13}$	123721.517	84.2	1.35	” †	”	”
E	$15_{4,12}$-$15_{3,13}$	123721.517	84.2	7.50	” †	”	”
E	$14_{2,12}$-$14_{1,13}$	123998.080	69.4	5.13	123998.2	0.04	
E	$14_{3,12}$-$14_{2,13}$	123998.080	69.4	5.13	” †	”	
E	$14_{3,12}$-$14_{1,13}$	123998.080	69.4	0.92	” †	”	
E	$14_{2,12}$-$14_{2,13}$	123998.080	69.4	0.92	” †	”	
A	$16_{4,12}$-$16_{4,13}$	124237.659	100.2	2.06	124237.0	0.05	CH_2CHCN v_{11}= 2
A	$16_{4,12}$-$16_{3,13}$	124237.659	100.2	9.52	” †	”	”
A	$16_{5,12}$-$16_{4,13}$	124237.669	100.2	9.52	” †	”	”
A	$16_{5,12}$-$16_{3,13}$	124237.670	100.2	2.06	” †	”	”
E	$9_{3,6}$-$8_{4,5}$	130741.908	35.8	10.80	...	...	U-line
E	$5_{4,2}$-$4_{1,3}$	130742.482	14.0	0.50	... †	...	”
E	$9_{3,6}$-$8_{3,5}$	131086.092	35.8	4.63	...	...	U-line
E	$24_{21,4}$-$24_{20,5}$	131086.767	300.8	15.10	... †	...	”
A	$9_{4,6}$-$8_{4,5}$	131088.231	35.9	4.75	131088.2	0.03	U-line
E	$21_{8,13}$-$21_{8,14}$	131292.010	187.6	3.20	131292.3	0.01	
E	$21_{8,13}$-$21_{7,14}$	131292.024	187.6	18.60	” †	”	
E	$21_{9,13}$-$21_{8,14}$	131292.385	187.6	18.60	” †	”	
E	$21_{9,13}$-$21_{7,14}$	131292.399	187.6	3.20	” †	”	
E	$10_{2,8}$-$9_{3,7}$	131449.963	39.1	15.60	...	...	CH_3NH_2
E	$10_{3,8}$-$9_{3,7}$	131450.249	39.1	5.68	... †	...	”
E	$10_{2,8}$-$9_{2,7}$	131452.020	39.1	5.68	... †	...	CH_2CHCN v_{11}=2
E	$10_{3,8}$-$9_{2,7}$	131452.306	39.1	15.60	... †	...	”
A	$9_{4,6}$-$8_{3,5}$	131576.929	35.9	10.60	131577.0	0.05	U-line
A	$10_{2,8}$-$9_{3,7}$	131674.811	39.2	15.30	131673.8	0.04	U-line
A	$10_{3,8}$-$9_{3,7}$	131675.331	39.2	5.90	” †	”	”
A	$10_{2,8}$-$9_{2,7}$	131678.247	39.2	5.90	131679.49	0.03	NH_2CHO
A	$10_{3,8}$-$9_{2,7}$	131678.766	39.2	15.30	” †	”	”
A	$21_{8,13}$-$21_{8,14}$	131720.651	188.0	3.66	131720.7	0.05	U-line
A	$21_{8,13}$-$21_{7,14}$	131720.687	188.0	18.20	” †	”	”
A	$21_{9,13}$-$21_{8,14}$	131721.470	188.0	18.20	” †	”	”
A	$21_{9,13}$-$21_{7,14}$	131721.506	188.0	3.66	” †	”	”
E	$20_{7,13}$-$20_{7,14}$	131954.946	166.9	2.85	...	...	$^{13}CH_2CHCN$
E	$20_{7,13}$-$20_{6,14}$	131954.948	166.9	16.40	... †	...	”
E	$20_{8,13}$-$20_{7,14}$	131955.034	166.9	16.40	... †	...	”
E	$20_{8,13}$-$20_{6,14}$	131955.037	166.9	2.85	... †	...	”
A	$20_{7,13}$-$20_{7,14}$	132507.582	167.4	3.31	132507.8	0.01	
A	$20_{7,13}$-$20_{6,14}$	132507.590	167.4	16.10	” †	”	
A	$20_{8,13}$-$20_{7,14}$	132507.789	167.4	16.10	” †	”	
A	$20_{8,13}$-$20_{6,14}$	132507.797	167.4	3.31	” †	”	
E	$19_{6,13}$-$19_{6,14}$	132514.297	147.3	2.48	...	...	$^{13}CH_3CH_2CN$, U-line
E	$19_{6,13}$-$19_{5,14}$	132514.297	147.3	14.30	... †	...	”
E	$19_{7,13}$-$19_{6,14}$	132514.316	147.3	14.30	... †	...	”
E	$19_{7,13}$-$19_{5,14}$	132514.316	147.3	2.48	... †	...	”
E	$12_{0,12}$-$11_{1,11}$	132810.366	42.7	25.90	132810.4	0.07	
E	$12_{1,12}$-$11_{0,11}$	132810.366	42.7	25.90	” †	”	
E	$12_{0,12}$-$11_{0,11}$	132810.366	42.7	7.33	” †	”	
E	$12_{1,12}$-$11_{1,11}$	132810.366	42.7	7.33	” †	”	
A	$12_{0,12}$-$11_{1,11}$	132850.106	42.8	24.90	132850.1	0.07	
A	$12_{1,12}$-$11_{0,11}$	132850.106	42.8	24.90	” †	”	
A	$12_{0,12}$-$11_{0,11}$	132850.106	42.8	8.31	” †	”	
A	$12_{1,12}$-$11_{1,11}$	132850.106	42.8	8.31	” †	”	
A	$19_{6,13}$-$19_{6,14}$	133190.972	147.6	2.93	133191.2	0.03	

Table B.5. continued.

Torsional substate	Transition $J_{K_a,K_c} - J'_{K'_a,K'_c}$	Predicted frequency (MHz)	E_{upp} (K)	$S_{ij}\mu^2$ (D^2)	Observed frequency (MHz)	T_{MB} (K)	Blends
A	$19_{6,13}$-$19_{5,14}$	133190.973	147.6	13.90	” †	”	
A	$19_{7,13}$-$19_{6,14}$	133191.019	147.6	13.90	” †	”	
A	$19_{7,13}$-$19_{5,14}$	133191.020	147.6	2.93	” †	”	
A	$6_{6,1}$-$5_{5,0}$	133251.594	22.0	11.00	133251.7	0.06	A-CH_3OCOH
E	$16_{3,13}$-$16_{3,14}$	133695.347	94.1	1.17	133696.2	0.04	CH3CHO v_t=2, CH_2CHCN
E	$16_{3,13}$-$16_{2,14}$	133695.347	94.1	7.72	” †	”	”
E	$16_{4,13}$-$16_{2,14}$	133695.347	94.1	1.17	” †	”	”
E	$16_{4,13}$-$16_{3,14}$	133695.347	94.1	7.72	” †	”	”
E	$15_{3,13}$-$15_{1,14}$	133957.571	78.3	1.79	133957.9	0.03	U-line
E	$15_{2,13}$-$15_{2,14}$	133957.571	78.3	1.79	” †	”	”
E	$15_{2,13}$-$15_{1,14}$	133957.571	78.3	1.79	” †	”	”
E	$15_{3,13}$-$15_{2,14}$	133957.571	78.3	1.79	” †	”	”
A	$8_{6,2}$-$7_{6,1}$	133960.025	33.9	2.75	...	...	U-line
E	$14_{2,13}$-$14_{0,14}$	134168.437	63.5	2.71	134168.4	0.02	
E	$14_{1,13}$-$14_{1,14}$	134168.437	63.5	2.71	” †	”	
E	$14_{1,13}$-$14_{0,14}$	134168.437	63.5	0.41	” †	”	
E	$14_{2,13}$-$14_{1,14}$	134168.437	63.5	0.41	” †	”	
A	$17_{4,13}$-$17_{4,14}$	134295.630	111.1	2.10	134295.5	0.05	
A	$17_{4,13}$-$17_{3,14}$	134295.630	111.1	9.56	” †	”	
A	$17_{5,13}$-$17_{3,14}$	134295.632	111.1	2.10	” †	”	
A	$17_{5,13}$-$17_{4,14}$	134295.632	111.1	9.56	” †	”	
E	$9_{4,5}$-$8_{5,4}$	139021.421	38.3	7.62	139021.8	0.05	
A	$8_{5,4}$-$7_{4,3}$	139043.733	31.8	6.42	139043.1	0.02	
A	$25_{11,14}$-$25_{11,15}$	139044.609	274.1	4.70	139045.0†	0.02	
A	$25_{11,14}$-$25_{10,15}$	139044.004	274.1	24.60	139045.0†	0.02	
E	$10_{3,7}$-$9_{4,6}$	141476.268	42.6	13.00	141476.5	0.03	
E	$10_{3,7}$-$9_{3,6}$	141542.966	42.6	5.28	...	...	U-line
E	$10_{4,7}$-$9_{3,6}$	141554.413	42.6	13.00	141554.4	0.03	
A	$10_{3,7}$-$9_{4,6}$	141775.598	42.7	12.80	...	...	U-line
A	$10_{4,7}$-$9_{3,6}$	141895.366	42.7	12.80	141895.7	0.02	
E	$11_{2,9}$-$10_{3,8}$	142091.560	45.9	17.80	142091.6	0.12	
E	$11_{3,9}$-$10_{3,8}$	142091.597	45.9	6.33	” †	”	
E	$11_{2,9}$-$10_{2,8}$	142091.846	45.9	6.33	” †	”	
E	$11_{3,9}$-$10_{2,8}$	142091.884	45.9	17.80	” †	”	
A	$11_{2,9}$-$10_{3,8}$	142313.602	46.0	17.50	142313.6	0.08	
A	$11_{3,9}$-$10_{3,8}$	142313.677	46.0	6.62	” †	”	
A	$11_{2,9}$-$10_{2,8}$	142314.122	46.0	6.62	” †	”	
A	$11_{3,9}$-$10_{2,8}$	142314.196	46.0	17.50	” †	”	
E	$20_{6,14}$-$20_{6,15}$	142559.736	160.6	2.37	142559.7	0.05	
E	$20_{6,14}$-$20_{5,15}$	142559.736	160.6	14.50	” †	”	
E	$20_{7,14}$-$20_{6,15}$	142559.736	160.6	14.50	” †	”	
E	$20_{7,14}$-$20_{5,15}$	142559.736	160.6	2.37	” †	”	
E	$12_{1,11}$-$11_{2,10}$	142764.642	48.2	22.70	...	...	$CH_3CH_2{}^{13}CN$
E	$12_{2,11}$-$11_{2,10}$	142764.642	48.2	7.34	... †	...	”
E	$12_{1,11}$-$11_{1,10}$	142764.643	48.2	7.34	... †	...	”
E	$12_{2,11}$-$11_{1,10}$	142764.643	48.2	22.70	... †	...	”
A	$20_{6,14}$-$20_{6,15}$	143281.081	161.0	2.99	143281.1	0.03	
A	$20_{6,14}$-$20_{5,15}$	143281.081	161.0	14.00	” †	”	
A	$20_{7,14}$-$20_{6,15}$	143281.089	161.0	14.00	” †	”	
A	$20_{7,14}$-$20_{5,15}$	143281.089	161.0	2.99	” †	”	
E	$13_{0,13}$-$12_{1,12}$	143461.524	49.6	30.80	143461.5	0.23	U-line
E	$13_{1,13}$-$12_{0,12}$	143461.524	49.6	30.80	” †	”	”
E	$13_{0,13}$-$12_{0,12}$	143461.524	49.6	5.29	” †	”	”
E	$13_{1,13}$-$12_{1,12}$	143461.524	49.6	5.29	” †	”	”
A	$19_{5,14}$-$19_{4,15}$	143846.989	141.3	11.80	143847.4	0.06	
A	$19_{5,14}$-$19_{5,15}$	143846.989	141.3	2.57	” †	”	
A	$19_{6,14}$-$19_{5,15}$	143846.990	141.3	11.80	” †	”	
A	$19_{6,14}$-$19_{4,15}$	143846.991	141.3	2.57	” †	”	
E	$16_{2,14}$-$16_{1,15}$	143914.403	87.7	2.12	143914.5	0.03	
E	$16_{3,14}$-$16_{2,15}$	143914.403	87.7	2.12	” †	”	
E	$16_{3,14}$-$16_{1,15}$	143914.403	87.7	3.97	” †	”	
E	$16_{2,14}$-$16_{2,15}$	143914.403	87.7	3.97	” †	”	
A	$18_{4,14}$-$18_{4,15}$	144342.667	122.5	2.12	144342.6	0.06	
A	$18_{4,14}$-$18_{3,15}$	144342.667	122.5	9.60	” †	”	
A	$18_{5,14}$-$18_{3,15}$	144342.667	122.5	2.12	” †	”	
A	$18_{5,14}$-$18_{4,15}$	144342.667	122.5	9.60	” †	”	

Table B.5. continued.

Torsional substate	Transition $J_{K_a,K_c} - J'_{K'_a,K'_c}$	Predicted frequency (MHz)	E_{upp} (K)	$S_{ij}\mu^2$ (D^2)	Observed frequency (MHz)	T_{MB} (K)	Blends
A	$17_{4,14}$-$17_{2,15}$	144775.558	104.7	1.80	144775.6	0.04	
A	$17_{3,14}$-$17_{3,15}$	144775.558	104.7	1.80	” †	”	
A	$17_{3,14}$-$17_{2,15}$	144775.558	104.7	1.80	” †	”	
A	$17_{4,14}$-$17_{3,15}$	144775.558	104.7	1.80	” †	”	
A	$16_{3,14}$-$16_{1,15}$	145152.355	87.7	3.00	145152.6	0.04	
A	$16_{2,14}$-$16_{2,15}$	145152.355	87.7	3.00	” †	”	
A	$16_{2,14}$-$16_{1,15}$	145152.355	87.7	3.12	” †	”	
A	$16_{3,14}$-$16_{2,15}$	145152.355	87.7	3.12	” †	”	
A	$9_{5,5}$-$8_{4,4}$	145205.349	38.5	7.95	145205.3	0.03	
E	$7_{6,1}$-$6_{5,1}$	148696.498	27.5	8.56	...	...	U-line
E	$26_{11,15}$-$26_{11,16}$	149276.449	292.4	4.08	149276.9	0.03	
E	$26_{11,15}$-$26_{10,16}$	149276.477	292.4	25.30	” †	”	
E	$26_{12,15}$-$26_{11,16}$	149277.070	292.4	25.30	” †	”	
E	$26_{12,15}$-$26_{10,16}$	149277.098	292.4	4.08	” †	”	
A	$7_{6,1}$-$6_{5,2}$	150908.093	27.5	8.87	...	...	U-line
E	$10_{4,6}$-$9_{5,5}$	151162.032	45.6	10.30	...	...	U-line
A	$10_{4,6}$-$9_{5,5}$	151326.876	45.8	10.00	151327.1	0.02	
A	$23_{8,15}$-$23_{8,16}$	152044.752	219.2	3.82	152044.9	0.03	
A	$23_{8,15}$-$23_{7,16}$	152044.753	219.2	18.30	” †	”	
A	$23_{9,15}$-$23_{8,16}$	152044.779	219.2	18.30	” †	”	
A	$23_{9,15}$-$23_{7,16}$	152044.780	219.2	3.82	” †	”	
E	$22_{7,15}$-$22_{7,16}$	152110.350	196.1	2.58	152110.6	0.02	CH_3CH_2CN, E-CH_3OCOH
E	$22_{7,15}$-$22_{6,16}$	152110.350	196.1	17.00	” †	”	”
E	$22_{8,15}$-$22_{7,16}$	152110.352	196.1	17.00	” †	”	”
E	$22_{8,15}$-$22_{6,16}$	152110.352	196.1	2.58	” †	”	”
E	$11_{3,8}$-$10_{4,7}$	152114.541	49.9	15.30	...	...	CH_3CH_2CN, E-CH_3OCOH
E	$11_{4,8}$-$10_{4,7}$	152116.337	49.9	5.93	... †	...	”
A	$22_{7,15}$-$22_{7,16}$	152736.196	196.6	3.44	...	...	CH_3OH
A	$22_{7,15}$-$22_{6,16}$	152736.197	196.6	16.20	... †	...	”
A	$22_{8,15}$-$22_{7,16}$	152736.203	196.6	16.20	... †	...	”
A	$22_{8,15}$-$22_{6,16}$	152736.203	196.6	3.44	... †	...	”
E	$20_{5,15}$-$20_{4,16}$	152998.019	153.8	12.70	...	...	CH_2CHCN v_{11}=2, $CH_3{}^{13}CH_2CN$
E	$20_{6,15}$-$20_{5,16}$	152998.019	153.8	12.70	... †	...	”
E	$20_{6,15}$-$20_{4,16}$	152998.019	153.8	1.69	... †	...	”
E	$20_{5,15}$-$20_{5,16}$	152998.019	153.8	1.69	... †	...	”
A	$10_{5,6}$-$9_{4,5}$	153251.768	45.8	10.10	153251.8	0.04	CH_2CHCN v_{11}=2, $^{13}CH_3CH_2CN$
E	$19_{5,15}$-$19_{3,16}$	153342.329	134.1	2.02	153342.6	0.05	
E	$19_{4,15}$-$19_{4,16}$	153342.329	134.1	2.02	” †	”	
E	$19_{4,15}$-$19_{3,16}$	153342.329	134.1	9.71	” †	”	
E	$19_{5,15}$-$19_{4,16}$	153342.329	134.1	9.71	” †	”	
A	$21_{6,15}$-$21_{5,16}$	153350.871	174.9	14.00	...	...	A-CH_3OCOH, E-CH_3OCOH
A	$21_{6,15}$-$21_{6,16}$	153350.871	174.9	3.04	... †	...	”
A	$21_{7,15}$-$21_{6,16}$	153350.872	174.9	14.00	... †	...	”
A	$21_{7,15}$-$21_{5,16}$	153350.872	174.9	3.04	... †	...	”
E	$13_{1,12}$-$12_{2,11}$	153413.859	55.6	25.10	153413.9	0.10	
E	$13_{2,12}$-$12_{2,11}$	153413.859	55.6	7.91	” †	”	
E	$13_{2,12}$-$12_{1,11}$	153413.859	55.6	25.10	” †	”	
E	$13_{1,12}$-$12_{1,11}$	153413.859	55.6	7.91	” †	”	
A	$13_{1,12}$-$12_{2,11}$	153545.713	55.7	24.30	153545.7	0.08	
A	$13_{2,12}$-$12_{2,11}$	153545.713	55.7	8.64	” †	”	
A	$13_{2,12}$-$12_{1,11}$	153545.714	55.7	24.30	” †	”	
A	$13_{1,12}$-$12_{1,11}$	153545.714	55.7	8.64	” †	”	
E	$18_{4,15}$-$18_{2,16}$	153630.344	115.3	0.16	153630.6	0.02	
E	$18_{3,15}$-$18_{3,16}$	153630.344	115.3	0.16	” †	”	
E	$18_{3,15}$-$18_{2,16}$	153630.344	115.3	8.81	” †	”	
E	$18_{4,15}$-$18_{3,16}$	153630.344	115.3	8.81	” †	”	
A	$20_{5,15}$-$20_{4,16}$	153896.648	154.1	11.80	...	...	U-line
A	$20_{5,15}$-$20_{5,16}$	153896.648	154.1	2.61	... †	...	”
A	$20_{6,15}$-$20_{5,16}$	153896.648	154.1	11.80	... †	...	”
A	$20_{6,15}$-$20_{4,16}$	153896.648	154.1	2.61	... †	...	”
E	$14_{0,14}$-$13_{1,13}$	154112.386	57.0	11.60	154110.7	0.24	$(CH_3)_2CO$
E	$14_{1,14}$-$13_{0,13}$	154112.386	57.0	11.60	” †	”	”
E	$14_{0,14}$-$13_{0,13}$	154112.386	57.0	27.40	” †	”	”
E	$14_{1,14}$-$13_{1,13}$	154112.386	61.1	27.40	” †	”	”
E	$14_{1,14}$-$13_{1,13}$	154112.386	61.1	5.84	” †	”	”
A	$14_{0,14}$-$13_{0,13}$	154150.659	57.1	3.36	154150.9	0.12	

Table B.5. continued.

Torsional substate	Transition $J_{K_a,K_c} - J'_{K'_a,K'_c}$	Predicted frequency (MHz)	E_{upp} (K)	$S_{ij}\mu^2$ (D^2)	Observed frequency (MHz)	T_{MB} (K)	Blends
A	$14_{1,14}$-$13_{1,13}$	154150.659	57.1	3.36	” †	”	
A	$14_{0,14}$-$13_{1,13}$	154150.659	57.1	35.60	” †	”	
A	$14_{1,14}$-$13_{0,13}$	154150.659	57.1	35.60	” †	”	
E	$7_{7,1}$-$6_{6,1}$	154354.509	29.0	13.20	154354.6	0.04	
A	$9_{5,4}$-$8_{5,3}$	154827.786	40.2	4.72	...	...	
A	$10_{5,5}$-$9_{6,4}$	155734.077	48.2	6.16	155734.2	0.03	U-line
A	$7_{7,0}$-$6_{6,1}$	156272.154	29.5	13.20	156271.9	0.03	
E	$27_{11,16}$-$27_{11,17}$	159543.987	311.7	3.96	159544.3	0.05	U-line
E	$27_{11,16}$-$27_{10,17}$	159543.991	311.7	25.60	” †	”	”
E	$27_{12,16}$-$27_{11,17}$	159544.098	311.7	25.60	” †	”	”
E	$27_{12,16}$-$27_{10,17}$	159544.102	311.7	3.96	” †	”	”
E	$11_{5,7}$-$10_{4,6}$	162455.164	53.4	12.60	...	...	CH_2CHCN v_{11}=2
E	$12_{3,9}$-$11_{4,8}$	162742.955	57.7	17.50	...	...	$^{33}SO_2$, E-CH_3OCOH
E	$12_{4,9}$-$11_{4,8}$	162743.218	57.7	6.57	... †	...	”
E	$12_{3,9}$-$11_{3,8}$	162744.751	57.7	6.57	... †	...	”
E	$12_{4,9}$-$11_{3,8}$	162745.014	57.7	17.50	... †	...	”
A	$22_{6,16}$-$22_{5,17}$	163403.945	189.2	14.10	...	...	U-line
A	$22_{6,16}$-$22_{6,17}$	163403.945	189.2	3.09	... †	...	”
A	$22_{7,16}$-$22_{6,17}$	163403.945	189.2	14.10	... †	...	”
A	$22_{7,16}$-$22_{5,17}$	163403.945	189.2	3.09	... †	...	”
E	$14_{1,13}$-$13_{2,12}$	164062.852	63.5	27.80	164062.9	0.13	
E	$14_{2,13}$-$13_{1,12}$	164062.852	63.5	27.80	” †	”	
E	$14_{1,13}$-$13_{1,12}$	164062.852	63.5	8.12	” †	”	
E	$14_{2,13}$-$13_{2,12}$	164062.852	63.5	8.12	” †	”	
E	$15_{0,15}$-$14_{0,14}$	164762.926	64.9	13.50	164762.5	0.25	U-line
E	$15_{1,15}$-$14_{1,14}$	164762.926	64.9	13.50	” †	”	”
E	$15_{0,15}$-$14_{1,14}$	164762.926	64.9	28.40	” †	”	”
E	$15_{1,15}$-$14_{0,14}$	164762.926	64.9	28.40	” †	”	”
A	$15_{0,15}$-$14_{1,14}$	164800.487	65.0	11.70	164798.1	0.33	U-line
A	$15_{1,15}$-$14_{0,14}$	164800.487	65.0	11.70	” †	”	”
A	$15_{0,15}$-$14_{0,14}$	164800.487	65.0	30.20	” †	”	”
A	$15_{1,15}$-$14_{1,14}$	164800.487	65.0	30.20	” †	”	”
A	$10_{7,3}$-$9_{7,2}$	170087.129	51.0	4.05	170087.3	0.13	
A	$8_{7,2}$-$7_{6,1}$	171324.610	35.7	11.30	...	...	U-line
E	$13_{3,10}$-$12_{4,9}$	173375.257	66.0	19.70	173375.6	0.31	
E	$13_{4,10}$-$12_{4,9}$	173375.293	66.0	7.20	” †	”	
E	$13_{3,10}$-$12_{3,9}$	173375.519	66.0	7.20	” †	”	
E	$13_{4,10}$-$12_{3,9}$	173375.556	66.0	19.70	” †	”	
E	$15_{1,14}$-$14_{1,13}$	174711.537	71.8	15.20	174711.6	0.42	CH_3OCH_3
E	$15_{2,14}$-$14_{2,13}$	174711.537	71.8	15.20	” †	”	”
E	$15_{1,14}$-$14_{2,13}$	174711.537	71.8	23.60	” †	”	”
E	$15_{2,14}$-$14_{1,13}$	174711.537	71.8	23.60	” †	”	”
A	$15_{1,14}$-$14_{1,13}$	174841.224	71.9	12.20	...	...	$^{13}CH_2CHCN$, $^{13}CH_3CH_2CN$,
A	$15_{2,14}$-$14_{2,13}$	174841.224	71.9	12.20	... †	...	E-CH_3OCOH
A	$15_{1,14}$-$14_{2,13}$	174841.224	71.9	26.50	... †	...	”
A	$15_{2,14}$-$14_{1,13}$	174841.224	71.9	26.50	... †	...	”
E	$16_{0,16}$-$15_{0,15}$	175413.122	73.4	44.70	...	...	CH_3CHO v_t=1, A-CH_3OCOH
E	$16_{1,16}$-$15_{1,15}$	175413.122	73.4	44.70	... †	...	”
A	$16_{0,16}$-$15_{1,15}$	175449.982	73.4	11.90	175449.7	0.35	U-line
A	$16_{1,16}$-$15_{0,15}$	175449.982	73.4	11.90	” †	”	”
A	$16_{0,16}$-$15_{0,15}$	175449.982	73.4	32.90	” †	”	”
A	$16_{1,16}$-$15_{1,15}$	175449.982	73.4	32.90	” †	”	”
A	$18_{0,18}$-$17_{0,17}$	196747.892	91.8	12.80	196748.1	0.10	
A	$18_{1,18}$-$17_{1,17}$	196747.892	91.8	12.80	” †	”	”
A	$18_{0,18}$-$17_{1,17}$	196747.892	91.8	37.80	” †	”	”
A	$18_{1,18}$-$17_{0,17}$	196747.892	91.8	37.80	” †	”	”
E	$9_{9,1}$-$8_{8,1}$	199873.852	47.1	17.60	199873.7	0.15	
E	$9_{9,0}$-$8_{8,0}$	200425.435	47.7	17.60	200425.7	0.24	
E	$14_{5,9}$-$13_{6,8}$	204171.089	84.3	16.80	...	...	$CH_3{}^{13}CH_2CN$, U-line
E	$14_{6,9}$-$13_{5,8}$	204213.479	84.3	16.80	...	...	CCS
A	$14_{5,9}$-$13_{6,8}$	204607.577	84.5	16.40	204607.2	0.07	
A	$14_{5,9}$-$13_{5,8}$	204666.712	84.5	7.39	204668.2	0.22	
E	$15_{4,11}$-$14_{5,10}$	204667.655	89.7	21.70	” †	”	
E	$15_{5,11}$-$14_{5,10}$	204667.686	89.7	8.07	” †	”	
E	$15_{4,11}$-$14_{4,10}$	204667.872	89.7	8.07	” †	”	
E	$15_{5,11}$-$14_{4,10}$	204667.903	89.7	21.70	” †	”	

Table B.5. continued.

Torsional substate	Transition $J_{K_a,K_c} - J'_{K'_a,K'_c}$	Predicted frequency (MHz)	E_{upp} (K)	$S_{ij}\mu^2$ (D^2)	Observed frequency (MHz)	T_{MB} (K)	Blends
A	$14_{6,9}$-$13_{5,8}$	204678.184	84.5	16.40	204677.9	0.09	
A	$15_{4,11}$-$14_{5,10}$	205023.758	89.9	21.10	205023.8	0.28	
A	$15_{5,11}$-$14_{5,10}$	205023.828	89.9	8.53	” †	”	
A	$15_{4,11}$-$14_{4,10}$	205024.197	89.9	8.53	” †	”	
A	$15_{5,11}$-$14_{4,10}$	205024.267	89.9	21.10	” †	”	
A	$16_{3,13}$-$15_{4,12}$	205571.050	94.3	25.80	205571.0	0.22	
A	$16_{4,13}$-$15_{4,12}$	205571.050	94.3	9.76	” †	”	
A	$16_{3,13}$-$15_{3,12}$	205571.051	94.3	9.76	” †	”	
A	$16_{4,13}$-$15_{3,12}$	205571.052	94.3	25.80	” †	”	
E	$17_{2,15}$-$16_{3,14}$	205962.120	97.5	37.30	...	...	CH_3CH_2CN, U-line
E	$17_{3,15}$-$16_{2,14}$	205962.120	97.5	37.30	... †	...	”
E	$17_{2,15}$-$16_{2,14}$	205962.120	97.5	4.18	... †	...	”
E	$17_{3,15}$-$16_{3,14}$	205962.120	97.5	4.18	... †	...	”
E	$12_{8,4}$-$11_{8,3}$	205963.499	71.6	4.96	... †	...	”
E	$18_{1,17}$-$17_{1,16}$	206655.181	100.1	1.33	206654.6	0.54	
E	$18_{2,17}$-$17_{2,16}$	206655.181	100.1	1.33	” †	”	
E	$18_{1,17}$-$17_{2,16}$	206655.181	100.1	46.10	” †	”	
E	$18_{2,17}$-$17_{1,16}$	206655.181	100.1	46.10	” †	”	
E	$13_{7,6}$-$12_{8,5}$	206803.225	80.6	6.91	206803.1	0.02	
E	$19_{0,19}$-$18_{0,18}$	207361.422	101.7	22.10	207361.6	0.22	
E	$19_{1,19}$-$18_{1,18}$	207361.422	101.7	22.10	” †	”	
E	$19_{0,19}$-$18_{1,18}$	207361.422	101.7	31.40	” †	”	
E	$19_{1,19}$-$18_{0,18}$	207361.422	101.7	31.40	” †	”	
A	$10_{8,3}$-$9_{7,2}$	208597.448	52.9	11.50	208597.5	0.29	
E	$10_{8,3}$-$9_{7,3}$	208736.402	52.4	10.50	208736.2	0.28	
A	$10_{8,2}$-$9_{7,3}$	212470.096	53.0	11.30	...	...	A-CH_3OCOH
A	$14_{6,8}$-$13_{7,7}$	214661.125	88.5	13.60	214660.6	0.32	A-CH_3OCOH
E	$15_{6,10}$-$14_{6,9}$	214760.818	94.6	7.75	214759.7	0.12	CH_3NH_2
E	$15_{5,10}$-$14_{5,9}$	214766.203	94.6	7.75	214766.4	0.13	U-line
E	$15_{6,10}$-$14_{5,9}$	214766.203	94.6	19.00	” †	”	”
E	$14_{7,8}$-$13_{6,7}$	214959.007	88.2	14.00	214959.0	0.14	
A	$16_{4,12}$-$15_{5,11}$	215642.336	100.2	23.30	215642.5	0.16	
A	$16_{5,12}$-$15_{5,11}$	215642.347	100.2	9.25	” †	”	
A	$16_{4,12}$-$15_{4,11}$	215642.406	100.2	9.25	” †	”	
A	$16_{5,12}$-$15_{4,11}$	215642.416	100.2	23.30	” †	”	
E	$17_{3,14}$-$16_{4,13}$	215931.507	104.4	29.20	215931.6	0.25	/g+−g-/-CH_3CH_2OH
E	$17_{4,14}$-$16_{4,13}$	215931.507	104.4	9.26	” †	”	”
E	$17_{3,14}$-$16_{3,13}$	215931.507	104.4	9.26	” †	”	”
E	$17_{4,14}$-$16_{3,13}$	215931.507	104.4	29.20	” †	”	”
E	$10_{9,1}$-$9_{8,1}$	216388.399	55.4	15.70	...	...	U-line
E	$18_{2,16}$-$17_{3,15}$	216607.211	107.9	36.20	216607.1	0.29	
E	$18_{3,16}$-$17_{2,15}$	216607.211	107.9	36.20	” †	”	
E	$18_{2,16}$-$17_{2,15}$	216607.211	107.9	8.21	” †	”	
E	$18_{3,16}$-$17_{3,15}$	216607.211	107.9	8.21	” †	”	
A	$18_{2,16}$-$17_{3,15}$	216811.791	108.1	12.50	216811.6	0.31	
A	$18_{3,16}$-$17_{2,15}$	216811.791	108.1	12.50	” †	”	
A	$18_{2,16}$-$17_{2,15}$	216811.791	108.1	31.80	” †	”	
A	$18_{3,16}$-$17_{3,15}$	216811.791	108.1	31.80	” †	”	
A	$19_{1,18}$-$18_{1,17}$	217428.127	110.6	20.20	217428.4	0.70	^{13}CN
A	$19_{2,18}$-$18_{2,17}$	217428.127	110.6	20.20	” †	”	”
A	$19_{1,18}$-$18_{2,17}$	217428.127	110.6	20.20	” †	”	”
A	$19_{2,18}$-$18_{1,17}$	217428.127	110.6	20.20	” †	”	”
A	$19_{1,18}$-$18_{1,17}$	217428.127	110.6	20.20	217428.3	0.70	HCC^{13}CN
A	$19_{2,18}$-$18_{2,17}$	217428.127	110.6	20.20	” †	”	”
A	$19_{1,18}$-$18_{2,17}$	217428.127	110.6	30.10	” †	”	”
A	$19_{2,18}$-$18_{1,17}$	217428.127	110.6	30.10	” †	”	”
A	$10_{9,2}$-$9_{8,1}$	217473.888	55.5	15.80	217474.2	0.15	
A	$10_{9,1}$-$9_{8,2}$	217714.818	55.5	15.80	...	...	U-line
E	$20_{0,20}$-$19_{0,19}$	218010.022	112.1	23.90	218010.0	0.21	
E	$20_{1,20}$-$19_{1,19}$	218010.022	112.1	23.90	” †	”	
E	$20_{0,20}$-$19_{1,19}$	218010.022	112.1	32.60	” †	”	
E	$20_{1,20}$-$19_{0,19}$	218010.022	112.1	32.60	” †	”	
A	$20_{0,20}$-$19_{1,19}$	218044.215	112.2	15.30	218044.4	0.46	
A	$20_{1,20}$-$19_{0,19}$	218044.215	112.2	15.30	” †	”	
A	$20_{0,20}$-$19_{0,19}$	218044.215	112.2	41.20	” †	”	
A	$20_{1,20}$-$19_{1,19}$	218044.215	112.2	41.20	” †	”	

Table B.5. continued.

Torsional substate	Transition $J_{K_a,K_c} - J'_{K'_a,K'_c}$	Predicted frequency (MHz)	E_{upp} (K)	$S_{ij}\mu^2$ (D^2)	Observed frequency (MHz)	T_{MB} (K)	Blends
E	$13_{7,6}$-$12_{7,5}$	219194.637	80.6	6.33	...	...	CH_2CHCN v_{11}=2, E-CH_3OCOH
E	$12_{8,5}$-$11_{7,4}$	220286.773	70.7	7.49	...	...	U-line
A	$13_{7,6}$-$12_{7,5}$	220336.860	80.8	6.58	220337.1	0.12	CH_2CHCN v_{11}=2
E	$14_{7,7}$-$13_{8,6}$	222456.760	91.5	10.50	222456.8	0.20	
E	$10_{10,1}$-$9_{9,1}$	222653.999	57.8	19.80	...	...	E-CH_3OCOH, E-$CH_3O^{13}COH$
A	$28_{7,22}$-$28_{5,23}$	223476.376	286.2	14.00	223476.4	0.12	U-line
A	$28_{6,22}$-$28_{6,23}$	223476.376	286.2	14.00	” †	”	”
A	$28_{6,22}$-$28_{5,23}$	223476.376	286.2	3.63	” †	”	”
A	$28_{7,22}$-$28_{6,23}$	223476.376	286.2	3.63	” †	”	”
E	$15_{6,9}$-$14_{7,8}$	224957.535	99.0	16.30	224957.6	0.16	
A	$15_{6,9}$-$14_{7,8}$	225435.035	99.3	16.00	...	...	U-line
E	$17_{4,13}$-$16_{5,12}$	225926.462	110.8	26.30	...	...	A-CH_3OCOH
E	$17_{5,13}$-$16_{5,12}$	225926.463	110.8	9.14	... †	...	”
E	$17_{4,13}$-$16_{4,12}$	225926.467	110.8	9.14	... †	...	”
E	$17_{5,13}$-$16_{4,12}$	225926.467	110.8	26.30	... †	...	”
A	$17_{4,13}$-$16_{5,12}$	226265.469	111.1	25.40	...	...	CH_2OHCHO, CH_3NH_2
A	$17_{5,13}$-$16_{5,12}$	226265.471	111.1	9.98	... †	...	”
A	$17_{4,13}$-$16_{4,12}$	226265.480	111.1	9.98	... †	...	”
A	$17_{5,13}$-$16_{4,12}$	226265.481	111.1	25.40	... †	...	”
E	$18_{3,15}$-$17_{4,14}$	226572.817	115.3	31.50	226572.6	0.11	
E	$18_{4,15}$-$17_{3,14}$	226572.817	115.3	31.50	” †	”	
E	$18_{3,15}$-$17_{3,14}$	226572.817	115.3	9.81	” †	”	
E	$18_{4,15}$-$17_{4,14}$	226572.817	115.3	9.81	” †	”	
A	$18_{3,15}$-$17_{3,14}$	226844.496	115.5	11.20	...	...	CH_3OH v_t=1, U-line
A	$18_{4,15}$-$17_{4,14}$	226844.496	115.5	11.20	... †	...	”
A	$18_{3,15}$-$17_{4,14}$	226844.496	115.5	30.10	... †	...	”
A	$18_{4,15}$-$17_{3,14}$	226844.496	115.5	30.10	... †	...	”
E	$19_{2,17}$-$18_{2,16}$	227251.864	118.8	3.30	227251.9	0.28	
E	$19_{3,17}$-$18_{3,16}$	227251.864	118.8	3.30	” †	”	
E	$19_{2,17}$-$18_{3,16}$	227251.864	118.8	44.00	” †	”	
E	$19_{3,17}$-$18_{2,16}$	227251.864	118.8	44.00	” †	”	
A	$38_{15,23}$-$38_{14,24}$	227453.385	605.2	33.60	227454.5	0.38	
A	$38_{15,23}$-$38_{15,24}$	227453.385	605.2	6.97	” †	”	
A	$38_{16,23}$-$38_{15,24}$	227453.385	605.2	33.60	” †	”	
A	$38_{16,23}$-$38_{16,24}$	227453.385	605.2	6.97	” †	”	
A	$19_{2,17}$-$18_{2,16}$	227454.435	119.0	20.50	” †	”	
A	$19_{3,17}$-$18_{3,16}$	227454.435	119.0	20.50	” †	”	
A	$19_{2,17}$-$18_{3,16}$	227454.435	119.0	26.70	” †	”	
A	$19_{3,17}$-$18_{2,16}$	227454.435	119.0	26.70	” †	”	
E	$20_{1,19}$-$19_{1,18}$	227948.547	121.4	0.21	227948.6	0.36	
E	$20_{2,19}$-$19_{2,18}$	227948.547	121.4	0.21	” †	”	
E	$20_{1,19}$-$19_{2,18}$	227948.547	121.4	53.00	” †	”	
E	$20_{2,19}$-$19_{1,18}$	227948.547	121.4	53.00	” †	”	
A	$20_{1,19}$-$19_{2,18}$	228073.754	121.6	15.90	228073.3	0.17	
A	$20_{2,19}$-$19_{1,18}$	228073.754	121.6	15.90	” †	”	
A	$20_{1,19}$-$19_{1,18}$	228073.754	121.6	37.40	” †	”	
A	$20_{2,19}$-$19_{2,18}$	228073.754	121.6	37.40	” †	”	
E	$21_{0,21}$-$20_{0,20}$	228658.172	123.1	17.30	228657.9	0.46	
E	$21_{1,21}$-$20_{1,20}$	228658.172	123.1	17.30	” †	”	
E	$21_{0,21}$-$20_{1,20}$	228658.172	123.1	42.00	” †	”	
E	$21_{1,21}$-$20_{0,20}$	228658.172	123.1	42.00	” †	”	
A	$21_{0,21}$-$20_{0,20}$	228691.729	123.2	1.21	228691.9	0.32	
A	$21_{1,21}$-$20_{1,20}$	228691.729	123.2	1.21	” †	”	
A	$21_{0,21}$-$20_{1,20}$	228691.729	123.2	58.10	” †	”	
A	$21_{1,21}$-$20_{0,20}$	228691.729	123.2	58.10	” †	”	
A	$14_{7,7}$-$13_{7,6}$	228744.365	91.8	6.88	228744.3	0.11	
E	$14_{11,3}$-$13_{11,2}$	229530.903	100.6	4.15	229530.9	0.03	
A	$14_{10,5}$-$13_{10,4}$	230766.574	97.7	5.32	230766.5	0.04	CH_2OHCHO
E	$11_{9,3}$-$10_{8,3}$	231462.153	63.5	13.40	231462.6	0.15	
E	$11_{9,2}$-$10_{8,2}$	232178.775	64.0	13.50	232178.7	0.30	
A	$15_{7,8}$-$14_{8,7}$	235019.381	103.2	12.90	235018.8	0.27	$CH_3CH_2C^{15}N$
E	$18_{4,14}$-$17_{5,13}$	236560.226	122.2	28.80	236560.3	0.37	
E	$18_{5,14}$-$17_{5,13}$	236560.226	122.2	9.54	” †	”	
E	$18_{4,14}$-$17_{4,13}$	236560.227	122.2	9.54	” †	”	
E	$18_{5,14}$-$17_{4,13}$	236560.227	122.2	28.80	” †	”	
A	$18_{4,14}$-$17_{5,13}$	236891.531	122.5	27.60	236891.6	0.26	

Table B.5. continued.

Torsional substate	Transition $J_{K_a,K_c} - J'_{K'_a,K'_c}$	Predicted frequency (MHz)	E_{upp} (K)	$S_{ij}\mu^2$ (D^2)	Observed frequency (MHz)	T_{MB} (K)	Blends
A	$18_{5,14}$-$17_{5,13}$	236891.532	122.5	10.70	” †	”	
A	$18_{4,14}$-$17_{4,13}$	236891.533	122.5	10.70	” †	”	
A	$18_{5,14}$-$17_{4,13}$	236891.533	122.5	27.60	” †	”	
E	$19_{3,16}$-$18_{3,15}$	237214.119	128.6	11.50	237214.0	0.82	E-CH_3OCOH v_t=2
E	$19_{4,16}$-$18_{4,15}$	237214.119	128.6	11.50	” †	”	”
E	$19_{3,16}$-$18_{4,15}$	237214.119	126.7	32.70	” †	”	”
E	$19_{4,16}$-$18_{3,15}$	237214.119	126.7	32.70	” †	”	”
A	$15_{7,8}$-$14_{7,7}$	237237.036	103.2	7.41	237236.7	0.21	A-CH_3OCOH, U-line
A	$20_{2,18}$-$19_{3,17}$	238096.658	130.5	50.10	...	...	CH_2CHCN v_{11}=1
A	$20_{3,18}$-$19_{2,17}$	238096.658	130.5	50.10	... †	...	”
E	$11_{10,2}$-$10_{9,2}$	238547.665	66.3	18.00	238548.6	0.19	U-line
E	$21_{1,20}$-$20_{2,19}$	238594.419	132.9	4.29	238594.5	0.30	
E	$21_{2,20}$-$20_{1,19}$	238594.419	132.9	4.29	” †	”	
E	$21_{1,20}$-$20_{1,19}$	238594.419	132.9	51.90	” †	”	
E	$21_{2,20}$-$20_{2,19}$	238594.419	132.9	51.90	” †	”	
A	$21_{1,20}$-$20_{1,19}$	238718.881	133.0	0.41	238718.1	0.35	HCCCN (v_4+3v_7)
A	$21_{2,20}$-$20_{2,19}$	238718.881	133.0	0.41	” †	”	”
A	$21_{1,20}$-$20_{2,19}$	238718.881	133.0	55.70	” †	”	”
A	$21_{2,20}$-$20_{1,19}$	238718.881	133.0	55.70	” †	”	”
E	$11_{10,1}$-$10_{9,1}$	238898.960	66.9	18.00	238900.1	0.31	NH_2CHO
E	$22_{0,22}$-$21_{1,21}$	239305.851	134.6	12.40	239305.9	0.20	
E	$22_{1,22}$-$21_{0,21}$	239305.851	134.6	12.40	” †	”	
E	$22_{0,22}$-$21_{0,21}$	239305.851	134.6	49.80	” †	”	
E	$22_{1,22}$-$21_{1,21}$	239305.851	134.6	49.80	” †	”	
A	$22_{0,22}$-$21_{1,21}$	239338.784	134.6	15.90	239339.1	1.13	$SO^{18}O$, U-line
A	$22_{1,22}$-$21_{0,21}$	239338.784	134.6	15.90	” †	”	”
A	$22_{0,22}$-$21_{0,21}$	239338.784	134.6	46.30	” †	”	”
A	$22_{1,22}$-$21_{1,21}$	239338.784	134.6	46.30	” †	”	”
A	$11_{10,1}$-$10_{9,2}$	240355.220	67.1	18.00	240354.8	0.09	
A	$28_{5,24}$-$28_{3,25}$	244417.721	264.2	4.68	244417.6	0.05	t-HCOOD
A	$28_{4,24}$-$28_{4,25}$	244417.721	264.2	4.68	” †	”	”
A	$28_{4,24}$-$28_{3,25}$	244417.721	264.2	7.43	” †	”	”
A	$28_{5,24}$-$28_{4,25}$	244417.721	264.2	7.43	” †	”	”
A	$12_{9,4}$-$11_{8,3}$	244747.138	73.6	11.50	244747.4	0.23	U-line
E	$11_{11,1}$-$10_{10,1}$	245444.940	69.6	22.00	245444.4	0.03	A-CH_3OCOH
E	$17_{6,11}$-$16_{7,10}$	246093.214	122.1	20.90	246093.6	0.12	
E	$17_{7,11}$-$16_{7,10}$	246093.991	122.1	8.65	” †	”	
E	$17_{6,11}$-$16_{6,10}$	246097.792	122.1	8.65	246098.5	0.23	
E	$17_{7,11}$-$16_{6,10}$	246098.569	122.1	20.90	” †	”	
A	$16_{7,9}$-$15_{8,8}$	246229.600	115.0	15.40	...	...	NH_2D
A	$16_{8,9}$-$15_{8,8}$	246370.321	115.0	8.03	246370.4	0.03	
E	$18_{5,13}$-$17_{6,12}$	246584.848	128.6	25.90	246585.3	0.36	
E	$18_{6,13}$-$17_{6,12}$	246584.851	128.6	9.45	” †	”	
E	$18_{5,13}$-$17_{5,12}$	246584.872	128.6	9.45	” †	”	
E	$18_{6,13}$-$17_{5,12}$	246584.876	128.6	25.90	” †	”	
A	$16_{8,9}$-$15_{7,8}$	246966.210	115.0	15.40	246966.5	0.28	CH_2CHCN v_{11}=2
A	$18_{5,13}$-$17_{6,12}$	246972.022	128.9	25.10	246971.9	0.26	A-$CH_3O^{13}COH$
A	$18_{6,13}$-$17_{6,12}$	246972.032	128.9	10.20	” †	”	”
A	$18_{5,13}$-$17_{5,12}$	246972.081	128.9	10.20	” †	”	”
A	$18_{6,13}$-$17_{5,12}$	246972.090	128.9	25.10	” †	”	”
E	$19_{4,15}$-$18_{5,14}$	247195.409	134.1	31.50	247195.5	0.41	A-$CH_3O^{13}COH$, A-CH_3OCOH
E	$19_{5,15}$-$18_{4,14}$	247195.409	134.1	31.50	” †	”	”
E	$19_{4,15}$-$18_{4,14}$	247195.409	134.1	9.75	” †	”	”
E	$19_{5,15}$-$18_{5,14}$	247195.409	134.1	9.75	” †	”	”
A	$19_{4,15}$-$18_{5,14}$	247519.427	134.1	29.70	...	...	HCOOH
A	$19_{5,15}$-$18_{5,14}$	247519.427	134.1	11.50	... †	...	”
A	$19_{4,15}$-$18_{4,14}$	247519.427	134.1	11.50	... †	...	”
A	$19_{5,15}$-$18_{4,14}$	247519.427	134.1	29.70	... †	...	”
A	$15_{10,6}$-$14_{10,5}$	247755.405	109.6	6.39	247755.9	0.10	$CH_3CH_2{}^{13}CN$
E	$20_{3,17}$-$19_{3,16}$	247855.202	138.6	39.00	247855.1	0.19	
E	$20_{4,17}$-$19_{4,16}$	247855.202	138.6	39.00	” †	”	
E	$20_{3,17}$-$19_{4,16}$	247855.202	138.6	8.14	” †	”	
E	$20_{4,17}$-$19_{3,16}$	247855.202	138.6	8.14	” †	”	
A	$20_{3,17}$-$19_{3,16}$	248118.794	138.9	12.50	248117.9	0.22	
A	$20_{4,17}$-$19_{4,16}$	248118.794	138.9	12.50	” †	”	
A	$20_{3,17}$-$19_{4,16}$	248118.794	138.9	34.60	” †	”	

Table B.5. continued.

Torsional substate	Transition $J_{K_a,K_c} - J'_{K'_a,K'_c}$	Predicted frequency (MHz)	E_{upp} (K)	$S_{ij}\mu^2$ (D^2)	Observed frequency (MHz)	T_{MB} (K)	Blends
A	$20_{4,17}$-$19_{3,16}$	248118.794	138.9	34.60	” †	”	
E	$21_{2,19}$-$20_{2,18}$	248539.582	142.2	22.90	... †	...	CH_2CHCN, CH_2CHCN v_{11}=2
E	$21_{3,19}$-$20_{3,18}$	248539.582	142.2	22.90	... †	...	”
E	$21_{2,19}$-$20_{3,18}$	248539.582	142.2	30.10	... †	...	”
E	$21_{3,19}$-$20_{2,18}$	248539.582	142.2	30.10	... †	...	”
A	$21_{2,19}$-$20_{2,18}$	248738.400	142.4	45.50	... †	...	CH_2CHCN v_{15}=1, E-CH_3OCOH
A	$21_{3,19}$-$20_{3,18}$	248738.400	142.4	45.50	... †	...	”
A	$21_{2,19}$-$20_{3,18}$	248738.400	142.4	7.52	... †	...	”
A	$21_{3,19}$-$20_{2,18}$	248738.400	142.4	7.52	... †	...	”
E	$22_{1,21}$-$21_{1,20}$	249239.716	144.9	1.32	249239.6	0.36	$CH_3CH_2{}^{13}CN$
E	$22_{2,21}$-$21_{2,20}$	249239.716	144.9	1.32	” †	”	”
E	$22_{1,21}$-$21_{2,20}$	249239.716	144.9	57.70	” †	”	”
E	$22_{2,21}$-$21_{1,20}$	249239.716	144.9	57.70	” †	”	”
A	$22_{1,21}$-$21_{1,20}$	249363.480	145.0	3.89	249363.3	0.26	
A	$22_{2,21}$-$21_{2,20}$	249363.480	145.0	3.89	” †	”	
A	$22_{1,21}$-$21_{2,20}$	249363.480	145.0	55.10	” †	”	
A	$22_{2,21}$-$21_{1,20}$	249363.480	145.0	55.10	” †	”	
E	$23_{0,23}$-$22_{1,22}$	249953.038	146.6	29.50	249953.1	0.18	
E	$23_{1,23}$-$22_{0,22}$	249953.038	146.6	29.50	” †	”	
E	$23_{0,23}$-$22_{0,22}$	249953.038	146.6	35.60	” †	”	
E	$23_{1,23}$-$22_{1,22}$	249953.038	146.6	35.60	” †	”	
A	$23_{0,23}$-$22_{1,22}$	249985.360	146.6	28.50	249985.0	0.94	CH_3CH_2CN, CH_3CHO v_t=1
A	$23_{1,23}$-$22_{0,22}$	249985.360	146.6	28.50	” †	”	”
A	$23_{0,23}$-$22_{0,22}$	249985.360	146.6	36.70	” †	”	”
A	$23_{1,23}$-$22_{1,22}$	249985.360	146.6	36.70	” †	”	”
A	$13_{9,5}$-$12_{8,4}$	252121.729	83.8	9.61	252121.8	0.37	U-line
E	$30_{6,25}$-$30_{4,26}$	252717.483	310.4	7.15	252717.3	0.07	$SO^{17}O$
E	$30_{5,25}$-$30_{5,26}$	252717.483	310.4	7.15	” †	”	”
E	$30_{5,25}$-$30_{4,26}$	252717.483	310.4	7.77	” †	”	”
E	$30_{6,25}$-$30_{5,26}$	252717.483	310.4	7.77	” †	”	”
A	$12_{9,3}$-$11_{8,4}$	252930.941	73.7	11.00	252931.1	0.22	$SO^{17}O$, U-line
E	$12_{10,2}$-$11_{9,2}$	254760.866	76.3	15.90	254761.9	0.09	A-CH_3OCOH
E	$16_{8,8}$-$15_{9,7}$	254762.997	118.5	12.50	” †	”	”
A	$14_{9,6}$-$13_{8,5}$	255150.318	94.9	9.04	255150.8	0.03	
A	$12_{10,3}$-$11_{9,2}$	255737.223	76.4	16.10	...	...	$CH_3CH_2{}^{13}CN$, U-line
E	$16_{9,8}$-$15_{9,7}$	255832.627	118.5	7.53	255831.9	0.12	CH_3CH_2CN
A	$16_{9,8}$-$15_{9,7}$	256156.115	118.9	7.72	256156.5	0.09	U-line
A	$12_{10,2}$-$11_{9,3}$	256500.454	76.4	16.00	...	...	E-CH_3OCHO v_t=1
E	$18_{6,12}$-$17_{7,11}$	256675.851	134.4	23.20	...	...	$^{13}CH_3OH$, $^{13}CH_3CH_2CN$
E	$18_{7,12}$-$17_{7,11}$	256675.975	134.4	9.23	... †	...	”
E	$18_{6,12}$-$17_{6,11}$	256676.628	134.4	9.23	... †	...	”
E	$18_{7,12}$-$17_{6,11}$	256676.752	134.4	23.20	... †	...	”
E	$20_{4,16}$-$19_{5,15}$	257831.354	146.4	34.60	...	...	E-CH_3OCHO v_t=1, $CH_3{}^{13}CH_2CN$,
E	$20_{5,16}$-$19_{4,15}$	257831.354	146.4	34.60	... †	...	E-CH_3OCOH
E	$20_{4,16}$-$19_{4,15}$	257831.354	146.4	9.47	... †	...	”
E	$20_{5,16}$-$19_{5,15}$	257831.354	146.4	9.47	... †	...	”
E	$22_{2,20}$-$21_{2,19}$	259182.541	154.6	1.55	259182.5	0.18	
E	$22_{3,20}$-$21_{3,19}$	259182.541	154.6	1.55	” †	”	
E	$22_{2,20}$-$21_{3,19}$	259182.541	154.6	54.40	” †	”	
E	$22_{3,20}$-$21_{2,19}$	259182.541	154.6	54.40	” †	”	
A	$22_{2,20}$-$21_{2,19}$	259379.607	154.8	14.30	259379.6	0.30	
A	$22_{3,20}$-$21_{3,19}$	259379.607	154.8	14.30	” †	”	
A	$22_{2,20}$-$21_{3,19}$	259379.607	154.8	41.60	” †	”	
A	$22_{3,20}$-$21_{2,19}$	259379.607	154.8	41.60	” †	”	
E	$16_{9,8}$-$15_{8,7}$	259547.792	118.5	12.70	259548.2	0.06	
A	$16_{8,8}$-$15_{8,7}$	259701.679	118.8	7.82	259701.5	0.18	CCS
E	$23_{1,22}$-$22_{2,21}$	259884.412	157.3	0.19	259884.6	1.6	CH_3CH_2CN v_{13}/v_{21}
E	$23_{2,22}$-$22_{1,21}$	259884.412	157.3	0.19	” †	”	”
E	$23_{1,22}$-$22_{1,21}$	259884.412	157.3	61.80	” †	”	”
E	$23_{2,22}$-$22_{2,21}$	259884.412	157.3	61.80	” †	”	”
A	$23_{1,22}$-$22_{2,21}$	260007.527	157.5	21.40	...	...	CH_3OCH_3, t-CH_3CH_2OH,
A	$23_{2,22}$-$22_{1,21}$	260007.527	157.5	21.40	... †	...	$CH_2{}^{13}CHCN$, $CH_2CH^{13}CN$
A	$23_{1,22}$-$22_{1,21}$	260007.527	157.5	40.50	... †	...	”
A	$23_{2,22}$-$22_{2,21}$	260007.527	157.5	40.50	... †	...	”
A	$24_{0,24}$-$23_{1,23}$	260631.436	159.1	20.30	260631.4	0.23	
A	$24_{1,24}$-$23_{0,23}$	260631.436	159.1	20.30	” †	”	

Table B.5. continued.

Torsional substate	Transition $J_{K_a,K_c} - J'_{K'_a,K'_c}$	Predicted frequency (MHz)	E_{upp} (K)	$S_{ij}\mu^2$ (D^2)	Observed frequency (MHz)	T_{MB} (K)	Blends
A	$24_{0,24}$-$23_{0,23}$	260631.436	159.1	47.70	” †	”	
A	$24_{1,24}$-$23_{1,23}$	260631.436	159.1	47.70	” †	”	
E	$12_{11,2}$-$11_{10,2}$	261346.426	78.9	20.20	261346.4	0.12	
E	$12_{11,1}$-$11_{10,1}$	261411.291	79.4	20.20	261411.3	0.26	
A	$15_{9,6}$-$14_{9,5}$	261925.438	108.5	7.75	261925.6	0.09	
A	$16_{12,4}$-$15_{12,3}$	264119.662	128.7	5.46	264119.9	0.05	
E	$17_{8,9}$-$16_{9,8}$	266467.040	131.3	15.20	266466.5	0.24	$CH_2{}^{13}CHCN$
E	$18_{7,11}$-$17_{8,10}$	266884.676	139.8	20.50	266884.4	0.06	
E	$18_{8,11}$-$17_{8,10}$	266887.840	139.8	8.97	266888.4	0.16	CH_2CHCN v_{11}=1
E	$18_{8,11}$-$17_{7,10}$	266904.991	139.8	20.50	266904.6	0.33	U-line
A	$18_{7,11}$-$17_{8,10}$	267389.203	140.2	20.00	267389.1	0.07	
A	$19_{6,13}$-$18_{7,12}$	267698.403	147.6	24.80	267698.2	0.85	$(CH_3)_2CO$
A	$19_{7,13}$-$18_{7,12}$	267698.449	147.6	10.50	” †	”	”
A	$19_{6,13}$-$18_{6,12}$	267698.679	147.6	10.50	” †	”	”
A	$19_{7,13}$-$18_{6,12}$	267698.726	147.6	24.80	” †	”	”
A	$18_{8,11}$-$17_{7,10}$	267425.544	140.2	20.00	267425.8	0.06	
E	$20_{5,15}$-$19_{6,14}$	267833.809	153.8	30.90	267834.1	0.18	
E	$20_{6,15}$-$19_{6,14}$	267833.809	153.8	10.20	” †	”	
E	$20_{5,15}$-$19_{5,14}$	267833.810	153.8	10.20	” †	”	
E	$20_{6,15}$-$19_{5,14}$	267833.810	153.8	30.90	” †	”	
E	$17_{9,9}$-$16_{8,8}$	267799.269	131.3	15.20	267799.3	0.15	
A	$20_{5,15}$-$19_{6,14}$	268198.078	154.1	29.40	...	...	CH_3CH_2CN, $^{13}CH_2CHCN$,
A	$20_{6,15}$-$19_{6,14}$	268198.079	154.1	11.70	... †	...	CH_2CHCN v_{11}=1
A	$20_{5,15}$-$19_{5,14}$	268198.080	154.1	11.70	... †	...	”
A	$20_{6,15}$-$19_{5,14}$	268198.080	154.1	29.40	... †	...	”
E	$21_{4,17}$-$20_{4,16}$	268467.608	159.3	11.80	...	...	CH_3OCH_3
E	$21_{5,17}$-$20_{5,16}$	268467.608	159.3	11.80	... †	...	”
E	$21_{4,17}$-$20_{5,16}$	268467.608	159.3	35.20	... †	...	”
E	$21_{5,17}$-$20_{4,16}$	268467.608	159.3	35.20	... †	...	”
A	$21_{4,17}$-$20_{4,16}$	268778.003	159.6	13.00	268778.0	0.40	
A	$21_{5,17}$-$20_{5,16}$	268778.003	159.6	13.00	” †	”	
A	$21_{4,17}$-$20_{5,16}$	268778.003	159.6	33.90	” †	”	
A	$21_{5,17}$-$20_{4,16}$	268778.003	159.6	33.90	” †	”	
A	$13_{10,4}$-$12_{9,3}$	269622.116	86.6	13.80	269622.4	0.39	
A	$12_{12,1}$-$11_{11,0}$	269701.395	83.4	24.20	269702.0	0.30	
A	$12_{12,0}$-$11_{11,1}$	269701.977	83.4	24.20	” †	”	
E	$23_{2,21}$-$22_{3,20}$	269824.844	167.6	28.40	269824.7	0.29	
E	$23_{3,21}$-$22_{2,20}$	269824.844	167.6	28.40	” †	”	
E	$23_{2,21}$-$22_{2,20}$	269824.844	167.6	30.40	” †	”	
E	$23_{3,21}$-$22_{3,20}$	269824.844	167.6	30.40	” †	”	
E	$13_{10,4}$-$12_{9,4}$	269900.783	86.0	12.60	269900.2	0.40	CH_3CH_2CN v_{13}/v_{21}
A	$23_{2,21}$-$22_{3,20}$	270020.235	167.8	28.70	270020.2	0.46	
A	$23_{3,21}$-$22_{2,20}$	270020.235	167.8	28.70	” †	”	
A	$23_{2,21}$-$22_{2,20}$	270020.235	167.8	30.10	” †	”	
A	$23_{3,21}$-$22_{3,20}$	270020.235	167.8	30.10	” †	”	
A	$24_{1,23}$-$23_{2,22}$	270650.996	170.5	24.40	270651.2	0.28	
A	$24_{2,23}$-$23_{1,22}$	270650.996	170.5	24.40	” †	”	
A	$24_{1,23}$-$23_{1,22}$	270650.996	170.5	40.50	” †	”	
A	$24_{2,23}$-$23_{2,22}$	270650.996	170.5	40.50	” †	”	
E	$25_{0,25}$-$24_{1,24}$	271245.857	172.1	62.10	...	...	A-CH_3OCOH
E	$25_{1,25}$-$24_{0,24}$	271245.857	172.1	62.10	... †	...	”
E	$25_{0,25}$-$24_{0,24}$	271245.857	172.1	8.86	... †	...	”
E	$25_{1,25}$-$24_{1,24}$	271245.857	172.1	8.86	... †	...	”
A	$25_{0,25}$-$24_{1,24}$	271276.991	172.2	23.70	271276.6	0.36	
A	$25_{1,25}$-$24_{0,24}$	271276.991	172.2	23.70	” †	”	
A	$25_{0,25}$-$24_{0,24}$	271276.991	172.2	47.20	” †	”	
A	$25_{1,25}$-$24_{1,24}$	271276.991	172.2	47.20	” †	”	
A	$17_{9,8}$-$16_{10,7}$	272567.754	135.3	10.70	272568.3	0.14	
A	$13_{9,4}$-$12_{8,5}$	277131.953	84.3	7.68	277134.6	0.44	U-line
E	$18_{8,10}$-$17_{9,9}$	277219.294	144.6	17.70	277219.6	0.27	A-CH_3OCOH, CH_2CHCN v_{11}=2
E	$13_{11,2}$-$12_{10,2}$	277306.696	89.6	18.20	277306.8	0.35	U-line
E	$19_{7,12}$-$18_{7,11}$	277433.861	153.1	9.55	277434.0	0.41	CH_2CHCN v_{11}=2
E	$19_{8,12}$-$18_{7,11}$	277434.406	153.1	22.80	” †	”	”
A	$20_{6,14}$-$19_{7,13}$	278288.141	161.0	26.90	278287.8	0.40	
A	$20_{7,14}$-$19_{7,13}$	278288.149	161.0	11.20	” †	”	
A	$20_{6,14}$-$19_{6,13}$	278288.188	161.0	11.20	” †	”	

Table B.5. continued.

Torsional substate	Transition $J_{K_a,K_c} - J'_{K'_a,K'_c}$	Predicted frequency (MHz)	E_{upp} (K)	$S_{ij}\mu^2$ (D^2)	Observed frequency (MHz)	T_{MB} (K)	Blends
A	$20_{7,14}$-$19_{6,13}$	278288.196	161.0	26.90	” †	”	
A	$21_{5,16}$-$20_{6,15}$	278815.884	167.5	31.50	278815.9	0.36	
A	$21_{6,16}$-$20_{6,15}$	278815.884	167.5	12.40	” †	”	
A	$21_{5,16}$-$20_{5,15}$	278815.884	167.5	12.40	” †	”	
A	$21_{6,16}$-$20_{5,15}$	278815.884	167.5	31.50	” †	”	
E	$22_{4,18}$-$21_{5,17}$	279103.851	172.7	49.80	279103.9	0.39	
E	$22_{5,18}$-$21_{4,17}$	279103.851	172.7	49.80	” †	”	
A	$22_{4,18}$-$21_{5,17}$	279407.813	173.1	13.10	279407.5	1.18	
A	$22_{5,18}$-$21_{5,17}$	279407.813	173.1	13.10	” †	”	
A	$22_{4,18}$-$21_{5,17}$	279407.813	173.1	36.70	” †	”	
A	$22_{5,18}$-$21_{4,17}$	279407.813	173.1	36.70	” †	”	
E	$16_{10,6}$-$15_{10,5}$	279544.740	123.5	7.79	279544.7	0.17	
E	$23_{4,20}$-$22_{4,19}$	279775.737	177.3	1.03	279775.6	0.08	
E	$23_{3,20}$-$22_{3,19}$	279775.737	177.3	1.03	” †	”	
E	$23_{3,20}$-$22_{4,19}$	279775.737	177.3	54.70	” †	”	
E	$23_{4,20}$-$22_{3,19}$	279775.737	177.3	54.70	” †	”	
A	$23_{3,20}$-$22_{4,19}$	280028.276	177.6	47.70	...	...	OCS v=2, CH_3OCH_3
A	$23_{4,20}$-$22_{3,19}$	280028.276	177.6	47.70	... †	...	”
A	$23_{3,20}$-$22_{3,19}$	280028.276	177.6	8.00	... †	...	”
A	$23_{4,20}$-$22_{4,19}$	280028.276	177.6	8.00	... †	...	”
E	$24_{2,22}$-$23_{3,21}$	280466.453	181.0	29.80	280466.5	0.34	
E	$24_{3,22}$-$23_{2,21}$	280466.453	181.0	29.80	” †	”	
E	$24_{2,22}$-$23_{2,21}$	280466.453	181.0	32.00	” †	”	
E	$24_{3,22}$-$23_{3,21}$	280466.453	181.0	32.00	” †	”	
A	$24_{2,22}$-$23_{2,21}$	280660.246	181.3	26.10	280660.3	0.37	
A	$24_{3,22}$-$23_{3,21}$	280660.246	181.3	26.10	” †	”	
A	$24_{2,22}$-$23_{3,21}$	280660.246	181.3	35.60	” †	”	
A	$24_{3,22}$-$23_{2,21}$	280660.246	181.3	35.60	” †	”	
E	$25_{1,24}$-$24_{2,23}$	281171.910	183.8	67.10	...	...	A-CH_3OCHO v_t=1, CH_2OHCHO
E	$25_{2,24}$-$24_{1,23}$	281171.910	183.8	67.10	... †	...	”
E	$25_{1,24}$-$24_{1,23}$	281171.910	183.8	0.69	... †	...	”
E	$25_{2,24}$-$24_{2,23}$	281171.910	183.8	0.69	... †	...	”
A	$25_{1,24}$-$24_{2,23}$	281293.865	184.0	15.70	281292.9	0.37	
A	$25_{2,24}$-$24_{1,23}$	281293.865	184.0	15.70	” †	”	
A	$25_{1,24}$-$24_{1,23}$	281293.865	184.0	52.00	” †	”	
A	$25_{2,24}$-$24_{2,23}$	281293.865	184.0	52.00	” †	”	
E	$26_{0,26}$-$25_{0,25}$	281891.449	185.6	73.80	...	...	CH_2CHCN
E	$26_{1,26}$-$25_{1,25}$	281891.449	185.6	73.80	... †	...	”
A	$26_{0,26}$-$25_{0,25}$	281922.005	185.7	2.55	...	...	$H^{13}COOH$
A	$26_{1,26}$-$25_{1,25}$	281922.005	185.7	2.55	... †	...	”
A	$26_{0,26}$-$25_{1,25}$	281922.005	185.7	71.30	... †	...	”
A	$26_{1,26}$-$25_{0,25}$	281922.005	185.7	71.30	... †	...	”
A	$15_{10,6}$-$14_{9,5}$	283973.174	109.6	9.88	283973.2	0.15	
A	$13_{12,2}$-$12_{11,2}$	284149.269	92.5	22.40	...	...	CH_3CH_2CN, $CH_2{}^{13}CHCN$
E	$14_{10,5}$-$13_{9,5}$	286621.043	97.2	5.61	286620.8	0.15	
A	$17_{10,8}$-$16_{9,7}$	286671.127	135.5	11.60	286670.7	0.35	U-line
E	$18_{10,9}$-$17_{10,8}$	287558.912	148.9	8.50	287559.0	0.15	U-line
A	$19_{9,11}$-$18_{9,10}$	288293.646	158.9	9.67	288293.8	0.22	
A	$19_{8,11}$-$18_{8,10}$	288369.783	158.9	9.67	288370.2	0.14	
A	$19_{9,11}$-$18_{8,10}$	288390.794	158.9	19.50	288391.0	0.41	
A	$20_{7,13}$-$19_{8,12}$	288453.601	167.4	24.40	288453.3	0.33	
A	$20_{8,13}$-$19_{8,12}$	288453.808	167.4	10.70	” †	”	
A	$20_{7,13}$-$19_{7,12}$	288454.748	167.4	10.70	” †	”	
A	$20_{8,13}$-$19_{7,12}$	288454.956	167.4	24.40	” †	”	
A	$21_{6,15}$-$20_{7,14}$	288885.666	174.9	29.10	288885.7	0.36	CH_3SH
A	$21_{7,15}$-$20_{7,14}$	288885.668	174.9	11.90	” †	”	”
A	$21_{6,15}$-$20_{6,14}$	288885.674	174.9	11.90	” †	”	”
A	$21_{7,15}$-$20_{6,14}$	288885.675	174.9	29.10	” †	”	”
A	$23_{4,19}$-$22_{5,18}$	290037.585	187.0	51.80	290037.4	0.32	U-line
A	$23_{5,19}$-$22_{4,18}$	290037.585	187.0	51.80	” †	”	”
A	$23_{4,19}$-$22_{4,18}$	290037.585	187.0	0.90	” †	”	”
A	$23_{5,19}$-$22_{5,18}$	290037.585	187.0	0.90	” †	”	”
E	$13_{13,0}$-$12_{12,0}$	290490.325	97.0	26.40	290489.9	0.64	
A	$24_{3,21}$-$23_{3,20}$	290663.786	191.6	22.20	290663.9	0.45	
A	$24_{4,21}$-$23_{4,20}$	290663.786	191.6	22.20	” †	”	
A	$24_{3,21}$-$23_{4,20}$	290663.786	191.6	36.40	” †	”	

Table B.5. continued.

Torsional substate	Transition $J_{K_a,K_c} - J'_{K'_a,K'_c}$	Predicted frequency (MHz)	E_{upp} (K)	$S_{ij}\mu^2$ (D^2)	Observed frequency (MHz)	T_{MB} (K)	Blends
A	$24_{4,21}$-$23_{3,20}$	290663.786	191.6	36.40	” †	”	
E	$26_{1,25}$-$25_{1,24}$	291814.665	197.8	64.00	291816.4	0.47	$CH_2CH^{13}CN$, HCOOD
E	$26_{2,25}$-$25_{2,24}$	291814.665	197.8	64.00	” †	”	”
E	$26_{1,25}$-$25_{2,24}$	291814.665	197.8	6.66	” †	”	”
E	$26_{2,25}$-$25_{1,24}$	291814.665	197.8	6.66	” †	”	”
A	$13_{13,1}$-$12_{12,0}$	92319.797	97.4	26.40	292320.2	0.88	U-line
A	$13_{13,0}$-$12_{12,1}$	92319.985	97.4	26.40	” †	”	”
E	$27_{0,27}$-$26_{0,26}$	292536.469	199.7	5.87	292536.2	1.00	CH_2OHCHO, U-line
E	$27_{1,27}$-$26_{1,26}$	292536.469	199.7	5.87	” †	”	”
E	$27_{0,27}$-$26_{1,26}$	292536.469	199.7	70.80	” †	”	”
E	$27_{1,27}$-$26_{0,26}$	292536.469	199.7	70.80	” †	”	”
A	$27_{0,27}$-$26_{0,26}$	292566.458	199.7	76.70	292536.2	1.00	
A	$27_{1,27}$-$26_{1,26}$	292566.458	199.7	76.70	” †	”	”
E	$14_{11,4}$-$13_{10,4}$	292714.351	100.0	15.70	292714.3	0.16	
A	$17_{10,7}$-$16_{10,6}$	296019.993	138.0	8.78	296020.3	0.12	
A	$19_{9,10}$-$18_{10,9}$	298506.849	163.6	16.60	298506.7	0.24	CH_3CH_2CN
A	$20_{8,12}$-$19_{9,11}$	298751.422	173.2	21.80	298751.6	0.11	
A	$19_{10,10}$-$18_{10,9}$	298789.508	163.6	9.36	298789.1	0.14	
A	$21_{7,14}$-$20_{8,13}$	299014.313	181.7	26.60	299014.4	0.27	
A	$21_{8,14}$-$20_{8,13}$	299014.349	181.7	11.40	” †	”	
A	$21_{7,14}$-$20_{7,13}$	299014.520	181.7	11.40	” †	”	
A	$21_{8,14}$-$20_{7,13}$	299014.556	181.7	26.60	” †	”	
E	$23_{5,18}$-$22_{5,17}$	299722.040	195.4	12.30	299721.5	0.64	
E	$23_{6,18}$-$22_{6,17}$	299722.040	195.4	12.30	” †	”	
E	$23_{5,18}$-$22_{6,17}$	299722.040	195.4	37.40	” †	”	
E	$23_{6,18}$-$22_{5,17}$	299722.040	195.4	37.40	” †	”	
E	$14_{12,2}$-$13_{11,2}$	299843.642	104.0	20.40	299843.7	0.38	
E	$24_{4,20}$-$23_{4,19}$	300375.414	201.0	21.00	300375.7	0.26	
E	$24_{5,20}$-$23_{5,19}$	300375.414	201.0	21.00	” †	”	
E	$24_{4,20}$-$23_{5,19}$	300375.414	201.0	34.60	” †	”	
E	$24_{5,20}$-$23_{4,19}$	300375.414	201.0	34.60	” †	”	
A	$24_{4,20}$-$23_{4,19}$	300667.116	201.4	0.50	300666.4	0.40	
A	$24_{5,20}$-$23_{5,19}$	300667.116	201.4	0.50	” †	”	
A	$24_{4,20}$-$23_{5,19}$	300667.116	201.4	55.10	” †	”	
A	$24_{5,20}$-$23_{4,19}$	300667.116	201.4	55.10	” †	”	
E	$25_{3,22}$-$24_{4,21}$	301052.921	205.7	61.60	301052.4	0.93	CH_2OHCHO
E	$25_{4,22}$-$24_{3,21}$	301052.921	205.7	61.60	” †	”	”
A	$14_{12,3}$-$13_{11,2}$	301460.317	104.3	20.50	301459.0	0.38	CH_3NC
E	$26_{2,24}$-$25_{2,23}$	301747.465	209.5	14.20	301747.5	0.67	
E	$26_{3,24}$-$25_{3,23}$	301747.465	209.5	14.20	” †	”	
E	$26_{2,24}$-$25_{3,23}$	301747.465	209.5	53.30	” †	”	
E	$26_{3,24}$-$25_{2,23}$	301747.465	209.5	53.30	” †	”	
A	$26_{2,24}$-$25_{2,23}$	301938.272	209.5	29.30	...	...	$(CH_3)_2CO$, U-line
A	$26_{3,24}$-$25_{3,23}$	301938.272	209.5	29.30	... †	...	”
A	$26_{2,24}$-$25_{3,23}$	301938.272	209.5	38.20	... †	...	”
A	$26_{3,24}$-$25_{2,23}$	301938.272	209.5	38.20	... †	...	”
E	$27_{1,26}$-$26_{1,25}$	302456.729	212.3	20.20	...	...	E-CH_3OCOH
E	$27_{2,26}$-$26_{2,25}$	302456.729	212.3	20.20	... †	...	”
E	$27_{1,26}$-$26_{2,25}$	302456.729	212.3	53.30	... †	...	”
E	$27_{2,26}$-$26_{1,25}$	302456.729	212.3	53.30	... †	...	”
A	$27_{1,26}$-$26_{2,25}$	302577.710	212.5	33.60	302577.5	0.41	
A	$27_{2,26}$-$26_{1,25}$	302577.710	212.5	33.60	” †	”	
A	$27_{1,26}$-$26_{1,25}$	302577.710	212.5	40.00	” †	”	
A	$27_{2,26}$-$26_{2,25}$	302577.710	212.5	40.00	” †	”	
E	$28_{0,28}$-$27_{1,27}$	303180.896	214.2	70.70	303180.8	0.82	
E	$28_{1,28}$-$27_{0,27}$	303180.896	214.2	70.70	” †	”	
E	$28_{0,28}$-$27_{0,27}$	303180.896	214.2	8.89	” †	”	
E	$28_{1,28}$-$27_{1,27}$	303180.896	214.2	8.89	” †	”	
A	$28_{0,28}$-$27_{1,27}$	303210.330	214.3	16.60	303210.7	0.36	
A	$28_{1,28}$-$27_{0,27}$	303210.330	214.3	16.60	” †	”	
A	$28_{0,28}$-$27_{0,27}$	303210.330	214.3	63.10	” †	”	
A	$28_{1,28}$-$27_{1,27}$	303210.330	214.3	63.10	” †	”	
E	$19_{10,9}$-$18_{11,8}$	306374.732	167.3	13.30	306374.8	0.40	$^{13}CH_3CH_2CN$
E	$14_{13,1}$-$13_{12,1}$	306460.811	107.8	24.60	306461.3	0.34	$CH_2{}^{13}CHCN$
E	$16_{11,6}$-$15_{10,5}$	306483.382	124.8	7.91	306483.6	0.19	

Note.- Emission lines of CH_3COOH in its ground torsional state ($v_t = 0$) shown in Fig. A.8. Column 1 indicates the symmetry substate of the torsional mode, Col. 2 gives the quantic numbers of the line transition, Col. 3 the predicted frequency in the laboratory, Col. 4 upper level energy, Col. 5 the line strength (Sijμ^2), Col. 6 observed centroid frequency (relative to a v_{LSR} of 7.5 kms^{-1}), Col. 7 main beam temperature, and Col. 8 shows the blending with other molecular species.
† blended with the previous line.

Table B.6. Lines of A-CH_3COOH and E-CH_3COOH in its first excited state $v_t = 1$.

Torsional substate	Transition $J_{K_a,K_c} - J'_{K'_a,K'_c}$	Predicted frequency (MHz)	E_{upp} (K)	$S_{ij}\mu^2$ (D^2)	Observed frequency (MHz)	T_{MB} (K)	Blends
A	$8_{0,8}$-$7_{1,7}$	89615.790	134.0	21.40	89616.9	0.02	
A	$8_{1,8}$-$7_{1,7}$	89615.790	134.0	0.23	”†	”	
A	$8_{0,8}$-$7_{0,7}$	89615.791	134.0	0.23	”†	”	
A	$8_{1,8}$-$7_{0,7}$	89615.792	134.0	21.40	”†	”	
A	$8_{1,7}$-$7_{2,6}$	98250.284	137.0	18.30	98250.5	0.02	
A	$8_{2,7}$-$7_{2,6}$	98250.300	137.0	0.48	”†	”	
A	$8_{1,7}$-$7_{1,6}$	98250.385	128.5	0.48	”†	”	
A	$8_{2,7}$-$7_{1,6}$	98250.400	128.5	18.30	”†	”	
A	$9_{0,9}$-$8_{1,8}$	100286.607	138.8	23.90	100286.4	0.03	
A	$9_{1,9}$-$8_{1,8}$	100286.607	138.8	0.64	”†	”	
A	$9_{0,9}$-$8_{0,8}$	100286.607	138.8	0.64	”†	”	
A	$9_{1,9}$-$8_{0,8}$	100286.607	138.8	23.90	”†	”	
A	$10_{1,10}$-$9_{1,9}$	110956.499	144.1	1.45	...	...	CH_3COOH
A	$10_{0,10}$-$9_{1,9}$	110956.499	144.1	26.00	...†	...	”
A	$10_{0,10}$-$9_{0,9}$	110956.499	144.1	1.45	...†	...	”
A	$10_{1,10}$-$9_{0,9}$	110956.499	144.1	26.00	...†	...	”
A	$10_{2,8}$-$9_{3,7}$	128521.154	151.6	20.90	128521.2	0.04	
A	$10_{3,8}$-$9_{3,7}$	128521.174	151.6	0.80	”†	”	
A	$10_{2,8}$-$9_{2,7}$	128521.272	151.6	0.80	”†	”	
A	$10_{3,8}$-$9_{2,7}$	128521.292	151.6	20.90	”†	”	
A	$25_{11,14}$-$25_{10,15}$	137506.799	380.8	28.70	137507.1	0.01	
A	$25_{12,14}$-$25_{11,15}$	137507.660	380.8	28.70	”†	”	
A	$11_{2,9}$-$10_{3,8}$	139239.342	158.2	23.80	139239.5	0.07	A-CH_2DCH_2CN
A	$11_{3,9}$-$10_{3,8}$	139239.346	158.2	0.76	”†	”	”
A	$11_{2,9}$-$10_{2,8}$	139239.362	158.2	0.76	”†	”	”
A	$11_{3,9}$-$10_{2,8}$	139239.366	158.2	23.80	”†	”	”
A	$12_{2,11}$-$11_{2,10}$	140986.735	161.0	2.11	140986.6	0.04	
A	$12_{1,11}$-$11_{2,10}$	140986.735	161.0	28.20	”†	”	
A	$12_{1,11}$-$11_{1,10}$	140986.736	161.0	2.11	”†	”	
A	$12_{2,11}$-$11_{1,10}$	140986.736	161.0	28.20	”†	”	
A	$13_{0,13}$-$12_{1,12}$	142960.828	163.1	32.50	142960.9	0.08	
A	$13_{1,13}$-$12_{0,12}$	142960.828	163.1	32.50	”†	”	
A	$13_{0,13}$-$12_{0,12}$	142960.828	163.1	3.62	”†	”	
A	$13_{1,13}$-$12_{1,12}$	142960.828	163.1	3.62	”†	”	
A	$14_{0,14}$-$13_{0,13}$	153627.207	170.5	18.80	153627.2	0.06	
A	$14_{1,14}$-$13_{1,13}$	153627.207	170.5	18.80	”†	”	
A	$14_{0,14}$-$13_{1,13}$	153627.207	170.5	20.20	”†	”	
A	$14_{1,14}$-$13_{0,13}$	153627.207	170.5	20.20	”†	”	
E	$11_{3,8}$-$10_{4,7}$	154548.638	155.8	15.00	154548.5	0.02	E-$CH_3OC^{18}OH$
A	$11_{4,7}$-$10_{5,6}$	157512.093	165.1	18.50	157512.2	0.05	
A	$12_{3,9}$-$11_{4,8}$	159083.049	169.5	23.40	159083.4	0.06	
A	$12_{4,9}$-$11_{4,8}$	159083.072	169.5	1.16	”†	”	
A	$12_{3,9}$-$11_{3,8}$	159083.170	169.5	1.16	”†	”	
A	$12_{4,9}$-$11_{3,8}$	159083.192	169.5	23.40	”†	”	
E	$13_{2,11}$-$12_{3,10}$	164977.374	166.9	22.40	164977.9	0.09	U-line
E	$13_{3,11}$-$12_{3,10}$	164977.397	166.9	7.01	”†	”	”
E	$13_{2,11}$-$12_{2,10}$	164977.491	166.9	7.01	”†	”	”
E	$13_{3,11}$-$12_{2,10}$	164977.514	166.9	22.40	”†	”	”
E	$14_{1,13}$-$13_{2,12}$	165022.332	169.1	27.00	165022.4	0.22	$SO^{18}O$
E	$14_{2,13}$-$13_{2,12}$	165022.332	169.1	8.52	”†	”	”
E	$14_{2,13}$-$13_{1,12}$	165022.332	169.1	27.00	”†	”	”
E	$14_{1,13}$-$13_{1,12}$	165022.332	169.1	8.52	”†	”	”
A	$15_{4,11}$-$14_{5,10}$	200681.028	200.5	28.50	200681.2	0.22	$^{13}CH_3CH_2CN$
A	$15_{5,11}$-$14_{5,10}$	200681.033	200.5	1.80	”†	”	”
A	$15_{4,11}$-$14_{4,10}$	200681.051	200.5	1.80	”†	”	”
A	$15_{5,11}$-$14_{4,10}$	200681.056	200.5	28.50	”†	”	”
A	$17_{2,15}$-$16_{2,14}$	203449.347	209.1	1.42	203449.5	0.23	
A	$17_{3,15}$-$16_{3,14}$	203449.347	209.1	1.42	”†	”	
A	$17_{2,15}$-$16_{3,14}$	203449.347	209.1	40.40	”†	”	
A	$17_{3,15}$-$16_{2,14}$	203449.347	209.1	40.40	”†	”	
A	$19_{1,18}$-$18_{2,17}$	215677.731	222.7	23.70	215677.8	0.38	CH_3CH_2CN
A	$19_{2,18}$-$18_{1,17}$	215677.731	222.7	23.70	”†	”	”
A	$19_{1,18}$-$18_{1,17}$	215677.731	222.7	26.90	”†	”	”
A	$19_{2,18}$-$18_{2,17}$	215677.731	222.7	26.90	”†	”	”
A	$20_{0,20}$-$19_{0,19}$	217607.963	225.5	20.80	217607.9	0.29	

Table B.6. continued.

Torsional substate	Transition $J_{K_a,K_c} - J'_{K'_a,K'_c}$	Predicted frequency (MHz)	E_{upp} (K)	$S_{ij}\mu^2$ (D^2)	Observed frequency (MHz)	T_{MB} (K)	Blends
A	$20_{1,20}$-$19_{1,19}$	217607.963	225.5	20.80	”†	”	
A	$20_{0,20}$-$19_{1,19}$	217607.963	225.5	35.60	”†	”	
A	$20_{1,20}$-$19_{0,19}$	217607.963	225.5	35.60	”†	”	
E	$17_{3,14}$-$16_{4,13}$	217875.073	210.9	28.60	217875.2	0.12	
E	$17_{4,14}$-$16_{4,13}$	217875.074	210.9	9.32	”†	”	
E	$17_{3,14}$-$16_{3,13}$	217875.079	210.9	9.32	”†	”	
E	$17_{4,14}$-$16_{3,13}$	217875.080	210.9	28.60	”†	”	
A	$18_{3,15}$-$17_{3,14}$	223473.929	226.1	37.60	223474.0	0.27	U-line
A	$18_{4,15}$-$17_{3,14}$	223473.929	226.1	37.60	”†	”	”
A	$18_{3,15}$-$17_{3,14}$	223473.929	226.1	4.10	”†	”	”
A	$18_{4,15}$-$17_{4,14}$	223473.929	226.1	4.10	”†	”	”
A	$19_{2,17}$-$18_{3,16}$	224820.963	230.2	16.10	...	...	g+-CH_3CH_2OH
A	$19_{3,17}$-$18_{2,16}$	224820.963	230.2	16.10	...†	...	”
A	$19_{2,17}$-$18_{2,16}$	224820.963	230.2	31.50	...†	...	”
A	$19_{3,17}$-$18_{3,16}$	224820.963	230.2	31.50	...†	...	”
A	$20_{1,19}$-$19_{1,18}$	226338.976	233.6	13.30	226338.9	0.45	U-line
A	$20_{2,19}$-$19_{2,18}$	226338.976	233.6	13.30	”†	”	”
A	$20_{1,19}$-$19_{2,18}$	226338.976	233.6	40.10	”†	”	”
A	$20_{2,19}$-$19_{1,18}$	226338.976	233.6	40.10	”†	”	”
A	$21_{1,20}$-$20_{1,19}$	236998.151	245.0	56.30	236997.9	0.16	
A	$21_{2,20}$-$20_{2,19}$	236998.151	245.0	56.30	”†	”	
E	$22_{0,22}$-$21_{0,21}$	239592.644	239.9	16.10	239592.8	0.22	
E	$22_{1,22}$-$21_{1,21}$	239592.644	239.9	16.10	”†	”	
E	$22_{0,22}$-$21_{1,21}$	239592.644	239.9	46.00	”†	”	
E	$22_{1,22}$-$21_{0,21}$	239592.644	239.9	46.00	”†	”	
A	$12_{11,2}$-$11_{10,1}$	244310.542	187.2	20.70	244311.1	0.15	
A	$20_{3,17}$-$19_{3,16}$	244889.621	249.1	11.60	244889.8	0.19	
A	$20_{4,17}$-$19_{4,16}$	244889.621	249.1	11.60	”†	”	
A	$20_{3,17}$-$19_{4,16}$	244889.621	249.1	35.90	”†	”	
A	$20_{4,17}$-$19_{3,16}$	244889.621	249.1	35.90	”†	”	
A	$21_{2,19}$-$20_{3,18}$	246179.204	253.3	19.20	246179.4	0.25	
A	$21_{3,19}$-$20_{2,18}$	246179.204	253.3	19.20	”†	”	
A	$21_{2,19}$-$20_{2,18}$	246179.204	253.3	34.10	”†	”	
A	$21_{3,19}$-$20_{3,18}$	246179.204	253.3	34.10	”†	”	
E	$17_{6,11}$-$16_{7,10}$	249386.058	229.2	19.80	...	...	A-CH_3OCOH
E	$19_{4,15}$-$18_{5,14}$	249396.528	241.0	30.60	249396.8	0.25	
E	$19_{5,15}$-$18_{5,14}$	249396.529	241.0	10.00	”†	”	
E	$19_{4,15}$-$18_{4,14}$	249396.535	241.0	10.00	”†	”	
E	$19_{5,15}$-$18_{4,14}$	249396.537	241.0	30.60	”†	”	
A	$18_{6,12}$-$17_{7,11}$	252180.413	244.0	30.30	252180.9	0.32	
A	$18_{7,12}$-$17_{7,11}$	252180.436	244.0	2.80	”†	”	
A	$18_{6,12}$-$17_{6,11}$	252180.514	244.0	2.80	”†	”	
A	$18_{7,12}$-$17_{6,11}$	252180.537	244.0	30.30	”†	”	
A	$23_{1,22}$-$22_{1,21}$	258310.421	269.3	25.00	258310.2	0.40	
A	$23_{2,22}$-$22_{2,21}$	258310.421	269.3	25.00	”†	”	
A	$23_{1,22}$-$22_{2,21}$	258310.421	269.3	37.10	”†	”	
A	$23_{2,22}$-$22_{1,21}$	258310.421	269.3	37.10	”†	”	
A	$20_{5,15}$-$19_{6,14}$	264064.114	263.3	36.50	264064.2	0.28	$(CH_3)_2CO$
A	$20_{6,15}$-$19_{6,14}$	264064.114	263.3	5.17	”†	”	”
A	$20_{5,15}$-$19_{5,14}$	264064.114	263.3	5.17	”†	”	”
A	$20_{6,15}$-$19_{5,14}$	264064.114	263.3	5.17	”†	”	”
A	$25_{0,25}$-$24_{0,24}$	257902.634	285.4	61.80	270902.8	0.39	
A	$25_{1,25}$-$24_{1,24}$	257902.634	285.4	61.80	”†	”	
A	$25_{0,25}$-$24_{1,24}$	257902.634	285.4	9.11	”†	”	
A	$25_{1,25}$-$24_{0,24}$	257902.634	285.4	9.11	”†	”	
A	$19_{7,12}$-$18_{8,11}$	272736.986	262.2	29.60	272737.1	0.44	U-line
A	$19_{8,12}$-$18_{8,11}$	272737.079	262.2	3.42	”†	”	”
A	$19_{7,12}$-$18_{7,11}$	272737.384	262.2	3.42	”†	”	”
A	$19_{8,12}$-$18_{7,11}$	272737.478	262.2	29.60	”†	”	”
A	$25_{1,24}$-$24_{2,23}$	279614.765	295.6	32.00	279614.7	0.48	$CH_3{}^{13}CH_2CN$
A	$25_{2,24}$-$24_{1,23}$	279614.765	295.6	32.00	”†	”	”
A	$25_{1,24}$-$24_{1,23}$	279614.765	295.6	35.90	”†	”	”
A	$25_{2,24}$-$24_{2,23}$	279614.765	295.6	35.90	”†	”	”
E	$19_{8,12}$-$18_{7,11}$	280729.453	260.6	21.40	280730.2	0.25	
E	$21_{5,16}$-$20_{6,15}$	280730.326	274.6	32.60	”†	”	
E	$21_{6,16}$-$20_{6,15}$	280730.328	274.6	10.70	”†	”	

Table B.6. continued.

Torsional substate	Transition $J_{K_a,K_c} - J'_{K'_a,K'_c}$	Predicted frequency (MHz)	E_{upp} (K)	$S_{ij}\mu^2$ (D^2)	Observed frequency (MHz)	T_{MB} (K)	Blends
E	$21_{5,16}$-$20_{5,15}$	280730.334	274.6	10.70	”†	”	
E	$21_{6,16}$-$20_{5,15}$	280730.336	274.6	32.60	”†	”	
E	$23_{3,20}$-$22_{3,19}$	281447.580	284.3	14.10	281447.7	0.40	$HC^{13}CCN$ v_6=1
E	$23_{4,20}$-$22_{4,19}$	281447.580	284.3	14.10	”†	”	”
E	$23_{3,20}$-$22_{4,19}$	281447.580	284.3	41.20	”†	”	”
E	$23_{4,20}$-$22_{3,19}$	281447.580	284.3	41.20	”†	”	”
A	$26_{0,26}$-$25_{1,25}$	281559.086	298.9	65.90	281559.2	0.18	t-CH_3CH_2OH
A	$26_{1,26}$-$25_{0,25}$	281559.086	298.9	65.90	”†	”	”
A	$26_{0,26}$-$25_{0,25}$	281559.086	298.9	7.94	”†	”	”
A	$26_{1,26}$-$25_{1,25}$	281559.086	298.9	7.94	”†	”	”
A	$20_{7,13}$-$19_{8,12}$	283560.644	275.8	32.40	283560.9	0.44	CH_2OHCHO
A	$20_{8,13}$-$19_{8,12}$	283560.666	275.8	3.49	”†	”	
A	$20_{7,13}$-$19_{7,12}$	283560.738	275.8	3.49	”†	”	
A	$20_{8,13}$-$19_{7,12}$	283560.759	275.8	32.40	”†	”	
A	$25_{2,23}$-$24_{3,22}$	288859.633	305.7	28.60	288860.0	0.27	
A	$25_{3,23}$-$24_{2,22}$	288859.633	305.7	28.60	”†	”	
A	$25_{2,23}$-$24_{2,22}$	288859.633	305.7	36.30	”†	”	
A	$25_{3,23}$-$24_{3,22}$	288859.633	305.7	36.30	”†	”	

Note.- Emission lines of CH_3COOH in its first torsional state (v_t = 1) shown in Fig.A.9. Column 1 indicates the symmetry substate of the torsional mode, Col. 2 gives the quantic numbers of the line transition, Col. 3 the predicted frequency in the laboratory, Col. 4 upper level energy, Col. 5 the line strength (Sijμ^2), Col. 6 observed centroid frequency (relative to a v_{LSR} of 7.5 kms^{-1}), Col. 7 main beam temperature, and Col. 8 shows the blending with other molecular species.
† blended with the previous line.

Table B.7. Lines of A-CH_3COOH and E-CH_3COOH in its second excited state $v_t = 2$.

Torsional substate	Transition $J_{K_a,K_c} - J'_{K'_a,K'_c}$	Predicted frequency (MHz)	E_{upp} (K)	$S_{ij}\mu^2$ (D^2)	Observed frequency (MHz)	T_{MB} (K)	Blends
E	$9_{1,9}$-$8_{0,8}$	103199.044	221.4	18.70	103.1994	0.02	
A	$12_{0,12}$-$11_{1,11}$	134315.650	219.1	22.70	134315.6	0.03	
A	$12_{1,12}$-$11_{1,11}$	134315.675	219.1	10.10	”†	”	
A	$12_{0,12}$-$11_{0,11}$	134315.734	219.1	10.10	”†	”	
A	$12_{1,12}$-$11_{0,11}$	134315.759	219.1	22.70	”†	”	
E	$11_{2,10}$-$10_{1,9}$	137941.083	237.8	19.30	137940.9	0.02	
A	$10_{2,8}$-$9_{3,7}$	137949.234	217.5	12.50	...	...	U-line
A	$13_{0,13}$-$12_{1,12}$	144975.035	226.1	24.50	144975.0	0.07	
A	$13_{1,13}$-$12_{1,12}$	144975.042	226.1	11.20	”†	”	
A	$13_{0,13}$-$12_{0,12}$	144975.059	226.1	11.20	”†	”	
A	$13_{1,13}$-$12_{0,12}$	144975.067	226.1	24.50	”†	”	
E	$12_{2,11}$-$11_{1,10}$	147739.567	244.9	21.90	147739.7	0.03	
A	$11_{2,9}$-$10_{3,8}$	148940.476	224.6	14.60	...	...	$CH_3CH_2{}^{13}CN$
E	$10_{6,4}$-$9_{6,4}$	153236.149	253.2	8.51	1532361.1	0.03	
E	$13_{1,12}$-$12_{1,11}$	157870.443	252.5	4.97	157871.6	0.10	U-line
E	$13_{2,12}$-$12_{1,11}$	157871.672	252.5	24.50	”†	”	”
E	$10_{4,6}$-$9_{4,6}$	159979.056	239.3	10.30	159979.1	0.05	
E	$14_{4,10}$-$13_{5,9}$	205895.128	277.0	12.60	205895.2	0.08	
A	$18_{1,17}$-$17_{2,16}$	210949.979	279.2	28.00	210950.1	0.20	
A	$18_{2,17}$-$17_{2,16}$	210949.982	279.2	18.50	”†	”	
A	$18_{1,17}$-$17_{1,16}$	210949.986	279.2	18.50	”†	”	
A	$18_{2,17}$-$17_{1,16}$	210949.989	279.2	28.00	”†	”	
A	$20_{0,20}$-$19_{1,19}$	219603.944	289.1	4.33	219603.8	0.16	
A	$20_{1,20}$-$19_{1,19}$	219603.944	289.1	51.70	”†	”	
A	$20_{1,20}$-$19_{0,19}$	219603.945	289.1	4.33	”†	”	
A	$20_{0,20}$-$19_{0,19}$	219603.945	289.1	51.70	”†	”	
A	$19_{1,18}$-$18_{2,17}$	221607.301	289.8	27.80	221607.3	0.15	
A	$19_{2,18}$-$18_{2,17}$	221607.302	289.8	21.60	”†	”	
A	$19_{1,18}$-$18_{1,17}$	221607.304	289.8	21.60	”†	”	
A	$19_{2,18}$-$18_{1,17}$	221607.306	289.8	27.80	”†	”	
A	$21_{0,21}$-$20_{1,20}$	230266.006	300.2	16.40	230266.4	0.34	
A	$21_{1,21}$-$20_{0,20}$	230266.006	300.2	16.40	”†	”	
A	$21_{0,21}$-$20_{0,20}$	230266.006	300.2	42.50	”†	”	
A	$21_{1,21}$-$20_{1,20}$	230266.006	300.2	42.50	”†	”	
E	$16_{9,7}$-$15_{9,6}$	239308.277	317.0	13.20	239308.2	0.14	
E	$22_{0,22}$-$21_{1,21}$	240281.623	331.6	27.90	240282.1	0.38	
E	$22_{0,22}$-$21_{0,21}$	240281.689	331.6	32.80	”†	”	
E	$22_{1,22}$-$21_{1,21}$	240282.734	331.6	32.90	”†	”	
E	$22_{1,22}$-$21_{0,21}$	240282.734	331.6	28.00	”†	”	
A	$21_{1,20}$-$20_{2,19}$	242927.233	312.6	3.11	242927.5	0.22	
A	$21_{2,20}$-$20_{2,19}$	242927.235	312.6	52.10	”†	”	
A	$21_{1,20}$-$20_{1,19}$	242927.244	312.6	52.10	”†	”	
A	$21_{2,20}$-$20_{1,19}$	242927.245	312.6	3.11	”†	”	
A	$19_{3,16}$-$18_{4,15}$	246481.996	309.9	26.90	246482.1	0.15	
A	$19_{4,16}$-$18_{4,15}$	246482.478	309.9	15.30	”†	”	
A	$19_{3,16}$-$18_{3,15}$	246483.288	309.9	15.30	246482.7†	0.12	
A	$19_{4,16}$-$18_{3,15}$	246483.770	309.9	26.90	”†	”	
A	$19_{4,15}$-$18_{5,14}$	258888.644	318.8	24.40	...	...	$^{34}SO_2$
A	$23_{1,22}$-$22_{2,21}$	264245.895	337.5	20.10	264245.4	0.39	
A	$23_{2,22}$-$22_{2,21}$	264245.896	337.5	40.90	”†	”	
A	$23_{1,22}$-$22_{1,21}$	264245.896	337.5	40.90	”†	”	
A	$23_{2,22}$-$22_{1,21}$	264245.896	337.5	20.10	”†	”	
E	$23_{2,21}$-$22_{3,20}$	274805.981	367.5	38.30	274806.6	0.18	
E	$23_{3,21}$-$22_{3,20}$	274806.480	367.5	18.30	”†	”	
E	$23_{2,21}$-$22_{2,20}$	274806.888	367.5	18.20	”†	”	
E	$23_{3,21}$-$22_{2,20}$	274807.387	367.5	38.30	”†	”	
A	$24_{1,23}$-$23_{2,22}$	274928.126	350.7	22.90	274928.3	0.27	
A	$24_{2,23}$-$23_{2,22}$	274928.126	350.7	41.00	”†	”	
A	$24_{2,23}$-$23_{1,22}$	274928.126	350.7	22.90	”†	”	
A	$24_{1,23}$-$23_{1,22}$	274928.126	350.7	41.00	”†	”	
A	$21_{4,17}$-$20_{5,16}$	279991.074	345.2	27.60	279992.0	0.18	$^{13}CH_2CHCN$
A	$21_{5,17}$-$20_{5,16}$	279992.133	345.2	16.80	”†	”	”
A	$21_{4,17}$-$20_{4,16}$	279993.781	345.2	16.80	279994.1†	0.19	”
A	$21_{5,17}$-$20_{4,16}$	279994.840	345.2	27.60	”†	”	”
E	$26_{0,26}$-$25_{1,25}$	282839.655	382.8	20.20	282839.7	0.27	t-HCOOD

Table B.7. continued.

Torsional substate	Transition $J_{K_a,K_c} - J'_{K'_a,K'_c}$	Predicted frequency (MHz)	E_{upp} (K)	$S_{ij}\mu^2$ (D^2)	Observed frequency (MHz)	T_{MB} (K)	Blends
E	$26_{1,26}$-$25_{1,25}$	282839.655	382.8	52.40	”†	”	”
E	$26_{1,26}$-$25_{0,25}$	282839.655	382.8	20.20	”†	”	”
E	$26_{0,26}$-$25_{0,25}$	282839.655	382.8	52.40	”†	”	”
A	$10_{10,1}$-$9_{9,0}$	283412.799	250.4	19.50	283412.9	0.18	
A	$10_{10,0}$-$9_{9,1}$	283412.822	250.4	19.50	”†	”	
E	$25_{1,24}$-$24_{2,23}$	284182.944	382.7	7.84	284183.1	0.16	
E	$25_{2,24}$-$24_{2,23}$	284183.053	382.7	57.10	”†	”	
A	$25_{1,24}$-$24_{2,23}$	285605.657	364.4	28.50	285605.9	0.31	
A	$25_{2,24}$-$24_{1,23}$	285605.657	364.4	28.50	”†	”	
A	$25_{1,24}$-$24_{1,23}$	285605.657	364.4	38.30	”†	”	
A	$25_{2,24}$-$24_{2,23}$	285605.657	364.4	38.30	”†	”	
A	$23_{3,20}$-$22_{4,19}$	288939.884	362.3	53.10	288940.1	0.36	U-line
A	$23_{3,20}$-$22_{3,19}$	288939.934	362.3	0.68	”†	”	”
A	$23_{4,20}$-$22_{4,19}$	288940.074	362.3	0.68	”†	”	”
A	$23_{4,20}$-$22_{3,19}$	288940.124	362.3	53.10	”†	”	”

Note.- Emission lines of CH_3COOH in its second torsional state ($v_t = 2$) shown in Fig.A.10. Column 1 indicates the symmetry substate of the torsional mode, Col. 2 gives the quantic numbers of the line transition, Col. 3 the predicted frequency in the laboratory, Col. 4 upper level energy, Col. 5 the line strength (Sijμ^2), Col. 6 observed centroid frequency (relative to a v_{LSR} of 7.5 kms^{-1}), Col. 7 main beam temperature, and Col. 8 shows the blending with other molecular species.
† blended with the previous line.

Table B.8. Spectroscopic lines of CH_2OHCHO in its ground state v_t=0.

Transition $J_{K_a,K_c} - J'_{K'_a,K'_c}$	Predicted frequency (MHz)	E_{upp} (K)	S_{ij}	Observed frequency (MHz)	T_{MB} (K)	Blends
$17_{3,14}$-$17_{2,15}$	90507.266	93.8	9.26	90507.3	0.02	
$24_{6,18}$-$24_{5,19}$	93048.504	191.6	18.82	93048.5	0.02	
$9_{0,9}$-$8_{1,8}$	93052.668	23.3	7.34	93052.8	0.03	
$10_{0,10}$-$9_{1,9}$	103391.279	28.3	8.37	103391.3	0.04	
$10_{1,9}$-$9_{2,8}$	103667.906	31.9	4.83	103668.0	0.02	
$10_{1,10}$-$9_{0,9}$	104587.696	28.4	8.39	104587.7	0.04	
$21_{6,15}$-$21_{5,16}$	106067.412	151.6	14.10	106067.3	0.02	
$16_{2,14}$-$16_{1,15}$	112341.668	80.1	5.82	112341.7	0.02	
$11_{5,7}$-$11_{4,8}$	112444.290	51.9	5.58	...	...	U-line
$14_{5,10}$-$14_{4,11}$	112472.780	73.8	7.74	112473.0	0.03	
$15_{5,11}$-$15_{4,12}$	113233.047	82.2	8.42	113233.0	0.03	
$11_{0,11}$-$10_{1,10}$	113569.526	33.8	9.40	113569.4	0.04	
$11_{1,11}$-$10_{0,10}$	114264.429	33.8	9.40	114264.5	0.09	
$12_{0,12}$-$11_{1,11}$	123646.727	39.8	10.42	123646.8	0.07	
$20_{3,17}$-$20_{2,18}$	126916.909	126.1	8.80	126916.9	0.03	
$12_{1,11}$-$11_{2,10}$	128797.109	44.4	7.03	128797.1	0.04	
$21_{5,17}$-$21_{4,18}$	133572.251	144.6	11.16	133572.3	0.06	CH_3CHO v_t=1
$19_{6,14}$-$19_{5,15}$	135013.714	128.1	10.89	135013.7	0.02	
$14_{6,8}$-$14_{5,9}$	135222.176	80.3	7.19	135222.1	0.03	
$20_{6,15}$-$20_{5,16}$	135833.351	139.4	11.58	135833.3	0.04	
$14_{6,9}$-$14_{5,10}$	136504.252	80.3	7.17	136504.7	0.04	U-line
$7_{3,5}$-$6_{2,4}$	138436.791	21.0	2.78	138436.6	0.03	
$9_{6,3}$-$9_{5,4}$	138830.859	46.9	3.46	138830.5	0.04	
$7_{6,1}$-$7_{5,2}$	139222.751	37.4	1.87	139223.0	0.04	U-line
$7_{6,2}$-$7_{5,3}$	139223.851	37.4	1.87	” †	”	”
$5_{4,1}$-$4_{3,2}$	146444.979	18.0	3.48	146445.0	0.06	E-CH3O13COH
$22_{3,19}$-$22_{2,20}$	149616.384	150.0	8.75	149616.8	0.03	(CH3)2CO
$28_{7,22}$-$27_{8,19}$	150032.481	257.8	3.24	150034.5	0.03	
$21_{7,14}$-$21_{6,15}$	150034.484	158.8	11.99	” †	”	
$15_{0,15}$-$14_{1,14}$	153597.997	60.5	13.44	153598.2	0.18	
$20_{7,13}$-$20_{6,14}$	153614.223	147.0	11.13	153614.6	0.04	U-line
$15_{1,15}$-$14_{0,14}$	153666.951	60.5	13.44	153666.8	0.08	
$26_{6,21}$-$26_{5,22}$	157736.896	218.9	14.21	157737.1	0.04	
$6_{4,3}$-$5_{3,2}$	157780.346	21.4	3.54	157780.2	0.09	CH_3OCOD, U-line
$18_{7,11}$-$18_{6,12}$	158399.310	125.0	9.53	158399.1	0.06	
$23_{3,20}$-$23_{2,21}$	160274.749	162.6	8.75	160275.1	0.07	He+ (34alpha)
$15_{2,13}$-$14_{3,12}$	160493.769	71.3	6.42	160493.9	0.15	
$17_{7,11}$-$17_{6,12}$	160694.045	115.0	8.76	160694.3	0.16	$CH_3{}^{13}CH_2CN$
$23_{4,20}$-$23_{3,21}$	163412.208	162.7	8.72	163412.2	0.08	U-line
$16_{0,16}$-$15_{1,15}$	163542.290	68.3	14.45	163542.2	0.33	U-line
$21_{3,19}$-$21_{2,20}$	163544.085	131.2	5.82	” †	”	”
$16_{1,16}$-$15_{0,15}$	163580.087	68.3	14.45	163580.1	0.17	
$15_{2,14}$-$14_{1,13}$	164047.051	66.5	10.28	164047.3	0.13	
$10_{7,3}$-$10_{6,4}$	164264.518	60.3	3.53	164265.3	0.11	
$10_{7,4}$-$10_{6,5}$	164265.723	60.3	3.53	” †	”	
$17_{3,15}$-$16_{2,14}$	198094.147	89.7	8.86	198093.9	0.11	A-CH_3OCOH v_t=1
$35_{8,28}$-$35_{7,29}$	198098.646	393.3	20.22	” †	”	”
$19_{1,18}$-$18_{2,17}$	202434.016	102.5	14.37	202434.0	0.19	
$19_{2,18}$-$18_{1,17}$	202701.919	102.5	14.38	202701.9	0.10	
$26_{9,18}$-$26_{8,19}$	205568.546	245.0	14.28	205568.3	0.13	
$18_{9,9}$-$18_{8,10}$	213181.620	144.2	8.19	213182.4	0.28	
$18_{9,10}$-$18_{8,11}$	213186.330	144.2	8.19	213186.7	0.28	
$21_{0,21}$-$20_{1,20}$	213191.865	114.7	19.47	213191.9	0.22	
$21_{1,21}$-$20_{1,20}$	213192.462	114.7	20.84	” †	”	
$21_{0,21}$-$20_{0,20}$	213192.986	114.7	20.84	213193.7†	0.22	
$21_{1,21}$-$20_{0,20}$	213193.582	114.7	19.47	” †	”	
$12_{4,9}$-$11_{3,8}$	213689.962	53.2	3.88	213690.0	0.10	$SO^{18}O$
$19_{3,17}$-$18_{2,16}$	214481.076	109.5	11.00	214481.2	0.20	
$11_{9,2}$-$11_{8,3}$	215150.266	85.8	2.81	215150.5	0.21	
$11_{9,3}$-$11_{8,4}$	215150.267	85.8	2.81	” †	”	
$21_{1,20}$-$20_{2,19}$	222352.417	123.4	16.40	222352.7	0.16	
$14_{4,11}$-$13_{3,10}$	223738.670	68.4	4.24	223738.9	0.22	
$22_{2,21}$-$21_{1,20}$	232335.444	134.5	17.42	232335.5	0.15	
$19_{10,9}$-$19_{9,10}$	238828.483	166.3	8.28	238828.6	0.33	CH_2CHCN v_{11}=1
$19_{10,10}$-$19_{9,11}$	238828.915	166.3	8.28	” †	”	”
$57_{14,43}$-$57_{13,44}$	238830.161	1047.9	38.88	” †	”	”

Table B.8. continued.

Transition $J_{K_a,K_c} - J'_{K'_a,K'_c}$	Predicted frequency (MHz)	E_{upp} (K)	S_{ij}	Observed frequency (MHz)	T_{MB} (K)	Blends
$40_{9,32}$-$39_{10,29}$	238830.660	510.8	3.92	” †	”	”
$17_{10,7}$-$17_{9,8}$	239540.065	145.7	6.80	239540.4	0.31	U-line
$17_{10,8}$-$17_{9,9}$	239540.118	145.7	6.80	” †	”	”
$22_{2,20}$-$21_{3,19}$	241131.867	142.8	14.15	241132.1	0.25	A-$^{13}CH_3OCOH$
$24_{0,24}$-$23_{1,23}$	242957.815	148.3	22.48	242958.4	0.32	
$24_{1,24}$-$23_{1,23}$	242957.904	148.3	23.84	” †	”	
$24_{0,24}$-$23_{0,23}$	242957.983	148.3	23.84	” †	”	
$24_{1,24}$-$23_{0,23}$	242958.072	148.3	22.48	” †	”	
$20_{4,17}$-$19_{3,16}$	245711.242	126.7	8.32	245711.5	0.34	$CH_2{}^{13}CHCN$
$24_{1,23}$-$23_{2,22}$	252131.626	158.3	19.43	252132.3	0.45	E-$^{13}CH_3OCOH$, CH_2CDCN
$24_{2,23}$-$23_{1,22}$	252147.029	158.3	19.43	252146.9	0.31	
$25_{1,24}$-$24_{2,23}$	262048.278	170.8	20.44	262048.1	0.69	
$25_{2,24}$-$24_{1,23}$	262056.817	170.8	20.44	262057.2	0.46	
$26_{0,26}$-$25_{1,25}$	262794.278	173.0	24.48	262794.8	0.35	
$26_{1,26}$-$25_{1,25}$	262794.302	173.0	25.83	” †	”	
$26_{0,26}$-$25_{0,25}$	262794.324	173.0	25.83	” †	”	
$26_{1,26}$-$25_{0,25}$	262794.349	173.0	24.48	” †	”	
$21_{11,10}$-$21_{10,11}$	263999.212	201.8	9.12	263999.3	0.19	
$21_{11,11}$-$21_{10,12}$	263999.311	201.8	9.12	” †	”	
$11_{6,6}$-$10_{5,5}$	266101.126	58.5	5.68	266101.7	0.35	
$24_{4,21}$-$23_{3,20}$	273970.301	175.7	12.70	273970.5	0.46	HCCCN v_5+v_7
$25_{12,13}$-$25_{11,14}$	288247.986	268.1	11.42	288248.5	0.14	
$25_{12,14}$-$25_{11,15}$	288248.136	268.1	11.42	” †	”	
$22_{12,10}$-$22_{11,11}$	289541.531	228.0	9.21	289541.9	0.51	
$22_{12,11}$-$22_{11,12}$	289541.539	228.0	9.21	” †	”	
$29_{0,29}$-$28_{1,28}$	292536.778	213.7	27.49	292536.5	0.98	CH_3COOH
$29_{1,29}$-$28_{1,28}$	292536.782	213.7	28.83	” †	”	
$29_{0,29}$-$28_{0,28}$	292536.785	213.7	28.83	” †	”	
$29_{1,29}$-$28_{0,28}$	292536.788	213.7	27.49	” †	”	
$12_{7,6}$-$11_{6,5}$	303089.537	73.1	6.65	303089.9	0.27	
$12_{7,5}$-$11_{6,6}$	303093.956	73.1	6.65	303094.2	0.46	CH_3SH v=0

Notes. Emission lines of CH_2OHCHO in its ground state (v_t=0) present in the spectral scan of the Orion-KL from the radio-telescope of IRAM 30m. Column 1 gives the quantic numbers of the line transition, Col. 2 the predicted frequency in the laboratory, Col. 3 upper level energy, Col. 4 the line strength, Col. 5 observed centroid frequency (relative to a v_{LSR} of 7.5 kms^{-1}) , Col. 6 main beam temperature, and Col. 7 shows the blending with other molecular species.
† blended with the previous line.

Bibliografía

B. Acke and M. E. van den Ancker. Resolving the disk rotation of HD 97048 and HD 100546 in the [O I] 6300 Å line: evidence for a giant planet orbiting HD 100546. *Astronomy & Astrophysics*, 449: 267–279, April 2006. doi: 10.1051/0004-6361:20054330. 47

M. Agúndez. Estudio de la química en la envoltura circunestelar irc+ 10216. 2009. 26

M. Agúndez, J. P. Fonfría, J. Cernicharo, J. R. Pardo, and M. Guélin. Detection of circumstellar CH_2CHCN, CH_2CN, CH_3CCH, and H_2CS. *Astronomy & Astrophysics*, 479:493–501, February 2008. doi: 10.1051/0004-6361:20078956. 174

L. J. Allamandola, M. P. Bernstein, S. A. Sandford, and R. L. Walker. Evolution of Interstellar Ices. *Space Sci. Rev.*, 90:219–232, October 1999. doi: 10.1023/A:1005210417396. 48

Héctor G Arce, Joaquín Santiago-García, Jes K Jørgensen, Mario Tafalla, and Rafael Bachiller. Complex molecules in the l1157 molecular outflow. *The Astrophysical Journal Letters*, 681(1):L21, 2008. 40

Peter William Atkins and Julio De Paula. *Química física*. Médica Panamericana, 2008. 35

Jacob WM Baars. *The paraboloidal reflector antenna in radio astronomy and communication*. Springer, 2007. 60

R Bachiller, SWCM Liechti, CM Walmsley, and F Colomer. Methanol enhancemant in young bipolar outflows. *Astronomy and Astrophysics*, 295:L51, 1995. 40

A. Bacmann and A. Faure. Complex organic molecules and star formation. In J. Ballet, F. Martins, F. Bournaud, R. Monier, and C. Reylé, editors, *SF2A-2014: Proceedings of the Annual meeting of the French Society of Astronomy and Astrophysics*, pages 3–8, December 2014. 45

A. Bacmann, V. Taquet, A. Faure, C. Kahane, and C. Ceccarelli. Detection of complex organic molecules in a prestellar core: a new challenge for astrochemical models. *Astronomy & Astrophysics*, 541:L12, May 2012. doi: 10.1051/0004-6361/201219207. 45

J. Ballesteros-Paredes, R. S. Klessen, M.-M. Mac Low, and E. Vazquez-Semadeni. Molecular Cloud Turbulence and Star Formation. *Protostars and Planets V*, pages 63–80, 2007. 20

J. Bally, A. Ginsburg, H. Arce, J. Eisner, A. Youngblood, L. Zapata, and H. Zinnecker. The ALMA View of the OMC1 Explosion in Orion. *Astrophys. J.*, 837:60, March 2017. doi: 10.3847/1538-4357/aa5c8b. 12, 18

John Bally and Hans Zinnecker. The birth of high-mass stars: Accretion and/or mergers? *The Astronomical Journal*, 129(5):2281, 2005. 21

John Bally, CR O'Dell, and Mark J McCaughrean. Disks, microjets, windblown bubbles, and outflows in the orion nebula. *The Astronomical Journal*, 119(6):2919, 2000. 13

John Bally, Adam Ginsburg, Devin Silvia, and Allison Youngblood. The orion fingers: Near-ir adaptive optics imaging of an explosive protostellar outflow. *Astronomy & Astrophysics*, 579:A130, 2015. 10, 11, 12, 18

Nadia Balucani. Elementary reactions and their role in gas-phase prebiotic chemistry. *International journal of molecular sciences*, 10(5):2304–2335, 2009. 181

P Bastien, J Bieging, C Henkel, RN Martin, T Pauls, CM Wamsley, TL Wilson, and LM Ziurys. Small scale clumping in the orion molecular cloud. *Astronomy and Astrophysics*, 98:L4–L7, 1981. 16

E. E. Becklin and G. Neugebauer. Observations of an Infrared Star in the Orion Nebula. *Astrophys. J.*, 147:799, February 1967. doi: 10.1086/149055. 12

CA Beichman, PC Myers, JP Emerson, S Harris, R Mathieu, PJ Benson, and RE Jennings. Candidate solar-type protostars in nearby molecular cloud cores. *The Astrophysical Journal*, 307:337–349, 1986. 11

MB Bell, PA Feldman, MJ Travers, MC McCarthy, CA Gottlieb, and P Thaddeus. Detection of $hc_{11}n$ in the cold dust cloud tmc-1. *The Astrophysical Journal Letters*, 483(1):L61, 1997. 39

T. A. Bell, J. Cernicharo, S. Viti, N. Marcelino, A. Palau, G. B. Esplugues, and B. Tercero. Extended warm gas in Orion KL as probed by methyl cyanide. *Astronomy & Astrophysics*, 564:A114, April 2014. doi: 10.1051/0004-6361/201321872. 17

A. Belloche, K. M. Menten, C. Comito, H. S. P. Müller, P. Schilke, J. Ott, S. Thorwirth, and C. Hieret. Detection of amino acetonitrile in Sgr B2(N). *Astronomy & Astrophysics*, 482:179–196, April 2008. doi: 10.1051/0004-6361:20079203. 38

A. Belloche, R. T. Garrod, H. S. P. Müller, K. M. Menten, C. Comito, and P. Schilke. Increased complexity in interstellar chemistry: detection and chemical modeling of ethyl formate and n-propyl cyanide in Sagittarius B2(N). *Astronomy & Astrophysics*, 499:215–232, May 2009. doi: 10.1051/0004-6361/200811550. 174

A. Belloche, H. S. P. Müller, R. T. Garrod, and K. M. Menten. Exploring molecular complexity with ALMA (EMoCA): Deuterated complex organic molecules in Sagittarius B2(N2). *Astronomy & Astrophysics*, 587:A91, March 2016. doi: 10.1051/0004-6361/201527268. 18

Arnaud Belloche, Holger SP Müller, Karl M Menten, Peter Schilke, and Claudia Comito. Complex organic molecules in the interstellar medium: Iram 30 m line survey of sagittarius b2 (n) and (m). *Astronomy & Astrophysics*, 559:A47, 2013. 174

Arnaud Belloche, Robin T Garrod, Holger SP Müller, and Karl M Menten. Detection of a branched alkyl molecule in the interstellar medium: iso-propyl cyanide. *Science*, 345(6204):1584–1587, 2014. 38

M. T. Beltrán, C. Codella, S. Viti, R. Neri, and R. Cesaroni. First Detection of Glycolaldehyde Outside the Galactic Center. *Astrophys. J. Lett.*, 690:L93–L96, January 2009. doi: 10.1088/0004-637X/690/2/L93. 174

Chris J Bennett and Ralf I Kaiser. On the formation of glycolaldehyde (hcoch2oh) and methyl formate (hcooch3) in interstellar ice analogs. *The Astrophysical Journal*, 661(2):899, 2007. 181

Edwin A Bergin, Sébastien Maret, Floris FS Van Der Tak, Joao Alves, Sean M Carmody, and Charles J Lada. The thermal structure of gas in prestellar cores: A case study of barnard 68. *The Astrophysical Journal*, 645(1):369, 2006. 25

H Beuther and Henrik Dahl Nissen. Identifying the outflow driving sources in orion-kl. *The Astrophysical Journal Letters*, 679(2):L121, 2008. 15

A. Blaauw. The O Associations in the Solar Neighborhood. *Annu. Rev. Astron. Astrophys.*, 2:213, 1964. doi: 10.1146/annurev.aa.02.090164.001241. 21, 22

Adriaan Blaauw. Ob associations and the fossil record of star formation. In *The physics of star formation and early stellar evolution*, pages 125–154. Springer, 1991. 22

G. A. Blake, C. R. Masson, T. G. Phillips, and E. C. Sutton. The rotational emission-line spectrum of Orion A between 247 and 263 GHz. *Astrophys. J. Suppl. Ser.*, 60:357–374, January 1986. doi: 10.1086/191090. 22

Geoffrey A Blake, EC Sutton, CR Masson, and TG Phillips. Molecular abundances in omc-1-the chemical composition of interstellar molecular clouds and the influence of massive star formation. *The Astrophysical Journal*, 315:621–645, 1987. 12, 14, 15, 16, 17, 18, 21, 174

Geoffrey A Blake, LG Mundy, JE Carlstrom, S Padin, SL Scott, NZ Scoville, and DP Woody. A λ= 1.3 millimeter aperture synthesis molecular line survey of orion kleinmann-low. *The Astrophysical Journal Letters*, 472(1):L49, 1996. 12

L. Blitz. Giant molecular clouds. In E. H. Levy and J. I. Lunine, editors, *Protostars and Planets III*, pages 125–161, 1993. 19

L. Blitz and J. P. Williams. Molecular Clouds. In C. J. Lada and N. D. Kylafis, editors, *NATO Advanced Science Institutes (ASI) Series C*, volume 540 of *NATO Advanced Science Institutes (ASI) Series C*, page 3, 1999. 19

Peter H Bodenheimer. Molecular clouds and the onset of star formation. In *Principles of Star Formation*, pages 37–91. Springer, 2011. 47

Ian A Bonnell, Matthew R Bate, and Hans Zinnecker. On the formation of massive stars. *Monthly Notices of the Royal Astronomical Society*, 298(1):93–102, 1998. 22

W. B. Bonnor. Boyle's Law and gravitational instability. *MNRAS*, 116:351, 1956. doi: 10.1093/mnras/116.3.351. 19

J. Bouwman, A. de Koter, C. Dominik, and L. B. F. M. Waters. The origin of crystalline silicates in the Herbig Be star HD 100546 and in comet Hale-Bopp. *Astronomy & Astrophysics*, 401:577–592, April 2003. doi: 10.1051/0004-6361:20030043. 48

N. Brouillet, D. Despois, A. Baudry, T.-C. Peng, C. Favre, A. Wootten, A. J. Remijan, T. L. Wilson, F. Combes, and G. Wlodarczak. CH_3OCH_3 in Orion-KL: a striking similarity with $HCOOCH_3$. *Astronomy & Astrophysics*, 550:A46, February 2013. doi: 10.1051/0004-6361/201219983. 22

P. D. Brown, S. B. Charnley, and T. J. Millar. A model of the chemistry in hot molecular cores. *MNRAS*, 231:409–417, March 1988. doi: 10.1093/mnras/231.2.409. 18, 46

RD Brown, JG Crofts, PD Godfrey, FF Gardner, BJ Robinson, and JB Whiteoak. Discovery of interstellar methyl formate. *The Astrophysical Journal*, 197:L29–L31, 1975. 174

S Brünken, H Gupta, CA Gottlieb, MC McCarthy, and P Thaddeus. Detection of the carbon chain negative ion c8h–in tmc-1. *The Astrophysical Journal Letters*, 664(1):L43, 2007. 39

GM Munoz Caro, UJ Meierhenrich, WA Schutte, B Barbier, A Arcones Segovia, H Rosenbauer, WH-P Thiemann, A Brack, and JM Greenberg. Amino acids from ultraviolet irradiation of interstellar ice analogues. *Nature*, 416(6879):403–406, 2002. 181

P Brandon Carroll, Brett A McGuire, Geoffrey A Blake, Aldo J Apponi, Lucy M Ziurys, and Anthony Remijan. The search for a complex molecule in a selected hot core region: A rigorous attempt to confirm trans-ethyl methyl ether toward w51 e1/e2. *The Astrophysical Journal*, 799(1):15, 2015. 172

P Caselli, TI Hasegawa, and Eric Herbst. Chemical differentiation between star-forming regions-the orion hot core and compact ridge. *The Astrophysical Journal*, 408:548–558, 1993. 44

Paola Caselli. Chemical processes in star forming regions. In *Cores to Clusters: Star Formation with Next Generation Telescopes*, page 47, 2005. 45

S Cazaux, AGGM Tielens, C Ceccarelli, A Castets, V Wakelam, E Caux, Berengere Parise, and D Teyssier. The hot core around the low-mass protostar iras 16293–2422: Scoundrels rule! *The Astrophysical Journal Letters*, 593(1):L51, 2003. 174

C. Ceccarelli, L. Loinard, A. Castets, A. G. G. M. Tielens, E. Caux, B. Lefloch, and C. Vastel. Extended D_2CO emission: The smoking gun of grain surface-chemistry. *Astronomy & Astrophysics*, 372:998–1004, June 2001. doi: 10.1051/0004-6361:20010559. 18

J Cernicharo. Internal iram report. *Granada: IRAM*, 1985. 58, 60

J. Cernicharo. Laboratory astrophysics and astrochemistry in the Herschel/ALMA era. In C. Stehlé, C. Joblin, and L. d'Hendecourt, editors, *EAS Publications Series*, volume 58 of *EAS Publications Series*, pages 251–261, February 2012. doi: 10.1051/eas/1258040. 52, 53, 65

J. Cernicharo, S. Perez-Martinez, E. González-Alfonso, S. J. Leeks, M. J. Sempere, T. Lim, B. Lefloch, and F. Najarro. The far-infrared spectrum of Orion-IRC2. In P. Cox and M. Kessler, editors, *The Universe as Seen by ISO*, volume 427 of *ESA Special Publication*, page 651, March 1999. 50

J. Cernicharo, M. Guélin, and J. R. Pardo. Detection of the Linear Radical HC_4N in IRC +10216. *Astrophys. J. Lett.*, 615:L145–L148, November 2004. doi: 10.1086/426439. 39

J. Cernicharo, M. Guélin, M. Agúndez, K. Kawaguchi, M. McCarthy, and P. Thaddeus. Astronomical detection of C_{4H^-}, the second interstellar anion. *Astronomy & Astrophysics*, 467:L37–L40, May 2007. doi: 10.1051/0004-6361:20077415. 39

J Cernicharo, N Marcelino, E Roueff, M Gerin, A Jiménez-Escobar, and GM Muñoz Caro. Discovery of the methoxy radical, ch3o, toward b1: Dust grain and gas-phase chemistry in cold dark clouds. *The Astrophysical Journal Letters*, 759(2):L43, 2012. 45

SB Charnley, AGGM Tielens, and TJ Millar. On the molecular complexity of the hot cores in orion a-grain surface chemistry as' the last refuge of the scoundrel'. *The Astrophysical Journal*, 399:L71–L74, 1992. 47

A. C. Cheung, D. M. Rank, C. H. Townes, D. D. Thornton, and W. J. Welch. Detection of Water in Interstellar Regions by its Microwave Radiation. *Nature, year = 1969, month = feb, volume = 221, pages = 626-628, doi = 10.1038/221626a0, adsurl = http://adsabs.harvard.edu/abs/1969Natur.221..626C, adsnote = Provided by the SAO/NASA Astrophysics Data System*. 27

AC Cheung, David M Rank, CH Townes, Douglas D Thornton, and WJ Welch. Detection of n h 3 molecules in the interstellar medium by their microwave emission. *Physical Review Letters*, 21(25): 1701, 1968. 27

E Churchwell, A Nash, J Rahe, CM Walmsley, O Lochner, and G Winnewisser. Abundances and excitation of interstellar methyl formate. *The Astrophysical Journal*, 241:L169–L174, 1980. 174

C. Comito, P. Schilke, T. G. Phillips, D. C. Lis, F. Motte, and D. Mehringer. A Molecular Line Survey of Orion KL in the 350 Micron Band. *Astrophys. J. Suppl. Ser.*, 156:127–167, February 2005. doi: 10.1086/425996. 22

P. C. Cortes, J. M. Girart, C. L. H. Hull, T. K. Sridharan, F. Louvet, R. Plambeck, Z.-Y. Li, R. M. Crutcher, and S.-P. Lai. Interferometric Mapping of Magnetic Fields: The ALMA View of the Massive Star-forming Clump W43-MM1. *Astrophys. J. Lett.*, 825:L15, July 2016. doi: 10.3847/2041-8205/825/1/L15. 20

L. H. Coudert, B. J. Drouin, B. Tercero, J. Cernicharo, J.-C. Guillemin, R. A. Motiyenko, and L. Margulès. The First Astrophysical Detection, Terahertz Spectrum, and Database for the Monodeuterated Species of Methyl Formate $HCOOCH_2D$. *Astrophys. J.*, 779:119, December 2013. doi: 10.1088/0004-637X/779/2/119. 18

A. Coutens, M. V. Persson, J. K. Jørgensen, S. F. Wampfler, and J. M. Lykke. Detection of glycolaldehyde toward the solar-type protostar NGC 1333 IRAS2A. *Astronomy & Astrophysics*, 576:A5, April 2015. doi: 10.1051/0004-6361/201425484. 174

John R Cronin and Sherwood Chang. Organic matter in meteorites: Molecular and isotopic analyses of the murchison meteorite. In *The chemistry of life's origins*, pages 209–258. Springer, 1993. 181

... Cuadrado, Sara. ...in prep. 2017. 40

A. M. Daly, C. Bermúdez, A. López, B. Tercero, J. C. Pearson, N. Marcelino, J. L. Alonso, and J. Cernicharo. Laboratory Characterization and Astrophysical Detection of Vibrationally Excited States of Ethyl Cyanide. *Astrophys. J.*, 768:81, May 2013. doi: 10.1088/0004-637X/768/1/81. 7, 18, 69, 174

P De Vicente, J Martín-Pintado, R Neri, and A Rodríguez-Franco. On the heating source of the orion kl hot core. *The Astrophysical Journal Letters*, 574(2):L163, 2002. 12

K Demyk, H MÄBDER, B Tercero, J Cemicharo, J Demaison, L Margulès, M Wegner, S Keipert, and M Sheng. Isotopic ethyl cyanide 13ch3ch2cn, ch313ch2cn, and ch3ch213cn: laboratory rotational spectrum and detection in orion. *Astronomy and astrophysics*, 466(1):255–259, 2007. 69, 174

K. Demyk, G. Wlodarczak, and M. Carvajal. Detection of vibrationally excited methyl formate in W51 e2. *Astronomy & Astrophysics*, 489:589–600, October 2008. doi: 10.1051/0004-6361:200809354. 7, 174

Walter Winston Duley and David Arnold Williams. Interstellar chemistry. *Inorganic Chemistry*, 1, 1984. 42

P. Ehrenfreund, S. B. Charnley, and O. Botta. A voyage from dark clouds to the early Earth. In M. Livio, I. N. Reid, and W. Sparks, editors, *Astrophysics of Life*, volume 16, pages 1–20, 2005. 41

Pascale Ehrenfreund and Steven B Charnley. Organic molecules in the interstellar medium, comets, and meteorites: a voyage from dark clouds to the early earth. *Annual Review of Astronomy and Astrophysics*, 38(1):427–483, 2000. 47, 49, 181

NR Erickson, PF Goldsmith, RL Snell, RL Berson, GR Huguenin, BL Ulich, and CJ Lada. Detection of bipolar co outflow in orion. *The Astrophysical Journal*, 261:L103–L107, 1982. 15

G. B. Esplugues, J. Cernicharo, S. Viti, J. R. Goicoechea, B. Tercero, N. Marcelino, A. Palau, T. A. Bell, E. A. Bergin, N. R. Crockett, and S. Wang. Combined IRAM and Herschel/HIFI study of cyano(di)acetylene in Orion KL: tentative detection of DC_3N. *Astronomy & Astrophysics*, 559:A51, November 2013. doi: 10.1051/0004-6361/201322073. 18

C. Favre, D. Despois, N. Brouillet, A. Baudry, F. Combes, M. Guélin, A. Wootten, and G. Wlodarczak. $HCOOCH_3$ as a probe of temperature and structure in Orion-KL. *Astronomy & Astrophysics*, 532: A32, August 2011. doi: 10.1051/0004-6361/201015345. 17, 22

D. F. Figer. The stellar Initial Mass Function in the Galactic Center. In E. Corbelli, F. Palla, and H. Zinnecker, editors, *The Initial Mass Function 50 Years Later*, volume 327 of *Astrophysics and Space Science Library*, page 89, January 2005. doi: 10.1007/978-1-4020-3407-7_13. 20

J Franco, G Tenorio-Tagle, P Bodenheimer, M Rozyczka, and IF Mirabel. On the origin of the orion and monoceros molecular cloud complexes. *The Astrophysical Journal*, 333:826–839, 1988. 11, 12

Helen J Fraser, Martin RS McCoustra, and David A Williams. The molecular universe. *Astronomy & Geophysics*, 43(2):2–10, 2002. 23, 26, 41

P. Friberg, A. Hjalmarson, S. C. Madden, and W. M. Irvine. Methanol in dark clouds. *Astronomy & Astrophysics*, 195:281–289, April 1988. 45

A Fuente, J Cernicharo, P Caselli, C McCoey, D Johnstone, M Fich, T van Kempen, Aina Palau, UA Yıldız, B Tercero, et al. The hot core towards the intermediate-mass protostar ngc 7129 firs 2-chemical similarities with orion kl. *Astronomy & Astrophysics*, 568:A65, 2014. 174

H.-P. Gail and E. Sedlmayr. The primary condensation process for dust around late M-type stars. *Astronomy & Astrophysics*, 166:225–236, September 1986. 47

H.-P. Gail and E. Sedlmayr. Dust formation in stellar winds. In G. E. Morfill and M. Scholer, editors, *NATO ASIC Proc. 210: Physical Processes in Interstellar Clouds*, pages 275–303, 1987. 47

FF Gardner and G Winnewisser. The detection of interstellar vinyl cyanide/acrylonitrile. *The Astrophysical Journal*, 195:L127–L130, 1975. 38, 174

Muriel Gargaud. *Encyclopedia of astrobiology*, volume 3. Springer Science & Business Media, 2011. 29

RT Garrod and E Herbst. Formation of methyl formate and other organic species in the warm-up phase of hot molecular cores. *Astronomy & Astrophysics*, 457(3):927–936, 2006. 44

TR Geballe and T Oka. Detection of h3 in interstellar space. *Nature*, 384(6607):334, 1996. 26

R Genzel and D Downes. Mass outflow in molecular clouds: A new phase in the evolution of newly-formed stars? *Highlights of Astronomy*, 6:686–706, 1983. 15

R. Genzel and J. Stutzki. The Orion Molecular Cloud and star-forming region. *Annu. Rev. Astron. Astrophys.*, 27:41–85, 1989. doi: 10.1146/annurev.aa.27.090189.000353. 7, 10, 12, 13, 18, 21

R. Genzel, P. T. P. Ho, J. Bieging, and D. Downes. NH3 in Orion-KL - A new interpretation. *Astrophys. J. Lett.*, 259:L103–L107, August 1982. doi: 10.1086/183856. 17

M. Gerin, F. Combes, G. Wlodarczak, T. Jacq, M. Guelin, P. Encrenaz, and C. Laurent. Interstellar detection of deuterated methyl cyanide. *Astronomy & Astrophysics*, 259:L35–L38, June 1992. 18

EL Gibb, DCB Whittet, ACA Boogert, and AGGM Tielens. Interstellar ice: The infrared space observatory legacy. *The Astrophysical Journal Supplement Series*, 151:35–73, 2004. 48

F. C. Gillett, W. J. Forrest, and K. M. Merrill. 8 - 13-micron spectra of NGC 7027, BD +30 3639, and NGC 6572. *Astrophys. J.*, 183:87–93, July 1973. doi: 10.1086/152211. 48

IL Goldberg and AW Mc Culloch. Annular aperture diffracted energy distribution for an extended source. 1968. 60

PF Goldsmith, R Krotkov, RL Snell, RD Brown, and P Godfrey. Vibrationally excited ch3cn and hc3n in orion. *The Astrophysical Journal*, 274:184–194, 1983. 12

Laura Gómez, Luis F Rodríguez, Laurent Loinard, Susana Lizano, Christine Allen, Arcadio Poveda, and Karl M Menten. Monitoring the large proper motions of radio sources in the orion bn/kl region. *The Astrophysical Journal*, 685(1):333, 2008. 11

Walter Gordy and Robert L Cook. *Microwave molecular spectra*. Wiley,, 1984. 30, 35, 36

N. Guessoum, P. Jean, and W. Gillard. Positron annihilation on polycyclic aromatic hydrocarbon molecules in the interstellar medium. *MNRAS*, 402:1171–1178, February 2010. doi: 10.1111/j.1365-2966.2009.15954.x. 48

Viviana V Guzmán, Jérôme Pety, Pierre Gratier, Javier R Goicoechea, Maryvonne Gerin, Evelyne Roueff, Franck Le Petit, and Jacques Le Bourlot. Chemical complexity in the horsehead photodissociation region. *Faraday discussions*, 168:103–127, 2014. 40

Martin Harwit. Large-scale distribution of far-infrared and submillimeter line emission. *Annals of the New York Academy of Sciences*, 395(1):56–63, 1982. 16

T Hasegawa, N Kaifu, J Inatani, M Morimoto, Y Chikada, H Hirabayashi, H Iwashita, K-I Morita, A Tojo, and K Akabane. Cs around orion-kl-a large rotating disk. *The Astrophysical Journal*, 283:117–122, 1984. 16

Eric Herbst. The chemistry of interstellar space. *Chemical Society Reviews*, 30(3):168–176, 2001. 43, 48, 49

Eric Herbst. Surface reactions in interstellar space. *Highlights of Astronomy*, 12:55–57, 2002. 43

Eric Herbst. Chemistry of star-forming regions. *The Journal of Physical Chemistry A*, 109(18):4017–4029, 2005. 23

Eric Herbst. Astrochemistry and star formation: Successes and challenges. *Reviews in Modern Astronomy*, 19:167, 2006. 23

Eric Herbst and William Klemperer. The formation and depletion of molecules in dense interstellar clouds. *The Astrophysical Journal*, 185:505–534, 1973. 16

Eric Herbst and Ewine F Van Dishoeck. Complex organic interstellar molecules. *Annual Review of Astronomy and Astrophysics*, 47:427–480, 2009. 26, 31, 43

W. Hermsen, T. L. Wilson, and J. H. Bieging. VLA maps of ammonia in Orion-KL - Fine-scale structure and geometry. *Astronomy & Astrophysics*, 201:276–284, August 1988. 17

Tomoya Hirota, Mi Kyoung Kim, Yasutaka Kurono, and Mareki Honma. A hot molecular circumstellar disk around the massive protostar orion source i. *The Astrophysical Journal Letters*, 782(2):L28, 2014. 22

Paul TP Ho and Alan Hildreth Barrett. A new dynamical model for the orion molecular cloud. *The Astrophysical Journal*, 224:L23–L26, 1978. 16

J Michael Hollas. *Modern spectroscopy*. John Wiley & Sons, 2004. 35

J. M. Hollis, F. J. Lovas, and P. R. Jewell. Interstellar Glycolaldehyde: The First Sugar. *Astrophys. J. Lett.*, 540:L107–L110, September 2000. doi: 10.1086/312881. 174

Jan M Hollis, Frank J Lovas, Philip R Jewell, and LH Coudert. Interstellar antifreeze: ethylene glycol. *The Astrophysical Journal Letters*, 571(1):L59, 2002. 38

JM Hollis, Francis J Lovas, Anthony J Remijan, PR Jewell, VV Ilyushin, and I Kleiner. Detection of acetamide (ch3conh2): the largest interstellar molecule with a peptide bond. *The Astrophysical Journal Letters*, 643(1):L25, 2006. 38

S Hotzel, J Harju, and M Juvela. The kinetic temperature of barnard 68. *Astronomy & Astrophysics*, 395 (1):L5–L8, 2002. 25

G. R. Huss, G. J. MacPherson, G. J. Wasserburg, S. S. Russell, and G. Srinivasan. 26Al in CAIs and chondrules from unequilibrated ordinary chondrites. *Meteoritics and Planetary Science*, 36:975–997, July 2001. doi: 10.1111/j.1945-5100.2001.tb01934.x. 47

Shu-ichiro Inutsuka. Present-day star formation: From molecular cloud cores to protostars and protoplanetary disks. *Progress of Theoretical and Experimental Physics*, 2012(1):01A307, 2012. 20, 21

W. M. Irvine. Extraterrestrial Organic Matter: A review. *Origins of Life and Evolution of the Biosphere*, 28:365–383, October 1998. 181

W. M. Irvine and A. Hjalmarson. The chemical composition of interstellar molecular clouds. *Origins of Life*, 14:15–23, December 1984. doi: 10.1007/BF00933635. 17

James H Jeans. The stability of a spherical nebula. *Philosophical Transactions of the Royal Society of London. Series A, Containing Papers of a Mathematical or Physical Character*, 199:1–53, 1902. 19

Lars EB Johansson, C Andersson, J Ellder, P Friberg, Å Hjalmarson, B Hoglund, WM Irvine, H Olofsson, and G Rydbeck. Spectral scan of orion a and irc+ 10216 from 72 to 91 ghz. *Astronomy and astrophysics*, 130:227–256, 1984. 16, 17, 21

D. R. Johnson, F. J. Lovas, C. A. Gottlieb, E. W. Gottlieb, M. M. Litvak, P. Thaddeus, and M. Guelin. Detection of interstellar ethyl cyanide. *Astrophys. J.*, 218:370–376, December 1977. doi: 10.1086/155691. 174

J. K. Jørgensen, M. R. Hogerheijde, G. A. Blake, E. F. van Dishoeck, L. G. Mundy, and F. L. Schöier. The impact of shocks on the chemistry of molecular clouds. High resolution images of chemical differentiation along the NGC 1333-IRAS 2A outflow. *Astronomy & Astrophysics*, 415:1021–1037, March 2004. doi: 10.1051/0004-6361:20034216. 40

J. K. Jørgensen, C. Favre, S. E. Bisschop, T. L. Bourke, E. F. van Dishoeck, and M. Schmalzl. Detection of the Simplest Sugar, Glycolaldehyde, in a Solar-type Protostar with ALMA. *Astrophys. J. Lett.*, 757: L4, September 2012. doi: 10.1088/2041-8205/757/1/L4. 174

JK Jørgensen, MHD van der Wiel, A Coutens, JM Lykke, HSP Müller, EF van Dishoeck, H Calcutt, P Bjerkeli, TL Bourke, MN Drozdovskaya, et al. The alma protostellar interferometric line survey (pils)-first results from an unbiased submillimeter wavelength line survey of the class 0 protostellar binary iras 16293-2422 with alma. *Astronomy & Astrophysics*, 595:A117, 2016. 174

Michael J Kaufman, David J Hollenbach, and AGGM Tielens. High-temperature molecular cores near massive stars and application to the orion hot core. *The Astrophysical Journal*, 497(1):276, 1998. 12

Kentarou Kawaguchi, Yasuko Kasai, Shin-Ichi Ishikawa, and Norio Kaifu. A spectral-line survey observation of irc+ 10216 between 28 and 50 ghz. *Publications of the Astronomical Society of Japan*, 47:853–876, 1995. 39

Mi Kyoung Kim, Tomoya Hirota, Mareki Honma, Hideyuki Kobayashi, Takeshi Bushimata, Yoon Kyung Choi, Hiroshi Imai, Kenzaburo Iwadate, Takaaki Jike, Seiji Kameno, et al. Sio maser observations toward orion-kl with vera. *Publications of the Astronomical Society of Japan*, 60(5):991–999, 2008. 10

Z. Kisiel, L. Pszczółkowski, B. J. Drouin, C. S. Brauer, S. Yu, J. C. Pearson, I. R. Medvedev, S. Fortman, and C. Neese. Broadband rotational spectroscopy of acrylonitrile: Vibrational energies from perturbations. *Journal of Molecular Spectroscopy*, 280:134–144, October 2012. doi: 10.1016/j.jms.2012.06.013. 37

D. E. Kleinmann and F. J. Low. Discovery of an Infrared Nebula in Orion. *Astrophys. J. Lett.*, 149:L1, July 1967. doi: 10.1086/180039. 7

Ralf Klessen and Andreas Burkert. Fragmentation in molecular clouds: The formation of a stellar cluster. *Interstellar turbulence*, page 272, 1999. 20

Kaori Kobayashi, Kazumi Ogata, Shozo Tsunekawa, and Shuro Takano. Torsionally excited methyl formate in orion kl. *The Astrophysical Journal Letters*, 657(1):L17, 2007. 174

Kurt W Kolasinski. *Surface science: foundations of catalysis and nanoscience*. John Wiley & Sons, 2012. 43

John D Kraus. Antennas. 1988. 60, 61

P. Kroupa. On the variation of the initial mass function. *MNRAS*, 322:231–246, April 2001. doi: 10.1046/j.1365-8711.2001.04022.x. 20

TBH Kuiper, B Zuckerman, and EN Rodriguez Kuiper. High velocity molecular emission in orion-a case for stellar winds. *The Astrophysical Journal*, 251:88–102, 1981. 15

ML Kutner, KD Tucker, G Chin, and P Thaddeus. The molecular complexes in orion. *The Astrophysical Journal*, 215:521–528, 1977. 12

J Kwan and N Scoville. The nature of the broad molecular line emission at the kleinmann-low nebula. *The Astrophysical Journal*, 210:L39–L43, 1976. 15

Sun Kwok. *Physics and chemistry of the interstellar medium*. University Science Books, 2007. 19, 20, 60

Charles J Lada. The formation of low mass stars: Observations. In *The Physics of Star Formation and Early Stellar Evolution*, pages 329–364. Springer, 1991. 22

Charles J Lada and Nikolaos D Kylafis. *The Origin of Stars and Planetary Systems*, volume 540. Springer Science & Business Media, 2012a. 11

Charles J Lada and Nikolaos D Kylafis. *The physics of star formation and early stellar evolution*, volume 342. Springer Science & Business Media, 2012b. 18

Richard B Larson. Turbulence and star formation in molecular clouds. *Monthly Notices of the Royal Astronomical Society*, 194(4):809–826, 1981. 20

J Lequeux. The interstellar medium, ed. *Lequeux, J*, 2005. 57, 62

Hua-bai Li, Alyssa Goodman, TK Sridharan, Martin Houde, Zhi-Yun Li, Giles Novak, and Kwok Sun Tang. The link between magnetic fields and cloud/star formation. *Protostars and Planets VI*, 1: 101–123, 2014. 11

A. López, B. Tercero, Z. Kisiel, A. M. Daly, C. Bermúdez, H. Calcutt, N. Marcelino, S. Viti, B. J. Drouin, I. R. Medvedev, C. F. Neese, L. Pszczółkowski, J. L. Alonso, and J. Cernicharo. Laboratory characterization and astrophysical detection of vibrationally excited states of vinyl cyanide in Orion-KL. *Astronomy & Astrophysics*, 572:A44, December 2014. doi: 10.1051/0004-6361/201423622. 7, 18, 84, 174

Tercero B. Cernicharo López, A. $C_2h_4o_2$ isomers in orion kl: Methyl formate, acetic acid, and glycolaldehyde. an overview of alma and iram 30m. in prep. 2017. 174

M.-M. Mac Low and R. S. Klessen. Control of star formation by supersonic turbulence. *Reviews of Modern Physics*, 76:125–194, January 2004. doi: 10.1103/RevModPhys.76.125. 20, 21

G. H. MacDonald, A. G. Gibb, R. J. Habing, and T. J. Millar. A 330-360 GHz spectral survey of G 34.3+0.15. I. Data and physical analysis. *Astronomy & Astrophysics Supplement*, 119:333–367, October 1996. 174

Jeffrey G Mangum and Yancy L Shirley. How to calculate molecular column density. *Publications of the Astronomical Society of the Pacific*, 127(949):266, 2015. 30, 34

N Marcelino, O Berné, and J Cernicharo. Large scale co emission in orion a: Star formation feedback on the molecular gas. In *IAU Symposium*, volume 280, page 246P, 2011. 15

L. Margulès, R. Motiyenko, K. Demyk, B. Tercero, J. Cernicharo, M. Sheng, M. Weidmann, J. Gripp, H. Mäder, and J. Demaison. Rotational spectrum of deuterated and ^{15}N ethyl cyanides: CH_3CHDCN and CH_2DCH_2CN and of CH_3CH_2C^{15}N. *Astronomy & Astrophysics*, 493:565–569, January 2009. doi: 10.1051/0004-6361:200810889. 69, 174

L. Margulès, A. Belloche, H. S. P. Müller, R. A. Motiyenko, J.-C. Guillemin, R. T. Garrod, and K. M. Menten. Spectroscopic study and astronomical detection of doubly ^{13}C-substituted ethyl cyanide. *Astronomy & Astrophysics*, 590:A93, May 2016. doi: 10.1051/0004-6361/201628309. 174

J. S. Mathis. Interstellar dust and extinction. *Annu. Rev. Astron. Astrophys.*, 28:37–70, 1990. doi: 10.1146/annurev.aa.28.090190.000345. 47

HE Matthews and TJ Sears. The detection of vinyl cyanide in tmc-1. *The Astrophysical Journal*, 272: 149–153, 1983. 174

R Mauersberger, C Henkel, CM Walmsley, LJ Sage, and T Wiklind. Dense gas in nearby galaxies. v-multilevel studies of ch3cch and ch3cn. *Astronomy and Astrophysics*, 247:307–314, 1991. 40

M. C. McCarthy, C. A. Gottlieb, H. Gupta, and P. Thaddeus. Laboratory and Astronomical Identification of the Negative Molecular Ion C_6H^-. *Astrophys. J. Lett.*, 652:L141–L144, December 2006. doi: 10.1086/510238. 39

David M Mehringer and Lewis E Snyder. The location of complex molecules in g34. 3+ 0.2: further evidence for grain-surface chemistry. *The Astrophysical Journal*, 471(2):897, 1996. 174

David M Mehringer, Lewis E Snyder, Yanti Miao, and Frank J Lovas. Detection and confirmation of interstellar acetic acid. *The Astrophysical Journal Letters*, 480(1):L71, 1997. 174

David M Mehringer, JC Pearson, Jocelyn Keene, and TG Phillips. Detection of vibrationally excited ethyl cyanide in the interstellar medium. *The Astrophysical Journal*, 608(1):306, 2004. 69, 174

K. M. Menten and M. J. Reid. What is powering the Orion Kleinmann-low infrared nebula. *Astrophys. J. Lett.*, 445:L157–L160, June 1995. doi: 10.1086/187913. 12

KM Menten, MJ Reid, J Forbrich, and A Brunthaler. The distance to the orion nebula. *Astronomy & Astrophysics*, 474(2):515–520, 2007. 10

Y. Miao and L. E. Snyder. Full Synthesis Observations of CH_3CH_2CN in Sagittarius B2: Further Evidence for Grain Chemistry. *Astrophys. J. Lett.*, 480:L67–L70, May 1997. doi: 10.1086/310624. 174

Glenn E Miller and John M Scalo. The initial mass function and stellar birthrate in the solar neighborhood. *The Astrophysical Journal Supplement Series*, 41:513–547, 1979. 20

S. L. Miller. A Production of Amino Acids under Possible Primitive Earth Conditions. *Science*, 117: 528–529, May 1953. doi: 10.1126/science.117.3046.528. 4

S. L. Miller and H. C. Urey. Organic Compound Synthesis on the Primitive Earth. *Science*, 130:245–251, July 1959. doi: 10.1126/science.130.3370.245. 4

YC Minh and William M Irvine. Upper limits for the ethyl-cyanide abundances in tmc-1 and l134n: Chemical implications. *Astrophysics and space science*, 175(1):165–169, 1991. 174

H Møllendal, L Margulès, A Belloche, RA Motiyenko, A Konovalov, KM Menten, and Jean-Claude Guillemin. Rotational spectrum of a chiral amino acid precursor, 2-aminopropionitrile, and searches for it in sagittarius b2 (n). *Astronomy & Astrophysics*, 538:A51, 2012. 181

H. S. P. Müller, A. Belloche, K. M. Menten, C. Comito, and P. Schilke. Rotational spectroscopy of isotopic vinyl cyanide, H_2CCHCN, in the laboratory and in space. *Journal of Molecular Spectroscopy*, 251:319–325, September 2008. doi: 10.1016/j.jms.2008.03.016. 174

Sebastien Müller, A Beelen, Michel Guélin, Susanne Aalto, John H Black, Françoise Combes, SJ Curran, Patrice Theule, and SN Longmore. Molecules at z= 0.89-a 4-mm-rest-frame absorption-line survey toward pks 1830- 211. *Astronomy & Astrophysics*, 535:A103, 2011. 40

PC Myers, M Heyer, Ronald L Snell, and PF Goldsmith. Dense cores in dark clouds. v-co outflow. *The Astrophysical Journal*, 324:907–919, 1988. 11

J. L. Neill, N. R. Crockett, E. A. Bergin, J. C. Pearson, and L.-H. Xu. Deuterated Molecules in Orion KL from Herschel/HIFI. *Astrophys. J.*, 777:85, November 2013. doi: 10.1088/0004-637X/777/2/85. 18

Albert Nummelin and P Bergman. Vibrationally excited vinyl cyanide in sgr b2 (n). *Astronomy & Astrophysics*, 341:L59–L62, 1999. 174

Karin I Öberg, Ewine F Van Dishoeck, and Harold Linnartz. Photodesorption of ices i: Co, no_2, and co_2. *Astronomy & Astrophysics*, 496(1):281–293, 2009. 181

Karin I Öberg, Viviana V Guzmán, Kenji Furuya, Chunhua Qi, Yuri Aikawa, Sean M Andrews, Ryan Loomis, and David J Wilner. The comet-like composition of a protoplanetary disk as revealed by complex cyanides. *Nature*, 520(7546):198–201, 2015. 39, 181

Masatoshi Ohishi and Norio Kaifu. Chemical and physical evolution of dark clouds molecular spectral line survey toward tmc-1. *Faraday Discussions*, 109:205–216, 1998. 39

E. C. Ostriker. Turbulence and magnetic fields in star formation. In S. S. Holt and L. G. Mundy, editors, *American Institute of Physics Conference Series*, volume 393 of *American Institute of Physics Conference Series*, pages 51–62, February 1997. doi: 10.1063/1.52734. 20

R Padman, PF Scott, DR Vizard, and AS Webster. Cs 5–4 observations of omc1: evidence for external heating of the quiescent gas. *Monthly Notices of the Royal Astronomical Society*, 214(3):251–270, 1985. 16

Marco Padovani, Daniele Galli, and Alfred E Glassgold. Cosmic-ray ionization of molecular clouds. *Astronomy & Astrophysics*, 501(2):619–631, 2009. 44

J. R. Pardo. *Estudios de la atmósfera terrestre mediante observaciones en longitudes de onda milimétricas y submilimétricas*. PhD thesis, 1996. 58, 60

J. R. Pardo, J. Cernicharo, F. Herpin, J. Kawamura, J. Kooi, and T. G. Phillips. Deuterium Enhancement in Water toward Orion IRc2 Deduced from HDO Lines above 800 GHz. *Astrophys. J.*, 562:799–803, December 2001. doi: 10.1086/323882. 58, 60

Juan R Pardo, José Cernicharo, Javier R Goicoechea, Michel Guélin, and Andrés Asensio Ramos. Molecular line survey of crl 618 from 80 to 276 ghz and complete model. *The Astrophysical Journal*, 661(1):250, 2007. 39

A. Pauls, T. L. Wilson, J. H. Bieging, and R. N. Martin. Clumping in Orion KL - 2-arcsecond maps of ammonia. *Astronomy & Astrophysics*, 124:23–38, July 1983. 17

R. L. Plambeck and M. C. H. Wright. Aperture synthesis maps of HDO emission in Orion-KL. *Astrophys. J. Lett.*, 317:L101–L105, June 1987. doi: 10.1086/184920. 18

R. L. Plambeck, M. C. H. Wright, D. N. Friedel, S. L. Widicus Weaver, A. D. Bolatto, M. W. Pound, D. P. Woody, J. W. Lamb, and S. L. Scott. Tracing the Bipolar Outflow from Orion Source I. *Astrophys. J. Lett.*, 704:L25–L28, October 2009. doi: 10.1088/0004-637X/704/1/L25. 15

R. L. Plambeck, A. D. Bolatto, J. M. Carpenter, J. A. Eisner, J. W. Lamb, E. M. Leitch, D. P. Marrone, S. J. Muchovej, L. M. Pérez, M. W. Pound, P. J. Teuben, N. H. Volgenau, D. P. Woody, M. C. H. Wright, and B. A. Zauderer. The Ionized Circumstellar Envelopes of Orion Source I and the Becklin-Neugebauer Object. *Astrophys. J.*, 765:40, March 2013. doi: 10.1088/0004-637X/765/1/40. 21

RL Plambeck, MCH Wright, WJ Welch, JH Bieging, B Baud, PTP Ho, and SN Vogel. Kinematics of orion-kl-aperture synthesis maps of 86 ghz so emission. *The Astrophysical Journal*, 259:617–624, 1982. 14

R. E. Pudritz, M. Klassen, H. Kirk, D. Seifried, and R. Banerjee. The Role of Magnetic Fields in Star Formation. In P. Petit, M. Jardine, and H. C. Spruit, editors, *Magnetic Fields throughout Stellar Evolution*, volume 302 of *IAU Symposium*, pages 10–20, August 2014. doi: 10.1017/S174392131400163X. 20

Ralph E Pudritz. Clustered star formation and the origin of stellar masses. *Science*, 295(5552):68–76, 2002. 21

Brati Sankar Ray. Über die eigenwerte des asymmetrischen kreisels. *Zeitschrift für Physik*, 78(1-2): 74–91, 1932. 36

M. J. Reid, K. M. Menten, L. J. Greenhill, and C. J. Chandler. Imaging the Ionized Disk of the High-Mass Protostar Orion I. *Astrophys. J.*, 664:950–955, August 2007. doi: 10.1086/518929. 21

A Remijan, LE Snyder, S-Y Liu, D Mehringer, and Y-J Kuan. Acetic acid in the hot cores of sagitarrius b2 (n) and w51. *The Astrophysical Journal*, 576(1):264, 2002. 174

A Remijan, LE Snyder, DN Friedel, S-Y Liu, and RY Shah. A survey of acetic acid toward hot molecular cores. *The Astrophysical Journal*, 590(1):314, 2003. 174

Anthony J Remijan, Friedrich Wyrowski, Douglas N Friedel, David S Meier, and Lewis E Snyder. A survey of large molecules toward the proto-planetary nebula crl 618. *The Astrophysical Journal*, 626 (1):233, 2005. 39

S. D. Rodgers and T. J. Millar. The chemistry of deuterium in hot molecular cores. *MNRAS*, 280: 1046–1054, June 1996. doi: 10.1093/mnras/280.4.1046. 18

R. W. Russell, B. T. Soifer, and S. P. Willner. The 4 to 8 micron spectrum of NGC 7027. *Astrophys. J. Lett.*, 217:L149–L153, November 1977. doi: 10.1086/182559. 48

P Schilke, TD Groesbeck, GA Blake, Phillips, and TG. A line survey of orion kl from 325 to 360 ghz. *The Astrophysical Journal Supplement Series*, 108(1):301, 1997. 174

W. A. Schutte and J. M. Greenberg. Explosive desorption of icy grain mantles in dense clouds. *Astronomy & Astrophysics*, 244:190–204, April 1991. 47

W. A. Schutte, P. A. Gerakines, T. R. Geballe, E. F. van Dishoeck, and J. M. Greenberg. Discovery of solid formaldehyde toward the protostar GL 2136: observations and laboratory simulation. *Astronomy & Astrophysics*, 309:633–647, May 1996. 47

E. Sedlmayr. From Molecules to Grains. In U. G. Jorgensen, editor, *IAU Colloq. 146: Molecules in the Stellar Environment*, volume 428 of *Lecture Notes in Physics, Berlin Springer Verlag*, page 163, 1994. doi: 10.1007/3-540-57747-5_42. 47

Y-S Jerry Shiao, Leslie W Looney, Anthony J Remijan, Lewis E Snyder, and Douglas N Friedel. First acetic acid survey with carma in hot molecular cores. *The Astrophysical Journal*, 716(1):286, 2010. 174

Frank H Shu, Fred C Adams, and Susana Lizano. Star formation in molecular clouds: observation and theory. *Annual review of astronomy and astrophysics*, 25(1):23–81, 1987. 19, 21

Ian WM Smith. Laboratory astrochemistry: gas-phase processes. *Annual Review of Astronomy and Astrophysics*, 49:29–66, 2011. 27

Ian WM Smith, Eric Herbst, and Qiang Chang. Rapid neutral-neutral reactions at low temperatures: a new network and first results for tmc-1. *Monthly Notices of the Royal Astronomical Society*, 350(1): 323–330, 2004. 39

Lewis E Snyder, David Buhl, B Zuckerman, and Patrick Palmer. Microwave detection of interstellar formaldehyde. *Physical Review Letters*, 22(13):679, 1969. 27

V. V. Sobolev. *Moving envelopes of stars*. 1960. 58

SW Stahler and F Palla. The formation of stars. 2005. *Cited on*, page 30, 2004. 10

J. Stutzki, R. Genzel, A. I. Harris, J. Herman, and D. T. Jaffe. First detection of HCN J = 9-8 (797 GHz) line emission - Very high densities in the Orion core. *Astrophys. J. Lett.*, 330:L125–L129, July 1988. doi: 10.1086/185219. 15

E. C. Sutton, G. A. Blake, C. R. Masson, and T. G. Phillips. Molecular line survey of Orion A from 215 to 247 GHz. *Astrophys. J. Suppl. Ser.*, 58:341–378, July 1985. doi: 10.1086/191045. 21

J. S. Sweitzer. On the excitation of interstellar ammonia in the Kleinmann-Low nebula. *Astrophys. J.*, 225:116–129, October 1978. doi: 10.1086/156473. 18

M. Tafalla, J. Santiago-García, P. C. Myers, P. Caselli, C. M. Walmsley, and A. Crapsi. On the internal structure of starless cores. II. A molecular survey of L1498 and L1517B. *Astronomy & Astrophysics*, 455:577–593, August 2006. doi: 10.1051/0004-6361:20065311. 45

S. Takano, Y. Sakai, S. Kakimoto, M. Sasaki, and K. Kobayashi. Detection of Methyl Formate in the Second Torsionally Excited State ($v_t = 2$) in Orion KL. *Publ. Astron. Soc. Japan*, 64:89, August 2012. doi: 10.1093/pasj/64.4.89. 174

Jonathan C Tan, Maria T Beltrán, Paola Caselli, Francesco Fontani, Asunción Fuente, Mark R Krumholz, Christopher F McKee, and Andrea Stolte. Massive star formation. *Protostars and Planets VI*, pages 149–172, 2014. 22

B. Tercero. *Condiciones físicas y químicas del gas alrededor de estrellas jóvenes masivas*. PhD thesis. 14, 15, 50, 51, 62

B. Tercero, J. Cernicharo, J. R. Pardo, and J. R. Goicoechea. A line confusion limited millimeter survey of Orion KL . I. Sulfur carbon chains. *Astronomy & Astrophysics*, 517:A96, July 2010. doi: 10.1051/0004-6361/200913501. 7, 16, 17, 22, 50, 51, 62, 69

B. Tercero, L. Vincent, J. Cernicharo, S. Viti, and N. Marcelino. A line-confusion limited millimeter survey of Orion KL. II. Silicon-bearing species. *Astronomy & Astrophysics*, 528:A26, April 2011. doi: 10.1051/0004-6361/201015837. 22, 51

B Tercero, I Kleiner, J Cernicharo, HVL Nguyen, A López, and GM Muñoz Caro. Discovery of methyl acetate and gauche ethyl formate in orion. *The Astrophysical Journal Letters*, 770(1):L13, 2013. 125, 174

B. Tercero, J. Cernicharo, A. López, N. Brouillet, L. Kolesniková, R. A. Motiyenko, L. Margulès, J. L. Alonso, and J.-C. Guillemin. Searching for trans ethyl methyl ether in Orion KL. *Astronomy & Astrophysics*, 582:L1, October 2015. doi: 10.1051/0004-6361/201526255. 22, 38, 132, 172, 174

L. Testi, J. C. Tan, and F. Palla. The near-infrared reflected spectrum of source I in Orion-KL. *Astronomy & Astrophysics*, 522:A44, November 2010. doi: 10.1051/0004-6361/201014497. 21

P Thaddeus. The prebiotic molecules observed in the interstellar gas. *Philosophical Transactions of the Royal Society B: Biological Sciences*, 361(1474):1681–1687, 2006. 27

A. G. G. M. Tielens and D. Hollenbach. Photodissociation Regions - Part Two - a Model for the Orion Photodissociation Region. *Astrophys. J.*, 291:747, April 1985. doi: 10.1086/163112. 18

A. G. G. M. Tielens and D. C. B. Whittet. Ices in star forming regions. In E. F. van Dishoeck, editor, *IAU Symposium*, volume 178 of *IAU Symposium*, page 45, 1997. 49

B. E. Turner. A molecular line survey of Sagittarius B2 and Orion-KL from 70 to 115 GHz. I - The observational data. *Astrophys. J. Suppl. Ser.*, 70:539–622, July 1989. doi: 10.1086/191348. 22

F. F. S. van der Tak, P. Schilke, H. S. P. Müller, D. C. Lis, T. G. Phillips, M. Gerin, and E. Roueff. Triply deuterated ammonia in NGC 1333. *Astronomy & Astrophysics*, 388:L53–L56, June 2002. doi: 10.1051/0004-6361:20020647. 18

E. F. van Dishoeck and G. A. Blake. Chemical Evolution of Star-Forming Regions. *Annu. Rev. Astron. Astrophys.*, 36:317–368, 1998. doi: 10.1146/annurev.astro.36.1.317. 46

Ewine F van Dishoeck. *The chemistry of diffuse and dark interstellar clouds*. Oxford University Press: Oxford, 1998. 28

A. I. Vasyunin and E. Herbst. Reactive Desorption and Radiative Association as Possible Drivers of Complex Molecule Formation in the Cold Interstellar Medium. *Astrophys. J.*, 769:34, May 2013. doi: 10.1088/0004-637X/769/1/34. 46

C. L. Verdes, A. von Engeln, S. A. Buehler, and A. Perrin. Partition function data and impact on retrieval quality for an mm/sub-mm limb sounder. *Journal of Quantitative Spectroscopy & Radiative Transfer*, 90:217–238, January 2005. doi: 10.1016/j.jqsrt.2004.03.012. 34

Serena Viti, Estelle Bayet, Thomas W Hartquist, Thomas A Bell, David A Williams, and Manda Banerji. Cosmic rays in the interstellar medium. In *Cosmic Rays in Star-Forming Environments*, volume 34, page 7, 2013. 44

SN Vogel, JH Bieging, RL Plambeck, WJ Welch, and MCH Wright. Differential rotation near the orion-kleinmann-low region aperture synthesis observations of hcn emission. *The Astrophysical Journal*, 296:600–605, 1985. 16

V. Wakelam, J.-C. Loison, E. Herbst, B. Pavone, A. Bergeat, K. Béroff, M. Chabot, A. Faure, D. Galli, W. D. Geppert, D. Gerlich, P. Gratier, N. Harada, K. M. Hickson, P. Honvault, S. J. Klippenstein, S. D. Le Picard, G. Nyman, M. Ruaud, S. Schlemmer, I. R. Sims, D. Talbi, J. Tennyson, and R. Wester. The 2014 KIDA Network for Interstellar Chemistry. *Astrophys. J. Suppl. Ser.*, 217:20, April 2015. doi: 10.1088/0067-0049/217/2/20. 47

C. M. Walmsley, W. Hermsen, C. Henkel, R. Mauersberger, and T. L. Wilson. Deuterated ammonia in the Orion hot core. *Astronomy & Astrophysics*, 172:311–315, January 1987. 18

Catherine Walsh, Tom J Millar, Hideko Nomura, Eric Herbst, Susanna Widicus Weaver, Yuri Aikawa, Jacob C Laas, and Anton I Vasyunin. Complex organic molecules in protoplanetary disks. *Astronomy & Astrophysics*, 563:A33, 2014. 39

N Watanabe, O Mouri, A Nagaoka, T Chigai, A Kouchi, and V Pirronello. Laboratory simulation of competition between hydrogenation and photolysis in the chemical evolution of h2o-co ice mixtures. *The Astrophysical Journal*, 668:1001–1011, 2007. 48

J. W. Waters. Absorption and emission by atmospheric gases. In M. L. Meeks, editor, *Astrophysics. Part B: Radio Telescopes*, pages 142–176, 1976. 34

Fred L Whipple. A comet model. i. the acceleration of comet encke. *The Astrophysical Journal*, 111: 375–394, 1950. 181

Fred L Whipple. A comet model. ii. physical relations for comets and meteors. *The Astrophysical Journal*, 113:464, 1951. 181

David A Williams and Eric Herbst. It's a dusty universe: surface science in space. *Surface Science*, 500 (1):823–837, 2002. 24

S. P. Willner, F. C. Gillett, T. L. Herter, B. Jones, J. Krassner, K. M. Merrill, J. L. Pipher, R. C. Puetter, R. J. Rudy, R. W. Russell, and B. T. Soifer. Infrared spectra of protostars - Composition of the dust shells. *Astrophys. J.*, 253:174–187, February 1982. doi: 10.1086/159622. 46

Thomas L Wilson, Kristen Rohlfs, and Susanne Hüttemeister. *Tools of radio astronomy*, volume 5. Springer, 2009. 60

Maria Womack, Lucy M Ziurys, and LJ Sage. N2h (+) in the orion ambient ridge-cloud clumping versus rotation. *The Astrophysical Journal*, 406:L29–L33, 1993. 16

M. C. H. Wright and R. L. Plambeck. Positions of the SiO masers in Orion-KL - Anisotropy on a scale of 70 AU. *Astrophys. J. Lett.*, 267:L115–L120, April 1983. doi: 10.1086/184014. 15

Yuefang Wu, Tie Liu, and Sheng-Li Qin. A study of dynamical processes in the orion kl region using alma—probing molecular outflow and inflow. *The Astrophysical Journal*, 791(2):123, 2014. 12

C. G. Wynn-Williams, R. Genzel, E. E. Becklin, and D. Downes. The Kleinmann-Low nebula - an infrared cavity. *Astrophys. J.*, 281:172–183, June 1984. doi: 10.1086/162086. 12

Satoshi Yamamoto. Chemistry of diffuse clouds. In *Introduction to Astrochemistry*, pages 65–90. Springer, 2017. 28

L. A. Zapata, J. Schmid-Burgk, and K. M. Menten. Orion KL: the hot core that is not a "hot core". 529: A24, May 2011. doi: 10.1051/0004-6361/201014423. 7, 12, 15, 18

Luis A Zapata, Johannes Schmid-Burgk, Paul TP Ho, Luis F Rodríguez, and Karl M Menten. Explosive disintegration of a massive young stellar system in orion. *The Astrophysical Journal Letters*, 704(1): L45, 2009. 15

B. Zuckerman and P. Palmer. On the Orion infrared nebula/molecular cloud. *Astrophys. J. Lett.*, 199: L35–L38, July 1975. doi: 10.1086/181843. 15

B. Zuckerman, T. B. H. Kuiper, and E. N. Rodriguez Kuiper. High-velocity gas in the Orion infrared nebula. *Astrophys. J. Lett.*, 209:L137–L142, November 1976. doi: 10.1086/182284. 15